MASSACHUSETTS INSTITUTE OF TECHNOLOGY
RADIATION LABORATORY SERIES

LOUIS N. RIDENOUR, *Editor-in-Chief*

TECHNIQUE OF MICROWAVE MEASUREMENTS

MASSACHUSETTS INSTITUTE OF TECHNOLOGY

RADIATION LABORATORY SERIES

Board of Editors

LOUIS N. RIDENOUR, *Editor-in-Chief*
GEORGE B. COLLINS, *Deputy Editor-in-Chief*

BRITTON CHANCE, S. A. GOUDSMIT, R. G. HERB, HUBERT M. JAMES, JULIAN K. KNIPP, JAMES L. LAWSON, LEON B. LINFORD, CAROL G. MONTGOMERY, C. NEWTON, ALBERT M. STONE, LOUIS A. TURNER, GEORGE E. VALLEY, JR., HERBERT H. WHEATON

---

1. RADAR SYSTEM ENGINEERING—*Ridenour*
2. RADAR AIDS TO NAVIGATION—*Hall*
3. RADAR BEACONS—*Roberts*
4. LORAN—*Pierce, McKenzie, and Woodward*
5. PULSE GENERATORS—*Glasoe and Lebacqz*
6. MICROWAVE MAGNETRONS—*Collins*
7. KLYSTRONS AND MICROWAVE TRIODES—*Hamilton, Knipp, and Kuper*
8. PRINCIPLES OF MICROWAVE CIRCUITS—*Montgomery, Dicke, and Purcell*
9. MICROWAVE TRANSMISSION CIRCUITS—*Ragan*
10. WAVEGUIDE HANDBOOK—*Marcuvitz*
11. TECHNIQUE OF MICROWAVE MEASUREMENTS—*Montgomery*
12. MICROWAVE ANTENNA THEORY AND DESIGN—*Silver*
13. PROPAGATION OF SHORT RADIO WAVES—*Kerr*
14. MICROWAVE DUPLEXERS—*Smullin and Montgomery*
15. CRYSTAL RECTIFIERS—*Torrey and Whitmer*
16. MICROWAVE MIXERS—*Pound*
17. COMPONENTS HANDBOOK—*Blackburn*
18. VACUUM TUBE AMPLIFIERS—*Valley and Wallman*
19. WAVEFORMS—*Chance, Hughes, MacNichol, Sayre, and Williams*
20. ELECTRONIC TIME MEASUREMENTS—*Chance, Hulsizer, MacNichol, and Williams*
21. ELECTRONIC INSTRUMENTS—*Greenwood, Holdam, and MacRae*
22. CATHODE RAY TUBE DISPLAYS—*Soller, Starr, and Valley*
23. MICROWAVE RECEIVERS—*Van Voorhis*
24. THRESHOLD SIGNALS—*Lawson and Uhlenbeck*
25. THEORY OF SERVOMECHANISMS—*James, Nichols, and Phillips*
26. RADAR SCANNERS AND RADOMES—*Cady, Karelitz, and Turner*
27. COMPUTING MECHANISMS AND LINKAGES—*Svoboda*
28. INDEX—*Henney*

TECHNIQUE OF MICROWAVE MEASUREMENTS

Edited by

CAROL G. MONTGOMERY

ASSOCIATE PROFESSOR OF PHYSICS
YALE UNIVERSITY

OFFICE OF SCIENTIFIC RESEARCH AND DEVELOPMENT
NATIONAL DEFENSE RESEARCH COMMITTEE

FIRST EDITION

NEW YORK AND LONDON
McGRAW-HILL BOOK COMPANY, INC.
1947

v. 11

TECHNIQUE OF MICROWAVE MEASUREMENTS

COPYRIGHT, 1947, BY THE
McGRAW-HILL BOOK COMPANY, INC.

PRINTED IN THE UNITED STATES OF AMERICA

All rights reserved. This book, or parts thereof, may not be reproduced in any form without permission of the publishers.

SCIENCE LIBRARY

MASS. INST. TECH.
JAN 2 1948
LIBRARY

THE MAPLE PRESS COMPANY, YORK, PA.

TECHNIQUE OF MICROWAVE MEASUREMENTS

EDITORIAL STAFF

C. G. Montgomery

D. D. Montgomery

Catherine F. Scott

CONTRIBUTING AUTHORS

R. Beringer
R. N. Griesheimer
D. Hamilton
R. A. Howard
G. N. Kamm
S. Katz
R. L. Kyhl
C. G. Montgomery
R. V. Pound
E. M. Purcell
R. M. Redheffer
E. Weber
H. R. Worthington
L. B. Young

FEB 20 1964

Foreword

THE tremendous research and development effort that went into the development of radar and related techniques during World War II resulted not only in hundreds of radar sets for military (and some for possible peacetime) use but also in a great body of information and new techniques in the electronics and high-frequency fields. Because this basic material may be of great value to science and engineering, it seemed most important to publish it as soon as security permitted.

The Radiation Laboratory of MIT, which operated under the supervision of the National Defense Research Committee, undertook the great task of preparing these volumes. The work described herein, however, is the collective result of work done at many laboratories, Army, Navy, university, and industrial, both in this country and in England, Canada, and other Dominions.

The Radiation Laboratory, once its proposals were approved and finances provided by the Office of Scientific Research and Development, chose Louis N. Ridenour as Editor-in-Chief to lead and direct the entire project. An editorial staff was then selected of those best qualified for this type of task. Finally the authors for the various volumes or chapters or sections were chosen from among those experts who were intimately familiar with the various fields, and who were able and willing to write the summaries of them. This entire staff agreed to remain at work at MIT for six months or more after the work of the Radiation Laboratory was complete. These volumes stand as a monument to this group.

These volumes serve as a memorial to the unnamed hundreds and thousands of other scientists, engineers, and others who actually carried on the research, development, and engineering work the results of which are herein described. There were so many involved in this work and they worked so closely together even though often in widely separated laboratories that it is impossible to name or even to know those who contributed to a particular idea or development. Only certain ones who wrote reports or articles have even been mentioned. But to all those who contributed in any way to this great cooperative development enterprise, both in this country and in England, these volumes are dedicated.

L. A. DuBRIDGE.

Preface

THE development and engineering of microwave radar equipment required that considerable effort be spent on improvements in the art of microwave measurements. New techniques had to be devised which were suitable for laboratory use, and these had to be modified and adapted for use in the field and in the factory. The necessity for the maintainance and the repair of military equipment imposed other special problems, and test gear had to be designed for these purposes also. A large portion of this test equipment was highly specialized and suited only for a particular purpose. No standard methods that were commonly acknowledged were available. Moreover, the precision and the convenience of operation of various pieces of measuring equipment varied widely. It has been attempted in the present volume to select for description those techniques and apparatus which are most likely to prove useful to future workers in the microwave field rather than to attempt a compilation that approaches completeness. Emphasis has been placed on laboratory equipment, since it is difficult to predict what future applications will be important.

Most of the methods to be described are based on the wave character of high-frequency currents, rather than on the low-frequency techniques of direct determination of current or voltage. The techniques to be described are grouped under four main headings:

I. Power Generation and Measurement.
II. Wavelength and Frequency Measurements.
III. The Measurement of Impedance and Standing Waves.
IV. Attenuation and Radiation Measurements.

Parts I and II need no further comment except that the measurements peculiar to radiation from pulsed generators are included as Chap. 7 of Part II. The numerous bridge measurements, so important in the low-frequency region, cannot be easily modified for microwave work, but analogous methods have been devised and show great promise for future development. These methods are discussed in Chap. 9 of Part III. The inclusion of the measurements of dielectric constant in Part III is based on the fact that it is the dielectric constant which determines the intrinsic impedance of a medium, since the permeability of nearly all

substances is very closely the same as that of a vacuum. Although attenuation and radiation measurements are essentially measurements of power, the special devices employed make it convenient to consider such measurements in a separate part.

It is a pleasure to acknowledge the cooperation of the many individuals who contributed to the preparation of this volume. In addition to those specifically named on a preceeding page in the list of authors and editorial staff, acknowledgement is due to Miss Ruth Kaufman for editorial assistance, to Mrs. Ruth Shoemaker who collated most of the photographs, and to Dr. V. Josephson for his able direction of the drafting staff.

CAROL G. MONTGOMERY.

NEW HAVEN, CONN,
February, 1947.

Contents

FOREWORD BY L. A. DUBRIDGE vii

PREFACE ix

CHAP. 1. INTRODUCTION 1

1·1. Microwaves 1
1·2. Microwave Measurements 2
1·3. The Detection of Microwaves 4
1·4. Microwave Cables and Connectors 8
1·5. Rigid Coaxial Lines 11
1·6. Waveguide Transmission Lines 13
1·7. Specialized Microwave Measurements 16

PART I. POWER GENERATION AND MEASUREMENT

CHAP. 2. POWER SOURCES 21

MICROWAVE OSCILLATORS 21

2·1. The Choice of a Microwave Oscillator 21
2·2. General Characteristics and Principles of Operation of the Reflex Klystron 24
2·3. More Detailed Characteristics of the Reflex Klystron 28
2·4. Frequency Multiplication in Detector Crystals 33
2·5. Specific Reflex-klystron Tube Types 34
2·6. The 723 Family of Reflex Klystrons 37
2·7. The Type 2K28 Reflex Klystron 41
2·8. The Type 417 Family 43
2·9. The Types 3K23 and 3K27 45
2·10. The Type 2K45 45
2·11. One-centimeter Reflex Klystrons 47
2·12. The Types 2K48 and 2K49 50
2·13. Reflex-klystron Power Supplies 51

FREQUENCY STABILIZATION OF ELECTRONICALLY TUNABLE MICROWAVE OSCILLATORS 58

2·14. General Description of Stabilization Circuits 60
2·15. The Microwave Discriminator 63
2·16. The D-c Stabilizer 67
2·17. The I-f Stabilization System 69
2·18. Electronic Circuits for I-f Stabilization 73
2·19. Results and Limitations of the Stabilization Systems 75

CHAP. 3. MICROWAVE POWER MEASUREMENTS 79
3-1. Introduction 79

POWER MEASUREMENTS AT LOW AND MEDIUM LEVELS 84
3-2. Bridge Circuits 84
3-3. Thermistor Parameters 89
3-4. Operation of a Thermistor in a Bridge Circuit 97
3-5. Audio-frequency Response of Bolometers 100
3-6. Temperature Compensation of Direct-reading Bolometer Bridges 103
3-7. The V-bridge 105
3-8. Temperature Compensation with Two Thermistor Disks 108
3-9. The Calculation of R-K Curves for Temperature Compensation 113
3-10. The W-bridge 118
3-11. The X-bridge 123
3-12. Self-balancing Bridges 127
3-13. Thermistor Mounts 130
3-14. Untuned Coaxial-line Thermistor Mount 132
3-15. A Double Thermistor Mount 136
3-16. Broadband Coaxial-line Thermistor Mounts 136
3-17. A 3-cm Thermistor Mount 139
3-18. Waveguide Thermistor Mounts 139
3-19. Impedance Variations of Thermistor Mounts 147
3-20. The Fishtail Mount 150
3-21. Thermistor Mounts for the 1-cm Band 151
3-22. Thermistor Power Monitors 155
3-23. Barretters 156
3-24. The Theory of Operation of a Barretter 161
3-25. Direct-reading Bridges for Barretters 169
3-26. Barretter–amplifier Combinations 171
3-27. Barretter Mounts 175
3-28. Load Lamps 180
3-29. Metalized-glass Bolometers 184
3-30 Thermocouple Power Detectors 187
3-31. The Use of Rectifiers for Power Indication 191

MEASUREMENT OF HIGH POWER 194
3-32. Water Loads 194
3-33. The Design of Water Loads for Coaxial Lines 195
3-34. Water Loads for Waveguide 199
3-35. Flow Systems for Water Loads 204
3-36. Thermopiles for Water Loads 211
3-37. The Use of Power Dividers for High-power Measurements . . . 213
3-38. Gas Loads 214
3-39. A Coaxial Wattmeter for Field Use 215
3-40. The Johnson Meter 216
3-41. Neon Tubes as Power Indicators 218

CHAP. 4. MICROWAVE SIGNAL GENERATORS 221
THE USE OF SIGNAL GENERATORS IN TESTING RECEIVERS 222
4-1. Receiver Noise Figures 222
4-2. Noise-figure Measurement with C-w Signal Generator 224

4·3. Noise-figure Measurement with Microwave Noise Source . . . 225
4·4. Measurements on Pulse Receivers . . . 226
4·5. Measurements with Pulsed Signal Generators . . . 228
4·6. Pulse-receiver Response to Frequency-modulated Signals . . . 230

The Design of Microwave Signal Generators . . . 234
4·7. Microwave Design Considerations for C-w and Modulated C-w Signal Generators . . . 234
4·8. Pulse Modulation of Oscillators . . . 237
4·9. R-f Leakage and Shielding . . . 240
4·10. Miscellaneous Features . . . 243
4·11. Calibration Procedures . . . 245

Practical C-w and Modulated-c-w Signal Generators . . . 247
4·12. A C-w, Pulse-modulated or F-m Signal Generator for the 3000-Mc/sec Region (the TGS-5BL Signal Generator) . . . 247
4·13. A Pulsed-lighthouse-tube Signal Generator for the 2700- to 2900-Mc/sec Region (TS-155) . . . 253
4·14. An F-m and C-w 9000-Mc/sec Signal Generator (TS-147) . . . 259
4·15. An F-m and C-w Signal Generator for the 24,000-Mc/sec Region 265

Microwave Noise Sources . . . 270
4·16. Noise Sources at Microwave Frequencies . . . 270
4·17. Thermal Noise Sources . . . 271
4·18. Shot-noise Sources . . . 273
4·19. Crystal Noise Source . . . 278

PART II. WAVELENGTH AND FREQUENCY MEASUREMENTS

Chap. 5. THE MEASUREMENT OF WAVELENGTH . . . 285
Cavities as Circuit Elements . . . 286
5·1. The Equivalent Circuit of a Single-line Cavity-coupling System 286
5·2. Transmission Through a Two-line Cavity-coupling System . . . 289
5·3. Frequency-pulling by Reactive Loads . . . 291

Normal Mode Fields in Some Cavities of Simple Shape . . . 293
5·4. Rectangular Parallelopiped . . . 294
5·5. The Right Circular Cylinder . . . 297
5·6. Coaxial Cylinders . . . 303
5·7. Other Shapes . . . 307
5·8. Cavities Containing Dielectric Materials . . . 307
5·9. Scaling Theorems and the Principle of Similitude . . . 308

Practical Wavemeter Circuits . . . 308
5·10. Transmission Cavity Wavemeter . . . 309
5·11. Reaction Wavemeter Terminating a Line . . . 311
5·12. Reaction Wavemeter on an E-plane Waveguide T . . . 314
5·13. Iris-coupled Wavemeter on Top of Waveguide . . . 316
5·14. Reaction Wavemeter on a Coaxial Stub . . . 318

PRACTICAL MICROWAVE WAVEMETERS 319
5·15. Coaxial Wavemeter for the 3- and 10-cm Regions 320
5·16. Right Circular Cylinder in TE_{011}-mode for the 3-cm Region . . 322
5·17. Right Circular Cylinder in TE_{011}-mode for the 10-cm Region (TS-270) 325
5·18. Right Circular Cylinder in TE_{11n}-mode for the 1-cm Region . . 327
5·19. Hybrid TE_{011}-mode Wavemeter for the 1-cm Region 328

MEASUREMENTS ON CAVITY-COUPLING SYSTEMS 330
5·20. Transmission Measurements with a Two-line Cavity 332
5·21. Standing-wave Measurements on Cavities 333
5·22. Phase Measurements 336
5·23. Decrement Measurements 340

CHAP. 6. FREQUENCY MEASUREMENTS 343
PRIMARY FREQUENCY STANDARDS 343
6·1. General Requirements 343
6·2. Microwave Frequency Generation 344
6·3. Design Considerations 345
6·4. Microwave Facilities at the National Bureau of Standards . . . 347
6·5. Crystal-controlled Oscillators 350
6·6. Reception of Standard-frequency Broadcasts 353
6·7. Frequency Dividers and Clocks 354
6·8. Tunable Oscillator 357
6·9. Audio Interpolation Oscillator 359
6·10. Comparison Oscilloscope 361
6·11. Variable-frequency Generation 365
6·12. Basic Types of Vacuum-tube Frequency Multipliers 365
6·13. Frequency Multipliers from 50 kc/sec to 5 Mc/sec 368
6·14. Frequency Multipliers from 6 to 24 Mc/sec 368
6·15. Frequency Multipliers from 24 to 96 Mc/sec 371
6·16. Frequency Multiplier from 96 to 288 Mc/sec 371
6·17. Frequency Multiplier from 288 to 864 Mc/sec 372
6·18. Harmonic Generation by Crystal Rectifiers and Velocity-modulated Frequency Multipliers 373
6·19. Frequency Range and Accuracy 375

RESONANT CAVITIES AS SECONDARY FREQUENCY STANDARDS 375
6·20. General Design Considerations 375
6·21. Partial-coaxial Cavities 377
6·22. TE_{011}-mode Cavities 379
6·23. Hybrid TE_{011}-mode Cavities 382

TEMPERATURE AND HUMIDITY EFFECTS FOR STANDARD CAVITIES 384
6·24. Temperature Effects 384
6·25. External Temperature Compensation 386
6·26. Humidity Effects 390

MEASURING EQUIPMENT AND TECHNIQUES 392
6·27. Standard Measurement Conditions 393
6·28. Spectrum-analyzer Techniques 393

6·29. Cavity Q-meter Technique 396
6·30. Cavity-comparator Technique 403

CHAP. 7. THE MEASUREMENT OF FREQUENCY SPECTRUM AND PULSE SHAPE 408

THE PRINCIPLES AND DESIGN OF SPECTRUM ANALYZERS 409
7·1. Formation of the Spectrum 409
7·2. General Theory of Operation 411
7·3. Determination of Sweep Frequency, Intermediate Frequency, I-f Bandwidth, and Video Bandwidth 416
7·4. Determination of the Sensitivity and I-f Gain Required for a Given Application 420
7·5. Stability Considerations in the Design of a Spectrum Analyzer 422

REPRESENTATIVE SPECTRUM ANALYZERS 423
7·6. The TSK-3RL 1-cm-band Spectrum Analyzer 423
7·7. The TS-148/UP 3-cm-band Spectrum Analyzer 429
7·8. The TSS-4SE 10-cm-band Spectrum Analyzer 434
7·9. The TSX-4SE Spectrum Analyzer 439
7·10. The TSK-2SE Spectrum Analyzer 440
7·11. Low-frequency Spectrum Analyzers Using Microwave Oscillators 441
7·12. Other Instruments Using the Spectrum-analyzer Principle . . 446
7·13. Echo Boxes 447

MEASUREMENTS WITH THE SPECTRUM ANALYZER 448
7·14. Interpretation of Spectra 448
7·15. Examples of Spectra of Pulses 449
7·16. Frequency and Frequency-difference Measurements 453
7·17. The Use of a Spectrum Analyzer as a Sensitive Receiver 455

THE R-F ENVELOPE VIEWERS AND OSCILLOSCOPES 455
7·18. The Components of an R-f Envelope Viewer 456
7·19. Crystal Detector with Video Amplifier 457
7·20. Vacuum-tube Detector with Video Amplifier 458
7·21. Diode Detectors Used at High Level 461
7·22. Diode Detectors for Frequencies Higher than 3000 Mc/sec . . . 464
7·23. Microwave Oscilloscopes 468

PART III. THE MEASUREMENT OF IMPEDANCE AND STANDING WAVES

CHAP. 8. MEASUREMENTS OF STANDING WAVES 473
8·1. Fundamental Relations 475
8·2. The Slotted Section and Traveling Probe 478
8·3. The Properties of the Slotted Line 480
8·4. The Properties of the Probe 483
8·5. The Design of Slotted Sections and Probes 488
8·6. Detectors and Amplifiers 496
8·7. Matched Loads and Other Accessories 503
8·8. Measurement of High Standing-wave Ratios 505
8·9. The Squeeze Section 507

8·10. Standing-wave Measurements at High Power 510
8·11. Continuously Indicating Standing-wave Detectors 511
8·12. Measurements on Lossless Devices 512

CHAP. 9. IMPEDANCE BRIDGES 515

BRIDGE ELEMENTS 516

9·1. The Side-outlet T 516
9·2. Analysis of the Operation and Properties of Side-outlet T's . . 517
9·3. Analysis of the Directional Coupler as a Bridge Element 522
9·4. T-construction 524
9·5. Matching Techniques for T's 525
9·6. Ring Networks and Coaxial T's 527

BASIC MEASURING TECHNIQUES 530

9·7. The Single-frequency Bridge 530
9·8. T-asymmetry 532
9·9. Bridge Balance and the Sliding Match 534
9·10. Magic-T Alignment 535
9·11. The Measurement of Large Reflections 536
9·12. Methods Which Provide Simultaneous Indications at Several Frequencies 537
9·13. Line Components 540

IMPEDANCE BRIDGES UTILIZING MODULATION-FREQUENCY DISCRIMINATION . 543

9·14. Microwave Sources 543
9·15. Line Components 544
9·16. Selective Amplifiers 545
9·17. Range of Measurement 547

IMPEDANCE BRIDGES THAT EMPLOY PULSE MODULATION 548

9·18. Microwave Sources 548
9·19. Line Components 549
9·20. Pulse Amplifier 550
9·21. Range of Measurement 551

IMPEDANCE BRIDGES UTILIZING PANORAMIC RECEIVERS 552

9·22. Microwave Sources and Local Oscillators 552
9·23. Line Components 554
9·24. Receiver 555
9·25. Range of Measurement 556

CALIBRATING DEVICES AND SOURCES OF ERROR 556

9·26. Adjustable Reference Mismatches 557
9·27. Fixed Mismatches and Calibrated Attenuators 557
9·28. Built-in Calibrators 558
9·29. Sources of Error 559

CHAP. 10. THE MEASUREMENT OF DIELECTRIC CONSTANTS . . . 561

INTRODUCTION 561

10·1. Derivation of Relations for Proceeding from Data to Results . . 562
10·2. General Considerations Influencing Choice of Method 568

METHODS DEPENDING ON TRANSMISSION IN GUIDE 570

10·3. Techniques for Phase Measurement 570

10·4. Techniques for Amplitude Measurement . . . 577
10·5. Details of Computation . . . 584
10·6. Uses . . . 591

MEASUREMENT BY TRANSMISSION IN FREE SPACE . . . 591
10·7. Experimental Procedure for Normal Incidence . . . 593
10·8. Computations for Normal Incidence . . . 597
10·9. Arbitrary Incidence . . . 599
10·10. Comparison with Optical Methods . . . 604
10·11. Uses . . . 605

GENERAL METHODS DEPENDING ON REFLECTION . . . 606
10·12. Interface Reflection . . . 606
10·13. Reflection Measurement in Free Space . . . 612
10·14. Change of Termination . . . 616
10·15. Short Circuit, Zero Reflection at Interface . . . 620

THE SHORT-CIRCUITED-LINE METHOD . . . 625
10·16. Theory . . . 625
10·17. Measurement Procedure . . . 633
10·18. A Few Sources of Error . . . 640
10·19. Modified Procedure for Low Power . . . 644
10·20. Uses . . . 654

CONCLUSION . . . 656
10·21. Resonant-cavity Methods . . . 657
10·22. Summary. Methods Tabulated . . . 666

BIBLIOGRAPHY . . . 672

PART IV. ATTENUATORS AND RADIATION MEASUREMENTS

CHAP. 11. MICROWAVE ATTENUATORS. CUTOFF ATTENUATORS . 679
INTRODUCTION . . . 679
11·1. Definitions of Attenuation . . . 679
11·2. General Design Considerations . . . 682

CUTOFF ATTENUATORS . . . 685
11·3. Principles of Cutoff Attenuators . . . 685
11·4. Purity of Useful Mode . . . 687
11·5. Separation of Undesirable Modes . . . 689
11·6. Principle of Mode Filtering . . . 693
11·7. Variation of Input Impedance with Close Coupling . . . 696
11·8. Impedance-matching Techniques . . . 700
11·9. Examples of Waveguide Attenuators for 3000 Mc/sec . . . 707
11·10. A Waveguide Attenuator for 9000 Mc/sec . . . 715
11·11. An Attenuator for 24,000 Mc/sec . . . 716
11·12. The Design of Cutoff Attenuators Using the TM_{01}-mode . . . 719

CHAP. 12. MICROWAVE ATTENUATORS. RESISTIVE ATTENUATORS 720
MATCHED TRANSMISSION-LINE TERMINATIONS . . . 720
12·1. Low-power Coaxial-line Terminations . . . 722
12·2. Low-power Waveguide Terminations with Polyiron . . . 726

12·3. Low-power Waveguide Terminations Which Use Other Lossy Materials 728
12·4. Low-power Terminations Using Metalized Glass 731
12·5. High-power Coaxial-line Loads 732
12·6. High-power Waveguide Loads 735

General Laboratory Attenuators 743
12·7. Cables as Coaxial Attenuators 743
12·8. Fixed Coaxial Pads 745
12·9. Fixed Waveguide Attenuators 747
12·10. Variable Waveguide Attenuators 748

Precision Metalized-glass Attenuators 751
12·11. Electrical Design of Coaxial-pad Inserts 752
12·12. Construction of Coaxial Fixed Pads 757
12·13. Performance Characteristics of Fixed Coaxial Pads 763
12·14. Variable Metalized-glass Coaxial Attenuators 769
12·15. Design of Elements for Waveguide Attenuators 774
12·16. Waveguide Pads of Fixed Values 781
12·17. Construction of Variable Waveguide Attenuators 784
12·18. Performance Characteristics of Variable Waveguide Attenuators 790

Power Dividers as Attenuators 799
12·19. Calibrated Pickup Probe 799
12·20. Directional Couplers 800
12·21. Bifurcated Lines 801
12·22. Branched Lines 803

Chap. 13. THE MEASUREMENT OF ATTENUATION 804
13·1. Direct Measurement of Power Ratio 805
13·2. Substitution Methods 808
13·3. Measurement of Attenuation by Standing-wave Effects 816
13·4. Measurement of Very Small Attenuation Values 821
13·5. Common Sources of Errors in Attenuation Measurements . . . 824
13·6. Calibration of Attenuation Standards 832
13·7. Calibration with Absolute Power Measurement 838
13·8. Calibration of Secondary Standards by the Substitution Method 841
13·9. Production Calibration 848

Chap. 14. DIRECTIONAL COUPLERS 854
14·1. Introduction 854
14·2. Equivalent Circuit of a Directional Coupler 855
14·3. The Bethe-hole Coupler 858
14·4. Branched-guide Couplers 866
14·5. Two-hole Couplers 873
14·6. Multiple-path Couplers 879
14·7. Reverse-coupling Types 883
14·8. Long-slot Couplers 885
14·9. Resistive-loop Couplers 891
14·10. General Theoretical Considerations 891
14·11. Measurements of the Properties of Directional Couplers 894
14·12. The Reflectometer 896

CHAP. 15. R-F PHASE AND PATTERN MEASUREMENTS 898
15·1. Terminology and Definitions 898
15·2. Pattern Intensity Measurements 900
15·3. The Measurement of Antenna Gain 907
15·4. Effect of Antenna Scattering in Gain Measurements 909
15·5. The Mirror Method of Gain Determination 911
15·6. Gain Determination by Pattern Integration 914
15·7. R-f Phase Measurements 915
15·8. Phase Apparatus for Point Sources 916
15·9. Frequency Sensitivity of Phase 917
15·10. Phase Apparatus for Line Sources 918
15·11. Phase-modulation Method 919

APPENDIX. MANUFACTURERS OF MICROWAVE EQUIPMENT 923
1. R-f Cables and Connectors 923
2. Waveguide and Rigid Coaxial Line and Connectors 923
3. Amplifiers and Power Supplies 924
4. Crystal Rectifiers 924
5. Oscillator Tubes 924
6. Power Measurements 924
7. Attenuators 925
8. Spectrum Analyzers 925
9. R-f Components 925
10. Wavemeters 925

MANUFACTURERS 925

INDEX 929

CHAPTER 1

INTRODUCTION

By C. G. Montgomery

1·1. Microwaves.—The spectrum of electromagnetic radiation may be divided into two parts that differ primarily in the principal methods for the detection of the radiation. The first of these regions, the optical region, extends from the shortest γ-rays, up through the ultraviolet and visual wavelengths, to some indefinite wavelength in the far infrared. In this region the elementary processes are discontinuous and must be described by the quantum theory. The methods of detection involve quantum effects—the photoelectric effect or photochemical processes in the human eye or in a photographic plate. In the second region, the phenomena are more directly associated with electrical effects. Radiation is detected by the transformation of the radiant energy into some mechanical motion—the deflection of a meter, the sound from a loudspeaker, or the motion of an electron beam that falls upon the screen of a cathode-ray tube. It is the short-wavelength end of this electrical region of the spectrum, the region of microwaves, that is the concern of this volume.

The microwave region extends from about 1000 Mc/sec to about 30,000 Mc/sec, a range of about five octaves. The range of wavelengths, from 1 to 30 cm, is identical with the range of dimensions of most experimental apparatus, and it is this circumstance that leads to a separation of the microwave region from the regions of longer wavelength. At low frequencies and long wavelengths, coils, condensers, and resistance elements are combined with vacuum tubes to form electrical networks, and the sizes of the components can be made small compared with the wavelength. If it were attempted to extend these techniques to the microwave region, the component parts would be much too small for practical application; therefore new techniques must be employed. Instead of circuits with lumped elements, circuits that are made up of transmission lines must be used. In fact, the process of separating a microwave circuit into component elements is one that must be applied with caution, and in many cases must be avoided altogether.

The strength of the interaction between the elements of a circuit—or, expressed in another way, the amount of the radiation—precludes the use of open wires to conduct microwave currents, and coaxial trans-

mission lines and hollow-pipe waveguides must be substituted. Emphasis is shifted from the currents flowing in the conductors to the electric and magnetic fields inside the pipes. The circuit elements take the form of obstacles placed within the transmission line, and the resonant combination of a coil and a condenser at low frequencies is replaced by a resonant cavity in the microwave region. Since at least one dimension of a resonant cavity must be of the order of half a wavelength, the long-wavelength limit of the region where microwave techniques are no longer very useful is the wavelength for which a resonant cavity becomes inconveniently large.

Vacuum tubes of the conventional type cannot be used in the microwave region both because the lead wires are too long and because the time of transit of the electrons between the electrodes in the tube is no longer short compared with the period of a wave. A new principle of operation must be invoked and tubes employing velocity-modulated electron beams are used. This principle is embodied in the klystron tubes that produce low and medium continuous-wave power and in the cavity magnetrons that furnish high power under pulsed operation. The high-frequency limit of the microwave region near 30,000 Mc/sec is set not because the dimensions of the circuits become too small, but because oscillator tubes, at the present time, have not been developed for shorter wavelengths. No doubt the near future will see the workable region extended. The natural limit of the microwave region where quantum effects prevail is already accessible at very low temperatures. In the customary notation, the significant parameter $h\nu/kT$ is unity for $\nu = 3 \times 10^{10}$ cps and $T = 1.3°K$.

1·2. Microwave Measurements.—The new techniques that are required for the transmission of microwaves must be accompanied by new techniques of measuring the transmission characteristics. Indeed the quantities that are useful to measure change as the frequency is increased. Measurements of the frequency of oscillation are replaced by measurements of wavelength; the fundamental quantities, current and voltage, cease to be significant in the microwave region, and the power and the phase of the waves become important. Physical quantities are characterized by four dimensions: mass, length, time, and charge. Since electro-mechanical phenomena are of little importance, microwave quantities may be characterized by only three. These three microwave "dimensions" can be taken as power, length, and frequency, and all microwave measurements may be reduced to measurements of three parameters.

The system of units that will be used throughout this volume is the rationalized practical MKS system. Microwave power is expressed in watts, or in multiples or submultiples of a watt, in megawatts (Mw),

kilowatts (kw), or milliwatts (mw); length is expressed in meters (m) or centimeters (cm); and frequency, in cycles per second (cps), kilocycles per second (kc/sec), or megacycles per second (Mc/sec). Some of the letter symbols most often used are given in Table 1·1. This table is not exhaustive, and most of the symbols are the commonly accepted ones. In the MKS system, the dielectric constant ϵ_0 of free space and the magnetic permeability μ_0 have not the value unity but are

$$\epsilon_0 = 8.85\ \mu\mu f/\text{meter},$$
$$\mu_0 = 1.257\ \mu h/\text{meter}.$$

These quantities often occur in the combination

$$\sqrt{\frac{\mu_0}{\epsilon_0}} = 377 \text{ ohms}.$$

Complex quantities will be used throughout without any distinguishing notation, and the complex conjugate of a quantity will be denoted by affixing an asterisk (*). In accordance with engineering practice, the time variation of a sinusoidally varying quantity is assumed to be $e^{j\omega t}$. This convention leads to the positive sign for the reactance of an inductance and for the susceptance of a capacitance, as indicated in the last two lines of Table 1·1.

TABLE 1·1.—LETTER SYMBOLS FREQUENTLY USED

Quantity	Symbol
Electric field	E
Magnetic field	H
Imaginary unit, $\sqrt{-1}$	j
Propagation constant, $\gamma = \alpha + j\beta$	γ
Attenuation constant	α
Phase constant or wave number, $2\pi/\lambda$	β
Wavelength*	λ
Wavelength in waveguide	λ_g
Frequency	ν, f
Angular frequency, $2\pi\nu$	ω
Voltage standing-wave ratio, VSWR	r
Reflection coefficient	Γ
Dielectric constant*	ϵ
Magnetic permeability*	μ
Relative dielectric constant,† or specific inductive capacity, ϵ/ϵ_0	k_e
Power	P
Impedance, $Z = R + jX$	Z
Admittance, $Y = 1/Z = G + jB$	Y

* When zeros are affixed to these symbols, the quantities refer to the values for free space.
† Throughout Chap. 10 the subscript e is dropped for convenience.

The new technique that contributed so largely to the opening of the microwave region was the utilization of the principle of velocity modulation for the production of continuous oscillations. Chapter 2 is devoted

to a description of low-power sources useful for microwave measurements. In Chap. 3 the methods of measurement of power are treated, and Chap. 4 contains a discussion of some of the microwave signal generators that have been used. Sources of noise power are also described, and here the atomic constants e and k, the electronic charge and Boltzmann's constant, are involved. The measurements of frequency and wavelength, the other fundamental quantities, are described in the next three chapters. Nearly all the new techniques that are encountered here rely upon frequency modulation of the oscillations. The microwave spectrum analyzer described in Chap. 7 has proved itself to be exceedingly versatile and useful. The remainder of the volume is devoted to measurements that combine power measurements with determinations of position and wavelength. The novel instruments include standing-wave detectors, directional couplers, and microwave bridge circuits or magic T's.

1·3. The Detection of Microwaves.—The presence of microwave radiation may be detected by electrical or by thermal methods. The electrical method distinguishes the microwave region of wavelengths from the optical region and involves the conversion of the microwave energy to a low, or perhaps zero, frequency by means of a nonlinear element and the detection of the energy by the ordinary low-frequency techniques. The thermal method is common to the whole electromagnetic spectrum and involves the conversion of the radiant energy to heat. The thermal method is the only method that admits of absolute calibration. The barretters, thermistors, and other thermometric devices are treated at length in Chap. 3 and need only be mentioned here. On the other hand, the electrical methods developed for microwave radiation represent a considerable advance in the art of measurement.

Frequency conversion, or demodulation, may be accomplished by any nonlinear electrical device, but the efficiency of conversion and useful frequency range vary greatly from one device to another. The most suitable conversion element for microwaves is a crystal of silicon with a tungsten cat whisker. Silicon to which a trace of impurity has been added is a semiconducting metal. If a very fine tungsten point makes contact with the surface of a crystal, the difference in work functions of the two metals causes a very thin boundary layer to be set up. This layer is unsymmetrical and the resistance of the contact depends on the sign and magnitude of the impressed voltage. Such a crystal rectifier is an excellent nonlinear device for microwave frequencies because the active region in the vicinity of the point of the whisker is extremely small. For microwave uses, crystals are packaged in small cartridges. Figure 1·1 shows cross sections of standard cartridge crystals that are useful for all but the highest microwave frequencies. The sensitive contact is adjusted during manufacture, and the space around the contact is

filled with wax. The resulting unit is stable, both electrically and mechanically. For wavelengths near 1 cm a second type of cartridge is used; this cartridge is shown in Fig. 1·2. The crystal is mounted at the end of a coaxial line of small diameter and the dimensions are so chosen that the coaxial line appears matched at a wavelength of 1.25 cm when the incident microwave power is 1 mw. Considerable effort has been expended on the development of crystal rectifiers of these types.

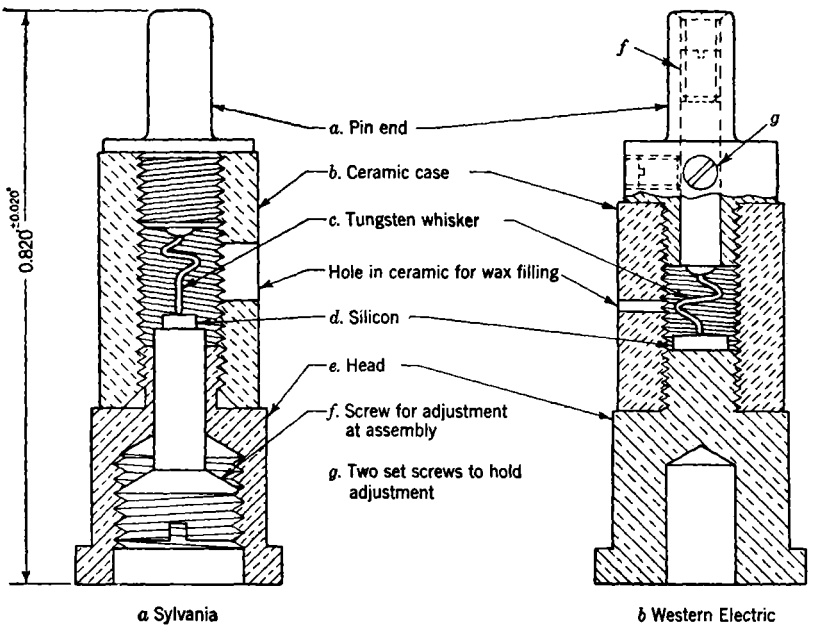

FIG. 1·1.—Standard ceramic-cartridge crystals.

Great improvements have resulted from this effort, both in the sensitivity of the rectifiers and in the ruggedness of the units.[1]

The ceramic cartridge crystals are of a size convenient for mounting as an extension of the center conductor of a coaxial line for wavelengths near 10 cm. A schematic drawing of such a mounting is shown in Fig. 1·3. The crystal is preceded by two slugs of metal or dielectric material which reflect microwaves incident upon them. The positions of the two slugs are adjustable and it is possible to arrange that the wave reflected by the crystal is canceled by the waves reflected from the slugs. When this is done all of the power traveling in the coaxial line is absorbed by the crystal, and the device is said to be matched. At higher frequencies,

[1] See *Crystal Rectifiers*, Vol. 15, Radiation Laboratory Series.

where waveguide is used for microwave transmission, the ceramic cartridge is mounted across the waveguide in the direction of the electric field. A crystal holder for wavelengths from 3.1 to 3.5 cm is shown in Fig. 1·4. The matching of the unit is accomplished by two adjustable screws preceding the crystal, and a variable short-circuiting plunger that terminates the waveguide line. A crystal holder of a third variety is shown in Fig. 1·5. The mount was designed for the shielded cartridge crystal of Fig. 1·2. The unit is a transition section from waveguide to coaxial line with the line terminated by the crystal cartridge. Impedance-matching is accomplished by two screws and a variable short circuit as in the other waveguide mount. The crystal holder was designed for a wavelength of 1.25 cm. Further details of crystal mounts may be found in other volumes[1] of the Series.

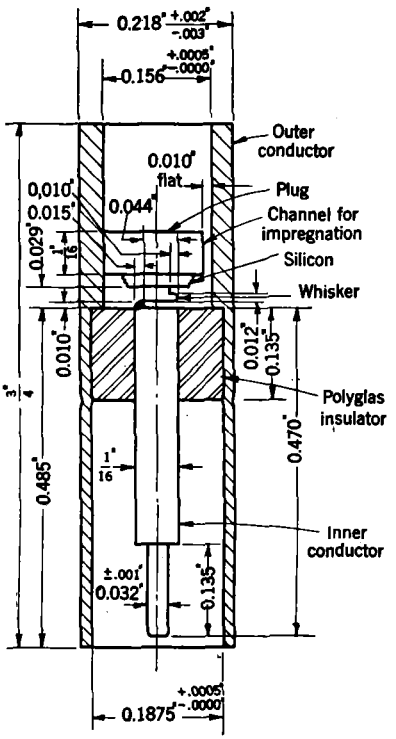

FIG. 1·2.—Shielded cartridge crystals for wave-lengths near 1 cm.

Crystals are often used as rectifiers to convert microwave energy to direct current. They are nearly square-law devices and deliver about 1 ma of current to a low impedance for 1 mw of microwave power. Unfortunately the deviations from square-law behavior are sufficiently large that calibration is essential for all but the most qualitative

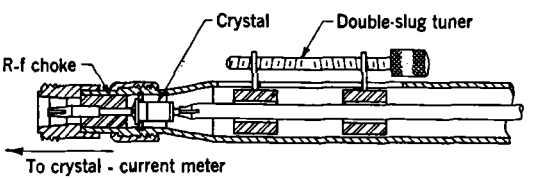

FIG. 1·3.—Coaxial-line mounting for ceramic-cartridge crystals with tuning elements for impedance-matching.

measurements. In a superheterodyne receiver, the crystal is used as a

[1] *Crystal Rectifiers*, Vol. 15, Radiation Laboratory Series. *Microwave Mixers*, Vol. 16, Radiation Laboratory Series.

mixing element. Power from a microwave oscillator, the local oscillator, is applied to the crystal together with the signal power. The difference frequency produced by the beating of the two microwave frequencies may be amplified and detected by ordinary low-frequency techniques. Some signal power is lost by this process, and the conversion loss of crystals at present is about 6 db. A summary of the properties of some of the various crystal types now available is given in Table 1·2. The first four types are designed for use as mixers; the last four types are intended to rectify to direct current. The type 1N32 differs from the type 1N27 in having approximately twice the sensitivity.

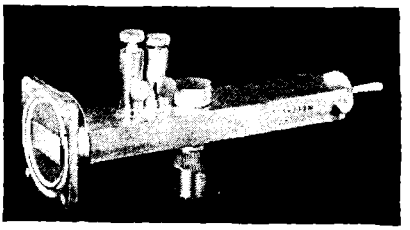

FIG. 1·4.—Crystal holder for use in the 3-cm region. The crystal is mounted directly across the waveguide.

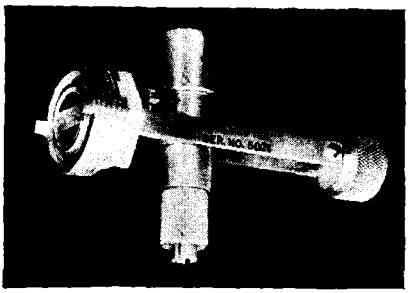

FIG. 1 5.—Holder for the shielded cartridge crystal. The crystal is inserted beneath the screw cap.

Vacuum tubes also have been used to rectify microwave currents. Because of the large transit time of the electrons between the grids of

TABLE 1·2.—PROPERTIES OF CARTRIDGE CRYSTAL UNITS

Crystal type	Cartridge	Use	Test frequency, Mc/sec	Maximum conversion loss, db
1N21B	Ceramic	Mixer	3,060	6.5
1N21C	Ceramic	Mixer	3,060	5.5
1N23B	Ceramic	Mixer	9,375	6.5
1N26	Coaxial	Mixer	24,000	8.5
1N27	Ceramic	Detector	3,295	
1N30	Ceramic	Detector	9,375	
1N31	Coaxial	Detector	9,375	
1N32	Ceramic	Detector	3,295	

the tubes, the conversion or rectification efficiency is low. Some of the r-f envelope viewers described in Chap. 7 employ vacuum tubes since the instruments are designed to work at high power levels, and sensitivity is not of great importance.

1·4. Microwave Cables and Connectors.—An important part of any experimental arrangement are the lines and cables used to connect the various pieces of equipment. At the long-wavelength end of the microwave region, flexible cables are commonly used for this purpose. A

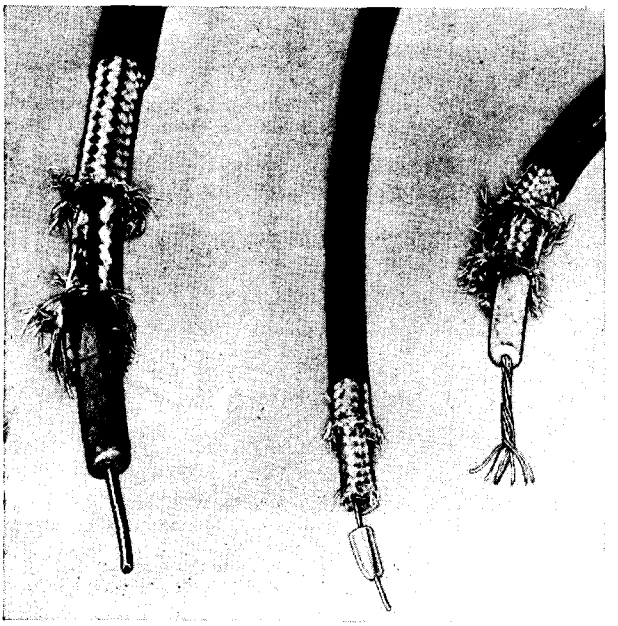

FIG. 1·6.—Microwave cables. The commonly used RG-9/U is shown on the right.

knowledge of the cables and the connectors and adapters that are available is very useful.[1] Figure 1·6 shows three cables with the ends spread apart to show the construction. The center cable in the photograph shows a beaded cable with "fish-spine" beads. Cables of this type are seldom used at wavelengths as short as those in the microwave region since the reflections from the beads are usually objectionable. Moreover, the beads are easily broken and the cable is not very rugged. More satisfactory cables are made with a solid flexible dielectric, usually polyethylene, as in the two other cables in the figure. A double layer

[1] Complete information on microwave transmission lines is given in Vol. 9 of the Radiation Laboratory Series. Flexible cables are discussed in Chap. 5 of that volume.

of braid forms the outer conductor of the cable, and the braid is covered by a protecting jacket and, sometimes, metal armor as well.

To facilitate production and to standardize transmission lines for the armed forces, the joint Army-Navy Radio Frequency Cable Coordinating Committee (ANRFCCC) was active during the war and established specifications for cables, connectors, and adapters for transmission lines of all types, including waveguides. A complete index[1] of r-f lines and fittings has been prepared by the committee and is a very useful source of information. To aid in identification and ordering, a number system has been established which is commonly used. Lines are described by a number such as RG-9/U (radio guide -9/universal), and fittings by UG-21/U (union guide -21/universal). Although the committee is a wartime agency and will soon cease to function, probably a new committee will be formed to continue the work.

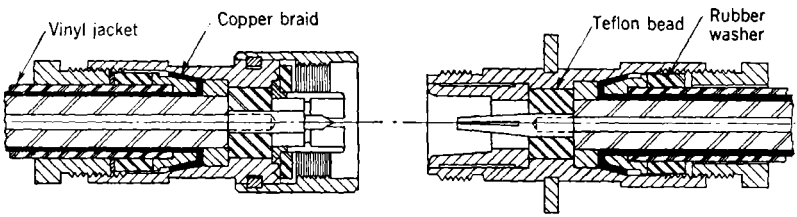

FIG. 1·7.—Type N connectors for microwave coaxial cable: UG-21B/U and UG-22B/U.

The cables most commonly used at microwave frequencies are the RG-9/U, RG-21/U, and RG-5/U cables. The RG-9/U cable is shown on the right side of Fig. 1·6. It has a diameter of 0.28 in. over the polyethylene dielectric, a characteristic impedance of 52 ohms, and a capacitance of 30 $\mu\mu f$/ft. The voltage rating is 4000 volts rms, but breakdown will occur in the connectors at a considerably lower voltage. This cable can be used with small losses down to a wavelength of 3 cm. The RG-21/U cable is similar to the RG-9/U cable except that the center conductor is made of nichrome wire, and a length of this cable can be used as an attenuator. The RG-5/U cabie has a smaller diameter, 0.185 in. over the dielectric, as well as a smaller center conductor; the impedance is also 52 ohms.

The usual connectors for the RG-9/U and RG-21/U cables are type N connectors. The latest designs for a plug and jack are shown in Fig. 1·7 and have the designations UG-21B/U and UG-22B/U. These connectors are designed to have a low reflection in the 10-cm region and also at wavelengths from 3.1 to 3.5 cm. At intermediate wavelengths

[1] "Index of Army-Navy R-F Transmission Lines and Fittings," Navships 900102, Army No. 71-4925, Washington, D.C., June, 1945.

the reflections are larger. The smaller RG-5/U cable is often used to connect to Sperry Klystrons and require an "SKL" fitting. Such a connector, the UG-275/U connector, is shown in Fig. 1·8. Many other cables, both larger and smaller, and the connectors for them are available, as well as adapters from one cable to another and to rigid lines, T's, and angle connectors.

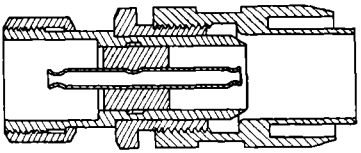

FIG. 1·8.—UG-275/U connector for use with RG-5/U cable to connect to Sperry Klystron tubes.

At frequencies below the microwave region, cables of higher characteristic impedance are used; 72 ohms is a common value. A reliable connector greatly facilitates experimental work and it is often desirable to use microwave cables and connectors for low-frequency circuits as well. Another series of connectors—the UHF connectors, which have

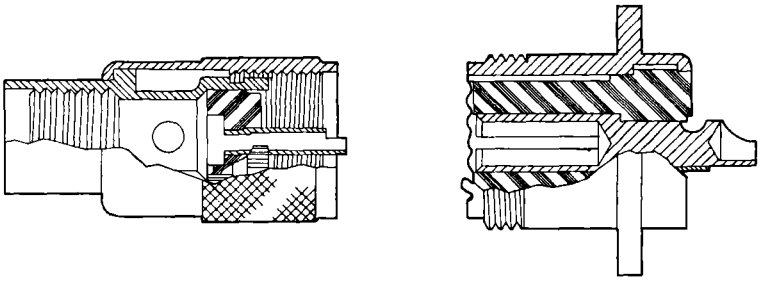

(a) (b)

FIG. 1·9.—UHF connectors, Navy types 49190 and 49194.

proved to be very satisfactory for low-frequency auxiliary equipment, can be used with RG-9/U cables and others. A plug and jack are shown in Fig. 1·9, Navy types 49190 and 49194 respectively. Figure 1·10 shows a bulkhead adapter for connecting two cables together. Adapters are also available from UHF fittings to type N connectors; Fig. 1·11 shows two of them. Low-frequency connectors are often made an integral part of microwave components. The crystal holder of Fig. 1·4 has a UHF jack mounted directly on the waveguide; the low-frequency connector shown in Fig. 1·5 is a small connector similar to a type N connector designated as a BNC or "baby type N" connector.

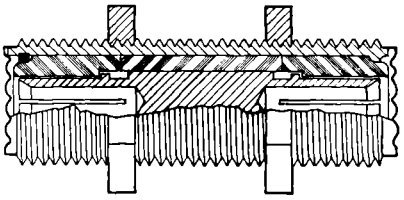

FIG. 1·10.—UHF bulkhead adapter.

Figure 1·12 shows a photograph of connectors of several types. At the left is a group of type N fittings, in the center are two UHF fittings, and on the right are two adapters from type N connectors to rigid coaxial line.

1·5. Rigid Coaxial Lines.—Many microwave transmission lines take the form of rigid coaxial lines with air as the dielectric between the inner and outer conductors. Air is used to minimize the losses in the line. The properties of the line and the characteristic impedance depend on

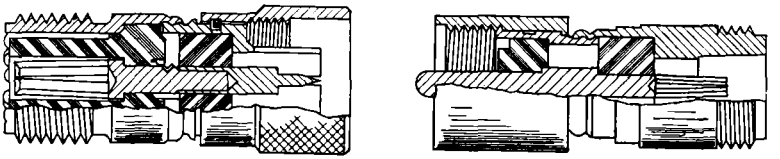

(a) (b)

FIG. 1·11.—Type N to UHF adapters, types UG-146/U and UG-83/U.

the diameters of the inner and outer conductors. Lines of standard sizes have been adopted, all of which have impedances near 50 ohms. This value represents a compromise between the dimensions that give a maximum power-carrying capacity and a minimum loss per unit length if either the outer diameter or the wavelength is held constant. The standard lines do not have an impedance of exactly 50 ohms, since the dimensions of the conductors are those of tubing that is readily available in standard sizes. Table 1·3 summarizes the properties of

FIG. 1·12.—Cable fittings. At the left are type N fittings; center, type UHF; right, adapters from type N to rigid coaxial line.

the rigid lines commonly used. The size of the line is specified by the outer diameter of the outer conductor.

Some means of supporting the inner conductor of the line is, of course, necessary. One method is to use dielectric beads of such a shape and size that no reflection takes place from the beads or from combinations of several beads. Figure 1·13 shows several forms of nonreflecting beads. Beads of all these types are often encountered. The bead of Fig. 1·13*d* is often split into halves to allow assembly of the line, although a joint in the center conductor is sometimes made at this point. It is difficult to

make bead-supported lines with very low reflection over a broad band of wavelengths. Moreover, the beads seriously reduce the power-handling capacity, as is evident from Table 1·3.

A second method for supporting the center conductor is by means of stub branches that are effectively a quarter-wavelength long. The branch line is in shunt with the main line, but the stub presents a very

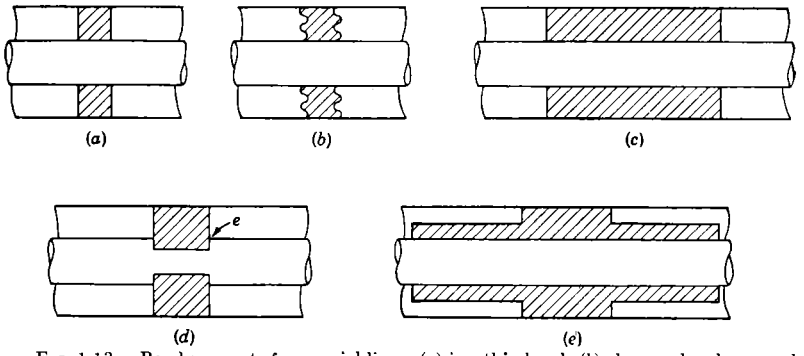

FIG. 1·13.—Bead supports for coaxial lines: (*a*) is a thin bead; (*b*) shows a bead grooved to increase the surface leakage path; (*c*) is a bead one-half wavelength long; (*d*) shows a bead with the center conductor undercut to maintain a constant impedance in the bead-filled section of the line; (*e*) shows a stepped bead three quarters of a wavelength long.

small admittance and has, consequently, little effect on the transmission at the design wavelength. The wavelength band over which the effect is small is, however, rather restricted. By means of an increase in the diameter of the center conductor of the main line, the bandwidth may be made much larger. A cross section of such a stub is shown in Fig. 1·14. The dimensions shown are for a $\frac{7}{8}$-in. line at a wavelength of 9.9

TABLE 1·3.—SOME CHARACTERISTICS OF COAXIAL LINES

Line size, in. OD	Wall thickness, in.	Inner-conductor diameter, in.	Impedance, ohms	Support	Theoretical maximum power, kw	Recommended maximum power, kw	Attenuation, db/m	Lowest safe wavelength, cm
$\frac{5}{16}$	0.025	0.125	44.4	Bead	140	5	0.021	1.70
$\frac{1}{2}$	0.032	0.1875	50.6	Stub	358	50	0.020	2.70
$\frac{3}{8}$	0.035	0.250	47.8	Bead	598	20	0.095	3.50
$\frac{7}{8}$	0.032	0.375	46.4	Stub	1310	200	0.066	5.28
$1\frac{1}{4}$	0.049	0.500	50.0	Stub	2530	400	0.045	7.18
$1\frac{5}{8}$	0.049	0.625	53.4	Stub	4200	600	0.033	9.30

cm. A single stub of this design produces a voltage standing-wave ratio of less than 1.02 for wavelengths from 8 to 12 cm.

A standard connector for $\frac{7}{8}$-in. line is shown in Fig. 1·15. Contact between the outer conductors is made with a taper joint, and contact between the inner conductors is made with a "bullet" with spring fingers. Both the male and female parts of this coupling are shown at the right of Fig. 1·12. With a polarized coupling such as this, it is desirable to have some convention to be followed in the assembly of lines. The convention adopted is that the power flow shall be from the male to the female coupling. This same convention is used for the connection of water pipes.

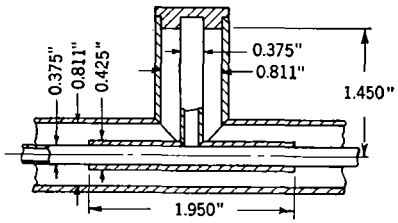

FIG. 1·14.—Broadband stub support for a $\frac{7}{8}$-in. coaxial line.

1·6. Waveguide Transmission Lines.—Although coaxial lines, both rigid and flexible, are adequate for the requirements of microwave transmission at long wavelengths and at power levels that are not too high, transmission of short wavelengths and high power must be accomplished through hollow-pipe waveguides. The waveguide has, almost universally, a rectangular cross section with a ratio of cross-sectional dimensions of about 2 to 1. Transmission takes place in the dominant mode which is designated as the TE_{10}-mode or H_{10}-mode. The electric field

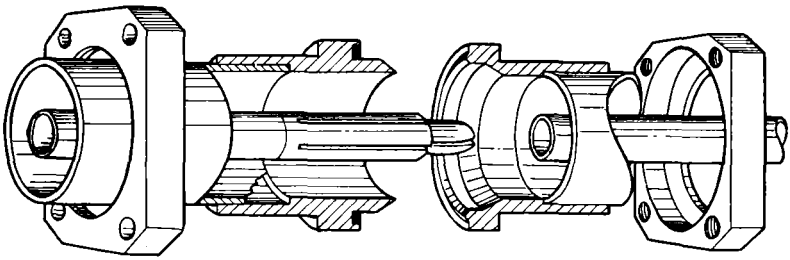

FIG. 1·15.—Connector for $\frac{7}{8}$-in. coaxial line.

is entirely transverse to the direction of propagation and is perpendicular to the broad face of the waveguide. The field strength has a maximum value at the center of the broad face, and decreases to zero at the side walls. The magnetic field is both transverse and longitudinal with respect to the waveguide axis and is perpendicular to the electric field. The magnetic field lines form closed contours in planes parallel to the broad faces of the waveguide. The wavelength λ_g in the waveguide is greater than the wavelength λ_0 in free space, and is given by the equation

$$\frac{1}{\lambda_g^2} + \frac{1}{4a^2} = \frac{1}{\lambda_0^2},$$

where a is the larger of the cross-sectional dimensions. For propagation to be possible in the dominant mode only, it is necessary that $2a > \lambda_0 > a$.

Standard sizes for waveguide transmission lines have been established and these sizes are given in Table 1·4. The wavelength band given extends from a wavelength 10 per cent less than the cutoff wavelength ($2a$) for the lowest mode to a wavelength 1 per cent greater than the cutoff wavelength (a) for the next mode. For a representative wavelength within this band, a value for the attenuation of a copper waveguide is given, and the maximum power P_{max} that can be transmitted without breakdown. The value of P_{max} is calculated on the assumption

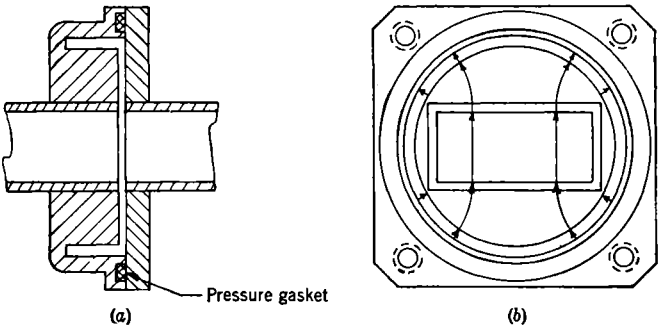

FIG. 1·16.—Choke-flange waveguide coupling.

that the breakdown field strength is 30,000 volts/cm and is independent of frequency. At the upper limit of the wavelength band given, the attenuation is roughly twice, and the power-handling capacity about half, the values at the lower limit.

Table 1·4 also lists the choke-flange couplings that are recommended for waveguides of each size. A choke-flange coupling is essentially a branch waveguide, one-half wavelength long, in series with the main waveguide. A coupling for waveguide is shown in Fig. 1·16*a*. For ease of manufacture the choke groove is circular. The radius and depth of the groove are so chosen that no current flows across the joint between the choke and the flange. Since no current flows, there is no need for an electrical contact at this point, and the connector makes a good joint even if no contact is made. In fact, flexible waveguides may be made by a series of choke-flange couplings held together by a flexible cover, with a slight spacing between the choke and flange units.[1] The choke

[1] See *Microwave Transmission Circuits*, Vol. 9, Radiation Laboratory Series, Chap. 5.

TABLE 1·4.—STANDARD RECTANGULAR WAVEGUIDES AND COUPLINGS

Waveguide Army-Navy Type No.	OD, inches	Wall, in.	Wavelength band, cm	Wavelength for P_{max} and loss, cm	P_{max}, Mw	Loss for copper, db/m	Choke coupling	Flange coupling	Design wavelength, cm	Bandwidth for $r < 1.05$, per cent
RG-48/U	3 × 1.5	0.080	7.3 –13.0	10.0	10.5	0.020	UG-54/U	UG-53/U	10.7	±15
							-200/U	-214/U	9.0	±15
	ID2.75 × 0.375	0.049	7.0 –12.6	10.0	2.77	0.058				
RG-49/U	2 × 1	0.064	4.8 – 8.5	6.5	4.86	0.031	-148/U	-149/U		
RG-50/U	1.5 × 0.75	0.064	3.6 – 6.3	5.0	2.29	0.063				
RG-51/U	1.25 × 0.625	0.064	2.9 – 5.1	3.2	1.77	0.072	-52/U	-51/U	3.20	
RG-52/U	1.0 × 0.5	0.050	2.3 – 4.1	3.2	0.99	0.117	-40/U	-39/U	3.20	±6
RG-53/U	0.5 × 0.25	0.040	1.07– 1.9	1.25	0.223	0.346	-117/U	-116/U	1 25	> ±2

groove of a coupling is a coaxial line. This line is operated, however, not in the lowest, or principal, mode but in the second or TE_{10}-mode. The fields excited in the choke groove are shown in Fig. 1·16*b*. Other choke couplings are shown attached to the crystal holders. Figure 1·4 shows a UG-40/U coupling; Fig. 1·5 shows a UG-117/U coupling.

Although the reflections from choke-flange couplings are usually completely negligible, it is desirable, for very precise measurements, to use a contact coupling such as shown in Fig. 1·17. To be satisfactory the surfaces at the joint must be flat, and sufficient pressure must be applied to ensure contact over the whole surface. The two waveguides

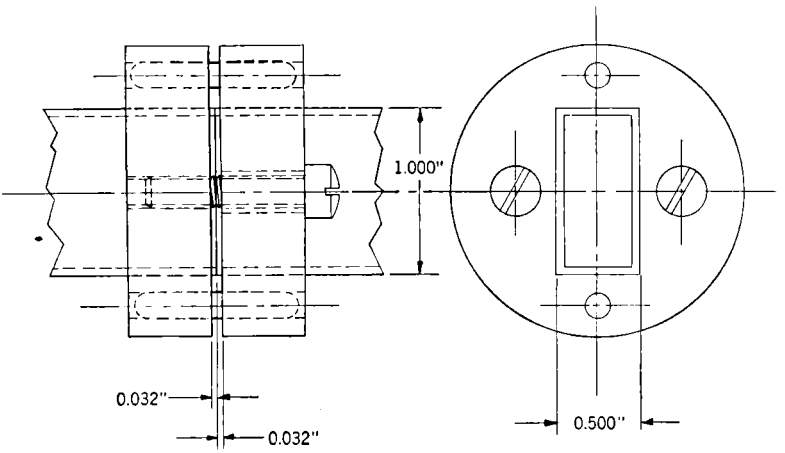

FIG. 1·17.—Contact coupling for precise waveguide measurements.

must also be accurately aligned. The pins in the coupling should be located by a jig that fits into the waveguide, and the screws that hold the coupling tight should not affect the alignment. A coupling of this type is not suitable for field use, since great care is necessary to make a good joint.

1·7. Specialized Microwave Measurements.—In a volume of this size, it is by no means possible to describe all the necessary techniques that are useful and necessary in the microwave region. The techniques that are used only for the study of special devices have, therefore, been omitted. A large number of these methods are given, however, in other volumes of the Radiation Laboratory Series. The theoretical background essential for most of the processes of measurements is discussed in Vol. 8. The properties of reflecting irises and other elements of microwave circuits are also to be found there, and a summary of the properties, with formulas and tables, is the subject of *The Waveguide Handbook*, Vol. 10. A discussion of irises for impedance-matching and the

description of tuners of various types are to be found in Vol. 9. Tuners are very widely used in many microwave measurements and form an essential part of the equipment of any microwave laboratory.

With the exception of power measurements and line terminations, little space has been devoted in this book to high-power equipment. The properties and testing of high-power magnetron oscillators are to be found in Vol. 6 of the Series; the modulators (pulsers) and the equipment for testing them are discussed in Vol. 5.

The measurements of the properties of microwave mixers are described in Vol. 16, and the radio-frequency and low-frequency properties of complete receivers are discussed in Vol. 23. Several volumes of the Series are devoted to the low-frequency circuits that are necessary auxiliary equipment for nearly all microwave devices. The alignment of amplifiers and the measurement of gain are treated in Chap. 8 of Vol. 18, and amplifier-noise measurements are described in Chap. 14 of the same volume.

The last two chapters of Vol. 12 describe the measurements of the properties of antennas in greater detail than does Chap. 15 of this volume. Experiments on the propagation of microwaves over the surface of the earth are described in Vol. 13.

The measurements made to determine the properties of gas-filled TR switching tubes and of duplexers are to be found in Vol. 14. The testing and maintainance of complete microwave radar systems are described in Vols. 1 and 2, and the testing of microwave beacons in Vol. 3.

A number of experiments have recently been made, or are now in progress, in a field that might be designated as microwave spectroscopy. The properties of substances in fields at microwave frequencies have considerable interest to physicists. These properties, however, are typical of the optical region of the electromagnetic spectrum and involve quantum effects. Consequently, a description of these experimental methods has been omitted here.

Most of the microwave apparatus during the war period was procured by the Army and Navy for military purposes and for the development of military equipment. Although a large number of manufacturers produced this equipment, it is not known at present what will be commercially available in the future. To aid prospective purchasers, however, a list of manufacturers and some of the microwave equipment that they produced during the war is given in Appendix A at the end of this volume.

PART I

POWER GENERATION AND MEASUREMENT

CHAPTER 2

POWER SOURCES

By Donald R. Hamilton and R. V. Pound

MICROWAVE OSCILLATORS

By Donald R. Hamilton

An obvious prerequisite to most of the measurements described in this book is a source of microwave energy. From the various factors involved there has developed a strong preference for the use of the reflex klystron oscillator as this source. For this reason most of the present chapter will be devoted to the reflex klystron and its associated equipment, but this will be preceded by a brief discussion of the behavior required of a source of power for measurements, and a comparison of the various basic types of microwave tubes on the basis of these criteria.

2·1. The Choice of a Microwave Oscillator.—The simplest requirement placed upon a signal source is that it generate sufficient power for the measurement in question—the more economically the better. For a simple standing-wave measurement, a few milliwatts of power in the transmission line of the standing-wave detector are sufficient. But in order that the process of measurement may not influence the signal frequency or amplitude, at least 10 db of attenuation are usually placed between source and point of measurement, which raises the requirement to a few tens of milliwatts. Very similar requirements are placed on the local oscillator in microwave receivers, so that many of the more common power sources are equally suitable for measurement work and as local oscillators. However, in measuring such things, for example, as attenuation or antenna patterns, a smaller fraction of the initially generated power is available to the final detector so that the initial power level needs to be increased by at least another factor of ten. But the latter measurements are rather less frequent than the multitudinous standing-wave measurements requiring tens of milliwatts.

The ease of modulation of this power is also frequently important. Ease of modulation may, of course, imply exact regulation of applied voltages. This is one of the reasons for a subsequent section on suitably regulated power supplies for such signal sources.

One of the commonest types of modulation is the simple square-wave on-off amplitude modulation at audio frequencies, which allows the use,

with the standing-wave detector, of an a-c amplifier instead of a d-c galvanometer. Amplitude modulation of the output power in microsecond pulses is somewhat similar to this; such pulses are necessary in a signal generator designed to produce a signal which simulates a received radar signal. The requirements in this case are the more stringent since times of the order of tenths of microseconds are of importance in producing an output pulse which duplicates the shape and duration of the applied pulse.

Frequency modulation of a signal is extremely useful in investigating any phenomenon involving frequency dependence; for example, in a spectrum analyzer (see Chap. 7) a reference signal swept in frequency is necessary. For such purposes, it is helpful to have the output frequency quite sensitive to some electrode voltage and to have the signal frequency depend nearly linearly on this voltage. Absence of amplitude modulation in the process is not so important since f-m receivers commonly make use of amplitude limiters in any case.

In addition to these matters of output power and modulation, there are a number of other fairly obvious criteria, such as the range of frequencies that the source may be tuned to generate, the ease of this tuning process, the number and difficulty of the adjustments that must be made for optimum operation, and the amount of mechanical skill required for constructing accessories. Further additions would begin to sound like the sermon of Calvin Coolidge's preacher who was "agin" sin.

To meet these requirements there are available three basic generators of microwave power: the microwave triode, the klystron, and the magnetron. The latter has been developed primarily as a high-power pulsed transmitter tube and so far remains an inherently higher power tube than is needed for most measurements.

The ingenious physical construction of the lighthouse tube has extended the practical operating range of the triode somewhat above 3000 Mc/sec. This physical construction requires an external cavity, however; the resulting problems of cavity construction and of good contact between cavity and tube are not too simple. By the adjustment of movable sections of the commonly used external cavity, tuning ranges of the order of 10 per cent may be obtained. At 3000 Mc/sec, output powers of the order of 125 mw may be obtained from the 2C40 lighthouse tube at a plate voltage of 250 volts. So far it has not been feasible to extend this range to the commonly used higher frequencies. As to modulation properties, microwave triodes have an output frequency which is quite insensitive to applied voltage. This has sometimes given rise to their use in field test equipment where constant frequency is desired and the cost of voltage regulation is an important criterion. Square-wave or pulsed-amplitude modulation is straightforward, and

with proper circuit adjustments satisfactory operation may be obtained with short pulses (cf. Sec. 4·8). Nevertheless, because of the complications of the circuits external to the vacuum tube, the difficulty of frequency modulation, and the upper limit to the operating frequency, the lighthouse tube has not come into general acceptance as a signal source for measurements.

Klystrons exist in a number of electrical and physical forms. There are amplifiers with power gains of 30 in the two-resonator form or 1000 in the three-resonator "cascade" amplifier. High-order multiplication of frequency is made possible by the waveform of the r-f current in a klystron. Klystron multipliers, preceded by conventional low-frequency multiplying stages, have been used for frequency multiplication from quartz-crystal-controlled oscillators up to microwave frequencies of the order of 9000 Mc/sec. The use of such frequency multipliers in frequency standards is discussed in Chap. 6. Also, at 3000 Mc/sec, two-resonator klystrons are available with output powers of the order of 15 to 20 watts.

For measurement purposes, however, the most generally useful type of klystron has been the reflex klystron oscillator. The word "reflex" derives from the fact that an electron beam passes once through a resonant cavity, then by means of a negative electrode, the "reflector," is made to return through this cavity on a second transit. Postponing for the moment a discussion of the operation of the reflex klystron, it is obvious that the use of one simple resonant circuit gives this oscillator a great advantage over the lighthouse tube or the two-resonator klystron oscillator, both in mechanical tuning range and in ease of tuning adjustment. It has also become common practice to place the resonant cavity within the vacuum envelope so that there are none of the mechanical complications of attaching an external cavity. At 3000 Mc/sec, and at comparable plate voltages, present-day reflex klystrons have only slightly less output power and efficiency than lighthouse tubes. However, triode efficiency drops sharply and reflex-klystron efficiency drops gradually with increasing frequency. Although at 3000 Mc/sec the maximum output power of current reflex klystrons is one-half watt as compared to the just-quoted 15 to 20 watts of the two-resonator klystron, in the 10,000 Mc/sec range one-quarter to one-half watt is still available from a reflex oscillator. Great difficulties of construction and tuning prevent the use of any two-resonator oscillators in this higher frequency range.

The output frequency of a reflex klystron is quite sensitive to the voltage applied to the reflector electrode, although in some tubes the sensitivity has been intentionally made small in the interests of stability. Change in frequency with applied voltage, known as "electronic tuning,"

obviously makes for easy frequency modulation, especially since the electrode to which the modulating voltage is applied draws no current. This last advantage is absent if the frequency is modulated, as it may be, by beam-voltage modulation. The same electronic-tuning effect is present in two-resonator klystron oscillators and may be enhanced by proper adjustment of the feedback, but the modulation must be applied to the beam voltage and the rate of change of frequency with voltage is less. Conversely, of course, the two-resonator tube is more stable in frequency. Frequency modulation of a reflex klystron is somewhat nonlinear and is accompanied by amplitude modulation to a degree which will be apparent from the later discussion. The two-resonator klystron may be adjusted to give a more linear characteristic with very little accompanying amplitude modulation.

On-off amplitude modulation of the square-wave or pulsed type is easily applied to a klystron or a triode by applying the same modulation to the plate voltage; in the reflex klystron similar modulation may also be applied to the reflector voltage. A normally loaded reflex oscillator will satisfactorily reproduce the shape and duration of the applied voltage pulse, as will a triode with proper circuit and feedback adjustments; a short buildup time is rather more difficult to obtain with present two-resonator klystrons.

The various points of comparison that have just been discussed are the basis for the general use of the reflex klystron in measurements at present. Specific data on the more common currently available tubes will be given in Table 2·1. In order to provide a general background for the reader, principles of operation and general characteristics of the reflex klystron will be discussed in the next section. More detailed information on klystrons and microwave triodes may be found in Vol. 7 of this series.

In addition to the signal sources just discussed, there is another means of obtaining signal power, which is primarily useful in initial work in new frequency bands for which no tubes are available; this is the technique of harmonic generation in crystal detectors. This technique will be discussed briefly following the section on principles of reflex-klystron operation.

2·2. General Characteristics and Principles of Operation of the Reflex Klystron.—The basic feature of any klystron is its utilization of "velocity modulation" and "bunching" to derive, from an input r-f voltage, an r-f intensity-modulated current with which to drive an output circuit. This is accomplished by substituting for the single cathode-grid control space of the triode a composite control space consisting of three separate regions: the cathode-anode region in which electrons receive their full d-c acceleration; the "r-f gap" in which these electrons are subjected to

an r-f field which does not turn them back but simply serves alternately to slow down or speed up the electrons (velocity modulation); and the "drift space" in which there may be d-c fields but no r-f fields, and in which the differences in electron velocities cause the electrons to form into groups or bunches (bunching). It is the increased physical size which this "division of labor" allows at a given frequency which makes the klystron work up to much higher frequencies than does the triode. An additional feature, common of course to the microwave art in general, is the use of cavity resonators for oscillator circuit techniques.

A schematic diagram illustrating the embodiment of these principles in the reflex klystron is shown in Fig. 2·1, in which the three regions of the control space referred to above are identified. In addition, it will be noted that the reflector electrode is operated at a potential negative with respect to the cathode; electrons which have passed through the r-f gap are therefore subject to a retarding electric field which, reversing their motion before they reach the reflector, returns them through the r-f gap.

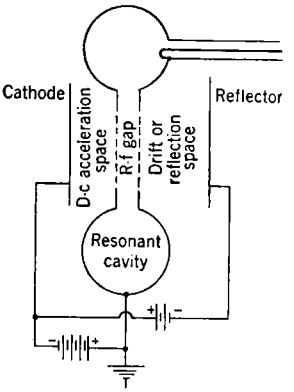

FIG. 2·1.—Schematic diagram of a reflex klystron.

Bunching; Phase Relations for Oscillation.—The process of bunching which takes place in the reflection space is illustrated in Fig. 2·2, in which electron position is shown as a function of time for a series of electrons which initially pass through the r-f gap at equal intervals. The slope of any one curve at any instant obviously corresponds to the velocity of the corresponding electron at that instant; the velocity modulation on first passage through the r-f gap appears as a change in slope at the gap. It will be seen that the faster the electron, the deeper it penetrates into the reflection space, and the longer the time taken to return to the r-f gap. The resulting bunching is apparent as the electrons make their second transit.

On the first trip through the gap as many electrons were speeded up, that is, gained energy at the expense of the r-f field, as were slowed down, that is, gave energy to the r-f field: the transactions balance to zero. But on the return passage through the gap the electrons are bunched. This "accounting" procedure of adding up the energy given to or taken away from each electron by the field will show a net profit or loss in the total energy of the beam, which must correspond to a loss or profit in the electromagnetic energy of oscillation stored in the resonant cavity. The net profit to the energy of oscillation will be greatest when the center of the bunch is slowed down most on its return passage. The

electron which forms the center of the bunch, and which made its first transit of the r-f gap at an instant of zero field, is shown with a heavy line in Fig. 2·2. As the figure is drawn, any small change in the total reflection transit time of the electron from its value of $1\frac{3}{4}$ cycles would clearly result in a diminution of the power delivered to the resonant circuit.

This example may be generalized to show that the delivery of power by the beam will be at a maximum whenever the d-c transit time in the reflection space is $(n + \frac{3}{4})$ cycles, where n is an integer. For a quarter cycle on either side of $(n + \frac{3}{4})$ cycles no delivery of power by the beam

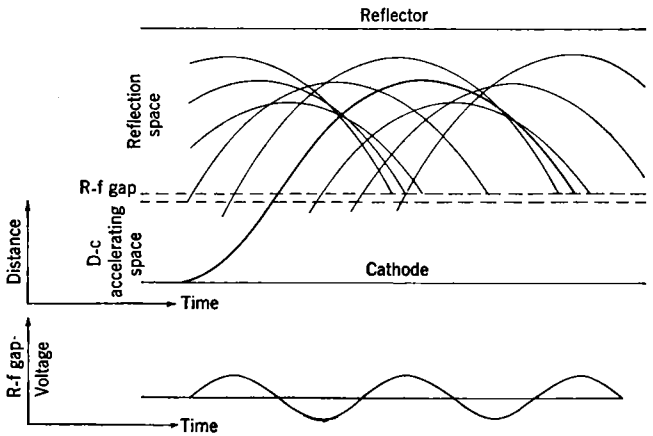

FIG. 2·2.—Applegate diagram illustrating velocity modulation and bunching in the reflex klystron. Trajectories are shown for a number of originally evenly spaced electrons, which form into bunches on the return transit because of velocity modulation on first transit of the gap.

is possible. This does not imply that the tube will always oscillate if this transit-time condition is met. For if the d-c beam current is too small, the power delivered by the bunched current to an infinitesimal r-f gap voltage may be less than the power dissipated in circuit and load losses in maintaining the gap voltage; in this case there will be no oscillation. Thus, given a transit time which lies in the vicinity of $(n + \frac{3}{4})$ cycles and therefore meets one of the necessary conditions for oscillation, a second condition is also necessary: the d-c beam current must exceed some minimum current called the "starting current," which depends upon circuit and external load and, incidentally, is inversely proportional to $(n + \frac{3}{4})$. If both conditions are satisfied, oscillation will always occur.

Reflector-mode Patterns and Mode Shapes.—Since transit time depends upon the reflector voltage V_R and the beam voltage V_0, oscillation is

allowed for some values of these voltages and not for others. A typical "mode pattern" is shown in Fig. 2·3, in which the regions of oscillation for a 2K25 klystron are indicated as shaded regions and are labeled with the corresponding values of n. It should be noted that the word "mode" is not used here in the sense of "normal modes of resonance of coupled circuits"; there is only one circuit, and the modes are distinguished by different transit times, not by different frequencies. The downward trend of the reflector voltage for a given mode as the beam voltage increases is a general characteristic of such patterns. Another general characteristic, not shown in Fig. 2·3, is an increase in the value of reflector voltage for a given mode as the mean klystron frequency is tuned upwards. And since transit time depends on reflector spacing, some fluctuation of mode position from tube to tube caused by mechanical tolerances is to be expected.

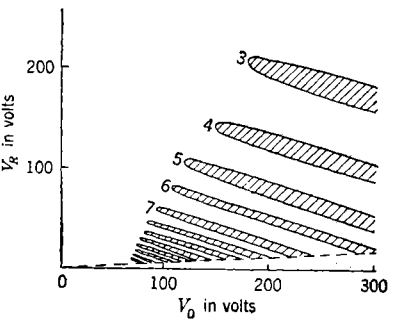

FIG. 2·3.—Reflector-mode pattern of the type 2K25 reflex klystron operating at 3.2 cm. The shaded areas correspond to those combinations of beam voltage V_0 and reflector voltage V_R at which oscillation occurs.

In Fig. 2·3, the modes of oscillation are shown as not extending to zero reflector voltage. This is not a true representation of fact; the modes usually extend through zero to positive reflector voltage. This is not shown in Fig. 2·3 because it is desired to draw attention to the fact that in making klystrons and in making the power supplies that operate them (see Sec. 2·13), it is assumed that they will be operated with the reflector sufficiently negative to draw no current. Current collected on the reflector may cause dangerous heating of the reflector, especially in conjunction with certain secondary-emission and power-supply phenomena; or it may give rise to unwanted reflector-voltage modulation. A slightly negative reflector may still collect electrons which have been accelerated in the r-f field.

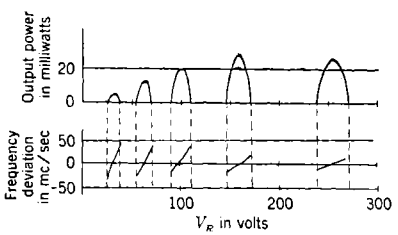

FIG. 2·4.—Output power and frequency of oscillation as functions of reflector voltage in the type 2K25 (723A/B) reflex klystron. Beam voltage 300 volts, $\lambda = 3.2$ cm.

Returning from this parenthetical admonition to the simple behavior shown in Fig. 2·3, it is apparent that for any given value of beam voltage there should be one or more ranges of reflector voltage in which oscilla-

tion will occur, and vice versa. This is illustrated in Fig. 2·4, which shows, for the type 2K25 klystron, the dependence of output power on reflector voltage for a given beam voltage. Moreover, as will be discussed in more detail later, the oscillation frequency varies with reflector

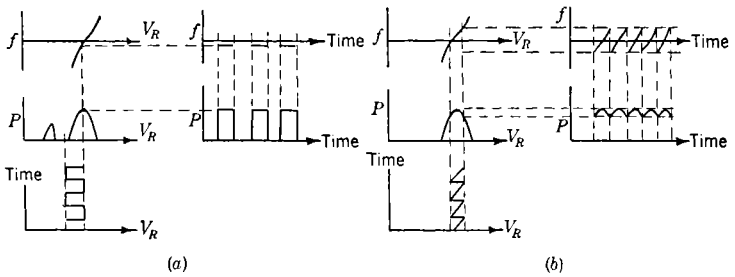

FIG. 2·5.—Amplitude- and frequency-modulation characteristics of the reflex klystron; (*a*) is for square-wave amplitude modulation; (*b*) for sawtooth frequency modulation.

voltage. This behavior is also indicated in Fig. 2·4. The tube characteristics exemplified in this figure will be discussed below. Meanwhile, it should be noted that the load into which the oscillator is working is constant in Fig. 2·4, and that a quantitatively, but not qualitatively, different result would be obtained if the load were changed in going from mode to mode.

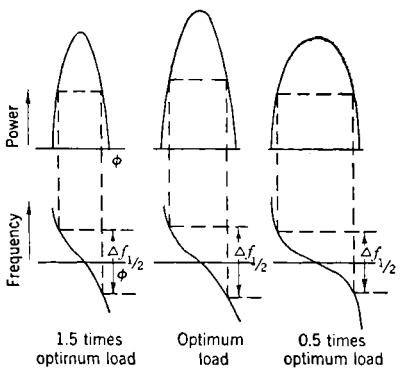

FIG. 2·6.—Universal mode curves for the reflex klystron for three different loads. Output power and relative frequency are shown as functions of relative reflection phase angle ϕ; graphical determination of half-power electronic-tuning range $\Delta f_{1/2}$ indicated by construction lines. Reflector voltage decreases with increasing ϕ.

Simple Modulation of the Reflex Klystron.—Even without going into the details of Fig. 2·4 in a quantitative manner, it is apparent how certain simple types of modulation, such as square-wave amplitude modulation or sawtooth frequency modulation, may be obtained by reflector-voltage modulation. The requisite reflector-voltage modulation and the resulting output waveform are indicated in Fig. 2·5.

2·3. More Detailed Characteristics of the Reflex Klystron. *Universal Mode Shapes.*—For many purposes involving a quantitative specification of such modulation, the behavior shown in Fig. 2·4 must be described in a more exact and quantitative fashion. It turns out, subject to some simple conditions which need not be stated, that the mode characteristics

of a reflex klystron may be represented by a single set of universal curves. Three such curves are shown in Fig. 2·6. The horizontal coordinate in these curves, denoted by ϕ, is the difference between the values of the transit angle (measured in radians at the center frequency) at the point in question and at the center of the mode; ϕ increases with decreasing reflector voltage. Since the transit angle changes by 2π radians in going from one mode to the next, the conversion from reflector volts to relative transit angle in such a diagram as Fig. 2·4 is a matter of straightforward interpolation. The different curves in Fig. 2·6 correspond to different external loads applied to the tube, as indicated in the figure. By a "heavy" or "large" load is meant one which necessitates a large starting current. At optimum load, the starting current is about 44 per cent of the operating current; hence at 1.5 and 0.5 times optimum load, the respective starting currents are 66 and 22 per cent of the operating current.

Electronic-tuning Characteristics.—It will be observed in Fig. 2·6 that while the output-power characteristics of the mode change in shape with change in load, the frequency characteristic simply changes its vertical scale factor; this frequency characteristic is given by the simple relation

$$\tan \phi = 2Q \frac{(f_0 - f)}{f_0}, \tag{1}$$

in which f is the frequency of oscillation, f_0 is its value at the center of the mode (resonant frequency of loaded cavity), and the circuit Q includes the effect of the load. Thus the Q's for the heavy, optimum, and light loads shown are in the ratio 0.67 to 1 to 2, and this is the vertical scale factor to which reference was made. A simple relation is obvious: the rate of electronic tuning at the center of the mode, expressed as fractional change in frequency per radian change in reflection transit angle, is given by

$$\frac{1}{f_0}\left(\frac{df}{d\phi}\right)_0 = -\frac{1}{2Q}. \tag{2}$$

In practice one is usually more interested in the total range of electronic tuning than in the tuning rate. The electronic-tuning range is normally specified as the difference in frequency, $\Delta f_{1/2}$, between the frequencies at which the power falls to half its maximum value. In Fig. 2·6 the graphical deduction of $\Delta f_{1/2}$ from the power and frequency characteristics has been indicated. It is apparent, in the first place, that the tuning range is much less dependent on the load and on the Q than is the tuning rate at the center of the mode. This is because the load giving the highest Q and the lowest tuning rate also allows oscillation over the largest range of phase, so that the effects of tuning rate and phase width

of the mode neutralize each other. In particular, the load for which the electronic-tuning range is a maximum gives the maximum output power. To verify further the essential simplicity of nature, it turns out to be true that $Q\Delta f_{\frac{1}{2}}/f_0 = 1.2$ at optimum load, that is, the electronic-tuning range at optimum load is approximately the bandwidth of the loaded cavity at this load (and only at this load).

In the case of optimum load, the mean electronic-tuning rate, averaged between half-power points, is

$$\frac{1}{f_0}\left(\frac{df}{d\phi}\right)_{av} = -\frac{1}{1.4Q}. \tag{3}$$

This is equivalent to saying that the frequency deviation at half power is about 40 per cent greater than it would be if the tuning rate at the center of the mode were followed throughout. If the frequency deviation is halved, the nonlinearity of electronic tuning is reduced to 11 per cent.

In practical cases the tuning rate, which is of interest, is expressed in megacycles per second per volt on the reflector; the conversion from the above form requires only the conversion already mentioned from transit angle to reflector voltage.

Electronic-tuning Hysteresis.—This discussion of mode shapes affords an opportunity for answering a question which was left unanswered at an earlier stage: What happens to the electrons which, having made two transits of the gap, go on to make further transits? Between grid absorption and electron-optical aberrations, not many electrons do make multiple transits; but this partially begs the question. Those electrons which do make three or more transits are the most common cause of occasional abnormalities of which an example is shown in Fig. 2·7. Such phenomena are collectively labeled "electronic-tuning hysteresis" since they include situations when the output power and frequency at a given reflector voltage depend upon the direction of approach to this reflector voltage. As mentioned in the later discussions of specific tube types, these effects have been largely eliminated from the more recent tubes by designing the electron optics to prevent multiple transits. They are also affected considerably by load and beam current and may usually be ameliorated by adjustment of these factors. In any case the remaining discussion of output characteristics will be for normally behaving modes such as those appearing in Fig. 2·4.

Load Effects.—All the comments which have so far been made about the effects of load on the operation of a reflex oscillator are based on the implicit assumption that this load is insensitive to frequency and nonreactive and that in all its effects it acts as if it were simply a resistance connected across the r-f gap of a klystron oscillator. In general, this

situation may be obtained only with special loading conditions and at a particular frequency; it is the exception rather than the rule.

One of the most convenient ways of presenting information on oscillator performance in the presence of more general loads is the so-called "Rieke diagram." This is a graphical presentation of the variation of any one oscillator characteristic—most commonly, output power or frequency—as a function of the load which the oscillator sees. This load may be described as a terminating impedance in the transmission line into which the oscillator is coupled; hence the most common way of specifying a load is by the magnitude and phase of the

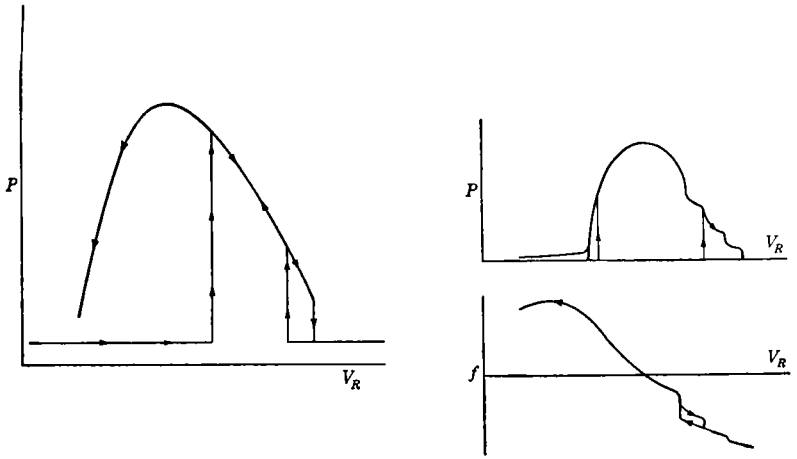

FIG. 2·7.—Examples of hysteresis and associated phenomena in reflex klystrons. Reflector voltage is being subjected to a sine-wave sweep. The arrows indicate the direction of motion of the trace. Reflector voltage is increasing to the left.

reflection coefficient which would produce the standing waves which are present in the line. The most common Rieke diagram is thus one in which the magnitude and phase of this reflection coefficient are used as polar coordinates to specify a load plane in which the contours of constant oscillator characteristic are plotted.

For an oscillator which has been designed with the effects of the load taken into account, optimum output power (and hence optimum electronic-tuning range) will occur at the center of the Rieke diagram, that is, for a matched transmission line. The Rieke diagrams for all such tubes are similar to each other. In Fig. 2·8 is shown such a Rieke diagram as measured for a type 723A/B klystron with fixed reflector voltage. For reference purposes, the contour of a constant voltage standing-wave ratio of 1.5 in the output transmission line (1-in. × $\frac{1}{2}$-in. waveguide) is shown; it is a circle concentric with the origin.

It will be observed that a voltage standing-wave ratio up to 1.5 has very little adverse influence on the output power. As the phase of this standing wave is changed, the frequency of oscillation is "pulled." At larger values of standing-wave ratio there is a region of the diagram, the "sink," for which the load is too heavy for oscillations to occur. But perhaps the most intriguing feature of Fig. 2·8 is the region behind the sink, where for a given load (a given point in the diagram) there are two different stable amplitudes and frequencies of oscillation. Without going into details, this phenomenon only occurs when the actual load is some distance away from the oscillator. A given geometrical distance

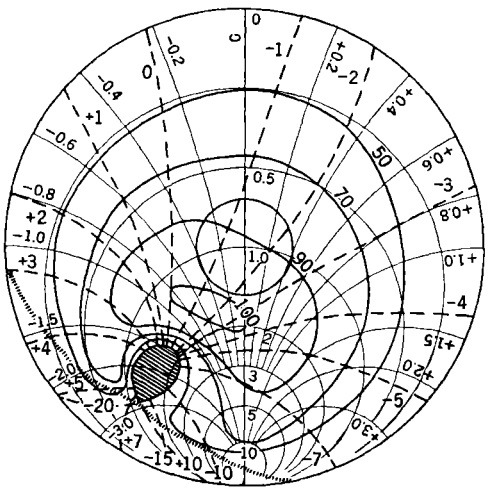

FIG. 2·8.—Rieke diagram for 723A/B reflex klystron ("250-volt mode"). Region of no oscillation cross-hatched; region of double-valued operation lies behind the heavy dotted line. Line length from tube to load is 10λ.

corresponds at different frequencies to different electrical distances (wavelengths); and when this variation of electrical distance becomes appreciable over the range of frequencies shown in the Rieke diagram, the "long-line effect" enters in as shown in the double-valued region of Fig. 2·8.

By comparison of a number of Rieke diagrams like Fig. 2·8, all taken at different reflector voltages, it would become apparent that one very painful effect of long lines (or, of course, of any frequency-sensitive load) is to cause hysteresis in the reflector-mode shape. A corollary to this is the occurrence of frequency discontinuities as the reflector voltage is varied. For all such ailments, the principal cure is to keep the distance from tube to load small and to keep the standing wave which the tube sees small.

Variation of Characteristics from Mode to Mode.—All the comments up to the present point have had to do with what happens within a single mode, with no mention of the differences between the modes which are apparent in Fig. 2·4. One simple difference is obvious. It has been seen that all modes at optimum load are supposed to have the same width in radians of transit angle; but since the modes are closer together at low reflector voltage, this is a region of more radians per volt and hence of modes narrower in voltage.

There are two much more basic differences between modes; namely, the maximum output power and the starting current for a given load are both inversely proportional to $(n + \frac{3}{4})$. The first point partially explains the variation of power from mode to mode in Fig. 2·4. The second says that the required optimum load is heavier for higher values of n, and hence that the electronic-tuning range is proportional to $(n + \frac{3}{4})$. Note that these comparisons of modes may not be carried out too closely in Fig. 2·4 when the same constant load is used for all modes.

Dynamic Modulation Characteristics.—The foregoing sums up briefly the static amplitude and frequency characteristics which are relevant to modulations such as those of Fig. 2·5. It is to be expected that the application of such static characteristics to dynamic modulation must break down when sufficiently high modulation rates or sufficiently rapid transients are considered. The following comments represent what is known about these points. Amplitude modulation begins to depart from static behavior when times comparable to the decay time of the loaded resonant cavity or frequencies comparable to the bandwidth of the cavity are involved. Thus, for example, at optimum load, the higher the electronic-tuning range the shorter the pulse buildup time. Frequency modulation, on the other hand, so long as it is carried out with small deviations of frequency about the maximum-power point, involves no time rate of change in the energy stored in the circuit and is, therefore, unaffected by circuit Q. The first limiting frequency which is encountered is probably the time of electron reflection, which is usually smaller than the circuit decay time by at least an order of magnitude.

2·4. Frequency Multiplication in Detector Crystals.—The end of the present section seems an appropriate place to summarize briefly the subject of frequency multiplication by means of detector crystals. This is a technique which is useful in working at a new frequency at which no electronic sources are yet available; it makes use of the distortion of an input sine wave in a rectifying crystal to generate harmonics of the input frequency.

A typical arrangement for accomplishing this is shown in Fig. 2·9. There are an input and an output line from the crystal. The input

line is coaxial and so dimensioned that it supports only the lowest coaxial mode at the harmonic frequency in question; it is then fitted with chokes which prevent any harmonic power from flowing into this line. The output line, on the other hand, is a waveguide which can transmit the harmonic but will not transmit the fundamental frequency. Preferably, the output waveguide presents a match looking from the crystal. For best harmonic generation, the two adjustable short circuits are necessary to adjust the standing waves in the vicinity of the crystal. Roughly speaking, their optimum adjustment is such that the crystal presents a match to the harmonic waveguide, at low power levels.

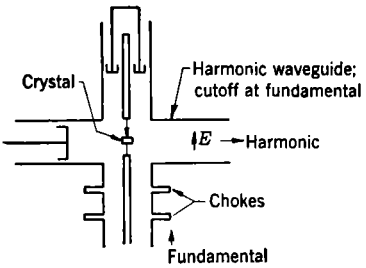

FIG. 2·9.—R-f circuit for frequency doubling in crystal detector.

With careful construction, adjustment, and selection of crystals such an arrangement has given a conversion loss of 10 db in going from 100-mw input power at 10,000 Mc/sec to 10-mw harmonic power at 20,000 Mc/sec. Less careful operation would probably give a 20-db loss; but the loss is diminished by use of a higher input power.

2·5. Specific Reflex-klystron Tube Types.—A number of reflex-klystron oscillators have been developed in recent years, mostly for use as local oscillators in superheterodyne receivers and as bench oscillators for test purposes. It is to be expected that eventually many of the currently available types will become obsolete. It nevertheless seems worth while to make a brief survey of the currently available types of tubes and their characteristics, both as an aid to prospective users and as a means of illustrating the foregoing discussion.

The properties of the tubes to be discussed are summarized in Table 2·1. An effort has been made in this table to give data corresponding to typical operation of typical tubes; the beam voltages and the currents are thus usually less than the maximum rated values, and the output power and the electronic-tuning range are in most cases some 30 to 50 per cent higher than the values required to pass the manufacturer's test specifications. A number of details relevant to the use of such tubes are omitted here and are available in the technical information sheets of the respective manufacturers, which should be consulted in any case before actually using the tubes.

When output power, electronic-tuning range, and electronic-tuning rate are given for a single frequency in the tuning range of the tube in question, this is so noted in the column headed "Notes"; additional comments on frequency dependence will usually be found in the text.

TABLE 2·1.—SUMMARY OF REFLEX KLYSTRON CHARACTERISTICS

Type no.	Frequency range, Mc/sec	Beam voltage, volts	Beam current, ma	Reflector voltage, volts	Power output, mw	Electronic tuning range, Mc/sec	Electronic tuning rate, Mc/sec per reflector volt	Mfr.	Notes
2K25 (723A/B)	8500–9660	300	22	110–170	28	45	2.2	BTL WE Raytheon	"160-volt mode"
				60–110	23	65	4.2	.....	"100-volt mode"
726C	2700–2960	300	22	90–130	120–200	30	0.9	WE	.....
726B	2880–3175	300	22	90–130	70–155	35	.....	WE	.....
726A	3175–3410	300	22	130–165	110	30	.....	WE	.....
2K29	3400–3900	300	22	90–172	75–150	48–34	1.7–0.7	BTL WE	.....
2K22	4300–4900	300	22	.....	(75)	.....	.....	BTL WE	.....
2K27	5200–5570	300	22	.....	(40)	.....	.....	BTL	.....
2K26	6250–7060	300	22	.....	(25)	.....	.....	BTL WE	.....
2K28 (707B)	1200–3750	250	25	110 230	70 110	21 22	0.85 0.60	Raytheon	3500-Mc/sec data

TABLE 2·1.—SUMMARY OF REFLEX KLYSTRON CHARACTERISTICS.—(*Continued*)

Type no.	Frequency range, Mc/sec	Beam voltage, volts	Beam current, ma	Reflector voltage, volts	Power output, mw	Electronic tuning range, Mc/sec	Electronic tuning rate, Mc/sec per reflector volt	Mfr.	Notes
2K41	2650–3320	1000	50	380	450	6	0.04	Sperry	$V_G = +40$
(417A)		400	..	50–180	55–35	8–3	0.27–0.10	.....	$V_G = +20$
2K39	7500–10300	1250	45	600	350	20	0.26	Sperry	.....
(419B)				350	270	40	0.50		
		700	19	40	70	6	0.6	.....	.....
2K42	3300–4200	1250	45	< 750	600	12	0.07	Sperry	.....
2K43	4200–5700	1250	45	< 750	600	17	0.15	Sperry	.....
2K44	5700–7500	1250	45	< 750	700	20	0.23	Sperry	.....
3K27	770–970	1000	60	< 600	1500	6	0.03	Sperry	.....
3K23	950–1150	1000	60	< 600	1500	6	0.03	Sperry	.....
2K45	8500–9660	300	25	95–145	30	45	0.7	BTL	Thermally
								WE	tuned
2K33	23600–24400	1800	8	100	20	40	1.5	Raytheon	.....
2K50	23500–24500	300	22	60–80	10	55	.....	BTL	Thermally
								WE	tuned
2K48	3000–5000	1000	10	75–300	20	. ...	.....	BTL	.....
								Sperry	
2K49	5000–10000	1250	12	50–350	10	.....	.....	BTL	.....
								Sperry	

When the behavior is known to be approximately uniform over the band (for example, ±15 per cent), a single average characteristic is given; otherwise the values at the lower and upper frequency limits of the band are given, in that order. When the data given cover a band of frequencies, as just discussed, the mean reflector voltages for the mode in question are given in the same order. These voltages are all negative with respect to cathode. Data are given only for the preferred or more commonly used reflector modes. There is usually considerable scatter about the stated voltages from tube to tube because of mechanical tolerances in reflector spacing. The electronic-tuning rate given is the average value for the electronic-tuning range, that is, electronic-tuning range divided by the difference between the half-power reflector voltages.

The abbreviations used under "Manufacturer" are, in full, as follows:

BTL—Bell Telephone Laboratories, 463 West St., New York, N.Y.

WE—Western Electric Co., 120 Broadway, New York, N.Y.

Sperry—Sperry Gyroscope Co., Great Neck, N.Y.

Raytheon—Raytheon Mfg. Co., Waltham, Mass.

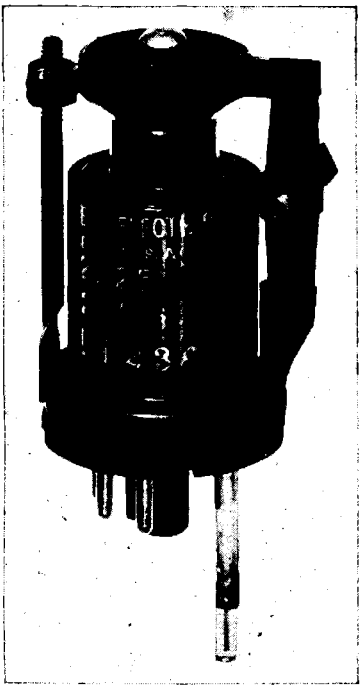

FIG. 2·10.—External view of the type 2K25 reflex klystron. Note coaxial output line protruding through the base.

2·6. The 723 Family of Reflex Klystrons.—The first eight tubes in Table 2·1 form a family of oscillators which are nearly identical in external appearance (see Fig. 2·10) and differ primarily in the size of the frequency-determining resonant cavity. This resonant cavity lies completely within the metal vacuum envelope so that these differences in size are not apparent externally. The frequency of oscillation is varied by turning a tuning screw which flexes the tuning bows on the side of the tube. This motion is transmitted to one of the grids forming the cavity gap, and in the process part of the vacuum envelope (and cavity wall) is slightly distorted. The reflector voltage is applied to the top cap. The r-f output lead is a coaxial line which passes out through the tube base at the usual position of the No. 4 pin. A schematic diagram of the

tube construction is shown in Fig. 2·11. More details concerning mechanical properties and r-f connections will be given after a discussion of the electrical properties.

The first tube of this series was the early form of the 2K25, the 723. There are two main differences between the 2K25 and the 723A/B: the 2K25 has a slightly wider tuning range and meets a minimum output-power specification of 20 mw throughout the band rather than at 9380

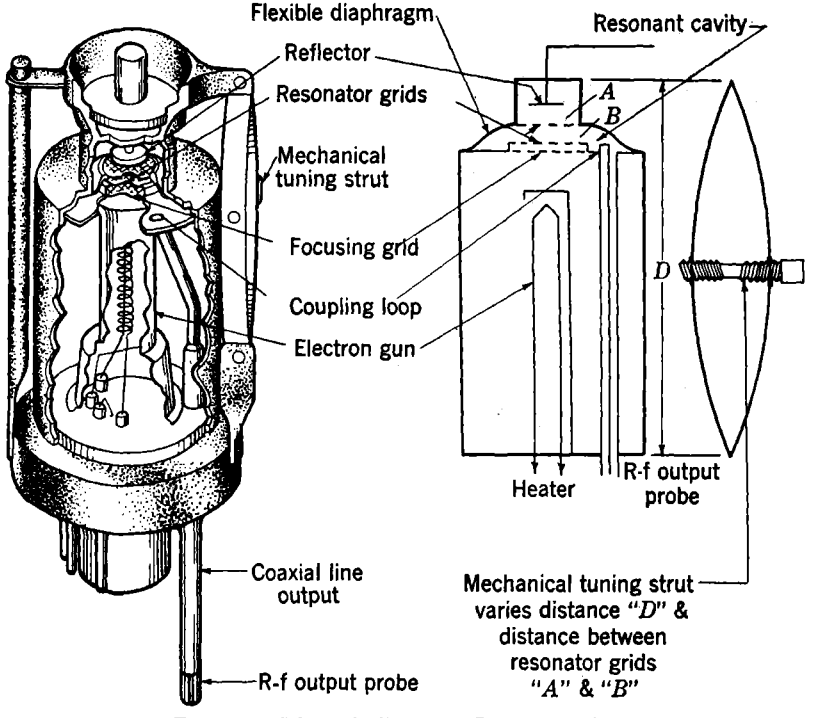

FIG. 2·11.—Schematic diagram of 723 construction.

Mc/sec alone, as is required of the 723A/B. The 723A/B is presumably obsolete.

All the tubes of this family operate at a normal voltage of 300 volts and a beam current averaging 22 ma. Modes of oscillation occur in the range of reflector voltage from 0 to 300 volts negative with respect to cathode. In this range there occur four or five modes in the 2K25 and two or three in the 726 and 2K29. In the 2K25, the two most commonly used modes are the "100-volt mode" and the "160-volt mode," so called from their mean position for an operating wavelength of 3.2 cm. In the 2K29 and 726, the phenomenon of electronic-tuning

hysteresis—which is present to a slight degree in the 2K25—becomes much more troublesome. Design features incorporated in the tubes to minimize this effect are not equally effective for all modes; therefore, in the 2K29 and the 726 there is a single recommended mode. A scatter of roughly ± 30 volts about the quoted reflector voltages may be expected from tube to tube in this family.

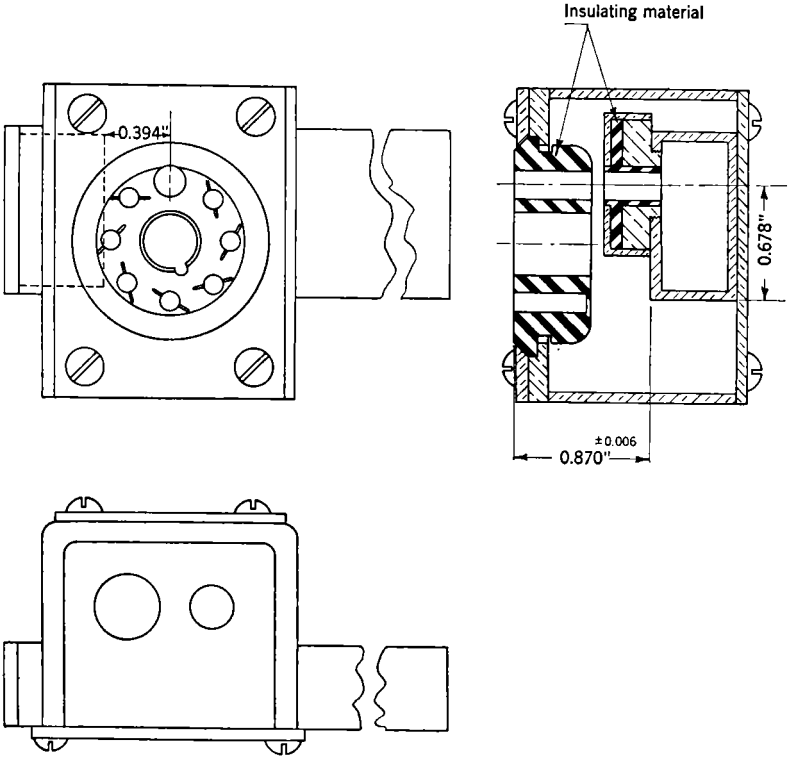

FIG. 2·12.—Schematic diagram of 2K25-to-waveguide socket and mount. Note the insulating bushing between waveguide and the tube for 2K25 output coaxial line; this acts as part of a choke joint and also serves to provide d-c insulation of the 2K25 from ground.

The 2K25 and 2K29 have been "preplumbed," by which it is meant that the r-f output leads have been designed to provide best oscillator performance when the tube works into a specified standard matched transmission line, as will be discussed shortly. The 726A, B, and C are not preplumbed, and if used with the r-f output fittings which are standard with the 2K29, require a matching transformer to obtain maximum output power.

The 2K22, 2K27, and 2K26 have been made only in limited produc-

tion and their properties are not so well defined as those of the tubes just discussed; therefore, only an approximate output power is indicated in Table 2·1.

The standard—and obvious—method of coupling power from the 2K25 to the 3-cm waveguide is indicated schematically in Fig. 2·12. The coaxial output line extends through a clearance hole in a conventional tube socket and projects into the waveguide in a direction parallel to the *E*-lines; the outer conductor of the line is then flush with the inner wall of the waveguide. For better electrical contact the connection

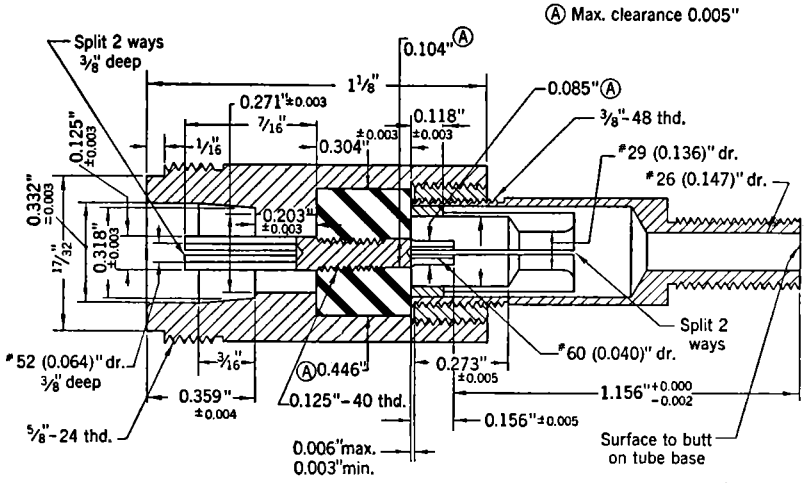

FIG. 2·13.—Recommended adapter from output line of 2K29 klystron to $\frac{5}{16}$-in. 50-ohm coaxial line (type N fitting). When this 50-ohm line is matched, optimum load is presented to the klystron. All metal parts are silver-plated brass. The dielectric is polystyrene.

between waveguide and outer conductor is a choke joint. If the waveguide is matched, the mount shown in Fig. 2·12 loads the 2K25 to maximum output power. It should be noted that any motion of the tube in its socket will change coupling and output power, and that any surface film of dirt on the polystyrene bead at the end of the coaxial line will cause r-f losses.

At 10 cm, for which the 726 and 2K29 tubes are designed, waveguide is not commonly used for these low powers. An adapter from the small $\frac{1}{8}$-in. line on the tube to some more standard line is therefore indicated. In Fig. 2·13 is shown an adapter to standard $\frac{5}{16}$-in. 50-ohm coaxial line, as recommended by the manufacturer. The 2K29 puts out practically its maximum power into a matched 50-ohm line through this adapter, and this is the condition under which the data in Table 2·1 were taken. The 726A, B, and C, as already noted, require an impedance transformer

to obtain the output power listed in the table. The electronic-tuning range quoted for the 726C corresponds to the load adjusted for maximum output power, while for the 726A and B it was obtained with the tube working into a matched 70-ohm line.

2·7. The Type 2K28 Reflex Klystron.—The next tube in Table 2·1 is the 2K28, the only one of those listed in which the resonant cavity does not lie completely within the vacuum. It is electrically comparable

FIG. 2·14.—Type 2K28 vacuum tube, showing copper disks protruding through glass vacuum envelope. In use, these disks are clamped to remainder of oscillator circuit, as in FIG. 2·16.

to, but chronologically earlier than, the 2K25 family. In the 2K28, as may be seen in Fig. 2·14, two copper disks that form part of the cavity walls project through the glass vacuum envelope; the surfaces which complete the cavity, of whatever form the surfaces may be, make contact with these projecting copper disks. One of the principal advantages of this construction, aside from ease of manufacturing, is the freedom it gives for choice of the external part of the resonant cavity to suit the application and the desired frequency of operation. Thus, although the most general application has been at the 10-cm band and above

2000 Mc/sec, oscillations have been obtained down to nearly 1000 Mc/sec by proper choice of external cavity. Near this frequency the (n = 1)-mode approaches zero reflector volts; and although the (n = 0)-mode may be operated at some frequencies below 700 Mc/sec, it is very unsatisfactory.

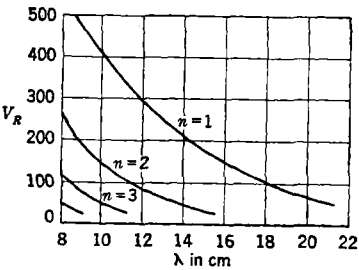

FIG. 2·15.—Reflector mode pattern for the type 2K28 klystron: dependence on wavelength of the reflector voltages at which the mode centers occur.

The 707B is an earlier form of the 2K28 which differs from it only in mechanical respects, being about 1½ in. longer and having slightly more drift of frequency with temperature in certain external cavities. In electronic characteristics and in dimensions relevant to the attachment of the cavity, the two types are identical. The most usual operating voltage for the 2K28 is that given in Table 2·1, 250 volts. The tubes may be operated at 300 volts but the electronic-tuning range is almost unaltered and the output voltage does not increase so fast as the input voltage. In the vicinity of 3000 Mc/sec there are two convenient modes corresponding to n = 2 and n = 3. Both have about the same electronic-tuning range; the (n = 2)-mode is, as usual, higher in output

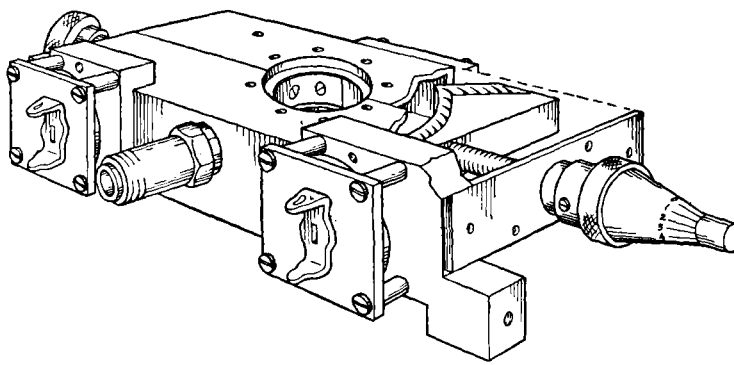

FIG. 2·16.—Tunable cavity for the type 2K28 klystron for the 8- to 12-cm region. Tuning is accomplished by motion of the sliding plungers at either end of the cavity, which is rectangular in form.

power and the (n = 3)-mode is higher in electronic-tuning rate. In Fig. 2·15 there is shown a typical relation between reflector voltage and wavelength for the various modes of oscillation of a 2K28. The most generally useful external cavity for use with the 2K28 over the 2500- to 3800-Mc/sec range is that shown in Fig. 2·16. This covers the stated

range by motion of the two sliding plungers in a rectangular waveguide, in the center of and transverse to which is clamped the vacuum tube.

For the much less frequent use at longer wavelengths the resonant cavity has usually consisted of a coaxial line folded back on the tube. One of the difficulties with such a circuit is a tendency toward oscillator operation in harmonic modes of the circuit, but this difficulty is not too serious since such modes of oscillation do not usually occur at the same reflector voltage as the fundamental mode. Electronic-tuning hysteresis is also somewhat greater with the ($n = 0$)- and ($n = 1$)-modes used at longer wavelengths.

2·8. The Type 417 Family.—Following the 2K28 in Table 2·1 is another sizable homogeneous family, the 2K41 (or 417A), the 2K39

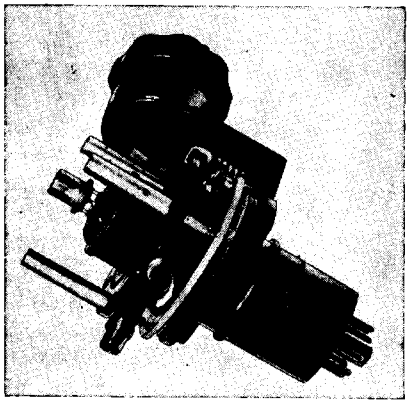

FIG. 2·17.—External view of the type 2K41 reflex klystron.

(419B), and a series of tubes intermediate in frequency between these two (the 2K42, 2K43, and 2K44). This family of tubes covers the band 2650 to 10,300 Mc/sec. Primarily a higher-voltage, higher-power, and more stable type of tube than those so far discussed, they operate at a maximum beam voltage of 1250 volts, at which the normal beam current is 45 ma. As is apparent in Table 2·1, the high beam impedance acts to diminish the electronic-tuning range and electronic-tuning rate; the higher d-c input voltage produces output powers of the order of $\frac{1}{3}$ to $\frac{3}{4}$ watt.

The 2K41, to which the other tubes of this family are externally quite similar, is shown in Fig. 2·17. The resonant cavity is completely enclosed by the metal vacuum envelope; its frequency is adjusted by a change in cavity-gap spacing accompanied by flexing of a diaphragm which is part of the cavity wall. This tuning is effected by relative motion of the two tuning rings which may be seen in Fig. 2·17; this

motion is controlled by a tuning knob. The solid and heavy construction of the tube and tuner contributes to mechanical and thermal stability.

In the 2K41, adjustment of the tuning knob alone covers the specified frequency band; in the other tubes, adjustment of the tuning knob alone covers about one-third of the total range, and the tuning screws must be adjusted to set the center point of this restricted range. This change to the full-range tuner distinguishes the 2K41 from the 417A which it supersedes. The latter also has a beam-voltage maximum of 1000 volts; otherwise the two differ only in minor details. The 2K39 and the 419B differ only in name. The output leads are in each case a coaxial line with a type SKL fitting. An adapter, JAN type UG-131/U, converts this to a type N fitting; or plugs JAN types UG-275/U and UG-276/U are used to go directly to JAN type RG-5/U flexible coaxial cable. The 2K41 has two output leads, the other tubes have one. None of the tubes are preplumbed, so that a coaxial matching transformer is used to obtain the optimum output data indicated in Table 2·1. With the 2K39, an adapter providing a matched transition from coaxial line to waveguide is needed in addition; such a transition is shown in Fig. 2·18. Since coaxial lines and coaxial transformers are lossy in the frequency range of the 2K39, the best arrangement for the 2K39 is probably one using as short a section of line from tube to waveguide as possible, followed by a matching transformer in the waveguide.

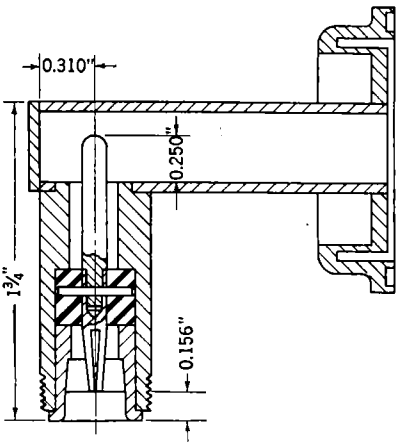

FIG. 2·18.—Schematic diagram of matched transition from $\frac{5}{16}$-in. 50-ohm coaxial line (type N fitting) to 1-in. by $\frac{1}{2}$-in. waveguide.

All of these tubes have control electrodes in the electron gun; the corresponding applied voltage V_G is given under "Notes" in Table 2·1. In the 2K41 this control electrode is a fine mesh control grid with a high-μ action; this control grid normally runs between 0 and +50 volts with respect to cathode. In the other tubes the auxiliary electrode is a focus ring which is normally run at cathode potential, but which has its own base pin so that it may be run at a nonzero voltage if control over the current is desired; this focus ring has a very low-μ action.

The electronic-tuning range and the output power quoted for the 2K41 at 1000 volts are not increased appreciably if the voltage is raised; nor do they drop very much if the voltage is lowered to 800 volts, but

if this is done, the necessary reflector voltage rises another 100 volts. The unusually low electronic-tuning rate of 0.04 Mc/sec per volt on the reflector should be noted.

The data given for 400 volts for the 2K41 correspond to the ($n = 4$)-mode, the mode which behaves in the most constant manner over the band. In the lower half of the stated frequency range, the ($n = 3$)-mode (180 to 380 reflector volts) has some 40 per cent more power and 55 per cent less electronic-tuning range.

The data for the 2K39 are self-explanatory. At 1250 volts there are two good modes; the ($n = 5$)-mode provides a marked increase of electronic tuning at little cost in output power. Output power is still appreciable in the ($n = 9$)-mode at 700 volts, but drops off very rapidly below this because of the coarseness of the tungsten vane grids which constitute the cavity gap. The data shown are for 9350 Mc/sec, near the upper end of the frequency band, because this is where the data are the most reliable and the applications most numerous; data at 8400 Mc/sec are closely similar to those shown. Output power and electronic-tuning range are higher at the center of the band and are dropping off rapidly at 9350 Mc/sec.

The 2K42, 2K43, and 2K44 are much newer tubes than the 2K41 and 2K39. They are very similar in all details to the 2K39, from which they are derived.

2·9. The Types 3K23 and 3K27.—In a sense, the 3K27 klystron shown in Fig. 2·19 and the 3K23 are members of the 2K41-2K39 family although they operate in the frequency range 770 to 1150 Mc/sec. They have the same general tuning arrangement and mechanical construction, somewhat enlarged because of the longer wavelength. Like the 2K41, they have a tuner which covers the whole frequency range by rotation of a single knob without other adjustments. The electron gun has a somewhat lower beam impedance (higher perveance) and normally operates at 1000 volts, 60 ma, with the low-μ focus ring connected to cathode. The 3K27 and 3K23 are not preplumbed; the output lead is a coaxial line of the same type as is used in the 2K41. Output power and electronic-tuning range average $1\frac{1}{2}$ watts and 6 Mc/sec over the tuning range. There is occasional electronic-tuning hysteresis.

2·10. The Type 2K45.—Both of the first two families of tubes discussed (the 723 and 417 families) included tubes at some or all of the frequencies between the 10-cm and the 3-cm bands. Both families are mechanically tuned and differ electronically in the features emphasized. A third type of tube is available in the 2K45, which is electronically quite similar to the 2K25 but is radically different in method of tuning. It is very likely that tubes similar to this type will be developed at other frequencies, thus building up a third family. The 2K50, to be discussed

shortly, is not quite in this same family, although it uses the same basic method of tuning; perhaps it is a first cousin to the 2K45.

The frequency of oscillation of the 2K45 is adjusted by the process of "thermal tuning"; by this is meant that the necessary mechanical distortion of the resonant circuit is produced by the thermal expansion of a tuning element. In the 2K45 and 2K50, the thermal expansion of this element is amplified mechanically before being applied to the resonant circuit. The thermal element is the plate of a "thermal tuning triode" which is built within the vacuum envelope which encloses the

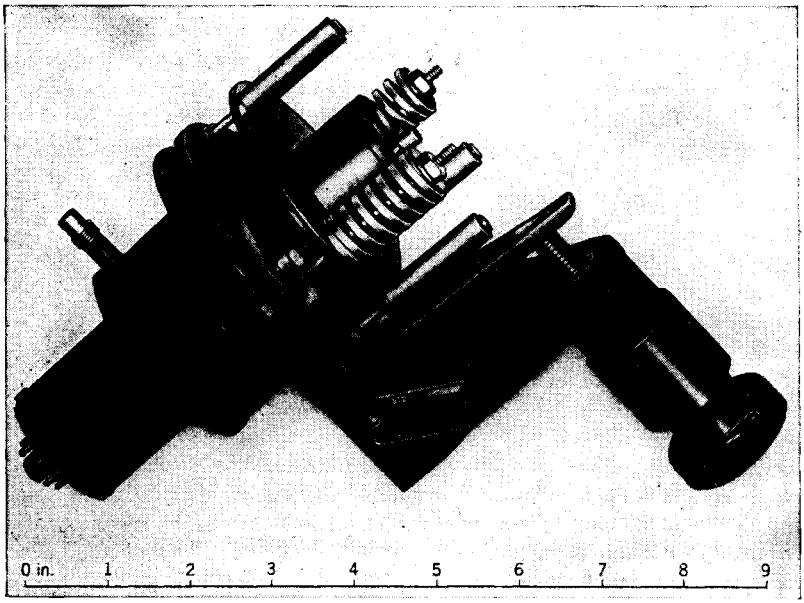

FIG. 2·19.—External view of type 3K27 reflex klystron. Note single-knob parallel-motion tuning mechanism.

oscillator; the anode and cathode of this triode are tied to the anode (resonator) and cathode of the klystron, respectively; a negative control grid varies the current flow to, and thus the temperature of, the thermal element. This control of frequency by a high-impedance electrode is a very desirable feature for circuit applications. A photograph of the tube is shown in Fig. 2·20.

In the 2K45, the thermal triode draws a maximum current of 20 ma at 300 volts, or 6 watts dissipation. This maximum current occurs at control-grid voltage about −5 volts with respect to cathode; −35 volts on the control grid reduces the thermal-anode current nearly to zero. This range of thermal control tunes the frequency at least over

the specified range 8500 to 9660 Mc/sec; and if, after the frequency has stabilized at one of these two limits, the tuning current is suddenly shifted to its maximum or minimum allowed value corresponding to the vicinity of the other end of the frequency scale, then the frequency is changed at such a rate that the specified range 8500 to 9660 Mc/sec is covered in not more than nine seconds.

As already noted, the 2K45 is electronically similar to the 2K25, although not identical to it. Electronic-tuning hysteresis has been practically eliminated for the 120-volt mode and the r-f output line has been very much improved electrically. The 2K45 is designed to operate into a mount such as that of Fig. 2·12.

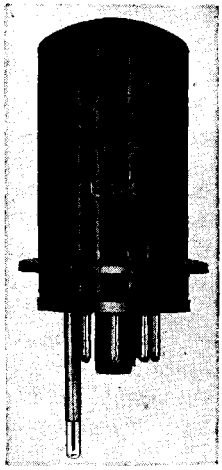

FIG. 2·20.—External view of the type 2K45 reflex klystron. Note the coaxial output lead extending through the base, and the absence of external tuning mechanism.

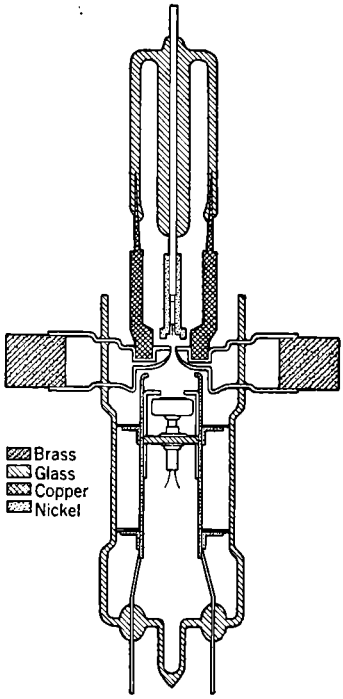

FIG. 2·21.—Schematic diagram of the type 2K33 reflex klystron. Rectangular waveguide leading from the radial transmission line is not shown.

2·11. One-centimeter Reflex Klytsrons.—The next two tubes in Table 2·1, the 2K33 and the 2K50, operate at 1 cm (24,000Mc/sec). The 2K33 is a high-voltage mechanically-tuned tube of simple construction which lends itself to quantity production. The 2K50 is a low-voltage thermally-tuned tube; both these features render the fabrication somewhat more complicated than that of the 2K33.

A schematic diagram of the 2K33 is shown in Fig. 2·21. This tube utilizes the same type of copper-disk construction as does the 2K28, with

a radical difference: the glass seal comes not inside the resonant cavity itself, but rather in a region outside the cavity which may be considered to be part of an impedance-matching transformer between the cavity and the rectangular-waveguide transmission line. Coupling out of the cavity is done by means of a quarter-wavelength section of radial waveguide formed by an indentation of corresponding length in one of the disks. The remainder of the impedance transformer is another section of radial waveguide bounded by a metallic wall formed by clamping a thick plate between the opposing disks. Out of this radial waveguide leads the usual rectangular waveguide. The present production tubes have, as an aid to impedance-matching, an additional section of rectangular waveguide diametrically opposed to the output line, and short-circuited by a movable plunger, called the "back plunger." The tube is tuned by a knob, the rotation of which causes flexing of one of the disks in the region of the impedance transformer, and thus causes a change in the cavity-gap spacing.

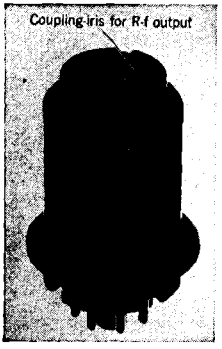

FIG. 2·22.—External view of type 2K50 reflex klystron. Note choke joint and glass window where the output transmission line passes through vacuum envelope at top of tube.

As an aid to focusing the beam through the very small hole (0.028-in. diameter) which forms the cavity gap, the electron gun has a focusing electrode. On current production tubes, there is stamped an optimum value of beam current (approximately 8 ma) for the operating beam voltage of 1800 volts; the focusing electrode voltage should be adjusted to give this current.

With proper values of beam current and adjustment of the back plunger, the output power and electronic range are quite uniform over the band. The tubes work into a matched load once the back plunger is adjusted.

In early tubes there was troublesome electronic-tuning hysteresis, which has since been removed by a change in design. There is still, however, some "thermal hysteresis"; the final distribution of beam current on the disks depends on reflector voltage, and the tube parts in the neighborhood of the beam have such small heat capacity that, if the reflector voltage is swept at 60 cps, a noticeable difference in the frequency of oscillation occurs at a given reflector voltage, depending on the direction of approach. This difference disappears with a 1000-cps sweep.

In contrast to the 2K33, the 2K50 achieves operation at a beam voltage of 300 volts by the use of fine tungsten grids for the cavity gap; this allows a larger beam and a smaller transit distance through the gap. An external view of the 2K50 is shown in Fig. 2·22; a schematic cross

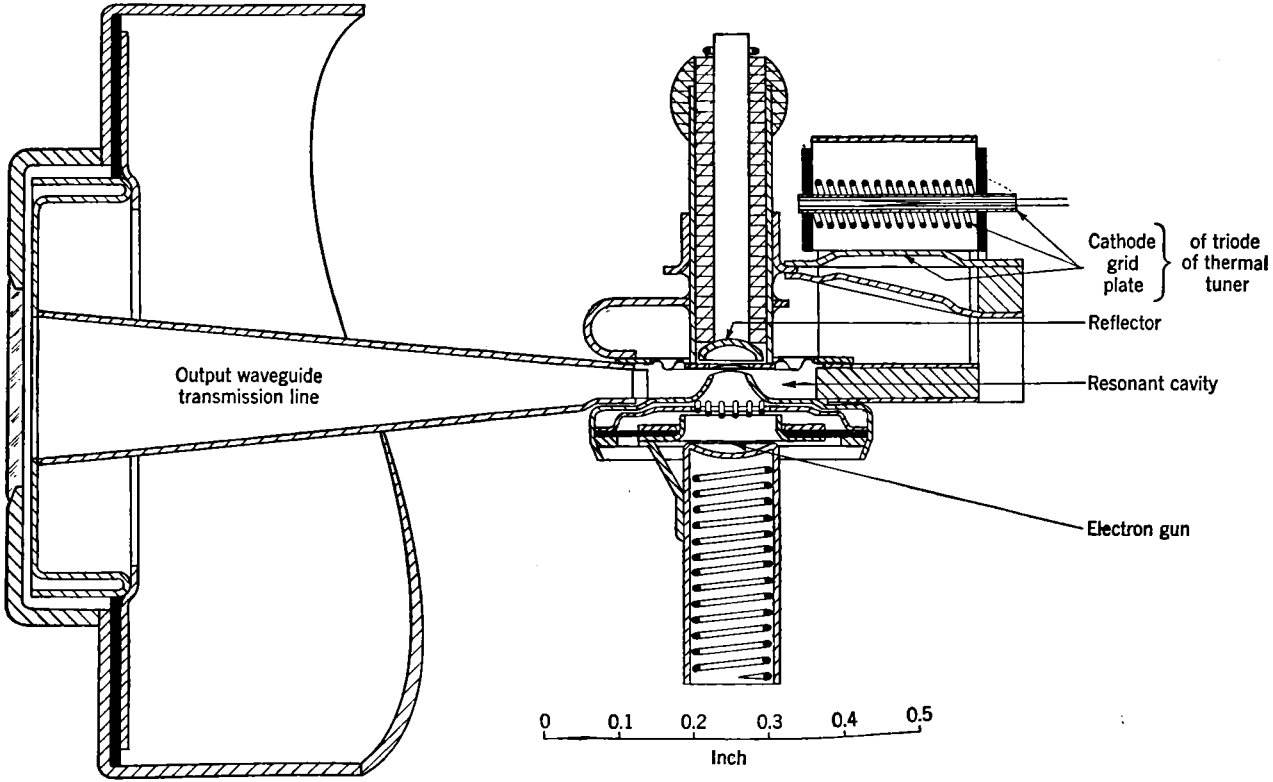

FIG. 2·23.—Schematic section of the type 2K50 reflex klystron. Note thermal-tuning mechanism and waveguide output line.

section is shown in Fig. 2·23. The output power is coupled directly to a tapered waveguide through an insert in the side of the cavity; the output waveguide ends at a choke flange inside a glass window which is at the top of the tube and is part of the vacuum envelope; in operation this window is butted up against another waveguide choke joint.

Tuning the frequency of oscillation is accomplished, as in the 2K45, by expansion of a thermal element which is the plate of a thermal tuning triode. The maximum power drawn by this thermal element is three watts. A variation of the thermal-triode control-grid voltage over the range 0 to −30 volts with respect to cathode covers a tuning range at least 60 per cent greater than the tuning range specified in Table 2·1 for r-f operation, 23,500 to 24,500 Mc/sec. If the control-grid voltage is suddenly changed from one to the other of the two values which correspond statically to this 60 per cent enlarged tuning range, the frequency passes through the 23,500- to 24,500-Mc/sec range in about two seconds. For the reflector mode specified, electronic-tuning hysteresis has been reduced almost to the vanishing point.

2·12. The Types 2K48 and 2K49.—The last two tubes in Table 2·1, the 2K48 and 2K49, together cover the frequency band from 3000 Mc/sec

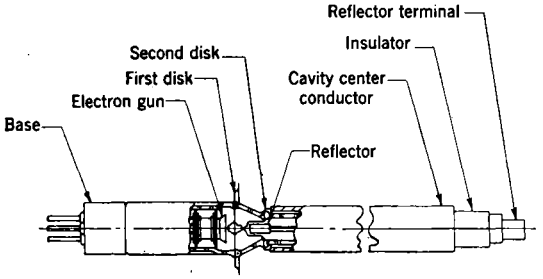

FIG. 2·24.—Cut-away view of the 2K49 tube.

to 10,000 Mc/sec; 3000 to 5000 Mc/sec is the operating range of the 2K48, 5000 to 10,000 Mc/sec that of the 2K49. In order to allow the tuning of the oscillator circuit over these wide bands, these oscillators are of the external-cavity type; the construction of the vacuum-tube part of the oscillator is such as to make convenient a resonant circuit which is a coaxial line enclosing the reflector leads. Sectional views of the vacuum tube by itself and placed in its associated coaxial cavity are shown in Figs. 2·24 and 2·25.

A single reflector mode, that for which $n = 1$, provides the optimum operation over the 3000- to 5000-Mc/sec band in the 2K48; the reflector voltage at which this mode occurs increases from 75 to 290 volts as the frequency is varied. In the 2K49 no one mode covers the whole band;

three modes corresponding to $n = 1$, 2, and 3 must be used. The corresponding reflector voltages range between 50 and 350 volts. The maximum beam voltage is 1500 volts for each tube.

The center conductor of the coaxial resonant cavity is an integral part of the vacuum tube. A resonant cavity of the type shown in Fig. 2·25 will of course resonate at a given frequency at a number of different plunger settings; the shortest possible cavity length consistent with mechanical requirements should be used. With the optimum inner diameter of one inch for the outer conductor of the coaxial line, the mode of oscillation with a cavity length of a quarter wavelength is used in the 2K48 and the mode with a three-quarter-wavelength cavity is used in the 2K49.

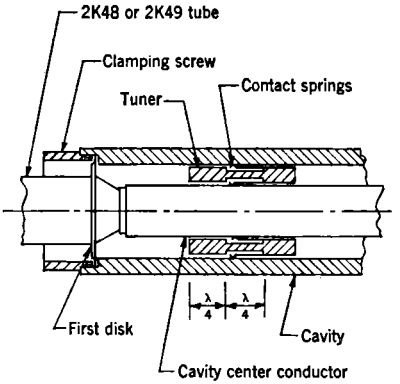

FIG. 2·25.—Arrangement of the 2K49 tube in its associated coaxial cavity. The tuner drive and support are not shown.

2·13. Reflex-klystron Power Supplies.—The general characteristics required of power supplies to operate these microwave oscillators are apparent. There are two principal voltages to be supplied—the beam voltage and the reflector voltage. The latter is applied to an electrode which normally draws only a few microamperes of current. Since the anode in a klystron is a somewhat sizable resonant circuit which usually forms part of the vacuum envelope, it is common practice to operate klystrons with the anode grounded. This may always be avoided if necessary, with a degree of inconvenience varying from tube to tube. Thus in the 2K25 (see Fig. 2·10) it is fairly simple to insulate the coaxial output line from the (grounded) waveguide into which this output line is inserted. The power supplies which will be discussed in detail are of the conventional type with high negative voltage.

As to other power-supply requirements, each tube of course requires a heater supply (6.3 volts alternating current); in addition, the type 2K41 normally requires a small positive control-grid voltage. Since one of the characteristics of the reflex klystron is sensitivity of frequency to beam and reflector voltages, these voltages must be regulated to a fraction of a volt. In addition to these necessities of life, it is very convenient to have included in the power supply some means for the square-wave amplitude modulation so commonly used in measurements.

Two power supplies which have been developed for reflex klystrons and which have received considerable use will be discussed shortly.

E. G. & G. LIBRARY
LAS VEGAS BRANCH

These power supplies use the conventional procedure of using a stepup transformer at line-frequency, then rectifying and regulating the transformer output voltage. Before launching into the details of these supplies, however, attention should be called to the so-called "r-f power supplies" which are discussed at more length in Vol. 22 of this series. In these supplies an unregulated low voltage is used to drive an r-f oscillator at a frequency of, for example, several megacycles per second. The tank coil of this oscillator serves as the primary of an air-core stepup transformer operating at radio frequency; the resulting high r-f voltage is then rectified in the usual manner to give high d-c voltage. The principal advantage of this scheme is the use of a small and light air-core transformer.

Returning to the subject of more conventional power supplies, it will be observed from Table 2·1 that a large number of the tubes there listed may be operated at 400 volts or below. For such tubes a very satisfactory power supply has been found to be the type TVN-7BL.[1] The output beam voltage of this supply is adjustable between 280 and 480 volts; this range is easily changed to 180 to 300 volts. The reflector-voltage range is -15 to -210 volts with respect to cathode. A positive control-grid voltage is available for the 2K41. A multivibrator type of square-wave generator with adjustable frequency is built into the supply, and its output voltage may be applied either to the control grid or to the reflector of the klystron.

A circuit diagram of this supply is given in Fig. 2·26. The main power supply, working from the two transformers T_1 and T_2 and a full-wave rectifier V_1, is separate from the square-wave modulator power supply which works from transformer T_3 and the full-wave rectifier V_2.

Control of the output voltage of the main supply is accomplished by tubes V_3 and V_4, a 6Y6G and a 6SJ7, respectively. The former acts as a current-regulator tube, the grid voltage of which is determined by the plate current of the 6SJ7 flowing through the bias resistor, R_2. An increase in the power-supply output voltage raises the grid voltage and plate current of the 6SJ7; the increased drop in R_2 changes the grid voltage of the 6Y6G negatively. For a given current delivered to the klystron cathode, this change in grid voltage must be countered by an increase in the drop across the 6Y6G; with proper circuit adjustment, this restores the output voltage to its original value.

The voltage which appears at the grid of the 6SJ7 is the difference between a positive voltage, taken from a voltage divider across the output voltage, and the fixed negative bias provided by V_5 and V_6, two 0C3/VR105 voltage-regulator tubes. The constant bias provided by these regulator tubes—in particular the independence of this bias on

[1] Manufactured by Browning Laboratories, Inc. Winchester, Mass.

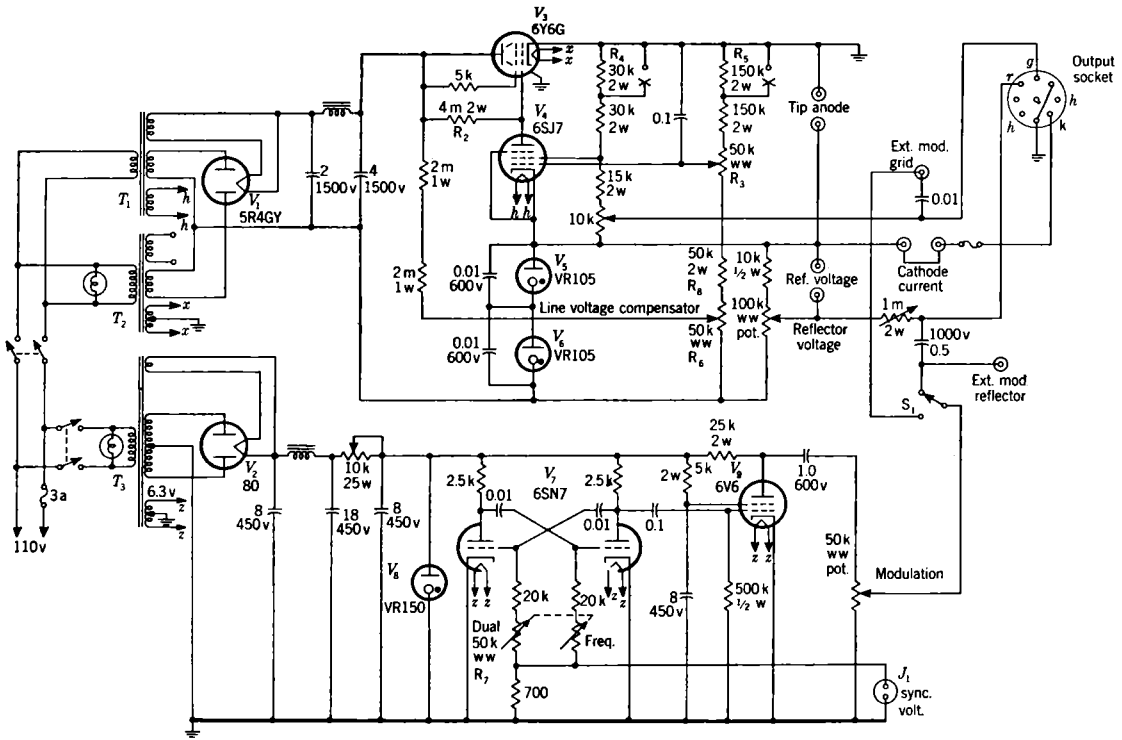

Fig. 2·26.—Circuit diagram for TVN-7BL power supply and square-wave modulator.

6SJ7 plate current—is essential to the operation of this system. Adjustment of the bias, by means of the variable resistor R_3, provides the means of controlling the output voltage of the power supply within the limits of 290 and 480 volts. If the resistors R_4 and R_5 are short-circuited, the output voltage range is 180 to 300 volts.

The variable resistor R_6 adjusts the feedback to the control tube and must be adjusted for the amount of feedback giving the best regulation. This adjustment, if impaired, is easily repeated by setting R_3 to give approximately the desired output voltage, then varying the input a-c voltage with a Variac. R_6 is then adjusted until the input variation produces no output variation.

As will be seen from the circuit diagram, the regulated reflector voltage is obtained by tapping off from a voltage divider placed across the two VR tubes.

The voltage supply for the square-wave modulator is regulated by tube V_8, a 0D3/VR150. Tube V_7, a 6SN7, and its associated circuit form a conventional multivibrator consisting of a two-stage resistance-capacitance-coupled amplifier with the output leads of the second stage connected to the input leads of the first. The dual adjusting control of the grid returns, R_7, adjusts the frequency of operation. In order to prevent the load from affecting the multivibrator frequency, the output voltage is taken from the buffer amplifier V_9, a 6V6 tube, which is in turn excited by the multivibrator.

This multivibrator may be synchronized with an external oscillator, by injecting a synchronizing voltage at J_1. Such synchronization is of course not necessary for operation.

The square-wave output voltage of the multivibrator is applied either to the klystron grid or to the reflector by switch S_1, and is capacitively coupled to these electrodes.

The one-megohm resistor in series with the reflector should be noted. This resistor is very convenient, but it means that one microampere flowing to the reflector will cause a one-volt change in reflector potential; hence the presence of resistor R_8 which keeps the reflector voltage at least 15 volts negative with respect to the cathode. At any reflector voltage there will be a few microamperes of reflector current caused by gas and leakage, but all tubes are required to pass close specifications on this leakage current.

In operating the high-voltage tubes, such as the 2K39, the power-supply problems are somewhat more complicated in detail although not in principle. In Figs. 2·27 and 2·28 are shown, respectively, the high-voltage power supply and the associated modulation circuits of a satisfactory power supply for these voltages as used in the SX-12 Klystron Signal Generator.[1] The power supply and modulation circuits are

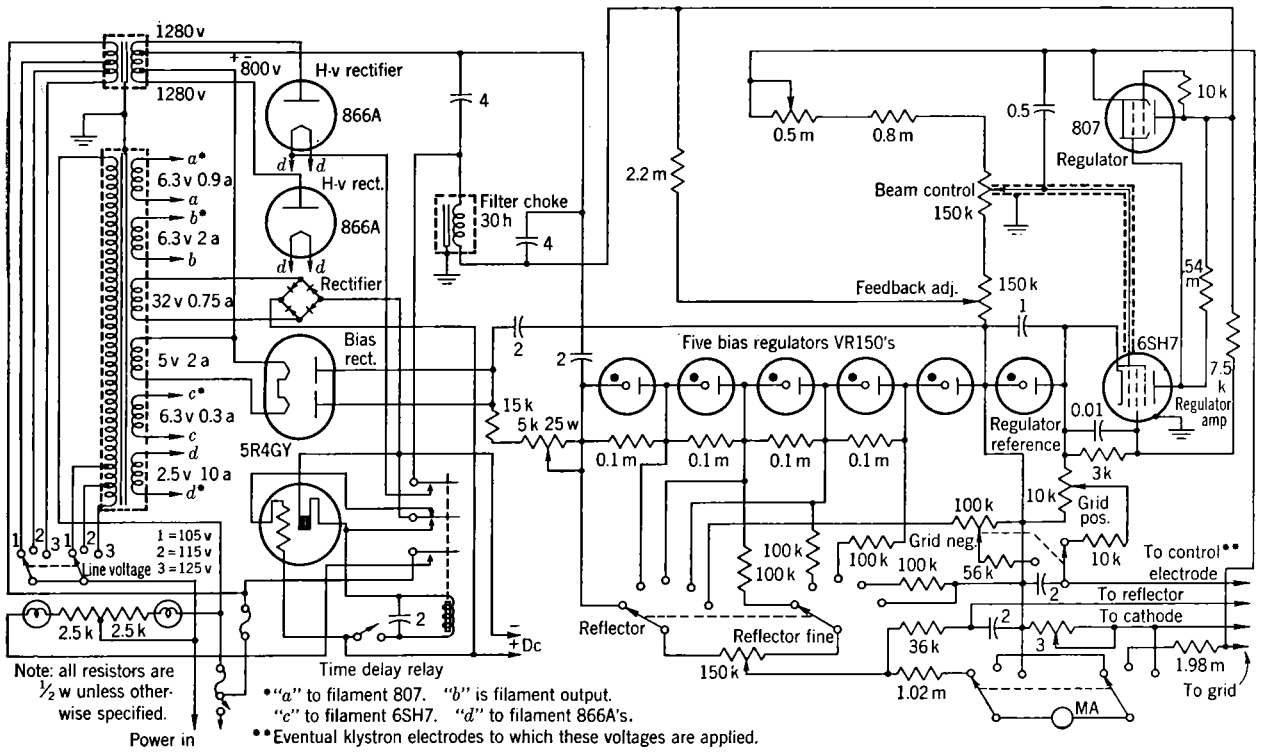

FIG. 2·27.—Mark SX-12 power supply, schematic diagram.

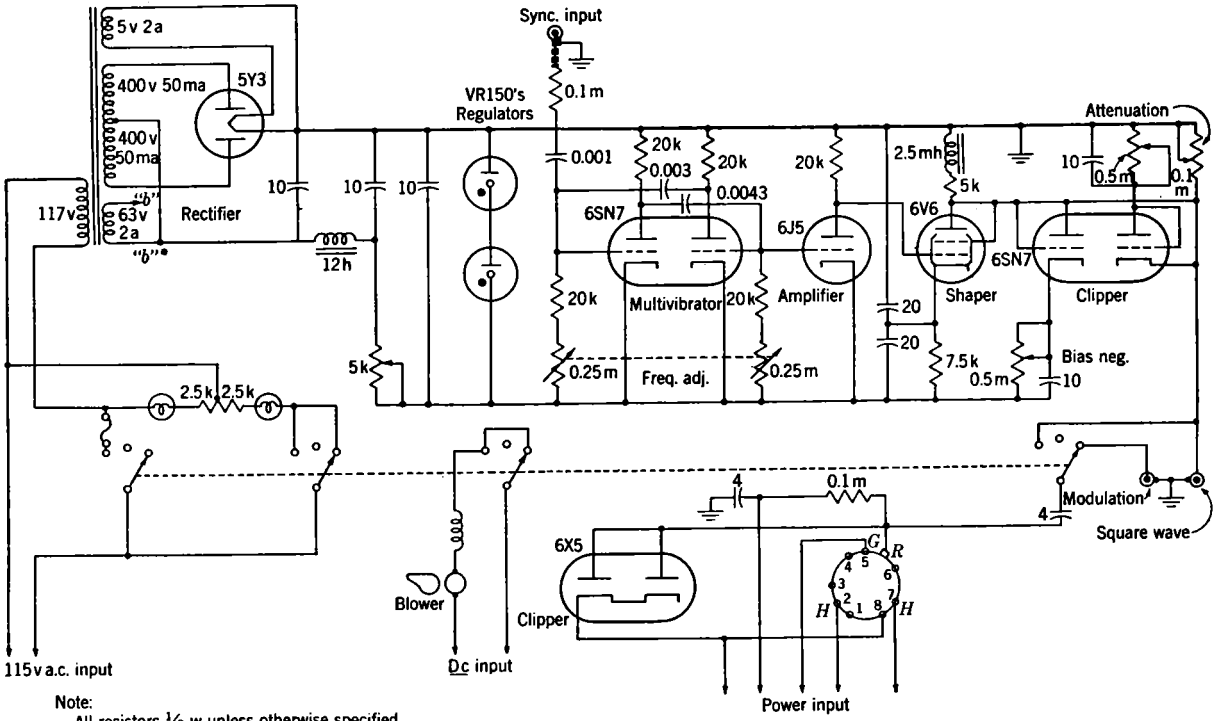

FIG. 2·28.—Mark SX-12 square-wave generator, schematic diagram.

shown in two figures as a matter of convenience. In Fig. 2·27, the schematic diagram of the high-voltage power supply and the leads for the output voltages which are eventually applied to the klystron are shown. In Fig. 2·28 the actual connections to the klystron socket are indicated.

Aside from the changes in tubes and components made necessary by the increased klystron current and voltage ratings, and aside from the time-delay relay arrangement, which is shown in Fig. 2·27, the electronically regulated high-voltage power supply of Fig. 2·28 is basically the same as that shown in Fig. 2·26 for the TVN-7BL power supply. Electronic voltage regulation is achieved in an identical manner by use of a regulator tube, the control grid of which is activated by a regulator amplifier; this regulator-amplifier tube in turn has its cathode voltage held at a given reference level by a VR tube. The same regulator-feedback adjustment is provided for compensating large line-voltage changes which alter VR tube characteristics.

In the TVN-7BL, the klystron cathode was connected to the cathode of the regulator amplifier and a (positive only) klystron-control-electrode voltage was derived from the same voltage divider which supplied the regulator-amplifier-grid voltage. The SX-12 is intended to be used with certain tubes (for example, 2K41, 2K39) which, in the aggregate, require that the power supply must therefore produce both positive and negative klystron control-electrode voltages. Hence the klystron cathode is now connected to the cathode of the regulator reference VR tube, and positive or negative control-grid voltages are derived by potentiometers across adjacent VR tubes. The regulated reflector voltage is similarly derived by potentiometers across VR tubes, as in the TVN-7BL, but, because a large negative reflector voltage is useful in obtaining the high-power modes of the type 2K39 klystron, five OD3/VR150's are used in series. A coarse switching adjustment and a fine potentiometer control of the reflector voltage are indicated in Fig. 2·27; padding resistors in the switching arrangement provide overlapping of the voltage ranges.

The resultant electrical characteristics of the output high voltage, as quoted by the manufacturer of the SX-12 klystron signal source, are as follows: beam voltage, +750 to +1250 volts at a maximum beam current of 50 ma; regulation, ±0.2 volts; ripple, 0.2 volts peak to peak; reflector voltage, 0 to −750 volts at a maximum reflector current of 1 ma; regulation, ±0.5 volts; ripple, 0.2 volts peak to peak. In connection with these characteristics, it is particularly to be noted (see Fig. 2·28) that, as in the TVN-7BL, a high resistance is provided in series with the reflector as an aid to reflector-voltage modulation. Thus, if reflector

[1] Manufactured by the Sperry Gyroscope Co., Great Neck, N.Y.

current above a few microamperes flows, undesirable reflector-voltage and frequency modulation results.

In Fig. 2·28 is shown a square-wave modulation circuit which has been developed for use with the klystron for which the high-voltage power supply of Fig. 2·27 is used; since some of these klystrons have modes of oscillation several hundred volts wide under conditions of maximum output power, a high-amplitude square wave is required for modulating these tubes. The square-wave generator shown has its own VR-tube-regulated voltage supply; the output square wave is provided by a multivibrator, amplifier, and square-wave shaper and clipper. The resultant square wave has times of rise and fall each equal to one microsecond. The frequency of the output square wave may be varied from 350 to 3500 cps by adjustment of the variable resistor indicated in Fig. 2·28. The amplitude of the square-wave modulation may be varied from 0 to 100 volts by adjustment of the indicated variable-resistance attenuator. The voltage square wave is capacitance-coupled to the reflector, with provision for switching to an external source of modulation if so desired.

If at any time during the modulation cycle the reflector is operated at a positive voltage with respect to cathode, sizable current will be drawn by the reflector. This is bad for several reasons. In the first place, heating of the reflector electrode and liberation of gas may take place. Even worse, when electrons are collected on a reflector which has a ratio of secondary electrons produced to primary electrons incident greater than unity, a net flow of electrons from reflector to anode may result. The net flow may cause the reflector to remain positive with respect to cathode regardless of any subsequent voltage modulation applied to the other end of the high resistance which is directly in series with the reflector. This is not only hard on the tube, but also output characteristics become very puzzling to the user, who thinks he knows what modulation he is applying to the reflector. Fig. 2·28 shows a diode clipper tube connected from cathode to reflector; this counteracts any reflector secondary emission and also prevents the reflector from becoming appreciably positive during modulation.

FREQUENCY STABILIZATION OF ELECTRONICALLY TUNABLE MICROWAVE OSCILLATORS

By R. V. Pound

Most automatic-frequency-control systems operate to minimize the difference between the frequency of an oscillator and that of some standard of reference. For most radar systems applications, the standard of reference is the local-transmitter frequency plus or minus the intermediate frequency and the AFC system can be thought of as a

difference-frequency system. The AFC system used for the beacon local oscillator of an airborne radar uses a precision resonant cavity as the standard of reference and can therefore be considered as an absolute-frequency system. The circuits commonly used for both of these systems, so-called hunting circuits (see Vol. 16, Chap. 7), function on information derived once per transmitter pulse or once per audio cycle and cannot, therefore, be expected to remove fluctuations in frequency that have periods comparable with the time between transmitter pulses, or with the audio-frequency period for the beacon AFC system. In fact, these circuits impose on the oscillator frequency modulation having a period of this order, and the resultant signal, although its average frequency is maintained with precision, covers a band of frequencies.

The conventional AFC systems used in broadcast receivers are different in principle in that a continuous source of error signal is available. The circuits usually used, however, have very long time constants and, consequently, are limited in the rate of change of frequency which they can correct. This situation is implied when the statement is made that the "d-c component" of the frequency-discriminator output voltage is applied as an error voltage for AFC purposes. The short-time frequency variation of the oscillator does not differ from the frequency variation without the AFC system.

The purpose of the frequency-stabilization circuits to be described here is different from that of the low-frequency circuits in that, in addition to maintaining a minimum difference in frequency from a standard reference cavity, they also remove frequency deviations, occurring at audio frequencies and higher, normally found in the output spectrum of a microwave oscillator. If a microwave oscillator is caused to maintain a steady average frequency, free from drifts caused by thermal, mechanical, or load-admittance changes, the output signal of the oscillator is usually found to be spread over a band of frequencies. This may be the result of frequency modulation by noise in the electron stream of the oscillator, by residual ripple on the supply voltage, by the a-c heater voltage, and by stray magnetic fields. Counteracting these sources of frequency modulation is the "flywheel" effect of the resonant-cavity "tank circuit" of the oscillator and its effectiveness is a function of the loaded Q of this resonator. Since only special types of cavities can be used in the oscillator, the tank-circuit Q is not usually very high compared with that of many microwave cavities. As a result, considerable care must be exercised to hold the oscillator frequency within one part in 10^6. Thus it would be difficult to keep a 9000-Mc/sec oscillator within a band of frequencies less than 10 kc/sec in width.

The stabilization systems to be described reduce the width of this frequency spectrum by a considerable factor. The long-time frequency

stability of the stabilized oscillator is almost completely determined by the stability of the reference cavity. The design of highly stable resonant cavities will not be discussed here, except to point out that cavities having zero, or very small, temperature coefficients of frequency can be made by the use of temperature-compensated tuning mechanisms built from materials having different temperature coefficients of linear expansion. The temperature coefficient of the cavity frequency can be reduced by making the cavity walls of Invar, or even fused quartz, lined with material of high electrical conductivity.

2·14. General Description of Stabilization Circuits.—Basically, the schemes of electronic frequency stabilization to be discussed here consist of a microwave circuit containing a high-Q reference cavity, and either

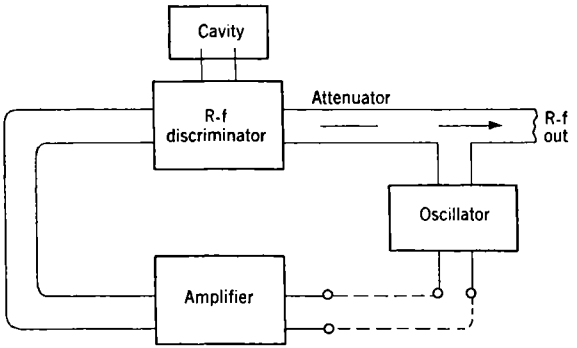

FIG. 2·29.—Block diagram of electronic frequency-stabilization system.

detectors or some other means for frequency conversion. A signal applied to this microwave circuit produces an output voltage which is a measure of the difference between the frequency of the signal and the resonant frequency of the cavity. This "error voltage" is then amplified and superimposed upon the supply voltage of an element of the oscillator, the potential of which controls the oscillator frequency. A block diagram illustrating this basic circuit is shown in Fig. 2·29.

Consider the situation that exists if the output terminals of the amplifying device are disconnected from the control terminals of the oscillator. If an a-c voltage were applied to the oscillator terminals, a frequency modulation would be produced which would in turn produce a large a-c output voltage from the amplifier. Ignoring the complex conversions of frequency occurring between the two terminal pairs, one may consider the device between them as a voltage amplifier. To produce stabilization it is necessary to connect the output terminals to the input terminals, which represents the limiting case of a negative feedback device. It is well known that if this is to be done without

singing around the feedback loop, rigid requirements are imposed upon the phase and amplitude characteristics of the amplifier. Since the feedback circuit must have a finite bandwidth, it must also have a cutoff characteristic at sufficiently high frequencies. It has been shown by Bode[1] that an amplifier containing coupling networks cannot have a phase shift less than an amount which can be specified for a "minimum-phase-shift" network. There is a definite relationship between the amplitude-vs.-frequency response and the phase shift at any given frequency for such a minimum-phase-shift network. To a good approximation, the phase shift in radians at a given frequency is given by

$$\phi = \frac{\pi a}{12},$$

where a is the rate of change of attenuation in decibels per octave of frequency.

For the stabilization circuit it is necessary, for greatest effect, that the output voltage from the amplifier have the inverse phase to that impressed upon the control element of the oscillator. To avoid singing, the voltage gain from the control-element terminals to the output terminals of the amplifier must fall to less than unity in the region of the high-frequency cutoff before a phase shift of π radians occurs. Thus the rate of change of attenuation with frequency cannot be allowed to be greater than 12 db per octave at frequencies below the frequency of unity gain. In the circuits to be described, this has been obtained by the use of relatively wide passbands throughout the circuits except at one point. The high-frequency cutoff is obtained by the use of an RC-circuit of fairly long time constant at the control element of the oscillator so that the rate of change of attenuation with frequency is less than 6 db per octave for most of the cutoff region.

It is probable that considerable improvement in the amount of gain which can be used and in the bandwidth over which it is effective could be obtained by a more elaborate application of the negative-feedback theory. Careful measurements of the phase-shift-vs.-frequency characteristics of the systems have not been made. Great emphasis should be placed upon the design of the amplifiers and associated circuits from the viewpoint of phase characteristics. A cutoff network based upon these characteristics should be designed. One difference between this type of negative-feedback device and the ordinary amplifier should be pointed out. For the negative-feedback device, it is not necessary that the feedback factor remain constant within the band in which stabilization is desired. Only when the phase shift exceeds $\pi/2$ is the stabilization

[1] H. W. Bode, "Relations Between Attenuation and Phase in Feedback Amplifier Design." *Bell Syst. Techn. J.*, 19, 421–454 (July, 1940).

effect lost completely. Since the major components of frequency modulation of the oscillator occur at the power-supply frequency and its first few harmonics, the stabilization system requires the highest gain at these frequencies.

The stabilization factor may be defined as follows. If, when the stabilization system is disconnected, the oscillator makes a frequency shift $d\nu_0$, and connection of the stabilizing circuit reduces the shift to $d\nu$, the stabilization factor for the system is

$$\frac{d\nu_0}{d\nu} = S. \tag{4}$$

This may be expressed in terms of quantities dependent on the major parts of the system. The frequency change $d\nu$ produces a change in output voltage from the amplifier of $A\,d\nu$, where A is the output-voltage change per unit frequency change and is dependent upon the gain of the amplifier, the characteristics of the cavity and associated microwave circuit, and the r-f input power to the microwave circuit. This voltage must produce a frequency change counteracting $d\nu_0$ and equal to $Af\,d\nu$, where f is the frequency change of the oscillator per unit change of applied voltage. Thus

$$\begin{aligned} d\nu &= d\nu_0 - Af\,d\nu \\ S &= \frac{d\nu_0}{d\nu} = 1 + Af \end{aligned} \tag{5}$$

The quantity f cannot be defined for the oscillator tube alone since the presence of a resonant cavity as a part of the load circuit of the oscillator can increase or decrease the value of f, depending upon the line length between the oscillator and the cavity. In Vol. 16, Sec. 4·8 it is shown that the presence of the cavity may produce frequency discontinuities in the oscillator output voltage unless a certain precaution is taken to restrict the rate of change of susceptance of the oscillator load. If the rate of change of susceptance is made just less than the limiting value, however, the rate of change of susceptance with frequency for the entire oscillator circuit, including its own cavity, becomes almost zero so that the quantity f is almost infinite. For a line length between the cavity and the oscillator which differs by a quarter wavelength from that showing the greatest tendency to produce discontinuities, the quantity f has only one-half the value that it has for the tube operated into a nonresonant load circuit. With a given amplifier, and a given coupling between the oscillator and the cavity circuit, the stabilization factor can vary with the cavity-to-oscillator line length, and thus with frequency, by a considerable factor. Hence, an amplifier gain or cavity coupling which satisfies the stability conditions for the negative-feedback device at one frequency may not at another. The best absolute stability

results with a cavity-to-oscillator line length which decreases the quantity f at the resonance frequency of the cavity, since the cavity coupling and amplifier gain can be increased to give the maximum electronic-stabilization factor compatible with the negative-feedback stability condition. Some stabilization of frequency, in addition to the electronic stabilization, is gained directly from the reaction of the high-Q cavity on the oscillator. For the line length giving discontinuities with the smallest coupling, on the other hand, the same electronic-stabilization factor can be obtained but the oscillator is made very much more unstable by the direct reaction of the cavity. These considerations are important only for oscillators having small output power and for which it is desirable to use as much coupling to the cavity as possible. For oscillators delivering 0.1 watt or more, sufficient decoupling could be used between the cavity and the oscillator so that the cavity need have very little influence on the electronic tuning or on the fundamental frequency stability of the tube.

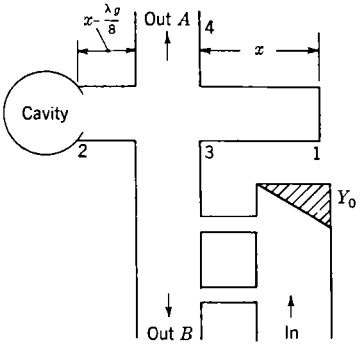

FIG. 2·30.—Microwave frequency discriminator.

2·15. The Microwave Discriminator.—One of the two stabilization circuits developed uses a circuit which is the microwave equivalent of the frequency discriminator used at low frequencies. A circuit with which a microwave frequency discriminator can be realized is shown in Fig. 2·30. This circuit uses a magic T as a bridge to compare the reflection of a cavity with that of a short-circuited line one-eighth wavelength long. A wave directed toward the junction of the T is applied by a directional coupler into arm 3 (H-plane arm) of the magic T. This excites waves in arms 1 and 2 of the T traveling outward from the junction. At frequencies far removed from the resonant frequency of the cavity, the cavity reflects almost exactly as though it were a short circuit in the plane of the coupling iris. At these frequencies, therefore, the two reflected waves in arms 1 and 2 return to the junction $\pi/2$ radians out of phase and excite waves of equal amplitude traveling outward in arms 3 and 4. Reflectionless detectors terminating these arms and having equal sensitivities would give equal output voltages. The difference between their output voltages would thus be zero.

At the resonant frequency of the cavity, the cavity admittance is a pure conductance, in the plane of the iris. Any wave reflected by the cavity at this frequency combines with the wave reflected from the short

circuit on the opposite arm of the T in such a way that waves of equal amplitude travel out of arms 3 and 4. The difference in detector output voltages is zero, although the output voltage for a single detector is different from the output voltage for frequencies far removed from resonance. For frequencies slightly removed from resonance, the reflection by the cavity is advanced or retarded in phase since the cavity admittance contains a capacitive or an inductive susceptance in addition to the conductance. On one side of resonance the detector on arm 4 receives increased power and the detector on arm 3 receives decreased power so that the difference in their output voltages is negative. For a frequency on the other side of resonance, the reverse is true and the difference in detector output voltage is positive. It is apparent that a curve of this difference voltage as a function of frequency must resemble the curves that are characteristic of the low-frequency discriminator circuit.

An analytical expression for the difference in powers incident upon the detectors on arms 3 and 4 may be derived with the aid of the admittance equations characteristic of the magic T. These are

$$\begin{aligned} i_1 &= \frac{\sqrt{2}}{2} j(e_3 + e_4) Y_0 \\ i_2 &= \frac{\sqrt{2}}{2} j(e_3 - e_4) Y_0 \\ i_3 &= \frac{\sqrt{2}}{2} j(e_1 + e_2) Y_0 \\ i_4 &= \frac{\sqrt{2}}{2} j(e_1 - e_2) Y_0, \end{aligned} \tag{6}$$

where i_1, i_2, i_3, and i_4 are the currents flowing into the upper terminals of terminal pairs 1, 2, 3, and 4 of an equivalent four-terminal-pair network, and e_1, e_2, e_3, and e_4 are the voltages across these respective terminal pairs. Using these equations, an expression for the power delivered to a load of admittance Y_4 on arm 4 from a generator of admittance Y_3 on arm 3 can be computed to be

$$P_4 = 4P_0 g_3 g_4 \left| \frac{Y_1 - Y_2}{(1 + Y_1 Y_4)(1 + Y_2 Y_3) + (1 + Y_1 Y_3)(1 + Y_2 Y_4)} \right|^2 \tag{7}$$

where Y_1 and Y_2 are the admittances terminating arms 1 and 2 respectively, g_3 and g_4 are the real parts of Y_3 and Y_4 respectively, P_0 is the power available from the generator connected to arm 3, and all admittances are expressed in units of Y_0.

For the discriminator circuit with matched detectors,

$$\begin{aligned} Y_3 &= Y_4 = 1 \\ Y_1 &= -j \end{aligned}$$

and

$$Y_2 = \frac{\delta_0}{\delta_1} + j\frac{2\Delta\nu}{\delta_1}, \tag{8}$$

where δ_0 and δ_1 are the reciprocals of the unloaded Q of the cavity and of the Q of the input circuit of the cavity with a matched waveguide generator, respectively; $\Delta\nu$ is $(\nu - \nu_0)/\nu_0$, the fractional difference in frequency from ν_0, the resonant frequency of the cavity. Using these in Eq. (7),

$$\frac{P_4}{P_0} = \frac{1}{2}\frac{1 + (\alpha + a)^2}{(\alpha + 1)^2 + a^2}, \tag{9}$$

where α is used for δ_1/δ_0 and a for $2\Delta\nu/\delta_0$. In an analogous manner, the power reflected back through arm 3 to the detector is

$$\frac{P_3}{P_0} = \frac{1}{2}\frac{1 + (\alpha - a)^2}{(\alpha + 1)^2 + a^2}. \tag{10}$$

If the detectors on both arms are square-law detectors (give output voltage proportional to the incident power) the difference between the output voltages is proportional to

$$\frac{P_4 - P_3}{P_0} = \frac{2\alpha a}{(\alpha + 1)^2 + a^2}. \tag{11}$$

Curves of this function, plotted against a for each of several values of α from 0.5 to 10, are given in Fig. 2·31. It is apparent that the maximum rate of change of output voltage with frequency for a given input power and unloaded Q occurs for α equal to unity. The maximum and minimum output voltages occur at a equal to $\pm(\alpha + 1)$ respectively, or at $\nu = \nu_0 \pm \nu_0/2Q_L$, where Q_L is the loaded Q of the cavity. The slope at the crossover point is

$$\left[\frac{d}{da}\left(\frac{P_4 - P_3}{P_0}\right)\right]_{a=0} = \frac{2\alpha}{(\alpha + 1)^2}.$$

If the detectors have a sensitivity of b volts per incident watt, the rate of change of output voltage with frequency is

$$\frac{dv}{d\nu} = \frac{4b\alpha Q_0 P_0}{(\alpha + 1)^2 \nu_0}.$$

In the 9000-Mc/sec region, wavemeter cavities have a Q_0 of 25,000, and for α equal to unity, b equal 1 volt/mw (1N23 crystal),

$$\frac{dv}{d\nu} = 2.78P_0 \qquad \text{volts per Mc/sec.}$$

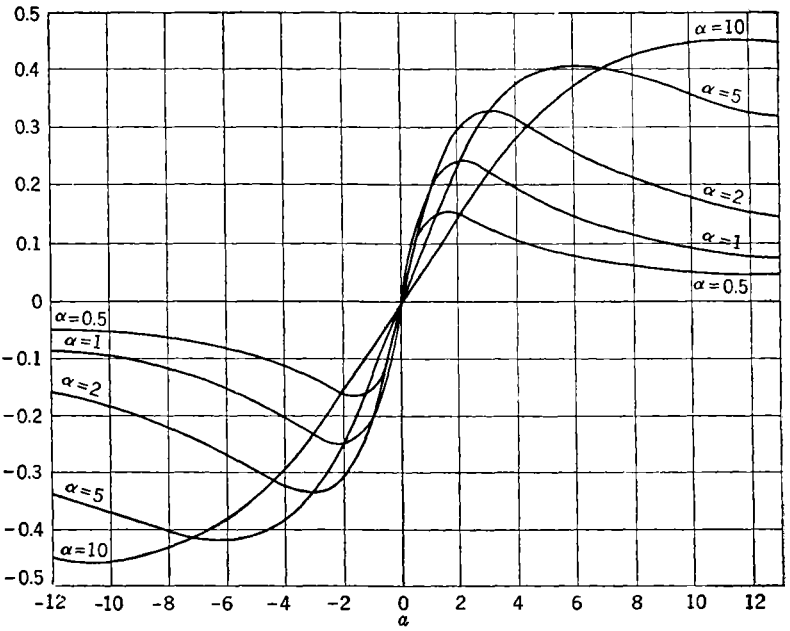

FIG. 2·31.—Output voltage vs. frequency for various cavity-coupling factors of a balanced magic-T discriminator.

With oscillator tubes like the 2K25 it can be shown (Vol. 16, Sec. 4·11) that about 18 db of attenuation are required between such a cavity and the oscillator, to avoid discontinuities. A rate of change of output voltage of 1.4 volts per Mc/sec can thus be obtained from a tube giving 30 mw of output power.

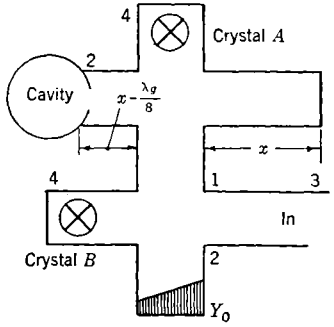

FIG. 2·32.—Microwave discriminator employing two magic T's.

Another form of the microwave discriminator is shown in Fig. 2·32. Here a second magic T is used, instead of the directional coupler, to isolate the input signal from the detector which receives the power reflected from the discriminator T. The input power is applied to arm 3. Arm 1 drives the discriminator T, arranged as before, and arm 2 is terminated with a matched dummy load. The detector for reflected power on arm 4 receives only half the reflected power. To get the balanced-discriminator action, the output voltage or the input power of

the detector on arm 4 of the discriminator T must be attenuated to half value. Since detectors of equal sensitivity are not likely to be found without selection of crystals, this attenuation, if made adjustable, affords a means of balancing the discriminator.

2·16. The D-c Stabilizer.—Frequency stabilization has been achieved with the microwave discriminators of Figs. 2·30 and 2·32, by the use of a d-c amplifier shown in Fig. 2·33, in the circuit shown in the block diagram of Fig. 2·34. The amplifier contains two push-pull stages, direct-coupled and with large cathode degeneration provided by the common cathode

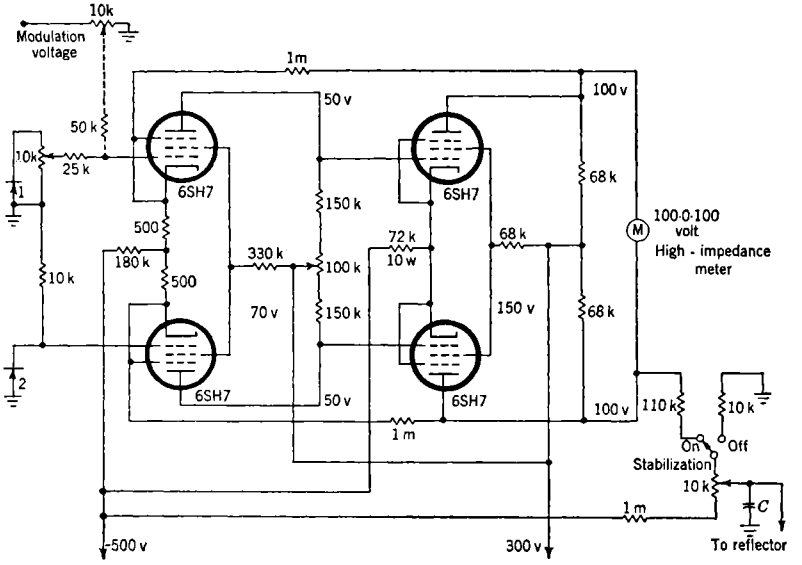

FIG. 2·33.—D-c amplifier for electronic frequency stabilizer.

resistors connected to a large negative voltage. Negative feedback from the plates of the output stage to the cathodes of the input stage establishes the voltage gain from input grids to output plates at 2000. Since the reflector of the 2K25 reflex oscillator to which the stabilization is applied must operate in the neighborhood of -100 volts (with the cathode at ground potential), and since it represents an unbalanced line circuit, the gain from the discriminator output voltage to the reflector is about 600. The stabilization factor is also 600 since the oscillator changes frequency by about 1 Mc/sec per volt on the reflector, and the discriminator output voltage changes at the rate of about 1 volt per Mc/sec with an amount of attenuation sufficient to avoid frequency discontinuities. Stability as a negative-feedback system is obtained by the large capacitance from the reflector to ground, which narrows the pass

band from that of the amplifier alone. Although this circuit begins to attenuate at a few hundred cycles per second, some stabilization of the oscillator frequency against frequency modulation at frequencies as high as 50 kc/sec is obtained since the attenuation increases at a rate less than 6 db per octave.

One very useful feature of the stabilization system is that the oscillator may be frequency-modulated at any frequency for which stabilization exists with stabilization acting throughout the cycle of the frequency-modulating signal. This is done by superimposing the modulating voltage on the output voltage of the frequency discriminator,

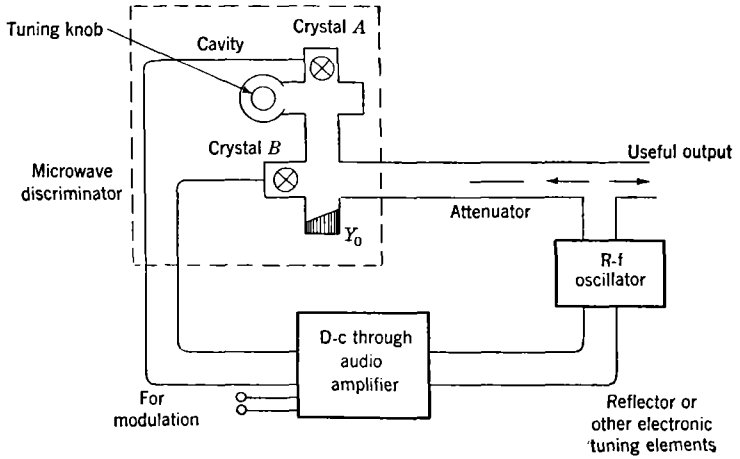

FIG. 2·34.—Block diagram of d-c stabilizer.

as indicated by the circuit in broken lines in Fig. 2·33. A change in the input voltage to the amplifier from this source produces a change in frequency only slightly less than sufficient to produce a discriminator-output change exactly counteracting the added voltage. Thus the circuit may be considered as a degenerative frequency-modulation device. The deviation is almost independent of the amplifier gain, the frequency-vs.-voltage characteristics of the tube, and the frequency of the modulating signal so long as it is within the band for which a reasonable stabilization factor exists. With the circuits described, a deviation almost independent of the frequency of the modulating signal is obtained for modulation frequencies from 0 to 50 kc/sec. The linearity of the modulation is the same as that of the discriminator characteristic and is quite good for deviations up to $\pm(\nu_0/4)Q_L$.

If the oscillator is locked through the stabilization circuit to the cavity, tuning of the cavity results in corresponding frequency changes

in the oscillator within the range of available electronic tuning. With control through the reflector this gives about 60-Mc/sec range of single-knob tuning of the system. For a wider range than this, a thermally-tuned tube may be used with the control voltage applied, at an appropriate d-c level, to the thermal-tuning element. With a 2K45 tube, for instance, the amplifier output voltage may be applied to the grid of the tuning triode as shown in Fig. 2·35. Fortunately, the reflector and the triode grid give a frequency change in the same direction as the change in their supply voltages and, therefore, the two control voltages may be derived from this same bleeder circuit. Diodes that limit the range of the voltages that can be applied to the triode grid are included for the protection of the tube and for the prevention of "motor boating" in and out of oscillation. Since the tuning rate per volt at the triode

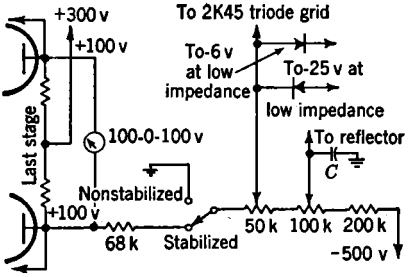

FIG. 2·35.—Supplementary circuit for wide-range single-knob tuning.

grid is very much higher than at the reflector, the frequency-stabilization factor is very large at very low frequencies. No singing occurs, however, because the time constant of the triode tuner is very long and thus the reflector control alone acts through the audio-frequency region and above. With this circuit a stabilized oscillator, tunable by a single knob over a 12 per cent range, can be obtained. The major difficulty encountered with this form of the system results from the change in electrical line length between the cavity and the oscillator with frequency. Since the rate of change of frequency with reflector voltage is influenced by the cavity and this line length, the gain of the system changes with frequency and an attenuation giving satisfactory operation at one frequency may give singing of the feedback circuit at another. For oscillators of higher power than the 2K45 this trouble would not be present.

2·17. The I-f Stabilization System.—Another circuit has been developed in order to circumvent the need for a d-c amplifier, which at best is troublesome, and to eliminate the use of crystals as detectors, in which application they have poor noise figures. A block diagram of this system

is shown in Fig. 2·36. The output signal of the microwave circuit is an i-f voltage which is dependent in sign on, and proportional in amplitude to, the imaginary part of the reflection coefficient of the high-Q cavity. After i-f amplification the output voltage is mixed with an i-f voltage of the same frequency in a lock-in mixer, and there results a d-c voltage that has the characteristics of a discriminator output voltage. This voltage can therefore be used as a control voltage for frequency stabilization.

Crystal B receives a signal containing one-half the input power to the T, at the frequency of the oscillator, together with two sideband signals, derived from modulation by crystal A of part of the wave incident

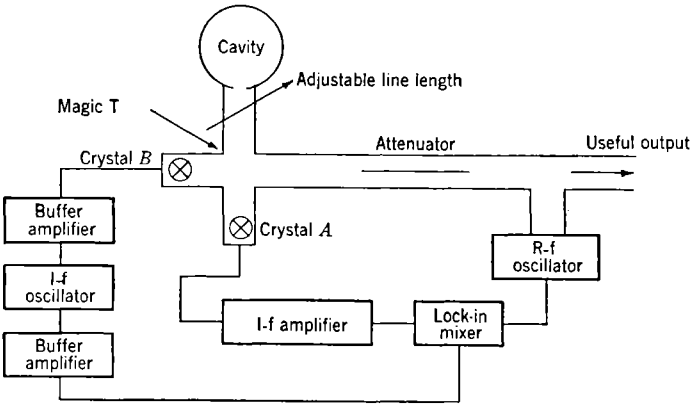

FIG. 2·36.—Block diagram of i-f stabilizer.

on crystal A reflected by the cavity. No carrier-frequency wave is reflected by crystal A since it is matched to the waveguide in the absence of an i-f voltage across its i-f terminals. Crystal B is so mounted that none of the oscillator signal incident upon it is reflected. Thus the total voltage arriving at crystal B is

$$E_B = \frac{\sqrt{2}}{2} E_0 \sin \omega_1 t + \frac{\sqrt{2}\, E_0 |\Gamma_c| m}{8} \{\sin [(\omega_1 + \omega_2)t + \delta] + \sin [(\omega_1 - \omega_2)t + \delta]\},$$

where E_0 is the voltage incident at the T, ω_1 is 2π times the oscillator frequency, ω_2 is 2π times the intermediate frequency, $|\Gamma_c|$ is the absolute value of the reflection coefficient of the cavity, m is the modulation coefficient for crystal A, and δ is a relative phase factor which depends upon the line lengths between the T and the cavity and the T and the modulator crystal, the phase characteristics of the T, and the phase of the reflection

coefficient of the cavity. The numerical factors are caused by the fact that power is divided by two for each transit through the T.

The output voltage from crystal B will contain terms found in the envelope of the superposition of these waves incident upon it. The square of the envelope E_t is

$$E_t^2 = \frac{E_0^2}{2}\left\{1 + \frac{|\Gamma_c|^2 m^2}{8} + \frac{|\Gamma_c| m}{2}\cos(\omega_2 t + \delta) + \frac{|\Gamma_c| m}{2}\cos(\omega_2 t - \delta) + \frac{|\Gamma_c|^2 m^2}{8}\cos 2\omega_2 t\right\}. \quad (12)$$

The terms in $|\Gamma_c|^2 m^2$ will be small in the region of resonance of the cavity since $|\Gamma_c|$ will be small and m must always be less than unity. The second harmonic does not pass through the amplifier so this term may be dropped. To this approximation the envelope is

$$E_t \approx \frac{E_0\sqrt{2}}{2}\{1 + |\Gamma_c| m \cos(\delta)\cos(\omega_2 t)\}^{1/2}. \quad (13)$$

For $|\Gamma_c|$ small compared to unity, a further approximation may be made by expanding the square root in a series and neglecting terms higher than the first power of $|\Gamma_c| m$. In this way the i-f voltage may be shown to be proportional to

$$E \approx \frac{E_0\sqrt{2}\,|\Gamma_c| m}{4}\cos(\delta)\cos(\omega_2 t). \quad (14)$$

Now suppose that the variable line length between the cavity and the T-junction is such that δ is an odd multiple of $\pi/2$ for a pure real reflection coefficient at the cavity. The product $|\Gamma_c| \cos\delta$ is the imaginary part of the reflection coefficient at the cavity and is

$$|\Gamma_c| \cos\delta = \operatorname{Im}\frac{Y_0 - Y_c}{Y_0 + Y_c}. \quad (15)$$

Using Eq. (8), $\alpha = \delta_1/\delta_0$, and $a = 2\Delta\nu/\delta_0$, this becomes

$$|\Gamma_c| \cos\delta = \frac{-2a\alpha}{(\alpha + 1)^2 + a^2}. \quad (16)$$

This is identical with the expression for the output voltage of the d-c discriminator. The output voltage of the lock-in mixer thus produces the desired type of control voltage. As in the case of the discriminator, the maximum rate of change of output voltage with frequency is obtained with α equal to unity. For this condition, $|\Gamma_c|$ goes to zero at the resonant frequency of the cavity, and therefore, in the region of resonance, the approximations neglecting terms in powers higher than the first of $|\Gamma_c|$

are valid. At the cavity resonance, the input voltage to the i-f amplifier goes to zero; just off resonance, this voltage is different from zero and has opposite phases on either side of resonance. The sense can be reversed by changing the cavity-to-T line length by a quarter wavelength; thus δ is changed by π radians. The sign of the error voltage produced by the lock-in mixer can be corrected to give stabilization.

The zero i-f signal at resonance is an important feature of this frequency-stabilization system. Zero is obtained even though the cavity reflection coefficient is not exactly zero at resonance. This fact permits the use of a large i-f gain without danger of overloading or of limiting in the amplifier or lock-in mixer. The phase of the reference voltage in the lock-in mixer is not of great importance since the i-f signal has either of two distinct phases, π radians different from each other. Thus the phase of the reference voltage that determines the sense of the error voltage affects only the gain of the mixer and does not affect the crossover frequency. In practice, it is found that neither of these things is exactly true. The gain can be made high enough so that a signal does exist at the resonant frequency of the cavity. This is probably caused by the slightly different efficiencies of the r-f circuit at the two sideband frequencies. If, for instance, the two sidebands are of slightly different amplitudes, the waves incident at the mixer crystal may be described by

$$E_B = \frac{\sqrt{2}}{2} E_0 \sin \omega_1 t + \frac{\sqrt{2}}{8} E_0 |\Gamma_c| m_1 \sin [(\omega_1 + \omega_2)t + \delta] + \frac{\sqrt{2}}{8} E_0 |\Gamma_c| m_2 \sin [(\omega_1 - \omega_2)t + \delta].$$

Using this equation, the equation corresponding to Eq. (13) can be shown to be

$$E_t \approx \frac{\sqrt{2}}{2} E_0 \left\{ 1 + |\Gamma_c| \left(\frac{m_1 + m_2}{2} \right) \cos \delta \cos (\omega_2 t) + |\Gamma_c| \left(\frac{m_1 - m_2}{2} \right) \sin \delta \sin (\omega_2 t) \right\}^{\frac{1}{2}}.$$

Thus there may be a signal with $\cos \delta$ equal to zero, but this signal is $\pi/2$ radians out of phase with the error-voltage signal. If the phase of the reference voltage in the lock-in mixer is adjusted to give exactly maximum error voltage, this extraneous signal produces zero voltage at the output terminals of the lock-in mixer. It can however limit the usable i-f gain by overloading the i-f amplifier. The closer $|\Gamma_c|$ is to zero at resonance, the smaller this extraneous signal will be.

The sideband signals arriving at the mixer crystal can be made to be zero at the cavity resonance even though $|\Gamma_c|$ is not zero. Since the

magic T is a bridge circuit, the modulator crystal receives a signal only when the admittance of the cavity arm is different from the admittance at a symmetrically chosen point in the mixer arm. For any α, the mixer could be tuned to balance the bridge at the resonant frequency of the cavity; no signal would be sent to the modulator crystal and no sideband signals would be produced.

2·18. Electronic Circuits for I-f Stabilization.—The i-f amplifier which has been used in several experimental stabilization systems has four stages of 6AK5 tubes in a stagger-tuned circuit having a pass band of 6 Mc/sec between half-power points centered at 30 Mc/sec. The 6AS6 tube, with the i-f amplifier output voltage applied to its control grid and the reference signal applied to its suppressor grid, is used as a lock-in mixer. The reference signal drives the suppressor grid beyond its linear region to such an extent that a change of several per cent in the plate current occurs upon application of the reference signal. The cathode of the 6AS6 is operated with a self-biasing resistor connected to −300 volts. Thus the plate voltage of about −150 volts may be used directly as the reflector voltage for a 2K25. Since the lock-in mixer can be operated at any d-c level, with appropriate bypass condensers, this system is considerably more flexible than the d-c system. It has been applied to tubes having reflector voltages of −1800 volts simply by providing high-voltage condensers.

The oscillator is a 6AK5 electron-coupled circuit operating at 30 Mc/sec and is contained, along with two 6AK5 buffer amplifiers, one for the modulator crystal and one for the lock-in mixer, in a well-shielded box. A filter circuit is used on the filament and plate-supply leads to minimize unwanted leakage. This filter circuit is made from a brass tube with feed-through disk condensers in three baffle plates and series i-f chokes between them.

To assist the alignment procedure, several metering circuits are used. The modulator-crystal rectified current and that of the mixer crystal can each be metered. A crystal detector is included in the i-f amplifier to allow observation of the i-f signal independent of phase, and a voltmeter is used to indicate the output voltage of the lock-in mixer. An independent reflector-voltage circuit is provided with a selector switch to allow the reflector to be connected either to this circuit or to the lock-in mixer plate. The adjustment of the length of line between the cavity and the magic T can be made by observation of the plate voltage of the lock-in mixer with the cavity tuned far from the r-f oscillator frequency. With moderate i-f amplifier gain the plate voltage of the lock-in mixer, for the correct line length, should be that obtained with zero amplifier gain. A deflection corresponding to the discriminator output is observed when the cavity is tuned through the oscillator frequency. The crossover

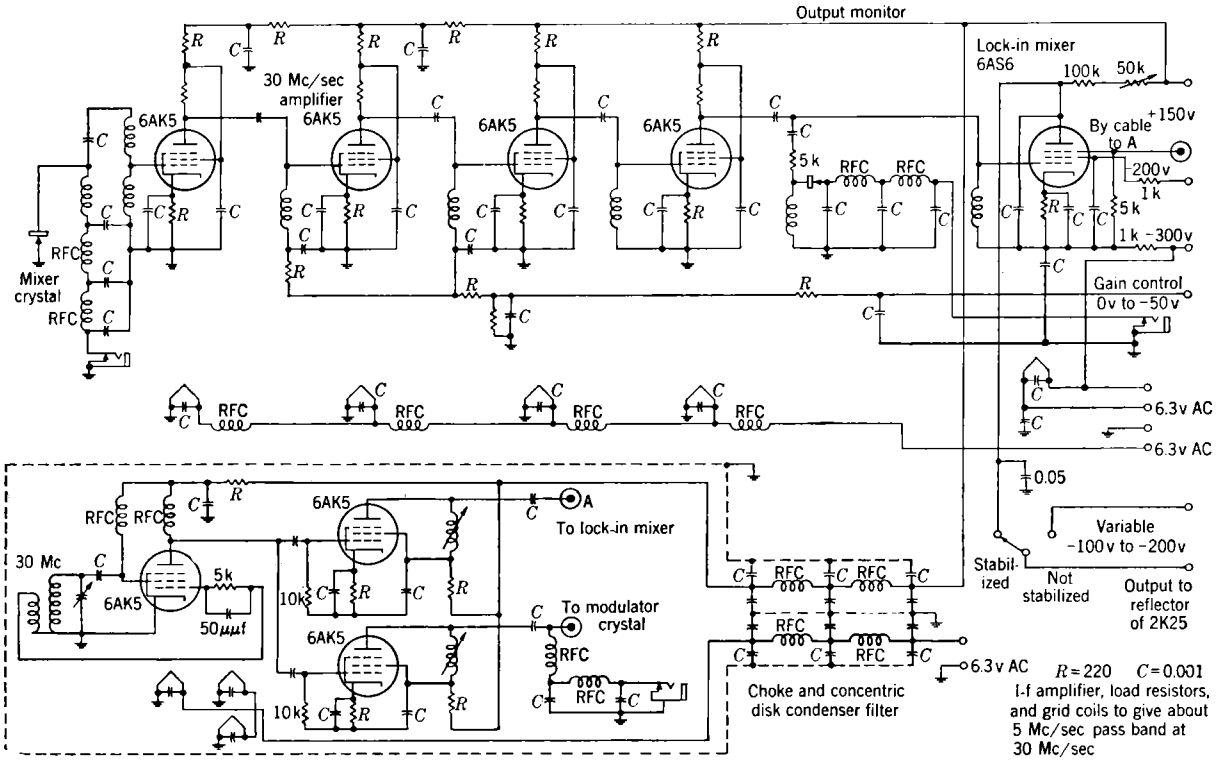

FIG. 2·37.—Circuit diagram of i-f stabilizer.

voltage can be made to equal the desired reflector voltage by adjustment of the plate load resistance of the lock-in mixer. The system can be locked by throwing the switch that connects the reflector to the lock-in mixer plate with the cavity set near the oscillator frequency. The amplifier gain can be increased as much as is compatible with the phase shift of the feedback loop. The circuits of these parts of the system are shown in Fig. 2·37.

It is also possible to produce frequency modulation with this system. One way in which this can be done is to apply the frequency-modulation signal as a bias voltage on the mixer crystal. If, in the absence of this voltage, this crystal is matched for the direct signal from the oscillator, it reflects in a manner corresponding to the instantaneous bias voltage. The reflected wave returns, in part, to the modulator crystal and becomes converted to sideband signals. A portion of these will return to the mixer crystal and change the i-f component in the envelope of signals arriving at the mixer crystal. This change will result in a shift in frequency by the amount required to make the sideband signals, developed from the wave reflected from the cavity, almost compensate for their presence. The largest deviation for a given amplitude of modulating signal will result if the line length from mixer crystal to modulator crystal is chosen to make the value of sin δ for these sideband signals equal to unity. The frequency deviation obtained is independent of the amplifier gain, of the reflector-voltage characteristics of the r-f oscillator, and of the amplitude and frequency of the i-f oscillator. To the extent that the reflection-coefficient change per unit bias-voltage change of the mixer crystal is independent of the incident power, the deviation is independent of the r-f oscillator output power. A deviation independent of the modulating frequency is obtained for all frequencies for which the stabilization factor is large compared to unity. The linearity of the modulation is dependent upon the change of the mixer-crystal impedance with bias voltage, a characteristic which has not been measured. An interesting property of this frequency modulation is that it could be used to measure a small change in the Q of the cavity. If, for instance, a medium of small loss were introduced into the cavity, a change in the frequency deviation resulting from a given modulation voltage could be observed by measurement of the output voltage of a conventional frequency-modulation receiver, adapted to receive the oscillator frequency.

2·19. Results and Limitations of the Stabilization Systems.—Most tests of these stabilization techniques have been made in the region of 9000 Mc/sec with 2K25 oscillator tubes. The tests were made by observation of the audio beat note between two identical systems. To avoid interaction of the two oscillators the beat note used was actually

in the region of 30 to 40 Mc/sec and was converted to audio frequency by the beat-frequency oscillator of a communications receiver.

With the d-c systems, a residual relative frequency deviation of plus and minus about 100 cps was observed under the best conditions. This deviation occurred at the power-supply frequency (60 cps) and harmonics of it and was probably caused by ripple in the amplifier voltages and by pickup of stray fields. In addition, there were slow changes, occurring over periods of a few seconds, of as much as 1 kc/sec, although the two oscillators remained within the audio-frequency spectrum of each other for many hours. No measurement of the long-time stability, independent of the cavity temperature, could be made since the best cavities available had a temperature coefficient of frequency of about 50 kc/sec per degree C.

The i-f systems gave an audio beat note having less than 50 cps frequency modulation at the power-supply frequency. No periodic changes of the sort observed with the d-c systems were observed and the only long-time drifts found could be attributed to the cavities. In both systems, mechanical stress on the r-f circuit parts would produce frequency changes, and heat transfer to the cavity from the hand produced a very perceptible frequency change. It is of interest to note that a motion of the end plate of one of the cavities of 10 angstroms would produce a frequency shift of 120 cps. If a device to measure very small dimensions were desired, a cavity having much greater sensitivity than this could be designed.

A limit is set, on the reduction in the width of the frequency spectrum of an oscillator which can be achieved with these systems, by the presence of noise in the output power of the crystal detectors and mixer and in the input power of the amplifiers. Increasing the amplifier gain beyond the point at which frequency deviations from other sources are made less than those resulting from this noise voltage would not produce an oscillator signal of more nearly constant frequency. In d-c systems, the noise voltage is very much larger than Johnson noise because the crystals, as detectors at a level of power of the order of a milliwatt, give a large noise-voltage contribution in the audio region and because the d-c amplifier is subject to drifts caused by cathode-emission changes. Measurements at the University of Pennsylvania have shown that the noise temperature of a crystal detector varies as $1/f$, where f is the audio frequency, and becomes very large at low frequency. This cannot hold to zero frequency, but it is probable that the observed frequency deviations occurring over periods of a few seconds were caused by this noise voltage. Since this voltage is so large, it is felt to be the limiting factor and no attempt has been made to use special d-c amplifier tubes of low drift.

The effect of the noise voltage is analogous to that of the frequency-

modulation voltage, and to account for a 1-kc/sec shift in frequency, with a discriminator output slope of 1 volt per Mc/sec, a noise voltage of 1 mv would be required. This is not in disagreement with the measurements at low audio frequencies. Special selection of the crystals might result in reduction of the frequency instability from this cause by a considerable factor.

In the i-f stabilization systems the situation is considerably better. No very-low-frequency drifts exist in the circuit ahead of the lock-in mixer. If the gain of the amplifier is large enough to make the amplified noise from the amplifier larger than a millivolt or so, it is improbable that cathode-emission drift would have any effect. The frequency deviations resulting from noise in the crystal and in the i-f amplifier may be calculated by replacing all of this noise by an equivalent r-f noise-voltage source and a perfectly noise-free frequency converter and i-f amplifier. The open-circuit mean-square noise voltage of this equivalent noise-voltage generator would be

$$\overline{E^2} = 4kTNRB, \tag{17}$$

where k is Boltzmann's constant, T is the absolute temperature, N is the over-all noise figure of the converter and i-f amplifier combination, R is an equivalent resistance for the waveguide characteristic impedance, and B is the equivalent noise bandwidth of the feedback system. This noise bandwidth is approximately the bandwidth for which the stabilization factor is greater than unity, since the lock-in mixer is operated as a linear mixer.

The presence of the noise voltage causes a frequency change developing an i-f signal voltage continuously compensating for the noise voltage. Therefore the equivalent open-circuit r-f signal-voltage generator, which depends upon frequency, is required. This can be found to be

$$E_s = \frac{2\sqrt{2\,E_0 m Q_0 \alpha}}{\nu_0(1+\alpha)^2}\,d\nu \tag{18}$$

from Eq. (14) and from the derivative of Eq. (11) with respect to frequency. Setting Eq. (17) equal to Eq. (18) and substituting for R

$$R = \frac{E_0^2}{P_0},$$

where P_0 is the input power to the magic T, the root-mean-square frequency deviation resulting from noise can be found to be

$$(\overline{d\nu_n^2})^{1/2} = \left(\frac{kTNB}{2P_0}\right)^{1/2} \frac{(1+\alpha)^2\nu_0}{\alpha m Q_0}. \tag{19}$$

In the systems described, N is about 10, B about 10 kc/sec, P_0 one milliwatt, α equal to unity, m almost unity. Q_0 is 25,000 and ν_0, 9000 Mc/sec. Putting these into Eq. (19), with kT equal to 4×10^{-21} joules, the root-mean-square frequency deviation is found to be

$$(\overline{d\nu_n^2})^{1/2} = 6.5 \quad \text{cps.}$$

Since this is somewhat less than the deviations observed, it is probable that improvement in the stabilization could be made if greater care were taken to remove sources of modulation at the power-supply frequency. Since the impedance of the mixer crystal is somewhat dependent upon the local-oscillator signal level, some frequency modulation might result from amplitude variation of the oscillator output voltage through the mechanism discussed for producing frequency modulation. The ripple voltage in the power supplies used on these systems was about 5 mv per hundred volts of d-c; 60-cycle heater voltages were used throughout.

CHAPTER 3

MICROWAVE POWER MEASUREMENTS

By R. N. Griesheimer

3·1. Introduction.—The measurement of power is one of the few fundamental measurements that can be made in the microwave region. In the much lower frequency regions, the audio-frequency region, for example, it is customary to measure voltage or current. In the i-f and r-f regions both voltage and power measurements are common, although the communications industry has shown a preference for power measurement on the basis that power is a more convenient and a more meaningful quantity to measure than voltage. The convenience is inherent in the fact that the specification of power is independent of the characteristic impedance of the transmission line, provided that the line is terminated by a matched impedance load. In contrast, a statement of voltage is meaningless without an accompanying specification of the line impedance. Power is considered a more meaningful quantity because the various line components—relays for example—are actuated by power and not by voltage. However, in the microwave region there is little or no basis for argument. The preference must be for power, because of the fact that the wavelengths are comparable to line dimensions and to the dimensions of the detectors that can be used for voltage or power measurement. Thus, any loop that might be used as a means for deriving a "loop-induced voltage" will, for adequate sensitivity, have a physical size comparable to the wavelength and the induced voltage gradient will therefore vary along the loop. Under such circumstances it is not possible to make an accurate voltage determination, but an accurate power measurement is still possible. In any attempt to measure voltage, an additional obstacle would be encountered—the difficulty of defining "voltage" for TM-modes in rectangular waveguides, where the curl component of the total electromagnetic field vector does not vanish anywhere across the waveguide, and voltage is therefore not equal to the simple line integral, $\int \mathbf{E} \cdot d\mathbf{s}$.

The techniques and equipment used for power measurement vary considerably with the level of power to be measured. For this reason it is convenient to divide the scale of average power into three arbitrarily defined regions: high-, medium-, and low-level power. Powers greater than one watt will be classed as high-level power; the range from 10 mw

to 1 watt will be referred to as medium-level power; 10 mw and less will lie in the low-level range. The range of medium-level power is the smallest, and will command the least attention in this chapter. As will be discussed in subsequent sections of the chapter, calibrated attenuators, power dividers, and similar devices may be used (usually with some sacrifice in accuracy) to measure high-level power with low-level detectors.

Since microwave power is often pulsed, it becomes necessary to differentiate between *average power* and *pulse power*. Both are time-averaged values, but differ with respect to the time interval involved in the averaging. If the power is averaged over the duration of a single pulse, the average is called *pulse power*. If the power is averaged over a period of time very large compared with the duration of a single pulse and with the time interval between successive pulses, the average is known as *average power*. Thus pulse power is always greater than average power except in the limiting case of unpulsed c-w operation where they become equal to each other and to the average power per cycle of oscillation. There is no ambiguity regarding the specification of pulse length if the pulse is rectangular. If the pulse is trapezoidal, it is customary to specify the pulse length as the time interval between the "half-altitude" points on the leading and trailing sides of the trapezoid. Available power detectors permit a direct determination of average power, but pulse power must be calculated from average power, pulse length, and pulse repetition frequency, according to the relation

$$P_0 = \frac{P}{\tau n}, \tag{1}$$

where

P_0 = pulse power, in watts.
P = average power, in watts.
τ = pulse length, in sec.
n = repetition frequency, pulses/sec.

Because of its great convenience in many calculations, the *dbm* (decibels with respect to 1 mw) unit of power has been been borrowed from the communications industry. Thus, for example, 1 mw is equivalent to 0 dbm, 1 watt equals +30 dbm, 10 μw correspond to −20 dbm. This unit of power facilitates calculations of power levels at various points along a transmission line which are separated by attenuating elements. For example, if the power incident on an 18-db attenuator is +13.5 dbm, the power level at the output terminals of the attenuator is quickly calculated as −4.5 dbm. The unit dbw—meaning decibels with respect to one watt—is also used.

Microwave power measurements are usually conducted by converting the high-frequency power into heat. In low- and medium-level power measurement the thermal energy is then used to effect a resistance change or to generate a thermal emf—either quantity being mensurable according to well-known d-c or a-f techniques. In high-level power measurement it is customary to make a calorimetric measurement of the thermal energy, using either water or a gas as the calorimetric fluid. The calorimetric technique is unsuited to low-power measurement because of the difficulty of making a simple yet accurate determination of a very small temperature rise. Conversely, the resistance element or thermocouple, which is physically small enough to avoid trouble from variations in skin depth with frequency, is too small to dissipate high power without suffering burnout. Other less commonly used techniques in microwave power measurement involve the conversion of power into light, as in lamp filaments, for example, and the use of crystal and diode rectifiers.

The bolometer, a small resistive element which is capable of dissipating microwave power and using the heat developed to effect a change in its resistance, is the most commonly used type of detector in low- and medium-level power measurement. There are a number of power detectors which must be classed as bolometers. Chief among these are the barretter and the thermistor. The barretter is an appropriately mounted short length of very fine wire, usually platinum, with sufficient resistance so that it can be impedance-matched as a termination for the transmission line. It has a positive temperature coefficient of resistance, typical of metals. In contrast, the thermistor consists of a tiny bead of semiconducting material which bridges the gap between two fine, closely spaced, parallel supporting wires. Effectively all of the resistance of the thermistor is concentrated in the bead material which has a negative temperature coefficient of resistance. The thermistor bead is usually installed in a small glass capsule for ease of mounting the element as a termination in the transmission line. Specially designed lamp filaments and metalized-glass tubes have also been used effectively as bolometers. The resistance change resulting from the dissipation of microwave power in the bolometer is commonly measured by using the bolometer as one arm of a d-c or a-f Wheatstone-bridge circuit.

The barretter and the thermistor are sensitive power detectors, and are capable of measuring as little as a few microwatts of power when used in properly designed bridge circuits. The thermistor is a somewhat more flexible device in that its resistance may be varied over an extremely broad range, depending on the magnitude of the bias current used. This is often a decided advantage in the broadband impedance-matching of the detector. Further, it leads to excellent overload and burnout

characteristics. The barretter has less desirable overload and burnout characteristics, and its operating resistance is confined to a considerably smaller range. However, barretters have the advantages that they can be made more reproducible in both sensitivity and impedance, and are less sluggish (that is, have a smaller time constant) than thermistors. Other kinds of bolometers and other low-power detectors usually suffer from one or more of the following: inadequate sensitivity, change in calibration with vibration or shock, objectionable overload and burnout characteristics, impedance characteristics that make broadband impedance-matching extremely difficult, or excessive variations of sensitivity and impedance from one element to the next.

In making absolute measurements of power there are a number of precautions that must be observed with regard to the choice of detector and the construction of the transmission-line housing or mount, as it is commonly called. In low-level power measurement with bolometers it is of prime importance that the sensitivity, in ohms per milliwatt, of the bolometer be independent of frequency. In other words, a milliwatt of microwave power must effect the same resistance change in the bolometer as a milliwatt of d-c power. In the use of a bolometer in a balanced bridge, the calculation of microwave power assumes this equivalence; in fact, there is no known way of measuring absolute power with bolometers that does not rely on the equivalence of the heating effects of d-c (or a-f) and high-frequency power. It is at once obvious that this condition cannot be met unless the bolometer is sufficiently small and its resistivity sufficiently great that the high-frequency currents are forced to flow throughout the volume of the bolometer element, rather than on its surface. The temperature gradients within the volume of the bolometer element and the exchange of heat with the surroundings will then be almost the same for d-c and high-frequency power, and the heating effects of the two will be closely equivalent.

In high-power measurement with water or gas loads, the chief problem is the typical calorimetric one of minimizing the heat exchange between the calorimetric fluid and its surroundings. That is, the temperature rise caused by the dissipation of the microwave power must be measured before any appreciable amount of the heat developed is conducted or radiated from the fluid. In either high- or low-level power measurements it is essential to match the power load to the transmission line—standing-wave-ratio measurements being used to guarantee that this condition is met. It is also essential that the mount for either the bolometer or the water load be carefully constructed so as to eliminate the possibility of microwave leakage into free space, and that there be no sources of power dissipation (for example, poor contacts, rusted metal conductors) other than that in the chosen power detector.

Usually there are three phases to the problem of developing equipment for microwave power measurement: (1) the choice of a suitable detector, (2) the design of a matched-impedance transmission-line housing or mount for the detector, and (3) the design of auxiliary circuits. Each phase involves a number of considerations, the more important of which will be listed to serve as an introduction to the discussions that comprise this chapter.

In low- and medium-level power measurement the choice of a suitable detector presents an interesting problem, particularly since a wide variety of detectors are available. The more important considerations involved in the choice are (1) the sensitivity of the detector, in ohms per milliwatt, (2) the suitability for absolute, as against relative, power measurement, (3) the overload and burnout characteristics, (4) the ease with which it can be impedance-matched over a broad band, (5) the variations in sensitivity and impedance characteristics within a large quantity of the detectors, (6) the availability, (7) the time constant, and (8) the complexity of the auxiliary circuit. A compromise is invariably necessary, since no one detector leads the field in all of these respects. The most important problem in detector-mount design is that of providing satisfactory impedance matching, usually over a broad wavelength band. It is often necessary to make a compromise between the desired bandwidth and the desired maximum allowable VSWR, so that the final design of the mount is influenced by the bandwidth requirements of the specific problem and the accuracy of power measurement. Thus, narrow-band and broadband mounts are evolved which have maximum allowable VSWR values of 1.10, 1.25, or 1.50, as the need for accuracy demands. The specific application also dictates the decisions in such other matters as the desirable transmission-line size and characteristic impedance, whether the mount may be tunable or must be pretuned, the extent to which it may suffer leakage of microwave power, and its maximum allowable physical dimensions.

The design of auxiliary circuits may often represent the most serious problem of all. For reasons previously stated, bolometers are the most commonly used detectors for low- and medium-level microwave power measurement, and are almost invariably installed in bridge circuits. However, since bolometers are temperature-sensitive elements, the bridge circuits, particularly those of the direct-reading type, must be temperature-compensated. Temperature variations affect both the sensitivity and balance of the bridge circuit, and the compensating devices must deal simultaneously with both problems. As the operating temperature range becomes larger, compensation becomes more difficult to achieve. It is also necessary to consider such problems as meter overload in the event of bolometer burnout, requisite voltage stability of the d-c and a-f

bridge supplies, and limitations on the current allowable for operation of the bridge.

In high-power calorimetric measurements there is no problem corresponding to the choice of a detector for low-power measurements. Water and certain gases (for example, ammonia gas) are satisfactory for microwave applications. Moreover, the thermopiles used in conjunction with water loads require simple auxiliary electrical circuits. There is, however, the design problem of a fluid-flow system for the water load which has no counterpart in the field of low-level power measurement. Finally, the major problem in high-power measurements centers around the design of the water load itself. Not only must the water column be properly impedance-matched, but additional precautions must be taken to avoid errors that may be caused by the exchange of heat between the water and its environment.

POWER MEASUREMENTS AT LOW AND MEDIUM LEVELS

3·2. Bridge Circuits.—The Wheatstone-bridge circuits in which bolometers are used may be operated either as balanced or unbalanced (direct-reading) bridges. When operating the circuit as a balanced bridge, the basic procedure involves balancing the bridge both with and without microwave power in the bolometer. The level or magnitude of the high-frequency power is determined from the difference in bolometer bias power between the two conditions of bridge balance. Direct-reading bridges are usually calibrated by means of a balanced bridge. A properly designed direct-reading bridge is closely linear in power, and a single calibration at full-scale deflection is often sufficient. The balanced bridge has the advantage of greater accuracy, but the direct-reading bridge is more convenient to use. There are certain fundamental principles in bridge design that apply both to balanced and to direct-reading bridges, and these will be reviewed prior to a discussion of the details of specific bridge designs.

It is, first of all, necessary to differentiate between two commonly used expressions for sensitivity, one pertaining to the bolometer, and the other to the bridge circuit in which the bolometer is used. Bolometer or *detector sensitivity* is usually expressed in ohms per milliwatt, and is the slope of the static curve of d-c resistance plotted against power for the detector. It is important to remember, particularly in the case of thermistors, that detector sensitivity can vary widely depending on the bias conditions (or operating resistance) of the detector. In contrast, *bridge sensitivity* is a measure of the bridge unbalance resulting from application of high-frequency power to the bolometer. It is often expressed as microamperes of meter deflection per milliwatt of microwave power. Bridge sensitivity is a function of many quantities includ-

ing detector sensitivity. It is not necessarily true, however, that the bolometer with the highest detector sensitivity will provide the greatest bridge sensitivity in a given bridge circuit.

Figure 3·1 represents a simple, unbalanced Wheatstone bridge, the bolometer arm of which has a resistance X. It is desired to calculate the several currents indicated in the diagram. Ohm's law provides the three equations necessary to calculate the three unknowns, i_1, i_2, and i_3. Thus,

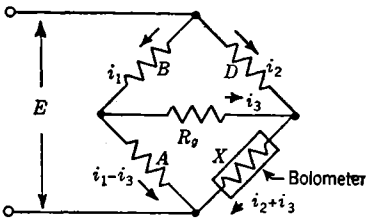

FIG. 3·1.—Diagram of unbalanced Wheatstone bridge.

$$\begin{aligned} Bi_1 + R_g i_3 &= Di_2, \\ A(i_1 - i_3) &= R_g i_3 + X(i_2 + i_3), \\ Bi_1 + A(i_1 - i_3) &= E. \end{aligned}$$

In order to achieve simplicity in the final expressions, assume that

$$A = B = D, \tag{2a}$$

$$X = A - \delta, \tag{2b}$$

$$\delta \ll A. \tag{2c}$$

Using determinants, the expressions may be calculated for the currents in various arms of the bridge,

$$i_3 = \frac{E\delta}{4A(A + R_g)}\left[1 + \frac{\delta}{4(A + R_g)} \cdot \frac{3A + R_g}{A}\right], \tag{3a}$$

$$i_2 = \frac{E}{2A}\left[1 + \frac{\delta}{4(A + R_g)} \cdot \frac{A + 2R_g}{A}\right], \tag{3b}$$

$$i_1 = \frac{E}{2A}\left[1 + \frac{\delta}{4(A + R_g)}\right], \tag{3c}$$

$$i_2 + i_3 = \frac{E}{2A} + \frac{\delta E(3A + 2R_g)}{8A^2(A + R_g)}. \tag{3d}$$

These equations apply for the condition of *small* bridge unbalance, and a constant driving voltage on the bridge terminals. As defined by Eq. (2*b*), the quantity δ is conveniently considered positive for thermistors, and negative for barretters. Further, if δ is small, as assumed in Eq. (2*c*), it is permissible to write

$$\delta = \frac{\partial R}{\partial P} \cdot \Delta P \qquad \text{ohms}, \tag{4}$$

where $\partial R/\partial P$ is an expression for the detector sensitivity, and ΔP is the increment of power resulting in a change in bolometer resistance

equal to δ. Thus, from Eqs. (3*a*) and (4), the bridge sensitivity may be written

$$\frac{i_3}{\Delta P} = \frac{E \cdot \dfrac{\partial R}{\partial P}}{4A(A + R_g)} \left[1 + \frac{\dfrac{\partial R}{\partial p}\,\Delta P}{4(A + R_g)} \cdot \frac{3A + R_g}{A} \right] \quad \text{amp/watt.} \quad (5)$$

The second term of the bracketed quantity in Eq. (5) may be dropped without sacrificing the validity of the equation for small meter deflections in sensitive bridge circuits. Thus, in its commonly considered form, the expression for bridge sensitivity becomes

$$\frac{i_3}{\Delta P} = \frac{E \cdot \dfrac{\partial R}{\partial P}}{4A(A + R_g)} \quad \text{amp/watt.} \quad (6)$$

It is apparent that if all factors were completely independent, increased bridge sensitivity would result from a larger driving voltage on the bridge or bridge current, decreased bridge-arm resistances, a *small* meter resistance, and increased detector sensitivity. However, the factors are usually not independent, and Eq. (6) must be interpreted with discretion. For example, bolometer A may have a greater detector sensitivity than bolometer B, but may have a higher operating resistance and may demand a smaller bridge current to balance the bridge at the operating resistance of the bolometer. Or, as is true for a thermistor, the detector sensitivity decreases as the operating resistance A decreases, and it is not obvious what combination of the two will lead to greatest bridge sensitivity for a given meter. In some instances additional bridge sensitivity may be derived from the use of bridge arms for which $A \neq B \neq D$. However, the gain is seldom large, and bridge circuits that use arms of different resistance values are usually designed to meet other demands, such as decreased bridge-current drain or greater meter protection in the event of bolometer burnout. Usually, bridge sensitivity is increased by using the meter of the lowest resistance and greatest current sensitivity which is sufficiently rugged. If this fails to provide adequate sensitivity, it is usually necessary to use an a-f voltage supply for the bridge so that the meter-arm unbalance may be amplified.

In the above discussion a constant voltage supply for the bridge has been assumed. However, if the supply impedance is not negligible, it must be noted that E will vary slightly with ΔP, increasing with ΔP if the bolometer is a barretter, and decreasing with ΔP if the bolometer is a thermistor. The effect is negligible when considering small unbalances of the bridge.

One of the interesting differences between barretters and thermistors involves the effect on bridge sensitivity caused by shunting the detector

element with an ohmic resistor. If a barretter is shunted with a resistor, a loss in bridge sensitivity results. However, bridge sensitivity can be increased by shunting a thermistor. The smaller the shunting resistance, the greater the increase in bridge sensitivity. Theoretically, there is no upper limit to the sensitivity that can be achieved in this way. It is possible to carry the phenomenon to a condition of instability for which the tiniest increment of high-frequency power will effect a violent off-scale meter deflection. Unfortunately, because of three serious disadvantages associated with the sensitivity increase, the principle is used only for relatively small sensitivity gains. The thermistor, under normal operating conditions, has a rather long time constant, and the sluggishness in the response of the bridge to a power change in the detector is increased appreciably by this scheme. Moreover, a serious departure from linearity in the calibration curve (that is, microwave power vs. meter deflection) of the bridge results, and the total bridge current needed is greatly increased.

Because of the infrequent use of the principle, it is hardly worth while to treat the phenomenon in mathematical detail. However, a simple qualitative explanation is appropriate. Consider first a bridge circuit, with an unshunted bolometer, which is initially balanced. If microwave power is applied to the bolometer, the detector resistance is changed not only by the microwave power, but also by the change in the d-c (or a-f) *bias* power in the detector. In other words, the microwave power effects a resistance change in the bolometer, which in turn incurs a change in the d-c power dissipated by the element. The change in d-c power may be positive or negative, depending on whether the bolometer has a positive or a negative temperature coefficient of resistance, and on the magnitude of the bolometer-supply impedance as measured at the *bolometer* terminals. Thus, if the bolometer has a constant-current supply, the d-c power increment will be positive for a barretter and negative for a thermistor. Conversely, if the bolometer has a constant-voltage supply, the d-c power increment will be negative for a barretter and positive for a thermistor. If the bridge arms are all equal to A at bridge balance, and if R_g again represents the meter resistance, the supply impedance measured at the bolometer terminals will vary between $A(A + 2R_g)/(3A + 2R_g)$ and $A(2A + 3R_g)/(2A + R_g)$, as the supply impedance measured at the bridge "battery" terminals varies between zero and infinity. Thus, if a high-impedance source drives the bridge, R_g must be small compared with A in order to make the d-c power increment negligible; conversely, if a low-impedance source drives the bridge, R_g must be made large compared with A in order to make the d-c power increment negligible. Finally, it is apparent that a small shunting resistance provides a low-impedance supply for the bolometer, thereby

effecting a negative d-c power increment (hence loss in bridge sensitivity) for the barretter, and a positive d-c power increment (or gain in bridge sensitivity) for the thermistor.

In the operation of a balanced bridge the linearity of the meter calibration is usually a meaningless consideration. In direct-reading bridges, however, it is an important consideration. Several factors influence the linearity of the calibration, and these deserve comment. The first condition demanded for linearity of the bridge calibration is linearity of the curve of detector resistance vs. power (R-P curve). An appreciable region of the R-P curve of the barretter is reasonably linear; however, the R-P curve of the thermistor is far from linear over any extended region. If the direct-reading bridge has a full-scale sensitivity of approximately 1 mw (microwave power), the error caused by the nonlinearity of the R-P curve of either the barretter or the thermistor is satisfactorily small. A bridge having a full-scale sensitivity of 5 to 10 mw will be nonlinear.

As previously discussed, the total power change in the bolometer is usually the algebraic sum of two components: the applied microwave power and an associated change in the d-c bias power. This second component may be used advantageously to improve the bridge sensitivity, but can adversely affect the linearity of bridge calibration. This follows because the d-c power increment is not linearly related to the magnitude of microwave power over a broad range of microwave power. The larger the d-c power increment associated with a given amount of microwave power, the greater the disturbing effect on the linearity of the bridge calibration.

There is a third source of nonlinearity in the calibration if the bridge supply is not a constant-voltage supply. The change in detector resistance with microwave power is reflected as a smaller change in the resistance of the whole bridge network, which necessitates a change of the driving voltage of the bridge. Since the sensitivity of any Wheatstone bridge is directly proportional to its driving voltage, the bridge sensitivity will be influenced by this effect. Usually it is of less importance than other sources of nonlinearity. The fourth source of nonlinearity in the calibration can pass almost without discussion. Nonlinearity in the calibration of the current of a cheap bridge meter can be a serious source of trouble, particularly in very sensitive bridges where other sources of nonlinearity are negligible.

Reference to Eq. (3a) reveals a fifth source of nonlinearity in the calibration. For large resistance changes, the meter deflection is not linearly related to the change in the resistance of the bolometer. Consequently, the bridge should be relatively sensitive if linearity of calibration is to be preserved.

A sixth source of nonlinearity in the calibration concerns the impedance-match of the bolometer at microwave frequencies. The microwave impedance is a complicated function of the d-c resistance of the bolometer. This impedance must be investigated over the entire resistance range corresponding to the limits of balance and full-scale deflection of the meter. A bolometer may be well matched at the resistance demanded for bridge balance, but may develop a sufficiently high standing-wave ratio at the resistance corresponding to full-scale deflection to cause appreciable error in power measurement. This error, because it is usually frequency-sensitive, can be particularly troublesome. Like most other sources of nonlinearity of calibration it must be circumvented by making the bridge as sensitive as possible. Thus, it is common practice to place a calibrated attenuator ahead of the detector mount so that power levels greater than 1 or 2 mw can be measured with accuracy by a direct-reading bridge. It is also customary to impedance-match the bolometer at a resistance corresponding to half-scale deflection, rather than at the resistance needed for bridge balance as is done in balanced-bridge practice.

Finally, in those bridge designs which employ an a-f instead of a d-c driving voltage so that the meter-arm voltage unbalance may be amplified, it is obviously important that the linearity of the amplifier be good.

In cases where it is impractical to make a point-by-point calibration of each bridge circuit, it is often possible to determine a point (usually one-half to three-quarters full-scale deflection) at which a one-point calibration will make the errors of nonlinearity approximately equally positive and negative.

3·3. Thermistor Parameters.—Bead thermistors are made of a semiconducting material involving a mixture of various metallic oxides such as nickel and manganese oxide, and in addition they contain finely dispersed metallic copper to increase the electrical conductivity of the material. In order to form the bead, two taut platinum-iridium wires, 0.001 in. in diameter, are stretched parallel to each other with a small, carefully controlled spacing between them. The mixture as a paste is daubed as a tiny "fly speck" at a spot on the wires. Surface tension shapes the drop into approximately a sphere that bridges the narrow gap between the wires. The bead is air dried, and subsequently sintered at an elevated temperature. Diagonally opposite tie-wire extensions are snipped and the bead cross section is that shown in Fig. 3·2. The bead is usually "loaded" with a skin film of glass to protect it from further oxidation at high temperatures, thereby adding greatly to the

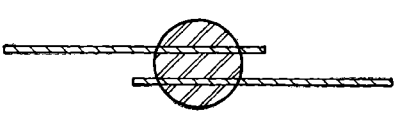

FIG. 3·2.—Diagram to illustrate construction of a bead thermistor.

long-term stability of the electrical characteristics of the bead. The two short tie-wire extensions are fastened to 0.030-in. tungsten-tipped nickel lead wires by a crimping operation, and an unevacuated glass capsule is heat-sealed to the lead wires. The final construction of a typical capsuled bead thermistor is shown in Fig. 3·3.

Disk thermistors are not used as power detectors, but are often used to temperature-compensate the direct-reading-bridge circuits that employ bead-thermistor detectors. Figure 3·4 shows a photograph of a typical disk thermistor. Disk thermistors are disk-shaped elements and vary considerably in size, depending on the electrical characteristics desired. Most of the disks used in temperature compensation of bridge circuits are approximately the size of a small coin. It is usually convenient to solder one side of the disk to a metal plate, using a special,

FIG. 3·3.—Photograph of a typical capsuled bead thermistor.

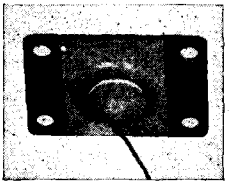

FIG. 3·4.—Photograph of a typical disk thermistor.

low-melting-point solder, and to use a lead wire soldered to the opposite face of the disk as a second terminal. Coatings of wax and paint are used to protect the disk from moisture.

The d-c characteristics of bead thermistors are conveniently plotted on double log-log graph paper which makes possible a quick determination of any one of the four pertinent quantities: resistance, voltage, current, or power. Figure 3·5 illustrates the use of such graph paper in plotting data on a V-519 glass-loaded thermistor bead, in air at atmospheric pressure.

A number of the interesting and important d-c characteristics of bead thermistors can be observed from the curves of Fig. 3·5. Three curves are shown to illustrate the effect of ambient (room) temperature on the d-c bead characteristics. The higher the temperature of the bead environment, the less the d-c power needed to operate the bead at a specified resistance. The resistance of the bead can be varied over wide limits by either ambient temperature or d-c power. The burnout resistance is less than 10 ohms, whereas the "cold" resistance, at negligible power dissipation, is about 1000 ohms. The *negative* temperature (or power) coefficient of resistance of the thermistor is clearly apparent. It is particularly important to note that the voltage drop across the thermistor passes through a maximum value as the current through the

bead is increased. At a specified bead voltage, the bead resistance, current, and power may have either of two possible values. The voltage and resistance of the d-c supply dictate the equilibrium condition.

The Bell Telephone Laboratories have developed a formula, Eq. (7), which expresses the resistance of the bead as a function of absolute

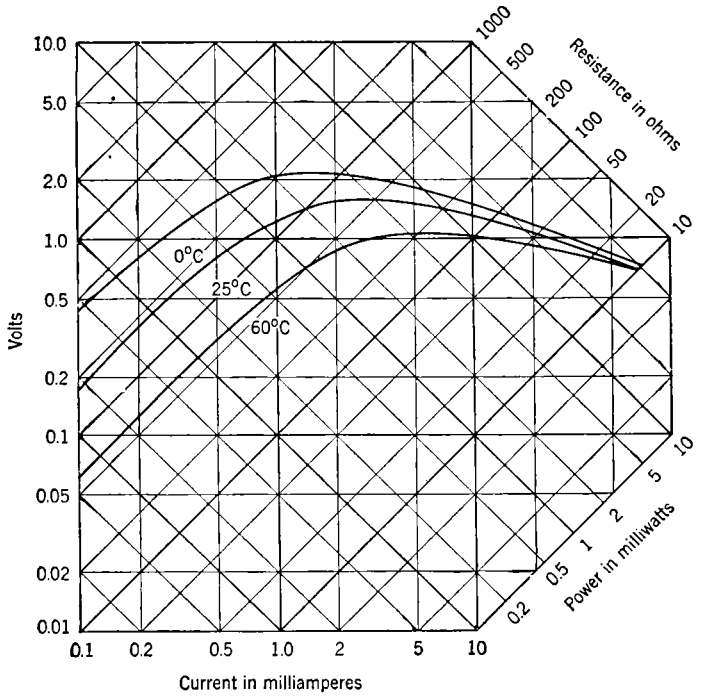

FIG. 3·5.—D-c voltage, current, resistance, and power data on a typical bead thermistor. (*Data by courtesy of Bell Telephone Laboratories.*)

temperature,

$$R = R_0 \exp\left[B\left(\frac{1}{K} - \frac{1}{K_0}\right)\right], \tag{7}$$

where

R = bead resistance at an absolute temperature K
R_0 = bead resistance at temperature K_0
B = a constant, expressed in degrees Centigrade.

Equation (7) may be rewritten as

$$R = Je^{B/K}, \tag{8}$$

where

$$J = R_0 e^{-B/K_0}. \tag{9}$$

Equation (8) is of limited use, however, since it does not differentiate between the effects of ambient temperature and of (RI^2)-heat dissipation on the resistance of the bead. If the reasonable supposition is accepted that the bead resistance depends only on its internal temperature regardless of the source of the thermal activity, Eq. (8) may be rewritten as

$$R = Je^{\frac{B}{K+CP}}. \tag{10}$$

The constant C is a simple proportionality factor, expressed in degrees per watt, which linearly relates the effects of ambient temperature and (RI^2)-heat dissipation on the resistance of the bead.

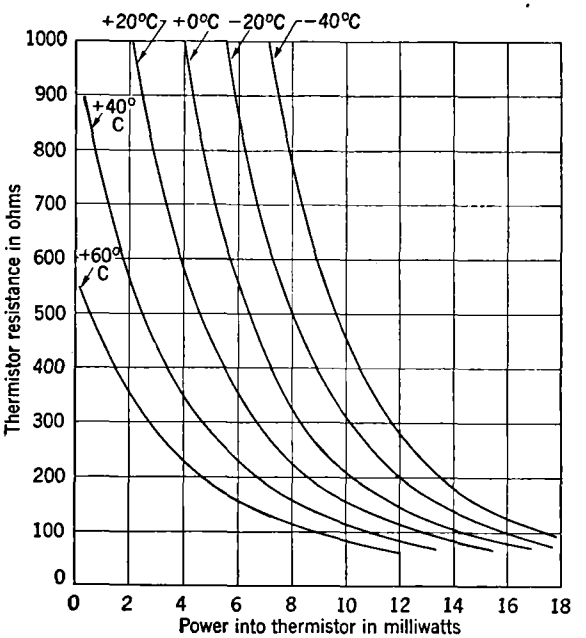

FIG. 3·6.—Temperature characteristics of a typical bead thermistor.

Justification for the use of a simple proportionality factor has been found in experimental data of the sort shown in Fig. 3·6. The resistance of a V-519 thermistor has been plotted against power, at six ambient temperatures, covering a range of 100°C in equal 20°C intervals. The curves should shift linearly, left to right, if the assumption involved in the use of C is a valid one. The observed shift is not quite linear, being slightly greater at high temperatures than at low temperatures, but is sufficiently linear to permit acceptance of Eq. (10) for many calculations.

The three fundamental parameters of the bead thermistor are J, B, and C. Parameter B is primarily a material constant, being determined largely by the composition of the thermistor mixture. It is dependent on temperature to a slight (and usually neglected) extent. Parameter J is primarily a geometrical constant, depending principally on such factors as the size of the bead, the spacing of wires within the bead, and the resistivity of the thermistor material. Parameter C is primarily a thermal constant, depending on such quantities as the thermal capacity and specific heat of the bead, the medium (usually air) in which the bead is immersed, and lead-wire conduction losses. It is temperature-sensitive to the degree made evident by the data plotted in Fig. 3·6.

Equations (8) and (10) are also valid for disk thermistors. Usually the value of C is small for a disk because it has a relatively large heat capacity. Since the current it carries is a few milliamperes, the product CP is negligible compared to the value of K, and almost all calculations involving disk thermistors may therefore be made with Eq. (8).

The values of J, C, and B of a thermistor may be experimentally determined as follows. If the d-c powers, P_1 and P_2, required to bring the thermistor to a resistance R_1 at temperatures K_1 and K_2, respectively, are measured, then by definition,

$$C = \frac{K_2 - K_1}{P_1 - P_2}. \tag{11}$$

To determine J and B it is necessary to use Eq. (10), which may be written as

$$(B) + (K + CP)(\ln J) = (K + CP) \ln R. \tag{12}$$

If C is determined from Eq. (11), Eq. (12) may be considered as an equation in two variables: B and $\ln J$. Therefore, if a third power measurement P_3 is made at a temperature K_3 and with the thermistor at a different resistance R_3, values for B and $\ln J$ may be obtained from

$$B = \frac{(K_1 + CP_1)(K_3 + CP_3)(\ln R_3 - \ln R_1)}{(K_1 + CP_1) - (K_3 + CP_3)}, \tag{13}$$

$$\ln J = \frac{(K_1 + CP_1) \ln R_1 - (K_3 + CP_3) \ln R_3}{(K_1 + CP_1) - (K_3 + CP_3)}. \tag{14}$$

The resistance R_1 is preferably chosen as the resistance at which the thermistor will be operated in the bridge circuit; R_3 is preferably 100 to 200 ohms greater. K_1 and K_2 are chosen as the extremes in temperature over which the bridge circuit must operate, with K_3 being chosen as an intermediate temperature. This selection of K and R values will lead to the most practical set of J, B, C values, since B and C are slightly temperature-dependent. It is advisable to operate the thermistor in a

precision balanced bridge while the data are being taken. This permits high accuracy in the determinations of R and P. Moreover, continued stability of the bridge balance over a long period of time guarantees that the bead has reached thermal equilibrium with its environment. Temperature data should be accurate to $0.1°K$.

When determinations of J, B and C are made, it is important to mount the bead in a manner similar to that in which it will be used. The environment of the bead affects the values of both J and C, particularly if the bead has no surrounding glass capsule. An illustration of the

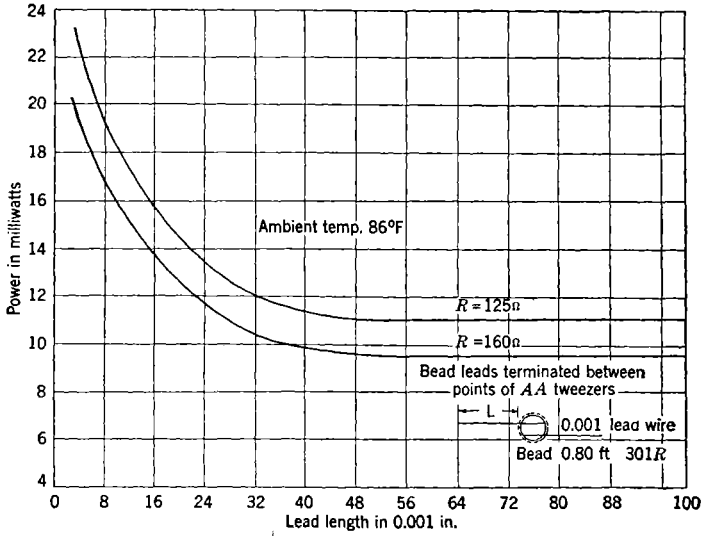

FIG. 3·7.—Power vs. tie-wire length of unmounted D-166382 glass-loaded thermistor bead in air. (*Courtesy of Bell Telephone Laboratories*).

effect of environment may be found in Fig. 3·7, which shows the influence of the length of the 0.001-in. tie wires on the d-c characteristics of the bead. The effect of increased conduction losses if the wire lengths are shorter than a critical value is readily apparent. If the thermistor (bead or disk type) is immersed in oil or water or a vacuum, the values of J and C will be changed appreciably from those that obtain in air. Occasionally a thermistor with d-c characteristics that are radically different from the average is found. Close inspection will often reveal that the bead is not centered within the air cavity of the glass capsule, but is in contact or near contact with the capsule wall. The increased conduction losses caused by contact can severely affect the d-c characteristics of the bead.

Considerable use will be made of Eq. (10) in subsequent sections

of the chapter, and hence the values of J, B, and C assume importance. The equation is particularly useful in the design of certain types of direct-reading thermistor bridge circuits, and in studying the effects of d-c thermistor tolerances on the temperature compensation of the circuits.

All disk thermistors have a value of B of 3890°C. Table 3·1 lists some of the disk thermistors that have been made by the Western Electric Company, together with their nominal values of J. The range of values

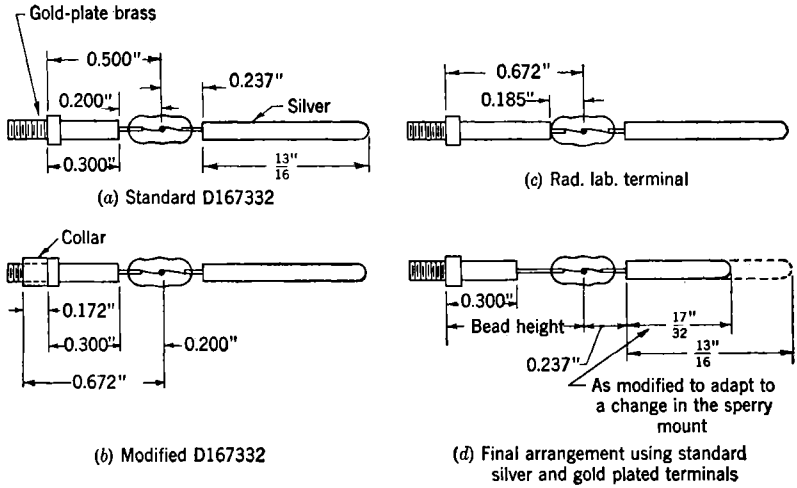

FIG. 3·8.—An assortment of BTL bead thermistors used in microwave power measurement.

of J listed does not typify the range that can be provided if need arises. Rather, these happen to be values of J that were required to meet specific design objectives.

TABLE 3·1.—VALUES OF J FOR AVAILABLE DISK THERMISTORS

Type No.	J Value
D-169227	0.447×10^{-3} ohm
D-167613	0.705×10^{-3} ohm
D-168391	1.52×10^{-3} ohm
D-168392	1.59×10^{-3} ohm
D-169228	2.82×10^{-3} ohm

Table 3·2 lists the values of J, B, C of V-519 bead thermistors. The average and extreme values have been calculated from the Western Electric production test specifications; the tolerances are stated in terms of power variations at given resistance and ambient temperature.

With very few exceptions, all bead thermistors that have been used in microwave power measurement are of the V-519 family. Many bead thermistors have been developed by the Bell Telephone Laboratories, and subsequently put into production by the Western Electric

Company. They differ in the capsule, in the length of platinum-iridium tie wires, in the design of built-up lead wires, and in other geometrical

TABLE 3·2.—CHARACTERISTICS OF V-519 BEAD THERMISTORS

	Average	Extreme no. 1	Extreme no. 2
J; ohms	0.555	0.750	0.228
B; °C	2,420	2,402	2,682
C; °C/watt	11,440	10,830	11,960

respects which are important from the point of view of microwave impedance matching. However, many bead thermistors use the V-519

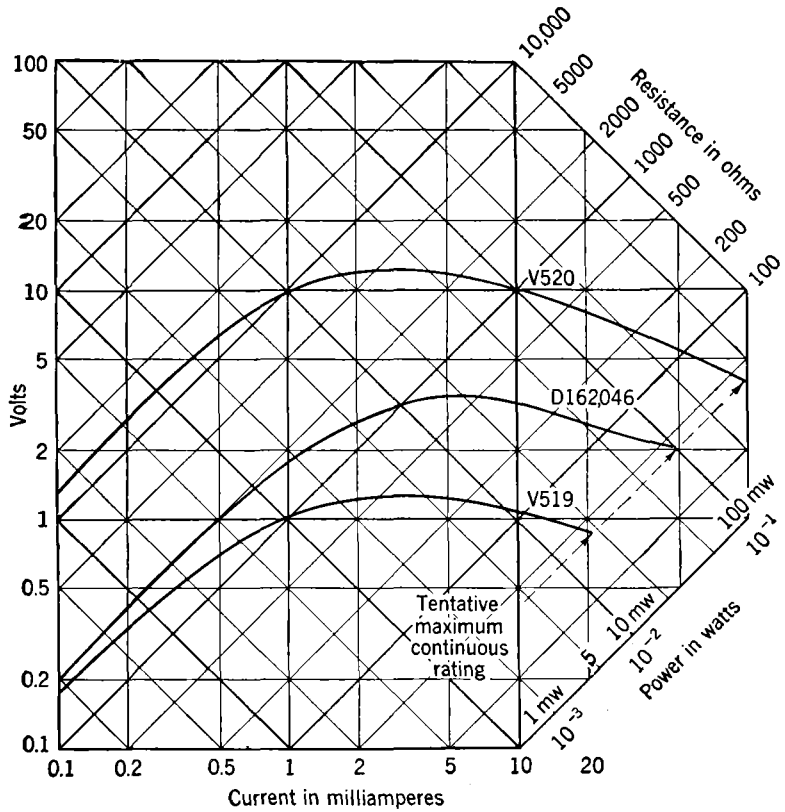

FIG. 3·9.—D-c characteristics of two high-power bead thermistors.

bead, and have the same d-c characteristics. Figure 3·8 shows a number of bead thermistors which are members of the V-519 family.

Brief investigations have been made of two high-power bead thermistors, the D-162046 and the V-520. The capsules are somewhat larger than those of the V-519 thermistor, but can be readily installed in 10-cm-band waveguide or coaxial-line mounts. The chief objection to large-bead thermistors is their excessive sluggishness. In most applications it is preferable to use the V-519 bead with calibrated attenuators to reduce the microwave power level. The d-c characteristics of the high-power beads are shown in Fig. 3·9, together with those of the V-519 for ready comparison.

3·4. Operation of a Thermistor in a Bridge Circuit.—Consider a simple series circuit consisting of a battery of potential E, a fixed resistance R_0, and a thermistor of resistance R. The voltage drop across the thermistor is given by

$$V = \frac{RE}{R_0 + R}. \tag{15}$$

To have a steady-state condition a second relation must be satisfied. Referring to Eq. (10), expressing P as V^2/R, and solving for V

$$V = \sqrt{\frac{R}{C}\left(\frac{B}{\ln \frac{R}{J}} - K\right)}. \tag{16}$$

A steady-state condition is reached when the thermistor resistance is such that the two expressions for V are equal. By plotting two curves of V vs. R, one from Eq. (15) and one from Eq. (16), the steady-state values of R and V may be determined from the point of intersection of the curves. Depending on which curve has the greater slope at the point of intersection, the steady-state condition may or may not be stable. In most bridge circuits, however, the equivalent series voltage and resistance of the d-c supply of the thermistor are such that the steady-state condition is stable, and there is a single crossover point for the two curves.

The resistance R_0 should be large enough to limit the series current to a value less than that required for burnout of the thermistor, which is slightly under 10 ohms.

The maximum voltage in the thermistor characteristic curve is commonly called the "hump" voltage. As may be seen from Fig. 3·5, its value depends considerably on the ambient temperature. A calculation of the hump voltage is of interest in the design of battery-operated direct-reading bridge circuits that must operate at low temperatures. In order to have long battery life and yet hold battery weight to a minimum, it is desirable to use low-voltage dry cells in such wattmeters. However, the battery emf must be large enough to guarantee that the thermistor can be biased "over the hump" at the lowest temperature, since the

operating resistance is almost always less than the value associated with the hump voltage.

The hump voltage, V_h, may be determined from Eq. (16) by differentiating V with respect to R, and setting $dV/dR = 0$. Thus,

$$V_h = \frac{1}{\ln \frac{R_h}{J}} \sqrt{\frac{BR_h}{C}}, \tag{17}$$

and

$$R_h = J \exp \left[\frac{B}{2K} \left(1 + \sqrt{1 - \frac{4K}{B}} \right) \right], \tag{18}$$

where R_h is the resistance of the thermistor at the hump voltage V_h. By substituting Eq. (18) in Eq. (17), an expression for V_h as a function of J, B, C, and K may be obtained. The value of V_h calculated from Eq. (17) may be compared with the value of V calculated from Eq. (15) under the condition $R = R_h$. The value calculated from Eq. (15) must of course be larger than that calculated from Eq. (17), if the thermistor is to be successfully biased over the hump. If it is not larger, it is impossible to balance the bridge. It is interesting to note that if the bridge cannot be balanced for this reason, it is possible to warm the thermistor mount by holding it tightly in a bare hand, balance the bridge at the elevated bead temperature, and maintain the balance after the temperature has dropped to its initial value. In other words, a battery potential inadequate to balance the bridge at a low temperature may nevertheless be capable of holding the bridge at balance if it has help in achieving the balance condition.

Although it is apparent from Fig. 3·5 that the resistance of a bead thermistor may be varied over a range of many hundreds of ohms, the practical operating range is confined to a fraction of this. If the thermistor is operated at too high a resistance it may be impossible to balance the bridge at a high temperature. For example, the 60°C curve in Fig. 3·5 demonstrates the impossibility of balancing a bridge that was designed to operate this particular thermistor at 700 ohms. If the operating resistance were 500 ohms, it would be possible to balance the bridge, but the bridge current and driving voltage would be so small that poor sensitivity would result. Conversely, at very low resistance levels (for example, 10 to 50 ohms) the bead is operated dangerously close to burnout. Moreover, broadband impedance-matching of the thermistor is extremely difficult at such low resistances. Experience has shown that a bead thermistor of the V-519 family should be operated within the range of 100 to 300 ohms in order to achieve the optimum set of conditions on bridge sensitivity, ease of impedance-matching the thermistor,

safety from overload or burnout of the thermistor, and ease in effecting temperature compensation for the bridge.

Bead thermistors of the V-519 family burn out at a resistance somewhat less than 10 ohms. Almost invariably the burnout is not within the sintered bead, but in one of the two 0.001-in. tie wires, halfway between the bead and the tie-wire junction with the larger 0.030-in. lead wire. If the burnout results suddenly from application of excessive power, the bead itself is apparently unhurt. On at least two occasions determinations of J, B, and C were made on bead thermistors, after which the thermistors were intentionally burned out by excessive power. The broken tie wires were spot-welded together and the data retaken. The changes noted were within the errors of measurement. Long-term application of power almost great enough to cause burnout can effect small changes in the values of J, B, and C of a bead; however, under normal conditions of use the beads can be considered to have very stable electrical characteristics.

All thermistor mounts share one desirable property which has become known as the "self-fusing" property. The burnout resistance of a thermistor is so much lower than the operating resistance (that is, 5 ohms compared with 150 ohms) that the mount impedance becomes badly mismatched before the thermistor can be burned out. As the mount mismatch increases, the generator delivers less power to the thermistor, so that a generator capable of delivering burnout power to a matched load will not necessarily burn out the mounted thermistor bead. Barretters do not share this advantage because of the much smaller difference between their operating and burnout resistance levels.

Bead thermistors of the type commonly used for microwave power detection are relatively sluggish devices. Resistance-frequency and reactance-frequency graphs for a typical V-519 thermistor show that the resistance is constant and the reactance zero at frequencies greater than a few cycles per second. Consequently, audio frequencies at 60 cps, or greater, may be used as sources of thermal energy for the bead. For example, the middle or bottom curve of Fig. 3·5 may be reproduced by maintaining a constant a-f power dissipation in the bead at 0°C while the d-c power variations are being made. The amount of a-f power required to reproduce the 60°C curve at 0°C depends on the value of C for this particular bead. This may be seen by writing Eq. (10) as

$$R = J \exp\left[\frac{B}{K + C(P_d + P_a)}\right] = J \exp\left[\frac{B}{(K + CP_a) + CP_d}\right], \quad (19)$$

where P_a is the a-f power dissipation in the bead, and P_d is the d-c power dissipation. For the example just cited P_a should be chosen so that

$$(K + CP_a) = 273 + 60.$$

3·5. Audio-frequency Response of Bolometers.—Although a V-519 thermistor responds only weakly to a-f voltages, a combination of a thermistor and an a-f amplifier has been used to advantage in making low-level pulse-power measurements. For example, in making production-line measurements of TR leakage power, a thermistor in a balanced-bridge circuit is used to measure the average power coupled through a standard hole.[1] The standard hole provides reproducible leakage from a transmission line carrying pulsed magnetron power. After the balanced-bridge measurement is made, the thermistor is switched to an amplifier circuit which is tuned to the pulse-repetition frequency. In order to preserve the microwave impedance-match of the thermistor, the amplifier bias current must be set at the same value required to operate the thermistor in the balanced bridge. The amplifier gain control is adjusted to make the amplifier read directly in pulse power, see Eq. (1). A 20-mw pulse-power signal for a $\frac{1}{2}$-μsec pulse at 1000 pps will provide an input voltage signal of 10 to 20 μv, depending on the magnitude of the thermistor bias current. This is adequate to operate a sensitive a-f amplifier. The amplifier calibration is checked periodically by measuring the leakage power from the standard hole. A barretter, because of its much smaller time constant, would provide a considerably larger voltage signal under the same operating conditions. However, the barretter, unlike the thermistor, does not have the ability to withstand large overloads without burnout, and every defective TR tube would result in a barretter burnout.

In order to understand certain phenomena that are troublesome in the design and use of sensitive a-c bolometer bridge circuits, it is necessary to probe into the mathematics of the periodic excitation of bolometers. It will be assumed that the bolometer time constant is large compared to the period of the modulation of the power, but is at the same time not a negligible factor. In other words, the average (internal) temperature of the bolometer will be large compared to the periodic variation of resistance. The rate of heat generation in the bolometer will be given by the product of the average bolometer resistance and the square of the bolometer current. Variations with resistance in the rates of heat generation and dissipation will be negligible second-order effects. The law of conservation of thermal energy demands that

$$(P - P_0)\, dt = H \cdot dT, \tag{20}$$

where P is the instantaneous power level, P_0 the average power level, H the heat capacity of the bolometer, and T the instantaneous temperature of the bolometer at the time t. For small periodic variations

[1] J. B. Wiesner, "Details of X-Band High Level TR Tube Test Bench," RL Report 417, February 3. 1944.

in temperature, it may be assumed that the bolometer resistance varies linearly with temperature, or

$$\frac{dR}{dT} = k, \tag{21}$$

where k is the dynamic temperature coefficient of resistance. If Eq. (21) is substituted in Eq. (20) and integrated,

$$R = R_0 + \frac{k}{H}\int_0^t (P - P_0)\, dt. \tag{22}$$

If the excitation of the bolometer is by an a-f current of constant amplitude,

$$I = I_0 \cos \omega t, \tag{23}$$

Eq. (22) may be written as

$$R \doteq R_0 + \frac{k}{H}\int_0^t \left(R_0 I_0^2 \cos^2 \omega t - \frac{I_0^2 R_0}{2}\right) dt,$$

or

$$R = R_0\left(1 + \frac{kI_0^2}{4H\omega} \sin 2\omega t\right). \tag{24}$$

From Eqs. (23) and (24) the expression for the voltage E appearing across the bolometer terminals becomes

$$E = I_0 R_0 \cos \omega t + \frac{R_0 k I_0^3}{8H\omega}(\sin \omega t + \sin 3\omega t). \tag{25}$$

If k is negative (the case of the thermistor), the equivalent circuit is shown in Fig. 3·10a, and

$$C_t = \frac{-8H}{kR_0 I_0^2}, \tag{26a}$$

$$E_t = \frac{R_0 k I_0^3}{8H\omega} \sin 3\omega t. \tag{26b}$$

If k is positive (the case of the barretter), the equivalent circuit is shown in Fig. 3·10b, and

$$L_b = \frac{8R_0 H}{kI_0^2}, \tag{27a}$$

$$E_b = \frac{R_0 k I_0^3}{8H\omega} \sin 3\omega t. \tag{27b}$$

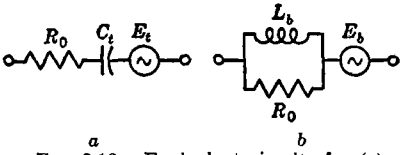

FIG. 3·10.—Equivalent circuits for (a) a thermistor and (b) a barretter excited by a constant-amplitude a-f current.

If d-c and a-f currents are applied simultaneously to the bolometer, a second generator is added in series with the first in the equivalent circuit.

For the thermistor, the second generator voltage E_t' is given by

$$E_t' = \frac{kR_0 I_0^2}{4H\omega} \sin 2\omega t, \tag{26c}$$

E. G. & G. LIBRARY
LAS VEGAS BRANCH

where i is the direct current through the bolometer. For the barretter, the second generator voltage E_b' is given by an equivalent expression

$$E_b' = \frac{kR_0 i I_0^2}{4H\omega} \sin 2\omega t. \tag{27c}$$

It is interesting to note that the apparent reactive elements L_b and C_t, behave as real reactive elements in that they are independent of frequency. However, they are unlike true reactive elements in that their magnitudes depend on I_0.

The above development has been necessary to demonstrate the following pertinent facts. If a bolometer is used as one arm of an a-c bridge circuit, and if the bridge is balanced for the fundamental a-c frequency, the third (in the a-c *and* d-c case, the second and third) harmonic will usually appear as an unbalanced voltage across the center of the bridge. Moreover, if the bridge is unbalanced for the fundamental frequency, this frequency will suffer a phase shift. The harmonic unbalance prevents a zero meter reading unless the a-f amplifier has good harmonic rejection. The phase shift of the fundamental frequency is troublesome in the design of self-balancing a-c bridge circuits which must use properly phased feedback loops.

It should be noted from Eqs. (26*b*), (26*c*), (27*b*), and (27*c*) that the amplitudes of the harmonic voltages can all be reduced by increasing the frequency. Thus, if an r-f current is modulated by an audio frequency, the radio-frequency component may be neglected and only the modulation envelope considered. If the r-f current is square-wave modulated, the power is then given by the Fourier series

$$P = P_0 + \frac{4P_0}{\pi}\left(\frac{\cos \omega t}{1} - \frac{\cos 3\omega t}{3} + \frac{\cos 5\omega t}{5} - \cdots\right). \tag{28}$$

If a d-c bias current i is used, Eq. (22) may be integrated and solved for the bolometer voltage E with the result

$$E = iR = iR_0 + \frac{4kiP_0}{\pi\omega H}\left(\frac{\sin \omega t}{1^2} - \frac{\sin 3\omega t}{3^2} + \frac{\sin 5\omega t}{5^2} - \cdots\right). \tag{29}$$

It is apparent from Eq. (29) that only odd harmonics of the modulation frequency are generated. The sign of k is of no importance. The Fourier expansion given in Eq. (29) will be readily associated with a triangular waveform.

If the skin depth for current in thermistor material at microwave frequencies is calculated, it is found to be in excess of the diameter of a V-519 bead. Consequently, a bead thermistor will be heated the same by microwave currents as by d-c currents, and it is a satisfactory detector for absolute power measurements. Careful comparisons of thermistors

and barretters in power measurements in the 3-cm and 10-cm bands have shown agreement between them that is well within experimental error. The glass loading and glass capsule of the thermistor are formed from a special low-loss Corning glass. The tie-wire losses are negligible except when the operating bead resistance is well under 100 ohms or when the frequencies are extremely high. There is, however, a question as to whether tie-wire losses are indeed negligible in the 1-cm band. This problem is discussed in detail in Sec. 3·21 in connection with 1-cm-band thermistor mounts.

3·6. Temperature Compensation of Direct-reading Bolometer Bridges.—There are two phases to the problem of temperature compensation for direct-reading bolometer bridges. It is desired that the bridge sensitivity should be independent of temperature changes, and that the bridge should not drift from a condition of balance to one of small unbalance as the ambient temperature varies. It should be emphasized that the techniques developed for temperature compensation in direct-reading bridge circuits do not provide perfect compensation. The circuits are almost invariably designed to have maximum effectiveness for the bolometer with average d-c and temperature characteristics, and the compensation for such a bolometer can usually be made very good. However, it is seldom desirable to adjust the circuits individually to take into account bolometer variations; consequently a compensating circuit designed for the detector with average characteristics may or may not be satisfactory for bolometers having characteristics of extreme values. Since most designs of direct-reading bridges to be discussed in this section and in Sec. 3·7 have been developed for quantity production, it is necessary to state specifications on temperature compensation that will apply to any thermistor or barretter that meets the d-c and temperature test specifications of the manufacturer.

The degree of difficulty involved in providing sensitivity compensation depends largely on the ambient-temperature range over which the bridge is expected to operate, and on the tightness of the tolerances in the test specifications of the bolometer. These same factors influence the problem of providing drift compensation, but there is an additional factor which often makes this problem more serious. Whereas sensitivity compensation is almost independent of the bridge sensitivity, the balance drift increases directly with bridge sensitivity. A given small change in ambient temperature will produce an unbalance deflection of the meter which is proportional to the bridge sensitivity.

Sensitivity compensation is essential, but drift compensation is merely desirable. Much time is saved in operation of the bridge if the drift compensation is good. For example, there is always a possibility that a small ambient-temperature variation may occur between the

time the d-c bridge is balanced and the time the meter deflection is noted after introduction of microwave power to the bolometer. Thus the power determination may be in error, and it is necessary to make a series of readings in order to ensure the correctness of the measurement. Satisfactory drift compensation avoids this repetition of measurements. Frequently the bridge must be transported from a warm room to a much colder outdoor location; an uncompensated bridge will drift rapidly for many minutes before the detector has reached temperature equilibrium and a stable bridge balance can be obtained. In some instances it is desirable to use a recording bridge meter to provide a continuous record of the variations in microwave power over long periods of time. In such an application, drift compensation becomes a necessity in order to avoid appreciable errors. Seldom is the drift compensation so good that the manual bridge-balance control (usually a d-c potentiometer) can be entirely eliminated. However, a single fine-adjustment control is quickly and easily used. Subsequent discussions of bridge designs will emphasize the techniques used to provide drift and sensitivity compensation. The remainder of this section will consider only thermistor bridges. These will be discussed in approximately the chronological order of their development in order to display better the logic underlying their development.

In considering sensitivity compensation it is essential first to understand *why* bridge sensitivity varies with temperature. Experimentally, it is found that the sensitivity of an uncompensated thermistor bridge (wherein balance is obtained by an adjustment of the bridge current) increases as the ambient temperature decreases. Neglecting the temperature coefficients of resistance of all elements except the thermistor, there are three potential explanations: (1) the detector sensitivity (in ohms per milliwatt) of the thermistor varies with temperature; (2) the resistance of the bridge supply and the thermistor-current supply varies with temperature because of the bridge-current adjustment; and (3) the driving voltage across the bridge terminals varies with temperature for the same reason.

If Eq. (10) is differentiated to obtain an expression for the detector sensitivity of the thermistor,

$$\frac{dR}{dP} = -\frac{cR}{B}\left(\ln\frac{R}{J}\right)^2 \qquad \text{ohms/watt.} \tag{30}$$

Since K does not appear in Eq. (30) it is to be concluded that the detector sensitivity of the thermistor is independent of ambient temperature provided that the resistance is held constant. This condition is met by the procedure of balancing the bridge at each and every temperature

before delivering microwave power to the thermistor. Consequently, the first of the above-mentioned possible explanations must be discarded.

It is found experimentally that the bridge sensitivity is markedly temperature-dependent even when the bridge- and the thermistor-current supplies have a high resistance. This high resistance is changed inappreciably when the bridge current is varied to effect balance over a wide temperature range, so that the second possible explanation is of minor importance.

Consistent with the third-mentioned possibility, it is found that bridge sensitivity varies directly with the bridge driving voltage, as the bridge driving voltage is changed by adjustment of the bridge current in traversing a wide ambient-temperature range. The first bridge design to utilize this observation in providing sensitivity compensation is described in the next section.

3·7. The V-bridge.—An example of a bridge with sensitivity compensation is known as the V-bridge. A circuit diagram of the bridge is shown in Fig. 3·11.

The V-bridge is designed to operate the bead thermistor Th_1 at a resistance of 200 to 300 ohms, depending on the optimum value for microwave impedance-matching. Potentiometer R_{14} is set accordingly. Cascaded voltage-regulator tubes provide a well-stabilized d-c bridge voltage that can be adjusted by R_4. The adjustment is such that the d-c bridge current will effect bridge balance at an ambient temperature somewhat in excess of the highest temperature at which the bridge is expected to operate. At lower ambient temperatures the d-c current is inadequate for bridge balance, and a-f (1000 to 2000 cps) power is superimposed on the d-c thermistor power in an amount sufficient to make the bridge balance. A 6J5 tube is used in a modified Wien-bridge circuit, with a suitable output transformer, to provide a stable a-f current. Potentiometer R_5 is used for manual adjustment of the bridge balance. With R_5 set at the middle of the range, and at an ambient temperature which is roughly at the middle of the operating temperature range, R_4 is adjusted for bridge balance. Thereafter the R_4 setting is left untouched, and all further balancing is conducted with R_5.

A d-c meter (200 μa full scale, 50 to 75 ohms coil resistance) is used as the bridge galvanometer. Full-scale sensitivity of the bridge is standardized at 2 mw by adjustment of the meter shunt R_{16}.

Since the bridge meter responds only to direct current, and since the d-c bridge driving voltage is maintained constant over the operating temperature range, the sensitivity of the bridge is relatively independent of temperature changes. It is essential, however, that the a-f supply impedance, as measured at the thermistor terminals, be kept close to the operating resistance of the thermistor. If this condition is not met, the

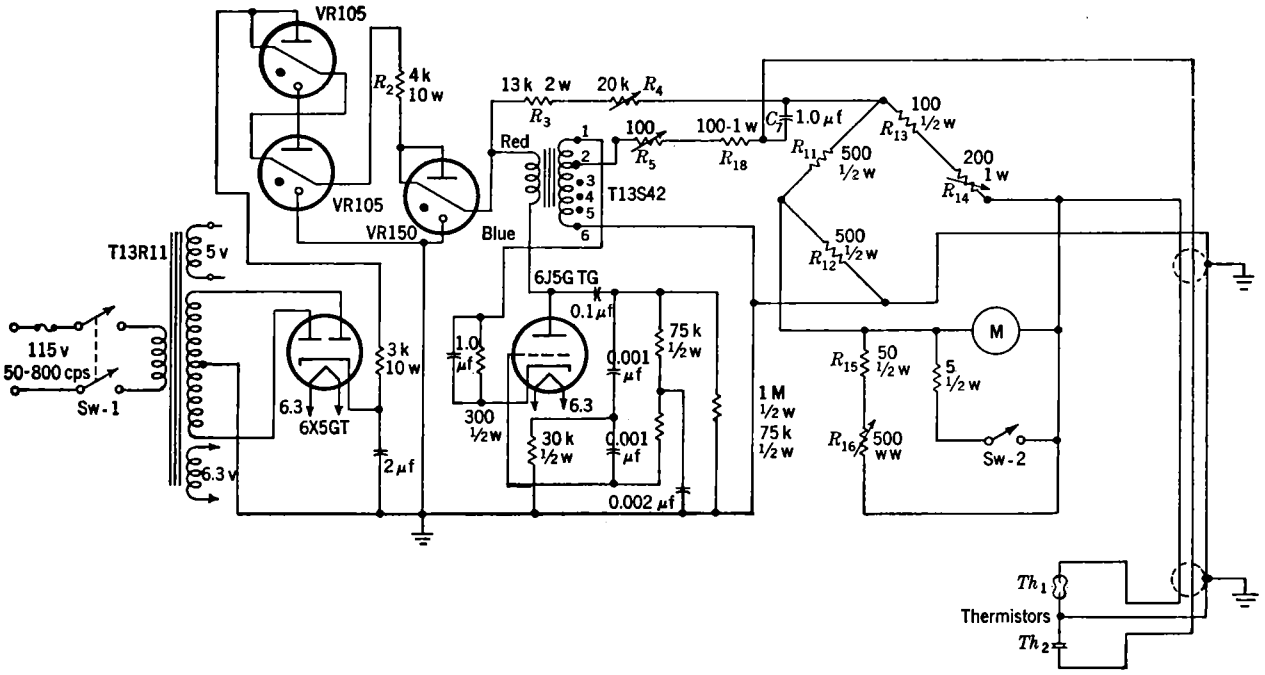

FIG. 3·11.—Circuit diagram of the direct-reading thermistor V-bridge.

a-f power in the thermistor will vary with the bridge unbalance and serious error can accumulate. A change in ambient temperature may occur between the times of bridge balance and bridge unbalance caused by the applied microwave power. Since the bridge must operate the bead at any place within the 200- to 300-ohm range, and since the a-f supply impedance also varies with temperature, some error in sensitivity compensation is thereby realized. The compensation achieved with this bridge design is $\pm \frac{1}{4}$ db over a temperature range from $-10°$ to $+60°$C, for any thermistor of the V-519 type. An uncompensated thermistor bridge would have a sensitivity variation in excess of ± 1 db over this same temperature range.

This circuit illustrates the first attempt to use a disk thermistor for drift compensation. The disk thermistor Th_2 is placed in parallel with the bridge network in the a-f bridge supply, and acts as a temperature-sensitive shunt element to control the a-f bridge voltage. As the ambient temperature increases, the resistance of the disk decreases. The disk therefore becomes a more effective shunt element, reduces the a-f current in the bridge network, and decreases the a-f power dissipation in the bead thermistor. For perfect drift compensation, the disk thermistor would have to limit the a-f power dissipation in the bead thermistor to the exact amount required for bridge balance at any ambient temperature. A bead thermistor of average J, B, C, values is used in designing the drift compensator, and a decade resistance box is placed in shunt with the bridge in the a-f bridge supply. Bridge balance is made over a wide temperature range by manual adjustment of the decade box, with the R_5 control left untouched at its midposition. The curve of decade-box resistance vs. ambient temperature must then be matched by the R-K curve of an available disk thermistor. It is convenient to prepare a family of curves with R_{18} as the parameter, and to select the value of R_{18} that provides an R-K curve that an available disk thermistor will match. Subsequent developments involving the use of disk thermistors in resistive T-networks have led to more accurate matching of the R-K curve, but the single D-167613 disk used in this circuit is surprisingly effective. The unbalance drift is less than $\pm \frac{1}{2}$ full scale at a sensitivity of 2 mw full scale over the temperature range of $\pm 35°$C. The maximum slope of the drift curve for any bead of the V-519 type is approximately 3.5 per cent of full-scale deflection per degree C. In the average bead for which the circuit is designed, with the bead operating at 250 ohms, the unbalance drift is $\pm \frac{1}{3}$ full scale, and the maximum slope 1.5 per cent of full scale per degree C.

Several factors collectively limit the maximum sensitivity of the V-bridge to approximately 1.7 mw full scale. The meter sensitivity cannot be increased appreciably without sacrificing the ruggedness

required if the instrument is to be readily portable. The d-c bridge driving voltage is relatively low because of the necessity of using a-f power, in part, to balance the bridge. The higher the maximum temperature at which the bridge must operate, the lower the d-c driving voltage that can be used. The a-f and d-c supplies provide sufficiently stable voltages for operation of the bridge at a 2-mw full-scale sensitivity, but any attempt to increase bridge sensitivity by using a much more sensitive galvanometer would cause trouble from inadequate voltage regulation. Finally, drift compensation by disk thermistors becomes increasingly more difficult at higher sensitivities because of the difficulty of maintaining the disk and bead thermistors in temperature equilibrium. The disk is installed on the outside of the metal mount for the bead thermistor, but the small temperature gradient that can exist between the disk and the bead becomes increasingly more significant and troublesome as the bridge sensitivity is increased.

The only front-panel controls on the V-bridge are the manual bridge-balance control R_5 and a push-button switch, Sw-2. This switch shunts the meter with a 5-ohm resistor, greatly decreasing the nominal sensitivity of the bridge. It is useful for indicating, *not* measuring, power levels of 2 to 50 mw. Further, if the microwave power level is not known approximately before measurement, it is wise to get a preliminary indication with the 5-ohm meter shunt in order to avoid a violent off-scale deflection of the sensitive meter.

The following changes in the circuit diagram shown in Fig. 3·11 permit the operation of the bead thermistor at 125 ohms in the V-bridge circuit: (1) change R_2 from 4000 to 2500 ohms; (2) change R_{11} and R_{12} from 500 to 300 ohms; (3) eliminate R_{18}; (4) set R_{14} at 25 ohms; (5) change C_1 from 1 μf to 2 μf; tap the a-f voltage off terminal 5 rather than terminal 2 of the secondary of the output transformer; (6) recalibrate.

The V-bridge has no self-contained calibration device. It is calibrated against a balanced bridge, and the calibration must be repeated if a new bead thermistor is installed.

3·8. Temperature Compensation with Two Thermistor Disks.—The most frequently voiced objections to the V-bridge have been its circuit complexity and its physical size. Whereas neither is objectionable for use of the bridge as a portable laboratory milliwattmeter, it is highly desirable that a milliwattmeter for field service be considerably smaller and simpler in design. The need for a simple, compact bridge circuit is also felt in the design of signal generators and field test sets. After considerable development work, the design of the "two-disk" thermistor bridge, which requires only direct current for its operation, evolved. In this circuit, sensitivity compensation is achieved by installing a disk thermistor in series with the bridge meter thereby making use of the fact

that bridge sensitivity can be controlled by adjustment of the meter-arm resistance. At the low ambient temperatures where an uncompensated bridge becomes more sensitive, the disk increases the meter-arm resistance to compensate. Similarly, constant sensitivity is maintained at high temperatures through the decrease in meter-arm resistance resulting from the reduced disk resistance. Drift compensation is achieved through the use of a second disk thermistor which is placed in shunt with the bridge, the technique being similar to that used for drift compensation in the V-bridge.

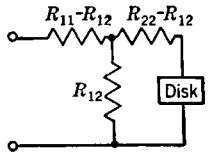

FIG. 3·12.—Resistive network for modifying the resistance-temperature characteristic of a disk thermistor.

The success of the design obviously rests on the resistance-temperature (R-K) characteristics of the two disk thermistors. The disk characteristic must match the R-K curve necessary for compensation, over the entire temperature range. A perfect match at all temperatures (hence perfect compensation) is not possible. However, by installing the disk in a network of ohmic resistors it is possible to match at several arbitrarily chosen points along the curve, and to have small errors at temperatures which lie between these points. It can be shown that a T-network, Fig. 3·12, is as general a network as need be used with a single disk thermistor.

Since there are four variables in the network, the three resistors and a disk of arbitrary J-value, it is to be expected that the desired R-K curve may be matched at four points. However, it is often satisfactory to match at three points, and thereby permit greater latitude in the choice of the disk thermistor. An available disk may suffice, and thereby obviate the need for manufacturing a special disk thermistor. This has been an important consideration since there must exist numerous variations of the two-disk bridge design to meet the various field and laboratory demands.

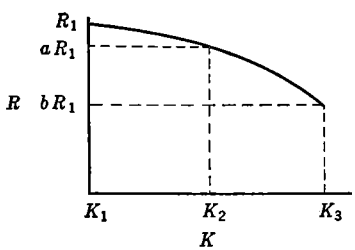

FIG. 3·13.—A resistance-temperature curve of the shape that can be matched by the network shown in Fig. 3·12.

If the R-K curve necessary for perfect compensation (drift or sensitivity) has been experimentally determined by the use of a decade resistance box, the problem is that of designing the circuit, Fig. 3·12, to match this curve. The curve to be matched is fortunately a smooth one in all but rare instances, and is of the form shown in Fig. 3·13.

Consider the network[1] as a two-terminal-pair network with the disk

[1] R. Krock and N. Painter, "The Two-disk D-c Thermistor Bridge Circuit," RL Report 502, Jan. 12, 1944.

thermistor connected to one pair of terminals. The network equations are

$$\begin{aligned} E_1 &= R_{11}I_1 + R_{12}I_2, \\ E_2 &= R_{12}I_1 + R_{22}I_2, \end{aligned} \tag{31}$$

where the resistance of the network as a whole is $E_1/I_1 = R$, and the resistance of the disk is

$$-\frac{E_2}{I_2} = Je^{B/K}. \tag{32}$$

With these substitutions Eq. (31) may be reduced to

$$(R - R_{11})Je^{B/K} + (R - R_{11})R_{22} + (R_{12})^2 = 0. \tag{33}$$

The quantities J, R_{22}, and $(R_{12})^2$ may be considered as the three variables. If three equations are made of Eq. (33) by substituting known resistances at known temperatures (see Fig. 3·13), values for the quantities may be determined as

$$\left.\begin{aligned} J &= \alpha(a - b)R_1e^{-B/K_1} \\ R_{22} &= \alpha\left[(R_{11} - aR_1)e^{\frac{B}{K_2}-\frac{B}{K_1}} - (R_{11} - bR_1)\right] \\ (R_{12})^2 &= \alpha(R_{11} - aR_1)(R_{11} - bR_1)e^{(\frac{B}{K_2}-\frac{B}{K_1}} - 1) \end{aligned}\right\}, \tag{34}$$

where α is a proportionality constant relating each variable to the corresponding cofactor of the first row of the determinant formed from Eq. (33).

From Eq. (34) it may be determined that

$$\left.\begin{aligned} R_{11} &= R_1\frac{Q_1}{P} \\ R_{22} &= \alpha R_1\frac{Q_2}{P} \\ R_{12} &= \sqrt{\alpha}\,R_1\frac{Q_3}{P} \end{aligned}\right\}, \tag{35}$$

where

$$\begin{aligned} P &\equiv Ma - (M - N)b - N \\ Q_1 &\equiv (M - N)a - Mb + Nab \\ Q_2 &\equiv (a - b)[(M - N)b - M(N + 1)a + (M + 1)N] \\ Q_3 &\equiv (a - b)\sqrt{MN(M - N)(1 - a)(1 - b)} \\ M &\equiv e^{\frac{B}{K_1}-\frac{K}{K_1}} - 1 \\ N &\equiv e^{\frac{B}{K_2}-\frac{B}{K_1}} - 1. \end{aligned}$$

For any physically realizable network $R_{12} \leqq R_{11}$, and $R_{12} \leqq R_{22}$. These conditions may be used to define the maximum and minimum values that

α may assume. Thus,

$$\left.\begin{aligned}\sqrt{\alpha_{max}} &= \frac{Q_1}{Q_3}\\ \sqrt{\alpha_{min}} &= \frac{Q_3}{Q_2}\end{aligned}\right\}. \tag{36}$$

It is not always possible to match a given R-K curve at three points. However, it is easy to determine whether a three-point match is possible. It has been shown in Eq. (36) that α must lie within a specified range if the required network is to be a physically realizable one. The limiting case must occur when $\alpha_{max} = \alpha_{min}$. If this equality is assumed, Eq. (36) may be reduced to a cubic in a and b. This cubic can be factored into a combination of a linear and a second-degree function that, when plotted on an a-b plane, defines a crescent-shaped area such as that shown in Fig. 3·14.

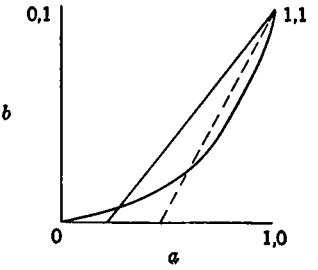

FIG. 3·14.—The crescent area in which the a-b points of Fig. 3·13 must fall if the R-K curve can be matched by the network of Fig. 3·12.

In the experimental R-K curve shown in Fig. 3·13, only those curves whose a-b points fall within this crescent area can be matched at the chosen three points. It is also possible to demonstrate that the dashed, straight line of Fig. 3·14 has special significance. The crescent area to the right of this straight line is concerned with matchable R-K curves having negative second as well as first derivatives; the crescent area to the left of the dashed line is concerned with curves having positive second but negative first derivatives. (No curves with positive first derivatives can be matched by a disk-thermistor network.) The slope of the dashed line (or its intercept along the a axis) is determined by the spacings of K_1, K_2, and K_3. For example, the intercept is $a = 0.5$ for $(K_2 - K_1) = (K_3 - K_2)$. The boundary curves which define the crescent are also dependent on K_1, K_2, and K_3.

The equations just stated are sufficient to permit calculation of the constants of the compensating network. However, a set of three graphs can be prepared from which the constants can be readily calculated by simple interpolation procedures. Such graphs are invaluable if there are numerous curves to be matched. To explain the origin and use of this set of graphs the following extension of the foregoing theory is necessary.

From Eqs. (35) and (36) the three pertinent equations may be restated,

$$\alpha_{min} = \left(\frac{Q_3}{Q_2}\right)^2, \tag{37}$$

$$\frac{R_{11}}{R_1} = \frac{Q_1}{P}, \tag{38}$$

$$\frac{R_{22}}{\alpha R_1} = \frac{Q_2}{P}. \tag{39}$$

The right side of each equation is a function only of a and b, once values have been assigned to B, K_1, K_2, and K_3. Hence it is possible on an a-b plane to plot a family of curves, each member of which has a definite value of α_{min}. Similar families of parametric curves can be drawn for R_{11}/R_1 and $R_{22}/\alpha R_1$.

Since values for a, b, and R_1 are known from the curve to be matched, the value of R_{11} can be obtained from the family of curves based on Eq. (38). By dividing Eq. (39) by Eq. (38), squaring, and multiplying by Eq. (37),

$$\left(\frac{Q_3}{Q_1}\right)^2 = \frac{1}{\alpha_{max}} = \alpha_{min}\frac{\left(\dfrac{R_{22}}{\alpha R_1}\right)^2}{\left(\dfrac{R_{11}}{R_1}\right)^2}. \tag{40}$$

By proper interpolation on each of the three prepared graphs values for α_{min}, $(R_{22}/\alpha R_1)^2$, and $(R_{11}/R_1)^2$ may be obtained. Then from Eq. (40), the value for α_{max} may be determined. In the first line of Eq. (34), J is expressed in terms of α and experimentally known constants. A value of α is selected which lies within the range defined by Eq. (36) and which requires the J-value of an available disk thermistor. From the set of curves based on Eq. (39), R_{22} may be calculated. The value of R_{12} may be determined by squaring Eq. (39) and multiplying by Eq. (37). The result, combined with the last line of Eq. (35), leads to

$$R_{12} = R_{22}\sqrt{\frac{\alpha_{min}}{\alpha}}. \tag{41}$$

This step completes the determination of the circuit constants.

It frequently happens that the calculated value of one of the network resistors is only a few ohms, and the resistor may therefore be eliminated. Similarly, it is usually possible to depart slightly from the calculated resistance value in order to use an RMA-standard resistor.

It should be pointed out that a four-point matching procedure does not extend the crescent area of Fig. 3·14 and therefore does not permit a wider variety of R-K curves to be matched than when three points are used.

It must be emphasized that these calculations neglect the heating effect of the current passed through the disk thermistor. This is certainly safe for the disk used for sensitivity compensation because the meter-arm currents are of the order of microamperes. The drift-compensator disk must pass currents, however, in the milliampere range, and care should be used

in selecting disks for this application. Regardless of the J-value, the disk must be sufficiently large, and hence have a sufficiently large heat capacity, to keep the product CP negligible compared with K. Fortunately, the drift-compensator disk carries the largest currents at high ambient temperatures where its resistance is lowest.

3·9. The Calculation of R-K Curves for Temperature Compensation. The above treatment of the problem of the design of a compensating circuit is based on an experimental determination of the R-K curve to be matched. This is a fundamental limitation because it is difficult to handle the tolerance problem in bead-thermistor characteristics. Whereas disk thermistors can be made uniform, the tiny beads are found to vary considerably in their ambient-temperature and d-c characteristics. Invariably there arises the problem of determining the success of the compensator circuits for limit beads in the bridge circuit, and such limit beads are seldom available for experimental tests. Consequently, it is often desirable to be able to *calculate* the R-K curves which must be matched. Such calculations must be based on known circuit quantities, including the values of J, B, and C of the bead thermistor used. Equations permitting these calculations can be used for other purposes. It is often desirable to calculate the range of the meter shunt resistance needed to standardize bridge sensitivity over the entire range of values of J, B, and C. Likewise, meter overload currents in the event of thermistor burnout, minimum supply voltage needed to avoid "hump trouble" at low ambient temperatures, and the maximum range of resistance variation needed in the manual bridge-balance control can be calculated.

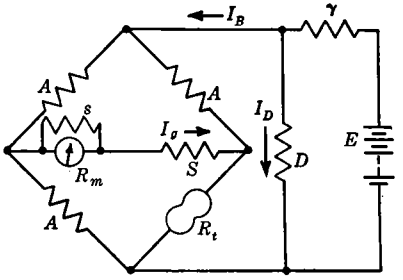

FIG. 3·15.—Diagram of two-disk bridge circuit with sensitivity compensator S and drift compensator D.

Consider the bridge circuit shown in Fig. 3·15 in which S and D represent respectively the sensitivity- and drift-network resistances. Both S and D vary with temperature, of course.

If the drift compensator is to maintain the bridge at balance, independently of temperature, then Ohm's law demands that

$$D = \frac{rA}{\dfrac{E}{2i_0} - (A + r)}, \tag{42}$$

where i_0 is thermistor current at bridge balance.

An expression for i_0 may be obtained from Eq. (10) by setting $R = A$,

and $P = Ai_0^2$, thus,

$$i_0 = \sqrt{\frac{1}{CA}\left(\frac{B}{\ln \frac{A}{J}} - K\right)}, \tag{43}$$

where the values J, B, and C are those of the bead thermistor.

From Eq. (42), with substitution for i_0 according to Eq. (43), the D-K curve that is to be matched by the drift compensator may be calculated. It is important to recognize that the values of r and E have an appreciable effect on the shape of the D-K curve required for perfect drift compensation, and some judgment is necessary in selecting the value for r. It is convenient to plot on the a-b plane the locus of the a-b points for D, as r is varied. The locus curve will intersect the crescent at some given value of r, and this places a limit on the value of r that will permit a matchable D-K curve. Deep within the crescent the matching problem is easy, particularly since the range of disk J-values acceptable for a three-point match is broader there than near the boundary of the crescent. Thus it is easier to select a standard disk. If the value of r (for a given E) is relatively small, it may be reasoned that the drift compensator draws large current. This is objectionable because either voltage-regulator tubes or batteries have limited current drain, and, as previously mentioned, the calculation can prove erroneous if the disk passes a large current. Finally, it must be remembered that the slope of the S-K curve for the sensitivity compensator depends on r. Consequently, a second locus curve on the a-b plane showing the locus of the a-b points of S as a function of r is needed to make the final decision. Usually the intercept of the D-K curve with the crescent boundary limits the maximum value of r, and the intercept of the S-K locus curve also limits the maximum value of r. The smaller of the two maxima dictates, of course.

The problem of calculating the S-K curve to be matched is more tedious than that of calculating the D-K curve. The steps involved are the following. Equation (10) may be rewritten as

$$R_T = J \exp\left[\frac{B}{K + C(P + p)}\right], \tag{44}$$

where P is the microwave power in the thermistor bead, and p the d-c power in the thermistor bead. If e_t and i_t represent, respectively, the thermistor bead d-c voltage and current,

$$\left.\begin{aligned} R_T &= \frac{e_t}{i_t} \\ p &= e_t i_t \end{aligned}\right\}. \tag{45}$$

If Eq. (45) is substituted in Eq. (44), and solved for P,

$$P = \frac{\frac{B}{C}}{\ln\left(\frac{e_t}{Ji_t}\right)} - e_t i_t - \frac{K}{C}. \tag{46}$$

A mesh-equation analysis of the unbalanced bridge circuit of Fig. 3·15 leads to the expressions for e_t and i_t

$$e_t = \frac{A^2E'}{2A(R_0 + A)}\left[1 - (3R_0R_g + 2AR_0 + 2AR_g + A^2)\frac{I_g}{AE'}\right] \tag{47}$$

$$i_t = \frac{AE'}{2A(R_0 + A)}\left[1 + (R_0R_g + 2AR_0 + 2AR_g + 3A^2)\frac{I_g}{AE'}\right], \tag{48}$$

where

$$E' \equiv \frac{E}{1 + \frac{r}{D}},$$

$$R_0 \equiv \frac{r}{1 + \frac{r}{D}},$$

$$R_g = S + \frac{sR_m}{s + R_m},$$

and

$$\frac{AE'}{2A(R_0 + A)} = i_0$$

as defined by Eq. (43).

The objective is an equation relating P to I_g, R_g, K and other circuit parameters including the values of J, B and C of the bead. Then, for given values of P and I_g (that is, constant bridge sensitivity) R_g (hence S) may be calculated as a function of K. Substitution of Eqs. (47) and (48) in Eq. (46) should accomplish this, but unfortunately the resulting equation, even with the simplifications resulting from the neglect of second-order terms, is extremely involved. It is preferable to plot curves of e_t and i_t against R_g, and to use these curves to plot P vs. R_g. The curves must be plotted for each of the three match points—K_1, K_2, and K_3. The procedure leads to the values of R_g (hence S) that the sensitivity compensator must meet at the three temperatures.

The procedure may be reversed and P calculated for known values of I_g, D, and S at any temperature. This is the technique used to study the success of drift and sensitivity compensators on limit beads after they have been calculated for a bead with average values of J, B, and C.

Although the equations presented above are applicable only to a

bridge with all arms equal at balance, it is possible to derive equivalent equations for a bridge using unequal arms. Many of the two-disk bridge-circuit designs use unequal arms, primarily to economize on bridge current, (see Table 3·3).

In the above theoretical treatment of the problem the effect of temperature on other circuit constants has not been considered. Bridge-arm and other resistors having small temperature coefficients of resistance are preferred. The effect of temperature on the resistance of the copper meter coil, however, is often not neglibigle, and the calculated S-K curve should be corrected to include this.

Bridge sensitivity is standardized in the two-disk circuit by selecting the proper value of s (the meter shunt) for the bead used. Since the parallel combination of meter and shunt is usually small compared with the resistance of S, this calibration technique has a minimum disturbing effect on the accuracy of the sensitivity compensator. Since the two-disk bridge circuit is not self-calibrating, it is desirable to install the meter-shunt resistances on the spare thermistor mounts. The shunts are made from the same wire used in winding the meter coils to avoid a temperature-dependent current split between the meter and the calibrating shunt. A nominal 200-μa, 68-ohm meter is used with the meter resistance set at 75 ± 1 ohms with a selected adjusting resistor. The normally large tolerances on meter coil resistance demand that this be done. All circuits must be checked for meter current in the event of thermistor burnout to be certain that the overload current is within the rating of the meter.

The sensitivity of the two-disk bridge circuit is commonly adjusted to 2 mw, full-scale deflection. Many of the factors which limit the maximum sensitivity of the bridge are identical with those already discussed in connection with the V-bridge. In addition, there is the obvious limitation on bridge sensitivity arising from the use of a sensitivity compensator which adds to the meter-arm resistance.

Experience has shown that better drift and sensitivity compensation can be realized if the bead thermistor is operated at a relatively low resistance. For example, if the thermistor can be impedance-matched for microwaves as well at 125 ohms as at 250 ohms, the 125-ohm operating resistance should be selected. At the lower resistance level the internal temperature ($K + CP$) of the bead depends more on the power-dissipation term, CP, and less on the ambient temperature K. Hence a given variation in K represents a smaller percentage variation of the whole, and the ambient-temperature variation proves less troublesome.

It is always possible in the two-disk bridge circuit to ground electrically the drift-compensator disk to the bead thermistor mount. This is desirable from the point of view of obtaining good thermal contact between the bead and the disk; however, the sensitivity-compensator disk cannot be

grounded to the bead mount. Since electrical insulators are usually poor thermal conductors, this poses a problem. Fortunately the d-c voltage between the sensitivity-compensator disk and ground is small, so that a very thin mica or polystyrene wafer is sufficient to insulate the sensitivity-compensating disk from the bead mount. If the mount is made of aluminum, the surface may be anodized in a thin film in order to provide the necessary insulation.

It is possible for a single disk thermistor (in a resistive T-network) to provide both sensitivity and drift compensation in a d-c bridge circuit. Since bridge sensitivity is dependent on the resistance of the bridge-current supply, it is possible to conceive a drift-compensating network which would vary this supply resistance in the exact manner necessary for simul-

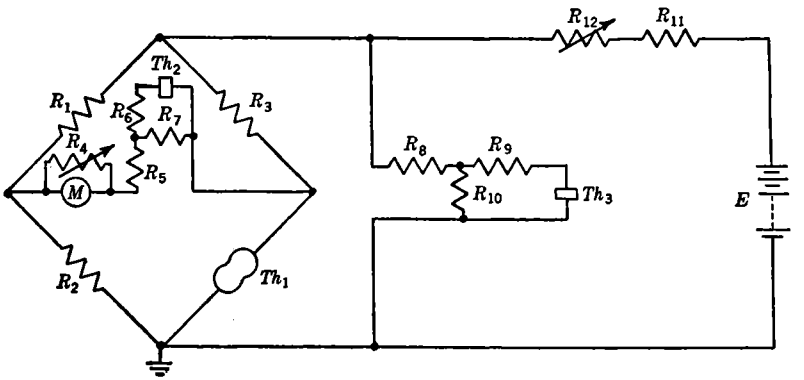

FIG. 3·16.—Circuit diagram of the two-disk thermistor bridge circuit (see Table 3·1 for circuit constants).

taneous sensitivity compensation. This condition has been met in a bridge circuit designed through the cooperative efforts of the Aircraft Radio Corporation and the Radiation Laboratory (see Table 3·3). Unfortunately the development came too late in the history of the Radiation Laboratory to permit a theoretical study of the conditions necessary to achieve these results with a single disk.

Figure 3·16 shows a detailed circuit diagram of the two-disk bridge circuit. The circuit constants are given in Table 3·3. The constants for four of the numerous two-disk circuits that have been developed are tabulated.

Any of the four bridge circuits will maintain the sensitivity constant to within $\pm \frac{1}{2}$ db over a 75°C ambient-temperature range for any bead thermistor in the V-519 family. The zero-drift specifications vary somewhat among the several circuits, but a typical specification is maximum drift of $\pm \frac{1}{2}$ full-scale deflection at a full-scale sensitivity of 2 mw. The

maximum slope of the drift curve is 3 per cent of full-scale deflection per degree Centigrade.

In conclusion, the two-disk bridge circuit represents a good compromise between accuracy of compensation and simplicity of design. The thermistor bridge circuits discussed in the following paragraphs are capable of greater accuracy and greater sensitivity, but involve relatively complicated and expensive circuit design.

TABLE 3·3.—CIRCUIT CONSTANTS APPLICABLE TO FIG. 3·16

	Circuit #1	Circuit #2	Circuit #3‡	Circuit #4
R_1	430 ohms	250 ohms	300 ohms	180 ohms
R_2	430	250	300	180
R_3	180	250	130	130
R_4	0–200	0–500	0–200†	0–200†
R_5	82	Zero	Not Used	Zero
R_6	120	20	Not Used	Zero
R_7	270	250	Not Used	130
R_8	33	40	Zero	Zero
R_9	Zero	36	200	82
R_{10}	15,000	475	620	780
R_{11}	330*	5000	7000	6500
R_{12}	0–400	0–750	0–1000	0–1000
E	6 volts	105 volts	150 volts	150 volts
M	75 ohms	68 ohms	75 ohms	75 ohms
T_1	Any bead thermistor in the V-519 family			
T_2	D-169227	D-168392	Not used	D-168392
T_3	D-169227	D-168391	D-168392	D-168391

* R_{11} shunts R_{12} in this case.
† R_4 in series with meter in this case.
‡ Example of the one-disk bridge circuit.

3·10. The W-bridge.—The direct-reading W-bridge, a circuit diagram of which is given in Fig. 3·17, is a thermistor bridge that has a maximum full-scale sensitivity of 0.1 mw. It differs from the V-bridge and two-disk circuits in that the initial bridge balance is made entirely with 2000-cps a-f power in the bead thermistor. The bridge unbalance is amplified, phase detected, and registered on a d-c milliammeter. A d-c calibrating signal is used to standardize the bridge sensitivity at the ambient temperature at which microwave power measurement is to be made. This technique circumvents the need for a sensitivity compensator of the sort discussed in connection with the two-disk bridge circuit. Compensating networks are not reliable at high sensitivities because of the slight temperature gradients that invariably exist between the detector element and the compensator. Drift control is realized by installing the thermistor mount in a thermostated oven, or, in many cases, in a box filled with rock wool to provide a very long thermal time constant.

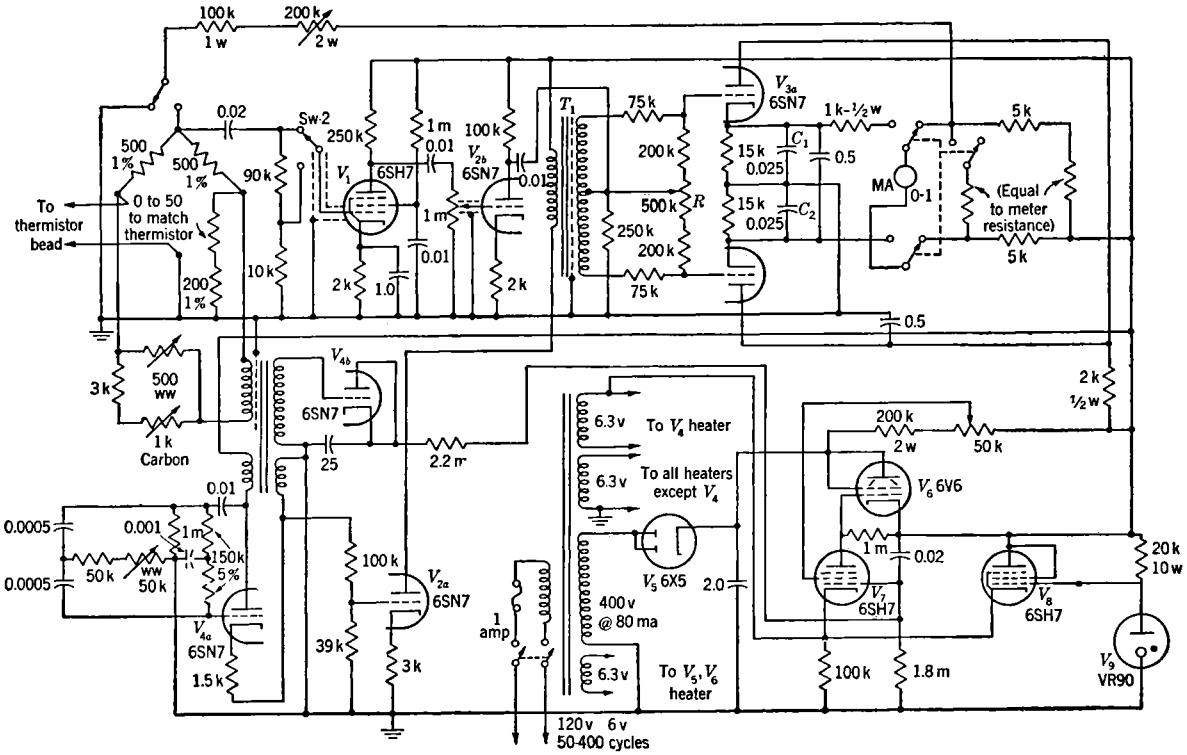

FIG. 3·17.—Circuit diagram of the direct-reading thermistor W-bridge.

The a-f oscillator in the W-bridge is a parallel-T feedback oscillator using one-half of a 6SN7 tube, V_{4a}. There are two feedback paths, one of which is the winding in the cathode circuit of the tube. It is in phase with the plate of the tube. The second feedback path is through two parallel *RC*-circuits—one being a low-pass filter, and the other a high-pass filter. Both *RC*-circuits are calculated so that $X_c = R$ at 2000 cps. At the crossover point the amplitude feedback is zero and the phase is indeterminate, passing from $-90°$ to $+90°$. Thus the arrangement represents a transformer feedback oscillator with a negative feedback circuit which prevents oscillation except at the one frequency at which the negative feedback voltage is zero. Since any distortion would represent frequency components other than 2000 cps, the output power will be very nearly a perfect sine wave. In order to stabilize the oscillator amplitude, a signal voltage from the oscillator is rectified and used to control the B+ voltage.

The amplifier consists of a 6SH7 pentode (V_1) followed by one half of a 6SN7 triode (V_{2a}), the other half of which is used as a buffer amplifier. In order to avoid any appreciable phase shift at 2000 cps, large coupling and bypass condensers are used. All leads from high-impedance points should be shielded to avoid a-f pickup.

A phase-detector circuit is necessary to indicate whether the resistance of the bead thermistor is greater than or less than that required for bridge balance. A signal from the oscillator is mixed with the amplified signal in transformer T_1. With no signal from the bridge, both grids of detector V_3 should receive equal signals, and R is adjusted to make certain of this. The cathodes remain at the same potential, and no current flows through the meter. Each positive peak charges up one of the condensers (C_1 or C_2), which discharges slowly during the remainder of the cycle. If the bridge is unbalanced, the amplified unbalance voltage has either the same or opposite phase as the plate of the a-f oscillator V_4. Since the voltage is applied to the center tap of the secondary of T_1, the entire secondary has this voltage. On the other hand, the signal applied from the oscillator through the buffer amplifier to the primary of T_1 will provide secondary voltages which are equal in magnitude, but 180° out of phase at the ends of the secondary winding. Center-tap signals from the unbalanced bridge will therefore increase the positive peak amplitude on one side of the center tap, and decrease it on the other. Finally, since the cathode voltage is proportional to the grid voltage, there will be a potential drop across the meter which indicates the degree of bridge unbalance. Since the meter impedance is low, the meter current is proportional to grid voltage up to nearly 2 ma, or twice full-scale deflection. The primary of T_1 is connected so that a decrease in thermistor resistance causes a positive meter deflection.

The bridge circuit is calibrated by first balancing with the audio fre-

quency, and then adding a known (100 μw) d-c power to the thermistor to produce a condition of unbalance. A variable gain control in the amplifier circuit is used to set the meter at the desired deflection. For example, if a 200-μw full-scale sensitivity is desired, the meter deflection would be set at one-half full scale when the 100-μw calibrating signal is applied. When calibrating, the 0- to 1-ma meter is switched from its amplifier-output position to the high-resistance d-c bridge supply. In this position it permits adjustment of the d-c current to the value required for the calibration. The calibrating current is calculated from Ohm's law, neglecting the fact that the thermistor resistance is slightly less than the balance value when the direct current is applied. The resulting error in power measurement

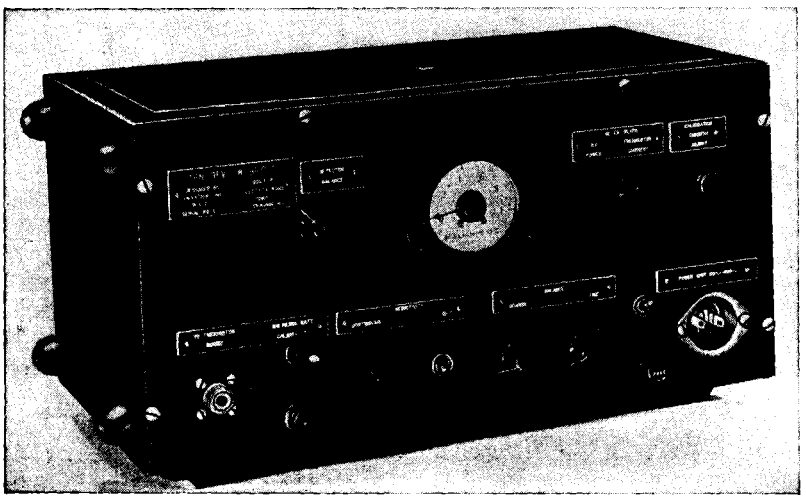

FIG. 3·18.—Photograph of the direct-reading thermistor W-bridge.

is less than 1 per cent if a 100-μw calibrating signal is used. If reduced sensitivity is desired, that is, 1 to 2 mw full scale, a push-button switch operating a 10:1 resistance divider in the amplifier circuit may be used when setting the gain control for a 100-μw calibrating signal. This technique avoids the appreciable error that would result if a 1- or 2-mw calibrating signal were used directly. When switched to the calibrating position, the meter is shunted so as to read the thermistor current directly.

In order to prevent heater-voltage changes in the oscillator from changing its output power, the B+ voltage is controlled by the oscillator voltage. This also makes the oscillator output voltage independent of loading. Tube V_{9}, one-half of a 6SN7 connected as a diode, is used to rectify the voltage from a 120-volt winding on the oscillator trans-

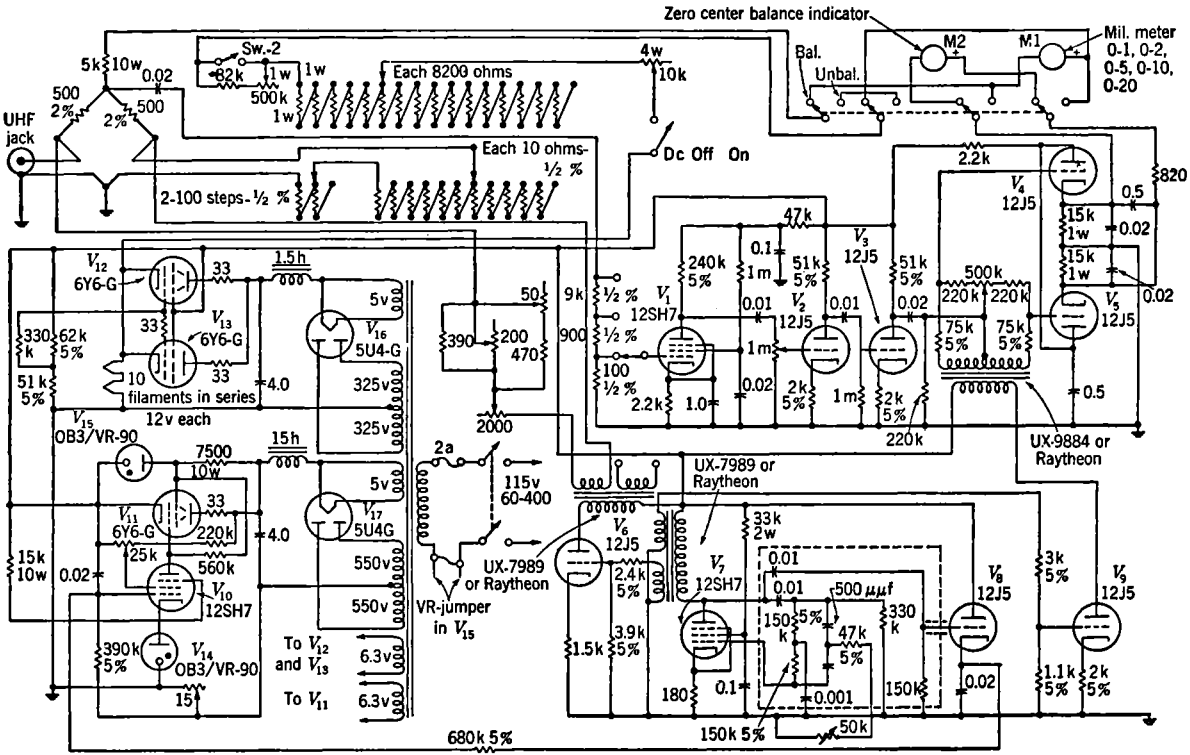

FIG. 3·19.—Circuit diagram of the thermistor X-bridge.

former. The rectified voltage controls the grid of the 6SH7 regulator, thereby making the B+ voltage vary to keep the a-f voltage constant. The diode is connected so that the grid is used as a plate, since this decreases the period of warm-up drift.

The bridge usually requires capacitance across the thermistor to effect a true balance for the fundamental a-c frequency. The third harmonic generated by the thermistor, when the bridge is balanced at full gain, is approximately 1 volt at the output terminals of the amplifier. The error caused is negligible at a 0.1-mw full-scale sensitivity.

The bridge is capable of operating a V-519 bead thermistor at any resistance within the range of 100 to 500 ohms. The accuracy of the bridge in the rated sensitivity range is limited only by the accuracy of the meter, bridge-arm resistances, and meter shunt. Figure 3·18 shows a photograph of the front panel of the W-bridge.

3·11. The X-bridge.—For some applications, for example the measurement of TR leakage power, the W-bridge does not have adequate sensitivity. To meet these needs a special, more complicated bridge circuit was developed which became known as the X-bridge. A circuit diagram of the X-bridge is given in Fig. 3·19.

The X-bridge is capable of a maximum full-scale sensitivity of 15 μw, but may be used at sensitivities as low as 2 mw full scale. In principle it is similar to the W-bridge, but in order to realize the greater sensitivity it has a higher-gain amplifier, and more stable d-c and a-f supplies. An additional front-panel control facilitates adjustment of the thermistor balance resistance in 10-ohm steps. Both a magic eye and a d-c, zero-center galvanometer are used to indicate bridge balance.

Unlike the W-bridge, the X-bridge may be used as a balanced as well as a direct-reading bridge. The initial balance is made with a-f power, and with the thermistor connected to the microwave source. When the microwave source is disconnected, balance is restored by adding d-c power. The magic eye is conveniently used for approaching the balance condition quickly, and the galvanometer is used in making the final exact balance.

It is almost essential that the thermistor mount be used in a temperature-stabilized oven when operating at or near the maximum sensitivity of the X-bridge. If this is done, the accuracy of the instrument is limited almost solely by the calibration accuracy of the d-c milliammeter. It is important that the bridge be balanced capacitively as well as resistively. If there is a large out-of-phase voltage at resistive balance, the amplifiers may be overloaded and may become nonlinear. At sensitivties greater than about 25 μw full scale, the large third-harmonic signal generated by the thermistor destroys the linearity between bridge sensitivity and amplifier gain. Consequently, direct calibration in this

power range is greatly preferable to using fixed gain steps in the amplifier circuit.

A fairly satisfactory oven for the thermistor mount can be designed around a simple bimetallic thermostat switch. A nichrome heating coil is wound around the outside of a tubular asbestos coil form; the thermistor mount is placed within the tube. A material such as rock

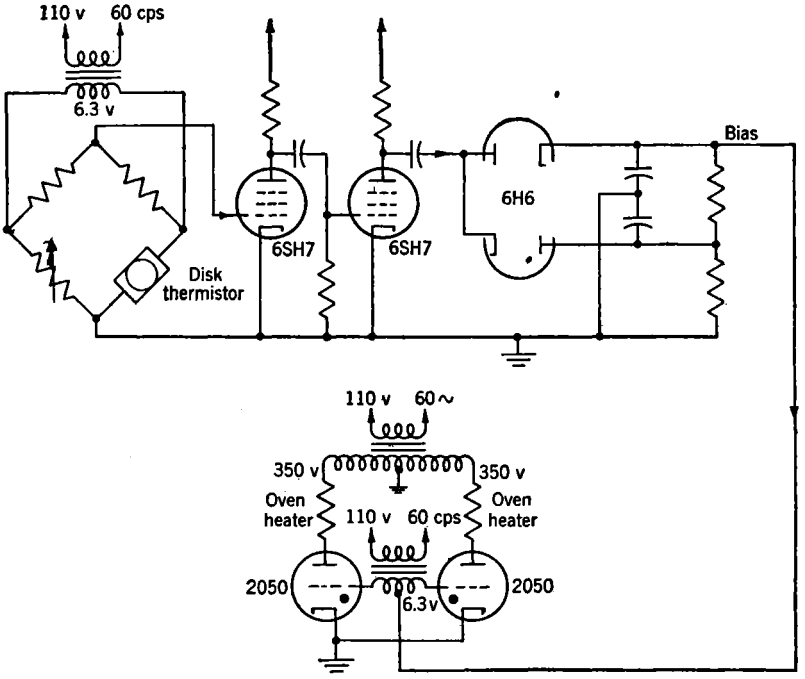

FIG. 3·20.—Schematic diagram of an oven temperature-control circuit using a disk thermistor as the control element.

wool is stuffed both inside and outside the coil form to reduce the tendency for "overshooting."[1] It is important to isolate the thermistor mount thermally from the microwave transmission line extending from the oven in order to avoid a direct conduction path of low thermal impedance. A length of coaxial cable or a section of metalized-plastic waveguide is effective for this purpose.

A more elaborate but more exact control of temperature can be realized by the use of a disk thermistor as the control element; see Fig. 3·20.

[1] "Notes on the Design of Temperature Control Units," General Radio Experimenter, Vol. XIX, No. 3, Aug. '44. Cambridge, Mass.

The disk thermistor constitutes one arm of an unbalanced bridge which is driven at 60 cps through a filament transformer. The disk is installed on the body of the bead-thermistor mount. Fluctuations in the temperature of the disk vary the output voltage of the unbalanced bridge. This output voltage is amplified and detected to provide a bias voltage which varies with temperature. The bias voltage controls the firing time of thyratrons whose plate supply is derived from a power transformer. Firing can be controlled over one-fourth of a cycle for each tube. Since the oven heaters constitute the load on the thyratrons,

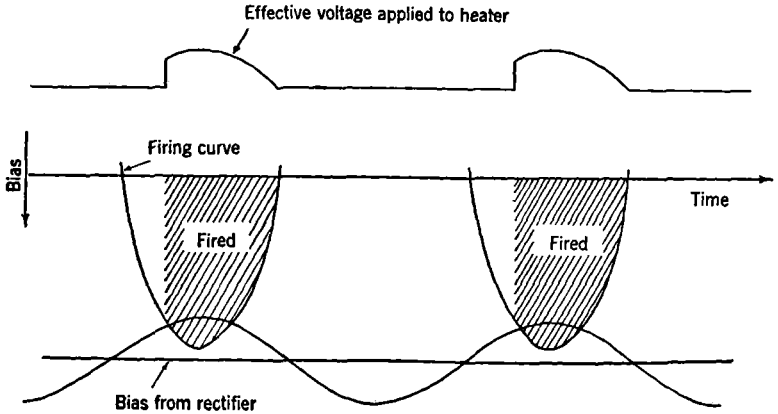

FIG. 3·21.—Diagram illustrating the action of thyratrons in the circuit of Fig. 3·20.

the average power supplied to the heaters can be varied by a factor of two.

The effective firing curve for one thyratron is shown in Fig. 3·21. By superimposing an a-c signal on the bias voltage, the intersection of the firing-signal and firing-voltage curves can be made more nearly normal, thus minimizing erratic firing. A filament transformer can be used for this purpose, as indicated in Fig. 3·20.

The oven used with the circuit can be very simple. Since no relays are involved the control is continuous, and no thermal insulation is needed between heaters and thermistor mount to reduce cycling effects. The resistance-wire heaters are tightly wound around the thermistor mount and coated with a paste which hardens to a porcelain-like material. The entire mount is then encased in a small box. A properly designed circuit of this type will hold the amplitude of the ambient-temperature cycle of the bead thermistor to within ± 0.1°C.

In this application of the disk thermistor it is not required that the disk and bead thermistors be at exactly the same ambient temperature. Rather, it is required only that the small temperature gradient between

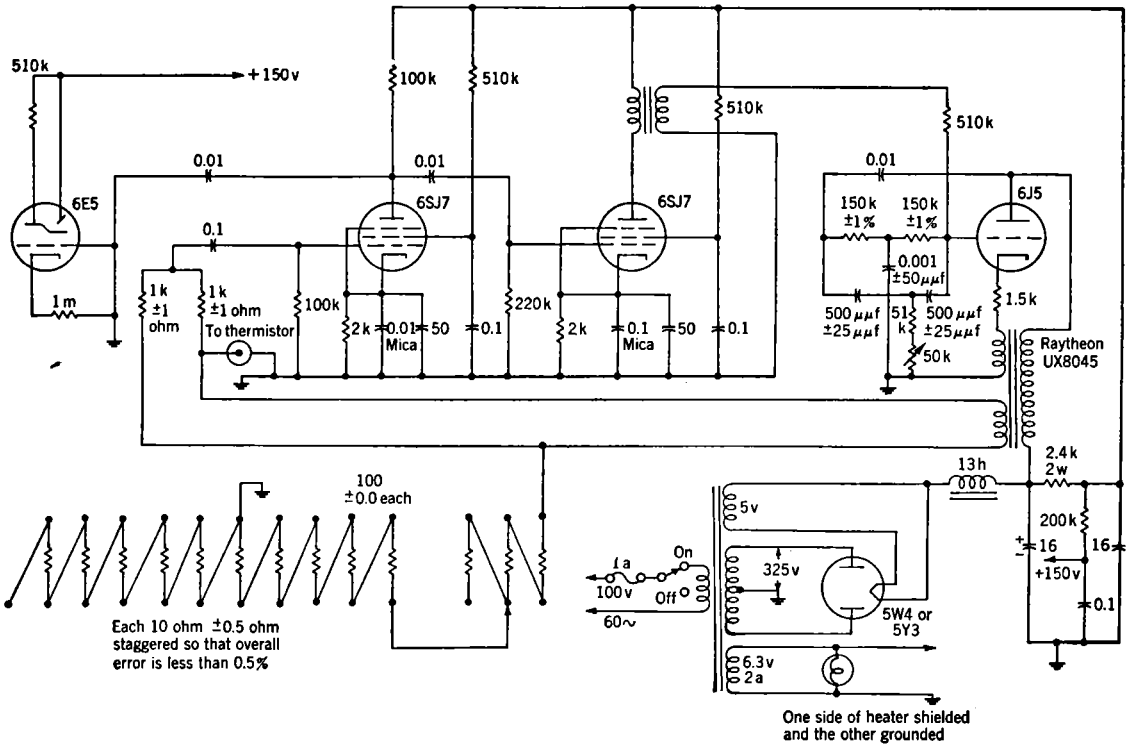

FIG. 3·22.—Circuit diagram of a self-balancing thermistor bridge.

the two be constant. This condition is readily met since the ambient-temperature range is extremely limited within the oven.

3·12. Self-balancing Bridges.—It is possible to design a self-balancing a-c bridge circuit[1] that utilizes the principle of negative feedback for control. Such a circuit is shown in Fig. 3·22. It was developed to serve as a tool for the microwave impedance-matching of thermistors. Many thermistor mounts have tuning mechanisms that must be adjusted for optimum broadband performance, and it is necessary to maintain the thermistor at a specified resistance while making these adjustments. This is conveniently accomplished by installing the thermistor in a self-balancing bridge circuit to obviate the necessity of frequent manual rebalance during this period of mount adjustment.

A 6J5 a-f oscillator, tuned to approximately 2000 cps, supplies bias power to the bridge. Any out-of-balance voltage across the bridge is amplified by two 6SJ7 stages, and is applied back to the grid of the oscillator so as to change the oscillator output voltage in the direction required to restore bridge balance. A twin-T resistance-capacitance feedback network is used to stabilize the oscillator frequency. This network includes a 0.1-megohm potentiometer to vary the oscillator output voltage. In order to minimize the feedback necessary to maintain bridge balance, the oscillator output voltage is advisedly adjusted to a level only slightly higher than that needed to balance the bridge at the *lowest* thermistor resistance to be considered. The first amplifier stage drives the grid of a normally open 6E5 magic-eye tube. Any appreciable out-of-balance voltage causes the 6E5 to bias itself to cutoff, and the eye closes. Consequently, the eye provides a convenient indication of the satisfactory operation of the bridge. Leads need not be shielded if they are short, but 60-cps pickup on the feedback leads can unbalance the bridge by changing the oscillator output voltage.

In practice, it is necessary to connect the thermistor and to set the resistance-level selector switches at the desired thermistor resistance. The circuit will hold the thermistor resistance within 2 ohms of the selector-switch setting—adequate control for ordinary requirements. No attempt has been made to modify this circuit to permit measurement of the microwave power that is dissipated in the bead while the mount is being adjusted. However, the Bell Telephone Laboratories have developed a self-balancing bridge for power measurement which utilizes a similar feedback loop to maintain the balance.[2]

The BTL bridge, like the V-bridge, relies on a constant d-c bridge driving voltage to maintain sensitivity independent of ambient temperature. Unlike the V-bridge, it uses a second bead thermistor rather than

[1] L. Mann, "Thermistor Bias Supply," RL Report 55-7/17/44A.

[2] "Temporary Instruction Manual for X-66399A Power Meter," BTL.

a disk thermistor as the control element for the a-f bridge power, and an a-f feedback loop to maintain automatically approximate bridge balance over a wide ambient-temperature range. The second or com-

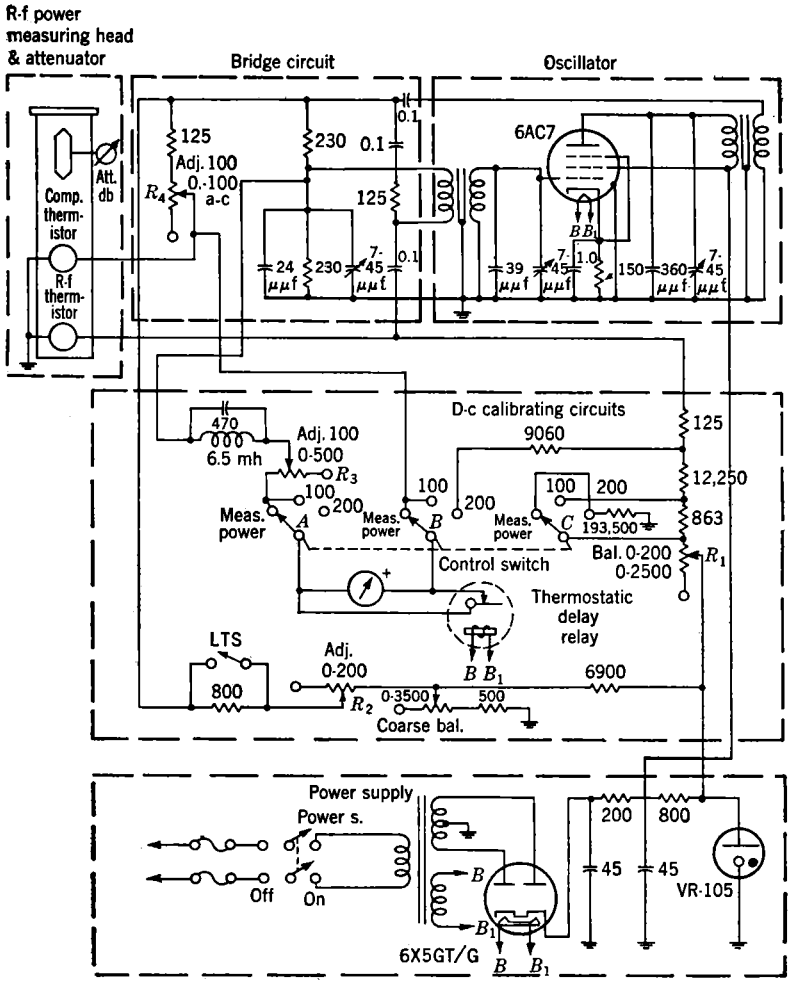

FIG. 3·23.—Circuit diagram of the BTL self-balancing thermistor bridge circuit.

pensating bead is installed in a separate "slave" bridge, as shown in Fig. 3·23.

The d-c power in the microwave bead is standardized at 7 mw with the d-c microammeter switched to the "200" position where it serves as a high-impedance voltmeter across the r-f thermistor. Since the r-f

bridge is *always* in balance, the bead resistance is known and the d-c power standardization can be made by adjustment of R_1 to place the correct d-c voltage across the r-f bead. When the control switch is turned to the MEAS-POWER position, the d-c voltage is unchanged. The total bead power required for balance of the r-f bridge is greater than 7 mw, hence the deficit must be met by the oscillator. However, the oscillator also transmits power to the bead in the compensating bridge. The amount is insufficient to balance the compensating bridge, and this deficit is corrected by varying the d-c power (R_2) until the meter reading indicates a condition of balance. At this point both bridges are balanced, each using a combination of alternating current and direct current to bring the thermistor to the desired resistance.

With the control switch set at the "100" position 8 mw of d-c power (an increase of 1 mw) flow into the r-f thermistor. The oscillator amplitude is reduced sufficiently to restore balance in the r-f bridge; however, this reduction in oscillator amplitude unbalances the compensating bridge. The resistance R_3 is then adjusted for a half-scale reading of the meter, thereby standardizing the bridge sensitivity at 2-mw full scale.

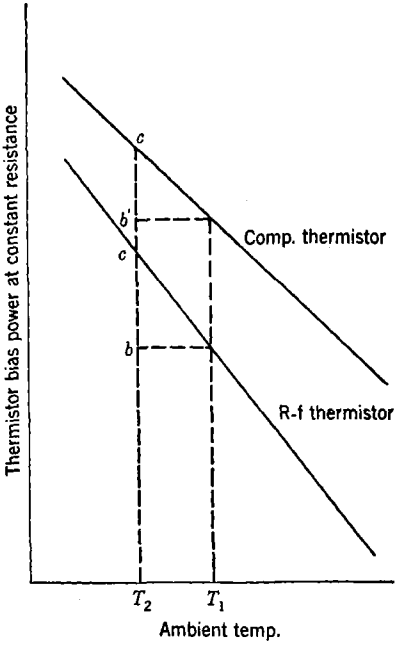

FIG. 3·24.—Diagram to illustrate principle of drift compensation in the BTL direct-reading thermistor bridge.

Although the a-f feedback loop will maintain balance of the r-f bridge over a wide temperature range, the slave bridge will not necessarily remain in balance throughout the whole of the same ambient-temperature range. Because of variations in the d-c characteristics of beads, some provision must be made in the circuit design to correct for these differences if the slave bridge is also to remain in balance. The solution of the problem is best explained by reference to Fig. 3·24.

Assume that two thermistors having characteristics as shown in Fig. 3·24 are placed in the bridge circuits. These characteristics show the variation in a-c thermistor power required to hold the thermistors at a constant value of resistance over a wide ambient-temperature range.

The slope characteristic (C-value of the bead) is constant and independent of the operating resistance of the bead. When the ambient temperature rises from T_2 to T_1, the a-c power required to hold the r-f bead at constant resistance decreases by an amount $b - c$. A proportional change in power occurs in the compensating thermistor, but since the slope of the curve of one thermistor is greater than that for the other a greater change in bias power is produced than is required for bridge balance. However, if R_4 is adjusted so that the proportion of a-c power into the two thermistors is correct for their individual slopes, the bridges will remain balanced for all variations in ambient temperature.

The sensitivity deviation with temperature is no greater than ± 0.1 db from $-40°C$ to $+55°C$. Over the same temperature range, the zero drift with no manual adjustments does not exceed ± 2.5 per cent full scale at a sensitivity of 2 mw full scale. An implicit advantage in this bridge design is the fact that the r-f thermistor is held at a constant resistance level; thereby the additional error introduced because the microwave impedance varies with varying bead resistance is avoided.

In addition to the circuits already discussed other direct-reading thermistor bridges have been developed which are simple variations of these designs. The development of thermistor-indicator circuits has progressed further than the development of thermistor mounts. Demands for increased bandwidth in the mounts will continue until a mount is developed that will be satisfactorily impedance-matched over the entire frequency spectrum from audio frequencies to microwave frequencies and beyond. On the other hand, a bridge design is relatively unaffected by bandwidth considerations and expansion of the present microwave region should offer no new problems in bridge design.

3·13. Thermistor Mounts.—The microwave transmission-line housing or "mount" for the thermistor is probably the most difficult design problem that arises in the development of thermistor equipment for microwave power measurement. The most obvious and most essential requisite of the mount is that it be closely matched to the characteristic impedance of the transmission line with which it is to be used. The exactness of the impedance match required is a function of the normalized generator impedance as measured at the input terminals of the thermistor mount. For example, if the generator is matched to the line, a thermistor mount having a voltage standing-wave ratio of 1.4 will cause an 8 per cent error in power measurement. However, if the generator VSWR is also 1.4, the error may lie anywhere within the range of 0 to 12 per cent, depending on the relative phase of the two mismatched impedances.

Tuning elements may be used to match the mount exactly to the transmission line at a specified microwave frequency. This is customary when the most accurate possible power determination is desired; how-

ever, it is more often true that a thermistor bridge must be operable over a broad frequency band with no frequency-dependent adjustments to complicate the operation. This demands a detector mount having a broadband impedance match. Unfortunately, from the viewpoint of the mount designer, the bandwidth requirements are often so broad that it is extremely difficult to maintain a close impedance match (hence negligible error in power measurement) throughout the frequency band. Consequently, it has been necessary to strive for the best possible broadband match realizable in the time alloted for the development, recognizing that the errors due to impedance mismatch at some frequencies will not be exactly negligible. In other words, accuracy is sacrificed for convenience in the operation of the equipment over a broad frequency band. These comments are considered necessary to justify the high maximum voltage standing-wave ratios that are accepted in some of the mount designs to be discussed.

The microwave leakage from or into the mount is important. If the power levels to be measured are very low or if the mount is to be used in a signal-generator power-monitoring circuit, it must be designed so that there is no effective leakage path in shunt with the thermistor. If the mount is to be used in a bridge circuit for absolute power measurement, it should not have any sources of power dissipation other than the thermistor. "Lossy" tuning elements and other defective electrical contacts must be carefully avoided.

For convenience in discussion, thermistor mounts may be classed as untuned, fixed-tuned, or tunable. An untuned mount is one that incorporates no *readily adjustable* tuning (or matching) element. It is designed so that the thermistor with average microwave characteristics is satisfactorily impedance-matched over the specified frequency band. Untuned mounts are commonly used in the 10-cm band and longer wavelengths, where the variations in the impedance characteristics of thermistors are relatively small. At shorter wavelengths it is usually necessary to use mounts of the other types. A fixed-tuned mount is one which incorporates tuning adjustments that are set in the laboratory for the individual thermistor and never changed. The adjustments are commonly made to effect a nearly perfect impedance match at the midband frequency, and the design of the mount dictates the extent of mismatch at the band edges. The tuning adjustments make possible some compensation for the variations in the microwave impedance characteristics of thermistors. Fixed-tuned mounts are commonly used at 3 cm and in the 1-cm band. Tunable mounts may be very similar to fixed-tuned mounts, except that the tuning adjustments are set for optimum impedance match at each frequency. The tuning mechanisms may be micrometer-operated so that tables of calibration

data can be prepared to facilitate proper settings at each frequency. Such a mount is advisable for use in precise power determinations where the broadband match of a fixed-tuned mount is not good enough. · Occasionally it is possible and practical, in balanced-bridge operation, to maintain a satisfactory impedance match over a broad band by varying the operating resistance (as a function of frequency) of a thermistor in a fixed-tuned mount. This is more convenient and economical than the use of an elaborate, calibrated tunable mount.

In general, two different approaches to the problem of designing fixed-tuned mounts have been tried, and each has its merits. In some instances it may be found preferable to design a preliminary untuned mount so that a reasonably satisfactory impedance match is obtained without resort to any tuning adjustments. The addition of tuning elements that introduce *small* reactance variations permit a more exact impedance match over a broader band. The tuners act simply as "trimmers," and are usually installed near the detector element. An alternative and sometimes necessary procedure is to accept an initially bad impedance match in the untuned mount, and to use high-reactance tuners, often placed an appreciable distance from the detector element, to effect the desired match. The success of the latter approach depends heavily on the impedance characteristics of the untuned mount as a function of frequency and on the reproducibility of the impedance characteristics of the detectors.

In waveguide mounts the operating resistance of the bolometer is customarily chosen at approximately the characteristic impedance of the waveguide. Experience has shown that this choice usually leads to optimum broadband matching. In coaxial lines the bolometer is more commonly operated at a resistance greater than the characteristic impedance of the line. The impedance of the line is so low, usually 50 ohms, that a thermistor would be operating too close to burnout and would demand excessive bridge current at this resistance level.

3·14. Untuned Coaxial-line Thermistor Mount.—Figure 3·25 shows the construction of an untuned thermistor mount developed for 10-cm-band use. This construction has been used in both $\frac{5}{8}$- and $\frac{7}{8}$-inch, 50-ohm coaxial lines. The center conductor of the mount is supported by a broadband quarter-wavelength stub. The thermistor is installed in series with the line at the end of a half-wavelength tapered section of the inner conductor. A 1- to 2-mil mica or polystyrene wafer, part (1), terminates the transmission line in a short circuit for microwaves and an open circuit for direct or audio-frequency current. In contrast, the stub line provides a short circuit or "return path" for direct current, and an open circuit for microwaves.

The small end of the truncated inner-conductor taper is drilled, and

two normal, diametrical saw cuts are made to form a set of four fingers to pressure-grip one of the thermistor lead wires. The opposite lead wire extends through a brass disk, part (2), which has a set of four coned contact fingers similar to, but shorter and stiffer than, those on the inner-conductor taper. The brass disk (4) which seats on part (2) has a drilled cone with a cone angle smaller than that of the fingers on disk (2). Consequently, pressure of part (4) against part (2) forces a firm grip on the thermistor lead wire. The polystyrene disk (6) and ring (7) prevent a d-c short circuit within the cap assembly. Parts (5) and (8) include the inner and outer conductors of a standard Amphenol or Selectar coaxial-line fitting to connect the thermistor to its bridge circuit.

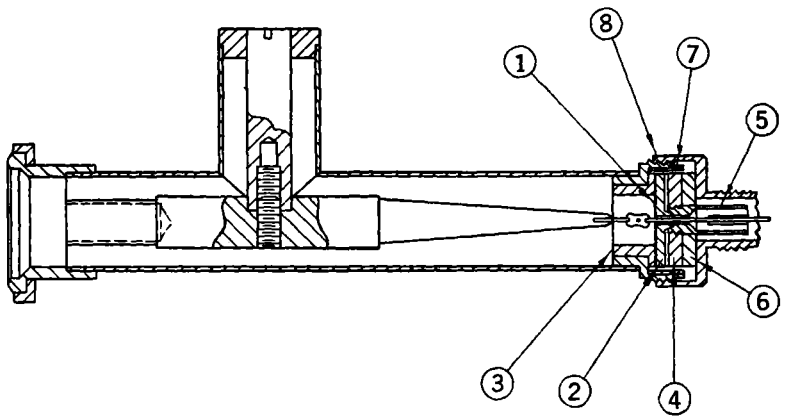

FIG. 3·25.—Drawing of a coaxial-line untuned thermistor mount for 10-cm band.

The impedance characteristics of the mount are influenced appreciably by the inner-conductor taper and by the choice of hole diameter in part (3). The taper length is chosen as $\lambda/2$ at the midband wavelength. The ID of sleeve (3) dictates the thermistor operating resistance at which best impedance-matching is realized. The optimum operating resistance is found to decrease with the ID of the sleeve, and this variable may be used effectively in designing a mount to operate with an available bridge circuit. Adjustment of this dimension affects both the distributed capacitance and distributed inductance of the short length of transmission line surrounding the thermistor capsule. At the same time, adjustment of the operating resistance of the bead influences both the reactive and resistive components of the series impedance caused by the bead. It is believed that a proper combination of the two factors results in a resonant circuit with a very low Q because of the loading provided by the bead. Such a low-Q resonant circuit in conjunction

with a line taper could be expected to present a broadband impedance match.

TABLE 3·4.—INFLUENCE OF THERMISTOR RESISTANCE ON VSWR OF UNTUNED THERMISTOR MOUNT

Resistance	100 ohms	150 ohms	200 ohms	250 ohms	300 ohms	350 ohms
VSWR at 9 cm	2.75	1.9	1.5	1.3	1.2	1.2
VSWR at 10 cm	2.45	1.7	1.4	1.25	1.3	1.4
VSWR at 11 cm	2.15	1.4	1.1	1.1	1.3	1.5

Table 3·4 shows the influence of the operating resistance of a D-166382 bead thermistor on the VSWR of a $\frac{7}{8}$-in. coaxial mount of the untuned type shown in Fig. 3·25. The tabulated data suggest 250 ohms as a desirable operating resistance. Table 3·5 demonstrates the broadband characteristics of the mount for twelve D-166382 beads chosen at random and operated at 250 ohms. The problem of thermistor variations is clearly apparent from the data of Table 3·5.

TABLE 3·5.—DATA TO ILLUSTRATE BROADBAND IMPEDANCE MATCHING OF UNTUNED $\frac{7}{8}$-INCH COAXIAL MOUNT, WITH TWELVE D-166382 THERMISTORS, OPERATED AT 250 OHMS

	8.0 cm	9.0 cm	9.8 cm	10.7 cm	11.6 cm	12.5 cm
Max. VSWR	1.28	1.27	1.30	1.23	1.15	1.14
Min. VSWR	1.07	1.12	1.10	1.07	1.05	1.05
Avg. VSWR	1.16	1.22	1.14	1.13	1.10	1.10

The installation of the bead in the untuned coaxial-line mount is extremely critical. It is necessary to make the sleeve, part (3), long enough to accept the longest glass capsule length within tolerances. Since these tolerances are large, some capsules will require that no more than 80 per cent of the sleeve length be used. In this case the capsule must be installed so that the bead within the capsule is as close as possible to the short-circuited end of the transmission line. The farther the bead is removed from the short circuit, the greater the reactance in series with it that is caused by the short-circuited length of transmission line. Table 3·6 illustrates the importance of proper positioning of the bead within the mount. The data were taken with a D-166382 thermistor operating at 250 ohms in an untuned $\frac{7}{8}$-in. coaxial-line mount. The gap distance mentioned in Table 3·6 refers to the gap between the end of the glass capsule and the mica wafer, part (1).

Comparable impedance matching has been obtained with $\frac{5}{8}$-in. untuned coaxial mounts. In both the $\frac{5}{8}$- and $\frac{7}{8}$-in. models, empirical

attempts were made to improve the impedance matching further by tapering the front end of sleeve (3). The blunt end shown in Fig. 3·25 was found to be as good as, or better than, any of several tapers that were tried.

TABLE 3·6.—INFLUENCE OF THE POSITION OF THE THERMISTOR WITH RESPECT TO THE SHORT CIRCUIT ON THE CHARACTERISTICS OF THE UNTUNED MOUNT. VALUES OF VSWR AT VARIOUS WAVELENGTHS

Gap distance, mm	8.0 cm	9.0 cm	9.8 cm	10.7 cm	11.7 cm	12.5 cm
0	1.22	1.15	1.12	1.09	1.09	1.09
1	1.35	1.30	1.25	1.16	1.04	1.04
2	1.5	1.35	1.20	1.17	1.03	1.06
3	1.55	1.5	1.35	1.17	1.05	1.09
4	1.6	1.5	1.4	1.22	1.06	1.09
6	2.0	1.9	1.65	1.33	1.19	1.22
8	2.5	2.1	1.95	1.55	1.31	1.35

This mount construction has maximum practicability in the 10-cm-band region. For wavelengths much longer than 10 cm, the $\lambda/2$ taper becomes objectionably long. For wavelengths much shorter than 10 cm the increasingly pronounced variations in the impedance characteristics of the thermistors demand a fixed-tuned or tunable mount design.

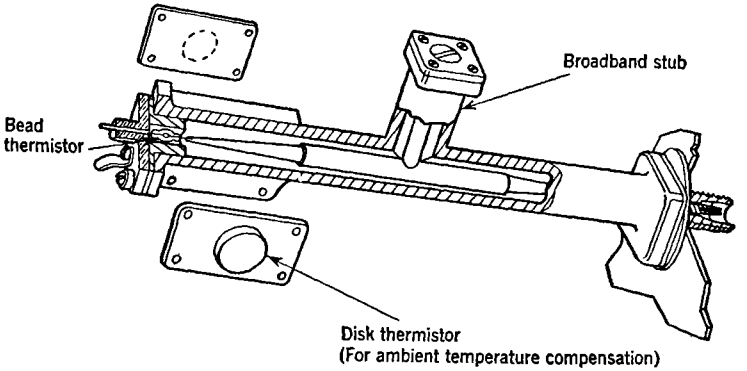

FIG. 3·26.—Drawing of the untuned coaxial thermistor mount with disk thermistors.

Figure 3·26 shows a drawing of the assembled untuned thermistor mount. The mount includes a built-in, constant-impedance taper from the $\frac{7}{8}$-in. coaxial line to a type N jack fitting. The brass block for mounting a disk thermistor is clearly shown. Such a design is used when it is necessary to connect the mount to a flexible microwave cable. However, flexible cables should be avoided in power measurements whenever

possible. Cable fittings often introduce appreciable reflections which effectively increase the VSWR of the thermistor mount.

3·15. A Double Thermistor Mount.—A British research agency, Radar Research Development Establishment, has designed a novel 70-ohm, coaxial-line thermistor mount[1] that uses *two* bead thermistors to dissipate the microwave power. The construction is shown in Fig. 3·27. The coaxial line is terminated by a T located in a round, pillbox cavity. The cavity is nonresonant, and the position of the bottom plate is said not to be critical. The thermistors are in parallel for microwaves but in series to direct current. The series combination comprises one arm of a d-c bridge circuit which uses disk thermistors for temperature compensation. The most interesting feature of this untuned mount is that the series combination of thermistors obviates the necessity of using a stub support for the d-c bridge return. In addition, no tapers are used, and the mount can be made extremely compact. The maximum VSWR of the mount is 1.25 over the 9- to 11-cm band.

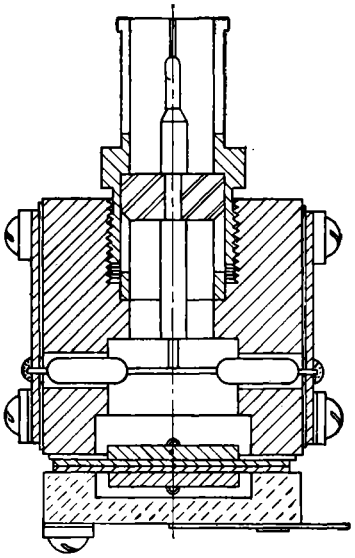

FIG. 3·27.—Section drawing of the Radio Research Development Establishment 10-cm-band thermistor mount.

3·16. Broadband Coaxial-line Thermistor Mounts.—A different technique for achieving broadband impedance matching has been used in a 30-cm band (780 to 900 Mc/sec) coaxial thermistor mount. A simple diagram of the construction is shown in Fig. 3·28.

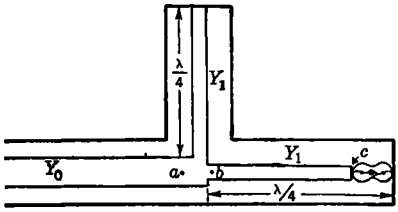

FIG. 3·28.—Diagram of a 1000-Mc/sec coaxial thermistor mount.

A stub and a series-transformer section, each $\lambda/4$ long, are used to impedance-match the thermistor. The bead is operated at a resistance *twice* the value of the characteristic impedance of the transmission line with which the mount is to be used. The design principle is valid only if this condition is met. As previously stated, there are objections to

[1] G. F. Gainsborough, personal communication.

operating a thermistor at a resistance as low as 50 or 70 ohms, the common values of the characteristic impedance for coaxial lines; however, operation of the bead at 100 or 140 ohms is not objectionable. The design principle involved is particularly applicable at relatively long wavelengths where the reactive component of the thermistor impedance is both small and relatively frequency-insensitive.

At the midband wavelength, the $\lambda/4$ stub has no influence on the input impedance of the mount, and the series transformer accomplishes the impedance match. If the mount were to be used as a narrow-band mount, it would be entirely satisfactory to follow elementary design practice and specify the characteristic impedance of the series transformer as the geometric mean of the desired input impedance of the mount and the thermistor impedance at point c in Fig. 3·28. However, for broadband use, there is an advantage to specifying a characteristic impedance for the transformer (and stub line) which is somewhat different from the geometric-mean value. Moreover, the stub and series transformer tend to cancel reflections at wavelengths removed from the midband wavelength.

Referring to Fig. 3·28, let Y_0 be the characteristic admittance of the line to the left of the stub, and let Y_1 be the characteristic admittance of both the stub and series-transformer sections of line. Let y_a, y_b, and y_c be, respectively, the admittances at points a, b, and c of the line to the right of these points. Let y_s be the admittance of the stub line. Then

$$y_a = y_b + y_s \tag{49}$$

$$y_s = -jY_1 \cot \beta l_0 = -j\frac{Y_1}{P}, \tag{50}$$

where

$$P \equiv \tan \beta l_0,$$

$$l_0 = \frac{\lambda_0}{4}.$$

The admittance y_c of the thermistor at point c can be transposed to point b by the equation

$$y_b = Y_1 \cdot \frac{y_c + jY_1P}{Y_1 + jy_cP}. \tag{51}$$

If Eqs. (50) and (51) are substituted in Eq. (49), and y_a is set equal to Y_0 since a match is desired,

$$Y_0 = Y_1 \frac{y_c + jY_1P}{Y_1 + jy_cP} - j\frac{Y_1}{P}. \tag{52}$$

If Eq. (52) is solved for y_c/Y_0,

$$\frac{y_c}{Y_0} = \frac{1 - j\dfrac{Y_1}{Y_0}\left(P - \dfrac{1}{P}\right)}{2 - j\dfrac{Y_0}{Y_1}P}. \tag{53}$$

By inspection of Eq. (53), it is apparent that if y_c/Y_0 equals $\frac{1}{2}$ (that is, the thermistor is operating at a resistance of $2Z_0$), and if the mount is impedance-matched, then

$$\frac{Y_0}{Y_1}P = 2\frac{Y_1}{Y_0}\left(P - \frac{1}{P}\right)$$

or,

$$P^2 = \frac{2Y_1^2}{2Y_1^2 - Y_0^2}. \tag{54a}$$

At the midband wavelength $P = \infty$, and

$$Y_1 = \frac{Y_0}{\sqrt{2}}. \tag{54b}$$

This is the result that the above-mentioned geometric-mean calculation gives. However, P^2 is approximately equal to 80 at the ends of the 780- to 900-Mc/sec band, and better broadband performance can be expected if

$$Y_1 = \frac{Y_0}{\sqrt{2}} \cdot \sqrt{\frac{80}{79}}. \tag{54c}$$

This technique of impedance matching leads to a VSWR-λ curve like that of the dashed curve in Fig. 3·29. In contrast, the solid curve in Fig. 3·29 is typical of a narrow-band mount. It is possible with a mount of this type to meet the specification of a maximum VSWR of 1.3 over the 780- to 900-Mc/sec band. However, it is necessary to use the mount as a fixed-tuned mount by making the stub length adjustable over a small range on each side of the nominal λ/4 length. This adjustment compensates effectively for thermistor impedance variations.

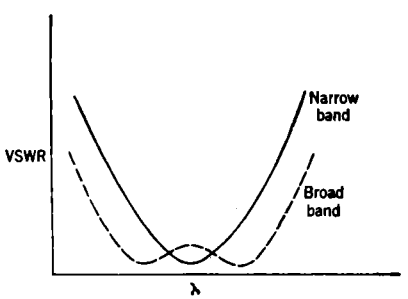

FIG. 3·29.—Typical VSWR-λ curves for narrow- and broadband thermistor mounts.

A number of variations on the stub—series-transformer matching technique have been developed. In some instances the thermistor is not placed at the short-circuited end of the transmission line as is done in the above-discussed coaxial mounts, but is located as much as λ/2 from the short circuit. The frequency-sensitive impedance of the line between the thermistor and the short circuit can be used as an additional variable in effecting a broadband impedance match. Also, in one design as a fixed-tuned mount, the position of the short circuit with

respect to the thermistor is often varied (as an end-plunger adjustment) to compensate for impedance variations in thermistors. The Bell Telephone Laboratories have made effective use of the frequency-sensitive impedance of such a line length in the design of several coaxial thermistor mounts. Table 3·7 lists the current series of BTL coaxial mounts, any one of which meets the specification of a maximum VSWR of 1.4 over the stated frequency band.

TABLE 3·7.—SUMMARY OF COAXIAL THERMISTOR MOUNTS DEVELOPED BY THE BELL TELEPHONE LABORATORIES

Frequency range, Mc/sec	Thermistor operating resistance, ohms
4000 to 5000	125
3400 to 4000	100
2400 to 3400	100
700 to 1500	100
50 to 500	Characteristic impedance of coaxial line.

3·17. A 3-cm Thermistor Mount.—A British laboratory, TRE, has devised a fixed-tuned coaxial thermistor mount for use in the 3-cm band. A 50-ohm coaxial line is joined to rectangular waveguide by a crossbar or doorknob type of adapter. The coaxial line is extended $\lambda/2$ from the adapter (to avoid high-order mode coupling) before the inner and outer conductors are reduced in diameter by conical tapers. The taper length is approximately one wavelength, and reduces the ID of the outer conductor from $\frac{1}{2}$ to $\frac{1}{4}$ inch. The inner-conductor taper terminates in small fingers. The thermistor capsule is installed in series with the inner conductor and is adjustable in position with respect to the short circuit at the end of the coaxial line. This adjustment serves as the sole tuning variable in the mount. It has been possible with this design to meet the matching specification of a maximum VSWR of 1.3 over the 3.13- to 3.53-cm band, including the effect of the imperfect waveguide-to-coaxial-line adapter. The thermistor is operated at 250 ohms.

3·18. Waveguide Thermistor Mounts.—In waveguide mounts the thermistor is installed across the waveguide with the lead wires parallel to the narrow sides of the waveguide. It is usually placed in the middle of the waveguide where the electric field is a maximum. The lead wires are customarily brought out through coaxial stubs—the construction suggesting an adapter from waveguide to coaxial line which is heavily loaded by the resistance of the thermistor bead. One lead wire is grounded to the waveguide, and the other is insulated from the waveguide for direct and audio-frequency currents. The waveguide is terminated in a short circuit placed at an appropriate distance from the thermistor.

Figure 3·30 shows schematic section drawings of two fixed-tuned designs of waveguide thermistor mounts for 3-cm-band use. The

narrow-band mount, developed by the Radiation Laboratory, uses an adjustable stub and an adjustable end-plunger for the waveguide short circuit. The stub length is approximately $\lambda/2$ for optimum match with a thermistor of average impedance characteristics. The two stub lengths, zero and $\lambda/2$, present short-circuit impedances to the thermistor. Consequently, the mount may be identified as a "short-short" or, simply, an "*S-S*" mount. In contrast, the second mount shown in Fig. 3·30 uses two $\lambda/4$ stubs which reflect open-circuit impedances to the ends of the thermistor capsule. This mount may be identified as an "*O-O*" mount. The *O-O* mount uses one adjustable stub and an adjustable waveguide shorting plunger. The Bell Telephone Laboratories were the first to use the *O-O* design, and other microwave research groups quickly followed their lead because of the increased bandwidth potentialities of the *O-O* design.

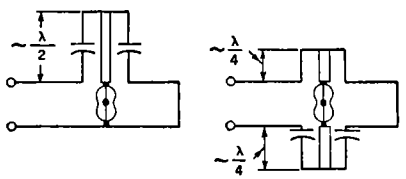

FIG. 3·30.—Section drawings of two rectangular waveguide thermistor mounts (narrow side views).

In the design of either the *O-O* or *S-S* mount, the objective is to make the change with frequency in the reactance of the stub lines counteract the change in the short-circuited length of the waveguide behind the thermistor. This is not *exactly* true because the thermistor bead has a frequency-sensitive impedance, and the prime objective, of course, is to maintain a matched mount impedance over a broad frequency band. It is fairly obvious, however, that the short-circuited lengths of coaxial stub lines and waveguide would seriously limit the bandwidth of the mount, were such a cancellation of reactances not possible. The rate of change of reactance with frequency of the short-circuited length of waveguide is dependent on the length of waveguide section involved. This length is set at the value required for midband match, and the associated rate of reactance change must be accepted, be it large or small. On the other hand, the rate of change of reactance with frequency in the stub line can be varied by selection of the characteristic impedance. Consequently, a means of matching the two rates in order to effect the desired cancellation of reactance changes exists.

In discussing waveguide thermistor mounts it is convenient to differentiate between the two quantities, mount admittance (or impedance) and thermistor admittance. The mount admittance is the quantity determined by a slotted-line measurement, and, unless otherwise specified, is referred to the plane of the thermistor bead. The thermistor admittance represents the contribution to mount admittance which is caused by the thermistor *and* the coaxial-line stub supports. Thermistor

admittance is calculated from mount admittance by subtracting from the latter the susceptance caused by the short-circuited length of waveguide behind the thermistor. The names of these admittance quantities have been loosely chosen, but their definitions are specific.

The effect of the several mount variables on thermistor and mount admittance can best be presented by reference to a series of admittance-

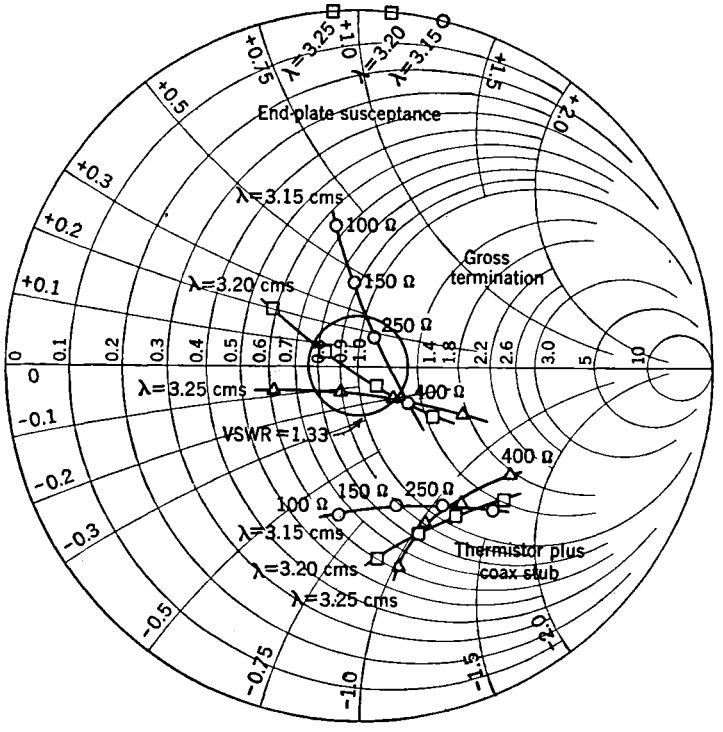

FIG. 3·31.—Admittance characteristics of a thermistor in the *S-S* mount.

circle diagrams.[1] Figure 3·31 shows both the thermistor and mount admittances as a function of λ and the operating resistance of the thermistor of a typical D-166382 thermistor in the *S-S* mount. The waveguide end-plunger has been adjusted so that the VSWR of the mount is under 1.35 over the 3.15- to 3.25-cm band, with the thermistor at a 250-ohm operating resistance. Several interesting observations may be made from Fig. 3·31. At any one wavelength it would be possible

[1] Figures 3·31 through 3·35 are taken from the final report: J. A. Becker, "The Investigation of the Effect of Manufacturing and Test Equipment Variables on the X- and K-Band Characteristics of Bell System Thermistors," NDRC No. 14-462, Bell Telephone Laboratories, July 30, 1945.

to obtain a perfect match by using the operating resistance of the thermistor and the end-plate adjustment as the two tuning variables. For example, at 3.20 cm a bead resistance of approximately 200 ohms would accomplish this. The marked frequency dependence of the mount admittance, particularly at relatively low thermistor resistances, is readily apparent; the mount is obviously not a broadband mount.

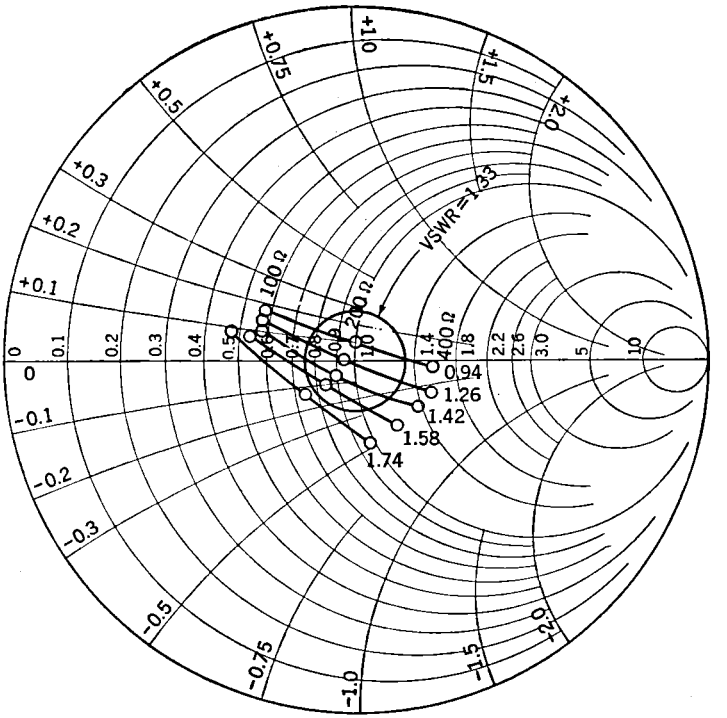

FIG. 3·32.—Effect of coaxial-stub length on the admittance characteristics of the *S-S* mount. Numbers adjacent to characteristics give stub lengths in centimeters.

The frequency sensitivity of the mount admittance is largely caused by the frequency dependence of the end-plate susceptance, since the points representing the 250-ohm thermistor admittance are much more closely grouped than the points representing the mount admittance.

Figure 3·32 shows the effect of stub tuning on the admittance characteristics of the *S-S* mount. The conductance component of mount admittance is particularly affected by the length of the stub line. Since most bridge circuits demand that the thermistor be operated at a specified resistance, the stub length and end-plate adjustment are the most commonly used tuning elements in the mount.

The end-plate adjustment should affect only the susceptance component of the mount admittance, unless the end plate is brought close enough to the thermistor to permit high-order mode coupling. However, it is possible for a sliding end-plunger which uses a tuned choke instead of contact fingers to effect a conductance as well as a susceptance change. Figure 3·33 illustrates this point.

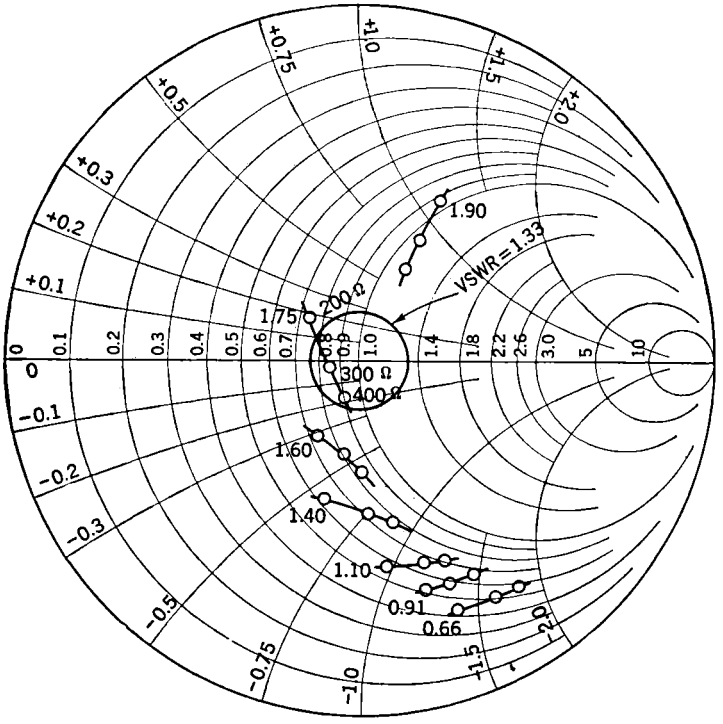

FIG. 3·33.—Effect of choke design end plate on the admittance characteristics of the *S-S* mount. Numbers adjacent to characteristics give the distance from the thermistor to the reflector in centimeters.

The effects of the coaxial-stub adjustment, end-plate adjustment and thermistor operating resistance on mount admittance are not vastly different in the case of the broader-band *O-O* mount. The additional bandwidth of the *O-O* mount is derived from the fact that the thermistor admittance shows mainly a conductance change (with λ) in the case of the *S-S* mount, and primarily a susceptance change in the case of the *O-O* mount. The susceptance change can be corrected over a broad frequency band by an end-plate susceptance of comparable magnitude and opposite sign. The conductance variation cannot be similarly

corrected, however. Figure 3·34 shows the plots of the mount admittance against frequency of several thermistors in an *O-O* mount. The curves tend to curl around the match point, $Y = 1 + j0$.

It is possible with the *O-O* mount to meet the specification of a maximum VSWR of 1.4 or less over the 3.13- to 3.53-cm band. The *S-S* mount will meet the specification of a maximum VSWR of 1.35 or less

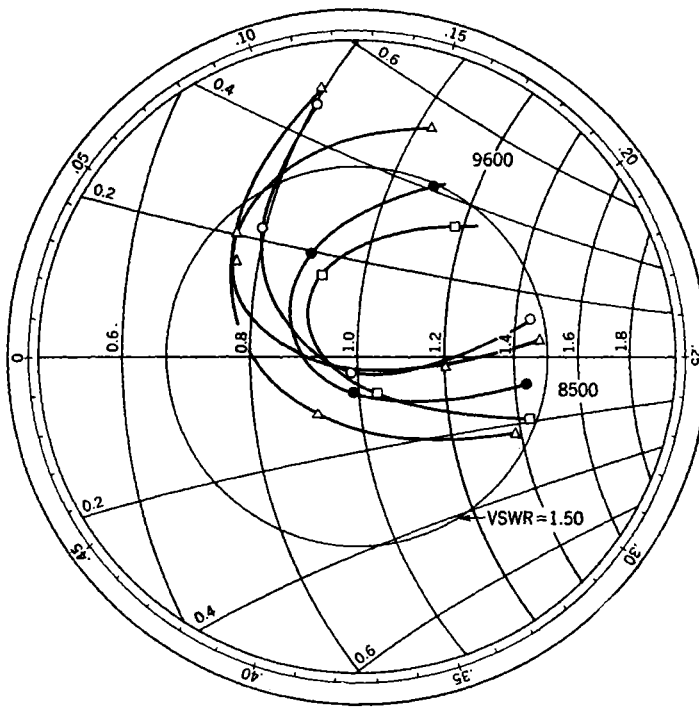

FIG. 3·34.—Mount admittance vs. frequency of several thermistors in an *O-O* mount.

over the narrower 3.15- to 3.25-cm band. These specifications are written so that most thermistors will meet them; a smaller percentage of thermistors will provide considerably better impedance matches than these VSWR values indicate.

When making the tuning adjustments to impedance-match a fixed-tuned mount, it is necessary to have some sort of impedance or VSWR indicator to indicate the progress of the adjustments. If a slotted line is used for this purpose, it is almost impossible to use more than two tuning variables. That is, the adjustment time may average 10 or more minutes when using a slotted line with a two-tuning-variable mount, and the inclusion of a third tuning variable would so greatly extend this time

that it is impractical to consider it. However, the development of the microwave impedance bridge (Chap. 9) has made possible the use of a third tuning variable—the vertical position of the thermistor bead (that is, bead height) within the waveguide. With this third tuning variable it is possible to reduce greatly the maximum VSWR specification for a given wavelength band. Moreover, all necessary tuning

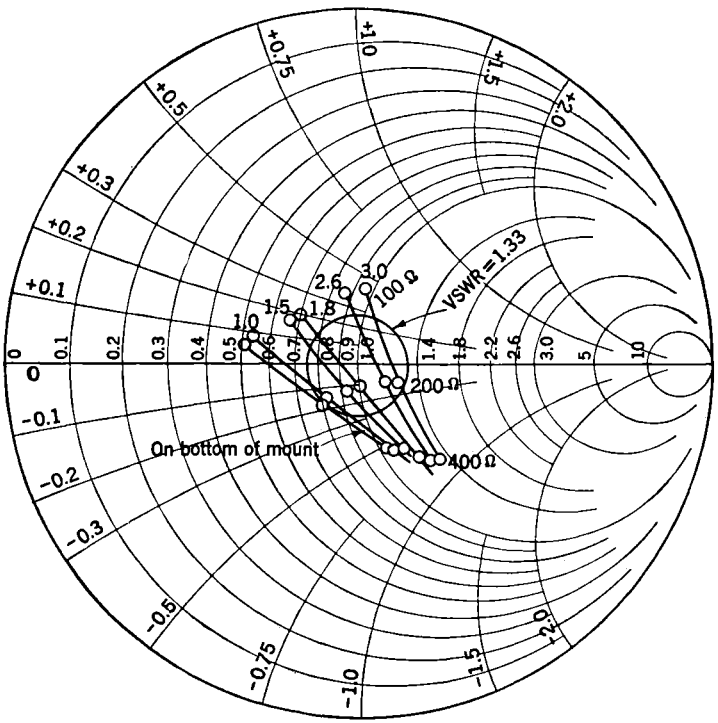

FIG. 3·35.—Effect of bead height on the mount admittance of the *S-S* mount. The numbers adjacent to the curves give the distances in millimeters from the end of the thermistor glass capsule to the bottom of the waveguide.

adjustments can be made, using the impedance bridge, in five minutes or less. Figure 3·35 shows the effect of bead height on the mount admittance of a D-166832 thermistor in an *S-S* mount. The effect in the *O-O* mount is approximately the same.

Figure 3·36 shows a detailed cross section (narrow-side view) of an *O-O* type of mount which has all three tuning variables. It has become known as the "tri-tuner" mount. The thermistor leads extend into $\lambda/4$ cup chokes to reduce microwave leakage into the stub lines. Bead height is adjusted by operation of the screw in the lower stub line. The

upper stub line is tuned by sliding the inner member along the thermistor lead wire and the bearing surface provided by the outer tube. The slidable end plate uses beryllium-copper contact fingers which are made $\lambda/2$ in length to guarantee a good short circuit at the tips of the contact fingers. Additional leakage protection is derived from the use of a polyiron sleeve (high d-c resistance, but high attenuation for microwaves) in the lower stub line, and a waveguide-beyond-cutoff extension of the outer tube of the upper stub line.

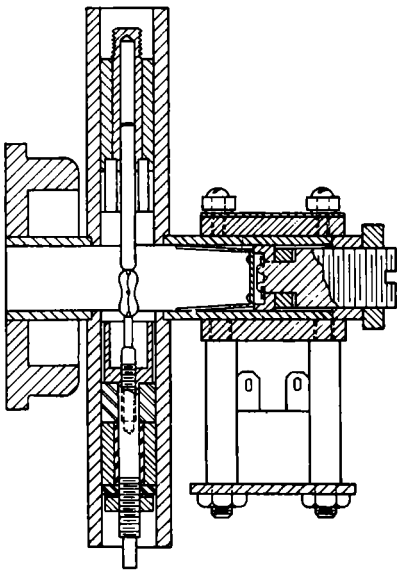

FIG. 3·36.—Drawing of the tri-tuner 3-cm-band thermistor mount.

It is possible with many thermistors using the tri-tuner mount to meet the specification of a maximum VSWR of 1·1 over the 3.13- to 3.53-cm band. In the worst case the maximum VSWR does not exceed 1.2 over this band. Moreover, these results may be obtained with operation of the thermistor anywhere within the resistance range of 100 to 300 ohms. Experience with the mount has shown that the thermistor should be lowered in the direction of the bottom stub line as the operating resistance of the bead is lowered. In the *O-O* mount using only two tuning variables, the bead height is standardized at a position which is optimum for the average thermistor. It is also possible, of course, to standardize on the upper stub length and to use bead height and end-plate adjustment as a set of two tuning variables.

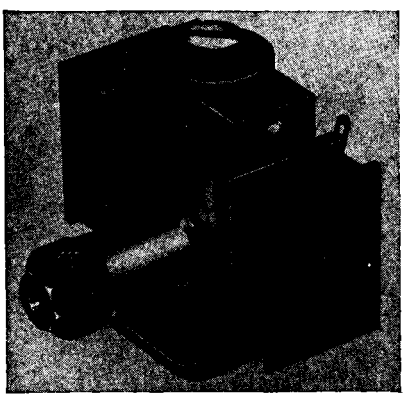

FIG. 3·37.—Photograph of an *O-O* 3-cm-band thermistor mount.

Figure 3·37 shows a photograph of an *O-O* thermistor mount. Disk thermistors, if desired, can be installed on the sides of the mount. The same technique for disk-thermistor mounting is used in the tri-tuner mount.

3·19. Impedance Variations of Thermistor Mounts.—Considerable research work has been done by the Bell Telephone Laboratories in investigating the sources of impedance variations in thermistors installed in *S-S* and *O-O* mounts.[1] The results of this work have made it possible for the Western Electric Company to improve their control on manufacturing variables, but troublesome impedance variations still exist.

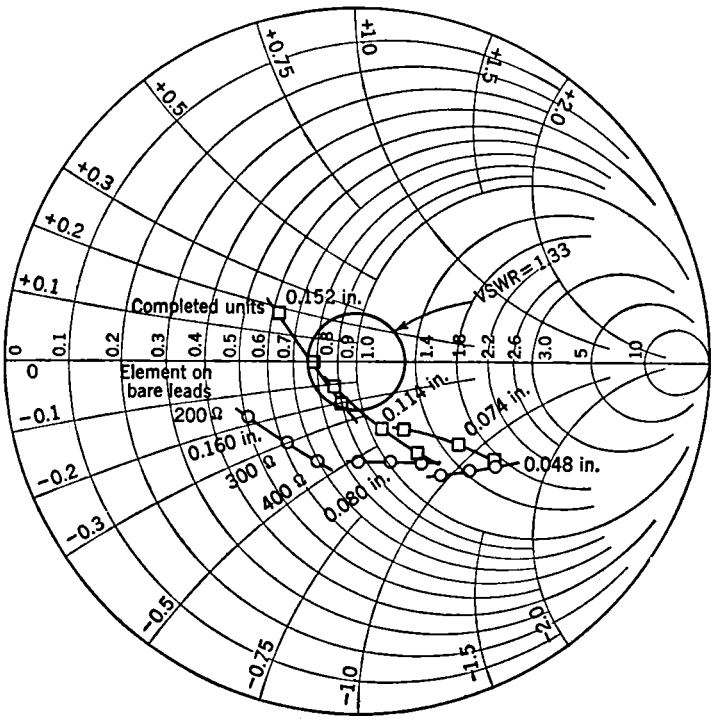

FIG. 3·38.—Effect of thermistor tie-wire length on mount admittance of an *S-S* mount for a wavelength of 3.20 cm.

Since most of the work in mount design has resulted from the necessity of studying match conditions for a large assortment of thermistors covering the range of anticipated impedance variation, it is worth while to review the more important conclusions presented in the BTL report. Further, the information should be valuable in selecting a proper thermistor mount for a new wavelength band.

One of the most important variables is the length of the 0.001-in.-diameter tie wires. These wires have an appreciable inductance at microwave frequencies. Further, the capacitance between the ends

[1] Becker, *loc. cit.*

(within the glass capsule) of the 0.030-in. lead wires must vary as the tie-wire length is altered. It is not easy to separate the two effects, but there appears to be little need for doing so since they are coexistent in manufacture. Figure 3.38 shows the effect of changing the tie-wire length on the mount admittance of an *S-S* mount. The effect of adding the glass capsule ("completed units") may also be seen. Small varia-

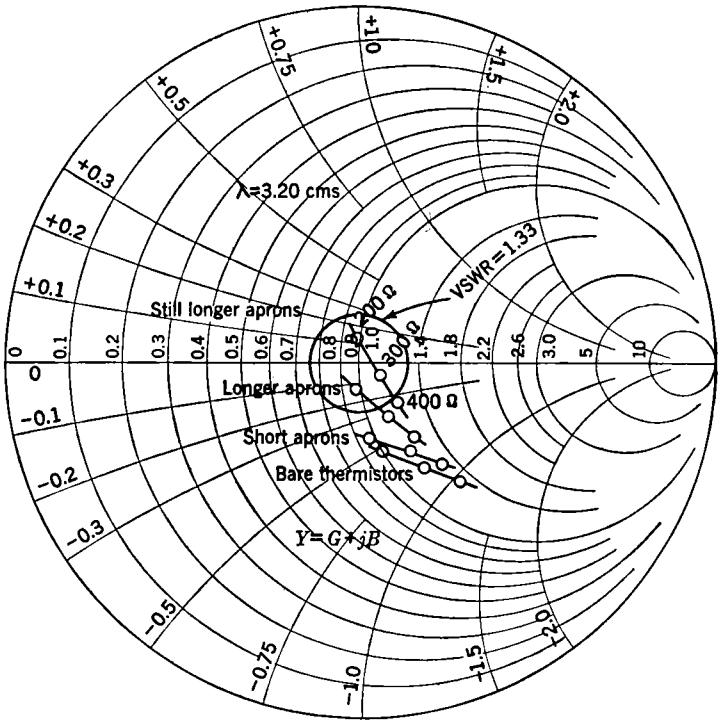

FIG. 3·39.—Effect on mount admittance of silver-paste aprons on the ends of the thermistor capsule.

tions in the mass of the glass capsule appear to affect the susceptance but not the conductance component of mount admittance. An increase in the mass of glass moves the susceptance toward a more positive point on the admittance diagram. This would be expected because of the additional capacitance due to the increased mass of dielectric.

Although no practical application has yet been made of the observation, it was found that thick silver-paste aprons on the ends of the glass capsule have an appreciable effect on the susceptance component of mount admittance. The apron capacitance accomplishes approxi-

mately the same result as increasing the mass of capsule glass. Figure 3·39 shows the effect of adding such aprons to the glass capsule.

There appears to be little direct connection between the d-c characteristics of the thermistor and its microwave impedance properties. Varying the percentage of copper oxide in the bead mixture has little effect on the final mount admittance, although this variation markedly affects the cold resistance (resistance at negligible current) of the bead. The size of the bead, however, has an important effect on the conductance component of the mount, with little or no effect on the susceptance component. The amount of glass loading on the bead and the sintering time and sintering temperature appear to be relatively unimportant variables.

Several attempts have been made to determine an equivalent circuit for the thermistor installed in a waveguide mount, but these have met with only partial success. For example, the simple circuit consisting of the thermistor admittance in series with the susceptance of the coaxial stub line, with the combination in parallel with the end-plate susceptance, can be used to predict the effect of end-plate and stub-line tuning on mount admittance. The thermistor itself is believed to have an equivalent circuit for microwaves similar to that shown in Fig. 3·40. The inductances L_1 and L_2 represent the inductances of the fine tie wires. The current flow through the bead follows two paths: the resistive path R_1 and the series RC-path in parallel with it. The RC-path is believed to represent the effect of the finite particle size of the sintered oxides within the bead. The current must in some cases bridge capacitive gaps caused by imperfect contact between adjacent particles of the mixture. The capacitance C_1 represents the combined effects of lead-wire capacitance and the dielectric of the glass capsule.

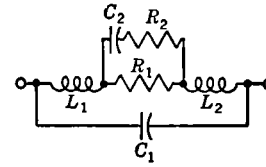

FIG. 3·40.—Proposed equivalent circuit for the thermistor.

Many of the more familiar broadbanding techniques are not practical for application to thermistor-mount design. For example, adapters[1] from waveguide to coaxial line can frequently be broadbanded by the proper placement of an iris or coaxial stub line of suitable susceptance. However, the variations in thermistor impedance are sufficiently great that such an iris can increase the mount mismatch for some thermistors while improving the match for others. This is particularly true if the iris or stub must be placed an appreciable distance ahead of the plane of the thermistor bead. An iris that could be readily adjusted in its position along the transmission line would undoubtedly be an effective

[1] F. L. Niemann, "S-Band Coaxial Line to Rectangular Waveguide Transitions," RL Report 802, Dec. 7, 1945.

tuning variable, but the mechanical and electrical problems of such a design have been too great to justify its careful investigation.

3·20. The Fishtail Mount.—A 3-cm-band rectangular waveguide mount, known as the "fishtail" thermistor mount, uses less conventional techniques for broadbanding. The section of waveguide between the thermistor and soldered end-plate is flared in the direction of the wide dimension of the waveguide. The flare increases the wide dimension to approximately twice its normal value, and extends over a length of 1.67 guide widths. The curvature follows the arc of a circle which is tangent to the waveguide at the plane of the thermistor where the flare

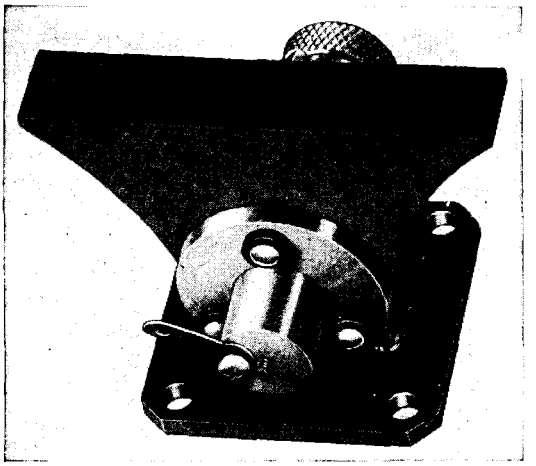

FIG. 3·41.—Photograph of the 3-cm-band fishtail thermistor mount.

is begun. The waveguide wavelength changes along the length of the flared region, and consequently the susceptance-frequency slope of the short-circuited length of waveguide is modified by the flare. The flared fishtail has been empirically shaped so that the susceptance of the short circuit approximately cancels the susceptive component of the thermistor admittance over a broad frequency band. Additional benefit is derived from placing the thermistor off-center, nearer one of the narrow sides of the waveguide than the other. This causes high-order modes to be set up, for which the flared termination acts as a resonant cavity. The susceptance-frequency characteristics of the back cavity are modified and an improvement of the susceptance cancellation results. The tuning variables in the mount are coaxial-stub length and bead height. It is possible with most thermistors to meet a specification of a maximum VSWR of 1.2 or less over the 3.13- to 3.53-cm band in this mount. Little use has been made of the fishtail mount because of an

unexplained resonance at approximately 3.10 cm, at which wavelength the VSWR often rises to very high values. Occasionally the resonance shifts into the 3.13- to 3.53-cm operating band for reasons not completely understood. Figure 3·41 shows a photograph of the fishtail mount.

3·21. Thermistor Mounts for the 1-cm Band.—Thermistor mounts for the 1-cm band are similar to 3-cm-band mounts, but their small physical dimensions preclude the use of a capsuled thermistor bead. Instead, the 0.001-in. tie wires are soldered or spot-welded to terminals that are an integral part of the mount. The mounts are mechanically designed so that they can be disassembled to facilitate the bead installation.

Figure 3·42 shows a cross section, looking into the waveguide end of a 1-cm-band thermistor mount. The bead is spot-welded halfway between the ends of the center conductors of the two coaxial stub lines. The stub lines are too small for sliding-plunger tuning. Consequently, a metal screw, projecting into the side of the lower stub line is used instead. Similarly, a screw is used to vary the susceptance of the short-circuited section of waveguide behind the thermistor. The latter screw projects through the center line of the broad dimension of the waveguide. A thin polystyrene sleeve and thin mica disk provide the necessary d-c insulation for the upper thermistor tie wire.

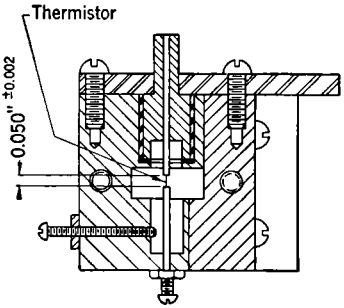

FIG. 3·42.—Drawing of a 1-cm-band waveguide thermistor mount.

The gap in which the thermistor bead is installed is small—0.050 in. The tie wires are not pulled taut prior to spot-welding, but are given a reasonable amount of slack. Each tie wire is approximately 0.030 in. long with the result that, with a 0.010-in. bead length, the total arc length is 0.070 in. The slack is necessary for two reasons, (1) to avoid snapping a tie wire when the mount is subjected to shock or vibration, and (2) to avoid excessive thermal conduction losses to the center-conductor supports. Figure 3·7 shows that the wires are shorter than is desirable from this latter point of view. In fact, two-disk bridge circuits using 1-cm-band mounts must take into account the somewhat smaller values of C of beads that are mounted in this way. The tie-wire inductance introduces greater reactance at the 1-cm band than at the 3-cm band, and the additional reactance associated with longer tie wires would seriously limit the broadband match of a mount of this type.

The desirable lengths and characteristic impedance of the stub lines have been experimentally determined. Optimum broadband impedance

matching is obtained with operation of the thermistor at a relatively low resistance, 100 to 150 ohms. At a standard operating resistance of 130 ohms many beads can be matched to a VSWR of 1.5 or less over a 2 per cent wavelength band centered at 1.25 cm.

The mount design has never been wholly satisfactory despite numerous attempts to improve it. The tiny No. 0-80 tuning screws must have an exceptionally snug fit in the threaded mount holes, must be free of dirt deposits, and must operate with negligible eccentricity. The various brass members of the mount must have accurately milled and cleaned machine fits. The microwave leakage was bad until it was found that an air-drying silver paste[1] is quite effective in electrically sealing the mount. Leakage was particularly bad in the vicinity of the end plate which is held by screws to the main body of the mount.

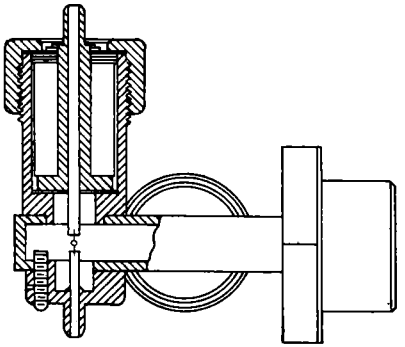

FIG. 3·43.—Drawing of a 1-cm-band thermistor mount. (Improvement on design shown in Fig. 3·42.)

An improved mechanical design of the 1-cm-band mount has been produced by the Aircraft Radio Corporation, Boonton, N. J. A section drawing is shown in Fig. 3·43. The shape of the stub has been changed and other alterations have been made to effect an improvement in impedance matching. With this design it is possible to meet a specification of a maximum VSWR of 1.4 or less over the 1.25 cm ± 2 per cent band.

The Bell Telephone Laboratories have designed a 1-cm-band thermistor mount that features a removable tunable coaxial stub line that houses the bead thermistor. The center conductor of the stub line extends as an antenna probe deep within the waveguide to within 0.020 in. of the bottom waveguide wall. The narrow gap between the end of the probe and the waveguide wall, together with an off-center positioning of the probe, leads to a broadband transition from waveguide to coaxial line. This, in fact, is the reason for the exceptionally good performance of the BTL mount. The thermistor-bead tie wires are soldered to the probe and to the cartridge case. The average thermistor bead in the BTL mount has a maximum VSWR of 1.4 over a ± 4 per cent band.

The problem of investigating thermistor impedance variations in the design of a 1-cm-band mount is extremely difficult. It is impossible

[1] Du Pont de Nemours Co., Wilmington, Del.

to remove an installed thermistor bead, and mount it again in exactly the same manner in the original or another mount. Likewise, it is difficult to determine allowable tolerances on the dimensions of various parts of the mount. Bead-impedance variations are, of course, more pronounced at 1 cm than at longer wavelengths. Collectively, these considerations explain why the design of the 1-cm-band mount has been a tedious and somewhat disconcerting task, and why the bandwidths that have been obtained are considerably less than those realized at 10-cm- and 3-cm-bands.

Thermistor beads that do not have the protection of a surrounding glass capsule are very sensitive to the cooling effect of air convection currents within the waveguide mount. This greatly aggravates the drift problem in the bridge circuit. It is advisable (even essential, at high bridge sensitivity) to seal the input end of the waveguide to the mount with a mica window or dielectric plug. The mica window, 0.001 in. thick to avoid reflections, may be installed at the choke-flange coupler at the input end of the mount. The dielectric plug may be fitted into the end of the mount and fills a short section of the waveguide ahead of the thermistor. Steps are cut into the ends of the plug to make it reflectionless. The dielectric material used has a negligible loss factor near 1.25 cm. Its temperature coefficient of expansion matches that of the waveguide walls, and a pressure fit is sufficient to hold it securely in position.

One problem has arisen in connection with 1-cm-band mounts. A comparison of the 1-cm-band thermistor mount with a water load assumed to be an absolute standard indicates that the 1-cm-band mount is lossy. That is, not all of the microwave power is dissipated in the bead, but some of it is lost in poor contacts and dissipative metal surfaces within the mount. Consequently, the 1-cm-band thermistor mount cannot be considered as an acceptable absolute standard for power measurement. The magnitude of the loss varies from mount to mount and depends largely on the excellence of the mechanical fits and on the surface cleanliness of the particular mount. The first indication of this loss resulted from calculations on the range of meter-shunt resistances needed to standardize the sensitivity of a two-disk bridge circuit using 1-cm-band beads of known values of J, B, and C. The calculated shunt resistances were much smaller than those found necessary when the bridge sensitivity was standardized against a water load. After eliminating other potential causes of the discrepancy, it was concluded that the mount must be lossy.

Barretters and thermistors installed in a mount of the same type (Fig. 3·42) were found to agree within the errors of power measurement, provided that the thermistor tie wires were held to within a total length

of 0.05 to 0.06 in. For tie-wire lengths as long as 0.10 in. the thermistor measured approximately 15 per cent less power than the barretter, indicating that there is some microwave power dissipation in the bead tie wires at 1-cm band. The thermistor bead with 0.05-in. tie wires was operated over a resistance range of 81 to 181 ohms; the power measured was unaffected by the operating resistance of the bead, provided the mount was tuned for match at each resistance level. These experiments prove nothing, however, regarding the suitability of either the thermistor (with short tie wires) or barretter as an absolute standard for power measurement.

A 1-cm-band thermistor mount of the type shown in Fig. 3·42 has been compared against a water load. The thermistor was operated in a d-c balanced bridge, all components of which had been checked against a precision potentiometer. The thermistor mount was sealed with silver paste, and the absence of microwave leakage was verified by moving absorbing and reflecting objects in the vicinity of the mount, with no consequent variations in the bridge-galvanometer reading. Troublesome video-frequency leakage from the magnetron modulator pulse was circumvented by installing a shielded bypass condenser in the d-c input cable to the bridge circuit. The water load used was one of the slot-coupled type (Sec. 3·34) which has no objectionable microwave leakage. A closed-flow system (Sec. 3·35) was used with the water load. A calibrated directional coupler was used to reduce the high-level magnetron power to the few milliwatts conveniently measured by the thermistor bridge. The final comparison between water load and thermistor involved a series of 10 runs. The power level measured by the thermistor was consistently lower than that measured by the water load; the values of the discrepancy varied from 15.8 per cent to 18.4 per cent, and averaged 17.2 per cent. An evaluation of all possible sources of error in both the thermistor and water-load measurements indicated that the apparent deviations could have corresponded to true deviations ranging from 12.9 per cent to 24.7 per cent. It is believed that lead-wire losses, tuning-screw losses, and losses in poor contacts within the mount are largely responsible for this.

The Bell Telephone Laboratories have also studied this problem, and report the following data on their 1-cm thermistor mount. A large number of mounts were compared with one another, with the following results: for 100 per cent of the mounts the maximum disagreement between any two was 0.3 db; for 90 per cent of the mounts the maximum disagreement between any two was 0.15 db. The maximum disagreement between a thermistor mount and a water load was 0.3 db. Thus, assuming the water load to be an absolute standard, the loss in the mounts varies from 0.15 to 0.3 db. It is the opinion of BTL that the

finger contacts in the coaxial tuning cavity were largely responsible for this.

3·22. Thermistor Power Monitors.—Special thermistor installations are sometimes used when the power delivered to a transmission-line load is to be monitored. For example, Fig. 3·44 shows a commonly used thermistor mount designed to monitor the output power from a 10-cm-band oscillator cavity. One lead wire of the capsuled bead is bent to form a pickup loop which projects, with proper orientation, into the cavity. The microwave short circuit is similar in construction to that used in 10-cm-band coaxial thermistor mounts. A polyiron sleeve is placed behind the short circuit to prevent any microwave leakage from traveling along the thermistor leads to the bridge circuit. The pickup loop should be as close to the thermistor bead as is physically possible.

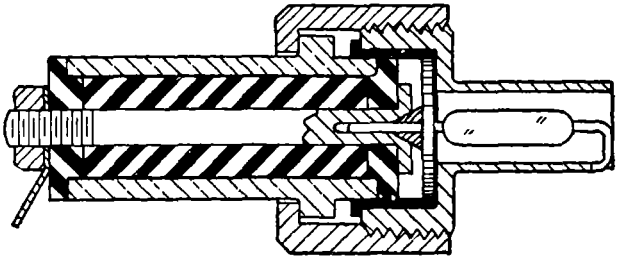

FIG. 3·44.—Thermistor mount for cavity power monitoring.

Since the loop seldom couples so tightly to the cavity that it presents a matched generator to the thermistor termination, it is important to minimize the coaxial-line length between bead and loop if the monitor is to be relatively frequency-insensitive.

An alternative power-monitor design which is mechanically more complicated but electrically more broadband is shown in Fig. 3·45. The tie wires of an uncapsuled bead thermistor are spot-welded to stud pins which are mounted in two parallel support wires. The pickup loop is formed by sandwiching thin polystyrene tape between bands of phosphor bronze ribbon, and cementing with polystyrene cement. The microwave bypass condenser, also formed with polystyrene tape and phosphor bronze ribbon, bands the vertical support wires together at the position of the thermistor. The whole assembly is installed in a threaded, polyiron-backed tube that screws into the oscillator cavity. The split-loop and bypass-condenser construction are so designed to avoid short-circuiting the bead to the d-c bridge supply. This mount design places the bead at the very base of the coupling loop, and in this respect is superior to the design shown in Fig. 3·44. It has the disadvantage that the uncapsuled bead is exposed to air convection currents within the cavity.

If a thermistor is installed parallel to and midway between the wide sides of a rectangular waveguide, it couples very loosely to the fields within the waveguide. Such a construction has been used for monitoring high-level power carried by a waveguide. Usually two thermistors are used, spaced $\lambda_g/4$ apart, so that their reflections cancel. The two may be used in series to form one arm of a bridge circuit, or the second thermistor may be entirely disconnected from any power supply. The advent of the directional coupler provided a preferable means of power monitoring, however, and interest in this thermistor mount was discontinued.

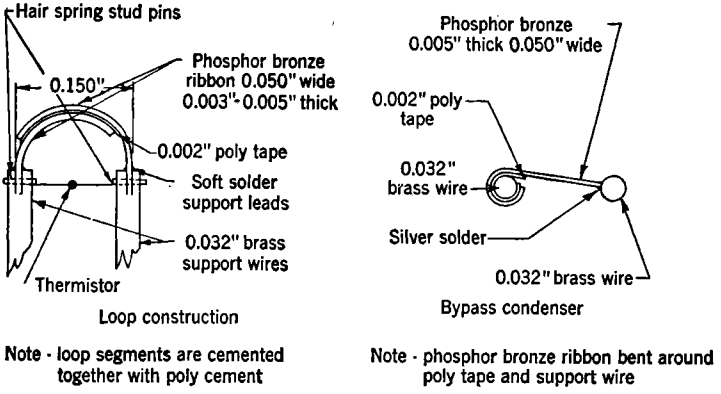

FIG. 3·45.—Uncapsuled-thermistor-bead mount for cavity power monitoring.

3·23. Barretters.—Barretters were used for microwave power measurement prior to the application of the thermistor to this purpose. In the early days of microwave developments the only commercially available barretters were the 5- and 10-ma Littelfuses and Buss fuses that had been designed primarily for the protection of sensitive milliammeters and other pieces of laboratory equipment. These were used with some success in microwave power measurement, but it was quickly realized that their construction was inherently bad from the viewpoint of microwave impedance-matching. The tiny platinum resistance wire is placed at right angles to the axis of the fuse capsule, and this produces a high reactance component of the fuse impedance. The VSWR of such a barretter in either a waveguide or coaxial-line mount is so high that impedance matching with tuners is a critical, painstaking manipulation. Moreover, the tuned match is extremely frequency-sensitive.

Recognizing the potentialities of properly constructed barretters, techniques for producing them in limited quantities were developed in the Radiation Laboratory. This development was also undertaken by

the Sperry Gyroscope Company, and by 1945 they were in a position to produce microwave barretters in sizable quantities. The Sperry No. 821 barretter has been used with a variety of mounts at wavelengths as short as those of 3-cm band. The 821 barretter is too large for use with wavelengths of 1-cm band and shorter.

The barretter construction technique to be described combines features of both the Sperry and Radiation Laboratory procedures. Although it is not suitable for quantity production, the technique is useful to an experimenter who finds it necessary to construct the barretters for his research work.

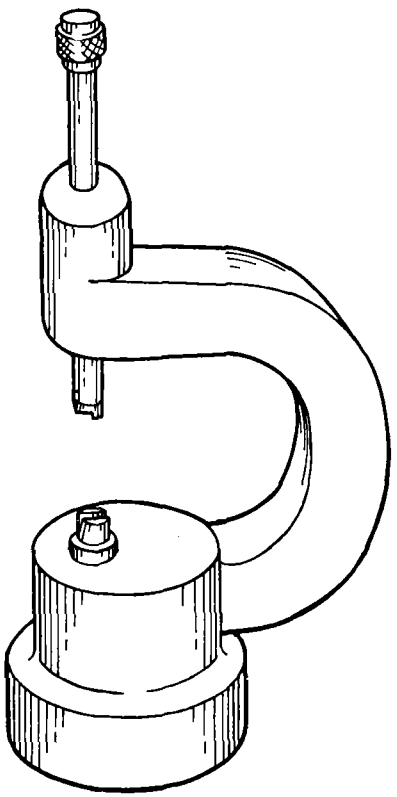

FIG. 3·46.—Staking tool used in barretter construction.

Platinum is the metal commonly used in forming barretter resistance wires. It is desirable to use a noble metal to avoid oxidation and other chemical action that would change the sensitivity of the wire. Of the noble metals, platinum has the most desirable set of physical properties such as resistivity, melting point, temperature coefficient of resistance, and tensile strength. The diameter of the wire commonly used for microwave barretter construction varies from 35 to 75 $\times$ 10^{-6} in. Such a fine wire can be seen with the naked eye only under intense illumination and is too fragile to handle when working with a magnifying lens. Consequently, it is customary to use Wollaston[1] wire, the fine platinum core of which is centered in a silver wire of approximately 0.001-in. diameter. The Wollaston wire can be mounted with relative ease, and an aqueous nitric acid solution is used to etch the silver from the platinum core. When a core diameter consistent with the desired detector sensitivity has been chosen, the resistance of the barretter can be adjusted by varying the etched length of Wollaston wire.

[1] Obtainable from Baker, Sigmund Cohn, and other platinum manufacturers.

The Wollaston wire may be spot-welded or soldered to the support leads of larger diameter. Two soldering techniques have been used: (1) tiny holes may be drilled into the ends of the support wires with a jeweler's drill, and the ends of the Wollaston wire seated into these holes for soldering, or (2) the end of the lead wire may be notched with a jeweler's staking tool (see Fig. 3·46), and the end of the Wollaston wire laid in the notch for soldering. A heated Nichrome wire is convenient for the soldering operation. A double-vise block is used to hold the lead wires in a straight, horizontal line with the short length of Wollaston wire between them. The two ends of the block are insulated from one another and a small d-c current can be passed through the wire during the etching period. Thus a constant check can be kept on the wire resistance, and the etching stopped at the right time.

The nitric acid solution used for etching is a mixture of equal parts by weight of cp nitric acid and distilled water. A small amount of wetting agent (for example, Aerosol) is added to the solution. This reduces the possibility of breaking the fine wire by surface-tension forces when it is removed from the acid solution. The amount of wetting agent to be used is best left to experiment, since the optimum amount seems to vary with the particular bottle of acid used. Excessive amounts of wetting agent cause the drop of acid to flood over the support vane used to bring it in contact with the wire. The etching time required is approximately five minutes.

A micromanipulator is an extremely valuable tool for use in the etching operation. Figure 3·47 shows one design of micromanipulator that has been very useful in this operation. Counterweighted arms, pivoting in ball and socket joints, are used to maneuver the etching arm into position beneath the wire. After these coarse adjustments have been made, micrometer-screw drives offering three degrees of translational freedom are used to contact the drop of acid solution with the wire. The etching arm consists of a dissecting needle with the tip stuck into a wedge-shaped piece of Plexiglas. The drop of acid solution is placed on the wedge and maneuvered into contact with the wire. The drop is smaller than the length of wire to be etched, so that it can be moved along the wire to etch the required length. If close resistance control is required, it is advisable to replace the arm-supported Plexiglas vane by an acid-filled capillary tube and to touch the fine capillary tip to the wire. It is convenient to have a low-power (20×) binocular microscope to view the work.

As the etching proceeds, gas bubbles are evolved which are clearly visible with the aid of a microscope. After the etching is completed, it is necessary to wash the wire before it dries; otherwise, silver nitrate crystals may form and break it. The Plexiglas wedge is flooded with

warm distilled water containing a wetting agent and carefully withdrawn from the wire. In order to remove the Plexiglas wedge without breaking the wire it is necessary for the Wollaston wire not to have been soldered to its supports under tension.

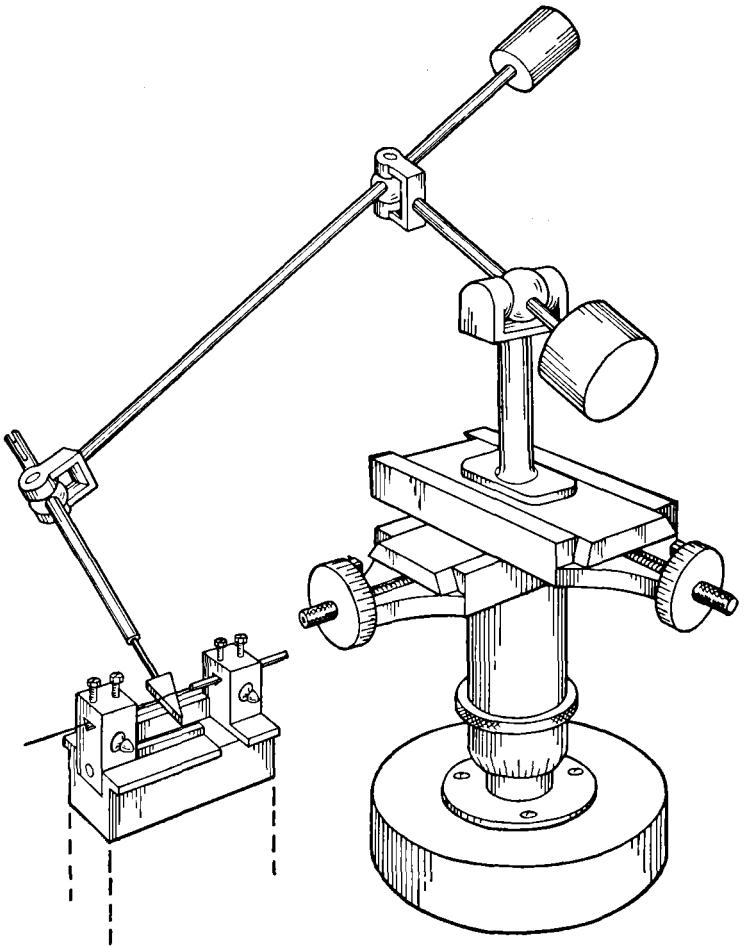

FIG. 3·47.—Sketch of micromanipulator used for etching Wollaston wire in barretter construction.

It is undesirable in most cases to stop the etching before the platinum core has been completely cleaned of silver. Specks of unetched silver will alloy with the platinum at high temperatures and change the characteristics of the wire. Thus overload power that is insufficient

to fuse the wire can still cause trouble by changing, for example, the calibration of a direct-reading barretter bridge.

In Fig. 3·47 one of the barretter lead wires supports a glass or polystyrene tube which can be slid over the short length of etched wire and cemented to the leads. The final construction outwardly resembles that of a capsuled thermistor bead with lead wires projecting from each end of the capsule. Attempts to heat-seal the glass tube to the lead wires have failed because conduction heating fuses too great a percentage of the wires. The Sperry type 821 barretter uses a copolymerstyrene capsule with a window that is cemented in place after the etching is completed. Figure 3·48 shows this construction.

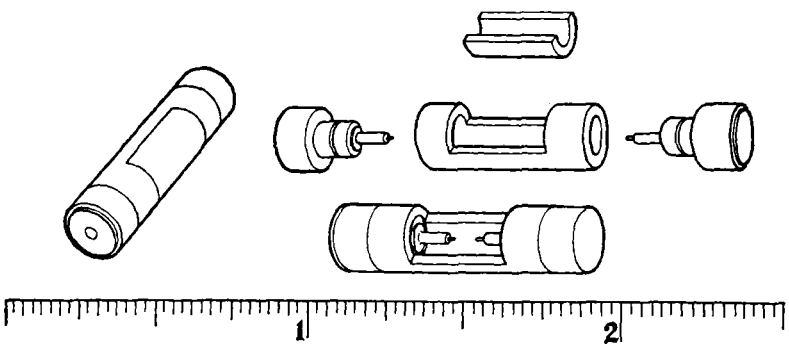

FIG. 3·48.—Drawing of the Sperry type 821 barretter capsule.

Unfortunately, the core diameter of the Wollaston wire often varies appreciably over a length of a few inches. Some lengths of wire have weak spots where the diameter is extremely small. Other pieces of wire, for reasons unknown, will not etch satisfactorily. Fortunately, the manufacturers of the wire have been sympathetic with the problems of the consumer and have not hesitated to exchange good wire for bad. The Sigmund Cohn Company, N.Y.C., has provided the following equation which relates the fusing current of a platinum wire to the diameter. A check on fusing current, using an etched length of several millimeters, offers a convenient check on diameter variations.

$$D = \left(\frac{C}{A}\right)^{2.4}, \tag{55}$$

where D is the wire diameter in inches, C is the current in amperes required to fuse, A is a constant equal to 5170 amp.

The barretter of the design that has the capsule cemented to its lead wires is only as strong as the cement. It must be handled carefully. The Sperry barretter, Fig. 3·48, is mechanically rugged, however. It

successfully withstands vigorous shock and vibration tests, and is satisfactorily waterproof. The fine platinum cores can be easily broken during the etching and washing process, but are surprisingly rugged after being capsuled. This ruggedness is achieved only if the Wollaston wire is installed with a slight sag; it does not resist tension greater than that caused by its own weight.

All 1-cm-band barretters have been made with uncapsuled Wollaston wires that are soldered or spot-welded to terminal posts within the waveguide mounts. The wires are etched after installation in the mounts. A reflectionless dielectric plug is fitted into the end of the mount to protect the wire mechanically, and also to protect it from cooling caused by air convection currents. Similarly, an uncapsuled Wollaston wire may be substituted for the thermistor bead in the coupling-loop design shown in Fig. 3·45.

Taylor-process wire, a fine platinum core in a quartz or glass sheath, holds some promise for barretter construction. Little is known about its usefulness for this application because it was not commercially available during the war.

3·24. The Theory of Operation of a Barretter.—The ideal microwave power detector would have a square-law response; that is, its resistance change would be directly proportional to the power dissipated in it. Square-law response is especially desirable in a bolometer, since it is the first requisite for linearity in the calibration of a direct-reading bolometer bridge. It may be seen from Eq. (30) that a thermistor is far from being a perfect square-law detector. The barretter more nearly meets this condition, and has an approximately linear curve of d-c resistance versus power over much of its resistance range. The steady-state d-c resistance-power curves of a number of barretters have been studied, and it has been shown that they can be reproduced accurately by curves calculated from the equation

$$R - R_0 = JP^n, \tag{56}$$

where R_0 is the cold resistance of a barretter in ohms and R is the barretter resistance when dissipating P watts. Values for a typical type 821 barretter are $R_0 = 115$ ohms, $n = 0.9$, and $J = 7.57$.

A general proof can be advanced[1] to demonstrate that a barretter cannot be a perfect square-law detector. Because of the conduction cooling of the element by its lead wires, a temperature gradient must exist along the length of the platinum wire. The resistance r per unit length of the wire is therefore a function of position as well as of current. For direct current, the power-resistance relation may be written

[1] E. Peskin, "Microwave Power Measurement with Bolometers," NDRC Report 14-529, Polytechnic Institute of Brooklyn, Oct, 31, 1945.

$$P = I^2 \int_{-s/2}^{s/2} r(I^2,x)\, dz = I^2 R(I^2).$$

Corresponding to each value of current is a value of resistance rise referred to R_0, the cold resistance of the barretter. Thus,

$$I^2 = f(R - R_0) = a_1(R - R_0) + a_2(R - R_0)^2 + \cdots . \quad (57)$$

The power dissipation in the barretter may be expressed as

$$P = I^2R = I^2(R - R_0) + I^2R_0. \quad (58)$$

Substitution of Eq. (57) in Eq. (58), and ordering of terms results in

$$P = a_1R_0(R - R_0) + (a_2R_0 + a_1)(R - R_0)^2 + (a_3R_0 + a_2)(R - R_0)^3 + \cdots . \quad (59)$$

Finally, since a_1 appears in the second term of the series expressed by Eq. (59), it is obvious that some deviation from a perfect square-law response exists.

When a barretter is used in a microwave power-measurement circuit, the deviation from square-law response is affected by the resistance of the bias-current supply. As discussed in Sec. 3·1, in general, the d-c bolometer power is changed when microwave power is introduced. Thus the *normal* deviation from square-law response, implicit in Eq. (56), must be differentiated from the *effective* deviation. The effective deviation includes the effect of the bolometer bias supply on the final resistance change resulting from application of the microwave power. If the resistance of the barretter bias supply is such that the d-c bias power is independent of the microwave power level in the barretter, then the so-called normal and effective deviations from square-law response become identical. The percentage deviation δ from square-law response is

$$\delta = \left(\frac{R_1 + \Delta R}{R_1} \cdot \frac{P_1}{P_1 + \Delta P} - 1 \right) 100, \quad (60)$$

where R_1 is the operating resistance of the barretter, P_1 is the d-c bias power at operating resistance, and ΔR is the change in barretter resistance caused by microwave power, ΔP.

For the type 821 barretter,

$$R_1 = 200 \text{ ohms}, \qquad P_1 = 16 \cdot 4 \text{ mw}$$
$$I = 9.06 \text{ ma}, \qquad t = 25°\text{C}.$$

For these values of the parameters, the Sperry Gyroscope Company has prepared a graph of Eq. (60) as a function of ΔP. This graph is shown in Fig. 3·49.

[1] "The Sperry Type 821 Barretter for Microwave Power Measurement and Detection," Sperry Gyroscope Company, Report No. 5244-1042, July 24, 1945.

Of direct interest is the calculation of the error in a direct-reading barretter bridge caused by the deviation from square-law response. It will be assumed that the normal and effective deviations are equal and that a barretter bridge circuit is used which is equivalent in operation to the thermistor W-bridge. The first bridge balance is an a-f balance, and d-c power is used as a calibrating signal. Calibration is effected for a full-scale meter deflection, and linear interpolation on the meter is used for power levels less than that corresponding to full-scale deflection. When microwave power is applied to the barretter, the bridge (by interpolation) reads P_m. Because of the deviation from square-law response, the meter deflection actually corresponds to a slightly different power level P_t. The percentage error, referred to full-scale deflection, is γ,

$$\gamma = \frac{P_m - P_t}{P_{dc}} \times 100 = \frac{P_m - P_t}{P_2 - P_1} \times 100, \qquad (61)$$

where P_1 is the a-f bias power for initial bridge balance, P_{dc} is the d-c calibrating power for full-scale deflection, and P_2 equals $P_1 + P_{dc}$.

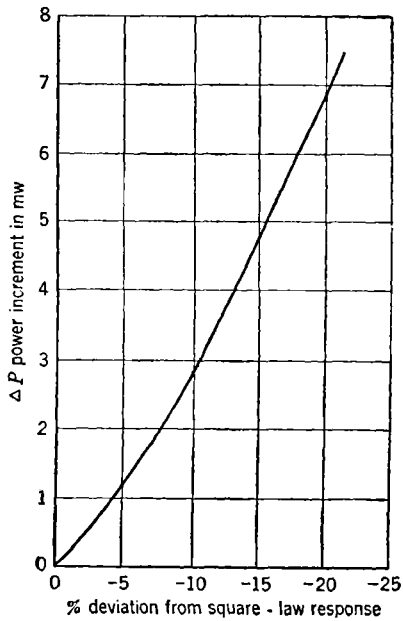

FIG. 3·49.—Barretter characteristic of incremental power vs. percentage deviation from square-law response.

The slope of the chord XY in Fig. 3·50 is given by

$$\tan \theta = \frac{R_2 - R_1}{P_2 - P_1}. \qquad (62)$$

If the R's in Eq. (62) are eliminated by application of Eq. (56),

$$\tan \theta = \frac{J(P_2^n - P_1^n)}{P_2 - P_1}. \qquad (63)$$

The resistance of the barretter for steady-state meter deflection with microwave power, R_3, is given by

$$R_3 = (P_m - P_1) \tan \theta + R_1. \qquad (64)$$

By substitution of Eqs. (56) and (63) in Eq. (64), the expression for

R_3 becomes

$$R_3 = \frac{J(P_2^n - P_1^n)(P_m - P_1)}{P_2 - P_1} + JP_1^n + R_0. \tag{65}$$

If Eq. (56) is solved for P_t in terms of R_3, and the value of R_3 according to Eq. (65) substituted,

$$P_T = \left[\frac{(P_2^n - P_1^n)(P_m - P_1)}{P_2 - P_1} + P_1^n\right]^{1/n} \tag{66}$$

Finally, by substitution of Eq. (66) in Eq. (61), the expression for γ is

$$\gamma = \frac{P_m - \left[\dfrac{(P_2^n - P_1^n)(P_m - P_1)}{P_2 - P_1} + P_1^n\right]^{1/n}}{P_2 - P_1} \times 100. \tag{67}$$

To illustrate the magnitude of this error, assume the following typical operating values: $P_1 = 8$ mw, $P_2 = 12$ mw, and $P_m = 10$ mw. Sub-

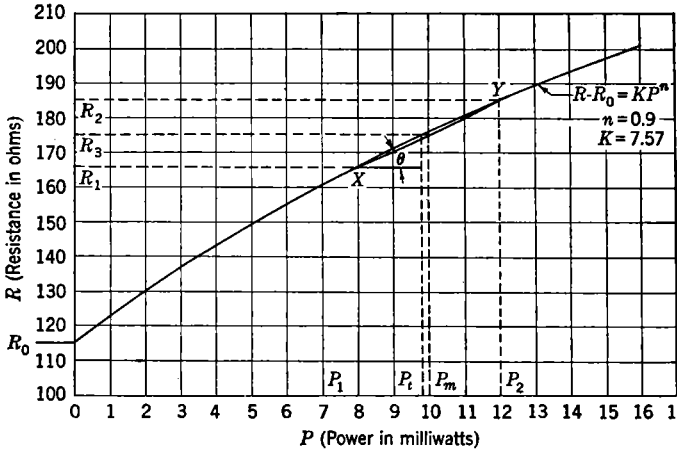

FIG. 3·50.—Barretter characteristic: steady-state resistance vs. power for Sperry type 821 barretter.

stitution of these values in Eq. (67), and the use of $n = 0.9$, gives γ a value of 2.5 per cent. Note that γ becomes zero for both zero and full-scale deflections, and has its maximum value when the microwave power is one-half the d-c power used for full-scale calibration. The deviation from square-law response is not important in balanced-bridge operation since the barretter is always operated at constant resistance.

Equation (56) may be differentiated to obtain an expression for the detector sensitivity of the barretter

$$\frac{dR}{dP} = nJP^{n-1} = \frac{n(R - R_0)}{P}. \tag{68}$$

Data taken on 60 Sperry type 821 barretters give values for detector sensitivity ranging from 4.17 to 4.88 ohms/mw, at an operating resistance of 200 ohms and a temperature of 25°C. The average value is 4.46 ohms/mw, and the mean deviation from the average is 2.75 per cent.

Figure 3·51 shows the dependence of the barretter bias power on ambient temperature for operation of the barretter at 200 ohms. The approximate linearity of the two curves suggests that Eq. (56) may be modified, as was the thermistor equation, to include the effect of ambient temperature T on the barretter resistance, thus,

$$R - R_0 = J\left(P + \frac{T}{C}\right)^n. \quad (69)$$

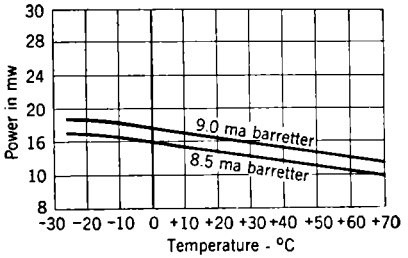

FIG. 3·51.—Barretter characteristic: ambient temperature vs. power required for 200-ohm operation.

The derivative of Eq. (69), dR/dP, can be expressed solely in terms of J, n, and $(R - R_0)$. This would indicate that the detector sensitivity of a barretter, at a given operating resistance, is independent of T. The extent of the error involved in assuming a linear relation between P and T is indicated by experimental data on dR/dP as a function of T. It has been found by the Sperry Gyroscope Company that dR/dP varies linearly with T within ± 3 per cent over a ± 50°C ambient-temperature range. This is not a large variation. Consequently, Eq. (69) can be considered valid for many approximate calculations.

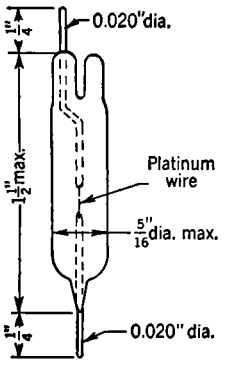

FIG. 3·52.—Evacuated high-frequency barretter manufactured by Tung-Sol Lamp Works, model B-100.

Convection cooling of the fine platinum wire has an important influence on the characteristics of the barretter. The detector sensitivity is greatly increased, and the time constant is increased. Little use has been made of evacuated barretter capsules because of their increased sluggishness. Barretters are usually used in applications where a fast response is desired, and thermistors are still preferred in applications where a longer time constant is not a handicap. The effect of altitude on the detector sensitivity of a barretter has not been studied, but should be of interest in connection with airborne-radar test equipment using barretters. The Tung-Sol Lamp Works has developed the evacuated barretter shown in Fig. 3·52. The resistance of the unit measured at a current of 0.5 ma is 200 ohms ± 25 per cent. The increase

in resistance due to skin effect is less than 1 per cent for frequencies up to 10,000 Mc/sec. The sensitivity is 4.5 μw for a 1 per cent change in resistance at the optimum bias current of 0.5 ma. The maximum current is 1.25 ma. The Radiation Laboratory has had no experience with the unit, but its physical size would seem to limit its usefulness to wavelengths of 10 cm and longer.

The time constant τ of the Sperry type 821 barretter is 320 μsec $\pm$ 10 per cent. It is determined from $\tau = \frac{1}{2\pi f}$, where f is the modulation frequency at which the demodulation sensitivity of the barretter is 3 db down from the value at 100 cps. Typical demodulation response curves for the barretter are given in Fig. 3·53. The curves were taken with a constant d-c bias current and an average resistance of 200 ohms. The carrier frequency was 10 Mc/sec and was modulated approximately 20 per cent by a sine wave. The power of the carrier was 1 mw. The two curves are expressed in decibels relative to the power in the fundamental at 100 cps.

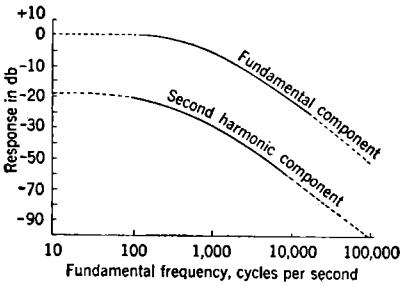

FIG. 3·53.—Barretter characteristic: demodulation response vs. modulation frequency.

The type 821 barretters are normally operated at 200 ohms, demanding a bias power of approximately 15 mw. The maximum safe power level (limited by alloying of silver specks with the platinum) is 32.5 mw. The power required to fuse the barretter wire is in excess of 50 mw.

The equivalence of the heating effects of direct current and microwave current, the requisite for application of the barretter to absolute power measurements, has been the subject of several investigations.[1] The treatment to be followed here is due to Feenberg.

If the wire is heated by direct current, the power dissipation is uniform throughout the cross section of the wire. The heat losses from the surface establish a condition in which the center of the wire is hotter than the surface. High-frequency currents, however, because of skin-depth considerations, generate heat at and near the surface of the wire. If the wire is thin, a negligible temperature gradient exists along the wire radius, and the temperature can be assumed constant throughout the cross section.

[1] H. E. Webber, "Power Measurement in the Microwave Region," Sperry Gyroscope Company, Report No. 5220-109, Mar. 9, 1943. E. Feenberg, "The Frequency Dependence of the Power-resistance Relation in Hot Wire Wattmeters," Sperry Gyroscope Company, Report No. 5220-108, Mar. 10, 1943.

In the case of high-frequency heating, the resistance R_a of the wire is given by

$$\frac{1}{R_a} = \frac{\pi a^2 \theta(T_a)}{l}, \tag{70}$$

where a and l are the radius and length of the wire, respectively, $\theta(T_a)$ is the electrical conductivity of the wire, and T_a is the absolute surface temperature required to dissipate the generated heat.

If the wire is heated by d-c power, the wire resistance R is given by

$$\frac{1}{R} = \frac{2\pi}{l} \int_0^a \theta(T) \cdot dr. \tag{71}$$

Since $\theta(T)$ varies inversely as the absolute temperature, for small variations in T,

$$\theta(T) = \theta(T_a) - \frac{\theta(T_a)}{T_a} \cdot (T - T_a).$$

Therefore,

$$\frac{R - R_a}{R_a} \approx \frac{1}{a} \int_0^a \frac{T - T_a}{T_a} \cdot dr. \tag{72}$$

It is possible to compute T as a function of r, the distance along the wire radius, by solving the heat equation in cylindrical coordinates.

$$k \frac{1}{r} \frac{d}{dr} \left(r \frac{d}{dr} T \right) = -p \approx -\frac{PJ}{\pi a^2 l}, \tag{73}$$

where k is the thermal conductivity of the wire in cal/°C sec cm, p is the heat production, in cal/sec cm^3, P is the total power dissipation, in watts, and J is 0.239 cal/joule.

The required solution of Eq. (73) is

$$T - T_a = \frac{-PJ(r^2 - a^2)}{4\pi a^2 l k}. \tag{74}$$

If Eq. (74) is substituted in Eq. (72), and integrated

$$R = R_a \left(1 + 0.013 \frac{P}{l k T_a} \right). \tag{75}$$

A 1-cm tungsten wire, dissipating 50 watts at 3000°C, has values of R and R_a which differ by only $\frac{1}{30}$ per cent. The difference is correspondingly small for a platinum wire operated at a high surface temperature.

The matter of different temperature gradients throughout the cross section of the wire is not the only concern, however. High-frequency standing waves may exist along the length of the barretter wire, and

consequently hot and cool spots may exist at the current loops and nodes. This condition does not exist for direct current, and its effect must also be considered. Bleaney[1] has treated this problem in considerable detail, and the results of his investigation will be summarized.

Like Feenberg, Bleaney treats the case of a wire thin enough so that the temperature rise due to r-f heating is uniform across the wire. He assumes that because the high-frequency power is small compared to the d-c bias power, it causes a small temperature rise. The change of high-frequency resistance with temperature does not materially alter the power developed at each point along the wire from a cosine-squared distribution. Because of the change in skin depth, the high-frequency resistance does not vary with temperature according to the same law as the d-c resistance. The development involves integrating the differential equation for the temperature distribution along the wire. If radiation losses are neglected and only conduction losses to the lead-wire supports are considered, the expression derived is

$$\frac{\left(\frac{\Delta R}{R_0}\right)_{r\text{-}f}}{\left(\frac{\Delta R}{R_0}\right)_{d\text{-}c}} = \frac{1 + \frac{3}{\phi^2}\cos 2\delta\left(\frac{\sin\phi}{4} - \cos\phi\right)}{1 + \frac{\sin\phi}{4}\cdot\cos 2\delta}, \tag{76}$$

where $\phi = 2\pi l/\lambda$, and l is the wire length. When the center of the wire is halfway between a current loop and node, $\cos 2\delta = 0$. When the center of the wire falls on a current loop or node, $\cos 2\delta = \pm 1$.

From Eq. (76) it may be demonstrated that

1. Regardless of wire length, the heating effects of direct and high-frequency current are exactly equivalent if the center of the wire is halfway between a current loop and node.
2. Regardless of wire length, the maximum error occurs if the center of the wire is coincident with either a current loop or node.
3. The error is zero for a wire the length of which is 0.96λ.
4. The maximum error (35 per cent) occurs for a wire slightly greater than $\lambda/2$ in length, with a current loop at its center. The barretter will indicate greater high-frequency power than it should, since the maximum heat is at the center of the wire where the leads cannot dissipate it effectively.

As the wire length is increased, lead-wire conduction losses become less important and radiation losses assume increased prominence. However, Bleaney concludes that radiation losses have a negligible effect

[1] B. Bleaney, "Power Measurements by Bolometer Lamps at 3-cm Wavelengths," Report CD Misc. 7, CVD Research Group, New Clarendon Lab., Oxford, England, Sept. 21, 1942.

on the conclusions stated above provided that the wire length is less than 0.96λ.

3·25. Direct-reading Bridges for Barretters.—Direct-reading barretter bridges are in most respects similar to direct-reading thermistor bridges. Barretters have a smaller detector sensitivity than thermistors, and consequently, d-c barretter bridges are usually less sensitive than d-c thermistor bridges. In order to achieve comparable sensitivity it is necessary to select the bridge-arm resistances so that the bridge driving voltage and bridge current are relatively large. The following data, applicable to the Sperry type 821 barretter, specify the approximate sensitivity of a d-c barretter bridge. With all bridge arms 200 ohms, and using a 200-ohm microammeter, the unbalance current caused by 1 mw of microwave power is 50 μa. The unbalance current increases to 100 μa in the limiting case of a zero-impedance meter. If two of the bridge arms are made higher in resistance, the bridge driving voltage must be increased, but the unbalance current for a 200-ohm meter can be increased to about 70 μa. In the more sensitive barretter bridge circuits which use audio frequencies with amplification, the frequencies must be higher than those used with thermistor bridges because of the much shorter time constant of the barretter.

Although no attempt has been made to do so, it is possible that the thermistor W-bridge, X-bridge, and self-balancing-bridge designs could be modified to adapt them for use with barretters. Among other things the modifications would include higher oscillator frequencies and a change in the phase of feedback voltages to take into account the fact that the barretter has a positive rather than a negative temperature coefficient of resistance. No attempt has been made to adapt disk thermistors to the temperature compensation of direct-reading barretter bridges, but there appears to be no fundamental reason why this cannot be done. The several barretter bridge designs to be discussed have all been contributed by the Sperry Gyroscope Company as a part of their general development of barretters for microwave power measurement. It will be observed that the bridge techniques used are somewhat different from those discussed in connection with thermistor bridges, but again, with proper modifications, these designs should be applicable for use with thermistors. All designs discussed use the Sperry type 821 barretter.

Figure 3·54 shows the circuit constants of a d-c barretter bridge of a simple type. This bridge was originally designed for monitoring microwave power at a level of 0.75 mw over the ambient-temperature range of $-40°$ to $+70°$C. This power level provides 20 per cent of full-scale deflection for an average barretter at 25°C. Variations in barretter sensitivity and in ambient temperature can cause a maximum error of ± 20 per cent referred to the average barretter operating at 25°C.

Partial sensitivity compensation is achieved by using copper resistors in two of the bridge arms. The difference in the temperature coefficients of resistance of copper and of manganin is sufficient to accomplish this. No drift compensation is included in the design since the bridge sensitivity is relatively low, and since a manual balance is made immediately prior to each microwave test. The meter has a resistance of 280 ohms $\pm \frac{1}{2}$ per cent, of which the copper coil has 180 ohms ± 10 per cent. The remainder of the resistance is composed of manganin.

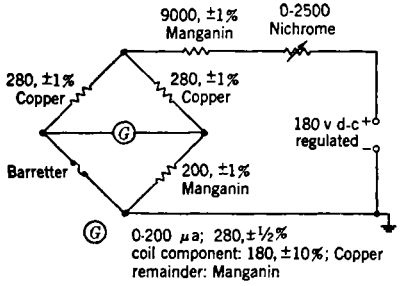

FIG. 3·54.—Sperry d-c barretter direct-reading bridge.

The barretter bridge shown in Fig. 3·55 is operated as a balanced bridge, but is nevertheless direct-reading in microwave power. The bridge is made self-calibrating through the use of a calibrating resistor and a d-c milliammeter. With the microwave power source disconnected from the barretter, the selector switch S is thrown to the calibrating-resistor position. The d-c bridge current is adjusted so that the milliammeter reads full-scale deflection—a current corresponding to 10 mw of d-c power in the calibrating resistor. When the barretter replaces the calibrating resistor, the d-c power is inadequate for bridge balance, and balance is achieved by superimposing some low-frequency r-f power on the d-c power in the barretter. If the resistance of the calibrating resistor is chosen the same as the resistance of the barretter at bridge balance, the d-c barretter power at the balance condition must be 10 mw. Introduction of microwave power unbalances the bridge, and balance is restored by reducing the d-c bridge current. The d-c milliammeter is calibrated (nonlinearly, of course) in terms of microwave power from 0 to 10 mw. It is convenient to use a zero-right milliammeter for this application so that the microwave power scale may be zero-left.

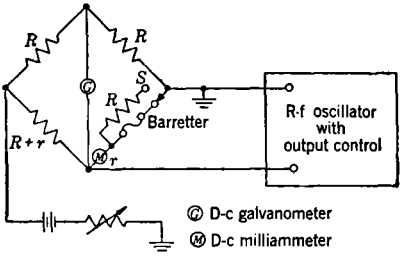

FIG. 3·55.—Sperry manually balanced barretter direct-reading bridge.

When the bridge is balanced, microwave power may be read directly from the milliammeter calibration to an accuracy of better than ± 10 per cent. It is essential, however, in this bridge design to use precision bridge-arm and calibrating resistors as well as an accurately calibrated

meter. The self-calibrating feature obviates the need for sensitivity compensation, and again, the bridge sensitivity is too low to demand drift compensation.

The self-balancing bridge shown schematically in Fig. 3·56 is powered partially by high-audio-frequency and partly by d-c power. The a-f oscillator is a regenerative amplifier deriving its feedback from the unbalance of the barretter bridge. The meter M responds to the a-f power delivered to the bridge, but is calibrated in terms of microwave power. The calibration is referred to an a-f power level of 10 mw, which is decreased by an amount equal to the level of microwave power when the bridge balances itself with the microwave source connected to the barretter. Corrections for barretter differences and ambient-temperature variations are made by changing the d-c power component. The bridge is operable over a wide range of sensitivities, with a maximum sensitivity of approximately 50 μw full scale. The high bridge sensitivity is obtained by increasing the d-c power component and by increasing the indicator sensitivity. As in the bridge design shown in Fig. 3·55, it is convenient to use a zero-right meter so that the microwave power scale will be zero-left. Design work on this bridge circuit is currently incomplete so that a detailed circuit diagram is not available.

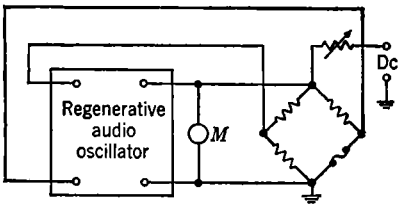

FIG. 3·56.—Sperry self-balancing barretter direct-reading bridge.

3·26. Barretter-amplifier Combinations.—Barretters have been used extensively in microwave measurements to indicate power-level ratios. For example, they are invaluable in studying antenna patterns, and are often used in attenuation measurements. In these applications the barretters are commonly biased with direct current and used with pulse- or square-wave-modulated microwave power so that the demodulation signal may be amplified. A typical arrangement of test gear involves a barretter in a microwave mount with a high-gain tuned preamplifier, the output voltage of which is registered on a logarithmic a-c voltmeter. With such an indicator it is possible to read power-level ratios directly in decibels. The relatively short time constant (high demodulation sensitivity) of the barretter makes it preferable to the thermistor for these applications. Crystals are excluded from consideration because they do not have a square-law response and are easily burned out by high pulse power.

Not only may barretter-amplifier combinations be used for power-level-ratio measurements, but they may also be used in place of bridge circuits for direct power measurement. The combination must be calibrated

against a balanced bridge, and thereafter the stability of the amplifier gain and of the barretter characteristics may be depended upon to maintain the calibration. High sensitivity is more easily achieved in this manner than with a bridge circuit. Moreover, there is less trouble from ambient-temperature variations. The chief disadvantages are that the combination is not self-calibrating unless a bridge circuit is appended, and that the method is applicable only with pulsed or modulated power.

The time constant of the barretter, as well as its detector sensitivity, influences the sensitivity of the barretter-amplifier combination. The normal variations in sensitivity to be expected are indicated by the data of

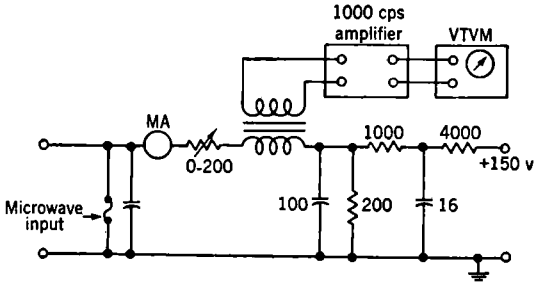

FIG. 3·57.—Barretter-amplifier combination used for microwave power measurement.

Table 3·8. One hundred Sperry type 821 barretters were tested in the circuit shown in Fig. 3·57. In making the tests the microwave input power was 100 per cent modulated by a 1000-cps square wave. The barretter bias current was fixed at 8.6 ma for all barretters, and the microwave power level was held constant. The data indicate that many barretters give an amplified signal that is within $\pm \frac{1}{2}$ db of the mean value for the hundred.

TABLE 3·8.—DATA ON THE REPRODUCIBILITY OF BARRETTERS USED WITH AN AMPLIFIER AND VACUUM-TUBE VOLTMETER

No. of barretters	Relative output reading
6	< 65
5	65– 70
16	70– 75
24	75– 80
26	80– 85
14	85– 90
5	90–100

It will be of interest to develop the theory of a barretter that is biased by a d-c voltage and subjected to pulsed microwave power. The rate of change of resistance of the barretter with time may be expressed as

$$\frac{dR}{dt} = \frac{dR}{d\theta} \cdot \frac{d\theta}{dH} \cdot \frac{dH}{dt}, \tag{77}$$

where R is the resistance of the barretter, t is the time, θ is the absolute temperature of the barretter wire, and H is the heat content of the wire. The heat capacity c_p of the wire is $dH/d\theta$. If Eq. (77) is solved for dH/dt,

$$\frac{dH}{dt} = c_p \cdot \frac{d\theta}{dR} \cdot \frac{dR}{dt}. \tag{78}$$

Equation (78) expresses the rate at which the wire is heated. Not all of the pulsed power is effective in heating the wire. Heat losses to the environment occur since the wire is not in an adiabatic system. As a first approximation ($\Delta\theta$ small), the losses may be expressed as

$$\frac{dH}{dt} = \alpha\Delta\theta = \alpha \frac{d\theta}{dR} \cdot \Delta R, \tag{79}$$

where α is the thermal conductivity of wire, and $\Delta\theta$ is the temperature difference between the barretter wire and its environment.

The microwave pulse input power P is the sum of the two dH/dt components expressed by Eqs. (78) and (79). Thus,

$$P = c_p \cdot \frac{d\theta}{dR} \cdot \frac{dR}{dt} + \alpha \frac{d\theta}{dR} \cdot \Delta R. \tag{80}$$

Since

$$\frac{d(\Delta R)}{dt} = \frac{dR}{dt},$$

Eq. (80) may be written as

$$\frac{d(\Delta R)}{dt} + \frac{\Delta R}{\left(\frac{c_p}{\alpha}\right)} = \frac{\frac{dR}{d\theta}}{c_p} \cdot P. \tag{81}$$

The differential equation given by Eq. (81) is analogous to that obtained for a simple parallel RC-network driven by a constant current generator. In establishing the analogy the correspondences are

1. The voltage drop across the RC-network corresponds to ΔR.
2. The current from the generator corresponds to P.
3. The capacitance corresponds to $c_p \cdot (d\theta/dR)$.
4. The resistance corresponds to $(1/\alpha) \cdot (dR/d\theta)$.

The integration of Eq. (81) leads to

$$\Delta R = s(P + ke^{-\frac{t}{\tau}}), \tag{82}$$

where

$$\tau = \frac{c_p}{\alpha},$$

the barretter time constant, and

$$s = \frac{1}{\alpha} \cdot \frac{dR}{d\theta},$$

a quantity proportional to the detector sensitivity of the barretter.

During the period of a pulse, the resistance of the barretter will increase exponentially according to Eq. (82). In the interim between successive pulses the resistance will decay exponentially. The decay will be less than the rise until a steady-state condition is reached, at which time they become equal. In this steady-state condition the resistance of the barretter (or the voltage drop across the wire) fluctuates between maximum and minimum values which may readily be determined by applying suitable boundary conditions to Eq. (82). Thus,

$$e_{max} - e_{min} = si_0P(1 - e^{-\frac{L}{\tau}}) \frac{[1 - e^{-\frac{(T-L)}{\tau}}]}{(1 - e^{-\frac{T}{\tau}})}, \tag{83}$$

where i_0 is the bolometer bias current in amperes, L is the pulse length in seconds, and T is the repetition period in seconds.

It may be observed from Eq. (83) that the amplitude of the demodulation signal is independent of the repetition period T either when $T \gg L$, or when $T \gg \tau$ and $(T - L) \gg \tau$. Thus, in order that the calibration of the barretter-amplifier shall be unaffected by variations in repetition rate, it is desirable that the pulse length and barretter time constant both be small compared to T. In this case Eq. (83) may be simplified to

$$e_{max} - e_{min} = si_0P(1 - e^{-\frac{L}{\tau}}) = si_0P\left(1 - 1 + \frac{L}{\tau} - \frac{L^2}{2\tau^2} \cdots\right)$$
$$= si_0P\frac{L}{\tau}\left(1 - \frac{L}{2\tau} \cdots\right). \tag{84}$$

Finally, if $L/2\tau \ll 1$,

$$e_{max} - e_{min} = \frac{si_0PL}{\tau}. \tag{85}$$

When using a Sperry type 821 barretter with 1-μsec pulses at a repetition rate of 1000 pps, Eq. (85) is valid. It should be noted that Eq. (85) specifies that the amplitude of the demodulation signal is directly proportional to PL, the pulse *energy* of a square pulse.

The detector sensitivity s of the barretter is somewhat temperature-sensitive so that the calibration of the barretter-amplifier combination depends to a small extent on temperature. The problem is not so severe as the problem of drift control in a bridge circuit that has a sensitivity comparable to that of the amplifier. Stability of the bias current is as critical as for bridge circuits.

A Fourier analysis of the steady-state exponential sawtooth wave for small duty cycles shows that the amplitude of the fundamental component is given by

$$e(t) = \frac{2si_0}{\tau} \cdot \left(\int_0^L P(t)\, dt \right) \cdot \frac{\left(\frac{\sin 2\pi t}{T} \right)}{\sqrt{\left(\frac{T}{\tau} \right)^2 + (2\pi)^2}}. \tag{86}$$

Hence the amplitude of the demodulation signal is not independent of the repetition period until $T^2 \ll 4\pi^2\tau^2$. When T is 500 μsec, a 10 per cent variation in T will effect a 1.6 per cent change in the amplitude of the demodulation signal.

There are several considerations with regard to amplifier design that deserve mention.[1] Since the amplitude of the fundamental component of the demodulation signal is not independent of repetition frequency whereas the amplitude of the sawtooth wave is, it is desirable to use a narrow-band amplifier. It has been pointed out that the barretter in this application is analogous to a parallel RC-network. Thus it acts as a simple low-pass filter with a time constant of 350 μsec. This corresponds to a half-power point of 1.6 kc/sec, and an amplifier with an upper pass band of 16 kc/sec can be used to get an acceptably accurate reproduction of the sawtooth. Since there are no components below the repetition frequency, the low-frequency half-power point need only be located sufficiently far below this frequency to cause negligible phase shift. It should not be made lower than necessary to avoid objectionable distortion of the sawtooth wave since the noise increases with bandwidth.

An acceptable amplifier design consists of three stages of 6AK5 tubes with a total voltage gain of 50,000, followed by a cathode follower which is used to drive the diode detector with a low-impedance source. The diode detector is of the voltage-doubling type, charging a condenser to the peak-to-peak voltage. A cathode-follower bridge is used to drive the output meter which is calibrated to read linearly in pulse power. Three per cent gain stability can be realized by using a feedback factor of approximately 20. A single-loop feedback arrangement gives adequate stability, but must be carefully shielded to avoid oscillation. Consequently, a double feedback loop using two L-pads may be preferable. The gain control may be installed in the cathode-follower driver or as an adjustable shunt on the output meter.

3·27. Barretter Mounts.—In the early days of microwave research when Littelfuse bolometers were popular for power measurement, the fuse capsules were installed in a coaxial-line mount of the type shown in Fig. 3·58. The 10-cm-band mount shown is tunable and has such a narrow bandwidth that it must be retuned at each new wavelength. The two tuning adjustments are an adjustable length of line adjacent

[1] R. S. Chaloff, R. J. Harrison, W. W. Mathison, G. B. Guthrie, "Design Proposal for AN/ALN-19A Check Set," RL Report 1062, Mar. 27, 1946.

to the fuse capsule and a tunable stub line at the opposite end of the mount. Both the stub and telescoping line stretcher are rack-and-pinion-driven. The 50-ohm, $\frac{5}{8}$-in. coaxial line is tapered from the right-angle T to a 50-ohm type N jack for cable connection.

The VSWR in the line between the fuse and the T is large. However, by adjustment of the line stretcher it is possible to make the admittance of the termination, referred to a point at the T, lie on the unit conductance circle. The stub may then be tuned to provide a susceptance of equal magnitude and opposite sign—the condition necessary to provide a matched-impedance mount. Because of the difficulty of making accurate VSWR measurements in $\frac{5}{16}$-in. line (cable size), the criterion for impedance match is more often taken to be the maximization

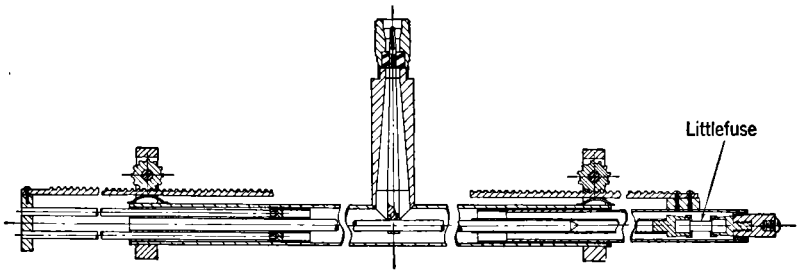

FIG. 3·58.—Section drawing of a 10-cm-band tunable Littelfuse mount.

of the power indication. As for coaxial-line thermistor mounts, the stub provides a return path for the d-c bridge current, and the polystyrene tape or mica provides a microwave short circuit but an open circuit for direct current.

There is nothing in the mount design shown in Fig. 3·58, aside from minor mechanical details, that characterizes it solely as a barretter mount. A thermistor could be used equally well in a mount of this type, but available broadband thermistor mounts are preferable for most purposes.

Littelfuses have also been installed in waveguide mounts; the method of installation is similar to that used in thermistor waveguide mounts. For example, Westinghouse Electric Corporation has designed a waveguide directional coupler for power-monitoring and automatic VSWR indication which uses specially selected Littelfuses. The impedance match is satisfactory for operation of the power monitor over the band from 2700 to 2900 Mc/sec. Similar to waveguide thermistor mounts, a fixed-tuned Littelfuse mount uses a tunable coaxial stub and a tunable waveguide end plunger.

Whereas the Littelfuse design does not lend itself to broadband impedance-matching in microwave mounts, the Sperry type 821 barretter has both desirable and reproducible microwave impedance characteristics.

The Sperry Gyroscope Company has developed a series of several barretter mounts, all of which use the type 821 barretter. The first in this series is a 3-cm-band waveguide mount, a section drawing of which is shown in Fig. 3·59.

The most interesting feature of the mount is the resonant iris (window)[1] that is used for broadband matching. The resonant iris acts as a parallel-resonant circuit shunting the waveguide. In the neighborhood of resonance the behavior of the resonant iris can be completely predicted if the resonant frequency, the unloaded Q, and the

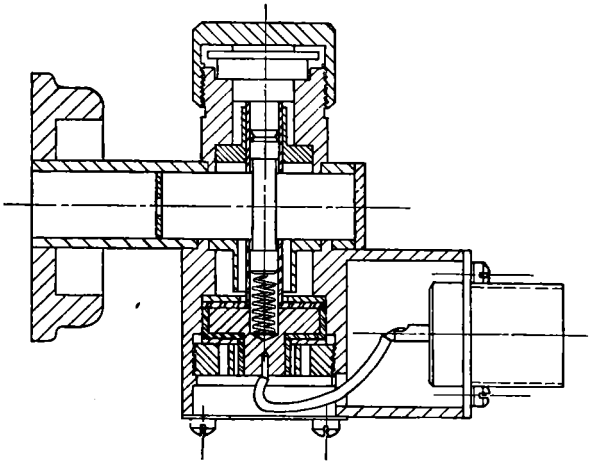

FIG. 3·59.—Section drawing of the Sperry type 82X barretter mount; 3-cm band, narrow-side view. (*Courtesy of Sperry Gyroscope Company.*)

characteristic impedance are known. For a narrow slot, resonance occurs when the slot length is approximately $\lambda/2$ in air. The losses in a well-soldered metal window are low, the unloaded Q is of the order of 1000, and the losses can be neglected. The characteristic impedance of a resonant circuit is defined as $\sqrt{L/C}$. For a window, the characteristic impedance is a function of the slot width and the thickness of the window. It increases with slot width, and decreases with increasing thickness of metal. The characteristic impedance is of prime importance in this application since it determines the shunting reactance offered by the window at frequencies off resonance.

Circle-diagram plots of impedance against frequency are conveniently used to determine the desirable characteristic impedance and the distance from the barretter at which the window should be placed. In order to realize the maximum possible bandwidth, it is found advisable to accept

[1] T. Moreno, "A Fixed-Tuned Broadband Wattmeter Using a Broadbanding Window," Sperry Report No. 5224-1003, June 19, 1944.

a small mismatch at midband in order to get a very low VSWR at wavelengths on *both* sides of the midband wavelength. The designer strives for a curve of VSWR against λ similar to the broadband curve shown in Fig. 3·29. If the susceptance-frequency characteristic of the window and the admittance-frequency characteristics of the mounted barretter are known, "cut and try" calculations with a circle diagram may be used to establish the iris location that gives the curve of the desired type. It is common at low-frequencies to overcouple two resonant circuits to obtain a broad double-humped bandpass characteristic. The window

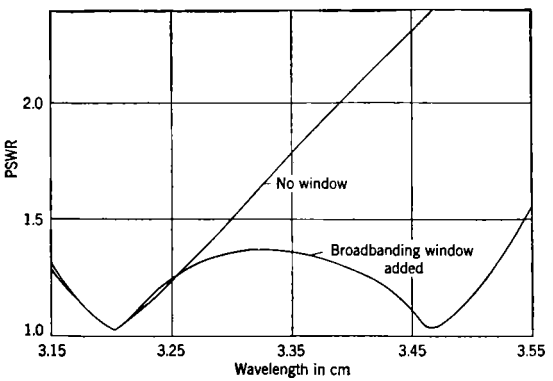

FIG. 3·60.—Effect of resonant iris on broadband match of type 82X barretter mount.

and the mounted barretter may be thought of as a pair of resonant circuits which, by proper coupling, can be made to give a double-humped curve of VSWR against λ like the one in Fig. 3·29.

In designing the type 82X mount to operate over the 3.13- to 3.53-cm band, it was found advisable to tune the iris to 3.2 cm. The $\sqrt{L/C}$ ratio of the resonant iris was so selected that its susceptance, properly located with respect to the barretter, provided a matched mount admittance at approximately 3.45 cm. Table 3·9 contains VSWR data taken with 16 type 821 barretters in the 82X mount that uses a fixed end-plunger position. It will be observed that the barretter mount has a

TABLE 3·9.—DATA ON VSWR OF 16 BARRETTERS IN THE TYPE 82X MOUNT

VSWR	Wavelength, cm.				
	3.13	3.24	3.33	3.43	3.53
Highest	1.29	1.15	1.23	1.18	1.27
Second highest	1.27	1.14	1.21	1.14	1.21
Average	1.20	1.09	1.15	1.10	1.13

bandwidth similar to that of the *O-O* thermistor mount. Figure 3·60 shows clearly the influence of the resonant iris on the broadband match of the mount.

In the mount of Fig. 3·59 microwave chokes are used at each end of the barretter capsule to reduce microwave leakage. The barretter is installed from the top of the mount, after removing the threaded plastic cap.

The Sperry Gyroscope Company has developed a 6-cm barretter mount in a 2- by 1-in. waveguide which meets the specification of a maximum VSWR of 1.5 over a ± 12 per cent wavelength band. It is similar in construction to the 3-cm-band type 82X mount.

Design work on a series of coaxial-line barretter mounts is currently in progress. It has been established that a low-resistance (for example, 125-ohm) barretter can be more easily broadbanded in a coaxial-line mount than can the 200-ohm type 821 barretter. There is an advantage in operating the wire at a resistance that is close to the characteristic impedance of the line. The disadvantage of a low-resistance wire is the decreased maximum power dissipation. Tests made over a 9- to 20-cm band with type 821 barretters in $\frac{1}{2}$-in. coaxial line have indicated the following results. With the microwave short circuit at one end of the capsule, there is a plane near the opposite end of the capsule at which the termination impedance is almost entirely real and changes very slowly with wavelength. This impedance is approximately 300 ohms when the wire is biased to 200 ohms. These conditions are relatively favorable for broadband matching.

Uncapsuled barretters are used in waveguides as small as 1-cm-band. It has been mentioned in Sec. 3·21 that barretter wires can be installed in a 1-cm-band thermistor mount, but the barretter installation will not be as broadband as the thermistor for which the mount was designed. A simple tunable 1-cm-band barretter mount can be constructed by placing an inductive-capacitive side stub an odd number of one-eighth waveguide wavelengths in front of the wire. When thus placed the matching stub will have low loss. The use of side stubs may be avoided if the dimensions of the bolometer wire are properly chosen. A wire that has a diameter smaller than the skin depth and that is mounted across a waveguide has a microwave resistance equal to the d-c resistance of the wire and a reactance equal to that of a perfectly conducting wire of the same diameter. For match, both the relative resistance and reactance should be about 0.5. The resistance is most effectively controlled by the diameter and length of the platinum wire; the reactance is controlled by the length of the choke or other structural arrangements which do not produce bad distributions of current along the wire (see Sec. 3·24).

3·28. Load Lamps.—Lamps, like barretters, are hot-wire bolometers. The chief distinction between the two is in wire diameter. Lamps usually use wires considerably larger in diameter than the wires used in barretter construction. Because of the larger wire diameters, lamps are capable of greater power dissipation than are barretters. They are usually medium-level power detectors, useful in the range of a few milliwatts to a few watts. Also, because of the larger wire diameters, many lamps cannot be used for absolute power measurements. The lamps used in microwave power measurements are usually evacuated to increase their sensitivity, but are occasionally gas-filled to increase the maximum safe power dissipation. They may be used in bridge circuits, as are barretters, or they may be used with photocells or optical pyrometers which measure the brilliance of their filaments.

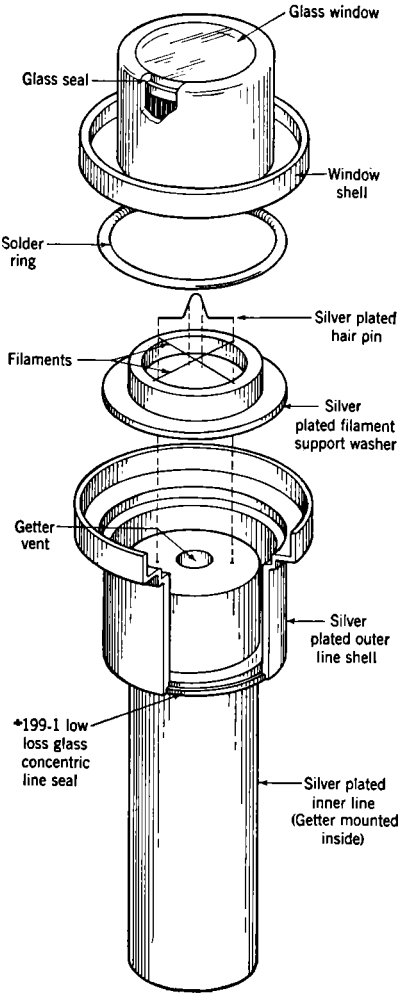

FIG. 3·61.—Construction of the General Electric Company L4PD load lamp.

The General Electric load lamps[1] have been extensively used for 10-cm-band power measurement, particularly in connection with the standardization of the output power of lighthouse-tube oscillators. The lamps are built as sections of coaxial line having glass seals between the inner and outer conductors to enclose the filament termination in a region of high vacuum. The termination consists of four equally spaced filaments mounted radially from the inner to the outer conductor. The end seal is made of glass to permit viewing the heated wire filaments. Figure 3·61 illustrates the construc-

[1] H. W. Jamieson and H. E. Beggs, "A New Power Dissipation Lamp for Microwave Applications," GE Data Folder No. 46248, Apr. 20, 1943.

tion of the lamp. The GE lamps are available in three wattage ratings. Table 3·10 summarizes the data for the three models.

TABLE 3·10.—WATTAGE DATA ON GE LOAD LAMPS

Model	Wattage			Visual glow at	Recommended wattage range
	For normal brilliancy	For 700°C	Max. for one hour life		
L4PD-1	1.5	0.04	3	40 mw	0.1- 2
L4PD-5	5.	0.1	10	100	0.5-7.5
L4PD-15	15.	0.25	30	250	2 -20

The lamps are commonly used with a barrier-layer photocell, the holder for which seats directly on the lamp at its window end. The lamp-photocell combination may be calibrated by dissipating known d-c power in the lamp; however, the d-c calibration is 8 to 10 per cent in error at 10-cm-band wavelengths because of losses in glass seals and metal contacts, and because the wires are larger in diameter than the skin depth of the microwave currents. This error has been experimentally determined by making the lamp and photocell holder watertight, immersing them in a water bath, and calorimetrically comparing the d-c and microwave power levels required for the same photocell current. When observed with an optical pyrometer, the filaments appear to be uniform in temperature with negligible end cooling. The calibration curve for the L4PD lamp is very nonlinear, as shown in Fig. 3·62.

Because of the filament shape, the L4PD lamps are not well impedance-matched. For example, the L4PD-5 gives a VSWR of 5 in a 50-ohm line at 500 Mc/sec, and the VSWR in the same line is about 10 in the 10-cm band. Tuning stubs and line stretchers are commonly used to maximize the input power to the lamps. The tuning adjustment is usually critical, and additional loss in poor tuner contacts is accepted.

In parallel with its program of barretter development, the Sperry Gyroscope Company has taken an active interest in microwave lamp investigations. In cooperation with the Aerolux Light Corporation they have developed a lamp suitable for installation in a $\frac{7}{8}$-in. or larger coaxial line. A typical lamp has a 0.0005-in. tungsten filament, approximately 1 cm long, which is enclosed in a cylindrical, side-exhausted glass bulb. Lead wires project from the ends of the bulb, as in the construction of capsuled thermistors, and the tungsten filament bridges the gap between the lead-wire ends. The lamps are installed in series with the inner conductor of the coaxial-line mount, in much the same manner as thermistors are installed in 10-cm band coaxial-line mounts. Maxi-

mum power dissipation for the filament is 0.5 watt in vacuum and 20 watts in hydrogen.

Since the filament resistance is low (6 ohms cold to 70 ohms at burnout) the lamps cannot be successfully broadbanded. A reasonably good match can be obtained, however, by the use of a single tuning adjustment, usually an end plunger which is adjusted to place a current loop at the filament. The resistivity of tungsten is sufficiently high that the diameter of a 0.0005-in. tungsten filament is no greater than the

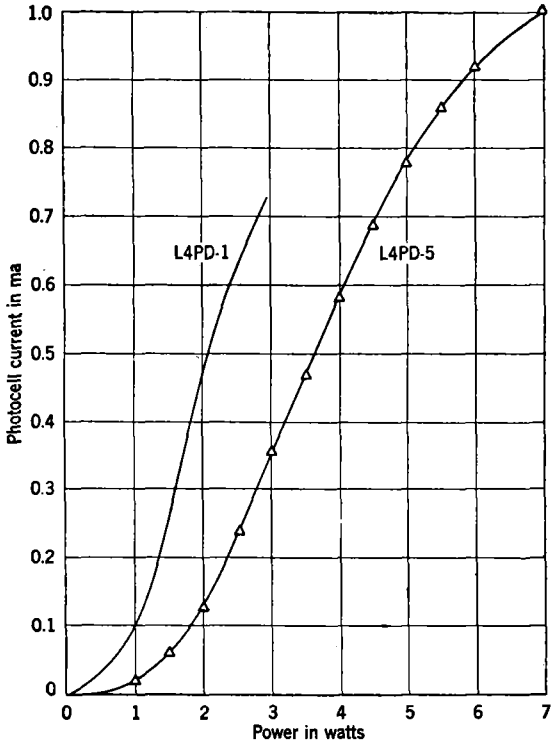

FIG. 3·62.—Representative calibration curves for General Electric Company load lamps.

skin depth at 10 cm. The lamps are used with balanced bridges and retuning is necessitated only by frequency changes and not by power-level changes.

Further study of the broadband matching problem has led to a radically different lamp structure. Since the development is not yet completed it is impossible to show an accurate sketch of its construction, but the drawing shown in Fig. 3·63 illustrates the more important features of a design by the Sperry Gyroscope Company.

The lamp filament (1) is a 0.1-in. length of 0.00175-in. carbon wire, or alternatively, a 0.25-in. length of 0.0005-in. tungsten wire, which is installed with duPont silver cement. It is contained in a 705 hard glass shell (2), which is heat-sealed to a silver-plated Kovar plug (4). The plug is shaped for easy pressure insertion into the inner conductor of the coaxial line. A 0.010-in. borated-copper wrinkled disk (3) is sealed between the two sections of the glass shell. When the lamp is installed the metal cap (5), separated into two parts by the insulation ring (8), screws onto the outer conductor. It thereby squeezes disk (3) between itself and metal ring (6). The high-frequency bypass condenser (7) is formed of anodized aluminum or borate block. The d-c path between the inner and outer conductors is completed by a stub cavity-coupling loop, or other arrangement.

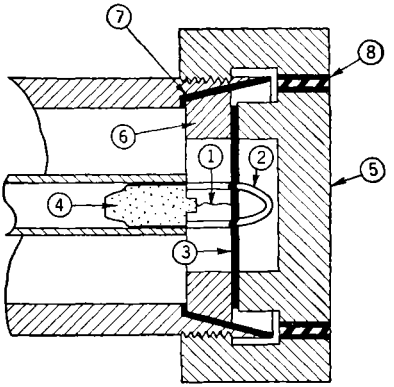

FIG. 3·63.—Sperry broadband lamp in coaxial-line mount.

The borated copper disk (3) terminates the line in a short circuit. This construction permits the filament wire to be located at a current loop that does not change position with frequency. The physical length of lamps with lead wires does not permit this. As in 10-cm-band coaxial-line thermistor mounts, the ID of metal ring (6) has a marked influence on the impedance match obtained. It is believed that the reduced outer diameter of the coaxial line introduces sufficient capacitance to resonate the inductance of the filament wire. The result is a low-Q circuit, heavily loaded by the resistance of the wire. The design is potentially capable of extreme bandwidth. One of the early research models has a VSWR less than 1.1 at 1000 Mc/sec, and less than 1.4 at 3000 Mc/sec. The maximum power capacity of the lamp is about 0.5 watt when evacuated and 5 watts when hydrogen-filled. The evacuated lamp with carbon filament has a detector sensitivity of approximately 33 ohms per watt.

The British have used a small lamp for power monitoring in one of their 10-cm-band signal generators. The microwave current flowing through the filament is used to excite fields in a waveguide-beyond-cutoff attenuator. The oscillator power is adjusted until the filament glow is barely perceptible. With the aid of a magnifying lens installed in a microscope tube directed at the filament, a trained operator can reproduce the setting to within a few tenths of a decibel. The monitoring arrangement is said to have small frequency sensitivity.

3·29. Metalized-glass Bolometers.—The Graduate Electrical Engineering Department of the Polytechnic Institute of Brooklyn has developed a bolometer[1] for medium-level power measurement at 10-cm-band which utilizes a tiny metalized-Pyrex tube as the detector element. The construction of the $\frac{5}{8}$-in. coaxial-line model is shown in Fig. 3·64. The inner conductor of the mount is supported by a broadband stub. The metalized-Pyrex tube, backed by a short circuit, terminates the line. Two $\lambda/4$ transformer sections, one of which is a small-diameter copper wire, are used for impedance matching. The bandwidth of the

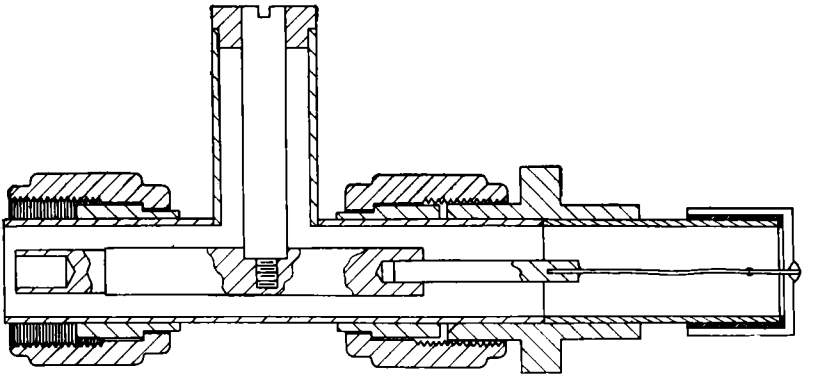

FIG. 3·64.—Section drawing of bolometer with metalized-glass tube.

PIB bolometer is as good as that achieved with thermistors in 10-cm-band coaxial-line mounts, or better. The calibration is stable, the overload characteristics are good, and the detector sensitivity is excellent for medium-level power measurements.

The Pyrex tube, drawn from standard 6-mm tubing, has an OD of 0.017 in. and a wall thickness of only 0.003 in. The exposed length of film is 0.7 cm. The heat capacity of the glass is small and the thermal lag of the element is not objectionable. For instance, with the 0.1- or 0.2-watt elements, less than 5 sec are required for a direct-reading bridge to reach final deflection, after application of the microwave power. The tube is metalized by baking a thin film of Hanovia No. 670 solution on the outer surface.

The procedures used for impedance-matching the element are of particular interest. The input impedance to an attenuating section of line at a point l cm distant from the short circuit which terminates it is given by

$$Z_i = Z_0 \frac{\sinh \alpha l \cdot \cos \beta l + j \cosh \alpha l \cdot \sin \beta l}{\cosh \alpha l \cdot \cos \beta l + j \sinh \alpha l \cdot \sin \beta l}. \tag{87}$$

[1] S. A. Johnson, "Metallized-Glass Bolometers," NDRC Report 14-524, Polytechnic Institute of Brooklyn, Oct. 31, 1945.

The input impedance for series-transformer matching should be real. Since there are only series losses in this bolometer design ($G = 0$), the condition that Z_i of Eq. (87) be real is that

$$\beta \sin 2\beta l = \alpha \sinh 2\alpha l, \tag{88}$$

where,

$$\alpha = \frac{\pi}{\lambda}\sqrt{2\sqrt{\sigma^2 + \sigma} - 2},$$

$$\beta = \frac{\pi}{\lambda}\sqrt{2\sqrt{\sigma^2 + \sigma} + 2},$$

$$\sigma = \frac{r\lambda}{2\pi Z_0} = \frac{L}{KZ_0},$$

$$Z_0 = 60 \ln \frac{d_1}{d_2}.$$

The diameter ratio of the conductors is d_1/d_2 and r is the resistance per unit length of line.

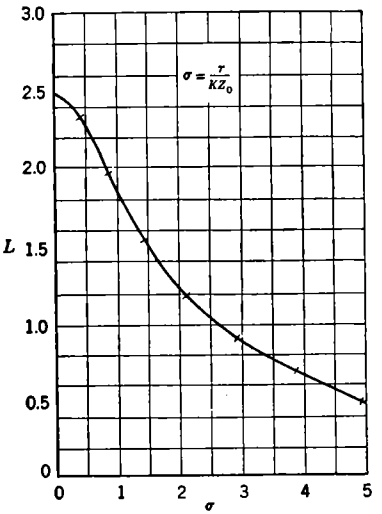

FIG. 3·65.—Length of short-circuited resistive line section to give a real input impedance.

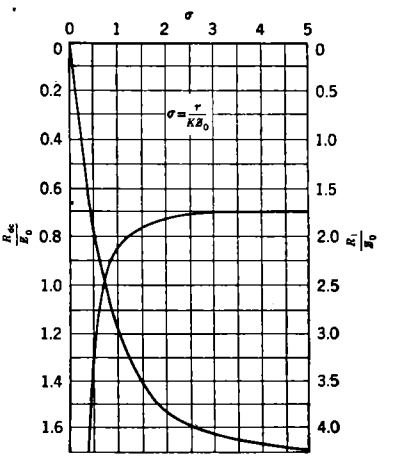

FIG. 3·66.—Input impedance to a short-circuited resistive line section at $\lambda = 10$ cm. The length of line is specified by Fig. 3·65.

If values are assigned to λ, r, and Z_0, a value for L, the length of line required to give a real input impedance, may be determined. Figure 3·65 shows a graph of L as a function of σ for $\lambda = 10$ cm. In Fig. 3·66 there are shown the corresponding values of R_i, the input resistance as computed from Eq. (87), together with values of the total d-c resistance R_{dc} of the length L of resistive center conductor. It is understood that data from Fig. 3·66 apply only when L is chosen from Fig. 3·65.

A value of $L = 0.7$ cm was chosen since this gives a value of R_i which is practically independent of small changes in R_{dc} (or r). Consequently, the mount impedance can be expected to be relatively independent of the power level measured with a direct-reading bridge. If the tube diameter is chosen as 0.017 in., thereby making Z_0 equal to 208 ohms, the other design data may be taken from the curves as follows:

$$\sigma = 3.73, \qquad R_i = 363 \text{ ohms}$$
$$r = 486 \text{ ohms/cm}, \qquad R_{dc} = 341 \text{ ohms}$$

In order to obtain the desired bandwidth, a pair of $\lambda/4$ transformer sections is used to match the element to the 50-ohm line with which the bolometer mount is used. The transformers are deliberately designed so that at the midband wavelength the input impedance of the mount is somewhat greater than that required for match, with the result that the reflections are reduced at the edges of the band. Figure 3·67 shows a comparison of the computed and measured values of the reflection coefficient for a typical bolometer.

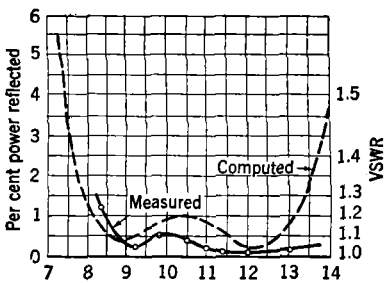

FIG. 3·67.—Calculated and measured VSWR-λ curves for metalized-glass bolometer. The wavelength scale is in centimeters.

Rose's metal is used for soldering the bolometer element to the end cap of the mount and to the copper-wire transformer section. Thus element replacement is not so simple as for a barretter or thermistor. After installation, the film is seasoned by passing 40 ma through it for 30 sec. After this treatment, the cold resistance of the film at 25°C is approximately 330 ohms.

The 0.1-watt (nominal rating) element burns out at approximately 0.8 watt, but power levels greater than 0.3 watt can effect a permanent change in the cold resistance. The detector sensitivity is approximately 220 ohms per watt.

The 0.1-watt bolometer is conveniently used in a direct-reading bridge having the resistances of all arms equal to 330 ohms, 20-ma bridge current (or 10-ma bolometer bias), and a 0-200-μa, 360-ohm bridge meter. Under these conditions the bridge sensitivity will be roughly 0.1 watt for full-scale deflection. No attempts have been made to introduce drift and sensitivity compensation in the bridge, but the methods discussed in the sections on thermistor bridges are in general applicable.

The PIB bolometer has been particularly useful in making laboratory measurements on the output power of the 10-cm-band local-oscillator

tubes. The detector sensitivity and 0.3-watt safe power dissipation place it in exactly the required range. When barretters or thermistors are used for this application, calibrated attenuators are required to reduce the power level to the range in which these bolometers operate. Further, the problem of zero drift in bridge operation is less troublesome if the power can be measured at a 0.1-watt rather than at a 0.001-watt level.

3·30. Thermocouple Power Detectors.—Relatively little use has been made of thermocouples as detectors in microwave power measurement, partly because of inherent limitations, but largely because the development of thermocouples specifically designed for microwave applications came too late in the progress of the war to attract great interest. Thermocouples may, however, assume increasing prominence in future microwave developments.

The greatest advantage associated with the use of the thermocouple is the simplicity of the indicator circuit. In contrast to the current supply and numerous bridge components required by the thermistor and barretter, only a millivoltmeter is required by the thermocouple. It may, however, have many disadvantages. Unless the thermocouple is used within a small fraction of the safe power range, the millivoltmeter calibration is apt to be objectionably nonlinear in microwave power, partly because radiation cooling at high temperatures is a more effective agent for heat dissipation than conduction or convection cooling at low temperatures. Also, since the internal resistance of the thermocouple varies with temperature (hence power level), the fraction of the thermal emf which is lost as a voltage drop across the thermocouple varies with the power level.

The sensitivity of the thermocouple is not comparable to that of a thermistor or barretter bridge unless an evacuated thermocouple capsule is used. Evacuated thermocouple capsules are not easily made as small as thermistor or barretter capsules; hence their use is limited to 10-cm band and longer wavelengths where waveguide and coaxial-line sizes are large enough for convenient mounting of the larger capsules. The more common directly heated thermocouples that use a pair of soldered or spot-welded wires have a d-c resistance of only a few ohms. Consequently, they are extremely difficult to broadband in a microwave mount, the characteristic impedance of which is much larger than the d-c resistance. Moreover, the wires used in construction are considerably larger in diameter than the skin depth at microwave frequencies. Whereas an extremely fine barretter wire can be made by etching Wollaston wire, it is not possible to fabricate a thermojunction with wires of such small diameter.

Many of these difficulties have been overcome in a series of thermo-

couples developed by the Bell Telephone Laboratories.[1] There are three types of thermocouples—the familiar, direct-heated two-wire thermocouple, the carbon-bridge thermocouple, and the resistive-bead thermocouple. All are contained in low-loss glass capsules with lead wires that project from the ends of the capsules. The carbon-bridge type consists of a length of fine carbon filament secured across a short gap between the thermocouple wires. The hot junction comprises the bridge and the connections to the wires. By the proper choice of the length and diameter of the filament, resistances of over 100 ohms can be obtained without too great a sacrifice in ruggedness. A large fraction of the input power is absorbed in the small volume containing the hot junction, and the sensitivity is about twice that of a simple two-wire element. The bead thermocouple includes a tiny glass bead coated with a thin metallic film in which the two wires of the thermoelement terminate. Most of the thermocouple resistance is concentrated in the bead film. The construction is rugged, and the film is sufficiently thin to avoid variation of skin depth with frequency.

One of the 100-ohm carbon-bridge thermocouples was calibrated at direct current and at 10 cm against a barretter. The two elements agreed within the experimental error of 2 to 3 per cent. No data of this sort are available for the bead thermocouple, although it seems reasonable that the agreement should also be good for this structure.

The conditions limiting the maximum safe power dissipation in a thermocouple are of interest. The resistance of a continuously overloaded thermocouple, immersed in air at atmospheric pressure, slowly increases because of oxidation of the wire. However, oxidation cannot occur if the capsule is evacuated, and slow sublimation of the wire sets the safe upper power limit in this case. An additional factor enters in the carbon-bridge thermocouple. An evacuated carbon-bridge thermocouple loses sensitivity without suffering a resistance change, when overloaded. This is probably caused by an outgassing of the carbon and a consequent pressure rise within the capsule. Unfortunately this occurs at a power level which is only a small fraction of that required for burnout.

The characteristics of a number of the BTL microwave thermocouples are summarized in Table 3·11. The list is by no means complete, but is intended to be representative of what has been accomplished. Since research on thermocouples is still continuing at the Bell Telephone Laboratories, it can be expected that further improvements will appear.

[1] J. A. Becker and J. N. Shive, "Thermocouples for Use as High Frequency Wattmeters," BTL Report MM-43-110-4, Mar. 4, 1943. J. N. Shive, "Temperature Coefficients of Sensitivity and Resistance, Overload and Burnout Data for Several Types of Ultra-high Frequency Thermocouples," BTL Report MM-43-110-18, June 23, 1943.

TABLE 3·11.—SUMMARY OF DATA ON A VARIETY OF BTL MICROWAVE THERMOCOUPLES

Unit no.	D-c resistance,* ohms	Sensitivity,*† mv/mw	Max. safe input power, mw.	Type	Environment
D-165747‡	5	0.4	50	Direct-heated	Air, atmos. press.
1170TC-40§	22	8.9	10	Direct-heated	Evacuated
1170TC-72	10	0.25	100	Direct-heated	Air, atmos. press.
1170TC-125	66	0.38	25	Bead	Air, atmos. press.
1170TC-129	42	0.38	25	Bead	Air, atmos. press.
1170TC-130	105	0.40	25	Bead	Air, atmos. press.
1170TC-148	120	2.7	25	Carbon-bridge	Evacuated
1170TC-160	24	4	10	Bead	Evacuated
1170TC-166	570	2.5	20	Carbon-bridge	Evacuated
1170TC-169	350	3.5	20	Carbon-bridge	Evacuated
1170TC-281	17	10	10	Direct-heated	Evacuated
1170TC-283	38	20	5	Direct-heated	Evacuated

* Approximate values, since they vary with power level.

† In some cases d-c data; in other cases low audio frequency. Microwave sensitivity may be several decibels lower in some models.

‡ Commercially available from Western Electric Co. Thermocouple mounted in a standard international silicon-crystal-rectifier cartridge.

§ Can be made available in a glass capsule mechanically interchangeable with that of the D-163903 bead thermistor.

If a thermocouple of thermal emf E and internal resistance R_c is connected to a meter having full-scale current sensitivity J and coil resistance R_M, the fraction n of full-scale deflection is given by

$$n = \frac{E}{J(R_M + R_c)}. \tag{89}$$

From Eq. (89) it may be seen that if $R_c \ll R_M$, the voltage sensitivity JR_M of the meter is the important factor in determining sensitivity. Conversely, if $R_M \ll R_c$, the current sensitivity J of the meter is the determining factor. The quantities J and R_M, are not necessarily independent variables if the size and ruggedness of the meter are to be held constant. Likewise, E and R_c are not necessarily independent. That is, smaller-diameter wire in a direct-heated thermocouple will increase R_c *and* E for constant microwave power dissipation. The calibration linearity is better if R_c is small compared to R_M, since variations in R_c with microwave power level have a negligible effect on n.

Early in the war the Bell Telephone Laboratories experimented briefly with 10-cm-band coaxial-line mounts for thermocouples, but

quickly abandoned the development in favor of bead-thermistor mounts. At that time the thermocouples available had many of the undesirable features discussed. A few tests were made at the Radiation Laboratory with thermocouples installed in thermistor mounts. A 38-ohm direct-heated thermocouple was installed in one of the 50-ohm, $\frac{7}{8}$-in. coaxial-line thermistor mounts designed for 10-cm-band use. The voltage standing-wave ratio was objectionably large, although it was observed that the admittance at the taper tip was constant at 0.4 ± 0.05 from 9.5 to 10.6 cm. Consequently, a change in the characteristic impedance of the line would result in a much better impedance match. A 200-ohm carbon-bridge thermocouple was installed in an *O-O* thermistor mount for the 3-cm band and, with an additional resonant iris, was matched to give a VSWR less than 1.5 over the 3.17- to 3.39-cm band. It was found, however, that the impedance match was very sensitive to microwave power level, and the effort was discontinued.

FIG. 3·68.—Photograph of thermocouple dipole.

The thermocouple dipole is an interesting adaptation of the thermocouple to microwave power measurement. The construction is best discussed by reference to Fig. 3·68, a photograph of the Philco design which was put into production by the National Union Radio Corporation.

The antenna is effectively a half-wavelength 10-cm-band dipole, the center of which is distorted into a long hairpin bend. The dipole is loaded by a thin, constantan wire which is arched across the gap at the center. To the center of this wire is spot-welded one end of a fine Chromel-P wire to form the hot junction of the thermocouple. The opposite end of the Chromel-P wire is tied to the top end of the vertical support rod, shown in the photograph. The thermocouple wires thus form a small T-structure with the curvature of the wires being of such nature that the T approximately fits the surface of a sphere of large diameter.

The dipole extracts power from free space, and the thermocouple current can be used as a rough measure of the microwave field strength at the location of the dipole. Therefore, if the dipole is always located in a fixed position with respect to a radar antenna, it can be used as a continuous monitor of the transmitter output power. The device is reason-

ably broadband, having an effective Q of approximately 10. The bulb surrounding the dipole is evacuated, and the time constant of the thermocouple is 15 to 30 sec. The sensitivity is approximately 0.1 mv/mw of microwave power. In establishing this sensitivity value it is necessary to measure the power delivered to a matched-impedance load by another dipole of equivalent gain connected to a coaxial line. The dipoles are mounted in absorbing corner reflectors.

Although specific mention has been made of constantan and Chromel P as the wires forming the thermojunction, it is of course possible to use other metal combinations. It is extremely important, however, to load the dipole with a wire having a very small temperature coefficient of resistance. The dipole is loaded in part by the resistive wire and in part by its own radiation resistance. In fact the equivalent circuit consists of a generator with an emf proportional to the electromagnetic field strength at the dipole which delivers current to a series combination of the load-wire resistance and the dipole radiation resistance. If the load-wire resistance is sensitive to the microwave power level, the power division between the two series loads will vary with the power level. This introduces a bad nonlinearity in the calibration curve of the dipole thermocouple.

Prior to the development of the directional coupler it was planned to make extensive field use of the thermocouple dipole. The directional coupler, however, offered a much more convenient and accurate means of monitoring radar transmitter power, and interest in the thermocouple dipole subsided.

3·31. The Use of Rectifiers for Power Indication.—Silicon crystals have been used to a limited extent as diode rectifiers in low-level power measurement. Like thermocouples, they offer the advantage of an extremely simple indicator circuit. Crystals are readily available for numerous mixer and video-frequency applications. Further, crystal cartridges can be made small enough for easy installation in transmission lines for 1-cm band and even shorter wavelengths. Unfortunately the disadvantages associated with crystal rectifiers greatly outnumber the advantages.

The crystal is applicable only to relative power measurements since it is necessary to calibrate the rectifier and the d-c microammeter against an absolute standard such as a balanced thermistor or barretter bridge. This fact alone would not seriously limit the usefulness of the crystal if the calibration were permanent. It is well known, however, that the calibration of a crystal rectifier may change appreciably if the crystal is subjected to shock, vibration, or overload. Any action which changes the condition of contact of the "cat whisker" against the rectifier surface

will change the calibration of the crystal. Although this fault alone is sufficient to make the crystal inadequate in most power-measurement problems, there are other serious objections.

At power levels of about 1 μw, crystals are very closely square-law detectors, but at power levels of about 1 mw, crystal response may deviate widely from the desirable square-law condition. Crystals vary widely in this respect; some are much worse than others. Crystals are difficult to match over a broad band because the impedance scatter at a given power level is very large, and because the impedance of a given crystal is relatively sensitive to power level. Consequently, there is no hope of obtaining the bandwidths that are possible with untuned and fixed-tuned barretter or thermistor mounts. The sensitivity of crystals as rectifiers varies tremendously. For example, tests on a large number of new 1N21 crystals showed variations of 10 to 1 in crystal current for a given microwave power level and in a tunable mount that provided matching for all crystals. Moreover, the sensitivity of a crystal rectifier is temperature-dependent. Finally, crystals may be damaged easily or burned out by high pulse power, even though the average power level is low. The above comments apply particularly to the 1N21 and 1N23 crystals. Little is known about the merits of the more recent welded-contact germanium crystals when used as rectifiers, but it is probable that they share at least some of the disadvantages common to the silicon type.

The advantages of crystal rectifiers make them particularly desirable when the problem is one of power indication rather than of power measurement. They are used extensively with wavemeters, for example, where a change in crystal current is used to indicate a condition of resonance. They are also used extensively with echo boxes as crude indicators of power level. The only important disadvantage of a crystal used with an echo box for spectrum analysis is its deviation from a square-law response, which tends to distort the spectrum. The time-delayed rise and decay of power in a high-Q echo box greatly protect the crystal against pulse-power burnout, and further protection may be derived from shunting the meter with a capacitance to avoid large video-frequency back voltages on the crystal. Crystals are used as rectifiers in receivers, but in this application the microwave power level is so low that the crystals have practically a square-law response.

Although no crystal mounts have been developed specifically for microwave power measurement, a variety of crystal mounts have been developed for general purposes.[1] These mounts do not have the bandwidths or low values of voltage standing-wave ratio that thermistor and barretter mounts possess unless 1 mw of power is incident on the crystal.

Vacuum-tube diode rectifiers have shown more promise than crystals

[1] See Vols. 15 and 16.

in microwave power measurements. Vacuum-tube diode rectifiers have more stable and less temperature-dependent calibrations than do crystals, and they can withstand greater overload abuse than crystals.

The General Electric Company[1] has used a modified GL-582 diode for monitoring the output power of a 10-cm-band signal generator. The diode is mounted with the cathode thimble in a waveguide, and the cathode-to-anode electron stream is used to excite an electromagnetic field in a waveguide-beyond-cutoff attenuator. The cathode of the diode is connected through an external resistor to a d-c meter and back to the tube shell. In order to complete the external d-c circuit between cathode and anode, a strip of Aquadag is painted on the glass cylinder of the tube between the anode and tube shell. The tube shell and cathode are insulated for direct current by an r-f bypass condenser built into the assembly.

Power from a 446-B oscillator is delivered through a coaxial line to the diode. The center conductor of the line connects to the anode of the diode, and the length of transmission line is made adjustable for tuning purposes. The meter current is used as an indication of the strength of the field excited in the waveguide-beyond-cutoff tube.

The GL-582 tube that was used in this design is no longer available. However, the 2B22 is mechanically and electrically equivalent to it except for the built-in cathode-to-shell bypass condenser. A suitable bypass condenser can be designed for the tube mounting. The GL-559 is the same as the 2B22 except for a larger diameter cathode structure. In addition, it is readily available.

The Radiation Laboratory has developed a 10-cm-band r-f envelope viewer (see Chap. 7) which uses a GL-559 diode in a tunable cavity. It is possible to calibrate the output voltage of the viewer as a function of the microwave input pulse power and to use the viewer for relative power measurements. A typical calibration curve[2] is shown in Fig. 7·33.

The diode may be used over a tremendous power range—from 20 or 30 mw to several hundred watts. The sensitivity of the diode as a power detector can be increased by the use of a larger load resistance, but this increases the rise time of the r-f envelope. The law of the diode is approximately

$$V \approx kP^{0.58} \tag{90}$$

where V is the output voltage of diode working into a 300-ohm load, P is the input pulse power in watts, and k is a constant. Consequently, if the output voltage is expressed in terms of the microwave pulse voltage

[1] G. E. Catalog No. 6933931 G2, "Standard Signal Generator, 8 to 12 cms."

[2] P. A. Cole, J. B. H. Kuper, and K. R. More, "Lighthouse R-f Envelope Indicator," RL Report No. 542, Apr. 7, 1944.

delivered to a matched-impedance load, an approximately linear calibration results. Equation (90) is not valid at low input power levels of 30 mw or less because of the zero current that is derived from contact potentials and initial velocity of the electron emission from the cathode.

The calibration of the diode is frequency-dependent because of changes in cavity coupling and changes in internal losses within the cavity and diode. The sensitivity of the diode is markedly dependent on the cathode emissivity, and the GL-559 diodes appear to vary considerably in this respect. The cavity is expensive and difficult to make and somewhat cumbersome to tune. The calibration is slightly temperature-dependent, and the zero current is an inconvenience at high sensitivities. For these and other reasons the cavity-mounted diode has not gained great popularity.

MEASUREMENT OF HIGH POWER

High-power measurements are concerned with average power levels of one to several hundred watts and with pulse power levels in the kilowatt range. With the single exception of lamps, all the power detectors that have been discussed are obviously incapable of dissipating many watts of power. Even lamps are of questionable usefulness because of the objectionable physical size of a design that is capable of dissipating a hundred watts for a long period of time. Consequently, an entirely different approach to the problem is necessary at these power levels. Since appreciable heat is developed by the dissipation of watts of power, it is at once evident that calorimetric techniques should be useful.

3·32. Water Loads.—The water load, most widely used detector for high-level microwave power, operates on a calorimetric principle. The power is totally absorbed in a matched-impedance section of transmission line that is wholly or partially filled with a flowing stream of water. The water itself dissipates all of the power, and the temperature rise in the stream is measured by calibrated thermocouples or thermistors. There are several procedures whereby the temperature rise may be related to the absolute microwave power level.

The design of a water load is analogous to that of a mount for a low-level bolometer. The impedance-matching and bandwidth are the most essential objectives. Instead of the problem of a temperature-compensated bridge circuit, the water load introduces the problem of a stable fluid flow circuit.

Since water is an ideal calorimetric fluid, it is fortunate that it also exhibits sufficient loss in the microwave region to make it an acceptable load material. Figure 3·69 shows a graph of the loss tangent[1] (tan δ) of

[1] The quantity, tan δ, is defined as the ratio ϵ''/ϵ', where the complex dielectric constant ϵ is defined as $(\epsilon' - j\epsilon'')$. Thus tan δ represents the ratio of the loss current to the charging current.

water as a function of frequency. In the frequency range up to about 10 Mc/sec, water shows the decreasing loss characteristic of a real conductivity. The space-charge polarization created by the unimpeded migration of charge carriers results in a frequency-independent conductivity. This condition demands that the loss tangent vary inversely proportionally to frequency. In the frequency range above 10 Mc/sec, the dipole characteristic of water predominates, and the loss tangent rises toward a maximum value which at room temperature is located above 30,000 Mc/sec. The dielectric constant of water is constant up to about 500 Mc/sec and slowly decreases to about half its original value at the frequency where tan δ is a maximum. The dielectric constant, like the loss tangent, is temperature-dependent. Approximate values of the dielectric constant, normalized with respect to the free-space value, are 86 at 1.5°C, 76 at 25°C, and 57 at 85°C, at 3000 Mc/sec.

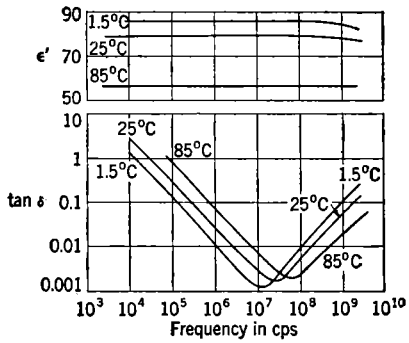

FIG. 3·69.—Loss tangent vs. frequency for distilled water. These data are taken from "Tables of Dielectric Materials," Report V, NDRC 14-237, Laboratory for Insulation Research, MIT, February, 1945.

At wavelengths considerably longer than microwaves the water load becomes objectionably long and impractical. In this case it is possible to consider an oil suspension of carbon particles as a substitute for the water, or it is possible to introduce an additional dissipative agent, for example, a highly resistive section of transmission line, which is cooled by the water stream.

3·33. The Design of Water Loads for Coaxial Lines.—In the design of water loads, attention must be given to several problems in addition to those of impedance-matching and bandwidth. As in a dry load, it is highly desirable that the power be dissipated uniformly along the length of the water column. If the input end of the water column carries the brunt of the power dissipation and if the temperature rise at that point is large, the resultant heat losses that occur prior to the thermometric measurement of the temperature rise can cause appreciable error in the power determination. Very large errors can result if the heat dissipation is so localized that superheating[1] of the water and steam generation result. Even under the circumstance of uniform power dissipation, it is important to reduce conduction and radiation losses to the minimum.

[1] C. J. Calbick, "Superheating of Water in Certain UHF Loads," BTL Report MM-43-140-63, Nov. 26, 1943.

The error caused by these losses is dependent on the method of calibration of the water load (see Sec. 3·35), and on the flow rate of the water column. "Dead pockets" should not exist in the flow stream between the thermocouple junctions, since such pockets usually suffer a high temperature rise and add to the undesirable heat losses. Microwave leakage from the water load can interfere greatly with other measurements that are being made in the vicinity of the load. The design of the load must be such that it will not arc at high pulse power levels. This is often a difficult design problem, and particularly so if the pulse power level is almost sufficient to cause arcing in the air-filled transmission line. Finally, the heat capacity of the load should be small so that a rise to the equilibrium temperature can be obtained quickly.

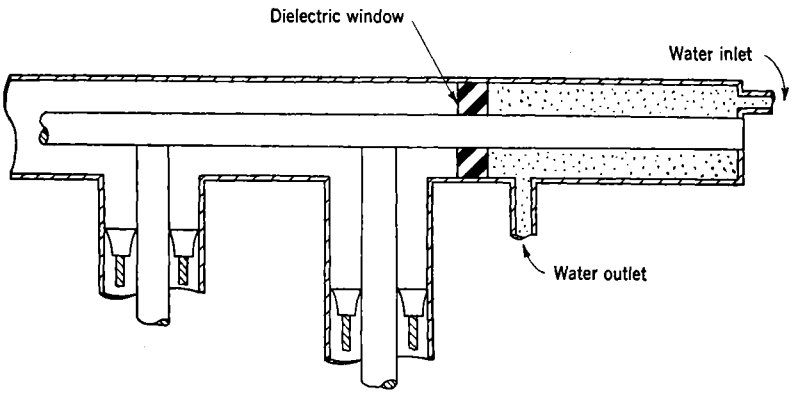

FIG. 3·70.—Early model of 10-cm-band coaxial water load.

A sketch of a 10-cm-band coaxial water load, perhaps the earliest, is shown in Fig. 3·70. A dielectric window has been cemented across the line to retain the water that is circulated through the terminal end of the coaxial container. The impedance-matching is effected with a pair of coaxial stub tuners. This design has many of the faults that can be found with water loads. The heat capacity of the load is so large that it is difficult to follow changes in power level having a period less than one minute. Consequently, the use of the tuners is extremely tedious, and the impedance-matching operation may require 5 or 10 minutes. The tuners can be dissipative, particularly if they are so adjusted that the finger contacts rest at a current loop in the stub line. The heat dissipation is nonuniform and is maximum at the input end. There is free heat interchange with the surroundings; dead pockets undoubtedly exist in the flow pattern. Arcing occurs at relatively low pulse power levels. This design furnishes a good example of how *not* to build a water load.

The 10-cm-band coaxial water load shown in Fig. 3·71 is a consider-

ably improved design. The broadband right-angle stub serves not only as a support for the inner conductor, but also represents a convenient means for bringing the water into the load. The tapered inner conductor fits into a glass tube, and is slotted to permit the water to flow from the interior into the glass tube, and thence out of the load. The taper serves several useful functions. When made sufficiently long, at least one wavelength, it is effective as a broadband impedance-matching transformer. It tends to distribute the power dissipation uniformly along the length of the exposed water column, and also to prevent arcing at operating pulse power levels since there are no sudden discontinuities in

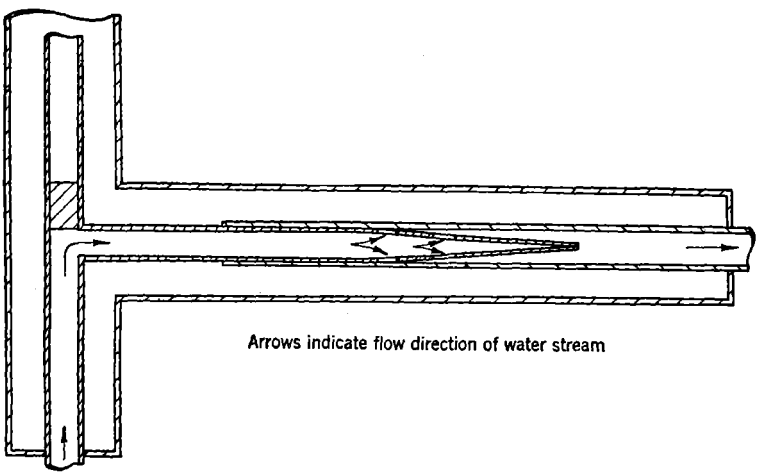

FIG. 3·71.—Improved 10-cm-band coaxial water load.

the line. In this design the taper must be long enough so that the attenuation of the water column over the length of the taper is sufficient to absorb the reflections from the open circuit at the end of the taper. The construction is also good from a calorimetric point of view since the heated water stream is confined primarily by glass of low thermal conductivity. The metal conduction losses would be increased if the water stream were directed opposite to the preferred direction shown by the arrows in Fig. 3·71.

A modification of the design shown in Fig. 3·71 allows the coned tip of the inner conductor to continue as a constant-Z_0 line to the end of the load. The intake and exhaust for the water stream can then be located together at the terminal end of the load, and there is no need to introduce the water stream through a stub line. It is probably a more convenient design to build and to use, but the opportunity for metal conduction losses along the length of inner conductor is increased. Either type of load

is well matched; for example, it is possible to meet a specification of VSWR < 1.05 from 9 to 11 cm.

At wavelengths considerably longer than those of the 10-cm band the taper length of the Fig. 3·71 design becomes objectionably long. For longer wavelengths it may be advisable to use step transformers for impedance matching. The Bell Telephone Laboratories have designed a 30-cm water load[1] which is similar to that shown in Fig. 3·70 except that the pair of tuning stubs and dielectric window are replaced by a Micalex or an F66 steatite $\lambda/4$ transformer section. The steatite is the prefera-

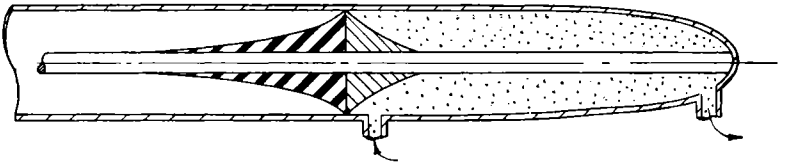

FIG. 3·72.—Water load for 1000 to 3000 Mc/sec developed by Radio Research Laboratory.

ble material from a machining viewpoint, and can be readily secured in the line with rubber cement. The VSWR of the load is less than 1.10 from 1040 to 1120 Mc/sec. In the design of quarter-wavelength transformer sections, it is desirable to select a material with a dielectric constant approximately 9, the geometric mean of the values for the air-filled and water-filled lines. Since numerous factors must be considered, for example, low attenuation constant, proper expansion coefficient and machineability, it may be necessary to select a somewhat smaller value of dielectric constant. An inner- or outer-conductor metal sleeve must be used with the plug in order to get the proper characteristic impedance in the transformer section.

The Radio Research Laboratory of Harvard University has developed a coaxial water load and associated closed-flow system[2] that can be used over the entire 1000- to 3000-Mc/sec band. The load is built in $\frac{5}{16}$-in., 50-ohm coaxial line with a 0.50-in. Chromax wire as the inner conductor. The water column need be only 9 in. long; the attenuation per wavelength in water at these frequencies is small, but the high dielectric constant of water effectively crowds many wavelengths within the specified physical length. The outer conductor is tapered into the inner conductor at the terminal end of the load in order to distribute the losses more

[1] R. C. Shaw and W. F. Bodtman, "Water-Cooled Load and Power Measuring Apparatus for Microwave Transmitters," BTL Report MM-42-160-141, Nov. 25, 1942. R. J. Kircher, BTL Report MM-32-160-187, Nov. 5, 1943. (Both reports have same title.)

[2] W. R. Rambo, "An R-F Wattmeter for the 1000mc–3000mc Range," RRL Report 411-209, June 22, 1945.

uniformly along the length of water column. The water column is confined in the line by a pair of fired TiO_2 tapers, installed with their bases together (see Fig. 3·72). The input taper used for impedance matching, is an exponential taper of 6-in. length. It proceeds from the inner to the outer conductor, where it is joined at the base with a shorter taper that noses into the water column. The shorter taper compensates for the variation of the dielectric constant of water with temperature, and thereby avoids dependence of the impedance match on power level and ambient temperature. The maximum VSWR of the load is 2 over the specified frequency range, and the average VSWR is 1.5. The maximum safe average power dissipation is 150 watts; no information is available on the maximum safe pulse-power rating.

3·34. Water Loads for Waveguide.—There is more latitude for ingenuity in the design of waveguide water loads, and a wider variety of

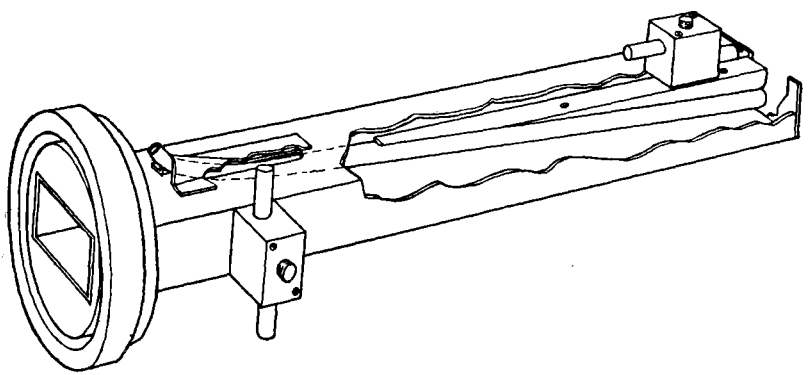

FIG. 3·73.—Radiation Laboratory 10-cm-band water load.

designs exists. An early Metropol-Vickers (British) 10-cm-band water load utilizes a pressure-molded polystyrene chamber which slips into a section of brass waveguide. The front end is wedge-tapered, from broad side to broad side of waveguide, for impedance matching. A dielectric partition along the axis of the waveguide divides the chamber into two sections, each with an approximately square cross section. The water stream is introduced at the rear end of the load, flows forward along one side of the partition, and returns along the other side. Except for the volume occupied by the thin-walled chamber and its partition, the waveguide section is completely filled with water. Polystrene has both low loss and low thermal conductivity, which make it a desirable dielectric for the application. The most important objections to the design are that arcing can readily occur at the leading edge of the taper, and that a stagnant, overheated pocket of water lies in the wedge tip behind the

leading edge of the taper. Increasing the taper length reduces the arcing, but increases the trouble from the water pocket. The 3-cm- and 10-cm-band waveguide water loads used in the Radiation Laboratory were designed as shown in Fig. 3·73. Rather than filling the entire waveguide section with water, the water is passed through a low-loss glass tube that slants across the waveguide from the center of one broad side to the center of the other. The combination of (1) slanting the tube, and (2) decreasing the bore toward the front end of the load provides both excellent impedance matching and reasonably uniform power dissipation along the length of the water column. The attenuation in the water column must be sufficient to absorb the reflections from the short circuit at the terminal end of the waveguide. An empirical approach is used to establish the optimum set of conditions on length, diameter, wall thickness, and tapering of the glass tube. The 10-cm-band and 3-cm-band loads both meet a maximum VSWR specification of 1.05 over the 9- to 11-cm and 3.13- to 3.53-cm bands, respectively. The tube shape that meets this broadband VSWR specification introduces no arcing problem at the pulse power levels of the best magnetrons available in 1945.

There is a practical restriction on the extent to which the bore of the tube may be tapered. If made too small, the flow through the tube may become turbulent at the flow rate required for the optimum temperature rise in the stream. In the 10-cm- and 3-cm-band designs the bore has not been reduced enough to get uniform power dissipation, and the front end of the water column develops somewhat more heat than the rear end. For this reason it is advisable to direct the water from the rear to the front of the load, since the hottest point in the stream should be closest to the hot thermojunction if heat losses occurring prior to the measurement of temperature rise are to be kept to a minimum.

A somewhat different approach to the problem has been taken by TRE.[1] They have designed a 10-cm-band water load,[2] Fig. 3·74, that relies on tapered waveguide dimensions rather than on a slanting of the tube to dissipate the power more uniformly along the length of the water column. The tapering in the resonant dimension increases the waveguide wavelength and decreases the energy velocity near the apex of the pyramid. This not only leads to more uniform power dissipation, but the effective electrical length of the pyramid is less than that of a waveguide of uniform cross section of the same physical length. It is believed that this accounts for the broadband properties of the load.

Two concentric glass tubes, supported by dielectric plates, carry the water into and out of the chamber. A capacitive iris is used for imped-

[1] Telecommunications Research Establishment, Malvern, Eng.

[2] "Power Measurement on 9 cm.," TRE Report No. G. 10/R 139/43, May 27, 1943.

ance-matching. Over an 8 per cent wavelength band the VSWR of the load is below 1.06. The load is recommended for use in the power range of 10 to 200 watts, average. The maximum safe pulse power rating is not available, but it is likely that arcing will occur at the iris if the pulse power level is high enough. At a flow rate of 5 cc/sec, and at an average power level of 100 watts, a steady-state temperature rise is reached in 10 to 15 sec. This figure is comparable with that for the slanted-tube design.

Another TRE water load, designed for 3-cm-band use, employs a hard silica-glass tube that is bent in the shape of a long hairpin. The plane of

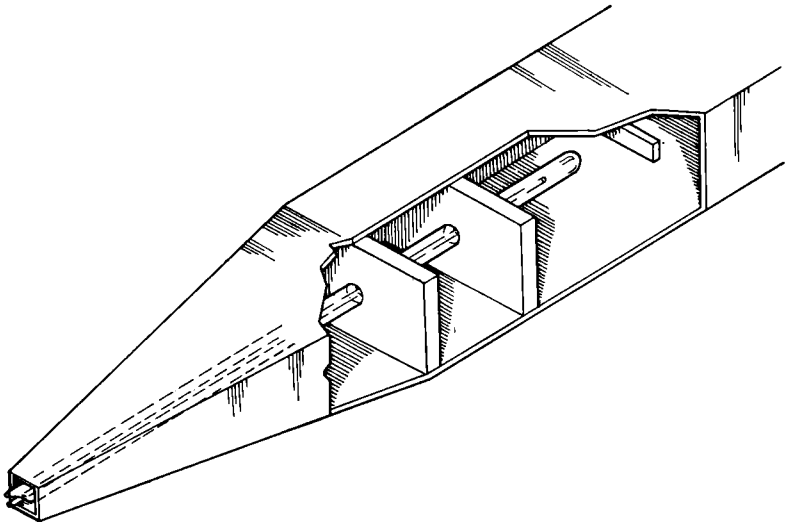

FIG. 3·74.—TRE 10-cm-band water load.

the hairpin parallels that of a narrow side of the waveguide, and lies near a side of the waveguide rather than at the center. Thin-walled, $\frac{1}{8}$-in. tubing is a desirable size for 1- by $\frac{1}{2}$-in. waveguide. In order to facilitate impedance matching the bend of the hairpin should be brought to a long, reasonably sharp point, rather than being smoothly rounded. The design has a VSWR less than 1.05 for a ± 4 per cent bandwidth. In 3-cm-band and smaller waveguides it is possible to support such a tube from the short-circuited end of the waveguide; at the 10-cm-band it would be necessary to support the longer tube with dielectric vanes that would probably decrease the bandwidth of the load. The hairpin is placed off center to get greater bandwidth, just as waveguide fixed-attenuator plates are positioned off center.

The Bell Telephone Laboratories have developed several slanted-tube

water loads;[1,2] the most interesting of these[2] is shown in Fig. 3·75. The glass flow tube is introduced through a channel and a slot cut in the bottom side of the waveguide. The channel is tapered so that it becomes shallower and broader toward the rear end of the load; the width of the slot increases with that of the wedge-shaped channel. The tube may also be tapered to a larger diameter toward the rear of the load. The construction represents an excellent means of bringing the tube into the waveguide without introducing reflections. The very small slot reflections are effectively canceled by placing their equivalent reflection $\lambda_g/4$ from the waveguide connection, which has a reflection coefficient of

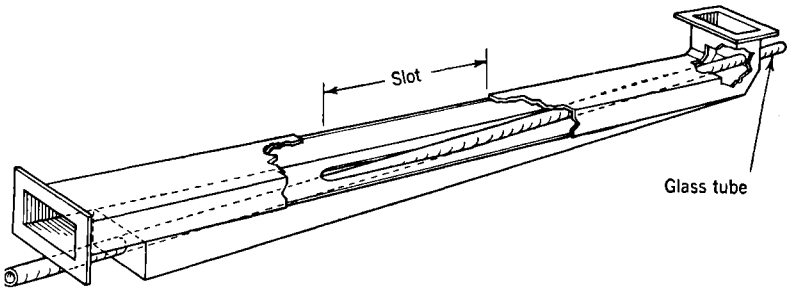

FIG. 3·75.—BTL 3-cm-band water load.

approximately the same amplitude. It is thereby possible to maintain the VSWR of the load below 1.02 over a 15 per cent band.

The load can be regarded as a matching section in which the water column is gradually exposed to the microwave field, and an attenuating section in which the water column is fully exposed to the field. The break comes approximately where the channel has a square cross section, or about one third of the distance from the front end of the channel to the rear of the load. Consequently, a shallower channel taper does not add proportionately to the total length of the load, and it is wise to make the taper a very gradual one.

The attenuation of the water column is approximately 1 db/cm, using 702P Nonex glass of 0.145 in. ID and normal wall thickness. Increasing the wall thickness increases the attenuation rate. The attenuation constant is roughly proportional to frequency. The total attenuation should be approximately 30 db to realize the low VSWR value quoted above.

The Westinghouse Electric Corporation has developed a useful 3-cm-

[1] N. Wax, "A Wide Range X-band Load," BTL Report MM-43-140-56, Nov. 5, 1943.

[2] C. J. Calbick, "Broadband UHF Calorimetric Load," BTL Report MM-44-140-76, Dec. 29, 1944.

band water load of extremely simple construction.[1] A short length of Pyrex tubing, $\frac{1}{4}$ in. OD and 0.93 mm capillary bore, extends across the waveguide through two directly opposite holes that are centered in the broad sides of the waveguide. An adjustable end-plunger provides an approximate impedance match; additional tuning screws are required for an exact match. The compensating advantage is that the response of the load is extremely fast because (1) only a few hundredths of a cubic centimeter of water are contained within the waveguide, and (2) the

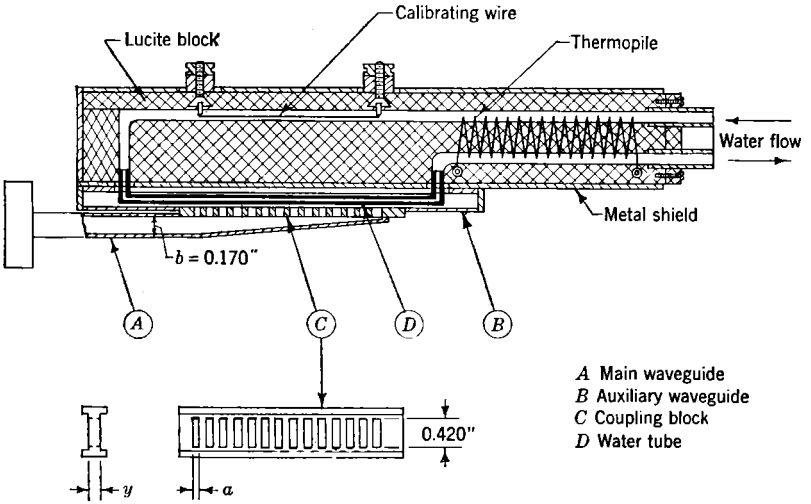

FIG. 3·76.—Water load for the 1-cm band.

thick-walled Pyrex tube has excellent heat insulating properties. In fact, the thermal time constant of the load is smaller than the time constant of the galvanometer used with its thermocouple. The thermocouple junctions are installed in rubber tubing at each end of the Pyrex tube.

The first Radiation Laboratory models of 1-cm-band water loads were patterned after the slanting-tube 10-cm- and 3-cm-band designs and the capillary-tube design. Because of the difficulty of scaling down the glass tube diameter proportionately with the decrease in waveguide dimensions, the design is much less satisfactory at 1-cm band than at longer wavelengths. A new design of water load,[2] based on the principle of the branched-guide directional coupler, subsequently replaced them. The details of this design are shown in Fig. 3·76.

[1] R. J. Schneeberger, "Capillary Tube Waveguide Power Measurer for Use at 3.20 cm," Westinghouse Research Report SR-142, Oct. 5, 1942.

[2] R. M. Walker, "K-Band High-Power Water Load," RL Report 723, May 10, 1945.

The glass-enclosed water column is contained in an auxiliary waveguide section that is coupled to the main waveguide by a linear array of 14 rectangular branches. The spacing and length y of the coupling branches are both chosen to be $\lambda/4$, with proper corrections for junction effects. These conditions (see Chap. 14) are optimum for impedance matching. If the wide dimensions of the main and auxiliary waveguides are the same but the narrow dimensions are b_A and b_B respectively, the percentage of the incident power coupled out per branch, P, is

$$P = \frac{a^2}{a^2 + 2b_A b_B}, \tag{91}$$

where a is the narrow dimension of the rectangular cross section of the coupling slots; $a = 0.061$ in., and it is assumed that the impedance looking either way from a point in the auxiliary waveguide is a match. Equation (91) suggests that the power coupled out per branch can be maintained constant by varying the dimension b_B, that is, by sloping the wall opposite the branches in the main waveguide. A linear slope approximately meets this condition—each branch coupling out 7.1 per cent of the total power to be absorbed.

Since the main line contains no dielectric or dissipative materials, the load should stand pulse power levels almost as high as those required for arcing in a uniform section of waveguide. No arcing was observed at a pulse power of 120 kw, the maximum available at the time of test. The VSWR of the load is less than 1.10 over an 8 per cent band.

A 16-junction copper-constantan thermopile and a heater wire for calibration are built into the load. They are mounted in a lucite block which provides good electrical and thermal insulation. Using a nominal flow rate of 3 cc/sec, a thermopile current of 60 μa with a 10-ohm meter results, for 20 watts average input power. The thermal time constant of the load is slightly less than one minute. The design has considerably less microwave leakage than many water loads because of the long length of water column that is enclosed by the metal shield around the load.

3·35. Flow Systems for Water Loads.—Flow systems of two kinds, open and closed, are used with water loads. In the open-flow system an elevated, continuously overflowing tank is used to maintain a constant pressure head on the stream flowing through the water load. In the closed-flow system the water is constantly recirculated through the load by means of a metering pump. Each method has its protagonists, and each has its advantages.

Discussion of the design objectives and design details of the two flow systems must be preceded by a discussion of the several methods of calibration used for water loads. The first of these involves a calculation of the microwave (average) power level from the formula

$$P = 4.18 m c_w \Delta T \quad \text{watts}, \tag{92}$$

where m is the speed of water flow (in g/sec) through the load, c_p is the specific heat of water (in cal/g°C), and ΔT is the temperature rise (in °C) due to absorbed microwave power. A thermopile is commonly used to measure the temperature rise, and a flowmeter or stop watch and a container of known volume is used to determine the flow rate. In addition to the errors inherent in the flow-rate and temperature-rise measurements, a calculation of P from Eq. (92) neglects any heat exchange that may occur between the water column and its environment throughout the length of flow line between the hot and cold junctions of the thermopile. This neglect may or may not be serious, depending on the construction of the specific water load. The thermopile is calibrated against a precision mercury thermometer by placing the cold-junction pairs in one water bath and the hot-junction pairs in another of somewhat higher temperature. The baths are well agitated, and care is taken that the junctions reach equilibrium temperatures at the time the galvanometer deflection is noted.

A second method of calibration involves the use of a heater coil which is installed in the flow stream immediately ahead of the water load and between the hot and cold thermopile junctions. Sixty-cycle power is applied to the heater coil through an accurate a-c wattmeter, and a Variac auto-transformer is used to adjust the power level. With an additional decade-box control of the thermopile meter sensitivity, it is possible to adjust the full-scale galvanometer deflection to correspond to any desired power level. The method avoids the necessity of calibrating the thermopile against a thermometer and avoids any measurement of flow rate. However, it *is* assumed that the flow rate is the same for the microwave power measurement as for the heater coil calibration. If the microwave power dissipation is reasonably uniform along the length of the water column exposed to the high-frequency fields, the problem of heat exchange with the environment is effectively solved. The heat exchange will be reasonably independent of whether the water column is heated by microwave or a-c power dissipation. This does not hold, however, if the power dissipation is badly nonuniform, and particularly if hot pockets exist in the flow stream near the input end of the load.

The heater-coil principle of calibration is most effective if the heater coil and thermojunctions can be built into the load as has been done in the 1-cm-band water load shown in Fig. 3·76. Accuracy is lost if the heater coil is located outside the load and heat exchange is possible in the length of flow line between the heater and the section of tubing exposed to the microwave fields. In such a case it is advisable to use the following modification of the heater-coil principle.

If the thermojunctions are not designed into the load, as shown in Fig. 3·76, it is customary to install them in a separate two-tube block that is mounted directly on the water load. The interior of the block can be the same as that portion of Fig. 3·76 concerned with the details

of the thermojunction installation in the lucite block. The flow of water is then directed through one tube of the block, through the water load, and back through the other tube of the block. The block can be removed from the water load and a thermally shielded, glass-enclosed heater coil substituted in the flow circuit for the water load. If the flow rate and a-c power are known, Eq. (92) can be solved for ΔT. This method offers a means of calibrating the thermopile without having to remove the junctions for immersion in water baths. The microwave power calculation may be based on Eq. (92), or the heat exchange may be assumed to be the same for the water load as for the calibration tube, in which case the second calibration method may be followed.

Such a calibration tube can be easily made by inserting a spiral nichrome coil into a glass U-tube and soldering or spot-welding the ends of the tube to heavy copper lead wires which are heat-sealed in the sides of the U-tube. The tube is placed in a cylindrical box stuffed with cotton, glass wool, or any material of low thermal conductivity and low heat capacity. Bakelite ends complete the box.

There is a third method of using a heater coil that is placed in series with the water load in the flow stream. Two identical thermocouples are used, one with junctions on each side of the heater coil, and one with junctions on each side of the water load. Alternatively, the thermal emf's of the two thermocouples may be placed in opposition across the terminals of a galvonometer, or the thermocouples may be used as two of the arms in a balanced-bridge circuit. In either case the a-c power is adjusted to restore balance after the microwave power dissipation in the load has caused a deflection. The microwave power level can be read directly from the a-c wattmeter, and the measurement is independent of flow rate. The null indicator, however, must be very sensitive for accuracy, and it is advisable to use a d-c photocell amplifier.

The problem of heat exchange between the exposed column of water and its environment deserves further discussion. If the water load is in thermal equilibrium with its environment at the existing ambient-temperature level, and if the water stream brought into the load is colder than ambient temperature, the water picks up heat between the two points of measurement (hot and cold junctions). Consequently, the thermopile meter will deflect despite the absence of microwave power dissipation. The effect is similar if the input stream is above the ambient-temperature level. When the load is absorbing power it would be ideal to have the input water stream as much below the ambient-temperature level as the exhaust stream is above it. The net heat exchange between the two points of measurement should then be zero. However, this is obviously impractical since the temperature of the input stream would have to be adjusted as a function of the microwave average power level. The best

compromise would involve bringing the water stream to ambient temperature level before directing it into the load. For this reason many water loads have several turns of copper tubing wrapped around them through which the water must flow before entering the load.

The flow rate should be adjusted so that the temperature rise in the stream is no more than a few degrees. The heat exchange by radiation is entirely negligible, and heat exchange by conduction is made less serious. The rate of heat loss by conduction, h, can be expressed in terms of the temperature rise ΔT in the stream by the equation

$$h = k_1\left(\frac{\Delta T}{2}\right), \tag{93}$$

where $\Delta T/2$ is the average temperature rise, and k_1 is the proportionality constant. It is also apparent that if ΔT is small, it varies directly with the microwave power level P, and inversely with the flow rate V; thus,

$$\Delta T = k_2\frac{P}{V}. \tag{94}$$

From Eqs. (93) and (94) it is shown that

$$\frac{h}{P} = \frac{K}{V}. \tag{95}$$

Therefore, the ratio of the rates of heat loss to heat generation can be reduced by increasing the flow rate. Other advantages accrue if the flow rate is fast and the temperature rise small. The thermal time constant of the load is reduced and the thermocouple meter is linear in power. The loss in sensitivity can be compensated by increasing the number of junction pairs in the thermopile and by using a more sensitive meter.

A number of design factors for flow systems must be considered. The flow rate should be adjustable over a 10-to-1 range so that, regardless of the microwave power level, the temperature rise in the load can be held within a desirable range. It must be large enough to be measured with accuracy, but not so large that the heat-exchange error is troublesome. The flow rate must be *stable* over long periods of time. A flowmeter giving results as accurate as the procedure of clocking a known volume or weight of the water has not been found. This procedure however, takes time and gives only an average value of flow rate. As previously mentioned, the water stream should be brought to room temperature before being directed into the load. A properly designed flow system can facilitate this. It is very important that the flow system contain some means of removing the air from the water stream. As the water is warmed the dissolved gas emerges in tiny bubbles. These bubbles cling to the sides of the flow line, increase the flow resistance, and thereby change the flow

rate in a constant-pressure flow system. If carried along by the water stream the bubbles effectively change the specific heat of the water [see Eq. (92)] and introduce error in the power calculation. If the situation is unusually bad, the flowmeter and the load itself can become clogged by gas bubbles.

Aside from the general considerations just discussed, there are few fixed rules that must be followed in the design of a flow system. Almost every experimenter in the field of high-power measurements has constructed a flow system, and has arranged it to meet his individual needs and desires. The details of one open and one closed system that have been used in the Radiation Laboratory will be discussed. These may be considered as representative of the construction of the two types.

The open-flow system is the simpler to assemble. An elevated tank, near ceiling level, is filled directly from the water main. The flow into the tank is adjusted so that there is always a slight overflow, thereby maintaining a constant pressure head on the flow line. The water passes through a long length of pipe to help bring it to room temperature (or heater coils may be used) and then flows through a bubble trap. The trap consists of a glass standpipe with input and exhaust lines at the base. A stopcock at the top facilitates periodic release of the gas trapped in the standpipe. Following the bubble trap is a flowmeter, preferably one of the Fischer and Porter rotameters. If the rotameter is not of the Stable-Vis type the calibration is temperature-dependent, and a thermometer must be inserted in the line immediately ahead of the rotameter. It frequently happens that algae collect in the glass rotameter tube, in which case it is necessary to clean it periodically with a weak acetic acid solution followed by a rinse in mild soap suds. It is possible to get automatic timing for a flow-rate check on the rotameter calibration by using a 30-sec electric clock to actuate a relay which in turn shifts the water jet into a special measuring sump for the 30-sec period. From the flowmeter the water is directed through the thermopile block and water load, and is then exhausted into the sewer.

The more complicated closed-flow system is diagrammed in Fig. 3·77. The flow through the system is maintained by a positive metering pump A of the gear type. For constant drive-shaft velocity the pump delivers a constant flow over a wide range of exhaust pressures. The pump is driven by an overpowered synchronous motor C, which operates through a gear box B. By changing the external gears and the internal reduction ratio of the gear box, it is possible to get six or more different flow rates. The total power required to operate the system is approximately $\frac{1}{2}$ kw at 60 cps and 110 volts.

The water flows from the pump through a safety valve D set for 15 lb/in.^{2} As an extra precaution a pressure switch E is included.

When the line pressure reaches 12 lb/in.^{2}, the switch actuates a relay which stops the motor C. The bubble trap F has a stopcock G in the line from the top of the trap. To remove the air collected in the trap, the motor is stopped, G is opened, the outlet H is closed off by folding the rubber tube back on itself, and the pump is started again. Water flows from the trap into the reservoir N. After the air is removed from the trap the motor is stopped before the stopcock is closed and the outlet line is opened. If a positive pressure is maintained on the intake side of the gear pump, very few bubbles will form in the water stream.

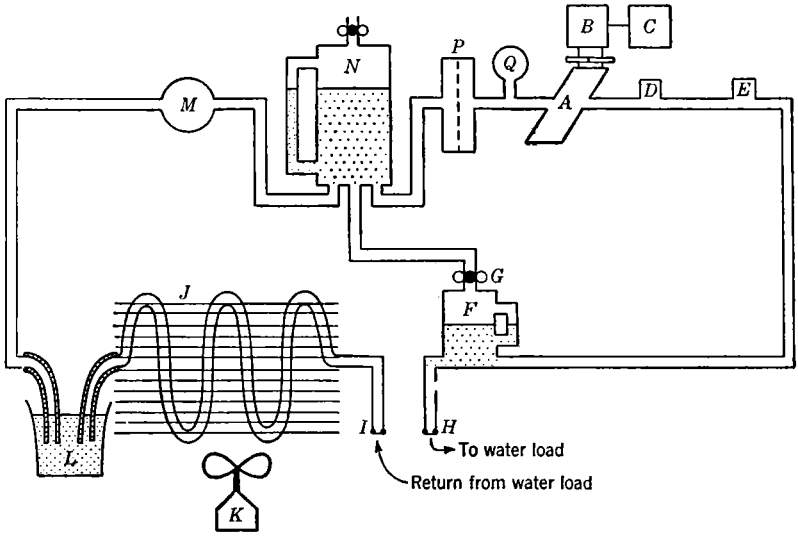

FIG. 3·77.—Diagram of a closed-flow system for use with water loads.

In a closed-flow system it is necessary to cool the water stream continuously to remove the heat formed by power dissipation in the load. An ordinary refrigerator condenser coil J cooled by a fan K is effective for this purpose. The effectiveness of the arrangement is shown in the fact that the equilibrium temperature rise in the stream is only 3°C when the load is dissipating 1-kw average power at a flow rate of 17 cc/sec. The flow line is broken at L to permit the occasional flow-rate measurements needed to check against wear in the pump gears. The water is introduced into the system at L. The reservoir capacity must be large enough to permit flow-rate measurements without draining the line.

A booster pump M sucks the water from L and delivers it to the reservoir N. The pump consists of a pair of automobile fuel pumps operated in parallel to provide the capacity needed for the fast flow rates.

The booster pump is driven by a cam mounted on the drive shaft extending from gear box B. Fuel pumps can work into any load pressure without producing damage, and without building up excessive pressures if the flow line becomes clogged. The pressure built up in the reservoir N forces the fuel pumps to deliver the same flow rate as the metering gear pump. The arrangement always maintains the desired positive intake pressure for the gear pump which is needed to avoid bubble formation in the stream. A pressure gauge Q is installed at the intake of the gear pump.

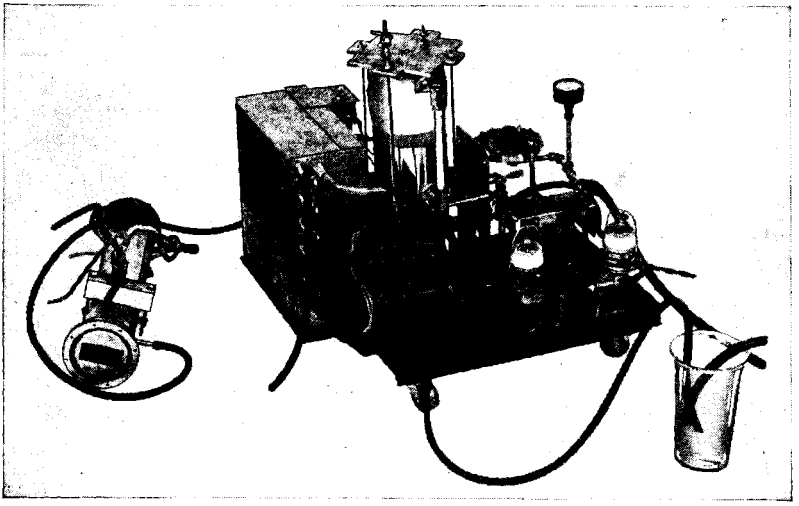

FIG. 3·78.—Photograph of an assembled closed-flow system.

It is important to install a filter P in the line ahead of the metering pump. Because of the minute clearances in the pump, a rust or grit particle can "freeze" the pump or cause enough wear to effect a flow-rate change. Since automobile oil filters were found to have too much flow resistance, a special filter was developed. A fine-mesh filter cloth is stretched across a flat cylinder and is supported by a series of radial rod spokes. Without the supports, the cloth would stretch so much under pressure that it would lie against the bottom of the cylinder, and effectively reduce the filtering area. As the filter clogs, the gauge Q shows a pressure drop, and the filter cloth should be cleaned or replaced.

If the critical parts of the gear pump are made of plain rather than stainless steel, the pump is subject to rusting. It has been found advisable in this case to substitute for water a 3 per cent aqueous solution of a commercial rust inhibitor known as Rust Master. The solution has the

same specific heat as water, and is as effective as water in dissipating microwave power.

Flow-rate variations in the closed-flow system are well under 1 per cent. As shown in Fig. 3·78, the whole flow system can be mounted on a base with rollers, and made readily portable.

3·36. Thermopiles for Water Loads.—The junctions of water-load thermopiles may either be immersed in the flow stream, or mounted on the outer surface of sections of the flow line. The immersion technique is more commonly used, although both methods are acceptable. Figure 3·79 shows the construction of a thermopile "block" in which the junctions are immersed in the flow stream.

Two parallel holes (channels) are drilled through a lucite or polystyrene block—one channel carrying water to the load, and the other

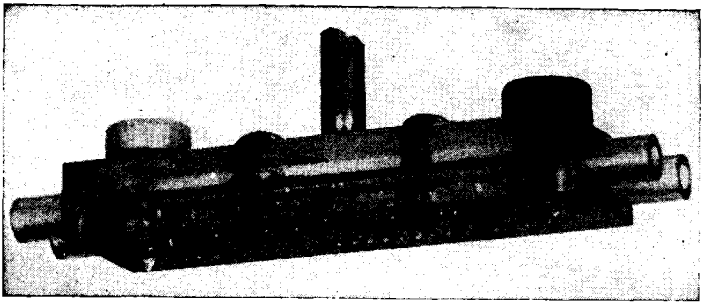

FIG. 3·79.—Water-load thermopile with junctions in the flow stream.

carrying the exhaust stream. A series of closely spaced, tiny holes are drilled into each channel to permit insertion of the junctions. The thermopile junctions, with wires properly shellacked to avoid the short-circuiting of any of the junctions, are sealed into the holes with polystyrene cement. The junctions project approximately to the center lines of the two channels.

In forming the series of thermopile junctions it is convenient to use a winding jig. Such a jig consists of a metal or fiber rod with an H-shaped cross section, notched at regular intervals along its length. By staggering the notches on opposite sides of the rod, it is possible to wind a wire (or ribbon) along and around the rod. The notches hold it securely in place. Similarly, a second wire can be wound along the rod, starting from the opposite end of the rod. The two wires touch in a series of X-shaped crossings extending in lines along the centers of the top and bottom sides of the H. The wires are soldered or spot-welded at all crossings. It is particularly easy to spot-weld because one electrode can be slipped into the bar, under the crossings. After all crossings are

spot-welded, they are snipped at the weld points. Consequently there are formed two identical thermopiles of the sort shown in the mounting in Fig. 3·79.

It is possible to construct the external-junction type of thermopile by a plating procedure.[1] Two thin-walled copper or silver flow tubes are coated with a thin layer of a lacquer No. E. P. 216 Formulation R.S. 57C (Dow Chemical Company), are wrapped tightly with a 0.005-in. thickness of Cellophane, and are then given another thin coat of lacquer. The coated tubes are mounted parallel to each other by means of a pair of dielectric spacers. A 0.004-in. constantan wire is wrapped in screw-thread fashion around the tubes, with the help of a winding fixture that holds the assembly securely in a slow-speed lathe. Each turn of wire encloses both tubes. The assembly is then floated as a raft on the surface of a silver-plating bath, so that one-half of each turn of wire may be plated with 0.002 in. of silver. Consequently, along each flow tube there is formed a series of silver-constantan junctions. It is therefore as little trouble to prepare a one-hundred-junction-pair thermopile as to prepare one with ten junction pairs. The turns should be as closely spaced as is consistent with freedom from short circuits. The assembly is installed in a Bakelite cylinder stuffed with glass wool or cotton.

In constructing any thermopile it is important to consider the magnitude of the heat transfer from the hot to the cold stream, through the thermopile wires connecting the two streams. Such calculations are easily made, and are important. For example, it is easily shown that the heat transfer through a number of parallel fine wires can be many times that through the dielectric separating the water streams. The greater the number of junction pairs, the longer or finer must be the wires between junctions if the net heat transfer is to be the same. Consequently the internal resistance of a thermopile increases faster than linearly with the number of junction pairs, and sensitivity increases more slowly than linearly.

The calibrations of thermopiles are remarkably stable. Corrosion is often a cause of trouble in the designs that permit the junctions to enter the flow stream. The corrosion is apparently the result of slow oxidation of the metals, and ultimately causes the junction to open-circuit. However, it is seldom that the calibration of a thermopile changes appreciably when the corroded junction is resoldered.

The Bell Telephone Laboratories have on occasion substituted thermistors for a thermopile.[2] One thermistor is installed in the input stream,

[1] Rita Hughes, "Thermopile for Use with R-F Water Loads," RL Group Report No. 55·1–10/26/45.

[2] R. C. Shaw and W. F. Bodtman, "Water-cooled Load and Power Measuring Apparatus for Microwave Transmitters"; BTL MM-42-160-141, Nov. 25, 1942.

and a second in the exhaust stream. The two thermistors comprise two arms of a bridge circuit that can be made extremely sensitive.

3·37. The Use of Power Dividers for High-power Mesaurements.—Whereas the water load has the unquestionable advantage of providing an absolute method of power measurement, the bulk and general inconvenience of its associated flow system relegate it primarily to use in the laboratory. Hence, considerable interest has been shown in alternative methods of high-power measurement, and particularly in those methods that are more adaptable to field usage, where simplicity in construction and operation, ruggedness, and portability are as important as accuracy.

Low-power bolometer bridges, together with calibrated attenuators or power dividers are frequently used instead of water loads. Attenuators of the high-power transmission type are infrequently used because of the difficulty of making their calibrations independent of temperature or power level. Power dividers, which allow most of the power to be dissipated in a well-matched high-power load and a small fraction of it to be measured directly by the low-power equipment, are frequently used. The power division can be accomplished with a variety of instruments, for example, the single probe, the double probe, the directional coupler, and the adjustable power divider.

The single probe may take the form of a capacitive probe, an inductive coupling loop, or a hole in the side of a waveguide. The coupling can be varied by rotating the loop or by adjusting the depth of insertion of the probe. The single-probe method of coupling demands that the transmission-line load be very well matched (for example, VSWR less than 1.02) in order to avoid objectionable error in the experimental determination of the coupling coefficient, and in order to avoid undue frequency sensitivity in the coupling. Even with a perfectly matched load the coupling can be expected to vary slowly with frequency. Further, the coupling must be loose enough (usually of the order of -30 db) so that the coupling element does not introduce appreciable reflections in the transmission line. Single-probe coupling is not recommended unless all power measurements are to be made at the calibration frequency.

In double-probe coupling two identical single probes, spaced $\lambda_g/4$ apart, are used. This spacing greatly minimizes the error due to a mismatched line termination, and also effects a cancellation of the reflections from the two coupling elements. Each coupling element transmits power to a detector, with the two detector output voltages being combined in the indicator circuit.

Directional couplers are discussed in Chap. 14. There are many types, and they can be designed for a wide range of coupling coefficients. They are not adjustable in coupling, but it is possible to add a

calibrated low-power attenuator between the directional coupler and the bolometer mount. Directional couplers of certain types have very desirable broadband coupling characteristics, as well as sufficiently high directivity to make the coupling coefficient satisfactorily independent of the voltage standing-wave ratio of the line termination. Directional couplers are usually the preferred type of power divider for this application.

The adjustable power divider (see Chap. 8, Vol. 9) involves a configuration of two ganged tuning stubs, an input line, and two output lines. Adjustment of the tuners varies the power division between the two loads; it is possible to direct any fraction of the input power into either of the loads. Through a proper choice of line lengths, the power divider may be designed so that, at the design frequency with both loads matched, the input impedance of the power divider will also be a match. Since both the calibration and the input impedance of the device are frequency-dependent, the power divider is of interest only if adjustable coupling at a given frequency is required.

There are fewer sources of error in the water-load measurement than in the measurement made with a bolometer bridge and directional coupler. In the water-load measurement the chief sources of error are in the flow-rate determination and in the a-c calibration of the water load. In the bolometer measurement the errors in the calibration of the directional coupler, the accuracy of the bridge-arm resistors and meter in the bridge circuit, and the errors due to microwave and video-frequency leakage must be considered. Errors in the directional-coupler calibration are the most serious of these, particularly if the coupling coefficient is 30 db or greater. It is often preferable to sacrifice the possibility of making absolute power measurements with the bolometer-coupler combination, and to calibrate the directional coupler against the water load for relative power measurements.

It is important to isolate the bolometer mount thermally from the high-power load on the main line of the directional coupler. The heat from the load can cause troublesome drift in the bridge balance. Sections of coaxial-line cable or metalized plastic waveguide are effective in minimizing heat transfer by conduction; inclosing the bolometer mount in a shiny metal box is effective in minimizing heat transfer by radiation.

3·38. Gas Loads.—An interesting gas load for high-power measurement has been developed by the Radio Corporation of America.[1] A cavity resonator filled with ammonia gas is used as the transmission-line load. In addition to dissipating the microwave power, the ammonia gas is used as the thermometric substance in a gas thermometer. A manom-

[1] W. D. Hersberger, "Ammonia-filled Resonators for Power Measurement," RCA Report PTR-10C, 9/13/43.

eter tube containing colored kerosene is connected to the resonator chamber, and the temperature rise is calculated from the pressure differential. Both tuned and untuned (multimode) resonators have been used. The tuned resonator has an adjustable end plunger, and a triple-screw tuner at its input end. Because of the low thermal capacity of the gas, the response of the thermometer is sufficiently rapid and the tuning adjustments present no problem. It is possible to base the power calculation on either the rate of temperature rise or the final equilibrium temperature of the gas.

The resonator is made of copper with an inner felt lining that increases the sensitivity of the thermometer at the expense of additional sluggishness in response. The heat dissipation is nonuniform throughout the resonator, and is a maximum at the center. The cooler ammonia layer near the copper wall limits the heat flow from the system more than the copper, since the thermal conductivity is relatively poor. The thin felt inner lining, together with an air blast against the outside of the resonator, prevents the copper losses from adding heat to the gas losses. Since the gas warms the felt appreciably, and since the several thermal capacities and the effect of convection currents are not well known, it is not possible to make accurate power calculations from data on the rate of pressure rise. It is therefore customary to calibrate the gas load against a bolometer or water load. A comparison of ammonia losses vs. copper losses may be obtained by a measurement of the change in input impedance when the ammonia is replaced by air. Both 3-cm-band and 1-cm-band gas loads have been used successfully by RCA.

3·39. A Coaxial Wattmeter for Field Use.—A crude but useful 10-cm-band field wattmeter has been made from a $\frac{7}{8}$-in. coaxial dry load and

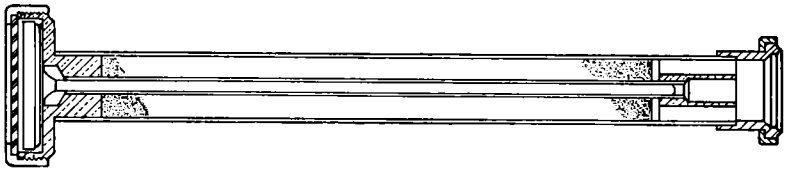

FIG. 3·80.—Dry calorimeter for high-power measurement.

a Weston all-metal thermometer. The thermometer is of the coiled-bimetal-strip type, with the strip housed near one end of a long metal tube which carries a dial indicator at its opposite end. The tube is inserted in the inner conductor of the load from the rear end of the load. The bimetallic element is thus located near the front end of the load where the temperature rise is a maximum. These construction features are shown in Fig. 3·80.

The usual radiating fins are removed from the load to increase its

sensitivity as a calorimeter. In use the calorimeter is placed on the end of the transmission line, the thermometer is read, and the power is applied. After an arbitrary one-minute interval the thermometer is read again. The temperature rise is proportional to the average power applied, with the proportionality constant being a function of the load and the material used in filling it. Each dry calorimeter is individually calibrated against a water load.

The test interval must be short enough to avoid a large temperature rise; otherwise the linearity between power and temperature rise is lost. Too short a test interval, however, or too small a temperature rise obviously introduces appreciable measurement errors. Consequently, the best values of such variables as the test interval, the thermal capacity of the load, and the sensitivity of the thermometer should be chosen in order to obtain maximum accuracy for a given average power level. The calorimeter shown in Fig. 3·80 has a sensitivity of approximately 2°F per watt of average power for a one-minute test interval.

3·40. The Johnson Meter.—Another high-power wattmeter that has met with limited popularity is the Johnson meter.[1] It is a power

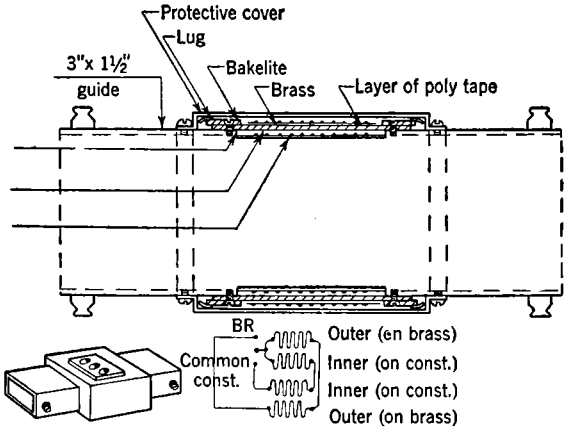

FIG. 3·81.—Construction of Johnson meter in 1½- by 3-in. waveguide.

monitor like the directional coupler and bolometer combination, since it requires only 1 per cent of the power rather than 100 per cent as do the water load, the gas load, or the dry load calorimeter. Figure 3·81 shows the construction of a Johnson meter for use in a waveguide transmission line.

A small section of the waveguide wall is removed and replaced with a section of high-resistance material, for example, a 0.015-in. sheet of constantan. It can be shown that, at magnetron power levels, enough

[1] M. H. Johnson, "Microwave Wattmeter," RL Report 239, Nov. 18, 1942.

heat is dissipated in the constantan to produce appreciable temperature changes. Since the conductivity of the brass waveguide is greater than that of the constantan section, a temperature differential will be maintained which can be used to give an indication of the power. A platinum resistance thermometer is used to measure this temperature differential; 200 ohms of 0.002-in. platinum wire is wound on the constantan section, and another 200 ohms is wound on the waveguide. These two windings serve as two of the arms of a Wheatstone bridge, as shown in Fig. 3·82.

The unbalance current in the bridge is directly proportional to the power in the transmission line to within a few per cent. The instrument may be calibrated against a water load, or by passing direct current or

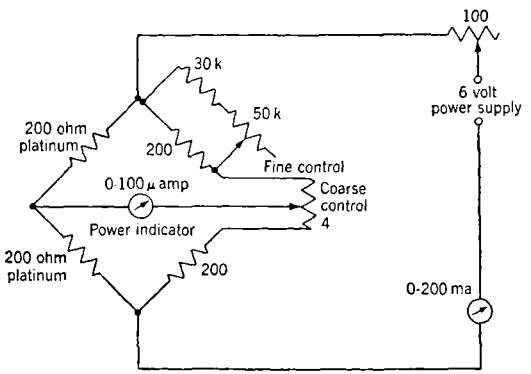

FIG. 3·82.—Diagram of the Johnson-meter bridge circuit.

low-frequency alternating current through the constantan. Heating by low-frequency current can be used on the 3-cm-band meters, but constructional details prevent its use on the 10-cm-band waveguide and coaxial-line meters. The coaxial meters are made in the same manner as the waveguide meters; that is, a thin sheet of constantan replaces the outer conductor and the platinum arm of the bridge is placed around it.

The thermal capacity of the active element is made as small as possible in order to speed up the response, but usually one to three minutes are required to get an equilibrium reading. Theoretically the Johnson meter is compensated for ambient-temperature variations because the two platinum windings are on a section of the transmission line, and any change in ambient temperature should affect both coils to the same degree. In practice, however, it is found that the drift condition is bad if the meter is located near the magnetron or a dissipative load where severe thermal gradients exist along the length of the transmission line.

3·41. Neon Tubes as Power Indicators.—Several attempts have been made to use neon tubes and lamps for relative high-power measurements. A glass capillary filled with neon,[1] inserted into a slot in a waveguide parallel to the axis of the waveguide, glows with an intensity dependent on the power level in the line. The intensity of the neon glow can be measured by a photocell. The chief trouble encountered is in obtaining properly reproducible neon tubes. A two-probe arrangement, with the energy coupled by the probes used to fire a pair of small neon bulbs, has also been tried. The probes are spaced $\lambda/4$ apart, and a single photocell views both bulbs. The difficulty with this arrangement lies mainly in the sensitive dependence of the coupling coefficient on the depth of probe insertion.

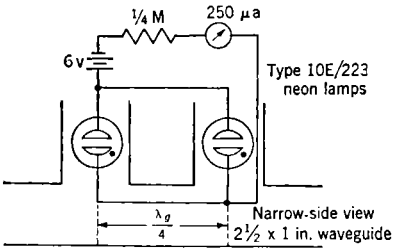

FIG. 3·83.—TRE neon-lamp arrangement for monitoring high power.

The British have also experimented with a double-probe neon-lamp arrangement,[2] as shown in Fig. 3·83. This device does not employ a photocell; the ionization current produced in lamps biased by a constant voltage and exposed to a high-frequency field is used as an indication of the power level. If a d-c voltage less than the d-c striking voltage is applied across the electrodes of the lamp, a current will flow. The d-c resistance of the lamp may be about 0.1 megohm, and the variation of this resistance with the microwave power level provides the desired indication. The lamps are adjusted to a standard power sensitivity and connected in parallel. Then the single meter reading gives the arithmetic mean response of the two lamps. Accuracies of ± 3 per cent relative to a water load are claimed.

It is of interest to investigate the accuracy obtainable with two neon lamps, rather than one, when the transmission-line termination is mismatched. The following development is not limited in application solely to neon lamps, but may be considered as a general comparison of the merits of single- and double-probe power taps.

Consider a transmission line carrying an incident voltage wave of unit amplitude, and a reflected wave of amplitude B. The voltage v at any point l along the line is given by

$$v = 1 + B \sin 2\beta l,$$

[1] J. M. Sturtevant, "Power Monitoring at 10 Cm," RL Group Report 82L-10, 8/24/43.

[2] "Power Measurement at 9 Cm," TRE Report No. G10/R139/43, May 27, 1943.

where

$$\beta = \frac{2\pi}{\lambda_g}.$$

The maximum and minimum values of v are $(1 + B)$ and $(1 - B)$, respectively, and the voltage standing-wave ratio r on the line is given by

$$r = \frac{1 + B}{1 - B}.$$

The product of the maximum and minimum values of v is the net power transfer along the line and is equal to $1 - B^2$. If it is assumed that the d-c ionization current in the lamp is directly proportional to the incident power (that is, the lamp is a square-law detector), the maximum and minimum current readings will lie between $(1 + B)^2$ and $(1 - B)^2$. The fractional error must then lie within the limits defined by

$$\frac{(1 + B)^2 - (1 - B)^2}{1 - B^2} = \frac{2B}{1 - B} = r - 1,$$

and

$$\frac{(1 - B)^2 - (1 - B^2)}{1 - B^2} = \frac{-2B}{1 + B} = \frac{1}{r} - 1.$$

Thus, for VSWR values of 1.1 or 1.2, errors of approximately ± 10 per cent or ± 20 per cent can occur.

For two lamps, spaced $\lambda_g/4$ apart, the line voltages at the positions of the lamps can be expressed as

$$v_1 = 1 + B \sin 2\beta l,$$

and

$$v_2 = 1 - B \sin 2\beta l.$$

The mean reading from the two lamps is given by

$$\frac{v_1^2 + v_2^2}{2} = 1 + B^2 \sin^2 2\beta l.$$

The fractional error is given by

$$\frac{(1 + B^2 \sin^2 2\beta l) - (1 - B^2)}{1 - B^2} = \frac{B^2}{1 - B^2}(1 + \sin^2 2\beta l)$$

$$= \frac{(r - 1)^2}{4r}(1 + \sin^2 2\beta l).$$

Thus the error, as a function of l, must lie between these limits:

$$\text{Maximum error} = \frac{(r - 1)^2}{2r},$$

$$\text{Minimum error} = \frac{(r - 1)^2}{4r}.$$

For $r = 1.1$, the error lies between $\frac{1}{4}$ per cent and $\frac{1}{2}$ per cent. For $r = 1.2$, the error lies between $1\frac{1}{4}$ per cent and $2\frac{1}{2}$ per cent. This is obviously a big improvement over the single-probe power tap.

Westinghouse Electric Corporation has also been interested in neon power indicators, and has developed a special neon tube[1] for the production-line bench-testing of magnetrons. The neon tubes are formed from one-foot lengths of 0.5-mm Pyrex tubing with a gas reservoir at one end and a tungsten electrode sealed into the other end. The conical tip of the electrode protrudes partially into the capillary and is needed to produce a potential gradient in the gas sufficient to start the discharge. A much smaller potential gradient can maintain it. The length of the gaseous discharge column measures the *pulse* power, since the ionization and deionization times of neon are presumably much less than the width of the pulse modulation envelope.

The tube is installed normal to the broad side of a waveguide, and protrudes a small distance into the guide. It is possible to match the tube to a VSWR of 1.5 or better by use of an adjustable end plunger and by variation of the depth of insertion of the tube. A water load is used as a primary standard for calibration purposes. It has been found that many tubes are erratic in performance, and that it is difficult to reproduce them in quantity.

By means of a rotating mirror, it is possible to observe the length of the discharge column for each individual pulse. It is thus possible to study whether the magnetron oscillates for each applied pulse, and the extent to which the output power varies with successive pulses.

[1] R. J. Schneeberger, "Neon Tube Power Indicator," Westinghouse Research Report SR-156, Dec. 1, 1942.

CHAPTER 4

MICROWAVE SIGNAL GENERATORS

By R. Beringer, C. G. Montgomery, R. A. Howard, and S. Katz

A signal generator is ordinarily understood to be a source of electrical power of known intensity, frequency, and modulation character. It differs from an *oscillator* or *generator* in that the power level is known and controllable. These conventions will be adopted in the following discussion of microwave signal generators.

The principal function of a microwave signal generator is to provide a signal of known character for the testing of receivers. As such receivers can differ greatly, and since the number of possible tests is unlimited, it is clear that there is no restriction on variety in signal-generator design. Signal generators may be designed to provide continuous-wave signals, short pulses of any shape, sinusoidal amplitude-or frequency-modulated signals, or even noise signals or noise-modulated signals; and all of these at any power level. In such a multitude of possibilities it is necessary to be arbitrary in the selection of topics and the way in which to treat them. The selection and presentation are highly colored by the problems which were met at the Radiation Laboratory in the course of a restricted development program. Even with such a narrow range of interest, reservations and apologies must be made for many of the devices to be described since they do not fulfill even these restricted design considerations in many instances.

To cite a single limitation, the microwave signal generators which have been developed at the Radiation Laboratory are usable over rather restricted frequency ranges, ± 10 per cent at most. There are no microwave signal generators that can compare in versatility with their low-frequency analogues. The accuracy of microwave signal generators is generally inferior to that commonly achieved at radio frequencies. These and other difficulties are indications of the newness of the microwave arts.

Receiver sensitivities are specified in terms of the smallest signal to which the receiver gives an unambiguous response; signals smaller than this limit are undetectable against the background of spontaneous fluctuations or electrical noise in the output voltage of the receiver,

For the best superheterodyne microwave receivers the noise background is of the order of 10^{-20} watt per cycle of receiver bandwidth when referred to the input terminals of the receiver. Hence, for such a receiver with a bandwidth of 10^6 cps, the ultimate sensitivity is about 10^{-14} watt. The controlled production of these very small signal intensities is perhaps the principal difficulty in signal-generator design. It requires the ultimate in careful design and calibration.

Specifically, there are two main classes of microwave signal generators: modulated or unmodulated continuous-wave signal generators and noise generators. The c-w signal generators involve a c-w oscillator, usually a velocity-modulation tube, an attenuating network, usually of variable insertion loss, a power monitor or absolute power meter, and often a frequency meter. These must be enclosed in a leak-proof box to which supply voltages are applied and out of which comes the signal. Since the oscillator level is 100 to 150 db above the required signal level, the shielding difficulties are considerable and have seldom been solved satisfactorily. In addition, the attenuators must be very carefully made since they are used to extrapolate the 70 to 120 db from the desired signal level to the power region where thermal elements can be used to measure the signal power in absolute units. These and other complications, especially the frequency sensitivity of the various components, make the design and calibration of such signal sources exceedingly difficult.

Some of these problems are avoided by the use of microwave noise sources in those cases where a continuous-wave signal is not required. Some noise sources are easily constructed and satisfactorily rugged and stable. In addition, some noise sources are absolute in the sense that they emit microwave noise of an amount given by physical constants and measurable parameters. Since the sources of noise are frequently just those which limit the sensitivity of receivers, the magnitude of the noise power is already in the range required for receiver-sensitivity measurements, and the sources need little or no shielding or attenuation. This may, however, be disadvantageous if larger intensities are required.

THE USE OF SIGNAL GENERATORS IN TESTING RECEIVERS

4·1. Receiver Noise Figures.—If it is desired to find the ultimate sensitivity of a microwave receiver, a cursory glance at the many receiver components and the multitude of forms which each can take is sufficient to prove that it is not easy to define this sensitivity unambiguously, much less to analyze the contributions from the several parts and characteristics of the receiver. Every receiver component from the input terminals to the observer is important to the problem and each receiver is, so to speak, a special case. This difficulty in assigning a simple scientific meaning to the ultimate sensitivity of a receiver has led to the definition

and measurement of another and more exact quantity, the *noise figure*[1] or noise factor of the receiver. This quantity provides a basis for comparing receivers and for the more complex study of the ultimate sensitivity of a particular receiver. A receiver which has no internal sources of noise is called a perfect receiver. The sensitivity of such a receiver is limited only by the thermal noise generated in the impedance of the signal source. Real receivers, having internal sources of noise, are less sensitive. These considerations are formulated mathematically in the following paragraphs.

For a linear-gain receiver[2] connected to a signal source, with s the available power from the signal source in the frequency range f to $f + \Delta f$, and Δn the available thermal noise power from the signal-source impedance in the same frequency range,

$$\Delta n = kT_0 \, \Delta f,$$

where k is Boltzmann's constant and T_0 is the absolute temperature of the signal-source impedance (usually taken to be 300°K). If the signal and noise powers as indicated by a wattmeter connected to the output terminals of the receiver are S and ΔN, respectively, in a frequency interval[3] f' to $f' + \Delta f$, it will be found that the noise-to-signal ratio $\Delta N/S$ is greater than $\Delta n/s$. The factor by which it is greater is defined as the *noise figure*,

$$F = \frac{\dfrac{\Delta N}{S}}{\dfrac{\Delta n}{s}}. \tag{1}$$

F is greater than unity except for a perfect receiver where F is equal to unity.

It is clear that F is a function of the signal-source impedance because S will depend on the "goodness of match" between the signal source and the receiver at the signal frequency f and at the image and harmonic frequencies, and the output noise ΔN will depend on the signal-source impedance. The complete dependence of F is so complex that at the present time the optimum signal-source impedance can be determined

[1] The treatment here follows that of S. Roberts, RL Report 293, Jan. 30, 1943. It is similar to that of H. T. Friis, *Proc. Inst. Radio Engrs*, 419 (1944).

[2] Linear-gain receivers are those for which the output power is proportional to the input power. This includes the more sensitive double-detection or superheterodyne class but excludes most single-detection receivers which are "square law."

[3] In double-detection receivers the frequencies f and f' differ; the former being called the radio frequency and the latter the intermediate frequency. The character of any modulation and Δf are the same, however, at these two frequencies.

only by experiment.[1] Because of this dependence of the noise figure on the signal-source impedance, it is necessary to specify and quote the signal-source impedance corresponding to a given noise-figure value.

The incremental-band noise figure of Eq. (1) is seldom used except in mathematical discussions. In practice, one is concerned with the so-called effective or average noise figure, the noise figure relevant to the entire acceptance band of the receiver. The average noise figure is computed by averaging F with respect to the receiver gain over the acceptance band of the receiver. If $G(f)$ is the receiver gain defined by $G(f) = S(f)/s(f)$, then the average noise figure is

$$\bar{F} = \frac{\int_0^\infty F(f)G(f)\,df}{\int_0^\infty G(f)\,df}. \tag{2}$$

In the following sections this quantity will be considered in connection with several ways in which it can be measured.

4-2. Noise-figure Measurement with C-w Signal Generator.—In the arrangement of Fig. 4-1, the receiver is presumed to include no detectors

FIG. 4-1.—Noise-figure measuring apparatus.

or other devices which mix signal and noise (i.e., no second detector for a superheterodyne receiver). If the acceptance band of the power meter is somewhat wider than the receiver pass band, in a frequency interval Δf of the pass band the output noise power as indicated by the power meter is

$$\Delta N = F\frac{S}{s}\Delta n = F\frac{S}{s}kT_0\,\Delta f;$$

consequently, the total indicated output noise power is

$$\begin{aligned} N &= \int_0^\infty F(f)\frac{S(f)}{s(f)}kT_0\,df \\ &= kT_0\int_0^\infty F(f)G(f)\,df. \end{aligned}$$

From Eq. (2) is obtained

$$\bar{F} = \frac{N}{kT_0\int_0^\infty G(f)\,df}. \tag{3}$$

[1] These matters are treated fully in Vol. 16 of this series.

If the receiver bandwidth B is defined as

$$BG(f_0) = \int_0^\infty G(f)\, df, \tag{4}$$

where f_0 is the midband frequency, the frequency at which $G(f)$ is a maximum, then Eq. (3) becomes

$$\bar{F} = \frac{N}{kT_0BG(f_0)}. \tag{5}$$

The noise figure F is measured in the following manner. With no signal emanating from the signal generator, the output power is N. A signal $s(f_0)$ of such a magnitude as to double the output power is introduced. Then

$$N = S(f_0) = G(f_0)s(f_0)$$

and Eq. (5) becomes

$$\bar{F} = \frac{s(f_0)}{kT_0B}. \tag{6}$$

Thus, if the available power from the signal generator for which the output signal-to-noise ratio is unity is known and B is measured, $\bar{F}$ can be found from Eq. (6).

Customarily a c-w signal generator has an attenuator calibrated in such a way that the available power can be changed and set to known values; and consequently, $s(f_0)$ is known. The bandwidth B can be found by measuring $G(f)$ throughout the receiver pass band by tuning the signal generator to a known set of frequencies or by using an f-m signal generator. For most superheterodyne receivers B is determined by the i-f-amplifier pass band, which is much narrower than the microwave bandwidth. In such instances B can be measured with an i-f signal generator.

4·3. Noise-figure Measurement with Microwave Noise Source.— Many noise sources have a uniform intensity over a frequency interval that is wider than the acceptance band of the receiver being tested. For a thermal noise source at temperature T, the available power in a frequency range Δf is just $kT\ \Delta f$. The *noise temperature* of the source is designated as T and completely characterizes the generation of noise signals. In the case of sources which are not thermal, this representation is still used, where T is the temperature of a thermal source having the observed available power. The noise temperature of a source may therefore be a real physical parameter or entirely fictitious.

The measurement of F with a noise source is very simple. The total output noise is

$$N = kT_0 \int_0^\infty G(f)F(f)\, df.$$

The total output signal is

$$S = kT \int_0^\infty G(f)\, df.$$

From Eq. (2) is obtained

$$\bar{F} = \frac{N}{kT_0} \cdot \frac{kT}{S} = \frac{T}{T_0} \cdot \frac{N}{S}.$$

If, as before, the signal source is adjusted so as to double the output noise, that is, $N = S$, then

$$\bar{F} = \frac{T}{T_0}. \tag{7}$$

It is seen that the bandwidth of the receiver does not enter into the measurement, and if the noise source is calibrated in noise-temperature units, $\bar{F}$ values are measurable directly.

It has been implicitly assumed that power is available from the signal source only at the signal frequency and not at any of the other frequencies to which the receiver is sensitive, such as harmonic or image frequencies. With noise sources this may not be the case and it is necessary to remove all but signal frequencies from the noise source or to make correction if they are present. If such contributions are present, the measured noise figure F' is related to that defined in Eq. (1) by

$$F = F' \frac{\Sigma G_j T_j}{G_{\text{sig}} T_{\text{sig}}}, \tag{8}$$

where the summation is carried over all frequencies to which the receiver responds. A simple case which occurs in practice is $G_{\text{sig}} = G_{\text{image}}$, $T_{\text{sig}} = T_{\text{image}}$, and $G_{\text{harmonic}} \approx 0$. Then Eq. (8) reduces to

$$F = 2F' = 2\frac{T}{T_0}. \tag{9}$$

An ideal noise source for receiver measurements is one for which the noise temperature is constant over the signal band of the receiver and zero everywhere else, thus avoiding the complications cited. Some noise sources, in particular those employing shot-noise vacuum tubes and resonant cavities, fulfill these conditions quite well.

4·4. Measurements on Pulse Receivers.—Microwave receivers for the amplification of short pulses have received considerable attention at the Radiation Laboratory. Most of the measurement techniques that will be treated were developed for this class of receiver and in some cases they apply only to these receivers. Some of the characteristics of microwave pulse receivers will be examined briefly.

A pulse receiver is a receiver that accepts a short pulse of microwave energy, amplifies it, and presents an amplified signal at a low frequency

whose envelope reproduces the shape of the pulse with good fidelity. Such receivers usually consist of a superheterodyne arrangement employing a crystal mixer driven by a c-w microwave oscillator as the first detector, a vacuum-tube i-f amplifier at ordinary radio frequencies, and a second detector which yields a d-c pulse. This pulse reproduces the microwave pulse shape to a degree that depends on the amplitude and phase response of the i-f amplifier. In particular, the acceptance band of the i-f amplifier must be of the order of $1/\tau$ cps in width, where τ sec is the length of the microwave pulse. The microwave circuits are almost

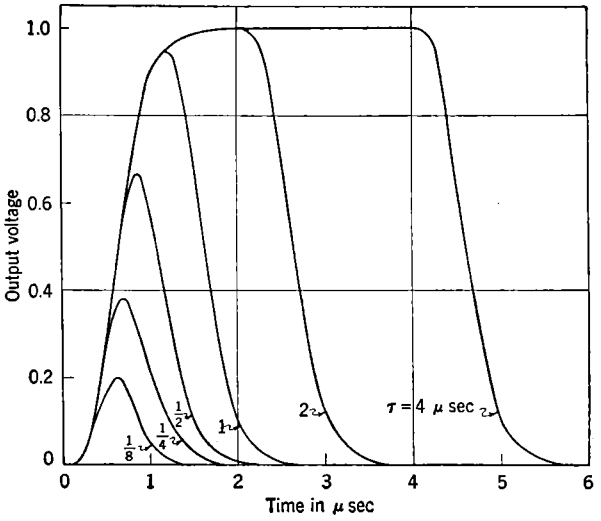

FIG. 4·2.—Output voltage from a 6-stage single-tuned i-f amplifier of 1-Mc/sec over-all bandwidth for rectangular voltage pulses starting at $t = 0$.

always much wider than this and do not limit the fidelity of the total system.

The theory and design of such amplifiers is treated elsewhere in this series and no more will be said than is necessary in order to understand the use of microwave signal generators in measuring their performance.

The Pulse Response.—The complete amplitude and phase characteristics of the receiver are necessary in solving the pulse-response problem; consequently, each receiver is a special case. The main points, however, can be illustrated with a single example. For a receiver having a 6-stage i-f amplifier that employs single-tuned coupling, that is, a simple shunt-resonant interstage coupling circuit, and having an over-all bandwidth B of 1 Mc/sec (total bandwidth between half-power points) Fig. 4·2 shows the normalized output voltage function for rec-

tangular pulses of various lengths τ but of equal amplitudes.[1] The main point of interest is the low output voltage and large distortion which result when the pulse length is too short for the receiver bandwidth in question. This condition should be avoided in testing receivers with pulsed signal generators.

4·5. Measurements with Pulsed Signal Generators.—Pulse receivers are frequently tested with pulsed signal generators since this most nearly reproduces the conditions under which the receiver is operated. The minimum detectable signal is very difficult to define and measure and depends markedly on receiver parameters and the observer. It is desirable, therefore, to find a more exact criterion which can be used with pulse receivers and the usual oscilloscope indicators. The so-called *tangential signal* has been found to be the best of such criteria. This is the signal that raises the observed noise amplitude by its own width as seen on an A-scope. This is shown in Fig. 4·3 for a square-law second detector. It is clear that there is no way in which to define this operation independently of the observer since there is no meaning to the "tops" of the noise peaks. Nevertheless, it is found that various observers agree upon the tangential signal strength and that the absolute value of the tangential signal is not a critical function of the various receiver parameters.

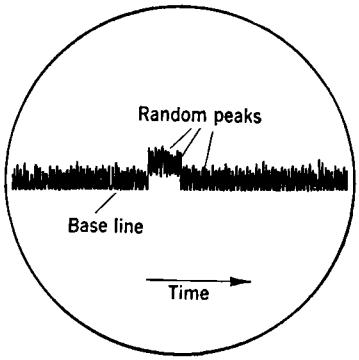

FIG. 4·3.—Tangential signal on an A-scope with a square-law second detector.

Such measurements have been reported[2] using a radar receiver of 4-Mc/sec bandwidth with rectangular pulses of 1 μsec duration occurring at a repetition rate of 1000 per sec. An A-scope with a sweep speed of 4.9 μsec/in. was used as the indicating device. It was found that each of seven experienced observers could repeat tangential-signal measurements with a standard deviation from the mean of less than 1 db for a variety of receiver-gain settings and intensities of the oscilloscope trace. The standard deviation in the mean for the seven observers was somewhat less than 2 db for the same experimental conditions. In these experiments the mean absolute value of the peak pulse power for the tangential signal was 9.2 db above the c-w power required to equal rms noise power measured as described in Sec. 4·1. It was also found

[1] The curves of Fig. 4·2 also represent the response of any 6-stage single-tuned amplifier, if the abscissas are in units of tB and the curves are labeled in units of τB.

[2] S. Katz, "Microwave Test Signals," RL Report 1023, Jan. 15, 1946.

that the tangential signal strength was quite insensitive to the pulse repetition rate for the range 200 to 4000 per sec. There are, however, no data on the way in which the pulse-length receiver-bandwidth product affects the tangential signal. This undoubtedly becomes important for pulses shorter than a certain critical value, perhaps of the order of $1/B$ as is seen by referring to Fig. 4·2. For very short pulses the amplitude is reduced and the shape is poor for exact measurements.

"Pulsed-off" Signal Generators.—One of the principal difficulties in designing microwave pulsed signal generators is the stringent requirement on the constancy of the pulse voltage applied to the klystron oscillator if frequency modulation during the pulse is to be avoided. Another difficulty is in the measurement of the peak pulse power. This is commonly accomplished by c-w operation of the oscillator on the assumption that the peak pulse power is equal to the c-w value which is measured with a thermal element. This is subject to error unless special circuits are employed to accomplish this condition. Even then it is difficult to be sure. Another way is to measure the average pulse power with a thermal element and to calculate the peak pulse power knowing the recurrence rate and pulse length. This is hard to do accurately for two reasons: (1) because the exact pulse shape, length, and separation must be known accurately; and (2) because the average pulse power is very small and difficult to measure.

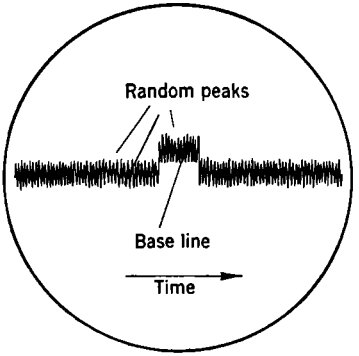

FIG. 4·4.—Pulsed-off tangential signal on an A-scope having a square-law second detector.

These problems are circumvented by the use of a "pulsed-off" signal generator, a generator that normally generates a continuous wave and which is pulsed out of oscillation for short lengths of time at some recurrence rate. If the oscillator is a reflex klystron, this is accomplished by putting onto the reflector a rectangular pulse (of either sign) sufficient in amplitude to drive the tube out of oscillation. The pulse need not have any particular shape but only steep sides, if rectangular pulses are to be generated. Since the oscillator is off for only a small fraction of the total time, the peak pulsed-off power is approximately equal to the average power and thus is easily measured.

Unfortunately, the use of such signal generators is not straightforward. In the first place, the character of the noise is changed by the c-w signal which is on between pulses. Secondly, the video characteristics of the

indication differ from those for a positive pulse, both between pulses (because of the c-w biasing of the second detector) and during the pulses. This is shown in Fig. 4·4 for a tangential signal on an A-scope having a square-law second detector. Very little experimental work has been done with pulsed-off signal generators. Available results indicate that tangential signals are of approximately the same peak power as for conventional pulsed generators.

4·6. Pulse-receiver Response to Frequency-modulated Signals.— Another way of avoiding some of the undesirable features of pulsed signal generators is by the use of a frequency-modulated signal source. With klystron oscillators, frequency modulation is easier to accomplish than good pulse modulation and the associated circuits are much simpler.

If the frequency of a signal generator is varied linearly with the time at a sufficiently high rate, the time variation of the output signal from a receiver is somewhat similar to its response for a rectangular pulse. If the signal voltage is the real part of

$$S = e^{j\theta},$$

where θ is the phase, the instantaneous frequency is $d\theta/dt$ and the average rate of change of frequency is

$$\frac{d^2\theta}{dt^2} = b.$$

If the rate of change of frequency is constant, then

$$S = e^{j(at+bt^2/2)},$$

where the frequency $\omega = a$ at $t = 0$. The frequency spectrum of this signal is given by the Fourier transform of S which is

$$\begin{aligned} g(\omega) &= \frac{1}{2\pi}\int_{-\infty}^{\infty} e^{j(at+bt^2/2)}\, e^{-j\omega t}\, dt \\ &= \sqrt{\frac{j}{2\pi b}}\exp\left[-j\,\frac{(a-\omega)^2}{2b}\right]. \end{aligned} \tag{10}$$

The amplitude of $g(\omega)$ is seen to be independent of the frequency.

The time response of the output voltage from a receiver having Eq. (10) as the input voltage is, of course, dependent on the amplitude and phase response of the receiver. The calculations are most easily made for a receiver having a Gaussian error-function amplitude response and linear or zero phase shift.[1] If B is the total bandwidth (in radians/

[1] This amplitude function is the limiting form for single-tuned stages in cascade. The phase shift of such a cascade, however, approaches ∞ with the number of stages and the Gaussian amplifier is not physically realizable. This is not serious in the present example.

sec), i.e., the interval between the frequencies where the voltage response is $1/\sqrt{2}$ times the maximum value, the gain of such an amplifier (output voltage divided by input voltage) is given by

$$H(\omega) = \exp\left[-2 \ln 2 \left(\frac{a-\omega}{B}\right)^2\right],$$

where a is the frequency at the band center. The output time response is given by

$$V(t) = \int_{-\infty}^{\infty} g(\omega)H(\omega)e^{j\omega t}\,d\omega$$
$$= \sqrt{\frac{1}{1-j\gamma}}\left\{\exp\left[-\frac{\gamma bt^2}{2(\gamma^2+1)}\right]\right\}\cdot\left\{\exp\left[jat+\frac{jbt^2}{2(\gamma^2+1)}\right]\right\}, \quad (11)$$

where $\gamma = 4 \ln 2 \dfrac{b}{B^2}$. The last exponential is the oscillating, frequency-modulated portion of the signal. It is noted that the modulation is less rapid than for $g(\omega)$ by a factor $f = (\gamma^2+1)^{-1}$. The first two terms represent the envelope of the f-m signal. The maximum value of this envelope occurs at $t = 0$, when the input signal has the same frequency as the center of the pass band of the receiver. The response is normalized so that $|V(t)| = 1$ for slowly modulated signals (small b). For rapid frequency modulation, $|V(t)| < 1$ by an amount given by the voltage attenuation A of the signal, where

$$A = Re\left(\sqrt{\frac{1}{1-j\gamma}}\right)$$
$$= \left[\frac{1+\sqrt{\gamma^2+1}}{2(\gamma^2+1)}\right]^{1/2}. \quad (12)$$

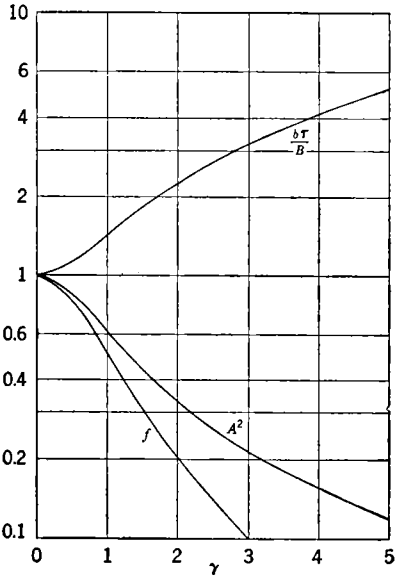

FIG. 4·5.—Parameters of output functions for a Gaussian receiver with an f-m input signal.

The time response of the output voltage is given by the first exponential in Eq. (11). It is seen to have the Gaussian form. This output voltage function can be characterized by a pulse duration τ sec, defined as the time duration between the points at which the output voltage is $A/\sqrt{2}$. This is

$$\tau = \frac{B}{b}\sqrt{\gamma^2 + 1} = \frac{4 \ln 2}{B}\frac{\sqrt{\gamma^2 + 1}}{\gamma}. \tag{13}$$

Figure 4·5 shows the quantities A^2, f, and $b\tau/B$ plotted against γ.

It is important to note that the output time functions for f-m and for rectangular-pulse inputs are somewhat different in form, especially for pulses long enough to be reproduced without great distortion. This is shown in Fig. 4·6 where four sets of output functions for rectangular-pulse and for f-m input functions have been plotted. The four output pulse functions are labeled with the input pulse durations in microseconds.

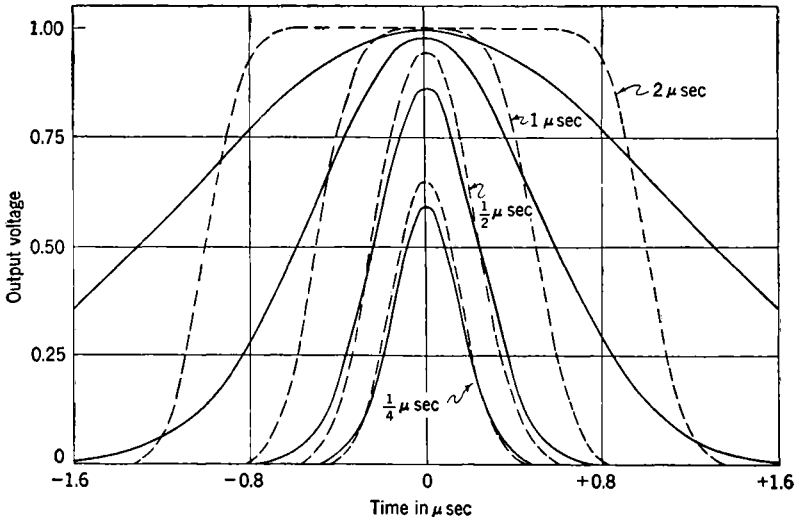

FIG. 4·6.—Pulse and f-m response of a Gaussian receiver of 2-Mc/sec bandwidth. Solid curves are f-m output functions and dotted curves are output functions for rectangular pulses whose output pulse durations are equal to the corresponding f-m pulse lengths. All curves are arbitrarily adjusted to be symmetrical about $t = 0$.

Each of the f-m output functions is calculated from Eq. (11) using a τ value which is equal to the output pulse duration of one of the rectangular-pulse response curves. The output pulse duration is defined as the time interval between the points at which the amplitude is equal to $1/\sqrt{2}$ of the maximum amplitude. Whereas the f-m response is always similar to the receiver bandpass function, the pulse function is more like a rectangular pulse, at least for long pulses. This difference in shape leads to some difference in the minimum detectable signal observed with pulse and with f-m signal generators. This difference seems to be small. For tangential signals there seems to be no detectable difference at least for the case of long pulses and slow frequency modulation such as the 2-μsec curve in Fig. 4·6.

Miscellaneous Measurements.—By use of an f-m signal generator receiver bandwidths can be measured with some accuracy. With the rate of change of frequency of the r-f signal properly adjusted, the receiver bandpass characteristic is displayed upon an oscilloscope. If a reaction wavemeter is included with the signal generator, this will cause a sharp notch in the pattern at the resonant frequency of the wavemeter. The width of the bandpass curve can be measured by moving this notch along the pattern and noting the wavemeter tuning. The bandwidth B as defined in Eq. (4) differs from the frequency interval between $1/\sqrt{2}$ voltage points (the so-called 3-db bandwidth). Table 4·1 illustrates the relation between these quantities for several simple cases.

TABLE 4·1.—RATIO OF BANDWIDTH B TO THE 3-DB BANDWIDTH

	Ratio
One single-tuned stage	1.57
Gaussian	1.06
Rectangular	1.00

An f-m signal generator also provides a convenient means of tuning the receiver. When the notch appears at the center of the bandpass characteristic, the frequency meter indicates the frequency to which the receiver is tuned. Conversely, the receiver may be adjusted so that, with the frequency meter tuned to a desired frequency, the notch appears at the center of the bandpass characteristic.

By a similar method, the operation of the automatic-frequency-control circuits of a radar receiver can be checked. Comparison of the frequency of the bandpass characteristic with the receiver frequency, under manual control and under automatic control, provides quantitative information about the locking of the automatic-frequency-control circuit. The behavior of the automatic-frequency-control circuits during actual operation can also be observed. If the transmitter frequency is varying because of a varying impedance in the transmission line, this is immediately obvious on the oscilloscope where the wavemeter notch moves relatively to the center of the receiver passband. A pulsed signal generator cannot yield such information.

There are other properties of receivers and receiving systems which may be measured with signal generators. The recovery time of a receiving system after a strong signal may be measured provided that the interval between the occurrence of the test signal and the initial trigger can be reduced to a small value. As the interval is reduced, the amplitude of the test signal decreases because of the reduced sensitivity of the receiving system. The interval at which the signal amplitude is one-half the value at full sensitivity is a useful measure of recovery time. Finally, signal generators facilitate the tuning of such frequency-

dependent components of a receiving system as the TR cavity. With the test signal displayed upon an oscilloscope, the frequency-critical components may be adjusted for maximum signal amplitude.

THE DESIGN OF MICROWAVE SIGNAL GENERATORS

4·7. Microwave Design Considerations for C-w and Modulated C-w Signal Generators.—The signal generators which have been built at the Radiation Laboratory for the testing of pulse receivers have been of three varieties: (1) continuous-wave, (2) rectangular-pulse-modulated continuous-wave, and (3) frequency-modulated continuous-wave. Usually in a given signal generator either c-w signals or one of the modulated forms can be produced by using a switching arrangement.

These generators employ a low-voltage r-f oscillator, usually a velocity-modulation tube, as the c-w source. The supply voltages are modulated for pulse or f-m operation. This oscillator signal is conveyed to the output terminals of the signal generator through a transmission line including attenuating elements and frequently a reaction wavemeter. Part of the oscillator signal is absorbed in a monitoring element, usually a thermal power-measuring element. This is frequently arranged so that the absolute value of the monitor power is related to the absolute level of the signal-generator output power. The r-f assembly consists, therefore, of four essential parts: an oscillator, an attenuator, a wavemeter, and a power monitor. The principal design problem is to construct and arrange these components so that a properly modulated signal of known frequency and power is available.

Suitable r-f oscillators are discussed in Chap. 2 and will not be listed here. Any oscillator capable of supplying a minimum of 10 mw over the frequency band in question, with good power and frequency stability, may be used.

At resonance the reaction wavemeter should produce a "dip" in the signal power of such a magnitude as to be easily detected by the power monitor when the wavemeter is tuned rapidly through the signal frequency. The resonance should also be broad enough in frequency to give a sufficient decrease in power when the frequency of very short pulses is measured. The decrease of power in this case is always smaller than for c-w power because of the reduced response of the wavemeter to the sideband frequencies of the pulse. On the other hand, the dip should be narrow enough for accurate frequency measurements. It has been found, in practice, that for c-w power a wavemeter dip of 50 per cent and a dip width of 0.01 per cent of the midband frequency satisfies these criteria. The response of the wavemeter for resonances in undesirable modes should be small compared with the response for the proper mode so that confusion will not result. When determining the frequency

of very short pulses, the lower Q of a spurious mode may result in a decrease in power as large as that caused by the proper mode, since a high-Q resonance affects only a small part of the frequency spectrum of the pulse.

The calibrated attenuator may be of any type provided that both ends present small voltage standing-wave ratios at all attenuation settings and frequencies within the band. Its variation of attenuation with frequency should be small. The power monitor may be conveniently arranged to give a full-scale deflection when the r-f power dissipated in the sensitive element, usually a thermistor, is 1.0 mw. The maximum voltage standing-wave ratio of the thermistor should also be small. If 1.0 mw is chosen as the reference power level, some means must be provided for reducing the power delivered by the oscillator to this level. This can conveniently be an auxiliary "power-set" attenuator.

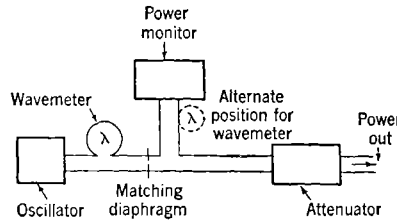

FIG. 4·7.—Schematic diagram of simple signal generator.

If the sole function of the signal generator is to provide a signal of known intensity and frequency, the design of the r-f circuit can be very simple. The wavemeter may be attached to the transmission line in one of the ways described in Chap. 5. The principal problem is to take a known portion of the oscillator power to be measured by the power monitor. One simple way of accomplishing this is shown schematically in Fig. 4·7. The oscillator is connected to one arm of a waveguide T-junction with the attenuator and power monitor attached to the other two arms. A matching transformer is provided so that the oscillator may work into a reflectionless load. A certain fraction of the oscillator power will go to the monitor, the remainder to the calibrated attenuator, the exact manner of division depending upon the variety of the T-junction used. The power division can be determined by a calibration of the device. The wavemeter is placed next to the oscillator in Fig. 4·7. In this way, when the wavemeter is tuned to resonance, both the power to the monitor and the power passing through the attenuator are reduced. The alternative placing of the wavemeter next to the power monitor, as indicated by dotted lines in the figure, is not satisfactory since the dip in the power through the attenuator would be very small.

Such a simple arrangement would be satisfactory for many laboratory uses. In commercially built equipment, however, the tendency has been to make a signal generator perform other functions. In particular, for the testing of radar systems, signal generators have been designed

so that the attenuator, power-measuring device, and wavemeter can also be used to measure the power and frequency of a signal from a source external to the signal generator (the radar transmitter). This greatly complicates the design of the r-f circuit. These difficulties will be outlined in more detail and specific examples of their solution will be given.

If power and frequency measurements are to be made on both an external source and the internal oscillator of a signal generator, it seems logical to use a symmetrical arrangement such as that shown in Fig. 4·7. It would be necessary to move the wavemeter to a symmetrical position at the junction. Such a signal generator is described in Sec. 4·14. The principal objection to power division by a T-junction is the inaccuracy introduced if the power monitor and attenuator are not perfectly matched. It may be shown that if appropriate reference planes are chosen in the arms of the junction, the equivalent circuit is the simple one shown in Fig. 4·8. The power delivered to the attenuator P_A can be simply written as

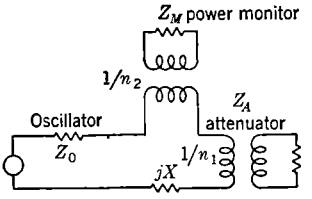

FIG. 4·8.—Equivalent circuit of T-junction used for power measurement.

$$P_A = P_M \left(\frac{Z_A}{Z_M}\right)\left(\frac{n_1}{n_2}\right)^2,$$

where P_M is the power absorbed by the monitor. If the voltage standing-

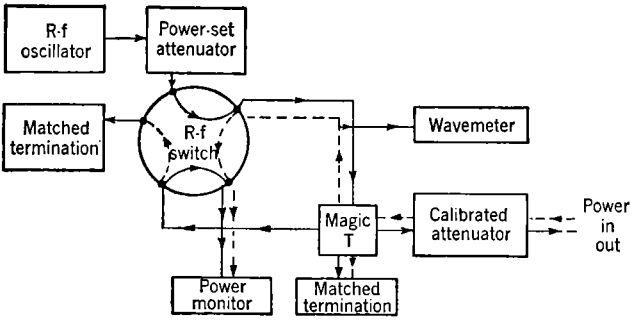

FIG. 4·9.—Signal generator using a magic T.

wave ratio of either the attenuator or power monitor is as large as 1.2, P_A will differ by one decibel from its value with matched components. Thus a calibration is essential for accurate work. The power division is, of course, a function of frequency. For greatest convenience of operation, this variation should be small.

The extreme sensitivity of the power division to reflections from the

individual components can be avoided by using more complicated arrangements. Three directional couplers (Chap. 14) and an r-f switch may be employed as described in Sec. 4·15 to avoid completely the effects of mismatch. Another possibility is to use a magic T for the power division, and a switch to interchange the position of the oscillator and power monitor. This arrangement is shown schematically in Fig. 4·9. A magic T has the property that power sent into one arm is divided equally between adjacent arms if these arms are terminated in matched loads. No power goes into the opposite arm (see Chap. 9). The r-f switch can be constructed similar to a stopcock using *E*-plane bends in waveguide. No signal generators using this r-f circuit are currently available.

4·8. Pulse Modulation of Oscillators.—To be useful, the pulse generated by a pulsed signal generator must simulate as closely as possible the characteristics of the signals for which the pulse receiver is used. Since the signal generator may be used to test receivers having widely different characteristics, it is usually desirable that the parameters of the pulse, such as length and recurrence rate, be variable. Furthermore, the timing of the test pulse should be synchronized with the presentation of the indicating system.

In the past, only two types of r-f oscillator tubes have been used in microwave signal generators, the reflex, velocity-modulated tube, and the so-called "lighthouse" tube. In the reflex, velocity-modulated tube, the frequency and output power depend critically upon the potential of the reflector electrode and only to a lesser extent upon the potential of the anode with respect to the cathode. By setting the reflector voltage accurately to a definite value during a very short interval of time, a pulse of r-f energy at the frequency determined by the reflector voltage is produced. If the pulse is to be rectangular and properly shaped, the voltage during the pulse must be very nearly constant, and the rise and decay time very short. At the end of the pulse the reflector voltage returns to a value at which the tube does not oscillate. Thus the oscillator is periodically turned on for a short time during the cycle. The amplitude of the pulse is determined by comparison with the power generated when the oscillator is producing a continuous-wave signal. The circuit constants of the signal generator are usually so adjusted that the peak amplitude of the pulse equals that of the continuous wave, which may be measured by means of the thermistor bridge in the signal generator.

Pulse-forming Stages.—Figure 4·10 shows the delay lines and switch tubes used to produce a voltage pulse. Normally the delay lines are charged to $B+$ potential. With the arrival of a positive trigger upon the grid of the gas-discharge tube A, the delay line selected by the *pulse-*

length switch discharges through the tube, causing an abrupt increase in cathode potential. The delay line discharges until the plate potential falls below the ionization point and the current is cut off. The cathode resistance is chosen so that the impedance of the discharge path is

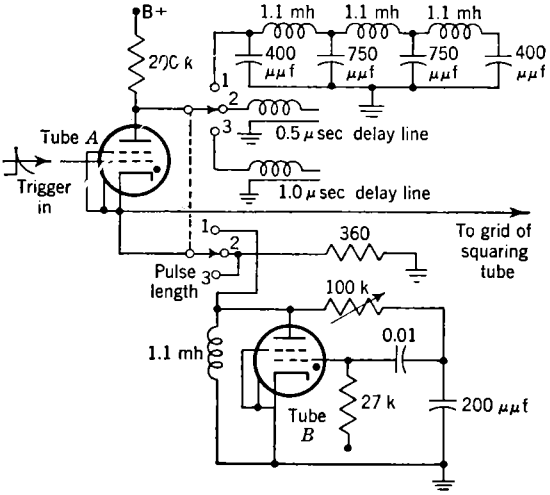

FIG. 4·10.—Pulse-forming network and switch tubes.

appoximately equal to the characteristic impedance of the delay line. Either of two delay lines (or more, if desired) are made available by switching.

For pulses of variable length (position 1 of the pulse-length switch), the front edge is produced in the same way as described above, with the 1.1-mh inductance as the load. The trailing edge is formed by the discharge of the gas tube *B*. The time interval between front and trailing edges is determined by the rate of change of bias controlled by the adjustment of the 100,000-ohm rheostat.

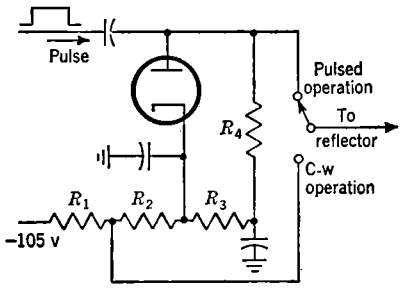

FIG. 4·11.—Diode clamping circuit.

To ensure that the d-c potential on the reflector of the r-f oscillator has the same value during the pulse as during c-w operation, a clamping circuit may be used, as shown in Fig. 4·11. The cathode of the diode is at a positive potential relative to the plate, and hence the diode conducts only during a positive pulse. The potentiometers are so adjusted

that, with the diode in a nonconducting state, the potential at the junction of R_1 and R_2 is equal to that at the junction of R_2 and R_3 when the diode is conducting.

Another method for generating a short voltage pulse uses a pulse multivibrator, shown in Fig. 4·12. With the arrival of a trigger upon the grid of one tube, one cycle of oscillation is produced, the multivibrator recovers, and remains quiescent until another trigger arrives. Potentiometer R_1 controls the duration of the pulse. The circuit constants may be so adjusted that when a single trigger is applied the multivibrator generates a train of pulses of short duration separated by 5 to 10 μsec. This type of modulation is often convenient, particularly in measurements of receiver recovery.

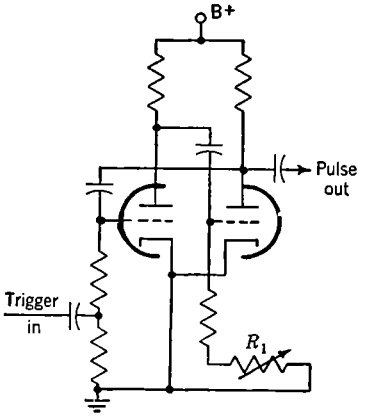

FIG. 4·12.—Multivibrator for producing pulses of variable length.

Synchronization of Pulses.—In testing pulsed radar systems it is necessary to synchronize the signal generator with the transmitter in order that the repetition rates of the system and signal generator are exactly the same. This synchronization is usually accomplished by trigger pulses formed in one part of the system and distributed to the other components. One common scheme is to use the trigger which operates the modulator of the transmitter to drive the pulse-generating circuit of the signal generator. Since this trigger may be either a positive or a negative one, some provision must be made so that the pulse-generating circuit can be actuated by either polarity. One method of accomplishing this is to have a selector switch and an inverter stage so that it is always possible to introduce a trigger voltage of the same polarity into the pulse generator. A modification consists of using an inverter-amplifier stage with a switching arrangement for applying a negative trigger to the cathode or a positive trigger to the grid so that in either case an amplified negative trigger is produced. This synchronization scheme requires a trigger cable connecting the transmitter with the signal generator.

A more convenient arrangement is to apply a small amount of the transmitter power to a crystal, amplify the resulting video pulse, and utilize this as the synchronizing signal. While the use of the signal generator is simplified by the elimination of the trigger cable and the trigger-polarity switch, the bulk of the set is increased slightly by the

addition of the video amplifier. The amount of power extracted from the line and applied to the crystal should be small enough so that no error is introduced in measuring the transmitter power. It should also be small enough so that the crystal will not be burned out with the largest transmitter power which is likely to be encountered. While it is simple enough to reduce the power coupled to the crystal to the required level, in doing so the output voltage of the crystal at minimum transmitter power is reduced to a very small amount. This requires that the video amplifier have a fairly large gain to produce a satisfactory synchronizing signal.

In some cases it is desirable to reverse the order of synchronization, and have the transmitter driven by a trigger generator which is part of the signal generator. An external cable connection must be provided for conducting the trigger voltage to the transmitter.

Not only must the signal generator be synchronized with the transmitter, but it is also necessary to have the signal separated in time from the transmitter pulse by a variable amount. Some delay circuit must therefore be placed between the trigger generator and the modulator of the signal generator, whether the trigger be generated internally or received from some external source. This delay circuit most commonly takes the form of a multivibrator of essentially the same type as that shown in Fig. 4·12. The rectangular pulse which the delay multivibrator produces is differentiated, and the pip caused by the trailing edge of the pulse is used to trigger the pulse generator. Thus, by varying the length of the pulse produced by the multivibrator, it is possible to alter the time interval between the signal and the transmitter pulse. A more detailed discussion of delay multivibrators for this application may be found in Vol. 22 of this series.

4·9. R-f Leakage and Shielding.—It is very important that the signal generator be well shielded, since the oscillator level is much greater than the signal level and signals can easily escape from the generator and find their way into the sensitive parts of the receiver being tested. Such spurious signals, even if small compared with the test signal, can introduce large errors in receiver measurements. This is illustrated by the following example. If P_L is the leakage power, and P_S the available signal power from the signal generator as measured at the receiver input terminals, and V_L and V_S the corresponding voltages, then the maximum and minimum values of the voltage at the receiver are

$$V_{max} = V_S + V_L$$

and

$$V_{min} = V_S - V_L.$$

If E is the error in decibels introduced by the leakage, the error cor-

responding to V_{max} is

$$E_+ = -20 \log_{10}\left(1 + \frac{V_L}{V_S}\right),$$

and that corresponding to V_{min} is

$$E_- = -20 \log_{10}\left(1 - \frac{V_L}{V_S}\right).$$

The actual error falls between E_+ and E_-. It is convenient to specify the error in terms of the ratio P_L/P_S or by the quantity

$$L = 10 \log_{10}\frac{P_L}{P_S} = -20 \log_{10}\frac{V_S}{V_L},$$

which is commonly called the "leakage," namely, the leakage power expressed in decibels below the signal power. The contours E_+ and E_-.

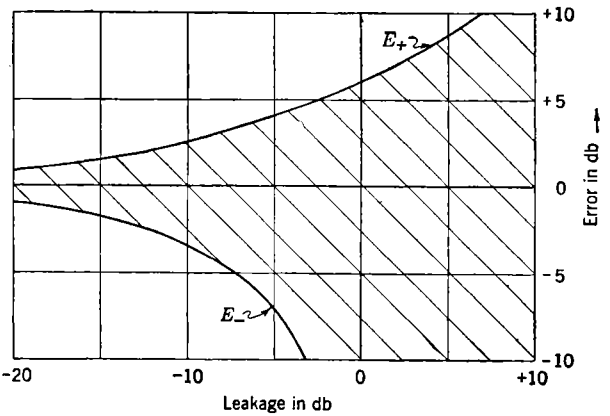

FIG. 4·13.—Errors due to leakage from a signal generator. E_+ curve is for leakage in phase with signal and E_- curve is for leakage 180° out of phase. Actual error will fall in shaded region.

vs. L are shown in Fig. 4·13. The actual error will always be inside of the shaded region.

The leakage from a signal generator can be measured with a calibrated, superheterodyne receiver. The receiver is connected to a flexible transmission line terminated in a small horn which is used to explore the region close to the signal generator. A small horn close to the source of leakage is more sensitive than a larger antenna several feet away.

Evidently, the smaller the power level of the test signal, the more damaging are the effects of leakage. It is, therefore, advantageous to use test signals which are large in amplitude, such as the tangential signal.

The sources of leakage in a signal generator are numerous. Leakage occurs at any imperfect waveguide junction, and through any small apertures in the r-f line. In most signal generators designed in the past, there has been leakage of r-f power at the back-plate of the thermistor mount and coaxial line by which the d-c power is supplied to the thermistor. Other sources of leakage have been the cover of the mount for the r-f oscillator tube, the junction of the tube mount and the exit transmission line, the waveguide choke-flange joints, and the openings for mechanical devices for driving the attenuator and tuning the r-f oscillator.

There are a variety of techniques which may be used to minimize leakage. In general, all joints, such as the threads of tube caps and the junctions of waveguide sections, should be as nearly mechanically perfect as is possible. The necessary apertures in the waveguide, such as a slot into which resistive attenuators are inserted, or the holes through which the supporting rods of an attenuator are moved, or the holes through which insulated wires pass must be very well shielded. It has been found that polyiron,[1] a material having a high attenuation for microwaves, provides an excellent means for absorbing leakage power. Thus, slots through which attenuator flaps move may be enclosed in polyiron; the dielectric material of insulated leads may be polyiron; and shafts may be sealed with polyiron washers.

Several techniques for reducing the leakage from waveguide fittings have been used. Among these are carefully constructed flanges making excellent contact with one another, and flange-choke combinations with a ring of metal textile in a shallow groove placed concentrically with and further from the guide axis than the choke groove. The metal textile ring consists of copper braid pressed into resilient rings which fit into this groove. When together, the choke and flange combination compress the ring, forming a very leakproof joint. In using a flange-to-flange combination, a thin washer has sometimes been used to compensate for the lack of parallelism. The metal textile ring is usually greatly superior to a solid washer. Thermistor mounts have been a great source of leakage in the past. The tunable back-plate and the coaxial line, whose center conductor is the d-c lead to the thermistor, were particularly objectionable. The tunable back-plate may be improved by careful soldering after the thermistor has been matched. Leakage from the coaxial line may be suppressed by the use of polyiron. A satisfactory method for suppressing leakage along a shaft is to make the shaft of plastic and to enclose it in a metal pipe in such a way that the combination is a waveguide below cutoff. Other materials that have been used to reduce the leakage from signal generators include steel wool, metal

[1] See Chap. 12; also Vol. 8, Chap. 11.

paint, and plaster of Paris impregnated with some lossy material such as graphite.

The best guarantees of negligible leakage are careful mechanical construction, the use of soldered joints wherever possible, the use of chokes and metal textile rings in waveguide connections, the use of polyiron washers and disks in movable components, and the use of polyiron strips to cover irises and slots in waveguide.

4·10. Miscellaneous Features.—The weight and the size of a laboratory signal generator are usually of little importance compared to accuracy. On the other hand, a test generator for field use should be light and compact for portability. The use of light metals for the panel, chassis, carrying case, and some of the r-f components is a great help in weight reduction. The other principal source of weight is the power transformer. The lower limit on transformer weight is determined primarily by the voltages it must be insulated to withstand, and the amount of power it must supply. By choosing an r-f oscillator which does not require high voltage and by choosing circuits which require a minimum amount of power, the weight of the test set can be minimized.

While the power-supply requirements on signal generators using lighthouse tubes are much less stringent than those for velocity-modulation tubes, the performance of the lighthouse-tube signal generators has not been sufficiently good to justify their use except in rare applications where higher power is required than can be obtained from velocity-modulation tubes. Since both the frequency and output power of velocity-modulation tubes are dependent on the voltages applied to the tube, the power supply for these tubes must be well regulated. In fact, it is sometimes necessary to stabilize the heater current for the tube. In thermally tuned tubes using direct heating of the tuning strut, the tuning current must be well regulated. Where triode tuning is used, as in the 2K50, the heater current as well as the plate voltage for the triode must be well regulated. Field-test generators should be designed to operate over a wide range of power frequencies (for example, 60 to 1600 cps) and should be insensitive to the waveform of the primary power source.

Where the output line of the signal generator consists of a waveguide junction, some provision should be made for keeping foreign matter, such as water and dirt, from entering the waveguide. This can be done by plugging the end of the waveguide with a piece of nondissipative dielectric shaped so that the standing-wave ratio is small when viewed from either side. Windows which are suitable for this purpose are described in Sec. 4·22 of Vol. 9 of this series.

The electrical connection between the signal generator and the device to be tested can take many forms. A direct connection to the

receiver necessitates disconnecting the receiver from its operating circuits, which is seldom convenient. A commonly used procedure for radar systems is to use a horn or dipole directed at the radar antenna and connected to the signal generator. This may, however, lead to serious errors. Space attenuation is often too great if the horn is placed a considerable distance from the antenna. If the horn is placed close to the antenna, it becomes extremely difficult to know the fraction of the signal power which is received. If the horn and antenna are separated by a distance greater than the extent of their wave zones, the space attenuation A in decibels is calculated from

$$A = 10 \log_{10} \frac{16\pi^2 d^2}{g_1 g_2},$$

where g_1 and g_2 are the gains, relative to an isotropic radiator, of the horn and antenna, and d is the distance between them. If the signal generator leaks, it is well to keep the leaking parts out of the antenna beam.

A more convenient and accurate method of introducing the signal into the transmission line of a radar system is by means of a directional coupler. Such couplers are described in Chap. 14 of this volume. It is good practice to install a directional coupler into the system permanently. The directional properties of the coupler cause the introduced signal to be propagated toward the receiver. By the same mechanism, only the transmitted wave from the system which is proceeding toward the antenna will be introduced into the test generator.

The most convenient method of conducting the signal power is by means of a flexible coaxial cable. The connections used for coaxial cables are usually mismatched to such an extent that the effect of additive reflections from the two ends of the cable and from the other imperfectly matched components can cause a serious variation in power output with frequency. To obtain the best accuracy, it is often necessary to calibrate the signal generator using the same cables and connections as are employed for the measurements. The transmission loss of flexible coaxial cables becomes greater at higher frequencies and cannot be used at frequencies much higher than 10,000 Mc/sec. Available types of flexible cables are discussed in Chap. 1 of this volume and in Chap. 5 of Vol. 9 of this series.

Waveguides are generally more satisfactory than cables from an electrical point of view, but they are less convenient to use. At frequencies much less than 8000 Mc/sec the size of waveguide necessary to transmit power without appreciable attenuation becomes too great to be practical. For the greatest versatility flexible waveguide should be used. A flexible guide, constructed of a spirally wrapped metal strip, is satisfactory for use at 10,000 Mc/sec. A guide made up of a series of

choke and flange joints (known as vertebrae) held in a rubber envelope is also satisfactory. Its transmission loss is not high and is not greatly affected by twisting and bending.[1] Flexible guides of both types leak power, the vertebral guide being the poorer in this respect. This leakage should be absorbed by a lossy covering material.

4·11. Calibration Procedures.—The procedures used in calibrating a signal generator depend, of course, on the device in question. There are certain similarities in the methods used if the discussion is limited to c-w and modulated c-w signal generators. For these classes there are three main points of interest: (*a*) the output signal power level, (*b*) its carrier frequency, and (*c*) the modulation characteristics.

The determination of the modulation characteristics is usually a question of design rather than one of calibration. For a c-w signal generator, the presence of modulation may be detected with a spectrum analyzer. If modulation is present, it may be eliminated by improved filtering of the supply voltages or by low-frequency shielding of the oscillator tube. For pulsed signal generators, the spectrum of the pulses or the time response of a receiver of known characteristics when excited by the generator may be observed.

It is usually desired to know the frequency of c-w or modulated c-w signals. This is often accomplished by including a cavity wavemeter in the signal-generator circuits. This wavemeter may be calibrated by any of the methods discussed in Chaps. 5 and 6. When a wavemeter is not included in the signal generator it is necessary to use an external wavemeter in the exit transmission line. Suitable circuits for this purpose are treated in Chap. 5. Such measurements can be used to calibrate roughly the tuning of the oscillator tube, which is frequently useful.

There are two principal forms of calibration of signal power which can be called *derived* and *direct* calibrations. A derived calibration is one in which power is measured in some part of the r-f circuit of the signal generator, and this value is used to calculate the available power at the output terminals when the circuit parameters are known—in particular the attenuation caused by power split and by the variable attenuator. For this purpose a thermal power-measuring element connected to a suitable bridge and indicator is often placed on a side stub connected to the r-f circuit in the signal generator. These devices are discussed in Chap. 3.

This derived calibration is usually supplemented by a direct measurement of the output signal power, in which case the internal power-measuring device becomes simply a monitor. The principal difficulty arises from the rather small output power that is usually available, particularly for pulsed signal generators. Direct measurements may be taken over

[1] Volume 9, Chap. 5 contains more complete descriptions of the several varieties of flexible waveguide.

the whole range of the variable attenuator at various frequencies or they may be made at a single point. If direct measurements are made at a single point, the attenuator must be calibrated by an auxiliary measurement or the attenuation may be calculated from the dimensions. For resistive attenuators it is necessary to calibrate the attenuator point by point.

Whether the calibration is derived or direct it is necessary to know the character of the modulation of the signal in order to interpret power measurements made with a thermal element. It is customary with f-m and pulsed signal generators employing klystron oscillators to provide for c-w operation and to assume that the f-m or peak pulse power is the same as the c-w value. With suitable pulsing and f-m circuits this is approximately correct. It is always subject to error, however, and consequently, it is more desirable to measure the f-m or peak pulse power directly. In the case of pulsed modulation this can be done by measuring the average power and deducing the peak power from the recurrence rate and pulse length and shape. This is frequently a difficult measurement because of the low value of available average pulsed powers. A more satisfactory measurement method is discussed in the following paragraphs.

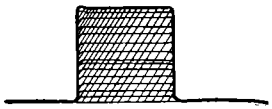

FIG. 4·14.—Effect of superposition of c-w and pulse signals.

In this method the peak power of a pulse is measured by mixing it with c-w power in a receiver. A relation between these two powers is derived so that a knowledge of the c-w level can be used to give the peak pulse power. Since the c-w power is easily measured, this is capable of considerable accuracy. By itself the c-w power produces no change in the output signal of the receiver;[1] that is, the baseline of an oscilloscope connected to the output terminals of the receiver remains unaltered. However, if c-w and pulsed power from two sources of exactly equal carrier frequency are applied to the mixer simultaneously, the video pulse appearing on the oscilloscope may be either positive, negative, or zero, depending upon the relative phase and amplitude of the two signals.

Suppose that the output signals from a pulsed and a continuous-wave generator, operating at exactly equal frequencies, are applied to a mixer and receiver. If the signals are equal in amplitude and in phase, the pulse and c-w signals combine to produce a positive video pulse, since the video output voltage changes only when the r-f pulse is applied. If the signals are out of phase and of equal amplitude, the two signals combine to produce a negative video signal. In practice, since the two sources cannot remain coherent, the video pulse appearing on the oscil-

[1] This measurement is carried out far above the noise level of the receiver.

loscope is composed of a series of horizontal lines representing combinations of the signals of arbitrary phases. If the r-f pulse amplitude is adjusted so that the modulation product appears as shown in Fig. 4·14,

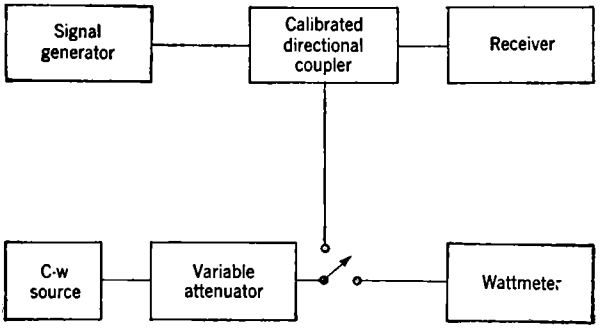

FIG. 4·15.—Block diagram of calibration equipment.

then the peak voltage of the pulse is twice that of the c-w signal, and the power during the pulse four times the c-w power. An operational block diagram of the calibrating equipment is shown in Fig. 4·15.

PRACTICAL C-W AND MODULATED-C-W SIGNAL GENERATORS

4·12. C-w, Pulse-modulated or F-m Signal Generator for the 3000-Mc/sec Region (the TGS-5BL Signal Generator).—This signal generator is designed to operate in the frequency range from 2400 Mc/sec (12.5 cm) to 3445 Mc/sec (8.7 cm). A front-panel view is shown in Fig.

FIG. 4·16.—TGS-5BL signal generator.

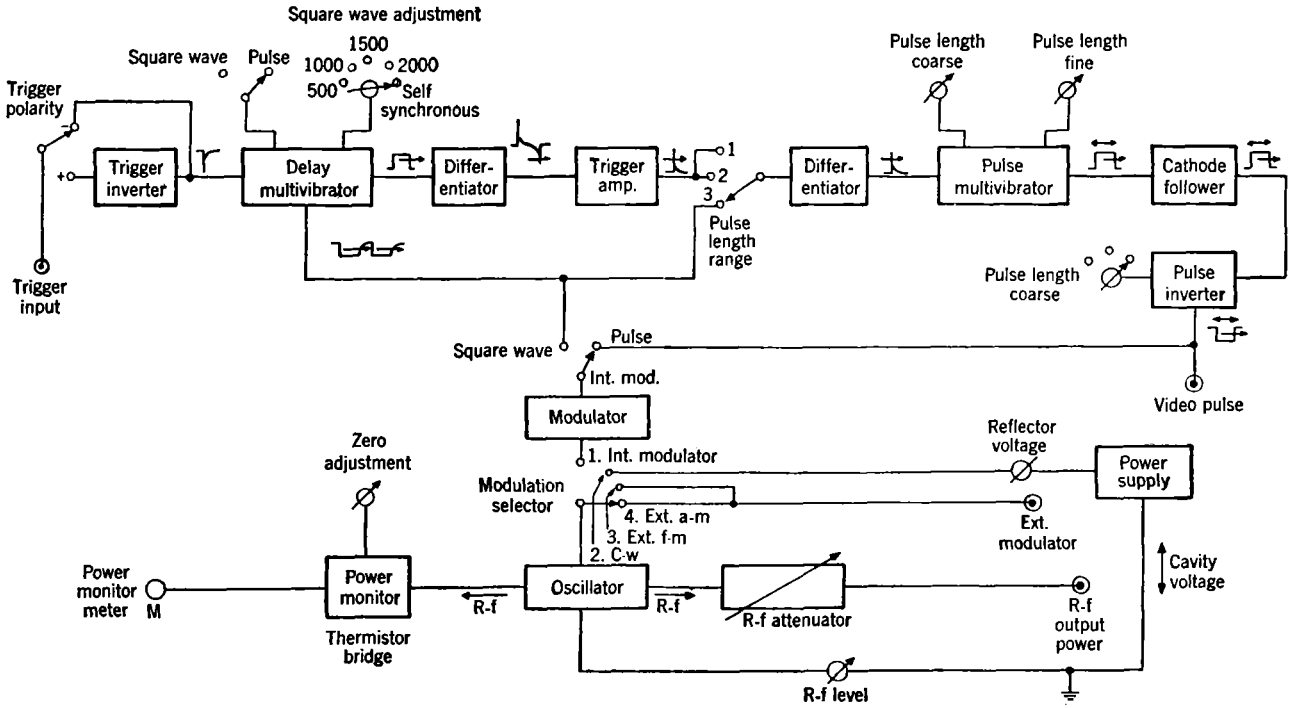

FIG. 4·17.—Block diagram of TGS-5BL signal generator.

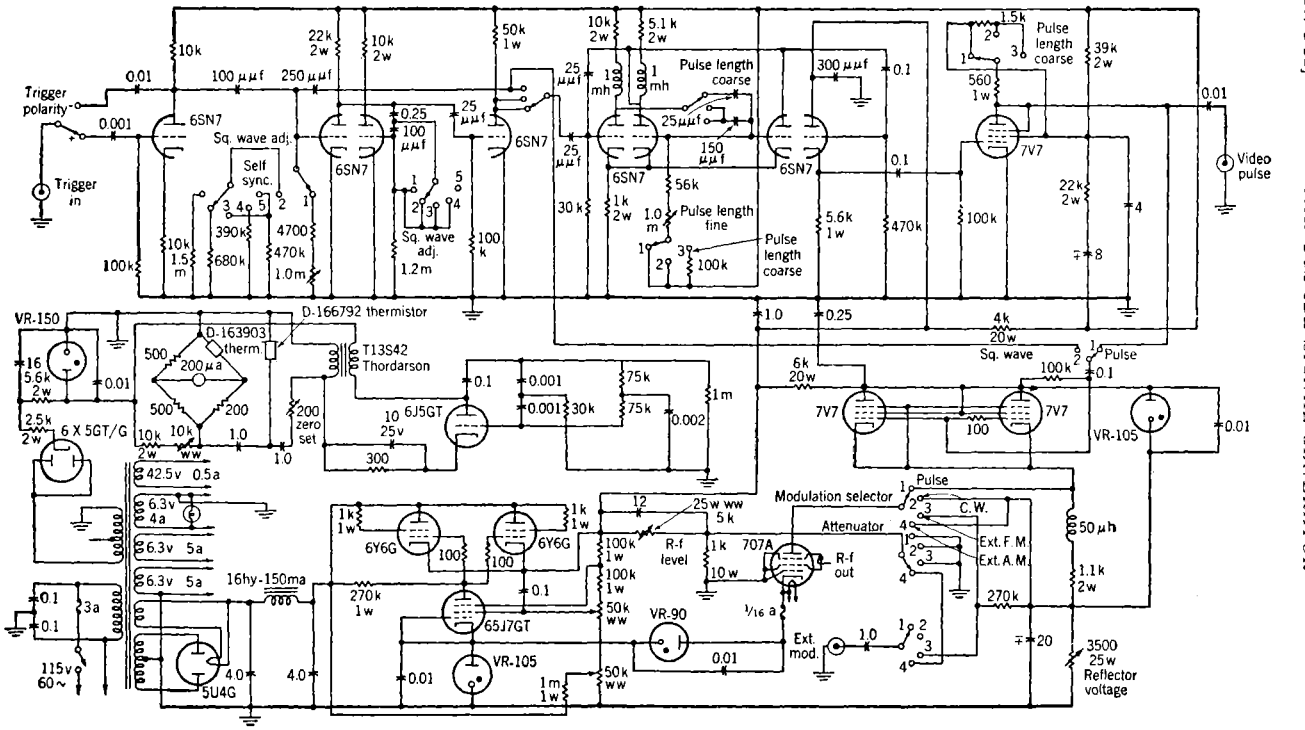

FIG. 4·18.—Circuit diagram of TGS-5BL signal generator.

4·16. Figure 4·17 is a block diagram of this equipment. No provision is made for measuring the input power from an external source. The equipment was designed for laboratory use only.

The circuit diagram for this signal generator is shown in Fig. 4·18 While this is largely self-explanatory, there are a few points to which it is worth calling attention. It will be noticed that a switch is provided so that when it is desired to go from c-w to pulsed operation, a voltage is applied to the reflector of the oscillator which prevents oscillation. The rectangular pulses remove this blocking voltage for short periods of time. This goes far toward avoiding the difficulties of a frequency

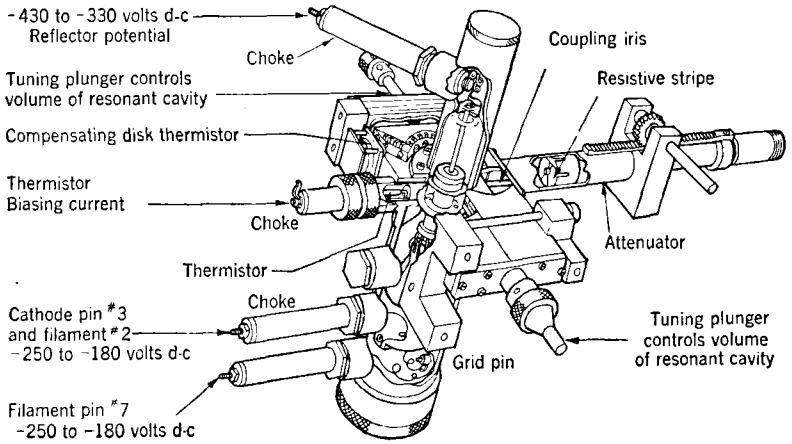

FIG. 4·19.—707B McNally cavity oscillator and associated r-f components.

change between the c-w and pulsed operation although there is still a small shift in frequency remaining.

External frequency-modulation voltage is applied to the reflector of the oscillator, but external amplitude modulation is applied to the grid which results in some frequency modulation. A selector switch permits square-wave modulation (50 per cent duty ratio) with the multivibrator running self-synchronously at about 1500 cps, or being triggered at any frequency from 500 to 2000 cps. The duration of the pulse from the pulsing multivibrator is determined partly by the duration of the trigger applied to it. For pulse lengths of 5 to 10 μsec, the trigger must be of several microseconds duration. A switching arrangement is provided to furnish this long trigger.

The oscillator is a 707B (McNally) reflex velocity-modulation tube with an external cavity. The oscillator and the arrangement of the other r-f components are shown in Figs. 4·19 and 4·20. As can be seen from Fig. 4·19, the cavity has straight sides and curved movable ends

in the form of tuning plungers. One of these plungers can be positioned at will and locked with a setscrew. The other is actuated by a micrometer drive which varies the wavelength over a band of about 2 cm. Thus, two positions of the semifixed plunger suffice to cover the whole frequency band. It would be desirable to have both plungers move out or in together, as the entire frequency range could be covered without resetting the second plunger. It would also result in more uniform variation of output power with frequency. These refinements were

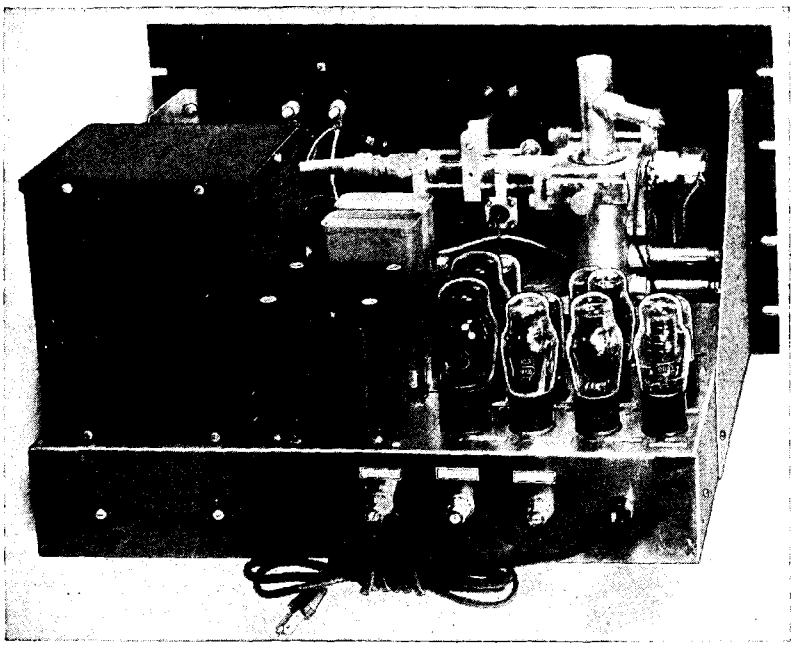

FIG. 4·20.—TGS-5BL signal generator, detailed view of mounting of cavity in the chassis.

foregone in the present case to gain mechanical simplicity. It will be seen from the block diagram, Fig. 4·17, that no means of determining frequency is provided in this signal generator. With a fixed setting of the back plunger, however, the micrometer driving the front plunger can be calibrated approximately in frequency. A typical frequency calibration chart is shown in Fig. 4·21.

The r-f power is adjusted to the reference level by adjusting the grid voltage of the 707B. Power monitoring is accomplished by extracting signal power from one side of the cavity and monitor power from the opposite side. The signal power is coupled out through a cutoff attenuator. The power monitor consists of a thermistor bead located as closely

as possible to its coupling loop. This thermistor forms one arm of a bridge circuit. It is driven by a constant d-c current so that its sensitivity is nearly independent of temperature, and compensated for ambient temperature effects by a 2000-cps current controlled by a disk thermis-

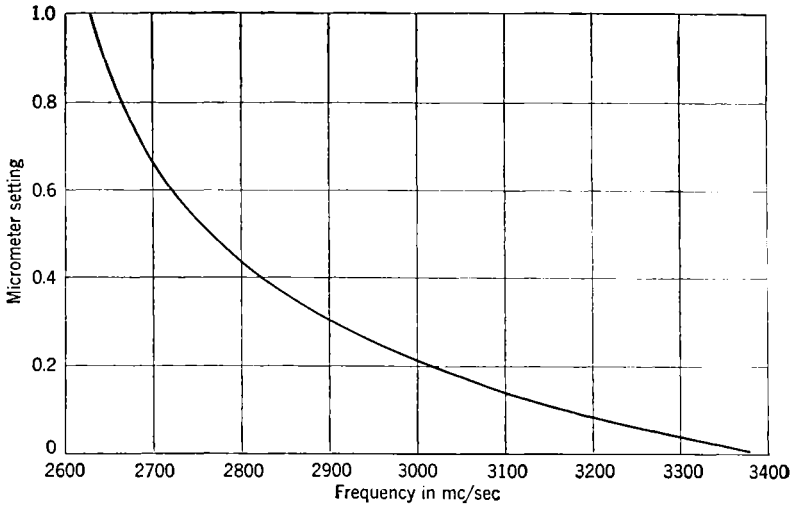

FIG. 4·21.—McNally-cavity micrometer setting vs. frequency.

tor. Figure 4·22 shows how the indicated power varies with the actual signal power when the output attenuator is set for minimum attenuation. The maximum signal power is about 1 or 2 mw. A somewhat more satisfactory method of calibration is to set the output attenuator to give 100 μw when the monitor reads half scale, and then set the attenuator

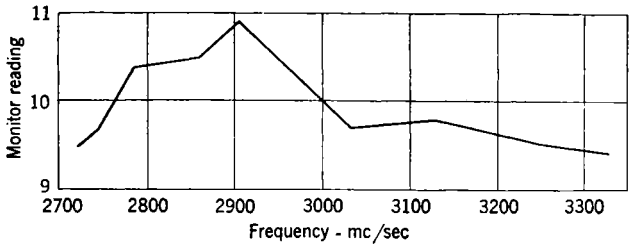

FIG. 4·22.—Frequency sensitivity of the power monitor in the TGS-5BL signal generator. The actual signal power is maintained constant as the frequency changes.

dial to read -10 dbm at this point. A typical calibration curve using this technique is shown in Fig. 4·23. It is desirable to have the monitor meter marked in + and $-$dbm as the output power of the oscillator at the edges of the frequency band is not always sufficient to give half-scale deflection on the monitor meter. The power-monitor meter may be

made to read linearly in dbm if the monitor coupling loop couples sufficient power out of the oscillator cavity.

The attenuator is of the cutoff type operating in the TE_{11}-mode. In order that the attenuator shall appear to be a generator of internal impedance approximately Z_0, the resistive attenuator insert is provided.

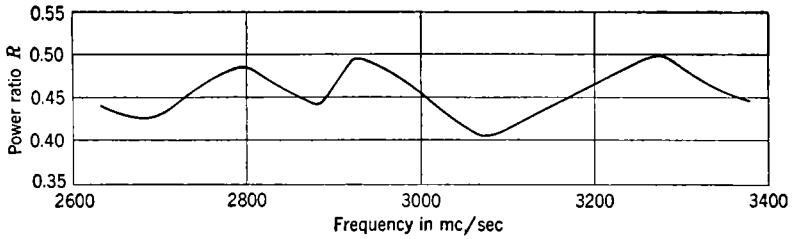

FIG. 4·23.—Frequency sensitivity of power monitoring in the TGS-5BL. The signal power is set to be 100μw when the attenuator dial reads −10dbm.

These resistive elements are easily burned out if several watts of power are accidentally fed into the signal generator from an external source. Because of the movement of the attenuator insert in the cutoff tube, it is necessary to have a length of flexible cable between the attenuator and the signal output jack.

There is probably some leakage of r-f power from the joint where the two halves of the cavity come together, some around the thermistor, and some around the attenuator insert. The voltage leads come out of the shield box through polyiron chokes.

4·13. A Pulsed-lighthouse-tube Signal Generator for the 2700- to 2900-Mc/sec Region (TS-155).—This is a signal generator with provi-

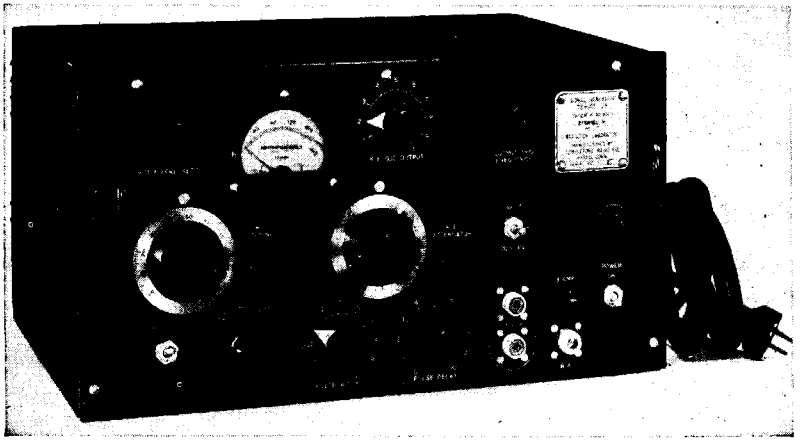

FIG. 4·24.—Front-panel view of the TS-155/UP signal generator.

sion for measuring power from an external source. A front-panel view of the set is shown in Fig. 4·24. It covers the frequency range from 2700 to 2900 Mc/sec and furnishes pulsed signals only. This generator employs a lighthouse tube with an external coaxial cavity. The frequency and amplitude of the oscillations of the lighthouse oscillator are rather insensitive to changes in plate voltage, which places rather lax requirements on the regulation of the power supply. Variations in construction of individual tubes has led to rather erratic performance of the microwave signal generators using them, such as failure to oscillate over the entire frequency band, and slow buildup in amplitude of oscillation when pulsed. Adequate shielding was provided by placing the tube and cavity assembly in a metal enclosure and bringing all lead

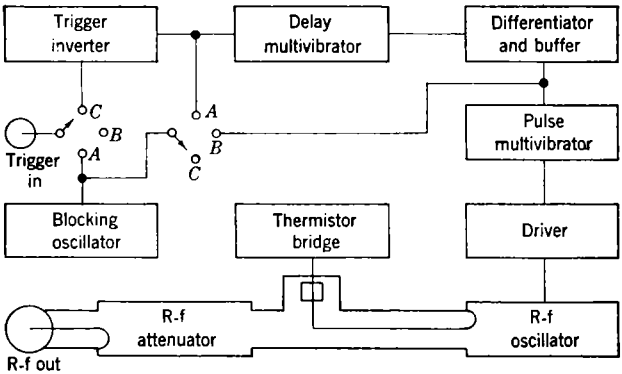

FIG. 4·25.—Block diagram of TS-155 signal generator.

wires and tuning controls out through polyiron chokes. The block diagram of this set is shown in Fig. 4·25.

The circuit diagram of the signal generator is shown in Fig. 4·26. The power supply is noteworthy only in the fact that so little attention is paid to voltage regulation. Two VR tubes are used, one to regulate the voltage for the thermistor bridge, and one to regulate the plate voltages of V_{1a}, V_{2a}, and V_{2b}, to prevent the pulse delay time from varying with power-line voltage.

The oscillator cannot be operated to produce a continuous wave but may be pulse-modulated at 120 to 2000 cps with either internal or external triggering. The internal trigger voltage is furnished by the blocking oscillator V_{5a}. When the selector switch is in the position for internal triggering, the trigger voltage is conducted also to the "trigger jacks" so that it may be used as a synchronizing signal to trigger an external transmitter. The external trigger pulse may be from 0.5 to 18.0 μsec long as measured between the half-voltage points, but the rise time to

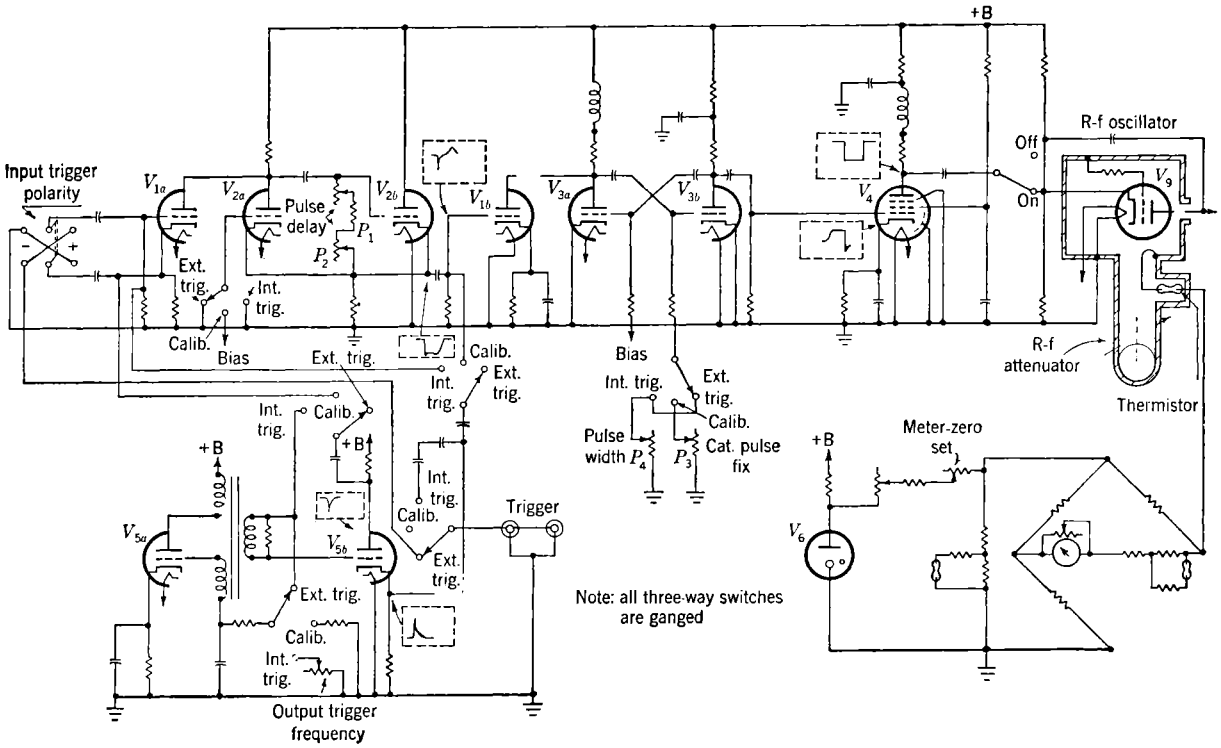

FIG. 4·26.—Circuit diagram of TS-155 signal generator.

10 volts must be less than 0.1 μsec. The amplitude may range from 10.0 to 100.0 volts.

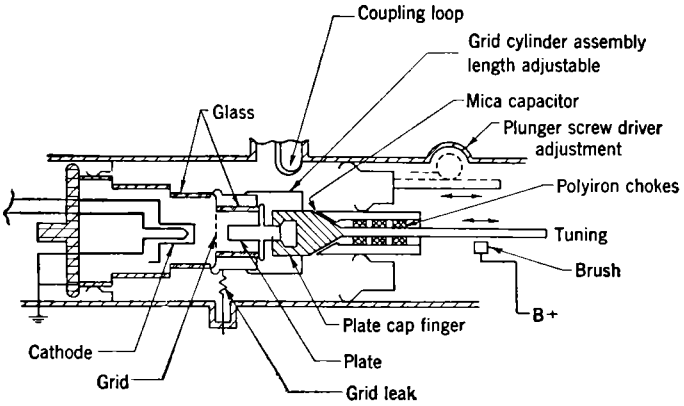

FIG. 4·27.—Schematic diagram of lighthouse-tube cavity, TS-155/UP.

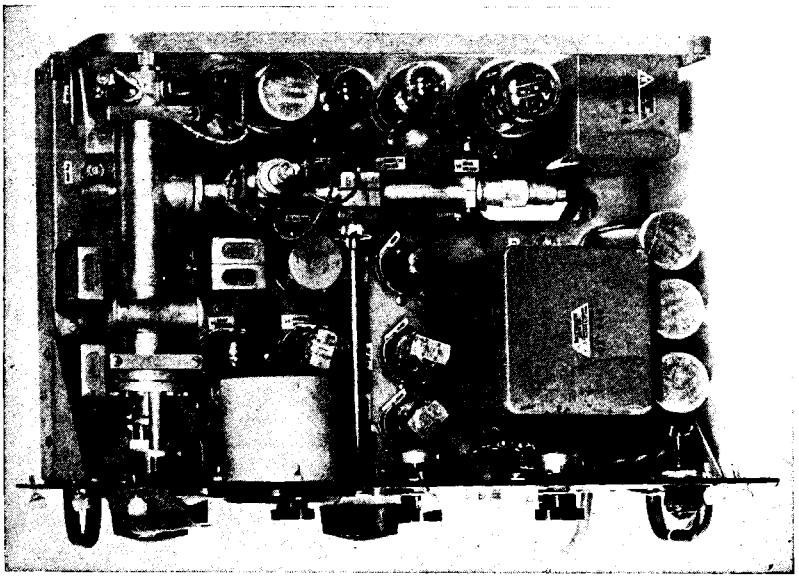

FIG. 4·28.—View of TS-155/UP signal generator showing r-f components.

The pulse may be delayed in any amount from 5 to 1800 μsec from the synchronizing trigger voltage at a repetition rate of 2000 cps. The delay range varies somewhat with repetition rate. The delay is varied by the potentiometers P_1, P_2 in the delay multivibrator $V_{2a} - V_{2b}$.

The pulse length is continuously variable from 0.75 to 6.0 μsec at a repetition rate of 2000 cps. The range of pulse lengths varies somewhat with repetition frequency. Pulse length is varied by means of the potentiometer P_4 in the multivibrator $V_{3a} - V_{3b}$. The resistor P_3 is set to give a fixed pulse length when the selector switch is set in the calibration position. In the calibration position, the multivibrator frequency is also set at about 650 cps so that the proper amount of average power is delivered to the thermistor power monitor for calibration. The shape of the r-f pulse is not all that might be desired. The pulse has a rise time of 0.25 μsec from 10 to 90 per cent voltage, and a fall time of 0.3 μsec from 90 to 10 per cent voltage.

The oscillator is a 2C40 lighthouse tube with adjustable coaxial cavities, as shown in Fig. 4·27. The arrangement of the oscillator and associated r-f components can be seen in Fig. 4·28, which is a top view of the signal generator. No provision is made for determining frequency in this equipment. The oscillator cavity can be adjusted until the power monitor shows a dip on input power. The output frequency of the oscillator is then near the frequency of the input signal. In testing radars, this is an aid in adjusting the test-signal frequency to that to which the receiver is tuned. The r-f power is adjusted to the reference level by varying the plate voltage of the oscillator with the selector switch in the calibration position. After the reference power level is set this way, the repetition rate and pulse length may be changed and the pulsed power will remain approximately the same.

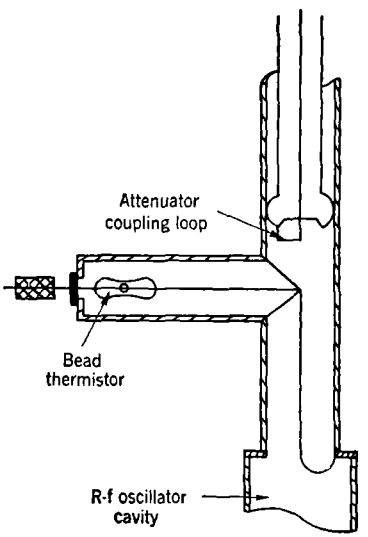

FIG. 4·29.—Schematic diagram of monitoring T-junction of the TS-155 signal generator.

Power is monitored by a temperature-compensated thermistor bridge. A loop couples power out of the coaxial cavity into a coaxial line. The center conductor of this line makes a right-angle bend and goes into a T-stub terminated by the thermistor. Power is radiated from this right-angle bend into the cutoff tube of the attenuator. This monitoring scheme is shown in Fig. 4·29. The variation in output power with frequency when the power monitor reads full scale and the attenuator is set at −20 dbm is shown in Fig. 4·30. Input-power measurements

may be made in the range from 0 to 200 mw. The attenuator is always set for minimum attenuation and the power level read from the monitor meter. Figure 4·31 is a typical calibration curve of input power for full-scale monitor reading. This monitoring scheme is obviously not well suited to input-power measurements.

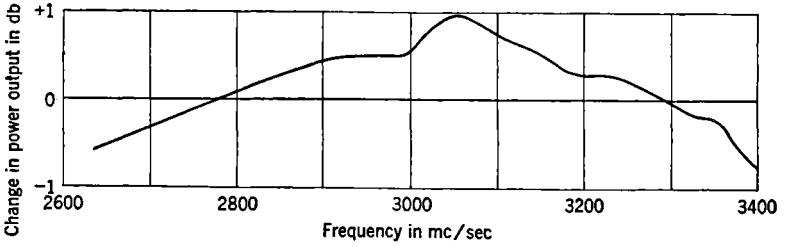

FIG. 4·30.—Power output vs. frequency, TS-155 signal generator. The power monitor reads full scale and the output attenuator is set to −20 dbm.

The attenuator is of the cutoff type operating in the TE_{11}-mode, with a resistive disk at the point of high impedance near the attenuator coupling loop. A flexible coaxial cable connects the attenuator insert to the output jack.

The r-f components are well shielded so that the detectable leakage power is less than −120 dbw. The heater-current leads for the 2C40 are brought out of the cavity through polyiron chokes. The plate rod, carrying the plate current, is brought through a reactance choke and a polyiron sleeve. The insulated thermistor lead passes through a polyiron choke. All other joints and connections are made to fit well and are assembled very tightly.

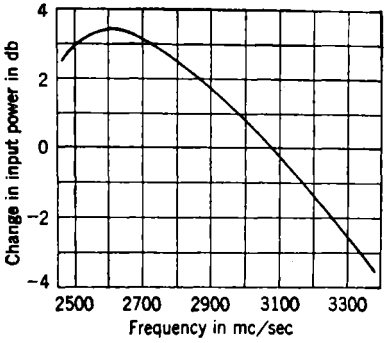

FIG. 4·31.—Calibration curve for power input vs. frequency, TS-155 signal generator.

Calibration of this set is complicated by the inability of the set to operate with the oscillator producing c-w power and by the large minimum attenuation of the attenuator. The repetition rate and the pulse length, as well as the average output power, must be accurately determined in order to determine the pulse power. The average output power is only about 2 to 3 μw, at most, and hence is difficult to measure even with a sensitive thermistor bridge. If the pulse power is determined at minimum attenuation, the signal is introduced into a spectrum analyzer.

The signal is compared with that from another oscillator whose output power is reduced by an accurately calibrated attenuator.

4·14. An F-m and C-w 9000-Mc/sec Signal Generator (TS-147).—This signal generator, a front-panel view of which is shown in Fig. 4·32,

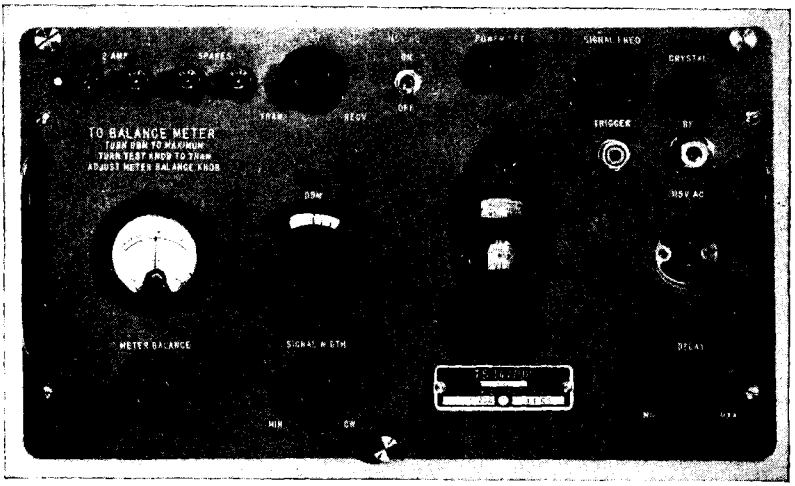

FIG. 4·32.—The TS-147/UP signal generator.

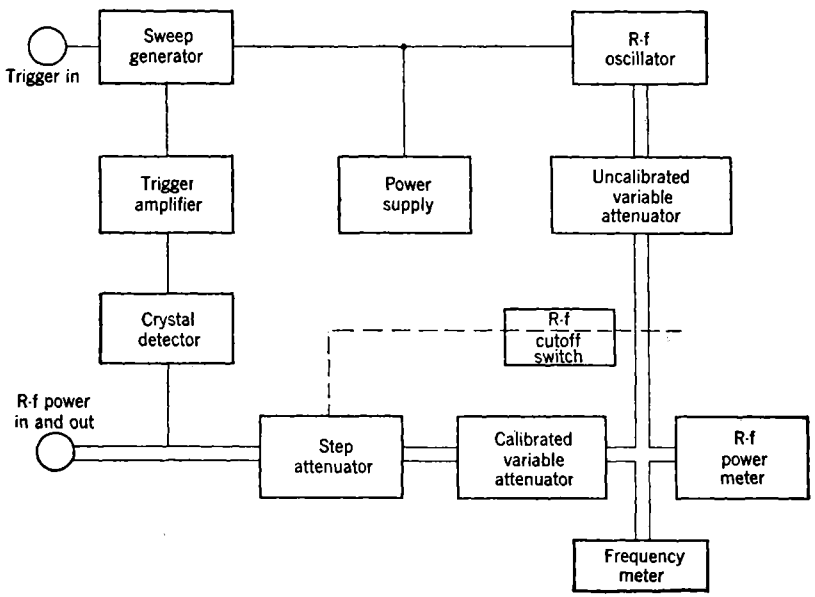

FIG. 4·33.—Block diagram of TS-147/UP signal generator.

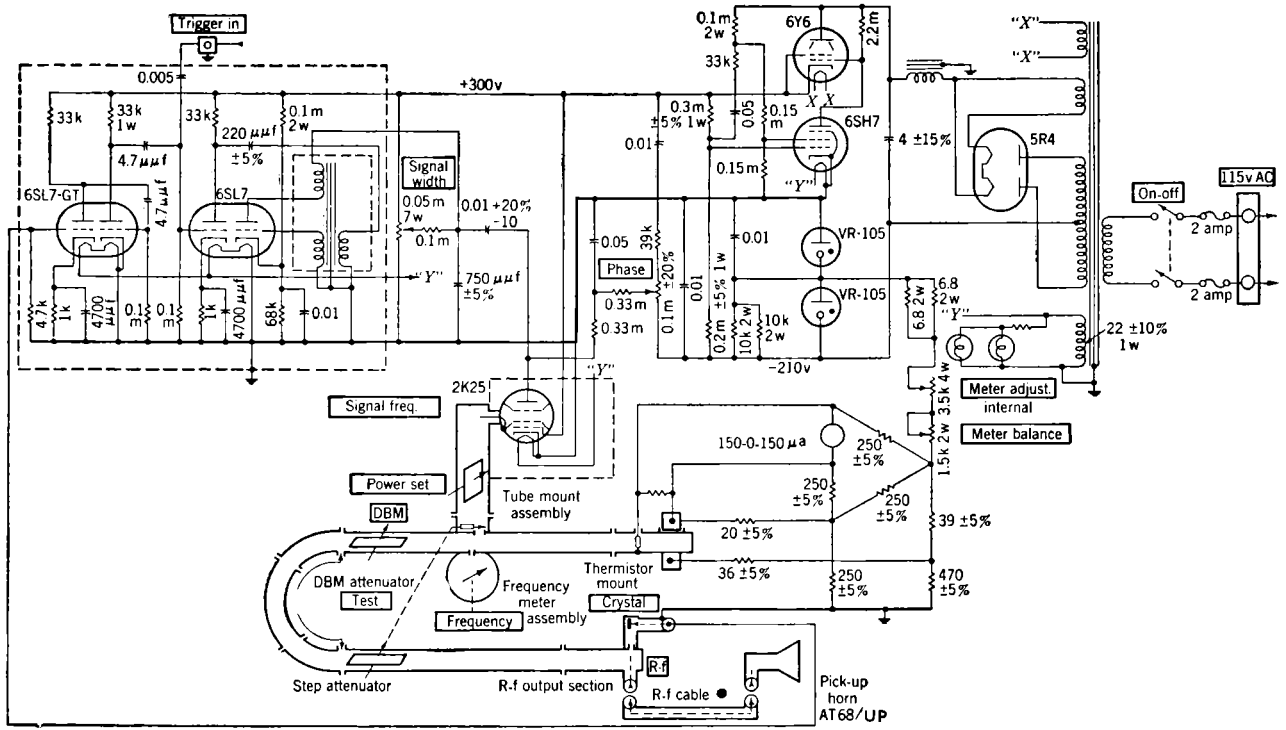

FIG. 4-34.—Signal generator TS-147/UP, circuit diagram.

was designed for measuring both input and output power and frequency in the frequency range from 8500 Mc/sec to 9600 Mc/sec. The block diagram of the set is shown in Fig. 4·33.

The generator may be operated to produce a continuous wave or f-m signals by means of a sawtooth voltage generated by a blocking oscillator.

Synchronization may be accomplished either by an external trigger voltage or by r-f pulses coming into the input-output jack of the signal

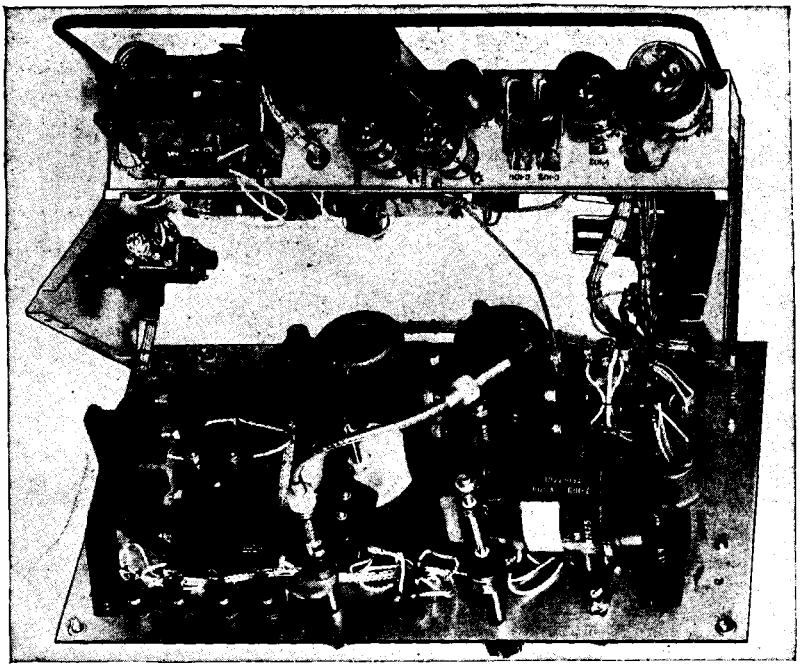

FIG. 4·35.—R-f components of the TS-147/UP signal generator. The waveguide and accessories are painted black.

generator. A small amount of the power coming from an external transmitter is coupled through a −35-db iris into a crystal rectifier. The video pulse from this crystal is amplified by the two-stage amplifier and is used in the same way as an external trigger voltage. Triggering takes place at r-f power levels of from 5 to 500 watts with pulses of 0.5- to 6-μsec duration. External positive trigger voltages of 10 to 50 volts and 0.5- to 20-μsec duration are capable of triggering the blocking oscillator. The sawtooth sweep voltage can be continuously adjusted to give sweep rates of 0 to 2 volts per μsec, which correspond to 0 to 6 Mc/sec per μsec of frequency modulation. The sawtooth sweep may be delayed

by any amount from 3 to 50 μsec after the triggering voltage. The circuit diagram is shown in Fig. 4·34.

The 2K25 oscillator is a reflex velocity-modulated tube with an antenna which radiates the power into rectangular waveguide. It is an internal-cavity tube with mechanical tuning. Figure 4·35 is a photograph showing the oscillator and other r-f components of the test set.

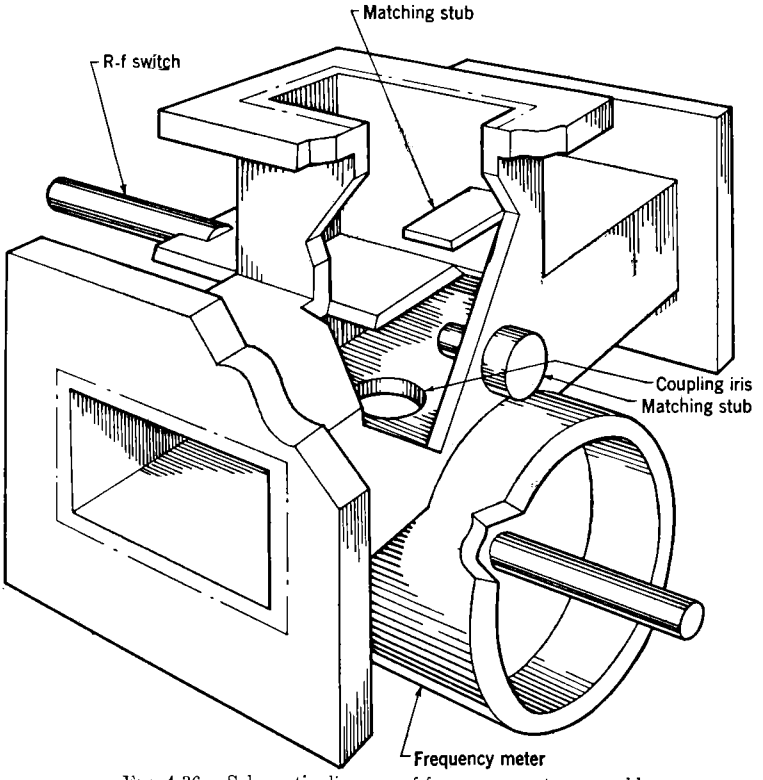

FIG. 4·36.—Schematic diagram of frequency-meter assembly.

The frequency meter is a cylindrical resonant cavity of variable length which normally operates in the TE_{011}-mode. It bears a spirally engraved dial with engraved marks 1 Mc/sec apart. It has an absolute accuracy of ±2.5 Mc/sec at 25°C and 60 per cent relative humidity. The relative accuracy is ±1.0 Mc/sec for frequency differences of less than 60 Mc/sec. The wavemeter is coupled to the waveguide by means of a hole in its side. Its response to c-w signals within the frequency band in spurious modes is at least 20 db less than the response in the TE_{011}-mode. The

variation in response with frequency on input signals is about ±15 per cent, but on output power the variation is about ±30 per cent.

As can be seen from Fig. 4·36, the wavemeter coupling iris is directly opposite the generator arm of a waveguide T. It will also be noticed that a small pin projects inward from one wall of the waveguide. This pin tends to match out the reactance of the wavemeter hole when the wavemeter is not resonant. The generator arm of the T may be closed off by an r-f switch, which is the movable metallic plate located just above the tuning pin.

A metalized-pyrex vane attenuator is used to reduce the r-f power to the reference level. Power is monitored by a thermistor and temperature-compensated bridge. A meter-shunt resistor is attached to the thermistor mount to compensate for the variation in sensitivity of different thermistor beads. In this way, the thermistor mount can be replaced in the field without having to recalibrate the power monitor. A noteworthy feature of the mount is the fact that there is very little leakage from it. Leakage is prevented by having a waveguide-beyond-cutoff tube extending beyond the coaxial tuning stub, and by surrounding the fixed coaxial stub with polyiron. The thermistor bridge is balanced when the reference power, 1 mw, is applied to the thermistor element. The meter-balance control decreases the d-c power to the thermistor by 1 mw. As a result the thermistor always has the resistance at which it was tuned for best match when the r-f power was measured. It should be noted, however, that when the set is switched to f-m operation, the average power delivered to the thermistor is very small; therefore, unless the bridge is rebalanced, the thermistor will not be at its proper value and its standing-wave ratio will probably be increased. This change in standing-wave ratio causes a change in the division of power at the T and a different proportion goes into the output line. For the same reason, replacement of the thermistor mount by one whose standing-wave ratio varies with frequency in a slightly different manner, even though it has a sensitivity-compensating meter-shunt resistor, alters the output power of the signal generator somewhat from that shown by the calibration curve which was made with the original mount. With the r-f switch closed, the T is cut off and the error of the thermistor in measuring input power is only that from reflection. Typical calibration curves for both input and output power are given in Fig. 4·37.

The two calibrated attenuators and the power-set attenuator are all metalized-pyrex vanes which are moved from the sidewall of the guide, where there is no electric field, to a point near the center of the guide, where the electric field is a maximum. The two calibrated attenuators are alike, except that one, known as a step attenuator, has only two positions differing in attenuation by 40 db. The other attenuator is

continuously variable over an approximate 40-db range. The frequency sensitivity of attenuation of this type of attenuator has the characteristic of being almost zero for minimum attenuation, increasing slowly to about the 20-db range, and then decreasing to nearly zero at about 40 db. Above 40 db, the frequency sensitivity increases more rapidly and is opposite in sign to that at attenuations less than 40 db. These facts dictated the use of a 40-db step attenuator, but the choice is a desirable one also from the standpoint of calibration as it divides the total attenuation into two nearly equal parts. When the selector switch is in the position for measuring input power, the step attenuator is in the position of minimum attenuation and input powers of +7 to +30 dbm can be measured. When the switch is in the position for testing receivers, the step attenuator is at the 40-db position and the output power may be

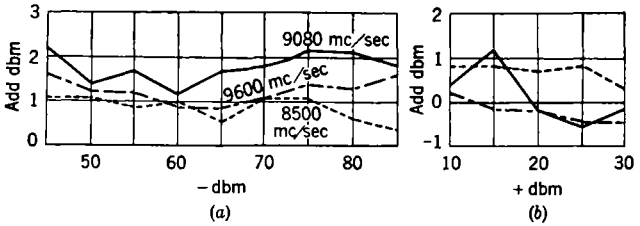

FIG. 4·37.—Sample calibration for a TS-147/UP signal generator; (*a*) gives the calibration for output power (*b*)for imput power.

varied from −42 to −85 dbm. When the switch is set at the third position, the step attenuator is at minimum value, giving output powers of approximately −7 to −30 dbm. The waveguide is terminated in a coaxial adapter. A flexible coaxial cable is used to conduct power into or out of the test set.

The set is well protected from r-f leakage by making each component leaktight. The leakage protection of the thermistor mount has already been described. The 2K25 is housed in a cast-aluminum cylinder, the lid of which has a polyiron choke-ring. The voltage leads are pressed into a single piece of nonconducting polyiron that fits tightly into a sleeve. The tuning adjustment is a bakelite rod passing through a long metal sleeve that acts as a waveguide beyond cutoff. The output antenna of the oscillator passes through a reactance choke before entering the waveguide. The video lead from the crystal passes through a polyiron choke. The waveguide sections each end in a flange. Each pair of flanges has a silver-plated washer (about 0.003 in. thick) clamped between the pair. No special precautions are taken to prevent leakage around the rods that actuate the attenuator strips other than having the parts fit tightly. The metal rod that operates the r-f switch passes through a polyiron block retained in a close-fitting sleeve.

4·15. An F-m and C-w Signal Generator for the 24,000-Mc/sec Region.—This signal generator produces signals and is designed for measuring the output power and frequency of transmitters in the region 23,500 Mc/sec to 24,500 Mc/sec. Figure 4·38 is a photograph of the front panel. A block diagram of this test set is essentially the same as that shown for TS-147 (Fig. 4·33) except for the arrangement of r-f components.

The circuit diagram of the signal generator is shown in Fig. 4·39, except for the power supply. The electrode voltages for the oscillator are electronically regulated, and a ballast lamp is provided to regulate

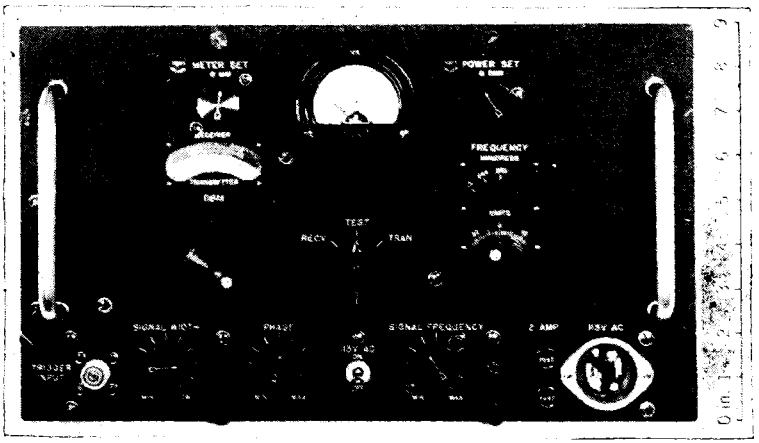

FIG. 4·38.—A 24,000-Mc/sec signal generator.

the heater current for the cathode of the triode tuner and the electron gun. This feature contributes a great deal to the frequency stability of the r-f oscillator.

The sawtooth sweep which is used to frequency-modulate the r-f oscillator is generated by a triggered blocking oscillator. An external trigger may be introduced, or if the set is connected to a transmitter which produces short pulses of r-f power, the blocking oscillator will be automatically triggered. This automatic triggering is accomplished by coupling a small amount of power from the main transmission line through a 43-db coupling iris into a crystal. The output voltage of this crystal is amplified by a 3-stage video amplifier and used as the trigger. Automatic triggering will take place at input powers ranging from 150 to 1000 watts.

The oscillator is a 2K50 internal-cavity, reflex, velocity-modulation tube with thermal tuning. The thermal-tuning current, which expands

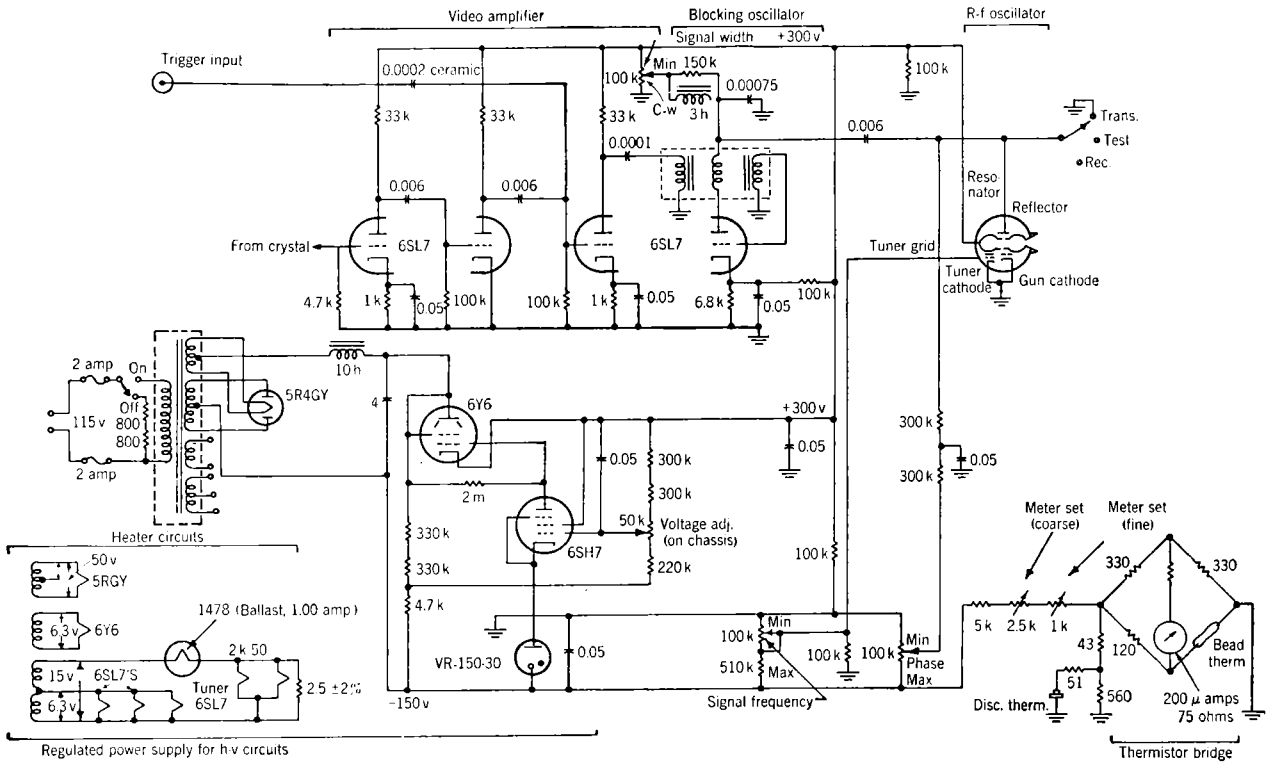

FIG. 4·39.—Schematic circuit diagram of the 24,000-Mc/sec signal generator.

a strut and distorts the oscillator cavity, is regulated by the grid voltage of a triode housed in the metal shell of the oscillator tube.

The frequency is determined by means of a cavity wavemeter. This is a hybrid cavity, being partly coaxial and partly cylindrical.[1] The frequency is read in megacycles per second, on a counter geared to the tuning rod, to an accuracy of less than 0.1 per cent at all parts of the band. While this accuracy is sufficient for most absolute frequency measurements, it is not good enough for many measurements of small frequency differences, such as between the transmitter and local-oscillator frequencies. Where higher accuracy is required, a calibration curve is furnished with the equipment. The wavemeter cavity and tuning rod

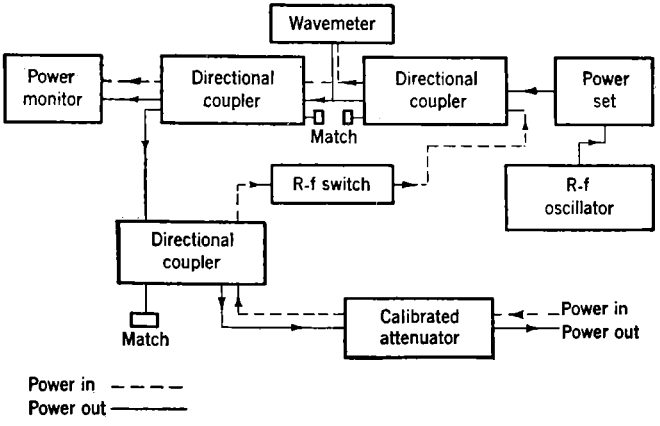

FIG. 4·40.—Block diagram showing directional-coupler arrangement.

are made of silver-plated invar to minimize the change in resonant frequency with temperature. The resonant frequency varies by about 14 Mc/sec from expansion when the temperature changes from −40° to +55°C. The maximum variation of the resonant frequency from humidity changes in the same temperature range is about 12 Mc/sec. In the worst case, these frequency variations are additive.

In order that the wavemeter give a dip on both input and output power, it is located between the input directional coupler (6-db coupling) and the output directional coupler (10-db coupling). In this way, the output signal passes first the wavemeter, then the first output coupler, and finally, the thermistor. An input signal, on the other hand, passes through the 6-db input coupler, then the wavemeter, and is finally absorbed in the thermistor. This can be seen at once in Fig. 4·40 which is a schematic drawing of the r-f circuit. Figure 4·41 shows in more detail how the switching is accomplished.

[1] See Sec. 5·19, for a description of this cavity.

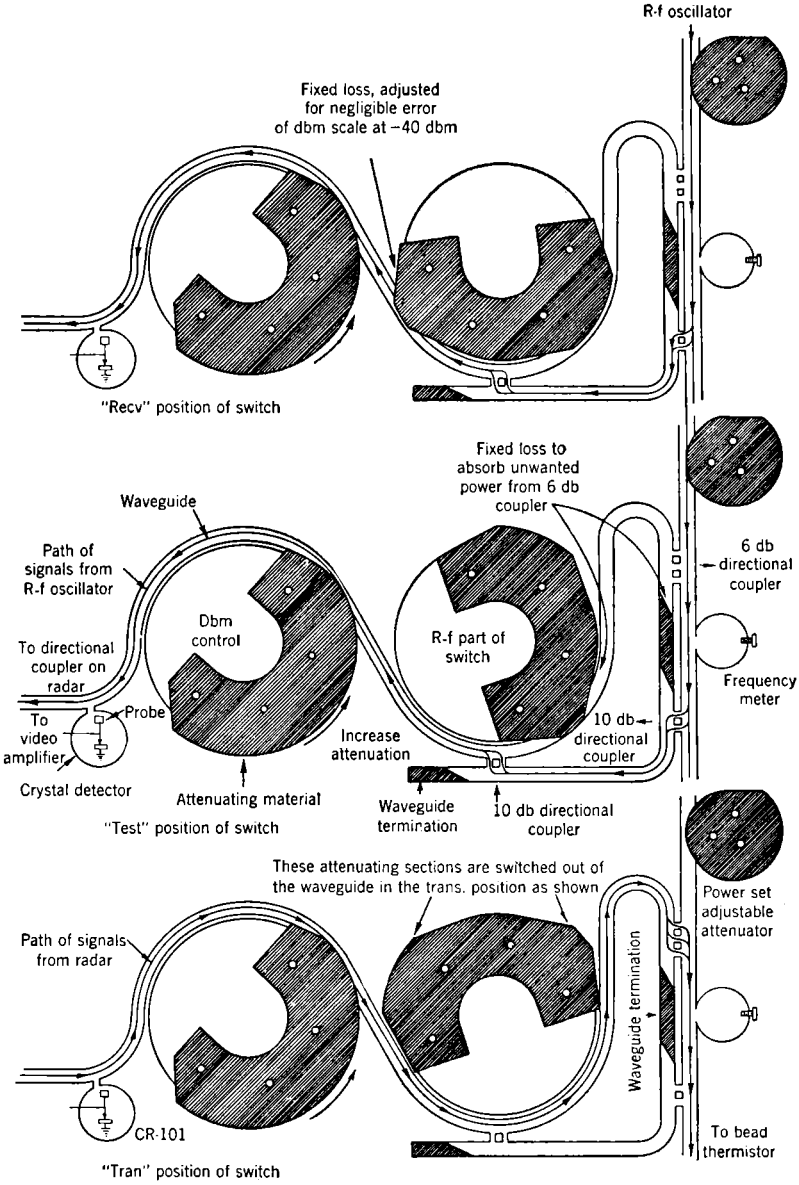

FIG. 4·41.—Schematic diagram of attenuators in the 24,000-Mc/sec signal generator.

An uncalibrated attenuator is provided so that the output power of the 2K50 may be cut down to 1 mw as shown on the power monitor. This attenuator, which is a dissipative-vane type, also provides padding which minimizes pulling of the oscillator by the wavemeter when it is resonant. This attenuator is marked POWER SET on the block diagram.

The power monitor is a thermistor used as one arm of a bridge circuit and compensated for thermal effects. The error from mismatch of this thermistor mount has a maximum value of about 7 per cent. The mechanical zero of the power-indicating meter is set with the needle pointing straight up. This point is marked 1 mw and 0 dbm. A METER SET knob is provided which varies the current to the thermistor bridge. This knob is adjusted to make the meter read 0 mw when the POWER SET attenuator is in the position of maximum attenuation. The effect is to reduce the d-c power to the thermistor by 1 mw. A lock is provided so that once the METER SET adjustment is made, it cannot be altered accidentally. The POWER SET attenuator is then adjusted until the meter reads 1.0 mw and locked. The bridge is now balanced and the thermistor resistance is that at which it was tuned for best match.

Errors that might arise from standing waves in the various transmission lines are avoided by the use of directional couplers. It is necessary to introduce an r-f switch (in this case a fixed attenuator with a carbonized vane) into the input power line in order to prevent errors from leakage of power around this path. This leakage power is caused by reflection from the thermistor mount, imperfect directivity of the 6-db coupler and reflection from the termination of the primary input power line. Because of the coherent nature of the leakage and the signal, the error may be much worse than it would seem at first glance. The directional couplers which are involved in the attenuation of input and output signals are of the branched-guide type because of their small variation of coupling with frequency, and the relatively good match that they present to the line.

The calibrated attenuator consists of a resistive strip that can be rotated into the common input-output waveguide. In this way the attenuator dial can be marked with a single set of marks and attenuations in decibels below 1 mw engraved on the upper half of the dial for receiver testing, while figures representing decibels above 1 mw are engraved on the lower half for use in testing transmitters. A fixed attenuator of the proper value is inserted into one of the waveguides by operation of the RECV-TRAN switch to make round attenuation figures (such as -60, $+30$) occur on the same calibration mark. This attenuator is removed from the power-output line in the TEST position of the RECV-TRAN switch so that the signal may be increased by approximately 17 db above the maximum *calibrated* signal level. The attenuation

figures marked on the dial of the calibrated attenuator refer to the ratio of the power at the output waveguide to the power measured by the thermistor. This includes the attenuation of directional couplers and fixed attenuators as well as the calibrated attenuator itself.

Since both coaxial cables and spirally wrapped flexible waveguides tend to be lossy and sensitive to flexing at these frequencies, a vertebrae-type flexible guide is furnished to connect the signal generator to the directional coupler of the transmitter or receiver waveguide or other test point. The output waveguide of the signal generator proper has a polyglas plug near its opening that prevents foreign matter from getting into the waveguide. This plug has matching steps on each side to minimize reflections from it.

The signal generator has been carefully designed to have a minimum of r-f leakage. The 2K50 tube is held in a leaktight aluminum shield and the voltage leads come out through polyiron chokes. The main body of the r-f circuit, which includes attenuators and directional couplers, is the most novel feature of this test set. The waveguides, including the directional couplers, are milled into two flat pieces of aluminum. The two pieces are then bolted tightly together to form the waveguides. The result is a very leaktight system. The wavemeter barrel is dropped through a hole in the aluminum plates and a take-up nut pulls it into such close mechanical contact with the plates that no leakage is detectable.

MICROWAVE NOISE SOURCES

4·16. Noise Sources at Microwave Frequencies.—The difficulties of calibration and construction of c-w signal generators have lent considerable favor to the use of noise sources, which are much more easily constructed and in some cases are considerably more rugged and stable. In addition, some noise sources are absolute in the sense that they emit microwave noise of an amount given by physical constants and measurable parameters. Such noise sources can rightly be considered as the ultimate standards of power measurement; consequently, apart from their convenience, noise sources are necessary tools in fundamental studies. Since the sources of noise are frequently just those which limit the sensitivity of receivers, the magnitude of noise power is already in the range required for the receiver measurements and the sources need little or no shielding or attenuation. This may, however, be disadvantageous if larger powers are required and constitutes perhaps the only serious limitation of noise sources.

It is convenient to divide noise sources into two categories, thermal sources and shot-noise sources. The physical mechanisms of noise production are quite different. Thermal sources are thermodynamic

systems and so are characterized by their absolute temperature T. Hot bodies such as incandescent filaments, hot transmission-line loads, furnaces, and the sun are practical examples of thermal-noise sources. Shot-noise sources employ moving electric charges, particularly electrons in vacuum tubes or metal-semiconductor contacts. Both thermal and shot-noise sources produce known amounts of noise, the former given by the equations of radiation theory and the latter by Schottky's equation or its modification. They are thus absolute sources. In practice, however, it is not always possible to apply the theory directly to the device in order to calculate the noise power generated. Such devices become secondary sources of noise and must be calibrated against some standard signal source. They may, however, retain the form of variation given by the theory so that extrapolation is possible around the calibration point.

A noise source and a load will be connected by a transmission system. It may be a simple transmission line or a complicated system of antennas, reflectors, transmission lines, or transformers. In any case, a cut can be made in the system at any point, dividing the load from the source. The terminals thus exposed are those of the source and the load. At the source terminals the available power in a frequency range df centered at the frequency f, for a thermal source at temperature T, is $kT\,df$. The quantity T is called the noise temperature of the source. In the case of sources which are not thermal this representation may still be used, and T becomes the temperature of a thermal source having the observed available power. The noise temperature of a source may therefore be a physical parameter of the source or entirely fictitious. In any case, the noise temperature of a source completely specifies the available power. The available power from a source of noise temperature T is the power absorbed by a load at 0°K having a bandwidth df at frequency f and having an impedance equal to the complex conjugate of the source impedance at the exposed terminals.

The load most frequently used in conjunction with a noise source is a receiver. The commonly accepted criterion of receiver performance, namely, the receiver noise figure, has been defined in Sec. 4·1.

4·17. Thermal Noise Sources. *Hot Transmission-line Loads.*—Perhaps the most absolute of the various noise sources is a matched transmission-line termination that can be heated to a known temperature. For calibrating receivers, the temperatures required may be quite high since noise figures of even the best receivers correspond to about 2000°K. For special receivers, designed for temperature measurement exclusively, the required temperatures are much lower. Dicke's microwave radiometer,[1] for example, requires a noise source only some 10 to 50° above room temperature.

[1] R. H. Dicke, "The Measurement of Thermal Radiation at Microwave Frequencies," RL Report 787, Aug. 22, 1945.

Payne-Scott[1] has described a 10-cm thermal noise source employing a tungsten-filament lamp mounted across a waveguide. The filaments are arranged in a cylindrical structure, the wires being parallel to the axis of the cylinder, and to the electric field in the waveguide. The author states that no appreciable power is absorbed in the glass envelope or lamp base, and that little difficulty was experienced in matching the device to the waveguide. Hansen[2] has described a hot load employing a heated filament as the central conductor of a coaxial transmission line. Noise in excess of that given by the filament temperature was observed, but no explanation was offered. Dicke[3] has constructed a very simple hot load for the calibration of a 1.25-cm radiometer. (See Fig. 4·42.) It consists of a carefully tapered polyiron plug fitted into a section of waveguide. With a suitable taper it is matched over a broad frequency band. A thermocouple or bimetallic thermometer is attached to the waveguide. The whole is surrounded by a heating coil and an insulating jacket. The load can be heated from 100° to 150°C without damaging the polyiron or affecting the match.

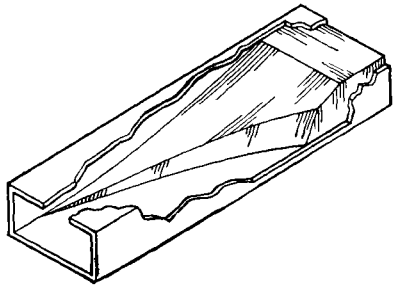

FIG. 4·42.—Tapered polyiron waveguide hot load.

The Sun.—The hot waveguide loads described are merely simple cases of thermal noise sources, which in general may take any form so long as an electrical connection can be made with a receiver. If the receiver is provided with a narrow-beam antenna, the sun is a suitable noise source. If the sun's temperature is T_s, the antenna gain G, and the solid angle of the sun Ω_s, then the available power at the receiver is

$$kT_s \frac{G\Omega_s}{4\pi}, \tag{14}$$

if there is no attenuating medium between the sun and the receiver, and provided that $G\Omega_s/4/ < 1$. This latter condition implies that the antenna pattern is broad compared with the aperture of the sun. If the reverse is true, the available power is just kT_s.

[1] Ruby Payne-Scott, "A Thermal Noise Generator for Absolute Measurement of Receiver Noise Factors at 10 cm," Radio Physics Laboratory Report 3924, May 29, 1944.

[2] W. W. Hansen, unpublished experiments reported in lectures given at RL Seminar.

[3] Dicke, *loc. cit.*

G. C. Southworth[1] has reported measurements on the noise from the sun at 10-, 3.2-, and 1.2-cm wavelengths. He finds the 10- and 3.2-cm measurements agree quite well with Eq. (14) using the optical values, $T_s = 6000°K$, and an angular sun diameter of 32′. He received, however, much less than the calculated noise at 1.2 cm. This has not been confirmed by the recent experiments of Dicke[2] with the 1.25-cm radiometer. Measurements[3] during the solar eclipse of July 9, 1945 were particularly sensitive to the sun's aperture which was found to be not greater than 10 per cent in excess of the optical value. The sun's temperature was measured as 10,000°K, considerably above the optical value and in the opposite direction from the discrepancy observed by Southworth. Much more work will be necessary to give a definitive answer to these difficulties.

In the wavelength region below about 2 cm, corrections must be applied[4] for the attenuation in the atmosphere when using Eq. (5). Also a correction must be made if any appreciable part of the antenna pattern falls on the terrestial objects for which the characteristic noise temperature may be in the range 100° to 300°K.

4·18. Shot-noise Sources.—Vacuum-tube noise sources have long been used at ordinary radio frequencies. In particular, the temperature-limited diode has served as an absolute source of noise for the calibration of receivers. At microwave frequencies, the shape of the conventional diode is not convenient because of the necessary smallness of the tubes and the distributed impedances of their leads, and other forms of vacuum-tube noise sources have been developed. Nevertheless, some attempts have been made to employ diodes. Breazeale and Beers[5] have described a diode which formed an integral part of the mixer circuit in a 10-cm receiver. The mixer was tuned for signal match with the diode in place. It was found that the diode current and noise temperature were roughly proportional. The device, however, was not convenient to tune and required its calibration *in situ*. The shot-noise source described by

[1] G. C. Southworth, J. Franklin Inst. 239, 285 (1945).

[2] R. H. Dicke, R. L. Kyhl, A. B. Vane, and R. Beringer, "The Absorption of Atmospheric Water-Vapor in the K-band Region," RL Report 1002, Jan. 15, 1946, *Phys. Rev.* **70,** 340 (1946).

[3] R. H. Dicke and R. Beringer, *Astrophys. J.* **103,** 375 (1946).

[4] J. H. Van Vleck, "Atmospheric Absorption of Microwaves," RL Report 175, Apr. 27, 1942; "Further Theoretical Investigations on the Atmospheric Absorption of Microwaves," RL Report 664, March 1, 1945. R. Beringer, "The Absorption of One-half Centimeter Electromagnetic Waves in Oxygen," RL Report 684, January 26, 1945, *Phys. Rev.* **70,** 53 (1946). Dicke, Kyhl, Vane, and Beringer, *loc cit.*

[5] W. M. Breazeale and Y. Beers, "Use of a Temperature-Limited Diode in Measurements of Noise Figures of Crystals," RL Report 294, Feb. 27, 1943.

Waltz and Kuper[1] is much more versatile. This source, which employs a shot-noise-excited, tuned cavity is commonly called the noise klystron.

Present noise klystrons are adapted from velocity-modulation oscillators. The electrons are accelerated from the cathode; some of them pass through the cavity gap, and are collected by the reflector, using the circuit of Fig. 4·43.

The electron beam induces shot-noise currents in the cavity which can be extracted in the usual way with loops, probes, or irises. All frequencies in the pass band of the cavity will be present, a spectrum several megacycles per second wide.

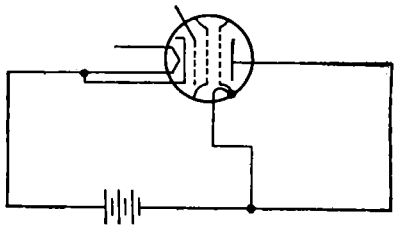

FIG. 4·43.—Circuit of a noise klystron.

The mode of noise production in the noise klystron is in some ways similar to that in a conventional diode. Fluctuations in the beam current, arising from the discreteness of the electronic charge, induce currents in the cavity as in the anode circuit of a diode. The roles of space charge and of transit time are somewhat different, however. Since no virtual cathode ever exists between the cavity grids, and since the radio-frequency circuit appears between these grids, there can be no compensation of fluctuation currents in the electron beam such as accounts for the space-charge reduction of diode shot-noise. The electron beam through that gap is therefore temperature-limited. Only if the grids are very poor will this be modified, and even in this case there will be little reduction because of the very large drift angles between cathode and cavity.

The transit-time effects observed in a conventional diode arise from the finite time required of an electron to traverse the cathode-anode space in the accelerating field. The transit-time reduction of noise is dependent on the form of this accelerating field and differs for different field configurations. In the noise klystron there is no accelerating field in the gap. It is necessary, therefore, to treat the noise production by a beam of electrons of essentially uniform velocity distributed at random in time.

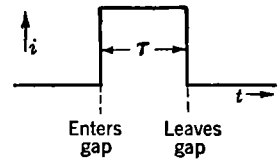

FIG. 4·44.—Current pulse in a noise klystron with perfect grids.

If the grids were perfect conductors of current, each electron would induce in the cavity a current pulse with straight sides and top as in Fig. 4·44 for which $\int_{-\infty}^{\infty} i(t)\,dt = e$ (electronic charge). In a frequency

[1] M. C. Waltz and J. B. H. Kuper, "Simplified Measurement of Receiver Sensitivities (S-Band Noise Sources)," RL Report 443, Sep. 17, 1943.

interval f to $f + df$ this gives a mean fluctuation current of

$$\overline{\Delta i^2} = 2eI\left(\frac{\sin\frac{\theta}{2}}{\frac{\theta}{2}}\right)^2 df, \tag{15}$$

where $\theta = 2\pi f\tau$ is the transit angle. This noise current is identified as a current generator appearing in shunt with the gap conductance, Fig. 4·45, which is made up of ohmic cavity losses and any loading caused by the beam. The available power from the device is $\overline{\Delta i^2}/4g$. Obviously $\overline{\Delta i^2}$ is reduced from its low-frequency value for any finite transit angle. This equivalent circuit has been checked by Waltz by measuring the output noise and the cavity bandwidth and calculating g from the bandwidth and gap capacitance.

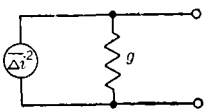

FIG. 4·45.—Equivalent circuit of noise klystron.

For a real tube with imperfect grids, the situation is quite similar except that the beam coupling coefficient is a more complicated function of the transit time since the electron current pulse has rounded corners that are caused by the field which leaks into the cavity before the electron enters and after it leaves the gap, as shown in Fig. 4·46. This will distort and remove the zeros in the beam-coupling coefficient. An exact calculation of this effect has not been made, largely because the device is not used as an absolute source, since the conductance g is not known with any certainty. Transit-time considerations are used only to select a region in which $\overline{\Delta i^2}$ is not a rapid function of the transit angle. For this purpose, the transit angle is calculated from

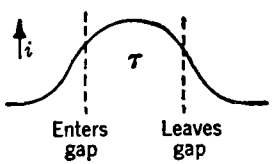

FIG. 4·46.—Current pulse in a noise klystron with imperfect grids.

$$\theta = \frac{2\pi fd}{5.96(10)^7\sqrt{V}}, \tag{16}$$

where d is the gap space in centimeters and V the electron energy in electron-volts.

Since the noise klystron is used as a relative source, the transit-time reduction in shot noise is not objectionable. The transit angle changes, however, with frequency and with changing gap space if the cavity is tuned in that manner, requiring that the device be calibrated anew at each frequency in the tuning range of the tube. It is therefore desirable to reduce θ as much as possible, usually by increasing the accelerating voltage as much as tube construction permits. The effects of transit time are illustrated in Fig. 4·47, which is taken from Waltz and Kuper, and in which the equivalent noise temperature is plotted vs. λ for different accelerating voltages at constant current.

Throughout a considerable range of cathode currents the equivalent noise temperature or output noise power is found to vary directly with cathode current as given in Eq. (15). For larger currents the noise saturates, the saturation current increasing with increasing acceleration voltage. This effect is not completely understood, but focusing difficulties play some part since the measured cathode current is not the true beam current and the cathode current will increase more rapidly

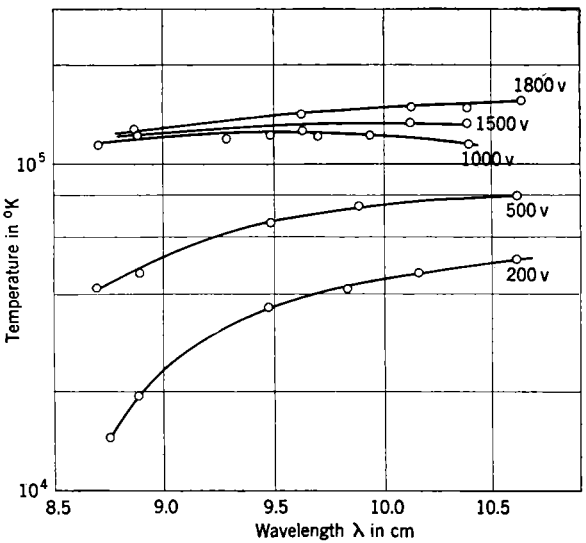

FIG. 4·47.—Noise temperature of a Sperry 417-A Klystron in the 10-cm region as a function of accelerator voltage and wavelength at a constant cathode current of 0.86 ma. This source had a measured bandwidth (to 3 db points) of 1.8 Mc/sec. Noise temperatures are referred to the cavity coupling loop, that is, corrected for cable loss.

than the beam current under defocusing conditions. Beam loading does not seem to be a contributing factor as measurements show no increase in cavity bandwidth with increasing cathode current. Figure 4·48 taken from Waltz and Kuper illustrates this effect.

A practical noise source for the 10-cm region can be easily constructed following Waltz and Kuper. A Sperry 417-A Klystron is connected as shown in Fig. 4·49 or Fig. 4·50. The coupling loop feeds a 50-ohm coaxial cable of some 5-db loss so that the device will appear as a matched source at signal frequency. The output noise is varied by changing the cathode temperature as in Fig. 4·49, or alternatively by adjusting the control-grid bias as in Fig. 4·50. These two methods give the same output noise for equivalent cathode currents. The curves of Fig. 4·47 and Fig. 4·48 were taken with such a tube. It is noticed that no accelerator-voltage regula-

tion is incorporated in the power supplies; it is unnecessary since the noise temperature is almost saturated with respect to accelerator voltage at 1500 volts. The device has a relatively broad band (2.5 Mc/sec to 3-db points), and displays the cavity resonance curve. Once it has been calibrated, it can be used over long periods of time under even extreme handling conditions, and it is certainly as stable as the best continuous-wave signal generator used under laboratory conditions.

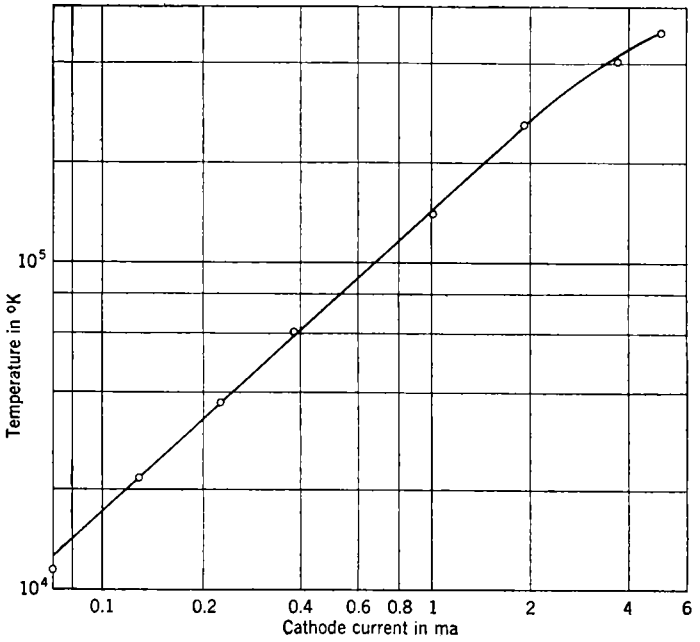

FIG. 4·48.—Noise temperature of a Sperry 417-A Klystron at 8.86 cm as a function of cathode current. Acceleration voltage is 1800 volts. Noise temperatures are referred to the cavity coupling loop, that is, corrected for cable loss.

A number of these 417-A Klystron noise sources have been constructed for receiver calibrations in the field. Recently, it was found that some tubes were unstable and did not have noise temperatures that were linear in cathode current. These tubes are, in general, gassy and thus precautions should be taken to obtain hard tubes.

In the 3-cm region similar noise sources have been constructed using Sperry 419 and Western Electric 723*A*/*B* Klystron tubes. Both tubes require very high voltages because of the rather large transit angles. At 2200 volts of accelerating potential, the 419 was still in a region of rather large transit angle and the output noise was a critical function of voltage

and frequency. The 723 tube does not permit accelerating voltages much above 750 volts and displays the same effect.

These difficulties are in accord with known grid spacings using Eq. (15). A tube with smaller grid gap is desired at this frequency. Transit-

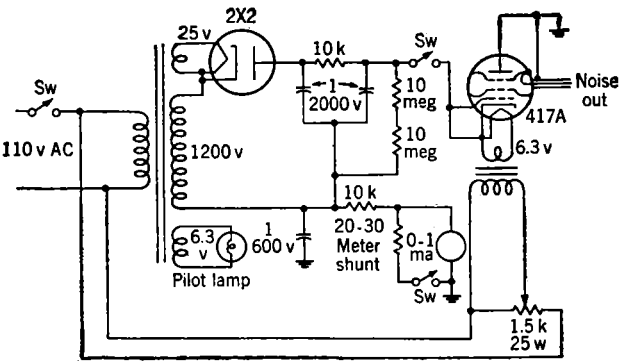

FIG. 4·49.—Cathode-temperature-controlled noise source and power supply.

angle considerations are quite stringent, especially for tubes in which the gap spacing increases with tuning to higher frequencies. Tubes essentially free of these effects could be built for the 10-, 3.2-, and 1.25-cm regions with gap spacings of 0.031, 0.010, 0.004 in. corresponding to $\theta = \pi/4$ at an accelerating potential of 1000 volts. At such a transit angle, doubling the gap space would reduce the output noise power by 15 per cent at most.

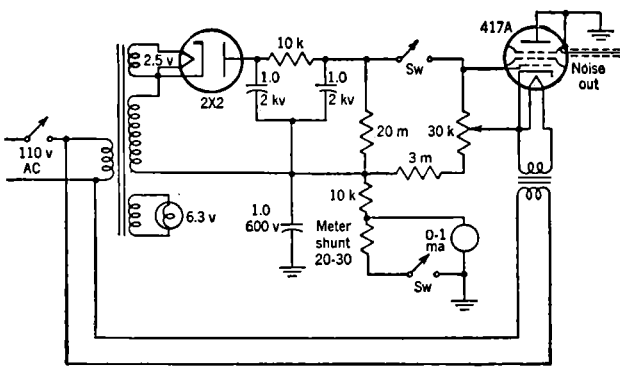

FIG. 4·50.—Grid-controlled noise source and power supply.

4·19. Crystal Noise Source.—It is generally known that the noise from a crystal mixer at ordinary radio frequencies is greater than that from a room-temperature resistor and that some part of this noise arises from the passage of electrons across the metal-semiconductor boundary

layer. Very high noise temperatures are observed, particularly for currents in the reverse or high-resistance direction. While this phenomenon may be troublesome in a crystal mixer, it offers a possible source of microwave noise, since the crystal also generates noise at microwave frequencies.

The behavior of electrons in a crystal boundary layer is in some ways similar to that in a diode. The electrons move through a region in which the electric potential is varying somewhat as in Fig. 4·51. The width of this boundary layer is rather small (10^{-6} cm).[1] Electrons will cross the barrier in both directions and for electrons moving from the semiconductor to the metal, the average distance which they must travel (10^{-8} cm) is small compared to their mean free path. Thus, as in a diode, the electrons move through a region in which the electric field is the dominant force.

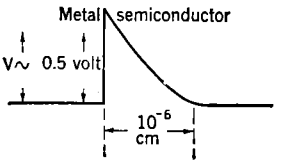

FIG. 4·51.—Metal semiconductor boundary layer with no applied potential.

When a potential is applied across the crystal, there will be a net current in the conventional direction. For reverse or back voltages applied, the current increases somewhat more rapidly than linearly with the voltage, largely because of the lowering of the barrier by the Schottky effect. The differential resistance slowly drops from say 10^4 ohms at 0 volts to 200 ohms at 5 volts in the back direction. Currents of several milliamperes are obtainable.

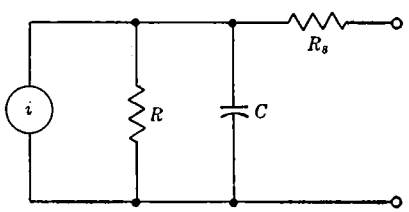

FIG. 4·52.—Equivalent circuit of crystal barrier.

These currents are composed of uncorrelated electrons since there are many electrons in the conductor band. These electrons induce shot-noise voltages across the barrier and electron transit-angles are negligible even at the highest microwave frequencies. The barrier should, therefore, behave as a temperature-limited diode with a noise temperature of

$$T = \frac{eIR}{2k} = 5800IR, \tag{17}$$

where I is the back-current and R the differential resistance of the barrier at that current.

Equation (17) is known to give the correct order of magnitude of

[1] H. A. Bethe, "Theory of High Frequency Rectifiers for Silicon Crystals," RL Report 184, October 29, 1942; "Theory of the Boundary Layer of Crystal Rectifiers," RL Report 185, November 23, 1942.

observed noise temperatures. It seems desirable, however, to modify this expression to take account of the spreading resistance R_s and the capacitance C associated with the barrier.. The equivalent circuit, instead of being simply a current generator in shunt with R, is more complicated (see Fig. 4·52). The noise temperature of this circuit is approximately

$$T = \frac{eIR}{2k(R_sR\omega^2C^2 + 1)} = \frac{5800IR}{(R_sR\omega^2C^2 + 1)}.$$

Figure 4·53 shows the variation of T with I for several 1N26 crystals; the measurements were made by R. H. Dicke at 1.25 cm.

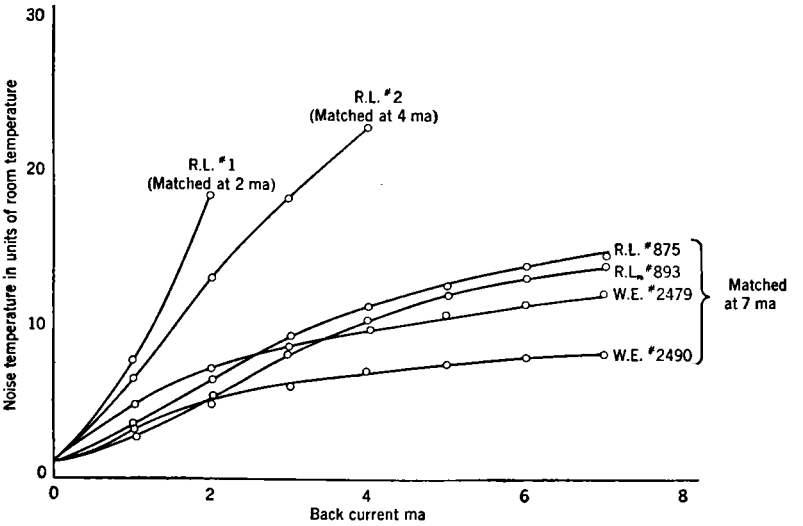

FIG. 4·53.—Noise temperatures of some 1N26 crystals at a wavelength of 1.25 cm.

In the calibration and use of noise crystals, several precautions must be observed. In the first place, a moderate back current, for example, 3 to 4 ma should be used. Higher currents cause instability in both the back resistance and the noise power. Furthermore, no sources of microwave power should be incident on the crystal. In particular, local-oscillator power from the receiver being tested will beat with the noise produced, giving very complicated effects. The circuit usually used is shown in Fig. 4·54. With the mixer M matched at the local-oscillator frequency, no local-oscillator power is incident on the noise crystal.

The noise temperature is usually calibrated with a receiver matched at signal frequency. The matching transformer is adjusted to match the noise crystal with the desired back current flowing. The line is

then broken at A and the noise-crystal circuit replaced by a matched load for the receiver noise-level measurement. This is better technique than turning off the noise current since the r-f noise-source impedance changes markedly with noise current. When measurements are made with an unmatched signal source, the noise source is replaced by a passive load having the noise-source impedance.

The bandwidth of a crystal noise source is largely determined by the crystal holder and passive circuit elements in the crystal cartridge. It will usually be very broad (2 per cent to 10 per cent). The noise at image frequency will, therefore, be essentially as large as at signal frequency and corrections must be made for it.

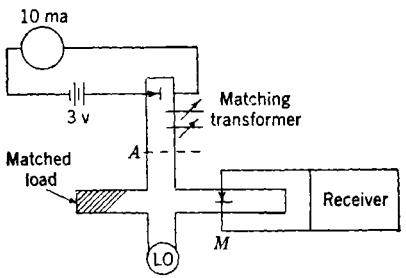

FIG. 4·54.—Circuit for measuring noise temperatures of crystals.

As the mixer is also usually broadband compared with signal-image separation, the correction is quite simple and Eq. (9) Sec. 4·1 can be used.

Noise crystals have been used somewhat in the 3-cm region, but chiefly in the 1-cm band. The results of Dicke and Pound give noise temperatures of 3000° to 6000°K for back currents of 3 to 5 ma at 1.25 cm with 1N26 crystals. Life tests were not entirely conclusive but indicate that the noise temperatures decrease and resistances increase during extended operation. At 3.2 cm, noise temperatures are generally higher, being 5000° to 9000°K for back currents of 3 to 4 ma with 1N23 crystals.

Before concluding, it should be mentioned that there is evidence of other than shot-noise contributions to crystal noise temperatures. For example, "burning" crystals with electrostatic discharges usually increases the noise. Also the observed noise temperatures are frequently in excess of those given by Eq. (17). Nothing quantitative is known of these contributions.

PART II

WAVELENGTH AND FREQUENCY MEASUREMENTS

CHAPTER 5

THE MEASUREMENT OF WAVELENGTH

By Robert Beringer

At ordinary radio frequencies, wavelengths or frequencies are often measured with a wavemeter that consists of a resonant circuit composed of inductances and capacitances. This is coupled to the source and to a device which indicates resonance in the circuit. With proper design, the system is resonant at a single frequency[1] for each set of inductance and capacitance values and it is possible to calculate the resonant frequency from a knowledge of these values. If the wavemeter is to be tunable, some means must be provided for varying the inductances and capacitances in a known manner. In addition a calibration point is sometimes provided by a comparison with a frequency standard.

At microwave frequencies such circuit elements lose their utility for a number of well-known reasons and it is common to build resonant circuits in the form of cavities. Under certain conditions it is possible to calculate the relevant circuit parameters of cavities from the dimensions, a practice which corresponds to the low-frequency calculation of inductance and capacitance from the dimensions of coils and condensers. In this sense a cavity is a standard circuit element, particularly convenient at microwave frequencies where frequency standards are rather difficult to build and operate.

Strictly speaking, a cavity is a dielectric region *completely* surrounded by conducting walls. The electromagnetic fields in such a region can assume a variety of spatial configurations. At certain frequencies and for certain configurations, the system is resonant; that is, electromagnetic energy is stored over time intervals long compared with the wave period. These resonant solutions are called the *normal modes* of the cavity. For a cavity of given dimensions the corresponding resonant frequencies and spatial configurations are completely specified. Conversely, for a given mode and resonant frequency, the dimensions are uniquely determined, making it possible to determine distances with the use of a frequency standard.

If the normal modes of a given cavity are examined, it will be found

[1] There will, in general, be other resonances at much higher frequencies. These are not given by the simple analysis in which coils and condensers are approximated by L and C.

that there is an infinite set of resonant frequencies having a lower bound but no upper bound. The least resonant frequency has a free-space wavelength of the order of the linear dimensions of the cavity for cavities of simple shape, so that resonant cavities are of a convenient size at microwave frequencies. Further, if the cavity size is altered in order to change the least resonant frequency by a few per cent, the mechanical displacement will be a few per cent of the linear dimensions and, for microwave frequencies, it will be easily measurable.

Of course, a complete cavity is of little use since means must be provided for coupling the cavity to the source and this involves a removal of a section of the cavity walls and the introduction of a coupling device (a probe, loop, or iris). These in turn are usually connected to transmission lines; one for each coupling. A system composed of such a cavity together with short sections of the coupled transmission lines is called a *cavity-coupling system.* A description of the use of such systems for wavelength indication is the purpose of this chapter.

Perhaps the most convenient way in which to analyze a cavity-coupling system is by the method of equivalent circuits. One finds the self-impedance and transfer impedance at certain terminals in the exit transmission lines and represents them by a low-frequency circuit composed of inductances, capacitances, resistances, transformers, and so forth. This analysis has been developed in Vol. 8, Chap. 7 and we shall not repeat it here; rather we shall merely review the results which are pertinent to the study of cavity wavemeters.

CAVITIES AS CIRCUIT ELEMENTS

5·1. The Equivalent Circuit of a Single-line Cavity-coupling System. The simplest cavity-coupling system is a cavity provided with a single

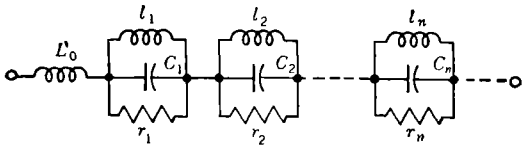

FIG. 5·1.—Impedance representation of a single-line cavity-coupling system at any terminal plane in the exit transmission line.

emergent transmission line coupled through a hole in the cavity wall by means of a probe, loop, or iris. This system constitutes a single-terminal-pair circuit. It has been shown (Vol. 8, Chap. 7) that, if the loss is not too high, all such systems can be represented by the circuits of Figs. 5·1 and 5·2 at an arbitrarily chosen terminal plane in the exit transmission line. The values of the circuit elements will, in general, depend on the choice of terminals, and in certain cases one or two of the

resonant elements may degenerate to a nonresonant element (by short-circuiting one of the L's or C's).

This general form of the equivalent circuit of a cavity-coupling system is of great utility since it embraces all systems, but it is a generality of form only. For any particular system the L's, R's, and C's must be found by the solution of a field problem or by experiment.

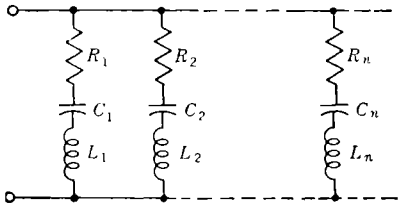

FIG. 5·2.—Admittance representation of a single-line cavity-coupling system at any terminal plane in the exit transmission line.

Impedance Functions near Resonance.—For most applications of cavities the behavior of the system near to a single resonant frequency is sufficient to give the desired results, in particular if this resonant frequency is well separated from its neighbors. In such cases the equivalent circuits of Figs. 5·1 and 5·2 are greatly simplified since all but one of the resonant elements can be replaced by nonresonant elements and these can be lumped into a single element. Thus the most general representations of a single-line

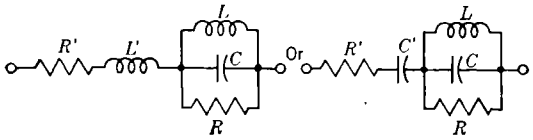

FIG. 5·3.—Impedance representation of a single-line cavity-coupling system near resonance.

cavity-coupling system are those of Figs. 5·3 and 5·4. These circuits can be further simplified by omission of the elements R' and r' since they are always small in a well-designed system, corresponding to the off-resonant losses in the transmission line and coupling. Furthermore, it can be

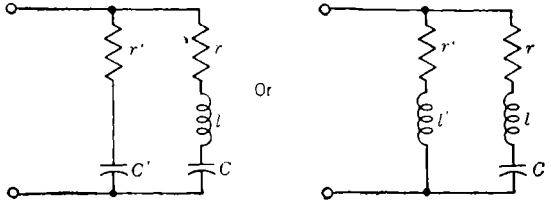

FIG. 5·4.—Admittance representation of a single-line cavity-coupling system near resonance.

shown that by proper selection of the terminal plane the equivalent circuit can be reduced to a simple series *RLC*-circuit or a simple parallel *RLC*-circuit.

This is seen by referring to a Smith impedance diagram. Consider a simple series *RLC*-circuit terminating a transmission line of charac-

teristic impedance Z_0. On a Smith impedance diagram, the input impedance of the circuit describes a locus like the circle (*a*) in Fig. 5·5, as a function of frequency. At the real axis, $\omega = \omega_0 = 1/\sqrt{LC}$, the resonant frequency of the circuit. If the circuit is shunted by a capacitor, the locus is a circle such as (*b*) in Fig. 5·5.[1] The new resonant frequency ω_0' is different from ω_0. The radius of the new circle is also different. If the simple *RLC*-circuit is shunted by an inductance, the circle will be shifted in a counterclockwise direction.

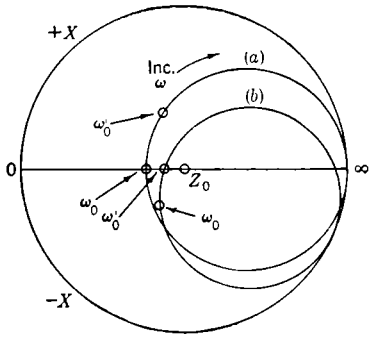

FIG. 5·5.—Loci of cavity-coupling-system input impedance on a Smith impedance diagram.

The circuits of Fig. 5·4 have been shown to be the most general representations of a cavity-coupling system near resonance. Hence loci such as (*b*) are the most general impedance contours for a cavity-coupling system near a particular resonance.

Since a change of reference terminals in the transmission line corresponds, to a first approximation, to simply rotating locus (*b*) around Z_0, it is evident that by a suitable choice of reference terminals any cavity-coupling system can be brought into the form of locus (*a*). Hence, any cavity-coupling system near resonance behaves as a simple series *RLC*-circuit at suitable terminals in the transmission line.

A discussion of the representations of Fig. 5·3 in terms of the Smith admittance diagram proceeds in an exactly parallel fashion.

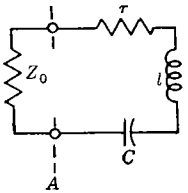

FIG. 5·6.—Equivalent circuit of cavity-coupling system terminated in Z_0 at a particular terminal plane.

Q-factors, Coupling Parameters, and External Loading.—It is common in the study of low-frequency resonant circuits and of cavity-coupling systems to specify the losses in the circuit by means of the *Q*-factor which is defined as

$$Q = 2\pi \frac{\text{energy stored}}{\text{energy dissipated per cycle}}. \qquad (1)$$

There are a number of *Q*-factors in common use which, for a cavity-coupling system, differ only in the sources of dissipation which are included in the denominator of Eq. (1). These are illustrated by a

[1] This is obtained by transforming (*a*) to the admittance plane, which consists of reflection of (*a*) through the point Z_0. The capacitive susceptance is then added, which rotates the admittance circle. This circle is then reflected back through Z_0 to obtain (*b*).

consideration of the circuit of Fig. 5·6, which is the equivalent circuit of a cavity-coupling system at certain terminals in a matched transmission line. The Q of the system to the right of line A is the so-called unloaded Q. It is

$$Q_u = 2\pi f_0 \frac{\frac{1}{2}lI^2}{\frac{1}{2}I^2 r} = \frac{\omega_0 l}{r}, \tag{2}$$

where $I \cos \omega_0 t$ is the driving current and $\omega_0^2 = 1/lC$. The Q of the entire circuit, including Z_0, is called the *loaded* Q. It is

$$Q_L = \frac{\omega_0 l}{r + Z_0} \tag{3}$$

$$= \frac{Q_u}{1 + \frac{Z_0}{r}}. \tag{4}$$

The *coupling parameter* is defined as $\beta = Z_0/r$ or as the normalized admittance, $Z_0/r = (1/r)/Y_0$, at resonance. Using this quantity Eq. (4) becomes

$$Q_u = (1 + \beta)Q_L. \tag{5}$$

The external or *radiation* Q of the circuit is defined as

$$Q_R = \frac{Q_u}{\beta}, \tag{6}$$

so that

$$\frac{1}{Q_L} = \frac{1}{Q_u} + \frac{1}{Q_R}. \tag{7}$$

It is clear that for the loaded Q all sources of dissipation are included in the denominator of Eq. (1). For the unloaded Q only sources interior to the cavity-coupling system are considered, while for the radiation Q the external losses alone are considered. The coupling parameter is, so to speak, the efficacy with which energy stored in the cavity-coupling system is coupled to the external load and dissipated there.

Our discussion considers only a single, simple model. It is not difficult, however, to formulate these Q's for an arbitrary resonant circuit. (See Vol. 8, Chap. 7.)

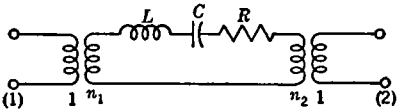

FIG. 5·7.—Equivalent circuit of a two-line cavity-coupling system at particular reference planes and near a particular resonance.

5·2. Transmission Through a Two-line Cavity-coupling System. The general impedance and admittance representations of cavity-coupling systems with more than one emergent transmission line can be derived with somewhat more difficulty. Near resonance these representations are rather simple for the case of small loss and negligible direct mutual

impedance between the two coupling lines. One form is shown in Fig. 5·7 for a particular choice of terminal planes in the emanating transmission lines. The transformers shown are ideal transformers, one of which can be eliminated by a transformation of impedance level.

Consider a transmission system including a two-line cavity-coupling system with its reference planes chosen as in Fig. 5·7. Let the generator and load impedances at these planes be real and given by R_G and R_L. This circuit is shown in Fig. 5·8. Transforming the load and generator

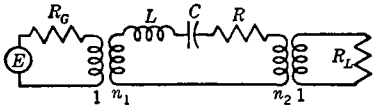

FIG. 5·8.—Equivalent circuit of a two-line cavity-coupling system at particular reference planes. Generator and load impedances R_G and R_L are real at these planes.

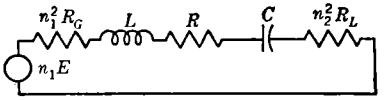

FIG. 5·9.—Alternative form for the circuit of Fig. 5·8.

into the resonant mesh, we have the circuit of Fig. 5·9. The unloaded Q is $Q_u = \omega_0 L/R$, corresponding to putting $R_G = R_L = 0$. The loaded Q is

$$Q_L = \frac{\omega_0 L}{R + n_1^2 R_G + n_2^2 R_L},$$

from which

$$Q_u = Q_L\left(1 + n_1^2 \frac{R_G}{R} + n_2^2 \frac{R_L}{R}\right).$$

The input and output coupling parameters are commonly defined in terms of a matched generator and load (i.e. $R_G = R_L = Z_0$). They are

$$\beta_1 = \frac{n_1^2 Z_0}{R},$$

$$\beta_2 = \frac{n_2^2 Z_0}{R}.$$

It is also customary to define the transmission through the cavity in terms of a matched generator and load. For this case the impedance of the mesh of Fig. 5·9 is

$$Z = R\left[(1 + \beta_1 + \beta_2) + jQ_u\left(\frac{\omega}{\omega_0} - \frac{\omega_0}{\omega}\right)\right],$$

and the power into the load impedance is

$$P_L = n_2^2 Z_0 |I|^2 = \beta_2 R |I|^2$$

$$= \frac{\dfrac{\beta_1 \beta_2 E^2}{Z_0}}{(1 + \beta_1 + \beta_2)^2 + Q_u^2\left(\dfrac{\omega}{\omega_0} - \dfrac{\omega_0}{\omega}\right)^2}.$$

The available power from the generator line is $\frac{1}{4}E^2/Z_0 = P_0$.

The transmission-loss function $T(\omega)$ is defined as P_L/P_0 or

$$T(\omega) = \frac{4\beta_1\beta_2}{(1 + \beta_1 + \beta_2)^2 + Q_u^2\left(\frac{\omega}{\omega_0} - \frac{\omega_0}{\omega}\right)^2}. \tag{8}$$

At resonance, the transmission loss is

$$T(\omega_0) = \frac{4\beta_1\beta_2}{(1 + \beta_1 + \beta_2)^2}. \tag{9}$$

Dividing Eq. (8) by Eq. (9), we have

$$T(\omega) = \frac{T(\omega_0)}{1 + Q_L^2\left(\frac{\omega}{\omega_0} - \frac{\omega_0}{\omega}\right)^2}.$$

Putting $\omega = \omega_0 + \Delta\omega/2$,

$$T(\omega) = \frac{T(\omega_0)}{1 + Q_L^2\left(\frac{\Delta\omega}{\omega_0}\right)^2}. \tag{10}$$

We see that $T(\omega) = \frac{1}{2}T(\omega_0)$ (i.e., half-power points of transmission) for $\Delta\omega/\omega_0 = 1/Q_L$. The frequency interval $\Delta\omega$ is frequently called the bandwidth of the cavity at the resonant frequency ω_0.

5·3. Frequency-pulling by Reactive Loads.—It is easily shown (Vol. 8, Chap. 7) that the resonant frequencies of a cavity-coupling system are functions of the reference-plane position in the emergent transmission line. Any change in line length changes the electric and magnetic energies stored interior to the reference plane and thus the resonant frequencies.

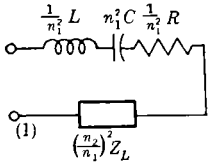

FIG. 5·10.—Circuit of Fig. 5·7 at terminals (1) when Z_L is placed across terminals (2).

If we have a cavity-coupling system with two or more emergent transmission lines, the resonant frequency looking into one of the lines depends on the load impedances on the other lines, and the frequency at which the cavity transmits a maximum of power depends on the load and generator impedances.

Consider a two-line cavity-coupling system. Near a particular resonance and at certain reference planes it can be represented by Fig. 5·7. For a particular choice of load impedance Z_L on terminals (2), Fig. 5·7 can be transformed to the circuit of Fig. 5·10 at terminals (1). The resonant frequency of this system is the frequency for which

$$\omega L - \frac{1}{\omega C} + n_2^2 X_L = 0 \tag{11}$$

is satisfied. In the case that $n_2^2 X_L \ll \omega L, 1/\omega C$, Eq. (11) may be solved

for the perturbed resonant frequency

$$\omega_R = \omega_0 - \frac{n_2^2 X_L}{2L}, \tag{12}$$

where $\omega_0^2 = 1/LC$. In terms of the coupling parameter $\beta_2 = n_2^2 Z_0/R$ and $Q_u = \omega_0 L/R$, we can write Eq. (12) as

$$\omega_R = \omega_0 \left(1 - \frac{\beta_2 X_L}{2Z_0 Q_u}\right). \tag{13}$$

The second term in the parentheses represents the frequency-pulling. This pulling is usually small but becomes important when cavities are used as accurate frequency meters. For example, if $\beta_2 = \frac{1}{2}$, $Q_u = 10^4$, and $X_L/Z_0 = 1$, then $(\omega_0 - \omega_R)/\omega_0 = 2.5 \times 10^{-5}$.

The pulling of a transmission cavity is evaluated in a similar way. At particular reference planes and near a particular resonance, a two-line cavity-coupling system with arbitrary loads is represented as in Fig. 5·8 with R_G and R_L replaced by Z_G and Z_L. Transforming Z_G and Z_L into the resonant mesh as in Fig. 5·9, we see that maximum power is absorbed by the load resistance R_L at a frequency which is the solution of

$$\omega L - \frac{1}{\omega C} + n_1^2 X_G + n_2^2 X_L = 0. \tag{14}$$

For $n_1^2 X_G$, $n_2^2 X_L \ll \omega L$, $1/\omega C$, the solution of Eq. (14) is given by

$$\omega_T = \omega_0 \left(1 - \frac{n_1^2 X_G}{2L\omega_0} - \frac{n_2^2 X_L}{2L\omega_0}\right). \tag{15}$$

In terms of $\beta_1 = n_1^2 Z_0/R$, $\beta_2 = n_2^2 Z_0/R$ and $Q_u = \omega_0 L/R$, Eq. (15) becomes

$$\omega_T = \omega_0 \left(1 - \frac{\beta_1 X_G}{2Z_0 Q_u} - \frac{\beta_2 X_L}{2Z_0 Q_u}\right). \tag{16}$$

The admittance case is treated in an analogous manner. If at some terminals the cavity-coupling system is representable as a shunt-resonant circuit, and if a load susceptance B appears at these terminals, then the resonant frequency of the system is

$$\omega_R = \omega_0 \left(1 - \frac{\beta B}{2Y_0 Q_u}\right). \tag{17}$$

The formulas (13) and (16) are carried over into the admittance case by replacing each X/Z_0 by its corresponding B/Y_0; signs remain unchanged.

Frequently in microwave circuits the series reactance is not known at the reference terminal for which Figs. 5·8 and 5·7 are valid. What is usually known is the standing-wave ratio of the generator and load impedances. Depending on the phase of these standing waves at the

reference terminals of Fig. 5·7, the pulling can vary from (*a*) none at all, corresponding to a maximum or minimum in the standing-wave pattern at the reference terminals, to (*b*) a maximum pulling, corresponding to $X/Z_0 = \pm(r^2 - 1)/2r$, where r is the VSWR corresponding to the reactance X. Therefore the extreme values of the resonant frequency corresponding to Eq. (13) are

$$\omega_R = \omega_0 \pm \omega_0 \frac{\beta_2(r_2^2 - 1)}{4Q_u r_2}. \tag{18}$$

The extreme values of the frequency for maximum transmission corresponding to Eq. (16) are

$$\omega_T = \omega_0 \pm \omega_0 \frac{1}{4Q_u}\left[\frac{\beta_1(r_1^2 - 1)}{r_1} + \frac{\beta_2(r_2^2 - 1)}{r_2}\right]. \tag{19}$$

NORMAL MODE FIELDS IN SOME CAVITIES OF SIMPLE SHAPE

The discussions thus far have been confined to the circuit aspects of cavity resonators. This study gave a number of results of considerable generality, in particular, the form of the equivalent circuit of a cavity at terminals in the emergent transmission lines. It was found that at certain terminals the cavity could be represented by an ensemble of simple series- or shunt-resonant circuits having certain Q's and resonant frequencies. The form of the resonant behavior of cavity-coupling systems is thus obtained, and with some restrictions it is the same for all systems. Various physical systems differ only in having a different set of resonant frequencies and associated Q-factors. These parameters are now to be discussed.

The determination of the resonant frequencies and associated Q's[1] of a cavity-coupling system is, of course, a field problem. In general, it is a very difficult problem, particularly if the cavity has a complex shape and if the coupling system is treated rigorously. Because of this difficulty, it is not usually solved. Instead, a much simpler system is considered, a system in which all transmission lines and coupling devices are removed and all walls are unbroken. With this simplification, it becomes possible to find the field solutions of cavities of regular shape such as rectangular parallelopipeds, right circular cylinders, spheres, and so forth.

These field solutions are very useful in the design of cavity systems. The resonant frequencies thus found are usually very nearly those of the complete system, since cavities are usually not coupled so tightly that an appreciable amount of the total stored energy resides in the external

[1] Throughout this section, which concerns isolated cavities, Q will always refer to the unloaded Q.

circuits. Likewise, the unloaded Q's calculated from the field equations do not differ greatly from those observed for the cavity-coupling system, since the coupling devices seldom distort the cavity fields appreciably.

These problems will not be solved in detail here. Many appear in the literature.[1] We shall merely tabulate the results after outlining briefly the methods used.

The first step is to find the normal-mode fields in a completely lossless cavity of the given shape. This involves solving Maxwell's equations subject to the boundary conditions that **E** be normal to all boundary surfaces and that **H** be tangential. The solutions can be written in several forms, but essentially they are a set of characteristic resonant frequencies and vector functions, **E** and **H**, describing the spatial configurations of the normal-mode fields.

Next, it is assumed that the introduction of loss by means of a finite wall conductivity does not change these normal-mode fields. The Q of the cavity, written as

$$Q = \frac{2}{\delta} \frac{\int_v H^2 \, dV}{\int_s H^2 \, dS},$$

is then computed using the normal-mode fields H and the known skin depth δ in the wall material. These are frequently expressed in terms of the dimensions of the cavity for each of the normal-mode fields. The quantity $Q\delta/\lambda$ is a function only of the relative dimensions or shape of the cavity and the form of the resonant mode.

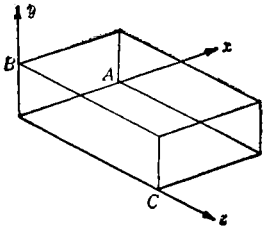

FIG. 5·11.—Rectangular-parallelopiped cavity.

5·4. Rectangular Parallelopiped.—The normal-mode fields are most easily found for the rectangular parallelopiped[2] and can be expressed in terms of sines and cosines. These fields are conveniently divided into two sets, transverse-electric and transverse-magnetic modes. They are transverse-with respect to the axis of reference which is taken to be along the longest dimension of the figure. In Fig. 5·11 this is the z-axis. The transverse-electric TE-modes have no **E** components along z, and transverse-magnetic TM-modes have no **H** components along z.

The next specification is in terms of the integers, l, m, n. These are

[1] For general review of field solutions see E. U. Condon, *Rev. Mod. Phys.*, **14**, 341 (1942) or W. W. Hansen, *J. Appl. Phys.*, **9**, 654 (1938).

[2] F. Bourguis, *Ann. Phys., Lpz.*, **35**, 359 (1939) and the review articles of Condon, *loc. cit.* and J. P. Kinzer, "Review of Information on Resonant Cavities," BTL, case 23458-5, Jan. 8, 1943. The treatment given here follows that of Kinzer.

defined as

l = number of half-period variations of **E** and **H** along x,
m = number of half-period variations of **E** and **H** along y,
n = number of half-period variations of **E** and **H** along z.

For a given set, the field is completely specified and the modes are designated as $TE_{l,m,n}$ or $TM_{l,m,n}$. The resonant frequencies are given by the equation,

$$\lambda = \frac{2}{\sqrt{\left(\frac{l}{A}\right)^2 + \left(\frac{m}{B}\right)^2 + \left(\frac{n}{C}\right)^2}} \quad \text{cm}, \tag{20}$$

where A, B, and C are in centimeters.

The normal-mode fields are given by the equations:

TE-modes

$$\left.\begin{aligned} E_x &= -\frac{k_2}{k}\cos k_1x \sin k_2y \sin k_3z \\ E_y &= \frac{k_1}{k}\sin k_1x \cos k_2y \sin k_3z \\ E_z &= 0 \\ H_x &= \frac{k_1k_3}{k^2}\sin k_1x \cos k_2y \cos k_3z \\ H_y &= \frac{k_2k_3}{k^2}\cos k_1x \sin k_2y \cos k_3z \\ H_z &= -\frac{k_1^2 + k_2^2}{k^2}\cos k_1x \cos k_2y \sin k_3z, \end{aligned}\right\} \quad \begin{aligned} &n > 0 \\ &l \text{ or } m > 0 \end{aligned} \tag{21}$$

TM-modes

$$\left.\begin{aligned} E_x &= \frac{k_1k_3}{k^2}\cos k_1x \sin k_2y \sin k_3z \\ E_y &= \frac{k_2k_3}{k^2}\sin k_1x \cos k_2y \sin k_3z \\ E_z &= -\frac{k_1^2 + k_2^2}{k^2}\sin k_1x \sin k_2y \cos k_3z \\ H_x &= -\frac{k_2}{k}\sin k_1x \cos k_2y \cos k_3z \\ H_y &= \frac{k_1}{k}\cos k_1x \sin k_2y \cos k_3z \\ H_z &= 0 \end{aligned}\right\} \quad \begin{aligned} &l > 0 \\ &m > 0 \end{aligned} \tag{22}$$

where $k_1 = l\pi/A$, $k_2 = m\pi/B$, $k_3 = n\pi/C$, $\lambda = 2\pi/k$, and

$$k^2 = k_1^2 + k_2^2 + k_3^2.$$

The restrictions, n, l or $m > 0$, for the TE-modes and, l, $m > 0$, for the

TM-modes, are introduced to avoid trivial cases in which all **E** or **H** field components vanish.

The quantity, $Q\delta/\lambda$, is commonly tabulated instead of Q, since this quantity is a function of only the mode and shape of the cavity. δ is the skin depth in centimeters in the cavity walls.

For the *TE*-modes,

$$Q\frac{\delta}{\lambda} = \frac{ABC}{4} \times \frac{(p^2+q^2)(p^2+q^2+r^2)^{3/2}}{AC[p^2r^2+(p^2+q^2)^2]+BC[q^2r^2+(p^2+q^2)^2]+ABr^2(p^2+q^2)}, \quad (23)$$

for (l and m) > 0;

$$Q\frac{\delta}{\lambda} = \frac{ABC}{2}\cdot\frac{(q^2+r^2)^{3/2}}{q^2C(B+2A)+r^2B(C+2A)}, \qquad \text{for } l=0; \quad (24)$$

and

$$Q\frac{\delta}{\lambda} = \frac{ABC}{2}\cdot\frac{(p^2+r^2)^{3/2}}{p^2C(A+2B)+r^2A(C+2B)}, \qquad \text{for } m=0, \quad (25)$$

where $p = l/A$, $q = m/B$, $r = n/C$.

For the *TM*-modes,

$$Q\frac{\delta}{\lambda} = \frac{ABC}{4}\cdot\frac{(p^2+q^2)(p^2+q^2+r^2)^{1/2}}{p^2B(A+C)+q^2A(B+C)}, \qquad \text{for } n>0; \quad (26)$$

and

$$Q\frac{\delta}{\lambda} = \frac{ABC}{2}\cdot\frac{(p^2+q^2)^{3/2}}{p^2B(A+2C)+q^2A(B+2C)}, \qquad \text{for } n=0. \quad (27)$$

The skin depth δ is given by the equation,

$$\delta = \sqrt{\frac{\lambda\rho}{120\pi^2\mu}} \quad \text{cm}, \quad (28)$$

where μ is the permeability of the wall material (or relative permeability in mks units), λ is the free-space wavelength in cm, and ρ is the resistivity of the walls in ohm cm. Table 5·1 gives the resistivities of some materials

TABLE 5·1.—D-C RESISTIVITY OF SOME COMMON METALS AND ALLOYS

Materials	ρ(at 20°C), ohm cm
Copper, commercial annealed	1.72×10^{-6}
Copper, pure annealed	1.69
Aluminum, commercial	2.83
Brass, various alloys	6 to 8
Silver, pure	1.63
Coin silver, annealed	1.87
Coin silver, hard drawn	2.1

commonly used in cavities. These depend on the purity and history of the material. All are at room temperature.

5·5. The Right Circular Cylinder.—The normal modes in the right circular cylinder[1] are also divided into *TE*- and *TM*-classes, where the axis of reference is along the cylinder axis (see Fig. 5·12). They are further specified in terms of three integers, l, m, and n, which are defined by

$l \equiv$ number of full-period variations of E_r with respect to θ,
$m \equiv$ number of half-period variations of E_θ with respect to r,
$n \equiv$ number of half-period variations of E_r with respect to z,

for *TE*-modes. For *TM*-modes, the integers are correspondingly defined in terms of the components of **H**.

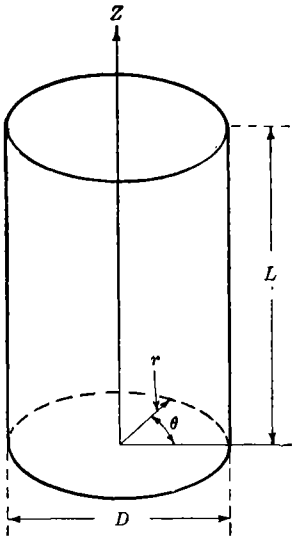

FIG. 5·12.—Right circular cylinder.

The normal-mode fields are expressed in terms of trigonometric and Bessel functions, and the resonant frequencies include the roots of Bessel functions. These latter are given by the equation,

$$\lambda = \frac{2}{\sqrt{\left(\frac{2x_{lm}}{\pi D}\right)^2 + \left(\frac{n}{L}\right)^2}}, \qquad (29)$$

for the free-space wavelength of the resonant frequencies. The quantities x_{lm} are:

$x_{lm} \equiv m^{\text{th}}$ root of $J_l'(x) = 0$ for the *TE*-modes;
$x_{lm} \equiv m^{\text{th}}$ root of $J_l(x) = 0$ for the *TM*-modes.

Values of a few of these roots are given in Table 5·2.[2] The equation for the resonant frequencies can also be written as

$$(fD)^2 = \left(\frac{cx_{lm}}{\pi}\right)^2 + \left(\frac{cn}{2}\right)^2 \left(\frac{D}{L}\right)^2, \qquad (30)$$

from which it is seen that $(fD)^2$ vs. $(D/L)^2$ is a straight line with intercept $(cx_{lm}/\pi)^2$ and slope $(cn/2)^2$. Plots of this type are called *mode charts*,

[1] F. Bourguis, *Ann. Phys., Lpz.*, **35**, 359 (1939); W. L. Barrow and W. W. Mieher, *Proc. Inst. Radio Engrs.*, **28**, 184 (1940); J. P. Kinzer, "Review of Information on Resonant Cavities," BTL, case 23458-5, Jan. 8, 1943. The treatment here follows Kinzer.

[2] Barrow and Mieher, *loc. cit.* These values for the most part agree with Kinzer *loc. cit.* and E. Jahnke and F. Emde "Funktionentafeln," Teubner, Leipzig, 1933.

and such a chart is shown in Fig. 5·13 for a few of the lower modes. Only the values 0, 1, 2 of n are shown.

Such mode charts are very useful in cavity design, for the observed resonant frequencies will usually lie close to those shown in the chart.

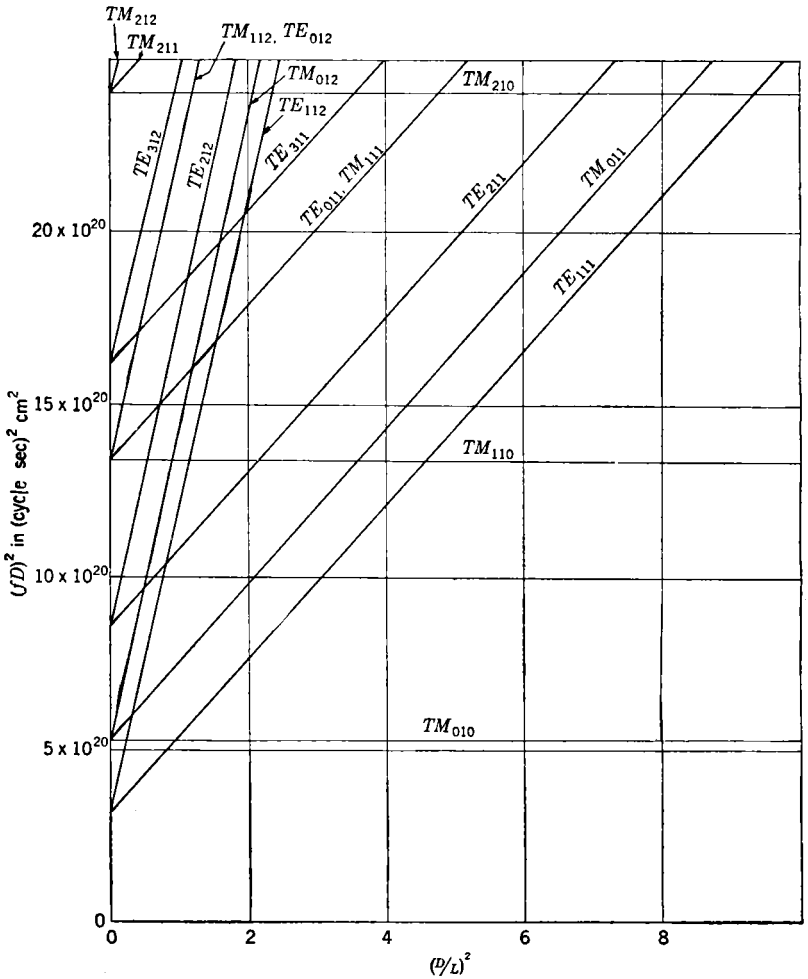

FIG. 5·13.—Mode chart for right circular cylinder.

For tunable cavities in which L is varied, one can see from the chart what modes are possible in the tuning range of the cavity, and steps can be taken to suppress any unwanted modes occurring in that range.

TABLE 5·2.—ROOTS OF $J_l(x)$ AND $J'_l(x)$

TE-mode	x_{lm}	TM-mode	x_{lm}
$11n$	1.841	$01n$	2.405
$21n$	3.054	$11n$	3.832
$01n$	3.832	$21n$	5.136
$31n$	4.201	$02n$	5.520
$41n$	5.318	$31n$	6.380
$12n$	5.332	$12n$	7.016
$51n$	6.415	$41n$	7.588
$22n$	6.706	$22n$	8.417
$02n$	7.016	$03n$	8.654
$61n$	7.501	$51n$	8.772
$32n$	8.016	$32n$	9.761
$13n$	8.536	$61n$	9.936
$71n$	8.578	$13n$	10.174
$42n$	9.283		
$81n$	9.648		
$23n$	9.970		
$03n$	10.174		

The normal-mode fields are given by the following equations. For the TE-modes,

$$\left.\begin{aligned} E_r &= -l\frac{J_l(k_1r)}{k_1r}\sin l\theta \sin k_3z \\ E_\theta &= -J'_l(k_1r)\cos l\theta \sin k_3z \\ E_z &= 0 \end{aligned}\right\}, \quad \begin{matrix} n > 0 \\ m > 0 \end{matrix} \tag{31}$$

$$\left.\begin{aligned} H_r &= \frac{k_3}{k}J'_l(k_1r)\cos l\theta \cos k_3z \\ H_\theta &= -l\frac{k_3}{k}\frac{J_l(k_1r)}{k_1r}\sin l\theta \cos k_3z \\ H_z &= \frac{k_1}{k}J_l(k_1r)\cos l\theta \sin k_3z \end{aligned}\right\}, \quad \begin{matrix} n > 0 \\ m > 0 \end{matrix} \tag{32}$$

For the TM-modes

$$\left.\begin{aligned} E_r &= -\frac{k_3}{k}J'_l(k_1r)\cos l\theta \sin k_3z \\ E_\theta &= l\frac{k_3}{k}\frac{J_l(k_1r)}{k_1r}\sin l\theta \sin k_3z \\ E_z &= \frac{k_1}{k}J_l(k_1r)\cos l\theta \cos k_3z \end{aligned}\right\}, \quad m > 0 \tag{33}$$

$$\left.\begin{aligned} H_r &= -l\frac{J_l(k_1r)}{k_1r}\sin l\theta \cos k_3z \\ H_\theta &= -J'_l(k_1r)\cos l\theta \cos k_3z \\ H_z &= 0 \end{aligned}\right\}, \quad m > 0 \tag{34}$$

where $k_1 = 2x_{lm}/D$, $k_3 = p\pi/L$, $k^2 = k_1^2 + k_3^2$, and $\lambda = 2\pi/k$.

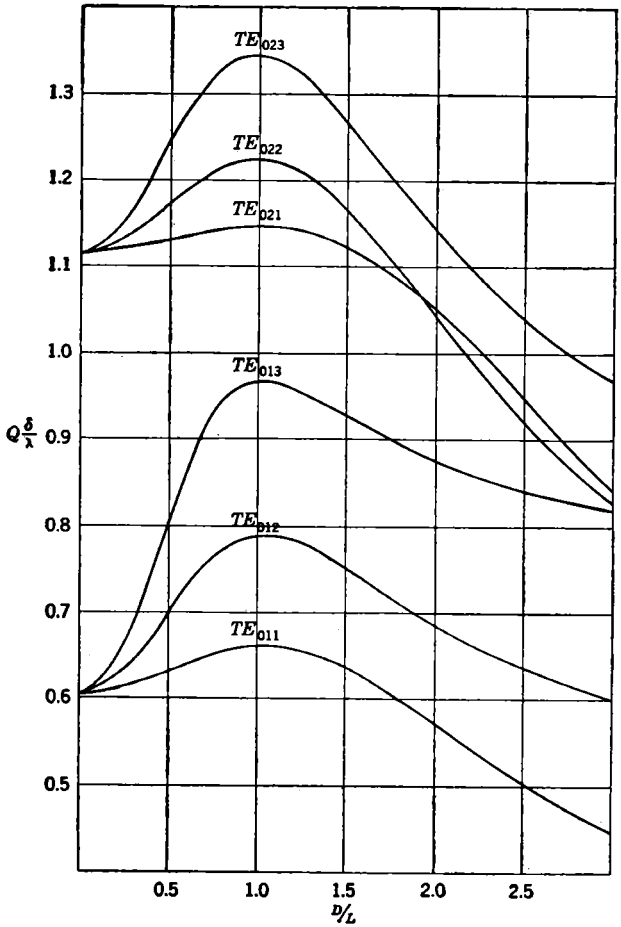

FIG. 5·14.—$Q\ \delta/\lambda$ vs. D/L for several TE_0-modes in a right circular cylinder.

The Q-factors are given by the following equations. For the TE-modes

$$Q\frac{\delta}{\lambda} = \frac{\left[1 - \left(\frac{l}{x_{lm}}\right)^2\right][x_{lm}^2 + p^2R^2]^{3/2}}{2\pi\left[x_{lm}^2 + p^2R^2 + (1 - R)\left(\frac{pRl}{x_{lm}}\right)^2\right]}, \tag{35}$$

and for the TM-modes

$$Q\frac{\delta}{\lambda} = \frac{\sqrt{x_{lm}^2 + p^2R^2}}{2\pi(1 + R)}, \qquad \text{for } n > 0, \tag{36}$$

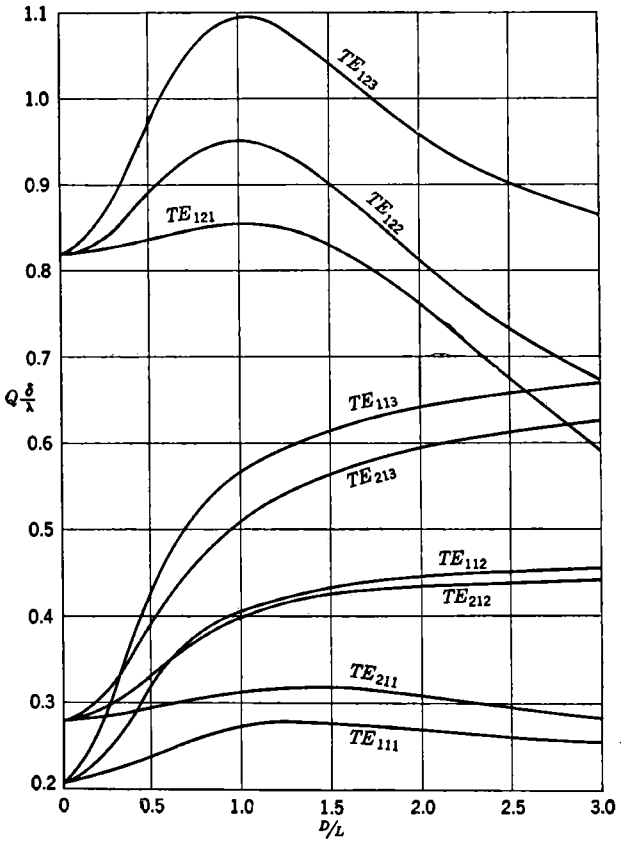

FIG. 5·15.—$Q\ \delta/\lambda$ vs. D/L for several TE-modes in a right circular cylinder.

and

$$Q\frac{\delta}{\lambda} = \frac{x_{lm}}{\pi(2+R)}, \qquad \text{for } n = 0, \tag{37}$$

where $R = D/L$ and $p = n\pi/2$.

These equations are represented graphically in Figs. 5·14, 5·15, and 5·16 where $Q\frac{\delta}{\lambda}$ values are plotted for several modes as a function of D/L.[1]

It can be seen from Fig. 5·14 or Eq. (35) that for a given TE_{0mn}-mode, $Q(\delta/\lambda)$ is a maximum for a square cylinder, that is, $D = L$.

[1] These curves are taken from Kinzer, *loc. cit.*

Consider, however, the more complicated question: for a given Q and λ, what mode and what shape give the minimum volume? Kinzer[1] has shown that the TE_{01n}-modes satisfy this criterion, at least for $Q(\delta/\lambda) > 0.75$ which is the usual case of interest. He finds that

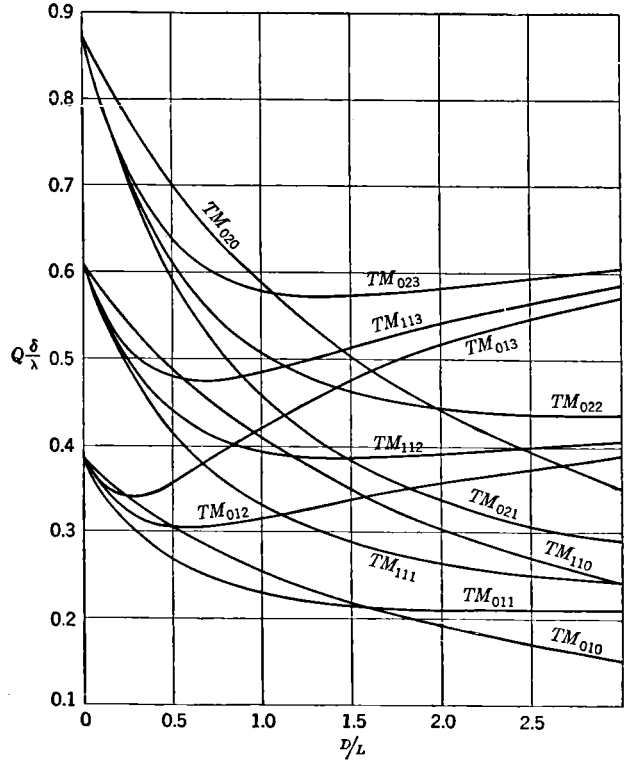

FIG. 5·16.—$Q\ \delta/\lambda$ vs. D/L for several TM-modes in a right circular cylinder.

$n = 1.626 \sin \phi/\cos^3 \phi$, where ϕ is a solution of the equation

$$5 \cos^3 \phi - 3 \cos^5 \phi = \frac{1.220}{Q\dfrac{\delta}{\lambda}}.$$

The corresponding diameter and length are given by

$$\frac{D}{\lambda} = \frac{1.220}{\cos \phi},$$

[1] J. P. Kinzer, "Cylinder Resonator of Minimum Volume for Given Q," BTL MM-43-3500-23, Apr. 6, 1943.

and

$$\frac{L}{\lambda} = \frac{0.813}{\cos^3 \phi}.$$

These results are presented in Fig. 5·17, where n, D/λ, and L/λ are

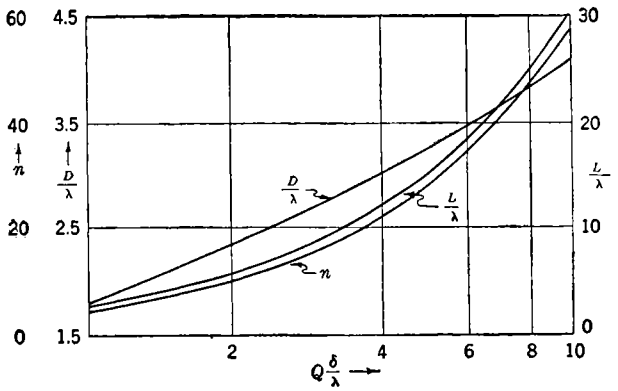

FIG. 5·17.—Cavity parameters for minimum volume for TE_0-modes.

plotted vs. $Q\frac{\delta}{\lambda}$ for the above conditions. This information is useful in designing very-high-Q cavities such as echo boxes. Of course, in using Fig. 5·17 one chooses the integral value of n nearest that taken from the ordinate scale.

5·6. Coaxial Cylinders.—The normal modes in the full coaxial resonator formed from concentric circular cylinders have been treated by several authors.[1] Cylindrical coordinates are used as in Fig. 5·18. The modes are divided into TE- and TM-modes and further specified by integers l, m, and n which are defined as in the cylindrical case.

The normal-mode fields and resonant frequencies contain Bessel functions and their roots. The resonant wavelengths $\lambda = c/f$ are given by

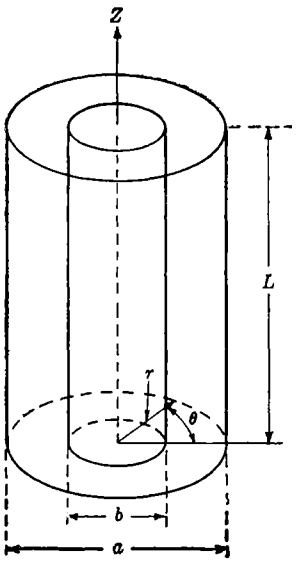

FIG. 5·18.—Coaxial resonator.

[1] F. Borguis, *Hochfrequenztechn. u Elektroakust.*, **56**, 47 (1940); W. L. Barrow and W. W. Mieher, *Proc. Inst. Radio Engrs.*, **28**, 184 (1940); J. P. Kinzer, BTL Case 23458-5, Jan. 8, 1943. The treatment here follows Kinzer.

$$\lambda = \frac{2}{\sqrt{\left(\frac{2x_{lm}}{\pi D}\right)^2 + \left(\frac{n}{L}\right)^2}}, \tag{38}$$

where x_{lm} are the roots of

$$J_l(x)N_l(\eta x) = J_l(\eta x)N_l(x), \qquad \text{for } TM\text{-modes}$$

and the roots of

$$J_l'(x)N_l'(\eta x) = J_l'(\eta x)N_l'(x), \qquad \text{for } TE\text{-modes.}$$

Here, $\eta = b/a$, and J_l and N_l are Bessel functions of the first and second kind respectively.

While it is possible to write Eq. (38) in the form of Eq. (30) and to construct mode charts therefrom, this procedure is cumbersome since a different chart must be constructed for each η-value. A better procedure

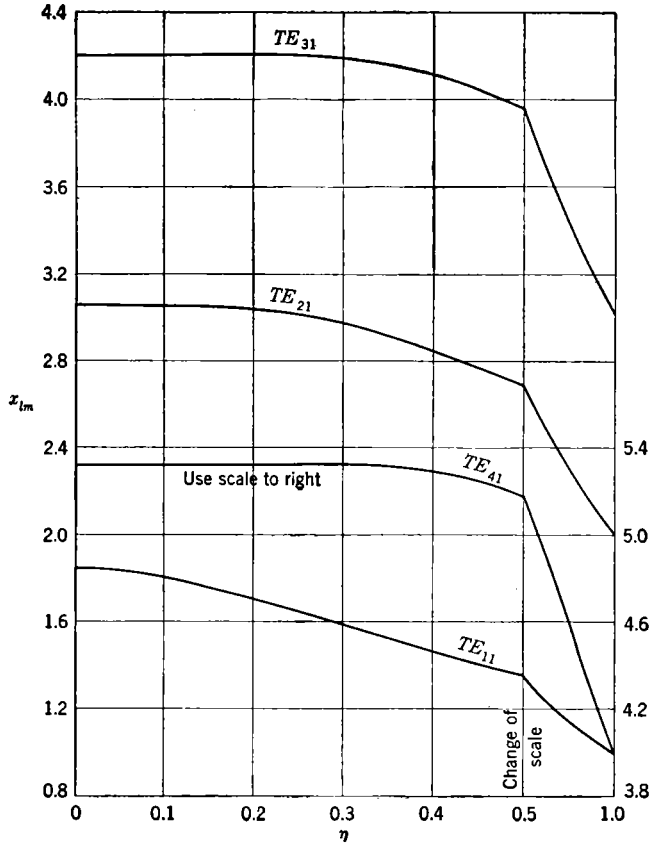

FIG. 5·19.—x_{lm} vs. m for TE-modes in coaxial-cylinder cavity.

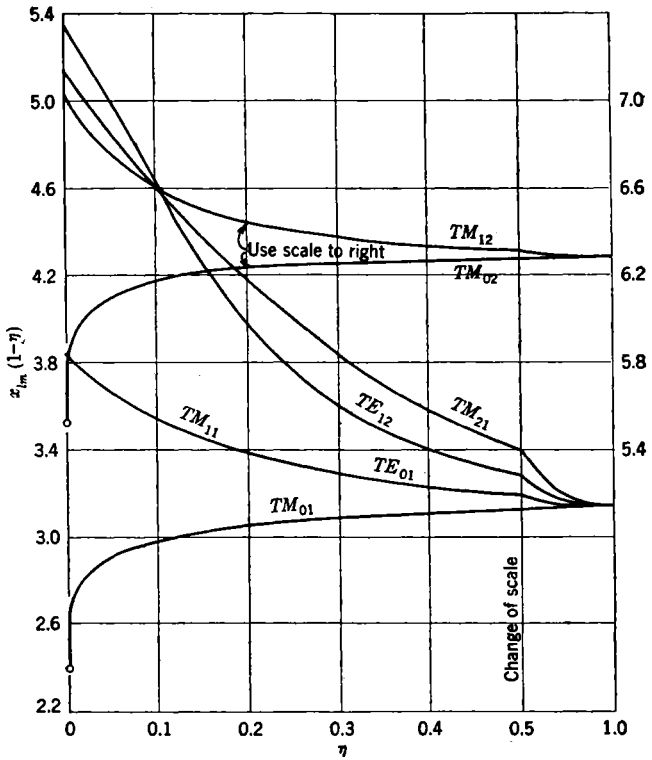

FIG. 5·20.—x_{lm} $(1 - \eta)$ vs. η for TM-modes in coaxial-cylinder cavity.

is to present graphs of x_{lm} vs. η for each of the modes as in Figs. 5·19 and 5·20.[1] From these, mode charts can be constructed for any given case.

For the TE-modes the fields are given by

$$\left.\begin{aligned} E_r &= -l\frac{Z_l(k_1r)}{k_1r}\sin l\theta \sin k_3z \\ E_\theta &= -Z_l'(k_1r)\cos l\theta \sin k_3z \\ E_z &= 0 \end{aligned}\right\} \tag{39}$$

$$\left.\begin{aligned} H_r &= \frac{k_3}{k}Z_l'(k_1r)\cos l\theta \cos k_3z \\ H_\theta &= -l\frac{k_3}{k}\frac{Z_l(k_1r)}{k_1r}\sin l\theta \cos k_3z \\ H_z &= \frac{k_1}{k}Z_l(k_1r)\cos l\theta \sin k_3z \end{aligned}\right\}, \tag{40}$$

where $Z_l(k_1r) = J_l(k_1r) - \dfrac{J_l'(x_{lm})}{N_l'(x_{lm})} \cdot N_l(k_1r)$.

[1] These figures are taken from Kinzer *loc. cit.*

For the TM-modes the fields are

$$\left.\begin{aligned} E_r &= -\frac{k_3}{k} Z_l'(k_1 r) \cos l\theta \sin k_3 z \\ E_\theta &= l \frac{k_3}{k} \frac{Z_l(k_1 r)}{k_1 r} \sin l\theta \sin k_3 z \\ E_z &= \frac{k_1}{k} Z_l(k_1 r) \cos l\theta \cos k_3 z \end{aligned}\right\} \tag{41}$$

$$\left.\begin{aligned} H_r &= -l \frac{Z_l(k_1 r)}{k_1 r} \sin l\theta \cos k_3 z \\ H_\theta &= -Z_l'(k_1 r) \cos l\theta \cos k_3 z \\ H_z &= 0 \end{aligned}\right\}, \tag{42}$$

where $Z_l(k_1 r) = J_l(k_1 r) - \frac{J_l(x_{lm})}{N_l(x_{lm})} N_l(k_1 r)$. In both the TE- and TM-modes,

$$k_1 = \frac{2x_{lm}}{a}, \qquad k_3 = \frac{n\pi}{L}, \qquad k^2 = k_1^2 + k_3^2, \qquad \text{and} \qquad \lambda = \frac{2\pi}{k}.$$

Kinzer gives the following formulas for $Q\frac{\delta}{\lambda}$. In the TE-modes,

$$Q\frac{\delta}{\lambda} = \frac{1}{2\pi} \cdot \frac{(x_{lm}^2 + p^2R^2)^{3/2}M}{x_{lm}^2(1 + \eta H) + p^2R^2 \frac{l^2}{x_{lm}^2}\left(1 + \frac{H}{\eta}\right) + p^2R^3M}, \tag{43}$$

where

$$H = \left[\frac{Z_l(\eta x_{lm})}{Z_l(x_{lm})}\right]^2, \qquad M = \left(1 - \frac{l^2}{x_{lm}^2}\right) - \eta^2 H \left(1 - \frac{l^2}{\eta^2 x_{lm}^2}\right),$$

and $R = a/L$ and $p = n\pi/2$. In the TM-modes,

$$Q\frac{\delta}{\lambda} = \frac{1}{2\pi} \cdot \frac{(x_{lm}^2 + p^2R^2)^{1/2}(1 - \eta^2 H')}{(1 + \eta H') + R(1 - \eta^2 H')}, \qquad \text{for } n > 0; \tag{44}$$

and

$$Q\frac{\delta}{\lambda} = \frac{x_{lm}}{\pi} \cdot \frac{(1 - \eta^2 H')}{2(1 + \eta H') + R(1 - \eta^2 H')}, \qquad \text{for } n = 0, \tag{45}$$

where $H' = [Z_l'(\eta x_{lm})/Z_l'(x_{lm})]^2$.

Kinzer states that the $Q\delta/\lambda$ values for TM_{0mn}-modes are not correct as $\eta \to 0$. Since the fundamental TEM- or TM_{00n}-mode is of considerable engineering interest, we will include an exact formula for this case. It is

$$Q\frac{\delta}{\lambda} = \frac{n}{4 + \frac{2L}{a} \cdot \frac{1 + a/b}{\ln a/b}}. \tag{46}$$

For a given λ, n, and outer-conductor diameter a, this Q is a maximum for $a/b = 3.6$.

5·7. Other Shapes.—Expressions for the Q-values and resonant fields have been worked out for several other shapes: the sphere,[1] the sphere with reentrant cones,[2] ellipsoidal-hyperboloid resonator,[2] and the partial-coaxial resonator.[3] None of these except the last-named have been used very much. The partial-coaxial TM_{001}-mode is used in klystron resonators. Partial-coaxial cavities in this and other modes are sometimes used as wavemeters, but no formulas for the normal-mode fields or Q-values are available.

5·8. Cavities Containing Dielectric Materials.—In the formulas which we have given for the resonant frequencies of cavities, it has been assumed that the cavities were empty; that is, a relative dielectric constant k_e of unity, where $k_e = \epsilon/\epsilon_0$. It is easy to extend these expressions to the case when $k_e \neq 1$.

Consider an arbitrarily shaped lossless cavity resonating at a frequency ω. Maxwell's equations in the cavity are

$$\text{curl } \mathbf{E} + j\mu\omega\mathbf{H} = 0, \tag{47}$$

$$\text{curl } \mathbf{H} - j\epsilon\omega\mathbf{E} = 0. \tag{48}$$

At resonance the stored electric and magnetic energies are equal and are given by

$$W_E = W_H = \tfrac{1}{2}\int_v \mu H^2\, dv = \tfrac{1}{2}\int_v \epsilon E^2\, dv. \tag{49}$$

Let us change the dielectric constant of the medium filling the cavity from ϵ to ϵ'. Also, change ω to ω' to restore resonance and the original spatial configurations of $\mathbf{E}$ and $\mathbf{H}$. Without loss of generality, we can keep $\mathbf{H}' = \mathbf{H}$. Then, from Eq. (49),

$$\int \epsilon E^2\, dv = \int \epsilon' E'^2\, dv,$$

and

$$\sqrt{\frac{\epsilon}{\epsilon'}} = \frac{E'}{E}.$$

[1] G. Mie, *Ann. Phys., Lpz.*, **25,** 377 (1908); S. Borguis, *Ann. Phys., Lpz.*, **35,** 359 (1939).

[2] W. W. Hansen and R. D. Richtmeyer, *J. Appl. Phys.*, **10,** 189 (1939).

[3] For cavities in TEM-mode, see W. W. Hansen, J. Appl. Phys., **10,** 38 (1939); *Microwave Transmission Design Data*, Publication No. 23-80, Sperry Gyroscope Company, Inc., N. Y., 1944; D. Alpert, "Design Characteristics of Resonant Cavities," Westinghouse Research Report SR-127, July 2, 1942. For partial-coaxial cavities, see W. L. Barrow and W. W. Mieher, Proc. Inst. Radio Engrs, **28,** 184 (1940).

From Eq. (48)

$$\frac{E'}{E} = \frac{\epsilon\omega}{\epsilon'\omega'},$$

and so,

$$\frac{\omega'}{\omega} = \sqrt{\frac{\epsilon}{\epsilon'}}. \tag{50}$$

Thus, if ω corresponds to $k_e = 1.00 \cdots$, the resonant frequency corresponding to k_e' is $\omega' = \omega/\sqrt{k_e'}$. In terms of free-space resonant wavelengths this can be written $\lambda' = \lambda\sqrt{k_e}$.

5·9. Scaling Theorems and the Principle of Similitude.[1]—Suppose we have an arbitrarily shaped cavity with lossless walls and let all dimensions be multiplied by a factor N. If **E** and **H** are also multiplied by N, and ω by $1/N$, Eqs. (47) and (48) are left invariant. From Eq. (49), we see that the condition for resonance is maintained. Hence, for any lossless cavity, if all dimensions are multiplied by a scale factor N, all resonant frequencies are divided by N, and the spatial configurations of the fields are similar.

If the cavity walls have a finite conductivity, it is seen that the skin depth is multiplied by a factor $\sqrt{N}$ when the dimensions are multiplied by N, keeping the conductivity constant. Thus, the fields in the walls are not scaled with those in the cavity and the scaling theorem is not obeyed. If, however, the resistivity is multiplied by the scale factor N, the skin depth is scaled by the factor N and the theorem is exact. Hence, if all dimensions of a cavity and the resistivity of the walls are multiplied by a factor N, then all resonant frequencies are divided by N, and the spatial configurations of all fields are similar. The Q of the cavity remains invariant.

For the usual high-Q microwave cavity, the resonant frequencies are affected very little by the finite wall conductivity, being almost the loss-free values. Hence, if all dimensions are multiplied by N, keeping the wall conductivity invariant, the resonant frequencies are multiplied, to a very good approximation, by $1/N$. The Q of the cavity is multiplied by a factor $\sqrt{N}$, since the spatial configurations of **E** and **H** are nearly similar, and the skin depth is multiplied by a factor $\sqrt{N}$.

PRACTICAL WAVEMETER CIRCUITS

A wavemeter is used to determine the frequencies of waves in a transmission system. This involves tuning or changing the resonant frequency of the wavemeter and noting the change in power absorbed by a load connected to the system. A knowledge of the circuit and the

[1] H. Konig, *Hochfrequenztechn. u. Elektroakust.*, **58**, 174 (1941) and review in *Wireless Engr.*, **19**, 216 (1942).

resonant frequency of the cavity-coupling system at some reference plane can then be used to determine the wave frequencies.

It is seen that this tuning procedure involves variables different from those used in the analysis of cavity-coupling systems, where the resonant behavior of fixed systems was studied. In all practical systems, however, a small change in source frequency is equivalent to a like change in the resonant frequency of the wavemeter, since the Q's, coupling parameters, and reference terminals change very slowly with frequency. Therefore, in the following discussion, source-frequency changes and wavemeter tuning will be used interchangeably at frequencies near a particular resonance.

While there exists an unlimited number of ways in which a cavity can be connected into a microwave transmission-line system, only a few simple forms are used for wavelength indication. Some of these have been discussed in previous sections; others will be introduced here. Although all of these circuits have certain features in common, it will be most convenient to discuss each independently.

5·10. Transmission Cavity Wavemeter.—An ideal circuit for a transmission wavemeter takes the form of Fig. 5·21. The generator frequency

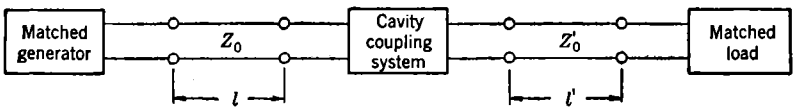

FIG. 5·21.—Transmission-wavemeter circuit.

is measured by changing the resonant frequency of the cavity in the region of the generator frequency until maximum power is transmitted to the load. The wavemeter setting corresponding to this maximum is an indication of the generator wave frequency.

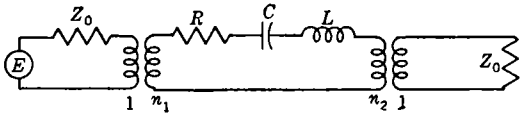

FIG. 5·22.—Representation of Fig. 5·21 at a particular set of reference planes.

At frequencies near a particular resonance and at particular reference planes in the input and output lines from the cavity, the circuit of Fig. 5·21 can be represented as in Fig. 5·22. Let the load be a power-measuring device. At frequencies far from resonance essentially no power is transmitted to the load. As the cavity is tuned to the frequency region of the incident waves, power will be transmitted to the load. This transmitted power is given in Sec. 5·2 and is

$$T(\omega) = \frac{4\beta_1\beta_2}{(1 + \beta_1 + \beta_2)^2 + Q_u^2\left(\frac{\omega}{\omega_0} - \frac{\omega_0}{\omega}\right)^2}, \tag{51}$$

where $T(\omega)$ equals the power into the load divided by the available power from the generator, $\beta_1 = n_1^2 Z_0/R$, $\beta_2 = n_2^2 Z_0'/R$, $Q_u = \omega_0 L/R$, ω_0 is the generator frequency, and ω the resonance frequency of the cavity, $\omega^2 = 1/LC$. Clearly, $T(\omega)$ is a maximum at $\omega = \omega_0$ and reduces to

$$T(\omega_0) = \frac{4\beta_1\beta_2}{(1 + \beta_1 + \beta_2)^2}. \tag{52}$$

The sharpness of resonance is given by the frequency difference between the points at which $T(\omega) = \frac{1}{2}T(\omega_0)$. This frequency difference is

$$\Delta\omega = \frac{\omega_0}{Q_L} = \frac{\omega_0(1 + \beta_1 + \beta_2)}{Q_u}, \tag{53}$$

the bandwidth of the cavity for transmission.

A typical transmission wavemeter is the TE_{011}-cavity described in Sec. 5·16. Its measured loaded Q is about 12,000, and its coupling parameters are equal and about 0.5. The bandwidth for

$$\frac{\omega_0}{2\pi} = f_0 = 9370 \text{ Mc/sec } (\lambda = 3.2 \text{ cm})$$

is, therefore, 0.78 Mc/sec, and the derived unloaded Q is 24,000; $T(f_0) = 0.25$ which is equivalent to a transmission loss of 6.0 db.

A wavemeter is usually calibrated with a standard or reference cavity which in turn is calibrated with a standard frequency source. A substitution method is often used, in which the standard cavity is substituted for the wavemeter in the circuit of Fig 5·21. Several precautions must be observed in this procedure. First, the generator frequency must be kept constant. Aside from thermal and power constancy, this implies that there be no reactance-pulling of the generator. This is usually accomplished by "padding" the generator with a bilaterally matched attenuator. Second, the reference and wavemeter cavities must not be subjected to reactive pulling, or must be pulled by equivalent amounts. If the cavities are identical (have equal Q_u's, couplings, and reference planes), they will be pulled equal amounts by reactive generator and load impedances. However, in general the cavities are not identical and the pulling will be different for the reference cavity and for the wavemeter. Thus the generator and load should be matched as well as possible.

The extreme values of the frequency for maximum transmission are given by Eq. (19), Sec. 5·3, in terms of the voltage standing-wave ratios,

r_1 and r_2, of the generator and load. The difference between this frequency and the frequency of maximum transmission with matched load and generator is

$$\delta = \pm\omega_0 \frac{1}{4Q_u}\left[\beta_1\left(r_1 - \frac{1}{r_1}\right) + \beta_2\left(r_2 - \frac{1}{r_2}\right)\right].$$

For the TE_{011}-cavity discussed above, this amounts to ± 0.018 Mc/sec for $r_1 = r_2 = 1.1$, and ± 0.15 Mc/sec for $r_1 = r_2 = 2.0$.

Transmission wavemeters are sometimes used on a side arm which is coupled to the main transmission line with a directional coupler. This is shown in Fig. 5·23 for a waveguide transmission-line circuit and directional coupler. Suitable couplers are discussed in Chap. 14.

This method of using a transmission wavemeter is very useful. There is no pulling of the cavity or change in transmitted power through the wavemeter by mismatched main-line loads. If the directional coupler is unidirectional and matched, the analysis of the wavemeter indication is the same as that of the preceding paragraphs since an equivalent matched generator appears at the output terminals of the directional coupler.

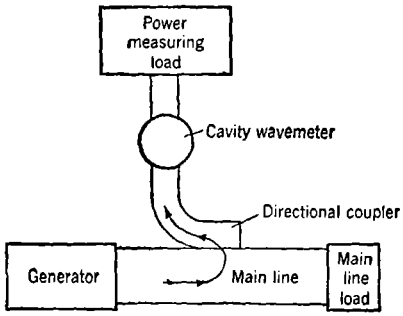

FIG. 5·23.—Transmission-wavemeter system coupled to the line with a "Bethe-hole" directional coupler.

5·11. Reaction Wavemeter Terminating a Line.—A circuit which has been used is shown in Fig. 5·24. As the cavity is tuned through the generator frequency the power absorbed by the load is changed. The form of this change depends on the line length l.

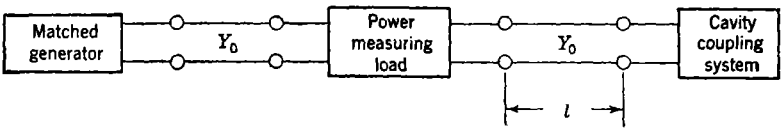

FIG. 5·24.—Reaction wavemeter terminating a line.

Frequently the power-measuring load is a crystal or bolometer, representable as a pure shunt admittance $g + jb$. If, the cavity-coupling system is representable at its terminals, as a shunt-resonant circuit, then Fig. 5·24 is equivalent to Fig. 5·25. The length l is usually chosen so that maximum power is absorbed in the load when the cavity is far off resonance. This occurs when the off-resonance cavity susceptance transformed to plane B is $-jb$, and $Y_c/b = \tan(2\pi l/\lambda_g)$. At the fre-

quency ω the cavity admittance at plane A is

$$Y' = \frac{1}{R} + j\omega_0 C\left(\frac{\omega}{\omega_0} - \frac{\omega_0}{\omega}\right),$$
$$\approx \frac{Y_0}{\beta}\left(1 + 2jQ_u\frac{\delta}{\omega_0}\right),$$

where $\beta = RY_0$, $Q_u = \omega_0 RC$, and $\omega = \omega_0 + \delta$. At plane B the cavity

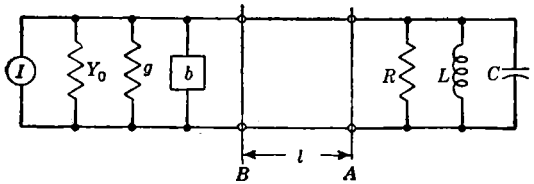

FIG. 5·25.—Circuit equivalent of Fig. 5·24 for a load admittance of $g + jb$.

admittance is

$$Y = Y_0\frac{1 + j\left(2Q_u\frac{\delta}{\omega_0} + \beta\frac{Y_0}{b}\right)}{\left(\beta - 2\frac{Y_0}{b}Q_u\frac{\delta}{\omega_0}\right) + j\frac{Y_0}{b}}.$$

The power into the load at the frequency ω is

$$P = \frac{I^2 Y_0}{(Y_0 + Y + g + jb)(Y_0 + Y^* + g - jb)}, \tag{54}$$

which reduces to

$$P_0 = \frac{I^2 Y_0}{(Y_0 + g)^2} \tag{55}$$

far off resonance. The ratio P_0/P gives the relative power into the load at any frequency.

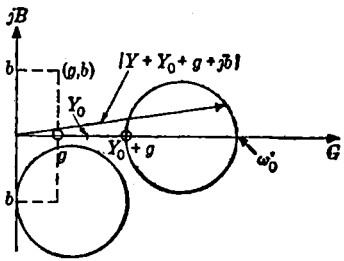

FIG. 5·26.—Vector representation of $(Y_0 + Y + g + jb)$.

The minimum power into the load occurs at the frequency for which $|Y_0 + Y + g + jb|$ is a maximum. On a (G,B) plane this quantity is the length of the vector shown in Fig. 5·26. This vector is a maximum and the absorbed power a minimum for the frequency ω_0' at which $(Y_0 + Y + g + jb)$ is pure real; that is, for

$$\frac{b}{Y_0} + \frac{\left(2Q_u\frac{\delta}{\omega_0} + \beta\frac{Y_0}{b}\right)\left(\beta - 2\frac{Y_0}{b}Q_u\frac{\delta}{\omega_0}\right) - \frac{Y_0}{b}}{\left(\beta - 2\frac{Y_0}{b}Q_u\frac{\delta}{\omega_0}\right)^2 + \left(\frac{Y_0}{b}\right)^2} = 0,$$

which occurs for

$$Q_u \frac{\delta}{\omega_0} = \frac{\beta b}{2Y_0}. \tag{56}$$

This frequency-pulling is the same as that calculated in Sec. 5·3. The power absorbed at this frequency, $\omega_0' = \omega_0 + (\omega_0 \beta b)/(2Y_0 Q_u)$, is

$$P_{\min} = \frac{I^2 Y_0}{\left[Y_0 + g + \frac{\beta}{Y_0}(b^2 + Y_0^2)\right]^2}.$$

and the ratio of this power to that absorbed far off resonance is

$$\frac{P}{P_0} = \frac{(Y_0 + g)^2}{\left[Y_0 + g + \frac{\beta}{Y_0}(b^2 + Y_0^2)\right]^2}. \tag{57}$$

The tuning curve of the power absorbed by the load is shown in Fig. 5·27. The bandwidth of the resonance is $\Delta\omega_0$ where $\delta = \Delta\omega_0/2$ is the solution of the equation

$$\frac{2}{|Y_0 + Y + g + jb|^2} = \frac{1}{(Y_0 + g)^2} + \frac{1}{\left[Y_0 + g + \frac{\beta}{Y_0}(b^2 + Y^2{}_0)\right]^2}.$$

This solution gives

$$\Delta\omega_0 = \frac{\omega_0}{Q_u} \frac{Y_0 + g + \frac{\beta}{Y_0}(b^2 + Y_0^2)}{Y_0 + g}.$$

The corresponding loaded Q of the resonance is

$$Q_L = Q_u \frac{Y_0 + g}{Y_0 + g + \frac{\beta}{Y_0}(b^2 + Y_0^2)}.$$

It should be noted that this reduces to $Q_u(1 + \beta)^{-1}$ for $b = 0$, $g = 0$. The same loaded Q is obtained for $b = \pm Y_0$, $g = Y_0$.

Clearly if $b = 0$ then $\delta = 0$, and the minimum power into the load occurs at the cavity resonance frequency ω_0. The corresponding line length for which the off-resonance cavity admittance transforms to zero at plane B is one-quarter of a wavelength. For this case the power into the load

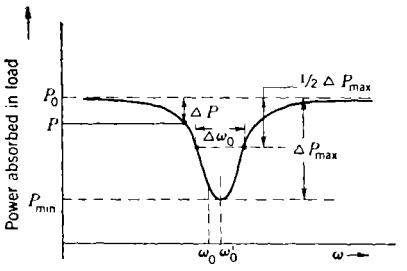

FIG. 5·27.—Power absorbed by the load in the circuit of Fig. 5·24.

at resonance, $\omega = \omega_0$, divided by the power into the load far off resonance is

$$\frac{P}{P_0} = \frac{(Y_0 + g)^2}{(Y_0 + g + Y_0^2 R)^2}.$$

This is easily verified directly by considering the circuit on resonance which is just Y_0, g, and $Y_0^2 R$ in parallel.

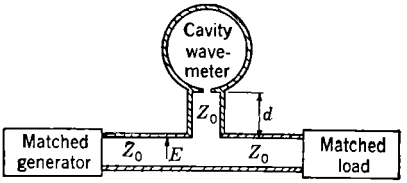

FIG. 5·28.—*E*-plane waveguide T-circuit with a reaction wavemeter.

For the TE_{011}-cavity, discussed in Sec. 5·16, with $\beta = 1$ and $Q_u = 24{,}000$ at 3.2 cm and for a 1N23 crystal in a standard waveguide holder for which $g = Y_0$, and $b = Y_0$, the frequency-pulling is 0.20 Mc/sec, $P_{\min} = (\frac{1}{4})P_0$ and $Q_L = 12{,}000$.

5·12. Reaction Wavemeter on an E-plane Waveguide T.—A convenient waveguide circuit for wavelength indication is of the form of Fig. 5·28. The line length between the junction and the cavity is chosen so that the load impedance seen by the generator is equal to Z_0 when the cavity is tuned far off resonance. This corresponds to a maximum power into the load. This absorbed power is reduced as the wavemeter is tuned to resonance.

At some particular reference planes, the T-junction is representable with an ideal transformer and series reactance. At these terminals, Fig. 5·28 can be represented by the circuit of Fig. 5·29. The line length l is chosen such that

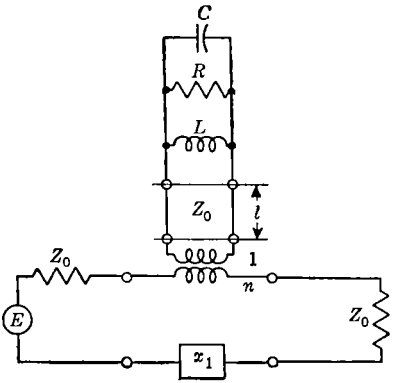

FIG. 5·29.—Circuit representation of Fig. 5·28 at particular reference planes.

$$\frac{x_1}{Z_0} = -n^2 \tan \beta l. \tag{58}$$

Transforming the cavity circuit into the main loop we have the circuit of Fig. 5·30, where

$$r + jx = n^2 Z_0 \frac{Z_c + jZ_0 \tan \beta l}{Z_0 + jZ_c \tan \beta l} = n^2 Z_0 \frac{Z_c - j\dfrac{x_1}{n^2}}{Z_0 - j\dfrac{Z_c x_1}{Z_0 n^2}}. \tag{59}$$

The cavity impedance is

$$Z_c \approx \frac{Z_0\beta}{1 + 2j\dfrac{\delta Q_u}{\omega_0}}, \tag{60}$$

where $\beta = R/Z_0$, $Q_u = \omega_0 RC$, and $\omega = \omega_0 + \delta$.

The power absorbed in the load is a minimum when the total loop impedance $2Z_0 + r + jx + jx_1 = Z$ has a maximum absolute value. This impedance is represented in the vector drawing of Fig. 5·31. This loop impedance has a maximum absolute value, and the power absorbed

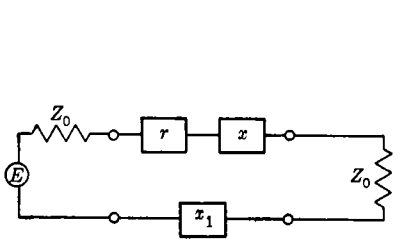

FIG. 5·30.—Alternative representation of Fig. 5·28 and Fig. 5·29.

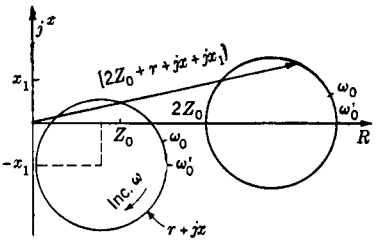

FIG. 5·31.—Vector representation of the loop impedance of Fig. 5·30.

in the load is a minimum for the frequency at which $jx + jx_1 = 0$. Solving for this condition from Eqs. (59) and (60), we obtain

$$\omega_0' - \omega_0 = \frac{\omega_0\beta}{2Q_u} \cdot \frac{x_1}{Z_0 n^2}. \tag{61}$$

For this frequency the total loop impedance Z is real and equal to

$$Z_{max} = 2Z_0 + Z_0\beta\left[n^2 + \frac{1}{n^2}\left(\frac{x_1}{Z_0}\right)^2\right]. \tag{62}$$

The power absorbed by the load at an arbitrary frequency is

$$P = \frac{E^2 Z_0}{ZZ^*} = \frac{E^2 Z_0}{(2Z_0 + r)^2 + (x + x_1)^2}. \tag{63}$$

Far off resonance this is

$$P_0 = \frac{E^2}{4Z_0}, \tag{64}$$

while at the frequency for which Eq. (61) is satisfied

$$P_{min} = \frac{E^2 Z_0}{Z_{max}^2} = \frac{E^2 Z_0}{\left[2Z_0 + Z_0\beta\left(n^2 + \dfrac{x_1^2}{n^2 Z_0^2}\right)\right]^2}. \tag{65}$$

The power absorbed by the load has the general shape of Fig. 5·27. The

position of ω_0' is given by Eq. (61). In general the curve is somewhat unsymmetrical about ω_0'.

Consider the function $\Delta P = P_{\min} - P$. The sharpness of the resonance is given by the rate of variation of this function with frequency. In fact, we may define a loaded Q for this wavemeter arrangement as $Q_L = \omega_0'/\Delta\omega_0$ where $\Delta\omega_0$ is the frequency range between the half-power points of ΔP. The frequencies $\omega_0' \pm \Delta\omega_0/2$ are the solutions of the equation

$$\frac{1}{ZZ^*} = \frac{1}{2(Z_{\max})^2} + \frac{1}{8Z_0^2}.$$

The solution of this equation is

$$\Delta\omega_0 = \frac{\omega_0}{2Q_u} \cdot \frac{Z_{\max}}{Z_0}. \tag{66}$$

Consider the TE_{011}-cavity discussed in Sec. 5·16 with $f_0 = 9365$ Mc/sec, $\beta = 1$, $Q_u = 23{,}000$, and an E-plane T in rectangular (0.900-in. by 0.400-in.) waveguide at this frequency for which $n^2 = 0.767$ and $x_1/Z_0 = 0.132$. The line length for which Eq. (58) is satisfied is $0.473\lambda_g$. This is the length from the reference plane of Fig. 5·29 to the plane at which the cavity is represented as a shunt-resonant circuit. Making correction for the positions of the reference planes of the T and the cavity, the physical line length shown in Fig. 5·28 is $.452\lambda_g = 2.03$ cm. For this system $P_{\min} = 0.513\ P_0$, and occurs at a frequency 9365 + 0.035 Mc/sec. The bandwidth of the resonance defined in Eq. (66) is $\Delta\omega_0/2\pi = 0.57$ Mc/sec. The resonance has the shape of Fig. 5·27.

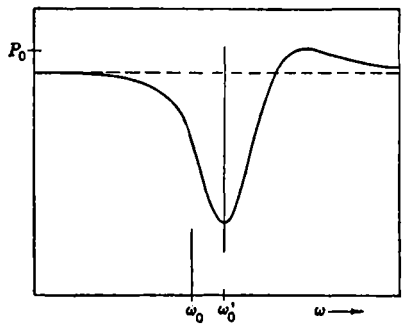

FIG. 5·32.—Schematic diagram of the power absorbed in the load of Fig. 5·28 in which d is chosen incorrectly.

The resonance curve (Fig. 5·27) for such a wavemeter circuit is almost symmetrical and the pulling is small when the line length is chosen according to Eq. (58). However, for other line lengths the resonance curve will become quite unsymmetrical and the power absorbed in the load, when the wavemeter is far from resonance, will be less than the available power. Such a resonance curve is shown in Fig. 5·32. This situation will always occur to some extent if the generator frequency is varied over a wide band without changing the physical line length in Fig. 5·28.

5·13. Iris-coupled Wavemeter on Top of Waveguide.—Of the several reaction wavemeter circuits commonly used, that of Fig. 5·33 is perhaps

the most satisfactory. The shunt capacitance is placed at the symmetry plane B to cancel the shunt inductance of the junction when the cavity is far off resonance. The series reactance X_s of the iris, as modified by the capacitive screw, still appears across the plane A. This series element has approximately the value of the off-resonance cavity reactance at the plane of the iris. It is part of the cavity-coupling system, and can be represented as a section of transmission line of characteristic impedance Z_0. This leads to the circuit of Fig. 5·34 at the reference planes A and B, where l is chosen such that

$$X_s = Z_0 \tan \beta l.$$

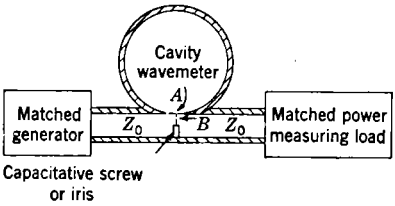

FIG. 5·33.—Iris-coupled wavemeter on top of waveguide.

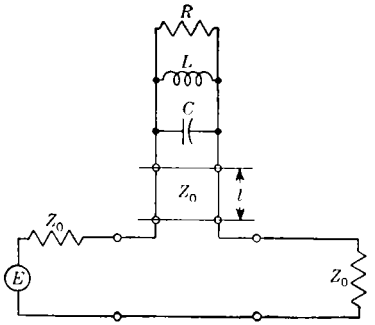

FIG. 5·34.—Circuit equivalent of Fig. 5·33 with $X_s = Z_0 \tan \beta l$.

The power absorbed by the load is

$$P = \frac{E^2 Z_0}{ZZ^*},$$

where

$$Z = 2Z_0 + Z_0 \frac{Z_c + jZ_0 \dfrac{X_s}{Z_0}}{Z_0 + jZ_c \dfrac{X_s}{Z_0}},$$

with $Z_c \approx \dfrac{Z_0\beta}{1 + 2j \dfrac{\delta Q_u}{\omega_0}}$, $Q_u = R\omega_0 C$, and $\beta = \dfrac{R}{Z_0}$.

Far off resonance, this becomes

$$P_0 = \frac{E^2 Z_0}{4Z_0^2 + X_s^2}.$$

The absorbed power is a minimum for

$$\omega_0' \approx \omega_0 + \frac{\omega_0 X_s}{2\beta Q_u Z_0}\left(\frac{4 - \beta}{4 + \beta} - \beta^2\right).$$

This minimum power is

$$P_{\min} \approx \frac{E^2 Z_0}{\left[2Z_0 + Z_0\beta + \left(\dfrac{X_s}{Z_0}\right)^2 \left(Z_0\beta + \dfrac{Z_0}{4 + \beta}\right)\right]^2}.$$

The maximum power is slightly greater than P_0. It is

$$P_{max} \approx \frac{E^2 Z_0}{\left[2Z_0 + \left(\frac{X_s}{Z_0}\right)^2 \frac{Z_0}{4+\beta}\right]^2},$$

and occurs far from ω_0. These points are illustrated in Fig. 5·35. In practice X_s/Z_0 is very small, and terms of the order of $(X_s/Z_0)^2$ are entirely negligible, so that $P_0 \approx P_{min} = E^2/4Z_0$ to a good approximation.

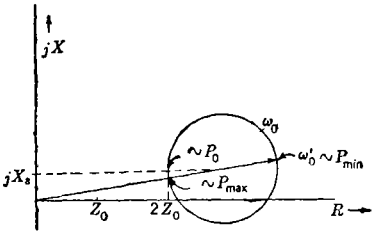

FIG. 5·35.—Vector diagram of the loop impedance of Fig. 5·34.

The tuning curve of the load power is very similar to that of Fig. 5·27. If we define the loaded Q as for Fig. 5·27, we get, to a very good approximation, $Q_L \approx \frac{Q_u}{1+\beta/2}$ which corresponds to a bandwidth of $\frac{\omega_0(1+\beta/2)}{Q_u}$.

5·14. Reaction Wavemeter on a Coaxial Stub.—In coaxial transmission systems it is convenient to use the circuit shown

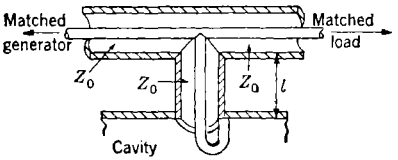

FIG. 5·36.—Reaction wavemeter on coaxial stub.

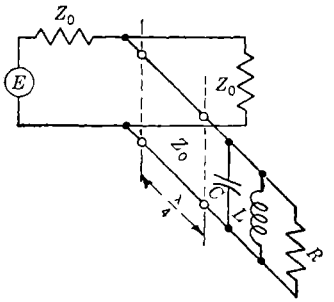

FIG. 5·37.—Equivalent circuit of Fig. 5·36.

schematically in Fig. 5·36. The line length l is chosen so that, when the cavity is far off resonance, the stub is an effective $\lambda/4$ in length; that is, the stub presents an infinite impedance in shunt with the main line. This gives the circuit of Fig. 5·37. Figure 5·37 can be transformed into the circuit of Fig. 5·38 if the change of stub line length with frequency is neglected. Here,

$$r = \frac{Z_0^2}{R}, \qquad \mathfrak{C} = \frac{L}{Z_0^2}, \qquad \mathfrak{L} = Z_0^2 C, \qquad \omega_0^2 = \frac{1}{LC} = \frac{1}{\mathfrak{L}\mathfrak{C}},$$

and $Q_u = \omega_0 RC = \omega_0 \mathfrak{L}/r$ and $\beta = R/Z_0 = Z_0/r$.

The power into the load at any frequency is

$$P_L = \frac{E^2}{Z_0} \cdot \frac{\left|\frac{Z_0 Z}{Z_0+Z}\right|^2}{\left|Z_0 + \frac{Z_0 Z}{Z_0+Z}\right|^2},$$

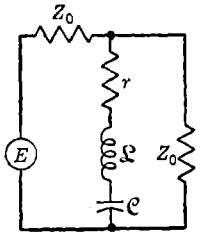

FIG. 5·38.—Alternative representation of equivalent circuit of Fig. 5·36.

where $Z = r + 2j\delta\mathfrak{L}$ in the region of resonance and $Z = j\infty$ far off resonance; here $\delta = \omega - \omega_0$. The expression for P_L reduces to

$$P_L = \frac{E^2}{Z_0} \cdot \frac{1 + 4\left(\frac{\delta Q_u}{\omega_0}\right)^2}{(\beta + 2)^2 + 16\left(\frac{\delta Q_u}{\omega_0}\right)^2}$$

in the region of resonance.

The load power is a minimum for $\delta = 0$, where

$$P_{\text{min}} = \frac{E^2}{Z_0} \cdot \frac{1}{(\beta + 2)^2}$$

and a maximum far off resonance, where it is

$$P_0 = \frac{E^2}{4Z_0}.$$

The tuning curve is similar to Fig. 5·27 with

$$\omega_0' = \omega_0.$$

Defining the bandwidth as for Fig. 5·27 we obtain

$$\Delta\omega_0 = \frac{\omega_0}{Q_u}\left(1 + \frac{\beta}{2}\right),$$

which corresponds to a loaded Q for the resonance of

$$Q_L = \frac{\omega_0}{\Delta\omega_0} = \frac{Q_u}{1 + \frac{\beta}{2}}.$$

This can also be written as

$$Q_L = Q_u\sqrt{\frac{P_{\text{min}}}{P_0}},$$

since

$$1 + \frac{\beta}{2} = \sqrt{\frac{P_0}{P_{\text{min}}}}.$$

PRACTICAL MICROWAVE WAVEMETERS

In this section several typical wavemeters will be described which have been designed and tested in the Radiation Laboratory. Each example will be chosen to illustrate a particular mode configuration and mechanical arrangement, any of which is suitable for general test purposes. In addition to a description of the mechanical and electrical features of each of these, theoretical Q values will be included, as well as experimentally observed values where they are known. Wherever important manufacturing techniques are known they will also be included.

A wavemeter consists of a cavity-coupling system having a variable or tunable resonant frequency. This is accomplished by displacing some part of the cavity walls, usually with a screw of known pitch. Some of these instruments are essentially self-calibrating in that enough pertinent dimensions are directly measurable to give the free-space wavelengths of the normal modes. These types were much used in the early days of the development of each of the microwave bands. Later, when standard frequency sources became available there was a general shift to wavemeters which required calibration point by point over the tuning range. These instruments frequently have more desirable mechanical and electrical properties than the self-calibrating variety.

The details of calibration and the standardization of frequency will not be treated at length since these matters are discussed fully in Chap. 6. The effects of temperature, humidity, and air pressure on the resonant frequencies of cavities will not be analyzed since these are also found in Chap. 6. The chief emphasis in this section will be on the physical and circuit aspects of some existing wavemeters.

5·15. Coaxial Wavemeter for the 3- and 10-cm Regions.—The coaxial wavemeter operating in the fundamental *TEM*-mode is a rugged and

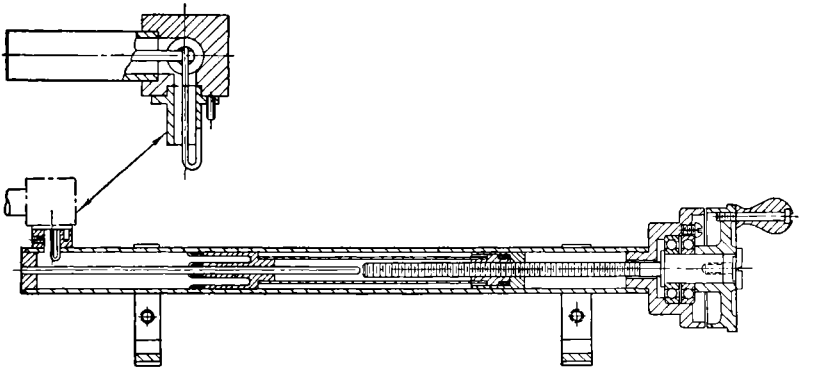

FIG. 5·39.—TFS-5 coaxial wavemeter for the 3000 and 10,000 Mc/sec regions.

dependable instrument, especially in the range up to 10,000 Mc/sec. Above this frequency the coaxial size becomes too small for convenience, and the drive mechanism must be too precise for easy manufacture.

The model shown in Figs. 5·39 and 5·40 is typical of these wavemeters. A short-circuiting plunger is caused to move along the axis of the coaxial cylinders, and a mechanism is provided for measuring this displacement. The wavemeter is coupled to an external coaxial line with a loop. At a reference plane slightly inside of the cavity the system can be represented by a shunt-tuned circuit. The system admittance is infinite at

this plane far off resonance and is pure real at resonance, which occurs when the cavity length is $d_0 \approx \lambda/2$. Successive resonances occur for cavity lengths of $d = d_0 + n\lambda/2$, where n is an integer.[1] Thus an observation of the plunger displacement between successive resonances gives the wavelength directly.

The plunger is driven with an accurately ground lead screw with a $\frac{1}{2}$-cm lead (the thread tolerance is ± 0.0005 inches per inch in manufactured units). This screw is attached to a dial divided into 50 equal

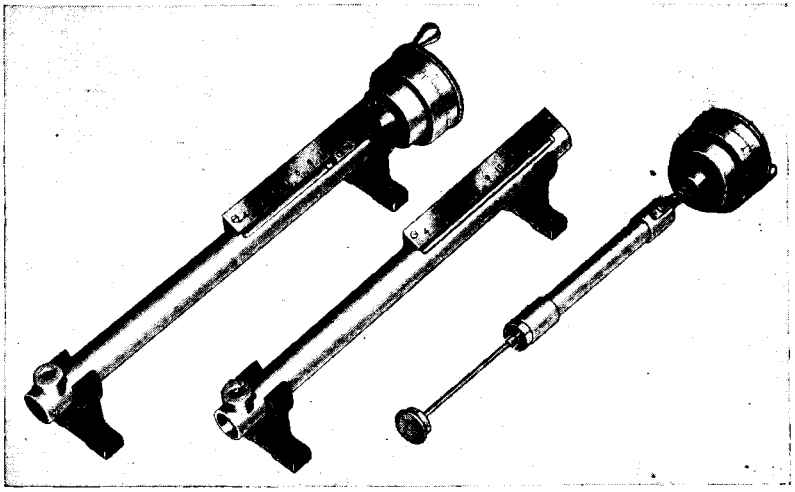

FIG. 5·40.—TFS-5 coaxial wavemeter.

divisions, each corresponding to 0.01 cm of thread lead. A dial vernier is provided for interpolation to 0.001 cm. The screw drives a nut which is attached to a tube which carries the short-circuiting plunger. The nut is kept from rotating by means of a block in a slot. The nut is split and loaded with a spring to eliminate end play. The slotted phosphor-bronze spring-finger plunger has an annular slot 1 in. deep behind the contact plane. This slot acts as a choke in the range $\lambda = 10$ cm where it is $\frac{1}{4}\lambda$ deep and in the range of $\lambda = 3.4$-cm where it is $\frac{3}{4}\lambda$ deep. The finger tips are chromium-plated for smooth sliding on the silver cavity walls.

The outer tube holds the drive mechanism and forms the outer conductor of the coaxial line. It is coin silver with an internal diameter

[1] Because of the finite loss in the coaxial line in the wavemeter, resonances are periodic with a period slightly smaller than $\lambda/2$. This error is, however, entirely negligible, being of the order of 10^{-5} per cent for a typical 3000 Mc/sec wavemeter.

of 0.625 in. The center rod is of coin silver and is 0.125 in. in diameter. At one end it is supported by a silver-plated plug which closes the cavity.

In the 10-cm region the cavity is one wavelength long near the center of the tuning range. The unloaded Q of a perfect coaxial line of silver of the dimensions given and of this length is 3,300 at $\lambda = 10$ cm. At $\lambda = 3.3$ cm this unloaded Q is 6,000. The increase is caused by the more favorable length and outer cylinder diameter at the latter wavelength.

The measured unloaded Q's fall far short of these theoretical values. For example, at $\lambda = 10.7$ cm, with the coupler shown in Fig. 5·39 and using the meter as a reaction device with matched generator and load, one measures $Q_L = 500$ and $\beta = 3.0$ at maximum coupling. This gives a deduced $Q_u = 1250$. The cause of this low value is not known but it seems probable that the plunger fingers are at fault, since such contacts are notoriously lossy. It would be better to use a choke plunger except that this would work only in certain frequency ranges.

Wavemeters of this type have been checked against a frequency standard. With well-constructed meters, wavelengths can be measured with an absolute accuracy of ± 0.05 per cent in the 3000-Mc/sec range, provided that backlash is eliminated by tuning to successive resonances in the same direction. The limiting accuracy is associated with both the Q of the resonance and imperfection in the lead screw.

The coupling to the wavemeter is adjustable by rotating the loop. Maximum coupling occurs when the loop is in a plane containing the axis of the cylinders, and corresponds to $\beta \approx 3$ in the 10-cm range for the loop shown. The coupling parameter can be reduced almost to zero by rotating the loop 90°.

The meter is usually used as a reaction device by coupling it to a coaxial line with a stub such as that shown in Fig. 5·39. In the 10-cm region the coupler shown satisfies the condition that the effective stub length is $\lambda/4$ far off resonance. This coupling scheme was treated in detail in Sec. 5·5. This wavemeter can also be used as a transmission wavemeter by introducing a second loop, usually in the fixed end.

5·16. Right Circular Cylinder in TE_{011}-mode for the 3-cm Region.—An iris-coupled right circular cylinder operating in the TE_{011}-mode has been extensively used as a wavemeter in the 10,000-Mc/sec region. The cavity may be coupled to one or more external waveguides. Tuning is accomplished by varying the length of the cavity. Figure 5·41 shows one model which has been manufactured in quantity. A photograph of this cavity is shown in Fig. 6·26. The plunger is advanced with a micrometer screw (40 threads per inch). A conventional micrometer head has often been used, although Fig. 5·41 shows a head with a special invar screw. Since no currents flow across the gap between the plunger and the cylinder for the TE_{011}-mode, no chokes are built into the plunger

and a simple plate will serve. All of the other modes which can become resonant in the tuning range of the cavity have currents across this gap and will excite the region behind the plunger. The polyiron absorbing disk on the back of the plunger dissipates these fields, thus lowering the Q's of these modes to very small values. Hence, for a fixed iris-coupling diameter, the coupling parameters for these modes are very small and the reaction on the external circuit is much reduced. Since none but the TM_{111}-mode can become simultaneously resonant with the

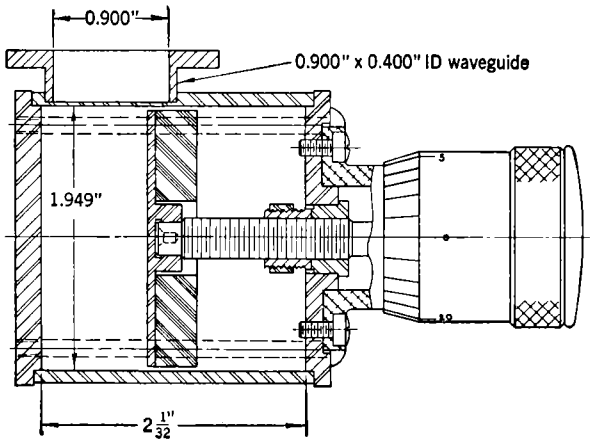

FIG. 5·41.—TFX-30 wavemeter for 10,000-Mc/sec region.

desired mode (TE_{011}), this mode-suppression technique prevents any detectable resonances other than the desired resonance and assures only one resonant frequency corresponding to each plunger displacement. In like manner, if the cavity is provided with two irises, the transmission is negligible for the unwanted modes. These transmission coefficients, which are easier to measure than the change in admittance as the cavity is tuned to a very low Q and weak resonance, have been studied and typical values are shown in Table 5·3.

TABLE 5·3.—TRANSMISSION THROUGH THE CAVITY OF FIG. 5·41 WITH POLYIRON MODE SUPPRESSOR

Mode	Transmission loss, db
TE_{011}	6.5
TE_{211}	> 33
TE_{311}	> 26
TE_{112}	> 50

The TM_{111}-mode requires an extra word of explanation. Since it is intrinsically degenerate with the TE_{011}-mode it will be simultaneously resonant at each plunger setting. Since it also has currents across the

gap it has a low Q, and, if excited, can lower the Q of the desired resonance. This is avoided by preventing its initial excitation by the iris and making sure that no cross coupling exists between it and the TE_{011}-mode. The former is accomplished by proper choice of the iris position, such as in Fig. 5·41. Cross coupling is avoided by keeping the end plates accurately perpendicular to the cavity axis and making the gap uniform. Considerable machining precision is required for these reasons.

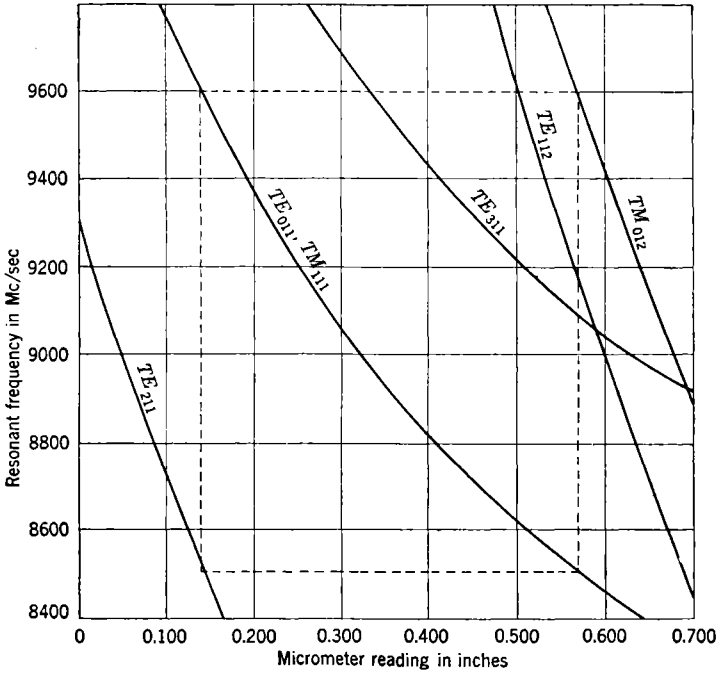

FIG. 5·42.—Experimentally observed mode chart for the wavemeter of Fig. 5·41.

The resonant wavelengths of the several possible modes are given only approximately by the formulas of Sec. 5·4 because of the iris and the gap. This necessitates an experimental determination of the resonant frequencies. Such results are shown in the mode chart of Fig. 5·42. The wavemeter is usually calibrated for the region inside of the dotted rectangle (8500–9600 Mc/sec). It was found possible to manufacture these wavemeters with sufficient precision so that a standard tuning curve (micrometer reading vs. resonant frequency) gave the true resonant frequency of any meter, to an accuracy ± 3 Mc/sec, provided the meter was adjusted to coincide with the standard at a single plunger setting. Details of this procedure are found in Chap. 6.

The invar cavity is finished internally by grinding, honing, or buffing all surfaces, copper plating (0.0003 in.), buffing or polishing, silver plating (0.0002 in.), and finally polishing. This procedure is meant to give a smooth, homogeneous silver surface of as high a skin conductivity as possible. Actually, little is known of how to produce plated surfaces of the lowest possible loss other than to ensure that the coating is free of fissures or rough spots. A high polish in itself may do little good.

The unloaded Q of a perfect right circular cylinder resonating in the TE_{011}-mode is given in Sec. 5·4. If we assume the d-c value for the conductivity of silver at 25°C, we find for the given dimensions that $Q_u = 27{,}400$ at 9365 Mc/sec (3.20-cm free-space wavelength in the standard atmosphere). The values of Q_u deduced from measurements of the loaded Q and coupling parameter sometimes approach this value. With coupling parameters of the order of unity, Q_u values as high as 24,000 have been observed. However, many cavities have much lower unloaded Q's sometimes traceable to poor plating or faulty alignment of the parts. There is some evidence that the deduced unloaded Q falls rapidly as the iris diameter is increased from that corresponding to $\beta = 1$. This may be due to increased excitation of the lossy TM_{111}-mode.

The reaction meters are provided with irises of 0.250-in. or 0.290-in. diameter and are mounted either on the top or at the end of a 0.900 by 0.400-in. (ID) waveguide. In the latter form the waveguide is made $\lambda_g/4$ long, for $\lambda = 3.2$ cm, and is provided with a flange for joining it to a waveguide circuit. Far off resonance no currents flow across this joint. The 0.290-in. iris diameter gives a coupling parameter of about unity, for meters with $Q_u \approx 23{,}000$ at $\lambda = 3.2$ cm, and somewhat less with inferior cavities. The loaded Q depends, of course, on the external circuit.

The transmission meters are provided with two 0.250-in. diameter irises feeding $\lambda_g/4$ sections of 0.900 by 0.400-in. (ID) waveguide. The best of these cavities have a transmission loss of 6.0 db at 3.2 cm corresponding to $Q_u = 23{,}000$, $\beta_1 = \beta_2 = \frac{1}{2}$, and $Q_L = 11{,}500$.

5·17. Right Circular Cylinder in TE_{011}-mode for the 10-cm Region (TS-270).—A TE_{011}-mode cavity similar to that described in Sec. 5·16 has been used in the 10-cm region as an echo box and a wavemeter. One form of this cavity is shown in Fig. 5·43. Tuning is accomplished by varying the cavity length between the limits shown in the figure, corresponding to resonant wavelengths of 10.3 to 11.2 cm. The plunger design follows that of Sec. 5·16. Coupling is provided by loops, one on the side and one on the top. The top loop is normally connected to a crystal detector whose output indicates resonance. The drive mechanism displaces the plunger without rotation, using a rotating micrometer screw attached to the main dial and a nut attached to the plunger.

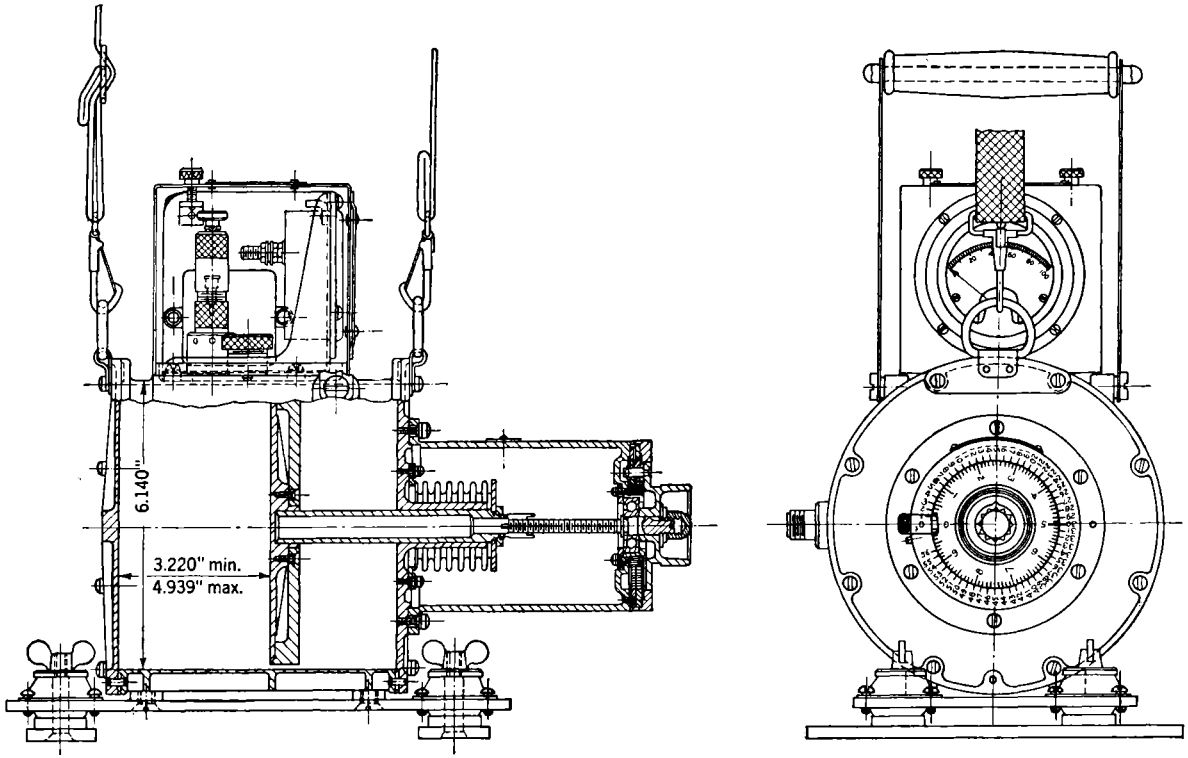

FIG. 5.43.—TE_{011}-mode cavity for the 10-cm region.

The main dial also drives a vernier dial through a gear reduction. The dials are calibrated in frequency and a calibration curve is supplied with the cavity. The cavity material is silver-plated bronze. It is sealed with rubber gaskets and a sylphon bellows.

The theoretical unloaded Q for a plunger setting at the center of the tuning range (2800 Mc/sec or 10.7 cm) is calculated from Fig. 5·14 to be 55,000 assuming pure silver walls. The loaded Q has been measured to be 42,000 with a total coupling coefficient of about 0.1 giving a deduced unloaded Q of 46,000. The application[1] of this cavity as an echo box is described in Vol. 22, Chap. 10.

5·18. Right Circular Cylinder in TE_{11n}-mode for the 1-cm Region.—A self-calibrating wavemeter operating in the lowest round-waveguide mode (TE_{11}) has been used in the 24,000-Mc/sec region. One form of this

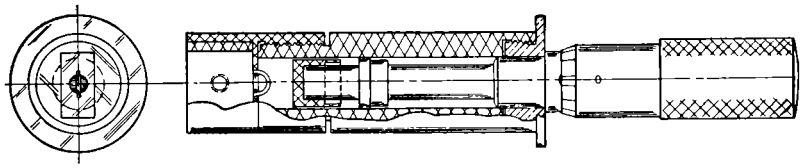

FIG. 5·44.—TFK-2 wavemeter for the 24,000-Mc/sec region.

cavity is shown in Fig. 5·44. A standard micrometer head is used to drive a choke plunger which is pressed on the spindle. Several successive resonances of the TE_{11}-mode occur in the $\frac{3}{4}$-in. tuning range. These lie $\lambda_0/2$ apart, and if the internal diameter of the cylinder is known, the free-space wavelength can be computed from the displacement corresponding to $\lambda_0/2$.

In Fig. 5·44 the cavity is excited from the end of a rectangular waveguide with an iris. This is suitable only for a reaction meter. Transmission meters are excited with irises $\lambda_0/4$ from the cavity end, one on either side of the cavity and in a median plane. The end-on coupling is largely magnetic and the electric vectors in the external waveguide and inside the cavity are polarized in the same direction. In the transmission cavity, the electric vector in the cavity lies in a plane perpendicular to the waveguide axis.

The horsehoe strap across the iris in Fig. 5·44 eliminates the double response which is sometimes observed in these wavemeters and which arises from ellipticity in the cylindrical cavity or in the plunger gap. This is seen as follows. In a perfect cavity any two TE_{11}-modes which are orthogonal can be used to describe the cavity fields, and since they

[1] Cf. also "Instruction Book for Model OBU-3 Echo Box Test Set," Ships 308-A, U. S. Navy Dept., June 15, 1944.

resonate at the same frequency they are indistinguishable from measurements in the external line. If the cylinder or the plunger gap is eccentric, the resonant frequencies of these two modes are split and they are polarized along the axes of the ellipse. Depending on the orientation of these axes with respect to the exciting waveguide more or less power will be coupled to each of the modes, but, in general, both will be coupled and two resonances will be observed in each $\lambda_g/2$ travel of the plunger (of the order of 5 to 14 Mc/sec apart for a group of manufactured units). The strap introduces a very large eccentricity which polarizes the two modes in planes parallel to and perpendicular to the electric vector in the external waveguide and splits them so far apart in frequency that no resistive coupling can introduce cross coupling. Only the mode polarized in the plane of the electric vector in the external waveguide is excited to any degree, and so the double resonance is eliminated.

All of the cavity parts are of pure silver. The tube is accurately broached and polished to a diameter of $0.375\ \binom{+.0005}{-.0000}$ in. The plunger is provided with a choke in the form of an annular cup $\lambda/4$ deep for $\lambda = 1.25$ cm. This is suitable since the fields excited in the plunger are in the coaxial TE_{11}-mode which has a wavelength very nearly λ for the dimensions used. The very-low-impedance line formed by the outside of the plunger and the cylinder improves the choke action, as it is $3\lambda/4$ in length. An absorbing disk is placed behind the plunger to eliminate resonances in the back cavity, which might conceivably be strong enough to give spurious indications.

In the 24,000-Mc/sec region the cavity is tunable to three resonances corresponding to the TE_{111}-, TE_{112}-, and TE_{113}-modes. The theoretical unloaded Q's of a perfect silver cylinder resonating in these modes are 8,200, 9,500 and 10,200 respectively. The experimental values deduced from measurements of loaded Q's and coupling parameters are very nearly as large as those calculated. In fact, they seem too large to be consistent with the added loss which must be introduced by the plunger. These measurements were taken with a 0.111-in.-diameter coupling hole. Typical measured values for the TE_{111}-mode are $Q_L = 3500$, $\beta = 1.3$, giving a deduced $Q_u = 8000$ for a resonant frequency of 24,000 Mc/sec.

5·19. Hybrid TE_{011}-mode Wavemeter for the 1-cm Region.—The wavemeters discussed thus far have all been of simple shape: coaxial and right circular cylinder. Above 20,000 Mc/sec, all of these simple cavities have too large a tuning rate (change in resonant frequency per unit displacement of a plunger) to be consistent with the available precision of drive mechanisms. This suggests a cavity in which only a part of the cavity wall is displaced, preferably in a region of low field intensity.

Such cavities nave been studied[1] for the case of a right circular cylinder tuned by a concentric cylindrical post somewhat shorter than the cavity. Such cavities are commonly called partial coaxial or hybrid cylindrical cavities.

It is seen by referring to the curves of Barrow and Mieher that the resonance frequency of the TE_{011}-mode in the right circular cylinder is displaced only a little by the post. The Q of this mode is, of course, quite high and should not be lowered very much by the post. Since the coaxial TE_{011}-mode as well as the TE_{011}-mode for the cylinder have circular currents in the end plates it is possible to introduce the post through a loose-fitting hole in one end plate without providing chokes or contact fingers. Figure 5·45 shows one form of the hybrid TE_{011}-mode cavity which has been used as a wavemeter in the 24,000-Mc/sec region.

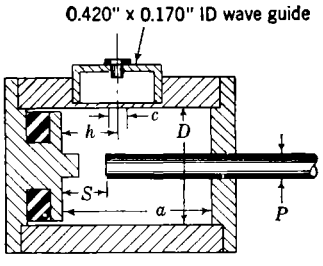

FIG. 5·45.—Hybrid TE_{011}-mode wavemeter or the 24,000-Mc/sec region.

Considerable cut-and-try work was done in the design of this cavity. Most of this was an effort to get a linear frequency-vs.-displacement curve so that an evenly divided dial could be calibrated directly in megacycles per second. Some work was also done to eliminate unwanted

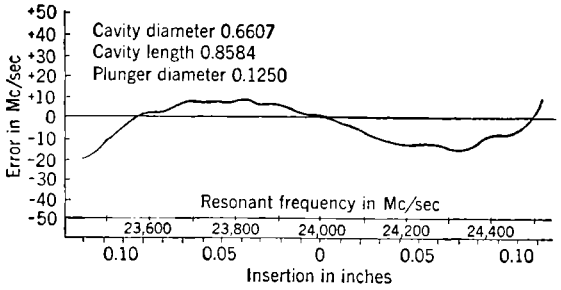

FIG. 5·46.—Error curve for cavity of Fig. 5·45, set at 24,000 Mc/sec, per revolution of 47-thread-per-inch plunger screw.

resonances, in particular that of the TE_{311}-mode, and to achieve a more constant coupling parameter and loaded Q throughout the tuning range. All of these problems are adequately solved in the model of Fig. 5·45.

The tuning post is driven by a 47-thread-per-inch screw giving a nominal tuning rate of 100 Mc/sec for each revolution. The post insertion is set so that the tuning rate is exactly the nominal value at

[1] W. L. Barrow and W. W. Mieher, *Proc. Inst. Radio Engrs*, N. Y. **28**, 184 (1940).

24,000 Mc/sec. An error curve showing the departure of this tuning rate from the nominal value is shown in Fig. 5·46. The small wiggles in the curve of Fig. 5·46 are due to eccentricity as the plunger rotates. At 24,000 Mc/sec the dimension S in Fig. 5·45 is approximately 0.37 inches. The exact insertion of the plunger at 24,000 Mc/sec is, of course, set by comparison with a frequency standard. It should be noted that the resonant frequency increases with increasing plunger insertion.

The cavity length is chosen so that no mode crossings occur within the tuning range (23,500 to 24,500 Mc/sec). The tuning rate is not appreciably influenced by this dimension but depends markedly on the post diameter which was chosen to give the smallest average departure from a tuning rate of 100 Mc/sec per revolution over the tuning range.

The iris opening is chosen to give a 50 per cent dip in transmitted power when the cavity is coupled to the top of the waveguide. This corresponds to a coupling coefficient of $\beta = 0.83$. This coupling is nearly constant (± 5 per cent) over the tuning range of the cavity.

The measured loaded Q of this cavity is $Q_L \approx 6{,}000$. Referring to Sec. 5·5 this corresponds to a deduced unloaded Q of 8500. This is much less than the theoretical value for the unloaded Q of a perfect silver cylinder in the TE_{011}-mode which is 19,600. However, the coaxial part of the cavity is very near or beyond cutoff for the coaxial TE_{011}-mode and the theoretical Q is much lower than the value for the cylinder.

MEASUREMENTS ON CAVITY-COUPLING SYSTEMS

The Q-factors and coupling parameters of cavity-coupling systems can be measured by a number of methods any of which can be placed in one of three categories.

First, there are measurements of power transmission, through or past a cavity, as a function of frequency or cavity tuning. With a two-line cavity, the transmission through the cavity is measured; with a single-line cavity a reaction circuit is used. These methods yield loaded Q-values using the formulas of Secs. 5·10 to 5·14.

In another class of methods, the magnitude and phase of the waves reflected from a cavity system are measured as a function of frequency or cavity tuning. The magnitude of the reflection is usually measured for high-Q systems where the reflection coefficient is a rapid function of frequency. For low-Q systems a measurement of the phase of the reflected waves is more convenient. When properly used these methods yield both Q_L and β.

For systems with very high Q-values neither of the above methods is satisfactory. With suitable apparatus however, it is possible to measure

the rate of decay of shock-excited fields in such cavity systems and hence to derive Q_L from decrement formulas.

In several of the methods mentioned it is desirable to have a signal source of very high frequency stability and preferably one which is tunable over a known range of frequencies. Crystal-controlled radio-frequency oscillators followed by a chain of frequency multipliers have been used for this purpose (see Chap. 6). These frequently have a very low output power so that highly sensitive receivers must be used as indicating devices. This difficulty has been overcome by using the multiplier output voltage as a locking voltage for a klystron multiplier, but the resulting apparatus is rather cumbersome. The stabilized

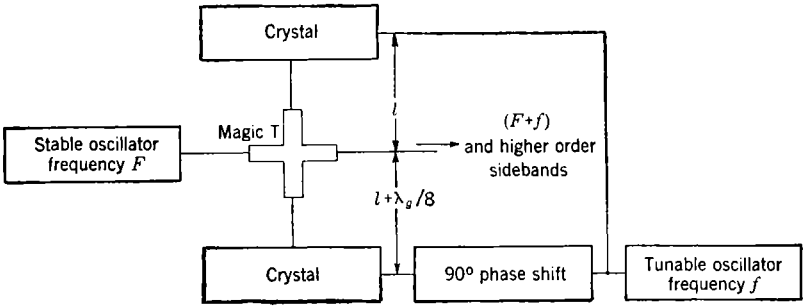

FIG. 5·47.—Tunable microwave frequency-stable signal source.

oscillators recently developed by Pound[1] are more convenient sources of frequency-stable signals. These devices are discussed in Chap. 2.

These stabilized oscillators can be tuned directly with the stabilizer cavity, which may be calibrated against a frequency standard (Chap. 6). This method is suitable if frequency differences need be known only with moderate precision ($\pm 10^5$ cps). For higher precision the tuning and calibration difficulties in this method are considerable and other tuning procedures are more attractive. One such method is the use of a single- or double-sideband modulator to put sidebands of known frequency separation on the stable signal. One or several of these sidebands can then be used as a variable-frequency source.

Figure 5·47 shows a tunable, frequency-stable source employing a single-sideband modulator, which is perhaps more desirable than other modulators since only one of the first-order sidebands (plus higher-order sidebands, in general) is emitted. The transmission-line circuits may be either waveguides or coaxial lines. The line lengths l and $l + \lambda_g/8$ are electrical or phase lengths to the crystal contacts. The crystals

[1] R. V. Pound, "An Improved Frequency Stabilization System for Microwave Oscillators," RL Report 837, Oct. 26, 1945; "An Electronic Frequency Stabilization System for c-w Microwave Oscillators," RL Report 815, Oct. 1, 1945.

must be accurately matched to the lines if no carrier is to be emitted. The signal frequency $F + f$ is varied by changing f which is produced by a calibrated radio-frequency generator. It is usually necessary to know with precision only differences in frequency so that F need be known only to within a few megacycles per second.

As the power level of f is increased, the level of $F + f$ increases until it is of the order of 4 db below the level of F for the optimum form of the time variation of the crystal impedance. The remainder of the carrier power is distributed into the $F - f$ sideband, which is lost in the oscillator, and higher-order sidebands, some of which are emitted. The main experimental problem is to obtain a signal level which is independent of modulation frequency, since otherwise the power must be monitored.

Of course, the circuit of Fig 5·47 is only one form of a variable-frequency sideband generator. Other and simpler forms using a single modulating crystal in which both sidebands are emitted are often quite satisfactory.

5·20. Transmission Measurements with a Two-line Cavity.—Any of the wavemeter circuits of Secs. 5·10 to 5·14 are suitable for measuring the loaded Q of a cavity system from the variation of transmitted power with frequency. Of these, the simplest is the two-line cavity with a matched generator and a matched load (Fig. 5·21). We have seen that the transmission loss (power into load divided by available power from generator) is

$$T(\omega) = \frac{4\beta_1\beta_2}{(1 + \beta_1 + \beta_2)^2 + Q_u\left(\frac{\omega_0}{\omega_0} - \frac{\omega_0}{\omega}\right)^2}$$

for this arrangement, where ω is the signal frequency and ω_0 the resonance frequency of the cavity (or vice versa). At $\omega = \omega_0$ this reduces to

$$T(\omega_0) = \frac{4\beta_1\beta_2}{(1 + \beta_1 + \beta_2)^2},$$

and the frequency difference between the points at which $T(\omega) = \frac{1}{2}T(\omega_0)$ is

$$2\delta_0 = \frac{\omega_0}{Q_L} = \frac{\omega_0(1 + \beta_1 + \beta_2)}{Q_u}.$$

In practice $2\delta_0/\omega_0$ is measured with a swept system (Sec. 6·31) or by measuring $T(\omega)$ point by point. In any case Q_L is given by the variation in $T(\omega)$. If β_1 and β_2 are also desired, it is necessary to make some other measurement such as the input and output impedances of the cavity at resonance.

The details of the apparatus will, of course, depend on the frequency range in question and individual preferences. However, they will all

resemble Fig. 5·48 to some extent. The signal source is some sort of tunable or swept-frequency stable oscillator. The receiver can be a crystal detector and d-c meter, or if modulation is employed, it can be an audio-frequency amplifier, a spectrum analyzer, or a conventional superheterodyne receiver, depending largely on the power available. If, for example, the available signal power is 10^{-3} watt, and if two 10-db pads are used, 100 μw are available at the receiver when the cavity is

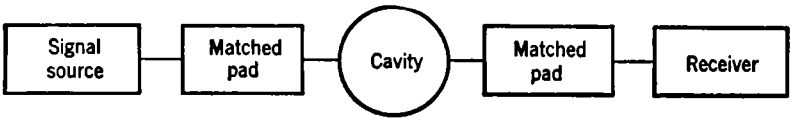

FIG. 5·48.—Transmission-loss apparatus.

removed, and a crystal detector can be used with cavities of reasonable insertion loss (20 db or less). The pads are made large enough to prevent frequency-pulling of the cavity and to assure that the cavity loads are each Z_0. If both the generator and load are reasonably matched something less than 10 db is entirely adequate. Without a stabilized oscillator large pads would be required to prevent frequency-pulling of the oscillator.

It is not necessary to discuss the measurement of Q_L with the other circuits of Secs. 5·10 to 5·14. The apparatus resembles that which has just been discussed. The loaded Q's are calculated from the formulas derived in the preceding paragraphs.

5·21. Standing-wave Measurements on Cavities.—The measurement of the amplitude or phase of waves reflected from a cavity-coupling

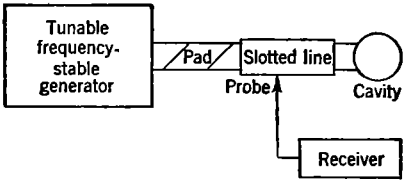

FIG. 5·49.—Apparatus for measuring standing waves from cavity.

system as a function of frequency yields both Q_L and the coupling parameter β. The amplitude measurements are most sensitive with high-Q systems, whereas phase measurements are better for low-Q systems. Either can be made with the apparatus of Fig. 5·49. The generator is any of those previously mentioned. It is usually provided with a pad of several decibels insertion loss, matched so that the cavity is loaded by the Z_0 of the exit cavity line. The slotted section is of coaxial line or waveguide and carries a scale for measuring phase. The receiver can be a crystal detector and d-c meter or an a-c amplifier if

the generator is modulated, or better, a spectrum analyzer or a superheterodyne receiver. If the superheterodyne receiver is used its local oscillator must track with the generator. Any of the usual methods can be used in comparing the maxima and minima of the standing-wave pattern to give the standing-wave ratio.

Amplitude Measurements.—The analysis of the amplitude of the standing-wave ratio to give Q_L and β is easily derived from the treatment in Secs. 5·1 and 5·2, and from the material of Chap. 8. It was shown that the VSWR of a terminating impedance Z in a transmission line of characteristic impedance Z_0 is

$$r = \frac{|Z + Z_0| + |Z - Z_0|}{|Z + Z_0| - |Z - Z_0|}, \tag{67}$$

or, in terms of admittances,

$$r = \frac{|Y + Y_0| + |Y - Y_0|}{|Y + Y_0| - |Y - Y_0|}. \tag{68}$$

At the reference plane at which the cavity-coupling system is representable as a simple series circuit the terminating impedance is

$$Z = R + jX \approx R + j2RQ_u \frac{\delta}{f_0},$$

where $Q_u = 2\pi f_0 L/R$ and $f = f_0 + \delta$, and Eq. (67) becomes

$$r = \frac{|\sqrt{(Z_0 + R)^2 + X^2}| + |\sqrt{(Z_0 - R)^2 + X^2}|}{|\sqrt{(Z_0 + R)^2 + X^2}| - |\sqrt{(Z_0 - R)^2 + X^2}|}. \tag{69}$$

For $\delta = 0$, Eq. (69) reduces to

$$r_0 = \frac{Z_0}{R}, \qquad \text{for } R < Z_0,$$

or

$$r_0 = \frac{R}{Z_0}, \qquad \text{for } R > Z_0.$$

At the frequencies $f_0 \pm \delta_1$, for which $2RQ_u(\delta_1/f_0) = \pm(Z_0 + R)$, Eq. (69) becomes

$$r_1 = \frac{1 + \left(\frac{R}{Z_0}\right) + \sqrt{1 + \left(\frac{R}{Z_0}\right)^2}}{1 + \left(\frac{R}{Z_0}\right) - \sqrt{1 + \left(\frac{R}{Z_0}\right)^2}} = \frac{1 + \left(\frac{Z_0}{R}\right) + \sqrt{1 + \left(\frac{Z_0}{R}\right)^2}}{1 + \left(\frac{Z_0}{R}\right) - \sqrt{1 + \left(\frac{Z_0}{R}\right)^2}}. \tag{70}$$

These frequencies $f_0 \pm \delta_1$ are those for which

$$\left|\frac{f_0}{\pm 2\delta_1}\right| = \frac{Q_u}{\frac{Z_0}{R} + 1} = \frac{Q_u}{\beta + 1} = Q_L, \tag{71}$$

where the coupling parameter β is defined in the usual way as Z_0/R. The procedure is to measure r as a function of frequency, to determine the minimum $r = r_0$, to calculate r_1 from this by Eq. (70), and to note the frequency separation $2\delta_1$ between the points at which $r = r_1$. From this one gets Q_L from Eq. (71), and since $r_0 = \beta$ or $1/\beta$, one gets β and Q_u as well. There is only one point of confusion in this procedure; it is necessary to determine whether $r_0 = \beta$ or $1/\beta$, that is, to determine whether $R > Z_0$ or $R < Z_0$. This is illustrated in Fig. 5·50. For locus (a), $R > Z_0$ and $r_0 = R/Z_0 = 1/\beta$. For locus (b), $R < Z_0$ and $r_0 = Z_0/R = \beta$. These two cases are best denoted by the following observation: for $r_0 = \beta$ the position of the minimum of the standing-wave pattern moves $\lambda_g/4$ as f goes from a value far off resonance to f_0; while for $r_0 = 1/\beta$ the minimum position is the same far off resonance as at f_0. It is to be noted however that r_1 is the same for $r_0 = \beta$ and for $r_0 = 1/\beta$.

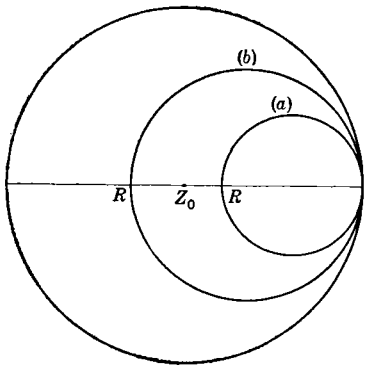

FIG. 5·50.—Impedance contours of cavity system near resonance.

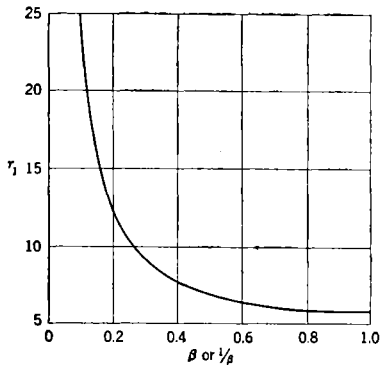

FIG. 5·51.—VSWR of cavity at frequencies $f_0 \pm \delta_1$, for which $Q_L = f_0/2\delta_1$, as a function of β or $1/\beta$.

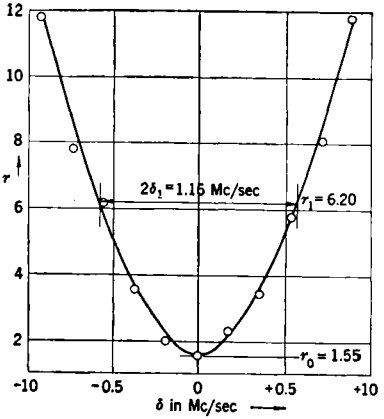

FIG. 5·52.—VSWR of a TFX-30EC cavity (0.2915-in.-diameter coupling hole) tuned to f = 9370 Mc/sec.

A plot of Eq. (70) is shown in Fig. 5·51. It is seen that r_1 is less than 10 in the range $0.26 < \beta < 3.85$. This is the most useful range for the procedure outlined above, and other methods or techniques should be used for larger values of r_1. One can, for example, choose some smaller

value for δ_1 and calculate the VSWR analogous to r_1 for this δ_1 as well as a new relation between Q_L and f_0/δ_1.

As an example of the procedure discussed, consider the data of Fig. 5·52 in which r is plotted vs. δ for a TFX-30 cavity tuned to $f_0 = 9370$ Mc/sec. The apparatus of Fig. 5·49 was used with a 723-A tube and a Pound stabilizer, tuned with a calibrated cavity. A spectrum analyzer was used as a receiver. The VSWR at resonance was $r_0 = 1.55$ and the minimum in the standing-wave pattern at resonance was at a distance $\lambda_g/4$ from the position of the minimum when the generator frequency was far off resonance (as in locus (*b*) Fig. 5·50.) Thus $\beta = 1.55$. For this value of β, r_1 is 6.20 (from Fig. 5·51) and the frequency separation is 1.16 Mc/sec. Thus $Q_L = 9370/1.16 = 8080$ and

$$Q_u = (1 + 1.55)8080 = 20{,}600.$$

The admittance case, proceeding from Eq. (68), is derived in an analogous manner. Here the loci of Fig. 5·50 are the admittance contours at a reference plane where the cavity system is representable as a simple shunt-resonant circuit, (*GCL*). The VSWR at resonance is

$$r_0 = \begin{cases} \dfrac{G}{Y_0}, & \text{for } G > Y_0, \\ \dfrac{Y_0}{G}, & \text{for } G < Y_0. \end{cases} \tag{72}$$

The coupling parameter is $\beta = Y_0/G$ which equals r_0 for $G < Y_0$ or $1/r_0$ for $G > Y_0$, corresponding to loci (*b*) and (*a*) respectively in a diagram identical with Fig. 5·50 for admittances. The VSWR at which $2GQ_u\,(\delta_1/f_0) = \pm(Y_0 + G)$ is given by

$$r_1 = \frac{1 + \left(\dfrac{G}{Y_0}\right) + \sqrt{1 + \left(\dfrac{G}{Y_0}\right)^2}}{1 + \left(\dfrac{G}{Y_0}\right) - \sqrt{1 + \left(\dfrac{G}{Y_0}\right)^2}} = \frac{1 + \left(\dfrac{Y_0}{G}\right) + \sqrt{1 + \left(\dfrac{Y_0}{G}\right)^2}}{1 + \left(\dfrac{Y_0}{G}\right) - \sqrt{1 + \left(\dfrac{Y_0}{G}\right)^2}}, \tag{73}$$

which is the same as the function of Fig. 5·51; and as before $Q_L = f_0/2\delta_1$, and $Q_u = (1 + \beta)Q_L$. This complete analogy between the impedance and admittance analyses is evident if one recalls that the shunt-resonant admittance function is given by transforming the series-resonant impedance function a distance $\lambda_g/4$ along the line and replacing all impedances Z by $1/Z = Y$, a procedure which to a first approximation gives an admittance locus identical to the original impedance locus.

5·22. Phase Measurements.—The loaded or unloaded Q of a cavity can also be found from the phase shift in the standing-wave pattern as a function of frequency in the region of resonance. For low-Q systems

which are tightly coupled ($\beta \gg 1$) these measurements are very sensitive whereas the magnitude of the VSWR changes very slowly with frequency.

The basis for the measurement is easily illustrated. Consider the impedance function of a single-line cavity-coupling system at a reference plane at which it is representable as a simple series *RLC*-circuit. This is

$$Z \approx R + j2RQ_u \frac{\delta}{f_0}, \tag{74}$$

where $Q_u = 2\pi f_0 L/R$ and $f = f_0 + \delta$. At a frequency shift $\delta_u = f_0/2Q_u$,

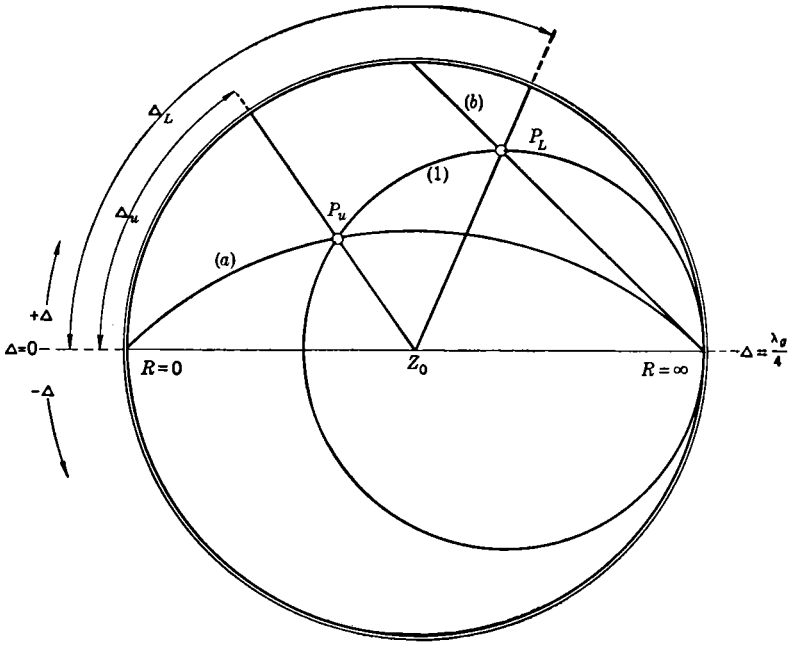

FIG. 5·53.—Smith impedance diagram showing the phase shift Δ_u in the standing-wave minimum for the frequency shift $\delta_u = f_0/2Q_u$; also the phase shift Δ_L for the frequency shift $\delta_L = f_0/2Q_L$.

$Z = R + jR$. The corresponding phase shift of the standing-wave minimum relative to the minimum position at resonance is most easily found with a circle diagram. Consider the construction of Fig. 5·53. Locus (1) represents the impedance function of Eq. (74). The intersection of this circle with locus (*a*) gives a point P_u at which $Z = R + jR$. The corresponding phase shift in the standing-wave minimum relative to the minimum position at resonance is Δ_u. A plot of $\Delta_{\min}/\lambda_g$ vs. R/Z_0 is shown in Fig. 5·54 for the above condition ($\delta_u = f_0/2Q_u$). It is to be

noted that all phase shifts are measured from the standing-wave-minimum position at resonance.

The conductance case is treated similarly. If terminals are chosen such that the cavity system is a simple shunt-resonant *GLC*-circuit,

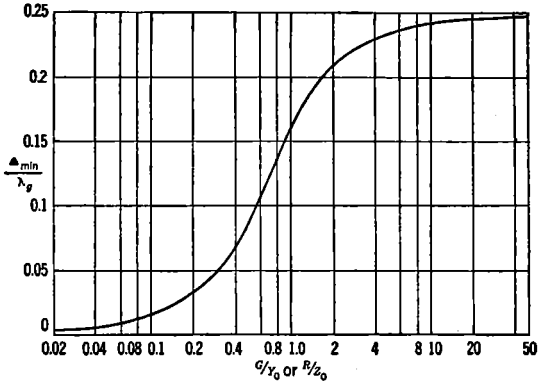

FIG. 5·54.—Shift in standing-wave minimum Δ_u/λ_g (relative to minimum position at resonance) corresponding to a frequency shift $\delta_u = (f_u - f_0) = f_0/2Q_u$.

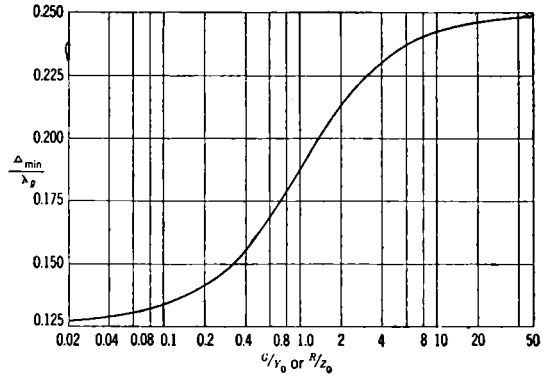

FIG. 5·55.—Shift in standing-wave minimum Δ_L/λ_g (relative to a minimum position at resonance) corresponding to a frequency shift $\delta_L = (f_L - f_0) = f_0/2Q_L$.

the admittance function is

$$Y \approx G + j2GQ_u \frac{\delta}{f_0}, \tag{75}$$

where $Q_u = 2\pi f_0 C/G$ and $f = f_0 + \delta$. At a frequency shift $\delta_u = f_0/2Q_u$ we have $Y = G + jG$. The corresponding shift in the standing-wave minimum relative to the minimum position at resonance is given in Fig. 5·54.

If the frequency shift δ_u is too small to be measured conveniently, the frequency shift $\delta_L = f_0/2Q_L$ can be used. At this frequency Eq. (74) becomes $Z = R + j(Z_0 + R)$. The corresponding shift in the minimum relative to the minimum position at resonance is given in the construction of Fig. 5·53 and is labeled Δ_L. Figure 5·55 is a plot of this shift vs. R/Z_0 or G/Y_0.

It is clear from the preceding paragraphs that one can conveniently get both Q_u and Q_L from phase measurements. If both of these are

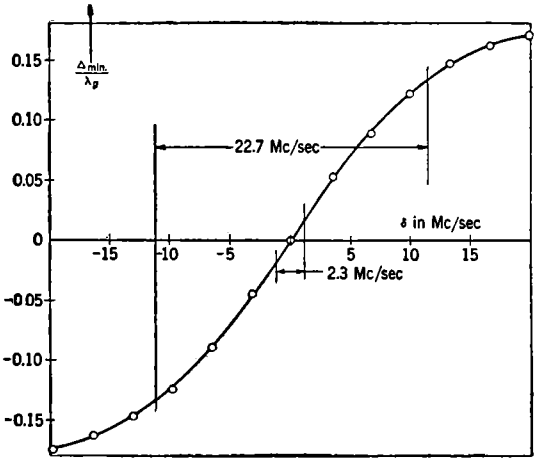

FIG. 5·56.—Measured phase shifts for a cavity resonating at 9370 Mc/sec with $G/Y_1 = 0.112$.

measured, one has a check on the conductance at resonance since

$$Q_u = Q_L(1 + \beta).$$

The above methods are illustrated by the data of Fig. 5·56 taken with a cavity resonating at $f_0 = 9370$ Mc/sec, with $G/Y_0 = 0.112$. From Fig. 5·54 we have $\Delta_u/\lambda_g = 0.018$ corresponding to $2\delta_u = 2.3$ Mc/sec, giving $Q_u = 9370/2.3 = 4070$. From Fig. 5·55, $\Delta_L/\lambda_g = 0.134$, corresponding to $2\delta_L = 22.7$ Mc/sec, giving $Q_L = 9370/22.7 = 413$. From these Q values, $\beta = \frac{4070}{413} - 1 = 8.9$ which checks with $Y_0/G = \beta = 8.9$.

In the foregoing treatment we have used phase shifts Δ_{min}/λ_g as phase angles between minimum positions. If there is no dispersion (that is, $\lambda = \lambda_g$) in the exit transmission line, the measured Δ_{min} values, in centimeters, can be used directly to give Δ_{min}/λ_g. However, if there is dispersion, this is subject to a correction depending on the ratio λ_g/λ, the total λ-interval experimentally used, and the number of wavelengths between the cavity and the measuring probe. In the case of very-low-Q

systems where a large λ-interval is used this may introduce an appreciable correction.

In order to avoid confusion arising from the algebraic sign of Δ_{min} let us consider $|\Delta_{min}|$. It is then true that the measured $|\Delta'_{min}|$ is always greater than or equal to the $|\Delta_{min}|$ which appears in all of the foregoing formulas. That is, the rate of change of phase with frequency is always increased by dispersion in the transmission line, a result which follows from Foster's reactance theorem. The correction which must be applied to $|\Delta'_{min}|$ is

$$\left|\frac{x}{\lambda_g}\Delta\lambda_g\right| = \left|\frac{x\lambda_g^2}{\lambda^3}\Delta\lambda\right| = \left|x\left(\frac{\lambda_g}{\lambda}\right)^2\frac{\Delta f}{f}\right|,$$

where x is the distance from the cavity to the probe.

5·23. Decrement Measurements.—For very-high-Q cavity systems, the frequency stability required to make transmission and standing-wave measurements becomes rather difficult to achieve. In such cases it may be more convenient to use decrement measurements. This has been extensively investigated in connection with the use of "echo boxes" for the measurement of radar-system performance. The point of view here is somewhat different from these studies which are concerned with the time required, after the termination of the transmitted pulse, for the signal from an echo box to decay to the minimum detectable receiver signal. From this time interval, an over-all figure of merit, including transmitter power and receiver sensitivity, can be found for the radar system, making use of a cavity of known Q-factor and coupling parameter. Here this problem is inverted to find the Q from decrement measurements.

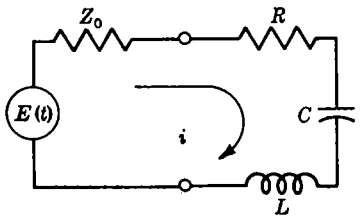

FIG. 5·57.—Equivalent circuit of cavity system at a particular reference plane.

Suppose that the cavity system in question has only one resonant mode in a certain frequency range. Then for these frequencies it is representable at certain reference terminals as a simple series- or shunt-resonant circuit. Let the cavity be connected to a matched generator of available power P_0. The circuit is that of Fig. 5·57 at a particular reference plane. Let $E(t)$ be a step function of amplitude

$$E_0 = 2\sqrt{2P_0Z_0},$$

starting at time $t = 0$ and of frequency ω. It is well known that if $\omega = \sqrt{\frac{1}{LC} - \frac{(R+Z_0)^2}{4L^2}}$ (the damped angular frequency of the loaded

cavity system) the current builds up according to[1]

$$i(t) = \frac{E_0}{R + Z_0}\left(1 - e^{-\frac{R+Z_0}{2L}t}\right)\cos \omega t. \tag{76}$$

If the generator is now extinguished at a time τ the current decays according to the law

$$i(T) = i(\tau)e^{-\frac{R+Z_0}{2L}T}, \tag{77}$$

where T is measured from the extinguishing time and $i(\tau)$ is the value of Eq. (76) at $t = \tau$.
Thus

$$i(T) = \frac{E_0}{R + Z_0}\left(1 - e^{-\frac{R+Z_0}{2L}\tau}\right)e^{-\frac{R+Z_0}{2L}T}\cos \omega t. \tag{78}$$

The decaying voltage measured across Z_0 is $E(T) = i(T)Z_0$ and the power absorbed in Z_0 is $P(T) = i(T)^2 Z_0$. Hence Eq. (78) becomes

$$\sqrt{\frac{P(T)}{P_0}} = \frac{2Z_0}{(R + Z_0)}\left(I - e^{-\frac{R+Z_0}{2L}\tau}\right)e^{-\frac{R+Z_0}{2L}T}.$$

In terms of the constants $Q_L = Q_u/(1 + \beta)$, $Q_u = \omega L/R$ and $\beta = Z_0/R$ this becomes

$$\sqrt{\frac{P(T)}{P_0}} = \frac{2\beta}{1 + \beta}\left(1 - e^{-\frac{\omega\tau}{2Q_L}}\right)e^{-\frac{\omega}{2Q_L}T}. \tag{79}$$

The decrement is obtained by measuring $P(T)$ at two times, T' and T''. The ratio of the corresponding $P(T)$ values is

$$\sqrt{\frac{P(T')}{P(T'')}} = e^{-\frac{\omega}{2Q_L}(T' - T'')}. \tag{80}$$

Equation (80) is of course directly obtainable from Eq. (77). The reason for deriving the complete expression Eq. (79) is so that the total time T can be calculated for a particular minimum detectable $P(T)$.

Consider a typical example in which $P(T)$ is detected with a superheterodyne receiver having a minimum detectable power of 10^{-12} watt. Let $\omega = 2\pi \times 10^{10}$ radian/sec $\tau = 10^{-5}$ sec $Q_L = 10^5$ $\beta = 0.1$ and $P_0 = 10^{-2}$ watt such as could be easily obtained from a reflex klystron. Then the time T required for the decaying signal to reach 10^{-12} watt is

$$T = \frac{2Q_L}{\omega}\ln\left[\sqrt{\frac{P_0}{P_t}}\cdot\frac{2\beta}{1 + \beta}\left(1 - e^{-\frac{\omega\tau}{2Q_L}}\right)\right]$$
$$= 3(10)^{-5} \text{ sec},$$

[1] For example, E. A. Guillemin, "Communication Networks," Vol. I, Wiley, New York, 1931, p. 92.

which should be ample for the measurement. Keeping other factors constant, if $Q_L = 10^4$ this interval decreases to $3(10)^{-6}$ sec, which is about as short as is convenient to measure.

An apparatus for measuring decrements could take the form of Fig. 5·58. The oscillator is a reflex klystron; the receiver is a conventional superheterodyne receiver with crystal mixer, an i-f amplifier 1-Mc/sec wide, a detector, and a video amplifier. The oscilloscope has a fast sweep

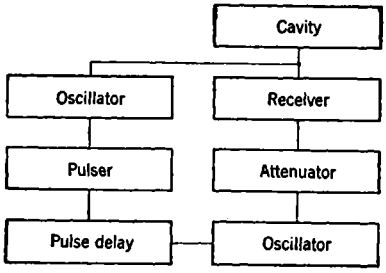

FIG. 5·58.—Apparatus for measuring decrements of cavity systems.

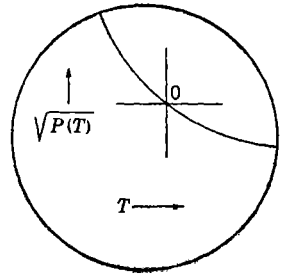

FIG. 5·59.—Oscilloscope pattern of decay of oscillating cavity.

circuit which is triggered by the modulator. The oscilloscope pattern is a plot of Eq. (79) with perhaps some nonlinearity in the voltage scale.

Such a pattern is shown in Fig. 5·59. One picks a certain fiducial mark such as O in Fig. 5·5. An attenuation of, for example, A db is then introduced in the receiver and the sweep delay is shortened by an amount ΔT sec, so as to restore the trace to its original position. Then from Eq. (80)

$$\frac{\omega}{Q_L} = \frac{2.303}{10}\frac{A}{\Delta T}. \tag{81}$$

For example if $A = 3$ db, $\omega = 2\pi(10)^{10}$ radian/sec, $Q_L = 5(10)^4$, the change in sweep delay is $\Delta T = 0.549$ μsec.

If the frequency of the oscillator is not constant from sweep to sweep the pattern of Fig. 5·59 will be fuzzy. However it will have a sharp edge (right-hand edge of trace shown) corresponding to the damped resonant frequency of the cavity since other frequencies will excite the cavity to a lesser degree.

CHAPTER 6

FREQUENCY MEASUREMENTS

By Louis B. Young

Associated with all electromagnetic phenomena are two quantities, frequency and wavelength, which are related by the velocity of light in the medium of propagation,

$$f = \frac{c}{\lambda}.$$

Either quantity may be chosen as a basis for standardization, but once this choice has been made, the other quantity must be derived from a knowledge of the velocity of light. Since this velocity is a function of the medium of propagation, the accuracy to which the dependent quantity may be determined hinges on the engineer's ability to correct the velocity in vacuum to fit his experimental conditions. Therefore standardization should be made on the quantity which requires the greatest accuracy in application. In addition, consideration must be given to the ease and accuracy of measurement of the quantity chosen for standardization.

It is apparent that frequency requires the greatest accuracy of measurement since the alignment of transmitters and receivers is dependent on it. Wavelength is the convenient quantity on which to base microwave impedance design problems, but the accuracy to which wavelength must be known is not nearly so great as in the case of frequency. The measurement of frequency involves a standard of time; that of wavelength, a standard of length. Standard time signals and standard frequencies whose submultiples agree precisely with standard time are made available by radio broadcast. Equally accurate standards of length are not readily available, and, if they were, the technique of the comparison of lengths, even in the microwave region, is not so easy nor capable of so great accuracy as that of frequency comparison. It is indeed fortunate that standards of frequency can be built with ease and accuracy since frequency must be known to great accuracy in application. Consequently, frequency has been chosen as a basis of standardization, and this chapter will deal with primary and secondary standards and with the measuring equipment developed to use them.

PRIMARY FREQUENCY STANDARDS

6·1. General Requirements.—A true primary frequency standard consists of a stable oscillator with which a clock is synchronized for

comparison with standard time. The National Bureau of Standards maintains seven crystal-controlled oscillators which are trimmed so that their mean frequency provides a time indication in exact agreement with astronomical observations of the U.S. Naval Observatory. One of these oscillators provides frequency multiples for radio transmission from Station WWV. By careful intercomparison of all seven oscillators, it is possible to avoid the use of an oscillator whose frequency has large cyclical deviations from the mean. The accuracy achieved in these transmissions is better than 1 part in 10^7.

Microwave frequency standards do not require such high accuracy because of the limitations placed on their utilization by existing measuring equipment and techniques. Therefore the elaborate means used to maintain the accuracy of the national standard of frequency can be omitted. In fact, a single crystal-controlled oscillator that can be monitored, relative to standard-frequency broadcasts, is an adequate basis for a microwave standard. Stability over long periods is highly desirable in the event that standard-broadcast reception is interrupted, but the only essential requirement is negligible frequency drift during a measurement.

6·2. Microwave Frequency Generation.—The frequency of the crystal oscillator is raised to the vhf region by means of vacuum-tube multipliers. The vhf multiple of the crystal frequency is raised to the microwave region by using a silicon crystal rectifier as a harmonic generator. These

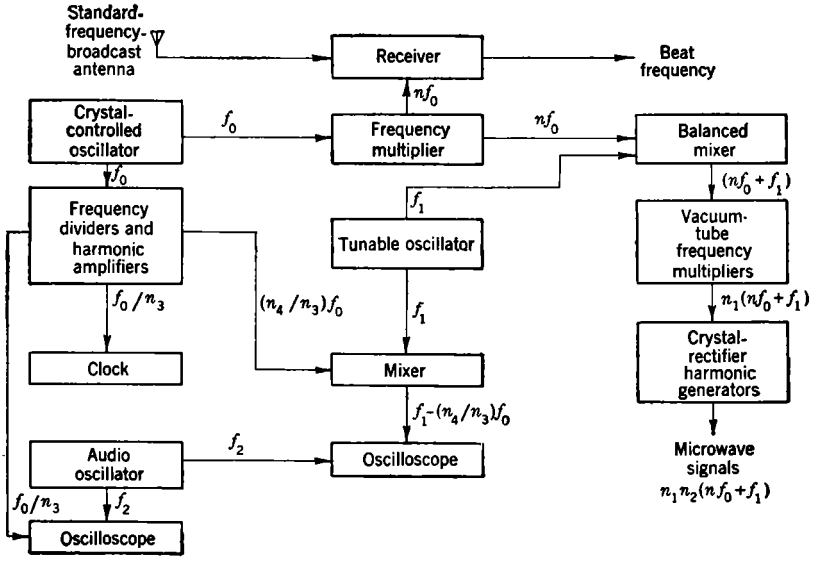

FIG. 6·1.—Microwave frequency standard.

harmonics represent a series of standard microwave frequencies that are spaced by the last vhf multiple of the crystal frequency. Such a standard is useful but lacks the versatility of one that can be varied to cover the entire microwave region.

Complete coverage is attained by multiplying a variable frequency rather than that of a crystal oscillator. The tuning range of this low-frequency source is chosen so that the ranges of microwave harmonics are overlapping. Multiples, submultiples, and known fractions of a crystal-controlled frequency are used to determine the variable frequency to a high degree of accuracy. The entire complex assembly necessary to produce a variable microwave frequency of predetermined accuracy has come to be known as a "primary frequency standard." Figure 6·1 indicates the functions of the various components of such a standard.

6·3. Design Considerations.—The variable frequency, which is multiplied to the microwave region, is obtained by mixing a multiple nf_0 of the crystal-oscillator frequency f_0 with the signal from a tunable oscillator of frequency f_1. The accuracy to which this variable base frequency is known depends to a large degree on the contribution and accuracy of the tunable oscillator. In order that this contribution may be small, the range of the variable frequency should be restricted as much as possible. The amount of restriction is determined by the frequency-multiplication process.

Vacuum tubes are employed to multiply the variable frequency $nf_0 + f_1$ so as to provide a vhf signal of frequency $n_1(nf_0 + f_1)$. Crystal rectifiers multiply this frequency to the microwave region by harmonic generation, and the microwave frequency is $n_1n_2(nf_0 + f_1)$. A microwave power of -70 dbw is available at the 40th harmonic ($n_2 = 40$) when 75 ma of rectified current is produced. This power is 50 db above the noise level of a spectrum analyzer (panoramic receiver). The utilization of higher-order harmonics results in lower output power which is inadequate for making measurements involving high insertion losses. The lowest-order harmonic $n_{2\min}$ that is utilized determines the variable-frequency range that is required for continuous microwave coverage, that is, overlapping ranges for successive harmonics. In order for the lowest and next-to-lowest harmonics to produce overlapping coverage,

$$n_1(n_{2\,\min})(nf_0 + f_1)_{\max} \geqq n_1(n_{2\,\min} + 1)(nf_0 + f_1)_{\min}.$$

This equation reduces to

$$\frac{(nf_0 + f_1)_{\max}}{(nf_0 + f_1)_{\min}} \geqq \frac{n_{2\,\min} + 1}{n_{2\,\min}}.$$

For example, if harmonics down to the 10th are utilized, the variable frequency must cover a 10 per cent range. However, the 10th through

40th harmonics of a vhf signal variable over a small range will not cover the entire microwave region. In fact, it is necessary to use three output signals in the vhf region to obtain complete and continuous microwave coverage.

Although the range of the variable frequency, and hence that of the tunable oscillator, is determined by the frequency-multiplication process, the actual frequency of the tunable oscillator is determined by other factors. Since the variable frequency is generated by a mixing process, undesirable frequency components tend to appear in the output signal. A balanced mixer may be used to eliminate the frequency component nf_0. Frequency components $nf_0 - f_1$, f_1, $2f_1$, and $2nf_0$ may be eliminated by using a double-tuned, low-Q mixer output circuit that has a pass band corresponding to the range covered by the variable frequency $nf_0 + f_1$. Response should be down 40 db at the difference frequency $nf_0 - f_1$. In order to satisfy all requirements it is advisable that

$$\frac{nf_0}{f_1} \leqq 5.$$

Consequently, the accuracy of the variable frequency is determined one-sixth by the tunable oscillator and five-sixths by the crystal-controlled oscillator.

The accuracy of the tunable oscillator's contribution depends on both its stability and accuracy of calibration. By careful protection of the components from sudden temperature changes and by voltage regulation, stability can be made such that the error caused by drift is negligible during a measurement. Calibration accuracy is the main factor, and maximum accuracy may be realized by calibration at the time of application rather than by dependence on a calibration curve.

Calibration is accomplished by measuring the frequency difference between known fractions of the crystal-oscillator frequency and the tunable-oscillator frequency. Multivibrators or regenerative modulators may be used to obtain submultiples f_0/n_3, of the crystal-oscillator frequency. Harmonics of these submultiples lie in the range of the tunable oscillator. The difference frequency is $f_1 - n_4 f_0/n_3$, and is measured by comparison with the frequency of an audio oscillator. If, for example, the $n_4 f_0/n_3$ components are harmonics of 2 kc/sec, then the audio oscillator must cover from 0 to 1 kc/sec, since the tunable-oscillator frequency can never be further than 1 kc/sec from a harmonic.

The audio oscillator is preferably of the beat-frequency type, for stability and for operation at very low frequencies. This oscillator will have sufficient accuracy if it is provided with a calibration curve which has points measured every 50 cps by comparison with the 50-cps signal derived from the crystal-oscillator frequency. The clock at the end of the

divider chain in Fig. 6·1 is not to determine accuracy, but rather to indicate if the operation of the equipment has been interrupted by a power-line failure or if the dividers have erratic behavior.

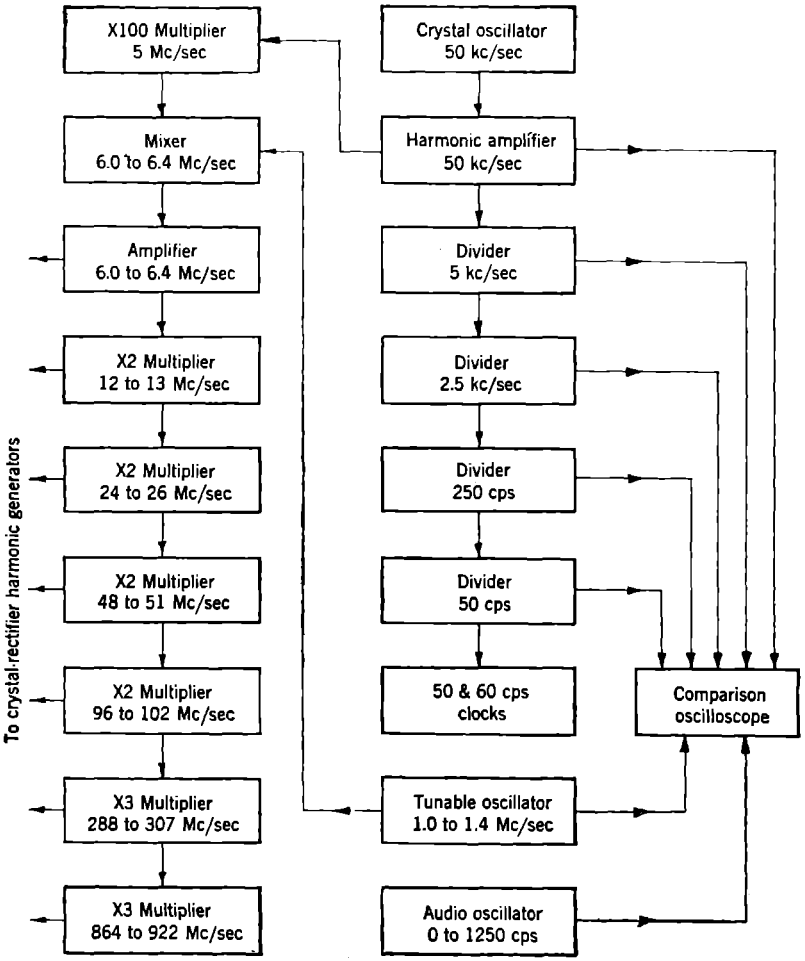

FIG. 6·2.—Block diagram for the Radiation Laboratory microwave frequency standard.

6·4. Microwave Facilities at the National Bureau of Standards.—As a result of the close cooperation between the Radio Section, National Bureau of Standards, and the Radiation Laboratory, both organizations developed frequency standards according to the general design considerations given in Sec. 6·3. Naturally the Bureau of Standards

generates more accurately known frequencies since their equipment is based on one of the seven 100-kc/sec crystal oscillators that determine the national standard of frequency. In addition to generating a variable frequency and multiplying it to the microwave region, they also multiply

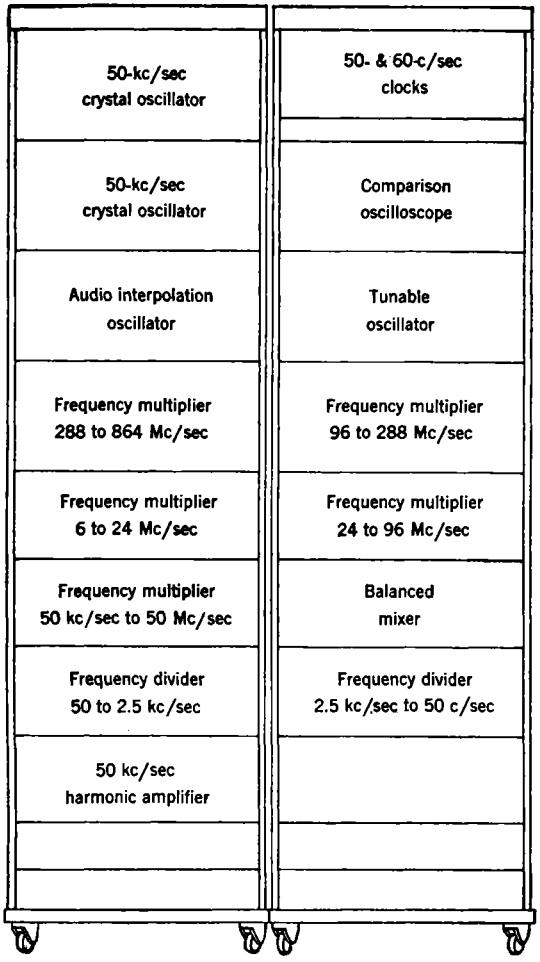

FIG. 6·3.—Key to Fig. 6·4.

the crystal-oscillator frequency in order to provide a series of microwave frequencies that are known to a very high degree of accuracy.

In order to utilize their precision frequencies, a shielded measurements room has been constructed in which both temperature and humidity are carefully controlled. The Radiation Laboratory has furnished

specialized equipment, such as a cavity Q-meter, and the Bureau itself has procured and improved all types of standard measuring equipment. Consequently, the Bureau is well equipped to provide a microwave calibration service, and to develop and improve the cavities that are used as secondary standards.[1]

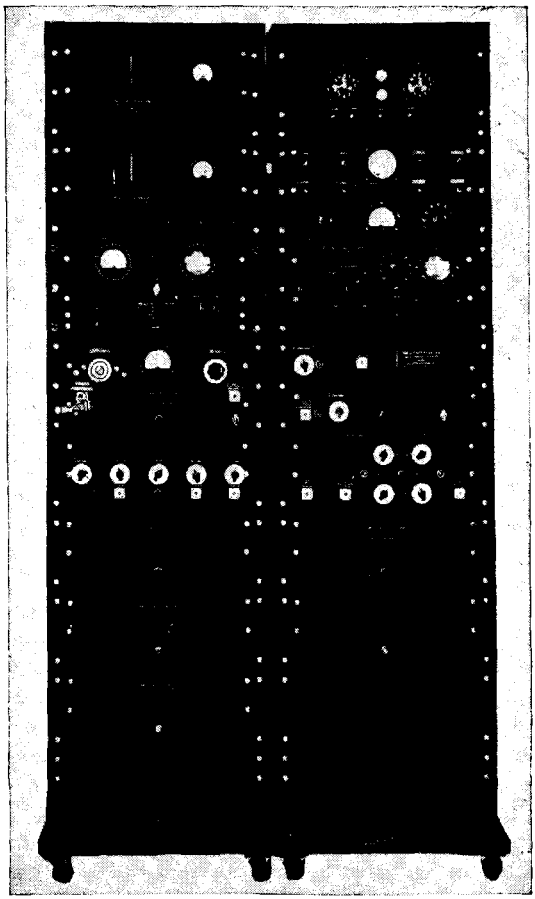

FIG. 6·4.—Radiation Laboratory microwave frequency standard.

RADIATION LABORATORY MICROWAVE FREQUENCY STANDARD

The general considerations for frequency standards are exemplified in detail by the Radiation Laboratory microwave frequency stand-

[1] In addition to these facilities, the Bureau is preparing to maintain microwave standards of power and attenuation.

ard.[1] Figure 6·2 indicates the components that are included and their relationships. Figures 6·3 and 6·4 show the arrangement of the panels in two 6-ft racks, the racks being bolted together and mounted on small trucks.

6·5. Crystal-controlled Oscillators.—Two crystal-controlled oscillators are shown although only one is actually used for frequency measurements. The extra oscillator is kept operating and provides a standby as well as a means of checking the first oscillator when poor radio reception prevents the use of standard-frequency broadcasts. Both oscillators are of the bridge type wherein the crystal is operated at series resonance. The crystal itself is maintained at nearly constant temperature in a thermostated oven. Both the circuit and the oven are similar to those used by the General Radio Company and the early Loran systems, since components from both sources were utilized. Figure 6·5 indicates, in simplified form, the circuit that is used. A Class A, r-f amplifier is followed by a triode phase inverter which drives a nearly balanced bridge, one arm of which is a series-resonant 50-kc/sec quartz crystal. The unbalance voltage developed across the bridge is coupled back to the input circuit of the r-f amplifier. The amplifier utilizes a resonant circuit for high gain and elimination of harmonics. One arm of the bridge is a tungsten-filament lamp whose resistance increases as more power is delivered to the bridge. This resistance change is such as to reduce the bridge unbalance, the feedback, and hence the power delivered to the bridge. Thereby, the lamp serves as a stabilizing element to maintain the oscillator output signal at constant amplitude. During oscillation, the net phase shift around circuit is zero, but variations in tubes or components may shift the phase slightly at one or more points in the circuit. In order to maintain oscillation, the frequency must change so that the crystal can introduce a compensating phase shift. However, since the crystal is equivalent to a very-high-Q series-resonant circuit, the frequency change need be but very slight. In fact, an ordinary series-resonant circuit is placed in series with the crystal in the bridge circuit to provide slight frequency adjustment. Variation of the capacitance from 300 to 525 $\mu\mu$f will change the resonant frequency only 12 parts in 10^6.

Actual circuit details for the crystal oscillator are shown in Fig. 6·6. The power supply is regulated by means of VR-tubes, although this precaution is not necessary for ordinary line-voltage fluctuations. The actual circuit also includes a voltmeter to monitor the oscillator, a cathode-follower output stage to isolate the oscillator from external loads, and components for the control of the crystal oven.

[1] P. A. Hower, "Radiation Laboratory Frequency Standard," RL Report 55·5-10/1/45.

The original alignment of a new oscillator may be facilitated by the use of a signal generator and oscilloscope. The circuit is broken, for example, at the input circuit of the r-f amplifier, and a 50-kc/sec signal is injected. The resonant circuit of the amplifier is tuned until there is no phase difference between the amplifier input signal and the bridge output signal. The circuit is reconnected for oscillation and the variable resistance in the bridge is adjusted until the output cathode follower delivers about 1 volt rms.

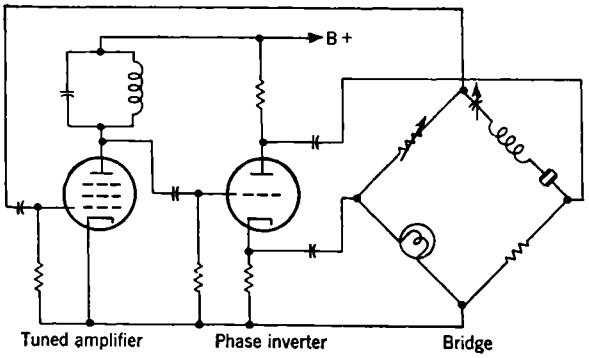

FIG. 6·5.—Simplified schematic for the crystal oscillator.

The 370-ohm resistor, which constitutes one arm of the bridge, is approximately equal to the resistance of the lamp when 1 volt rms is impressed across the lamp terminals.

The quartz crystal is mounted in a supersonic chamber and this assembly is placed in a thermostated oven consisting of two aluminum castings separated by asbestos insulation. Heater elements are placed around the outer casting and are separated from it by a narrow air space. The whole assembly is inclosed in a balsa-wood box. A mercury thermostat that operates on a temperature differential of ± 0.1°C is fastened in good thermal contact to the outer aluminum casting. This thermostat operates a sensitive relay which controls power to the heater elements through a power relay. The entire oven has sufficient thermal mass and insulation so that the temperature of the crystal is held to 60 ± 0.05°C. This temperature control combined with the bridge-type oscillator results in a stability of better than ± 5 parts in 10^7. By checking against standard-frequency broadcasts, it is not difficult to adjust the oscillator so that the mean frequency is 50 kc/sec ± 2 parts in 10^7. Therefore, over long periods of time, the over-all accuracy can be relied upon to be better than ± 7 parts in 10^7. If greater accuracy is desired, adjustment relative to standard-frequency broadcasts can be made at the time of use. The long-period accuracy is usually sufficient, however, and is highly

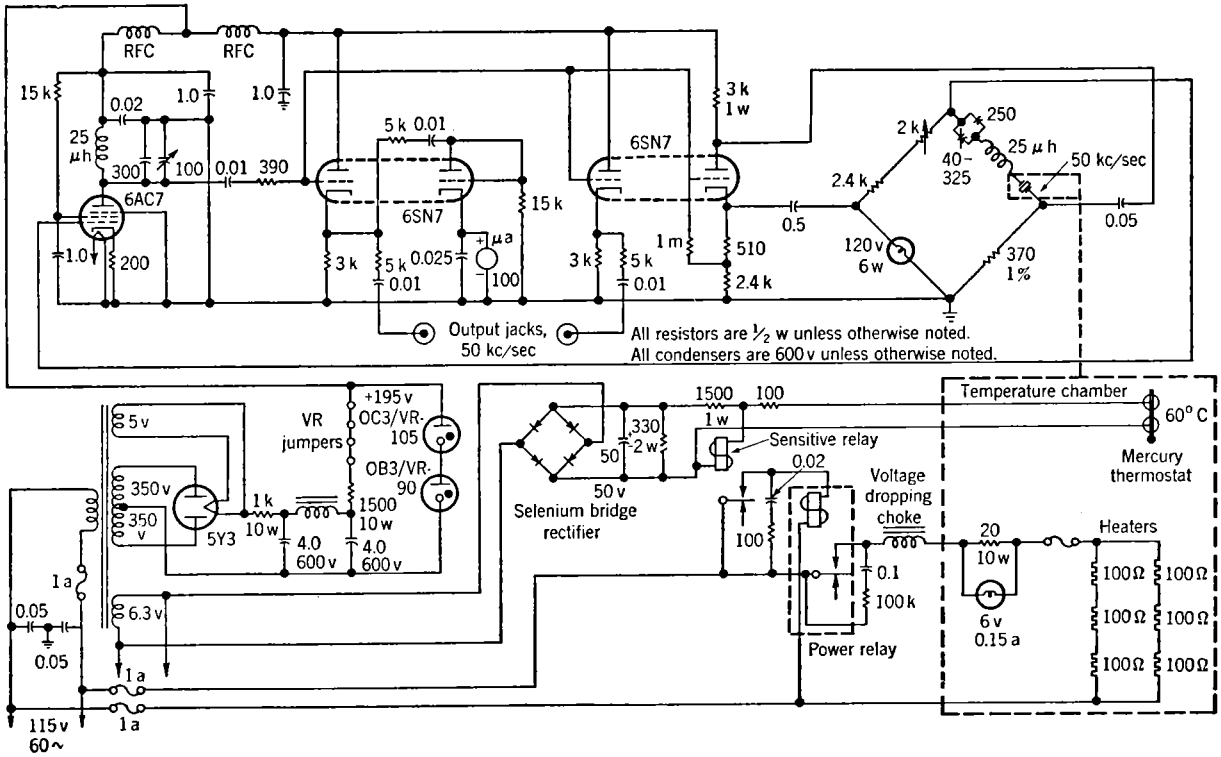

FIG. 6·6.—Crystal oscillator.

desirable in localities where standard-frequency broadcasts are often obscured by radio interference.

6·6. Reception of Standard-frequency Broadcasts.—Figure 6·2 does not indicate any means for checking the accuracy of the crystal oscillator. Any good communications receiver will have sufficient sensitivity to produce a reasonable indication of the carrier-level meter when tuned to the 2.5-, 5-, 10-, or 15-Mc/sec broadcast by WWV. Two of these transmissions are always on the air, modulated with 4000 cps, 400 cps, and pulses that mark the seconds, all derived from the national standard of frequency. Time signals mark the beginning of each 5-min period by complete removal of the modulation. In the Radiation Laboratory

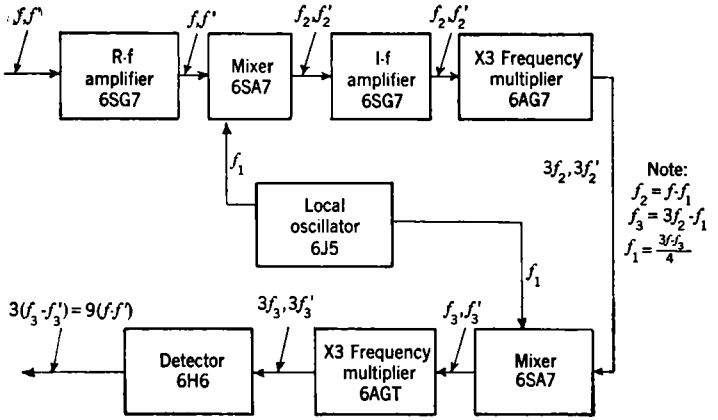

FIG. 6·7.—Comparison receiver.

standard, the crystal frequency of 50 kc/sec is multiplied to 5 Mc/sec, not only to provide a base to which the tunable-oscillator frequency is added to form the variable frequency but also to provide a signal for comparison with the 5-Mc/sec standard transmission. However, even when the crystal frequency has its maximum deviation from 50 kc/sec, the beat frequency in the receiver is but a few cycles. Frequency multiplication of the two 5-Mc/sec signals would increase the difference, but the r-f amplification preceding multiplication would be prohibitive. However, an effective multiplication without regeneration difficulties is possible with a receiver such as that indicated in Fig. 6·7. A heterodyne detector is used to reduce the carrier frequencies without reducing their difference frequency in order to divide the amplification preceding multiplication between stages at different frequencies. A choice of 1 Mc/sec for f_3 will keep all other frequencies below 5 Mc/sec, while the original difference frequency is multiplied by a factor of nine.

6·7. Frequency Dividers and Clocks.—The output signal from the crystal oscillator is coupled to a "harmonic amplifier" that generates 50-kc/sec square waves by amplification and clipping. Before clipping, an output jack is provided for the amplified 50-kc/sec signal that is used to drive the first fixed-frequency multiplier. Two output jacks are provided to couple square waves to the comparison oscilloscope and to the first frequency divider. Frequency division from 50 kc/sec to 50 cps is accomplished in four steps by means of synchronized multivibrators. Figure 6·8 with Table 6·1 shows the circuit details of the frequency divider, and Fig. 6·9 shows the circuit for the power amplifier that drives the 50-cps clock at the end of the divider chain. For each multivibrator the natural frequency and the amount of synchronizing signal are both adjustable. Cathode followers are used to couple successive dividers and to provide signals for the comparison oscilloscope. Both grids of the multivibrator tubes are synchronized in phase to favor division by an even integer; grids are synchronized 180° out of phase to favor odd division. An unregulated power supply delivering 250 volts will suffice to operate the dividers since synchronization is unaffected by ordinary line-voltage fluctuations. At the end of the divider chain, a 6V6 beam tetrode with a reactive load provides a distorted sine wave with sufficient power to drive a 50-cps synchronous-motor clock.

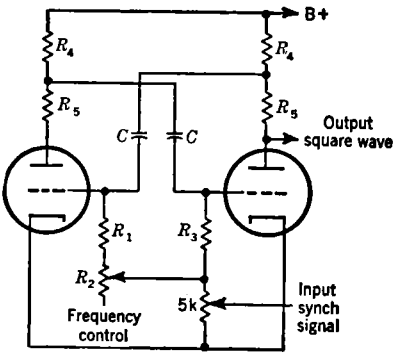

FIG. 6·8.—Frequency divider, 50 kc/sec to 5 kc/sec to 2.5 kc/sec to 250 cps.

TABLE 6·1.—CIRCUIT CONSTANTS FOR FIG. 6·8
The values of R are in thousands of ohms; C is in microfarads

	50 to 5 kc/sec	5 to 2.5 kc/sec	2500 to 250 cps
R_1	10	18	75
R_2	50	20	20
R_3	13	30	91
R_4	16	15	12
R_5	25	27	30
C	0.0036	0.0043	0.022

The 50-cps clock is mounted on a panel beside a 60-cps clock which is operated from the regular power line. A push-button switch on the

panel removes the 50-cps driving voltage, thereby retarding the clock. Another push button replaces 50-cps power with 60-cps power, thereby advancing the clock. By means of these two push buttons, the 50-cps clock may be set to close agreement with standard time signals. A quick comparison of the two clocks indicates whether or not the frequency dividers are operating properly. Both the 60-cps clock and a

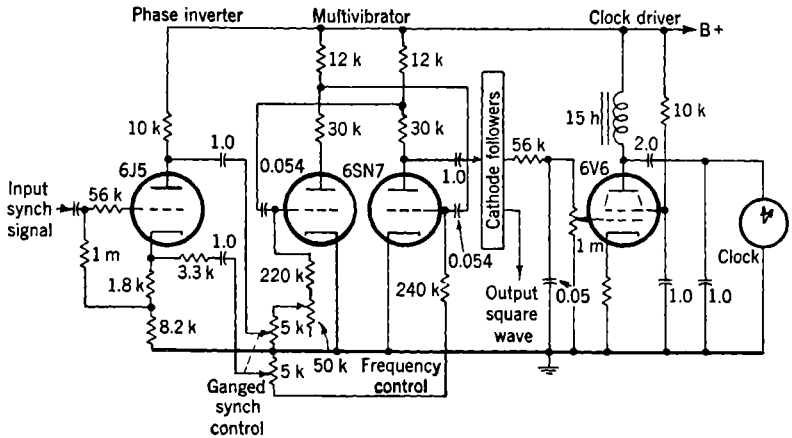

FIG. 6·9.—Frequency divider, 250 cps to 50 cps.

green pilot lamp are connected to the power line through the contacts of an a-c relay which is held closed by the presence of line voltage. If line voltage is interrupted, the clock stops and the green lamp is extinguished. When line voltage is restored, the clock and green lamp will operate only after a reset button is pressed to energize the relay. Until the reset button is pressed, the restored line voltage operates a red pilot lamp, thus indicating that the power has been interrupted. The 60-cps clock indicates the time of power failure and thereby is useful in estimating the state of stability of the crystal oscillators. The time lost by the 50-cps clock indicates the duration of the power failure.

The National Bureau of Standards avoids the synchronization problems of multivibrators by using regenerative modulators as frequency dividers. Four copper-oxide rectifiers are arranged to form a balanced modulator. As is characteristic of such a device, one of the two input frequencies is suppressed in the output signal. In this case, that input frequency closest to the desired output frequency is suppressed. Several of these modulators may be coupled to an amplifier as is shown schematically in Fig. 6·10. The output signal of each modulator is amplified and provides an input signal for another modulator. Into one modulator is fed the signal to be divided, thus providing a master control signal for the

entire system. If this signal is removed, the device stops. In fact, a push-button switch in the power supply is often necessary to shock the device into operation when the control frequency is present. In the

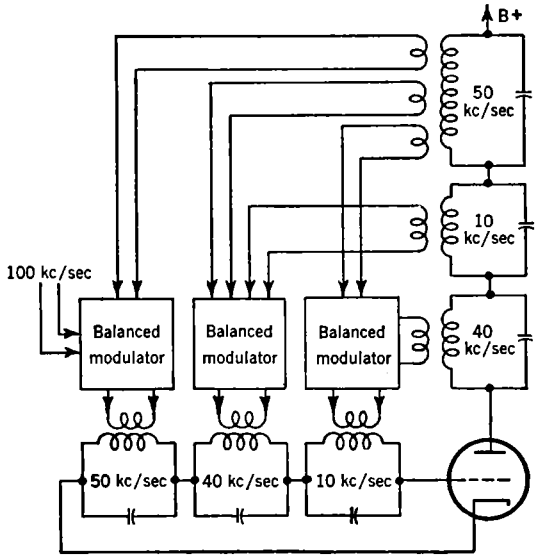

FIG. 6·10.—Regenerative-modulator frequency divider.

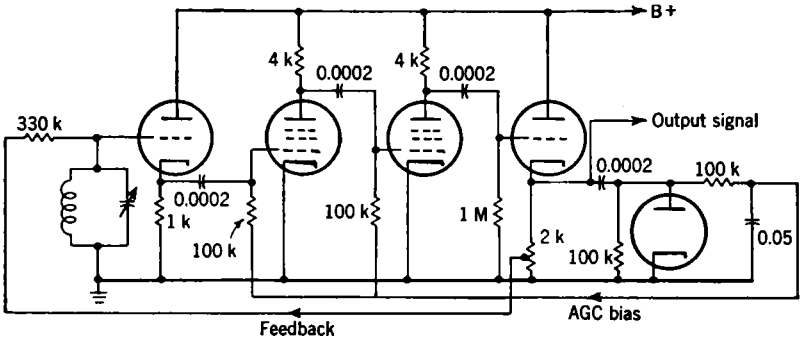

FIG. 6·11.—Tunable oscillator, simplified schematic.

case of the multivibrator divider, the system will continue to operate, but at its natural frequency, when the synchronization is removed. The regenerative modulator shown in Fig. 6·10 is representative of but one of many possible combinations. Those used by the Bureau of Standards operate over a two-to-one variation in amplifier supply voltage with but a slight phase shift of the output frequency. Although this system of

frequency division seems preferable to the multivibrator type, it is more difficult to construct because of the tuned circuits involved.

6·8. Tunable Oscillator.—As indicated in Fig. 6·2, the tunable oscillator furnishes a frequency that is variable from 1.0 to 1.4 Mc/sec. This frequency is mixed with the 5-Mc/sec multiple of the crystal-oscillator frequency to provide a frequency that is variable from 6.0 to 6.4 Mc/sec. It is this resultant frequency that is multiplied to the microwave region, and therefore it must have great stability. Accordingly, the prime design consideration for the tunable oscillator is stability. Figure 6·11 illustrates the general type of oscillator that is used. A parallel-resonant circuit works into a cathode follower to minimize loading and to prevent variations in tube characteristics from affecting the resonant frequency of the tuned circuit. The cathode-follower output signal is amplified by two video stages whose gain is stabilized by AGC. A portion of the amplifier output signal is coupled back to the resonant circuit in order to sustain oscillation.

Actual circuit details for the tunable oscillator are shown in Fig. 6·12. The resonant circuit is more complex than that shown in Fig. 6·11 in order to provide vernier tuning and somewhat uniform impedance over the tuning range. Four coils are employed which consist of solid copper wire wound on $1\frac{1}{2}$-in. diameter polystyrene forms. These coils are switched to provide four bands, each of which covers a range of 100 kc/sec. Ten different values of fixed capacitance can be switched so as to be in parallel with the particular coil that has been selected. This 10-position switch serves to subdivide the 100-kc/sec bands into parts that are approximately 10 kc/sec each. Finally, a precision variable condenser is used to tune the oscillator over the particular 10-kc/sec subdivision that has been selected. For this purpose, the effective capacitance of a General Radio precision condenser is reduced by series padding so that the tuning rate corresponds to 10 cps per dial division. All coils and fixed condensers are mounted in a thermally insulated box. A thermostated oven is not employed since gradual drift is more tolerable then small, but rapid, oscillating changes in frequency.

The resonant circuit is direct-coupled to the grid of the 955 cathode follower. The dynamic input capacitance is degenerated so that the static capacitance of 1 $\mu\mu$f is essentially all that the tube contributes to the resonant circuit. The output impedance of this cathode follower is sufficiently low so that input impedance of the first video amplifier is unimportant. The video amplifiers are shunt-compensated, however, and hence variations in input impedance of the second video amplifier will cause phase-shift variations. Input impedance variations will occur because of power-supply variations, AGC-bias variations, drafts, and tube aging. Consequently, the power supply is well regulated, and the

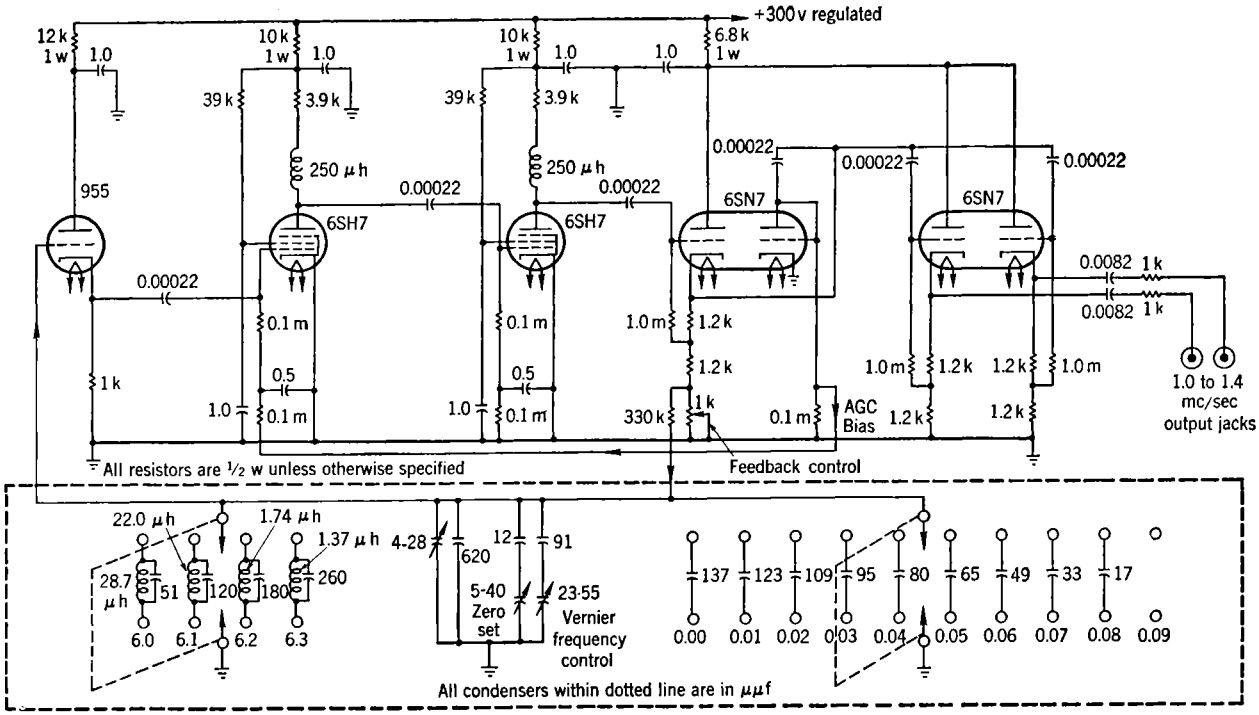

FIG. 6·12.—Tunable oscillator.

filaments of the tubes are operated from a Sola regulating transformer. The tubes are covered with shield cans to minimize the effects of sudden drafts of air.

The output signal of the second video amplifier is coupled to a cathode follower whose high input impedance minimizes the dynamic effects that might cause phase variations at this point. This cathode follower thus isolates the amplifier from the AGC diode and the output cathode followers. The feedback to the tuned circuit is tapped off the load resistor of the cathode follower at a low-impedance point. An isolating resistor whose resistance is large compared to the impedance of the resonant circuit is inserted in the feedback path. The amount of feedback is adjusted by short-circuiting a portion of the 1K potentiometer. In this way the capacitance from the moving contact to ground is eliminated. To minimize phase shift in the feedback lead, the 330K isolating resistor is soldered to the potentiometer. The lead wire to the resonant circuit has capacitance to ground, but this capacitance does not vary and constitutes part of the resonant circuit.

The video amplifiers are designed so that they provide excessive gain when no AGC is applied. The feedback is adjusted to provide about -5 volts of AGC bias, and hence about 5 volts peak of output signal.

This oscillator provides an output signal that is stable to ± 1 cps over long periods of time. Consequently, the accuracy of its contribution to the resultant microwave frequency depends to a large extent on the accuracy to which its relatively low frequency can be determined.

6·9. Audio Interpolation Oscillator.—The frequency of the tunable oscillator is determined by measuring the frequency difference between it and a harmonic of the 2.5-kc/sec submultiple of the crystal-oscillator frequency. Accordingly, the interpolation oscillator must cover a range from 0 to 1250 cps. In order to facilitate the generation of low-frequency signals and to provide good stability, the oscillator is of the beat-frequency type.

Figure 6·13 indicates the circuit details. The two oscillators operate at about 30 kc/sec. Each oscillator is similar to the tunable oscillator described in Sec. 6·8 and the same design considerations apply. The same type of regulated power supply is used and a Sola filament transformer is employed to regulate heater voltage. A General Radio precision condenser is used in the resonant circuit of the variable oscillator so that the tuning rate is 1 cps per dial division.

In order to minimize interaction both oscillators are coupled to a 6SA7 mixer through cathode followers. Interaction between the two oscillators results in their locking to the same frequency as the beat frequency approaches zero. Therefore, in order to generate as low an audio frequency as possible, all components are carefully shielded. In

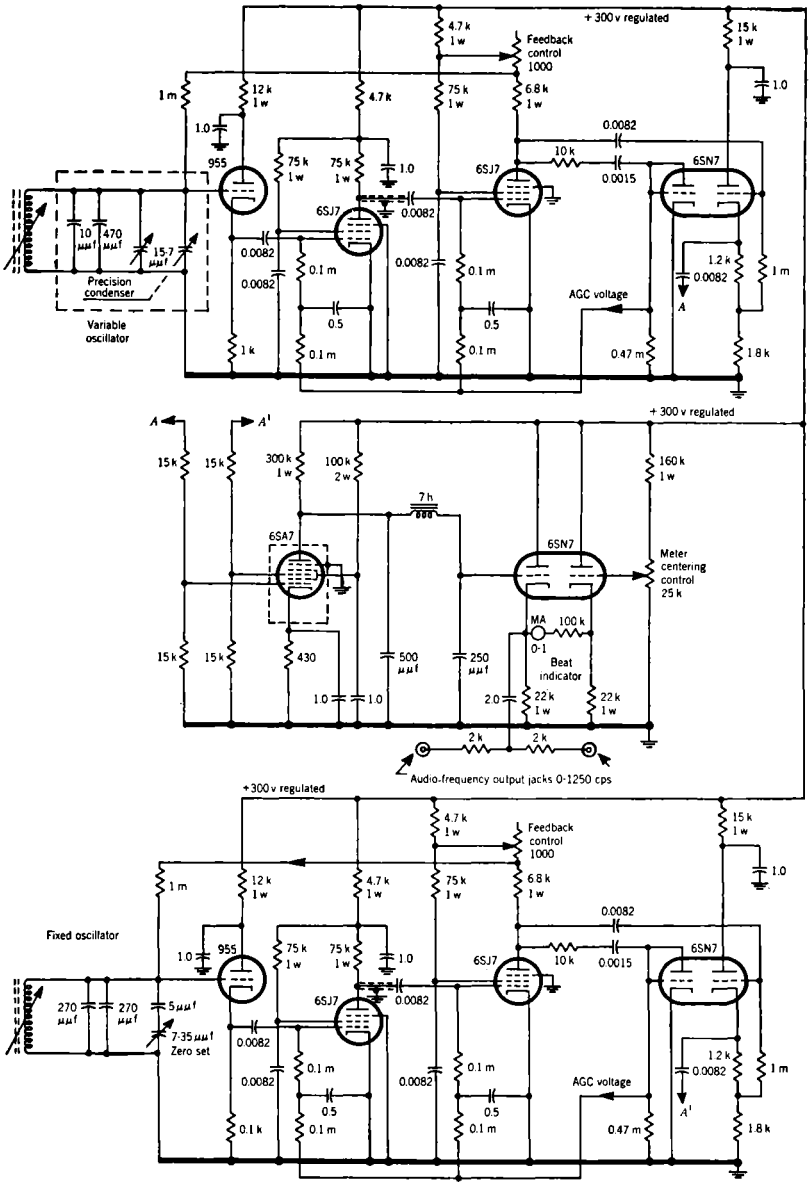

FIG. 6·13.—Audio interpolation oscillator.

fact, the bottom of the chassis is broken up into shielded compartments which separate the components common to each oscillator. Also the input level of each signal applied to the 6SA7 mixer is kept below 2 rms volts to reduce coupling through the mixer.

The output signal of the mixer is coupled to a cathode-follower output stage through a low-pass filter whose high-frequency cutoff occurs at 1500 cps. For low audio frequencies, the mixer is essentially direct-coupled to the cathode follower. Another triode is used in conjunction with the output stage to form a circuit that will indicate zero beat. A meter is connected between the two cathodes, and the grid bias of the

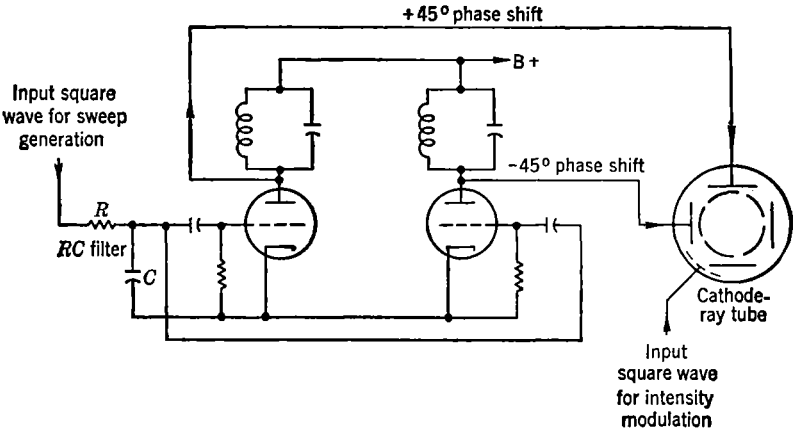

FIG. 6·14.—Comparison-oscilloscope components for checking frequency dividers.

auxiliary triode is adjusted so that the meter deflects either side of midscale.

The oscillator is calibrated every 50 cps by means of Lissajous patterns formed with the 50-cps submultiple of the crystal-oscillator frequency. The precision tuning condenser is sufficiently uniform so that the audio-frequency calibration is known to ± 2 cps. The stability of the oscillator is ± 0.1 cps over long periods of time. In fact, it will be within ± 1 cps of zero beat when first turned on after long inoperative periods.

6·10. Comparison Oscilloscope.—This unit facilitates checking the frequency dividers and calibrating the audio interpolation oscillator and the tunable oscillator. Its functions could be performed by means of a commercial oscilloscope and communications receiver, but the procedure would be much more difficult and time consuming.

Figure 6·14 is a simplified schematic of the components that are used to check correct frequency division. The output square wave of a divider

is coupled to the horizontal and vertical amplifiers of the cathode-ray tube through an *RC*-filter. Consequently, the effective input signal to the amplifiers is essentially the fundamental frequency of the square wave. The amplifiers work into highly reactive loads that are adjusted so that there is a 90° phase shift between the two sine-wave signals that are applied to the deflection plates, thus producing a circular pattern. Simultaneously, the output square wave of the preceding frequency divider is used to intensity-modulate the cathode-ray tube so that the circular pattern is divided into segments whose number is equal to the ratio of the two frequencies. This indication may be interpreted more quickly and easily than the conventional Lissajous figure.

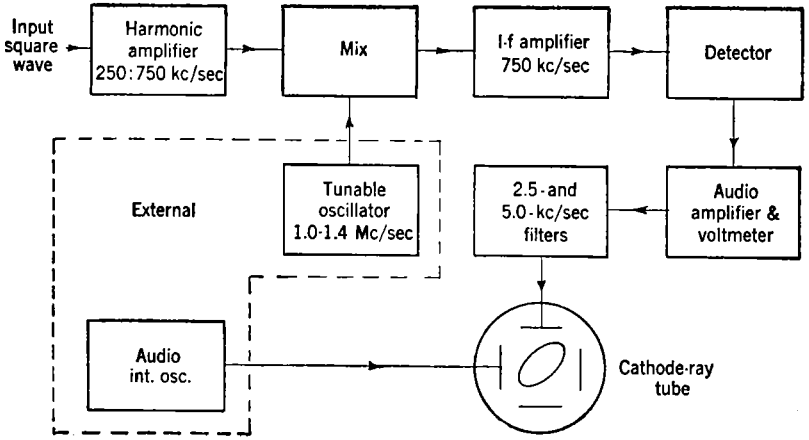

FIG. 6·15.—Comparison-oscilloscope components for tunable-oscillator calibration.

Even a complex Lissajous figure may, however, be used easily to check the calibration of the audio interpolation oscillator. An output square wave from a frequency divider is filtered and amplified so that, for example, a 50-cps signal provides horizontal deflection for the cathode-ray tube. The audio-oscillator signal provides vertical deflection and a Lissajous figure is established. Since the oscillator calibration is accurate to ± 2 cps, the frequency ratio indicated by the Lissajous figure need not be calculated in order to determine the frequency of the check point. That is, if the audio oscillator is tuned until the pattern is stationary, the error in dial calibration is but one or two divisions.

The third and most important feature of the comparison oscilloscope is the circuit that facilitates determination of the tunable-oscillator frequency. Figure 6·15 indicates the functions of the various circuit components. A 2.5-kc/sec square wave from the frequency dividers is coupled to a harmonic amplifier whose pass band is 250 to 750 kc/sec.

Harmonics within this band are coupled to a heterodyne mixer whose local-oscillator signal is supplied by the tunable oscillator. The mixer output signal is coupled to an i-f amplifier which passes frequencies in the range of 750 ±5 kc/sec. Consequently, several frequencies are present in the i-f channel. Some of these frequencies are square-wave harmonics that lie within the i-f pass band and are coupled directly through the mixer to the i-f channel without frequency conversion. Another i-f signal results from heterodyning a square-wave harmonic with the tunable-oscillator frequency. Accordingly, several beat frequencies appear in the detector output signal and hence in the output signal of the audio amplifier. Signals appear at 2.5 and 5 kc/sec and represent difference frequencies between harmonics of the 2.5-kc/sec square wave. These signals are removed by audio filters tuned to 2.5 and 5 kc/sec. Another audio signal appears which is the frequency difference between a square-wave harmonic and the i-f signal produced by heterodyning some other square-wave harmonic with the tunable-oscillator frequency. This audio frequency lies between 0 and 1250 cps and is equal to the frequency difference between the tunable-oscillator frequency and the multiple of 2.5 kc/sec that is nearest to it. Since the tunable oscillator is very stable and since provision is also made to check it against multiples of 5 and 50 kc/sec, the frequency of the nearest multiple of 2.5 kc/sec is readily determined.

The actual frequency of the tunable oscillator is the frequency of the nearest multiple of 2.5 kc/sec plus or minus the audio beat frequency that falls in the range of 0 to 1250 cps. The beat frequency is measured with the audio interpolation oscillator by forming a simple Lissajous figure. In the case of beat frequencies less than 2 cps, a voltmeter attached to the audio amplifier is used to determine the beat note. The meter will indicate zero beat at intervals corresponding to one-half the fundamental frequency of the input square wave. When harmonics of the 2.5-kc/sec square wave are used, the frequency of the tunable oscillator may be determined to the accuracy of the crystal oscillator at intervals of 1250 cps. The circuit details are shown in Fig. 6·16.

In the method described above, the 100th through the 300th harmonics of the 2.5-kc/sec square wave are used. If the tunable-oscillator frequency were compared with square-wave harmonics in an ordinary receiver, the 560th harmonic of 2.5 kc/sec would have to be utilized. Therefore, it is apparent that the heterodyne method reduces the requirements on the square-wave harmonic content and on the frequency response of the associated circuits.

The operation of the equipment could be improved by restricting the pass band of the beat-frequency amplifier that follows the special receiver. The i-f amplifier has a pass band of about 10 kc/sec, and consequently it

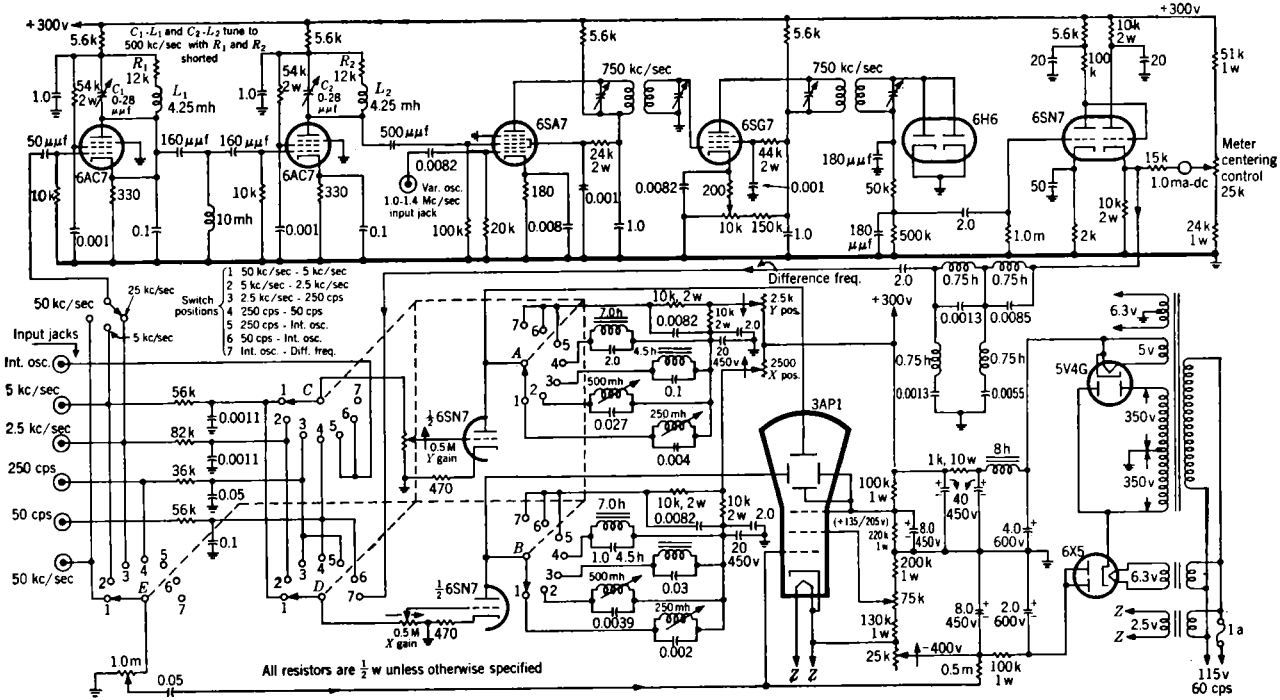

FIG. 6·16.—Comparison-oscilloscope circuit details.

provides nearly equal amplification for the 298th through the 302nd harmonic of 2.5 kc/sec. Similarly, the i-f amplifier will pass five other signals which are produced by heterodyning the tunable-oscillator frequency with lower square-wave harmonics. All of these signals are mixed in the second detector and all possible difference frequencies result. For example, if the tunable-oscillator frequency is 1.0 kc/sec above the nearest multiple of 2.5 kc/sec, audio frequencies of 1.0, 1.5, 2.5, 3.5, 4.0, 5.0, 6.0, 6.5, 7.0, 8.5, 9.0, . . . kc/sec will appear in the detector output signal. If the audio amplifier were cut off sharply at 1300 cps, a much clearer signal would appear on the cathode-ray tube for comparison with the audio interpolation oscillator.

6·11. Variable-frequency Generation.—The variable frequency that is multiplied to the microwave region is generated in the balanced mixer of Fig. 6·17. The output signal from the tunable oscillator is mixed with the 5-Mc/sec multiple of the crystal oscillator to produce a signal that is variable from 6.0 to 6.4 Mc/sec.

The 5-Mc/sec signal is obtained from the frequency multiplier described in Sec. 6·12. The multiplier output signal contains frequencies other than 5 Mc/sec, so a selective amplifier precedes the mixer and provides a pure 5-Mc/sec signal of about 40 volts rms. This signal is coupled to the mixer by means of a cathode follower. The cathode follower is also coupled to an output jack, thus providing a 5-Mc/sec signal for comparison with the standard-frequency broadcast from Station WWV. The resistor in series with the output lead prevents an external short circuit from affecting the mixer.

The mixer consists of two 6SA7 tubes whose plates are coupled in push-pull to a bandpass output circuit. A pass band from 6.0 to 6.4 Mc/sec is obtained by resistive loading and tight coupling to the output line which, in turn, is tightly coupled to the next tuned circuit. The 5-Mc/sec input signal does not tend to appear in the push-pull output circuit since this signal is applied to grids that are driven in phase. The tunable-oscillator signal is applied to mixer grids that are driven in push-pull by a triode phase inverter, but this frequency does not appear in the output signal because of the plate-circuit selectivity. In fact, since the 5-Mc/sec signal is eliminated by balancing the mixer, the plate-circuit selectivity is completely adequate to remove all other undesirable frequencies from the output signal.

6·12. Basic Types of Vacuum-tube Frequency Multipliers.—Vacuum-tube multipliers are essentially Class C r-f amplifiers in which the plate circuit is resonant at some multiple of the input frequency. Class C operation is preferred because of the high harmonic content of the resultant plate-current pulse. Multiplication can be performed by factors up to 5 before the harmonic content of the output signal is so low that the

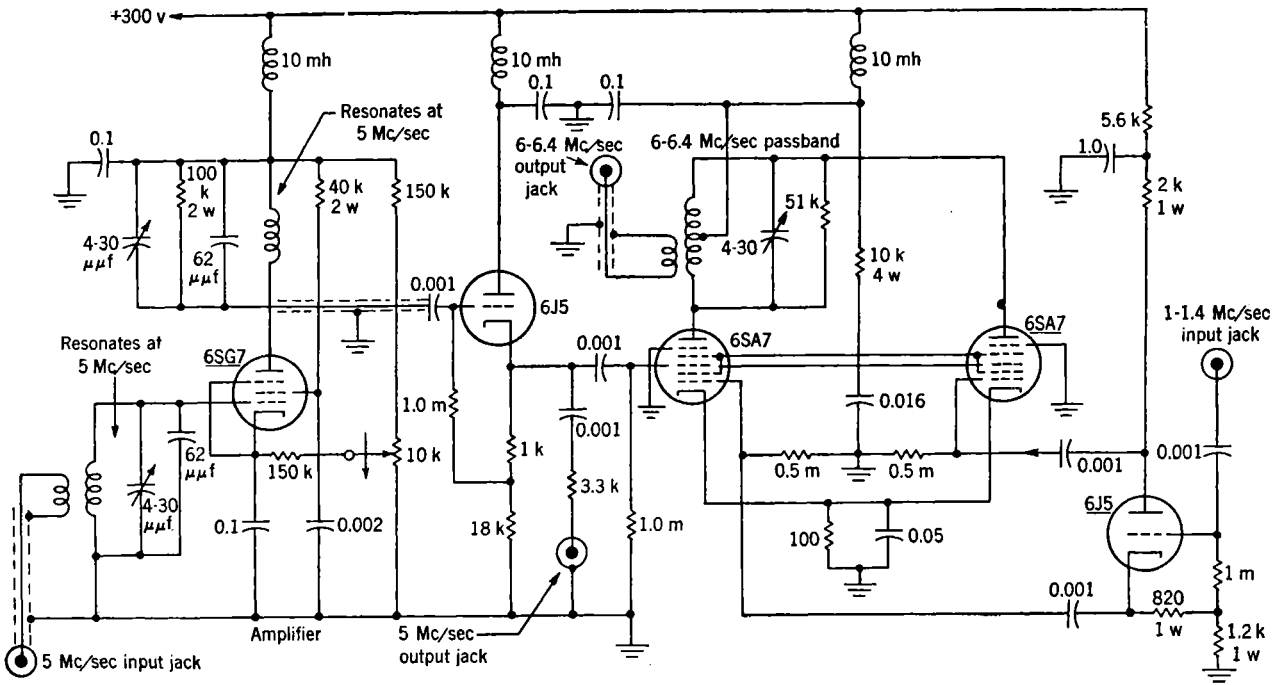

FIG. 6·17.—Variable-frequency generation

plate circuit can no longer discriminate successfully against the fundamental frequency and other harmonics. The elimination of these undesirable frequencies is very important since they produce cross-modulation in the next multiplier, and spurious microwave signals result. For example, if the first multiplier is a quadrupler whose input frequency is 5 Mc/sec, inadequate plate-circuit selectivity will result in output frequencies at 15 and 25 Mc/sec as well as at 20 Mc/sec. Since the next multiplier—in this case a quintupler—is also a nonlinear device, it will

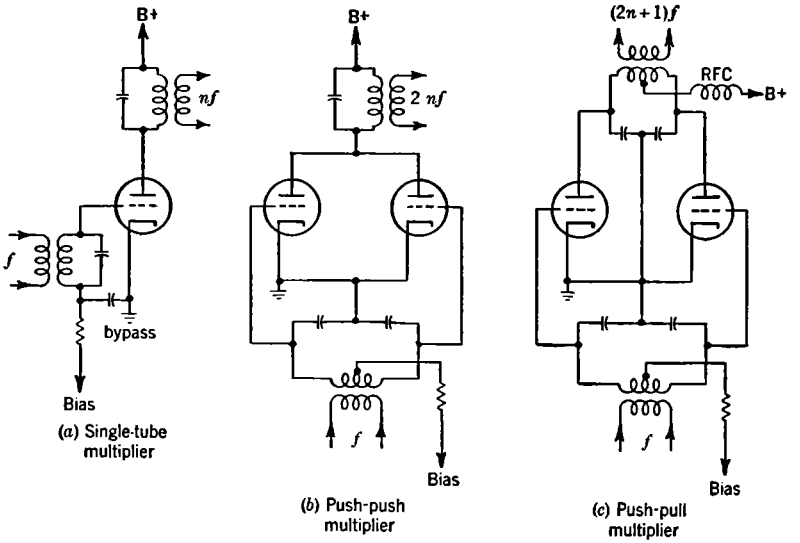

FIG. 6·18.—Basic types of frequency multipliers.

detect difference frequencies of 5 and 10 Mc/sec. These difference frequencies will modulate the output signal to produce a spectrum that contains frequencies of 90, 95, 100, 105, and 110 Mc/sec. This process is repeated in successive multipliers until the microwave output signal is not a single frequency but a series of indistinguishable frequencies that occur at 5-Mc/sec intervals. It is apparent from this example that selectivity is most important in the early stages of multiplication. Fortunately, the early multipliers operate in a frequency range where loosely coupled circuits and selective amplifiers may be used easily to improve discrimination.

The simplest multiplier is the single-tube circuit of Fig. 6·18. Sufficient fixed bias is provided so that the tube does not exceed its rated dissipation when the excitation is removed. When excitation is supplied, the resistance of the grid leak is adjusted so that the self-bias provides

optimum harmonic generation at the output frequency. Since all harmonics of the input frequency tend to appear in the output signal, a high-Q plate circuit is a prerequisite for successful operation.

Increased discrimination and output power are realized by the push-pull and push-push circuits of Fig. 6·18. In the case of the push-pull multiplier, all even harmonics of the input frequency are canceled in the output circuit; hence, a multiplier of this type is well suited for triplers and quintuplers. Also the push-pull circuit performs well at high frequencies since the effective output capacitance is one-half that of a single tube.

The push-push multiplier is so named because like current pulses flow through the plate circuit corresponding to each half cycle of the input frequency. Push-push operation is used for doublers and quadruplers since only even harmonics tend to appear in the output signal. The circuit is seldom used for vhf multipliers since the effective output capacitance is twice that for a single tube. Only a very small inductance is needed to resonate with this large output capacitance above 100 Mc/sec, and the resultant Q and selectivity are rather poor.

6·13. Frequency Multipliers from 50 kc/sec to 5 Mc/sec.—The crystal-oscillator frequency is multiplied to 5 Mc/sec by means of a push-push quadrupler followed by two push-pull quintuplers. The circuit details are shown in Fig. 6·19. The push-pull drive for the quadrupler is obtained from a triode phase inverter. A resistor is placed in series with the lead from the phase-inverter cathode in order to equalize the driving impedances for the two halves of the quadrupler. The plate circuit is resonant at 200 kc/sec and is link-coupled to the next multiplier, a quintupler.

The two quintuplers are alike except for their tuned circuits. All coils are made by winding a single layer of heavy copper wire on a polystyrene rod. All tuned circuits are shielded to minimize spurious coupling of undesirable frequency components. The 6AG7 tubes provide sufficient amplification so that the interstage coupling is relatively small, the tuned circuits are relatively independent, and the selectivity is reasonably good.

6·14. Frequency Multipliers from 6 to 24 Mc/sec.—The two push-push doublers of Fig. 6·20 are used to raise the variable frequency from the region 6.0 to 6.4 Mc/sec to the region of 24.0 to 25.6 Mc/sec. The output signal of the mixer, which generates the variable frequency, is coupled to an r-f amplifier that provides sufficient driving signal for the first doubler. Again 6AG7 tubes are employed and the stages are link-coupled. Except for the r-f amplifier input circuit, all resonant circuits are provided with front-panel tuning controls whose calibrations are sufficiently accurate to eliminate the necessity of tuning indicators.

The r-f amplifier provides an output signal in the range from 6.0 to

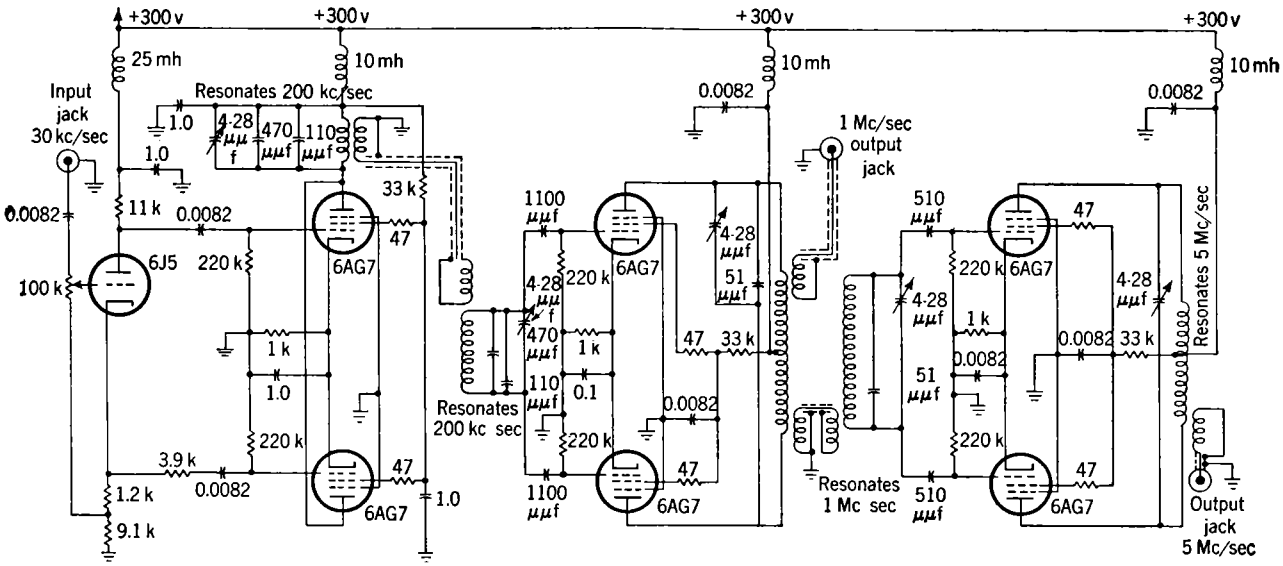

FIG. 6·19.—Frequency multipliers from 50 kc/sec to 5 Mc/sec.

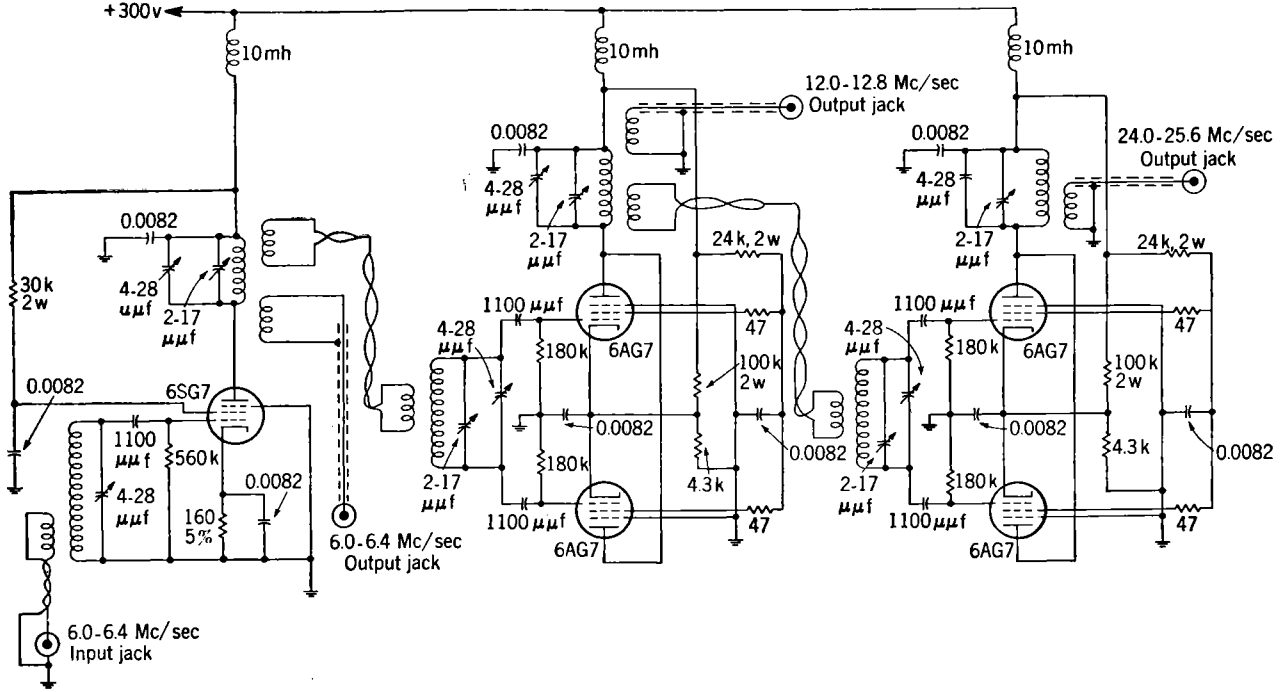

FIG. 6·20.—Frequency multipliers from 6 to 24 Mc/sec.

6.4 Mc/sec; the first doubler provides a signal in the range from 12.0 to 12.8 Mc/sec; the second doubler provides an output signal in the range from 24.0 to 25.6 Mc/sec.

6·15. Frequency Multipliers from 24 to 96 Mc/sec.—Two push-push doublers are employed to multiply 24 Mc/sec by a factor of four. In this frequency range, 832 twin-tetrodes are used because their input and output capacitances are approximately one-half those of the 6AG7 pentode. Also, the 832 tube has an internal bypass condenser for the screen grids. The use of an external condenser often causes instability.

Circuit details are shown in Fig. 6·21. All resonant circuits are tunable from the front panel, and small pilot lamps are coupled to the circuits for visual tuning indication. Tuning indication of this type is much easier to use than a d-c ammeter, especially in plate circuits.

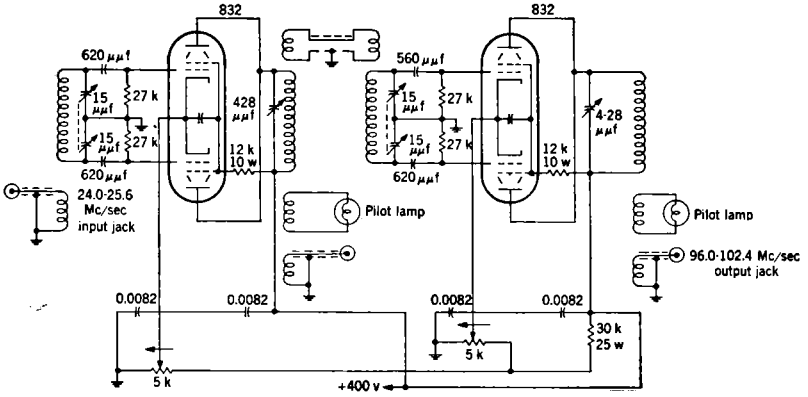

FIG. 6·21.—Frequency multipliers from 24 to 96 Mc/sec.

The first doubler provides an output signal in the range 48.0 to 51.2 Mc/sec; the second doubler provides an output signal in the range from 96.0 to 102.4 Mc/sec.

6·16. Frequency Multiplier from 96 to 288 Mc/sec.—In this frequency range the push-pull tripler of Fig. 6.22 is used in order to obtain the low output capacitance offered by push-pull operation. The input circuit employs a self-supported three-turn coil as inductance for the resonant circuit. The plate circuit employs a short-circuited transmission line which appears inductive and resonates with the combined capitance of the tubes and a split-stator tuning condenser. This condenser is mounted as close as possible to the plate leads emerging from the 832 envelope. The resonant lines are made from $\frac{1}{4}$-in. silver-plated rods which are spaced about 2 in. apart. The length of the resonant section is about 4 in.

Both the grid and plate circuits are tunable from the front panel, and

two pilot lamps are coupled to the resonant circuits for tuning indication. The grid circuit is below the chassis; the plate circuit, above the chassis. Both circuits are completely shielded to minimize radiation and pickup. The output signal is in the range from 288.0 to 307.2 Mc/sec.

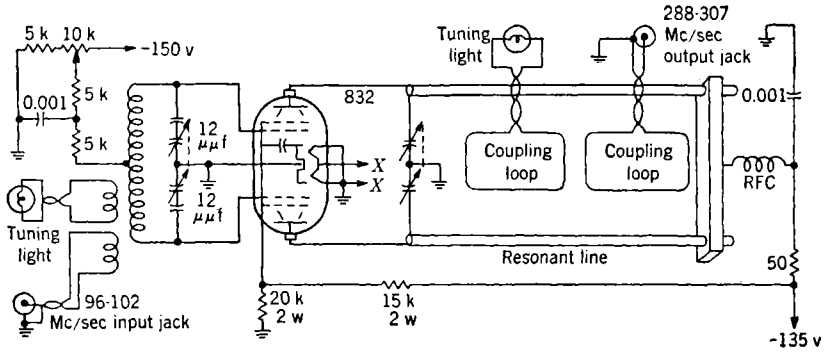

FIG. 6-22.—Frequency multipliers from 96 to 288 Mc/sec.

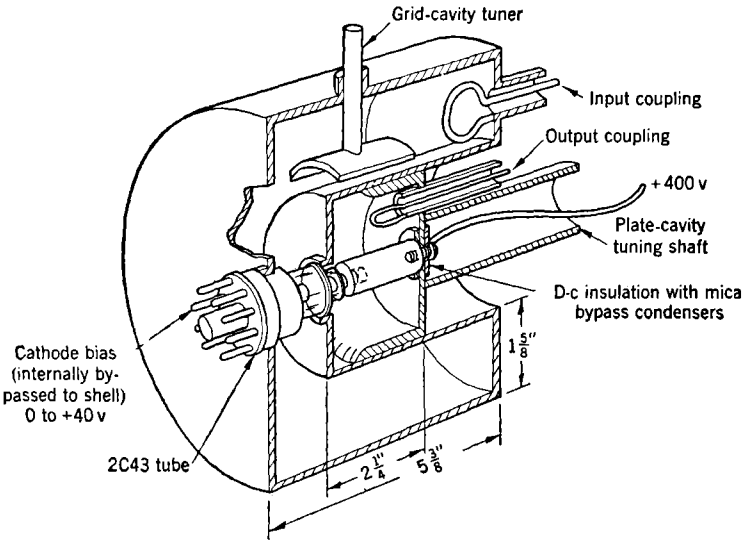

FIG. 6-23.—Frequency multipliers from 288 to 864 Mc/sec.

6-17. Frequency Multiplier from 288 to 864 Mc/sec.—A single-tube tripler is used in this region and employs a 2C43 lighthouse triode with coaxial grid and plate cavities. The details are shown in Fig. 6-23.

The grid circuit is formed by a section of $5\frac{1}{4}$-in. diameter tubing connected to the tube shell, and by a section of 2-in. diameter tubing con-

nected to the grid. Thus, the grid circuit is equivalent to a short-circuited coaxial line whose outer conductor is connected to the triode cathode and whose inner conductor is connected to the triode grid. Both conductors of the coaxial line have contact fingers to provide good connections with the tube that is inserted through the outer conductor. Grid excitation is supplied through a large coupling loop near the short-circuited end of the cavity. Tuning is accomplished by moving a curved plate toward, or away from, the inner conductor of the line. A front-panel control rotates a cam which, in turn, moves the rod supporting the tuning plate. Bias is applied to the cathode since the grid is at ground potential. It is insulated from, and bypassed internally to, the shell of the tube.

The plate circuit is formed by a section of 2-in.-diameter tubing connected to the triode grid and by a section of $\frac{1}{2}$-in.-diameter rod connected to the triode plate. The plate circuit is equivalent to a short-circuited coaxial line whose outer conductor is connected to the triode grid and whose inner conductor is connected to the triode plate. At the output frequency the grid circuit offers little impedance and the grid is essentially at a-c cathode potential. Thus, the plate cavity is nearly equivalent to a resonant circuit connected between plate and cathode. This circuit is tuned by varying the length of the short-circuited coaxial line. Actually the outer conductor is formed by two cylinders of nearly the same diameter, one sliding within the other. A good electrical connection between the two cylinders is ensured by means of contact fingers. Voltage is supplied to the triode plate through the inner conductor of the coaxial line. This conductor is insulated from, but bypassed to, the outer conductor at the plate that short-circuits the r-f line. Since the inner conductor is fastened rigidly to the outer conductor, beryllium-copper fingers are provided so that the inner conductor can slide with respect to the triode plate cap when the cavity is tuned. Only $\frac{1}{4}$ in. of axial movement is required to cover the range from 864.0 to 921.6 Mc/sec. Consequently, a micrometer drive is used to control this movement.

The output signal is coupled inductively from the plate cavity by a loop and is applied to a crystal-rectifier harmonic generator through a filter which makes it possible to monitor the rectified current.

6·18. Harmonic Generation by Crystal Rectifiers and Velocity-modulated Frequency Multipliers.—The last step in frequency multiplication to the microwave region is accomplished by harmonic generation in a silicon crystal. Crystal rectifiers of types 1N21, 1N23, and 1N26 are employed and mounted in holders similar to those used for microwave mixers. The vhf signal is applied to the crystal through the i-f output jack of the mount, and microwave harmonics of this signal are propagated down the microwave transmission line. If this is a coaxial line, stub supports serve as filters to remove the input frequency and its first few

harmonics. If the transmission line is waveguide, its own transmission characteristics provide adequate filtering. In practice, the 10th through the 50th harmonics of the vhf input signal have been used. The Radiation Laboratory standard utilizes the 15th through the 43rd harmonics of the output signals from the various vacuum-tube frequency multipliers. Experience has shown that in this range the harmonic amplitude is inversely proportional to the harmonic number. Microwave output powers of -50 to -70 dbw are obtained if the vhf input power is sufficient to produce 50 to 80 ma of rectified current.

Since the output signal from a crystal recfifier contains a series of microwave frequencies, a transmission frequency meter or cavity may be inserted in the output line to discriminate against unwanted harmonics. A low Q and an approximate frequency calibration can be tolerated as long as low insertion loss and a wide tuning range are realized.

Klystron triplers may also be used for frequency multiplication.[1] These tubes are similar to double-cavity klystrons except that the catcher cavity is resonant at the third harmonic of the buncher cavity. If a submultiple of the input frequency is applied to the accelerating grid, the tube is phase-modulated. Consequently, a series of microwave frequencies appear in the output signal, their number and amplitude being dependent on the Q of the output cavity and the index of modulation. Although a frequency multiplier of this type provides a larger power than does the crystal rectifier, the alignment of the cavities is critical, and the multiplier is difficult to use.

TABLE 6·2.—FREQUENCY RANGE COVERED BY HARMONIC GENERATION

Input frequency, Mc/sec		Output frequency, Mc/sec		Harmonic	
Min	Max	Min	Max	Min	Max
6.0	6.4	90.0	185.6	15	29
12.0	12.8	180.0	371.2	15	29
24.0	25.6	360.0	742.4	15	29
48.0	51.2	720.0	1484.8	15	29
96.0	102.4	1440	4403	15	43
288.0	307.2	4320	13209	15	43
864.0	921.6	12960	32256	15	35

[1] E. Ginzton, A. Harrison, R. Hatch, "A Frequency Standard in the Microwave Region," Report 105-5220, Measurements Development Laboratory, Research Laboratories, Sperry Gyroscope Company, Inc., Feb. 20, 1943; E. Feenberg, "Bunching Theory for Two Resonator Klystron Multipliers," Report 5221.117, Tube Development Laboratory, Research Laboratories, Sperry Gyroscope Company, Inc., May 23, 1944.

6·19. Frequency Range and Accuracy.—By utilizing harmonics of all frequencies in the multiplier chain, the Radiation Laboratory standard provides complete coverage from 90 to 32,000 Mc/sec. Table 6·2 indicates how this coverage is attained.

Since microwave signals are generated by frequency multiplication of a signal that is variable from 6.0 to 6.4 Mc/sec, the useful accuracy of the standard depends on the stability and accuracy of measurement of this variable frequency. Table 6·3 indicates the maximum uncertainty, in cycles per second, in the variable frequency, that are contributed by the various components. According to the table, the standard-frequency signals are accurate to at least ± 1.1 parts in 10^6. That is, a 3000-Mc/sec signal is known to ± 0.003 Mc/sec; a 9000-Mc/sec signal, to ± 0.01 Mc/sec; and a 27,000-Mc/sec signal, to ± 0.03 Mc/sec. The probable errors are, of course, much less than these maximum uncertainties.

TABLE 6·3.—UNCERTAINTY OF 6-MC/SEC VARIABLE FREQUENCY

Contributing factors	Uncertainty, cps
Stability of crystal oscillator	± 2.5
Mean frequency of crystal oscillator	$+1$
Stability of tunable oscillator	± 1
Stability of audio interpolation oscillator	± 0.1
Frequency of audio interpolation oscillator	± 2
Maximum uncertainty	± 6.6
Probable uncertainty	± 3.5

RESONANT CAVITIES AS SECONDARY FREQUENCY STANDARDS

Resonant cavities are ideally suited for secondary frequency standards since they are simple, compact, portable, and relatively inexpensive. During the war they were used almost exclusively for the production-line calibration of frequency meters, beacon-frequency reference cavities, and AFC cavities. Because of their compactness and portability, they were used to check the alignment of equipment in the field. Despite this usefulness, however, many existing cavity designs will prove inadequate as peacetime laboratory standards because they are subject to temperature and humidity effects. At the close of the war the ideal cavity had not been realized, but new developments indicate that much improved models are feasible.

6·20. General Design Considerations.—In order to be considered a standard of frequency, the resonant frequency of a cavity must remain unchanged despite the physical and electrical conditions imposed upon it. Temperature compensation or thermostated ovens must be employed to avoid frequency changes resulting from expansion or contraction. A small change in cavity dimensions produces a large change in resonant frequency. Consequently, temperature compensation is successful only when close tolerances and uniformity of materials are maintained. It is

difficult enough to obtain uniform raw materials, but it has been even more difficult to reproduce, cavity to cavity, the effects of machining, soldering and aging. Manufacturing processes not only change the characteristics of the basic materials, but also introduce unknown small quantities of other materials and strains which are not relieved even after several temperature cycles. A thermostated cavity avoids the difficulties of temperature compensation but results in a bulky device that is not readily moved from place to place.

In addition to temperature effects, humidity effects must be eliminated since the water-vapor content of the air within the cavity affects the dielectric constant and thereby affects the resonant frequency. Sealing and subsequent evacuation is the best, but the most difficult, solution to the humidity problem. Cavities usually include a tuning mechanism as well as one or more couplings. All these openings must be sealed, but it is highly desirable that the cavity remain tunable after sealing. Sealing techniques must not affect temperature compensation or introduce strains, and no hygroscopic material may be used within the cavity. All seams and joints must be vacuum tight if absolute freedom from humidity effects is expected.

In order to be most useful and to minimize production costs, a standard-cavity design should provide tuning over a wide frequency range with fairly uniform electrical characteristics. Loaded Q and transmission loss (or input conductance) must always provide a sharp resonance indication at the frequency of the signal transmitted through (or past) the cavity. This effect is achieved by properly placing the coupling loops or holes so that, as the cavity is tuned across the band, coupling changes compensate changes in unloaded Q. A sharp resonance indication requires a high loaded Q, which may be realized by loose coupling to a cavity of high unloaded Q. Although loose coupling increases the loaded Q and minimizes frequency pulling by external loads, transmission loss is increased accordingly.

Sensitive measuring equipment can tolerate considerable loss through a cavity, however, and a sharp resonance indication and freedom from frequency pulling are the most important characteristics. The resonant mode should provide a loaded Q sufficiently high so that the corresponding pass band is not more than 10 times the desired accuracy.[1] Also a mode should be chosen which allows a simple tuning mechanism that does not introduce uncertain electrical contacts at high-current points. Once a cavity design is chosen, it should be examined to determine the frequencies at which the cavity will resonate in other modes. The cavity should be free of the effects of other modes throughout its frequency range and

[1] The accuracy of resonant-frequency measurement is discussed in Sec. 6·28.

preferably mode-free over the frequency range of the oscillator with which it is used.

False responses can be minimized by selectively absorbing energy from the undesired modes without interfering with the desired mode. However, absorbing material must be nonhygroscopic in order to avoid humidity effects. Another mode-suppression technique employs slots or gaps which are cut in the cavity and thereby change its effective dimensions for the undesired modes. Accordingly, the cavity may be made resonant in these modes at frequencies well outside the operating range.

In summary, a standard cavity should provide a high loaded Q, low transmission loss, small couplings to external loads, a simple tuning mechanism, a broad tuning range, freedom from the effects of other modes, temperature compensation, and vacuum-tight seals for freedom from

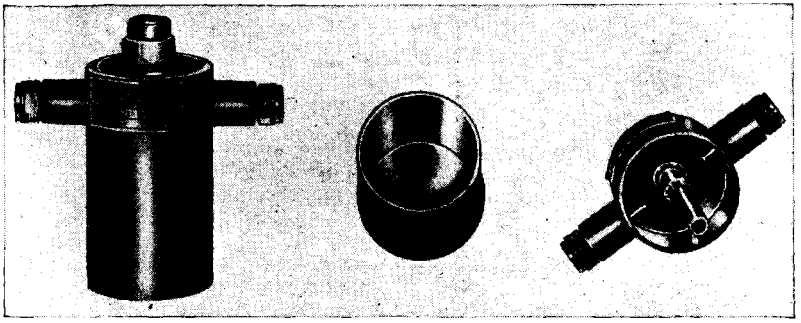

FIG. 6·24.—Partial-coaxial standard cavity.

humidity effects. A practical design must effect a compromise between satisfying these many requirements and avoiding the consequent difficulties of manufacture.

6·21. Partial-coaxial Cavities.—The cavity shown in Figs. 6·24 and 6·25 approximates a three-quarter-wavelength short-circuited coaxial line that has a lumped capacitance added to the open end.[1] This design is used to cover the frequency range from 2700 to 3400 Mc/sec by employing two models of different lengths. Production models were designated TFS-10 and were used primarily as beacon-reference and filter cavities. However, they also represent the most satisfactory standard-cavity design that has been developed for this frequency range.

As shown in Fig. 6·25, the cavity is tuned by varying the length of the center conductor. The tuning rate varies from 750 to 1500 Mc/sec per in. of shaft motion. Contact fingers are placed at a low-current point, approximately one-quarter wavelength from the short-circuited end of the cavity. The effective electrical position of the fingers varies with fre-

[1] This mode is described in Chap. 5.

quency, however, and, in order to keep them always in a low-current region, two cavities of different lengths were designed. The short cavity is tunable from 3000 to 3400 Mc/sec; the long model, from 2700 to 3050 Mc/sec. The contact fingers are one-quarter wavelength from the short-circuited end at 2850 and 3200 Mc/sec for the long and short models, respectively. Also, the long and short cavities have their coupling loops

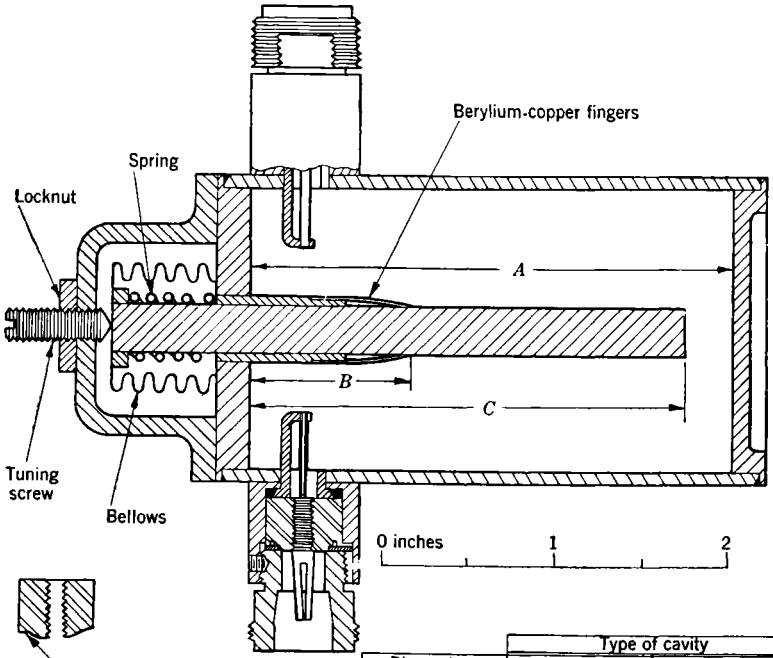

Dimensions		Type of cavity	
		Short	Long
A		2.870	3.406
B		0.915	1.050
C	Min.	1.970	2.506
	Max.	2.570	3.106

FIG. 6-25.—Mechanical dimensions for TFS-10 cavities.

and relative dimensions chosen so that together they provide a wide frequency range without unreasonable variations in Q and transmission loss.

The unloaded Q of this cavity is about 6000 if the interior is silver-plated and the contact fingers are made of heat-treated beryllium-copper. Depending on the orientation of the coupling loops, the loaded Q will lie between 650 and 3000. When the loops are oriented for standard-cavity use, a loaded Q of 3000 and a transmission loss of 6 db result.

An approximate temperature compensation has been achieved by

making the body of the cavity from ordinary steel and the center conductor from invar steel. The resultant frequency shift with temperature is about +5 kc/sec per degree C, the cavity being somewhat overcompensated. This overcompensation could be reduced by simply making part of the invar center conductor from brass or from the material of the body, steel. The preferable method for temperature compensation is that described in Sec. 6·25.

The cavity is sealed for evacuation by soldering a spring-loaded bellows around the tuning mechanism and by using glass beads to support the coupling loops. These beads provide a Kovar-glass seal at both the inner and outer conductors, and were manufactured by the Corning Glass Company. However, the use of glass beads, instead of the conventional polystyrene bead, introduces an impedance transformation that reduces the effective coupling-loop area. Loops that provide an insertion loss of 6 db with polystyrene beads provide a loss of 10 db with glass beads.

From the standard-cavity viewpoint, the most serious defect of the present design is the coaxial fittings. Waveguide is large and cumbersome in this frequency range, hence the use of 50-ohm coaxial cables. The connectors of both the cables and the cavity wear and cause large and unreproducible impedance mismatches, and the resultant frequency pulling is significant. It might be advisable to provide resistive padding between the cavity coupling loops and the coaxial connectors. The padding might well be in the form of a lossy center conductor that is made by evaporating metal on glass.[1] Although at first thought the use of padding may seem undesirable, this is a false impression since at least 10 db and preferably 20 db of attenuation should be provided on each side of the cavity in order to isolate it from the oscillator and the detector when making reliable frequency measurements. It is obviously advantageous to incorporate this padding as an integral part of the cavity.

6·22. TE_{011}-mode Cavities.—Right-cylindrical cavities that operate in the TE_{011}-mode have been used extensively in the frequency range from 7900 to 9700 Mc/sec. They are easy to construct and can be provided with a simple tuning mechanism that does not require the use of contact fingers. However, cylindrical cavities do support more than one resonant mode, even over relatively small frequency ranges, and hence require mode-suppression techniques.

All cavities of this type are tuned by the axial movement of a piston which constitutes one end of the cylinder. A small gap about $\frac{1}{16}$ in. between the piston and sidewall does not affect the operation since no currents flow across the corners of the TE_{011}-mode cavity. A standard micrometer thread is usually used to provide uniform motion. Vernier tuning is achieved by threading a rod through the main tuning shaft so

[1] Metalized-glass attenuators are discussed in Chap. 12.

that the end of the rod projects into the cavity from the piston. The tuning rate depends on the effective amount of the rod that is in the cavity. Since there are no radial currents across the end of a TE_{011}-mode cavity, contact fingers between the rod and piston are unnecessary. In practice a $\frac{1}{32}$-in. gap is left between the two parts. The double tuning mechanism, however, does not lend itself to standard sealing techniques. The simplest method for sealing the tuning mechanism is the spring-loaded bellows described in Sec. 6-21 for the TFS-10 cavity. If vernier tuning is desired, a second screw with fine, ground threads may be inserted through the main tuning screw.

The cavity may be inductively coupled to external loads in two ways. In the first method, which applies to either a transmission or a reaction cavity, waveguide is butted against a circular iris in the side of the cavity so that the broad dimension of the waveguide is parallel to the axis of the cylinder. The distance from the cavity to the waveguide flange is important only for the reaction cavity. This cavity is usually coupled to the main transmission line by means of a waveguide T. The effective distance between the cavity and the transmission line is made one-half wavelength so that resonance produces a reduction in power delivered to the load.

The second method of coupling applies only to the reaction cavity. The cavity and waveguide are milled and soldered together so that the circular iris is centered on the broad face of the waveguide. The axis of the cylinder is parallel to the broad dimension of the waveguide, and the effective distance between the cavity and the waveguide is zero. Thus the frequency sensitivity of the T-method is avoided. A small inductive post in the waveguide below the coupling iris will help to compensate for the impedance mismatch produced by the hole when the cavity is not resonant.

The coupling irises are usually sealed by soldering Kovar-glass disks over the holes on the outside of the cavity. Since this operation is done after the waveguide has been hard-soldered to the cavity, it is difficult to obtain a tight joint. Induction-heating techniques have been used to provide localized heating for this soldering operation.

The TE_{011}-mode cavity has a theoretical unloaded Q of about 30,000, if the inside surface is silver. Practical cavities have an unloaded Q of about 20,000. The inability to achieve the theoretical Q remains unexplained. Perhaps the buffing operations are imperfect and the silver-plated interior is not sufficiently uniform. Naturally the cavities are not perfectly symmetrical. The effect of the degenerate TM_{111}-mode associated with the TE_{011}-mode is unknown but may be appreciable. Measurements have shown that apparently identical cavities have unloaded Q's which vary from 15,000 to 25,000. The conventional coupling holes

of $\frac{1}{4}$-in. diameter load the cavity so that a loaded Q of about 10,000 and a transmission loss of about 6 db are realized. As in the case of the TFS-10 cavity discussed in Sec. 6·21, it is recommended that resistive attenuators of at least 10 db be attached permanently to the cavity.

Spurious-mode suppression is the major problem for TE_{011}-mode cavities. Because of their symmetry, they will resonate at several frequencies within the range of the oscillators that are used to excite them.[1] A slight separation of the TM_{111}- and TE_{011}-modes may be achieved by spherical curvature of the end of the cavity. In many production models, a polyiron disk was attached to the back of the piston. Energy

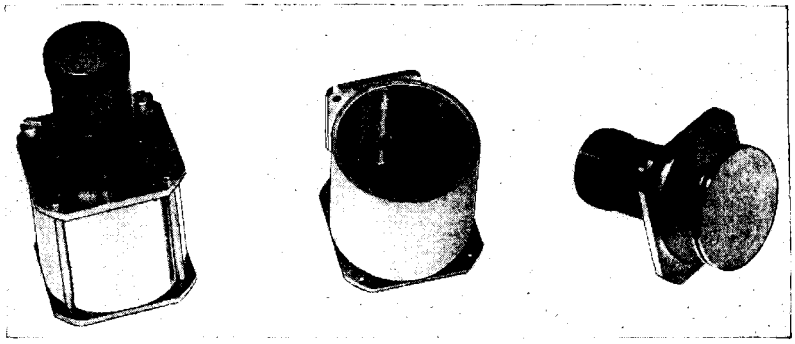

FIG. 6·26.—TE_{011}-mode cavity covering the frequency range from 7900 to 8500 Mc/sec

that is coupled into the back cavity is absorbed by the polyiron disk, if electric currents tend to cross the gap between piston and sidewall. However, the use of polyiron proved unsatisfactory in sealed cavities since the polyiron occluded water vapor. Perhaps a metalized-glass plate similar to those used in resistive attenuators would provide a satisfactory, nonhygroscopic absorber for the back cavity.

The cavity shown in Fig. 6·26 employs a choke cut in the edge of the piston in order to shift the TE_{311}-mode approximately 100 Mc/sec. This is a typical example of an undesired mode that causes trouble even though shifted outside the calibrated frequency range of the cavity. When the micrometer is set for resonance at 7900 Mc/sec in the TE_{011}-mode, the cavity is also resonant in the TE_{311}-mode at 8560 Mc/sec, just outside the calibrated range. An oscillator designed for use in this band will probably tune to 8560 Mc/sec. If so, the cavity can indicate falsely that the oscillator is at 7900 Mc/sec. Since this type of error can be very costly, it is often advisable to measure the approximate wavelength with, for instance, a coaxial wavemeter or slotted section.

Over a very narrow range of frequencies, some undesired modes can be shifted by making the back cavity resonant. As seen from the main

[1] Modes which may exist in cavities are discussed in Chap. 5.

cavity, the gap between piston and wall represents a high impedance that shifts modes which require currents across the cavity corners. In the case of transmission cavities, the relative orientation of the input and output coupling holes can be used to minimize transmission in nonsymmetrical modes.

Successful temperature compensation[1] of these cavities was never realized because they did not exhibit reproducible expansion characteristics. Standard cavities were made originally from all-invar parts except for

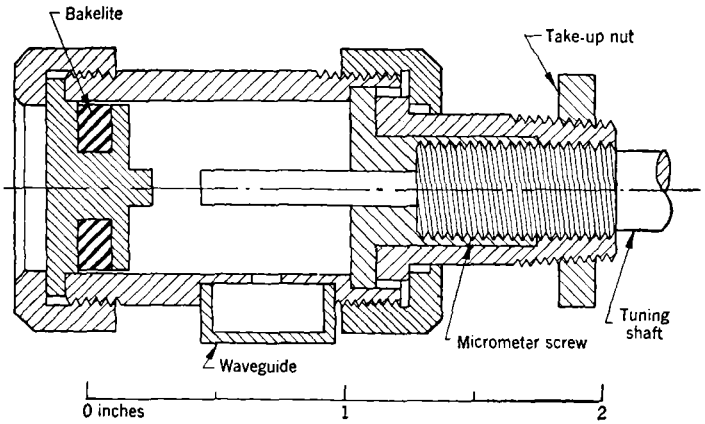

FIG. 6·27.—Hybrid TE_{011}-mode cavity.

the waveguide and its flanges. The cavities behaved, however, as if they were made from a material whose coefficient of expansion was two to four times that of invar. Many factors can be involved. Time did not always permit aging the invar as recommended by its manufacturer. Hard-soldering requires that the cavity be heated until cherry red. Invar is a critical material and slight changes in composition, as may result near the soldered joints, will change its characteristics. The brass waveguide and flanges may introduce unknown strains during changes in temperature. As a result compensation by inserting a section of brass in the tuning shaft was not reproducible.

6·23. Hybrid TE_{011}-mode Cavities.—These cavities are used in the frequency range from 23,500 to 24,500 Mc/sec and differ from the ordinary TE_{011}-mode cavity in that the field configuration[2] is slightly distorted by coaxial rods which are attached to the ends of the cavity as indicated in Fig. 6·27. The cavity is tuned by varying the insertion

[1] Section 6·24 discusses the temperature coefficient of frequency for a TE_{011}-mode cavity.

[2] The hybrid TE_{011}-mode is discussed in Chap. 5.

of one of these rods. The tuning rate is fairly linear, and simple, direct-reading dials can be utilized for frequency meters.

Spurious modes have been discovered in this cavity, despite the Bakelite absorber that is coupled to the cavity by means of a narrow gap which does not affect the operating mode. Also, a mode-crossing was observed which produced an uncertain resonance indication over a small part of the tuning range. One experimenter removed this mode-crossing by omitting the short, fixed coaxial rod, and reported that no other detrimental effects were introduced.

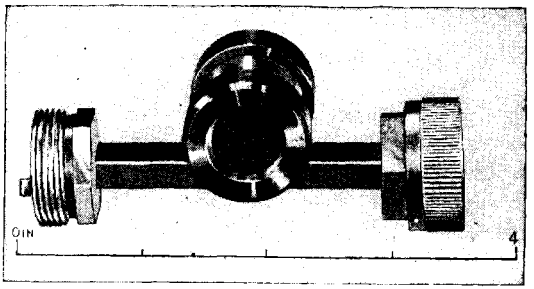

FIG. 6·28.—Standard cavity for the frequency range from 23,500 to 24,500 Mc/sec.

The only standard-cavity design using this mode is shown in Fig. 6·28. It is an all-invar cavity, but is unsealed and uncompensated for thermal expansion. Five fixed-tuned models were built with tuning rods of various lengths so that the resonant frequencies were distributed uniformly throughout the frequency range. The cavities are mounted directly on the broad face of the waveguide to produce a reaction resonance indication. The mounting is like that described in Sec. 6·22 for the TE_{011}-mode cavities, except that a capacitive, rather than an inductive, post is used to match out the reactance of the coupling hole. The coupling-hole diameter is about $\frac{1}{8}$ in., and the resultant loading reduces the unloaded Q of 15,000 to a loaded Q of about 6000.

No transmission cavities have been built but the same size coupling hole would serve equally well. Because of the small hole size, it probably would be simpler to seal the waveguide than the cavity. Kovar-glass seals could be placed between metalized-glass attenuators and the cavity. In this way, the frequency-pulling caused by the seals would be a permanent effect, and the combined mismatches of the seals and the cavity would be isolated from the generator and detector by the pads. The sealed tuning mechanism could be of the spring-loaded-bellows type as was suggested for the partial-coaxial cavities. In any case, the Bakelite absorbing material should be replaced by a nonhygroscopic absorber such as metalized glass. Temperature compensation could be achieved by

using external differential expansion to move the tuning shaft as discussed in Sec. 6·25.

TEMPERATURE AND HUMIDITY EFFECTS FOR STANDARD CAVITIES

The resonant frequencies of some cavities can change as much as 1 part in 10^3 as a result of thermal expansion and variation of the water-vapor content of the atmosphere within the cavity. Consequently, true standard cavities should be sealed and temperature-compensated. However, the ordinary frequency meters, which are calibrated by means of standard cavities, are not usually sealed. In order to avoid production-line corrections for temperature and humidity effects, these frequency meters are calibrated against standard cavities which undergo the same effects. For purposes of standardization, the standard cavities are adjusted to resonate at the desired frequencies at 25°C and 60 per cent relative humidity. Since these atmospheric conditions cannot usually be realized at the time of cavity adjustment, the cavities are made resonant at frequencies which differ from the desired frequencies by amounts corresponding to the temperature and humidity effects. The cavities are adjusted under nonstandard conditions so that they resonate at the desired frequencies under standard conditions, and a clear knowledge of temperature and humidity effects is necessary.

6·24. Temperature Effects.—If all dimensions of a lossless cavity are scaled proportionally, the resonant wavelength is scaled by the same factor. When a homogeneous cavity undergoes thermal expansion, all dimensions are increased by a factor $(1 + \alpha)$ per degree C, where α is the linear coefficient of expansion for the material. That is,

$$\frac{\lambda + \Delta\lambda}{\lambda} = (1 + \alpha) \text{ per degree C.}$$

Since frequency and wavelength are related according to

$$f = \frac{c}{\lambda},$$

it follows that

$$\frac{\Delta f}{f} = -\frac{\Delta\lambda}{\lambda + \Delta\lambda} = -\frac{\alpha}{1 + \alpha} \text{ per degree C.}$$

Since α is a very small quantity, the thermal coefficient of frequency is very nearly

$$\frac{\Delta f}{f} = -\alpha \text{ per degree C.}$$

Although the scaling principle is exact only when skin-depth effects are included, they can be omitted with negligible error in the case of high-Q cavities.

Unfortunately the thermal coefficient of expansion is useful only for estimating the frequency coefficient since truly homogeneous cavities of known expansion coefficients are not realized in practice. Small amounts of solder and manufacturing processes often change a low expansion characteristic so that the frequency coefficient is two or three times that predicted. Also, the frequency-pulling effects of external loads vary with temperature and effectively change the frequency coefficient. For example, TE_{011}-mode standard cavities were made in quantity from all-invar parts except for the waveguide transmission lines attached to them. Although the expansion coefficient for invar is 0.8×10^{-6}, the average frequency coefficient for these cavities was -2×10^{-6}. Individual frequency coefficients varied from this value by factors as large as 2, caused in part by improper sealing which introduced humidity, as well as temperature, effects.

However, if a TE_{011}-mode cavity is made from a high-expansion material—for example, steel for which $\alpha = 12 \times 10^{-6}$—then the frequency coefficient is more nearly $-\alpha$. Since the resonant frequency decreases with the height of the cylindrical cavity, a portion of the tuning shaft can be made from a higher-expansion material in order to effect internal compensation. If this portion has a coefficient α_1 and a length l, differential expansion will effectively move the piston an amount $-(\alpha_1 - \alpha)l$. This motion will change the resonant frequency an amount

$$-(\alpha_1 - \alpha)l\left(\frac{\partial f}{\partial h}\right),$$

where $\partial f/\partial h$ is the tuning rate, and h is the height of the cavity. The total frequency change will be

$$(\Delta f)' = -\alpha f - (\alpha_1 - \alpha)l\left(\frac{\partial f}{\partial h}\right),$$

and the frequency coefficient is

$$\left(\frac{\Delta f}{f}\right)' = -\alpha - \frac{(\alpha_1 - \alpha)l}{f}\left(\frac{\partial f}{\partial h}\right) \text{ per degree C.}$$

For compensation, this coefficient is zero and the ratio of expansion coefficients is

$$\frac{\alpha_1}{\alpha} = 1 - \frac{f}{l}\left(\frac{\partial h}{\partial f}\right).$$

The compensation cannot be perfect over the entire tuning range because $(f/l)(\partial h/\partial f)$ does not remain constant. Consequently, it is wise to start with a cavity of low-expansion material. Compensation is determined by cut-and-try methods since spurious effects are prominent and render calculation almost useless.

In the case of the partial-coaxial cavity, a decrease in the length of the center rod increases the resonant frequency. Therefore, if the center rod is made of a low-expansion material, differential expansion effectively shortens the center rod and provides temperature compensation. The field configuration for this mode is very complex, and the frequency coefficient of a compensated cavity is best determined experimentally. A cavity with a steel body ($\alpha = 10 \times 10^{-6}$) and invar center rod (effective $\alpha = 2 \times 10^{-6}$) has a frequency coefficient of $+1.6 \times 10^{-6}$ per degree C. By an approximate method, the coefficient for a steel-and-invar combination was calculated to be $+6 \times 10^{-6}$ per degree C. The factors neglected in the approximation tend to make the result even larger, and the discrepancy is another example of the large spurious effects which are too complex and numerous to calculate. Only a few cavities of this type were built, and data are insufficient to indicate that the frequency coefficient of $+1.6 \times 10^{-6}$ per degree C is really reproducible. If the compensation is reproducible, it may be improved further by changing the cavity dimensions slightly.

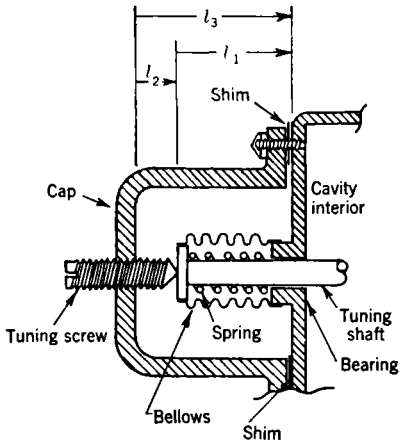

FIG. 6·29.—External temperature compensation for standard cavities.

In the case of the hybrid TE_{011}-mode cavity, the field configuration is such that the coaxial conductor has but little effect on the resonant frequency. In fact, even at 24,000 Mc/sec a conventional thread can be used for the tuning drive and yet a relatively low tuning rate is realized. The tuning effect is so complex and the dimensions are so small that internal temperature compensation is not practical.

6·25. External Temperature Compensation.—If all parts of a cavity are made from a material for which the expansion coefficient α_1 is larger than 10×10^{-6}, then spurious effects will be small and the frequency coefficient will be very nearly equal to $-\alpha_1$. Consequently, the calculations are simple when temperature compensation is applied to the tuning shaft external to the cavity. If the cavity is sealed by means of a spring-loaded bellows as shown in Fig. 6·29, the differential expansion of the shaft, screw, and cap can provide compensation.

The expansion coefficients and effective lengths of the shaft, screw, and cap are designated by the subscripts 1, 2, and 3, respectively. Positive

axial motion is into the cavity. The tuning shaft is made of the same material as the cavity in order to ensure a homogeneous interior. When the assembly undergoes a temperature change, the shaft experiences an effective movement

$$\Delta l = \alpha_1 l_1 + \alpha_2 l_2 - \alpha_3 l_3.$$

As indicated in Fig. 6·29,

$$l_1 + l_2 = l_3,$$

so that

$$\Delta l = (\alpha_1 - \alpha_2) l_1 + (\alpha_2 - \alpha_3) l_3. \tag{1}$$

This motion changes the resonant frequency an amount

$$\Delta l \left(\frac{\partial f}{\partial l}\right).$$

The expansion of the cavity changes the frequency an amount $-\alpha_1 f$ so that the net frequency change is

$$\Delta f = -\alpha_1 f + \Delta l \left(\frac{\partial f}{\partial l}\right).$$

The fractional frequency change is

$$\frac{\Delta f}{f} = -\alpha_1 + \frac{\Delta l}{f} \left(\frac{\partial f}{\partial l}\right).$$

For perfect compensation there is no frequency change and

$$\frac{\Delta l}{f} \left(\frac{\partial f}{\partial l}\right) = \alpha_1. \tag{2}$$

In order that the compensation may be successful over the tuning range, Δl must vary as the cavity is tuned. The nature of this variation depends on the tuning characteristic. Conversely, Eqs. (1) and (2) determine the tuning characteristic for which uniform compensation may be achieved. Differentiation of Eq. (1) gives

$$\frac{\partial(\Delta l)}{\partial l} = \alpha_2 - \alpha_1, \tag{3}$$

and differentiation of Eq. (2) gives

$$\frac{\partial(\Delta l)}{\partial l} = \alpha_1 \frac{\partial}{\partial l} \left(\frac{f}{\partial f / \partial l}\right). \tag{4}$$

Equations (3) and (4) may be combined and integrated to give

$$\frac{f}{\partial f / \partial l} = \frac{\alpha_2 - \alpha_1}{\alpha_1} l + C_1, \tag{5}$$

where C_1 is a constant. Equation (5) may be rearranged and integrated to give

$$\ln f = \frac{\alpha_1}{\alpha_2 - \alpha_1} \ln \left(\frac{\alpha_2 - \alpha_1}{\alpha_1} l + C_1 \right) C_2,$$

where C_1 and C_2 are constants. This equation is equivalent to

$$f^{\left(\frac{\alpha_2 - \alpha_1}{\alpha_1}\right)} = kl + C,$$

where k and C are constants. Thus, uniform compensation is feasible for a cavity whose tuning characteristic is of the general form

$$f^n = kl + C, \tag{6}$$

if α_1 and α_2 are chosen so that

$$n = \frac{\alpha_2 - \alpha_1}{\alpha_1}. \tag{7}$$

However, since the expansion coefficients are positive and not zero, Eq. (7) requires[1] that

$$n > -1.$$

Equations (1), (2), and (7) may be combined to give

$$\frac{\alpha_3}{\alpha_2} = 1 - \frac{nl_1 + f \dfrac{\partial l}{\partial f}}{(n+1)l_3}. \tag{8}$$

This equation suggests making the cap and screw of the same material so that $\alpha_2 = \alpha_3$. Accordingly, Eq. (8) gives the shaft length as

$$l_1 = -\frac{f}{n}\left(\frac{\partial l}{\partial f}\right), \tag{9}$$

which requires a negative tuning rate for $n > 0$ and a positive tuning rate for $0 > n > -1$.

Equations (7) and (8) may be combined to give

$$\frac{\alpha_3}{\alpha_1} = \frac{(n+1)l_3 - nl_1 - f \dfrac{\partial l}{\partial f}}{l_3}.$$

This equation suggests making the cap and shaft of the same material so that $\alpha_1 = \alpha_3$. Accordingly, the length of the screw is given as

$$l_2 = l_3 - l_1 = \frac{f}{n}\left(\frac{\partial l}{\partial f}\right), \tag{10}$$

[1] The case of $n = 0$, that is, $\alpha_1 = \alpha_2$, is treated separately in a later part of this section.

which requires a positive tuning rate for $n > 0$ and a negative tuning rate for $0 > n > -1$.

When $n = 0$, that is, $\alpha_1 = \alpha_2$, Eq. (5) becomes

$$\frac{f}{\frac{\partial f}{\partial l}} = C_1,$$

which may be rearranged and integrated to give

$$\log f = C_3 l + C_4,$$

where C_3 and C_4 are constants. Thus, if a cavity has a tuning characteristic so that a graph of $\log f$ versus l gives a straight line, uniform compensation is achieved by making the shaft and screw of the same material. Accordingly, Eqs. (1) and (2) may be combined to give the length of the cap as

$$l_3 = \left(\frac{\alpha_1 f}{\alpha_1 - \alpha_3}\right)\frac{\partial l}{\partial f}, \tag{11}$$

which requires $\alpha_1 > \alpha_3$ if the tuning rate is positive, and $\alpha_1 < \alpha_3$ if the tuning rate is negative.

Although uniform compensation cannot be achieved if $n \leqq -1$, this case is important because it includes, for example, the pure coaxial cavity. Since the resonant wavelength is proportional to the length of the cavity, the tuning characteristic is of the form

$$\frac{1}{f} = kl + C, \tag{12}$$

and $n = -1$. Differentiation of Eq. (12) gives

$$\frac{\partial f}{\partial l} = kf^2,$$

which may be combined with Eq. (2) so that

$$\Delta lkf = \alpha_1.$$

This equation indicates that Δl should decrease as the frequency increases, that is, as the cavity is lengthened. If the tuning rate is positive, this effect is realized by making the cap and screw of the same material so that only the shaft length is effective in producing compensation. At one frequency, perfect compensation is achieved by making the shaft length

$$l_1 = \left(\frac{\alpha_1 f}{\alpha_1 - \alpha_3}\right)\frac{\partial l}{\partial f},$$

where $\alpha_1 > \alpha_3$. This expression results from a combination of Eqs.

(1) and (2) when $\alpha_2 = \alpha_3$. If the tuning rate is negative, Δl will decrease as the frequency increases when the screw provides compensation. The cap and shaft are made of the same material, and $\alpha_1 = \alpha_3$. At one frequency, perfect compensation is achieved when the length of the screw is

$$l_2 = \left(\frac{\alpha_1 f}{\alpha_2 - \alpha_1}\right)\frac{\partial l}{\partial f},$$

where $\alpha_1 > \alpha_2$.

Although uniform compensation over the tuning range cannot be realized for all cavities, optimum compensation results when the materials and dimensions are chosen to be compatible with the requirements imposed by the tuning characteristic. Consequently, when designing a compensated cavity, the tuning characteristic should be examined by plotting frequency vs. shaft position on logarithmic or semilogarithmic graph paper. If the major portion of the resultant curve is a straight line, its slope is equal to the exponent n that is used in the equations for uniform compensation. Even in this case, however, uniform and exact compensation is difficult to realize because of variations in materials, tolerances, and the effects of manufacturing processes. Accordingly, it is desirable to provide shims of cap material between the cap and cavity as shown in Fig. 6·29. These shims are included in the calculations, but later may be made of high- or low-expansion material in order to improve compensation at some particular frequency.

6·26. Humidity Effects.—In a resonant cavity, the energy stored in the electric field is equal to that stored in the magnetic field. The energy stored in each field is a function of frequency, and that stored in the electric field is a function of the dielectric constant of the medium within the cavity. Consequently, when the dielectric constant varies, the frequency of excitation must be varied until the energies stored in the two fields are again equal and resonance is restored. For all practical cavities in which the medium does not introduce excessive and variable loss,

$$\frac{f_0'}{f_0} = \sqrt{\frac{k_e}{k_e'}},$$

where f_0' is the resonant frequency corresponding to a new dielectric constant, k_e'.

Accordingly, the fractional frequency change is one half the fractional change in dielectric constant, that is,

$$\frac{\Delta f}{f} = -\frac{1}{2}\frac{\Delta k_e}{k_e}.$$

However, this equation is of general use in the laboratory only when easily measured quantities, such as temperature and relative humidity, are related to the dielectric constant in a simple manner. Since this is

not the case, the nomograph of Fig. 6·30 was prepared for laboratory use.

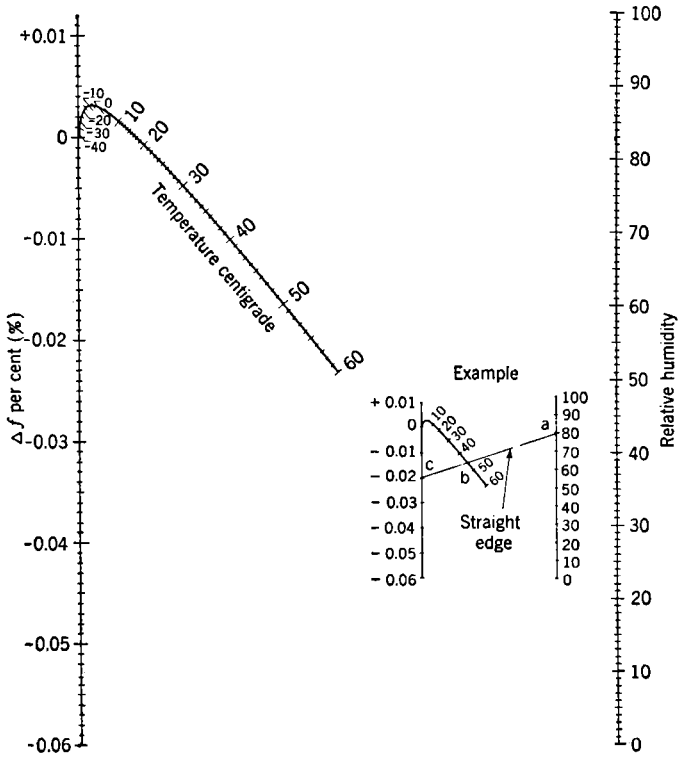

FIG. 6·30.—Humidity-effect nomograph.

The calculations are based on an empirical equation[1] which relates the dielectric constant of air to temperature and partial pressures of dry air and water vapor, that is,

$$k_e = 1 + 210 \times 10^{-6} \frac{P_a}{T} + 180 \times 10^{-6} \left(1 + \frac{5580}{T}\right) \frac{P_w}{T},$$

where T is the absolute temperature, P_a is the partial pressure of dry air in millimeters of mercury, and P_w is the partial pressure of water vapor in millimeters of mercury. The nomograph is normalized relative to 25°C

[1] A. C. Strickland, "The Dielectric Constant of Water Vapour and its Effect upon the Propagation of Very Short Waves," RRB 1594, Radio Department, National Physical Laboratory, Radio Research Board, Department of Scientific and Industrial Research, May 11, 1942. This is a British Report. The humidity effects based on this equation have been verified experimentally at the Radiation Laboratory.

and 60 per cent relative humidity, which are standard measurement conditions. Since the dielectric constant increases with the total water content of the air, the largest effects occur when the relative humidity is 100 per cent at high temperatures.

In the case of sealed cavities which are evacuated, small leaks are readily detected with ordinary frequency meters because of the large frequency changes produced by the humidity effect. If cavities are sealed merely to prevent the internal atmosphere from changing, small leaks are not readily detected unless the external conditions differ considerably from those at the time of sealing. Consequently, it is a good idea not only to seal cavities but to evacuate them as well.

It should be borne in mind that the humidity effects described in this section are relatively simple in principle and do not include the effects of molecular resonances which occur in some parts of the microwave spectrum.

MEASURING EQUIPMENT AND TECHNIQUES

Accurate frequency measurements usually fall into two classes: those in which the resonant frequency of a cavity is determined with the signal from a primary standard, and those in which the cavity frequency is determined by comparison with a standard cavity. For the first class of measurement, a spectrum analyzer (panoramic receiver) provides a sensitive indication of the transmission of, or reaction on, the standard signal by the cavity. The accuracy of this method is limited because the rate of change of transmission, or reaction, with frequency is zero at resonance. On the other hand, the rate of change is a maximum at the half-power frequencies of the cavity, and a factor of 10 in accuracy is gained by using images of the standard-frequency signal, the images being separated so as to occur at the cavity half-power points. This cavity Q-meter technique is so named because Q may be determined simultaneously from a knowledge of resonant frequency and pass band.

The simplest way to align two cavities to the same frequency is to allow them to react successively on the transmission line between an f-m oscillator and a detector. The detector output signal is coupled to an oscilloscope so that the pattern is a plot of reaction versus frequency. Accuracy is limited by the ability to judge when the peaks of the two reactions are coincident. A small displacement of the two peaks will produce merely a slight shift in the peak of the composite reaction. On the other hand, a small displacement is easily observed if the cavities are coupled to separate transmission lines and detectors. A common f-m oscillator is used, and electronic switching in the oscilloscope provides superposition of the two reaction patterns. This is the cavity-comparator technique.

However, even the most accurate standards and measuring techniques are of little value if the resonant frequencies of cavities are affected in an uncontrolled manner by temperature, humidity, and external loads. Obviously, standard conditions must be established and recognized.

6·27. Standard Measurement Conditions.—In order to minimize frequency errors caused by temperature and humidity effects on unsealed and uncompensated cavities, standard conditions were chosen to represent typical operating conditions. The choice of 25°C and 60 per cent relative humidity was made by the Radiation Laboratory where the first calibration service was initiated. The Radio Section of the National Bureau of Standards now maintains this service and continues to use these standard conditions. The conditions mean that cavities are adjusted so they resonate correctly at 25°C and 60 per cent relative humidity. Since these conditions are not always realized at the time of adjustment, a cavity is purposely misaligned by an amount corresponding to its temperature and humidity effects. Naturally this procedure introduces some error, and the best results are obtained with sealed and compensated cavities. The humidity effect is the same for all unsealed cavities but the temperature effect is often individual. Consequently, when a cavity is submitted for calibration, its temperature coefficient of frequency should be furnished to, or requested of, the test laboratory.

The ideal solution to the problem of standardizing the effects of external loads would be to terminate all transmission lines with their characteristic impedances. The practical solution is to use resistive attenuation between the cavity and external loads. The amount of attenuation depends on that tolerable and the reflection coefficients of the loads which are to be isolated.

Cavity Q-meters and comparators can tolerate about 32 db of attenuation between oscillator and detector. Since transmission cavities may have an insertion loss of about 7 db, about 25 db are left for isolation. A reflex oscillator is very poorly matched to the transmission line, but a crystal detector can be matched so that its VSWR does not exceed 1.10. Consequently, most of the attenuation should go between the oscillator and cavity. If well-matched 17- and 8-db attenuators are placed on the oscillator and detector sides respectively, the cavity will be coupled to loads whose voltage standing-wave ratios will not exceed 1.05.[1] Well-matched attenuators can be made from long, tapered pieces of resistance-strip material or polyiron, and frequency pulling by external loads will be minimized as much as possible.

6·28. Spectrum-analyzer Techniques.—Equipment is arranged as indicated in Fig. 6·31 if the standard-frequency signal is to be transmitted through or past the cavity. Many commercial spectrum analyzers have

[1] Frequency pulling as a function of load reflection is discussed in Chap. 5.

cutoff attenuators between the r-f input jack and the mixer, and the attenuator insertion loss effectively lowers the sensitivity. For frequency measurements, optimum sensitivity is necessary in order to allow adequate attenuation on either side of the cavity, and it is common practice to remove the cutoff attenuators from spectrum analyzers.

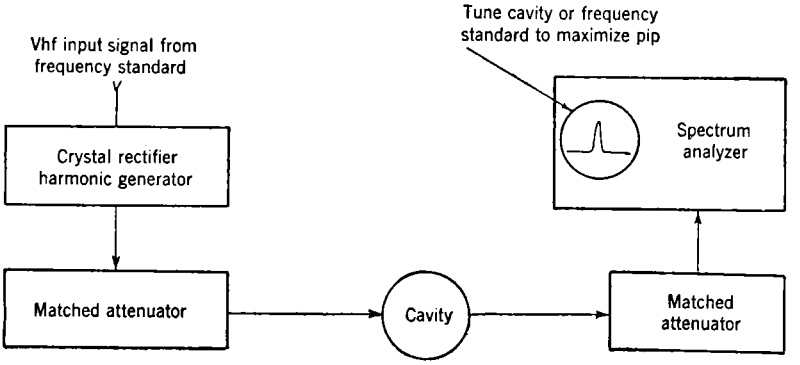

FIG. 6·31.—Spectrum-analyzer technique.

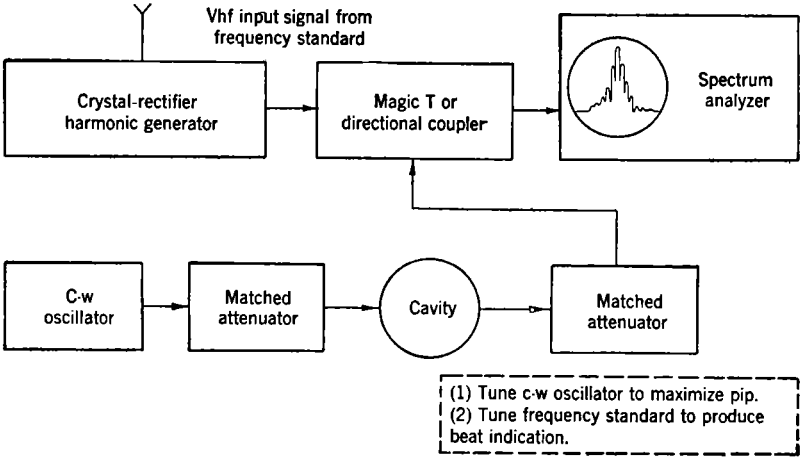

FIG. 6·32.—Auxiliary-oscillator technique.

If the sensitivity is still inadequate, an auxiliary c-w oscillator may be used as indicated in Fig. 6·32. The frequency standard is tuned so as to beat with the c-w signal transmitted through the cavity. Care must be taken not to use the beat which occurs between image frequencies in the spectrum analyzer. The two possible beat patterns are shown in Fig. 6·33. When the two input frequencies are nearly equal, the beat frequency is independent of the local-oscillator frequency; when the

frequencies are images, the beat frequency changes as the local oscillator is swept across its range. If the auxiliary oscillator is unstabilized, the beat indication will not persist for much longer than 2 or 3 min. Frequency coincidence can be estimated to about ± 10 kc/sec.

The accuracy of cavity resonant-frequency measurement depends also on the observer's ability to judge when the transmitted signal is maximized. If the spectrum analyzer has a linear heterodyne receiver,

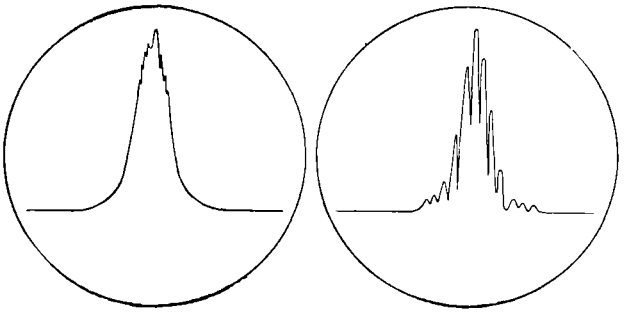

FIG. 6·33.—Spectrum-analyzer beat-frequency indications.

the height of the c-w pip is roughly proportional to the r-f input voltage.[1] For high-Q cavities, the relative voltage in the neighborhood of resonance is very nearly

$$V = \frac{V_0}{Q_L \sqrt{\frac{1}{Q_L^2} + \left(\frac{f}{f_0} - \frac{f_0}{f}\right)^2}},$$

where V_0 is the voltage at the resonant frequency f_0, f is the observed frequency, and Q_L is the loaded Q of the cavity. Since

$$\Delta f = f_0 - f,$$
$$\Delta h = h_0 - h,$$

and

$$V \propto h,$$

then

$$\frac{\Delta f}{f_0} = \frac{1}{Q_L} \sqrt{\frac{\Delta h}{2h_0}},$$

where $\Delta f/f_0$ is the fractional frequency error corresponding to a pip-height error $\Delta h/h_0$. A careful observer can detect a 2 per cent variation in pip height so that

$$\frac{\Delta f}{f_0} = \frac{1}{10Q_L}.$$

[1] It is assumed here that both the first and the second detectors are nearly linear. If they are not linear, the accuracy will be greater than that which is calculated.

6·29. Cavity Q-meter Technique.—The components for the Q-meter method are shown in Fig. 6·34. R-f power from an f-m oscillator is transmitted through the test cavity to a crystal detector. The detected signal is amplified and provides vertical deflection for the cathode-ray tube so that the resultant pattern is the bandpass characteristic of the cavity. The f-m oscillator also serves as the local oscillator for a heterodyne receiver whose intermediate frequency is adjustable and whose pass band is very narrow. The intermediate frequency is sufficiently low so that the f-m local oscillator produces i-f signals when it is either above

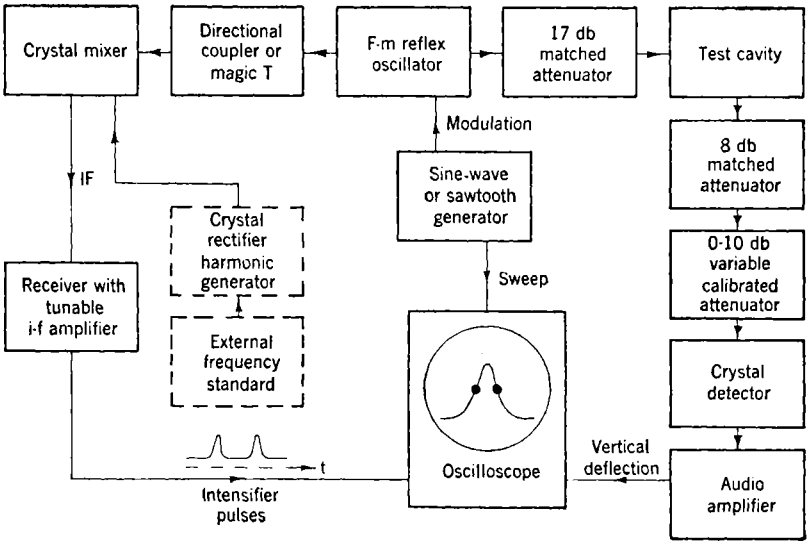

FIG. 6·34.—Components for cavity-Q-meter method.

or below the input frequency. The video output signal consists of pips similar to those produced by a spectrum analyzer. These pips are used to intensity-modulate the cathode-ray tube, thus producing spots on the bandpass characteristic. If the standard-frequency input signal corresponds to the resonant frequency of the cavity, the spots are equidistant from the base line. If the receiver is adjusted so the spots occur at the cavity half-power points, their frequency separation is equal to the bandwidth and is twice the intermediate frequency of the receiver. Loaded Q is measured as the ratio of resonant frequency to bandwidth.

The actual arrangement of the circuit components is shown in Fig. 6·35.[1] The power supply is not indicated but is designed to operate both

[1] The Radiation Laboratory has furnished a cavity Q-meter of this type to the National Bureau of Standards.

mechanically and thermally tuned reflex oscillators. Frequency modulation is accomplished by varying the oscillator reflector voltage. Either sine-wave or sawtooth modulating signals may be used.

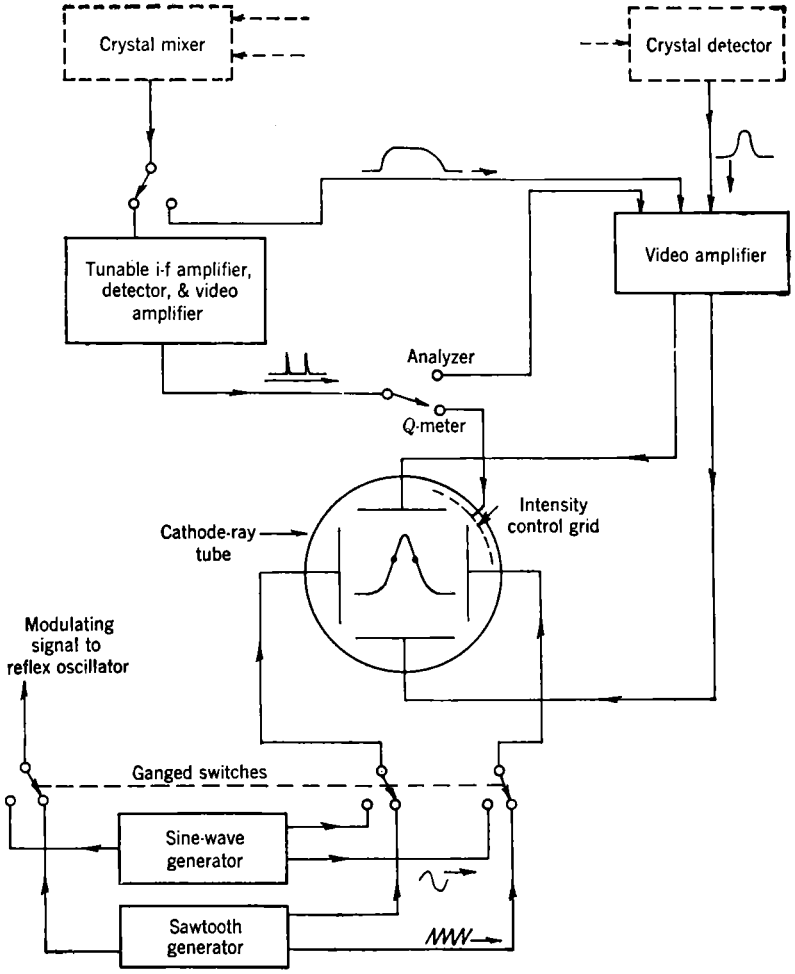

FIG. 6·35.—Arrangement of circuit components for cavity Q-meter.

Sine-wave modulation provides a double trace and produces two pairs of spots if the amplifiers introduce distortion or effectively delay the spots by poor video response. Measurement error can be avoided by using the mean positions of spot pairs. A phasing control is provided so that amplifier phase shift and oscillator hysteresis may be compensated

and the two patterns may be superimposed. However, the sine-wave modulation produces a faster sweep at the center of the screen than does a sawtooth modulation of the same recurrence frequency. Accordingly, better video response and a wider i-f pass band are required. The wider i-f pass band produces broader spots so that some accuracy is lost. Consequently, a compromise has been effected.

Amplifier response and i-f bandwidth are chosen for optimum operation when sawtooth modulation is used. That is, negligible error occurs

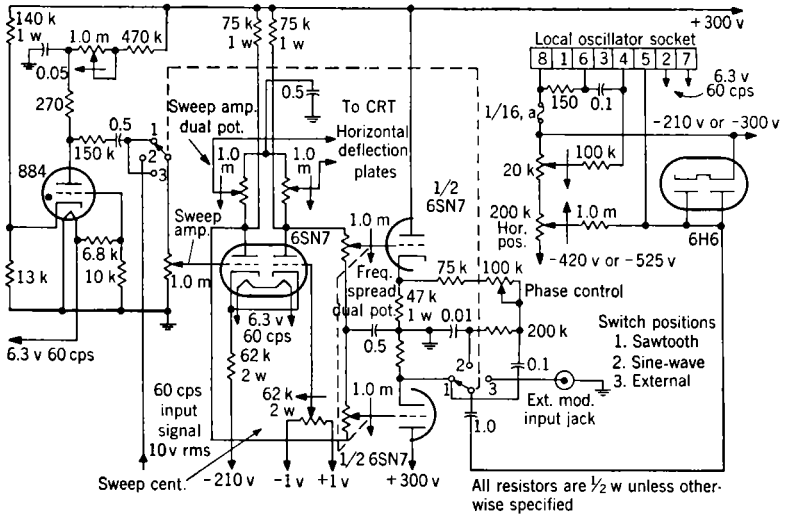

FIG. 6·36.—Modulation and sweep circuits for cavity *Q*-meter.

for sawtooth modulation. This may be checked against the mean position of the spot pairs when sine-wave modulation is employed. Spot pairs result because the simpler circuit design for sawtooth operation is inadequate for optimum sine-wave operation.

Modulation and sweep-circuit details are shown in Fig. 6·36. A selector switch provides a choice of a 60-cps sine-wave signal, a 60-cps sawtooth signal, or some external signal. A sawtooth recurrence frequency of 60 cps is chosen for three reasons: instability from 60-cps hum modulation is eliminated by synchronization; the low recurrence frequency reduces the high-frequency response requirements for the video amplifiers; and a narrow receiver pass band can be utilized.

The sawtooth signal is generated by means of a standard thyratron circuit which uses a fraction of the heater voltage for synchronization. When the thyratron fires, a positive pulse is developed across the cathode-bias resistor. This pulse is applied to the CRT cathode and blanks the

return trace. The sawtooth signal is applied to a cathode-coupled push-pull amplifier which is direct-coupled to the CRT horizontal deflection plates and the grids of two cathode followers. The output signal from one of the cathode followers is applied to the oscillator reflector. A clamping diode prevents the reflector from being driven positive with respect to the cathode. The entire sweep is centered on the CRT screen by varying the bias of one push-pull amplifier tube. This control, however, does not appear on the front panel. The horizontal-positioning control is actually the reflector-voltage control for the oscillator. Reflector-voltage variations shift the pattern with respect to the sweep since they shift the operating frequency with respect to the modulation.

When sine-wave modulation is employed, the cathode-follower output signals are applied to a phase-shift network. The output signal from this network is used to modulate the oscillator, and since only small phase variations are necessary to superimpose the two patterns, the amplitude variation is negligible. Another set of contacts (not shown in Fig. 6·36) on the selector switch removes the CRT blanking signal for sine-wave operation.

The receiver for the Q-meter, shown in Fig. 6·37, consists of a tunable i-f stage, three bandpass stages, a diode detector, and video amplifiers. The i-f input impedance is that of a 50-μh choke and is equal to about 100 ohms at 300 kc/sec, the lowest intermediate frequency. The choke offers even less impedance to crystal-current variations and minimizes the shock excitation of the i-f amplifier when the oscillator is overmodulated and drops out of oscillation. In order to facilitate oscillator alignment, crystal current may be returned to ground through the input resistor of the vertical amplifier. Figure 6·38 indicates this circuit and the switch which short-circuits the crystal current to ground in normal operation. When crystal current is coupled to the vertical amplifier, the CRT pattern indicates relative output power from the oscillator as a function of frequency.

Only the first stage of the i-f amplifier is selective and effective in determining the intermediate frequency. The tuning range is divided into four bands as indicated in Fig. 6·37. The selectivity of each band is such that there are at least 25 cycles of the intermediate frequency in the modulation envelope corresponding to an output pip. Coils, tuning condenser, and band switch are mounted in a separate shielded box and are connected to the receiver strip by means of a short, shielded cable. The cable enters the strip at the tube socket of the first stage to prevent regeneration. The tuning range of the receiver permits cavity-bandwidth measurement between 0.6 and 12.2 Mc/sec.

Two video stages follow the second detector and the output signal is coupled to a phase inverter. The positive pips from the plate of the

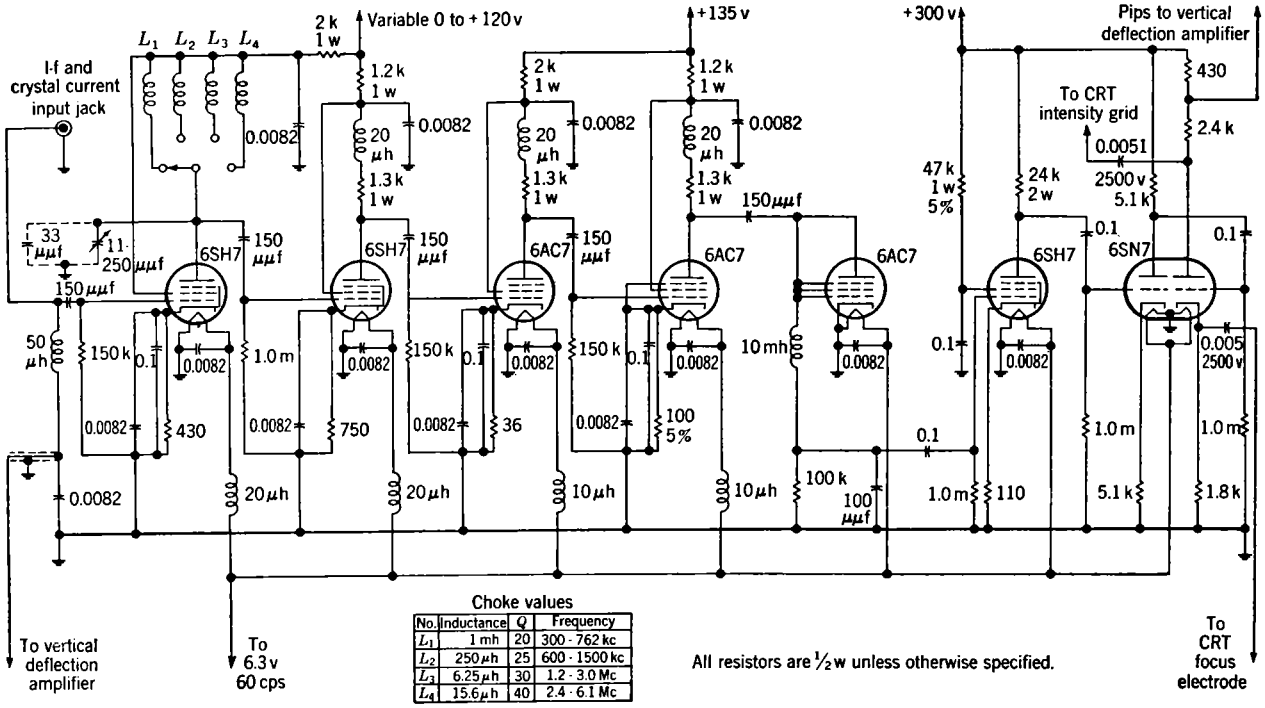

Choke values

No.	Inductance	Q	Frequency
L_1	1 mh	20	300 - 762 kc
L_2	250 μh	25	600 - 1500 kc
L_3	6.25 μh	30	1.2 - 3.0 Mc
L_4	15.6 μh	40	2.4 - 6.1 Mc

FIG. 6·37.—Receiver for cavity Q-meter.

phase inverter are coupled to the CRT intensity grid but are limited to a peak amplitude of 15 volts to prevent exceeding the CRT bias. The negative pips from the cathode of the phase inverter are coupled to the CRT focus electrode in order to maintain focus during intensification. Also, these negative pips may be coupled to the vertical amplifier so that the instrument may be used as a spectrum analyzer. Receiver sensitivity (barely discernable pip) is about −110 dbw.

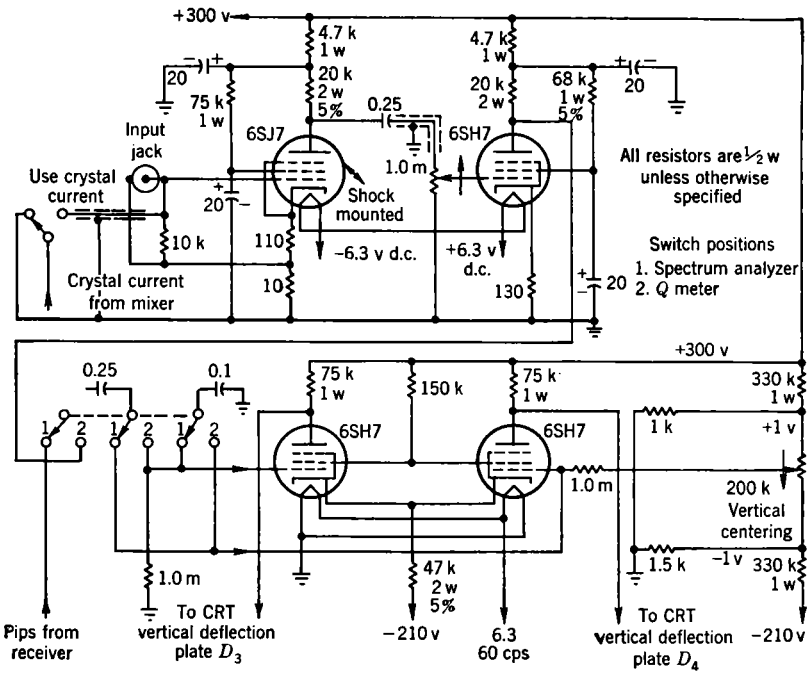

FIG. 6·38.—Vertical-deflection amplifier for cavity *Q*-meter.

The vertical amplifier, shown in Fig. 6·38, consists of two *RC*-coupled stages and a cathode-coupled push-pull amplifier which is direct-coupled to the CRT vertical-deflection plates. The first stage is shock-mounted, and the input circuit is decoupled from chassis ground to eliminate the effects of ground currents. Hum modulation resulting from a-c heater operation is eliminated by using well-filtered direct current from a selenium rectifier. The amplifier has negligible phase shift at the recurrence frequency, 60 cps, and its response is uniform to 20 kc/sec. The response falls to half power at the frequencies 2 cps and 60 kc/sec.

The CRT circuit is conventional and hence is not shown. A 5BP1 tube is used to obtain good focusing. The cathode is operated at −1700

volts and the intensifier ring at 1500 volts. For optimum focusing, the second anode is operated at +150 volts, the average potential of the direct-coupled deflection plates.

Typical CRT patterns are shown in Fig. 6·39. Spot pairs appear since sine-wave operation is assumed. For bandwidth measurement, the half-power level is established by means of the calibrated attenuator of Fig. 6·34. Since the crystal detector is very nearly a square-law detector, the half-power level will be half amplitude for the pattern In order to be sure that the pattern reaches the baseline, the f-m oscillator should have a large frequency deviation. If this is true, shifting

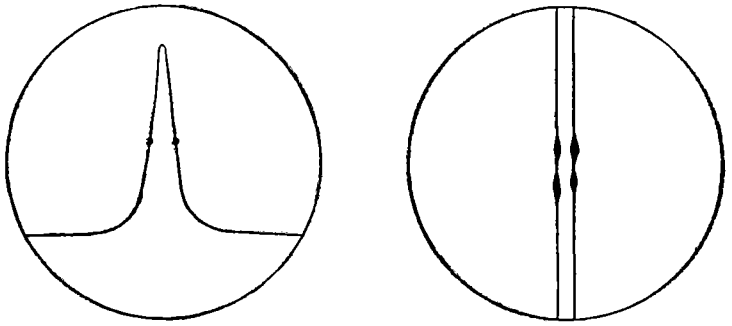

FIG. 6·39.—CRT patterns for cavity Q-meter. The pattern on the left is for bandwidth measurements, that on the right for frequency measurements.

the pattern along the baseline should not produce any vertical motion. Since the baseline is not clamped, however, attenuating the signal will produce some vertical motion of the baseline, and this motion must be included in the half-power level determination. When the half-power level is established, the receiver is tuned until the spots coincide with the half-power points and bandwidth is read from the receiver calibration. The accuracy of the measurement is essentially that of establishing the half-power level and probably will not be better than ± 7 per cent.

Figure 6·39 also shows the CRT pattern that is used for resonant-frequency measurement. The f-m oscillator has a small frequency deviation in order to obtain the best possible spots, and the horizontal amplitude is reduced to produce a very narrow pattern. Large vertical deflection is used and spots appear somewhat blurred even though their time duration is very short. The frequency standard or cavity is tuned until the spot pairs are matched. The sensitivity is sufficiently high so that manually squeezing a cavity will produce appreciable spot-pair separation. The accuracy of measurement depends on the Q of the cavity and the minimum discernable spot-pair separation.

For a transmission cavity which may be regarded as a lumped-

constant circuit coupled to matched transmission lines by ideal transformers,

$$\frac{\Delta P_{\frac{1}{2}}}{P_{\frac{1}{2}}} = \frac{\Delta f_{\frac{1}{2}}}{f_{\frac{1}{2}}} \left(\frac{\frac{f_{\frac{1}{2}}}{f_0} + \frac{f_0}{f_{\frac{1}{2}}}}{\frac{f_{\frac{1}{2}}}{f_0} - \frac{f_0}{f_{\frac{1}{2}}}} \right),$$

where $P_{\frac{1}{2}}$ is the power delivered to the matched line at the half-power frequency $f_{\frac{1}{2}}$. For high-Q cavities, this relation may be approximated by

$$\frac{\Delta P_{\frac{1}{2}}}{P_{\frac{1}{2}}} = \frac{\Delta f_{\frac{1}{2}}}{f_{\frac{1}{2}}} \left(\frac{f_0}{f_{\frac{1}{2}} - f_0} \right).$$

Since

$$Q_L = \frac{f_0}{2(f_{\frac{1}{2}} - f_0)},$$

then

$$\frac{\Delta P_{\frac{1}{2}}}{P_{\frac{1}{2}}} = 2Q_L \frac{\Delta f_{\frac{1}{2}}}{f_{\frac{1}{2}}}.$$

For the cavity Q-meter the vertical deflection d from the baseline is proportional to power, and the fractional frequency change at the half-power points is equal to the fractional change in resonant frequency. Accordingly, the equation may be written

$$\frac{\Delta f_0}{f_0} = \frac{1}{2Q_L} \frac{\Delta d}{d}.$$

Usually the vertical deflection from the baseline to half-power level is 5 in., and the minimum discernable spot separation is 0.2 in. so that Δd is 0.1 in. The resultant accuracy is

$$\frac{\Delta f_0}{f_0} = \frac{1}{100Q_L},$$

which is 10 times greater than that for the spectrum-analyzer technique where a similar 2 per cent variation in deflection is assumed discernable.

6·30. Cavity-comparator Technique.—Figure 6·40 indicates the method by which two cavities are aligned to the same frequency and their relative Q's and transmission losses are compared. A reflex oscillator is frequency-modulated by applying a sawtooth signal to its reflector. A recurrence frequency of 120 cps is used in order to eliminate, by synchronization, the instability produced by hum modulation. An oscillator with twin output jacks, or a magic T or directional couplers, is used to divide the oscillator output power between two channels. Power transmitted by each cavity is detected, and the detected signals are amplified, mixed, and applied alternately to the CRT vertical-deflection

plates. Alternate presentation of the two bandpass characteristics is achieved by electronic switching. A symmetrical multivibrator is synchronized with the sawtooth generator and provides a square wave which is applied to the mixer circuit.

The important circuit details are shown in Fig. 6·41. The regulated power supplies (omitted from the diagram) are designed to operate both

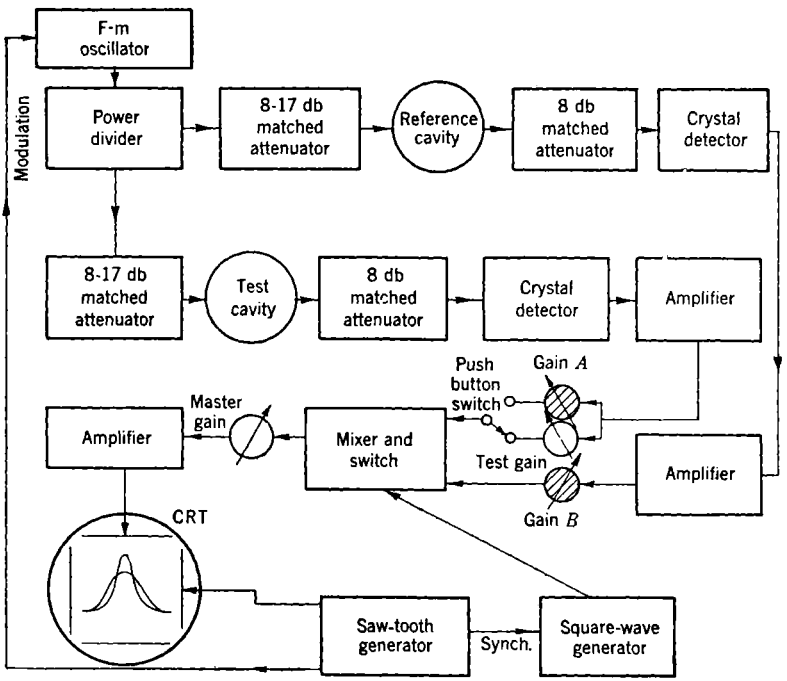

FIG. 6·40.—Cavity-comparator technique.

mechanically and thermally tuned oscillator tubes. The sawtooth generator (also not shown) is similar to that of Fig. 6·36, except that synchronization is accomplished by coupling a fraction of the 120-cps power-supply ripple to the thyratron control grid.

The input circuits of the amplifiers are isolated from ground by 10-ohm resistors to eliminate the effects of ground currents. Ground currents are exceptionally bad if the heater current flows through the ground lead to the oscillator. Type 6J7 tubes are used for the first amplifier stages since they introduce less hum modulation than other pentodes. Even less hum modulation is encountered if type 6F5 (metal envelope) triodes are used for the first stages. Their relatively high input capacitance is unimportant because of the low impedance of the crystal detector

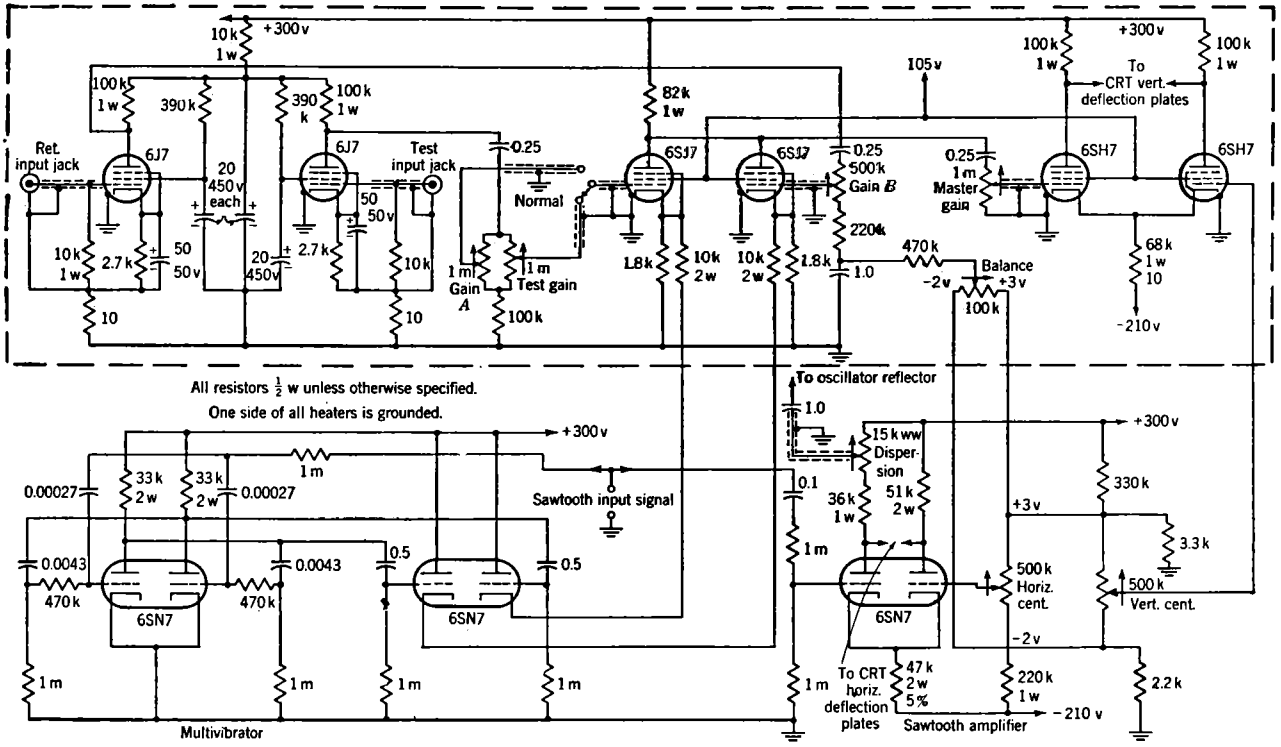

FIG. 6·41.—Circuit details for cavity comparator.

as a video generator. Each 6J7 stage has a voltage gain of 31 which can be duplicated by 6F5 tubes.

Mixing is accomplished by applying the two signals to 6SJ7 pentode amplifiers which have a common plate-load resistor. Switching is accomplished by direct-coupling the 6SJ7 cathodes to cathode followers which are coupled to the multivibrator. The two CRT patterns are adjusted for a common baseline by means of a balancing control which

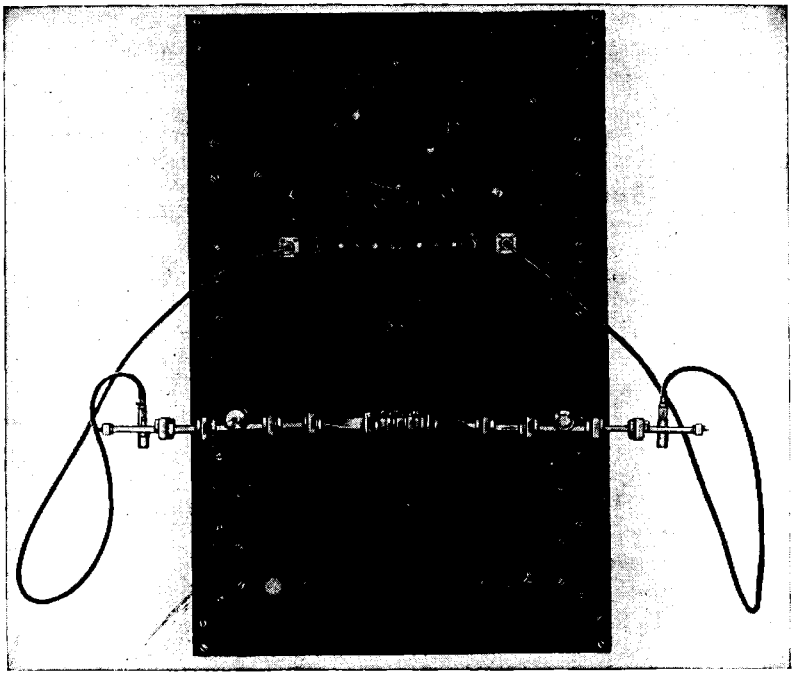

FIG. 6·42.—TFU-1RL cavity comparator.

varies the grid bias for one 6SJ7 tube of the mixing circuit. Balancing makes the plate currents of the mixing tubes equal. The mixer output signal is applied to cathode-coupled push-pull amplifiers which are direct-coupled to the CRT deflection plates. Horizontal deflection is achieved in a similar manner, and the CRT circuit is similar to that described for the cavity Q-meter. As in the case of the Q-meter, the reflector voltage of the oscillator effects horizontal positioning. The complete equipment is shown in Fig. 6·42 with microwave components for the frequency range from 23,500 to 24,500 Mc/sec.

For frequency or Q comparison the test gain control of Figs. 6·40 and 6·41 is adjusted so that the patterns have nearly equal amplitude.

For relative transmission-loss comparison, gains A and B (screwdriver adjustments) are set so that the two channels provide equal deflections under similar conditions. That is, the two gain controls are set so that the reference cavity produces equal deflections when inserted in either channel. When the test cavity is in place and the push-button switch is depressed, the relative amplitudes indicate relative power losses since the crystal is very nearly a square-law detector.

When two similar cavities are adjusted to resonate at the same frequency, a misalignment of 1 per cent of the bandwidth may be detected. Consequently, the accuracy of the technique is

$$\frac{\Delta f_0}{f_0} = \frac{1}{100Q_L},$$

which is the same as for the cavity Q-meter. That is, two cavities may be tuned to the same frequency as accurately as the resonant frequency of one can be measured.

CHAPTER 7

THE MEASUREMENT OF FREQUENCY SPECTRUM AND PULSE SHAPE

By George N. Kamm

The wide use of pulses in the applications of microwaves demands new techniques for the measurement of the characteristics of the pulses. Three instruments are available for these purposes: the spectrum analyzer, the r-f envelope viewer, and the r-f oscilloscope.

The spectrum analyzer is a device for the analysis of spectra of pulsed oscillators. It presents visually on a cathode-ray-tube screen the distribution in frequency of the r-f power of the pulse. A spectrum analyzer is an electronic instrument that incorporates a narrow-band superheterodyne receiver. The receiver is electronically tuned in frequency by applying a linear modulating voltage to the local oscillator. The same sawtooth voltage is applied to the horizontal deflecting plates of a cathode-ray tube. The output signal of the receiver is applied to the vertical-deflecting plates to produce a plot on the tube, which indicates power vertically and frequency horizontally.

Although originally designed specifically for spectrum analysis, the analyzer has proved to be a highly versatile r-f measuring instrument and has found wide use as such at the Radiation Laboratory and elsewhere. As a sensitive r-f detector, it may be used to align and check the operation of radar sets and to measure frequency and frequency differences, standing waves, and attenuation. This principle of an electronically tuned receiver has been incorporated into several special types of test equipment.

An r-f envelope viewer presents on a cathode-ray-tube screen the shape of the envelope of the radio-frequency pulse. The r-f envelope shows directly the amplitude modulation of the pulse, its time of rise, its time of fall, and any slope or oscillation on the top of the pulse, but it does not indicate anything about the frequency modulation during the pulse.

R-f oscilloscopes attempt to show the waveform of the microwave signal directly. They represent obvious extensions of the techniques so commonly employed in the low-frequency region. These extensions are difficult and relatively little effort has been spent in their development.

THE PRINCIPLES AND DESIGN OF SPECTRUM ANALYZERS

7·1. Formation of the Spectrum.—The spectrum analyzer is intended for use with pulsed r-f oscillators used in radar sets. The pulses of these oscillators are very short, ranging from 0.1 μsec to several microseconds in length, and there is a relatively long time between pulses, ranging from 500 to 2500 μsec. The i-f amplifier of the spectrum-analyzer receiver is narrow compared to the spectrum width but is still sufficiently broad so that the transient generated by a pulse has decayed entirely before the next pulse occurs. Therefore, although the pulse is repeated, the response of the analyzer to each pulse is the same as if it were a single nonrepeated pulse.

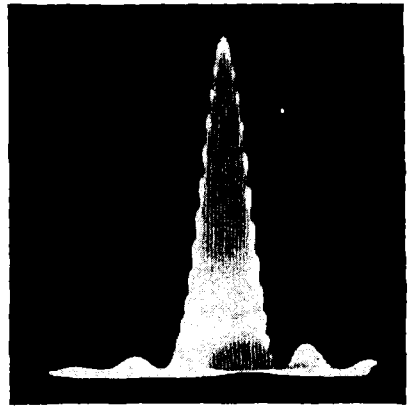

FIG. 7·1.—Spectrum of a 1-μsec rectangular r-f pulse as seen on a TS-148/UP spectrum analyzer.

The method of Fourier analysis shows that a single nonrepeated voltage transient may be expressed as the summation of the voltages of sine and cosine waves with incremental frequency differences over all frequencies from zero to infinity. The amplitude of these voltages as a function of frequency is the frequency function. The square of the absolute value of the frequency function is the power spectrum which is seen on the analyzer screen.

A receiver that has a sufficiently wide bandwidth to include the total range of the frequency function and has a linear phase response would reproduce the original form of the pulse except for a time delay. The spectrum-analyzer i-f bandwidth, however, is made very narrow and does not respond to the entire frequency function but only to a very narrow section of it, a section sufficiently narrow to represent, for practical purposes, the value of the frequency function at a single frequency. This narrow band of frequencies is likewise the equivalent of an r-f pulse, but one much longer in duration and lower in voltage than the original pulse. This longer pulse, rectified by a square-law detector, gives a transient pulse on the cathode-ray-tube screen proportional to the power spectrum at the frequency for which the receiver is tuned. To produce the complete spectrum the analyzer is slowly swept in frequency, while the horizontal deflection is varied in synchronism. A succession of transients appears on the screen, which resemble a picket

fence, and the envelope of the transients is proportional to the power spectrum. For small ranges of frequency the horizontal deflection is accurately proportional to frequency. Figure 7·1 is a photograph of the spectrum, as seen on a TS-148/UP spectrum analyzer, of a 1-μsec rectangular pulse having negligible frequency modulation. Although in the photograph the individual transients composing the spectrum cannot be clearly seen, examination of the edges of the spectrum will show that it is composed of such transients.

The reception of c-w signals by the spectrum analyzer is very easily explained. If the analyzer sweeps through the c-w signal slowly, the

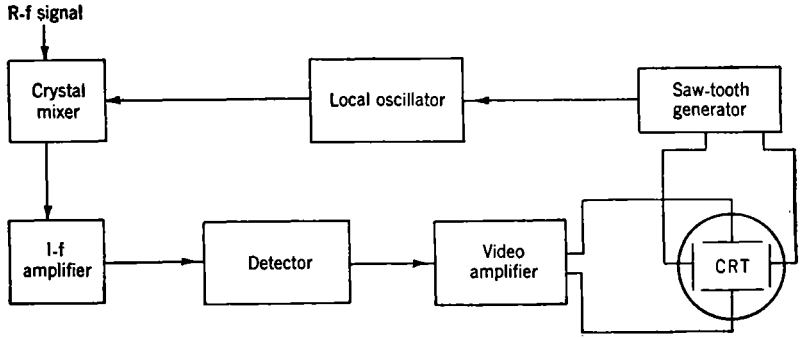

FIG. 7·2.—Basic circuit for a spectrum analyzer.

transient appearing on the screen will be just a plot of the pass band of the receiver. If the sweep is rapid, the transient may not reach its full amplitude and the amplitude becomes a function of the sweep rate. When seen in conjuction with pulsed spectra, a c-w signal can usually be identified by observing that there is a break in the baseline; for the pulse transients, which are faster, no such break is seen.

A block diagram of the basic circuit of a simple spectrum analyzer is shown in Fig. 7·2. The sawtooth generator at the upper right supplies the horizontal-sweep voltage of the cathode-ray-tube indicator. This voltage is also applied through a potentiometer to the reflector of the reflex local-oscillator tube, thus frequency-modulating the tube in accordance with the sawtooth waveform. The local-oscillator power is supplied to the crystal mixer (upper left) where it is combined with the incoming signal. If the frequency difference between the local-oscillator and signal frequencies is equal to the i-f frequency, a difference signal is produced which is proportional to the r-f signal and which is amplified by the i-f amplifier. The bandwidth of the i-f amplifier is purposely made much more narrow than that of a conventional radar receiver in order to achieve good resolution of the spectrum. The i-f amplifier may amplify at a

single frequency as in the TSS-4SE spectrum analyzer or it may use two intermediate frequencies, that is, it may have a second mixer to convert the signal to a still lower frequency. The TS-148/UP and the TSK-3RL spectrum analyzers are of this type.

Following the i-f amplifier and usually incorporated in the i-f-amplifier unit is the detector. The detector is usually operated at a small signal level so that its output voltage will be approximately square-law; however, the square-law characteristic cannot be relied upon for accurate measurements of the spectrum, and some method of calibration should be used. A video amplifier follows the detector to amplify the output voltage of the detector to a level suitable for the cathode-ray tube.

This is the basic circuit for a spectrum analyzer and shows the elements which cannot be omitted. However, more elements can be, and usually are, added to make the analyzer more useful, easier to operate, or to adapt it to a particular application. The modifications are sometimes so many and so great that it is difficult to recognize the basic spectrum analyzer. The section on applications of spectrum analyzers and the description of particular models of analyzers will illustrate the multitudinous additions and adaptations which are possible.

7·2. General Theory of Operation.—To illustrate the quantitative relations in the formation of the spectrum, the frequency functions representing two simple transients will be considered. The first transient is a rectangular r-f voltage pulse of length τ, symmetrically located with respect to the axis $t = 0$. For the duration of the pulse, the voltage is defined as $f(t) = A \cos \omega_0 t$. Fourier's integral theorem for a nonperiodic transient states that

$$f(t) = \int_{-\infty}^{\infty} a(\omega) e^{j\omega t}\, d\omega,$$

and (1)

$$a(\omega) = \frac{1}{2\pi} \int_{-\infty}^{\infty} f(t) e^{-j\omega t}\, dt.$$

For a symmetrical transient this simplifies to the form

$$f(t) = 2 \int_{0}^{\infty} a(\omega) \cos \omega t\, d\omega,$$

and (2)

$$a(\omega) = \frac{1}{\pi} \int_{0}^{\infty} f(t) \cos \omega t\, dt,$$

where $a(\omega)$ is the frequency function.

For the rectangular r-f pulse just mentioned, $a(\omega)$ has the form

$$a(\omega) = \frac{A}{\pi} \int_{0}^{\tau/2} \cos \omega_0 t \cos \omega t\, dt,$$

and if $\omega_0 \gg 1/\tau$,

$$a(\omega) = \frac{A\tau}{4\pi} \frac{\sin\ (\omega_0 - \omega)\ \frac{\tau}{2}}{(\omega_0 - \omega)\ \frac{\tau}{2}}. \tag{3}$$

The power spectrum $|a(\omega)|^2$ is given by

$$|a(\omega)|^2 = \frac{A^2\tau^2}{16\pi^2} \frac{\sin^2\ (\omega_0 - \omega)\ \frac{\tau}{2}}{(\omega_0 - \omega)^2\ \frac{\tau^2}{4}}. \tag{4}$$

The form of this function is shown in the graph, Fig. 7·3, of $\sin \pi x/\pi x$, where $x = (f_0 - f)\tau$. It may be noted that the first zero of the frequency function is at $x = 1$, or $|(f_0 - f)| = 1/\tau$, and the difference in frequency

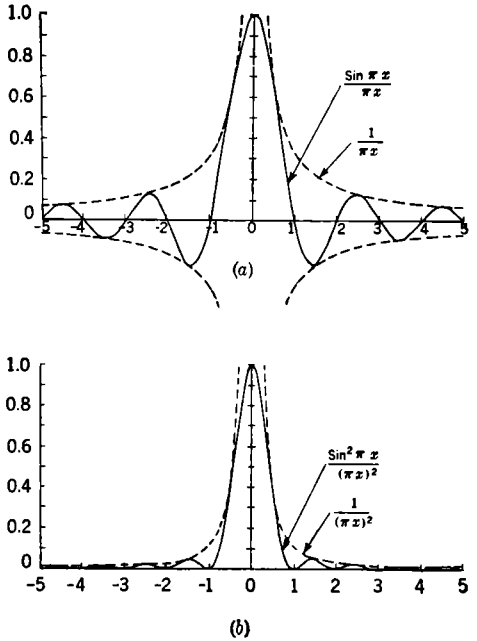

FIG. 7·3.—Graphs of $\sin \pi x/\pi x$, $\sin^2 \pi x/(\pi x)^2$.

between the first two zeros is $2/\tau$. Also plotted in Fig. 7·3 is the function $|a(\omega)|^2$, or $\sin^2 \pi x/(\pi x)^2$, which gives the power spectrum. The similarity of this figure to the spectrum photograph, Fig. 7·1, should be noted. A pulse 1 μsec long will have 2 Mc/sec between the first zeros of the spectrum and a pulse $\frac{1}{4}$ μsec long will have 8 Mc/sec.

The second r-f transient to be considered is the pulse with an error-function amplitude modulation. This waveform is unique in that $f(t)$ and $a(\omega)$ have the same form. The function $f(t)$ is given by the expression

$$f(t) = A' e^{-(kt)^2} \cos \omega_0' t. \tag{5}$$

The frequency function has the form

$$a(\omega) = \frac{A'}{\pi} \int_0^\infty e^{-(kt)^2} \cos \omega_0' t \cos \omega t \, dt,$$

and, assuming that $\omega_0' \gg 1/k$,

$$a(\omega) = \frac{A'}{4k\sqrt{\pi}} e^{-\left(\frac{\omega - \omega_0'}{2k}\right)^2}. \tag{6}$$

The usefulness of the expression for $a(\omega)$ in Eq. (6) is that it approximates the admittance function of the i-f amplifier. Many single-tuned stages, each tuned to the same frequency, have a pass band that approximates this admittance function as a limit, as the number of stages increases indefinitely. The frequency function representing the r-f transient at the output terminals of the i-f amplifier is the product of the admittance function and the frequency function of the r-f pulse. Since the i-f bandwidth is sufficiently narrow that $a(\omega)$ for the r-f pulse is essentially constant over that bandwidth, the expression $a(\omega)$, derived for the error-function pulse, is the form of the frequency function of the r-f transient of the i-f amplifier. The admittance function of the i-f amplifier is

$$g(\omega) = e^{-\left(\frac{\omega - \omega_0'}{2k}\right)^2},$$

corresponding to a transient

$$f(t) = 4k\sqrt{\pi}\, e^{-(kt)^2} \cos \omega_0' t.$$

If the receiver is tuned to a frequency ω in the region of the spectrum of the rectangular pulse, the frequency function at the output terminals of the i-f amplifier is given by

$$a(\omega) = \frac{A\tau}{4\pi} \frac{\sin (\omega_0 - \omega_0') \frac{\tau}{2}}{(\omega_0 - \omega_0') \frac{\tau}{2}} e^{-\left(\frac{\omega - \omega_0'}{2k}\right)^2},$$

and the corresponding transient is

$$f(t) = \frac{A\tau k}{\sqrt{\pi}} \frac{\sin (\omega_0 - \omega_0') \frac{\tau}{2}}{(\omega_0 - \omega_0) \frac{\tau}{2}} e^{-(kt)^2} \cos \omega_0' t. \tag{7}$$

The bandwidth of an amplifier is usually defined as the difference in frequencies for which the voltage amplitude is $1/\sqrt{2}$ times the maximum amplitude. This definition applied to the admittance function gives for the bandwidth the expression

$$\Delta f = \frac{2k}{3\sqrt{\pi}}.$$

This is not exact but is in error by only 0.3 per cent. If $f(t)$ in Eq. (7) is expressed in terms of i-f amplifier bandwidth, and if the frequency to which the analyzer is tuned is denoted by ω in place of ω_0', the result is

$$f(t) = \frac{3A\tau\Delta f}{2} \frac{\sin (\omega_0 - \omega)\frac{\tau}{2}}{(\omega_0 - \omega)\frac{\tau}{2}} e^{-\left(\frac{3\Delta f\sqrt{\pi}}{2}t\right)^2} \cos \omega t.$$

Detected by a square-law detector, the transient applied to the oscilloscope screen is

$$f(t) = \frac{9A^2\tau^2\Delta f^2}{4} \frac{\sin^2 (\omega_0 - \omega)\frac{\tau}{2}}{(\omega_0 - \omega)^2\frac{\tau^2}{4}} e^{-\left(\frac{3\Delta f\sqrt{\pi}}{\sqrt{2}}t\right)^2}. \tag{8}$$

The envelope of the peaks of the transients has the form

$$f(t) = \frac{9A^2\tau^2\Delta f^2}{4} \frac{\sin^2 (\omega_0 - \omega)\frac{\tau}{2}}{(\omega_0 - \omega)^2\frac{\tau^2}{4}},$$

which is proportional to the power spectrum of the rectangular pulse given in Eq. (4).

Besides showing analytically that the envelope of the transients appearing on an analyzer screen actually gives the power spectrum, the expression for $f(t)$ just developed shows the loss of sensitivity of the analyzer caused by its narrow bandwidth. If the i-f amplifier had infinite bandwidth and no phase distortion, it would reproduce the original pulse exactly with an amplitude a proportional to A. With the same gain but a narrow bandwidth the transient amplitude is given by $3a\tau\Delta f/2$, when the analyzer is tuned to the center of the spectrum. The loss of sensitivity in voltage is

$$\alpha = \frac{3\tau\Delta f}{2}, \tag{9}$$

and the loss of sensitivity in power is

$$\beta = \alpha^2 = \frac{9\tau^2\Delta f^2}{4}. \tag{10}$$

A spectrum analyzer having a bandwidth of 50 kc/sec, when viewing an r-f pulse of $\frac{1}{2}$-μsec length, would experience a reduction of sensitivity[1] by a factor 1.4×10^{-3} in power or 28 db. In the discussion it was assumed that the admittance function of the i-f amplifier had a phase function equal to zero. This amounts to neglecting the time delay

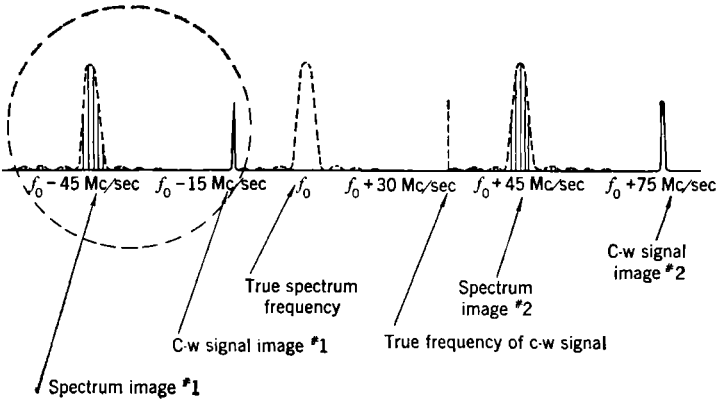

FIG. 7·4.—The spectra of a $\frac{1}{4}$-μsec rectangular r-f pulse and a c-w signal 30 Mc/sec higher in frequency as they would appear on the spectrum-analyzer screen. The intermediate frequency is 45 Mc/sec.

between the occurrence of the original pulse and the response of the i-f amplifier, an easily justifiable procedure.

Although the foregoing calculations do not assume that a superheterodyne receiver was used, the method applies equally well to that case and gives the same result, except that a superheterodyne receiver responds to more than one frequency. Both frequencies, $f_{LO} + f_{if}$ and $f_{LO} - f_{if}$ (where f_{LO} is the local-oscillator frequency and f_{if} the resonant frequency of the i-f amplifier) may beat with f_{LO} to produce f_{if}, which is amplified. The resultant spectrum is plotted not against the resonant frequencies of the receiver but against the local-oscillator frequency, which differs from them by the i-f frequency. Figure 7·4 shows the relation of the image spectra to the true spectrum frequency. The sweep range of the analyzer is limited and it is impossible to see the whole pattern at once, but by tuning the local oscillator any section of it can be seen. Such a typical section is shown by the dashed circle.

It should be noted that a superheterodyne receiver is sensitive to more than the two image frequencies shown in Fig. 7·4. For example, the frequencies $f_{LO} \pm f_{if}/2$ are amplified as well as the frequencies $f_{LO} \pm f_{if}$.

[1] The effect on the spectrum amplitude of changing the pulse length is illustrated by the spectra shown in Fig. 7·29. The pulse lengths are 0.5, 0.99, and 2.0 μsec; the attenuations necessary to equalize the amplitudes of the spectra closely approximate 0, 6, and 12 db as would be expected from Eq. (10).

If the signal is strong, the difference frequency $f_{if}/2$ is produced and is multiplied by the mixer crystal to produce f_{if} which then is amplified. Similarly the analyzer will respond to $f_{LO} \pm f_{if}/n$ to produce nth-order images. Although those higher-order images are of much lower amplitude than the first-order images they may be observed when a c-w signal of large amplitude is present, and frequently cause considerable confusion. Figure 7·5 is a graph of higher-order images as observed on a TSX-4SE

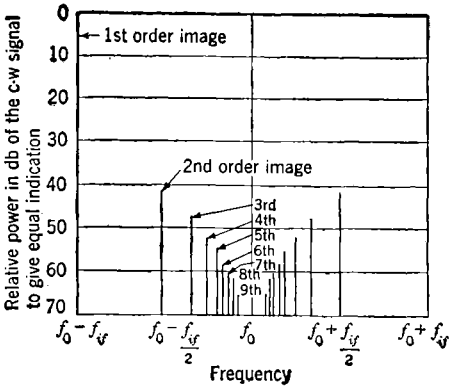

FIG. 7·5.—High-order images in the TSX-4SE spectrum analyzer.

spectrum analyzer. Frequency is plotted horizontally, f_0 being the frequency of the c-w signal. The images are spaced symmetrically about f_0. Plotted vertically is the number of decibels by which the c-w power must be increased for the nth-order image to give the same deflection as the first-order image.

7·3. Determination of Sweep Frequency, Intermediate Frequency, I-f Bandwidth, and Video Bandwidth.—Although the components of a spectrum analyzer and their functions have been discussed, nothing has been said about the design of the components to adapt the analyzer for a particular application. Although a single spectrum analyzer is frequently used to perform a large number of functions, the analyzer will be a more useful tool if it is designed to meet specific applications. If a pulse signal is used for radio transmission, the energy of the pulse should be confined to the narrowest possible band of frequencies in order to avoid loss of signal at the receiver. The spectrum analyzer provides the most direct and the simplest way of determining the frequency distribution of power in the r-f pulse. The manner in which the r-f pulse source dictates the design of the spectrum analyzer will now be described.

The local oscillator should be tunable throughout the frequency range of the r-f signals to be observed and the range of the frequency sweep should cover the principal region of the spectrum; for the rec-

tangular pulse at least three or four zeros should be visible on either side of the center lobe (see Fig. 7·1).

The spectrum as seen on the screen of the cathode-ray tube consists of a pattern of vertical transients, the envelope of which corresponds to the power spectrum of the pulse. Since each transient is produced by a single r-f pulse, the period of the transients is the repetition period of the r-f pulses. The separation of the transient pulses on the screen is determined by the sweep length in centimeters, the sweep frequency of the receiver, and the repetition frequency of the r-f pulses. If these quantities are designated as b, f_s, and f_r, respectively, the separation of the pulses in centimeters is bf_s/f_r, assuming that the voltage applied to the horizontal deflecting plates is a linear sawtooth waveform. The number of pulses in a single sweep is f_r/f_s.

To achieve adequate detail in the spectrum it is desirable that the number of transients in the region between the third minima of the spectrum be 50 or more (see Fig. 7·4). If this region covers the CRT screen, a sweep frequency of 10 cps is required for a pulse repetition frequency of 500 per sec, slow enough for the eye to see the spot of light moving across the screen. On the other hand, if the pulse repetition frequency were 1000 cps, an equivalent resolution would be achieved with a sweep frequency of 20 cps which would result in a barely detectable flicker. It might be argued that the number of transients appearing on the screen per unit time is independent of sweep frequency, hence the appearance of the spectrum should likewise be independent of repetition frequency. Actually when the sweep frequency is low enough in relation to the decay times of the CRT screen and the eye for a flicker to be observed, the eye sees a single sweep as a unit. The spectrum will appear more empty as the sweep frequency is increased. Of course the situation is changed when a screen having long persistence (such as a P7 screen) is used in place of the more usual P1 screen. The sweep frequency can then be varied over a much wider range without affecting the detail of the spectrum. In fact some very pretty spectra may be observed on a long-persistence screen. Such a screen, however, is a disadvantage when there is a frequency drift of the spectrum analyzer or of the pulse source or when it is desirable to change the tuning rapidly.

It is thus evident that the choice of sweep frequency is governed by the pulse repetition frequency and the type of cathode-ray-tube screen used. To make maximum use of the detail afforded by the spectrum analyzer, the spectrum should be expanded until only the main lobe and the first few minima are seen on the screen at one time. Since a particular reflector voltage, and thus a particular position on the screen, corresponds to a unique frequency, the form of the spectrum will be

independent of the exact waveform of the sweep voltage. There are two reasons for making the horizontal sweep a linear sawtooth waveform. First, any other choice would make the spacing of the transients vary across the screen and, second, a fast return trace is necessary since thermal effects in the oscillator would otherwise cause a slightly displaced spectrum to appear on the return trace.

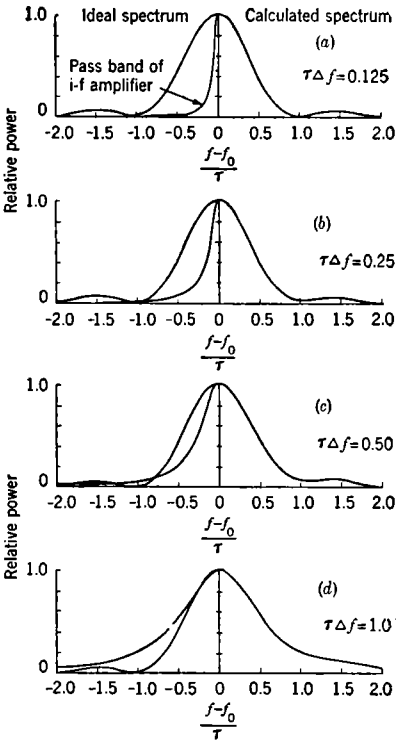

FIG. 7·6.—The effect of spectrum-analyzer bandwidth on the shape of the spectrum of a rectangular r-f pulse as it appears on the analyzer screen. The pulse length is τ sec, the bandwidth of the i-f amplifier is Δf cps.

As the proper choice of sweep frequency is dictated by the repetition rate of the r-f pulse signal, similarly, the proper choice of i-f frequency and i-f bandwidth is dictated by the pulse length. The lowest repetition rate of the pulse signal determines an upper limit for the sweep frequency. Likewise, the longest pulse length to be used determines the maximum value of the bandwidth of the i-f amplifier in order that the spectrum as seen on the analyzer screen be a true reproduction of the power spectrum. The shortest pulse length, on the other hand, determines the minimum intermediate frequency which may be used in order to avoid appreciable overlapping of the image spectra.

For a rectangular r-f pulse the width of the spectrum is increased as the pulse length is decreased. The frequency difference between first minima is equal to $2/\tau$, where τ is the pulse length in seconds. Thus, for a 1-μsec pulse the frequency difference between minima is 2 Mc/sec, while for a 5-μsec pulse, it is 0.4 Mc/sec. To achieve adequate resolution of the spectrum, the bandwidth of the i-f amplifier must be narrow compared to $2/\tau$. In Sec. 7·2 it was assumed that the i-f bandwidth Δf was infinitely narrow compared to $2/\tau$; in practice, however, if $\tau\Delta f$ is made 0.1 or less, it is not possible to detect the difference between the form of the spectrum and that of the spectrum function. The graphs in Fig. 7·6 show the effect of changing $\tau\Delta f$. It will be noticed that the

spectrum does not become worse rapidly and that the first effect to be seen is that the minima are no longer zero.

The achievement of adequate separation of the image spectra places a lower limit on the intermediate frequency which may be used. For a rectangular pulse, Fig. 7·3, the power in the fourth side lobe of the spectrum is about one-third of one per cent of the power at the spectrum center. Therefore, no appreciable overlapping of the spectra will occur if side lobes beyond the third overlap the third and lower side lobes of the other image. This condition requires the intermediate frequency to be equal to or greater than $4/\tau$, twice the separation of the first minima. Figure 7·7 shows the appearance of the images in this case.

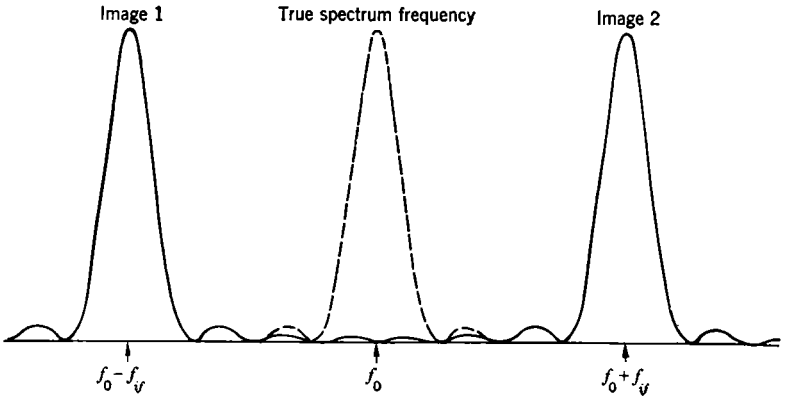

FIG. 7·7.—Appearance of the spectrum of a rectangular r-f pulse when the intermediate frequency of the analyzer is twice the separation of the first minima.

Since the pulse length determines the limits for the i-f bandwidth and the intermediate frequency, it is clear that the range of pulse lengths which must be accommodated will determine jointly maximum i-f band and minimum intermediate frequency. If the range of pulse lengths to be used is large, complications may arise in the design of the i-f amplifier. To consider a particular case, let the range of pulse lengths be from 5 to $\frac{1}{2}$ μsec. This requires an i-f bandwidth of 20 kc/sec or less and an intermediate frequency of 8 Mc/sec. It would be difficult to build an i-f amplifier at 8 Mc/sec with such a narrow bandwidth but the problem could be solved by using a double intermediate frequency; that is, amplifying at 8 Mc/sec, then converting to a still lower frequency where the narrow bandwidth could be achieved. Two of the spectrum analyzers to be described later use an i-f amplifier of this type.

It should be made clear that it is the i-f bandwidth and not the bandwidth of the video amplifier which determines the resolution of the spectrum. All of the spectrum resolution has been accomplished by

the time the signal reaches the detector. The video amplifier should amplify the transient signal without excessive loss in amplitude because of its bandwidth. Other than this, the characteristics of the video amplifier are of relatively little importance, since the exact form of the transient is never observed.

7·4. Determination of the Sensitivity and I-f Gain Required for a Given Application.—A spectrum analyzer is usually designed for use in a wide variety of applications requiring different sensitivities. Consequently, the sensitivity is made variable by means of r-f attenuators and an i-f gain control. The maximum sensitivity is, of course, dictated by the application requiring the greatest sensitivity.

The spectrum analyzer, like all other receivers, has a limit imposed upon its sensitivity by noise. For the design of spectrum analyzers for any given application, it is necessary to know the value of this limit. Since the analyzer is seldom used at very high sensitivity the mixer and input stages need not usually be designed as carefully as those for radar receivers.

A signal equal in power to noise produced in the receiver will have a power

$$S = NF,$$

where N is the noise power of an ideal receiver and F is the noise figure of the actual receiver. N is calculated from

$$N = kT\Delta f,$$

where

k = Boltzmann's constant, 1.37×10^{-23} joule/° Kelvin
T = Temperature in degrees Kelvin
Δf = Noise bandwidth of the receiver.

If $T = 293$°K (20°C), and $\Delta f = 100$ kc/sec, $N = 4.03 \times 10^{-16}$ watt or -154 dbw. A typical analyzer receiver may have a noise figure of 20 db, or $10 \log_{10} F = 20$. A signal equal to noise then would have a power of -154 dbw $+20$ dbw $= -134$ dbw, or expressed as decibels below one milliwatt, -104 dbm. If it is required, for example, that the fluctuations caused by noise be 3 per cent or less in power, and it is assumed arbitrarily that the peak power of noise is 4 times the rms value, the ratio of necessary signal power to noise power is 4 to 0.03, or 21 db. The r-f sensitivity of the analyzer should be made not greater than -83 dbm.

In viewing spectra of magnetrons, high sensitivity is not required since more than enough power is available. The problem in this case is that of introducing enough attenuation between the magnetron and the mixer crystal to ensure linear mixing, which requires that the signal power be small relative to the local-oscillator power. An initial attenuation of 20 or 30 db is usually achieved by a directional coupler which

extracts a small part of the power incident upon it from the magnetron. Thereafter, resistive or cutoff attenuators in the analyzer reduce the power to the required level.

To illustrate the determination of the required i-f sensitivity for a pulsed r-f signal, consider the case of a low-power oscillator, with a peak power of 10 mw, producing a rectangular pulse of 1 μ sec duration with no frequency modulation. The spectrum analyzer has a bandwidth of 50 kc/sec. If the output power of this oscillator is attenuated by 20 db before reaching the crystal mixer in the analyzer, this peak signal power of 0.1 mw meets the requirements of being small compared with the local-oscillator power which is usually about 1 mw.

The gain of the crystal is defined as the ratio of available i-f power from the crystal mixer to the available r-f power. The gain differs with the type of crystal and with the individual crystal but may be taken to be about 0.25.

Assuming that the form of the pulse is not modified by transmission through the r-f section and the crystal, there will appear at the input terminals of the i-f amplifier an i-f pulse with a peak power of 25 μw. The crystal impedance may be about 400 ohms, in which case the peak voltage will be 0.1 volt. However, the i-f amplifier must have a sensitivity considerably greater than 0.1 volt because of the loss in signal amplitude by transmission through the narrow-band filter.

In Sec. 7·2, an expression was developed for the peak voltage amplitude of the r-f transient at the output terminal of the i-f amplifier relative to the peak voltage, if the video amplifier has a wide response, and the receiver is tuned to the center frequency of the initial r-f pulse. This expression is

$$\alpha = \tfrac{3}{2}\tau\Delta f.$$

Substituting in this formula an i-f bandwidth of 50 kc/sec and a pulse duration of 1 μsec, $\alpha = 7.5 \times 10^{-2}$ is obtained. The i-f amplifier must, therefore, be designed to have a sensitivity at least as great as 7.5 mv.

Another use to which the spectrum analyzer is frequently put is the detection of leakage signals from a c-w local oscillator, so that the frequency and operation of the oscillator may be judged without removing the oscillator from the circuit in which it is being used. The sensitivity required of the analyzer is about -70 dbm or 10^{-10} watt. Assuming, as before, a gain of 0.25 for the crystal mixer and a resistance of 400 ohms, the i-f voltage sensitivity must be 10^{-4} volt, or 0.1 mv. For reception of c-w signals the output indication is independent of the i-f bandwidth; in fact, as will be seen in the next section, it would be desirable from considerations of stability to make the i-f bandwidth large.

A spectrum analyzer should have a maximum sensitivity dictated by the application which requires greatest sensitivity, whereas for other

uses, the sensitivity must be decreased either by reducing the i-f gain or introducing r-f attenuation. The i-f gain, however, must not be reduced so far that the peak r-f power will produce nonlinear distortion in the mixer crystal. If a large amount of r-f attenuation is to be used, care must be taken to minimize leakage. If this is not done, the leakage signal may obscure the input signal; similarly if attenuation measurements are to be made, leakage will cause completely erroneous results.

To illustrate the design for two applications, assume that a spectrum analyzer is to be used to detect c-w leakage signals requiring a c-w sensitivity of -70 dbm and also for viewing pulses from a 5-kw r-f source through a 20-db directional coupler. The pulse duration is 1 μsec and the spectrum-analyzer i-f bandwidth is 50 kc/sec. A possible solution of this problem is to use an i-f gain control which will vary the c-w voltage sensitivity of the i-f amplifier from 10^{-4} volt for c-w measurements to 7.5×10^{-3} volt for pulse measurements. Zero r-f attenuation would be used for c-w measurements; however, an attenuation of 57 db would be needed to reduce the 50-watt peaks from the directional coupler to the 10^{-4} watt necessary to avoid distortion in the mixer. If the analyzer is to be used at intermediate sensitivities, both the i-f gain and r-f attenuator must be variable, since the i-f gain control alone cannot cover 57 db. If desired, a step r-f attenuator might be used.

7·5. Stability Considerations in the Design of a Spectrum Analyzer.—There is no theoretical reason why a spectrum analyzer cannot be built with a bandwidth of 2 kc/sec for the analysis of 50-μsec pulses, assuming that such pulses can be obtained without having the frequency modulation completely obscure the pattern. However, in practice considerable difficulty is encountered because of the instability of the frequency-modulated local oscillator. Reflex oscillators of the type used in spectrum analyzers at microwave frequencies sweep over tens of megacycles per second and have reflector sensitivities of several megacycles per second per volt. Ripple voltage from the power supplies, heater-voltage changes, thermal-drift effects, and microphonics all contribute to distort the spectrum badly, or to cause it to drift rapidly off the screen Thus, unless a special stabilized local oscillator is used, such an analyzer is not practical.

If a spectrum analyzer is to be used for long pulses, supply voltages must be carefully regulated. For example, assume a reflector sensitivity of 3 Mc/sec per volt and a 2-μsec pulse. The spectrum will not be badly distorted if the frequency modulation of the local oscillator is limited to 4 per cent of the frequency difference between the first minima of the spectrum. The frequency modulation must be limited to 40 kc/sec, or the reflector modulation to 0.013 volt, which would result from a sine-wave modulating voltage of 4.6 mv rms. The stability of cavity voltage

is almost as important as reflector voltage. Frequently, heater voltage also must be regulated.

Frequency modulation caused by instability is also important in the reception of c-w signals. If the sweep frequency is synchronized with the supply frequency and the sweep expanded to give a clear indication of the form of the signal, frequency modulation due to the supply frequency will appear as changes in the width of the signal as the signal is moved across the screen by changing the reflector voltage.

The major importance of frequency modulation when viewing a c-w signal lies in the following effect. When the sweep frequency is high the amplitude and form of the output transient cease to be independent of the sweep speed because of the limiting response time of r-f and video amplifiers. Since the output transient is a function of the sweep speed (inverse square if the sweep speed is very high), its amplitude becomes a function of the frequency modulation of the sweep. It is easily observed that the amplitude of a c-w signal decreases as the sweep frequency or sweep speed expressed in megacycles per second per centimeter on the screen is increased beyond a certain point. If frequency modulation is present, the amplitude of the signal will fluctuate violently even though the signal strength is far above noise. If the sweep speed is suddenly increased a small transient results; if it is suddenly decreased there is a larger transient. The effect is of importance when the analyzer is used as a c-w detector, as it makes accurate amplitude measurements difficult. The effect can be minimized in two ways, by decreasing the sweep speed, or by increasing the bandwidth of the i-f amplifier, both of which methods lengthen the transient. It is better to increase the bandwidth since the requirements for frequency stability are thereby reduced. A spectrum analyzer for c-w measurements should have as wide a bandwidth as possible.

REPRESENTATIVE SPECTRUM ANALYZERS

The general theory of operation of a spectrum analyzer and the formation of the spectrum have been discussed in some detail, the functions of the components have been explained, and the principles of their design have been developed enough to permit the selection of a suitable analyzer or the designing of one for a specific need. Representative spectrum analyzers will now be described, particularly those which are of late design or those to which the reader may have access.

7·6. The TSK-3RL 1-cm-band Spectrum Analyzer.—The first spectrum analyzer to be described is the TSK-3RL (Radiation Laboratory designation). This has been chosen not for its availability but because it is of recent design and illustrates the application of the principles of design developed in Secs. 7·3 to 7·5; in addition, it is the one with which

the author has had the closest connection. Only a limited number of TSK-3RL analyzers have been produced.

General Description.—The TSK-3RL is a 1-cm spectrum analyzer designed for use with radar equipment in the range 23,500 to 24,500 Mc/sec. It is intended mainly to serve two specific functions: to analyze the spectra of magnetrons with pulse lengths varying from 1 to 0.1 μsec, and to permit the observation of the c-w signals from radar and beacon local oscillators, thus enabling them to be tuned properly.

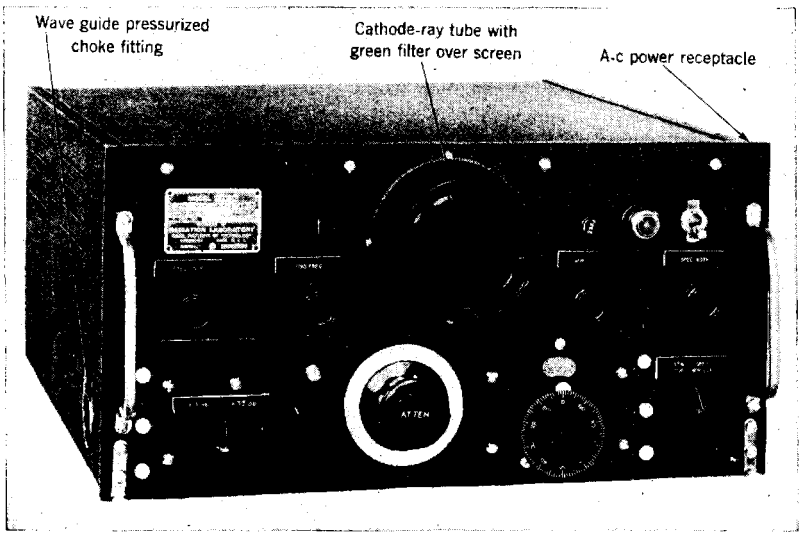

FIG. 7·8.—Control panel of TSK-3RL 1-cm spectrum analyzer.

The TSK-3RL spectrum analyzer is designed to operate from a power supply of 105 to 125 volts, 50 to 1200 cps. The power consumption is less than 150 watts. The bandwidth of the i-f amplifier is approximately 100 kc/sec. The i-f amplifier has two intermediate frequencies, the first being 45 Mc/sec and the second, after the second mixer, 6.5 Mc/sec. The sensitivity required for a c-w signal to give a 1-in. deflection is greater than −66 dbm. Besides spare parts the analyzer is furnished with a 1-cm-band pickup horn and a 2-ft length of flexible waveguide to aid in picking up the leakage signal from the radar local oscillator.

Physical Description.—The spectrum analyzer is built in a standard aircraft-rack assembly and has over-all dimensions of $15\frac{1}{2}$ in. wide, 8 in. high and $17\frac{1}{2}$ in. deep. The weight of the analyzer proper is 31 lb. The plywood carrying case has dimensions, 20 in. wide, 13 in. high, and $21\frac{3}{4}$ in. deep. It contains compartments for spare parts and cables. The combined weight of the analyzer, spare parts, and carrying case is 58 lb. Figure 7·8 shows the front control panel of the TSK-3RL analyzer.

Components of the TSK-3RL Analyzer.—The analyzer is swept in frequency by modulating the high-frequency local oscillator. The high-frequency local-oscillator tube used in the TSK-3RL is a type 2K50 reflex klystron. This tube may be rapidly modulated over an extreme range of 100 Mc/sec by applying the modulating voltage to the reflector. Tuning of this tube over the band is accomplished by an auxiliary "tuning triode" in the same envelope. The grid voltage of this triode controls the plate dissipation, thus expanding the plate element and thereby mechan-

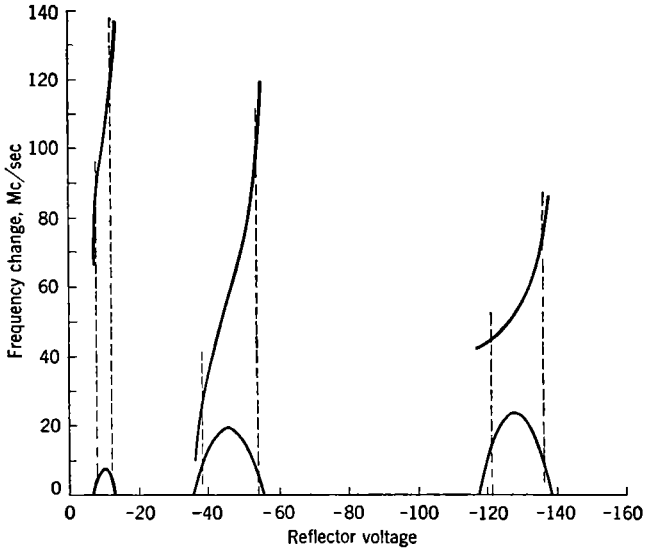

FIG. 7·9.—Modes of the 2K50 oscillator. The upper curves represent frequency change; the lower curves represent relative power.

ically tuning the oscillator section. The construction of the gun and tuner sections of the 2K50 tube is shown in Fig. 2·23. Figure 2·22 is a photograph of the 2K50 tube. The 2K50 operates with a cavity voltage of 300 volts, a gun-cathode current less than 25 ma, and has an output power greater than 10 mw at the center of the band. A negative voltage change on either reflector or tuner grid has the effect of increasing the frequency. There may be more than one mode of oscillation for this tube. These modes are in general characterized by different output powers, different maximum frequency ranges, and different values of the electronic tuning. The mode for which the tube was designed is characterized by moderate output power and a maximum frequency range. The modes of the 2K50 in frequency and output power are shown in Fig. 7·9.

Referring to the block diagram for TSK-3RL, Fig. 7·10, it will be seen that the modulating voltage for the reflector is derived from the

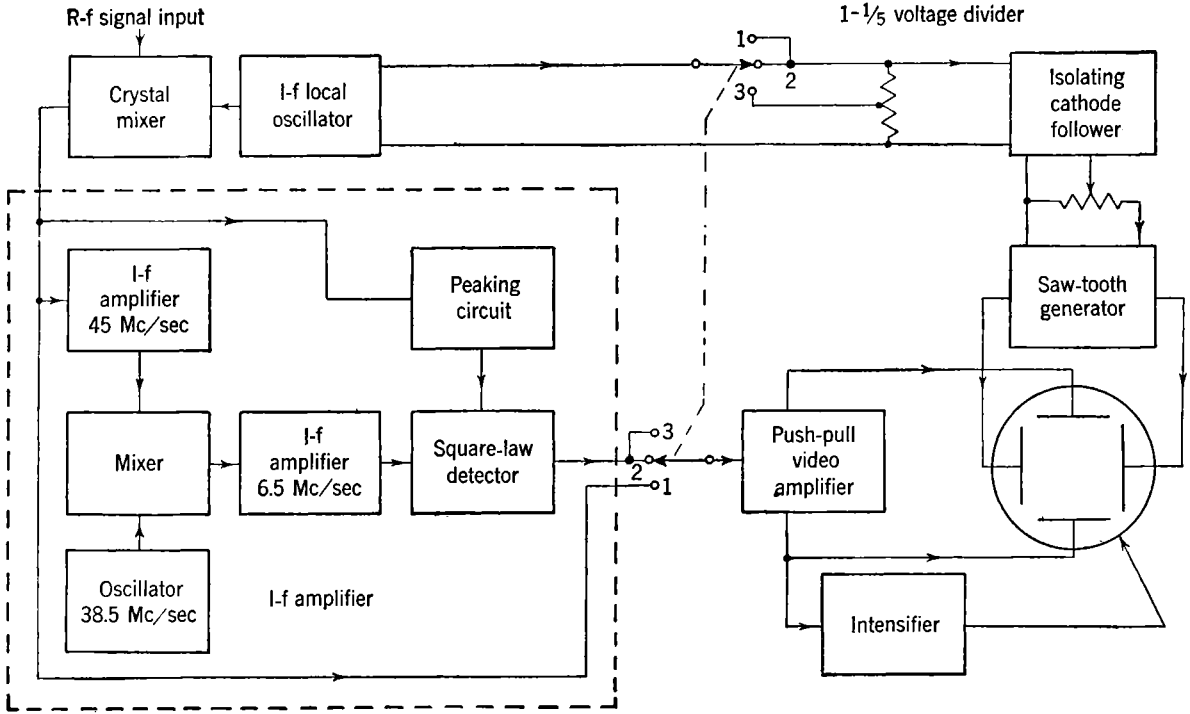

FIG. 7·10.—Block diagram for TSK-3RL 1-cm spectrum analyzer.

sawtooth generator. The sawtooth generator consists of a thyratron in a circuit providing push-pull deflection for the cathode-ray tube. An isolating cathode-follower provides sawtooth output voltage to the voltage divider and the reflector.

The local-oscillator output signal and the r-f input signal are combined in the crystal mixer, and the difference frequency, if it lies in a narrow band centered at 45 Mc/sec, is amplified by the i-f amplifier. The two image frequencies are $f_{if} + 45$ Mc/sec and $f_{if} - 45$ Mc/sec and

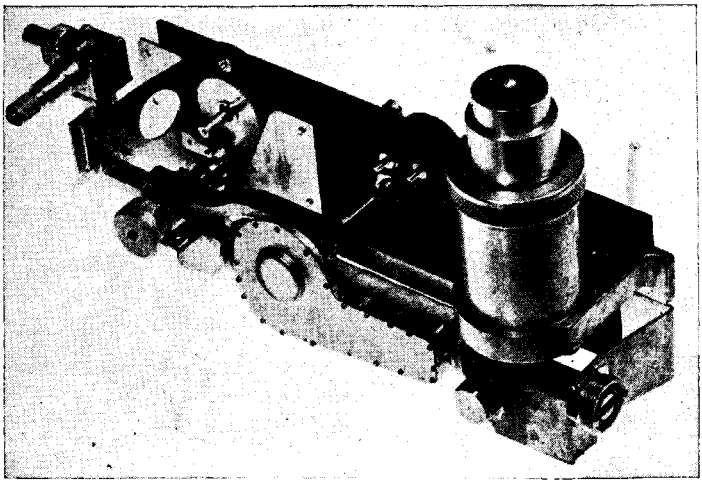

FIG. 7·11.—Photograph of TSK-3RL r-f circuit.

are spaced by 90 Mc/sec. The i-f bandwidth of 100 kc/sec is achieved by the use of the double-frequency i-f amplifier. Since the longest pulse length to be observed is 1 μsec, the condition that $\tau_{max}\Delta f \leqq \frac{1}{10}$ developed in Sec. 7·3 is satisfied; also since the shortest pulse is 0.1 μsec, the condition $f_{if} \geqq 4/\tau_{min}$ is also satisfied. The exact frequency 45 Mc/sec for f_{if} is chosen so that with either 30- or 60-Mc/sec radar receivers a local-oscillator signal is found 15 Mc/sec distant from a spectrum image. A square-law detector gives an output signal proportional to power of the r-f signal. A pair of pentodes with cathode phase inversion serves as the video amplifier and gives push-pull vertical deflection which aids considerably in focusing the spectrum.

Since the presentation of an r-f pulse is a short transient, to obtain sufficient light intensity to see this transient easily an intensifier circuit has been incorporated to brighten the trace for the duration of the transient. To intensify the trace and at the same time preserve optimum focus, an out-of-phase signal is simultaneously applied to the focus electrode.

The three-position switch on the front panel has the following functions. In the first position a plot of crystal current (a function of r-f power) versus reflector voltage is presented on the screen. The frequency-meter marker pip appears superimposed on the crystal current which greatly facilitates adjusting the analyzer. The second position provides normal operation; in the third position the reflector modulation voltage is changed and the sweep is expanded by a definite factor (approximately five).

A very important part of a spectrum analyzer is the r-f circuit. The r-f circuit of TSK-3RL is shown as a photograph in Fig. 7·11 and in block diagram form in Fig. 7·12. The r-f circuit is mounted on a removable section of the front panel for ease of assembly. The function which the

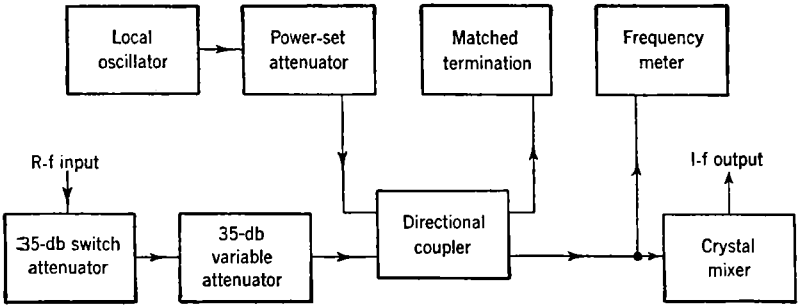

FIG. 7·12.—Block diagram for the TSK-3RL r-f circuit.

r-f circuit performs is the mixing of the incoming r-f signal with the local-oscillator signal to produce a beat-frequency signal that can be amplified. Because of the wide range of power encountered, the input signal passes through two r-f attenuators on its way to the crystal mixer. The first of the two attenuators is a switch attenuator, which introduces an attenuation of 35 db when in the ON position. The second is a calibrated continuously variable attenuator with a maximum attenuation of 35 db or more. The total maximum attenuation of 70 db with the additional attenuation of 20 db in the directional coupler in the radar set would reduce a 50-kw peak signal to a 50-μw peak signal that is sufficiently small to preserve linearity in the mixing. The local-oscillator power required is about 1 mw. The output power from the local oscillator, however, is many times that value, being 10 mw or more. Local-oscillator power is introduced into the crystal mixer through a directional coupler of 7 db coupling and is adjusted to the proper value by the power-set attenuator. The directional coupler prevents coupling between the local oscillator and the r-f input line, and makes the local oscillator relatively independent of impedance changes such as those occurring when the analyzer is being operated with zero r-f attenuation.

The frequency meter is of the reaction type and is connected between the directional coupler and the crystal mixer. In this location it can cause a dip in either the local-oscillator power or the signal power. The dip in the local-oscillator power amounting to perhaps 25 per cent causes a transient in the crystal current as the local oscillator sweeps through the cavity frequency. This transient when differentiated and introduced on the screen along with the spectrum provides a convenient frequency marker. The frequency has been zero-set at midband and reads directly in megacycles per second on a compound dial. For highest accuracy a correction should be applied to the reading. The bandwidth of the marker pips is about 3 Mc/sec. For frequency-difference measurements, the intermediate frequency may be used as a standard and it is more accurate than the frequency meter. Any two corresponding images will be separated by twice the intermediate frequency or 90 Mc/sec. This frequency difference may be used to calibrate part of the frequency-meter dial. To increase the accuracy of measurements of small frequency differences the sweep-expansion feature was developed. This feature permits calibration of the sweep by means of a large frequency difference and allows measurements to be made with a sweep expanded by a definite multiple of the original length.

Operating Controls of the TSK-3RL Analyzer.—Only the controls necessary for actual operation appear on the front panel. Other preset controls are mounted below the chassis. The analyzer is designed in such a manner that frequency increases from left to right on the screen and clockwise rotation of oscillator-frequency or spectrum-center control causes the spectrum to move to the right. Clockwise rotation of the frequency-meter dial moves the marker to higher frequency. Clockwise rotation of the variable attenuator and the i-f gain control increases the sensitivity. However, the OFF position of the switch attenuator is in the counterclockwise direction.

The front panel controls are the following: (1) oscillator frequency (bias on the tuner section of the 2K50), (2) spectrum center (reflector voltage), (3) spectrum width (sawtooth amplitude), (4) i-f gain, (5) crystal-current—spectrum-normal—spectrum-expanded switch, (6) attenuator (variable), (7) +0 db to +35 db (switch attenuator), (8) frequency meter, (9) focus and power. The preset controls are vertical-centering, horizontal-centering, intensity, 300-volt adjustment, and power-set (local-oscillator attenuator).

7·7. The TS-148/UP 3-cm-band Spectrum Analyzer.—The TS-148/UP (Army-Navy designation) was chosen as a representative 3-cm-band spectrum analyzer because more of these sets have been produced than any other 3-cm-band spectrum analyzer. In addition the TS-148/UP is smaller, more compact, and gives a better spectrum than the TSX-4SE

(Radiation Laboratory designation), the other 3-cm-band analyzer which is in extensive use. The TS-148/UP, however, does not supersede the TSX-4SE as the latter has somewhat greater sensitivity, is provided with a calibrated cutoff attenuator, and is much better shielded against leakage. The TS-148/UP was designed and produced by Westinghouse

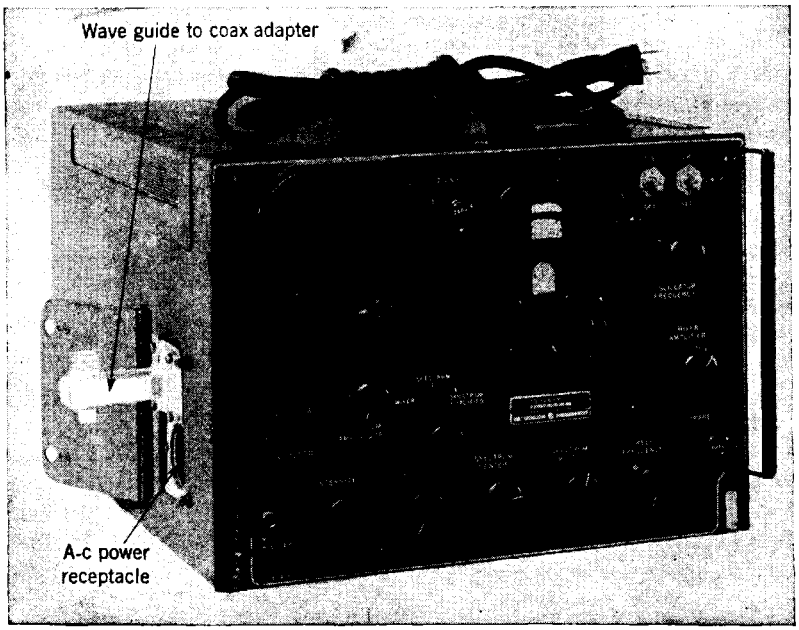

FIG. 7·13.—Photograph of front view of TS-148/UP.

Electric and Mfg. Co. with Radiation Laboratory as advisor. The TSX-4SE was designed by Radiation Laboratory and built by Sylvania Electric Products Co.

General Description.—The TS-148/UP spectrum analyzer is designed for use with radar and beacon equipments within the range of frequencies 8460 to 9630 Mc/sec. It is intended to permit the observation of pulsed or c-w signals in this range and the accurate measurement of their frequencies. The operation and the method of presentation of the spectrum are the same for the TS-148/UP as for the TSK-3RL. The TS-148/UP analyzer operates from a power supply of 105 to 125 volts, 50 to 1200 cps; the power consumption is 125 watts. The intermediate frequency is 22.5 Mc/sec and the bandwidth is 50 kc/sec; the i-f amplifier is of the double-frequency type, the second intermediate frequency being 3 Mc/sec. The sensitivity, which is -60 dbm for a minimum discernible c-w signal,

is sufficient to pick up a magnetron spectrum at a distance from the antenna. For stable coupling, however, the recommended method is to use a directional coupler. In addition to the usual functions, the analyzer may be used as a frequency-modulated signal generator to set the resonant frequency of cavities such as TR switches, wavemeters, and echo boxes. In addition to the ordinary spare parts and cables, the analyzer is provided with a pickup horn, a 6-ft horn cable, and a 15-in. length of flexible

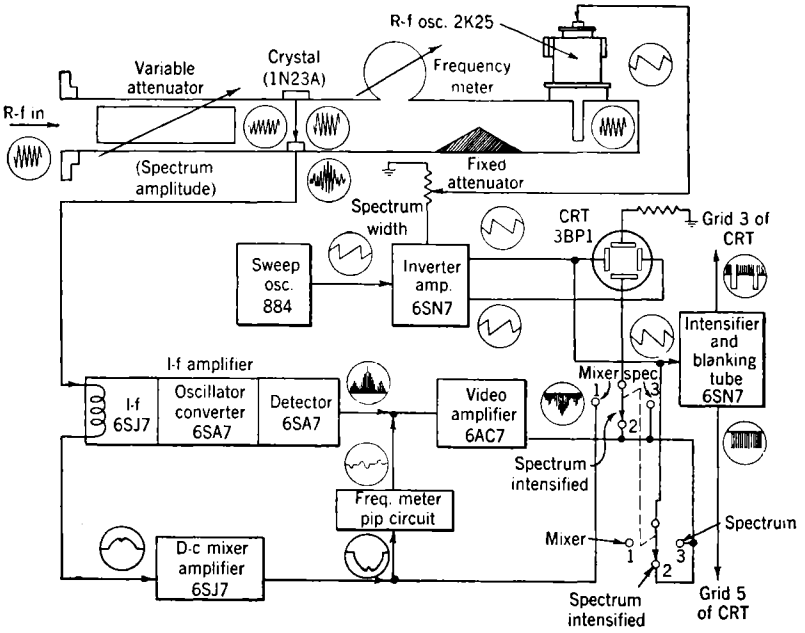

FIG. 7·14.—Block diagram of TS-148/UP spectrum analyzer.

waveguide. A front view of the TS-148/UP spectrum analyzer is given in Fig. 7·13. The spectrum analyzer proper has over-all dimensions of 9 by 13 by 14 in. and weighs 38 lb. Together with all spare parts and mounted in its carrying case the weight is about 70 lb. The dimensions of the carrying case are $25\frac{9}{16}$ by 18 by $13\frac{1}{2}$ in.

Components of the TS-148/UP Analyzer.—A block diagram of the components of TS-148/UP analyzer is shown in Fig. 7·14, and the circuit diagram is given in Fig. 7·15. The analyzer uses a mechanically tuned local oscillator, type 2K25, which has some advantage over a thermally tuned tube in that the frequency change is instantaneous when the oscillator-frequency control is turned. A photograph and a diagram of the internal construction of the 2K25 will be found in Figs. 2·11 and 2·10.

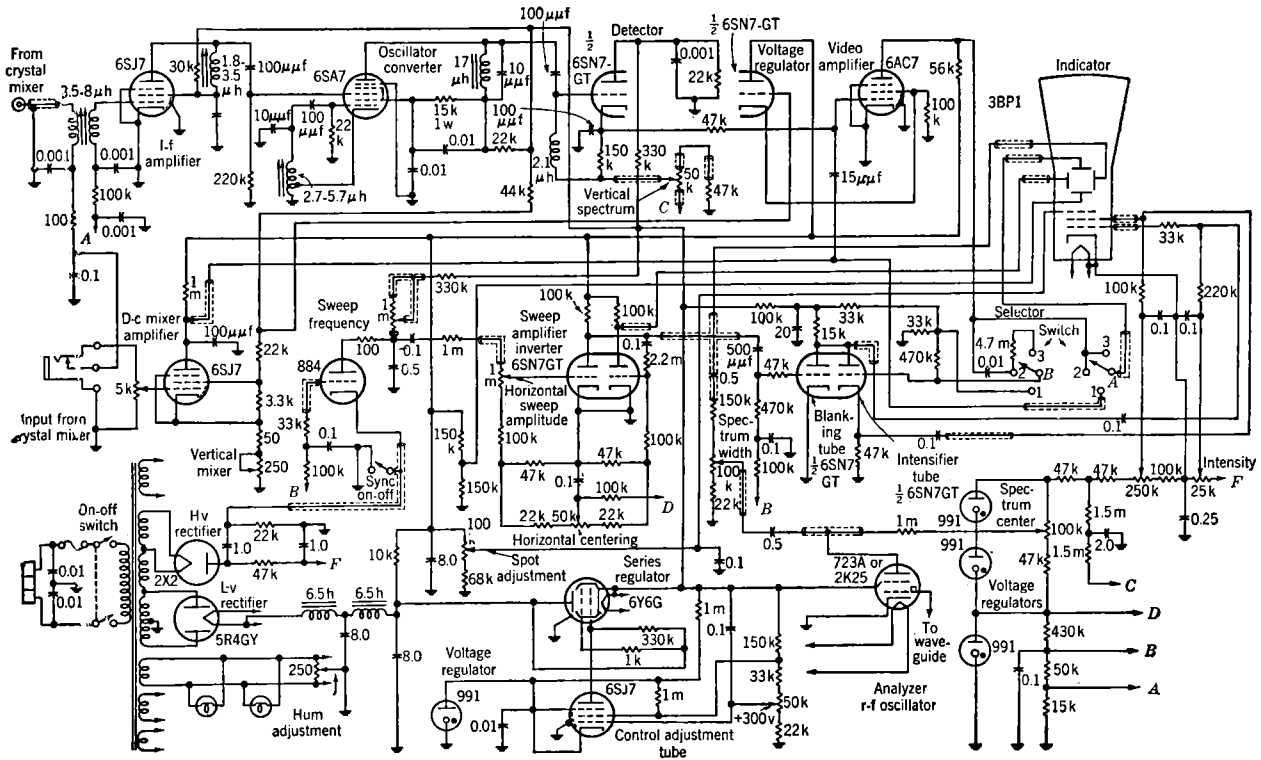

FIG. 7·15.—Circuit diagram of the TS-148/UP analyzer.

The oscillator can be frequency-modulated over a range up to 40 or 50 Mc/sec. The modulating voltage is derived from a sweep generator through an amplifier. The amplifier with a phase inverter provides push-pull horizontal deflection for the cathode-ray tube. The sweep frequency is continuously variable from 10 to 20 cps and can be synchronized with the line frequency.

The i-f amplifier operates at a frequency of 22.5 Mc/sec, which was chosen so that with $\frac{1}{4}$-μsec pulses the image spectra would be adequately separated and so that with either 30- or 60-Mc/sec radar intermediate frequencies a local-oscillator image would be 15 Mc/sec distant from a spectrum image. The output of the 22.5-Mc/sec amplifier is applied to an oscillator-converter stage that mixes the signal with a 19.5 Mc/sec locally generated signal to produce a 3-Mc/sec difference frequency. The sharply tuned bandpass characteristic of the oscillator-converter output-coupling circuit produces the narrow filter characteristic that is required. The 50-kc/sec bandwidth allows adequate resolution of pulses up to 2-μsec duration. The i-f output signal is applied to an infinite-input-impedance detector which is in turn directly connected to the video amplifier. The advantage gained by direct coupling is that, in the presence of large signals, the baseline remains fixed. The high-frequency response of the video amplifier is such that the i-f bandwidth is the limiting factor in the shape of a transient signal.

A separate high-gain direct-coupled amplifier is employed to amplify the crystal-current pattern; thus the crystal-current pattern also has a fixed baseline. A double-triode circuit is incorporated to blank the return trace and to intensify the transient signals.

The block diagram, Fig. 7·14, also shows the r-f circuit, which differs from that used in TSK-3RL. The r-f circuit of TS-148/UP is adapted for use both as a signal generator and as a spectrum analyzer. The crystal mixer does not terminate the r-f line but has local-oscillator power incident upon it from one direction and signal power from the other, through a variable attenuator with a range of 3 to 70 db. The frequency meter is connected between local oscillator and crystal mixer with a fixed attenuator between to prevent reaction on the local oscillator. A frequency-meter marker pip is generated in the usual manner and is introduced on the screen along with the spectrum. The bandwidth of the frequency meter used in TS-148/UP is much narrower than that of the frequency meter in TSK-3RL, being less than 0.5 Mc/sec. There is therefore no reason for an expanded-sweep switch. The frequency meters are individually calibrated and read directly in megacycles per second on a spiral dial.

The front-panel controls of TS-148/UP are similar to those of TSK-3RL except for the absence of an i-f-gain control and a switch attenuator.

Figure 7·16 is a photograph of the spectrum of $\frac{1}{2}$-μsec pulse from a TS-13 pulsed-signal generator as seen on the screen of a TS-148/UP spectrum analyzer. The sweep frequency has been synchronized with the repetition frequency. This photograph is typical of spectrum presentation on the TS-148/UP and shows the effectiveness of the intensifier in making the spectrum as bright as the baseline. The kink in the baseline at the center of the spectrum is the frequency-meter marker pip. A marker as sharp as this permits rather accurate frequency measurement. Note that the minima of the spectrum do not go to zero indicating frequency modulation on the pulse; also, the asymmetry of the spectrum, indicative of amplitude modulation, may be noted.

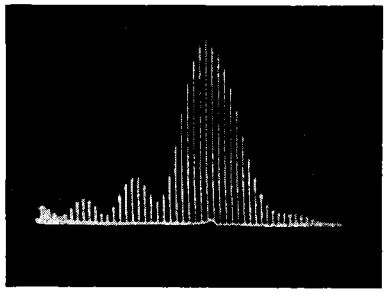

FIG. 7·16.—Spectrum of a $\frac{1}{2}$-μsec r-f pulse as seen on a TS-148/UP spectrum analyzer.

FIG. 7·17.—Front panel of TSS-4SE.

7·8. The TSS-4SE 10-cm-band Spectrum Analyzer.—The 10-cm-band spectrum analyzer that has been chosen for description is the TSS-4SE (Radiation Laboratory designation). It was selected because it is the most recently designed 10-cm-band analyzer and is most likely to be available (approximately 200 have been made to date), and also because it contains a frequency-marker oscillator and double r-f input circuit. These features are lacking in the other analyzers discussed. The TSS-4SE spectrum analyzer was designed by Radiation Laboratory and produced at Sylvania Electric Products, Inc.

General Description.—The TSS-4SE analyzer was designed primarily for laboratory use. There was no need therefore for it to be small and compact. The TSS-4SE analyzer is mounted in a steel cabinet that has the following over-all dimensions: 19$\frac{1}{2}$ in. high, 22 in. wide, and 17 in. deep. The weight is 105 lb. A photograph of the instrument is given in Fig. 7·17.

The TSS-4SE spectrum analyzer is intended for observation of the spectra of microwave signals in the frequency range 3650 Mc/sec (8.2 cm) to 2400 Mc/sec (12.5 cm). The bandwidth of the i-f amplifier is 50 kc/sec,

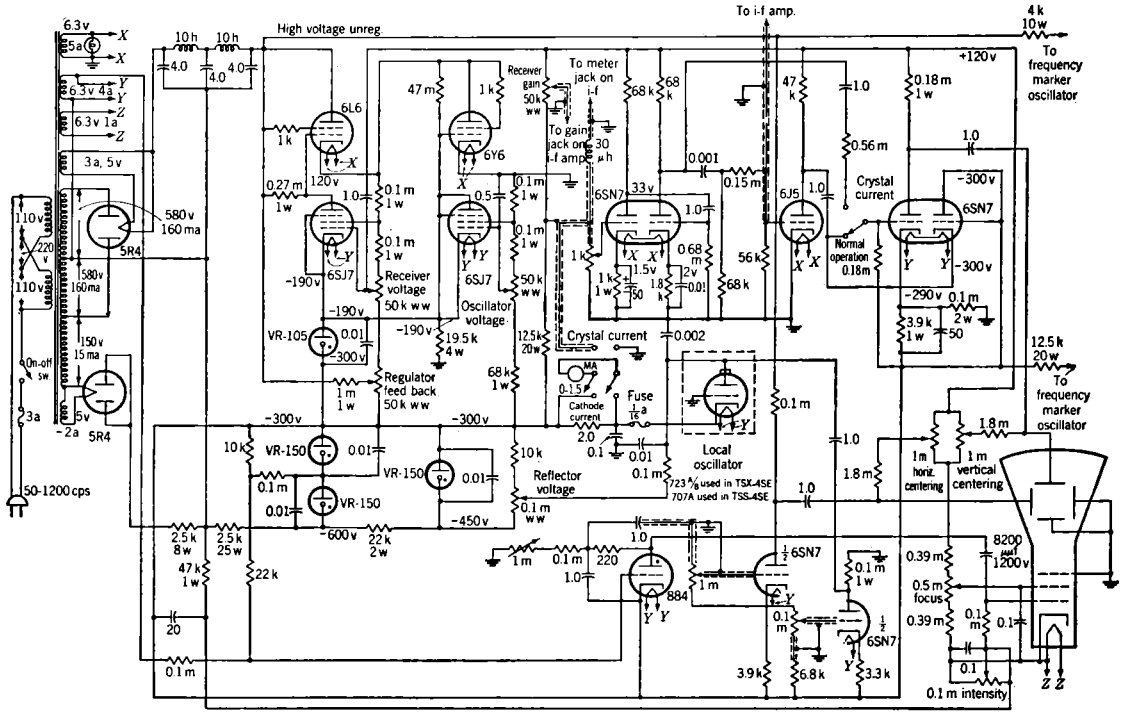

FIG. 7·18.—Circuit of the main chassis, spectrum analyzers TSS-4SE, TSX-4SE, and TSK-2SE.

enabling the analyzer to give an accurate presentation of the spectra of rectangular pulses up to 2-μsec duration. The intermediate frequency is 20 Mc/sec, which is adequate to give good separation of the image spectra of pulses as short as 0.2 μsec. The gain of the i-f amplifier is 125 db and gives adequate sensitivity for all ordinary measurements.

Besides the frequency-marker circuit, this analyzer differs from others in the use of double input terminals, each with a separate attenuator, in the addition of a milliammeter to read either crystal-mixer current or local-oscillator-tube cathode current, and in the omission of a built-in

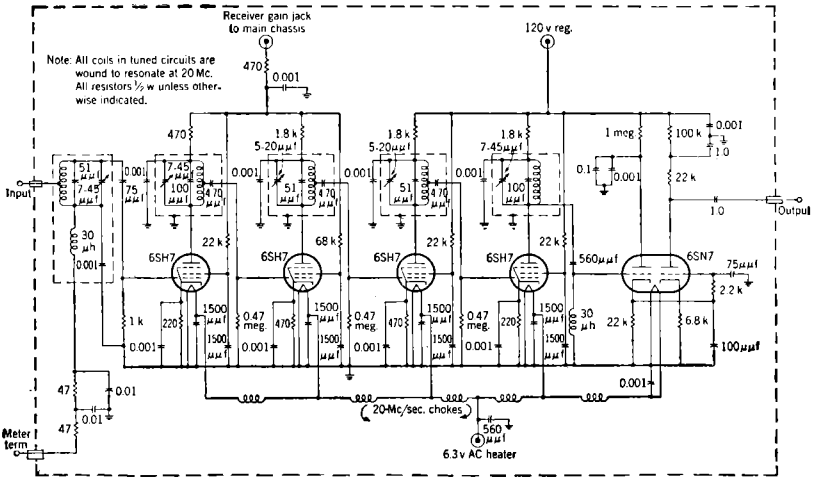

FIG. 7·19.—Circuit of the i-f amplifier used in spectrum analyzers TSS-4SE and TSX-4SE.

cavity frequency meter. The TSS-4SE analyzer has no provision for intensification of the spectrum, which makes the photographing of spectra rather difficult.

Figure 7·18 is the circuit diagram of the main chassis of the TSS-4SE and Fig. 7·19 is the circuit diagram of the i-f amplifier. These same circuits are used in the TSX-4SE analyzers. The TSS-4SE analyzer will operate from a power supply of either 115 volts or 230 volts and over a frequency range from 50 cps to 1200 cps.

The Local Oscillator.—The local-oscillator tube used in the TSS-4SE analyzer is the 707B reflex klystron. The large frequency range is attained by the use of a tunable cavity external to the tube envelope. To achieve better shielding this cavity completely encloses the tube and the power leads are brought through r-f filters. A range in wavelength of about 2 cm can be covered by the micrometer screw which is mounted on the front panel. This range may be centered by adjusting the band-

setting control at the rear of the cavity assembly. The maximum tuning range of the local oscillator is about 40 Mc/sec by reflector tuning.

The Frequency-marker Oscillator.—The TSS-4SE spectrum analyzer has no frequency meter for direct frequency measurements and for such measurements an external oscillator, either calibrated in frequency or provided with a frequency meter, must be employed. This is one reason for the two input terminals to the analyzer. For frequency-difference

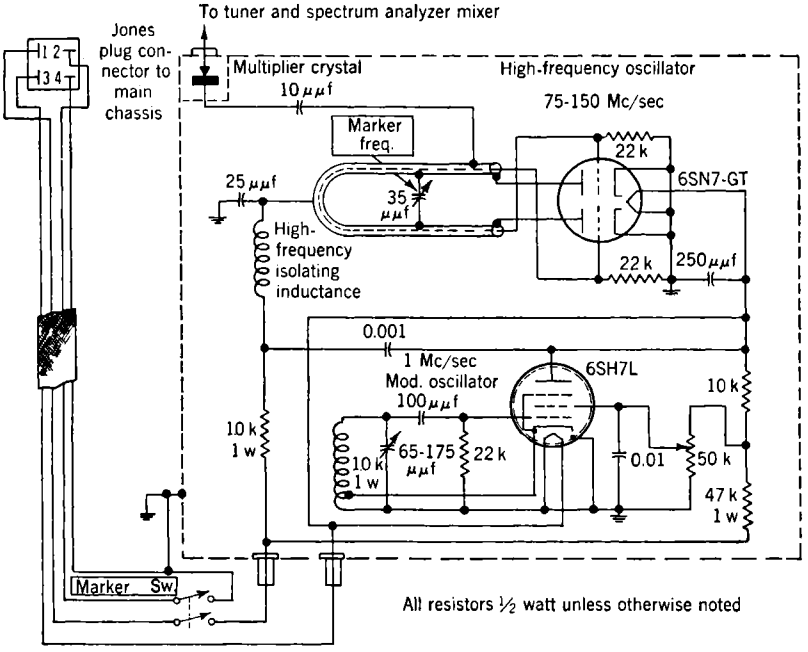

FIG. 7·20.—Circuit of the frequency-marker oscillator used in TSS-4SE.

measurements, however, the TSS-4SE analyzer has a frequency-marker oscillator that produces a series of pips on the oscilloscope screen having a frequency separation of 1 Mc/sec. With these, frequency-difference measurements on a spectrum can be made with ease. These marker pips are produced by a tunable high-frequency oscillator with a range from 75 to 150 Mc/sec heavily modulated by a second oscillator operating at 1 Mc/sec to produce both frequency and amplitude modulation. The circuit diagram is shown in Fig. 7·20. The output signal of the modulated oscillator is applied to a crystal multiplier (type 1N21A) to produce harmonics in the tuning range of the spectrum analyzer. The amplitude of the marker pips decays on either side of the center frequency but this is desirable, since it avoids confusion produced by the images of the pips.

The marker pips can be made to fall in any part of the band by adjusting the MARKER-FREQUENCY control, and their amplitude can be controlled by the double-stub tuners labeled MARKER AMPLITUDE. The plate voltage to the marker oscillator is controlled by a push-button switch. The pips may either be used directly for frequency-difference measurement or they can be used for calibrating the frequency scale.

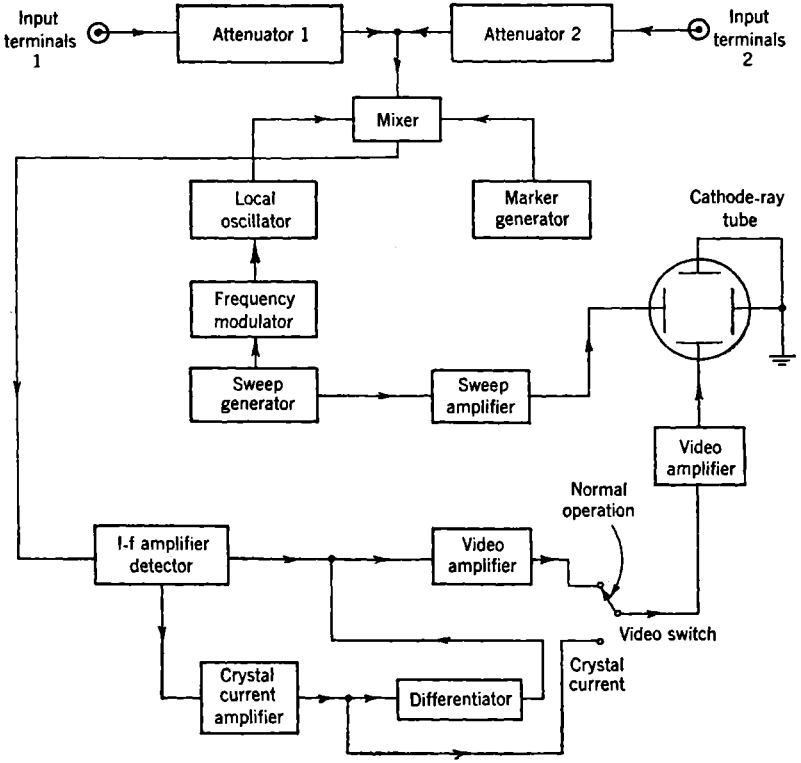

FIG. 7·21.—Block diagram of the TSS-4SE spectrum analyzer including r-f circuit.

The R-f Circuit.—The block diagram of the complete analyzer, Fig. 7·21 shows the interconnection of the components of the analyzer that have been described and shows the r-f circuit as well. The two coaxial input terminals to the spectrum analyzer lead to a waveguide-beyond-cutoff attenuator and from the attenuator to the crystal mixer where the two input signals and the harmonics of the marker oscillator are all mixed with the signal from the local oscillator, the difference frequencies being applied to the i-f amplifier. The mixer crystal and the frequency-multiplier crystal, both type 1N21A, are separate crystals. Coaxial lines

and flexible coaxial cables are used to interconnect the parts of the r-f circuit resulting in a maze of cables in the interior of the cabinet.

The two cutoff attenuators have dials which read from 0 to 100. Beyond the reading 20, the scale is linear in decibels, the attenuation being 1 db per division. At the reading 20, the insertion loss of the attenuator is about 38 db. In spite of the high minimum attenuation, the linear calibration is a convenience, and the analyzer is still sufficiently sensitive for all ordinary measurements.

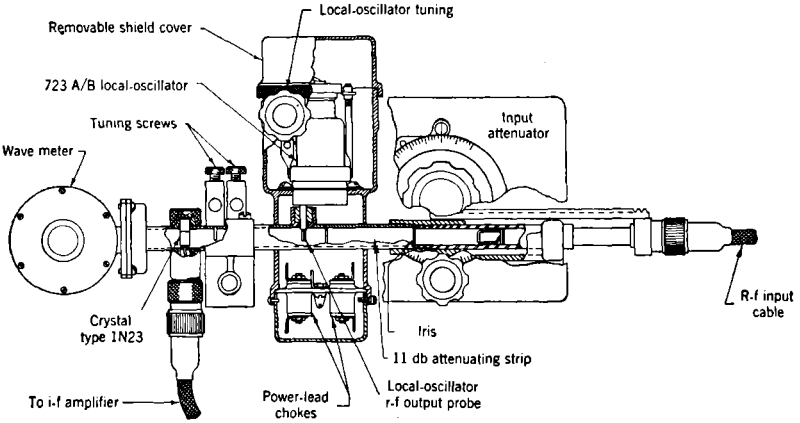

FIG. 7·22.—R-f circuit of TSX-4SE spectrum analyzer.

7·9. The TSX-4SE Spectrum Analyzer.—This 3-cm-band spectrum analyzer deserves a brief comment because it has been made in considerable quantities (over 450 have been made to date by Sylvania Electric Products, Inc.) and because the circuits and i-f amplifier are identical to those of the TSS-4SE analyzer. The difference is in the r-f circuit, which has one input terminal and no marker oscillator, but has, instead, a high-Q frequency meter which may be used to produce frequency-meter marker pips in the manner described for the TS-148/UP analyzer. The r-f circuit is simply a section of waveguide to which are connected in order the coaxial input terminal, the cutoff attenuator, the frequency-modulated local oscillator, the crystal mixer, and the frequency meter terminating the line. The improved shielding and the linearly calibrated waveguide-beyond-cutoff attenuator make the TSX-4SE analyzer superior to the TS-148/UP analyzer for many laboratory measurements. The attenuator calibration is 1 db per division beyond 15 on the dial. The range of the frequency meter and of the analyzer when a 2K25 tube is used as a local oscillator is 8500 Mc/sec (3.53 cm) to 9600 Mc/sec (3.13 cm). A diagram of the r-f circuit which is mounted on the front panel is given in Fig. 7·22. The circuit diagram is given in Figs. 7·18 and 7·19.

7·10. The TSK-2SE Spectrum Analyzer.—The TSK-2SE Spectrum analyzer (Radiation Laboratory designation) is of considerable interest because of the special principle that it employs. This analyzer has the same circuits as TSX-4SE but is adapted to 1-cm-band operation by the addition of a special r-f circuit and the substitution of a 40-Mc/sec i-f amplifier. The unusual feature of this analyzer is the use of a local oscillator at 3-cm band for the reception of signals at 1-cm band. This principle allows one to build spectrum analyzers for frequencies for which local-oscillator tubes are not available.

The R-f Circuit.—The local oscillator used is a WE 169618 reflex klystron, which has a tuning range of 7690 to 8330 Mc/sec. The output power of this tube is applied to a 1N26 crystal in the 1-cm-band waveguide. This crystal performs both the function of a frequency tripler and of a 1-cm-band mixer. The effective frequency range of the analyzer is then the range of the third harmonic of the local oscillator, or 25,000 to 23,070 Mc/sec.

Figure 7·23 is a drawing of the r-f circuit showing the essential parts. At the left is the 3-cm-band local oscillator in its shield can. The oscillator output voltage is applied to the transformer past the 3-cm-band frequency meter, which is tunable over the range 7833 to 8167 Mc/sec, but is calibrated in terms of the third harmonic or from 23,500 to 24,500 Mc/sec. This frequency meter is essentially the same as the one used in the TSK-3RL, scaled up by a factor of three. At resonance the frequency meter behaves as a high impedance in series with the line and thus decreases the power being transmitted to the transformer and the crystal. The dip in the crystal current is amplified and used as a frequency-meter marker in the same manner as in other analyzers. Up to this point a large-size 3-cm-band waveguide has been used; however, the multiplier and mixer crystal are mounted in the 1-cm-band guide. A transformer section of coaxial line is used to introduce the 3-cm-band power to the crystal. The input attenuator is in the 1-cm-band waveguide and is a dissipative-flap attenuator. It is well shielded and has a range from 0 to about 30 db.

The operation of this analyzer, except for tuning procedures, is the same as if it were an ordinary 1-cm-band analyzer. The plunger in the 3-cm-band guide is normally tuned to maximize crystal current, and the plunger in the 1-cm-band guide is tuned to maximize the deflection caused by the incoming signal.

In order to use the analyzer with pulses as short as 0.1 μsec, the intermediate frequency must be 40 Mc/sec. The i-f bandwidth is 160 kc/sec, limiting its use to pulse lengths less than 1 μsec. The circuit diagram of the i-f amplifier is given in Fig. 7·24.

The TSK-2SE was developed at a time when it was doubtful whether

the low-voltage 1-cm-band oscillator (type 2K50) would be available or could be used for analyzers. The principle, however, is of interest to those desiring an analyzer for measurements in a frequency range for which no local oscillator is available.

7·11. Low-frequency Spectrum Analyzers Using Microwave Oscillators.—The TSK-2SE is an example of an analyzer used at a frequency higher than the local-oscillator frequency. In a similar manner, a

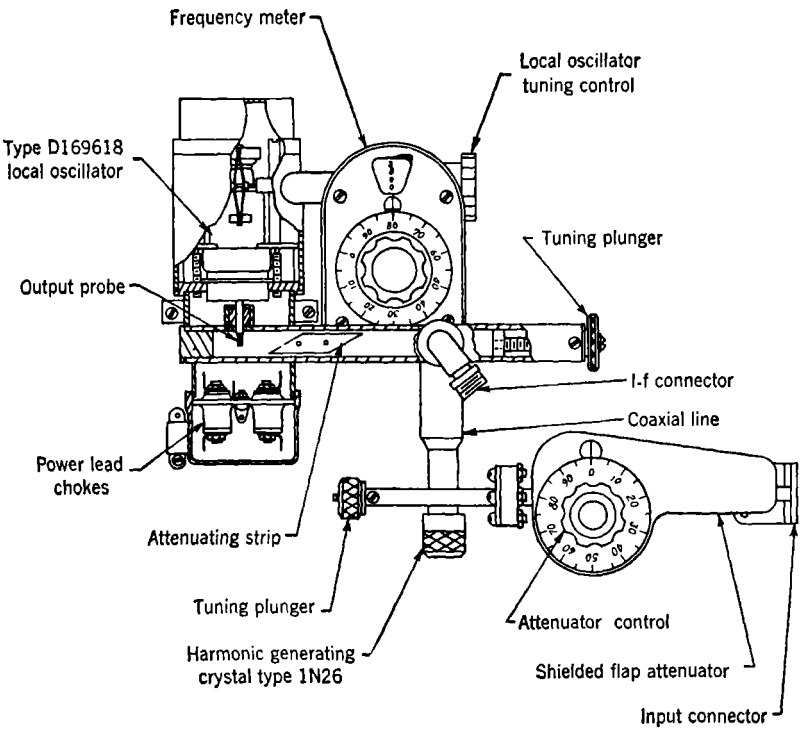

FIG. 7·23.—R-f circuit of the TSK-2SE spectrum analyzer.

spectrum analyzer can be built for use with frequencies lower than the local-oscillator frequency by beating the frequency-modulated local oscillator with a c-w oscillator to produce a frequency-modulated difference signal. This low frequency can serve as the local-oscillator signal for the reception of low-frequency signals. The TSS-4SE analyzer has, in fact, been used at frequencies of about 1000 Mc/sec without change, simply by introducing into one output attenuator a c-w signal of such frequency as to produce a beat frequency of about 1000 Mc/sec with the local oscillator of the analyzer. There is, of course, a loss of sensitivity

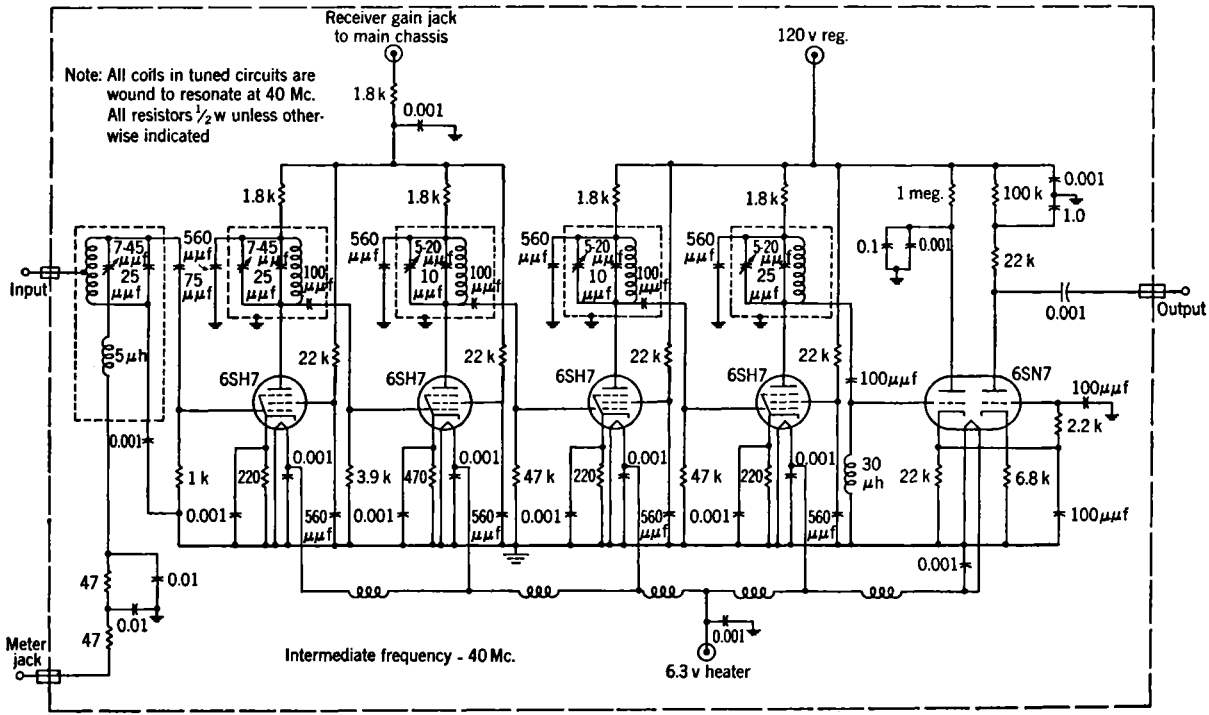

FIG. 7·24.—Circuit diagram of i-f amplifier used in the TSK-2SE spectrum analyzer.

in this arrangement and the insertion loss of the input attenuator is higher at the lower frequency.

The RP-347 Spectrum Analyzer.—A spectrum analyzer using this principle has been designed by the General Electric Company Research Laboratory on an NDRC contract, and is known as Project RP-347. Using two 2K25 3-cm local-oscillator tubes, it can be used for the analysis of spectra having a carrier frequency of from 100 to 1500 Mc/sec. By frequency-modulating both local oscillators, out-of-phase spectra as wide as 70 Mc/sec may be observed. The sensitivity is such that signals having greater than 250 μv across a 50-ohm line (−89 dbw) may be analyzed.

The operation is as follows: The two local-oscillator signals and the incoming low-frequency signal are mixed together in a single crystal. If the difference frequency of the two local oscillators differs from the signal frequency by the intermediate frequency or 40 Mc/sec, that signal is amplified and presented on the cathode-ray-tube screen after the manner of the other analyzers. The i-f amplifier operates at two frequencies as does that of the TSK-3RL and has a bandwidth of 80 kc/sec, which is sufficiently narrow to provide adequate resolution of spectra broader than 2 Mc/sec.

The operation of this analyzer is essentially the same as that of any other, and this analyzer is sensitive to image frequencies in the same manner. If the signal frequency f_s = 500 Mc/sec, and if the difference frequency $|f_1 - f_2|$ is swept about the point f_s − 40 Mc/sec, then the image frequency that could give an equal response at the same position on the screen would have a frequency f_s − 80 Mc/sec. Similarly, higher-order images can occur such as f_s − 20 Mc/sec, f_s − 60 Mc/sec, f_s − 13 Mc/sec, f_s − 53 Mc/sec, and so forth, if their amplitude is great enough. If the tuning is such that $|f_1 - f_2|$ = 40, 20, 13 Mc/sec, and so forth, a large signal will be passed through the i-f amplifier. By using the low-frequency image, however, ideally, signals down to zero frequency could be viewed.

This analyzer and the one to be described next have been developed for observation of the spectra of sources covering a broad region of frequency such as electrical equipment generating r-f interference or noise. Their relative lack of stability and poor resolution precludes their use for precise measurements on low-frequency signals.

The RP-392-K Spectrum Analyzer.—An alternative way of making a low-frequency spectrum analyzer using microwave oscillators and microwave techniques is to amplitude-modulate the output voltage of a microwave oscillator at a low frequency to produce a microwave sideband, the spectrum of which can be analyzed in the same manner as any other microwave spectrum.

The Research Laboratory of General Electric Company has designed a low-frequency spectrum analyzer, type RP-392-K, which uses this principle and thus corrects several disadvantages of the RP-347 analyzer. The RP-392-K analyzer uses two 1-cm oscillators and covers a range of 10 to 3000 Mc/sec with a frequency spread variable from 10 to 60 Mc/sec. The sensitivity achieved is such that a signal of 100 μv across a 50-ohm line (-97 dbw) gives a response twice noise on the cathode-ray-tube screen. The design is such that no images or spurious signals occur inside a range of 30 db from the desired signal. In spite of its relative complication the first model was built in a standard 19-in. panel cabinet 20 in. high, a size comparable to the TSS-4SE analyzer. The weight is 135 lb.

The operation of the analyzer can be understood from the block diagram, Fig. 7·25. The first local oscillator which is frequency-modulated and tunable over the range 24,600 to 21,600 Mc/sec is combined with the low-frequency input signal in the first crystal to give an amplitude-modulated output signal. This local oscillator is a type 1462, the developmental version of the 2K50 thermally tuned tube described in connection with TSK-3RL. The component of the high-frequency sideband, which has a frequency of 24,600 Mc/sec, passes through a frequency filter to the mixer or demodulator crystal which is supplied with c-w local-oscillator power by a second 2K50 oscillator operating at 24,715 Mc/sec. This oscillator is automatically stabilized to the frequency of a cavity tuned to 24,715 Mc/sec. The difference frequency between the c-w local oscillator at 24,715 Mc/sec and the signal frequency applied to the second crystal is amplified by a 115-Mc/sec i-f amplifier, which has a bandwidth of 200 kc/sec. After amplification the signal is presented as a vertical deflection on the 5-in. cathode-ray-tube screen. To the horizontal plates is applied a sweep signal proportional to the frequency modulating the first local oscillator. The crystal-current pattern from the first crystal is amplified by a separate amplifier and provision is made for presenting it on the oscilloscope screen. It is a considerable aid in tuning the system.

For measuring the frequency of the first local oscillator and as an aid in aligning the system, a tunable cavity frequency meter is provided. A frequency-marker pip is presented on the oscilloscope which may be calibrated directly in signal frequency. The positioning of the cavities making up the bandpass filter is such that they behave as coupled circuits with critical coupling. For frequencies other than the desired band the filter behaves as a short circuit at the first crystal, thus the image 230 Mc/sec away from the signal frequency is eliminated as well as the higher-order images. The positioning of the local-oscillator tubes is such that at 24,600 Mc/sec the energy will be directed to the proper channels and not be dissipated in the local-oscillator tubes.

The second local oscillator is stabilized to the resonant frequency of a

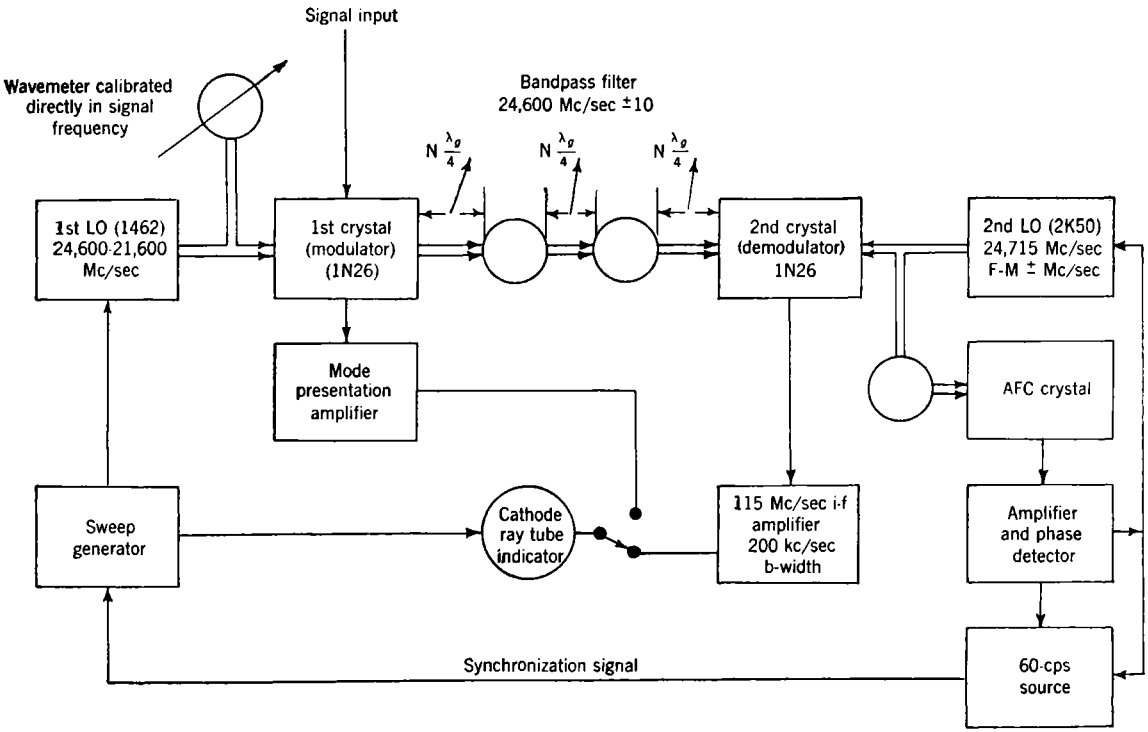

FIG. 7·25.—Block diagram of the wide-range spectrum analyzer type RP392K.

cavity tuned to 24,715 Mc/sec. The stabilization is obtained in the following manner: The oscillator is frequency-modulated by ±1 Mc/sec at a 60-cps rate and the output power passed through the transmission AFC cavity to a crystal detector. The output power of the crystal is compared in phase and amplitude with the original source of 60-cps voltage by the phase detector and the d-c bias produced is applied to the reflector to correct the frequency. When the oscillator is centered at the resonant frequency, no 60-cps signal is produced by the AFC crystals, whereas, on one side of resonance a 60-cps signal of one phase is produced and on the other side a 60-cps signal of opposite phase. After detection no bias is produced at resonance, and off resonance a d-c bias is produced whose sign depends on the direction of detuning.

Instead of a square-law scale as most analyzers have, this analyzer has a logarithmic scale which is accurate over a range of 25 db; hence signals anywhere in this range appear on the screen.

An earlier model used a frequency marker which is a very interesting device. An open-end coaxial wavemeter was shock-excited by a spark gap operating at a repetition frequency of about 10 kc/sec, and produced a series of pips on the screen, the envelope of which would be the cavity response. In this manner, a marker tunable from 500 to 3,500 Mc/sec was produced.

If this analyzer were built using microwave stabilized oscillators such as those described by R. V. Pound in Chap. 2 and if a receiver with higher resolution were employed, such a spectrum analyzer might be sufficiently stable to be useful for accurate measurement work over the whole range of microwave frequencies.

7·12. Other Instruments Using the Spectrum-analyzer Principle.—An instrument that is based on a spectrum analyzer is the TBX-1BR microwave impedance bridge. The basic part of this instrument is the symmetrical magic T. Simultaneous measurements can be made at three widely separated frequencies by using three frequency-modulated source oscillators and three c-w local oscillators tuned to the proper frequencies. The presentation on the oscilloscope is in the form of three c-w signals, the amplitudes of which are a function of the voltage standing-wave ratios. The impedance bridge is described in Chap. 9.

Another instrument that is similar in operation to a spectrum analyzer is the cavity-comparator type TFU-1RL, a unit for the comparison of resonant frequencies of transmission cavities or frequency meters. The cavity comparator resembles an analyzer in having a frequency-modulated oscillator and a presentation on a cathode-ray-tube screen with frequency plotted horizontally. It lacks an i-f amplifier, however, and has instead a vertical deflection representing the transmission of the cavity. On successive sweeps the transmission of first one cavity and

then the other is presented giving a double trace with two pips which can be accurately superimposed. This instrument is discussed in Sec. 6·30.

Another instrument that is a true spectrum analyzer but which has a unique presentation is the cavity Q-meter intended for measuring cavity frequency and the frequency difference between half-power points. The presentation is a cavity-transmission curve like that in the cavity comparator with the following modification. It has been mentioned in a number of places in this chapter that the intermediate frequency of the receiver provides a calibration for frequency-difference measurements since two image spectra are separated by twice the intermediate frequency. In the cavity Q-meter a tunable calibrated low-frequency receiver is used as the i-f amplifier and a tunable calibrated microwave oscillator is used for the signal source. The receiver output signal is used to intensity-modulate the oscilloscope producing two bright spots on the screen centered about the c-w signal frequency and with a separation twice the intermediate frequency. These spots can be moved to coincide with the half-power points of the cavity transmission characteristic and the resonant frequency and Q of the cavity are easily determined from the intermediate frequency and the frequency of the c-w signal. The cavity Q-meter is described in Sec. 6·29.

7·13. Echo Boxes.—Another method to measure the spectrum of an r-f pulse employs an echo box. An echo box is a tunable, high-Q, transmission cavity with a crystal rectifier and microammeter coupled to it. When the echo box is connected by a directional coupler to the pulsed oscillator of a radar set, tuning the echo box will give an indication on the microammeter of power as a function of frequency. Until rather recently echo boxes were not suitable for spectrum analysis because the Q's of the echo boxes available were too low to present spectra in sufficient detail. Now, however, echo boxes with bandwidths of about 100 kc/sec are available at both 10-cm and 3-cm bands. In terms of resolution these boxes are comparable to electronic spectrum analyzers. The advantage of the echo box as a spectrum analyzer for field use is its portability and the fact that it requires no power to operate. Since a radar set often contains a permanently installed echo box, it is used widely for spectrum analysis.

An echo box for spectrum analysis should be strongly built, should possess a smooth driving mechanism, and should have a tuning rate of less than 10 Mc/sec per dial revolution. The type TS-218A echo box, having a tuning range of 8990 to 9170 Mc/sec, is an example of a good echo box for this region. For the band 2700 to 2900 Mc/sec the type TS-270 box is available and is described in Sec. 5·17 and shown in Fig. 5·43. The deflection of the meter of the echo box is proportional to peak power, to repetition rate, and to the square of the pulse length. The sensitivity

is then expressible in milliwatt-microseconds, a figure of 200 being representative. The meter deflection is approximately linear in power but must be calibrated for accurate measurement work.

It is usually more difficult to interpret a spectrum when using an echo box than when using a spectrum analyzer, since it is necessary to plot the spectrum from individual observations. With the spectrum analyzer, on the other hand, the spectrum may be seen at a glance and a judgment made as to whether it is good or poor. Furthermore, an analyzer does not require direct connection to the radar set. Most service personnel who have both instruments available prefer to use the spectrum analyzer. For laboratory use the much greater sensitivity of the analyzer, its versatility, and the fact that one analyzer will cover a frequency range for which many echo boxes would be needed, all dictate the use of the electronic spectrum analyzer. However, for the analysis of extremely short pulses, such as the spike in the leakage energy from a TR switch, the width of the spectrum may exceed the tuning range of an electronic analyzer, and an echo box, or a wavemeter cavity, can be employed.

MEASUREMENTS WITH THE SPECTRUM ANALYZER

7·14. Interpretation of Spectra.—A voltage that is a function of time may be expressed by Fourier's integral theorem as a summation of frequencies in the form

$$F(t) = \int_{-\infty}^{\infty} a(\omega)e^{j\omega t}\,d\omega,$$

where

$$a(\omega) = \frac{1}{2\pi}\int_{-\infty}^{\infty} F(t)e^{-j\omega t}\,dt.$$

The spectrum function $a(\omega)$ is in general a complex function of the form $a(\omega) = a_1(\omega) + ja_2(\omega)$; it may also be expressed as an amplitude spectrum and a phase spectrum as follows

$$|a(\omega)| = [a_1(\omega)^2 + a_2(\omega)^2]^{1/2}, \qquad \theta(\omega) = \tan^{-1}\frac{a_2(\omega)}{a_1(\omega)}.$$

A spectrum analyzer performs in effect the above integration to obtain the amplitude spectrum $|a(\omega)|$, and gives a plot of $|a(\omega)|^2$, the power spectrum. Since a spectrum analyzer responds only to the amplitude spectrum of an r-f transient, information as to the phase spectrum is lost and the question arises whether the transient $F(t)$ is uniquely determined by the amplitude spectrum. Actually, more than one phase function can be associated with an amplitude spectrum to produce a real function $F(t)$. A simple example is the obvious fact that the amplitude spectrum does not depend on the time of occurrence of the pulse. Introducing a time delay t_0 amounts to multiplying $a(\omega)$ by $e^{-j\omega t_0}$, but $|a(\omega)|$ is unchanged

since $|e^{-j\omega t_0}| = 1$. Another example is the case of a pulse with no frequency modulation but linear amplitude modulation. The spectrum is symmetrical and is unchanged whether the slope of the pulse is positive or negative. A third example is the case of a pulse with no amplitude modulation but with linear frequency modulation. The spectrum is likewise unchanged when the slope of the frequency modulation is reversed. Other examples could be mentioned but these will illustrate the point. Even though the amplitude spectrum does not determine the form of the r-f pulse, it gives very useful information and, when correlated with other information such as the amplitude modulation measured with an r-f envelope viewer or r-f oscilloscope and the characteristics of the pulsed oscillator, may serve adequately to explain the nature of the r-f pulse.

When considering the response of a receiver to an r-f pulse it is clear that the power spectrum as seen on the analyzer screen does not determine the response of the receiver, but a knowledge of the spectrum will indicate the required bandwidth of the receiver in order that considerable loss of energy will not occur. If a considerable amount of frequency modulation is present the energy of the pulse may be spread over such a wide frequency band that a receiver designed to receive such a pulse without frequency modulation will respond to only a small portion of the power received.

One of the principal uses of spectrum analyzers is to check the spectra of radar transmitters to see that no excessive frequency modulation exists and that the magnetron is operating stably. Magnetrons are usually modulated by a flat-topped current pulse having short times of rise and fall. A flat-topped current pulse is desirable because the frequency of a magnetron varies with the current and if the current pulse is not reasonably constant, frequency modulation will be introduced. Moreover, some regions of the voltage-current characteristic are associated with instability or a change in the mode of oscillation, and to avoid these regions the current pulse should rise rapidly to its maximum and remain constant. It has been found, however, that with some magnetrons the operation is unstable if the rate of rise is larger than a certain amount. Most magnetrons operating properly will produce a spectrum very similar to that of the rectangular pulse with no frequency modulation. A spectrum of this sort is considered good. If the spectrum differs from this form it may be the result of amplitude modulation, frequency modulation, or a combination of the two.

7·15. Examples of Spectra of Pulses.—The section following is a detailed consideration of the spectra in Fig. 7·26. The spectra are power spectra; that is, $|a(\omega)|^2$ is plotted against frequency difference from the carrier frequency. The spectra are shown for specific values of pulse

length and frequency modulation but they may be interpreted for different pulse lengths in the following way. Multiplying the pulse length by a factor a is equivalent to multiplying the frequency scale by $1/a$ and multiplying the frequency modulation Δf by $1/a$.

Figure 7·26*a*.—This is the spectrum of a rectangular pulse with neither amplitude modulation nor frequency modulation during the pulse. The form of the spectrum is $\sin^2 \pi x/(\pi x)^2$ and it is obviously symmetrical. Minima in the spectrum occur at ± 1 Mc/sec, ± 2 Mc/sec, ± 3 Mc/sec,

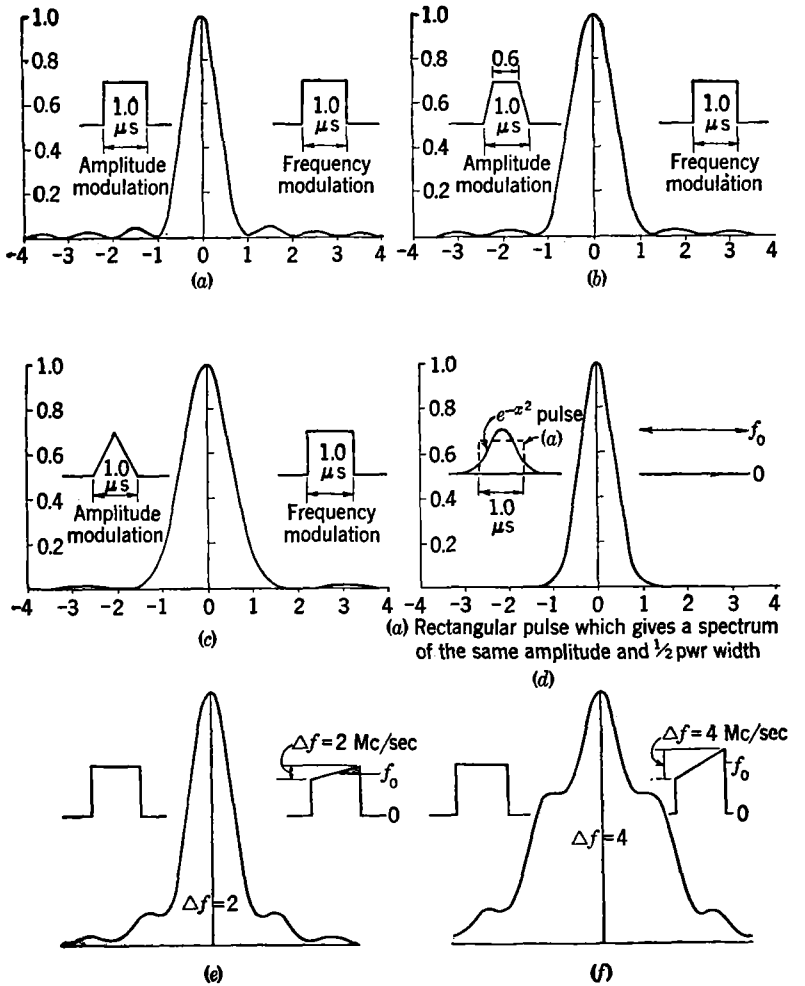

(a) Rectangular pulse which gives a spectrum of the same amplitude and ½ pwr width

(d)

FIG. 7·26.—Representative pulse

and so forth. This is representative of the spectrum of a properly operating magnetron or of a good pulsed test oscillator.

Figure 7·26*b*.—The spectrum of a symmetrical trapezoidal voltage pulse with no frequency modulation. The pulse is 1 μsec wide at the base and 0.6 μsec at the top and hence is effectively shorter than a 1-μsec rectangular pulse and accordingly the first minima occur at frequencies

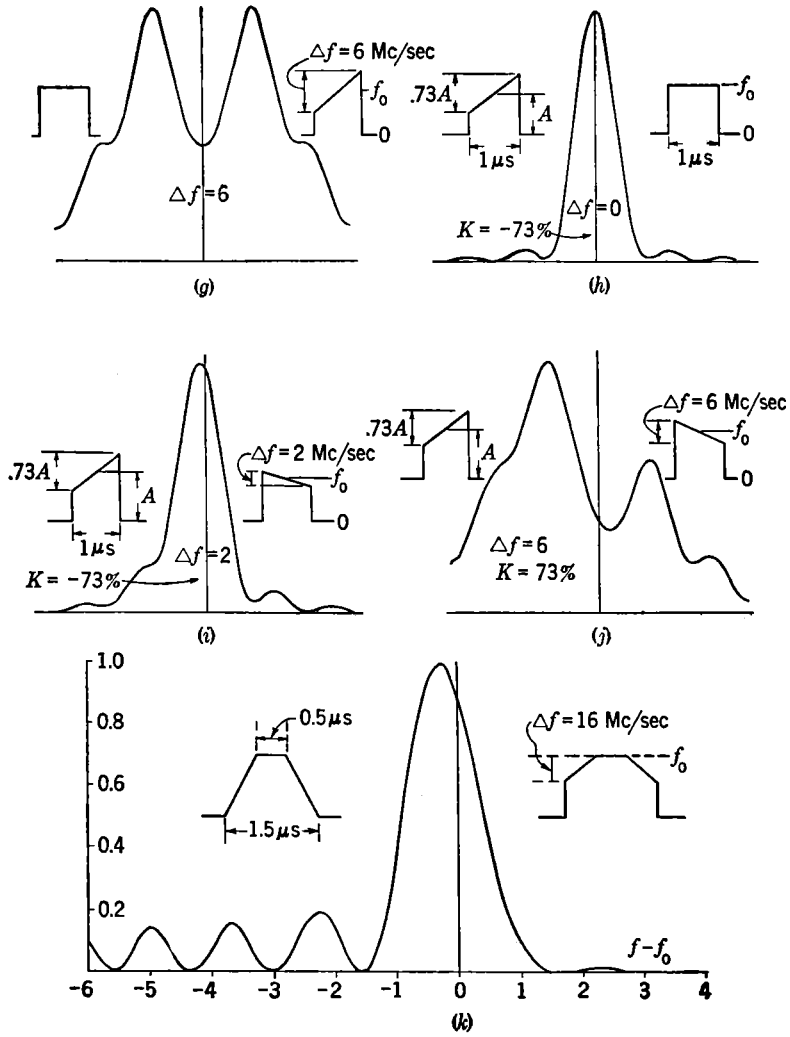

spectra; explanation in text.

which differ by somewhat more than 2 Mc/sec. The most notable change in the shape of the spectrum is a reduction of amplitude of the side lobes relative to the center lobe.

Figure 7·26*c*.—The spectrum of a symmetrical triangular voltage pulse with no frequency modulation. The pulse being 1 μsec wide at the base is effectively shorter than a 1-μsec rectangular pulse, and hence the first minima are at frequencies differing by more than 2 Mc/sec. The minima occur at ± 2 Mc/sec, ± 4 Mc/sec, and so forth. In this case the side lobes are practically negligible.

Figure 7·26*d*.—An error-function voltage pulse (e^{-x^2}) with no frequency modulation. A transient of this type is unique in the fact the spectrum has the same form as the transient. Accordingly, the spectrum has no side lobes although it extends to $\pm \infty$. Actually the portion of the spectrum beyond $f - f_0 = \pm 1.5$ Mc/sec is negligible. The pulse illustrated is the one that has a spectrum of the same amplitude and half-power width as the 1-μsec rectangular pulse shown by the dotted lines *a*. The shape of the center region of the spectrum is almost identical with that of the rectangular pulse spectrum Fig. 7·26*a*. Since the pass band of a series of single-tuned circuits approximates the error function, this was chosen for the discussion in Sec. 7·2 on the theory of operation.

Figure 7·26*e,f,g*.—A rectangular pulse with no amplitude modulation during the pulse but with varying amounts of linear frequency modulation. The first effect of increasing the frequency modulation is to raise the minima and they are no longer zero. This means that less energy is present in the center lobe. As the modulation is increased, the secondary maxima rise until they engulf the center, creating two peaks rather than one. With higher modulation three or more pairs of prominent peaks may exist with the result that very little energy is located in the central region. All these spectra are symmetrical and would be unchanged if the frequency modulation were reversed in sign. Spectra of this sort are rather commonly seen. Spectrum *e* would be classed as good, *f* as fair, and *g* as poor.

Figure 7·26*h*.—A linearly sloping pulse with amplitude modulation of 73 per cent and no frequency modulation. This spectrum is very similar to that of the rectangular pulse *a*, the only difference being that the minima are not quite zero. The shape of the spectrum is not greatly altered even when the modulation is 200 per cent (sawtooth waveform). Since there is no frequency modulation the spectrum is symmetrical; if the slope of the pulse were reversed the spectrum would be unchanged.

Figure 7·26*i,j*.—A linearly sloping pulse linearly frequency-modulated. In the case of linear frequency modulation with no amplitude modulation the spectrum was symmetrical, that is, qualitatively, frequencies $f_0 + f_1$ were not preferred to frequencies $f_0 - f_1$. Here, how-

ever, frequencies at which the pulse has higher amplitude are preferred to frequencies at which the amplitude is low and the effect is to move the maximum in the direction of the preferred frequency and to give an unsymmetrical spectrum. The amplitude modulation is the same as in *h* and the spectra are shown for two values of frequency modulation, 2 and 6 Mc/sec per μsec. At the higher modulation there is a resemblance to *g* but the spectrum is still distorted in the direction of the preferred frequency. In the case shown, the frequency is lowest where the amplitude is highest with the result that the spectrum is pushed in the direction of lower frequency. It is obvious that the same spectrum would occur if the amplitude and frequency modulations were both reversed in sign. If one only were reversed the spectrum resulting would be a mirror image of that shown.

Figure 7·26*k*.—A trapezoidal pulse trapezoidally frequency-modulated. The same sort of qualitative argument that applied in *i* and *j* can be used here. A large part of the pulse is rectangular so that a main lobe resembling that of a rectangular pulse is obtained. The frequency modulation causes a shift of the spectrum in the low-frequency direction but the effect is not so pronounced as it would be if the amplitude were unmodulated. The effective width of the pulse is between 0.5 and 1.0 μsec as indicated by the position of the zeros. This is a form of spectrum which is very commonly observed from magnetrons and pulsed low-power oscillators. The almost complete absence of side lobes on one side and side lobes larger than usual on the other is typical. An example of such a spectrum is shown in Fig. 7·16 of Sec. 7·7.

In correlating spectra with the r-f pulses that produce them a few generalizations may be made. When the frequency modulation is zero, changing the shape of the amplitude modulation while keeping the effective pulse width constant alters the relative sideband amplitudes but has little effect on the main lobe. This may be seen from spectra *a*, *b*, *c*, *d*, and *h* of Fig. 7·26. It will be observed also that each of the spectra is symmetrical. In fact, it is true in general that in the absence of frequency modulation any r-f pulse will produce a symmetrical spectrum. From spectra *e*, *f*, and *g* of Fig. 7·26 it is evident that in the case of no amplitude modulation a linear frequency modulation will result in a symmetrical spectrum. In general, with no amplitude modulation, a frequency modulation that is an odd function about the center of the pulse will produce a symmetrical spectrum. Frequency modulation has the effect of broadening the spectrum and is usually more serious than amplitude modulation. Most magnetron spectra observed can be explained qualitatively in terms of frequency modulation alone.

7·16. Frequency and Frequency-difference Measurements.—One of the measurement applications for which the analyzer is well adapted is

the comparison in frequency of two oscillators of slightly different frequencies. The coincidence of frequency of two c-w signals is very precisely indicated by the coincidence of the two patterns on the analyzer screen. If the two signals are stable and of comparable amplitude, a comparison can be made with frequency error small compared to the bandwidth of the i-f amplifier. For example, if the bandwidth is 100 kc/sec the comparison of two 3,000-Mc/sec signals can be made with a precision of three parts per million.

If one signal is from a calibrated signal generator with an attenuator, then measurements may be made of the frequency of any signal within the tuning range of both the calibrated signal and the spectrum analyzer. An example of the use of this method of frequency comparison is the microwave frequency standard discussed in Sec. 6·28. In this case, the calibrated signal source is a very-high-order harmonic of a very stable low-frequency oscillator. It is clear that the method of frequency measurement by comparison with a calibrated c-w signal is applicable to the measurement of modulated signals as well as c-w signals and could, for example, be used to make frequency measurements on the spectrum of the pulsed oscillator. In making frequency measurements by this method special care must be exercised in selecting the correct image for comparison, otherwise the results will be in error by twice the intermediate frequency. If the frequencies being compared are identical, only one other image will be found, and if the two signals are not quite coincident, the frequency difference will be the same on the other image. If, however, the incorrect image has been chosen, tuning the spectrum analyzer will disclose two additional images spaced twice the intermediate frequency from the central images. If one oscillator is slightly detuned the center image will be double while the others will remain single. Care must also be exercised that a higher-order image is not chosen for comparison. Another way of detecting true coincidence of two c-w signals is to observe carefully the pattern produced when the two signals are superimposed. If the two frequencies are nearly identical, the pattern will appear as a modulation of the difference frequency if the difference frequency is low enough; if the two signal frequencies are separated by twice the intermediate frequency, the beat frequency is a function of the analyzer tuning. In the first case, the pattern produced will show a definite modulation filling the area; in the second case, the pattern will be blurred.

The frequency of oscillators may be measured by the frequency meter contained in most spectrum analyzers. A frequency-meter marker pip when set to coincidence with a signal on the screen of the analyzer does not read the signal frequency, but instead the frequency of the local oscillator when the signal is being received. The cavity frequency is then

different by the intermediate frequency from the desired signal frequency. The best method of measuring the signal frequency is to set the frequency-meter marker pip first at one image and then at the other, adding the readings and dividing by two. This procedure does not depend on knowledge of the intermediate frequency or on the linearity of calibration of the frequency meter.

7·17. The Use of a Spectrum Analyzer as a Sensitive Receiver.—Another measurement application of the spectrum analyzer is as a sensitive c-w detector in bench test work. Most bench test work is done with a square-wave-modulated oscillator, a crystal or bolometer detector, and a high-gain sharply tuned audio amplifier. Much of this work can be done also with a spectrum analyzer which has the advantages of a wider range of sensitivity and much lower noise. Bolometer bridges, measuring i-f power directly, may be built into analyzers, and they give an easily measurable output indication accurately linear in power. The analyzer has the disadvantage that a calibrated i-f gain control is more difficult to construct than an a-f gain control. In consequence, r-f attenuators are used which are usually either of the resistive type or of the waveguide-beyond-cutoff type. The resistive type is usually calibrated using a bolometer and audio amplifier, whereas the calibration of a cutoff attenuator is linear and determined by the dimensions. Because of its sensitivity and wide range, an analyzer is a good instrument for measuring high standing-wave ratios. For the same reason the analyzer is very useful as an attenuator comparator. Standard attenuators calibrated by other means can be used in conjunction with an analyzer to calibrate other attenuators. In all accurate measurements of attenuation very great precautions must be taken to avoid leakage from the source around the attenuator and into the analyzer mixer. An analyzer specifically designed for use as a sensitive detector in the manner described has somewhat different requirements than an analyzer for use with pulsed signals. The leakage attenuation into the analyzer must be very high, and, as explained in Sec. 7·5, more stable operation can be obtained by the use of a wide i-f bandwidth. The intermediate frequency is relatively unimportant in this case.

The spectrum analyzer will probably be of considerable use in demonstration lectures to illustrate the methods of Fourier analysis of transient phenomena. It is well adapted to the study of modulation, both in amplitude and in frequency. The modulation sidebands can be seen directly and their amplitudes determined.

THE R-F ENVELOPE VIEWERS AND OSCILLOSCOPES

An r-f envelope viewer is a device that presents on an oscilloscope screen a plot of the amplitude modulation of an r-f pulse or transient

as a function of time. In its usual form it consists of a diode or crystal to rectify the r-f signal and, where the signal amplitude is small, an amplifier to bring the amplitude to such a value as will give a reasonable deflection on a cathode-ray tube. The cathode-ray oscilloscope must have a triggered sweep that can be started before the occurrence of the transient being observed, in order that the whole of the transient may be seen.

In the study of r-f pulsed oscillators, the spectrum analyzer and the r-f envelope viewer are two very useful instruments which complement each other in the information they give about the pulse. The r-f envelope viewer shows the exact shape of the pulse, that is, its amplitude modulation, whereas the spectrum analyzer gives a visual plot of the power distribution of the pulse in frequency. Frequency modulation during the pulse is not indicated by the r-f envelope viewer, whereas it is very sensitively indicated by the spectrum analyzer. The form of the amplitude modulation of a pulse affects the r-f spectrum, but it is not possible to interpret the spectrum to find the exact shape of the pulse producing it. In investigating the behavior of a pulsed oscillator, such as a magnetron, the current pulse, the r-f envelope, and the r-f spectrum must all be studied. The shape of the rising edge of the pulse is important in the explanation of the magnetron's operation and in applications where precise timing is required. Oscillations, or a slope on the top of the pulse, which may be caused by improper operation of the modulator and which may result in frequency modulation, are clearly indicated by the r-f envelope viewer. By correlating the information given by the r-f spectrum, the current pulse, and the r-f envelope with data on the voltage, current, and frequency relations of a pulsed oscillator such as a magnetron, an adequate explanation of its operation may be given.

An instrument very similar in function to the r-f envelope viewer but possessing certain advantages is the r-f oscilloscope. Whereas the r-f envelope viewer rectifies the signal and presents a video pulse on the cathode-ray tube, the r-f oscilloscope uses the r-f voltage to deflect the electron beam directly. If the time resolution is sufficiently high, the waveform of the r-f voltage is obtained. If the resolution is not high enough the picture obtained is a solid image, brighter on the edges where the trace is slower, the envelope of which indicates the amplitude modulation. Since the use of amplifiers and the RC time constants associated with diode circuits are avoided, the r-f oscilloscope can give a superior presentation of very short transients. For a cathode-ray tube to be useful as an r-f oscilloscope, the deflecting system must be designed so that the electrons pass by the deflecting plates before the r-f voltage on the plates has changed appreciably.

7·18. The Components of an R-f Envelope Viewer.—The basic parts of an r-f envelope viewer are the r-f detector, the cathode-ray tube and

its associated power-supply circuits, the sweep circuits for producing and synchronizing the linear sawtooth waveform and for intensifying the sweep for its duration, and the video amplifier.

An r-f envelope viewer is usually made by incorporating the r-f detector in an oscilloscope unit designed for the viewing of rapid transients. Such an oscilloscope is the synchroscope of which two models, the P4 and the Model 5, have been used extensively at the Radiation Laboratory. Both perform essentially the same functions. A synchroscope generates one trigger pulse, which starts the equipment producing the transient, and a second trigger pulse, which is so timed that it may be made either to precede or to follow the first pulse. This second pulse starts the linear sweep generator, which produces the horizontal sweep on the oscilloscope. In this manner, the beginning and any portion of the transient may be observed. A synchroscope may also be triggered externally by the transient to be observed. Because of the delay in starting the sweep and intensifier circuits, the very beginning of the transient cannot be observed. Since it is the beginning of the r-f pulse that is frequently of the most interest, an r-f envelope viewer is seldom used in this manner. To avoid excessive light on the screen the beam is cut off except during the sweep. A synchroscope will operate without external triggers at repetition frequencies of 500, 1000, 2000, and 4000 cps, or it will operate at any frequency from 50 to 5000 cps by using either an external sine-wave generator or an external trigger. Both the P4 and the Model 5 synchroscopes produce a horizontal sweep of about 4 in. on a 5-in. cathode-ray tube. The P4 synchroscope has available sweep speeds up to about 1.7 in. per μsec and the Model 5 up to 5 in. per μsec. The Model 5 has push-pull horizontal deflection whereas the P4 has single-end deflection and, therefore, a poorer image. In addition, the Model 5 synchroscope has a more precise delay circuit and a faster-rising output trigger pulse. Because of its higher resolution the Model 5 synchroscope is to be preferred for studies of fast transients. The operation of the circuits of the P4 and Model 5 synchroscopes is described in Chap. 6 of Vol. 22 in this series, and will not be discussed in detail here. Emphasis will be placed on the associated r-f circuits.

R-f envelope viewers may be divided into three classes, those using a crystal detector and video amplifier, those using a vacuum-tube detector and video amplifier, and those using a diode detector at high level where a video amplifier is not needed. These will be taken up in turn.

7·19. Crystal Detector with Video Amplifier.—A very simple sort of r-f envelope viewer may be made by adding a video amplifier to a P4 synchroscope and using an ordinary crystal as an r-f detector. Such an r-f envelope viewer is very sensitive, is approximately linear with power if the amplifier has sufficiently high gain, and can be made to

operate at any band where a crystal detector is available. The crystal-detector mount usually does not need to be tuned over the band of frequencies for which it was designed.

A video amplifier for use with crystals has been designed and is frequently incorporated in a P4 synchroscope. The combination is intended for viewing the r-f pulses from test oscillators and signal generators. The video amplifier has a voltage gain variable from 200 to 2000. At minimum gain the bandwidth is from 160 cps to 8.2 Mc/sec, and at maximum gain the upper limit is reduced to 5.4 Mc/sec. The amplifier is designed for use with a negative input signal. The input

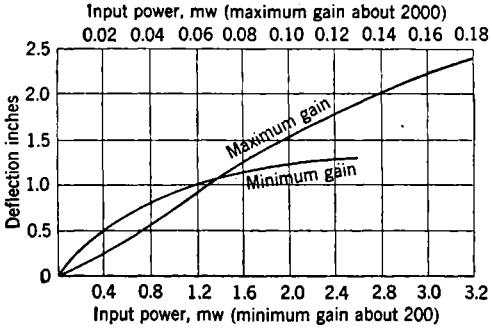

FIG. 7·27.—Calibration of a crystal r-f-envelope viewer with video amplifier.

impedance consists of a 1000-ohm resistor shunted by about 18 $\mu\mu$f. The undistorted output signal of the amplifier is 140 volts. Figure 7·27 shows the linearity and sensitivity of this amplifier used with a 10-cm-band crystal. If the cable connecting the crystal detector to the video amplifier is 12 in. long or less, the response will be essentially unaltered.

7·20. Vacuum-tube Detector with Video Amplifier.—An r-f envelope viewer for 10-cm band, which will also function at 3-cm band, can be made using a type 954 acorn pentode as a detector and amplifying the output signal by a video amplifier. Such a detector and video amplifier are easily installed in a P4 synchroscope. The r-f power is applied to the grid of the detector by means of a 50-ohm coaxial line. At the end of the inner conductor there is a set of spring jaws that grip the grid lead of the tube. The jaws are fastened to the inner conductor through a semiflexible coupling to allow for variations in individual tube dimensions. Since the tube does not properly terminate the line, a 50-ohm resistive disk is placed across the line ahead of the tube. The voltage standing-wave ratio is usually less than 1.7 over most of the 10-cm band and about 1.2 at the band center. The amplitude control is a bias potentiometer in the detector circuit. The video amplifier following

the detector consists of a 6AC7 and a 6AG7 tube. The bandwidth is about 5 Mc/sec.

This r-f envelope viewer is not so sensitive as the type using a crystal but this is not an important disadvantage if a source of adequate power is available, for example, a pulsed magnetron oscillator. The coupling to the r-f envelope detector may be effected by a pick-up antenna, by a probe in the r-f line with an attenuating cable, or by a directional coupler. A vacuum-tube detector has an advantage over a crystal detector in that it is not easily damaged by overload.

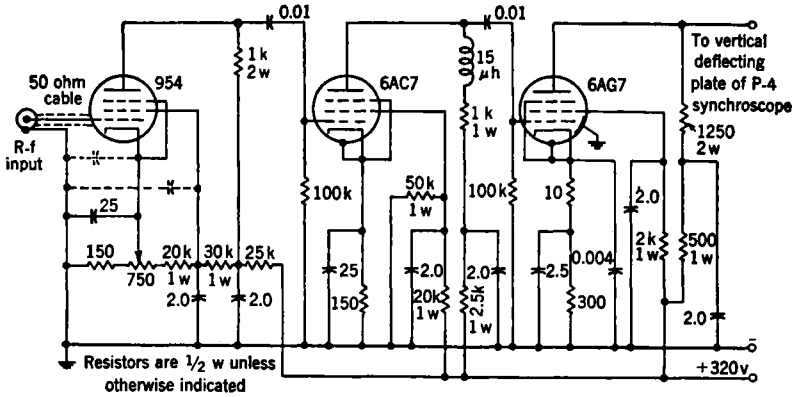

FIG. 7·28.—Detector and video amplifier for P4-E synchroscope and r-f envelope viewer.

Under some operating conditions the output voltage is approximately linear with input power. If the r-f envelope viewer is to be used to measure power accurately, however, an individual calibration is desirable. Because of differences in tubes a new calibration should be made if the detector is replaced. A circuit diagram of the detector and video amplifier used in the P4-E synchroscope is shown in Fig. 7·28.

The P4-E synchroscope and r-f envelope viewer are not satisfactory, as they stand, for making accurate measurements on r-f pulsed signals from magnetrons. The relatively long leads from the amplifier to the deflecting plates introduce stray inductance that distorts the image and may be a source of extraneous signals picked up from high electric fields near by. The amplifier must be shielded carefully and r-f and video-frequency grounds must all be short and made with heavy wire. It is desirable that the horizontal deflection leads be shielded. When all this is done, very acceptable pictures of r-f pulse envelopes may be obtained. Some typical results are shown in Fig. 7·29. Included are spectra, current pulses, and r-f envelopes for a 3-cm-band magnetron operated at three different pulse lengths. Current and r-f envelope

pulses have the same scale in time, the pairs of exposures being made successively with the same operating conditions. The r-f envelope pulse is seen to follow the current pulse quite exactly and to reproduce its oscillations. Since during the time of the r-f pulse the voltage is practically constant, the current pulse is a representation of the input power to the magnetron, and if the magnetron efficiency were constant, the r-f output would be expected to be similar in form. The fact that the

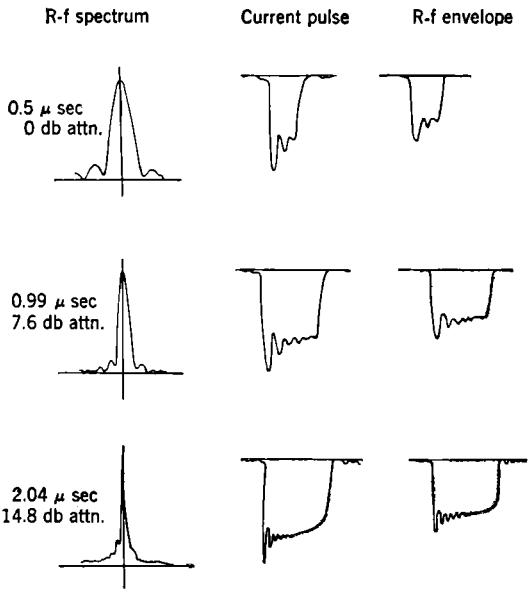

FIG. 7·29.—Representative spectra, current pulses, and r-f envelopes for a WE-725A magnetron using an aircraft modulator and pulse transformers. The r-f envelope viewer is a modified P4-E synchroscope.

r-f envelope follows the current pulse faithfully is an indication that the r-f envelope viewer gives a deflection roughly proportional to power. As the pulse length is increased the spectrum width between minima is decreased, and the spectrum amplitude is increased as indicated by the additional attenuation required to equalize the peak deflection. Equation (10), Sec. 7·2 shows that the amplitude of the transient on the spectrum-analyzer screen (deflection proportional to power) is proportional to the square of the pulse width. If this peak deflection were held constant as the pulse width was doubled, an attenuation of 6 db would have to be introduced. Figure 7·29 shows that this is, in fact, the case The somewhat distorted shape of the spectrum of the 2-μsec pulse is probably the result of a slight amount of frequency modulation. This is

not definite, however, as the spectrum analyzer bandwidth might have been broader than 50 kc/sec and this could cause a similar effect.

7·21. Diode Detectors Used at High Level.—Crystal and vacuum-tube detectors which must be used with a video amplifier are capable of showing the general form of r-f pulses of about 1 μsec. Because of the limited bandwidths that can be attained consistent with a reasonable gain, a video amplifier may seriously modify the form of a pulse. An amplifier with a 5-Mc/sec bandwidth and no overshoot will considerably modify the shape of a 1-μsec pulse and will completely distort a 0.1-μsec pulse. Amplifiers may be built having bandwidths of 15 Mc/sec or more, but even these are frequently not adequate for a detailed study of the pulse shape.

A typical problem that arises is the study of the starting behavior of pulsed magnetron oscillators. A magnetron does not start instantaneously when the applied voltage reaches the operating value. This delay is called the starting time, and for the 10-cm-band magnetrons it varies from 0.01 to 0.08 μsec. To measure accurately the starting time of a magnetron of 0.01 μsec, the resolving power of the r-f envelope viewer must be 0.01 μsec or less. A time of rise of 0.01 μsec requires a video amplifier having a bandwidth about 30 Mc/sec with good phase response. Since this is difficult to achieve, the video amplifier is omitted and a diode detector is used at a high enough power level to give a direct indication. A 10-cm-band detector that uses a type 2B22 lighthouse diode at high level is satisfactory. If such a detector is connected to a Model 5 synchroscope having a sweep speed of 5 in. per μsec, the shape and timing of the r-f pulse are not observably distorted. The r-f pulse has a shape similar to the current pulse and starts at the same time except for the delay in the attenuating cable connected to the r-f detector. Figure 7·30 shows three examples of typical voltage, current, and r-f pulses. The voltage and current pulses are shown above and voltage and r-f pulses are shown below in proper time relationship. The normal starting voltage V_0 and the starting time are indicated.

The r-f envelope detector with which the waveforms of Fig. 7·30 were observed uses the type 2B22 lighthouse diode in a low-Q tunable cavity. The power is coupled in by a capacitive probe. In this manner an output signal of several hundred volts could be obtained which is sufficient for deflecting a cathode-ray tube directly. The lighthouse diode and the cavity used are shown in Figs. 7·31 and 7·32. The object of the design is to provide a reasonably low-Q r-f circuit having an output connection with the lowest practicable capacitance. Connection is made from the end of the inner plate cylinder to one of the deflecting plates and from the outside cylinder to the other plate and ground. Since it is of utmost importance to minimize capacitance and stray inductance, the connec-

tions to the deflection plates are made as short as possible, and the cavity is mounted in the synchroscope box. The total capacitance is about

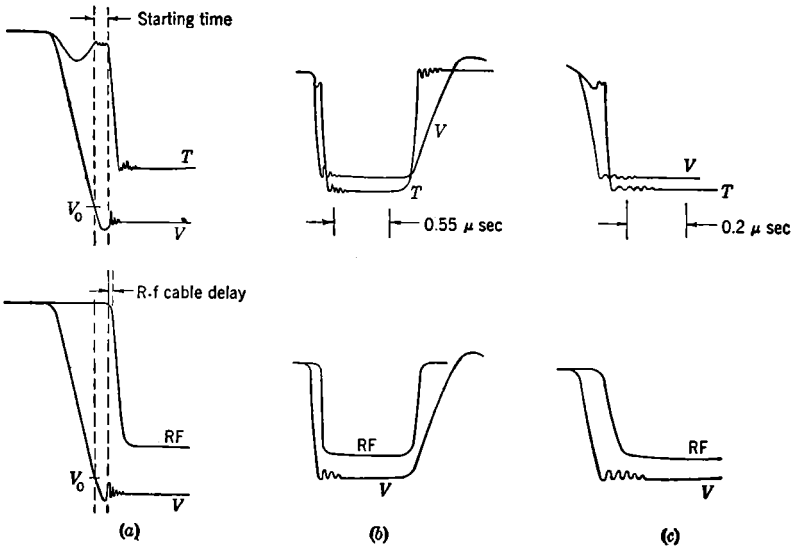

FIG. 7·30.—Voltage, current, and r-f pulses of 10-cm magnetrons. R-f envelope viewer using a 2B22 diode at high level was used in conjunction with a Model 5 synchroscope.

20 $\mu\mu$f. The cavity operates in the $\frac{3}{4}\lambda$-mode and has ample tuning range for the entire 10-cm band. Since the Q is low, the plunger and push rods provide fine enough control. Modification of the cavity for longer wave-lengths would be very simple.

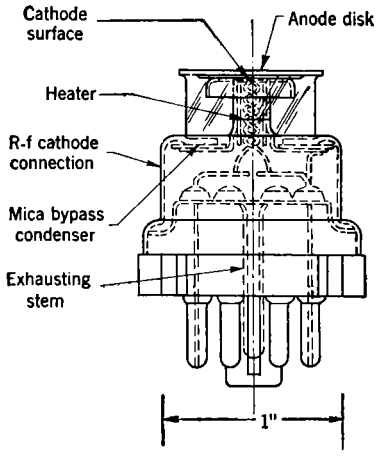

FIG. 7·31.—Type 2B22 lighthouse diode.

A requirement for good sensitivity is that the diode have adequate cathode emission. It was found that those tubes with highest conductance gave the greatest output signal. The major compromise in the design which had to be made was the choice of the diode load resistor. For resistances below 600 ohms, the sensitivity rises rapidly as the resistance is increased, indicating an improvement in rectification efficiency. The rise time, however, also increases and a compromise value of 300 ohms was chosen. A typ-

ical calibration under these conditions is given in Fig. 7·33. The approximate relation between input power and output voltage is given by $V = KP^{0.58}$.

The intrinsic rise time of the envelope viewer is determined by a combination of the r-f-circuit Q and the bandwidth of the video circuit. The Q of the r-f circuit is about 25, which at 3000 Mc/sec represents an

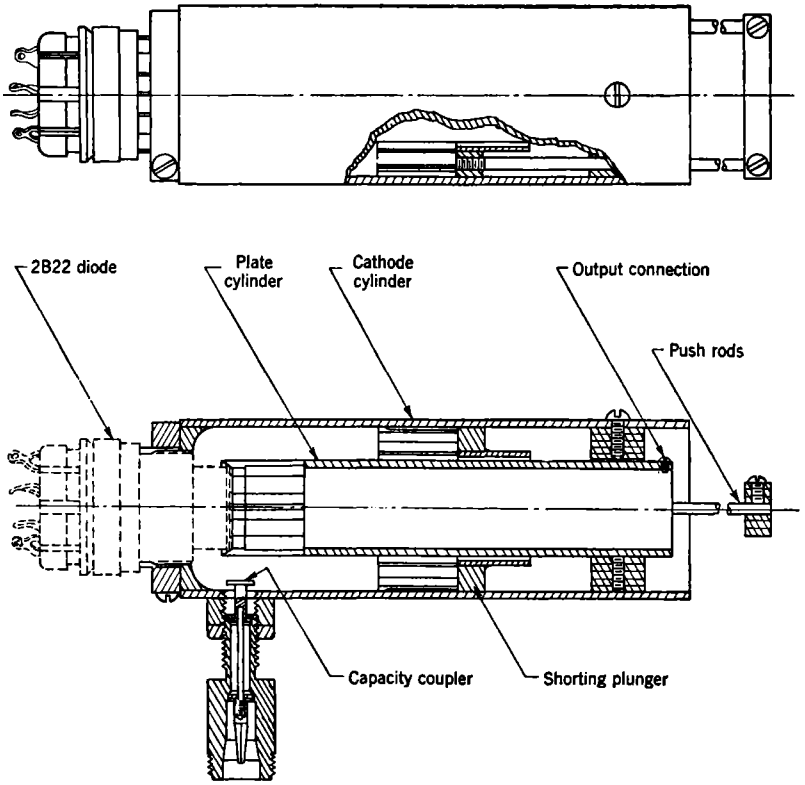

FIG. 7·32.—Cavity for use with lighthouse diode.

r-f bandwidth of 120 Mc/sec or an equivalent video bandwidth of 60 Mc/sec. The bandwidth of the video circuit consisting of a resistance of 300 ohms shunted by 20 $\mu\mu$f is 26.5 Mc/sec. This bandwidth could be improved somewhat by a peaking circuit, but a good phase response must be preserved. The bandwidth is thus limited by the video response. The rise time associated with a bandwidth of 26.5 Mc/sec is about 0.013 μsec, which is considerably shorter than the rise time of the r-f envelope viewer using a 954 tube with an amplifier.

In making measurements of very short time intervals with a fast oscilloscope and r-f envelope viewer, it is necessary to consider the length of the transmission lines connecting the pulse source to the oscilloscope and r-f envelope viewer. For example, in the measurement of the starting time of the r-f and current pulses of a magnetron, care must be taken to make all the cable lengths equal, or to correct for a difference in length. An extra 5-ft length of video or r-f cable will introduce a delay of 0.008 μsec.

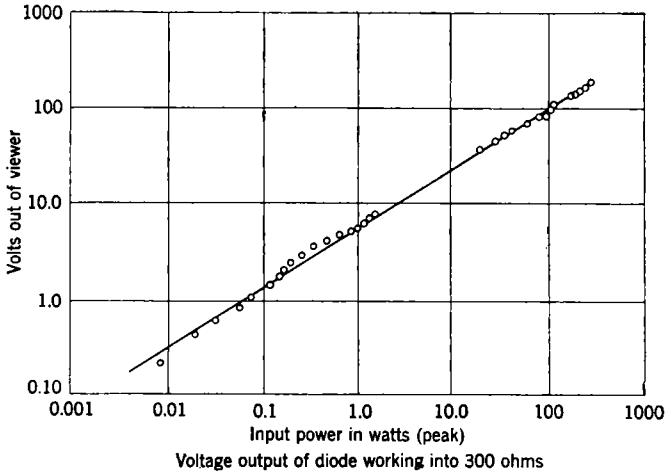

FIG. 7·33.—Typical calibration for the lighthouse-tube r-f envelope viewer.

7·22. Diode Detectors for Frequencies Higher than 3000 Mc/sec.—The lighthouse-tube r-f envelope detector was designed for 10-cm-band operation or, with modification, for use at lower frequencies. Operating on the same principle but with a different tube, r-f envelope viewers have been built for the 3-cm and the 1-cm bands. Basic to the operation of these detectors is a very small diode with cylindrical cathode and anode having a spacing of 0.002 in. The shunt capacitance of the tube is 4 $\mu\mu$f. The tube, which is still developmental, is the size of a standard crystal cartridge and is mounted across the waveguide in the manner of a crystal mixer. The tube is manufactured by RCA and has the type number R6271. Illustrations of the size and construction of the tube will be found in Figs. 7·34 and 7·35. The waveguide mounts for the tube at 3-cm band and 1-cm band are shown in Figs. 7·36 and 7·37, respectively. These mounts are similar to crystal mounts, except that provision must be made for the longer exhausting seal on the lower end of the tube and the structure and seals at the upper end. A plunger behind the tube and two tuning screws ahead of it serve to match the tube to the waveguide. The Q of either the 3-cm- or 1-cm-band mount

is such as to be equivalent to a video bandwidth of 150 Mc/sec. An output voltage of about 100 volts may be obtained on either band, although the sensitivity is different. This diode may of course be used at the 10-cm band as well. For the conditions of a 300-ohm load resistance and an output voltage of 100 volts, the sensitivities at the three bands are: one watt per volt at 10 cm (comparable to the 2B22), 12.5 watts per volt at 3 cm, and 75 watts per volt at 1 cm. In spite of the low

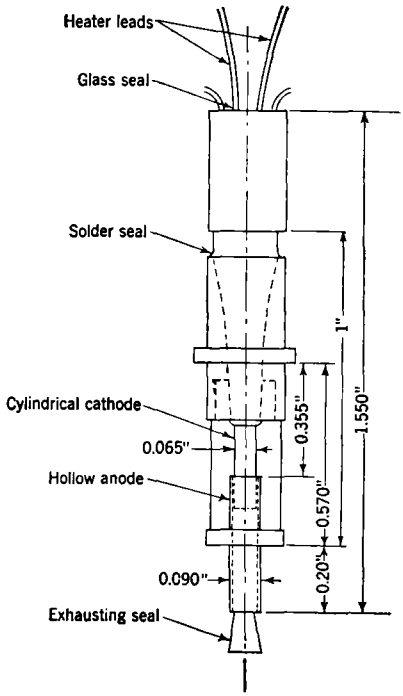

FIG. 7·34.—Type R6271 diode.

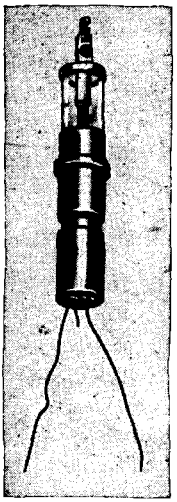

FIG. 7·35.—Type R6271 diode.

efficiency at 1-cm caused by transit-time effects, the tube is still of use if adequate power is available. The maximum power that may be applied to the diode is determined by the plate dissipation. At high frequencies the efficiency is so low that it may be assumed that the input power is dissipated in the tube itself. Although the maximum ratings have not been determined, if the anode is cooled adequately by the spring fingers that grip it in the mount, two watts is probably a safe value. The peak power is limited by the value at which sparking between the electrodes occurs. As with the 2B22 diode and cavity, the video bandwidth is determined by the total shunt capacitance of the circuit and the load resistor since the r-f bandwidth is not a limiting factor. The total capacitance including the cathode-ray-tube deflecting plates may be about 15 $\mu\mu$f with careful design. Where high resolution is important and sensitivity and deflection amplitude are secondary, the load resistance

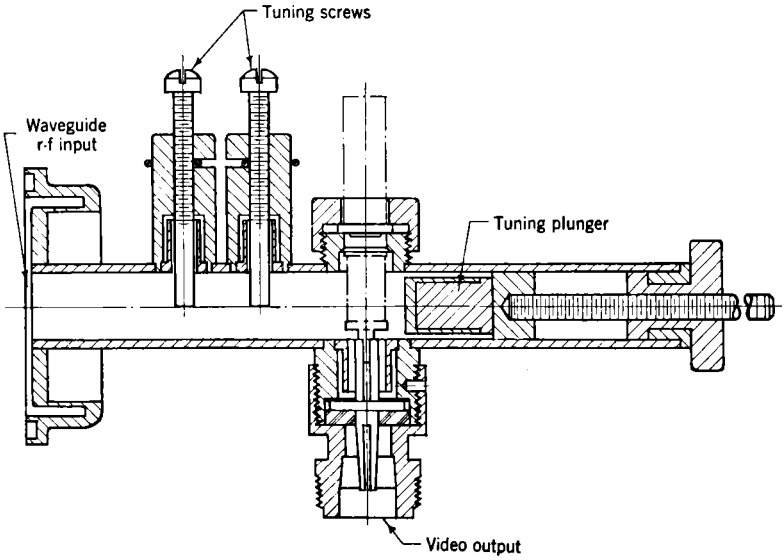

FIG. 7·36.—R-f envelope detector for 3-cm wavelengths using an R6271 diode.

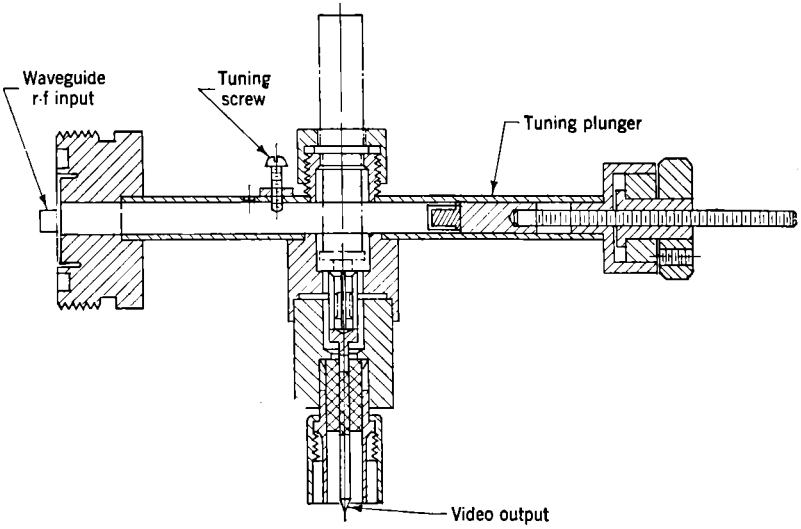

FIG. 7·37.—R-f envelope detector for wavelengths near 1 cm using an R6271 diode.

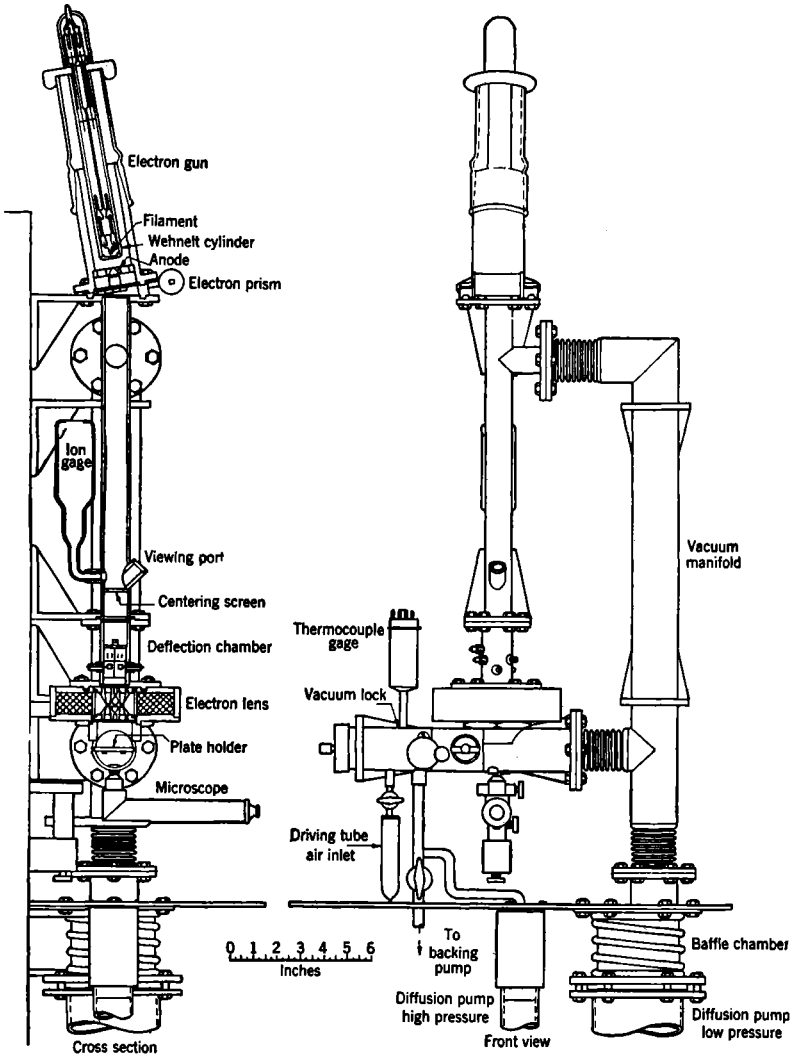

FIG. 7·38.—Diagram of high-speed oscillograph.

may be decreased to 100 ohms which would result in a video bandwidth of about 100 Mc/sec.

When measurements of rapid transients are to be made with extreme precision, it is necessary to ensure that the resolution of the image is not affected by the transit time of the electrons through the deflecting plates of the cathode-ray tube. The accelerating potential (cathode to second

anode) used in the Model 5 synchroscope is about 1300 volts, whereas the deflecting plates are about 3 cm long. The transit time of an electron is then 0.002 μsec, somewhat shorter than the limit of resolution of that synchroscope. If it were important to reduce the transit time, this could be done by raising the accelerating potential or by using a different cathode-ray tube.

7·23. Microwave Oscilloscopes.[1]—The fundamental limiting factor in the use of oscilloscopes to observe microwave oscillations or very fast transients is the distortion resulting from the finite length of time required for the electrons to traverse the deflecting field. It may be easily seen[2]

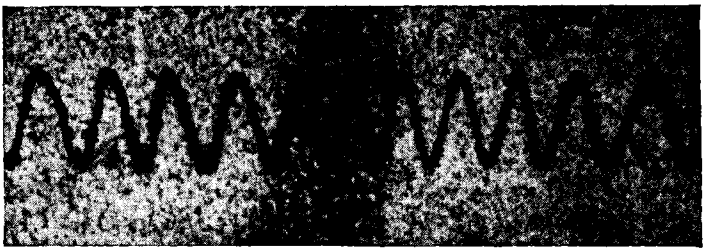

FIG. 7·39.—Oscillogram of 3000-Mc/sec wave.

that the ratio $s(f)$ of the deflection sensitivity at the frequency f to the d-c sensitivity is given by

$$s(f) = \frac{\sin \pi ft}{\pi ft} \tag{11}$$

where t is the transit time of the electrons through the deflecting plates. For good sensitivity the transit time must be reduced by using electrons with a high velocity and short deflecting plates. Two such oscilloscopes have been recently built which merit description.

The first[3] of these employs a very fine electron beam at high velocity that impinges directly on a photographic plate and the oscillogram is viewed with a microscope after exposure. The beam diameter is about 10^{-2} mm and the accelerating potential 50 kv. The length of the deflecting plates is 0.5 mm. Hence the transit time is about 4×10^{-11} sec. The sensitivity $s(f)$ therefore has its first zero at a frequency of 25,000 Mc/sec. For a 3000-Mc/sec signal, the sensitivity is nearly 97 per cent of the d-c sensitivity.

A very rapid sweep is produced by a simple RC-network discharging through a spark gap. A reasonably linear writing speed of 5×10^8 cm/sec can be obtained. A cross-sectional view of the oscilloscope is shown in

[1] By C. G. Montgomery.

[2] H. E. Hollman, *Hochfrequenztechn Elektroakust.* **40,** 97 (1932).

[3] Gordon M. Lee, "Development of a High-speed Oscillograph," Doctor of Science thesis, Massachusetts Institute of Technology, 1944.

Fig. 7·38. An oscillogram of a 3000-Mc/sec wave is shown in Fig. 7·39.

The second oscilloscope[1] uses a tube of the more conventional type. It was developed jointly by the Radiation Laboratory and Allen B. Du Mont Laboratories, Inc.[2] An electron beam of about 1-mm diameter is accelerated to 5000 volts before it passes through the deflecting plates

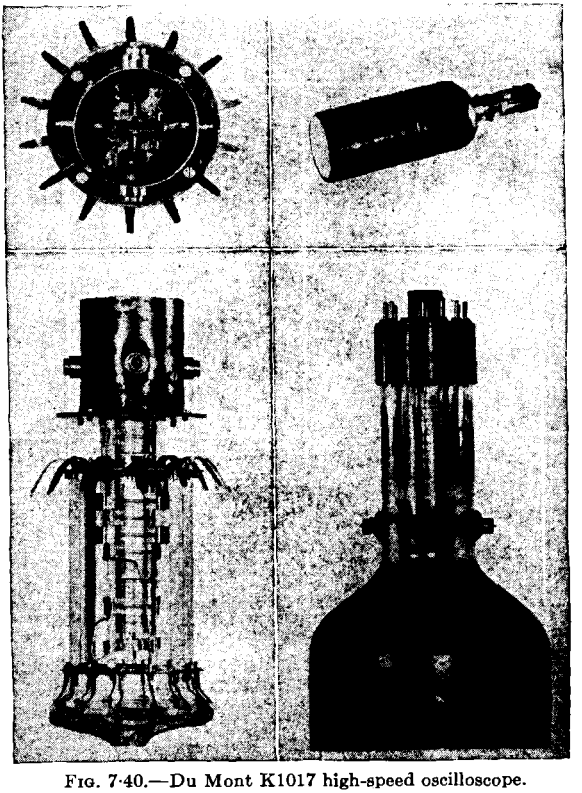

FIG. 7·40.—Du Mont K1017 high-speed oscilloscope.

and then falls through an additional potential difference of 20,000 volts before it strikes a fluorescent screen of the conventional variety. The deflecting plates are 8 mm long and separated by 0.050 in. The transit time is about 3×10^{-10} sec and the first zero of the relative sensitivity occurs at 5000 Mc/sec. At 1000 Mc/sec the sensitivity is 95 per cent of the d-c value. The deflection sensitivity is about 175 volts/in. Figure 7·40 shows a photograph of the cathode-ray tube. This instrument has not been used much up to the present time, but it seems likely that the oscilloscope tube may soon be commercially available.

[1] cf. Vol. 22, Sec. 6·7 of this series.

[2] Tube type K1017.

PART III

THE MEASUREMENT OF IMPEDANCE AND STANDING WAVES

CHAPTER 8

MEASUREMENTS OF STANDING WAVES

By E. M. Purcell

If a uniform transmission line is excited by a generator at a frequency that is not too high, the steady state can be described by saying that there are two waves on the line, one running in each direction. The amplitude of each of these waves can be associated with some quantity characteristic of the electromagnetic field, such as the electric field strength at some arbitrarily selected location on a cross section of the transmission line. With this understanding, the amplitude of the waves may be formally described, at any point along the line and at any time, by complex numbers A and B, which refer to the wave running from the generator and the wave running toward the generator, respectively. If the positive x direction is pointed away from the generator,

$$\begin{aligned} A &= A_0 e^{j\omega t - \gamma x}, \\ B &= B_0 e^{j\omega t + \gamma x}. \end{aligned} \tag{1}$$

The instantaneous magnitude of the electromagnetic field quantity to which the amplitude refers is understood to be the real part of A, or of B. The numbers A_0 and B_0 depend on choice of the zero points for the measurement of time and distance. The quantity γ is called the propagation constant of the wave; it depends upon the properties of the transmission line, and upon the frequency. It is customary to denote the real and imaginary parts of γ by α and β, that is,

$$\gamma = \alpha + j\beta. \tag{2}$$

If the transmission line is lossless, $\alpha = 0$, and $\beta = 2\pi f/v$, where v is the phase velocity of a wave on the line at frequency f. If attenuation along the line must be reckoned with, $\alpha > 0$; there is then an exponential decrease of the absolute magnitude of A, and a corresponding increase of the absolute magnitude of B, as x increases.

The total amplitude, $A + B$, at some point along the line, is the quantity of interest and more particularly the time average of some function of $|A + B|$, for the instruments are not, as a rule, capable of following the rapid variations at frequency f. Suppose for definiteness that something proportional to the time average of $|A + B|^2$ can be measured, the result of one such measurement being a single real number

which will be called P_s and which will be a function of x, although not, of course, a function of t. Then,

$$P_s \propto |A_0 e^{-\gamma x} + B_0 e^{+\gamma x}|^2. \tag{3}$$

In general, P_s will display maxima and minima as x is varied; it may be said that there are *standing waves* on the line. From the variation of P_s with x it is possible to deduce the ratio of A_0 to B_0, which is a complex number, and also γ, if necessary. This is the object of all standing-wave measurements. Such measurements are useful because knowledge of A_0/B_0, together with γ, suffices to determine completely the properties of the termination of the transmission line at the prevailing frequency.

In most microwave measurements it is permissible to neglect the attenuation in the transmission line itself and to assume that

$$\gamma = j\beta = j2\pi f/v.$$

This may seem at first rather surprising if one is accustomed to associate high losses with high frequencies, in consequence of the decrease of skin depth with increasing frequency. The significant quantity, however, is the attenuation per wavelength and for transmission lines of a *given size* this decreases, with increasing frequency, as $1/\sqrt{f}$. Microwave transmission lines are not much smaller in cross section than lines used at much lower frequencies, as a rule, and hence the approximation made by neglecting the attenuation is much better than it would be at low frequencies. As the high-frequency end of the microwave spectrum is approached, however, transmission lines (which in most cases take the form of hollow waveguides) must be made smaller to avoid the possibility of propagation in higher modes, and the attenuation per wavelength increases, approximately as $\sqrt{f}$. But even at 30,000 Mc/sec the ratio of α to β is usually less than 10^{-3}. The effect of line attenuation upon standing-wave measurements will be considered briefly later; in most of what follows it will be neglected.

It has already been suggested that, if the frequency is too high or the transmission line too large in cross section, propagation of energy in more than one mode may be possible. In that case the two waves of Eq. (1) do not suffice to describe conditions within the line, and other waves must be included. For an introduction to this special problem which will not be treated here, the reader is referred to Chap. 10 of Vol. 8.

It will be assumed throughout the chapter that the electromagnetic fields under examination correspond to a steady state, which is equivalent to the assumption that a single sharply defined frequency is involved. Nevertheless, the results can be applied, in many cases, to a modulated signal. This is allowable when the modulation frequencies concerned

are much lower than the carrier frequency, as is almost always true in the microwave region.

8·1. Fundamental Relations.—If γ is known in advance, the result of a measurement of the standing-wave pattern on a line at a fixed frequency with a given load can be expressed by a single complex number, the ratio of B to A, the amplitudes appearing in Eq. (1), at some selected point on the line. From this number the ratio of B to A at any other point can be computed from Eq. (1). In particular, the value of B/A at the load can be found, which is, by definition, the complex reflection coefficient Γ_L of the load,

$$\Gamma_L = \left(\frac{B}{A}\right)_L. \qquad (4)$$

More generally B/A at any point x on the line can be called the reflection coefficient of the remainder of the line terminating in the load.

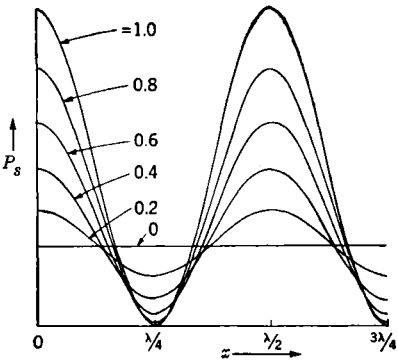

FIG. 8·1.—Variation of probe power P_s with position of probe. The parameter is Γ_0.

The form of the standing-wave pattern, that is, the curve of P_s as a function of distance x along the line, can be derived at once from Eq. (2). For simplicity let the origin of x be taken at a point where B/A is the positive real number Γ_0. Then,

$$\begin{aligned} P_s &= \text{constant} \times [(1 + \Gamma_0)^2 \cos^2 \beta x + (1 - \Gamma_0)^2 \sin^2 \beta x] \\ &= \text{constant} \times (1 + \Gamma_0 + 2\Gamma_0 \cos 2\beta x). \end{aligned} \qquad (5)$$

The curves in Fig. 8·1 show how P_s varies with x for certain values of Γ_0. No significance is ordinarily attached to the absolute magnitude of P_s in a standing wave, but the *relative* magnitudes of the waves of Fig. 8·1 are correct for the case of a matched generator. That is to say, the "constant" in Eq. (5) is the same for all the curves of Fig. 8·1, corresponding to constant amplitude of the wave running *from* the generator.

It must be remembered that the form of the standing-wave pattern actually observed will resemble a P_s curve only if the indication is proportional to the square of the total amplitude of the waves. The discussion in this chapter will be based on this special case, for the most part, both because the analysis is simpler, and because the detectors that are actually used can, with certain precautions, be made to approximate this response law very closely.

The features of the standing-wave pattern which are most easily

measured are the ratio of the maximum to the minimum reading, $P_{s_{max}}/P_{s_{min}}$, and the position of a maximum or a minimum along the line. The ratio, $P_{s_{max}}/P_{s_{min}}$, is called the power standing-wave ratio, whereas $\sqrt{P_{s_{max}}/P_{s_{min}}}$ is called the voltage standing-wave ratio, sometimes abbreviated VSWR, and denoted by the letter r,

$$r = \sqrt{\frac{P_{s_{max}}}{P_{s_{min}}}} = \frac{|A| + |B|}{|A| - |B|}. \tag{6}$$

The connection between r and $|\Gamma|$ is particularly simple; it is at once evident from Eq. (5) that

$$r = \frac{1 + |\Gamma|}{1 - |\Gamma|}; \qquad |\Gamma| = \frac{r - 1}{r + 1}. \tag{7}$$

The phase angle of the reflection coefficient of the load can be determined by observing the distance between the load and the nearest *minimum* in P_s. If this distance is denoted by x_{min} and if the reflection coefficient of the load is written $\Gamma = |\Gamma|e^{i\theta}$, then

$$\theta = 2\beta x_{min} \pm \pi. \tag{8}$$

It is often convenient to describe the load by its impedance Z_L or its admittance Y_L measured, respectively, in units of the characteristic impedance or the characteristic admittance of the line. The relation between these dimensionless quantities and Γ is

$$\Gamma_L = \frac{Z_L - 1}{Z_L + 1} = \frac{1 - Y_L}{1 + Y_L}. \tag{9}$$

If the dimensions of the transmission line and the load are small compared to a wavelength, the quantity Z_L appearing in Eq. (9) is the ratio of two impedances, that of the load and that of the line, which are uniquely defined in terms of voltage and current. Equation (9) can be derived by applying the boundary conditions on voltage and current which the load imposes. In a waveguide transmission line or circuit, voltage and current cannot be given a unique and universally useful definition. Equation (9) is to be regarded as *defining* Y and Z in terms of Γ. The introduction of the impedance concept does not increase the amount of information made available by a standing-wave measurement, but it does facilitate the comparison of the system under investigation with equivalent circuits composed of transmission lines and lumped impedances, the analysis of which, in turn, is readily carried out by familiar methods.

It is helpful to adopt a method of plotting the results of a series of standing-wave measurements which displays all of the information obtained. A natural way to do this is to plot the quantity $\Gamma = |\Gamma|e^{i\theta}$ in

the complex plane, with Γ the reflection coefficient at some selected reference point on the line. Often it is convenient to choose as this reference point the termination of the line. All values of Γ will fall on or within the unit circle, at least for passive terminations, and the diagrams take the form of Fig. 8·2*a*. Through the relations between $|\Gamma|$ and r,

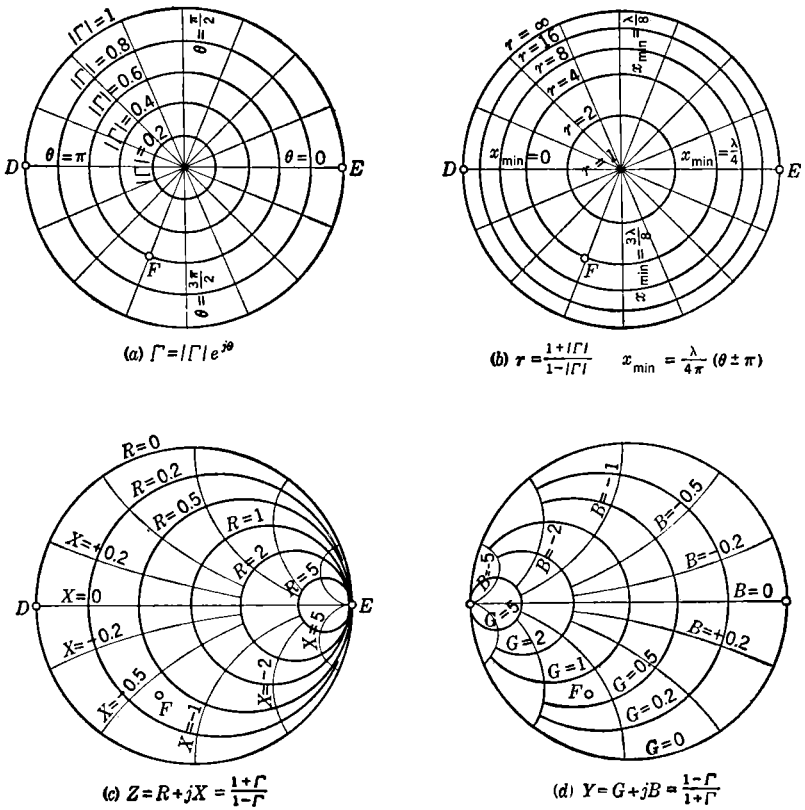

FIG. 8·2.—Representation of properties of the load by points in the complex plane; (*a*) reflection coefficient, (*b*) standing-wave ratio and minimum position, (*c*) impedance, (*d*) admittance.

and between θ and $x_{\min}$, another set of lines and circles can be drawn in the same complex plane from which r and $x_{\min}$ can be read directly. This new grid is shown in Fig. 8·2*b*. The quantity $x_{\min}$ is understood to be positive when it represents the distance between the reference point on the line and a minimum in P_s located between the reference point and the generator. The location of a point in the Γ-plane can also be described in terms of the impedance Z, or the admittance Y, seen at the

reference point in the line, by imposing on the Γ-plane the curves of Fig. 8·2*c* or Fig. 8·2*d*.

For example, the points *D*, *E*, and *F* which appear in each of the plots may be considered. The point *D*, in each plot, corresponds to a short circuit, $\Gamma = -1$, at the reference position, hence to a *zero* in P_s at that point, with $r = \infty$. The same point in Figs. 8·2*c* and *d* is to be interpreted as zero impedance and infinite admittance, respectively. The point *E* represents an open circuit at the reference position, giving $r = \infty$, with $x_m = \lambda/4$, $Z = \infty$, $Y = 0$. For the point *F*, for which $\Gamma = 0.6e^{j\frac{11\pi}{8}}$, the minimum in P_s occurs $\frac{3}{16}\lambda$ from the reference position, measured toward the generator, $r = 4$, $Z = 0.35 - j0.61$ and

$$Y = 0.76 + j1.31.$$

The diagrams of Fig. 8·2*c* and *d* are the so-called "Smith charts"[1] for impedance and admittance, respectively. They have proved to be very useful in microwave work because, being based on a plot in the Γ-plane, they permit line-length transformations to be effected by simply rotating the whole diagram. The reader may have noted that one additional convention has been introduced without warning, which is that the quantity P_s refers to the transverse electric field in the line. This convention is established when it is stated that $P_s = 0$ at a short circuit. It is consistent with the use of electric antennas, or probes, projecting in through the wall of the guide to pick up the signal eventually indicated as P_s. As will be seen in the following sections, a probe of this type is almost universally favored in microwave measurements, and therefore the convention adopted is natural and convenient.

8·2. The Slotted Section and Traveling Probe.—The instrument that has been most widely used for the measurement of standing waves consists of a section of transmission line or waveguide into which a small antenna, or *probe*, can be introduced through a slot. The probe extracts a small fraction of the power flowing in the transmission line, and is connected to an external circuit containing a rectifier, sometimes an amplifier, and a meter. By moving the probe along the slot, which is parallel to the axis of the line, the field in the interior of the line is explored and a curve similar to those of Fig. 8·1 is obtained. The simplified diagrams in Fig. 8·3 show the arrangement of the probe and the slot in a coaxial-line standing-wave instrument and in a waveguide instrument.

The slot is cut so that it runs parallel to the lines of surface current flow associated with the electromagnetic field in an unslotted line or guide, and its presence modifies the original field configuration only to a minor extent. The current flow in a coaxial line in the principal mode is,

[1] Phillip H Smith, *Electronics*, January, 1939, and January, 1944.

of course, directed exclusively parallel to the axis, and a longitudinal slot anywhere on the periphery is allowable. In a rectangular waveguide carrying the dominant mode (TE_{10}) the slot must be located at the center of either of the two broad walls of the guide, as is at once evident from a consideration of the electromagnetic field configuration for this mode.

The slot should be long enough to permit observation of at least one maximum and one minimum in P_s regardless of the position of the standing-wave pattern relative to the slot. Reference to Fig. 8·1 shows that the minimum probe travel thus required is half a wavelength. In

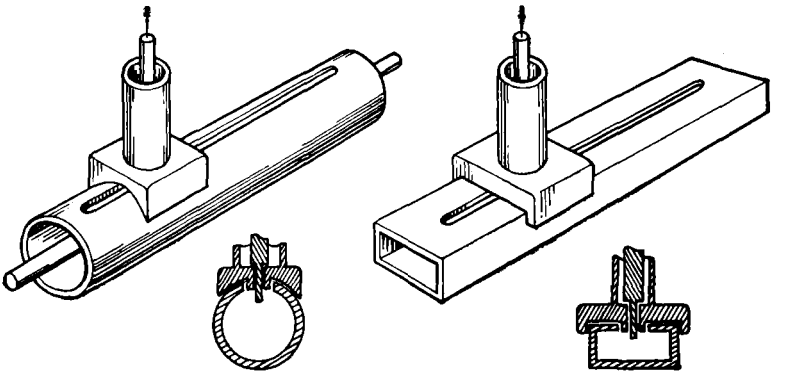

FIG. 8·3.—Slotted section with probe (*a*) coaxial line, (*b*) waveguide.

practice, a considerably longer probe travel is advantageous, for the observation of several maxima and minima affords a useful check on the instrument and allows a more accurate determination of the wavelength in the slotted section. It is usually easy to provide this additional length, and most microwave slotted sections permit a probe travel of $1\frac{1}{2}$ to 3 wavelengths.

The probes shown in Fig. 8·3 are called electric probes because the power that is withdrawn to the indicating circuit depends on the intensity of the electric field at the probe. A magnetic probe, consisting of a small loop antenna could be used instead, and has occasionally been used. The construction of a very small loop that responds only to the magnetic component of the field within the transmission line is difficult, however, if the line leading from the probe out to the detector is a *coaxial* line. There are practical reasons for preferring the coaxial line (rather than a shielded pair, for example) for this function, and the magnetic probe is thereby ruled out in most cases.

Little has been said about the indicating circuit itself, the function

of which is to detect the power picked up by the probe, perhaps to amplify it, and to provide a meter indication proportional to $|A + B|^2$ or to some other known function of $|A + B|$. This part of the instrument will be considered in a later section. For the present, the probe will be regarded simply as a load on the main transmission line, and it will be assumed that the ultimate meter reading is proportional to the power absorbed by this load.

The slotted-section technique is based on two assumptions: first, that the slotted line itself can be treated as a uniform lossless transmission line; second, that the presence of the probe does not seriously modify the electromagnetic field in the line. The validity of these assumptions is restricted by several factors which must be carefully examined if the best use is to be made of such an instrument, and which must be taken into account in the design of slotted sections and probes. The disturbing influences to be reckoned with are of two kinds: those which cannot be avoided so long as the probe and slot are of finite size and a finite amount of power is required to actuate the indicator, and those which can be blamed on accidental mechanical irregularities, departures from perfect symmetry, and so on. In the following sections effects of the first sort will be examined.

8·3. The Properties of the Slotted Line.—The effect of a longitudinal slot in the outer conductor of a coaxial line is to change the characteristic impedance of the line slightly, and to introduce a finite, but usually negligible, loss. The change in impedance can be understood by recalling that the characteristic impedance of a line consisting of two parallel cylinders, which need be neither circular in cross section nor coaxial, is uniquely determined by the capacitance of the line per unit length.[1] The creation of the slot reduces slightly the capacitance per unit length. The magnitude of the effect is given approximately by the following formula which was derived for the case of an infinitely thick outer conductor as in Fig. 8·4*a*.

$$\frac{\Delta Z_0}{Z_0} = \frac{1}{4\pi^2} \frac{w^2}{R_2^2 - R_1^2}. \tag{10}$$

Here ΔZ_0 is the change in characteristic impedance, R_1 and R_2 are the radii of the inner and outer conductors, respectively, and w is the width of the slot. For a wall of finite thickness the effect will be only slightly larger. The only significant consequence of a change in characteristic impedance is that a small reflection of the waves in the line will occur where the slot begins and again where it ends. The reflection coefficient will be, in absolute value, $\frac{1}{2}\Delta Z_0/Z_0$ from Eq. (10). For very precise work the effect might prove troublesome. It can be avoided, if neces-

[1] It is assumed that the magnetic permeability of the intervening medium is fixed.

sary, by compensating the change in impedance caused by the slot by an increase in the diameter of the inner conductor.

In a waveguide slotted section, the presence of the slot affects the propagation constant of the line, as well as the characteristic impedance. The guide wavelength λ_g' in a slotted guide differs slightly from the guide

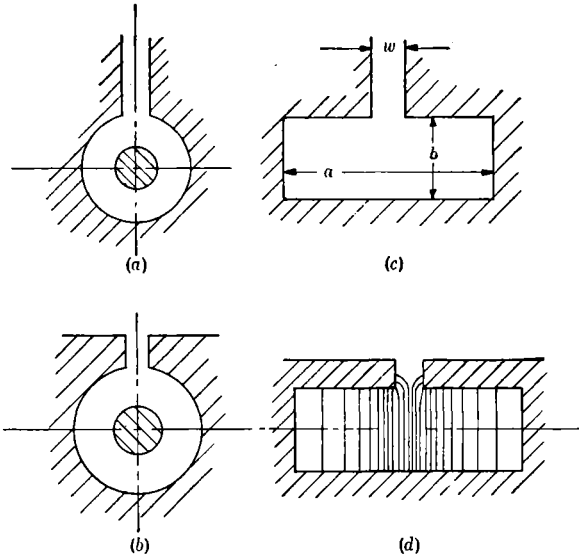

FIG. 8·4.—Cross section of slotted coaxial line and slotted guide.

wavelength λ_g in a guide of the same cross section but without a slot. The magnitude of the effect for a rectangular guide of width a, height b, and slot of width w, (see Fig. 8·4) is given approximately by

$$\lambda_g' = \lambda_g \left(1 + \frac{w^2 \lambda_g^2}{8\pi b a^3}\right). \tag{11}$$

Expressed in another way, the slotted guide of width a acts like an ordinary guide of width

$$\left(a - \frac{w^2}{2\pi b}\right).$$

Equation (11) was derived for a guide of infinite wall thickness, but can be used without significant error when the thickness is of the order of magnitude of the slot width, as is usually the case. The change in λ_g for most slotted sections amounts to less than 1 per cent. It causes no difficulty because the guide wavelength in a slotted section can and should be determined by direct measurement, where high accuracy is required. The wave-impedance of the guide will be increased by the

same factor $\left(1 + \frac{w^2\lambda_g^2}{8\pi b a^3}\right)$; as a consequence a small reflection may be expected at the beginning and at the end of the slot, as in the case of the coaxial slotted section.

The electric field will penetrate the slot to some extent and unless the wall is infinitely thick the field will extend into the exterior region with consequent loss of power by radiation. This effect, however, is ordinarily immeasurably small, for when the wall thickness is comparable with the slot width, the slot acts as a waveguide far beyond cutoff for the penetrating field, which may be thought of as a *TM*-wave in the parallel-plate transmission line formed by the sides of the slot. The attenuation of this wave in a direction normal to the axis of the line or guide is so rapid that the coupling to the exterior region is of no practical importance. The actual field configuration must resemble that sketched in Fig. 8·4*d*.

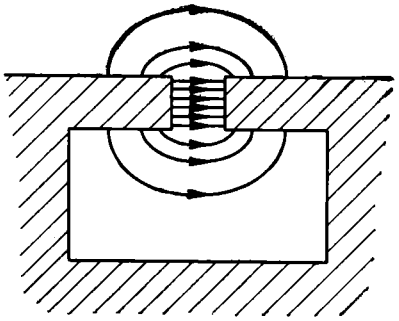

FIG. 8·5.—Electric field in a slot wave.

The slotted waveguide has another property that occasionally makes itself evident. A new mode of propagation is made possible by the presence of the slot. The field configuration of this mode is sketched in Fig. 8·5. It will be noted that the symmetry of the field is such that it cannot be excited by a wave incident in the TM_{01}-mode unless the cross section of the guide departs in some way from perfect symmetry, as, for example, if the slot is slightly off center. The possibility of departures from symmetry cannot be ignored in practice. Even weak excitation of the mode of Fig. 8·5 may have a disturbing effect upon the standing-wave measurement through a resonance effect like that which can occur in a waveguide section carrying several modes, one of which cannot be propagated in the sections immediately preceding and following. That is to say, the *slot waves*, as the oscillations in this mode will be called, are totally reflected at each end of the slot, and although energy is lost by radiation, to some extent, a pronounced resonance reaction upon the primary TE_{10}-wave is sometimes observed when the length of the slot is an integral multiple of half the guide wavelength for this mode. Moreover, the slot is divided into two sections by the probe and carriage (see Fig. 8·3). As the probe travels, the lengths of these sections vary, allowing full opportunity for a slot-wave resonance if the slot wave is excited.

The cutoff wavelength for the slot wave can be calculated by an application of formulas derived for the series waveguide T. If the thickness of the waveguide wall is t, and if w denotes the slot width with a and b as the waveguide dimensions, the cutoff wavelength λ_c for the slot wave is given implicitly by the relation

$$\cot\left(\frac{\pi a}{\lambda_c}\right) = \frac{2b}{\lambda_c}\left[2\ln\left(\frac{0.372b\lambda_c}{w^2}\right) + \frac{2}{\sqrt{1-\left(\frac{2b}{\lambda_c}\right)^2}} + \frac{2\pi t}{w}\right]. \qquad (12)$$

For typical guide and slot dimensions, Eq. (12) is satisfied by a value of λ_c which is considerably larger than $2a$. That is, the guide wavelength of the slot mode is shorter than the guide wavelength of the TE_{10}-mode in the guide. For example, the dimensions $a = 0.84\lambda_0$, $b = 0.34\lambda_0$, $t = w = 0.08\lambda_0$ lead to $\lambda_c = 6.0\lambda_0$. The slot-wave resonance, in this case of a relatively wide slot, is damped by radiation to the extent that the associated Q is about 7.[1]

Slot-wave resonances are not excluded from coaxial-line slotted sections even though, in the absence of the slot, only the principal mode is allowed. The Formula (12) applies approximately in this case, if a represents the mean circumference and b the distance between inner and outer conductors.

In all cases, of course, perfect geometrical symmetry of the slotted section and the probe will prevent excitation of the slot mode and will ensure that the slotted section behaves as a uniform, nearly lossless transmission line supporting only one mode of propagation.

8·4. The Properties of the Probe.—An ideal probe would be one whose presence in no way altered the fields within the transmission line and which, nevertheless, provided an indication of the intensity of the electric field within the line. The ideal is unattainable, and in fact for rough measurements only is it permissible to neglect the effect of the probe upon the line. Fortunately it is not difficult to analyze the action of the probe if two assumptions are made: (1) The probe and any associated high-frequency circuit components can be included in the complete microwave circuit of generator, transmission line, and load without introducing nonlinear circuit elements. This means that the line which connects the probe antenna to the external detecting circuit presents, as seen *from the probe*, an impedance which is independent of the amplitude

[1] The formulas used in deriving the properties of the slot wave were taken from *The Waveguide Handbook*, Vol. 10 of the Series, Sec. 10·4a. The slot is treated as the perpendicular branch of an E-plane T terminating in a transition to an infinite guide of infinite height. The loading referred to is also derived from this model and is given approximately by $Q = \lambda_c^2/2\pi^2 ab$.

of excitation. (2) The dimensions of the probe in a direction parallel to the slot are small compared with a wavelength.

The first assumption is not, as might at first be supposed, incompatible with the use of a crystal detector to rectify the signal picked up by the probe. The signal is required to be very weak for other reasons, and the detector then appears to the *microwave line* as a linear load. The second assumption is very well fulfilled also in most instruments.

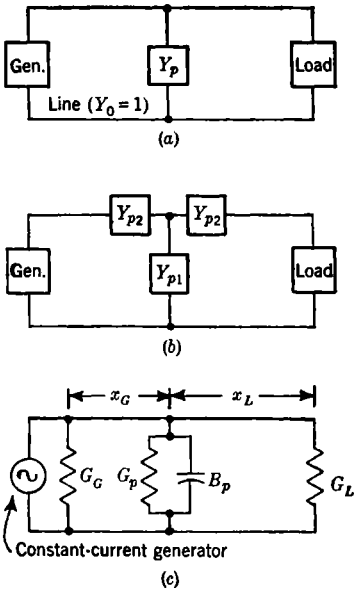

FIG. 8·6.—Equivalent circuit for the probe; in (*a*) and (*c*) the probe is represented as a simple shunt admittance $Y_p = G_p + jB_p$.

As a direct consequence of assumptions (1) and (2), the probe can be represented as a simple shunt admittance connected across the transmission line or waveguide, and the complete equivalent circuit takes the form shown in Fig. 8·6*a*. Had assumption (2) not been made, it would have been necessary to adopt a more complicated equivalent circuit for the probe, such as the T-network of Fig. 8·6*b*.

In Fig. 8·6*c*, the probe admittance Y_p is separated into a conductance G_p and a susceptance B_p. The power extracted by the probe is that dissipated in G_p and although this power, in the actual probe, may not all reach the detector because of ohmic loss in the probe circuit, it may still be assumed that the final indication P_s is proportional to $e_p^2 G_p$ where e_p is the voltage across the line at the probe position. The representation of the probe as a *shunt* element is not the only possibility, but it is convenient because of the convention already adopted that the probe reading refers to the transverse electric field, that is, that the probe is actually an electric antenna.

The influence of the probe upon the observed standing-wave pattern can now be analyzed by expressing the power dissipated in the conductance G_p as a function of the position of the probe on the line, the load admittance Y_L, and the generator admittance Y_L. The case $Y_L = 1$, that of a *matched* generator, will be considered first. The distance between generator and probe will be denoted by x_G and the distance between probe and load by x_L. It will suffice to consider Y_L as real, writing it as G_L, since any load of complex admittance will give rise to the same standing-wave pattern as some real load, except for a

shift of the pattern along the line. Alternatively, it may be said that x_L is measured between the probe and a point on the line at which the admittance of the remainder of the line, terminating in the load, is real and of magnitude G_L.

A straightforward application of the transmission-line relations now leads to an expression for the power absorbed in G_p, which apart from an irrelevant constant factor involving the generator current, the efficiency of the detector, and so forth can be identified with P_s, the probe reading.

$$P_s \propto \frac{G_p(1 + G_L^2 \tan^2 \theta)^2}{[1 + G_L + G_p + G_L(1 + G_L + G_pG_L) \tan^2 \theta]^2 + [B_p + (1 - G_L^2) \tan \theta + B_pG_L^2 \tan^2 \theta]^2}. \quad (13)$$

The angle θ has been written in place of $2\pi x_L/\lambda_0$. That P_s does not depend on x_G is the result of assuming a matched generator.

Consider first the case $G_L = 0$. Eq. (13) becomes

$$P_s \propto \frac{G_p}{(1 + G_p)^2 + (B_p + \tan \theta)^2}. \quad (14)$$

The standing-wave pattern displays zeros for $\tan \theta = \infty$, a condition that does not involve B_p and G_p. In other words, the zeros in the standing-wave pattern appear just where they would if the probe were idea ly infinitesimal. The *maxima*, however, are shifted, since they are located by the condition $\tan \theta = -B_p$, rather than $\tan \theta = 0$, and the pattern as a whole is distorted compared to that which would be observed with an infinitesimal probe. Figure 8·7 displays a rather extreme case of such distortion, observed with a probe for which B_p was about 0.5. The circles are experimental points.

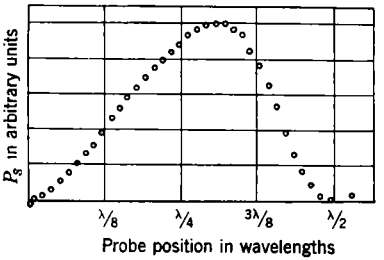

FIG. 8·7.—Observed standing-wave pattern showing distortion by probe susceptance. Circles are experimental points.

The shift in the maximum affords a direct measure of B_p. The maxima will be shifted toward the load if B_p is positive. The degree of asymmetry can also be specified by comparing values of P_s measured at two points $\lambda/8$ to either side of a minimum, where $\tan \theta = +1$ and -1, respectively. The ratio ρ of the two readings will be

$$\rho = \frac{(1 + G_p)^2 + (B_p - 1)^2}{(1 + G_p)^2 + (B_p + 1)^2},$$

or approximately, if G_p and B_p are small,

$$\rho = 1 - 2B_p.$$

If G_L is not zero, the probe admittance may be expected to affect the measured standing-wave ratio r_m, as well as the positions of maxima and minima. The shifts in maxima and minima can be computed from Eq. (13). The shift of the minimum from the "true" position, that is, from the position where a minimum would be found with an infinitesimal probe, may be denoted by $\delta_{\min}$ and the shift of the maximum by $\delta_{\max}$.

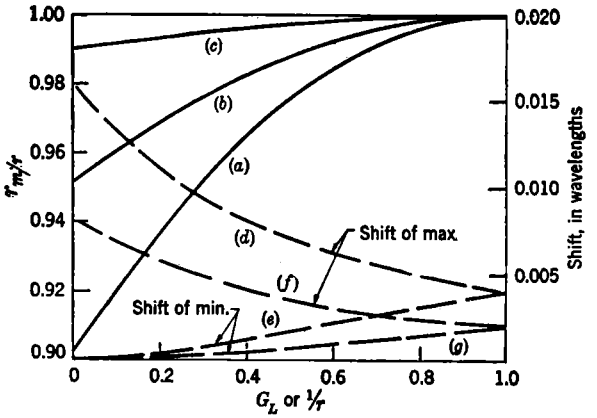

FIG. 8·8.—Solid curves show effect of probe conductance G_p on measured standing-wave ratio r_m as a function of G_L, with $B_p = 0$. Curves (*a*), (*b*), (*c*) are for $G_p = 0.1$, 0.05, and 0.01, respectively. Dashed curves show effect of B_p in shifting maximum and minimum. Curves (*d*) and (*e*) are for $B = 0.1$; curves (*f*) and (*g*) for $B = 0.05$.

If B_p and G_p are both small, by differentiation of Eq. (13) the following formulas for the case $G_L \leqq 1$ are obtained,

$$\frac{\delta_{\min}}{\lambda_g} = \frac{G_L^2 B_p}{(1 + G_L)^2}, \tag{15}$$

$$\frac{\delta_{\max}}{\lambda_g} = \frac{B_p}{(1 + G_L)^2}. \tag{16}$$

These relations are plotted in Fig. 8·8. For $G_L \geqq 1$ the subscripts *min* and *max* need only be interchanged, or, what amounts to the same thing, G_L be replaced by $1/G_L$. Thus, the shift of the minimum is in general *less* than the shift of the maximum, and when the standing-wave ratio is large ($G_L \ll 1$ or $G_L \gg 1$), the shift of the minimum is very small indeed. Moreover, to the first order, the minimum shift and the maximum shift depend only on B_p. It is in fact readily shown from Eq. (13) that if $B_p = 0$, both shifts are zero, no matter how large G_p. It is obvious from these results that a large value of B_p is undesirable and that in any case the

location of the *minimum*, rather than the *maximum*, should be used to establish the phase of the reflection coefficient of the load in a standing-wave measurement.

It must also be expected that the measured standing-wave ratio r_m will differ somewhat from the value r which would be observed with an infinitesimal probe. This effect is due both to G_p and B_p, and if G_p and B_p are of the same order of magnitude, the analysis is tedious and the result rather complicated. Only the case of $B_p = 0$ will be discussed. It has been pointed out that it is desirable to reduce B_p and in most cases this can be done by a tuning adjustment in the probe circuit. If $B_p = 0$, Eq. (13) yields immediately

$$\frac{r_m}{r} = \frac{1 + G_L + G_p G_L}{1 + G_L + G_p} \tag{17}$$

for $G_L \leqq 1$. Since $r = 1/G_L$ when $G_L \leqq 1$, the result can also be written

$$\frac{r_m}{r} = \frac{1 + r + G_p}{1 + r + rG_p}. \tag{18}$$

The observed standing-wave ratio is always less than the true standing-wave ratio if $B_p = 0$. The solid curve in Fig. 8·8 is a plot of the formula just given.

The quantity G_p is a particularly significant parameter, for it determines the amount of power extracted by the probe. For example, if the load is matched ($G_L = 1$) and if $G_p \ll 1$, G_p is identical with the fraction of the power flowing toward the load which is diverted by the probe to the measuring circuit. It is therefore appropriate to call G_p the *coupling coefficient* of the probe. Every standing-wave measurement poses the problem of a compromise between a very small coupling coefficient, which would make severe demands on the sensitivity of the indicating circuit or upon the output power of the generator, and a larger coupling coefficient necessarily accompanied by larger discrepancies between the measured and the true standing-wave ratio. Where the compromise is to be struck depends, of course, on the circumstances—the degree of accuracy sought, the power available, and so forth. The point that must be emphasized here is that a compromise cannot be avoided; both the power extracted and the error in r_m depend directly on G_p. It is not possible to construct a probe that has a coupling coefficient of 0.05 without introducing across the line a conductance $G_p = 0.05$.

Two probes that are adjusted to have the same G_p can differ only in the value of B_p, no matter how dissimilar their physical appearance; if B_p can be tuned to zero for each, the probes will be electrically identical. These conclusions, of course, hold only if the probe can be considered a simple shunt circuit; this is allowable in nearly all practical cases because the

dimensions of the probe, in a direction parallel to the slot, are small compared to a wavelength.

If the generator is not matched ($G_G \neq 1$), the formula for the power dissipated in the probe conductance necessarily becomes very complicated, involving G_G, B_G, G_p, B_p, G_L, and both x_G and x_L. B_G could of course be eliminated by a suitable choice of the point to which x_G is measured. Only a special case will be considered, that of a matched load $G_L = 1$, and a probe of zero susceptance $B_p = 0$. As the probe is moved, maxima and minima will be observed in P_s, despite the fact that $G_L = 1$, because a change in x_G changes the load on the generator. The apparent standing-wave ratio r_a is

$$r_a = \frac{1 + G_G + G_p}{1 + G_G + G_p G_G}, \qquad \text{for } G_G < 1. \tag{19}$$

Thus, for $G_p = 0.1$, $G_G = 0.5$, an apparent standing-wave ratio of 1.03 would be observed. The error due to a mismatched generator decreases as G_p, the probe coupling, is decreased. The example just discussed shows how the degree of mismatch might be found, if G_p were known, or conversely how G_p might be measured if G_G were known; in both cases a matched load is utilized.

An exhaustive analysis of more general cases which cannot be treated here, together with abundant experimental data, has been given by Redheffer and Dowker.[1]

8·5. The Design of Slotted Sections and Probes.—The most important requirements that must be satisfied in designing a slotted section and traveling probe can be stated in this way: (1) A cross section of the guide and probe assembly, at the plane containing the probe, should display perfect symmetry about the axis of the probe over all regions accessible to the electromagnetic field associated with the guide. (2) The cross-section view must not be altered in any way as the probe travels along the slot. A cross section of a typical instrument is shown in Fig. 8·9, with certain details omitted which are of no concern in this discussion. The requirements stated apply to the region below line A-A including the gap between the guide and probe carriage.

The effect of any specified departure from symmetry and uniformity is easily understood in a qualitative way. In general, lack of symmetry causes excitation of the slot wave described in Sec. 8·3. A change in the depth of penetration of the probe, or of the dimensions of the guide near the probe, as the probe moves, results in a variation in the probe admittance Y_p. It is not unusual to discover a small systematic effect of this sort, a gradual and uniform increase or decrease of G_p with distance along

[1] Y. Dowker and R. M. Redheffer, "An Investigation of RF Probes," RL Report 483-14, Feb. 6, 1946.

the slot, for which faulty alignment of the ways upon which the probe carriage moves is often to blame. In a coaxial slotted section such a "slope effect" may be observed if the axes of the inner and outer conductor and the path of the probe are not everywhere parallel.[1]

Thus good *mechanical* design is extremely important. The method of construction should be one which lends itself to the maintenance of close tolerances on all critical dimensions not easily adjustable.

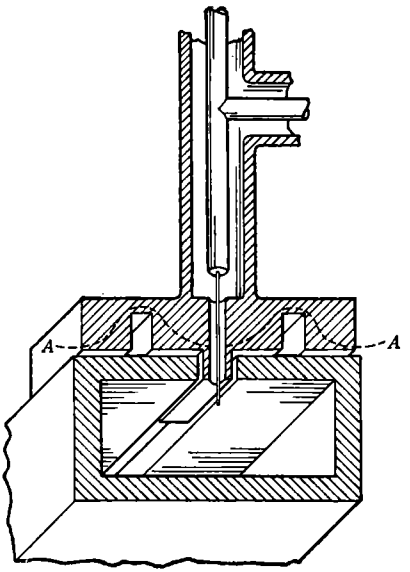

FIG. 8·9.—Shielded probe in slot.

The means for guiding and moving the probe require more careful attention than might at first be supposed. It should be possible to move the probe easily and rapidly over the whole length of the slot, and immediately thereafter to set the probe very precisely at some position. The position of the probe, in accurate work, should be indicated directly and legibly with an error of not more than a few thousandths of a wavelength. The way in which this problem is solved varies widely with the accuracy sought, the wavelength range for which the instrument is intended, and with the inclination and ingenuity of the designer. Only a few general remarks can be made here on the subject.

[1] If the probe penetration is not too small, it has been found empirically that it is more important to maintain a uniform distance between the end of the probe and the inner conductor than to maintain uniform penetration in the event that inner and outer conductor are not parallel. It is difficult, however, to make general statements about a problem in which so many parameters are involved.

At wavelengths of 10 cm or greater, no elaborate driving mechanism is required, as a rule. The probe carriage can be moved by hand, directly, and its position read with sufficient accuracy on a vernier scale. Likewise the tolerances on dimensions are not beyond normal machining practice with the possible exception of the dimension that controls the depth of penetration of the probe in a coaxial instrument. Instruments designed for shorter wavelengths usually embody a reduction in the driving mecha-

FIG. 8·10.—Standing-wave detector for 1.25 cm. The detector which connects to the square flange is not shown.

nism, and for wavelengths shorter than 3 or 4 cm, amplification of the position reading is almost necessary. A simple screw reduction is not suitable for it does not allow rapid traversal of the entire slot. In several instances a rack and pinion drive, with separate means for registering the probe position, has been satisfactory. In the standing-wave detector for use at 1.25-cm wavelength, shown in Fig. 8·10, a setting and reading accuracy of 0.001 in. is attained without sacrificing the possibility of rapid motion. A friction drive kinematically equivalent to a rack and pinion, but free from backlash,[1] is used; the position of the carriage is indicated by a commercial dial gauge permitting a travel of one inch and reading directly in thousandths of an inch.

[1] Backlash in the drive would not affect the accuracy of position measurement, but it could be a minor annoyance in setting the probe on a sharp minimum.

Instruments of recent design are provided with accurate ways that define the path of the probe carriage. In general, the tendency has been toward a more massive construction, similar to that of other precision instruments. This tendency reflects the increasing interest in, and usefulness of accurate impedance measurements, as well as the progress to higher frequencies.

The requirement of symmetry can be made less stringent by certain modifications in the design of the probe and probe carriage. Indeed experience has shown that these modifications are necessary at short wavelengths in order to achieve a reliable instrument at reasonable cost. Of the features referred to, all of which are visible in Fig. 8·9, the most important is the probe *shield*. The probe-shield is the tongue of metal, integral with the probe carriage, which projects into the slot; its lower surface is level with the inner wall of the waveguide. The probe wire runs through a small hole in this shield. The presence of the shield greatly reduces the chance of exciting slot waves through lack of symmetry in the probe. The length of slot filled by the tongue is usually made half a wavelength to minimize the effect of reflections at the ends of the tongue.

It will be noted that no part of the probe carriage in Fig. 8·9 touches the slot or the top of the guide. A positive clearance is maintained on both sides of the shielding tongue and beneath the carriage. It is easier to maintain this clearance with a tolerance of a few thousandths of an inch than to assure intimate but freely sliding contact everywhere between the carriage and shield, and the guide. If such an attempt were made, the location of the *actual* point of bearing, and hence of electrical contact, would depend on minute irregularities, and the electrical symmetry of the system would be jeopardized.

If the two modifications mentioned are introduced, the narrow gap on either side of the probe shield will be excited to a slight extent by the primary wave in the guide. The excitation can be thought of as arising from the current which tends to flow across the narrow gap between the guide and the probe shield. If the probe wire were withdrawn, the current would be merely that required to charge the lower surface of the probe shield. To this must be added, when the probe is inserted, the input current to the probe line. The effect of this current ordinarily predominates. A rough calculation indicates that the probe current exceeds the shield current in a typical case if $G_p > 0.005$. Thus, two impedance elements, corresponding to the impedance of the two gaps, one on either side of the probe shield, are in effect connected in series with the probe; if these impedances vary, the probe power will change. To avoid any such effect, the "transmission line" represented by the continuation of the gap into the space beneath the probe carriage is

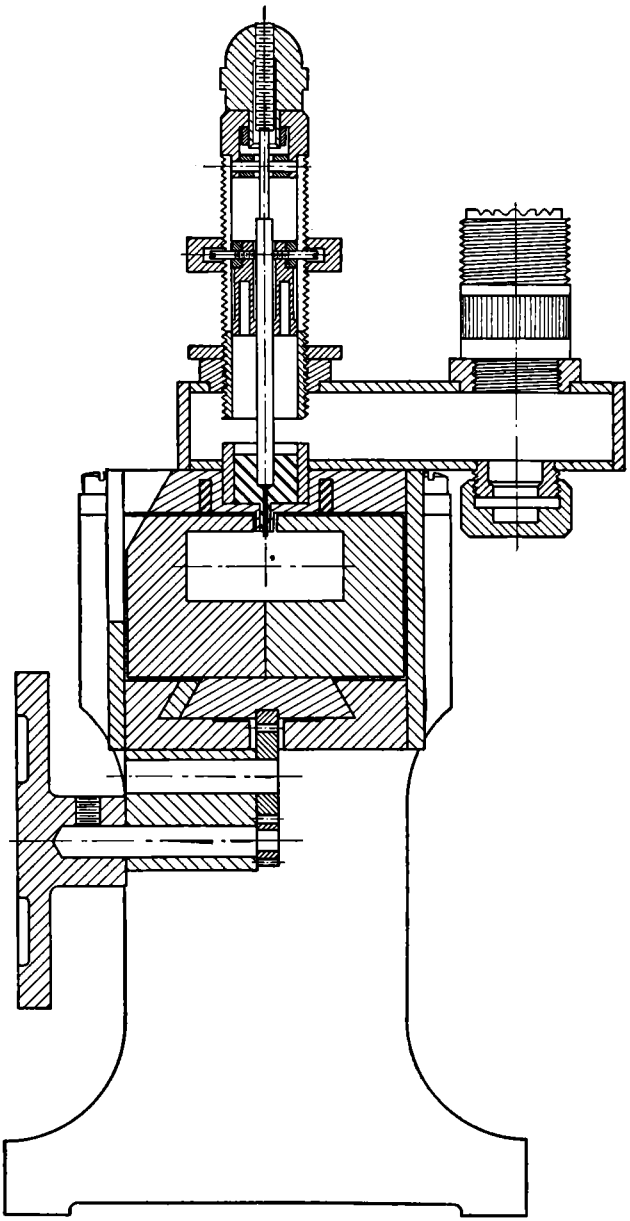

FIG. 8·11.—Cross section of standing-wave detector for 3.2-cm wavelength

terminated in an open circuit approximately $\frac{1}{4}\lambda$ from the gap, which results in a very *low* impedance at the gap itself. The open-circuit termination is provided by a quarter-wave trap consisting of a longitudinal groove in the bottom of the probe carriage. In the instrument shown in Fig. 8·11 the groove is filled with dielectric to save space; the depth is $(\lambda/4)(1/\sqrt{k_e})$. The distance between the mouth of the groove and the lower edge of the shield, which is nominally $\lambda/4$, is not critical, as the characteristic impedance of the transmission line is very small.[1]

The probe is ordinarily adjustable in its penetration; this is the easiest way to vary the probe coupling, or probe conductance G_p. In general, B_p will be found to change as the probe penetration is varied, and provision must be made for an additional adjustment which will allow B_p to be made small at any setting of the probe depth. The cross section of a 3-cm standing-wave instrument, Fig. 8·11, shows such a tuning device, in this case a coaxial stub on the probe line with a movable plunger. The probe itself is the projecting end of a thin central rod which can be extended or withdrawn by the screw adjustment at the top of the coaxial stub. It should be clear from the discussion in Sec. 8·4 that any further adjustments would be redundant; the characteristics of the probe are entirely determined by G_p and B_p.

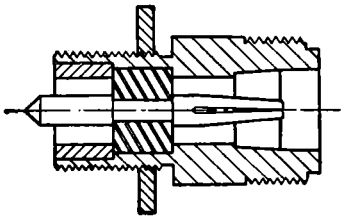

FIG. 8·12.—Attachment for standing-wave detector shown in Fig. 8·11 to allow r-f power from the probe to be sent through a cable.

Certain other features of the instrument of Fig. 8·11 are worth noting. The carriage moves on dovetail ways and is driven by a rack and pinion with an intermediate idler gear whose chief function is to make the sense of the motion the natural one. The short auxiliary guide to which the probe couples is provided with a mount for a cartridge crystal rectifier; an interchangeable fitting allows r-f power to be led off through a suitable cable to a remote rectifier or mixer, if desired. The attachment for this purpose is shown in Fig. 8·12. Finally, the slotted guide itself is made of two blocks joined together; these blocks can be cut from the same milled section, which ensures a highly symmetrical guide and slot. A photograph of the complete instrument is shown in Fig. 8·13.

Figure 8·14 shows in cross section the probe assembly belonging to a 10-cm coaxial slotted section. The probe was designed for the measure-

[1] The basic wavelength is the *free-space* wavelength, where excitation of the gap by the probe current is concerned, because the mode excited in the gap transmission line corresponds nearly to the dominant mode in a parallel-plate transmission line with open sides.

ment of very small reflections in a line of unusually small diameter ($\frac{5}{16}$ in.); it therefore had to meet exacting requirements.

The internal dimensions of the guide in a waveguide slotted section are usually determined in advance by the existence of standard guide dimensions for the frequency range to be covered. In any case the limitations are identical with those which apply to waveguide in general, namely, the dimensions must be small enough to exclude the possibility of propagation by higher modes at the short-wavelength end of the range, and yet

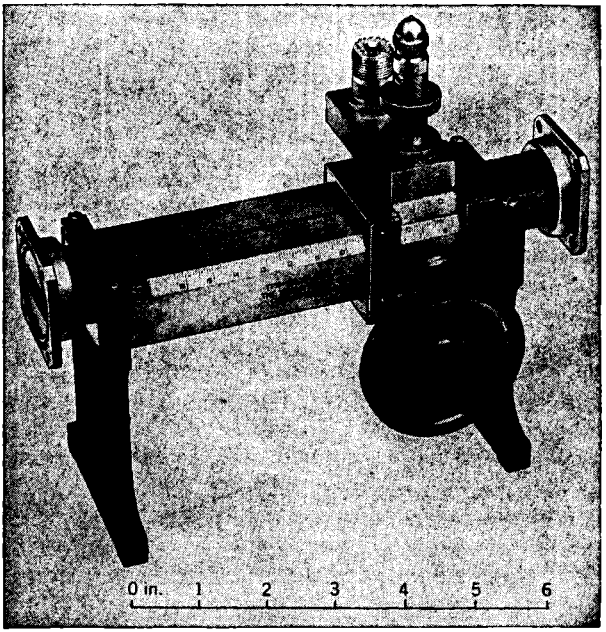

FIG. 8·13.—Standing-wave detector for 3.2-cm wavelength.

large enough to be comfortably far from cutoff for the longest wavelength. In coaxial slotted sections the upper limit of size is set by the occurrence of the lowest mode other than the principal coaxial mode. This next higher mode must be guarded against more carefully in slotted coaxial line than in an ordinary unslotted line, for the presence of the slot represents a departure from axial symmetry favorable for the excitation of the mode in question. The cutoff wavelength for the mode is approximately equal to the mean circumference of the line, $\pi(R_1 + R_2)$, where R_1 and R_2 are the radii of the inner and outer conductor. The true value of λ_c differs from $\pi(R_1 + R_2)$ by less than 3 per cent for $1 \leqq R_2/R_1 \leqq 15$.

The support of the inner conductor in a coaxial slotted section poses a

problem which is already familiar to the microwave engineer but which is particularly acute here since, as has been seen, the accuracy of the standing-wave measurements depends to a large degree on the uniformity of the cross section. Three methods of support for the inner conductor should be mentioned: (*a*) support by low-reflection beads, or insulators at either end of the section; (*b*) support by $\lambda/4$ stubs; (*c*) support by the device under test, or "cantilever" support. In every case the requirements of low reflection are most severe at the *load* end of the line; as has been shown in Sec. 8·4, the effect of a mismatched *generator*, which would be equivalent to a reflecting support at the generator end, is small.

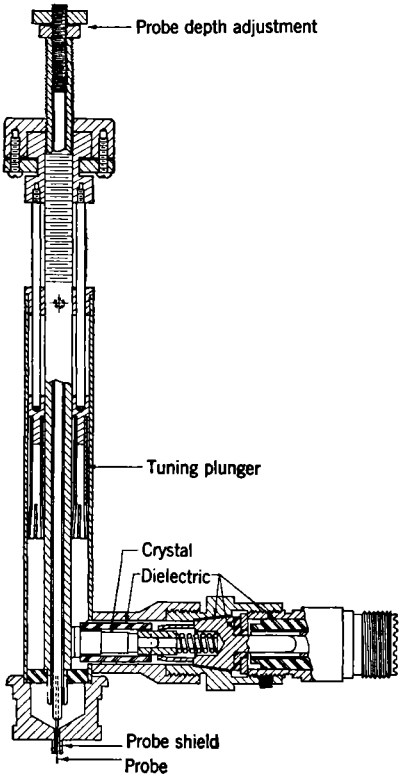

FIG. 8·14.—Cross section of 10-cm probe.

Method (*c*) is a rough-and-ready method suitable for measurement of low precision. Quarter-wave stubs provide rigid support if the line diameter is not too small compared to the stub length. Broadband stubs (see Vol. 9 Sec. 4·4) are used in most cases; the frequency sensitivity of an uncompensated $\lambda/4$ line would be objectionable. The 10-cm instrument in Fig. 8·15 has a stub-supported center conductor, and is provided in addition with an adjustable two-stub transformer by means of which residual reflections between slotted section and load can be matched out. Less use has been made of reflectionless insulators, which, beginning with a simple half-wave bead, can be elaborated, with varying degrees of frequency compensation.

Finally, attention must be paid to the junction between the slotted section and the device under test. The limit of accuracy in the measurement of standing-wave ratios near unity is often set by the small reflection from an imperfect junction. For extremely precise work in waveguides, a tightly clamped butt joint between ground flat surfaces, with some positive means for alignment, is probably the best solution. For most

measurements the standard guide coupling, whatever it may be, is of course preferred, for convenience.

8·6. Detectors and Amplifiers.—The power that is diverted from the slotted line by the probe ultimately causes deflection of a meter or an oscilloscope trace. The important characteristics of the apparatus by which the conversion from r-f power to meter deflection is accomplished are (1) the over-all *sensitivity* of the detecting system, and (2) the *response law*, that is, the nature of the function that connects probe power with meter reading. The problem is not the same as that of r-f power *measurement* although in principle any of the methods for absolute power measurement described in Chap. 3 are applicable. The difference is that relative power measurements only are required and these must be made rapidly and conveniently.

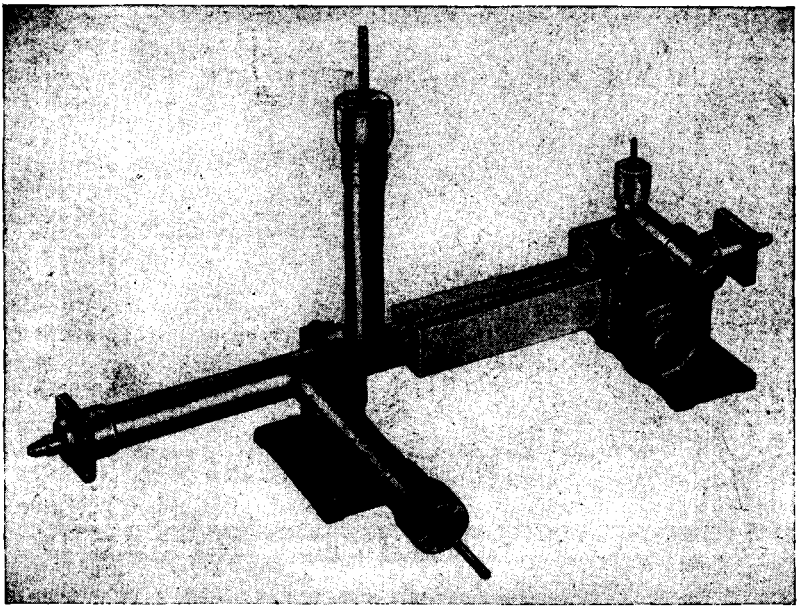

FIG. 8·15.—Coaxial standing-wave detector for 10-cm wavelength.

High sensitivity is an advantage that can be utilized in several ways. Obviously, the output power required of the generator depends inversely on the sensitivity of the detecting system. But even if the output power of the generator seems adequate, it may be desirable to isolate the generator from the line by attenuating pads in order to avoid frequency changes caused by a changing load, or to satisfy the condition $G_G = 1$, or both. Also, the errors attributable to the presence of the probe in the line rapidly

become smaller as G_p, and hence the power available from the probe, are reduced. Finally, the measurement of large standing-wave ratios taxes the sensitivity of the system because the amplitude of the field in the line near a voltage minimum is very small compared to the amplitude observed with the same generator power when the load is matched.

Whatever the form of the function connecting the probe power with the meter indication, the standing-wave patterns obtained with the system can be interpreted if the system has been calibrated over the range of probe power covered by the measurements. A calibration can be obtained, for example, by terminating the slotted section in a short circuit and recording the meter reading as a function of probe position. The variation of probe power with distance is especially simple in this case; it is described by $\sin^2 (2\pi x_p/\lambda_g)$, if G_p can be neglected, or, in the next higher approximation by

$$P_s \approx \sin^2 \frac{2\pi x}{g}\left(1 - 2G_p \sin^2 \frac{2\pi x}{\lambda_g}\right). \tag{20}$$

In each case B_p has been assumed to be zero. It is then a straightforward procedure to construct a calibration curve by which subsequent measurements can be reduced to some selected basis.

The question of the response law is thus one of convenience only. Nevertheless, the inconvenience of the procedure just outlined is formidable, particularly if the calibration has to be repeated for different ranges of probe power, and repeated again after any significant alteration in the detecting and amplifying system such as replacement of a crystal detector. Most workers have therefore preferred detectors, or detector-amplifier combinations, for which the response, if not accurately proportional to the probe power, is at least a simple function of the probe power over a wide range. For example, it may be possible to represent the final meter deflection D fairly accurately over some range by a simple power law, such as

$$D = k|A + B|^{\mu}, \tag{21}$$

where A and B represent the amplitudes of the waves in the line, as in Sec. 8·1, and μ is a constant. If μ is very nearly 2, the response is said to be approximately *square law* in the range in question. Even if the square law is only approximately obeyed, it may be permissible to assume $\mu = 2$ when dealing with standing-wave ratios near unity. It is easy to see that the error made in supposing that $\mu = 2$ when the response, in fact, should be represented by $\mu = 2.3$, for example, increases rapidly as the standing-wave ratio r increases.

Detector and amplifier systems that have found general use in microwave standing-wave measurements can be grouped in three categories, more or less in order of increasing sensitivity and complexity.

1. Unmodulated source; crystal detector followed by d-c meter or d-c amplifier and meter.
2. Modulated source; crystal detector or bolometer, followed by a narrow-band amplifier at the modulation frequency.
3. Unmodulated source; superheterodyne receiver employing crystal mixer, local oscillator, and second detector.

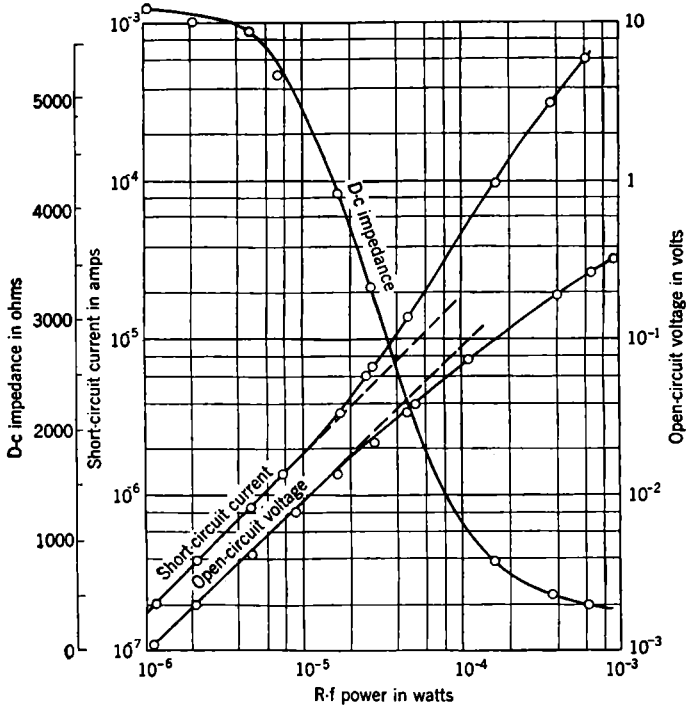

FIG. 8·16.—The rectification properties of a silicon crystal at 3300 Mc/sec.

A crystal rectifier connected to a suitable meter is perhaps the simplest indicating device. The sensitivity that can be achieved with standard microwave crystals is of the order of 1 μa of rectified current (into a low-impedance load) for 1 μw of r-f power absorbed in the crystal. The rectified current is in most cases very nearly proportional to the power absorbed for powers not greater than a few microwatts, but the response law of a new crystal should be checked before accurate measurements are undertaken. The r-f impedance of the crystal is substantially independent of the power level below a few microwatts, and it may be assumed that the response law is not affected by tuning the r-f parts of the probe circuit.

Figure 8·16 is a graph of the characteristics of a silicon crystal rectifier at 3300 Mc/sec. It will be observed that the response is nearly square-law below 10 μw. The sensitivity of this particular sample is however not typical of the best obtainable since it is considerably less than 1 amp/watt. The crystal types which are preferable as detectors are those selected for this property: types 1N27 and 1N32 for 10 cm, types 1N30 and 1N31 for 3 cm.

The meter that measures the rectified current should have a sensitivity of 10 μa for full-scale deflection, or better, not more than a few hundred

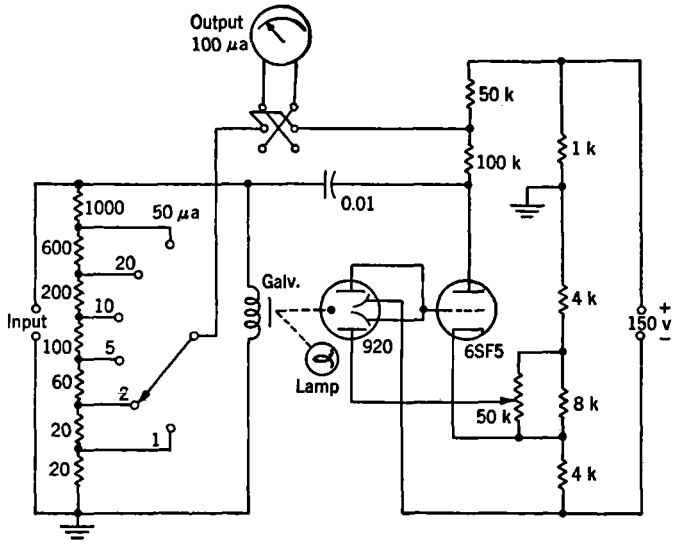

FIG. 8·17.—A galvanometer-amplifier; in effect, a microammeter of very low input resistance.

ohms resistance, and a reasonably short period. Galvanometers of the taut-suspension type which satisfy these requirements are available commercially. A sensitivity of 1 μa full scale, with a period of about 3 sec, can be obtained in an instrument rugged enough for general laboratory use.

Much higher *current* sensitivity could be provided by a conventional d-c amplifier, but the crystal is not a constant-current source. Reference to Fig. 8·16 shows that the maximum open-circuit voltage obtainable under the power limitation imposed is only a few millivolts. Little is to be gained therefore by using a direct-coupled d-c amplifier.

A device that avoids the well-known limitations of the conventional amplifier is the galvanometer-amplifier, the circuit of which is shown in Fig. 8·17. The input current, in this case the rectified current from the

crystal, tends to deflect the mirror of the galvanometer that is connected across the input terminals. Deflection of the mirror alters the light distribution on the double photo-cell, which displaces the grid potential of the amplifier tube. The output current of the tube is connected back in such a way as to restore the galvanometer to its zero position. The negative feedback is so strong that the current through the galvanometer remains negligibly small at all times. Very nearly all of the input current, therefore, flows through the tapped resistance at the left; the potential difference between the input terminals is practically zero, and the input and output currents are related by a constant factor depending only on fixed resistances. An additional capacitive feedback path of higher gain is provided to eliminate hunting in the servo system. The device is, in effect, a microammeter of high sensitivity and zero resistance. The response time is that of the output meter; the natural period of the galvanometer plays no role whatever. A discussion of the galvanometer-amplifier, and modifications thereof, can be found in Vol. 18 Sec. 12·16.

Modulation of the r-f source makes it possible to use a-c amplification of the signal from the probe. How modulation can be applied to a microwave oscillator has already been explained in Chap. 2. For standing-wave measurements the percentage of amplitude modulation should be large, but frequency modulation is to be avoided, for a frequency change displaces the standing-wave pattern along the line. Therefore "on-off" modulation, with a square modulation envelope, is preferred. The modulation frequencies ordinarily used are in the audio-frequency range. The difference in frequency between the resulting modulation sidebands and the carrier is entirely negligible, in contrast to frequency differences of many megacycles per second which may arise from changes in the applied potentials of the oscillator during operation.

Demodulation of the signal picked up by the probe can be effected in various ways. A *crystal* detector can be used, connected directly to a tuned audio-frequency amplifier. A *bolometer* can also be used if the response time is not too long compared to the modulation period. A suitable type is the fine-wire *barretter* described at length in Chap. 3. A voltage is applied to the barretter from a d-c source; the temperature changes caused by the absorption of r-f power in the barretter wire are manifested as periodic changes in resistance, and consequently the current through the wire has a component at the modulation frequency. If the temperature change during each cycle is small, the response is accurately square-law, which is one of the principal advantages of the barretter over the crystal. In addition to this advantage, the barretter is less vulnerable to burnout by high pulse power, and is therefore always to be preferred to the crystal when the modulation has the form of short, widely spaced pulses.

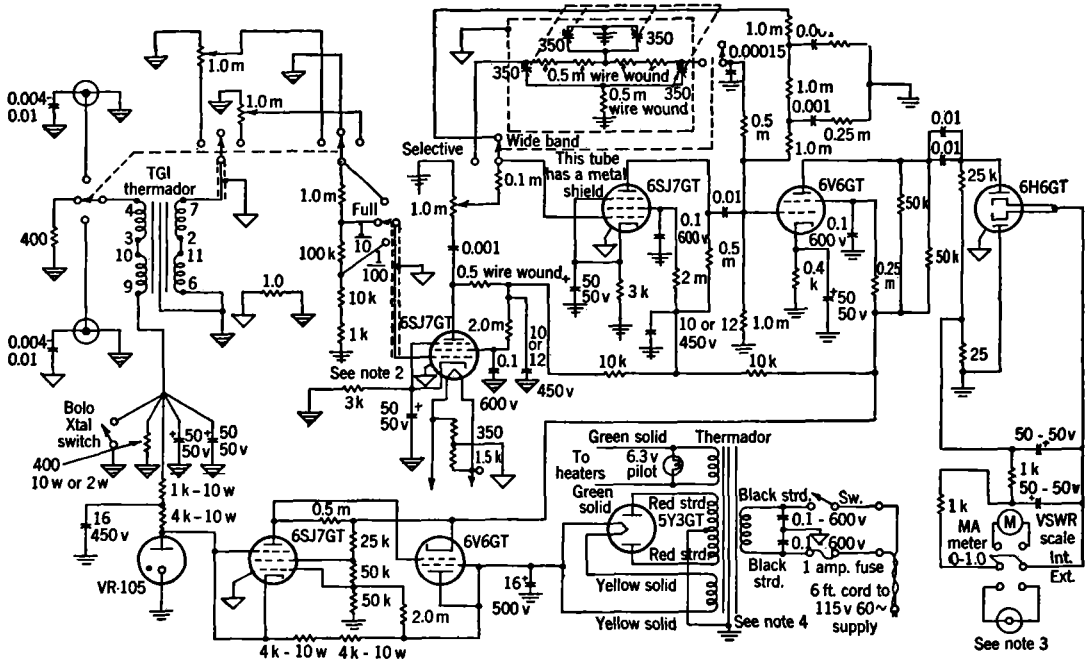

Grounds shown as ⏚ made to one common point not on chassis.
Grounds shown as ⏚ tied to a second common point not on chassis.
Grounds shown as ⏚ and those above tied together with jumper wires.
Grounds shown as ▽ tied to chassis at most convenient point.

FIG. 8·18.—Twin-T amplifier. Notes: (1) Transformer and input connectors insulated from chassis and grounded to a common point with wire. (2) This tube has metal shield and is cushion-mounted. (3) This connector must be insulated from chassis. (4) Transformer spaced from chassis by $\frac{1}{4}$-in. bakelite plate. Case connected to ground system through only one mounting screw.

A tuned amplifier that has been used successfully in conjunction with both crystals and bolometers is shown in Fig. 8·18. The tuning has two advantages; it not only eliminates much extraneous interference, but reduces the effect of any frequency modulation that may occur during the rise and fall of the modulating square wave. If neither the rise nor the fall of the modulating voltage that is applied to the source occurs instantaneously, a brief period of oscillation at a frequency other than that prevailing during the main portion of the *on* period may sometimes be observed during the rise, and again during the fall. This spurious signal, after demodulation, will have its strongest component at *twice* the modulation frequency, if the on and off periods have equal length, and will be suppressed, relative to the fundamental, in the tuned amplifier. The frequency selectivity of the amplifier of Fig. 8·17 is provided by a twin-T feedback network applied to the second stage. For a discussion of the principles governing the design of twin-T feedback amplifiers, the reader is referred to Vol. 18, Chap. 11. The circuit of Fig. 8·18 has been carefully designed to avoid ground currents that might result from indiscriminate grounding of points nominally at ground potential.

Sensitivity far exceeding that of the methods so far discussed can be achieved with a "double detection" system, that is, a microwave superheterodyne receiver consisting of a crystal mixer, local oscillator, i-f amplifier, second detector, and some form of indication. The *spectrum analyzer* described in Chap. 7, which is basically just such a receiver, is ideal for the purpose. At least up to the second detector the response of the system is accurately proportional to the input signal power. The excellent power sensitivity, however, (of the order of 10^{-13} watt ultimate sensitivity) allows the problem of the response law to be avoided, or, more precisely, to be transferred to an r-f attenuator. The power picked up by the probe is transmitted through an adjustable attenuator to the input terminals of the spectrum analyzer. A reading is taken by adjusting the attenuator to bring the final output indication to some chosen reference level. A standing-wave ratio is thus determined directly by the difference between two settings of the attenuator. A wide range, in decibels, is available, and consequently high standing-wave ratios can be measured reliably. The attenuator is usually of the waveguide-beyond-cutoff type (see Chap. 11) and requires no calibration. It is the rather high minimum attenuation of such *absolute* attenuators which restricts the application of the method to systems of high sensitivity.

It is characteristic of the spectrum analyzer that the frequency of the local oscillator is continually swept over a range of many megacycles per second. In the application under discussion, this feature makes accurate tuning of source to receiver, or vice versa, unnecessary, and provides incidentally a continual check on the spectral purity of the source.

The methods so far described are not the only ones which have been or could be used, for, as mentioned at the beginning of this section, the only essential requirement is the measurement of relative power at microwave frequencies. For example, the thermistor bridge discussed in Chap. 3 is well suited for standing-wave measurement in some circumstances. The task of reviewing each of the power-measurement methods discussed in Chap. 3, with a view toward their application in standing-wave measurement is, however, left to the reader.

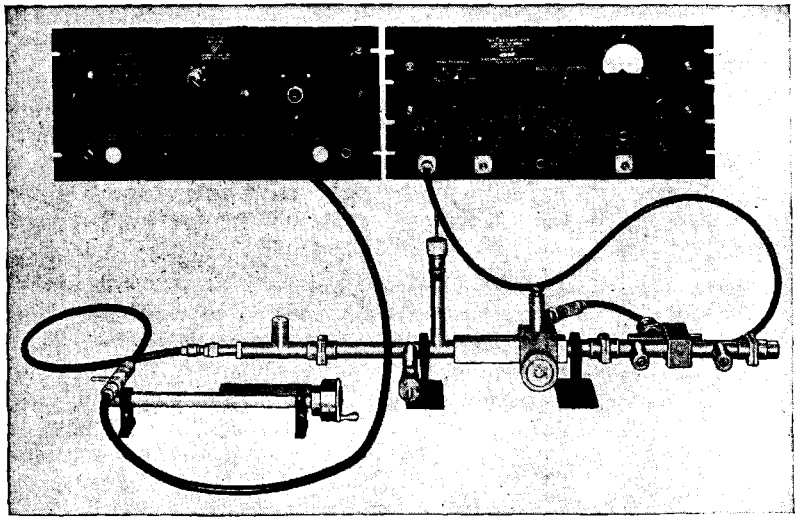

FIG. 8·19.—Assembled apparatus for standing-wave measurement at 10-cm wavelength. The amplifier is the twin-T amplifier whose circuit diagram appears in Fig. 8·18.

A typical assembly of equipment for standing-wave measurement in coaxial line is shown in Fig. 8·19. The unit at the upper left provides square-wave-modulated r-f power from a 10-cm klystron. The power is transmitted by cable to a coaxial wavemeter and thence to the slotted section. The tuning stubs in the slotted section are used here to match the generator to the line. The device under test appears at the right. The rectified crystal current is led to the twin-T amplifier at the upper right.

8·7. Matched Loads and Other Accessories.—As in many other experiments it is helpful and sometimes necessary to check the standing-wave instrument, and the technique, against a standard. The calibration of a crystal by means of a short-circuit termination has been mentioned in the preceding section. A somewhat similar procedure was suggested in Sec. 8·4 as a means by which the magnitude of the probe susceptance

B_p could be found. In each case a short-circuit termination, ideally one without loss, is required. If, as in those two cases, the termination need not be movable, a short length of guide or coaxial line closed by a soldered end-cap is adequate. In other cases a movable short circuit, that is, a plunger, is needed. For example, the generator admittance Y_G can be measured by determining the height of the maximum in P_t for several positions of a terminating plunger.

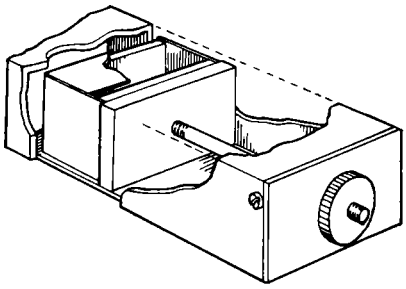

FIG. 8·20.—A short-circuiting plunger with a choke trap consisting of an anti-resonant box.

The design of a plunger that is easily movable and yet produces a practically total reflection is not a simple matter. The problem of the design of a plunger is discussed at length elsewhere (Vol. 9 Chap. 8). The most successful wave-guide plungers have been those in which actual mechanical contact between plunger and guide walls, where r-f currents are to flow, is avoided by the use of chokes, or traps. In other words, there are no sliding electrical contacts. A plunger of this type is shown in Fig. 8·20. Many other designs have been tried and it is not easy to select the best.

A *calibrated* plunger provides a short circuit whose position is accurately measurable and which can be used to establish a reference position with respect to which the equivalent line length between the probe and some other unknown load can be determined. The reflection from a noncontact plunger may occur as if it were from a conducting plane slightly displaced from the actual plunger face. For very accurate work the difference must be taken into account.

A *matched load* is the standard of reference when standing-wave ratios near unity are being measured. At microwavelengths, fortunately, a tapered absorber is not inconveniently long. A tapered load that has a very small reflection coefficient can be fashioned from almost any lossy material, such as wood, hard rubber, or any of the special materials developed for microwave absorbers if the taper is made several wavelengths long and the onset of the absorption at the input end of the absorber is very gradual. If somewhat more care is taken the over-all length of the absorber can be reduced (see Chap. 12).

The reflection coefficient of the absorbing load is easily measured if the absorber can slide along within a uniform guide or line. This is easily arranged in the case of the tapered loads mentioned. With a fixed probe, and constant generator power, variations in probe power which are observed as the load alone is moved can only be caused by a reflection

from the load. Thus, small reflections from connections, from the end of the slot, or other irregularities cannot mask the small reflection from the load itself, and it is possible by repeating this test after judicious alterations in the shape of the tapered load to arrive at a very well-matched condition with the reflection coefficient of the load less than 0.01. Such a load can then be used to check the uniformity of probe coupling along the slot, the reflection from connectors, and other disturbances which may interfere with the measurement of very small reflection coefficients.

8·8. Measurement of High Standing-wave Ratios.—The standing-wave ratio r increases rapidly as the reflection coefficient of the load approaches one. If $|\Gamma| = 0.9$, $r = 19$ and r^2, the ratio of maximum to minimum probe power, is almost 400. To measure r^2 directly by any of the methods previously described, other than the one that makes use of a spectrum analyzer and an r-f attenuator, is almost out of the question. The range over which the detector would be required to respond according to an accurately determined law is too great. There is, however, another procedure by which r^2 can be determined from measurements in a restricted power range. The procedure, in short, consists in examining the standing-wave pattern in the immediate neighborhood of a voltage minimum.

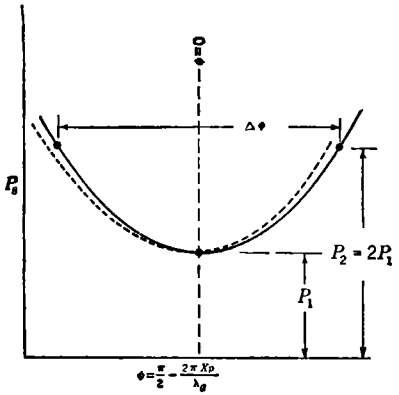

FIG. 8·21.—Variation of probe power in the neighborhood of a minimum.

In the neighborhood of a minimum, if $G_L < 1$, $\tan\theta$ in Eq. (13) can be replaced by $1/(\pi/2) - \theta$. If the angle $(\pi/2) - \theta$ is denoted by ϕ, P_s after substitution is

$$P_s \propto \frac{G_p(G_L^2 + \phi^2)^2}{[\phi^2(1+G_L+G_p)+G_L(1+G_L+G_pG_L)]^2+[\phi^2B_+ + (1-G_L^2)\phi + B_pG_L^2]^2} \quad (22)$$

To consider the simplest case first, suppose that $B_p = 0$, $G_L \ll 1$, $G_p \ll 1$, and take only terms of the lowest order in G_L, G_p, and ϕ. Equation (22) then becomes simply

$$P_s \propto G_L^2 + \phi^2. \quad (23)$$

The curve of P_s versus probe displacement (measured by ϕ) is a parabola, the solid curve in Fig. 8·21. Measurement of P_s at three positions suffices to determine the parabola. A method that is often used is to measure P_s at the minimum, that is, P_1 in Fig. 8·21, then to determine the width

of the curves $\Delta\phi$ between points of twice the minimum height. In this case, Eq. (23) yields directly

$$G_L = \frac{1}{r} = \frac{\Delta\phi}{2}. \tag{24}$$

In terms of the directly measured probe displacement Δx_p between points of twice minimum value

$$G_L = \frac{1}{r} = \frac{\pi \Delta x_p}{\lambda_g}. \tag{25}$$

For example, if the separation so measured is $0.01\lambda_g$, $r = 32$ is obtained.

The inclusion of higher-order terms modifies Eq. (23) only slightly, as does the effect of finite probe susceptance, which will be considered first. If B_p is no longer neglected, the following is derived from Eq. (22), instead of Eq. (23);

$$P_s \propto (G_L^2 + \phi^2)\left(1 - \frac{2B_p G_L^2 \phi}{G_L^2 + \phi^2}\right). \tag{26}$$

For the range of ϕ involved in the twice-minimum procedure, $|\phi| \leqq G_L$. The correction term $2B_pG_L^2\phi/(G_L^2 + \phi^2)$, therefore, does not exceed B_pG_L. Moreover, this correction term is an odd function of ϕ and the effect is merely to distort the pattern as indicated by the dotted curve in Fig. 8·21, without changing (except in a still higher approximation) the separation of the twice-minimum points. Thus, the effect of probe susceptance upon the measurement of r by this method is, in practice, negligible, even though B_p may be as large as unity.

The correction for terms of higher order in G_L and G_p is also small. A calculation based on Eq. (22) shows that a determination of G_L by the twice-minimum procedure using Eq. (24) leads to a result which is too large by the factor $[1 + G_L^2(\frac{1}{2} + G_p)]$. The error in G_L, or in r, is, therefore, less than 1 per cent for $G_L < 0.14$ $(r > 7)$ if $G_p \ll 1$. It may be noted at this point that the error made in replacing $\tan\theta$ by $1/\phi$ is also less than 1 per cent for $r > 7$ and is in the direction to make the measured value of G_L too small.

Since the correction term $G_L^2(1 + G_p)$ is not significantly larger if G_p is made fairly large, *strong probe coupling* is permissible. This makes the demands on the sensitivity of the detector less severe. In fact, a condition as extreme as $G_p = 1$, $B_p = 1$ is not objectionable.

By the procedure just outlined, the necessity of measuring the probe power at widely different power levels is avoided. On the other hand, the method requires accurate measurement of small probe displacements. If many measurements of this type are contemplated, it may be worth while to construct a special slotted section equipped with a micrometer drive operating over a short distance.

In the measurement of high standing-wave ratios it is not always permissible to neglect, as has been done so far in this chapter, the attenuation in the guide or line between the probe and the load. The effect is easily taken into account. Suppose that a wave traveling from the probe to the load is attenuated in amplitude by the factor f, which can be computed readily if the properties of the line are known. If Γ'_L is the measured reflection coefficient of the load, the true reflection coefficient of the load Γ is clearly

$$\Gamma = \frac{\Gamma'}{f^2}. \tag{27}$$

Similarly, the measured standing-wave ratio r_m is related to the standing-wave ratio r, which would be observed if the line were lossless, by

$$r_m = \frac{r + 1 + f^2(r - 1)}{r + 1 - f^2(r - 1)}. \tag{28}$$

A totally reflecting termination ($r = \infty$) at the end of a line causing attenuation will give rise to a standing-wave ratio

$$r_m = \frac{1 + f^2}{1 - f^2}. \tag{29}$$

Thus the attenuation in a line or guide can be found by measuring the standing-wave ratio at the entrance to a section of the line which is terminated in a short circuit. The method described in this section is well suited to this particular problem. Similar problems arise in the investigation of dielectrics at microwave frequencies (see Chap. 10).

8·9. The Squeeze Section.—If the generator is matched ($Y_G = 1$), the probe power depends not upon X_G, the distance between generator and probe, but only upon X_L, the distance between probe and load (Sec. 8·1). For that reason, it is possible to ignore the change in X_G which accompanies the change in X_L as the probe is moved. Obviously, then, the same variation in probe power would be observed if X_L were changed without changing X_G, that is, if the length of line between the load and a *fixed* probe were varied. A coaxial transmission line of variable length is a rather cumbersome affair involving telescoping joints. In waveguide, however, the dependence of phase velocity upon the width of the guide makes it possible to achieve an equivalent result by very simple means. A small change in the width of the guide changes also the *electrical* length.

A guide of variable width can be made by cutting a long narrow slot in each of the broad sides of an ordinary rectangular waveguide. The width is varied by squeezing the split guide, and the device is usually called a *squeeze section*. The change in width is not the same at all points of course, but is greatest at the midpoint of the section where the squeezing

constraint is applied and decreases toward either end of the slot. This effects a very gradually tapered transition, and is just what is needed to avoid reflections. In every cross section taken through the squeezed guide the slots will be centrally located, if they were so originally; hence the loss of power through the slot will be negligibly small as explained in Sec. 8·3. Thus the squeeze section, simple as it is, fulfills the requirements of an ideal line stretcher in all respects but one—the relation between the squeezing displacement and the resulting change in electrical length is only approximately linear, and cannot be easily computed with great accuracy as it depends on the shape assumed by the stressed guide.

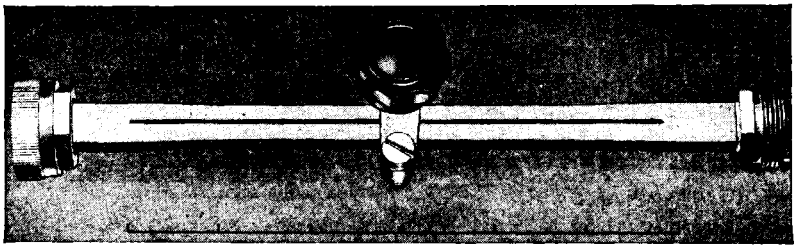

FIG. 8·22.—Squeeze section for 1.25-cm wavelength. The scale marks are inches.

A squeeze section designed for 1.25-cm wavelength is shown in Fig. 8·22. The squeezing is accomplished by links through which passes an eccentric shaft with a knob. The mechanism ensures that the guide will neither be squeezed nor dilated beyond fixed limits, but of course introduces further nonlinearity in the connection between the motion introduced by the operator and the change in electrical length thereby effected. Other examples use a screw drive, which is better adapted to calibration; in the simplest of these the elasticity of the guide itself is relied upon to expand the guide as the screw pressure is relaxed.

Standard 1.25-cm guide (0.420 in. inside width) is so wide that a relatively large change in width is needed to produce a considerable change in λ_g. For this reason, the section shown in Fig. 8·22, although made from standard guide, is actually reduced in width, even in its relaxed condition, over most of the slot length. This is accomplished in manufacture by cutting preliminary slots, then annealing the guide near the ends of the slots and squeezing the slots shut irreversibly by forces applied near the ends. The slots are then milled out to a final width of $\frac{1}{16}$ in. If it is important to conserve length, as in this case, the internal width of the squeeze section, in its relaxed condition, should be 0.70 to $0.75\lambda_0$, as a general rule.

For the purpose of preliminary design the electrical length of a squeezed guide can be estimated roughly by assuming that over the length of the slot it is equivalent to a uniform guide whose width is the arithmetic

average of the actual widths at the center and at the end of the slot, respectively. A squeeze section made from standard 1.25-cm guide (not "pre-squeezed" as was the one in Fig. 8·22) with 0.0625-in. slots 10 in. in length changed in electrical length by 5.24 radians when squeezed shut at the center. This figure is the result of a direct measurement at $\lambda_0 = 1.25$ cm. The approximate method of calculation recommended above predicts a change of 4.65 radians.

For the use of the squeeze section in standing-wave measurements, the section is connected between the load and the probe shown in the diagram of Fig. 8·23. The probe is fixed and usually consists merely of a small hole coupling to a branch guide that is soldered to the main guide and terminated in the detector. The admittance of a probe of this type is adjustable only by tuning the branch guide; usually no provision is made for such tuning. More elaborate coupling circuits could be used instead; the hole has the advantage of simplicity and of a predictable admittance. With the generator matched the ratio of maximum to minimum probe power, observed as the electrical length of the squeeze section is varied, is the standing-wave ratio r.

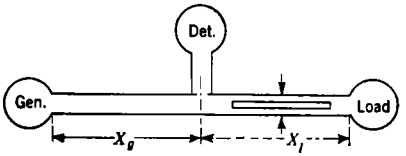

FIG. 8·23.—A diagram illustrating the use of a squeeze section.

The *phase angle* of the reflection coefficient of the load is not so easy to find. Perhaps the most direct method is the following: Adjust the squeeze section to minimize the probe power. Then replace the load with a plunger, and move the plunger to reduce the probe power to zero. The plunger is now an integral number of half wavelengths from the probe, and the distance between the plunger face and the former position of the load is equivalent to $X_{\min}$ in the traveling-probe type of measurement.

It must be emphasized that the requirement of a matched generator is much more stringent here than in the traveling-probe method. There the load in the generator changed as the probe moved only because of a finite probe admittance Y_p. Here the distance between the generator and the load Y_L is changing and the error caused by a mismatched generator vanishes only as $Y_L \to 1$. The method is for that reason best suited to the examination of nearly matched loads, as in routine testing of components that must satisfy some specification of maximum allowable standing-wave ratio.

The squeeze-section method has been highly refined by N. I. Korman[1] and applied to the measurement of very small reflection coefficients. The reader is referred to his report for further analysis of the method and

[1] N. I. Korman, "A Precision Standing-wave Detector for Waveguides," RCA Report TR-12-C, Nov. 27, 1942.

for important variations in the method, including the use of a squeeze section on either side of the probe.

8·10. Standing-wave Measurements at High Power.—In testing pulsed microwave transmitters and also in testing many microwave transmission systems during actual operation, or under conditions resembling actual operation, it becomes necessary to measure the standing-wave ratio in a line in which the pulse power is very high. Certain problems which arise deserve mention in this chapter.

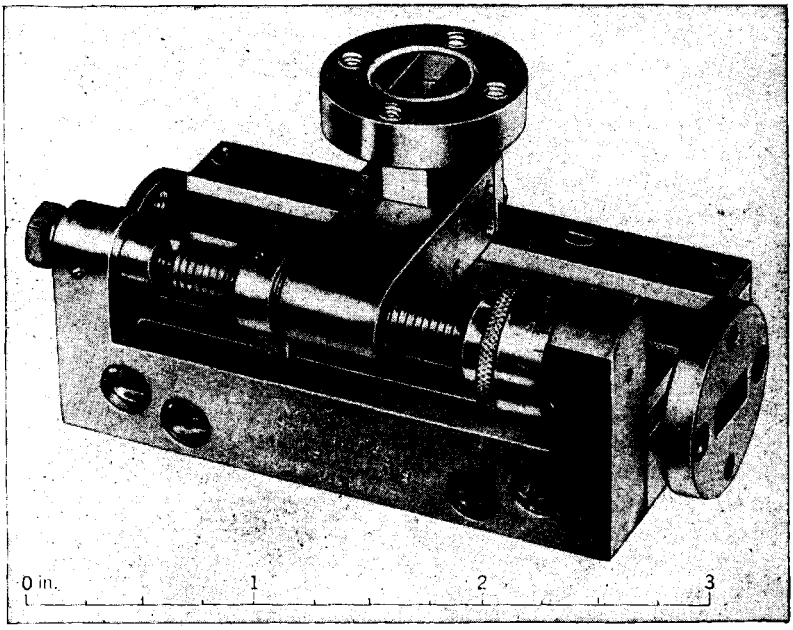

FIG. 8·24.—High-power standing-wave detector.

In the first place it is clear that the requirements on the detecting system are now rather different. Extreme sensitivity is not needed. Instead a detector is required which will withstand relatively high pulse power but will show adequate response to much lower *average* power. A bolometer or a thermistor bridge may be used, for example, coupled in either case very loosely to the line ($G_p \ll 1$) and perhaps protected additionally by an attenuating pad in the probe circuit.

The purpose of the test usually forbids the use of an attenuating pad at the generator end of the line. Therefore, the errors which may be caused by a mismatched generator must be guarded against.

The chief difficulty, however, is voltage breakdown, or sparking, at the probe or slot. The conventional probe is a fine wire projecting slightly

into the guide at a point where the electric field is most intense; there is also a concentration of the field at the inner corners of the slot and at the ends of the probe shield. The usual slotted section, in other words, is not designed to transmit high power, and will break down electrically at a power level considerably lower than that which regular transmission-line components will withstand.

The only steps which can be taken to raise the breakdown limit, as long as the conventional design is adhered to, are the obvious ones of enlarging the dimensions and rounding the corners of any necessary projections, rounding the edges of the slot, and so on. If these precautions are not enough it may be necessary to devise a traveling probe of different type.

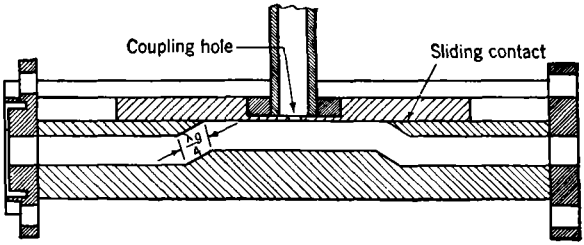

FIG. 8·25.—Cross section of high-power standing-wave detector.

One such design has been worked out with notable success by A. Nordsieck of the Columbia Radiation Laboratory.

Nordsieck's instrument, shown in Fig. 8·24, is a radical departure from previous methods in this respect: the part that travels includes the whole top surface of the waveguide. The probe is merely a small hole in this surface connecting to a branch guide and thence to a detector. In order to bring the inner surface of the guide up to a level accessible to this "cover plate" (see Fig. 8·25) the guide makes two jogs. Each jog is designed to be reflectionless, or nearly so, by spacing successive bends $\lambda_g/4$ apart.

The crucial problem raised in this design is that of electrical contact, for now the sliding part makes contact with the main body of the guide at a point where the current flow is large. This problem was solved by providing hard, smooth, extremely flat surfaces on the contact members. The surfaces were ground, chromium plated, and lapped, to a tolerance of 0.0002 in. in flatness. It was found possible to obtain a smoothly sliding joint that displayed no sparking at powers up to 100 kw and behaved in other respects as a perfect electrical contact.

8·11. Continuously Indicating Standing-wave Detectors.—It would often be helpful to the experimenter if he could see the entire standing-wave pattern at a glance, without the necessity of successive measurements of probe power. If, for instance, he is trying to match the

terminating device by means of tuning adjustments, after each adjustment a new measurement of r must be made. It does not suffice merely to set the probe at a minimum and then maximize the meter reading by tuning adjustments (although an adjustment in that direction is a good first step) because the adjustments will in general alter the phase as well as the magnitude of the reflection coefficient of the load. There is, therefore, some reason to desire what might be called an *automatic*, or perhaps better, a *continuously indicating* standing-wave detector. There are several more or less obvious ways to build such a device, which will be briefly described.

A standing-wave detector employing a continuously and rapidly movable probe was designed at the Telecommunications Research Establishment. The slotted portion of the main guide followed a semicircular arc, the plane of the circle lying in the plane of the electric field in the guide. The slot was in the inner face and continued a short way beyond the ends of the semicircular arc. This allowed a probe mounted on an arm extending from the center of the arc to move into the slot at one end, travel around the semicircular arc, and emerge from the slot at the other. The probe arm revolved continuously and the rectified crystal current was led to an ordinary oscilloscope upon which the standing-wave pattern was displayed.

A device designed by G. E. Mueller, of the Bell Telephone Laboratories employed a long squeeze section bent into a hairpin shape and vibrated rapidly by a cam arrangement. Again the detector output voltage could be displayed on an oscilloscope.

H. E. Kallmann of the Radiation Laboratory has described an automatic standing-wave detector[1] in which rapid "line stretching" was accomplished by a rotating dielectric disk which dipped into the waveguide through a slot. The waveguide was bent into a circular arc, permitting a considerable length of the periphery of the disk to be used. This instrument included a special peak-voltmeter circuit, the output voltage of which depended on the difference between maximum and minimum probe power. A single meter was calibrated to read r directly after a preliminary normalizing procedure.

8-12. Measurements on Lossless Devices.—Many microwave circuit elements can be treated as lossless devices that serve to connect together two or more uniform waveguides or transmission lines. A junction of waveguides, for example a waveguide T, is such a device. A transition between a waveguide and a coaxial line, a tuning post, an inductive iris, the series-parallel T described in Chap. 9, are other examples. Each of these is equivalent to an electrical network having n pairs of terminals

[1] H. E. Kallmann, "Matchmeter," RL Report 705, Apr. 9, 1945.

when n is the number of transmission lines or waveguides connected together by the device.[1] It has been found possible, and convenient, to describe the electrical properties of such a device at a single frequency by an *equivalent circuit*, an n-terminal-pair network made up of lumped impedance elements. The representation of a lossless device will of course contain reactive elements only. In many cases the *form* of an appropriate equivalent circuit can be deduced from general theoretical considerations but the magnitude of the elements usually cannot be found without solving a complicated electromagnetic boundary-value problem. Then arises the problem of determining the value of the equivalent-circuit parameters experimentally by suitable measurements. It is the purpose of this section to call attention to a method which is especially well suited to the purpose.

A representation of some given device will contain a limited number of parameters. A lossless two-terminal-pair device (sometimes called a *four-terminal* device) requires for its description three parameters, which might be the elements of an equivalent T-, or those of an equivalent π-network; other representations are possible, also, but in every case *three* quantities have to be determined by measurement. A way in which this might be done is to find the input impedance at one terminal pair by means of a standing-wave measurement for each of three arbitrarily selected terminating impedances. The information obtained would suffice to fix the circuit parameters with an accuracy which would depend on the accuracy of the standing-wave measurement, and upon the way in which the various values of the terminating impedance were chosen.

Now the device itself is lossless, and advantage can be taken of this circumstance by making the terminating impedance a pure reactance in each case. The input impedance is necessarily a pure reactance also, the standing-wave ratio is infinite, and the standing-wave measurement consists merely in locating the *minimum position*. When the standing-wave ratio is high, it is easy to locate the minimum with precision, and the true minimum position coincides with the apparent minimum position even for strong probe coupling (Sec. 8·8). The response law of the detector, which is the chief source of uncertainty in the measurement of finite standing-wave ratios, has no influence on the measurement. Also it should be noted that the reactive termination of the circuit under test is the easiest sort of known, variable termination to provide. All that is needed is a calibrated plunger (Sec. 8·7).

When the circuit possesses more than two terminal pairs, the procedure is to terminate all but two of these in plungers which for the time being are left fixed. The resulting two-terminal-pair device is then examined by

[1] It is assumed here that in each of the lines or guides only one propagating mode can exist. A guide carrying two modes must be counted as two terminal pairs.

the method already described, and from these measurements three numbers, in general, are derived. The process is repeated for other settings of the plungers that terminate the remaining pipes until enough information has been acquired to fix the values of all equivalent-circuit parameters.

The deduction of the circuit parameters from the measurements of minimum position *vs* plunger setting deserves more attention than can be allotted to it in this chapter, which is concerned only with standing-wave measurements. Of the numerous procedures that might be followed, one or two are superior in affording not only maximum accuracy and convenience, but a thorough check on the internal consistency of the data.

CHAPTER 9

IMPEDANCE BRIDGES

By Louis B. Young[1]

A multifrequency impedance bridge provides simultaneous indications of the power reflected from some test piece at three or more frequencies. Such a device is extremely useful in the development of r-f components which must be well matched over a wide range of frequencies. For example, power detectors such as thermistors are not exactly reproducible in their r-f characteristics and so are mounted in holders that have two or three tuning adjustments. When a slotted section is used in the matching procedure, the mount is tuned for an optimum midband match, and then is checked at the band extremes. If the match is not acceptable at one extreme, it is difficult to make an improvement without adversely affecting the match at the opposite extreme. Another measurement is necessary to check this effect, and the procedure becomes one of successive approximations. On the other hand, when an impedance bridge is used, an optimum match across the band is readily achieved since the effects of tuning may be visualized simultaneously at three or more frequencies.

An impedance bridge consists of three groups of components: r-f sources, the bridge element, and the detector-indicator. Of these, the bridge element is the most interesting since it must couple to the detector only that power which is reflected from the test piece. Although both side-outlet T's and directional couplers can satisfy this requirement, the T is preferred because its selective properties result from symmetry and hence are not frequency-sensitive, an important consideration for multifrequency bridges. In addition to the discrimination requirement, the bridge element must be matched looking back from the test piece, and the coupling to the detector must be independent of the phase of the wave reflected from the test piece. In the case of the side-outlet T, techniques that match it over a wide frequency range also tend to introduce asymmetry and hence impair discrimination. Accordingly, the design of practical impedance bridges often effects a compromise between the errors resulting from asymmetry and mismatch.

[1] The author is indebted to W. E. Waller for assistance in preparing the material that describes bridge elements and basic measuring techniques.

BRIDGE ELEMENTS

9·1. The Side-outlet T.—The waveguide side-outlet T consists of an E-plane T and an H-plane T arranged as shown in Fig. 9·1. By virtue of the symmetrical construction, a wave coupled into arm 3 will divide between arms 1 and 2, but will not cross-couple into arm 3 if all arms are coupled to matched generators or matched loads. This property may be shown qualitatively by coupling coherent generators of arbitary phase to arms 1 and 2. The waves that they excite in the waveguide are indicated by the solid and dashed vectors, respectively. The orientation of the vectors is unchanged in the process of coupling into the H-arm, and the resultant wave amplitude is $\sqrt{2}$ times the original amplitude of the input waves (since even power split at a T-junction corresponds to a voltage split by a factor $\sqrt{2}/2$). When the input waves are coupled from the side arms into the E-arm, the vectors swing around the corners to produce two waves of equal amplitude but opposite phase. Hence, there is no resultant wave in the E-arm. Now, by reciprocity, if a wave of relative amplitude equal to $\sqrt{2}$ is coupled into the H-arm, equal waves of unit amplitude and equal phase will be propagated in the side arms, but no wave will be propagated in the E-arm.

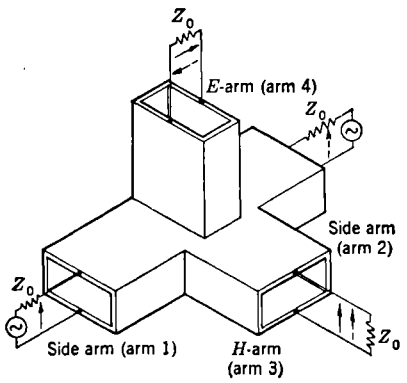

FIG. 9·1.—Side-outlet T.

By reversing the phase of the generator coupled to arm 2, a similar argument will show that when power is coupled into the E-arm, it divides between the side arms with no cross-coupling to the H-arm. It should be noted that the waves propagated in the side arms are of opposite phase.

By coupling arbitrary generators to the E- and H-arms, the same method of argument can be employed to show that there is no cross-coupling between the two side arms. This is an important property since it means the impedance seen looking into either side arm is a function of the E- and H-arms and is independent of the load on the opposite side arm.

In a bridge element, power is coupled into arm 3 or 4 from the r-f sources, and out of arm 4 or 3 to the detector. A matched termination is placed on arm 2 and it becomes the reference arm. The test piece is coupled to arm 1 and it becomes the test arm. Since there is no cross-coupling between arms 3 and 4, and since no power is reflected from the

reference termination, the only power coupled to the detector is that reflected from the test piece. When the test piece is matched, the bridge is balanced and no power reaches the detector.

However, the simple side-outlet T fails in one respect. Even with matched loads on all arms, the impedance seen looking into the test arm is not a match. Consequently, when the test piece is not matched, interaction between the T and test piece makes the power delivered to the detector dependent on the phase of the test-piece reflection coefficient. This trouble can be alleviated by tuning the E- and H-arms so that a match is seen looking into the test arm. Unfortunately, this procedure does not necessarily result in matches looking into the *E*- and *H*-arms, a highly desirable property when the T is used with variable attenuators that are calibrated for use in a matched line.

Consequently, it is wise to tune the *E*- and *H*-arms for matches looking into them. It is a property of the T that such a matching procedure automatically results in matches seen looking into the side arms. If the resultant T is matched looking into all arms, it is referred to as a magic T.

9·2. Analysis of the Operation and Properties of Side-outlet T's.— The side-outlet T may be regarded as an eight-terminal network in which the four terminal pairs represent the four waveguide arms. The amplitude of the wave out of any terminal pair may be related to the amplitudes of the waves coupled into all pairs by a simple linear combination of these input amplitudes, each being multiplied by an appropriate proportionality constant. For example,

$$E_{o1} = S_{11}E_{i1} + S_{12}E_{i2} + S_{13}E_{i3} + S_{14}E_{i4},$$

where E_{o1} is proportional to the amplitude of the wave out of the test arm, E_{i1} is proportional to the amplitude of the wave incident on the test arm (reflected from the test piece), S_{11} is the complex reflection coefficient seen looking into the test arm, E_{i2} is proportional to the amplitude of the wave incident on the reference arm (reflected from an imperfect reference termination), S_{12} is the complex amplitude transfer coefficient between the test and reference arms, and so on for the other coefficients. The E's are proportional to wave amplitudes by a constant which is chosen so that $|E|^2$ is equal to the incident or reflected power. Similar equations can be written for the other three arms, and the like-numbered S's are reflection coefficients whereas the unlike-numbered S's indicate coupling between two arms. Again it is assumed that all arms are coupled to matched generators or loads when the proportionality constants are defined. The constants from the output amplitude equations may be arranged to form the so-called *scattering matrix*. Before writing the matrix, however, it is useful to examine the effects of sym-

metry and reciprocity. From symmetry,

$$S_{11} = S_{22},$$
$$S_{13} = -S_{23},$$

and

$$S_{14} = S_{24}.$$

From reciprocity, if all lines have the same characteristic impedance,

$$S_{12} = S_{21},$$
$$S_{13} = S_{31},$$
$$S_{14} = S_{41},$$
$$S_{23} = S_{32},$$
$$S_{24} = S_{42},$$

and

$$S_{34} = S_{43}.$$

Accordingly, the scattering matrix is written

$$\begin{pmatrix} S_{11} & S_{12} & S_{13} & S_{14} \\ S_{12} & S_{11} & -S_{13} & S_{14} \\ S_{13} & -S_{13} & S_{33} & S_{34} \\ S_{14} & S_{14} & S_{34} & S_{44} \end{pmatrix}. \tag{1}$$

This is a unitary matrix of which two theorems are true:

Theorem I. The sum of the squares of the absolute magnitudes of any row or column is equal to unity.

Theorem II. For any pair of rows (or columns), the sum of the products of each S in one row (or column) with the conjugate of the corresponding S in the other row (or column) is equal to zero.

These two theorems may be applied to the scattering matrix to prove six statements that are important for impedance-bridge design.

Statement I: If a T is matched looking into arms 3 and 4, there is an equal power split between arms 3 and 4 for power reflected toward the T from a test piece on arm 1. That is, if

$$S_{33} = S_{34} = 0,$$

then

$$|S_{14}| = |S_{13}|.$$

This statement is proved by applying Theorem I to columns 3 and 4 of Matrix (1).

Statement II: Even if the E- and H-arms do not appear matched looking into the T, there is no cross-coupling between the E- and H-arms. That is, even if

$$S_{33} \neq 0$$

and

$$S_{44} \neq 0,$$

still

$$S_{34} = 0.$$

This statement is proved by applying Theorem II to columns 3 and 4 of Matrix (1).

Statement III: If the E- and H-arms appear matched looking into the T, there is no cross-coupling between the side arms, and the side arms appear matched looking into the T. That is, if

$$S_{33} = S_{44} = 0,$$

then

$$S_{12} = 0,$$
$$S_{11} = 0,$$

and

$$S_{22} = 0.$$

This statement is proved by applying Statement II to Matrix (1) to give

$$\begin{pmatrix} S_{11} & S_{12} & S_{13} & S_{14} \\ S_{12} & S_{22} & -S_{13} & S_{14} \\ S_{13} & -S_{13} & S_{33} & 0 \\ S_{14} & S_{14} & 0 & S_{44} \end{pmatrix}. \tag{2}$$

Application of Statement I and Theorem I to columns 1 and 4 will prove that $S_{12} = 0$ and $S_{11} = 0$. Application of Theorem I to rows 1 and 2 will prove that $|S_{11}| = |S_{22}|$ so that $S_{22} = 0$.

Statement IV: If a T is matched looking into the side arms, the VSWR's looking into the E- and H-arms are equal, but not necessarily unity. That is, if

$$S_{11} = S_{22} = 0,$$

then

$$|S_{33}| = |S_{44}|.$$

This statement is proved by applying Theorem I to columns 3 and 4 of Matrix (2).

Statement V: If a T is matched looking into the side arms, there is an even power split between arms 3 and 4 for power reflected toward the T from a test piece on arm 1. That is, if

$$S_{11} = S_{22} = 0,$$

then

$$|S_{13}| = |S_{14}|.$$

This statement is proved by applying Theorem I to columns 1 and 2 of Matrix (2).

Statement VI: If the T is matched looking into the side arms, but not matched looking into the E- and H-arms, there can be cross-coupling

between the side arms. That is, if

$$S_{11} = S_{22} = 0,$$

but

$$S_{33} \neq 0$$

and

$$S_{44} \neq 0,$$

then

$$S_{12} \neq 0.$$

This statement is proved by applying Theorem I and Statement V to Matrix (2) and $|S_{12}| = |S_{33}|$.

When a T is used as a bridge element, it is convenient to assume that a matched generator supplies a wave of unit amplitude incident on arm 3, that is, $E_{i3} = 1$, and that a matched detector is coupled to arm 4, that is, $E_{i4} = 0$. If the reference match has a reflection coefficient Γ_m and is coupled to arm 2, then

$$E_{i2} = \Gamma_m E_{o2}.$$

If the test piece has a reflection coefficient Γ_t and is coupled to arm 1, then

$$E_{i1} = \Gamma_t E_{o1}.$$

When these values are substituted in the equations defined by Matrix (2), the solution of the equations gives the wave amplitude delivered to the detector as

$$E_{o4} = \frac{S_{13}S_{14}(\Gamma_m - S_{11}\Gamma_m\Gamma_t + S_{12}\Gamma_m\Gamma_t - \Gamma_t)}{(1 - S_{12}\Gamma_m)(1 - S_{11}\Gamma_t) - S_{12}^2\Gamma_m\Gamma_t}. \tag{3}$$

If the reference match is perfect, $\Gamma_m = 0$, and Eq. (3) becomes

$$|E_{o4}| = \frac{|S_{13}| \cdot |S_{14}| \cdot |\Gamma_t|}{|1 - S_{11}\Gamma_t|}. \tag{4}$$

Application of Theorem I to columns 3 and 4 of Matrix (2) gives

$$|S_{13}| = \left(\frac{1 - |S_{33}|^2}{2}\right)^{1/2},$$

and

$$|S_{14}| = \left(\frac{1 - |S_{44}|^2}{2}\right)^{1/2}.$$

Substitution in Eq. (4) gives the maximum and minimum values for the power delivered to the detector, that is,

$$P = \frac{1}{4}(1 - |S_{33}|^2)(1 - |S_{44}|^2)\frac{|\Gamma_t|^2}{1 \pm |S_{11}\Gamma_t|^2}. \tag{5}$$

The terms involving S_{33} and S_{44} are not important since they merely represent inefficient power transfer if the T is not matched to the generator and detector. The power delivered to the detector is seen to be proportional to the fractional power reflection, $|\Gamma_t|^2$, from the test piece. If the T is not matched looking into the test arm, however, there will be interaction between the T and test piece so that the power to the detector is not independent of the phase of the reflection from the test piece. This "phase error" is represented by the term involving $|S_{11}\Gamma_t|$ and is illustrated by Fig. 9·2.

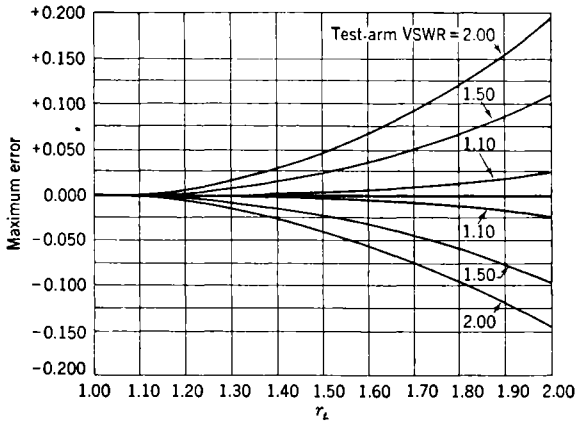

FIG. 9·2.—Effect of T-mismatch on the measurement of r_t.

If the reference match is imperfect ($\Gamma_m \neq 0$), matters are not so simple. The effect of the imperfect reference match can be seen by considering a magic T for which S_{11}, S_{22}, S_{33}, S_{44} and S_{12} are zero. In this case Eq. (3) becomes

$$E_{o4} = \tfrac{1}{2}(\Gamma_m - \Gamma_t),$$

and the maximum and minimum values of power to the detector are given by

$$P = \tfrac{1}{4}(|\Gamma_t| \pm |\Gamma_m|)^2.$$

If the reference-match VSWR is less than 1.02, and if the VSWR of the test piece does not exceed 2, then $|\Gamma_t| \cdot |\Gamma_m| \ll 1$. Accordingly, the apparent standing-wave ratio of the test piece lies between $r_t r_m$ and r_t/r_m.

If the T is not magic, this is still a good approximation for the apparent VSWR since the cross-coupling between the side arms and secondary reflections from the reference match are small if r_m is less than 1.02. It should be noted that, since the phase error results from the mismatch

seen looking into the side arms, in practice this error may be increased if the generator and detector are not matched to the line.

9·3. Analysis of the Directional Coupler as a Bridge Element.—A directional coupler may be represented as an eight-terminal network as shown in Fig. 9·3. The amplitude transfer coefficient between the two lines is defined as

$$K = \frac{E_{o3}}{E_{i1}} = \frac{E_{o4}}{E_{i2}},$$

with all lines coupled to matched generators or loads. The directive property of the coupler is defined as

$$d = \frac{E_{o4}}{E_{o3}}$$

when the generator is coupled to pair 1. The reflection coefficient of

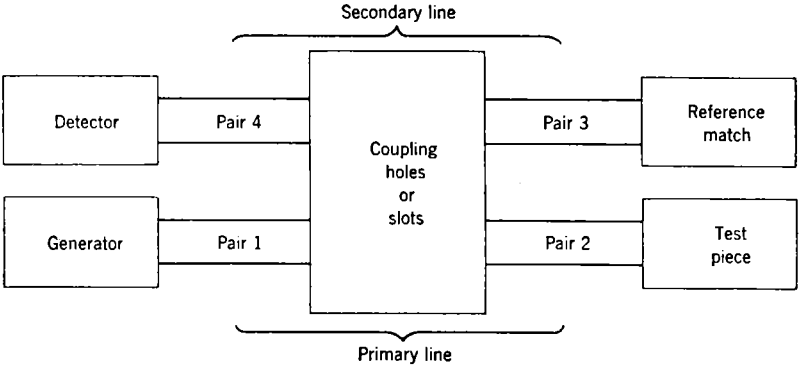

FIG. 9·3.—Directional coupler as a bridge element.

the slots is Γ_c; that of the reference match, Γ_m; and that of the test piece, Γ_t. If the generator and detector are matched to the line,

$$E_{o3} = K(E_{i1} + dE_{i2}).$$

Since

$$E_{i3} = \Gamma_m E_{o3},$$

substitution for E_{o3} gives

$$E_{i3} = \Gamma_m K(E_{i1} + dE_{i2}).$$

This wave is incident in the direction of the detector, but is reduced by coupling to the primary line and reflection by the slots. If small secondary reflections and couplings are ignored,

$$E_{o4} = \beta E_{i3} + KE_{i2} + KdE_{i1},$$

where

$$|\beta|^2 = 1 - |K|^2 - |\Gamma_c|^2$$

for conservation of energy. Also,

$$E_{o2} = \beta E_{i1} + \Gamma_c E_{i2}.$$

Since

$$E_{i2} = \Gamma_t E_{o2},$$

substitution for E_{o2} gives

$$E_{i2} = \frac{\Gamma_t \beta E_{i1}}{1 - \Gamma_c \Gamma_t}.$$

Substitution for E_{i2} gives

$$E_{o4} = \beta \Gamma_m K E_{i1} + \frac{\beta \Gamma_m K d \Gamma_t (1 - K) E_{i1}}{1 - \Gamma_c \Gamma_t} + \frac{K \Gamma_t \beta E_{i1}}{1 - \Gamma_c \Gamma_t} + K d E_{i1}.$$

Since the second term is smaller than all others by factors $\Gamma_t d$, $\Gamma_m d$ or $\Gamma_m \Gamma_t$, the equation for E_{o4} may be approximated by

$$E_{o4} = K E_{i1} \left(\Gamma_m \beta + \frac{\Gamma_t \beta}{1 - \Gamma_c \Gamma_t} + d \right).$$

Accordingly, the maximum and minimum values of the voltage to the detector are given by

$$|E_{o4}| = |K| \cdot |E_{i1}| \left(\frac{|\beta| \cdot |\Gamma_t|}{1 \pm \Gamma_c \Gamma_t} \mp |\beta| \cdot |\Gamma_m| \mp |d| \right).$$

Since $|\beta|$ is very nearly unity, the phase error and imperfect-reference-match error enter in the same way as in the case of the T. Although Γ_c is much smaller than S_{11} for an unmatched (not magic) T, a T can usually be matched so that the phase error is as small as in the case of a coupler. The important factor is the term d, which makes the coupler undesirable as a bridge element.

A good directional coupler has a directivity that is 30 to 35 db over a narrow band. Over a wide band, however, the directivity often is as low as 15 or 20 db for part of the band. This corresponds to $|d| > 0.1$, and the maximum error in measuring r_t can be a factor of 1.22. Even if the directivity is 35 db, the error can be as large as a factor of 1.04. That the error is frequency-sensitive is an intrinsic property of the directional coupler. This error in the case of a coupler results from direct-coupling between the generator and the detector. In a T, an analagous error enters if the T is asymmetrical and there is cross-coupling between the E- and H-arms. Since the effect results only from asymmetry, however, it is not frequency sensitive, and T's can be constructed commercially so that the error from asymmetry does not exceed a factor of 1.01. This corresponds to a directivity of 52 db for a directional coupler.

9·4. T-construction.—Four fundamental processes have been used to manufacture waveguide T's. They are (1) fabrication from rectangular tubing, (2) electroforming, (3) die-casting, and (4) milling channels in a block of metal split into two halves.

Figure 9·4 shows a T fabricated from 1- by $\frac{1}{2}$-in. rectangular tubing. Since the characteristic impedance of the lines depends on the dimensions, 6-in. lengths of tubing are broached to tolerances of $+0.002$ and -0.000 in. The positive tolerance results from the outward bowing of the tubing after broaching. The three pieces are jigged and soldered, and extreme

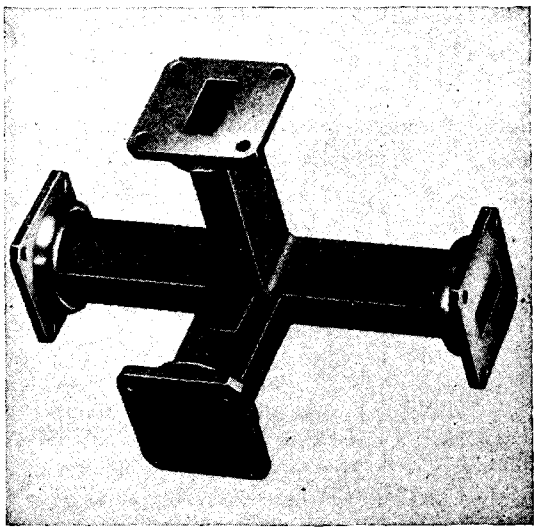

FIG. 9·4.—T fabricated from broached tubing.

care is taken not to warp the tubing during soldering. In order to avoid introducing asymmetry no matching irises or posts are used. This type of construction is well suited for large waveguide, $1\frac{1}{2}$ by 3 in., for example, but is not precise enough for $\frac{1}{4}$- by $\frac{1}{2}$-in. waveguide.

It was hoped that electroforming would facilitate the manufacture of small waveguide T's, but this was not the case. If a removable matrix is used, it must be made from three pieces whose assembly is subject to asymmetry. If the matrix is made as one piece and is dissolved after electroforming, a new matrix is necessary for each T and production costs are increased. Also, it is difficult to "throw" metal into the sharp corners of the T, and the resultant structure is mechanically weak.

Die-casting is a satisfactory solution for quantity production. The finished product is as good as the die, and slots may be cast into which matching irises may be driven. Irises are usually placed so close to the

T-junction that they introduce some asymmetry, which varies from T to T. Measurements indicate, however, that the error in measuring r_t can be as small as a factor of 1.005.

In small quantities, satisfactory T's can be made by milling channels in a block as shown in Fig. 9·5. It is difficult to insert matching irises, and r-f leakage and alignment are additional problems. Nevertheless, T's have been made whose r_t-error from asymmetry did not exceed a factor of 1.01.

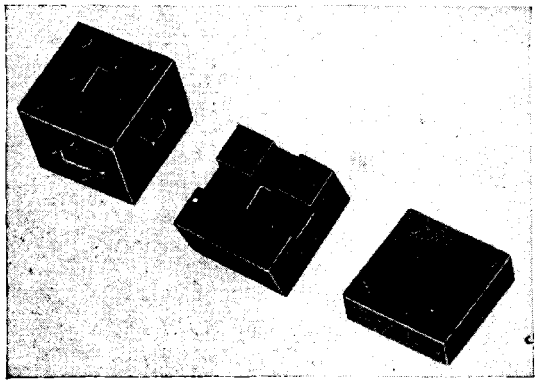

FIG. 9·5.—T made by milling channels in a block.

9·5. Matching Techniques for T's.—A T that appears matched looking into all arms is called a "magic" T. It is desirable to make a magic T in order to avoid three sources of error in measuring the voltage standing-wave ratio of a test piece. There is cross-coupling between the side arms of an unmatched T and interaction between the T and the test piece. Also, if a variable, calibrated attenuator is coupled to the E- or H-arms, interaction with the T will change the effective attenuation. Although it is desirable to match a T, the problem is not simple. To match a T over a wide band requires that the matching elements be placed as close as possible to the T-junction. If elements are placed in or near the junction, asymmetry is often introduced and this new source of error may overshadow those eliminated by matching the T.

Figure 9·6 indicates the success with which a post and iris may be used to match a T made from 1½- by 3-in. waveguide. The dimensions and positions of the matching elements are shown in Fig. 9·7. The post is 0.375 in. in diameter and 1.750 in. high. The iris is made from 0.032-in. stock.

Figures 9·8 and 9·9 indicate the post-and-iris scheme as applied to a ½- by 1-in. waveguide T. The post is 0.125 in. in diameter and 0.650 in. high. The iris is made from 0.032-in. stock.

T's made of $\frac{1}{4}$- by $\frac{1}{2}$-in. waveguide have been matched by using two irises. Figures 9·10 and 9·11 indicate the dimensions and success of matching. The irises are made from 0.020-in. stock.

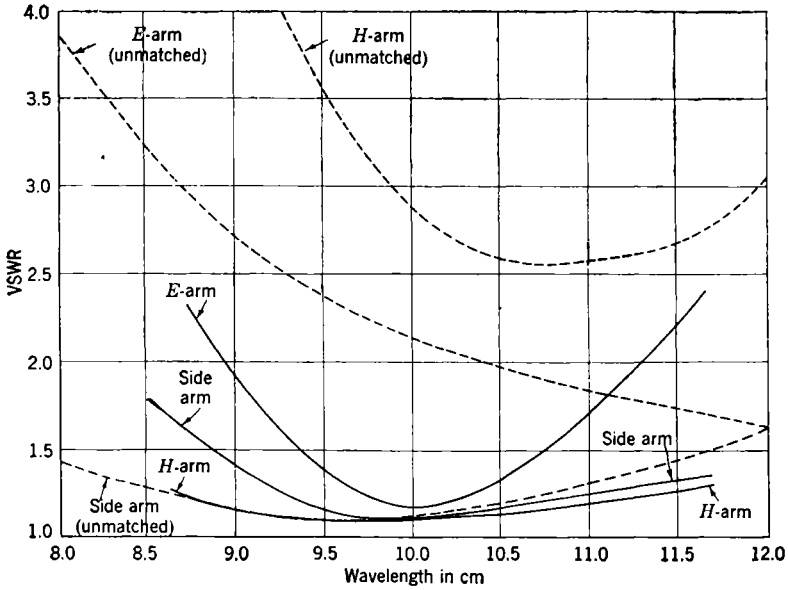

FIG. 9·6.—Effects of a post and iris for matching a $1\frac{1}{2}$- by 3-in. waveguide T.

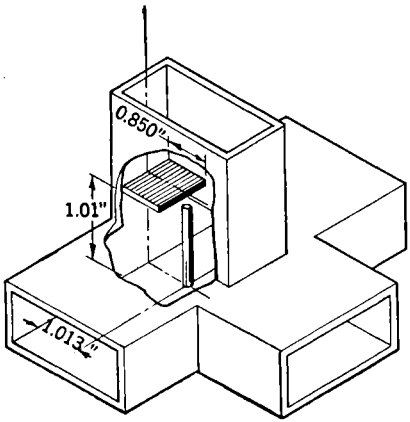

FIG. 9·7.—Positions of post and iris for matching a $1\frac{1}{2}$- by 3-in. waveguide T.

A British scheme for matching T's is shown in Fig. 9·12. Both side arms and the *H*-arm have the narrow dimension reduced by a factor of two through one-quarter-wavelength transformers. A circular block

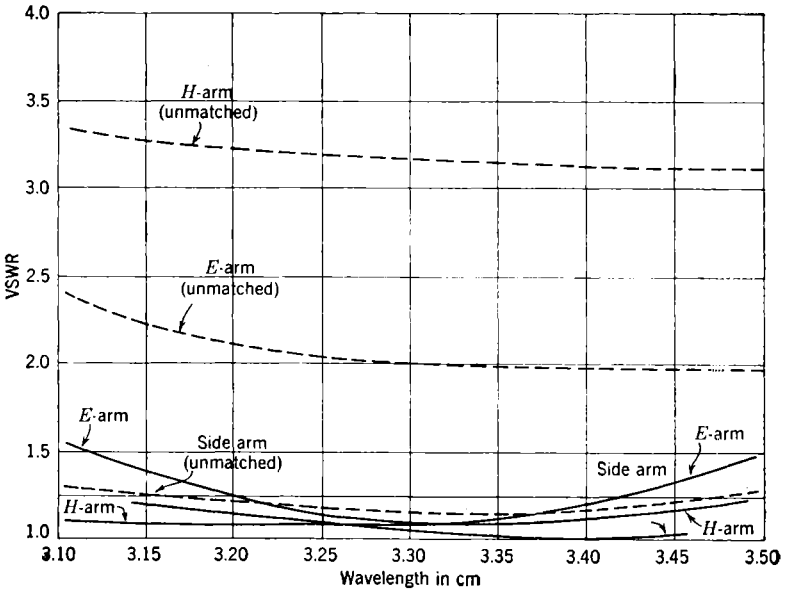

FIG. 9·8.—Effects of a post and iris for matching a 1½- by 1-in. waveguide T.

and post are mounted so that the post projects into the *E*-arm. All arms have VSWR's not exceeding 1.07 from 3.1 to 3.3 cm when the terminals are ½- by 1-in. waveguide. Although no additional data are available, the technique would seem to be equally applicable to other sizes of waveguide.

When a post is employed as a matching element, it can also be used to correct asymmetry. If the post is fastened to the waveguide by means of a pin which allows it to rotate eccentrically, this movement may be used to compensate asymmetry and to eliminate cross-coupling without appreciably affecting the impedance match.

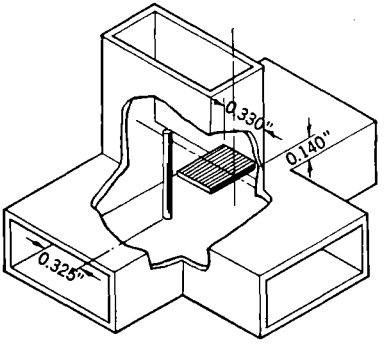

FIG. 9·9.—Positions of post and iris for matching a ½- by 1-in. waveguide T.

9·6. Ring Networks and Coaxial T's.—Figure 9·13 illustrates both waveguide and coaxial ring networks that are analogous to T's and may be used as bridge elements. Their selective properties result from the spacings of the arms and hence are frequency sensitive. However, it is easy to match the devices over a wide range of frequencies.

For example, the waveguide ring network consists of E-plane T's, with the result that the impedance looking into a junction from a side arm is the sum of the impedances seen looking both ways into the ring

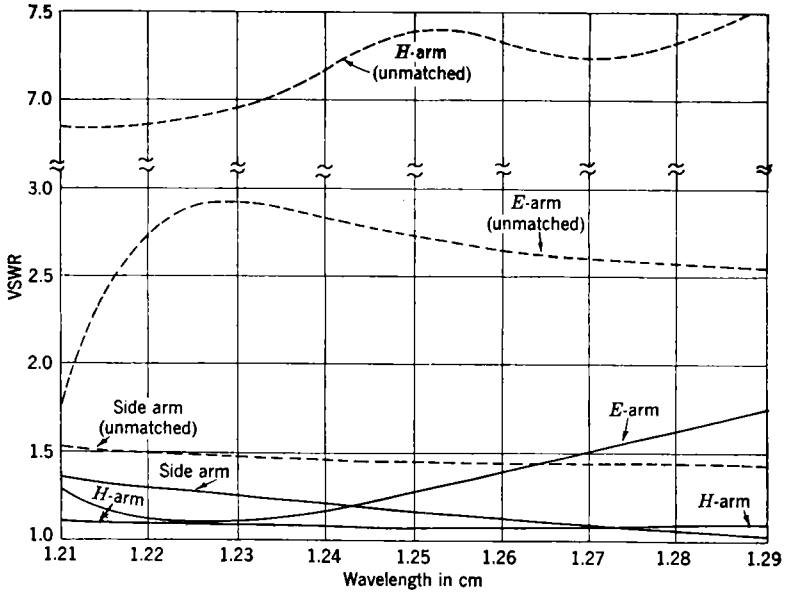

FIG. 9·10.—Effect of irises for matching a $\frac{1}{4}$- by $\frac{1}{2}$-in. waveguide T.

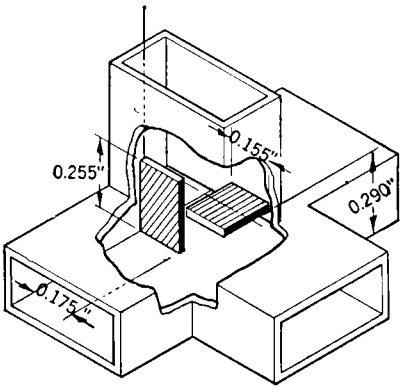

FIG. 9·11.—Positions of matching irises for $\frac{1}{4}$- by $\frac{1}{2}$-in. waveguide T.

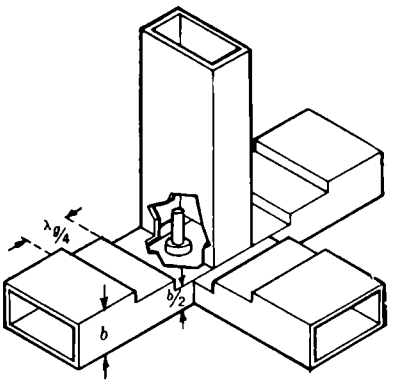

FIG. 9·12.—British method for matching waveguide T's.

from the junction. If power is coupled into arm 1, no power is coupled out of arm 3 since wave interference effectively short-circuits junction 3. Consequently, junctions 2 and 4 see an open circuit when looking toward

junction 3, and only the side arms determine the impedances of junctions 2 and 4. Looking into junction 1 from its side arm, there appear, in series, the characteristic impedances of arms 2 and 4 transformed through

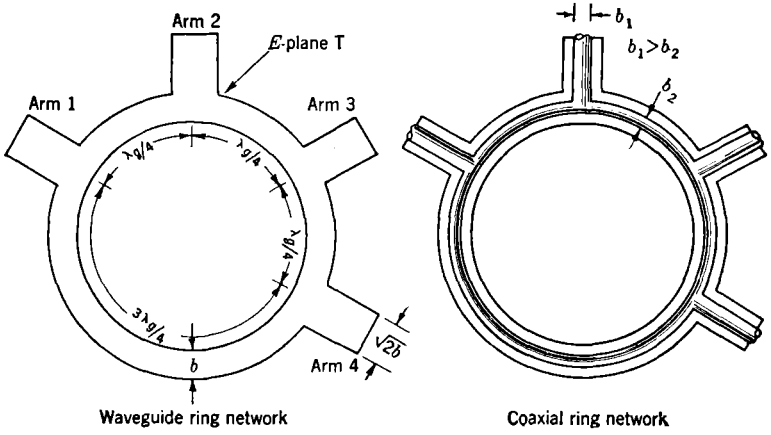

FIG. 9·13.—Waveguide and coaxial ring networks.

the ring to junction 1. If the characteristic impedance of the ring is smaller than that of the side arms by a factor $\sqrt{2}$, the transformations through the ring will result in matches looking into the side arms. Thus, matching is accomplished simply by choosing the proper characteristic impedance for the ring. In the case of the coaxial ring network, an analogous argument shows that the diameter of the inner conductor should be smaller for the ring than for the side arm.

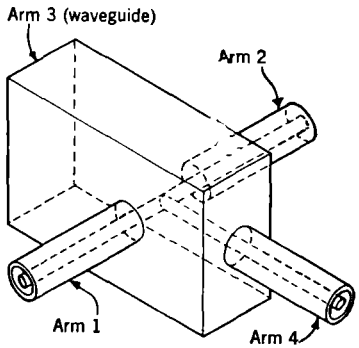

FIG. 9·14.—Coaxial T.

Waveguide ring networks have been made so that the side arms were of ½- by 1-in. waveguide[1] and the impedance ratio was exactly $\sqrt{2}$ Fortunately, over a wide frequency range the VSWR's looking into the side arms did not exceed 1.20.

While the ring network is one solution to the coaxial-T problem, Fig. 9·14 illustrates another possibility. Unfortunately, no data are available to describe its properties.

[1] This ring network resulted from duplexer developments which are described in Vol. 14, Chap. 8.

BASIC MEASURING TECHNIQUES

Ordinary bench test equipment, such as that indicated by Fig. 9·15, is used for single-frequency operations. The components are essentially those used for slotted-section measurements. If a greater power range is desired, the r-f source may be a c-w oscillator and the detector may be a receiver or spectrum analyzer. The calibrated r-f attenuator is important for many basic measurements since the output power from a T

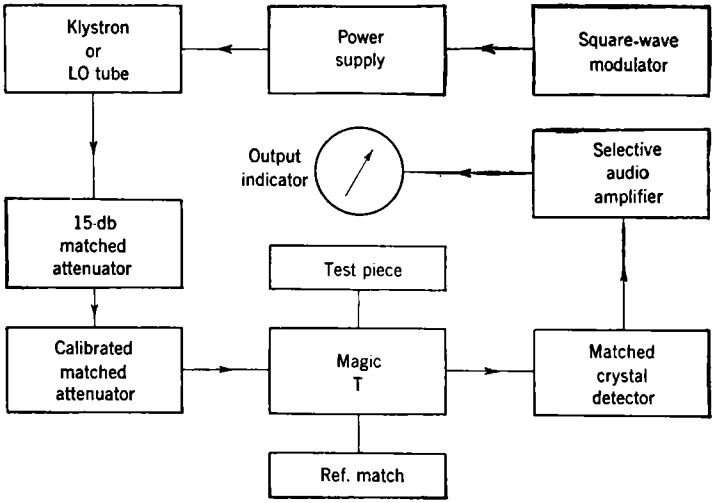

FIG. 9·15.—Typical equipment for basic measurements.

is related to the test-piece standing-wave ratio in a very definite manner. If a bolometer or crystal detector of known law is employed, the r-f attenuator may be replaced by an i-f or a-f attenuator although the range of attenuation measurement may not be large enough to permit the measurement of very small standing-wave ratios.

9·7. The Single-frequency Bridge.—At a single frequency it is possible to match a T so that it is truly "magic," that is, matched looking into all arms. If unit power is incident on the bridge from a matched generator, the power to a matched detector is, from Eq. (5) Sec. 9·2,

$$P = \frac{|\Gamma_t|^2}{4}, \tag{6}$$

where Γ_t is the reflection coefficient of the test piece. This expression requires a symmetrical T and perfect reference match. Although neither requirement can be realized in practice, the cross-coupling that results from asymmetry can be cancelled by tuning the reference match so that

it introduces a compensating reflection. If asymmetry does not affect power division, the attenuation between the input and output powers is

$$n = 20 \log_{10} |\Gamma_t| - 6.0 \quad \text{db.} \tag{7}$$

However, asymmetry does affect the power splits and so alters the 6-db term in Eq. (7). If the T is well matched and only slightly asymmetrical, the coupling between the E-arm and the test arm will be proportional

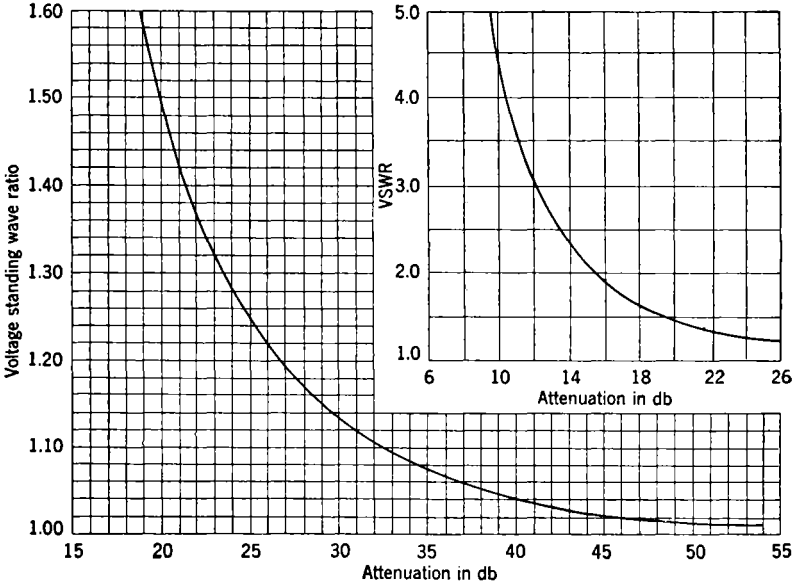

FIG. 9·16.—r_t vs. equivalent line attenuation.

to $(\frac{1}{2} + \delta)$, and that between the H-arm and the test arm will be proportional to $(\frac{1}{2} + \epsilon)$. If the test arm appears matched looking into the T and if the cross-coupling between the side arms is negligible, conservation of energy requires a power division between the E- and H-arms so that

$$1 = (\tfrac{1}{2} + \delta) + (\tfrac{1}{2} + \epsilon)$$

when unit power is coupled into the test arm. Accordingly, $\epsilon = -\delta$, and the 6-db term will be in error by an amount proportioned to δ^2, which is negligible for small amounts of asymmetry.

Since the voltage standing-wave ratio of the test piece is

$$r_t = \frac{1 + |\Gamma_t|}{1 - |\Gamma_t|},$$

a graph of r_t vs. equivalent line attenuation may be plotted as in Fig. 9·16. The measurement of r_t simply amounts to measuring attenuation through the T and reading the corresponding r_t from the graph.

The attenuation measurement may be made in several ways depending on the range of the voltage standing-wave ratio to be measured. A matched bolometer detector followed by a selective amplifier and audio attenuator or logarithmic voltmeter will provide a range of about 45 db with an accuracy of ± 0.2 db. This allows the measurement of standing-wave ratios exceeding 1.02 and means, for example, that an r_t of 1.500 will appear to be between 1.485 and 1.515. If smaller standing-wave ratios are to be measured, an r-f attenuator can be calibrated in two steps by the bolometer method. With this higher-range attenuator, a more sensitive detector such as a heterodyne receiver or spectrum analyzer should be coupled to the bridge.

The bridge-attenuation measurement necessitates disassembly of the components in the process, and this is usually an undesirable operation. The measurement can be broken effectively into two steps by using a reference mismatch. An iris is placed ahead of a well-matched termination in broached waveguide, and the standing-wave ratio of the combination is measured by attenuation through the T or by means of a slotted section. If the reference-mismatch VSWR is 1.30, the attenuation is 23.7 db; if the VSWR is 1.50, the attenuation is 20.0 db. Consequently, the attenuation measurement is not difficult.

The reference mismatch and the test piece are alternately coupled to the bridge, and the relative output powers from the bridge are compared by means of an r-f or a-f attenuator. The amplifier or spectrum analyzer is used merely as a reference indicator, and the r_t is determined from Fig. 9·16. If the reference-mismatch VSWR is 1.20, an r_t range from 1.06 to 1.90 may be covered by measuring relative attenuation of ± 10 db.

For this small range, a crystal may be assumed to be a square-law detector without excessive error for production testing of line components. An r_t of 1.06 may appear to be between 1.05 and 1.07, and an r_t of 1.70 may appear to be between 1.60 and 1.80. A good audio attenuator may be installed in the selective amplifier that follows the crystal detector, and its dial may be calibrated directly in r_t.

These techniques are accurate only when the T is well matched and asymmetric cross-coupling is eliminated. Although this can be accomplished at a single frequency, over a wide frequency range errors result from the T-mismatch, an imperfect reference match, the asymmetric cross-coupling, and the frequency sensitivity of the r-f attenuator; and these errors can combine to produce a large over-all error. Consequently, the wideband bridge is recommended for production testing and impedance-matching, and the single-frequency bridge is recommended for precision laboratory measurements, especially those involving small reflections.

9·8. T-asymmetry.—Cross-coupling between the *E*- and *H*-arms is caused by T-asymmetry, and the effect may be measured or eliminated

by using a termination that is tunable about the characteristic impedance of the line. For example, this termination is coupled to arm 2 and a well-matched load (VSWR < 1.01) is coupled to arm 1; power is coupled into the H-arm, and the termination is tuned until there is no resultant wave out of the E-arm. This effect is shown in Fig. 9·17 where the wave-amplitude subscripts T, A, and M refer to signals produced by the termination, asymmetry, and the imperfect reference match, respectively.

Now if the side arms have equal electrical lengths, interchanging the tunable termination and reference match will simply reverse the phases of e_T and e_M. In this case, the resultant wave amplitude in the E-arm

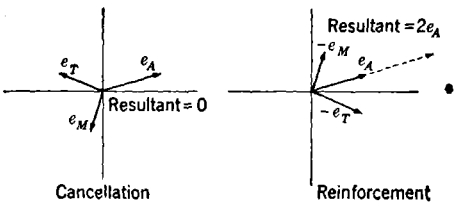

FIG. 9·17.—Cancellation and reinforcement of asymmetric cross-coupling by reflections from the side-arm terminations.

is twice that from asymmetry as shown in Fig. 9·17. This output wave is equivalent to that produced by some test piece that is coupled to a perfect bridge. The equivalent r_t can be determined from attenuation through the T or by using a reference mismatch in conjunction with a calibrated attenuator. However, since the output voltage is twice that resulting from asymmetry, 6 db must be added to the measured amount of attenuation in order to obtain the r_t equivalent to the signal caused by asymmetry.

Although asymmetry affects the power division within the T, no appreciable error is introduced in the measurement of the equivalent r_t. The side arms must have equal electrical lengths, however, or appreciable error may be introduced. The electrical length of a side arm is dependent on not only the physical length, but the average width of the waveguide as well. If the T is made of $\frac{1}{2}$- by 1-in. waveguide, and if the side arms differ in length by 0.005 in., the error in measuring an asymmetric VSWR of 1.01 will not exceed ± 0.0001. If the asymmetric VSWR is 1.02, the error will not exceed ± 0.0002. If the T is made of $\frac{1}{4}$- by $\frac{1}{2}$-in. waveguide, and if the side arms differ in length by 0.002 in., the error in measuring an asymmetric VSWR of 1.02 will not exceed ± 0.0004 and will be less if the equivalent r_t is smaller. If one side arm of a $\frac{1}{2}$- by 1-in. waveguide T has an average deviation of 0.001 in. from the correct width, the error in measuring an asymmetric VSWR of 1.02 will not exceed ± 0.0004 and will be less if the equivalent r_t is smaller. If one side arm of a $\frac{1}{2}$- by 1-in.

waveguide T has an average deviation of 0.001 in. from the correct width, the error in measuring an asymmetric VSWR of 1.02 would probably be too small to detect. If one side arm of a $\frac{1}{4}$- by $\frac{1}{2}$-in. waveguide T has an average deviation of 0.007 in. from the correct width, the error will not exceed ± 0.0004. Thus, if close mechanical tolerances are observed, no appreciable error is caused by the unequal lengths of the side arms. The effect of unequal arms may be detected by beginning the asymmetry measurement with the tunable termination first on one side arm, and then on the other.

The major error in the measurement of asymmetry is caused by incorrect waveguide dimensions at the output-terminal planes of the side arms. Since asymmetry is defined as a function of the output wave when perfect terminations in correct-size waveguide are coupled to the side arms, the definition includes reflections from discontinuities at the output terminals of the side arms. Since these reflections do not result from asymmetry within the junction, however, their effect must be small for the measurement to be indicative of the junction asymmetry. If the T is made of $\frac{1}{2}$- by 1-in. waveguide, and if the narrow dimensions of the side-arm output terminals differ by 0.0004 in., the error in measuring the asymmetric VSWR will be about ± 0.001. For $\frac{1}{4}$- by $\frac{1}{2}$-in. waveguide T's, the error will be ± 0.0023. If the T is made of $\frac{1}{2}$- by 1-in. waveguide, and if the wide dimensions of the side arms differ by 0.0004 in. at the output terminals, the error will be ± 0.001. If the wide dimensions differ by 0.0003 in. for a $\frac{1}{2}$- by $\frac{1}{4}$-in. waveguide T, the error is again ± 0.001. If the output terminals differ from the correct dimensions by equal amounts, no error will be incurred in the measurement of asymmetry, but error may be introduced when the T is used to measure this standing-wave ratio of a test piece. In summary, if the tolerances given in the preceding paragraphs are observed, an asymmetric VSWR of 1.01 can be measured to ± 0.002 for $\frac{1}{2}$- by 1-in. waveguide T's, and to ± 0.004 for $\frac{1}{4}$- by $\frac{1}{2}$-in. T's. If similar tolerances are observed for $1\frac{1}{2}$- by 3-in. waveguide T's, the error will not be appreciable.

9·9. Bridge Balance and the Sliding Match.—Because of the cross-coupling that results from an asymmetrical T-junction, a bridge will appear unbalanced even if all arms are coupled to perfectly matched generators or loads. The bridge may be balanced by tuning the reference match, which is slightly imperfect anyhow, so that it produces a reflection that cancels the cross-coupling. Balancing should result in no output signal from the bridge when a perfect match is coupled to the test arm. Since a completely reflectionless termination is not realizable in practice, a "sliding match" is used instead.

The sliding match consists of a well-matched termination which may be moved lengthwise in a waveguide casing. The termination may be

a tapered piece of polyiron which is machined for a sliding fit. If the casing is made from broached or precision-drawn waveguide, and if the termination is a close fit, only the phase of the reflection varies when the termination is moved. A good termination should produce a VSWR less than 1.02, and the casing should allow a motion of at least one-half the wavelength in the line. As the termination is moved over this range, its impedance will describe a circle whose center is the characteristic impedance of the line.

If the bridge is unbalanced when the termination is moved, the reflection from the sliding match will add to, or subtract from, the unbalance signal, and the output power from the bridge will vary. If the bridge is balanced, the output signal will not vary since it results only from the sliding-match reflection, which is variable in phase but constant in amplitude.

The sliding match can be used not only to facilitate bridge balance but to measure unbalance as well. The maximum and minimum output powers are measured as the sliding match is moved, and these values are converted to equivalent r_t's by means of Fig. 9·16. If the signal caused by bridge unbalance is less than that resulting from the sliding-match reflection, the equivalent r_t for bridge unbalance is

$$\sqrt{r_{max}/r_{min}},$$

and the sliding-match standing-wave ratio is

$$\sqrt{r_{max} \cdot r_{min}}.$$

If the bridge unbalance produces the larger output signal, the relations are reversed.

9·10. Magic-T Alignment.—Although the matching techniques described in Sec. 9·5 provide reasonably good operation over a wide range of frequencies, a single-frequency bridge can be matched almost perfectly by means of tuning screws. Since frequency sensitivity is unimportant, the screws may be placed sufficiently far from the T-junction so that no asymmetry is introduced. The screws should be placed in the *E*- and *H*-arms, and matching these arms automatically results in matches looking into the side arms. The easiest method of alignment is to couple the *E*- and *H*-arms alternately to another impedance bridge and to adjust them independently for minimum power reflection. Although the side arms should be coupled to well-matched terminations during this procedure, the unused *E*- or *H*-arm need not be terminated. If the radiation from the unused arm interferes with the detector by means of coupling through the intervening space, this arm may be short-circuited with a metal plate without affecting the matching procedure for the other arm.

It should be remembered that even though the T is matched according to this procedure, it will not appear matched looking into the side arms unless the *E*- and *H*-arms are coupled to a matched generator and a matched detector. For single-frequency bridges, the detectors can be matched by means of tuning screws. Although a matched generator could be achieved also by reactive tuning elements, these elements might impair the operation of those low-voltage oscillators (types 2K25 and 2K50), for example) that are purposely mismatched to the line for stability as well as power considerations. Even when tuners are used to obtain the optimum operation of high-voltage tubes, such as the 2K39, the oscillator is not necessarily matched to the line. Therefore, a matched generator is best achieved by inserting resistive attenuation between the oscillators and the T.

9·11. The Measurement of Large Reflections.—Both the amplitude and phase of large reflection coefficients can be measured if the reference match is replaced by a short circuit whose position is adjustable relative to the T-junction. The test piece is coupled to one side-arm of a magic T, and the position of the short circuit on the opposite arm is varied until the output wave is minimized. Accordingly, the attenuation through the T is

$$20 \log_{10} (|\Gamma_s| - |\Gamma_t|) - 6.0 \quad \text{db},$$

where Γ_s and Γ_t are the reflection coefficients of the short circuit and the test piece. If the short circuit provides total reflection ($\Gamma_s = 1$), then the attenuation is a measure of $1 - |\Gamma_t|$. If the side arms of the T have equal or known electrical lengths, the position of the short circuit is indicative of the phase of Γ_t.

Since this technique involves large reflections, the T, the generator, and the detector must all be very well matched. Also, asymmetric cross-coupling must be compensated since the output signal will be small for large values of Γ_t. Compensation is achieved in several steps. First, the bridge is matched and balanced as described in the preceding sections; the matching screws are placed in the *E*- and *H*-arms, and the balancing screws, in the reference arm. Second, the sliding match on the test arm is replaced by a load which is tuned until the output signal is zero, thus indicating a perfect match. Third, the termination on the reference arm is replaced by the sliding match, and the resultant output signal is caused only by asymmetry, reference-arm screw reflections, and the sliding-match reflection. If the screws are adjusted until the amplitude of the output signal is unaffected by moving the sliding match, this signal results only from the sliding-match reflection, and asymmetry is compensated. The important fact is that the T is still compensated when the reference arm is short-circuited.

If high accuracy is desired in the measurement of Γ_l, the loss in the sliding short circuit must be considered. A good short circuit employs chokes, rather than contact fingers, and will produce a standing-wave ratio of about 50 db. Consequently, $|\Gamma_s|$ will be about 0.994. This can be measured with a T whose reference arm is short-circuited by a plate soldered to the waveguide.

DESIGN CONSIDERATIONS FOR MULTIFREQUENCY IMPEDANCE BRIDGES

The first design consideration for multifrequency impedance bridges is usually the selection of the process that provides simultaneous indications at several frequencies. The detector-indicator circuits, are therefore

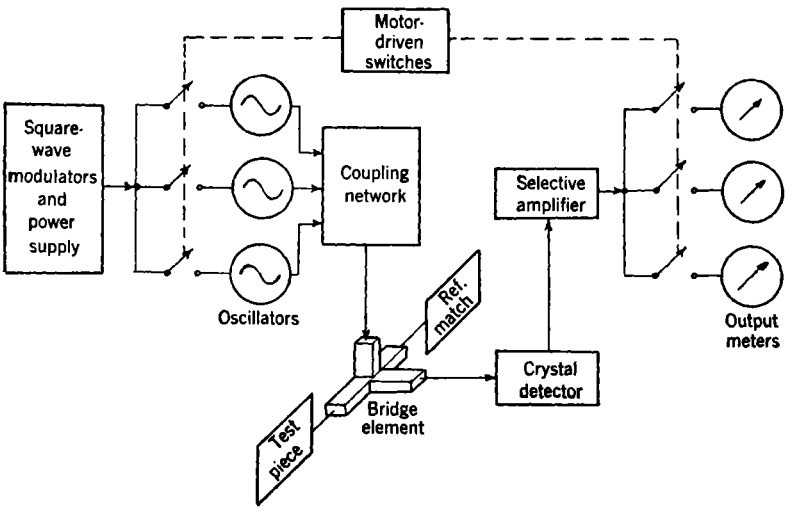

FIG. 9·18.—Simple multifrequency bridge that utilizes mechanical switching.

often predetermined, and the selection of the r-f oscillators, the coupling networks, and the other line components usually effects a compromise between accuracy and range of measurement. Although complexity, cost, and application are important, they are commonly the results of, rather than the prerequisites for, the preliminary design considerations.

9·12. Methods Which Provide Simultaneous Indications at Several Frequencies.—The simplest method for providing multifrequency operation is a slight elaboration of the single-frequency bridge. Figure 9·18 illustrates the method in which three oscillators are coupled to the bridge by directional couplers or magic T's. By means of a motor-driven mechanical switch, the oscillators are turned on and off in sequence, and the amplifier is coupled, in turn, to each of the three output meters.

This effect may be achieved electronically as shown in Fig. 9·19.

Three oscillators are square-wave modulated at audio rates which are not multiples of one another, and the amplifier uses three selective output channels to discriminate between the different modulation frequencies. Because of the good sensitivity afforded by a crystal detector and selective amplifier, low-voltage oscillators will deliver sufficient r-f power, and a common power supply can be used for all circuit components. If the crystal is operated as a square-law detector, an audio attenuator may be used as a calibrating device, and the number of r-f line compo-

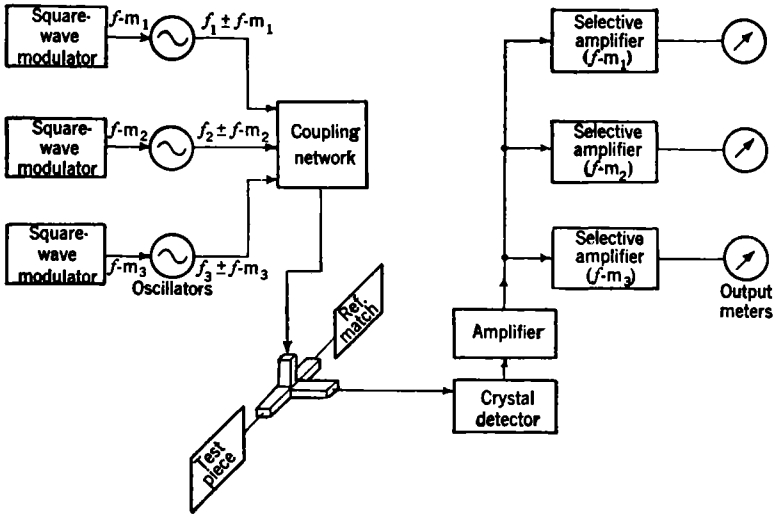

FIG. 9·19.—Multifrequency bridge that employs modulation-frequency discrimination.

nents may be held to a minimum. Both the microwave and the circuit techniques are extremely simple, and consequently, this type of bridge is recommended for applications where the investment in test equipment and its maintenance must be minimized.

A better visual presentation is obtained with a cathode-ray tube since the indications can be spaced more closely than in the case of meters. Figure 9·20 illustrates a pulse-modulated impedance bridge in which the oscillators are pulsed sequentially to provide a time separation of the corresponding pips that appear on the cathode-ray tube. Unfortunately, high-voltage oscillators are necessary to compensate for the inherent low sensitivity of the wide-band pulse amplifier, and the circuits associated with these oscillators and the cathode-ray tube make the cost and the complexity relatively high. On the other hand, these disadvantages are somewhat offset by the desirable presentation and the ease of operation; and the pulse-modulated bridge is well suited for commercial applications.

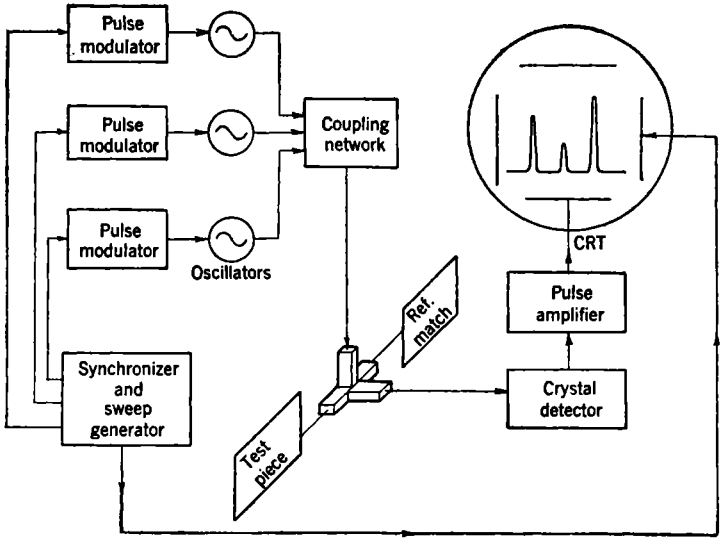

FIG. 9·20.—Multifrequency bridge that employs pulse modulation.

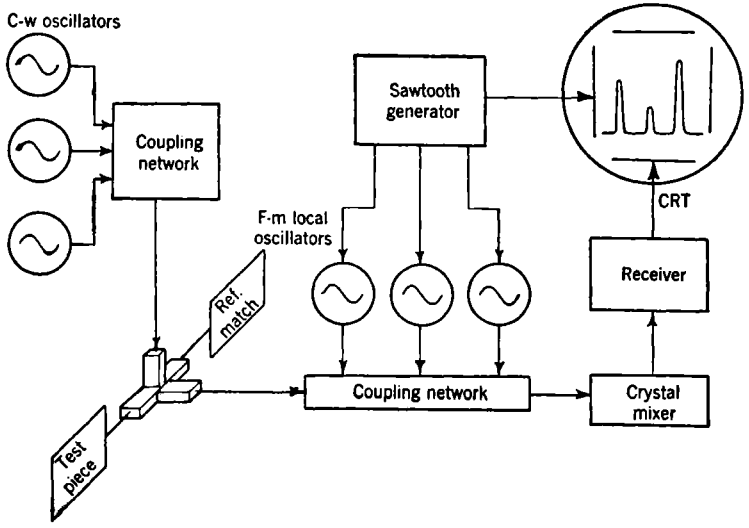

FIG. 9·21.—Multifrequency bridge that utilizes a panoramic receiver.

A similar CRT presentation is obtained with impedance bridges that employ panoramic receivers. Figure 9·21 illustrates this method in which three frequency-modulated local oscillators are coupled to a common mixer. It is also possible to use f-m sources instead of f-m local oscillators, thus minimizing spurious responses. The principle of operation is the same in both cases. Corresponding pairs of c-w and f-m oscillators are tuned so that the frequency difference between each pair is equal to the intermediate frequency at some point in the modulation cycle. Since these difference frequencies vary with time, i-f pulses are generated, and hence video output pulses result. Although the high sensitivity of the heterodyne receiver provides a large range of measurement, the use of local oscillators and their coupling networks results is a considerable increase in cost. Also, the current capacity of the power supply must be increased because of the additional oscillators. If a wide-band i-f amplifier is used for stability considerations, the current drain from the power supply will be still greater.

From an operational viewpoint, the panoramic impedance bridge is also the most complex. Commercial models provide hinged covers for the oscillator-voltage controls, and these covers are closed following alignment by an engineer. However, sometimes the oscillators drift in frequency, and their harmonics cross-modulate in the mixer and block the receiver, thus confusing the test-line operator. In general, panoramic impedance bridges are best suited for use by persons of engineering caliber who willingly tolerate the greater complexity for the increased accuracy and the greater sensitivity.

9·13. Line Components.—Coupling networks should introduce minimum insertion loss in order to allow the measurement of very small test-piece reflections, but should provide maximum isolation between oscillators. Both magic T's and directional couplers can be used. Directional couplers usually introduce an attenuation of at least 10 db, whereas T's introduce only 3 db. However, T's must be provided with matching elements and do not always lend themselves to mechanical arrangements in which oscillator tuning shafts must be brought out through a front panel. Directional couplers can provide 40 db of isolation between oscillators—a value that is also easily realized by T's, even those that have considerable asymmetry.

Although any number of directional couplers may be inserted in a common line, each magic T is used to couple two sources to a common line. If four oscillators are used, they may be coupled in pairs to two T's, and these T's may be coupled to a third T in order to obtain all signals in a common line. In this case, the attenuation between each oscillator and the main line is 6 db, only 4 db less than that for directional-coupler networks. If several directional couplers are inserted

in a common line, however, their individual reflections may combine so that, at some frequencies, the whole assembly, when viewed from the bridge, may appear as a very poorly matched generator. In practice, it is often possible to space the couplers so that their reflections tend to cancel rather than to reinforce. In general, matched T's provide less insertion loss than directional couplers, but a less desirable mechanical arrangement; directional couplers provide a desirable mechanical arrangement, but introduce more loss than matched T's and require judicious spacing.

Included among the line components are several attenuators, both fixed and variable. Since a crystal detector may produce a VSWR as large as 4.0 over part of a wide frequency range, it is usually padded by about 10 db of resistive attenuation in order that the VSWR, as seen from the bridge, shall not exceed 1.1. If the output powers from the oscillators are not controlled electronically, a variable attenuator can be inserted between each oscillator and the coupling network. At minimum attenuation, these attenuators should have negligible insertion loss in order to allow the measurement of small test-piece reflections. Under these conditions there is little attenuation between the oscillators and the T, and the line appears badly mismatched looking back from the T. Although the phase error tends to increase because of this mismatch, it also tends to be reduced because under these conditions a small reflection is being measured. When a larger reflection is being measured the phase error tends to increase, but sometimes the power-level attenuators can be adjusted to provide more isolation between the oscillators and the T. This increased isolation reduces the mismatch as seen looking back from the T, and consequently tends to reduce the phase error.

For example, consider a T that is matched so that the VSWR looking into all arms does not exceed 1.10 when all arms are coupled to matched generators or matched loads. The detector is isolated from the T by 10 db of attenuation so that the VSWR, as seen from the T, does not exceed 1.10. If the power-level attenuators are adjusted for the measurement of small reflections, the attenuation between each oscillator and the T may not exceed 10 db. If the coupling network alone produces a VSWR of 1.10, the VSWR, looking back from the T, can be as large as 2.20, but probably will not exceed 1.80. With E- and H-arms coupled to impedances that produce VSWR's of 1.10 and 1.80, the VSWR that is seen looking into the test arm can be increased from 1.10 to 1.65. Consequently, if an r_t of 1.02 is measured, the phase error will cause the test-piece reflection coefficient to be measured in error by a factor of 1.003, and the error in the measurement of r_t is unimportant.

Now suppose that when the bridge is used to measure an r_t of 1.6, the power-level attenuators can be adjusted to provide at least 20 db

of attenuation between each oscillator and the T. The VSWR seen looking back from the T will probably not exceed 1.15, and the VSWR looking into the test arm of the T will not exceed 1.30. Consequently, the phase error will cause the apparent r_t to fall between 1.57 and 1.62. Unfortunately, other design factors, such as the method of calibration and the over-all sensitivity, often restrict the isolating attenuation to values much less than 20 db.

If an r-f attenuator is incorporated in the bridge as a calibration device, it should be placed between the T and the detector. In this position it will be coupled to more nearly matched lines than if it were placed on the generator side of the T. Accordingly, its calibration will be much more reliable. However, if r_t is 1.60, the VSWR looking back into the T can be as large as 1.50. In bridge designs that can tolerate more line attenuation, a 5-db fixed attenuator is placed between the T and the variable attenuator so that the VSWR of 1.50 is reduced to 1.14.

All line components must furnish good protection against r-f leakage. Even if the coherent leakage is 10 db below the signal level at the detector, the signal can be changed about ± 3db by the leakage. If this condition exists when r_t is 1.02, the measured value will be between 1.01 and 1.03. Since the total line attenuation is not less than 65 db between the oscillators and the detector for an r_t of 1.02, the leakage protection for this example is at least 75 db. If the calibration device is an audio attenuator or logarithmic voltmeter, the signal level at the detector increases 25 db when r_t is 1.60. Although the effect of the leakage is less prominent, the measurement of large test-piece reflections is more sensitive to attenuation error. Hence, the apparent r_t will be between 1.59 and 1.61, and 75 db of leakage protection may be adequate for some applications.

If an r-f attenuator is used as a calibration device, however, the detector is used merely to indicate a reference level, and hence operates at the same signal level regardless of the test-piece reflection. Consequently, the effect of leakage is always the same, and the leakage protection must be increased to about 100 db if an r_t of 1.60 is to fall between 1.59 and 1.61.

Optimum leakage protection is achieved by carefully shielding the oscillators and by providing good electrical contacts at all junctions. All electrical leads to the oscillators should enter the shield cans through coaxial fittings that have polyiron bushings between the conductors. It is usually advisable to wrap the polyiron bushings with two or three layers of varnished cambric in order to obtain greater protection against voltage breakdown. All oscillator tuning shafts and attenuator drive pins should pass through bearings that have polyiron bushings. Waveguide choke joints may be sealed by inserting a metal-textile (woven

metal strands) gasket in the choke groove. Larger gaskets can be used to seal the oscillator shield cans. Flat gaskets of metal shim-stock should be avoided since they are easily burred, scarred, and spoiled.

IMPEDANCE BRIDGES UTILIZING MODULATION-FREQUENCY DISCRIMINATION

The principle of operation for bridges that utilize modulation-frequency discrimination is described in Sec. 9·12 with reference to Fig. 9·19. The circuit components of this bridge can be essentially those used in bench test equipment for the measurement of standing waves by means of slotted sections. Many of the design features apply equally well to bridges that employ a mechanical switch to operate, in sequence, the oscillators and their corresponding output meters. In this bridge, however, a single amplifier channel is used since all oscillators can use the same modulation.

9·14. Microwave Sources.—Reflex oscillators that deliver about 25 mw of microwave power are commonly used because they are economical from the standpoint of power-supply and modulator requirements, and from the standpoint of replacement. In order to use a common power supply for all circuit components, it is desirable to operate the oscillator cathodes at ground potential and their cavities at +300 volts. The 2K25 and 2K50 tubes can be used for the 9000- and 24,500-Mc/sec regions, respectively, since the cavity (tube shell) is easily insulated from the line components. The selection of a tube for the 3000-Mc/sec region is more difficult since the 2K28 (707B) tube requires an external cavity that is usually large and difficult to insulate, especially when equipped with a micrometer-driven tuning mechanism. Although the 726 tube has its cavity as an integral part, the coaxial output fitting requires that insulating devices be provided for the coaxial line. The alternate solution is the common one: A negative-voltage power supply is used, and the oscillator cavity is operated at ground potential.

Reflex tubes are usually modulated by applying a square-wave signal to the oscillator reflector. In order to avoid frequency modulation, the square wave should have sufficient amplitude so that the oscillator drops out of oscillation for alternate half cycles. However, the amplitude also must be limited so that the tube will not be driven into the next lower mode of oscillation. When adjusting the amplitude of the modulating signal, the output signal from the detector of the bridge should be coupled to an oscilloscope in order to detect overmodulation. A diode may be connected between the reflector and the cathode of the tube in such a way that the reflector cannot be driven positive with respect to the cathode. Simple, but adequate, modulators consist of unsynchronized multivibrators which are designed so that their recurrence

frequencies are slightly adjustable in order to achieve correspondence with the selective-amplifier channels. The adjustment, however, should be limited so that the recurrence frequencies cannot be multiples of one another.

9·15. Line Components.—Since individual gain controls can be inserted in each channel of the selective amplifier, the r-f attenuators that are commonly used to adjust the power level may be eliminated. However, if the calibration technique is dependent on the law of the detector, error may be incurred when the different signals at the detector are not comparable in amplitude. If the power-level attenuators are omitted, and if magic T's are used for coupling networks, the bridge T may be isolated from the oscillators by only 3 or 6 db. In this case it is advisable to provide 5 to 10 db of matched attenuation in the main input line to the bridge. Correspondingly, 10 db of attenuation should be placed between the T and the detector in order that the VSWR should not exceed 1.10 looking from the T toward the detector.

Either a crystal or a bolometer may be used as a detector. Although bolometers are less sensitive than crystals and may be more difficult to procure, they have the advantage of a truly square-law behavior over a wide range of power. This fact is useful for calibration methods which utilize the law of the detector, but in many cases, the slight error that results from the uncertain law of the crystal detector will be tolerated to realize the greater sensitivity. If a calibrated r-f attenuator is used, the law of the detector need not be known, and the crystal is preferred.

Although waveguide line components are used with waveguide T's, coaxial line components will save considerable space for bridges that operate in the region of 3000 Mc/sec. Directional couplers have been designed with terminals that mate with standard 50-ohm cable plugs. If the components are connected with short cables, a good mechanical arrangement usually can be attained. Fixed attenuation may be in the form of lossy cables or coaxial metalized-glass pads. Coaxial crystal holders and double-stub tuners are also standard components for 50-ohm line.

Reaction frequency meters or wavemeters are preferable to transmission types and should be coupled to the line just ahead of the detector. In this way, any mismatch that is introduced is isolated from the T by the 10-db pad.

Leakage protection is not difficult since the sensitivity of the crystal detector and conventional amplifier produces full-scale meter deflection for an input power of about -80 dbw. This level is about 35 db above the sensitivity of a heterodyne receiver, and is comparable to that used for slotted-section measurements. As in the case of slotted-section measurements, no appreciable leakage error results when only a simple

shield can (no gaskets or polyiron bushings) is placed over the oscillator. The input power leads to the oscillator run through a shield which is soldered to the tube mount, so that r-f leakage power must pass through the cable where much of it is dissipated in the insulating material. If moving a sheet of metal in close proximity to the various line components does not produce any noticeable output-meter fluctuation, the leakage protection usually meets the requirement of 100 db as specified in Sec. 9·13.

Although ordinary mixer crystals (types 1N21, 1N23, and 1N26) are often used as detectors, better results are obtained when special video crystals can be employed. Types 1N27 and 1N32 are used for the 3000-Mc/sec region; the type 1N31, for the 9000-Mc/sec region. Unfortunately, no video crystals have been produced for the 24,500-Mc/sec region.

9·16. Selective Amplifier.—The ordinary selective amplifier that is used for slotted-section measurements consists of a well-shielded input transformer, a pentode amplifier, a second pentode amplifier that includes a twin-T feedback network, a beam-tetrode power amplifier, a full-wave diode rectifier, and a d-c meter. This conventional design is commonly used with a 1N21, 1N23, or 1N26 crystal detector, and provides full-scale meter deflection when the average power incident on the detector is about −80 dbw. Although this standard and proved design can be modified for impedance bridges, a much-improved design is feasible. In the audio range of frequencies, sensitivity is usually limited by microphonics, flicker effect, and harmonics of the power-line frequency rather than thermal noise. These effects are considerably reduced if the recurrence frequencies are increased, from the usual 500 to 1000 cps, to 15 to 20 kc/sec, and the multivibrator requirements are not increased appreciably. If the input transformer is replaced by a shielded preamplifier, less pickup and several other advantages result.

If the crystal detector is direct-coupled to the grid of the first amplifier, the open-circuit output voltage from the crystal is realized. Since conventional input transformers present a load impedance of about 400 ohms to the crystal whose video impedance is between about 2000 and 20,000 ohms, the input voltage will be increased by at least a factor 6. If a video crystal (1N27, 1N31, or 1N32) is used, the sensitivity will be increased by between 4 and 8 db. The first stage should use a tube, possibly a 6F5 triode, that has low microphonics, little hum modulation, and a low equivalent-noise resistance. The preamplifier should provide one or two stages of amplification, and a cathode-follower output stage is recommended. The effects of the power-line frequency and its harmonics are minimized if a 60-cps filter is inserted in the supply-voltage input lead, and if the heaters are operated from a selenium

rectifier. Small bridge rectifiers will deliver 12 volts and will operate both preamplifier stages if the heaters are connected in series. The effects of ground currents can be minimized by isolating the input stage from ground by means of a small resistance. Naturally the tubes should be shielded and shock-mounted, and the entire unit should be mounted close to the crystal detector.

The audio attenuator should precede the selective channels, and should be matched or calibrated for a particular load impedance. If a high-impedance network is used, the low output impedance of the preceding cathode follower need not be considered in the attenuator design. Each selective channel may consist of a buffer amplifier, a

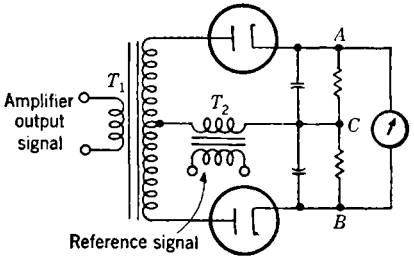

FIG. 9·22.—Coherent-signal detector.

selective amplifier, and a coherent-signal detector. If the twin-T networks are aligned carefully with the aid of standard audio test equipment, Q's of 50 may be realized.

The greatest improvement over the conventional amplifier may be achieved through the use of a coherent-signal detector. In fact, the use of a coherent-signal detector even with conventional circuits is strongly recommended since it will reduce the pass band to about 1 cps. The twin-T selective stages should not be omitted since they remove a great deal of noise and interference prior to the detector. The principle of operation of the coherent-signal detector is illustrated by the simple diode circuit of Fig. 9·22 which is the equivalent of a hybrid coil or a low-frequency magic T. The output signal from the amplifier is coupled into T_1, and the resultant voltages between A and C and between B and C are equal and cancel unless a reference signal is coupled into T_2. If the reference signal is coherent with some component of the amplifier output signal, and if the two signals have the proper relative phase, the reference signal will reinforce the coherent component of the amplifier signal for one diode, but will reduce the component presented to the other diode. Consequently, coherent signals produce a net voltage between A and B, and if the signals have the proper relative amplitudes, the

meter deflection will be proportional to the coherent component of the amplifier output signal.

In practice, the reference signal is obtained by filtering the output signal from a multivibrator. The resultant signal is passed through a variable phase-shift network which is adjusted for maximum meter deflection. The simple circuit of Fig. 9·22 may have many variations. The transformers may be replaced by vacuum-tube circuits, and the diodes may be replaced by triodes, pentodes, or pentagrid tubes. The use of two tubes is recommended since the zero set of the meter will, in that case, be less subject to power-line variations.

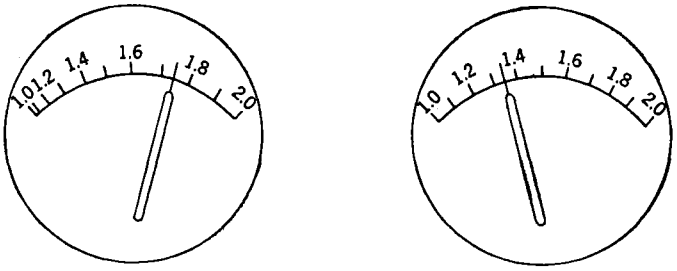

FIG. 9·23.—Meter scales for use with a square-law detector.

If the selective amplifier is constructed in accord with the previous design considerations, it should be possible to realize a stable full-scale meter deflection for r-f power levels as low as −90 to −100 dbw.

Since the detector is very nearly a square-law device, and since this amplifier is very linear, the output meters can be calibrated in terms of r_t. A cramped scale results, as shown in Fig. 9·23, but it may be expanded by altering the shape of the pole pieces.

9·17. Range of Measurement.—Since each r-f oscillator delivers square-wave-modulated power at an average power level of −20 dbw, and since the crystal detector and conventional amplifier provide full-scale meter deflection when the received power level is −80 dbw, a line attenuation of 60 db can be tolerated. If the attenuation between each oscillator and the T is 15 db, and if the attenuation between the T and the detector is 10 db, an attenuation through the T of 37 db corresponds to full-scale deflection. However, since $\frac{1}{5}$-scale deflection can be used as a reference level, the attenuation through the T can be 44 db.

If calibration is made relative to a reference mismatch whose VSWR is 1.20, the corresponding attenuation through the T is 27 db. If the reference deflection is $\frac{1}{5}$ scale, the calibrating attenuator can have an

insertion loss that is equivalent to a line attenuation of 17 db. Since this effective attenuation is reduced in order to regain reference deflection when the test-piece reflections are small, r_t's down to 1.025 can be measured. If the calibrating attenuator can increase the effective line attenuation 11 db (relative to that when the VSWR is 1.20), then a maximum r_t of 2.00 can be measured.

Although the calibrating attenuator is useful for accurate measurements, the meter is used to judge the success of test-piece matching procedures. If the meter is modified so that its sensitivity decreases with increasing deflection, and if the reference deflection is still $\frac{1}{3}$ scale, then the scale can be nearly linear in r_t from 1.0 to 2.0.

Since a bridge T cannot be balanced perfectly over a wide range of frequencies, the sensitivity of the system is not always the limiting factor in the measurement of small reflections. In many cases the bridge unbalance is equivalent to an r_t of 1.02, and consequently it is hardly worth while to extend the calibration below an r_t of 1.05. If the lower limit is set at 1.05, the calibrating attenuator need introduce only 11 db of loss at the reference VSWR of 1.20, and an additional safety margin of 6 db is realized. However, in order to maintain the signal level in the range of square-law detection, it may be advisable to insert a variable level-set attenuator between each oscillator and the coupling network. If the amplifier provides a stable full-scale indication at -90 dbw instead of -80 dbw, the isolating attenuations between the T and the oscillators and detector can be increased, for example, 6 and 4 db, respectively, and the phase error will be reduced.

IMPEDANCE BRIDGES THAT EMPLOY PULSE MODULATION

The principle of operation for pulse-modulated impedance bridges is discussed in Sec. 9·12 with reference to Fig. 9·20. Several r-f oscillators are pulsed in sequence, and their output signals are coupled through the bridge T to a crystal detector. The detector is followed by a pulse amplifier which provides vertical deflection for a cathode-ray tube. The amplitudes of the resultant pips that appear on the cathode-ray tube indicate the amount of power reflected from the test piece at several corresponding frequencies.

9·18. Microwave Sources.—Because a pulse amplifier has a wider pass band and hence less sensitivity than a selective audio amplifier, the pulse method and the modulation-frequency method will provide comparable over-all sensitivities only if the pulsed oscillators deliver relatively higher powers. When a reflex oscillator is employed, the available pulse power is usually no greater than the available c-w power since the modes of oscillation, as well as the dissipation, determine the maximum voltages that may be applied to the tube. Whereas low-

voltage local-oscillator tubes can be used for the modulation-frequency method, the pulse method employs tubes that require voltages in the range of 1000 to 2000 volts. Since these tubes have beam currents between 50 and 100 ma, a large power supply is necessary unless the tubes are turned off, as well as driven out of oscillation, between pulses. Consequently, anode or grid modulation is preferred to reflector modulation, and the recurrence frequency should be as low as possible.

In order that a single power-supply design can serve equally well for different sets of r-f components, it is wise to choose tubes that have similar d-c characteristics. Over the frequency range from 3300 to 10,300 Mc/sec, the 2K42, 2K43, 2K44, and 2K39 tubes are a good choice since they will deliver about 250 mw. They operate with about 1250 volts applied to the anode, draw a beam current of about 45 ma, and have a focus electrode whose bias may be varied to control beam current. Since this bias may be slightly negative, pulsing may be accomplished with a high-impedance modulator; that is, no driving power is required.

The 2K33 tube, which operates in the 24,500-Mc/sec region, may be pulsed in a similar manner, but requires 1800 volts. The beam current is only about 8 ma, and the output power does not often exceed 25 mw. Although the output power is no greater than that which can be obtained from a low-voltage tube, a high-voltage power supply that employs an oscillator can be equipped with plug-in coils in order to allow the use of this tube.[1]

The 2K41 tube, the present design for an output power of 250 mw from 2650 to 3320 Mc/sec, has a mesh grid instead of a focusing ring. This grid is operated at a positive bias of between 0 and 50 volts. Since considerable grid current is drawn, a modulator must be capable of supplying an 80-volt pulse at about 17 ma. Since the average power consumption is very low, these drivers can be operated from the common low-voltage power supply in the bridge without increasing its capacity. The drivers can be coupled to the multivibrators which serve as modulators for the oscillators of other types, and can be mounted beside the 2K41 tubes so that they are part of the r-f package for the 3000-Mc/sec region.

If a conventional regulated supply is used, it is probably more economical to design it for 1250 volts, and use 2K50 tubes instead of 2K33's. Accordingly, the low-voltage supply is designed to withstand the current drain of the 2K50's, and modulation is applied to the reflector electrodes.

9·19. Line Components.—With a few exceptions, the line components for pulse-modulated bridges are the same as those discussed in Sec. 9·15 for the modulation-frequency method. The high-voltage reflex oscil-

[1] A power supply of this type is described in Chap. 2.

lators are not designed to operate with a matched load, and hence double-stub tuners should be inserted between each oscillator and the line. Also, these tubes have coaxial output fittings so that waveguide-to-coaxial-line adapters are necessary in many cases.

Since the oscillators are coupled to the other line components by means of cables, they may be mounted on the front panel and enclosed by a common shield. Good shielding is necessary because these tubes do not have all-metal shells and there is considerable r-f leakage from the glass portions.

Many of the high-voltage oscillators are still being improved and redesigned, and hence the available output power may vary considerably from tube to tube. Consequently, level-set attenuators should be installed between each oscillator and the coupling network. For this purpose, frequency sensitivity and gradual changes in attenuation are unimportant, and satisfactory attenuators can be made in which the absorbing elements are tapered strips of resistance-card material. For coaxial-line components, a cam-driven flap of this material may be inserted through slots in the outer and inner conductors.

9·20. Pulse Amplifier.—In order to provide reasonable reproduction of the pulse, arbitrary limits place the lower cutoff frequency at five times the recurrence frequency, and place the upper cutoff frequency at about 1.5 times the reciprocal of the pulse duration. The pulse will rise rather slowly, and the trailing edge will have considerable overshoot. This overshoot is not troublesome since it can be removed by a diode which also clamps the CRT baseline against the effects of varying pulse amplitudes.

If the duty ratio is limited to $\frac{1}{150}$ by the power-supply requirements, then for a given quality of pulse reproduction the narrowest pass band is realized at the lowest possible recurrence frequency. Although this consideration produces a narrow pass band, optimum sensitivity may not be realized because considerable instability is introduced in the lower audio-frequency range by the power-line frequency and its harmonics, by microphonics, and by flicker effect. On the other hand, above 25 kc/sec, sensitivity is determined primarily by statistical noise, and increasing bandwidth results in decreasing sensitivity.

Consequently, optimum sensitivity can be realized if the lower cutoff frequency is about 10 kc/sec. This means that a recurrence frequency of 2000 cps and a pulse duration of 33 μsec can be used, and the upper cutoff frequency for the amplifier will be 45 kc/sec. If the detector is a video crystal with a figure of merit of at least 50, a sensitivity of -91 dbw can be realized. However, the minimum usable signal is about 10 db above the noise level, so that a useful sensitivity of -80 dbw is achieved. Figure 9·24 shows a pulse amplifier that is slightly less sensitive because

it is designed for a recurrence frequency of 60 cps and a 100-μsec pulse. The cutoff frequencies are 300 and 15,000 cps.

In Sec. 9·16 the full-scale sensitivity of an ordinary selective amplifier was given as −80 dbw, and it is mentioned later that this sensitivity is greater than that of a pulse amplifier. This statement is still true since

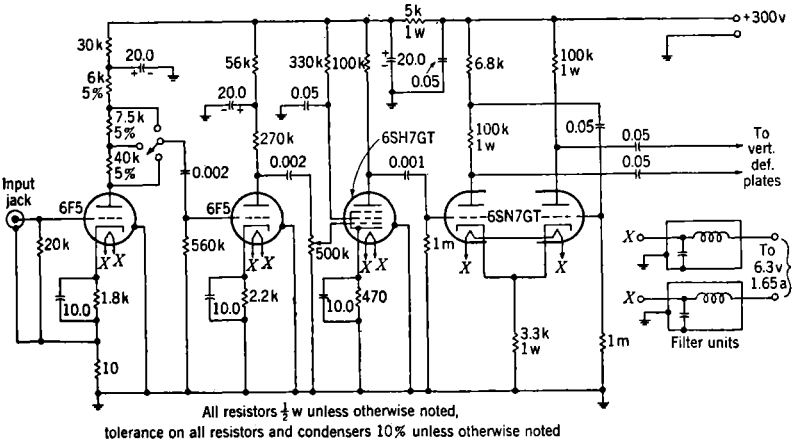

FIG. 9·24.—Typical pulse amplifier.

a power level of −80 dbw produces the minimum usable pip for a pulse-modulated bridge, not a stable full-scale indication as for the modulation-frequency bridge.

9·21. Range of Measurement.—Since each r-f oscillator will deliver a pulse power of −6 dbw, and since a power level of −80 dbw produces the minimum usable pip, a total line attenuation of 74 db can be tolerated. If the attenuation between each oscillator and the bridge T is 15 db, and if that between the T and the detector is 10 db, an attenuation of 49 db through the T can be measured. Since an attenuation of 46 db corresponds to an r_t of 1.02, the range of measurement is limited by other factors, such as bridge unbalance.

If a minimum r_t of 1.02 is to be measured, 3 db of line attenuation are available as a margin of safety. If the minimum r_t is 1.05, the attenuation through the T is 38 db, and the isolating attenuation may be increased about 10 db in order to reduce the phase error.

Calibration may be achieved in a manner similar to that described in Sec. 9·17 for the modulation-frequency bridge. Accurate measurements are made by using an a-f or r-f attenuator in conjunction with a reference mismatch. The face of the cathode-ray tube may be calibrated to judge the success of test-piece matching procedures, but, as in the case

of the linear meter, the calibration will be nonlinear. This problem may be alleviated somewhat by providing a double scale as shown in Fig. 9·25. The left-hand scale is used with a reference mismatch that produces a VSWR of 1.20, and calibration is made at maximum deflection. In order to use the right-hand scale, without the necessity of recalibration, a switch can be employed to reduce the amplifier gain by a factor of 10.

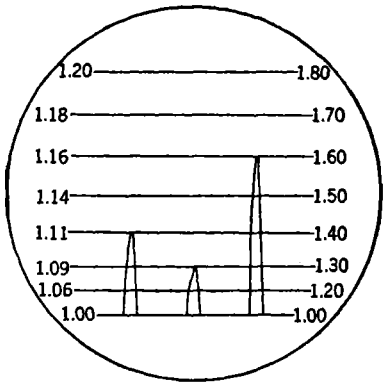

FIG. 9·25.—CRT calibration for pulse-modulated impedance bridges.

IMPEDANCE BRIDGES UTILIZING PANORAMIC RECEIVERS

Chronologically, panoramic bridges were developed first because receiver components were available and because adequate sensitivity is assured even with low-power oscillators as microwave sources. The principle of operation is described in Sec. 9·12 with reference to Fig. 9·21. Although pulse-modulated bridges have been engineered in view of production, the TBX-1BR bridge shown in Figs. 9·26 and 9·27 is the only type that has been produced commercially. It operates in the frequency range from 8500 to 9600 Mc/sec, and was produced by the Boonton Radio Corporation for the Radiation Laboratory.

9·22. Microwave Sources and Local Oscillators.—Low-voltage reflex oscillator tubes such as the 2K28, 726, 2K25, or 2K50 may be used as microwave sources and local oscillators for the heterodyne receiver. By operating the oscillator cathodes at ground potential, a common power supply may be used for the receiver and other low-voltage circuits. Since the tube shells will be 300 volts above ground, good insulation must be provided between the mechanical tuning shafts and the tubes. Also, because of the high sensitivity of the receiver, the oscillators should be provided with all the leakage-protection devices described in Sec. 9·13.

A total of six oscillators, three of which are frequency-modulated, is required to produce indications at three microwave frequencies, and it is not surprising that spurious signals result because of cross-modulation in the crystal mixer. Since no spurious signal can exceed the fundamental components introduced by the r-f oscillators, and since the frequency-modulated oscillators are more likely to produce spurious responses, there is a definite advantage to modulating the microwave sources because their signals are attenuated about 85 db before reaching the detector. Consequently, the main problem is the c-w local-oscillator

signals and their harmonics that can cross-modulate at a level high enough to block the receiver. This difficulty was removed from the TBX-1BR bridge by using a motor-driven switch that operated the local oscillators sequentially instead of simultaneously.

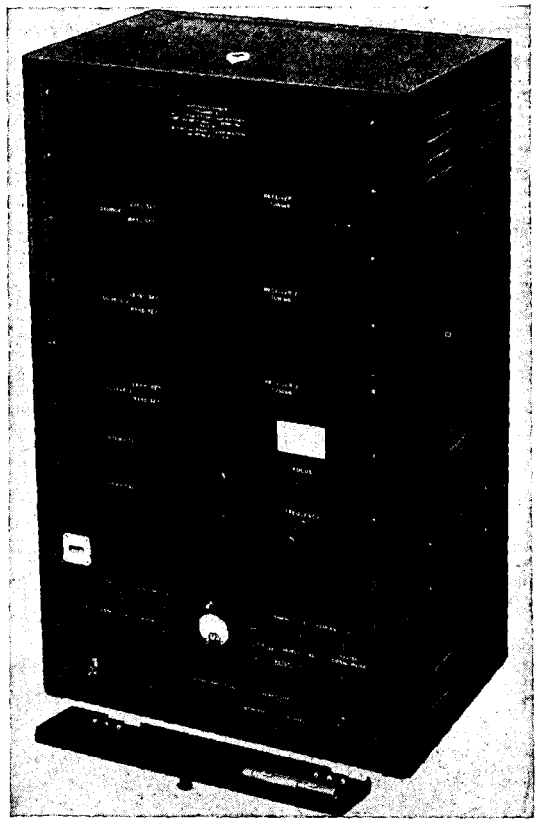

FIG. 9·26.—Front view of TBX-1BR impedance bridge.

The microwave sources are frequency-modulated by applying sawtooth signals to the reflector electrodes. The total frequency deviation is about 10 Mc/sec in order to generate pips each of which occupies about 10 per cent of the CRT horizontal trace. The horizontal position of each pip is controlled by adjusting the d-c reflector voltage for the corresponding microwave source. Reflector-voltage variations shift the pip with respect to the sweep since they shift the operating frequency with respect to the modulation.

9·23. Line Components.—Since the heterodyne receiver provides more than adequate sensitivity, the line components may include sufficient attenuation so that the impedance mismatches of the oscillators and the detector do not increase the phase error excessively over that which results from the T itself. This may be achieved on the input side

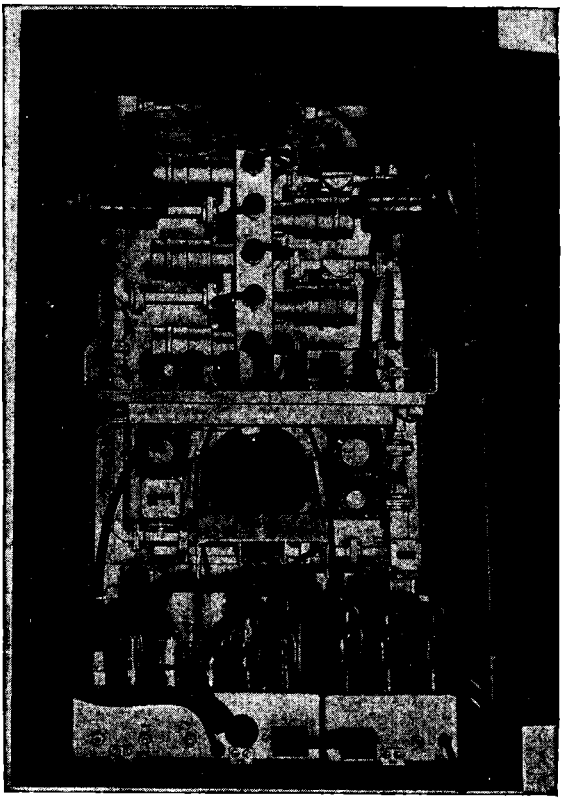

FIG. 9·27.—Rear view of TBX-1BR impedance bridge.

of the T by coupling the oscillators to the input line by 12-db directional couplers, and by inserting 10 db of matched attenuation between the couplers and the T. If the couplers are so spaced that their individual reflections do not combine adversely, the VSWR looking back from the T will not exceed 1.05. If the detector is preceded by 13 db of matched attenuation, the VSWR seen by the output arm of the T will not exceed 1.05. Although the coupling networks and the isolating attenuators have introduced 35 db of the line attenuation, the high sensitivity of the

system will still allow the use of level-set attenuators which normally are adjusted for 5 db of attenuation in order to compensate for decreases in the output powers from the oscillators.

The r-f components of the TBX-1BR impedance bridge exemplify the good mechanical arrangements that can be achieved with directional couplers. Since this bridge uses an unmatched side-outlet T, the isolating attenuation is particularly important in order to prevent an already large phase error from increasing. As shown in Fig. 9·27, the microwave sources deliver power through their level-set attenuators to the 11-db directional couplers on the right-hand side of the photograph. Power from the couplers is attenuated approximately 4 db by a metalized-glass pad, and then enters the *E*-arms of the T. Output power from the *H*-arm is attenuated about 4 db by another pad and is coupled through a 10-db directional coupler to the crystal mixer. The isolating pads are adjustable from nearly 0 to 6 db. Since they introduce small reflections themselves, and since the mismatches that they isolate vary slightly from one unit to another, the pads are adjusted for an optimum match looking into the test arm of the T. This adjustment is made with the aid of another impedance bridge. Between the isolating coupler and the mixer are the directional couplers by which the local oscillators are coupled to the mixer. These couplers and tube mounts are identical with those used for the microwave sources, and production costs are minimized by using a common design for the two similar functions. Note that the reaction frequency meter is placed between the isolating coupler and the local oscillators, and, accordingly, the reaction on a pip indicates the frequency of the signal transmitted through the T. If the meter were placed next to the mixer, it would cause confusion by producing reactions when tuned to the local-oscillator frequency.

The T is oriented so that the test arm protrudes through the front panel, and the reference match is coupled to the open junction which appears in Fig. 9·27. No r-f attenuator is included as a calibrating device, but it could be installed by removing the 4-db pad that follows the T. When used with a reference mismatch whose VSWR is 1.20 the attenuator must provide 11 db of attenuation at the reference level in order to measure an r_t as small as 1.05. In addition to serving as a calibrating device, this attenuator would provide increased isolation when the phase error tends to be large, and less isolation, but more sensitivity, when the phase error tends to be small.

9·24. Receiver.—Although the TBX-1BR impedance bridge employed a standard W-5 i-f amplifier and preamplifier in order to expedite production, a more suitable receiver could be designed for this application. The W-5 receiver strip and preamplifier provide 7 i-f stages, a diode detector, and two video stages. The intermediate fre-

quency is 30 Mc/sec, and the bandwidth is about 2 Mc/sec. Since a recurrence frequency of 60 cps is used in order to synchronize hum modulation, it is necessary to modify the video amplifiers designed for radar applications. This receiver provides a reliable sensitivity of about −120 dbw, and very stable operation at a microwave power level of −100 dbw. A more suitable receiver would provide a narrower pass band and hence could achieve greater sensitivity. The limit to which the pass band may be narrowed is determined by the duration of the i-f pulse that is generated. If the recurrence frequency is 60 cps, the pulses can have long durations, and the instability that tends to result from hum modulation is eliminated by synchronization. In addition, a more selective receiver is more economical since a high gain per stage can be realized with low current drain from the power supply.

9·25. Range of Measurement.—Since the microwave sources deliver power at a level of −16 dbw, and since the receiver has a sensitivity of −120 dbw, a line attenuation of 104 db will result in a signal equal to noise. If the line components introduce 38 db of attenuation, and if a signal level 20 db above noise is chosen from stable operation, the test-piece reflection must be large enough so that the attenuation through the T does not exceed 46 db. This corresponds to a minimum r_t of 1.02. If an r-f calibrating attenuator precedes the mixer, 6 db of isolating attenuation can be removed on the output side of the T, and the lower limit for r_t is 1.01. Over a wide range of frequencies, bridge unbalance usually will not justify extending the calibration to this low limit.

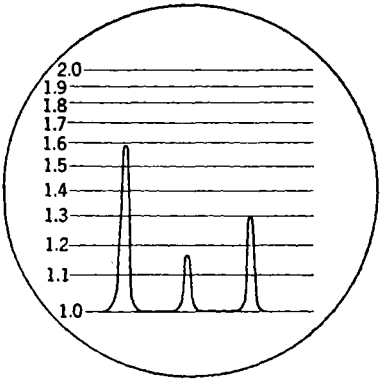

FIG. 9·28.—CRT calibration for panoramic impedance bridge.

If the receiver is linear, the CRT deflection is proportional to the magnitude of the test-piece reflection coefficient. Accordingly, a screen calibrated for r_t would appear as shown in Fig. 9·28.

CALIBRATING DEVICES AND SOURCES OF ERROR

There are three methods by which an impedance bridge can be calibrated in terms of r_t. An adjustable load can be calibrated and coupled to the bridge to produce an indication equal to that produced by the test piece. Although this is not a desirable method for measuring r_t, it is a convenient way of establishing an acceptance level for produc-

tion testing. A more desirable method uses a reference mismatch and a variable calibrated attenuator. The attenuator introduces or removes an amount of line attenuation equivalent to the ratio of the reference-mismatch and test-piece power reflections. However, this calibrating method necessitates coupling an accessory to the bridge. The ideal method is one in which a calibrating signal is produced by merely turning a switch while the test piece can remain coupled to the bridge. Since r_t is related to attenuation through the T, this method is achieved by using an r-f switch to direct the power around the bridge element and to the detector through an attenuation equivalent to some reference standing-wave ratio.

9·26. Adjustable Reference Mismatches.—The adjustable reference mismatch that was developed for use with the TBX-1BR impedance bridge consists of a micrometer-driven steel rod that protrudes from a well-matched polyiron termination. The combined reflections of the rod and the termination produce a voltage standing-wave ratio that is very nearly proportional to the micrometer adjustment from 1.20 to 1.50. The reflecting elements slide within the waveguide casing, and the effects of phase error and bridge unbalance may be averaged by "phasing" the reflection to produce maximum and minimum indications.

Since the device is frequency-sensitive, individual calibration charts were prepared. Each chart was a family of constant-VSWR contours for corresponding frequencies and micrometer settings. Although single-frequency plots of VSWR versus micrometer setting produced smooth, reproducible curves, the final charts were very erratic. The cause of these variations has not been determined completely, but their existence makes the device of dubious value. In addition, although the data were reproducible on the same day, the hygroscopic nature of the polyiron made the calibration subject to humidity conditions.

9·27. Fixed Mismatches and Calibrated Attenuators.—The simplest fixed mismatch can be made by placing an iris just ahead of a well-matched termination. The iris is soldered in place and then filed until the desired reflection is produced. Although the device will be frequency-sensitive, this variation can be minimized by making the reflection from the termination very small, by placing the iris very close to the termination, and by keeping the iris flat. Another type of mismatch can be made from a purposely mismatched resistive attenuator. Some of the absorbing material is removed from the leading edge of the strip, and the position of the strip in the waveguide is adjusted to produce the desired reflection. If the line is short-circuited at some point after the strip, the position of the terminating plate may be adjusted so that its reflection, reduced by the attenuating strip, is of the proper phase to minimize the over-all frequency sensitivity.

If an audio or video attenuator is used with the reference mismatch, the law of the detector must be known accurately. The attenuator can be made sufficiently accurate so that the detector law is the important factor. Measurements indicate that at low power levels, a crystal is very nearly a square-law detector. If the power level is increased 20 db from about −80 dbw, a crystal detector and audio attenuator will measure the increase as about 18 db, an error of about 2 db. Although this error in attenuation may seem large, the error in measuring r_t will not be excessive for production-testing applications.[1]

If a calibrated r-f attenuator is employed, the law of the detector is unimportant, but the problem of frequency sensitivity arises. Actually,

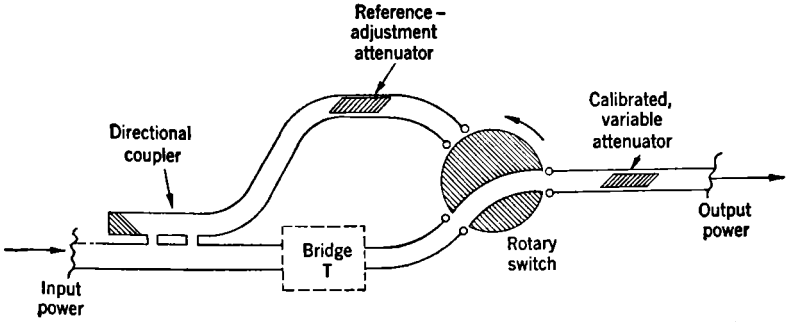

FIG. 9·29.—Built-in calibrator that employs a single directional coupler.

the frequency sensitivity of total attenuation is not important if a range of about 20 db can be obtained for which the slope of the calibration curve is frequency-insensitive. This procedure requires that some additional loss can be tolerated and that the power levels at each frequency can be adjusted to compensate for the frequency sensitivity of total attenuation. Metalized-glass attenuators are somewhat frequency-sensitive as to both total and incremental attenuation, and the calibration curves at different frequencies cross over one another. Consequently, it is desirable to plan a crossover region that corresponds to the attenuation at the reference level.

If the calibration is to cover a range of r_t from 1.05 to 1.90, a logical choice for the reference-mismatch VSWR is 1.20. In this case the calibrated attenuator must provide deviations of ±11 db, and the drive mechanism can employ a special cam so that the scale is linear in r_t. This scale can be made sufficiently expanded so that the error in reading is negligible.

9·28. Built-in Calibrators.—A directional coupler and r-f switch may be used as shown in Fig. 9·29 to bypass the T and to provide a signal equivalent to that produced by, for example, an r_t of 1.20. The

[1] The magnitude of the error in r_t is mentioned in Sec. 9·7.

line attenuation equivalent to an r_t of 1.20 is 26.8 db, and the small trimming attenuator is adjusted accordingly. The coupler should be designed to provide an attenuation of about 25 db. There are other arrangements of the components, such as interchanging the coupler and switch, that will work almost as well. For most cases, considering the usual mismatches in the various line components, the arrangement shown will minimize the error caused by reflection losses. R-f leakage must be minimized in all cases, and a coupler design, such as the Schwinger type, should be chosen in order to avoid the necessity of a correction curve for the frequency sensitivity of coupling.

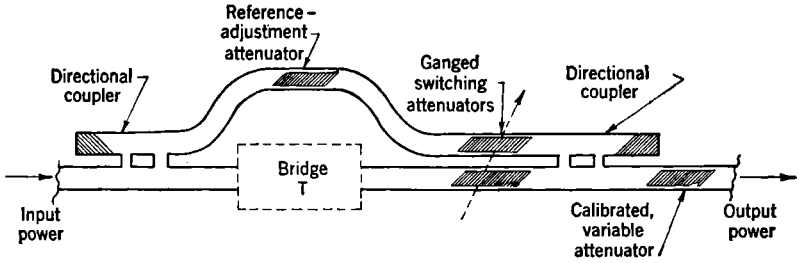

FIG. 9·30.—Built-in calibrator that employs two directional couplers.

A similar method is shown in Fig. 9·30. Two directional couplers are employed, and switching is accomplished by two attenuators which are operated by a single cam drive so that attenuation is introduced in one line as it is removed from the other line. The attenuators should be variable from about 0 to 40 db. This method may prove more expensive from the standpoint of components, but different designs can be chosen for the two couplers so that their frequency sensitivities tend to cancel.

Since the errors resulting from the calibrated attenuator are the same for this as for other methods of calibration, the error of interest is that incurred in the reference-level determination. If it is assumed that a VSWR of 1.20 can be measured to ± 0.01 by, for example, slotted-section techniques, then the built-in calibrator must have its insertion loss of 27 db known to ± 0.40 db for comparable accuracy. This accuracy applies to matched line components, and since reflection losses can be between 0 and 0.15 db in practice, the attenuation should be measured to ± 0.25 db. It was shown in Sec. 9·7 that a slightly asymmetrical T does not introduce appreciable power-split error, and hence this error is not considered here.

9·29. Sources of Error.—Although the sources of error can be enumerated, it is difficult to estimate the over-all error unless a specific bridge design is considered. In general, the output signal from bridge unbalance

will be equivalent to an r_t of between 1.01 and 1.02. If a rotating post within the T, or an adjustable reference match, is employed, a sliding match can be used on the test arm to facilitate optimum bridge balance at several frequencies simultaneously. By following this procedure and by checking it over the entire operating range of frequencies, bridge unbalance should not exceed 1.01.

Phase error is given by Fig. 9·2 and amounts to ± 0.01 when r_t is 1.60 and the VSWR looking into the test arm is 1.10. This is a very well-matched T, and does not include the reflections from a mismatched generator and mismatched detector. In practice the VSWR looking into the side arm may be 1.50 and the corresponding phase error is ± 0.036 for an r_t of 1.60. For small test-piece reflections, the phase error is usually unimportant.

The other main source of error is the method of calibration. For accurate measurements, the detector is used as a reference indicator whose level can be reproduced to approximately 1 per cent. A reference mismatch, or built-in calibrator, is used with a calibrated attenuator to measure r_t. If the reference level corresponds to a VSWR of 1.20, it can be determined to ± 0.01. If the attenuation relative to this level is known to ± 0.1 db, an r_t of 1.60 will be in error by ± 0.008. For small r_t's the attenuation error is unimportant. If a reference mismatch is used which is not of the sliding type, the phase error can enter into the calibration procedure. In estimating over-all error, however, this factor will not be included since a sliding mismatch or built-in calibrator could be employed.

Over-all error for a multifrequency impedance bridge is shown by Table 9·1. Errors that might arise from r-f leakage, incorrect side-arm dimensions, instability, and an illegible attenuator dial are not considered. Also, it must be remembered that the errors in the table apply only to the hypothetical bridge considered in this section.

TABLE 9·1.—PROBABLE ERROR FOR TYPICAL IMPEDANCE BRIDGE

Source of error	Error in r_t	
	$r_t = 1.05$	$r_t = 1.60$
Bridge unbalance equivalent to an r_t of 1.01	±0.011	±0.017
Phase error for test-arm VSWR = 1.50	0.000	0.036
Reference-level reproducibility of 1 per cent	0.000	0.004
Reference VSWR = 1.20 ± 0.01, or equivalent attenuation	0.002	0.035
Calibrated attenuator error of ±0.1 db	0.000	0.008
Maximum error	±0.013	±0.100
Probable error	±0.011	±0.054

CHAPTER 10

THE MEASUREMENT OF DIELECTRIC CONSTANTS

By R. M. Redheffer

INTRODUCTION

In an ordinary material, which is the only type to be considered here, the electromagnetic field equations are linear, and the properties of the material that are relevant to a study of these equations may be completely specified by two complex constants. These constants, called the *complex dielectric constant* and the *complex permeability*, are designated respectively by ϵ_0 and μ_0 (real) for free space and by ϵ and μ (complex) for the material; ϵ and μ are usually separated into real and imaginary parts, with the notation

$$\epsilon = \epsilon' - j\epsilon'' = \epsilon'(1 - j \tan \delta) = \epsilon_0 k_e(1 - j \tan \delta), \qquad (1)$$
$$\mu = \mu' - j\mu'' = \mu_0.$$

The equation for μ is true for most nonmetallic materials, including all those with which the present discussion will be concerned. The dimensionless quantity $\tan \delta$ in Eq. (1) is called the *loss tangent;* it is equal to the power dissipated divided by the power stored per cycle (Refs. 2b to 5b)[1] and is thus a measure of the energy lost in the form of heat when a wave is propagated through the material. The quantity k_e, likewise dimensionless, is properly called the *specific inductive capacity;* in the present text, however, k will be written in place of k_e and referred to simply as the *dielectric constant.* Since the parameters ϵ_0 and μ_0 for free space are known, being in fact determined by the choice of measuring units, it is clear that the two constants k and $\tan \delta$, rather than ϵ' and ϵ'', may be used to specify any given material, and these quantities will be taken as fundamental throughout the ensuing discussion.

For reasons which are too well known to require enumeration here the values of k and $\tan \delta$ are frequently required in both industrial and laboratory work. With especial regard to experimental procedures as well as theoretical principles, and with emphasis on results rather than on derivations, it is the purpose of the present chapter to describe the chief means by which these parameters are evaluated at microwave frequencies. Certain of the methods of measurement in the microwave

[1] All references in text are to the Bibliography at the end of chapter.

region are similar, as far as principles are concerned, to the standard techniques used in other frequency ranges. For various reasons, however, there is little in common besides this similarity of principle, the details of equipment and procedure being different from those of either the ordinary electrical or the optical frequencies. The necessity of preventing radiation requires rather extensive modification of the low-frequency techniques. The optical methods, on the other hand, are not directly applicable because of the reduced sample dimensions, as measured in terms of wavelengths, and, until recently, because of the difficulty of obtaining a constant frequency from a microwave generator. The method of detection is unlike those customarily used in either the low- or high-frequency ranges, moreover, as are the procedures for determining impedance or wavelength; and for microwaves, resonant-cavity techniques may be used which would be impractical in other cases. Because of these differences, microwave measurement of k and tan δ should be approached as a field of study in its own right, even though the same problem has been extensively investigated for neighboring ranges of the spectrum.

10·1. Derivation of Relations for Proceeding from Data to Results.— Since the electromagnetic behavior of the material is completely specified by the parameters in question, it is possible to find their values by many different methods; in principle, practically any measurable effect the material may have on an electromagnetic field can be used for such a determination. If a wave of known wavelength λ is incident upon a plane sheet of known thickness d, for example, there will be a certain transmission coefficient $te^{-it'}$ and a certain reflection coefficient $re^{-ir'}$, all quantities permitting direct measurement. In principle, any two of the four values t, r, t', and r' usually suffice to determine both k and tan δ, whereas if tan δ is known to be negligible, only one measurement is needed for k. There is, to be sure, an ambiguity in that an infinite set of values of k and tan δ will reproduce the observed data; but this difficulty, which is often encountered when the minimum possible number of measurements are used, may be avoided in practice by making a suitable estimate of the true value, or by repeating the measurement with slightly different initial conditions as will be described. It is clear that the experiment can be performed at a known angle of incidence θ_0 or in a waveguide of known properties; and, instead of a direct measurement of t, t', r, and r', a determination of related quantities, such as the angle of incidence for minimum reflection, the thickness for minimum reflection, or the cutoff wavelength of the filled guide, can be made. Further variation may be obtained by changing the so-called "termination" of the sheet which, instead of being backed by free space or by a matched load, may be backed by any suitable source of reflection; for

example, it may be backed by a second sheet similar to the first, by a metal plate, or by a termination that eliminates the reflection at the second air-sample interface. In all such cases two electrical measurements usually suffice to determine both k and tan δ, whereas with negligible loss only one measurement is required for k.

Because of this great variety of methods which, in principle, make possible the evaluation of k and tan δ, it is inexpedient to derive the necessary theoretical expressions afresh for each case. Such an approach not only leads to an exposition of excessive length, but also obscures

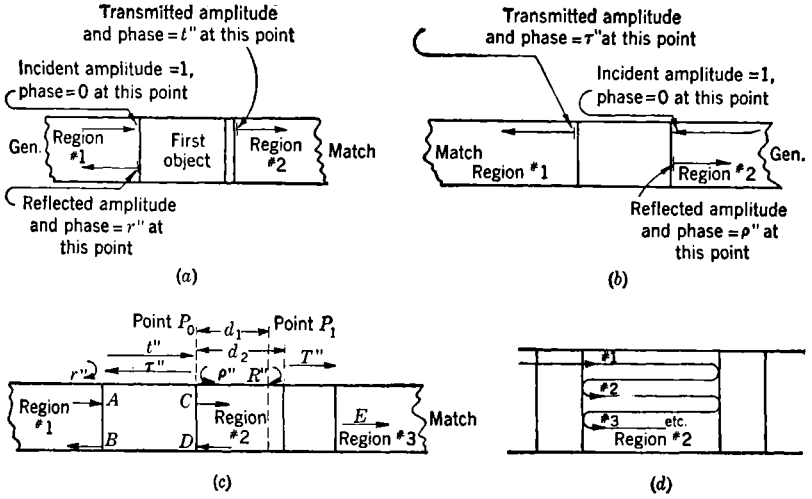

FIG. 10·1.—Reflection and transmission coefficients for one or two objects.

the underlying unity of the methods, giving an impression of complete independence that does not correspond to the facts. Instead of this procedure of obtaining each equation from first principles as it is required, the following four results are presented, which are found to include every relation for the transition from measured to desired quantities which will be needed in twenty-eight of the thirty methods here considered.

A Basic Configuration.—If the complex transmitted and reflected amplitudes in Fig. 10·1 are proportional to the incident amplitudes, and if the fields in the indicated regions of Fig. 10·1*c* can be resolved into one or two waves as there shown, then the complex amplitude of the resultant wave moving from left to right at point P_0 of that figure will be given by

$$C = \frac{At''}{1 - \rho''R''e^{-2j\beta d_1}}, \tag{2}$$

where

$$j\beta = \frac{2\pi}{\lambda_2} \tag{3}$$

and λ_2 is the wavelength in region No. 2, which is assumed to be lossless. The complex coefficients t'', τ'', r'', ρ'' are defined in Figs. 10·1*a* and *b*, and R'' and T'' are to be similarly interpreted; the propagation constant for general media is defined in the next section.

Because of the importance of this result in the sequel, two derivations of it are given. Thus, the wave in question is equal to the sum of waves (1), (2), (3), · · · in Fig. 10·1*d* provided the sum is evaluated with due regard to phase; thus (cf. Ref. 7*b*),

$$C = At'' + At''(R''\rho''e^{-2j\beta d_2}) + At''(R''\rho''e^{-2j\beta d_2})^2 + \cdots + ,$$

which is equivalent to Eq. (2), since the series is obviously convergent. For the second derivation, it should be noted that the amplitudes A, B, · · · satisfy the relations (Ref. 6*c*)

$$\begin{aligned} D &= R''e^{-2j\beta d_2}C, \\ C &= At'' + D\rho'', \\ B &= Ar'' + D\tau'', \\ E &= T''e^{-j\beta d_2}C, \end{aligned} \tag{4}$$

by virtue of the superposition principle and the definition of t'', τ'', · · · . The solution of this system for C/A again gives Eq. (2).

If the wave in region 2 is allowed to travel to the second source of reflection, and through it,

$$\frac{E}{A} = \frac{t''T''e^{-j\beta d_2}}{1 - \rho''R''e^{-2j\beta d_2}} \tag{5}$$

is obtained for the transmission coefficient of the whole arrangement; and similarly,

$$\frac{B}{A} = r'' + \frac{R''t''\tau''e^{-2j\beta d_2}}{1 - \rho''R''e^{-2j\beta d_2}} \tag{6}$$

for the over-all reflection. Analagous procedure gives D, the amplitude of the wave moving from right to left at point P_0 of the figure. If this is added to the amplitude C, with due regard to phase, the field at the arbitrary point P_1 between the two objects, Fig. 10·1*c* is

$$\frac{At''e^{-j\beta d_1}[1 + R''e^{-2j\beta(d_2 - d_1)}]}{1 - \rho''R''e^{-2j\beta d_2}}. \tag{7}$$

These equations, which are immediate corollaries of the fundamental Eq. (2), may also be derived from the system of Eq. (4); their relevance to the theory of dielectric measurement will become apparent in the ensuing discussion.

Interface Reflection.—Like Eq. (2), the following result also will be used repeatedly for relating k and $\tan \delta$ to measured quantities: If a plane wave is incident normally on the interface between two lossless dielectrics k_1, k_2, then the complex reflection coefficient will be given by

$$r_i e^{-ir'_i} = \frac{\sqrt{k_1} - \sqrt{k_2}}{\sqrt{k_1} + \sqrt{k_2}}, \tag{8}$$

and the complex transmission coefficient by

$$t_i e^{-it'_i} = 1 + r_i e^{-ir'_i} = \frac{2\sqrt{k_1}}{\sqrt{k_1} + \sqrt{k_2}}. \tag{9}$$

The wave is assumed to be traveling from the medium with constant k_1 to that with constant k_2. The variation of r_i, or $t_i - 1$, with k_1/k_2 is shown in Fig. 10·2*a*. A special case of the Fresnel equations, this result may be found in any text on optics; it is rigorously derived in Ref. 1*b*.

Arbitrary Incidence or Waveguide.—There will frequently be occasion to analyze measurements made in waveguide or at arbitrary incidence, as well as those for free space at normal incidence. On the other hand, a separate derivation of the results appropriate to these modified situations is undesirable for reasons already stated. It is easily shown, however, that any relation of the type under consideration here may be used in these more general circumstances, if β of Eq. (2) and its corollaries, and k of Eqs. (8) and (9), be replaced by appropriate quantities as indicated in Table 10·1 (cf. also Fig. 10·2*b*).

TABLE 10·1.—EQUIVALENCE RELATIONS FOR OBTAINING EQUATIONS AT ARBITRARY INCIDENCE OR IN GUIDE FROM THOSE FOR FREE SPACE AT NORMAL INCIDENCE

Situation	To obtain the correct expression for the given situation, k in the free-space normal-incidence equation must be replaced by	The propagation constant β must be taken as the following, if k is the dielectric constant of region No. 2 in Fig. 1*c*
Free space, normal incidence; or coaxial line, fundamental mode	k	$\frac{2\pi\sqrt{k}}{\lambda}$
Waveguide propagating a TE-wave with cutoff wavelength λ_c for the mode in question; or free space, incidence θ, E-vector polarized perpendicular to plane of incidence	$\frac{k-p}{1-p}$	$\frac{2\pi\sqrt{k-p}}{\lambda}$
Same, propagating a TM-wave; or parallel polarization in free space	$k^2\,\frac{1-p}{k-p}$	$\frac{2\pi\sqrt{k-p}}{\lambda}$

The symbol p of the table stands for the squared ratio of free-space to cutoff wavelength,

$$p = \left(\frac{\lambda}{\lambda_c}\right)^2, \tag{10}$$

whenever the equations are concerned with waveguide (Ref. 27*b*). When the result is for free space, on the other hand, p is defined as

$$p = \sin^2 \theta, \tag{11}$$

where θ is the angle of incidence. This abbreviated representation, which will be used throughout the present chapter, is possible because the condition $\sin \theta = \lambda/\lambda_c$ leads to an exact equivalence between the results for free space and waveguide without further complication; perpendicular polarization corresponds to a *TE*-wave, parallel polarization to a *TM*-wave. Like the equivalence relations of Table 10·1, this one is actually of considerable generality, applying to any series of parallel plates with arbitrary thicknesses and dielectric constants (cf. Refs. 6*b*, 7*b*, and 8*b*). Since *TE*-waves have apparently been most often used in practice, all waveguide results in the present text are presented for *TE*-waves alone, unless the contrary is expressly stated; the extension to *TM*-waves is readily made by means of Table 10·1 if it should become necessary. The waveguides customarily used in dielectric measurement are coaxial, circular, or rectangular; and the cutoff wavelengths for the lowest (or most commonly used) mode in these three cases are respectively infinity, 1.706 times the inside diameter, and 2.000 times the larger of the two inside widths. The quantity p for waveguide is thus determined whenever λ is known, since these dimensions of the guide are readily measured. An alternative procedure which is sometimes more accurate is to determine the guide wavelength λ_g, for example as twice the difference between successive minima, and then to evaluate p by the relation

$$p = 1 - \left(\frac{\lambda}{\lambda_g}\right)^2.$$

Equipment and methods for finding the free-space wavelength are described in Chap. 5.

Loss.—Although the general expression Eq. (2) assumes nothing about loss, those of the foregoing relations which involve k explicitly are valid only when $\tan \delta = 0$. To the three fundamental results, Eq. (2), Eq. (8), and Table 10·1, must therefore be added a fourth which will allow the case $\tan \delta > 0$ to be taken into account. The equivalence relation here is even simpler than those for arbitrary incidence or waveguide, namely,

$$k(1 - j \tan \delta) \equiv (k \sec \delta)e^{-j\delta} \tag{12}$$

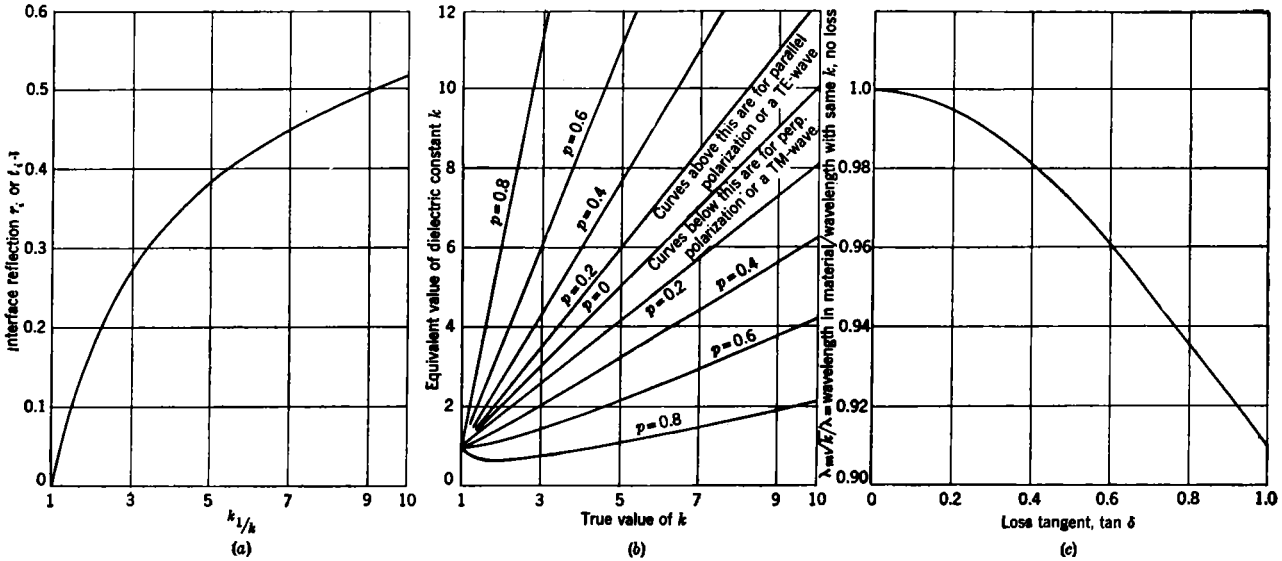

FIG. 10-2.—A few general relations for dielectric materials. (*a*) Interface reflection for a lossless sheet in free space at normal incidence. (*b*) The equivalent dielectric constant (Table 10-1) for arbitrary incidence or for waveguide. (*c*) The effect of conductivity on wavelength: incidence is normal, sheet is in free space.

replaces k wherever it appears. This procedure, which follows easily from relations derived in Ref. 1*b*, applies without error to any result based on Maxwell's equations, provided only that the original equation for zero loss be written in complex form; specifically, no separation of real and imaginary parts or taking of absolute values can have occurred at any point in the derivation. When Eq. (12) is used in conjunction with Table 10·1, the operations must be carried out in the proper order. Thus, starting with the equation in complex form the relations of Table 10·1 should be used to obtain the complete result for zero loss, and then k is replaced in this expression by its complex analogue. The reverse order of substitution will not in general give the correct result.

10·2. General Considerations Influencing Choice of Method.—In the foregoing discussion a number and variety of methods were noted by which k and $\tan \delta$ may be determined. Five or ten different possibilities were specifically mentioned, each of which may in turn be carried out by a number of experimental techniques. These methods themselves are only representative of the many which may be used. Besides affecting the general treatment of derivation, this diversity of method also shows that some criterion for selection is much to be desired.

Practical Considerations.—In a consideration of requirements, it should be noted that the choice of method will depend to a large extent upon the type of work contemplated; a method which is satisfactory in research is sometimes undesirable for routine measurement, and conversely. Further subdivision is found when the preparation of the sample is considered, an operation which often takes more time than the actual process of measurement. Thus, a method requiring rod-shaped samples is almost impossible to use with certain types of laminates, which are ordinarily supplied in sheet form; but on the other hand, free-space methods, which require fairly large sheets, are inconvenient when the temperature and humidity are to be controlled or when the material is not available in quantity. The choice of method is likewise influenced by the properties of the material itself, apart from its form or availability; for example, those with high losses are not always conveniently treated by the methods used for low-loss materials, and similarly, materials of low dielectric constant ($k < 2$), which are often inhomogeneous, are most accurately measured by methods utilizing a large sample, with the consequence that an average result is obtained. Still another item influencing the utility of a given method is the type of equipment available; for example, it may or may not be easy to change the oscillator wavelength, the use of a traveling probe may be recommended or prohibited for various reasons, or the transmitter output power may be sufficient for some methods but not for others. The evaluation of the methods described in the ensuing discussion is based on considerations

of this type, which have been found of considerable practical importance in certain cases.

Theoretical Requirements.—Before these methods are discussed in detail it is perhaps worth while to consider the respective roles played by the two parameters being measured, as this question too has considerable influence on the choice of procedure. First, it is found, in general, that the effect of k cannot be separated rigorously from that of $\tan \delta$, since any electrical phenomenon that depends upon the one will likewise depend to some extent upon the other. Quantitative consideration of the relations given in Ref. 1*b* or Eq. (12) easily leads to

$$\kappa = \left(\frac{2\pi}{\lambda}\right)\sqrt{6k \sec \delta}\, e^{-\frac{j\delta}{2}}, \tag{13}$$

$$\kappa = \left(\frac{2\pi}{\lambda_m}\right)\left[1 - j \tan\left(\frac{\delta}{2}\right)\right], \tag{14}$$

where λ is the wavelength in free space, λ_m in the material, and κ is the propagation constant as usually defined. In other words, multiplication by $e^{-j\kappa d}$ gives the change in amplitude and phase experienced by a plane electromagnetic wave when propagated a distance d through the material. The wavelength λ_m is inversely proportional to the real part of κ,

$$\lambda_m = \left(\frac{\lambda}{\sqrt{k}}\right)\left[\frac{\sqrt{\cos \delta}}{\cos\left(\frac{\delta}{2}\right)}\right], \tag{15}$$

whereas the imaginary part gives a measure of the attenuation. Briefly, if the wave is propagated a distance λ_m,

the phase increases by 2π radians; (16)

the amplitude is multiplied by $e^{-2\pi \tan (\delta/2)}$. (17)

These two effects, phase and attenuation, depend upon λ_m, which involves both k and $\tan \delta$; and hence k cannot be determined from a single measurement of phase alone nor $\tan \delta$ from a measurement of amplitude alone; a simultaneous solution is necessary for the general case.

Although separation of k and $\tan \delta$ in this sense is impracticable with the exact equations, it is feasible if certain approximations are allowed. In most cases of practical interest $\tan \delta$ is small compared with unity, and the expansion of λ_m (Ref. 1*b*) may be written

$$\lambda_m = \frac{\lambda}{\sqrt{k}}\left[1 - \frac{\tan^2 \delta}{8} + O(\tan^4 \delta)\right] \tag{18}$$

for the wavelength in the material, where, as elsewhere in this chapter, the symbol $O(x)$ means "terms of the order of x." To the extent that

$\tan^2 \delta$ may be neglected, λ_m depends on k alone, and many equations giving k from measured quantities will in fact be the same as they are when $\tan \delta = 0$ (cf. Fig. 10·2*c*). This approximation is the basis of a procedure often used in optics, where the effect of loss is considered for questions involving attenuation but is ignored for both measurement and computation of the index of refraction. In microwave work the approximation $\tan^2 \delta \approx 0$ is equally useful; not only does it facilitate computation, but it allows the proper choice of the general type of measurement to be made for determining each of the two parameters. It should be noted from Eqs. (17) and (18) that any effect depending primarily on wavelength may lead to an accurate method of finding k; and once k has been determined, any effect depending primarily on power absorption may be expected to give $\tan \delta$. Although derived here only for plane waves in an infinite medium, considerations of this sort are shown by Table 10·1 to be qualitatively valid for the majority of configurations encountered in the actual process of microwave measurement, and they will be frequently used in the following sections.

METHODS DEPENDING ON TRANSMISSION IN GUIDE

When $\tan \delta = 0$ it is readily shown that k can be determined by measurement of either the amplitude transmission t or the phase shift t'. Upon more detailed examination, however, it is found that determination from t is, in general, considerably less accurate than determination from t', even in the assumed situation $\tan \delta = 0$; and when this condition is only approximately satisfied, which is always the case in practice, the errors are found to be much increased, being of the order of $\tan \delta$ in the first case, $\tan^2 \delta$ in the second. For the determination of loss, on the other hand, the situation is reversed, measurement of t giving an accurate, measurement of t' an inaccurate, result. Because of these considerations, which, incidentally, agree with the discussion of the relative effect of the two parameters, it will be assumed throughout the present section that k is to be determined from t', whereas $\tan \delta$ is to be found from t.

10·3. Techniques for Phase Measurement.—Measurement of t may be made with the equipment of Fig. 10·3*a*. The procedure as described in Ref. 6*a* is to adjust the phase shifter for minimum voltmeter reading (1) when the sample is not present, and (2) when it is present; the setting of the phase shifter should be noted in each case. With the arrangement of Fig. 10·3*b*, the phase difference corresponding to these two settings is then determined or, when many measurements are to be made, the equipment may be completely calibrated. If Δ denotes the difference in probe position for the two settings in the equipment of Fig. 10·3*b*, then Eq. (16) combined with Table 10·1 gives the relation plotted in

Fig. 10·4,

$$k = 1 + \left(\frac{\Delta}{d}\right)\left(2 + \frac{\Delta}{d}\right)(1 - p), \tag{19}$$

for waveguide propagating a TE-wave (Ref. 6a). There is a certain ambiguity in the value of Δ, as anticipated in the introduction, for the addition of $n\lambda_g$ has no apparent effect on the relative phases of the two waves, so that Δ may be increased or decreased by this quantity at discretion. The ambiguity may be resolved by estimating the dielectric

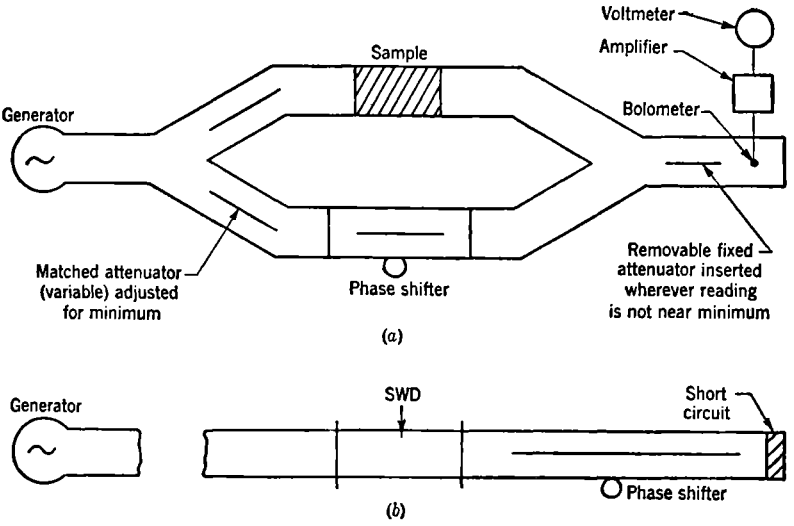

FIG. 10·3.—Measurement of k by phase shift in guide.

constant, or by repeating the measurement with a different sample thickness.

R-f Errors.—The foregoing discussion is intended to illustrate principles only, and it includes a number of tacit assumptions that are not necessarily satisfied in practice. In deriving Eq. (19) it is assumed, for example, that the phase shift on transmission through a sheet of thickness d is exactly equal to $2\pi d/\lambda_m$, that is, to the phase shift obtained for propagation a distance d through an infinitely long medium. This relation, which is physically equivalent to neglecting the reflection r_i at the two air-sample interfaces, may be shown to be true without error if and only if the thickness is an integral number of quarter wavelengths,

$$d = \frac{n\lambda}{4\sqrt{k - p}} \qquad (n = 0, 1, 2, \cdots), \tag{20}$$

or the dielectric constant is unity, $k = 1$. In other cases, the error may be exactly compensated by a procedure similar to that to be described for the same error in free-space measurement; or it may be reduced to negligible proportions by the use of a sufficiently long sample. If the use of a long sample is impracticable, Δ may be taken as the average of the two values found for two values of d differing by approximately $\lambda_m/4$. With this procedure (Ref. 6*a*), it is not difficult to show that the

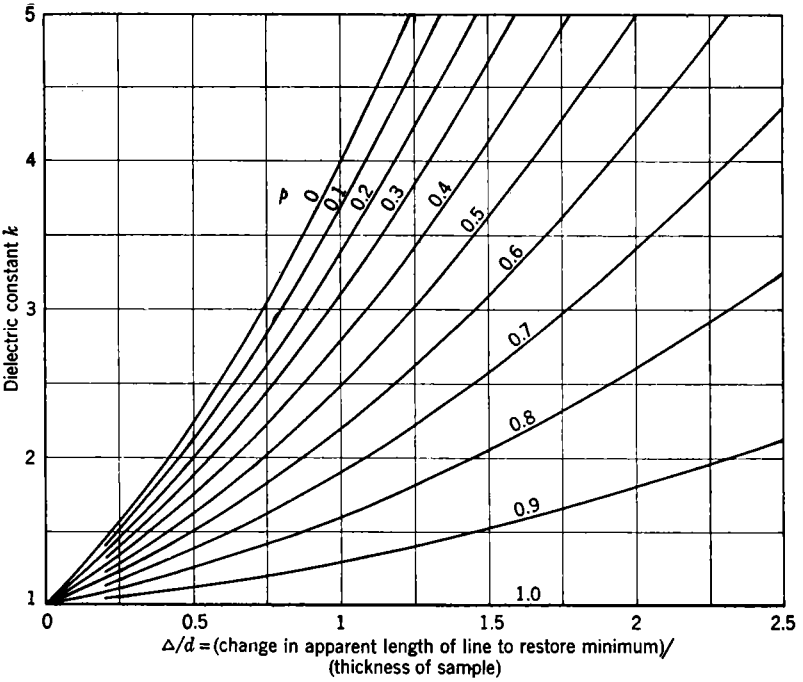

FIG. 10·4.—Dielectric constant vs. phase shift in guide.

deviation in the final value of Δ will be of the order of r_i^4, if r_i is the reflection at the interface between material and air. The deviation as found from a single measurement is of the order of r_i^2.

Closely analogous to the above error is the error due to reflection from the Y-joints of the equipment, which is shown by Eq. (5) to be of the second degree in the three variables: reflection of sample, combined reflection of first Y-joint and attenuator, and reflection of second Y-joint. The error is therefore small when these joints are moderately well matched, and all terms that involve the sample reflection r become of the fourth degree (Ref. 4*a*) when two measurements are taken with a quarter-wave displacement of the sample and the results are averaged. The use

of a magic T for these Y-joints will also decrease the error in certain cases. If still further accuracy is desired, at least for the shorter wavelengths, it is a simple matter to design attenuators giving a standing-wave ratio not much over 1.01 in power, although the design of well-matched joints and indeed of most other r-f components is difficult. In such cases it is sometimes helpful to precede each source of unwanted reflection by an attenuator, as suggested by Fig. 10·5. Except for terms of the order of T^2AJ, it follows from Eq. (6) that

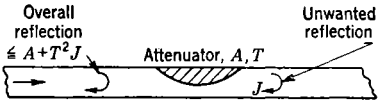

FIG. 10·5.—Use of an attenuator to reduce reflection.

$$\text{Over-all reflection} \leqq A + T^2J, \tag{21}$$

for such an arrangement, if T is the transmission coefficient of the attenuator and A and J are respectively the reflection coefficients of the attenuator and termination. To apply this principle to the case at hand two attenuators are added to the right-hand Y-joint of Fig. 10·3*a*, located more or less symmetrically with respect to those already present, which are necessary in any case to prevent interaction between the two branches of the circuit.[1]

Additional r-f error is contained in the assumption of a constant generator frequency. Clearly, if this frequency is not the same when the readings are taken with and without the sample, or when the phase shifter is calibrated, than Δ will be in error by a corresponding amount. The error of calibration due to this difficulty is usually negligible in practice, and if necessary, it may be compensated by using appropriate values of the wavelength. Error due to frequency drift occurring in the actual process of measurement, on the other hand, may become serious if no precautions are taken in the design of the equipment. With A and B as the lengths of the two branches of the circuit (Fig. 10·3*a*), it is not difficult to show that the error in Δ is given by

$$\frac{(B - A)(\Delta\lambda)}{\lambda(1 - p)} + O[(\Delta\lambda)^2], \tag{22}$$

where $\Delta\lambda$ represents the difference in transmitter wavelength with and without sample. The effect of the sample has been neglected, a procedure that is usually justified in calculations of this sort; it is discussed briefly in connection with Eq. (43). Since the error is proportional to $(B - A)$, it may become large when the equipment is used for measuring

[1] In Ref. 6*a* a set of values of k versus d was obtained without isolation of this type and the measured values varied from 2.4 to 3.1. When a single attenuator was added to the equipment, however, all values fell between 2.59 and 2.65. Except for this one change, the addition of an attenuator, identical equipment was used in both cases.

gases, and on the other hand the error is practically zero, independently of the total lengths A and B of either guide, when these lengths are equal. It is evident, then, that equipment of this type should be designed to be symmetrical; the two branches should not only use guides with the same internal dimensions (as here assumed) but also have substantially the same length. Of course such considerations are relevant only when the transmitter is moderately unstable, permitting a frequency drift of perhaps one part in five or ten thousand; instability of this or higher order was often encountered when the work here presented was first carried out. Recently, however, methods have been found by which the frequency of a klystron transmitter can be stabilized to within one part in 10^8, and if such equipment is used for dielectric measurement the expedients here described are unnecessary. In the present chapter this remark applies whenever questions of frequency stability are discussed.

Other Errors.—If the error due to loss, which is of the order of $\tan^2 \delta$ and negligible for our present purposes, is omitted, the above discussion summarizes the significant r-f errors in the derivation of Eq. (19) from measured quantities. Besides these errors, some inaccuracy due to the equipment and the experimental procedure is inevitable; much of this may be avoided by the use of precision instruments and sufficient care in taking the readings. The standing-wave detector used to calibrate the phase shifter, for example, must have the same internal width as the guide containing the sample; or, if not, the measured value of Δ, as determined from Fig. 10·3*b*, should be corrected by the relation

$$\Delta_{\text{true}} = (\Delta_{\text{measured}}) \left(\frac{\lambda_g}{\lambda_s} \right), \tag{23}$$

where λ_s is the wavelength in the standing-wave detector, and λ_g that in the portion of guide which is to contain the sample. The remaining details of the proposed method of calibration are similar to those of the short-circuited-line method for measuring dielectric constants, which will be discussed subsequently. Other procedures are possible; for example, the meter reading may be taken as a function of the position of the phase shifter with the guide empty, and the resulting sine curve may be used to determine the relative phases of the two waves. Partly because the attenuation depends to some extent on phase-shifter setting, however, this method is usually less accurate than that of Fig. 10·3*b*. A third procedure, of course, is to use a phase shifter that is known to be linear and hence to require no calibration. Such a device is described in connection with free-space measurement.

Throughout the foregoing analysis it was assumed that the physical lengths of all waveguides remained unchanged while the experiment

was being carried out. In normal circumstances such an assumption is justified whenever the r-f paths are sufficiently short, since the actual (as well as the percentage) expansion due to temperature variation will then be very small. As in the case of frequency instability, however, to which the present effect has a certain formal resemblance, it is found that variation due to temperature changes may become serious whenever the path differences are large. Such large differences are likely to occur in the measurement of gases. Thus, the error results from the magnitude of the change in length and may be considerable for moderate temperature variation when the original length is large. It must be noted too that the cutoff wavelength λ_c depends on the temperature. The result of this variation, which happens to enhance the effect of the change in length, is to alter the guide wavelength in accordance with Table 10·1. It has already been shown that the error resulting from a change of wavelength is proportional to path difference [Eq. (22)]. A precise expression for the particular effect in question, may be obtained by replacing $\Delta\lambda/\lambda$ in Eq. (22) by $d\Delta T$, with the result

$$\text{Error in } \Delta = \alpha(B - A)\,\frac{(\Delta T)}{(1 - p)} + O(\alpha^2),$$

where α is the coefficient of expansion for the metal of which the guide is made, ΔT is the temperature change in units appropriate to the value of α chosen, and $(B - A)$ represents the difference in geometrical path lengths as shown in Fig. 10·3*a*. This result, which does not assume a rectangular guide, takes account of the change in λ_c as well as of that in $(B - A)$; the effect of the sample itself is neglected as in the derivation of Eq. (22), however, and α is assumed independent of temperature over the range ΔT.

Since the error is proportional to $(B - A)$, the equality of paths should be retained regardless of the over-all length required, and since the error is proportional to ΔT, compensation may be necessary, even with small path differences, when the dependence of k and $\tan\delta$ on temperature is being investigated (cf. Ref. 16a). Since the value of ΔT is usually known, in order to compensate the error the measured value of Δ may be corrected, and either the computed or the measured values of d and λ_c appropriate to the new temperature may be used in all calculations. For such a procedure only approximate values for α of the sample and the guide are required; in fact the value for the guide may be evaluated in terms of the shift in Δ with temperature. Any error from clearance, produced by the difference of expansion of the guide and the sample, may be compensated as described subsequently, if necessary, although the effect due to temperature alone is completely negligible in ordinary practice. If a complete curve of k vs. temperature is taken,

such a condition requires merely that the setting be repeated without the sample and that d and λ_c be evaluated from time to time as the experiment progresses. When practicable, this procedure is usually preferred. The same or substantially equivalent methods are valid for estimating or compensating the effect of temperature in all methods to be considered.

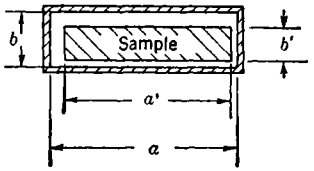

FIG. 10·6.—Clearance in a rectangular waveguide.

A third source of error is the clearance between the sample and the guide, which is necessarily present to some extent in all methods not carried out with the sample in free space. Although the exact theoretical results are available for the situation illustrated in Fig. 10·6, it suffices here to give the empirical equation

$$k_{\text{true}} = (k_{\text{measured}} - 1)\frac{b}{b'} + 1, \tag{24}$$

which has been experimentally verified in a number of cases (Ref. 4*a*). The stated dependence on b' is suggested by the uniformity of the E-field in the vertical direction; that the result is substantially independent of a' for small clearance, follows from the fact that the field is zero at the sides of the guide. Corrections for clearance may be given in other cases, for example, for round or coaxial waveguides, although it is usually necessary to assume that the sample is centered for an exact theoretical derivation. It must be mentioned that errors from clearance can be greatly reduced by use of a mode in which the E-field is tangential to the inner surface of the guide at all points. The field must then be nearly zero at the edges of the sample, and hence, for all dimensions, a reduction of error is obtained which is similar to that noted in connected with dimension a' of Fig. 10·6. An example of such a mode is the TE_{01}-mode in circular waveguide, which was suggested and actually used in Ref. 13*a* as a means of eliminating this source of error.

A final error is found in the actual process of determining Δ, as the phase shifter evidently cannot be adjusted exactly to give minimum power. This error is reduced to a small value, however, if the waves in the two branches of the equipment have amplitudes so nearly equal that the minimum meter reading is practically zero. The result may be magnified by an increase of over-all gain or, what is essentially the same thing, by the use of a logarithmic meter, and hence a small change in setting of the phase shifter suffices to produce a large change in meter reading. Because the minimum can be made very small by appropriate adjustment of the variable attenuator in Fig. 10·3*a*, the only obvious limitation to the accuracy that may be obtained (with constant generator

frequency) is set by the transmitter power and the signal-to-noise ratio of the receiver. In practice, however, it is not usually possible to obtain zero both with and without the sample, as the transmission coefficient t is less than unity. Since the phase shift of an attenuator depends upon its setting, moreover, this difficulty cannot be completely overcome by any simple procedure. It may be partially obviated by adjusting the attenuator initially to give somewhat too little power in one branch when the sample is not present, and somewhat too much when it is. This adjustment, which is made by observing meter reading vs. attenuator position, depends for its efficacy upon the fact that t is usually close, even though not exactly equal, to unity. The error in Δ is thus made negligible compared with the other errors, for most applications, especially if the sample is reasonably long. The increase in accuracy here described is, of course, obtained only when the phase shifter is set for minimum or near-minimum meter reading; in particular, the whole method of measurement is inaccurate if the attempt is made to set on a maximum. It is perhaps worth noting that transmission errors have much in common with errors encountered in the other procedures to be investigated; these other errors may often be treated by the same methods or even by the same equations that are presented in detail here.

10.4. Techniques for Amplitude Measurement.—The general procedure used and the chief difficulties encountered when k is found by measurement of transmission in guide have been indicated. With regard to the question of loss, from Eqs. (12), (13) and Table 10·1,

$$\tan \delta = -\frac{\lambda \sqrt{k - p} \ln t}{\pi k d} + O(\tan^2 \delta) \tag{25}$$

may be obtained for $\tan \delta$ in terms of the amplitude transmission coefficient t, if it is assumed for the moment that no power is reflected at the interface between air and medium.

Direct Measurement of Transmission.—To measure t directly the procedure suggested in Fig. 10·7*a*, may be used, which leads to

$$t^2 = \left[\frac{\text{receiver reading with sample}}{\text{receiver reading without sample}}\right] \times \left[\frac{\text{monitor reading without sample}}{\text{monitor reading with sample}}\right] \tag{26}$$

whenever second-order terms in the generator reflection, the sample reflection, and the reflection of the termination may be neglected. As previously, all terms except the product of the generator reflection and the reflection of the termination are reduced to the fourth degree if the experiment is repeated with a quarter-wavelength displacement of the sample. When the isolating attenuator is properly designed and placed

in the position shown, rather than in the fixed part of the line as might perhaps seem more natural, then it is seen from Eq. (21) that this product term will be negligible irrespectively of slight inaccuracies in the joints. Quantitative evaluation of the maximum error in this and similar methods of transmission measurement may be made by means of Table 10·2 if A is is taken to mean the reflection from the sample. The effect of detector nonlinearity is the same for measurement of transmission

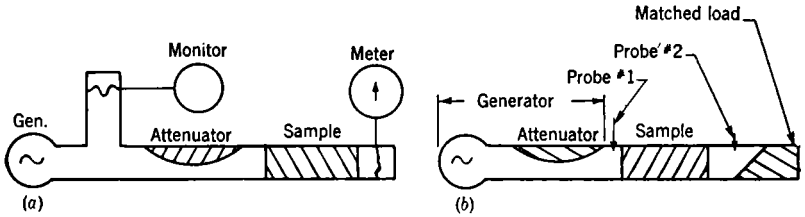

FIG. 10·7.—Direct measurement of transmission.

by this method as for measurement of a power standing-wave ratio by the maximum-to-minimum technique. The ratio of transmissions for different sample lengths is often required rather than the actual value of the transmission, and a modified procedure that eliminates error from the terminating reflection may then be employed. Thus, instead of reducing this reflection to a zero or near-zero value, the phase may be adjusted in such a way as to maximize the receiver reading; or, what is nearly the same thing, the bolometer may be matched to generator plus sample rather than to the line. For the validity of either procedure, it is necessary and sufficient that the reflection of generator plus sample be constant, a condition that will usually be realized only when the sample transmission is so low that the over-all reflection r nearly equals the interface reflection r_i. Thus, the method should not be used for short low-loss samples. Another property of this method which makes it unsuitable for such samples is that the transmission of the phase shifter itself will depend to some extent upon the setting; the change in transmission so introduced must be compensated by previous calibration unless it is negligible in comparison with the change in transmission being measured. The error from generator reflection persists in general even with this modified procedure, but if the sample has low transmission—which is a desirable property with this method in any case—then the error is eliminated whenever the distance from the generator to the nearest sample interface is held constant. It must be mentioned again, however, that the ratio of two transmissions only is considered here. The procedures outlined in this paragraph are incorrect when the value is desired in an absolute sense. An illustration of the correct application of the

method is given in Ref. 8*a*, where the loss tangent of water is evaluated.

Still a third method of finding t directly is suggested in Fig. 10·7*b*, for which a relation is given in Ref. 17*a*,

$$t = \left[\frac{\sqrt{\text{max}} + \sqrt{\text{min}} \text{ for probe \#2}}{\sqrt{\text{max}} + \sqrt{\text{min}} \text{ for probe \#1}}\right] \div [\text{same, without sample}], \quad (27)$$

with an apparent error of the order of the sample reflection times the reflection of the termination independently of generator mismatch. Unlike the procedures hitherto described, however, this one involves the use of a traveling probe, which is shown in Ref. 5*a* to lead to large inaccuracy in certain cases. The fractional error is of the second degree in the five quantities: reflection of generator, reflection of first probe, reflection of sample, reflection of second probe, reflection of load; several of the terms involving probe reflection remain of the second degree, in general, even if an average with quarter-wavelength displacement is taken. The need for reducing this source of reflection is thus apparent.

Measurement of the Difference between Transmission and Unity.— Although the foregoing methods of finding t are simple and direct, they are not entirely satisfactory when the loss is low. Thus, it is seen from Eq. (25) that it is essentially $1 - t$ rather than t which is desired, with the result that the fractional error in $\tan \delta$ greatly exceeds that in t when $t \approx 1$. To overcome this difficulty the bridge method previously described may be used, which gives $1 - t$, essentially, rather than t. Thus,

$$1 - t = \frac{2m}{M + m}, \quad (28)$$

where M^2 is the maximum, m^2 the minimum meter reading observed as the setting of the line stretcher is changed with the sample in place, if the variable attenuator has been adjusted to give a minimum of zero with the sample removed. To avoid overloading the detector, the maximum M^2 is taken with the fixed attenuator present, the minimum m^2 with it absent; the true maximum for substitution in Eq. (28) is then equal to the measured maximum divided by the transmission coefficient of the attenuator.

Such a procedure reduces errors due to nonlinearity, as may be easily shown, but its indiscriminate use is likely to lead to errors of another kind. Thus if the insertion of an attenuator reduces the power by a given amount in Fig. 10·8*a*, it causes, in general, a different reduction in Fig. 10·8*b*; the ratio of power with and without the attenuator is, however, independent of probe position in both cases. For quantitative treatment T^2 is defined as the ratio of powers with and without attenuator in Fig. 10·8*a*, τ^2 as the ratio in Fig. 10·8*b*, R as the amplitude reflection coefficient

for the load, G for the generator, and A for the attenuator. If the attenuator is not symmetrical, A is the reflection coefficient from the right for the first situation, from the left for the others in Table 10·2. With the aid of this table, in which only the last two entries are approximate, the attenuation is found to be independent of the position of the attenuator, of the position of the load, and of the magnitude of the reflection from the load if, and only if, two of the three quantities A, R, and G are equal to zero (Ref. 2*a*). In particular, the generator must be matched to the line rather than to the load if the errors for high standing-wave ratios are not to be prohibitively large; the corresponding reduction in available power leads to complications in certain cases.

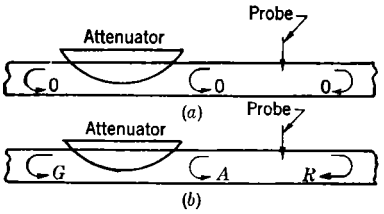

FIG. 10·8.—Typical application of an attenuator.

TABLE 10·2.—THEORETICAL ERRORS INTRODUCED BY IMPROPER USE OF AN ATTENUATOR

Situation	Least possible value of T/τ	Greatest possible value of T/τ	Extremes possible in ordinary cases
$G = 0$, R and A finite	$(1 - RA)^2$	$(1 + RA)^2$	Yes
$R = 0$, G and A finite	$(1 - GA)^2$	$(1 + GA)^2$	Yes
$A = 0$, G and R finite	$\left(\frac{1 - RGT}{1 + RG}\right)^2$	$\left(\frac{1 + RGT}{1 - RG}\right)^2$	No
$A = 0$, G and R finite, phase shift through attenuator same as for empty line	$\left(\frac{1 + RGT}{1 + RG}\right)^2$	$\left(\frac{1 - RGT}{1 - RG}\right)^2$	Yes
G, R, A, finite $T \ll 1$	$\left(\frac{1 - RA}{1 + RG}\right)^2 (1 - GA)^2$	$\left(\frac{1 + RA}{1 - RG}\right)^2 (1 + GA)^2$	Yes, for certain attenuator lengths.
$T \ll 1$, generator initially matched to load	$\frac{(1 - RA)^4}{(1 - R^2)^2}$	$\frac{(1 + RA)^4}{(1 - R^2)^2}$	Yes

If the calibration of the variable attenuator is known, an alternative procedure is to adjust the attenuator for zero minimum with and without the sample, whereupon the ratio of the attenuator transmissions for the two cases is easily seen to be equal to the transmission desired; that is,

$$t = \frac{T_1}{T_2}, \tag{29}$$

if t is the transmission coefficient of the sample, as usual, and T_1, T_2 are those of the attenuator when adjusted to give a minimum meter reading of zero with and without the sample, respectively. The chief advantage of this procedure over those discussed hitherto is that the result is now independent of the linearity of the receiver. This independence of linearity is characteristic of all procedures that merely require two readings to be equalized, and, although not explicitly mentioned in all cases, it is of frequent application in the present discussion. Error from reflection is again given in Table 10·2.

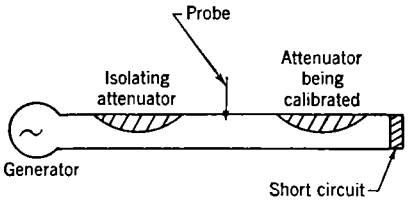

FIG. 10·9.—Calibration of a low-loss nonreflecting attenuator.

Because the range of attenuation is small for most applications, the calibration may be carried out by the method suggested in Fig. 10·9; from Eq. (6) with $r'' = \rho'' = 0$

$$T^2 = \frac{[(\text{SWR}) - 1]}{[(\text{SWR}) + 1]} \tag{30}$$

is obtained for the attenuator transmission T in terms of the measured standing-wave ratio. The error in the method of Fig. 10·9 due to attenuator reflection, which must be small anyway for the application suggested, is shown by Eq. (6) to be of the first degree when a single measurement is made, of the second if two measurements are averaged with a quarter-wavelength displacement. When the attenuation exceeds 1 db, the measurement of the standing-wave ratio must be carried out by taking maximum and minimum meter readings, as usual, whereas for lower attenuation, the procedure is preferably that described in connection with the short-circuited-line method. In the first case probe errors are of the order of the product of the reflection being measured and the probe reflection; in the second they are negligible (Ref. 5*a*). From this and other considerations it is concluded, finally, that the attenuator should be calibrated by one of the methods of Fig. 10·7 for moderate or large attenuation, and by the method of Fig. 10·9 for small attenuation.

Thus far it has been assumed that the transmission coefficient of the phase shifter is independent of setting, which is actually not the case in normal practice. The error due to this variation may be shown to be

negligible when t' is being considered, but when t is to be found by the method just described the error must be considered in somewhat greater detail. By application of Eq. (28) to the situation illustrated in Fig. 10·3*b* it is a simple matter to calibrate the phase shifter, and the transmission, although not constant, is then known as a function of the setting. With this information available the error due to the effect in question is readily corrected by the relation

$$t = \frac{(Mt_1 - mt_3)}{(Mt_2 + mt_2)}, \tag{31}$$

which replaces Eq. (28), and by

$$t = \frac{T_1 t_1}{T_2 t_2} \tag{32}$$

instead of Eq. (29). In these equations, which are valid without appreciable error if the reflection from the phase shifter may be neglected,

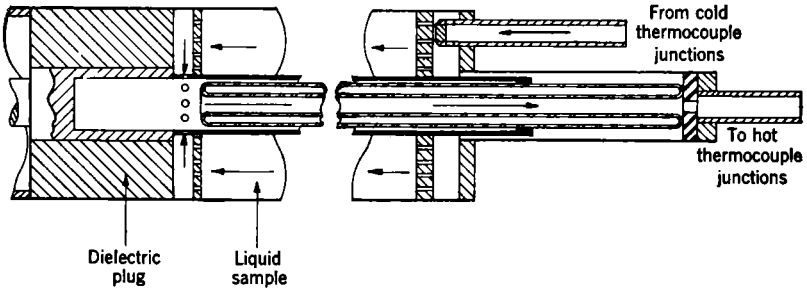

FIG. 10·10.—A calorimeter for measuring loss.

t_2 is the transmission of the phase shifter when it is set for minimum reading with no sample, and t_3 and t_1 are the transmissions when it is adjusted for maximum and minimum readings, respectively, with the sample in place.

A Calorimeter Method.—Attention hitherto has been confined to the standard methods of r-f power measurement. Partly because of its novelty one other procedure is considered which requires none of the r-f components that have played an essential role in the foregoing discussion. With the procedure in question, developed in Ref. 15*a*, the temperature change caused by the r-f power absorbed is measured, and from this temperature change the loss tangent of the material is obtained (see Fig. 10·10). If $(\Delta T)_t$ denotes the difference between input and output temperatures at time t after the r-f power is turned on, a plot of $(\Delta T)_\infty - (\Delta T)_t$ vs. t is a straight line on semilogarithmic paper with slope s given by

$$s = -2\alpha \frac{q}{A},$$

where A is the cross-sectional area of the coaxial line, q the rate of flow of liquid, and α the attenuation constant, defined by the relation

$$E(x) = E(0)e^{-\alpha x},$$

which gives the amplitude $E(x)$ at point x inside the liquid. The foregoing result was obtained for the period of temperature rise. After the steady state has been reached the transmitter may be turned off. The temperature difference will now decrease exponentially, in such a way that $(\Delta T)_t$ vs. t will be a straight line with the same slope as that formerly obtained for $(\Delta T)_t - (\Delta T)_\infty$. As a check for experimental accuracy, the slope s is evaluated in practice by both methods. The method appears to be most feasible in coaxial line, since the center conductor supplies a convenient return path; in this case Eq. (17) of the introduction, together with the above equation, gives the simple result

$$\sec \delta = 1 + \frac{1}{8}\frac{1}{k}\left(\frac{\lambda s A}{\pi q}\right)^2$$

for sec δ in terms of the measured quantities s, A, q, and k, provided the first three are expressed in a consistent system of units.

The experimental procedure is to measure the temperature difference at regular intervals from the time at which the transmitter was turned on, with due care to keep the input power and rate of flow constant. From a logarithmic plot of temperature difference vs. time, the slope s is obtained. The quantities A and q, and with them the ratio A/q, giving the velocity of the liquid, are determined by standard methods, whereas k is found by a separate r-f measurement of the type considered elsewhere in this chapter.

The foregoing discussion gives only the essentials of the method, and it remains to consider the conditions for its validity. In the first place, the power was assumed to be traveling in a direction opposite to that of the liquid flow, as illustrated in Fig. 10·10. It was shown in Ref. 15*a* that this condition is the most satisfactory experimentally; it leads to a time constant that is smaller than that obtained in other circumstances, and that is, moreover, independent of the length of the liquid column. The limitation on this last statement is that the length must be sufficient to absorb practically all the r-f power, that is, a traveling wave must exist in the sample rather than a standing wave, and only negligible power must reach the termination. This condition, which requires either very long or very lossy samples, seriously restricts the utility of the method, apart from the fact that it is applicable to liquids only. The use of a short circuit for the termination, if accompanied by a suitable modification of the theory, could be expected to allow lengths half as great as those otherwise permitted; but the restriction on length would still be incon-

venient for most materials. Another assumption was that the flow is laminar, a condition which need be only approximately satisfied in practice and which is sufficiently assured by the proper design of the end plates. Local velocity variations with time must be avoided, however, and precautions must be taken to prevent heat interchange between the input and output pipes. In conclusion, the method has the disadvantages of giving loss alone, and of applying only to a very special type of sample. Its accuracy is apparently not sufficient, moreover, to permit measurement of small losses. On the other hand it is advantageous in that it requires no r-f equipment besides the generators, and it has a certain theoretical interest in that it can be used for absolute power measurement. Henceforth, however, only the more familiar r-f techniques will be described. The following discussion is not intended to apply to the calorimeter method.

10.5. Details of Computation.—It is possible to determine transmission with considerable accuracy. Most causes of error noted above in connection with t', such as clearance or generator instability, are relatively less serious for t, and may be corrected when necessary in the same way as before. For the computation of tan δ from the accurate value so obtained, however, it may be observed that the simple equation given for this purpose is actually incorrect in many cases. By analogy to the procedure used in deriving Eq. (19), the interface reflection r_i was neglected and the attenuation was computed as though the wave were simply traveling a distance d through a continuous medium. In the equation for k, Eq. (19), the error due to this neglect of r_i was found to be of the second order and to be, moreover, rigorously equal to zero for many values of the thickness. In the present case, on the contrary, not only does the error persist for all values of d, but the change in t due to interface reflection—far from being negligible—is often fifty or a hundred times greater than the change due to a nonzero tan δ. In other words the terms neglected in the derivation of Eq. (25) are usually more significant than the terms retained, and the need for further investigation is clear.

Exact Solution.—In the first place, the problem may be solved exactly by the relations given in the Introduction. Thus, if $r_i e^{-jr_i'}$ and $t_i e^{-jr_i'}$, as given by Eqs. (8) and (9), are substituted for the quantities t'', T'' and ρ'', r'' of Eq. (5),

$$te^{-jt'} = \frac{4\sqrt{k}e^{-j\beta d}}{(\sqrt{k}+1)^2 - (\sqrt{k}-1)^2 e^{-2j\beta d}} \tag{33}$$

is found to be the complex transmission coefficient of a single lossless sheet of thickness d, when a plane wave is incident normally upon it in free space (Ref. 1*b*). The corresponding equation for guide is obtained

from Table 10·1, and finally application of Eq. (12) to the resulting expression gives the general relation for arbitrary loss. The two noncomplex equations eventually obtained in this way are unfortunately transcendental as well as simultaneous; they may, however, be solved graphically or by successive substitution. In this latter case use is made of the fact that the computation of k is practically independent of $\tan \delta$, and an accurate value may be found directly by Eq. (19). This preliminary value for k is then substituted in the final form of Eq. (33), which thereupon becomes quadratic and may be solved by elementary methods. With $\tan \delta$ equal to the value thus obtained instead of zero, Eq. (33) is used to find a more accurate k, and so on. The process converges rapidly in most cases; in fact, as was observed in connection with Eq. (19), the first value of k, computed for $\tan \delta = 0$, will ordinarily be correct within the experimental error.

Although numerical solution of Eq. (33) is not convenient, the values of both k and $\tan \delta$ are obtained in principle from the measured quantities t, t', d, λ. If conductor losses be dealt with as suggested, no theoretical error is introduced in the transition from data to results. Of course the experimental errors remain, however, and upon more detailed investigation it is found that those in $\tan \delta$ will be excessive for all but certain limited ranges of the parameters. Thus, the percentage change in t or $1 - t$ caused by a positive rather than a zero value of $\tan \delta$ is usually small; conversely, a small change in the measured transmission will often lead to a large, or even infinite, percentage error in $\tan \delta$. In this situation, which is the usual case for arbitrary values of d and moderate loss, the present method of loss measurement is relatively useless whether or not the exact equation be employed.

Low Transmission.—To obtain a large percentage change in a measured quantity, as $\tan \delta$ increases from zero to a finite value, two procedures may be used, namely, a large value of d, or a lossy sample may be taken so that the change will actually be great in magnitude; or a sample that will have almost complete transmission for zero loss may be used, so that the percentage change in $1 - t$ caused by $\tan \delta$ will be large whether or not the actual magnitude is large. The first situation is expressed by the inequality

$$\exp\left[\left(\frac{-2\pi d}{\lambda_m}\right)\left(\tan\frac{\delta}{2}\right)\right] \ll 1 \tag{34}$$

for which Eq. (5) leads to

$$te^{-j\psi'} \approx (1 - r_i^2 e^{-2jr_i'}) e^{\left(-\frac{2\pi jd}{\lambda}\right)\sqrt{k(1-j\tan\delta)+p}}, \tag{35}$$

instead of the exact equation corresponding to Eq. (33). Equation (35), which is valid whether the wave be TE or TM, suggests that the measure-

ments be repeated with two different values of d, as such a procedure will eliminate r_i or r_i' and lead to a nontranscendental solution for both k and tan δ without further approximation of any kind. Thus,

$$k = 1 + \left(\frac{\Delta}{d}\right)\left(2 + \frac{\Delta}{d}\right)(1 - p) - \left[\frac{(\lambda \ln t)}{(2\pi d)}\right]^2, \tag{36}$$

$$\tan \delta = \left(\frac{2}{k}\right)\left(1 + \frac{\Delta}{d}\right)\sqrt{1 - p}\,\frac{(\lambda \ln t)}{(2\pi d)}, \tag{37}$$

where d now stands for the difference between the two values of d, Δ for the difference in the two values of Δ, and t for the ratio of the two values of t. For its validity this equation requires only that interaction between the two faces of the sample be negligible; in particular, it is not even assumed that tan δ is less than unity. To compute k and tan δ the result for zero loss is obtained, Eq. (19), to which Eq. (34) evidently reduces whenever $\tan^2 \delta = 0$; and from this the term indicated in Eq. (36) is subtracted. Having thus found k, tan δ may be computed from Eq. (37), which is equal to the square root of the correction term already found, multiplied by an easily computed factor. As may be seen from Eq. (5), the theoretical error in Eqs. (36) and (37) is of the order of

$$r_i^2 \exp\left(-\frac{4\pi d}{\lambda_m} \tan \frac{\delta}{2}\right),$$

or somewhat less if the two values of d differ by $n\lambda_m/2$. The experimental errors will be relatively small for the assumed situation, as the effect being measured is large in both percentage and magnitude.

The method just described was used in Ref. 8*a* to evaluate the loss tangent of water, for which the transmission is low enough to satisfy all the requirements noted above. It was verified that p can be neglected when k is sufficiently large, a result which is evident from Eq. (35) or from Table 10·1 of the present text. The equations appropriate to free space were used accordingly in Ref. 8*a* even though the measurement was carried out in guide. Such a procedure, it is perhaps worth mentioning, is usually valid for the propagation constant alone; the effective k used for interface reflection involves $(1 - p)$ as a factor, and hence the dependence must be retained regardless of its magnitude (Table 10·1).

With the propriety of the simplified equations for $p = 0$ verified, the presence of negligible interaction between the sample faces, which follows theoretically from Eq. (34), was checked experimentally. To this end a complete curve of transmission vs. thickness, rather than only two points as hitherto described, was obtained (see Fig. 10·11*a*), and log t was plotted as shown in Fig. 10·11*b*. The thickness itself, which was

too small to measure directly, was obtained as the quotient of the volume of the water and its surface area. If Eq. (35) of the present text is valid, then a curve of the type given in Fig. 10·11*b* should be a straight line.

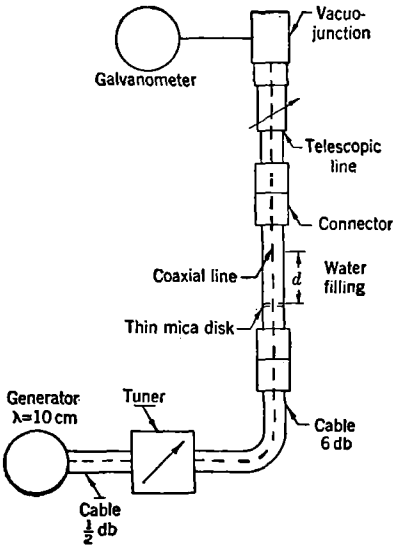

FIG. 10·11*a*.—Use of transmission in coaxial line to determine the loss tangent of water (from Ref. 8*a*).

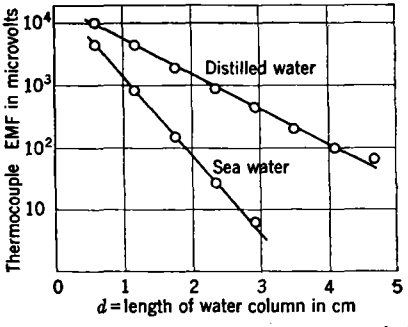

FIG. 10·11*b*.—Data obtained with the apparatus shown in Fig. 10·11*a*.

It may be shown, conversely, that if this curve is a straight line, then Eq. (35) is valid. With axes chosen to give such a linear relation, the best-fitting curve is particularly easy to find by least-square methods. The slope of this best-fitting curve (that is, straight line) gives the proper values for substitution in Eq. (35). No error is introduced by the mica partition, for Eq. (5), which leads immediately to Eq. (35), assumes

nothing about the origin of t'', r'', T'', R''. Thus, Eq. (35) and the cancellation attendant upon taking the ratio of t's, remain valid for the present situation if $t_i e^{-j\psi_i}$ be interpreted as the transmission coefficient of the three-medium transition from air to mica to water. Similarly, the error term $r_i^2 \exp [-(4\pi d/\lambda_m) \tan \delta/2]$ remains valid if r_i be taken as the over-all reflection of the same three-medium transition.

This investigation described in Ref. 8*a*, which has been here discussed in some detail, was carried out with regard to water alone, but many of the principles employed have a general validity that is relevant to less specialized problems and may well be given a place in the present discussion. Such a principle is embodied in the use of a complete curve of k or tan δ vs. some easily varied parameter (Fig. 10·11*b*); not only does it give a check for certain inaccuracies but it often leads to an increase in accuracy by virtue of the well-known behavior of probable error in such circumstances. Similarly, cancellation of the effect of the mica separator, which is shown by Eq. (5) to be obtained regardless of the transmission or loss, is often found for extraneous effects of this sort if a ratio is taken as here described. A third principle, which is likewise of general utility, is the modification of procedure and theory to suit the special problem at hand. Thus, the fact that k was large in this particular case permitted use of the somewhat simpler free-space equations; similarly, the fact that the interface reflection is large with k large suggested that the maximizing procedure described, rather than some other method, be used for finding the transmission. And finally, the fact that the sample was a liquid permitted use of a novel and accurate method of measuring the thickness. Although they are not specifically mentioned here with every method treated, it is clear that such procedures, and similar ones which will suggest themselves to the reader, are sometimes of considerable utility in dielectric measurement.

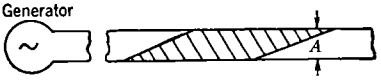

FIG. 10·12.—Use of tapered ends to eliminate interface reflection.

Moderate or High Transmission.—It frequently happens that the loss is too low for Eq. (34) to be satisfied with conveniently small values of d. In this case a large magnitude for the measured effect of tan δ cannot be obtained, but it is still possible to obtain a large percentage effect by the procedure outlined above. Specifically, a sample is used that would have high transmission for zero loss, whereupon the value of $1 - t$, which can be measured directly, will depend critically on tan δ. Thus, instead of measuring a large quantity with high accuracy a small quantity is measured with moderate accuracy, an operation which is considerably more practicable. To achieve the desired characteristics of the sample the technique suggested in Fig. 10·12 may be used, where

reflection at the air–sample interfaces is practically eliminated by the taper.[1] Higher modes are obviated when the inner dimension A of the guide satisfies the condition

$$A < \frac{\lambda}{2\sqrt{k}}, \tag{38}$$

and in other particulars the equipment remains as described above. There is an error in t caused by the less-than-unity transmission of the taper, which is eliminated by the following procedure: two measurements with different values of d are taken and the difference between these values, the difference between corresponding Δ's, and the ratio of the t's are used rather than the quantities themselves in Eqs. (36) and (37). The conditions for validity and errors are the same as before but where the accuracy was formerly attained by making $d \tan \delta$ large, it is now attained by making r_i small. It should be observed that Eq. (37) reduces to Eq. (25) whenever $\tan^2 \delta \approx 0$, although the symbols must be given their present significance of differences or ratios. Despite the fact that complete neglect of r_i is inadmissible, it is thus apparent that appropriate experimental conditions allow the treatment of the theory as if it were indeed a valid approximation. It is in this sense that Eq. (25) may be considered correct.

Half-wavelength Sample.—Although the foregoing techniques arose from experimental necessity rather than from theoretical convenience, they actually led to much more manageable relations than those obtained for the general case. The need for having $1 - t$ depend critically on $\tan \delta$ suggests one other specialization of this type, which likewise gives simple theoretical relations, namely, a sample with $d = n\lambda_m/2$ may be used. The necessary preliminary estimate of λ_m causes no difficulty, as it depends primarily on k, which may be determined with an arbitrary value of d. Thus a simplified form of the exact expression for Eq. (33) is obtained, which reduces to

$$t = \frac{4ae^{-b}}{(a+1)^2 - (a-1)^2 e^{-2b}}, \tag{39}$$

$$a = \sqrt{\frac{k-p}{1-p}}, \qquad b = \frac{k\pi n}{2(k-p)} \tan \delta,$$

when $\tan^2 \delta = 0$, as may be seen from Refs. 6*b* and 8*b*. The two results are compared in Fig. 10·13, where the elementary quadratic Eq. (39) is shown to be valid in all cases not covered by Eq. (34). Although

[1] This method of measurement, with an E-plane taper to eliminate interface reflection, was suggested and used by E. L. Younker (Ref. 6*a*). Waveguide transmission was apparently used to determine $\tan \delta$ for solid low-loss materials in Refs. 17*c*, 18*c*, though no description of procedure is given.

the thickness for maximum transmission is an exact half-wavelength only when tan $\delta = 0$, the deviation is negligible for the present application; hence the value of t for substitution in Eq. (39) may be most accurately determined by measuring transmission vs. thickness near $d = n\lambda_m/2$.

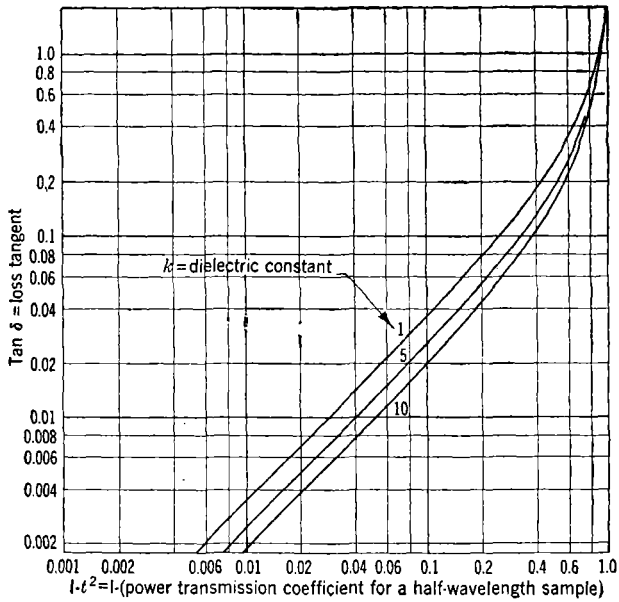

FIG. 10·13.—Exact and approximate curves for tan δ from the transmission of a half-wavelength sample. If the approximate equation is valid, these curves may be used for a sample of thickness $n\lambda_m/2$ provided tan δ is replaced by n tan δ.

Wall Losses.—The loss introduced by the waveguide itself has hitherto been neglected, although it is frequently comparable with that of the sample. This loss is not the same with the filled as with the empty guide, for not only are the energy relations changed by the presence of a dielectric, but the field in the sample is often a standing-wave field rather than the traveling-wave field formerly obtained. The error is accordingly not canceled by the bridge procedure as would perhaps be expected, and special compensation is necessary.

If the *empty* guide were completely lossless,

$$(\tan \delta_{\text{measured}}) = (\tan \delta_{\text{sample}}) + (\tan \delta_{\text{wall}}) \tag{40}$$

would be obtained[1] when measuring the transmission of the sample con-

[1] This method of treating wall losses, which will be repeatedly used in the present text, is due to A. R. von Hippel (Ref. 1*a*).

tained in a piece of the actual lossy guide. The condition of zero loss for the empty guide may be simulated if the substitution is made

$$t = t_{\text{measured}} \cdot \exp\left[\left(-\frac{\pi d}{\lambda}\right)(\tan \delta_{\text{wall}})\sqrt{1-p}\right], \tag{41}$$

and hence wall losses may be readily corrected whenever $\tan \delta_{\text{wall}}$ is known. To determine this parameter, t is measured for two widely differing lengths of empty guide, whereupon the appropriate form of Eq. (25), with $k = 1$ and t = ratio of transmissions, gives the desired result. Since the loss is of concern here rather than k, the large path difference used for finding $\tan \delta_{\text{wall}}$, with consequent magnification of the effect of frequency drift, causes no undue error in normal practice.

10·6. Uses.—The utility of the present method lies chiefly in two characteristics, namely, it does not require a probe of any sort and sharpness of resolution may be attained even with great path lengths. The first characteristic is relevant because of the demonstrated superiority of the short-circuited-line method presently to be described which, however, requires a traveling probe. Although standard at the longer wavelengths, equipment of this type is not easily designed for wavelengths much below one centimeter. On the other hand, it is precisely in this range of very short wavelengths, for which d may be much greater than λ_1 that the present method appears to best advantage.

The second property, independence of path length, is particularly useful for the study of gases, in which the necessarily long guides, with their attendant high losses, give such a broad minimum with the short-circuited-line method as to render it practically useless. Transmission techniques are open to no such objection, the sharpness of the minimum depending on waveguide attenuation only to the extent that this attenuation reduces the available power. For measurement of gases, incidentally, not only is the advantage just described obtained, but also most of the sources of error, including all those involving r_i, are negligible since $k \approx 1$.

MEASUREMENT BY TRANSMISSION IN FREE SPACE

In all methods requiring the use of a guide, the preparation of the sample usually takes much more time than the actual process of measurement. If the methods are modified as suggested in Fig. 10·14 this preliminary step is eliminated for most production materials that are normally supplied in sheet form, and the resulting saving of time is considerable. Besides this increase in speed and simplicity, the experimental procedure, which is evident from the preceding discussion and from Fig. 10·14, has the additional advantages that there are no errors from clearance and that systematic error from other causes may be

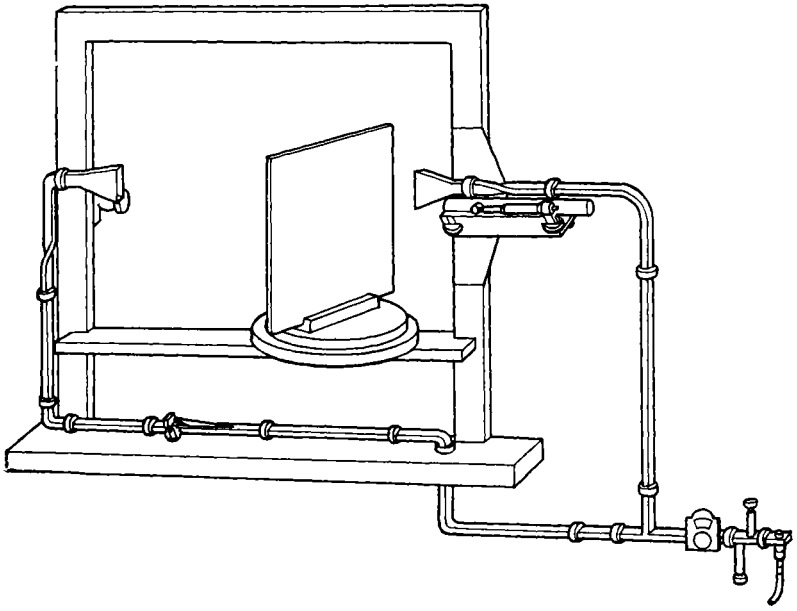

FIG. 10·14*a*.—Equipment for measurement of phase in free space.

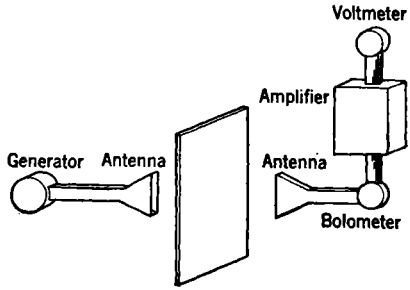

FIG. 10·14*b*.—Equipment for measurement of transmission in free space.

conveniently investigated by the use of several angles of incidence. If p is set equal to zero in Eq. (19), or by direct calculation from Eq. (15) with $\delta = 0$, the relation

$$k = \left(1 + \frac{\Delta}{d}\right)^2, \qquad \theta_0 = 0, \tag{42}$$

results as an approximate equation for the dielectric constant k in terms of the sample thickness d and the phase difference Δ obtained for the air gap with and without sample (Ref. 6*a*). The details for more rigorous

calculation will be given; it suffices here to observe simply that k can be determined once Δ is known.

10·7. Experimental Procedure for Normal Incidence.—Although much of the discussion given in Secs. 10·3 to 10·5, including almost all results on amplitude measurement, applies without change to the present situation, there are a few differences for phase measurement which are of sufficient importance to be mentioned explicitly. With regard to the equipment itself (cf. Ref. 6*a*), a sufficiently long guide must be used in Fig. 10·14*a* to avoid undue strain as the micrometer setting is altered; the horn must be constrained to move in a straight line without nodding; and the micrometer itself must be aligned parallel to the direction of this motion. With these precautions, the first important difference between this and the previous techniques is that the present equipment need not be calibrated and Δ may be read directly from the micrometer. Unlike those customarily used in waveguide work, moreover, a phase shifter of this type gives an accurately symmetrical minimum; hence the position may be computed as the average of two values for equal meter readings, (see Fig. 10·15). This process leads to a significant increase in accuracy by virtue of the nonzero derivative (cf. Sec. 10·3). With drift eliminated as described later, absolute accuracies of the order of 0.0005λ are found to be attainable with relatively crude equipment, and the sensitivity is such that a single sheet of paper inserted in the air gap may increase the meter reading by a factor of ten.

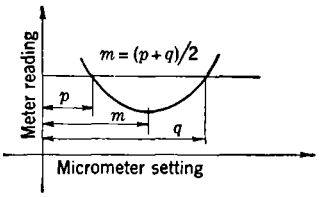

FIG. 10·15.—The location of the minimum of a symmetrical curve by using points of nonzero slope; $m = (p + q)/2$.

Inconstant Frequency.—With such precision the effect of drift becomes increasingly important; on the other hand, the expedient of using equal paths no longer avails for the equipment of Fig. 10·14. Upon calculation of the derivative, the equation

$$a = 2b + c\sqrt{1 - p} \tag{43}$$

should be satisfied for minimum sensitivity to drift (Ref. 6*a*), in which case

$$c' = c\left[\frac{\lambda\lambda'}{\lambda_c^2} + \sqrt{(1 - p)(1 - p')}\right], \tag{44}$$

for the change c to c' in micrometer setting produced by a change of λ to λ' in transmitter frequency when the sample is not present. An exact criterion of this kind of course depends to some slight extent on the material between the horns, and is moreover impossible to satisfy exactly

for two different materials, for example, for air alone and at the same time for air plus dielectric. As a compromise adjustment for this effect, which is of secondary importance, a value may be given to a slightly higher than that indicated by Eq. (43). A similar method is applicable to the waveguide equipment already treated, although for all ordinary work it is unnecessary in either case.

If the equipment is designed with paths of equal geometrical or electrical lengths, rather than with paths satisfying Eq. (43), the equations corresponding to Eq. (44) indicate considerably greater sensitivity to drift, as would be anticipated from the nonzero derivative. By Table 10·3, which gives a comparison of such equations with that just obtained, it is seen that the optimum condition Eq. (43) is satisfactory even with rather unstable oscillators, and that these other conditions may on the contrary lead to large errors in practical work (cf. Ref. 6*a*). Unlike the result for waveguide measurement, the present relations sug-

TABLE 10·3.—THEORETICAL EFFECT OF FREQUENCY DRIFT IN FREE-SPACE EQUIPMENT

Transmitter wavelength, in.	Change in micrometer setting for minimum, c = 22 in., λ_c = 0.84 in.		
	Equal geometrical lengths, $a = 2b + c$, in.	Equal electrical lengths, in.	Correct adjustment, in.
0.5000	0.000000	0.000000	0.000000
0.5001	0.001100	0.002442	0.000000
0.5005	0.005412	0.012100	0.000002
0.5010	0.010736	0.024112	0.000013
0.5100	0.110638	0.245256	0.002442

gest that complete insensitivity to drift is unattainable even when the effect of the sample is neglected. From more detailed analysis it is indeed found that such insensitivity may be achieved if, and only if, every guide with a given dielectric and λ_c in one branch of the circuit be balanced by a similar guide of the same length in the other. For the present case, a second air gap would be required, which would be inconvenient in normal practice.

Errors Similar to Those in Guide.—Except for inaccuracy specifically caused by the use of a guide, which is not found in the free-space measurement, the errors are essentially the same as those described in Secs. 10·3 to 10·5. Analogous to the clearance error, for example, is the error produced by diffraction around the edge of the sample, which is discussed quantitatively in what follows. For our present purposes, the error analogous to clearance may be eliminated altogether if the sample is

sufficiently large. Besides this error, which is corrected without the use of accurately prepared samples, additional inaccuracy occurs as before from interaction between various parts of the equipment. In Ref. 6*a* it is shown theoretically and experimentally that the effect of interaction between the two antennas is practically negligible. By the methods of Refs. 6*a* and 7*a* it is also possible to eliminate error from the interaction between antenna and sample. Thus, a graph of measured Δ vs. the distance from sample to antenna should theoretically[1] be a sine curve, nearly, with period $\lambda/2$, as is seen from Ref. 7*a*. Hence the procedure previously advocated for compensating Y-joint reflection likewise applies in the present instance, that is, Δ may be taken as the average of the two values found for a quarter-wavelength motion of the sample (Ref. 6*a*). Other details of this sort need not be reiterated here; in particular the comments of Sec. 10·5 relative to the measurement of tan δ remain valid for free space.

Spherical Wavefront.—A source of error which is unlike interaction in that it has no analogue for waveguide work is the fact that the wavefront incident on the sample is essentially spherical rather than plane. As is seen from Fig. 10·16, the effect is qualitatively similar to that obtained by taking a number of readings for various angles of incidence near normal and averaging the results in some suitable way. To the extent that this simple mechanism represents the true effect it can be said, by virtue of Eqs. (47) and (52) and the accompanying remarks, that the error in practice will usually be very small. It may be investigated experimentally by taking measured k or tan δ vs. the distance from transmitter to sample, a procedure which was suggested and used in Ref. 14*a*.

Besides thus changing the "effective angle of incidence" (if one may be permitted such a term for waves which are not plane), the spherical phase-front has the added effect of producing inverse-distance attenuation; hence the amplitude distribution through the sample will not have the uniformity hitherto assumed, even along the axis. Points off the axis are illuminated nonuniformly in accordance with the antenna pattern, an effect commented on in Ref. 7*a*. Whether significant error from this attenuation would be encountered in practice is a matter not easy to determine with assurance, although the similarity of propagation constants for plane and spherical waves would indicate that no appreciable error should be observed when interface effects are negligible. For moderately thin samples the effect in question would likewise be expected to be small, a conclusion which has been verified experimentally in that the results are independent of both thickness and angle of incidence (cf. Refs. 6*a*, 7*a*, and Sec. 10·18). It is worth noting, incidentally, that

[1] That such behavior is found in practice is verified by the curves of Fig. 19c.

this inverse-distance attenuation gives a simple and accurate method of investigating the receiver characteristics. Thus, if the antennas are sufficiently far apart for the application of Fraunhofer theory, if they are kept oriented for maximum pickup, and if care is taken to avoid interference between the antennas themselves (Ref. 7*a*) or from surrounding objects, then a log-log plot of receiver reading vs. the distance between antennas should be a straight line with slope equal to the law of the detector. Such a curve was actually obtained in Ref. 14*a*, and used as a check on the linearity of the receiving system.

In connection with error from the spherical wavefront it is natural to inquire whether more accurate results will be obtained, for given antenna separation, with the sample near the receiver than with the

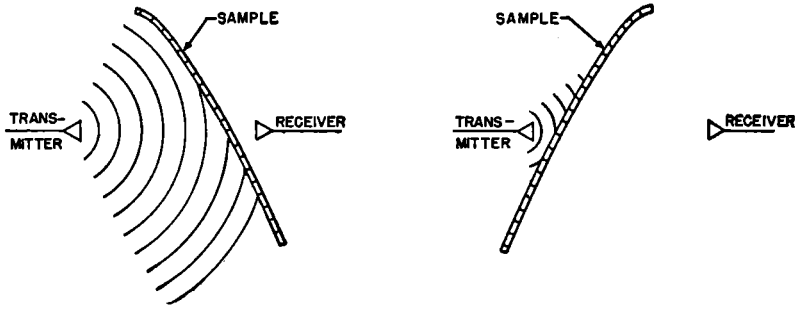

FIG. 10·16.—Spherical wavefront obtained in free-space measurement. The sample is shown as curved to indicate the generality of the result in the text, which is valid for such samples or for arbitrary incidence, and to illustrate the nature of the symmetry required.

sample near the transmitter. Intuitively an affirmative answer would perhaps be expected to this question, since the incident wave certainly becomes more nearly plane, both in phase and in amplitude, as the distance from sample to transmitter increases (Fig. 10·16). Despite this intuitive reasoning, however, the two positions are found to be essentially equivalent whenever the antennas are alike: for the situation of Fig. 10·16*b* can then be obtained from that of Fig. 10·16*a* by merely reversing the direction of power flow. If the general reciprocity theorem is applied to the system when the sample is not present, and then when it is, the ratio of complex transmission with sample to that without, which is the measured transmission coefficient, will be the same in Fig. 10·16*a* as in Fig. 10·16*b*. It follows that Δ and t are both unchanged, and hence the error due to the curved wavefront is presumably the same in both cases. Some slight error in this argument is to be anticipated in that one of the antennas is moved during the measurement, though the qualitative conclusion is not thereby invalidated. In practice, nevertheless, the sample should be placed nearer to the receiver, though for an

entirely different reason (Ref. 6*a*), namely, to prevent the so-called "pulling" of the microwave generator.

10·8. Computations for Normal Incidence.—The calculation of k from Δ may be made, in principle, by setting $p = 0$ in the waveguide equations, which then become equally valid for free space. Because of the restrictions introduced by having the sample in sheet form, however, these relations are for the most part rather inappropriate and therefore may be supplemented with equations specifically derived for the case at hand. The restrictions in question chiefly involve the sample thickness d, which can be given fairly large values and changed at will in guide, but which is usually small and difficult to change for free space. With the choice of d thus circumscribed, the analogue of Eq. (19), Eq. (42), is quite inaccurate theoretically, a situation that is the more serious in view of the high precision possible experimentally. For quantitative consideration Eq. (42) actually represents the exact limiting value (always neglecting $\tan^2 \delta$) which would be approached as d approaches infinity; and when d approaches zero, on the other hand, this exact limiting value is given by

$$k = 1 + \frac{2\Delta}{d},$$

as can be seen by Ref. 6*a* or by Eq. (45). In intermediate cases Eq. (33) gives the transcendental but real equation

$$\left(\sqrt{k} + \frac{1}{\sqrt{k}}\right) \tan\left(\frac{2\pi d\sqrt{k}}{\lambda}\right) = 2 \tan t', \tag{45}$$

which is likewise exact for $\tan^2 \delta = 0$ and which may be solved by graphical means (Fig. 10·17). With a direct solution of this kind, however, the plot required for accurate work is of almost prohibitive size, and therefore another procedure is sought.

Method Permitting Accurate Graphical Computation.—If Eq. (42) and Eq. (45) are combined (Ref. 6*a*),

$$\Delta_{\text{meas}} - \Delta_{\text{desired}} = \frac{\lambda}{4} - d\sqrt{k} - \left(\frac{\lambda}{2\pi}\right) \tan^{-1}\left[\frac{2\sqrt{k}}{1+k} \cot\left(\frac{2\pi d\sqrt{k}}{\lambda}\right)\right] \tag{46}$$

is obtained for the difference between the Δ's which would lead to Eq. (42) and the true value of Δ as actually measured. From this equation, which is plotted in Fig. 10·18, the value of the error in question cannot only be estimated but can also be corrected. Thus, the value of k is found from Eq. (42), which usually gives a value accurate enough for negligible error in Eq. (46). From Eq. (46) or from Fig. 10·18 the desired value of Δ may be obtained and substituted in Eq. (42) to find the true value of k. Although essentially a process of successive sub-

stitution which may be indefinitely continued, the values converge so rapidly that a single operation suffices for practically all cases. By virtue

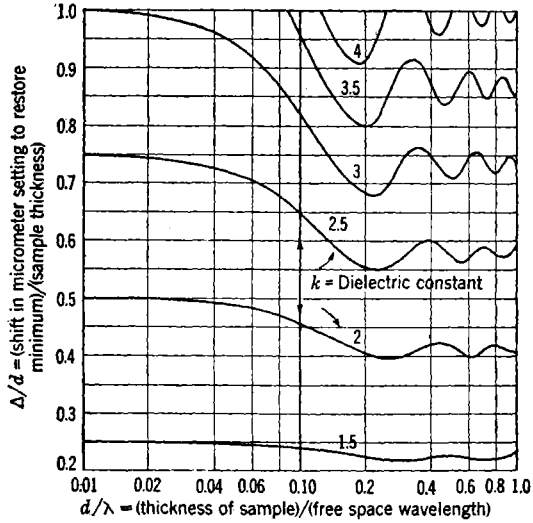

FIG. 10·17.—Exact relation between k and Δ for free space, normal incidence, and negligible $\tan^2 \delta$.

of the equivalence relations of Table 10·1, this method of compensation may also be applied to measurements in guide, although the use of samples thin enough to make such a procedure necessary is not particularly to be recommended.

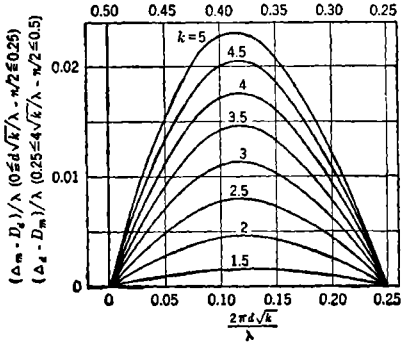

FIG. 10·18.—Error in approximate equation as a function of thickness and dielectric constant. The quantity Δ_m is equal to the measured value of Δ and Δ_d represents the desired value, that is, the value of Δ for which $k = (1 + \Delta/d)^2$.

Loss.—It has so far been assumed that $\tan^2 \delta \approx 0$. In the few cases for which this assumption is not valid certain of the waveguide equations may be used, although the expedients suggested for eliminating the effect of r_i in guide are usually no longer practicable here. Similarly, it is not usually possible to obtain a large effect from $\tan \delta$ in free space, unless the sample happens to be such that $d = n\lambda_m/2$. For this case Eq. (33) gives the required result implicitly, Eq. (39) explicitly, and in other cases the free-space method should not be used at normal incidence for finding loss. If $\tan \delta$ is already

known, however, its effect on the measured value of k may be compensated, the procedure being to use $(1 + r_i)^2/(1 - r_i)^2$ in place of k in Fig. 10·18, d/λ_m in place of $d\sqrt{k}/\lambda$, and from the value of k thus obtained to subtract the correction term of Eq. (36) with $p = 0$. Such complications seldom arise, however, in ordinary practice.

It must be mentioned that there is one notable exception to these inconveniences that are usually attendant upon free-space measurement of tan δ. The exception in question concerns the sample itself, which may be readily and accurately measured provided it is sufficiently lossy for the validity of Eq. (34) with manageable values of d, and of such a form (almost necessarily liquid) that d may be easily changed, and available in sufficient quantity to permit use of a sample large enough to obviate diffraction. With such samples the procedure suggested for comparable circumstances in guide is valid for free space as well; in particular the calculations may be made by Eqs. (36) and (37) with the symbols as there defined and with $p = 0$. Of course the number of materials fulfilling the above requirements is somewhat limited, although the requirements are admirably met by water, which was successfully investigated (Ref. 14*a*) by the free-space method as described here. For reasons already mentioned, however, free-space measurement of tan δ is not to be recommended as a procedure of general utility.

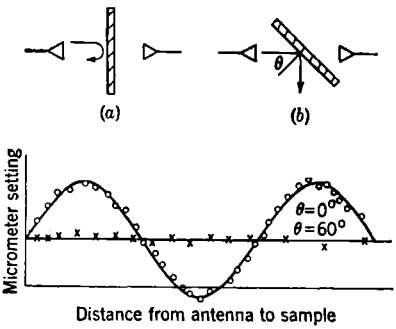

FIG. 10·19.—Interaction between sample and antenna at arbitrary incidence. (*a*) Normal incidence. (*b*) Not normal incidence. (*c*) Micrometer setting vs. sample position at $\lambda = 1.25$ cm. Points are experimental, curve is best-fitting sine curve with period $\lambda/2$.

10·9. Arbitrary Incidence.—Although error due to interaction may be canceled with the foregoing procedures, the labor of experiment and computation is considerably increased. The possibilities of the free-space method are not exhausted by the foregoing discussion, however, since the process of measurement is often more convenient and accurate at arbitrary than at normal incidence. In this case the errors due to interaction are automatically eliminated. Thus, instead of returning to the antenna, as in Fig. 10·19*a*, the wave reflected from the sample is directed away from the equipment as shown in Fig. 10·19*b*, and thus the measured value of Δ should be substantially independent of sample position. That such is the case in practice is shown in Fig. 10·19*c*; it is therefore unnecessary to duplicate the measurement with a quarter-wavelength

displacement when the incidence is far from normal. The appropriate form of Eq. (42) with either polarization may be written

$$k = 1 + 2\left(\frac{\Delta}{d}\right)\cos\theta + \left(\frac{\Delta}{d}\right)^2, \tag{47}$$

for incidence θ and negligible interaction between the sample faces (see Fig. 10·20). The equation may be obtained by setting $p = \sin^2\theta$ in Eq. (19), or directly by Eq. (42) and the β-equivalence of Table 10·1, since the phase is measured perpendicular to the wavefront in free space

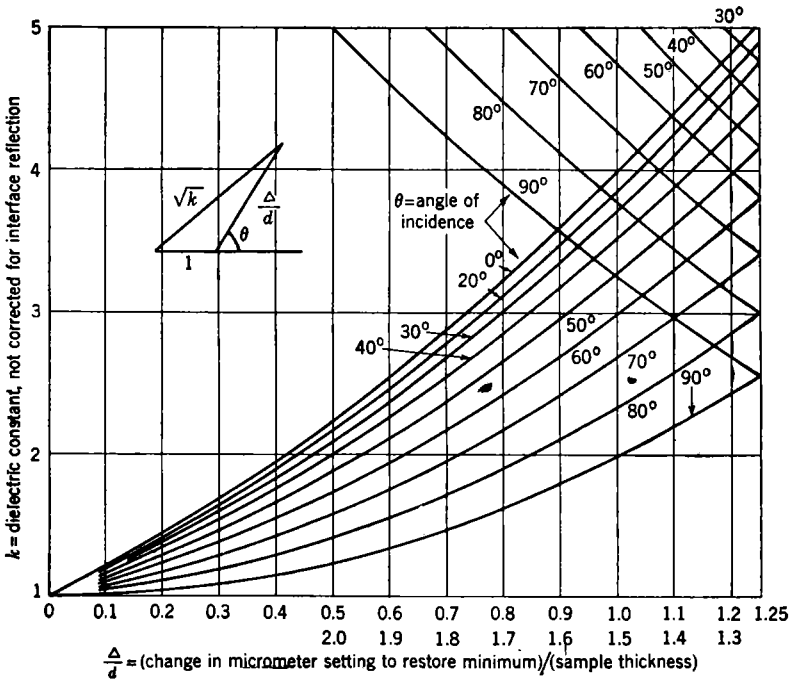

FIG. 10·20.—Approximate curves giving dielectric constant in terms of the phase shift at arbitrary incidence in free space.

and perpendicular to the sample in guide. Thus, the value of Δ in the earlier result or in the table corresponds to $\Delta\cos\theta$ in the present case, a substitution which is frequently necessary in progressing from normal incidence or guide equations to those of the type in question here.

Interface Reflection.—Like interaction between sample and antenna, the interaction between the two faces of the sample, which necessitated the correction associated with Fig. 10·18, may be eliminated automatically by the use of arbitrary incidence in many cases. For quantitative

investigation (cf. Refs. 7*b*, 6*a*),

$$\frac{\lambda}{2\pi} \sin^{-1} r_i^2 \approx \frac{\lambda}{2\pi} [r_i^2 + O(r_i^6)] \tag{48}$$

is found to be the maximum error in Δ due to r_i as the thickness is changed. This expression follows directly from Eq. (5) and is correct without approximation in guide as well as for arbitrary incidence at either polarization in free space, if the appropriate value of r_i be used in each case. From the curves of Fig. 10·21 it is seen that the error is much larger for

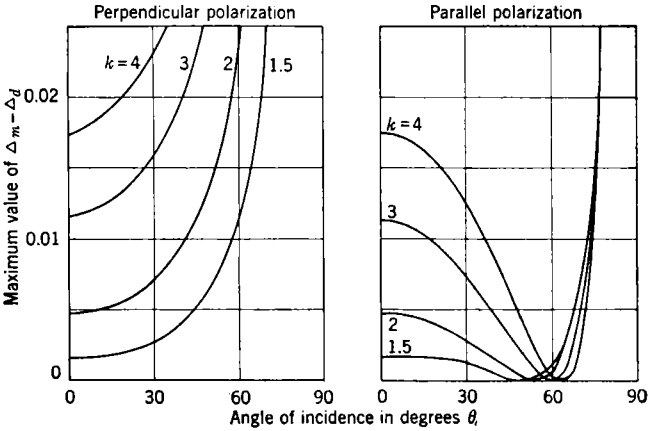

FIG. 10·21.—Maximum error in Δ due to interface reflection for polarization perpendicular or parallel to the plane of incidence.

perpendicular than for parallel polarization, in agreement with the well-known behavior of interface reflection; with parallel polarization the error is zero, as it should be, when θ equals the polarizing or Brewster angle,

$$\theta_b = \tan^{-1} \sqrt{k}. \tag{49}$$

In practice it is inconvenient to set θ to this value exactly, particularly when k is unknown; however, the error is so small that the exact determination of the proper θ is unnecessary in any case. For example, if $\theta = 60°$ is taken independently of Δ, the maximum possible error is shown by Fig. 10·21*b* to be less than 0.001λ whenever $1 \leqq n \leqq 4.5$, an error which is negligible for all but the most exacting work. If for any reason θ must be very far from θ_b, however, the correction of Fig. 10·18 may also be used at arbitrary incidence by means of the substitutions of Table 10·1. Such a situation arises when the sample is unusually thick, as the beam shift, due to refraction, will then lead to erroneous results whenever θ deviates appreciably from zero (cf. Ref. 6*a*). It is worth

remarking that a similar reduction of interface reflection is obtained when a TM-wave is used in a guide giving an appropriate value of p, though such a procedure has apparently not yet been used in practice.

Loss.—The reduction of r_i obtained with incidence other than normal may also be applied to measurement of loss, which satisfies

$$\tan \delta = -\frac{\lambda \ln t}{\pi k d}\frac{\sqrt{k-p}}{k} + O(\tan^2 \delta),\ (\theta \approx \theta_b),$$
$$= -\frac{\lambda \ln t}{\pi d\sqrt{k+1}} + O(\tan^2 \delta),\ (\theta = \theta_b), \qquad (50)$$

whenever θ is sufficiently near to θ_b. In the few cases for which neglect of $\tan^2 \delta$ is inadmissible the appropriate relation may be obtained by Eqs. (12) and (33) and Table 10·1, with due regard to the mode of measuring Δ [cf. Eq. (47) and accompanying remarks]. In both Eqs. (47) and (50) it is worth noting that change of polarization affects only the error term r_i, not the value of the main expression; hence the presence of slight cross-polarization may be justifiably neglected.

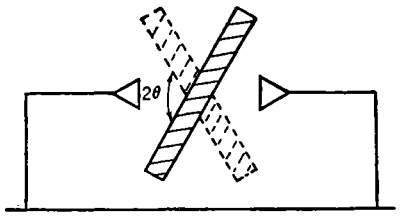

FIG. 10·22.—Determination of the true angle of incidence.

Measurement of Angle of Incidence.—With the above procedure it is necessary to know the true value of θ, which cannot be found by geometrical measurements alone. For this reason it is advisable to modify the normal-incidence technique, taking θ rather than the micrometer setting as the variable used to minimize the received power. Thus, θ is set at about 60°, or at any other desired value, and the micrometer is adjusted for minimum. With this fixed micrometer setting, θ is adjusted for minimum reading on the original and on the other side of $\theta = 0$, as suggested in Fig. 10·22, the fixed attenuator being inserted during the transition. The average of the two values so obtained is the true angle of incidence (Ref. 6*a*), and Δ is found, as usual, from the fixed micrometer setting as compared with that obtained without the sample. Because $\cos \theta$ varies so slowly when θ is near zero, this difficulty does not arise with the normal-incidence method, that is, Eq. (42) remains valid over a range of perhaps $\pm 10°$ in most cases, and hence the adjustment may be made by inspection (cf. Eq. (52)).

Sample Size.—Besides this extra difficulty in determining θ_0, the use of arbitrary incidence has the disadvantage of leading to large errors from diffraction in certain cases. Although the error can still be eliminated when the sample is sufficiently large, the size required is often prohibitive for materials not in industrial production. At the shorter

wavelengths this diffraction effect should theoretically depend chiefly upon the projected width of the sample, the minimum permissible size being accordingly given by an equation of the form

$$\text{Minimum permissible width} = A \sec \theta, \tag{51}$$

with the constant A depending only on the sample position and type of equipment. That such intuitive results are valid in practice is verified

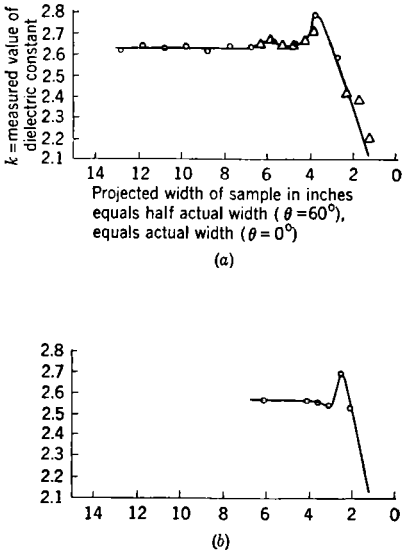

FIG. 10·23.—Effect of diffraction on apparent value of k, as measured by the phase shift for transmission in free space. In a the distance from the center of the sample to the receiver is 4.5 in.; the circles are for $\theta = 0°$, the triangles are for $\theta = 60°$. In b the center of the sample is 0.5 in. from the receiver, and $\theta = 0°$.

by Fig. 10·23a, where a curve of measured k vs. projected width is seen to be nearly the same at $\theta = 0$ as at $\theta = 60°$. For this particular case the constant A of Eq. (51) happens to be about 7 in. when the axis of rotation is 4.5 in. from the antenna, and about 4 in. when the distance is 0.5 in. (Fig. 10·23b). This decrease of A with the distance to the nearest antenna is likewise to be expected intuitively; obviously the axis and antenna should in practice be as close as the construction of the system will permit. Although no reliable method of compensation has been found, curves of the type shown in Fig. 10·23 permit estimation of the error in question or, alternatively, of the sample size required to reduce this error to negligible proportions, and only one or two curves are required for any given equipment. If it is desired merely to verify that the particular sample used is sufficiently large, without determining

the minimum size, a nontransmitting sample of the same size may be substituted. If the receiver reading is zero, independently of the micrometer setting, the size is ample. Such a procedure is described for checking the amplitude measurement in Ref. 14*a*.

10·10. Comparison with Optical Methods.—Before the subject of transmission as a means of determining k is left, a brief comparison of the microwave techniques described here with the closely analogous interferometer procedures of optics will be given. In optics the phase is usually measured by counting interference fringes, whereas in microwave techniques the micrometer setting is adjusted for minimum received power. The results obtained in the optical region are evidently considerably less accurate; phase errors of many degrees are possible. With microwave techniques, accuracies of the order of 0.1° are regularly obtained. In optical work, moreover, the effects of interaction are neglected, all results being computed from Eq. (42) or similar equations without correction of any kind; but this source of error has been considered in detail and compensated for in the microwave procedures just outlined.

From this superficial examination it might perhaps be concluded that optical methods usually lead to less precise values for k than those obtained with microwaves. Actually, however, such is far from the case. In fact, optical methods usually give two or three more significant figures than are at present attainable in the microwave region, quite irrespective of the inaccuracies noted. The approximate relations for k', the numerical error in k, may be written

$$k' \approx \left(\frac{2}{d}\right)\left[\left(\cos\theta + \frac{\Delta}{d}\right)\left(\Delta' - \frac{d'\Delta}{d}\right) - \theta'\Delta\sin\theta\right],$$

and

$$k' \approx \left(\frac{2\sqrt{k}}{d}\right)[\Delta' - d'(\sqrt{k} - 1)], \qquad \theta = 0, \tag{52}$$

in terms of Δ', d', θ', the numerical errors in Δ, d, θ respectively. From this equation it is seen, among other things, that the error depends on the ratios Δ'/d, d'/d; it does not depend on the angular errors Δ'/λ, d'/λ. Thus, although Δ' can be measured with only moderate angular accuracy at optical frequencies, it can be measured with high accuracy in length; it is in this sense that accuracy is required by Eq. (52). Looking at the question from a different point of view it may be said that the actual phase change Δ, in degrees, is extremely large for optical work, and hence an error Δ' of ten or twenty degrees is a negligible fraction of the total. From still a third point of view it may be found that Δ is really its measured value, which is less than a wavelength, plus a term $n\lambda$; although n is usually zero or a small integer in microwave work, it may

be as high as 10,000 in optics. By far the greater contribution to the Δ substituted in Eq. (47) accordingly comes from $n\lambda$, which is accurately known because λ is; and a given percentage error in the measured quantity Δ will therefore lead to a smaller percentage error in $\Delta + n\lambda$. Such considerations all depend on the fact that $d \gg \lambda$, and it is this condition that gives to optical methods their superior accuracy. Such a condition is unattainable to anything like the same extent with microwaves. The advantage of greater accuracy in phase measurement and in computation, then, is more than offset by the decreased sample thickness as measured in terms of wavelengths; whereas the refinements here mentioned would perhaps affect the eighth significant figure in optics, and could be ignored, they will usually affect the second or third figure in microwave work, and must be retained.

10·11. Uses.—The experimental and theoretical procedures for determining k by measurement of transmission in free space having been indicated, the applications will be discussed briefly. There are two characteristics of especial interest, namely, the method entails no preparation of the sample, and the phase shifter can be designed in such a way as to require no calibration. Because of this first property the method is particularly suitable for routine testing, in which a large number of determinations are to be made in a short time. Although many applications are of this type, it is often desirable to achieve great accuracy in a few determinations. The free-space method offers certain advantages here also, as the errors all decrease with increasing sample thickness and there are no serious systematic errors. In particular, there are no errors from clearance if the sample is sufficiently large. Accuracies of the order of a few tenths of one per cent are readily achieved for thick low-loss samples, and variation of θ, which is quite convenient in practice, leads to independent values of k as a check for consistent error. These advantages of having the sample in free space and unprepared are especially noteworthy for the measurement of certain materials. For those such as glass, which cannot be machined, the method is often convenient, and similarly for materials which are not strictly uniform, where the use of a large area automatically gives an average determination, which is often desirable. Examples of such materials are low-density materials, certain laminates, plain or conducting cloth, and wood. In particular for oriented materials, such as wood, it is possible to take a complete curve of k vs. the direction of polarization, although this presents considerable difficulty with any waveguide or cavity method.

The foregoing advantages follow from the fact that the sample need not be accurately machined to fit a cavity or guide. When combined with the fact that no calibration is required, this property shows the

method to be particularly applicable at the shorter wavelengths; with negligible error in d, θ, λ and with a given angular error in Δ, the error in k is directly proportional to λ. Moreover, difficulties from diffraction decrease rapidly as the frequency increases. Apart from this increase in accuracy, the equipment is suitable for use at the shorter wavelengths because of the simplicity of the r-f components required. Given a suitable generator, it is sufficient to have unmatched T-joints, simple horns, variable attenuators, and some means of measuring power, all of which are relatively easy to make in small sizes. In particular, no slotted section, probes, or phase shifters are required either for calibration or for measurement.

To these advantages must be added the corresponding disadvantages. For example, the use of large samples in sheet form is not only possible, but necessary; hence small samples or materials available only in the form of rods cannot be tested. Similarly, the increase in accuracy found with thick samples, which is easily attained in guide, is usually impracticable in free space. Even though the higher precision of Δ compensates this difficulty to some extent, it is nevertheless found that accurate results cannot be achieved with very thin sheets. Such considerations are particularly true of $\tan \delta$, in which the only compensating feature analogous to this higher accuracy of Δ is the slight advantage of having zero wall losses. And finally, instead of saying that the method improves with decreasing wavelength it may be said that it deteriorates with increasing wavelength; not only is the precise measurement of Δ more difficult, but errors from diffraction and stray radiation may become prohibitively large. At the same time the alternative waveguide and cavity methods become more accurate. It may be concluded that the present method is suitable for measurement at short wavelengths only.

GENERAL METHODS DEPENDING ON REFLECTION

10·12. Interface Reflection.—The discussion has hitherto been concerned solely with transmission. As noted, however, both k and $\tan \delta$, in principle at least, can be likewise determined from reflection. This procedure may well be considered in greater detail.

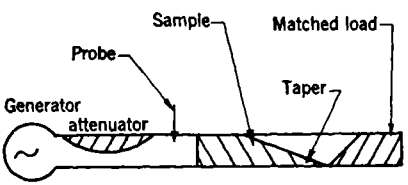

FIG. 10·24.—Experimental procedure for measuring interface reflection.

Waveguide.—With the arrangement of Fig. 10·24 it is clear that the complex interface reflection $r_i \exp(-jr_i')$ is obtained, which gives k

and tan δ by the exact Eqs. (54) and (55) for coaxial line. The corresponding result for waveguide in general is somewhat complicated, and therefore terms of the order of $\tan^2 \delta$ are neglected to obtain the approximate forms (cf. Fig. 10·27)

$$k \approx \frac{(1 + r_i)^2 - 4r_i p}{(1 - r_i)^2} \tag{53}$$

$$\tan \delta \approx \frac{k - 1}{k} \sqrt{\frac{k - p}{1 - p}} \tan r_i',$$

which follow easily from Eqs. (8), (12) and Table 10·2. Like Eqs. (54) and (55), these relations lead to simple numerical calculations. They

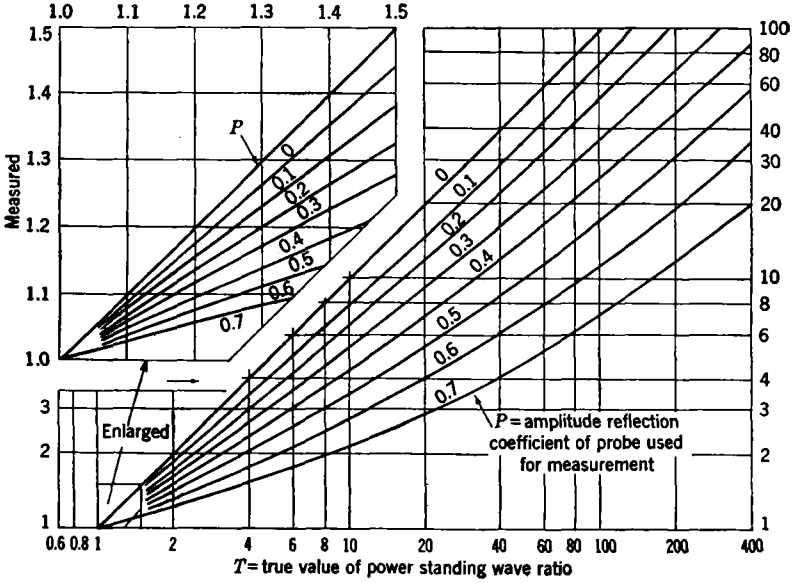

FIG. 10·25a.—Effect of probe reflection on apparent power standing-wave ratio; theoretical true vs. measured power standing-wave ratio with generator matched to line.

show that loss is determined from the phase shift r_i', essentially, whereas k is found from the absolute magnitude of r_i. To cancel the small reflection from the taper, the measurement is repeated with d replaced by $d - \lambda_m/4$, and to cancel the error due to load reflection the measurement is repeated with a quarter-wavelength motion of the sample as a whole. As an alternative procedure, which is especially useful when the measured reflection is small, the probe may be kept stationary, with the generator matched to the line, and the ratio of the maximum to the minimum probe reading may be taken as the sample is moved. A rather

detailed account of this and other methods of measuring small reflections or the associated phase shifts is given in Ref. 4*a*. Similarly, errors due to the measuring probe are discussed at length in Ref. 5*a*; if $Pe^{-iP'}$ is the probe reflection, it is sufficient here to observe that the fractional error in r_i is of the order of $r_i P \cos P'$, when the generator is matched to the line, whereas that in r_i' is negligible in comparison with the other errors. If the generator is matched to the load and if the probe is tuned

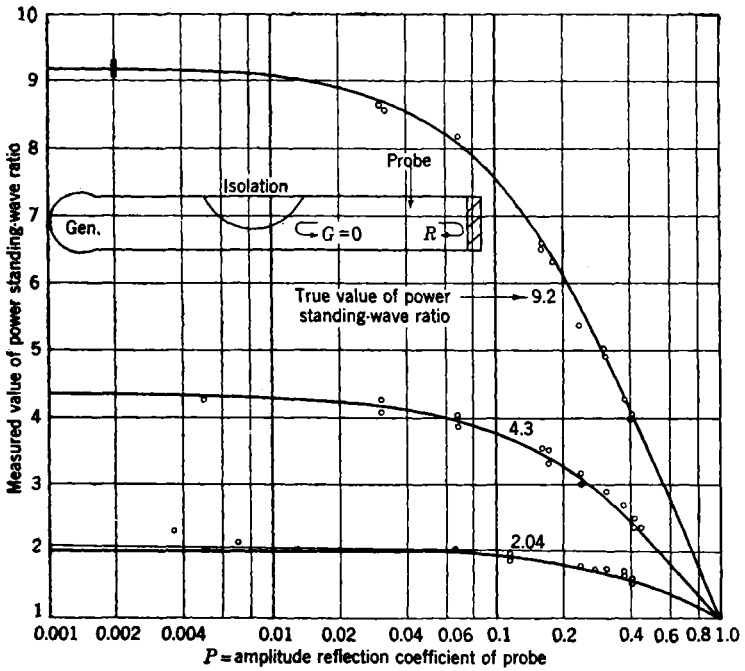

FIG. 10·25*b*.—Effect of probe reflection on apparent power standing-wave ratio; comparison of theory and experiment, generator matched to line.

for maximum pickup, which conditions should both be satisfied in good practice, then the error in reflection may be corrected by the curves of Fig. 10·25*a*. Experimental illustrations showing the general behavior are given in Figs. 10·25*b*, *c*. Wall losses are compensated by extrapolating the measured reflection to the sample interface, as described in Sec. 10·18, and subtracting (tan δ_{wall}) from (tan $\delta_{measured}$).

Interface reflection in guide was used in Ref. 11*a* to evaluate the dielectric constant and loss tangent of water, which is one of the few materials giving a sufficiently high reflection for accurate results. Precautions were taken to avoid error from probe reflection, and other r-f errors were investigated by the use of several depths for the water column. Because

of the high attenuation it was unnecessary to use a tapered sample. Loss was determined by the phase shift, as here described, and k was found from r_i. The size of waveguide used, combined with the large value of k, permitted substitution of the free-space equations, Eqs. (54) and (55), for the guide equation, Eq. (53). The method seemed to be satisfactory in this case. It was similarly used in Ref. 16*a* to determine k for water, although tan δ was found by a procedure presently to be described rather than by the phase shift r_i'. The general utility of this

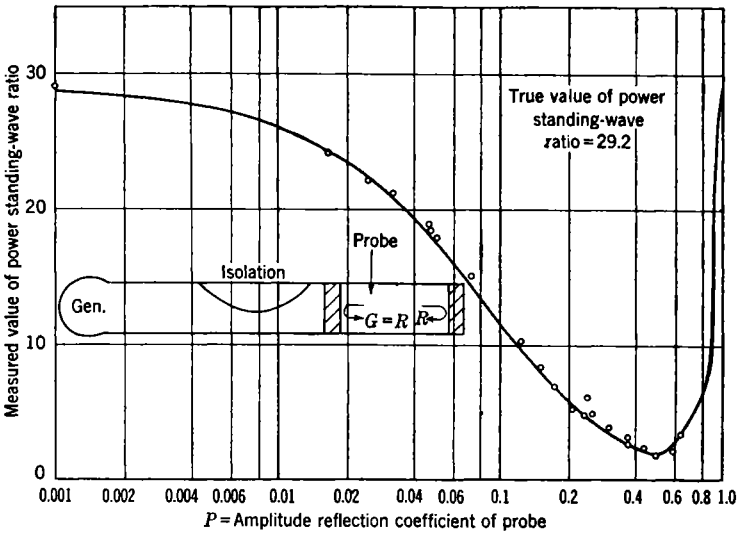

FIG. 10·25c.—Effect of probe reflection on apparent power standing-wave ratio; comparison of theory and experiment, generator matched to load.

interface method will be commented upon; the examples here cited show, for certain circumstances at least, that it can be successfully used in practical work.

Free Space.—In the course of the foregoing discussion it was noted that the methods depending on transmission in guide could be readily extended to free space—the process being regarded as an extension, despite the slight simplification of theory, because of the nonstandard experimental techniques required. A similar extension may be made for the methods just described; as before, it is found to lead to certain advantages, as well as disadvantages, not offered by the waveguide procedure. If Eq. (12) is substituted in Eq. (8), the following equations are obtained (cf. Fig. 10·26):

$$k \sec \delta = \frac{1 - 2r_i \cos r_i' + r_i^2}{1 + 2r_i \cos r_i' + r_i^2}, \tag{54}$$

$$\sin\left(\frac{\delta}{2}\right) = \frac{1}{2}\left(\sqrt{k \sec \delta} - \frac{1}{\sqrt{k \sec \delta}}\right) \tan r_i' \tag{55}$$

for tan δ in terms of $r_i e^{-jri'}$, the interface reflection when the incidence is normal in free space. Since the right-hand side of Eq. (54) involves measured quantities only, the need for simultaneous solution is obviated when the results are presented in the form here given. Thus, $k \sec \delta$ is obtained from Eq. (54), and is substituted in Eq. (55) to find sin $(\delta/2)$ which in turn gives δ, the loss tangent tan δ, and the term sec δ required to complete the computation of k.

With arbitrary incidence the corresponding equations are somewhat involved, and, as in the derivation of Eq. (53), terms of the order of $\tan^2 \delta$ are neglected to obtain

$$k = \frac{A(1 + \sqrt{1 - 4p(1-p)/A}}{2(1-p)}, \tag{56a}$$

where

$$A = \frac{(1 + r_i)^2}{(1 - r_i)^2}$$

and

$$|k - pk - p| \gg \tan \delta.$$

Similarly, when

$$|(k-1)(k-2p)(k-pk-p)| \gg \tan \delta,$$

$$\tan \delta = \frac{\sqrt{k-p}\,(k-1)(k-pk-p)}{\sqrt{1-p}\,(k)(k-2p)} \tan r_i' \tag{56b}$$

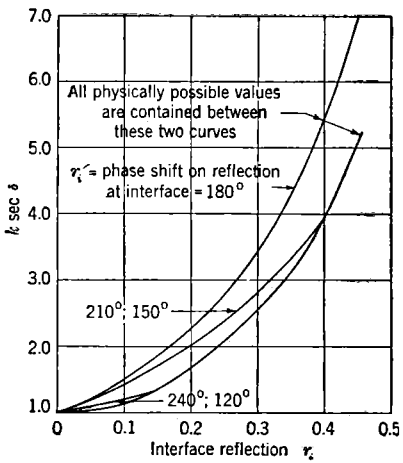

FIG. 10·26.—Dielectric constant vs. interface reflection for arbitrary loss in free space at normal incidence.

is found for polarization parallel to the plane of incidence. The result for perpendicular polarization is given, to the same approximation, by Eq. (53). Both equations, plotted in Fig. 10·27, follow from Eqs. (8) and (12) and Table 10·1. Parallel polarization admits a possibility not presented by any of the other conditions in that the effective dielectric constant for zero loss would be unity at the polarizing angle θ_b, which is found when p satisfies

$$p = \frac{k}{k+1}, \tag{57}$$

as is seen by setting the effective

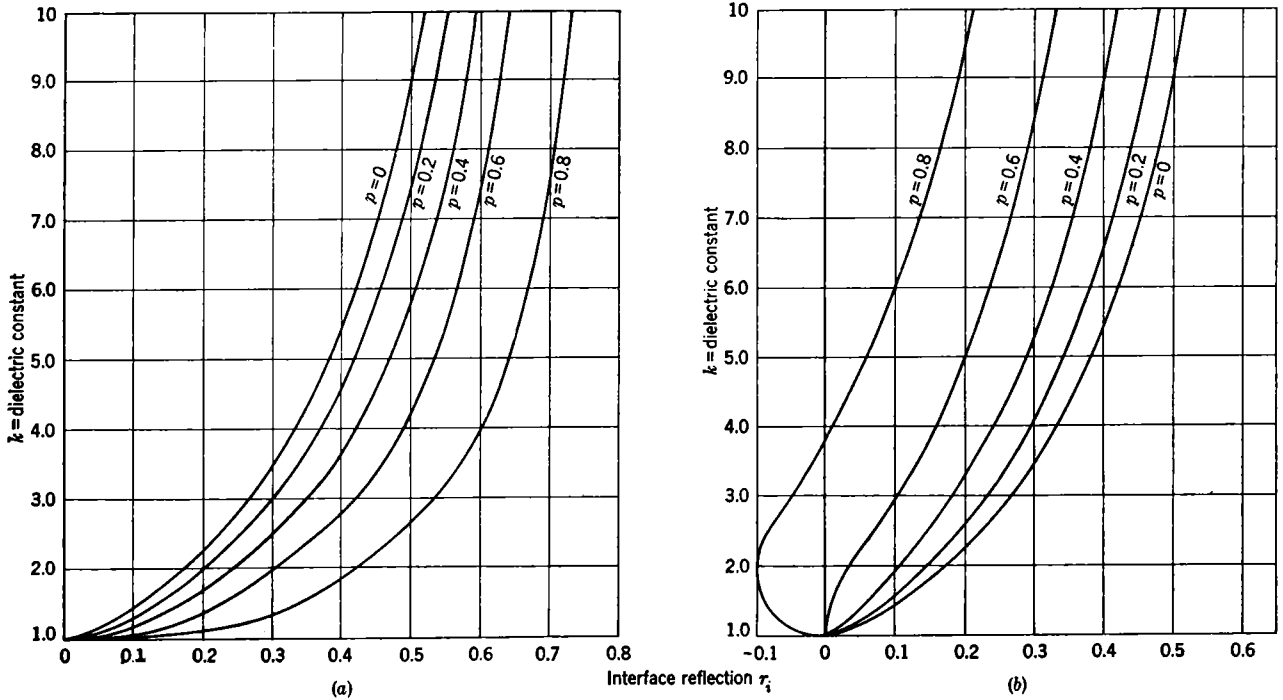

FIG. 10·27.—Dielectric constant vs. interface reflection for low-loss materials at arbitrary incidence or in waveguide. (*a*) Perpendicular polarization or *TE*-wave. (*b*) Parallel polarization or *TM*-wave.

value equal to unity in Table 10·1, or by Eq. (49). With this angle of incidence (which may be found with sufficient accuracy by taking reflection vs. angle over a small range and noting the minimum value) the approximations used in the derivation are incorrect; instead of Eq. (56), the equations obtained are

$$\tan \delta = \frac{4kr_i}{k-1}, \qquad p = \frac{k}{k+1}, \tag{58}$$

if again terms of the order of $\tan^2 \delta$ are neglected. Thus, the amplitude of the interface reflection cannot be used to determine loss, in general, as it involves only the small quantity $\tan^2 \delta$; but if parallel polarization is used and the angle of incidence is adjusted in accord with Eq. (49), then on the contrary, the amplitude reflection not only depends on the first power, but is directly proportional to it. The situation is unique in that it represents perhaps the only case in which small loss may be accurately determined from measurement of amplitude reflection without the use of a short circuit or its equivalent. Of course these results concerning parallel polarization are equally valid for waveguide propagating a TM-wave, although TM-waves have apparently not been used in experimental work.

10·13. Reflection Measurement in Free Space.—Turning now to the question of free-space measurement, three different methods are available from current practice.

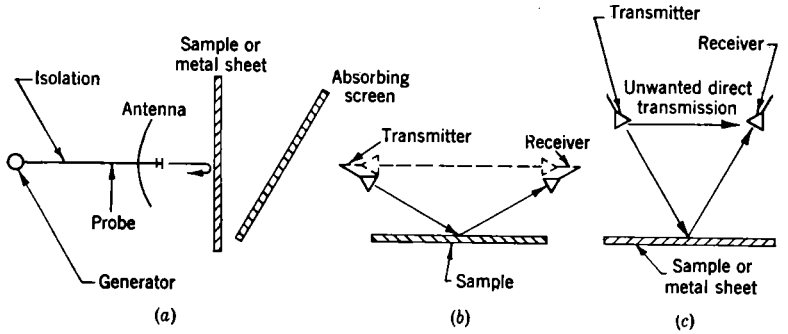

FIG. 10·28.—Equipment for reflection measurement in free space: (*a*) normal incidence, (*b*) incidence far from normal, and (*c*) general case.

Normal Incidence.—The first of these methods is to measure the reflection in the line from the sample, then from a metal sheet, as shown in Fig. 10·28*a*. If the antenna is matched to free space, the ratio of the two measured reflections gives the reflection coefficient desired (Refs. 7*a*, 20*a*). The dependence on sample size is investigated in some detail elsewhere (Ref. 7*a*). The sample may be considerably smaller than is permissible with transmission; a safe criterion is to have it cover the

antenna aperture if in the Fresnel region, and a larger area if in the Fraunhofer region. The effect of sample curvature is likewise investigated theoretically and experimentally in Ref. 7*a*, where the error is found to be theoretically negligible whenever the product of the radius of curvature of the surface and the wavelength is greater than one hundred times the square of the radius of the antenna for a paraboloidal antenna. Error from interaction between antenna and sample is canceled in the usual way by repeating the measurement with a quarter-wavelength displacement and using the average of the two values so obtained, rather than either value alone, as the measured reflection. Additional error is noted when the angle of incidence is not the same for the metal sheet as for the sample; thus, (Refs. 7*a*; 20*a*)

$$\text{(Measured reflection in amplitude)} = \text{(constant)(reflection coefficient of sample)}\ P(\theta), \quad (59)$$

where $P(\theta)$ is the one-way secondary power pattern of the antenna and θ is the (small) angle between the electrical axis and the normal to the sheet. Essentially the same result is obtained for the methods considered below, if θ is suitably interpreted. Because erratic values with a metal sheet are obtained at the shorter wavelengths, this method is suitable only when the microwave frequency is relatively low; even then a certain amount of care must be exercised since the measured power standing-wave ratio is usually small.

Incidence Far from Normal.—The foregoing procedure is operable only when the incidence is normal. With the arrangement of Fig. 10·28*b*, however, reflections in more general circumstances may be determined; the procedure as described in Ref. 14*a* is to compare the reflected power (solid path in the figure) with that received directly (dotted path). To check for cross-polarization, which is of moment whenever the incidence is far from normal, the ratio of maximum to minimum received power is noted as one of the antennas is rotated about its axis (Refs. 14*a*, 22*a*); with suitable antennas the ratio so obtained should be of the order of 10^3 or higher. The experiments of Ref. 14*a* were all carried out with perpendicular polarization; if the polarization is parallel, as required, for example, by Eq. (58), it is clear that error from cross-polarization becomes considerably more serious. Thus, the interface reflection is now higher for the unwanted component, whereas previously the reverse was the case.

A second source of error is the simultaneous presence of both direct and reflected waves, an effect which is unavoidable in that any real antenna has but limited directivity. This difficulty was considered in Ref. 14*a*, the procedure being to take reflection vs. angle and to draw a

smooth curve through the mean of the points so obtained. It was expected that the error in question would be sometimes positive, sometimes negative, and would thus be averaged out by the procedure described. An alternative—or rather a supplementary—method of cancelation is to change the distance from the receiver to the transmitter or the metal sheet, as the case may be, and to use the average of the maximum and minimum received amplitudes so obtained in all equations. Such a procedure, which is closely analagous to that to be treated in detail, will lead to slightly different values for the average path length with the direct and reflected waves—a difference which is present to some extent in any case. The attendant error may be corrected by the relation

$$\text{(Receiver reading with path length } D) = \text{(receiver reading with length } D') \left(\frac{D'}{D}\right)^2, \quad (60)$$

which is valid whenever the antennas are sufficiently far apart for inverse-distance attenuation (Refs. 7*a*, 14*a*). A square-law detector is assumed, and the receiver reading is taken as proportional to the received r-f power. As was the case for direct measurement of transmission, here too the error is the same as that in the power standing-wave ratio, and hence the discussion may again be deferred. Strictly speaking, the path length D must be measured from the effective center of the antenna (Ref. 7*a*), though for our present purposes it suffices to measure D from the antenna aperture.

Incidence Not Normal but Otherwise Unrestricted.—When the incidence is near normal, it is impracticable to send the power directly from the transmitter to the receiver along the dotted path in Fig. 10·28*b*. Thus, although error from interference between the two antennas may be canceled out by the usual quarter-wavelength motion (cf. Ref. 7*a*), error caused by the now great difference in path lengths cannot be compensated for by Eq. (60), which is valid only in the Fraunhofer region. To obviate this difficulty a metal plate may be used as before, the reflection coefficient being again obtained as a ratio of two measured values (Refs. 7*a*, 14*a*, 20*a*). The sources of error are for the most part similar to those already described, and, with one exception, they need not be reconsidered here. The exception concerns the problem of direct pickup between antennas, which is made more serious than before by their increased proximity in spite of the large angle in the secondary pattern at which it must occur (Ref. 14*a*). If A or A' denotes the amplitude of this directly transmitted wave, after it has entered the r-f line of the receiver, and if B or B' is proportional to the amplitude of the reflected wave, the unprimed quantities referring to the metal sheet, the primed ones to the dielectric, then the received power will be given approximately by (Ref. 14*a*)

$$\begin{aligned}\text{receiver reading} &= \left|A + \frac{B}{D}e^{-\frac{2\pi jD}{\lambda}}\right|^2 \\ &= \left|A' + \frac{B'}{D}e^{-\frac{2\pi j(D-C)}{\lambda}}\right|^2,\end{aligned} \tag{61}$$

where D again stands for the total length, between suitably chosen end points, of the r-f path. The constant C is necessary because the phase shift on reflection from the sample need not be the same as that for the metal. The ratio B'/B may be determined from Eq. (61), since this is easily seen to be equal to the reflection coefficient of the material. Such a determination was made in Ref. 14*a* by adjusting D for maximum receiver reading M^2, M'^2 in each case, whereupon second-order terms may be neglected (Ref. 14*a*), and

$$\frac{B'}{B} \approx \frac{M'}{M}\left(1 + \frac{C}{D}\right)\left(1 + \frac{AD}{B}\right)\left(1 - \frac{A'(D+C)}{B'}\right) \tag{62}$$

is the desired ratio B'/B in terms of the variables of Eq. (61), if D now stands for the particular value of D which gave a maximum with the metal sheet. With regard to inverse-distance attenuation, the unknown quantities AD/B, $A'(D + C)/B'$ are then determined from the ratio of maximum to minimum received power with the metal sheet or sample, as the case may be, and substituted in Eq. (62).

Although this method has been used with success it is somewhat complicated in practice. The following procedure, which is simpler and more consistent with the experimental techniques developed in this chapter, is presented. For compensating error from extraneous r-f power, it is required that an average of two readings be obtained, with the error positive for one reading and negative for the other. It is instructive to investigate the same operation as applied to Eq. (61). Since it may be assumed that $A < B/D$ and $A' < B'/D$, Eq. (61) gives

$$\begin{aligned}M + m &= B\left(\frac{1}{D + \lambda/8} + \frac{1}{D - \lambda/8}\right) \\ M' + m' &= B'\left(\frac{1}{D + C + \lambda/8} + \frac{1}{D + C - \lambda/8}\right),\end{aligned} \tag{63}$$

if D stands for the average of the two lengths noted for M and m and if M and M' are the maximum, m and m' the minimum receiver readings obtained by changing the distance to the metal sheet and to the sample, respectively. Thus both of the unknown amplitudes A and A' have been eliminated. From Eq. (63)

$$\frac{B'}{B} = \frac{M' + m'}{M + m}\left(1 + \frac{C}{D}\right) + e \tag{64}$$

is obtained for the desired ratio B'/B, with the error-term e easily shown to be $\leqq (\frac{1}{32})(\lambda/D)^3$ since $|C|$ may be assumed $\leqq \lambda/8$. Besides having the small coefficient $\frac{1}{32}$, this error term is of the third degree in a quantity whose square was neglected throughout the previous calculation; hence it may be justifiably ignored. Equations (62) and (64) are, of course, valid whether the antennas or the sample be moved to change D; they may also be used when only one antenna is moved, provided the amplitudes A, A' remain substantially constant.

Phase.—Phase may be determined in principle by comparing the minimum positions for metal and dielectric in Fig. 10·28*a*, as described in Ref. 7*a*, or by the free-space bridge method applied to the systems of Figs. 10·28*b* and *c*. Because of the low standing-wave ratio, the first method is very inaccurate, however, and both methods present certain difficulties in that the metal surface, if employed, must be placed precisely at the position formerly occupied by the sample. In using free-space reflection, therefore, the amplitude alone is usually measured, and the transmission or some other easily measured property is relied upon for the information that would normally be obtained from r_i'. This is the procedure followed in Ref. 14*a*, where the free-space methods here outlined were used to evaluate the dielectric constant and loss tangent of water. Because of the high loss the equations were too complicated for convenient simultaneous solution, and instead a graphical method was adopted, which is of sufficiently general application to be given a place here. The slope of the transmission curve was determined experimentally, whereupon Eq. (35) of the present text became an implicit relation between k and $\tan \delta$, and the locus of values could be plotted as a single curve. Next, the interface reflection r_i was obtained experimentally, and a similar locus derived therefrom. The computations are relatively convenient in each case; the intersection of the two loci gives the true values of both k and $\tan \delta$.

10·14. Change of Termination.—In transmission measurement nothing is usually gained by use of an unmatched termination for the sample; indeed, whether it be part of the sample itself or of the r-f measuring equipment, such a termination was found in the foregoing pages to be a serious source of error, and much of the experimental procedure was accordingly designed to simulate the condition of zero reflection for both sample and load. With reflection, on the other hand, quite the opposite behavior is found to prevail. Not only is it permissible to use an unmatched termination (with suitable changes in the theory, of course) but it is often necessary for the attainment of high accuracy. Such questions perhaps merit further consideration.

Terminations Not Containing a Short Circuit.—One of the simplest unmatched terminations is the second interface of the sample itself,

which need not be tapered as shown in Fig. 10·24. Instead of interface reflection, it is the over-all reflection $re^{-jr'}$ for an entire sheet of material that is obtained here. This reflection in turn may be evaluated

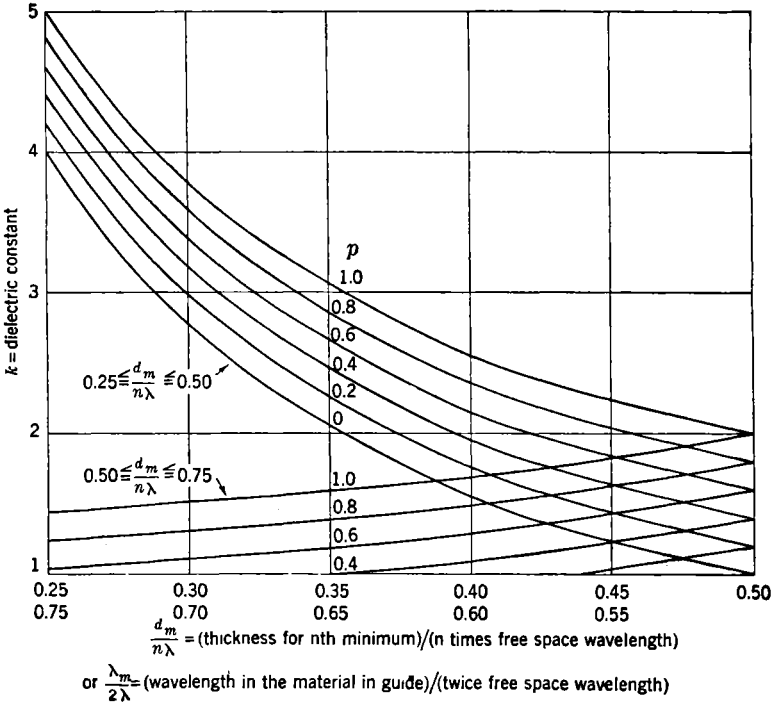

FIG. 10·29.—Dielectric constant vs. thickness for minimum reflection or vs. wavelength in the material.

by substituting $t_i e^{-jt_i'}$, $r_i e^{-jr_i'}$ as obtained from Eqs. (8) and (9) for t'', T''', τ'' and r'', R'', ρ'' in Eq. (6). Thus (Ref. 1*b*)

$$re^{-jr'} = -\frac{(k-1)(1-e^{-2j\beta d})}{(\sqrt{k}+1)^2 - (\sqrt{k}-1)^2 e^{-2j\beta d}} \tag{65}$$

is found for zero loss and normal incidence, with the result in more general circumstances to be derived as usual from Eq. (12) and Table 10·1. Equation (65) easily leads to

$$\left(\sqrt{k} - \frac{1}{\sqrt{k}}\right) \sin\left(\frac{2\pi d\sqrt{k}}{\lambda}\right) = \pm \frac{2r}{\sqrt{1-r^2}},$$

$$k \approx 1 + \frac{r\lambda}{\pi d}, \qquad d \ll \lambda, \tag{66}$$

for the amplitude, and the corresponding result for phase is given by Eq. (45) with $t' = r' + \pi/2$ (cf. Refs. 20*a*, 8*b*). In particular, the thickness d_m for minimum reflection gives a relation plotted in Fig. 10·29,

$$k = \frac{(n\lambda)^2}{(2d_m)^2} + p, \tag{67}$$

and the maximum reflection r_M gives the relation

$$k = \frac{1 + r_M(1 - p)}{1 - r_M}. \tag{68}$$

In Fig. 10·30 are plotted curves showing this function, for the general case of waveguide. Besides being nontranscendental, Eq. (67) is superior

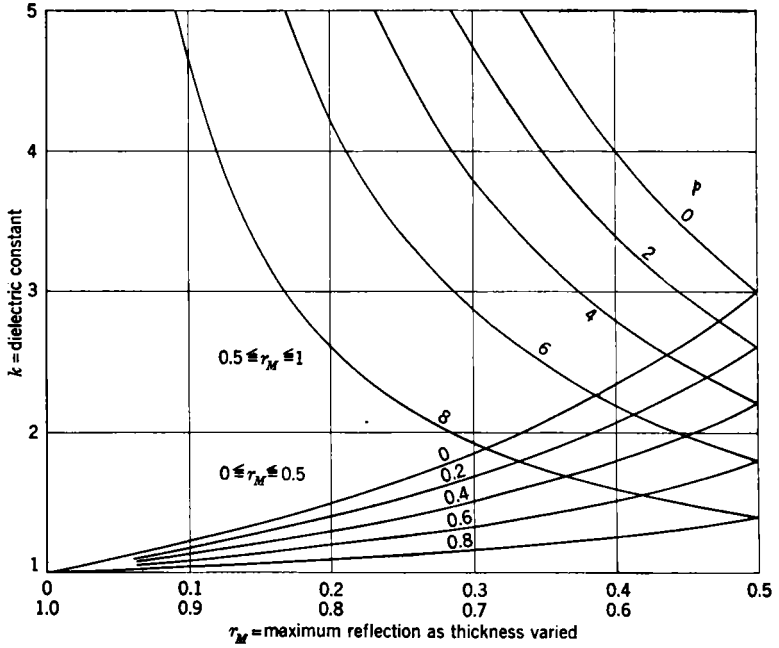

FIG. 10·30.—Dielectric constant vs. maximum reflection in waveguide.

to Eq. (60) because a large reflection can be measured with greater percentage accuracy than a smaller one, as may be easily shown (Ref. 2*a*), and because the derivative of the final result with respect to d is zero, the error due to inaccuracy in measuring the thickness is minimized. This process of maximizing the reflection while minimizing the derivative may be extended to several samples. Thus, if each of n sheets has its thickness adjusted for maximum reflection, then the reflection for the

whole series in free space will be maximum when the sheets are uniformly spaced exactly a quarter-wavelength apart. The over-all reflection so obtained equals the maximum reflection attainable with a single sheet of dielectric constant k^n (Ref. 8*b*).

A Digression Concerning Merit.—The use of various terminations in reflection procedure has been briefly considered; first a termination which matched out the reflection of the second interface was assumed, then one which consisted of this second interface itself, and finally a special case of a termination consisting of extra samples similar to the original one. Each of these terminations, as it happens, has actually been used in practice. Thus, the first occurred in sources already quoted; the second [Eqs. (66) to (68)] was studied in Refs. 6*a*, 21*b*, the approximate form of Eq. (60) being given in Refs. 6*b*, 21*b*; and the third has been used in unpublished laboratory work. There is apparently but one other termination, namely, a short circuit at some point behind the sample, which has been used in the measurement of dielectrics by reflection methods, and this termination is discussed in detail in Sec. 10·15.

Before proceeding to this final method, however, the merit of those just described will be considered. In the first place, the use of interface reflection has led to accuracy of the order of $\pm \frac{1}{2}$ per cent in practical work (Ref. 14*a*), and measurement of the over-all reflection of an entire sheet can likewise give precision of this order (cf. Refs. 4*a*, 7*a*). Such accuracy compares favorably with that obtained by the best methods at present available. Hence, inquiry should be made to determine whether it is a general property of these reflection techniques, or whether it is caused by an unusually favorable set of special circumstances. That the accuracy is caused by special circumstances is easily seen for the interface method; the material used was water, for which the interface reflection and loss are both high. Large reflection is desirable, although perhaps not absolutely necessary (Ref. 4*a*) for accurate measurement in guide. With ordinary precautions in evaluating the reflections usually encountered, k could hardly be determined to more than two figures, and because of the difficulty of measuring the minimum position associated with a moderate power standing-wave ratio, the loss $\tan \delta$ will usually fare even worse. Similarly, the use of interface reflection in free space is not only inaccurate, in general, but impossible to use, for the effect of the second interface cannot be eliminated when the sample is of ordinary thickness and moderate loss. Free-space measurement, in particular, permits no matching device analogous to the taper shown in Fig. 10·24. Hence for the high values of k or $\tan \delta$ obtained in the special investigations cited above, the interface method presents many advantages, but when regarded as an over-all procedure of general utility, it is nevertheless inferior to the methods presently to

be described. Similar considerations apply to the other methods, for example, to measurement of reflection for the complete sample and use of the approximate Eqs. (66) to (68), or their precise analogues for finite loss.

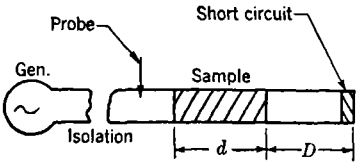

(a) General case

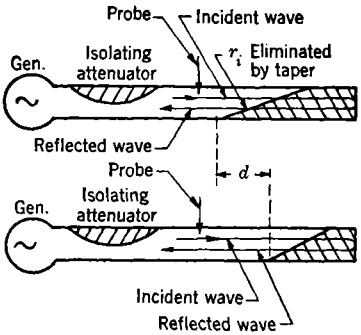

(b) Tapered sample. Repeat experiment with different length to cancel effect of taper

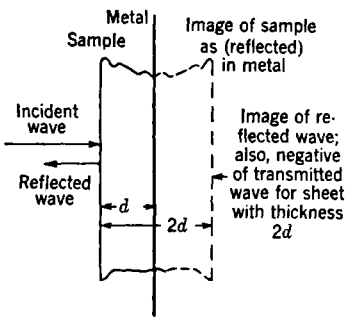

(c) Interpretation by the method of images. Zero reflection at the interface is assumed here.

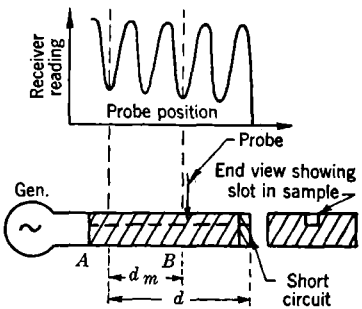

(d) Probe moving within the sample

FIG. 10·31.—The general short-circuited-line method; and two special forms of it which illustrate principles and lead to simple calculations. (a) General case. (b) Tapered sample. (c) Interpretation by the method of images. (d) Probe moving within the sample.

Since the emphasis here is upon techniques that are applicable in general, the discussion may proceed forthwith to methods using a short circuit.

10·15. Short Circuit, Zero Reflection at Interface.—By the equipment of Fig. 10·31*a* the reflection coefficient and minimum position may be obtained for the short-circuited line with and without the dielectric sample, whereupon from Eq. (18) and the accompanying remarks it is

seen that the change in minimum position gives k, essentially, whereas the change in reflection coefficient gives tan δ. The general arrangement of Fig. 10·31*a*, for which the interface reflection r_i has not been eliminated, is discussed at length in the following sections. For our present purposes a qualitative description of the type just given is sufficient.

From this so-called "short-circuited-line method," which was developed by A. R. von Hippel and his associates (Refs. 1*a*, 2*b*, 3*b*, 5*b*), many advantages are obtained over the mere measurement of r_i or r. Not only do given errors in measurement usually lead to smaller errors in the result, but these measurements themselves may be carried out with far greater accuracy. Instead of being perhaps 3 or 4, the power standing-wave ratios are now anywhere from 10^3 to 10^7, with a corresponding increase in the accuracy with which minimum position, and hence k, may be determined. For tan δ the situation is analogous to that noted in connection with Fig. 10·12, where it was found desirable to have $t = 1$ when tan $\delta = 0$. Here $R = 1$ for zero loss, if R is the amplitude reflection of sample and short circuit; hence the error in tan δ is comparable with that in $1 - R$, which may be measured directly. Thus, instead of measuring a minute variation in a large quantity, as is necessary for finding tan δ from r or r_i, the actual value of a small quantity is measured, a procedure which here too, as with t above, is more accurate.

Methods Using a Probe.—There is indeed more than a superficial similarity between this procedure and the transmission procedures hitherto described, although the wave now traverses the sample twice instead of once. This equivalence, intuitively evident in any case, becomes formally exact when r_i is negligible, for the solution is then given, without further approximation, by Eqs. (36) and (37), with $2d$ written in place of d and with R, the over-all reflection of sample and short circuit, in place of t. The quantity Δ represents twice the difference in minimum positions with and without the sample (cf. Fig. 10·31*c*). These results, which follow by setting $r'' = \rho'' = 0$, $t'' = 1/\tau''$, $R'' = -1$ in Eq. (6), may be used for actual measurement if the effect of r_i be properly eliminated. Thus, when $k \approx 1$, the usual quarter-wavelength change is made in d. For general values of k the same effect is achieved by the use of two measurements with a tapered sample (Fig. 10·31*b*). When the quarter-wavelength change is made, the average of the two computed values is used; when the tapered sample is used, the difference of the two d's and the ratio of the two R's are substituted, rather than the quantities themselves, into the equation. Wall losses are compensated, *mutatis mutandis*, by the procedure of Secs. 10·5 or 10·18. This is true of all the methods of this section.

A second method of achieving much the same result is given in Fig.

10·31*d*, where the measuring probe is so located that the measured reflection must be completely independent of r_i. This property, which is easily proved by Eq. (7) of the introduction, also follows from the well-known fact that the impedance of a termination depends only on the termination, not on the items that may have preceded it in the line. In terms of the measured reflection at the point A, which is a distance d from the short circuit (Fig. 10·31*d*), the transmission equations of the foregoing pages, with the substitutions described in the above paragraph, will again give k and tan δ. The result involves no theoretical approximation.

As far as the present theory is concerned, the choice of point A is arbitrary; in particular, it need not be at a voltage node as shown in Fig. 10·31*d*. But when measurement instead of theory is considered, the advantage of this choice becomes at once apparent, for the reflection, as well as the phase, cannot be readily determined at any other points of the line. In connection with measurement procedure it is worth noting also that, for measurement of reflection at a point within the sample as here required, it will not do to take the ratio of maximum to minimum power in the conventional manner, since the attenuation produced by the sample may become appreciable over the region thus traversed by the probe. Instead the procedure to be discussed is used noting that Eq. (79) for reflection in terms of the width at twice minimum is valid here if λ_v be replaced by λ_m, the wavelength in the material in guide. The dielectric constant k may usually be determined first from the minimum position alone. After k has been thus determined, λ_m is computed without difficulty, and with λ_m known the reflection is obtained from Eq. (79), which in turn gives tan δ by the procedure outlined. If the loss is so high that it appreciably affects the value of λ_m—which is almost never the case in practice—then the equations are transcendental; they may, however, be solved by successive substitution in the manner suggested for Eq. (33).

The foregoing method neglects loss in the short circuit itself, which is not compensated even when tan δ_{wall} is subtracted from tan $\delta_{measured}$ as prescribed. To obviate this difficulty the reflection may be measured at two points, for example, A and B of Fig. 10·31*d*; d is taken now as the distance d_m between the points, and the reflection as the ratio of the two measured values. Because of the need for a slot in the sample, the method of Fig. 10·31*d* is not well suited for measurement at very short wavelengths, although the same or a similar procedure appears to have been employed successfully (Ref. 17*c*) for measurement of k in the 3-cm range. Since the slot is in a region of maximum field, the error is probably somewhat larger than that for an equivalent area spread over the top of the sample. In other words, the present failure of the sample

to fill the guide completely is more serious than the ordinary clearance problem. It must be mentioned, however, that this method has an outstanding advantage over all the others involving a short circuit in that the character of the load does not change while the measurements are being made. The results for different sample lengths or for sample and guide need not be compared. The necessity for generator isolation is thus materially reduced, since the free-space wavelength can be measured while the sample is in place.

The use of a probe and a short circuit for dielectric measurement as described permits a physical interpretation somewhat different from the one here given. Thus, the problem has been regarded as analogous to transmission, a procedure which was made plausible by Figs. 10·31*b,c,d* and which was proved by Eq. (6). If the dielectric constant is considered, however, the method of Fig. 10·31*d* may be interpreted as a means of measuring the wavelength in the material, without regard either to transmission or to reflection as such. For negligible $\tan^2 \delta$ the distance between the ith and $(i + n)$th node is equal to $n\lambda_m/2$, and hence k is given by the relation plotted in Fig. 10·29 and Eq. (67), with $d_m = d$. This point of view, which is the one adopted for such methods in Ref. 6*a*, may be used here and in the following paragraphs to supplement the transmission analogy noted. The wavelength presentation is in some respects the simpler when loss is not in question, whereas the transmission analogy is to be preferred for the general case.

Methods Not Using a Probe.—At short wavelengths the design of traveling probes becomes difficult, and methods have accordingly been devised for obtaining the necessary information by other means. Several of these methods have already been described in the foregoing sections of the present text, with regard to measurement of both transmission and reflection. For the present situation, in which the sample is followed by a short circuit, the procedure suggested in Fig. 10·32*a* may be used. As the plunger and with it the sample are moved along the line, the receiver reading will take on maximum or minimum values; the difference between plunger positions for corresponding values will be equal to $\lambda_m/2$, and k is thus to be found from Eq. (67). In other respects too the method is equivalent, as far as principles are concerned, to that of Fig. 10·31*d*. Thus, it is possible to imagine the sample and plunger positions held constant while the generator and receiving system are moved; all theoretical relations or procedures for the previous case are therefore applicable here. With regard to actual operation in practice, however, there are several differences in addition to the valuable property of not requiring a traveling probe. The line leading to the load is of variable length, for example, with the result that the usual measures must be taken to prevent interaction between the two components of the system—in the present

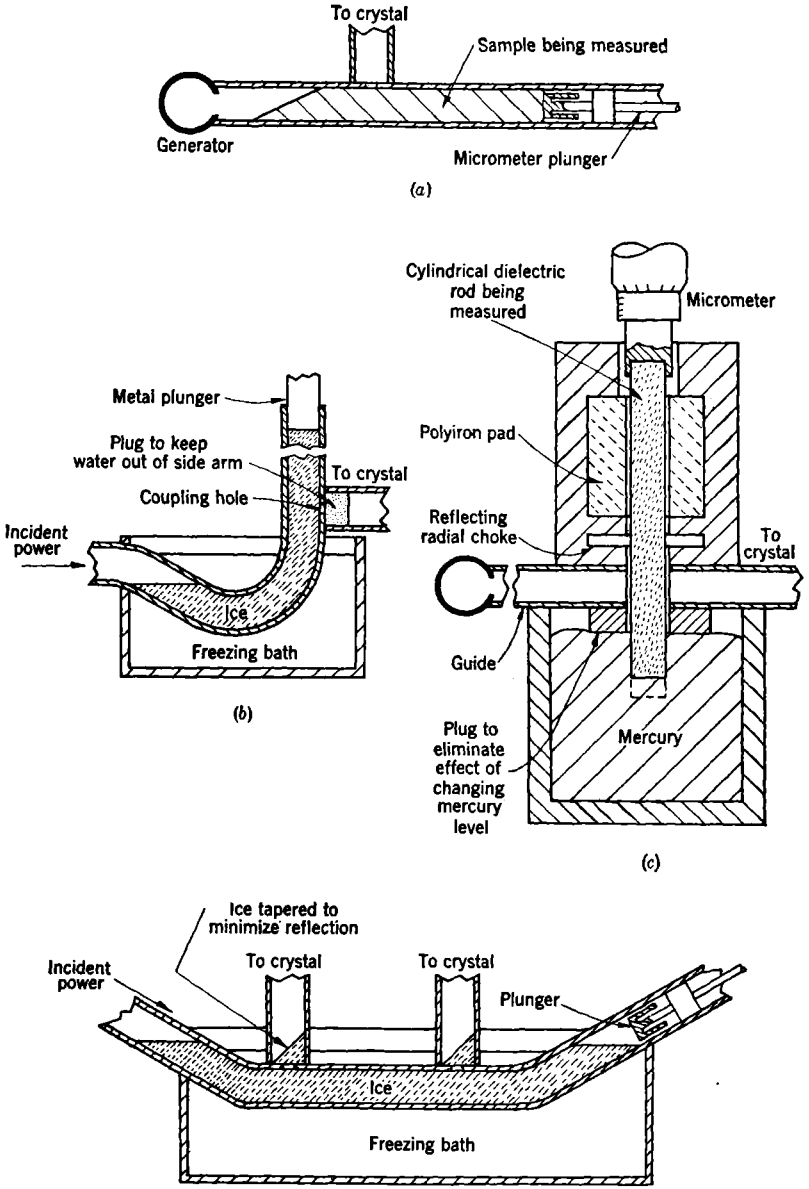

FIG. 10·32.—Methods of making measurements on a sample, backed by a short circuit, without the use of a probe.

case, between generator and load. Added to this requirement, which is essentially that the generator reflection must be small, is a second requirement that the sample be tapered, for the sidearm, corresponding to the probe in Fig. 10·31*d*, has a relatively high reflection of its own. Partly because of this reflection the method is found not to be satisfactory for evaluation of loss; its originator, E. L. Younker, has used it successfully, however, for measurement of k (cf. Ref. 6*a*).

In Ref. 16*a* the foregoing procedure was modified as illustrated in Fig. 10·31*d* and used for measurement of the delectric constant of ice. The plunger is now moved by melting the sample, which thus changes in length while the interface position remains constant; but in all respects relevant to the present discussion the method is equivalent to that of Fig. 10·32*a*. A second modification, developed by E. L. Younker and E. M. Purcell (cf. Ref. 6*a*) is represented in Fig. 10·32*c*, where the use of a mercury well eliminates error due to clearance. The samples, which must be in the form of rods, should be of a diameter D satisfying

$$0.765\lambda \geqq D\sqrt{k} \geqq 0.585\lambda$$

to permit propagation at one and only one mode; but in other respects the theory and equations remain the same as for Fig. 10·31*a*. A final modification (Ref. 16*a*), which gives information on tan δ rather than on k, is that shown in Fig. 10·32*d*. The ratio of maximum to minimum power is taken, first in one side arm and then in the other, as the plunger is moved. From this the ratio of the reflection coefficients at the two points is computed and the procedure thenceforward is the same as that described in connection with Fig. 10·31*d*.

THE SHORT-CIRCUITED-LINE METHOD

10·16. Theory.—Although sufficiently exact for numerical computation when $r_i = 0$, the precise analogy to transmission is no longer obtained when $r_i > 0$. The following relation, however, which is suggested by Fig. 10·31*c*, may be proved by direct substitution from Eqs. (33), (65), and (69):

$$\left.\begin{array}{l}\text{Complex reflection for a sheet of}\\ \text{thickness } d \text{ backed by a metal}\\ \text{plate } (D = 0)\end{array}\right\} = \left\{\begin{array}{l}\text{Complex reflection minus com-}\\ \text{plex transmission for a similar}\\ \text{sheet of thickness } 2d \text{ backed}\\ \text{by a matched load.}\end{array}\right.$$

A special case of a similar result which has been proved from the relations of the Introduction, this equation is easily shown, by the methods here adapted for such extension, to be valid without error for lossy materials in waveguide or at arbitrary incidence. This affords another proof

of the unity so often observed in the present text, in that the relations for the short-circuited-line method are contained in those for a single sheet. Of course the details of actual computation require further study, which will be given in the present section; as far as principles are concerned, however, the equivalence has been completely established.

General Considerations.—From the result just stated, it may be shown that one of the most significant practical differences between the short-circuited-line method and transmission methods is the behavior of errors. Thus, when dealing with transmission, it was found necessary to have $1 - t$ small, so that the measured effect would be due to tan δ alone. This condition, which arose through experimental requirements, immediately led to the theoretically simple situations $r_i \approx 0$ (tapered sample) or $r \approx 0$ (half-wavelength thickness). It was therefore unnecessary to give a detailed consideration of rectangular samples for general values of d. When dealing with reflection, on the contrary, no such artifices are required to achieve experimental accuracy; the quantity $1 - R$ will automatically approach zero with tan δ, irrespective of the value of d or r_i. Physically, this behavior follows from the fact that all power not measured must now be absorbed, since none is transmitted through the termination; but in the transmission measurement the power not measured could be either reflected or absorbed. The use of tapered samples, samples an integral number of half wavelengths long, or the other modifications heretofore described, is therefore unnecessary with the short-circuited-line method, and an investigation of the theory for the general case (Fig. 10·31) is well worth while.

If a lossless sheet is backed immediately by a metal plate in free space, the normal-incidence reflection $Re^{-jR'}$ for the whole is given by

$$Re^{-jR'} = -\frac{(\sqrt{k} - 1) + (\sqrt{k} + 1)e^{-2j\beta d}}{(\sqrt{k} + 1) + (\sqrt{k} - 1)e^{-2j\beta d}}, \tag{69}$$

as is seen if values from Eqs. (8) and (9) are substituted for t'', τ'', $\bar{\tau}''$ and ρ''; and R'' is set equal to -1 in Eq. (6). By reference to Eq. (12) and Table 10·1, the exact solution is obtained for the general case represented with $D = 0$ in Fig. 10·31*a*. The equation so obtained can be put into strikingly simple form without approximation of any kind; whether in free space or guide, the entire problem reduces to the transcendental equation (Refs. 2*b*, 5*b*)

$$\frac{\tanh(ae^{jb})}{ae^{jb}} = ce^{jd}, \tag{70}$$

where c and d are known and a and b are required. Since it involves but two variables, the left-hand side of Eq. (70) may be plotted or tabu-

lated without difficulty (Ref. 5*b*) and thus, in principle at least, a general solution of the problem with arbitrary thickness, interface reflection, and loss is obtained. It is worth noting that the short-circuited-line method, or modifications of it, are apparently the only ones for which the general equation simplifies in this way. Although simple results can be found for the other methods, they depend upon neglect of $\tan^2 \delta$, elimination of r_i, or some similar artifice.

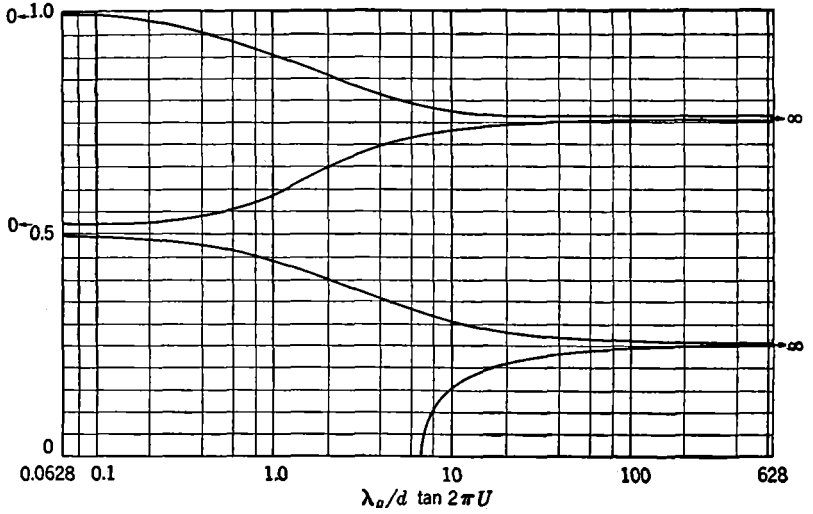

FIG. 10·33.—A plot of $2\pi \tan x/x$ giving the general solution of Eq. (71); $x = 2\pi V$.

In spite of this increased simplicity (as compared with the corresponding result for other methods) actual computation from Eq. (70) leads to a certain amount of difficulty in practice. The mathematical methods whereby such difficulty is circumvented are not relevant in a discussion of measurement procedure, and are moreover described at length elsewhere (Refs. 1*a*, 2*b*, 5*b*). It therefore suffices here to point out the existence and theoretical advantages of Eq. (70). Attention is henceforward confined to the case $\tan^2 \delta = 0$, which leads to simple relations, and actually includes most situations of practical interest. The results, to this approximation, are given in Refs. 26*b*, 9*b*, and, together with correction terms for more accurate approximation, in Ref. 22*b*:

$$\frac{\tan 2\pi V}{V} = \frac{\lambda_g}{d} \tan 2\pi U, \tag{71}$$

$$\tan \delta = W\left(\frac{k-p}{k}\right) \frac{4\pi \csc 4\pi U}{4\pi V \csc 4\pi V - 1} \tag{72}$$

The quantities U, V, W are given by

$$U = \frac{(\Delta + d)}{\lambda_g},$$

$$V = \frac{d\sqrt{k - p}}{\lambda}, \tag{73}$$

$$W = \frac{1}{\pi}\frac{1 - R}{1 + R},$$

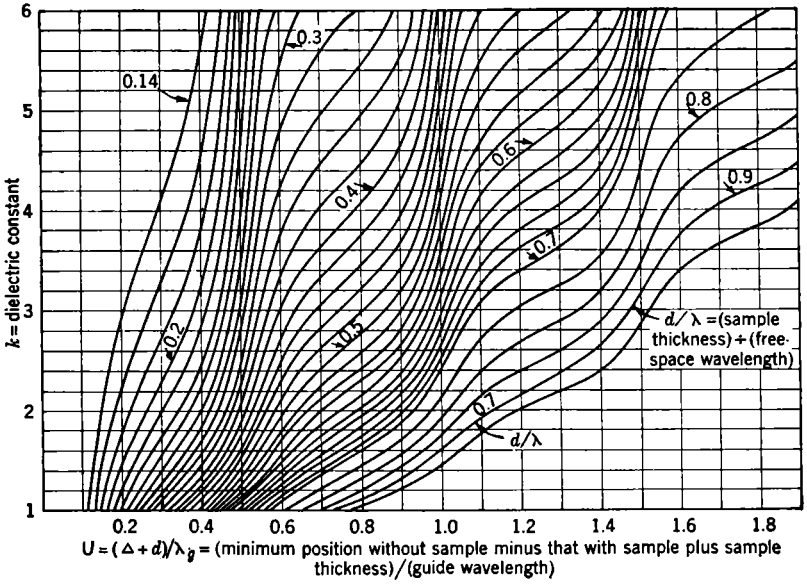

FIG. 10·34.—Explicit curves of k vs. measured quantities, valid for $p = 0.345$.

in terms of the amplitude reflection coefficient R and the shift in minimum position Δ produced by insertion of the sample. Although transcendental, Eq. (71) is readily solved by graphical means; indeed, a plot of $(\tan x)/x$ is all that is required (Fig. 10·33). When much work is to be done for a given value of p, however, it is expedient to give a less general presentation such as that shown in Fig. 10·34. The equation for $\tan \delta$ is likewise solved conveniently by means of graphs; because of periodicity, a single set of curves covering a limited range suffices for all cases (Fig. 10·35). When the thickness is an integral number of quarter wavelengths, this graph cannot be accurately read; but its equation then takes the simpler forms

$$\tan \delta \approx \frac{W\lambda^2}{kd\lambda_g}$$

$$\tan \delta \approx W\frac{\lambda_g}{d}\left(\frac{(k - p)}{k}\right), \tag{74}$$

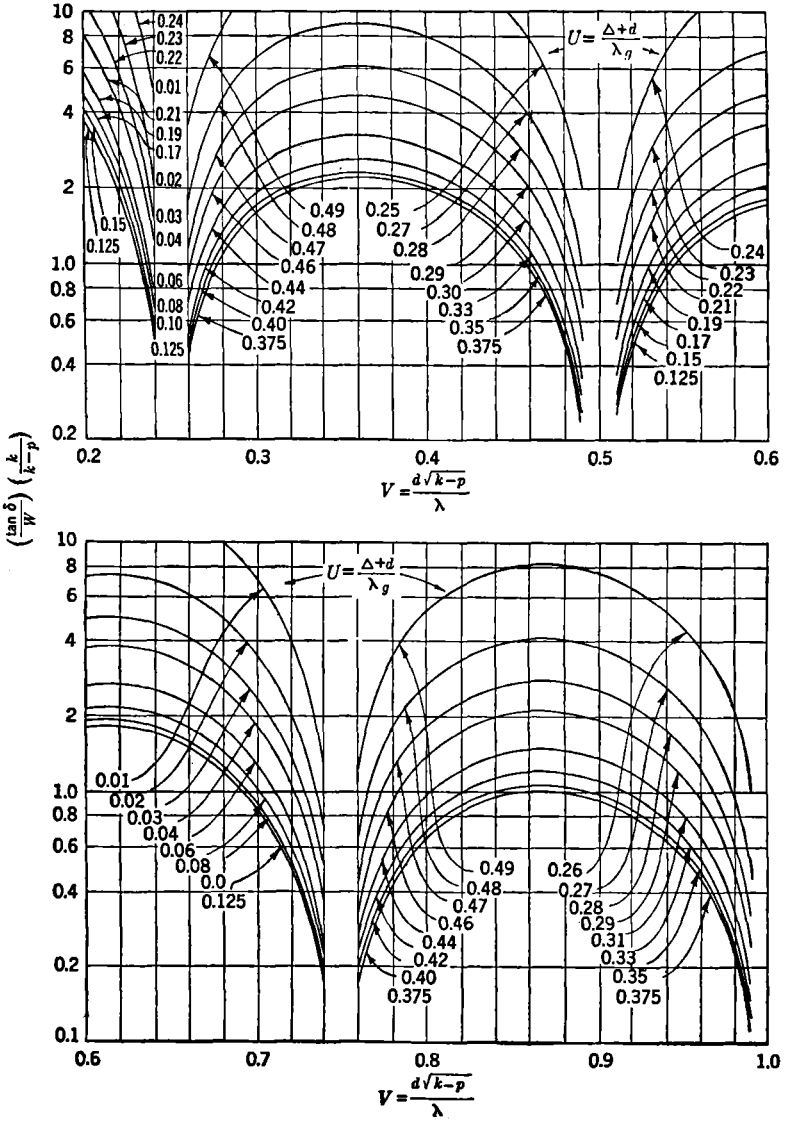

FIG. 10-35.—Curves for computation of tan δ, valid for all values of p.

and graphical computation is less convenient than direct computation for this case. The error is less than 5 per cent in the first equation when $0.73 < V < 0.77$, in the second when $0.48 < V < 0.52$. Wall losses are compensated as described in Sec. 10·18.

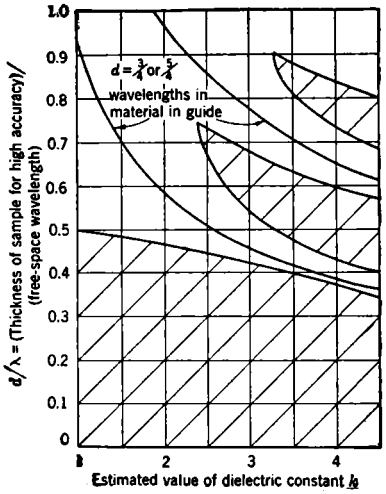

FIG. 10·36*a*.—Value of sample thickness for maximum accuracy with short-circuited-line method. Condition for minimum slope in Fig. 10·34. The slope is greater than 60° in the shaded region, less than 60° elsewhere.

Thickness for Maximum Accuracy.—In the transmission method, the accuracy of k, for given experimental errors, increases steadily as d increases, although of course errors due to clearance are not thus reduced. In the present case, no such steady decrease of errors is obtained. As is seen from Fig. 10·34, regions of high accuracy alternate with those of lower accuracy; only the general trend is preserved. Closer scrutiny of this effect, which is caused by the nonzero value of r_i, shows that the errors in k caused by errors in Δ are minimized if the thickness is an odd number of quarter wavelengths (Ref. 5*b*). Thus, Eq.

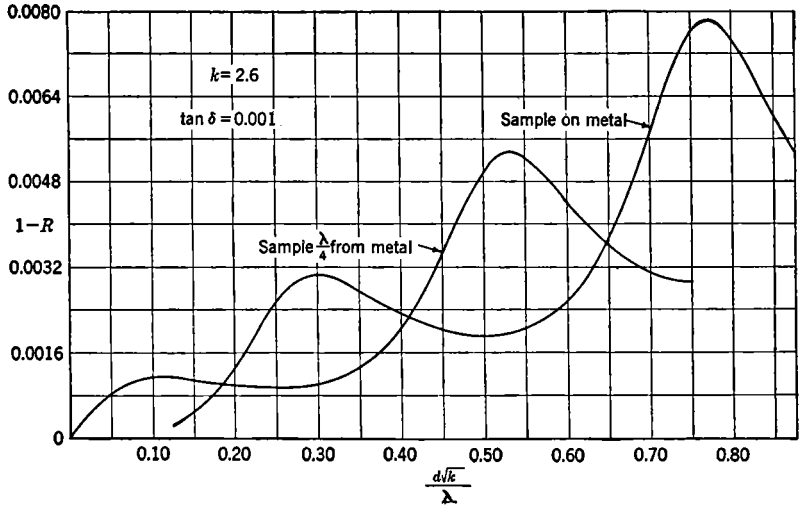

FIG. 10·36*b*.—Relation of the measured quantity $(1 - R)$ to sample thickness.

(20) with n odd is the condition for minimizing the slope of the curves in Fig. 10·34. To estimate the permissible deviation, a point on the curve may be found where the slope has some preassigned constant value; although highly arbitrary, such a procedure does give an indication of the general behavior (Fig. 10·36*a*). The same condition maximizes the value of $1 - R$ and thus minimizes the error in tan δ (cf. Ref. 5*b* and Fig. 10·36*b*). On account of these considerations, which are shown by Fig. 10·36*c* to be important in practice as well as in theory, the original data should fall in a restricted region of the curves. For purposes of computation this restricted region may be plotted on an expanded scale, as shown in Fig. 10·37, the remainder of the curves being omitted. Alternatively, a preliminary value of k may be obtained with any thickness, this preliminary value may be used to satisfy Eq. (20), and the final values of k and tan δ may be computed from the resulting simplified form of Eq. (70). The merit of this procedure (cf. Refs. 5*b*, 24*b*) is most evident when $\tan^2 \delta \neq 0$, as the computations are then greatly facilitated. For low-loss materials of the type here considered, however, the equations are sufficiently simple in the first place without this experimental complication; and in most cases k can be estimated well enough beforehand to come within the range required by Figs. 10·36*a* and 10·37.

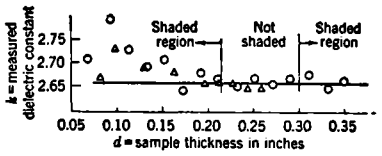

FIG. 10·36*c*.—Measured dielectric constant vs. sample thickness at $\lambda = 1.25$ cm.

Before this question of the optimum value for d is left, it should be noted that another consideration will lead to the opposite conclusion from the one just obtained. Thus, an error is produced by irregularity in the air—sample interface or by a failure to have it perpendicular to the waveguide axis; this error will presumably be minimum when the interface is in a region of minimum field (Ref. 13*a*). The "optimum" thickness on this basis is an integral number of half wavelengths, $d = n\lambda_m/2$, a value that is also obtained for k by maximizing the slope in Fig. 10·38 rather than in Fig. 10·34 (cf. Ref. 18*b*). Thus, the previous argument is to be regarded with a certain diffidence in some cases.

Gap between Sample and Short Circuit.—The foregoing results assume that the sample is immediately followed by the short circuit, which is perhaps the most convenient situation in practice. There may, however, be a gap between sample and termination, as shown in Fig. 10·31*a*, and it is of interest briefly to consider this new arrangement. It is clear that the necessary theoretical relations are contained in the introduction for that case also; it suffices in fact to substitute $r'' = \rho'' = r$ as determined by Eq. (65), $t'' = \tau'' = t$ as found from Eq. (33), and

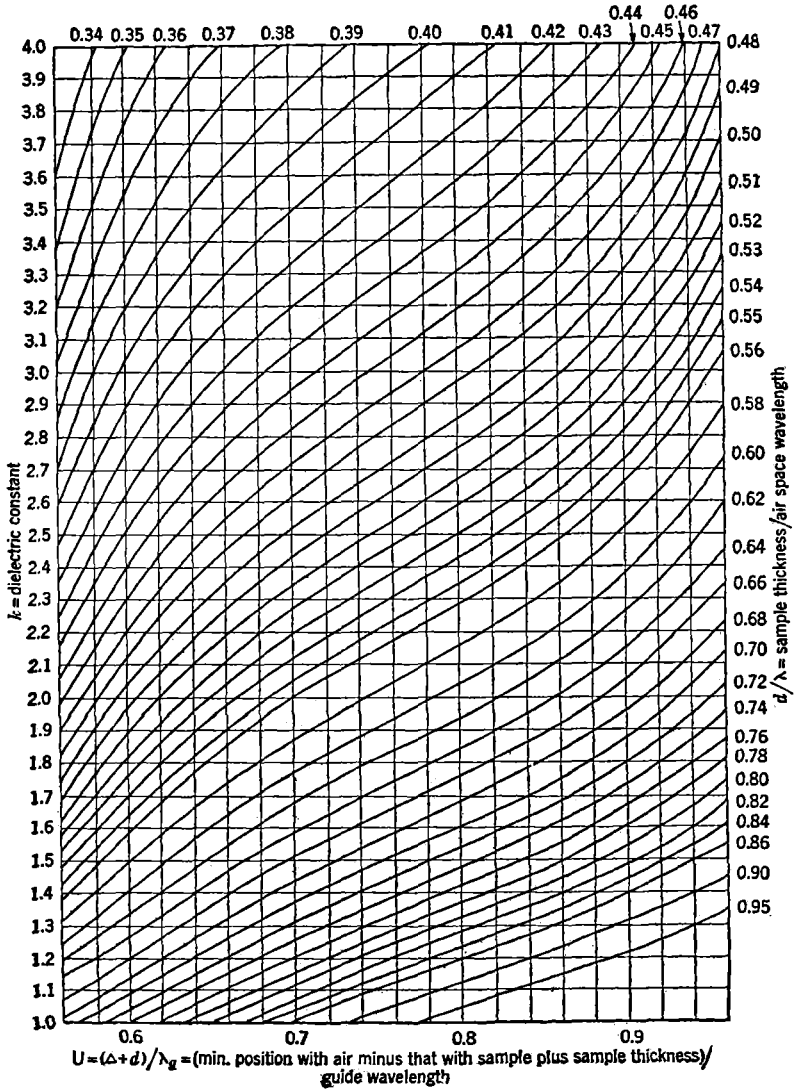

FIG. 10·37.—Expanded chart for computation of k when $p = 0.345$, giving region of high accuracy only.

$R'' = e^{-\frac{4\pi jD}{\lambda}}$, for the variables of Eq. (6), which then gives B/A, the over-all reflection of sample and short circuit in the free-space analogue of Fig. 10·31*a*. The extension to guide is made in the usual way; specifically t and r are taken appropriate to that case and λ is replaced by λ_g

in the relation for R''. Since it illustrates no new principles, and is moreover rarely used in practice, the somewhat complicated relation so obtained is omitted (see Ref. 5*b*). The exact solution, however, leads to an equation of the form of Eq. (70). Perhaps the most significant change, from a practical point of view, is in the behavior of errors. Thus, the optimum thickness is found to be an odd number of quarter wavelengths when $D = 0$; but if on the other hand $D = (2n + 1)\lambda_g/4$, then the optimum thickness for both k and $\tan \delta$ is an even number of quarter wavelengths (Ref. 5*b*) (cf. Ref. 5*b* and Fig. 10·36*b*). For a thin sample, near-optimum accuracy is obtained if the location of the sample is symmetrically disposed about an antinode (cf. Ref. 12*b*), but for practical

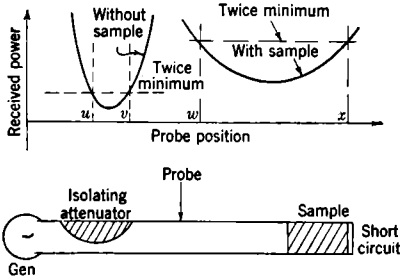

FIG. 10·38.—Measurement of reflection by taking probe positions at which the power equals twice its minimum value.

work the two values $D = 0$ or $D = \lambda_g/4$ are usually sufficient. It must be noted, in this connection, that the reflection for several values of D may be taken (Refs. 19*a*, 23*b*) and that k and $\tan \delta$ may be computed by relations somewhat different from those given here. It is not apparent, however, that any appreciable advantage is obtained thereby, and the duplication of effort, the need for moving the sample, and the difficulty of compensating for wall losses between sample and short circuit are undesirable in practical work.

10·17. Measurement Procedure.—Hitherto theoretical methods of finding k and $\tan \delta$ from the measured quantities R and Δ have been considered. The experimental techniques merely concern the problem of impedance measurement, for which a number of different methods are available from current practice. Free-space methods have been considered in detail, and no new problems are presented by the short-circuited-line procedure. In fact the experimental operations are somewhat easier to perform than in other methods, since the metal plate can remain stationary at all times, while the sample is placed on it or removed as required. The problem of locating sample and metal at precisely the same distance from the antennas, which is one of the chief difficulties of measuring phase in free space, accordingly does not arise in

the short-circuited-line method. A similar advantage is that the reflection of the combination of sample and metal is usually about the same as that from metal alone, and thus a sharp minimum for phase measurement can be obtained in both cases.

Direct Measurement of Standing-wave Ratio.—Perhaps the most widely known of the waveguide methods is that in which the maximum and minimum received powers, M^2 and m^2, are measured as the probe is moved along the line, whereupon the reflection is computed from

$$R = \frac{(M - m)}{(M + m)}, \tag{75}$$

and Δ is determined by setting the probe on a minimum. Despite its general acceptance, this method has certain shortcomings for the case at hand. In the first place, r-f detectors obey the square law only approximately, and often the voltage V from the detector is

$$V \propto E^{\alpha}, \tag{76}$$

where E is the electric field in the r-f line. If $\alpha \neq 2$, such a relation never gives true proportionality of r-f power and receiver reading, and it is apparent that both the magnitude and the percentage error approach infinity with power standing-wave ratio, no matter how small the deviation of α from the ideal value 2 may be. Nor is it easy to correct the error by evaluation of α and by use of Fig. 10·39, for α is likely to depend on field strength over the wide ranges encountered in the present application, since a detector sufficiently sensitive to respond to the minimum is usually overloaded at the maximum. For the measurement of high-power standing-wave ratios by the proposed method a calibrated attenuator must be used in somewhat the same manner as that previously described for transmission; specifically, the maximum when the attenuator is present and the minimum when it is absent are measured—a procedure which introduces new errors, however, in accordance with Table 10·2.

From the foregoing it appears, first, that errors due to nonlinearity become excessive when high standing-wave ratios are measured by the maximum-to-minimum technique; and second, that these errors can be reduced by the use of an attenuator, although a certain amount of care must be exercised in this operation. Direct measurement of high standing-wave ratios in the manner described is open, however, to still another objection, namely, in the derivation of Eq. (75) not only is the voltmeter reading assumed to be proportional to the r-f power at the probe but also it is assumed that this r-f power itself remains unchanged when the probe enters the line. For quantitative investigation, the generator may be regarded as matched to the line, $G = 0$, which condition has just been shown to be desirable in any case. The true value

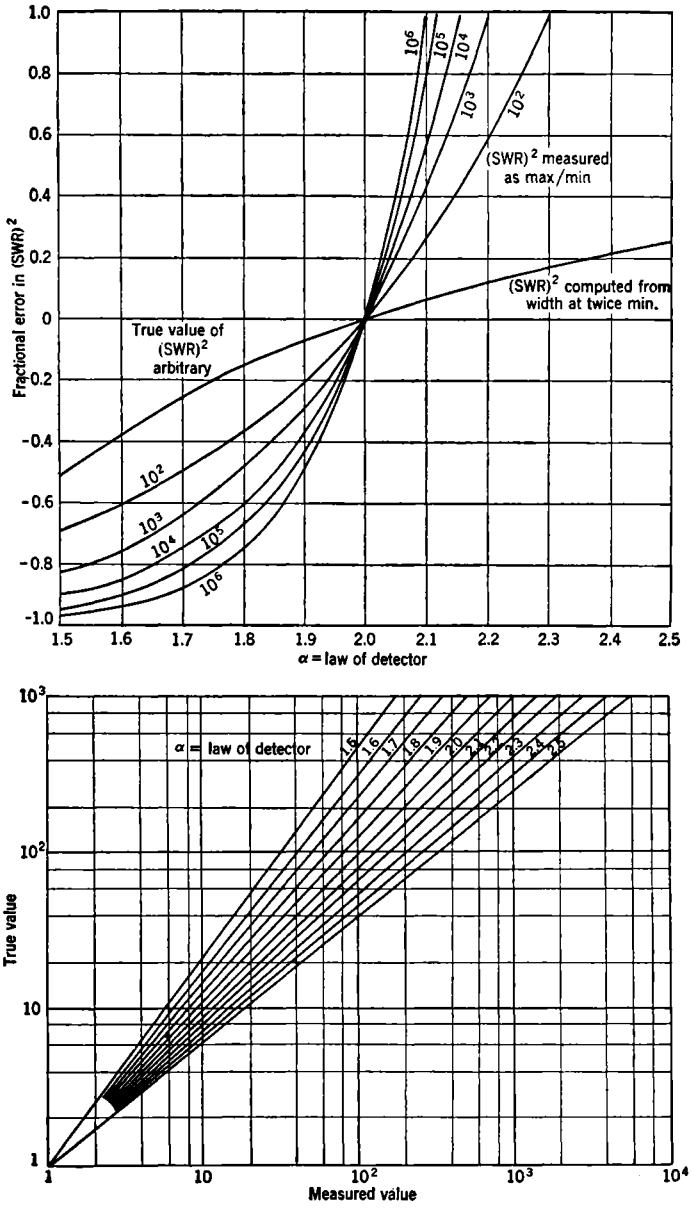

FIG. 10·39.—Theoretical effect of detector nonlinearity on certain r-f measurements. Lower curves: Effect on power transmission as measured directly; or on power reflection as measured at incidence far from normal; or on $(SWR)^2$ as measured by the maximum-minimum technique. Upper curves: Comparison of the effects of nonlinearity in the maximum-minimum method of reflection measurement and measurement from the width

of the reflection R may be assumed to differ but slightly from unity. By the methods of Ref. 5*a*, or directly from Eq. (7) of the present text, the relation plotted in Fig. 10·40 is obtained,

$$\text{fractional error in } (1 - R) = -2\,\frac{P + \cos P'}{1 + 2P\cos P' + P^2}, \qquad (77)$$

or, for $P' = \pi$,

$$\text{fractional error} = \frac{2P}{1 - P}, \qquad (78)$$

for the fractional error in $1 - R$ produced by a thin probe with reflection coefficient $Pe^{-jP'}$. Equation (78) is usually valid if the probe is tuned

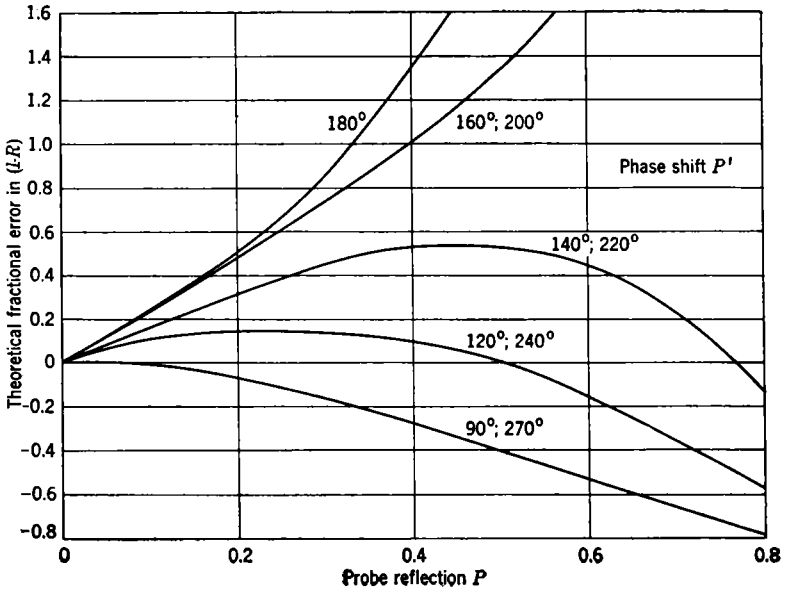

FIG. 10·40.—Fractional error in $(1 - R)$ produced by a probe reflection P exp (jP') when a high reflection R is measured by the maximum-minimum technique and the generator is matched to the line.

for maximum pickup, as was shown in Ref. 5*a*, where it was also found that the dependence of P on the probe depth δ is essentially exponential:

$$P = Ae^{B\delta}. \qquad (79)$$

The error in minimum position is also given in Ref. 5*a*; it is of the order of $P \sin P' (1 - R)^2$ and is entirely negligible here.

When added to those just obtained, this result on probe reflection permits numerical estimates of the over-all error to be anticipated in ordinary practice. Suppose, for example, that a power standing-wave ratio of 10^5 is to be measured directly as the quotient of maximum and

minimum. If no attenuator is used it is seen that a detector law of 2.02 (instead of 2.00) leads to an error of 26 per cent in the final result, exclusive of inaccuracy caused by the probe. To avoid this error, an attenuator known to have exactly 40 db attenuation and a reflection coefficient, from either side, of 0.01 per cent in power is used. Error due to nonlinearity is now reduced to about 5 per cent. Since an attempt to match generator to load, if successful, might lead to an error of over 10^5 per cent upon insertion of the attenuator, the generator is isolated by an attenuator whose reflection is likewise 0.01 per cent in power. The maximum error due to reflection is then about ± 8 per cent, as seen by Table 10·2; thus the over-all error is now 12 per cent instead of 26 per cent. To either figure must be added the inaccuracy due to the probe, however, which is shown by Eq. (78) to be about 30 per cent in power standing-wave ratio if the probe reflects as much as 0.5 per cent in power. With these rather conservative estimates for detector law and reflection coefficients, errors as high as 40 to 50 per cent may be expected in the final power standing-wave ratio if it is measured by the procedures here described.

Computation from Width at Twice Minimum.—The foregoing method has been considered in some detail, partly because it is standard practice for most types of reflection measurement, and partly because the excellent alternative method developed by A. R. von Hippel (Refs. 2*b* to 5*b*) can be properly appreciated only after a discussion of the sort just given. In this alternative method the probe positions u and v at which the power has twice its minimum value are measured as illustrated in Fig. 10·38. If a lossless line, exact linearity of all receiver components, and zero probe reflection may be assumed, then the expression

$$(SWR)^2 = 1 + \csc^2\left[\frac{\pi(v-u)}{\lambda_g}\right] \approx \frac{1}{[\pi(v-u)/\lambda_g]^2} \tag{80}$$

is obtained for the standing-wave ratio produced by the termination. The approximate Eq. (80) is valid with an error less than 1 per cent whenever the standing-wave ratio is greater than 133, and it will henceforward be treated as a strict equality. In terms of the measured positions u and v without the sample, w and x with the sample (Fig. 10·38) the quantities U and W of Eq. (73) take the form

$$U = [(u+v) - (w+x) + 2d]\frac{1}{2\lambda_g}, \tag{81}$$

$$W = \frac{(x-w)}{\lambda_g}, \tag{82}$$

and preliminary computation of the reflection coefficient R is unnecessary in practice. It must be mentioned, incidentally, that the three quantities $1/(SWR)$, $(1 - R)$, and $(x - w)$ all vary in approximately the same way. As is seen from Eqs. (75) and (80) they are in fact almost proportional whenever $R \approx 1$. Hence the fractional error of any one is nearly equal to that of any other; and the three quantities shall therefore be regarded as interchangeable. Whichever one happens to give the simplest result for the problem at hand should be used.

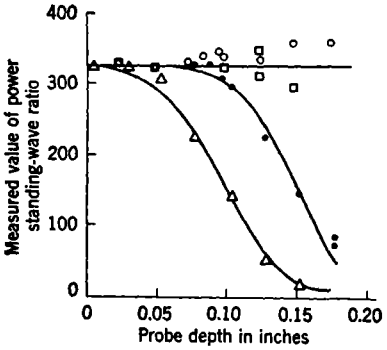

FIG. 10·41.—Experimental comparison of the effects of probe penetration on $(SWR)^2$ as measured by the maximum-minimum and twice-minimum techniques in guide at $\lambda = 3.2$ cms. The points ○, □ represent values taken by the twice-minimum method with the generator matched to the line and load, respectively, while the points ●, Δ represent corresponding results as measured by the maximum technique. The curves are theoretical with the constants A, B of Eq. (79) adjusted for optimum fit, the same values being used for each curve; data from Ref. 6*a*.

In a consideration of experimental errors, it is found that those discussed in the preceding paragraphs are practically eliminated by the method in question. The effect of nonlinearity is represented by

$$\text{fractional error in } (SWR)^2 = 2 - 2^{2/\alpha}, \quad (83)$$

for example, which is shown in Fig. 10·39*b*. In view of the low fields and small variations here encountered, moreover, the parameter α may be expected to be constant and to deviate but slightly from its ideal value 2, whereas in the former situation the reverse was the case. There is no occasion to use an attenuator in the manner previously described, and this source of error is eliminated. From the fact that the probe is in a region of low field it may be concluded (Ref. 5*b*) that these errors too, although not obviated entirely, are greatly reduced. Intuitive reasoning of this sort is indeed verified by quantitative calculation. Probe errors with a matched generator are completely negligible in the sense that the approximations made in the derivation of Eq. (80) are equally valid whether P be zero or positive (Ref. 5*a*). In other words, irrespective of the value of P', the only terms in $1 - R$ which are affected by probe reflection are terms of the order of $1/(SWR)^3$ or higher, and are of no significance here. That this relative insensitivity to probe reflection is found in practice is verified by Fig. 10·41.

Power Level for Optimum Accuracy.—This superiority of the alternative method is not confined to measurement of standing-wave ratios, but is

found for the minimum position as well. Thus, instead of a setting on a point of zero slope being attempted, two points for which the slope is positive are averaged, a procedure that is feasible by virtue of the symmetrical curve shape (cf. Fig. 10·15 and accompanying remarks). If the determination of minimum position is considered in more detail, the error in position is found to be about equal to that in the two measurements of distance v and u. These errors will be least if the power level at which they are made is such that the slope of the curve of meter-needle displacement vs. distance is a maximum. If the meter is linear, the maxi-

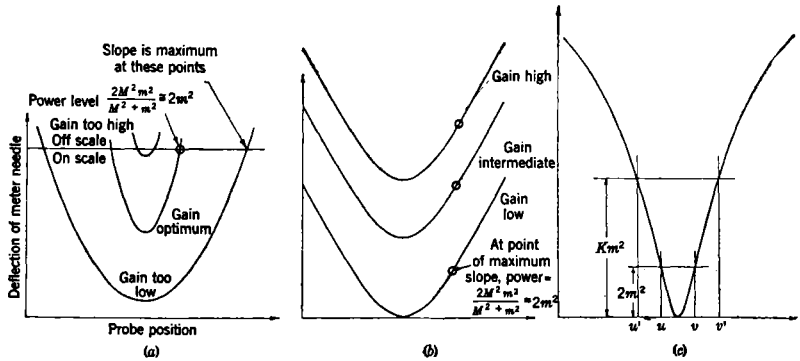

FIG. 10·42.—Conditions on receiver gain and portion of curve selected, to obtain optimum accuracy. (*a*) Effect of gain on slope with a linear meter. (*b*) Same, logarithmic meter. (*c*) Measurement of width at twice minimum from that at K times minimum.

mum of the curve will be far off scale in normal practice, and the points of greatest slope occur at full-scale deflection. As the gain is increased, this maximum slope will likewise increase up to a certain point, then decrease to zero when the minimum itself causes a full-scale deflection. Quantitative investigation shows this point of maximum slope to occur at the harmonic mean of maximum and minimum as illustrated in Fig. 10·42*a*. To determine phase with optimum accuracy when a linear meter is used for large standing-wave ratios the gain should be adjusted until the minimum leads to half-scale deflection, and the two probe positions that are then found to lead to full-scale deflection should be averaged. If the meter is logarithmic rather than linear, all properties relevant to the present discussion are independent of receiver gain (Fig. 10·42*b*), in contrast to the results noted. When the derivative is maximized, however, the harmonic mean of maximum and minimum represents the condition for maximum slope and hence, as before, the optimum points for high standing-wave ratios are the ones actually used. The methods and results of this paragraph are valid for any curve which approximates a parabola near the minimum.

The question of slope is somewhat more complicated when the width of the curve rather than minimum position is considered. Thus, if the length of a segment is measured at a power level K times the minimum, as shown in Fig. 10·42*c*, then the desired twice-minimum segment is given by (Ref. 2*a*)

$$v - u = \frac{\lambda_g}{\pi\sqrt{K-1}} \sin\frac{\pi(v'-u')}{\lambda_g} \approx \frac{(v'-u')}{\sqrt{K-1}} \qquad (v'-u') \ll \lambda, \quad (84)$$

and the error in $v - u$ is thus less than that in $v' - u'$ by a factor $\sqrt{K-1}$, approximately. For this reason greater accuracy is sometimes achieved by taking one-third the width at ten times the minimum, for example, rather than by direct measurement of the width at twice the minimum. Despite the fact that the end points of such a segment are determined with less accuracy than is the case for $v - u$, the additional error is often more than compensated by Eq. (84). No such desirable behavior is found for errors from nonlinearity, however; instead of Eq. (83),

$$\text{fractional error in } (SWR)^2 = \frac{K - K^{2/\alpha}}{K-1}. \qquad (85)$$

The expedient of Fig. 10·42*c* is to be recommended, then, only for unusually low-loss samples that give a minimum too narrow to be measured with precision, and only when the detector is accurately linear. In other cases the increase in accuracy, if obtained at all, would scarcely warrent the added complications.

10·18. A Few Sources of Error. *Impurity of Generator Output Power.* It has been assumed throughout the foregoing discussion that only a single frequency is generated by the source of r-f power. The output power of a modulated klystron does not always satisfy this condition, however, but sometimes has components at frequencies different from the fundamental. This behavior is the result of improper modulation of the generator (Ref. 1*a*); it is quite different from the normal presence of harmonics in the frequency spectrum of a pulse. Since they deal chiefly with generator adjustment or design rather than with measuring techniques, methods of correction are not included here (cf. Ref. 1*a*). It is of interest, however, to investigate the effect as to order of magnitude, an investigation that is readily made by Eq. (7) of the Introduction. As described in Ref. 1*a*, the r-f power is not present simultaneously at two different frequencies, but rather one frequency exists for alternate pulses of the modulator, or one frequency at one point of each pulse, a different frequency at a later point of the same pulse. For approximate quantitative computation, therefore, powers are added instead of amplitudes, and the meter reading is assumed to be the sum of the values for the two individual frequencies. With such an approach neither equal

resonance of the cavity nor equal sensitivity of the receiving system need be assumed, and in addition, the power need not be equally divided between the two frequencies. If the load reflection is independent of frequency over the small variation in question, then

$$\frac{1}{(SWR)^2_{\text{measured}}} = \frac{1}{(SWR)^2_{\text{true}}} + \frac{1}{1-p}\left(\frac{\pi X}{\lambda}\right)^2\left(\frac{2\rho}{1+\rho^2}\right)^2\left(\frac{\Delta f}{f}\right)^2 \quad (86)$$

gives the measured standing-wave ratio at a distance X from the interface in terms of its true value, and the ratio ρ^2 of received powers at frequencies $f, f + \Delta f$. The error in minimum position is of the order of Δf; but when the results for sample and short circuit are compared, the error is found to be nearly the same in both cases and thus to cancel out.

The result of Eq. (86) was obtained for direct measurement of the power standing-wave ratio as the ratio of maximum to minimum. If the power is set equal to twice its minimum value, however, and the above assumptions are retained, an identical expression is found for the error, except that the power standing-wave ratios are replaced by the squares of the twice-minimum widths as given by Eq. (80). Thus, direct measurement of the standing-wave ratio and computation from the width of the curve are equivalent as far as sensitivity to impurity of the frequency is concerned (Ref. 2*a*). The error in width, which has been seen to be essentially equivalent to that in $1/(SWR)$, is proportional to the right-hand term of Eq. (86) if the error is small compared with the actual width; but if the reverse is the case then the error is proportional to the square root of this term. In particular, for a perfect short circuit, which gives a true width of zero,

$$\text{measured width} = \left(\frac{X}{1-p}\right)\left(\frac{2\rho}{1+\rho^2}\right)\left(\frac{\Delta f}{f}\right). \quad (87)$$

The first factor shows that the error increases as the average frequency approaches the cutoff wavelength of the guide, and that it is proportional to the distance from the minimum to the sample; the second indicates that the error is proportional to the geometric mean of powers at f and $f + \Delta f$ divided by the arithmetic mean; from the last factor it is seen that the error is proportional to the percentage change in frequency, $\Delta f/f$. These remarks apply to the general case of nonzero width, if the error in width and each factor mentioned are squared. For example, if the frequency is 3000 Mc/sec and $p = \frac{1}{2}$, the measured width at the second minimum for a perfect short circuit [Eq. (87)] is found to be about 0.0019 in. when the power ratio ρ^2 is unity and the frequency difference is $\frac{1}{2}$ Mc/sec, whereas it is 0.001 in. when this difference is $\frac{1}{4}$ Mc/sec. If the true width is 0.002 in., however, then the error becomes 0.0007 or 0.0002 in., respectively. These computed values are consistent with the experimental

results of Ref. 1*a*, where a transmitter bandwidth of $\frac{1}{4}$ Mc/sec was found to be satisfactory and a bandwidth of $\frac{1}{2}$ Mc/sec caused a noticeable increase in the measured width of the curve.

Wall Losses.—The foregoing errors occur in the actual process of finding U and V. When the quantities k and tan δ, are computed from these measured quantities, an additional error is found to be introduced by the neglect of wall losses. To correct this error much the same procedure is used as for transmission. The data are manipulated to obtain the values for lossy guide surrounding the sample, lossless guide elsewhere, and the computed result is interpreted by Eq. (40). With the short-

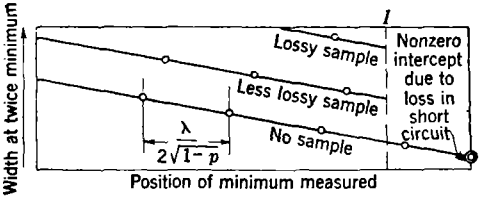

FIG. 10·43.—Detailed behavior of width at twice minimum.

circuited-line method the calculation (Ref. 1*a*) is particularly simple. As illustrated in Fig. 10·43, the width at twice minimum increases almost linearly with distance from the short circuit (Ref. 5*b*), and the curves for different terminations are all parallel to one another. Both results have been verified by experiment; theoretically they follow from the fact that tan δ_{wall} is small enough to give exp (tan δ_{wall}) $\approx 1 -$ (tan δ_{wall}). With such linear dependence it is a simple matter to extrapolate the minimum width from the point at which it actually occurred to the air—dielectric interface I of the figure. Although appropriate only to point I for lossy guide, this same extrapolated width would be appropriate to any point when the guide leading to the sample is lossless. With this procedure, which neglects the small loss in the short circuit, it is found (Ref. 1*a*) that tan δ equals the value of tan δ as obtained from Eq. (72) with extrapolated width, minus tan δ_{wall}. The quantity tan δ_{wall} is obtained from

$$\tan \delta_{wall} = D(1 - p) \tag{88}$$

if D represents the difference in the W's obtained, either with or without the sample, for the kth and $(k + n)$th minima. Losses in the $(v - u)$ length of guide over which the probe moves are neglected, as well as all wall losses, in computing phase. These approximations were also used in the transmission methods already described; that they are justified is easily proved theoretically. Additional verification is given in Fig. 10·44, where neglect of loss is actually permissible over a portion of line much larger than the length $(v - u)$ in question here.

Insufficient Power.—A third source of error sometimes encountered is the frequency shift produced by the changing character of the load, or, with adequate isolation, the increase in apparent signal due to receiver noise. Thus, the short-circuited-line method differs from the others mentioned in that it leads to high mismatches that are of variable phase. Hence, whereas isolation of the generator was formerly of only secondary importance, it is now necessary to provide the requisite stability, for

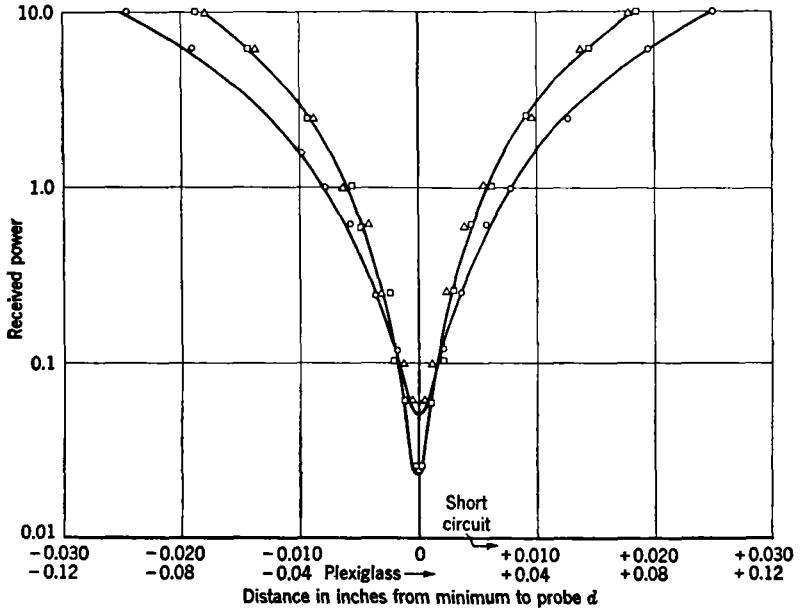

FIG. 10·44.—Experimental verification that neglect of loss is permissible in the region traversed by the probe. The points are experimental at $\lambda = 3.2$ cm; the curve is theoretical, matched at two points. The triangles are for the probe near the short circuit, the squares are for the probe a half wavelength farther from the short circuit, and the circles are for plexiglas plus short circuit.

despite the high and variable mismatch, the generator frequency must be the same when the two measurements are taken with and without sample. Even if the receiving systems were of equal sensitivity in both cases, the short-circuited-line method would require more power, for a given signal-to-noise ratio, than methods depending on transmission. In actual practice, however, this difference in available transmitter power caused by the need for isolation is enhanced by a similar difference in the receiving equipment. Thus, for transmission, a bolometer or similar device is used, placed in the line at the antinode of a short circuit, with the result that most of the r-f power actually contributes to receiver

reading. In the short-circuited-line method, on the other hand, the role taken by the bolometer is now taken by a traveling probe, which responds to only a small fraction of the total power available. Indeed it has been shown (Ref. 5*a*) that a thin probe cannot remove more than one-fourth of the power from the line, irrespective of its depth, and that the figure in ordinary practice is considerably less than this. Because of this combined loss of transmitter power and receiver efficiency it is found, at the higher frequencies, that klystron oscillators usually provide insufficient power[1] for the short-circuited-line method to be successfully used. A magnetron transmitter leads to no improvement, as the use of a bolometer instead of a crystal, necessitated by the short pulse, offsets the gain in transmitter power by a corresponding decrease in detector sensitivity (Ref. 6*b*). In principle the power standing-wave ratio may be increased by artificial means, and thus the need for readings at low power is avoided; for example, a poor short circuit may be used or a quarter-wave sheet of lossy material may be placed between the sample and the termination (Refs. 23*b*, 24*b*). Such expedients, however, are easily seen to destroy the inherent accuracy of the method. Thus, the value of tan δ depends essentially on the difference of the two widths when the sample is present or removed (Ref. 23*b*). Not only will this difference be small when the sample has loss low enough to require an artificial increase, but the original measurement of the width loses accuracy because of the decreased slope. These considerations are not to be confused with those of the foregoing discussion, where it was found preferable to adjust d for a large value of $(1 - R)$. The increase in $(1 - R)$ there obtained was entirely due to the desired quantity tan δ, whereas it is now the result of the introduction of an extraneous loss that must be later subtracted. In view of these problems, then, there is need for a modified procedure that will give essentially the same information as that obtained from the points u, v, w, x, of Fig. 10·38, but which will nevertheless presuppose no knowledge of the minimum.

10·19. Modified Procedure for Low Power.—Determination of the minimum position $(u + v)/2$ presents no difficulties. If the attenuation is neglected in the part of the line in which the measurement is made (not in the load, nor in the line leading to it) it may be shown that the average of any two suitable probe settings for which the voltmeter readings are equal will give the minimum position. This is true independently of the law of the detector. Although the condition of maxi-

[1] This problem has been recently attacked by electronic methods that are quite different from the r-f methods to be considered here. Besides being at present incomplete, however, such procedures are concerned chiefly with the means of power detection or with receiver design. As far as r-f dielectric measurement itself is concerned they suggest no new principles, and are therefore omitted from the present discussion.

mum slope is no longer obtained, the curve is steep enough to give accuracy adequate for most purposes, and there is some compensation too in that fluctuations from noise are reduced. That such considerations are valid in practice was verified in Ref. 2*a*, where accuracies of the order of $\pm 0.0002\lambda$ for a short circuit and $\pm 0.0004\lambda$ for a sample were consistently obtained at power levels 20 to 25 db above the minimum.

Derivation.—From the ease with which the minimum position $(u + v)/2$ may be found at low power it might be expected that equally

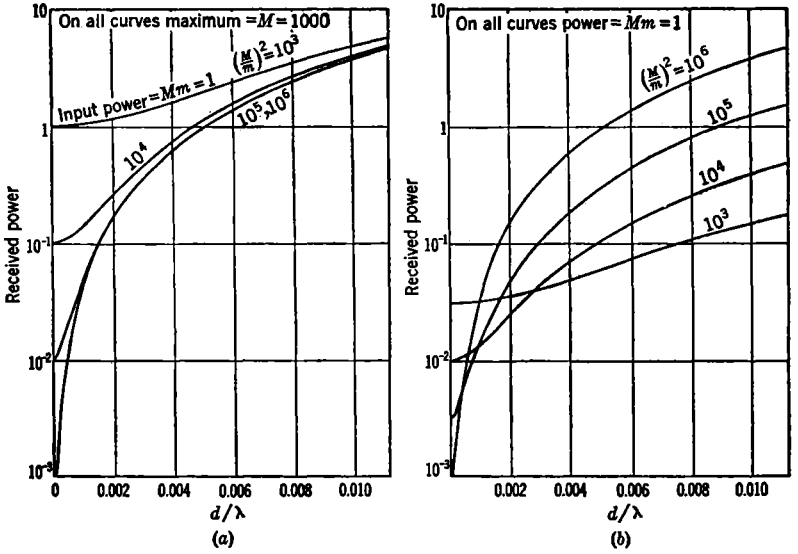

FIG. 10·45.—Comparison of probe power vs. position when maximum is constant (*a*) and when input power is constant (*b*).

simple methods would give the width of the curve $(v - u)$. Thus, since the general equation for probe power vs. position is known, the entire curve may be determined—and with it the twice-minimum points—by making any two independent measurements; for example, the width at a known fraction of the maximum power may be measured, or the two widths for any known power ratio. Despite the simplicity and similarity to the procedure for minimum position, however, such expedients are unsuccessful in practice; as was shown in Ref. 2*a*, the experimental errors are multiplied by 100 or 1000 in typical cases. Upon closer investigation it is found that there is nothing surprising in this behavior of errors, since the shape of the power-vs.-distance curve near the maximum is practically the same for all large values of the standing-wave

ratio (Fig. 10·45*a*). It is therefore impossible to measure high reflections at low power by any method depending on shape alone.

If the net input power were kept constant, however, the height of the curve (not its shape) would show a marked dependence upon standing-wave ratio even near the maximum, as is seen by Fig. 10·45*b*, and the use of some sort of matching device is at once suggested. It is found, in principle, that only approximate matching suffices for measurement of the net input power, and hence for accurate determination of $1 - R$ (Ref. 2*a*); but in practice there are large errors from tuner loss, and the necessary adjustments are somewhat inconvenient (Ref. 3*a*). Without changing the essential features of the method, however, these difficulties may be obviated by the procedure suggested in Fig. 10·46*a*, in which a curve of power vs. phase of generator mismatch with constant probe position is measured. By inspection of Eq. (7) a relation for the r-f power at the probe is obtained, and from this is found the theoretical equation of the curve just described, if the receiver reading is assumed to be proportional to r-f power. The curve of power vs. phase of the generator mismatch is thus shown to be inversely proportional to a curve of power vs. probe position with a load reflection RG, if G is the coefficient for the moving mismatch (Ref. 2*a*). From this property, which is illustrated in Fig. 10·46*a*, it follows that the behavior of the one curve near the maximum is essentially the same as the behavior of the other near the minimum. Thus,

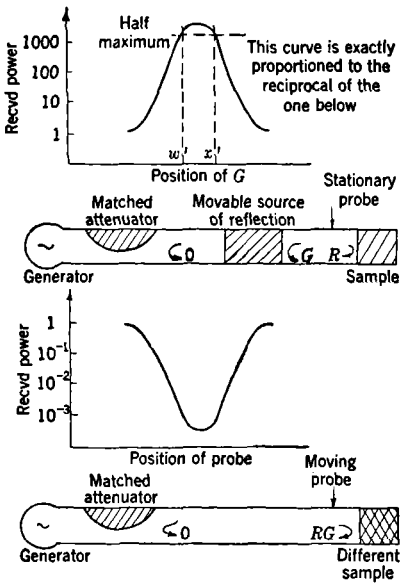

FIG. 10·46.—Modified short-circuited-line method. Diagram illustrating principles.

$$(x - w) = (x' - w') - (x_G - w_G), \tag{89}$$

after making the same approximation as that used for Eq. (80). In Eq. (89) the quantities $(x - w)$, $(x_G - w_G)$ are the widths at twice minimum which would be found in a curve of power vs. probe position with load reflections of R and G, respectively, and $(x' - w')$ is the measured width at half maximum found in a curve of probe power vs. the position of G (Fig. 10·46*a*). The equations for the unmodified short-

circuited-line method, Eqs. (71), (72) and all others, are valid here. If u' and v' denote the two positions at half maximum without the sample, and w', x' the positions with the sample, then

$$U = \frac{[(u' + v') - (w' + x') + 2d]}{(2\lambda_g)}, \tag{90}$$

$$W = \frac{[(x' - w') - (v' - u')]}{\lambda_g}, \tag{91}$$

instead of Eq. (81). Equation (91) follows directly from Eq. (89), and Eq. (90), which is evident by inspection of Fig. 10·46*a*, may be proved by Eq. (7).

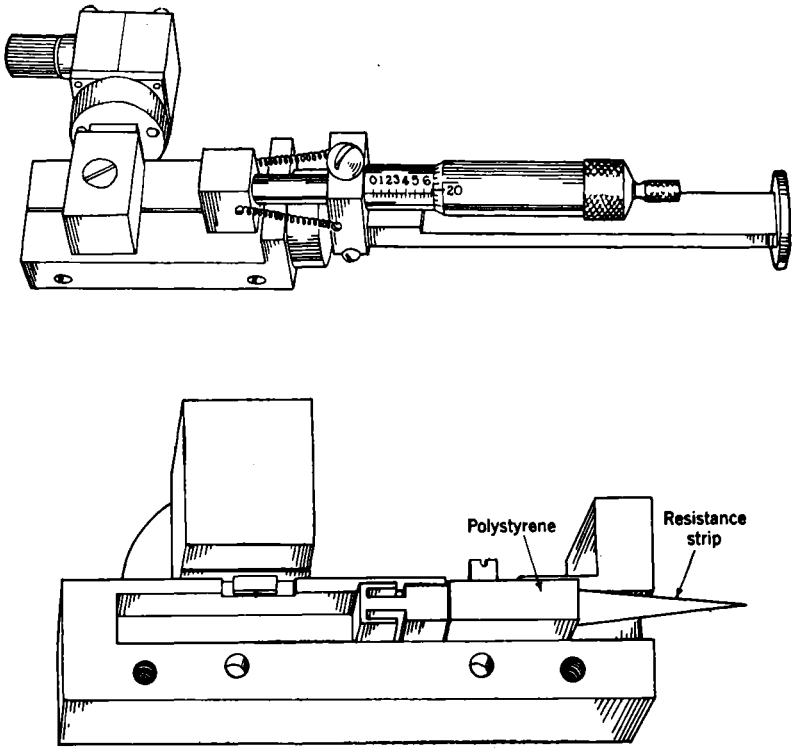

FIG. 10·46*b*.—Modified short-circuited-line method. Diagram showing details of equipment.

Power Gain.—Up to this point it has been shown that the alternative procedure of Fig. 10·46*a* gives all data needed for computation of k and tan δ by the unmodified short-circuited-line method. The errors are not excessive, being essentially the same as those in the unmodified

method with R replaced by RG. It remains to investigate the power requirement, which is determined by the equation

$$\text{Power at minimum} = (1 - R)^2, \tag{92}$$

with the generator matched to the line, and

$$\text{Power at minimum} = \frac{(1 - R)}{(1 + R)}, \tag{93}$$

with the generator matched to the load. The latter condition may be approximated in practice by use of a plunger similar to that of Fig. 10·46*b* (cf. Refs. 2*b*, 25*b*). With a lossless source of reflection G, on the other

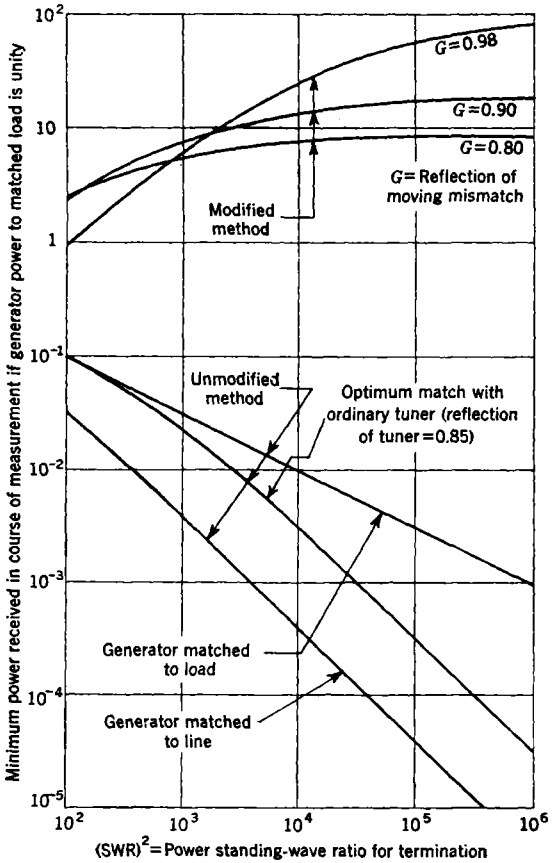

FIG. 10·47.—Comparison of power requirements in modified and unmodified methods.

hand, the modified method gives

$$\text{Power at half maximum} = \frac{(1 - G^2)(1 + R)^2}{2(1 - RG)^2} \tag{94}$$

for the power at half maximum which, like Eq. (93), represents the smallest power level required for measurement. In Eqs. (92), (93) and

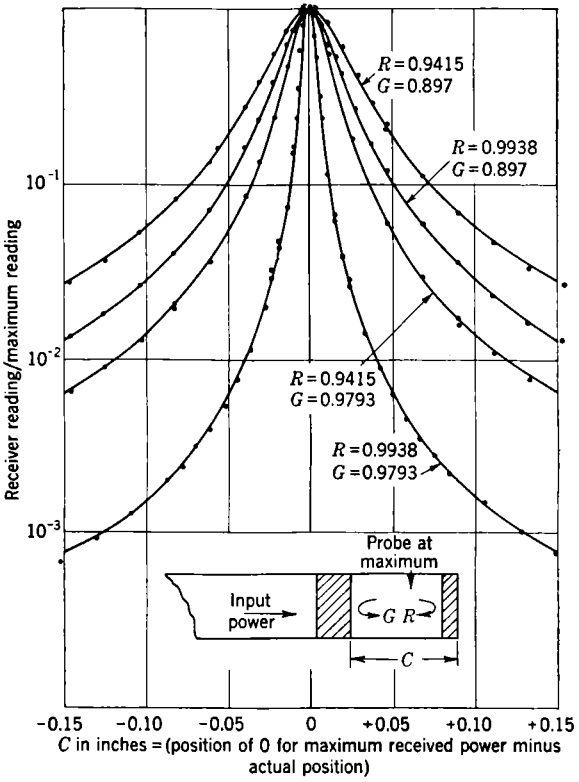

FIG. 10·48.—Detailed comparison of experiment and theory for modified short-circuited-line methods. The points are experimental, the curves are theoretical from independent measurements of R and G.

(94) the received power for the isolated generator connected directly to a matched load has been taken as unity. These results are compared in Fig. 10·47, where the modified method is seen to be operable at relatively low power; there is in fact a power gain, so that if the power be sufficient to give a reading with a matched load it will usually be more than sufficient to permit measurement of high power standing-wave ratios. In contrast to the behavior of most other methods for reflection measurement, moreover, the available power is found to increase rather

than to decrease as the load reflection approaches unity. With very large G, Eq. (94) can be used for measurement of R, if the value of G is known and the generator is supplied with a suitable monitor (cf. Ref. 2*a* and Table 10·4).

Accuracy in Practice.—In regard to the question of error it may be observed that the foregoing results are correct without theoretical approximation, irrespective of probe position and of the loss associated with G, if line losses may be neglected and if power is propagated in only one mode. Thus, in practice, a low-loss source of reflection G is used with the probe set on or near the maximum to increase the available power; no theoretical error is incurred by a failure to satisfy these conditions. Experimental verification is given in Fig. 10·48, where the values of G

TABLE 10·4.—COMPARISON OF FOUR METHODS FOR MEASURING HIGH REFLECTIONS

Termination	Value of G used					
	0.897		0.9490		0.9793	
	Without sample	With sample	Without sample	With sample	Without sample	With sample
$(u - v)$ as computed from maximum/minimum.	0.0020 in.	0.0180 in. 0.0171	0.0023 in.	0.0166 in.	0.0020 in.	0.0175 in.
$(u - v)$ as computed from over-all maximum, Eq. (83).	0.0020	0.0198 0.0151	0.0011	0.0154	0.0014 0.0014	0.0174
$(u - v)$ as obtained by modified method, Eq. (78).	0.0016	0.0168	0.0017	0.0169	0.0017	0.0168
$(u - v)$ as measured directly by unmodified method.	0.0013	0.0168 0.0178	0.0016	0.0171	0.0015	0.0170

and R used for the theoretical curve were independently measured by the twice-minimum procedure. An additional check on the theory is given in Table 10·4, which compares the twice-minimum widths as obtained by direct measurement, by the standard maximum or minimum technique, by Eq. (94) and by the modified method, Eq. (84).

The theoretical and experimental accuracy of the method naturally presupposes that the conditions for its use are satisfied in practice. The

probe reflection must be negligible, the value of G must remain constant, and the slopes must be such that the true points at half maximum can be accurately determined. The true points can be determined whenever RG is sufficiently large, the slope on a logarithmic meter being in fact equal to that obtained in the twice-minimum method for a reflection of this magnitude. The discussion of Fig. 10·42 is therefore essentially valid for this case also; in particular, the points of optimum accuracy for determining minimum positions are the half-maximum points actually used. The value of the maximum slope so obtained increases steadily with G, and for this reason it is desirable to give G as large a value as is convenient. Such a condition not only gives greater accuracy but also leads to a higher output power, as the attendant loss in the transmission of G is usually more than compensated by the increased resonance effect of the cavity (Fig. 10·47). It is worth noting too that Eq. (84) involves the same approximation applied to RG as was applied to R in the derivation of Eq. (81). Hence RG must be greater than 0.84 if the error is not to exceed 1 per cent. With sufficiently large G (0.95 to 0.98), but not otherwise, the inequality is usually satisfied. When R is so small that this is not the case, the exact equation analogous to Eq. (79) may be used or the comparatively small standing-wave ratio may be measured directly.

Probe Errors.—Since the measurement is carried out in a region of high field, the impurity of the frequency might be expected to be less important and probe errors more important than in other cases. This latter conclusion was quantitatively verified in Refs. 2*a*, 5*a*, 6*a*. Thus, when the probe is at the maximum, the equation

$$(R_{\text{measured}}) = R\sqrt{\frac{1 + 6P\cos P' + 9P^2}{1 - 2P\cos P' + P^2}}, \qquad P(1 - R) \approx 0 \qquad (95)$$

$$(R_{\text{measured}}) = R\frac{(1 - P)^2}{1 + RP} - P, \qquad P' = \pi$$

give the measured reflection coefficient in terms of its true value R and the probe reflection $Pe^{-iP'}$. This result may be derived from the relations of the Introduction; the measured reflection is in fact equal to that for the probe and termination together, which is given by Eq. (6) with $t'' = \tau'' = 1 - Pe^{-iP'}$, $r'' = \rho'' = Pe^{-iP'}$, $R'' = R$, $d = 0$—the last two substitutions being valid because the probe position is that for maximum power. In the course of dielectric measurement, the difference of the two determinations with and without sample is measured, a procedure that is found to cancel out the first-order terms in probe reflection (Ref. 5*a*). The probe insertion must still be less than that permitted by the unmodified method; but so great is the power gain that an improvement of 20 to 30 db is obtained even with the probe sufficiently retracted to

lead to negligible error. Experimental examples are given in Fig. 10·49; the curves are computed from an equation analogous to Eq. (84).

Errors from Moving Plunger.—As was observed, the reflection G must be both high and constant, because a low value leads to small slopes and invalidates the approximation made in Eq. (89), and a value that varies with position will introduce errors in accordance with the same equation. To obtain a large value a choke-plunger short circuit may be used as shown in Fig. 10·46*b*. For constancy, accurately machined

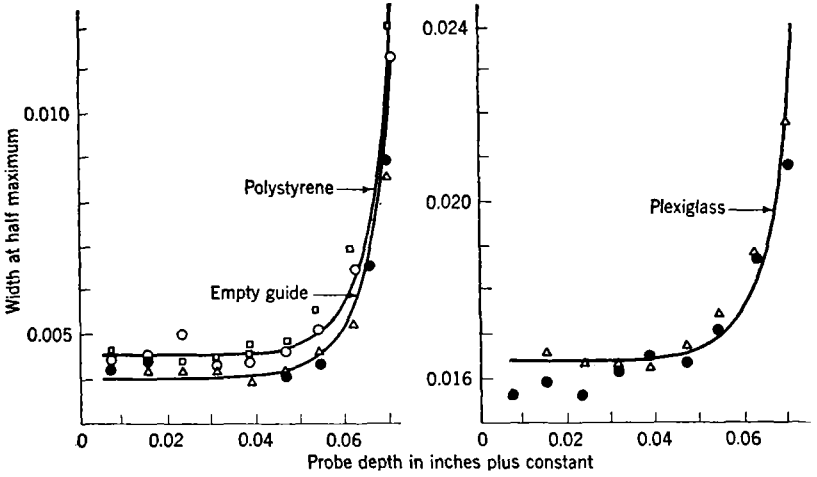

FIG. 10·49.—Effect of probe depth on measured width of curve at half maximum power (modified method). The points ○, ● are measured directly and the points □ △ are determined from the width at one-tenth maximum. The curves are theoretical, computed as in Fig. 10·41.

parts and a generator matched to the line are used. With regard to constancy, the error in G is found to be approximately

$$\text{Error} = \pm G_1 T_G^2, \tag{96}$$

if T_G^2 is the power transmission coefficient of G, and G_1 is the reflection looking into the generator as shown in Fig. 10·50. The use of a large

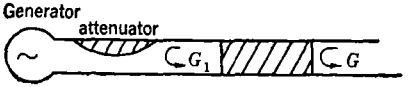

FIG. 10·50.—Generator reflection G_1.

G is thus recommended to reduce T_G^2, as well as for the reasons just mentioned. For further reduction a small attenuator may be added as shown in Fig. 10·46*b*. If this small attenuator has a one-way power transmission of 0.2, for example, then the error from G_1 is reduced by a

factor of five; a power standing-wave ratio of 1.05 for G_1 is now no more serious than one of 1.01 was before. The power requirement is not increased, since the need for generator insolation is obviated in proportion as the attenuation associated with G becomes large.

Radiation.—Even with these two requirements of accurate machining and low $G_1T_G^2$ both satisfied, however, there may still be a slight error from radiation. Thus, the current lines are strictly parallel to the slot only when it is infinitely narrow; in actual practice there is always a certain amount of leakage. To avoid the consequent interference of G with the performance, the dimensions are adjusted in such a way as to have the choke plunger entirely enclosed at all times; that is, it is never allowed to extend to either of the two slots as G is moved (Ref. 2*a*). Error from radiation is further decreased by the use of a narrow slot and by arranging the probe carriage in such a way as to cover it completely for all probe positions. This expedient is of value only when error from variable contact is less serious than that from radiation, which appears to be the case at least for the shorter wavelengths (Ref. 2*a*). Radiation from slots causes difficulty in maintaining G constant and in measuring high standing-wave ratios. Radiation is present whenever slotted equipment is used, for example, the phase shifters illustrated in connection with the transmission method. It may be eliminated by similar procedures in these other cases, of course, although the effect is usually negligible for all work not involving high reflection.

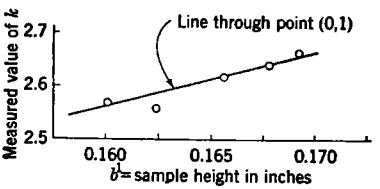

FIG. 10·51.—Experimental effect of clearance on measured value of k in rectangular guide at $\lambda = 1.25$ cm. Points are experimental, curve empirical as given by Eq. (24).

Errors Analogous to Those Previously Discussed.—Most of the errors discussed heretofore are peculiar to reflection measurement. Because of the above-mentioned analogy between reflection and transmission procedure, other errors are similar to those previously discussed and need not be considered in detail. From clearance, for example, the behavior shown in Fig. 10·51 is obtained. Although presented only for the modified method, the same result would evidently have been obtained with the maximum/minimum or twice-minimum techniques, as is seen by Table 10·4 and the accompanying remarks. Similarly, the treatment of wall losses, although slightly complicated by the term $(x_G - w_G)$ of Eq. (89), is still analogous to the procedures heretofore described. If linear variation like that of Fig. 10·43 is assumed, the half-maximum width is extrapolated without sample to the position at which the maximum occurred with sample, whereupon the term in question

is canceled by subtracting the two widths. To this difference must be added the change in width due to loss in the portion of line containing the sample, which is given by

$$\text{Change in width} = \frac{2Dd}{n\lambda_g}, \tag{97}$$

if D represents the difference in the two widths found, either with or without sample, for any two positions of G differing by $n\lambda_g/2$. The modified width so obtained is then substituted in Eq. (72) and finally the computed value of tan δ is corrected by Eq. (40), where tan δ_{wall} is found from Eq. (88) with D defined as in Eq. (97). As before, the loss in computing phase and in the portion of line over which G moves in a single measurement has been neglected, and the error is entirely negligible (cf Fig. 10·48). Strictly speaking, the present procedure is also incorrect in that it assumes the loss in the short circuit to be the same with and without sample, but the error so introduced usually does not exceed that in the unmodified method, where loss due to the short circuit was neglected altogether. In fact, the former assumption is sometimes the more accurate, especially when $\sqrt{k} \approx 1$. In such circumstances the method of compensation suggested for the modified method may be profitably applied to the unmodified method as well, the procedure being in all respects the same as that just described.

10·20. Uses.—One of the more important characteristics of the short-circuited-line method is that it requires only a relatively small sample for precise measurement—a length of $\lambda_m/4$ or, at the higher frequencies, of $3\lambda_m/4$, being sufficient for high accuracy. This property of the method is due partly to the fact that the wave traverses the sample twice and partly to the increase of the standing-wave ratio usually found with decreasing sample length. Thus, although the measured effects, width and shift of minimum position, are smaller with a short sample, these measurements themselves may be made with correspondingly higher accuracy. Since the method requires only small samples, it is thus especially satisfactory for research and other work involving materials not available in quantity.

A related advantage is found in the location of the sample, which is placed at the end of the line rather than at some intermediate point as in the other methods discussed hitherto. The method is accordingly adapted to experiments in which the temperature is to be controlled, and is to be recommended especially for measurement of liquids. For such measurement the transmission methods can usually be used, if at all, only with clumsy expedients that are inconvenient and in general introduce considerable error. With the short-circuited-line method it suffices merely to have the equipment vertical (Refs. 1*a*, 5*b*). Because

of surface tension there is difficulty in deciding on a precise value for d, but this is a magnitude rather than a percentage error and may therefore be reduced by the use of a long sample, since the error in both k and $\tan \delta$, due to a given magnitude error in d, approaches zero as d increases indefinitely. A second expedient, by which the error is eliminated altogether, is the use of a window of mica or some other suitable material, a procedure that also prevents condensation of the liquid in the upper part of the guide. A detailed account of equipment for such measurements and of means for compensating the electrical effect of the window is given in Ref. 1*a*.

The short-circuited-line method, besides using a small and easily accessible sample, gives high accuracy both theoretically and practically, particularly at wavelengths not much below 10 cm. Thus, the sources of error are few and well defined. Instead of a host of extraneous reflections, as in the transmission methods, only the probe reflection exists, and this has been shown, for the unmodified method at least, to be completely negligible in practice. Similarly, no calibration is required for the r-f components, and the detector itself may deviate widely from linearity with but slight effect on the measured results. Because of the relatively short sample permissible, errors from clearance are readily minimized, and because of the high standing-wave ratios, the necessary measurements of field can be carried out with considerable accuracy. If care is taken in the machining of the equipment and the sample, this method is found to be about as accurate as any other for the measurement of k, and perhaps more accurate than any other for $\tan \delta$. With regard to this last, in particular, not only is the general behavior of the errors favorable, but the theoretical compensation of the effects of r_i and wall losses is found to be both possible and relatively convenient without approximation of any kind, provided that the short circuit itself produces negligible loss. In other words, the exact equation, with all parameters arbitrary, assumes the simple and manageable form of Eq. (70).

Only the unmodified method is clearly superior in regard to loss measurement; errors in the modified method are no longer eliminated with the same simplicity, and those remaining after compensation are usually somewhat higher because of the inconstancy of G and the decreased slope of the curve. The modified method, nevertheless, offers an advantage not possessed by any of the other methods discussed so far in that it is operable even when the power is insufficient to give a receiver reading when the line is matched. Although found only in the modified method, this characteristic of low power requirement is perhaps of sufficient importance to be set down as a fourth advantage peculiar to the short-circuited-line procedure.

In a consideration of the unfavorable properties of the method, it is observed that it has a failing common to all procedures not carried out in free space inasmuch as it presupposes an accurately prepared sample. At best a tedious process, this preparation becomes exacting for short wavelengths, and it is at these short wavelengths that the alternative free-space methods appear to best advantage. A second disadvantage, which again is especially noteworthy at the short wavelengths, is that a considerable supply of accurately machined equipment is required; in particular, a traveling probe of some sort is required for either method, and an accurately constructed reflector G is required as well for the modified procedure. A third disadvantage is the high power requirement of the unmodified method, which is surmounted by the suggested modification only with an attendant loss in accuracy for $\tan \delta$. And finally, the method is unsuitable for measurement of gases: the use of a short sample is not only permissible but imperative if the standing-wave ratio is not to become too small, and the path lengths of 500 to $2000\lambda_m$ required for even moderate accuracy in measurement of gases would lead to prohibitively low values from the effect of line losses alone.

CONCLUSION

Retrospect.—In the course of the foregoing pages the great variety of experimental techniques by which dielectric measurement can be made in the microwave region was noted; and at the same time an equally great uniformity in the theoretical principles required was observed. The equations for every method were, in fact, deduced from Eq. (2) of the Introduction with its corollary Eqs. (5), (6), and (7), and from Eq. (8) with the supplementary results, Eqs. (9), (12), and Table 10·1. Not only did these few relations suffice for the transition from data to results in ideal circumstances, but they also allowed an investigation of many of the sources of r-f error. An illustration of this repeated application of a few simple equations is found in the modified short-circuited-line method just considered; and the deviations for this method, which is of importance in the sequel, may be summarized in the following manner. The first step was the computation of r_i from Eq. (8); with r_i known, the corollaries of Eq. (2) gave both reflection and transmission for a lossless sheet of arbitrary thickness in free space. In the situation in which the sheet is followed at a distance D by a metal plate, it was found that this more difficult configuration also depended for its solution upon Eq. (2), the extension to lossy materials in guide being made by Eq. (12) and Table 10·1. The fact that the measuring probe has, in general, a nonzero reflection led to the investigation of the consequent error—a computation which required only that the over-all reflection of probe and

termination be computed, which could accordingly be done by the same methods. The next step was to relate receiver reading to plunger position, a problem that was likewise solved by a corollary of Eq. (2); and finally the error due to generator reflection was investigated by the same means. This uniformity of theory has been noted for each of the other methods, the derivations from Eqs. (2) and (8) being, in fact, more immediate than in the case described.

To the mathematical equivalence just observed must be added a similar correspondence in the physical principles required. Thus, the last procedure was proved essentially equivalent to the short-circuited-line method; the only change was in the actual manner of obtaining the data since all relations between measured quantities, k and tan δ, were the same in the two cases. The short-circuited-line method, in turn, was seen to be closely related to the transmission procedures with which the present discussion was begun; as far as principles are concerned, the equivalence was established on both intuitive and mathematical grounds, the chief difference again consisting in the method of obtaining the data. Moreover, the two transmission methods, free space and waveguide, are evidently equivalent to each other in all essentials; and, with the exception as before of measurement technique, they are likewise equivalent to the standard interferometer methods of physical optics. If the relatively unimportant procedures discussed in Secs. 10·12 to 10·14 are omitted the methods hitherto considered may be regarded as forming a sort of sequence: from the familiar technique of optics to its microwave analogue, transmission in waveguide or free space; from this to the short-circuited-line method, where the "transmitted" and incident waves are compared on the generator side, rather than on the load side, of the sample; and from the short-circuited-line method to the modified procedure last described.

10·21. Resonant-cavity Methods.—This modified procedure, which requires a high mismatch on both sides of the sample, permits continuation of the sequence mentioned, making a simple and natural transition from the elementary methods first discussed to the apparently more difficult ones forming the topic of this section.

Methods Included in Preceding.—In the resonant-cavity method of Fig. 10·52*a* the plunger position is adjusted for resonance with and without the sample; the change in position gives k, essentially, and tan δ is found from the change in resonant current (cf. Eq. (94)) or from the width of the resonance curve (cf. Eq. (92)). This procedure, discussed at length in Ref. 18*b*, is evidently equivalent to that of Fig. 10·46*a*; the only change is to introduce the generator power by a second probe or coupling loop rather than by the transmission of the plunger. The entire discussion of Sec. 10·19 is therefore valid almost word for word

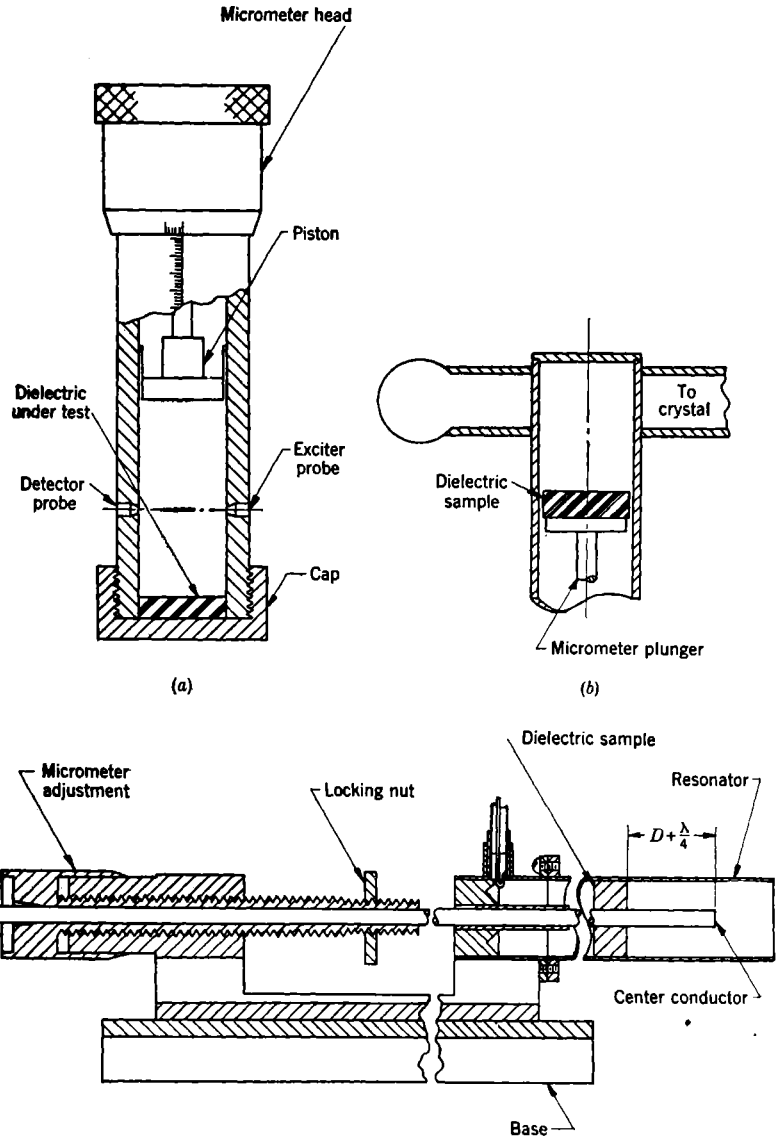

FIG. 10·52.—Resonant-cavity methods. In (*c*) a second coupling loop, not shown, is placed 90° from the first. The resonator may have an open end, as shown, or may be closed.

in the present case, and Eqs. (71) and (72) again give k and tan δ (Ref. 18*b*), whenever terms of the order of $\tan^2 \delta$ may be neglected. The same remarks apply to the method of Fig. 10·52*b* developed in Ref. 13*a*; and because of the complete equivalence to what has gone before it is unnecessary to present more than the most cursory discussion of either method. It is observed, however, that these methods are superior to the former insofar as the equipment is considerably easier to construct. Instead of a traveling probe, for example, there is a simple coupling loop; and the sliding plunger, which need not be adjusted to have a constant nonzero transmission, may have a reflection coefficient of unity. For this reason the plunger is more easily designed and its reflection more easily maintained constant. There is, on the other hand, some slight disadvantage in that the received power is not usually the maximum possible. Thus, neither the penetration of the coupling loops nor their position is adjustable, and, since the position of the minimum will depend on the sample, it is clear that the two loops will not generally be on an antinode. Moreover, when the loops are near a node, an increase in coupling, which is then permissible, cannot be obtained. In other words, the coupling coefficient must be sufficiently small to permit operation at an antinode even when the loops are actually located near the minimum. In the previous method no such difficulty was found, and there was also a possible advantage in that only one source of extraneous reflection (the probe) was required, rather than two.

Difficulty due to variation of the minimum position may be obviated, in principle, by using two traveling probes in place of the coupling loops of Fig. 10·52*a*. A better method, however, is that suggested in Fig. 10·52*c* (Refs. 11*b*, 12*b*, 15*b*, 16*b*, 17*b*, 12*c*, 18*c*) where the two loops are located at the short circuit and hence are always at a node. The length of the line is changed, but the distance from the sample to one end remains constant. Whether this constant distance happens to be measured to the generator end or the load end is unimportant in this discussion, for in either case the opposite end of the line may be replaced by a short circuit shifted a distance zero or $\lambda_g/4$ according to whether this opposite end was itself a short or open circuit. The method is thus seen again to be equivalent to that of Sec. 11·19; if the fixed distance from the sample to the end of the line is represented by 0 or $\lambda/4$ plus the distance D of Fig. 10·31*a*, as shown in Fig. 10·52*c*, then the whole of the foregoing theory applies without approximation to the present case. It is observed in passing that the methods of Fig. 10·52 may be used with variable frequency rather than variable length—a remark which applies to almost all the methods here considered. In principle, the free-space wavelength λ is adjusted for resonance with and without the sample. At the same time the resonant current or the width at half

maximum is noted. For the empty guide of resonant length $n\lambda_g/2$ the width Δl, when the length l is variable, is related to that found when λ is variable by the approximate equation (Ref. 12*a*)

$$\Delta l \text{ for half power} = \left(\frac{n}{2}\right)\left(\frac{\lambda_g}{\lambda}\right)^3 \times \Delta\lambda_{\text{half power.}} \tag{98}$$

This is seen by differentiating the relation of Table 10·1 for waveguide in terms of free-space wavelength. In a similar manner the change $\Delta\lambda_g$ in guide wavelength needed to restore resonance after insertion of the sample is related to the change in length Δl by

$$(\Delta l) = -\frac{n(\Delta\lambda_g)}{2}, \tag{99}$$

where Δl is measured at the wavelength that gave resonance when the sample was in place, and n, as before, represents the number of antinodes in the resonating empty guide. This last equation is valid

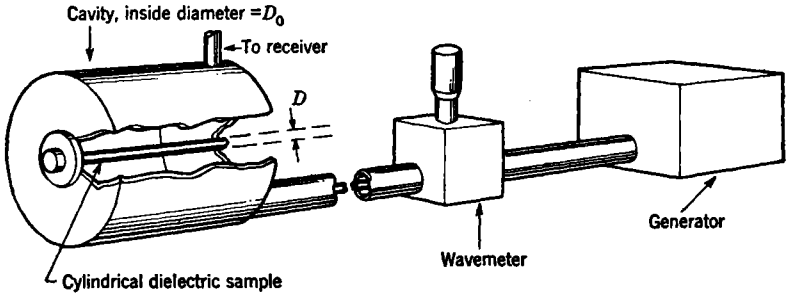

FIG. 10·53*a*.—A resonant-cavity method using cylindrical samples and variable frequency, Ref. 9*a*.

without approximation, whereas Eq. (98) is to be used only when terms containing the square of the width may be neglected—a situation which is, as will be shown, the only one that should be allowed to occur. Equation (98) may be regarded as correct, to a first approximation, when the sample is in place, although a rigorous treatment is made difficult by the fact that the total electrical length, which is involved in the constant n of the equation, then depends in a complicated way on the frequency. The maximum power, however, is the same for variable frequency as for variable length (cf. Ref. 12*a*); hence Eq. (94) may be used without change in either case. The merit of using a variable frequency will be commented upon; it is sufficient to note that the foregoing results may be used in this case also, provided that the resonant width is suitably determined, the equivalent change in length is computed from Eq. (99), and the parameter λ in all equations is taken as equal to its value for resonance when the sample is in place.

A Method Not Included.—The summary dismissal of the resonant-cavity methods shown in Fig. 10·52 was possible because of their close similarity to procedures already discussed. In the method of Fig. 10·53 it is found that the general form cannot readily be subsumed in this way; there is, however, a special case that has considerable practical importance and is at the same time amenable to treatment by the elementary methods hitherto employed. This special case, which forms a convenient introduction to the general method, is found when the resonator is entirely filled with the material being tested so that, with the notation of Fig. 10·53, $D = D_0$. Although its attainment with solid samples is somewhat inconvenient, such a condition is easily obtained in practice whenever the sample happens to be in liquid or gaseous form. With all air-dielectric boundaries perpendicular to the axis of the system, this special configuration is now included among those

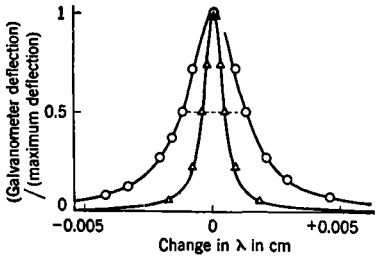

FIG. 10·53*b*.—Example of resonance curves, received power vs. λ, for the empty cavity (triangles) and for the cavity containing a dielectric sample (circles). The points are experimental, the curves theoretical fitted at the half-maximum points.

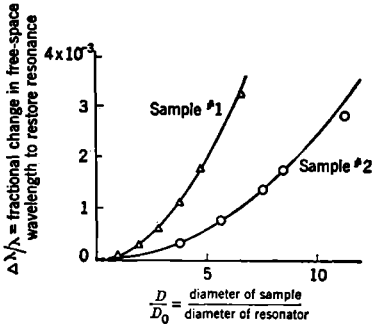

FIG. 10·53*c*.—Experimental verification of Eq. (105*a*) for two dielectric materials. The points are experimental and the curves are calculated from Eq. (105*a*).

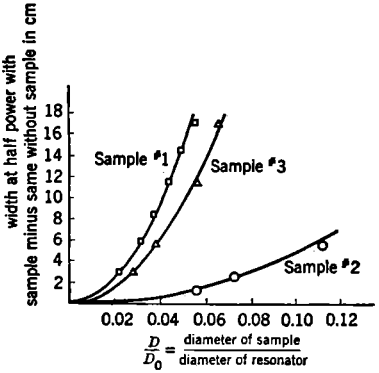

FIG. 10·53*d*.—Experimental verification of Eq. (105*b*) for three materials. The theoretical curves are determined from the best experimental value of tan δ.

hitherto treated; and the condition for resonance is thus seen to be (cf. Ref. 12*a*)

$$(\text{length of resonator}) = \left(\frac{n}{2}\right)(\text{wavelength in material in guide}), \quad (100)$$

whence is obtained

$$k = \left(\frac{m}{n}\right)^2 \left(\frac{\lambda}{\lambda_0}\right)^2 + \left[1 - \left(\frac{m}{n}\right)^2\right] \left(\frac{\lambda}{\lambda_c}\right)^2, \tag{101}$$

$$k = \left(\frac{\lambda}{\lambda_0}\right)^2, \qquad m = n, \tag{102}$$

for the dielectric constant k in terms of the resonant (free-space) wavelengths λ, λ_0, with or without the sample, and the ratio m/n of the number of antinodes in the filled or empty guide. The normal situation is represented by the case $m = n$, for which the equation takes the simple form Eq. (102) given in Refs. 10*a*, 10*b*, 17*b*. Equations (101), (102) are valid only for negligible $\tan^2 \delta$; the general result is obtained by substituting an appropriate value for guide wavelength in Eq. (100), as computed from Eq. (12) and Table 10·1. It must be noted, however, that Eq. (100) itself ceases to be valid for very lossy samples; the condition of resonance, as determined by maximum power, gives a length somewhat smaller than the length there indicated.

For the loss tangent (Refs. 10*b*, 13*b*, 14*b*, 17*b*),

$$\tan \delta = \frac{\Delta\lambda}{\lambda} - \left(\frac{\Delta\lambda}{\lambda}\right)_0, \tag{103}$$

where the first term stands for the width of the resonance curve at half power divided by the resonance wavelength for the actual sample (Fig. 10·39*b*), while the second is the corresponding quantity for a hypothetical sample with the same dielectric constant but zero loss. With negligible $\tan^2 \delta$ this second quantity is equal to the corresponding result for the empty resonator multiplied by $\sqrt{k}$ (Ref. 17*b*). Instead of taking the width of the resonance curve, the following relation (Ref. 10*a*) may sometimes be used,

$$\frac{\text{Width for first sample}}{\text{Width for second}} = \frac{\text{power at resonance for second}}{\text{power at resonance for first}}. \tag{104}$$

This equation gives the ratio of widths in terms of the received power at resonance. Besides requiring use of a monitor, the procedure has the disadvantage of being relative only, with the result that one of the widths must be directly measured in any case. After such a determination is made, however, the evaluation of the other is sometimes facilitated.

The foregoing discussion has been devoted to the special case for which the sample entirely fills the resonating chamber, and the relations obtained were both convenient and elementary. In the general situation of Fig. 10·53*a*, on the other hand, the corresponding results become considerably more complex than any hitherto encountered. Not only are the equations for both k and $\tan \delta$ transcendental even when

$\tan^2 \delta = 0$ (see Refs. 14*b*, 19*b*, 20*b*), but they involve too many parameters to be readily solved by graphical methods. Moreover, the functions themselves are not elementary; instead of the exponential or circular functions that have hitherto sufficed in all cases, Bessel functions must be used. These difficulties, noted when $\tan^2 \delta$ is set equal to zero, are naturally enhanced when a truly general computation is attempted; for not only will the equations be transcendental involving functions which are not elementary, but the arguments of these functions will be complex as well. It is clear, then, that any theoretical investigation aiming at completeness will necessarily be somewhat involved. Before embarking on such an enterprise, it is perhaps worth while to consider the experimental conditions imposed on the method in question. Thus, with some of the transmission procedures considered above it was found that the quantity $r_i e^{-d \tan \delta}$ should be small for experimental convenience. Hence the theory could justifiably be confined to the simple relations obtained when this condition is satisfied. A similar approach is found valid for the present method too, in that the general situation is somewhat impracticable from an experimental standpoint irrespective of its theoretical difficulty. Before extending the theory, therefore, the question of experimental procedures is to be considered.

In the first place it is noted that variation of frequency presents considerable difficulty when the range of variation is large. With the microwave generators available at present a change of much over twenty per cent is hardly feasible, and for convenience the figure should be considerably less than this. Even the small variation required to measure the width presents certain problems, in that due care must be taken to ensure constant output of the generator and constant sensitivity of the receiving equipment, or of the monitor if one is used, over this range. There is, moreover, a theoretical objection in that both k and $\tan \delta$ depend on frequency, although this objection is somewhat academic in ordinary practice (cf. Ref. 9*a*). A more serious problem occurs, however, when the empty resonator rather than the filled is considered, for the frequency shift so required will, in general, be far beyond the capacity of most microwave generators to achieve, apart from incidental difficulty due to frequency sensitivity of the r-f components. To obviate this difficulty the resonant wavelength for the empty guide may be computed, instead of measured, easily and accurately from Eq. (100) whenever the resonator length is known. This length is so chosen that resonance is obtained, with the sample in place, at a frequency that is within the range of the generator and that is also sufficiently close to the frequency at which the values of k and $\tan \delta$ are desired. In this way the measurement of k is carried out with but slight change of frequency, even when the difference as given by Eq. (102) is large. Such a procedure, which

was used with success in Refs. 10*b* and 14*b*, requires knowledge of the approximate value of k and demands that the resonator length be adjusted accordingly, since different lengths are necessary for different samples.

The foregoing limitations were concerned chiefly with the dielectric constant, as it is this parameter rather than loss that is primarily determined from the frequency shift [cf. Secs. 10·3 to 10·6 and Eq. (102)]. For measurement of tan δ, however, another difficulty is encountered in that Eq. (103) presupposes knowledge of the width for a hypothetical sample with the same dielectric constant as that of the original sample, but of zero loss. Of course, no such sample can be actually produced and measured, and the question must be considered in more detail. Theoretically this hypothetical loss may be computed from the dimensions of the resonator and the conductivity (or more particularly, the so-called "skin depth") of the walls (Refs. 10*b*, 13*b*, and 14*b*), but such a computation neglects all extraneous losses, including those from the junctions and coupling loops. For this reason it is found that the values computed differ perhaps by a factor of two from the ones actually measured (Refs. 10*b* and 14*b*). In Ref. 14*b* it was assumed, therefore, that the ratio of computed to measured width would be the same for the empty cavity as for the cavity filled with the hypothetical lossless dielectric; but, as was there observed, no proof has been obtained, nor is it to be supposed that such a procedure is of general validity. Even if it be permissible, however, there is still difficulty because the determination of width for the empty cavity itself must be made at a frequency that is too far from that with the sample to be readily attained in practice. To obviate this added difficulty a new and larger cavity that will resonate at a convenient wavelength when empty, may be constructed and from measurement on this new cavity the width that would have been obtained for the original one can be estimated. Although such a procedure has been actually used (Refs. 10*b* and 14*b*), the inconvenience as a matter of general practice is evident.

From this discussion, much of which applies to all methods using a variable wavelength, it is seen that considerable experimental difficulty is often to be anticipated in the method of Fig. 10·53; and although such difficulty can be circumvented by various devices, these devices are sufficiently inconvenient to be of but limited utility. Instead of seeking a general theory, therefore, the problem is to find the particular circumstances in which the method appears to best practical advantage. Once this has been decided, the special theory appropriate to that case may be exhibited in simple form. The complications noted consisted chiefly in the large frequency change for proceeding from the filled to the empty guide, and in the difficulty of computing a sort of "comparison loss"

corresponding to the empty-guide loss. Both difficulties would be obviated if, and apparently only if, the character of the resonator were not appreciably changed by insertion of the sample. In other words, the resonant wavelength should remain nearly the same, and the loss when empty should be nearly the same as the loss when filled by a lossless sample of the same dielectric constant. These conditions are met whenever $k \approx 1$; in particular for a gas the method is most convenient and was used for such measurement in Refs. 10*a* and 12*a*. The length rather than the frequency, however, is varied in Ref. 12*a*. After it was verified that no undue absorption was to be anticipated from dry air at the frequency used, the width for the empty resonator was taken as equal to the value for the air-filled resonator, and this value was substituted for the second term of Eq. (103). Because of the low dielectric constant, such a procedure was entirely justified in that case. The remainder of the measurement too could be carried out with ease, since all frequency shifts were very small; and k was readily computed from Eq. (102). In Ref. 12*a* the accuracy was increased by use of a large cavity, and due precautions were taken to prevent oscillation at unwanted modes (cf. Ref. 13*b*). The method is in many respects the best for measurement of gases; not only is the cavity airtight whenever the coupling loops are suitably sealed off, but also the method allows accuracies that are scarcely attainable by other procedures. The power requirement is not excessive, and the equipment itself, which requires no moving plunger, is perhaps as simple as any hitherto discussed.

It is not necessary to use materials of low dielectric constant; a sample of such small diameter may be used that the resonant frequency is only slightly affected. There is, to be sure, a limit to the reduction that is permissible in good practice, since both the frequency shift and the rod diameter must be known within a small percentage error, rather than a small absolute error, if accurate results are to be obtained; for diameters $D \approx 0.05D_0$ this effect is still of secondary importance when the sample is accurately machined. For a TM-wave the general equation takes the simple form (Refs. 9*a* and 14*b*)

$$k \approx 1 + 0.538\left(\frac{D_0}{D}\right)^2\left(\frac{\lambda}{\lambda_0} - 1\right), \quad D \ll D_0, \tag{105a}$$

$$\tan\delta \approx 0.269\left(\frac{D_0}{D}\right)^2\left(\frac{\Delta\lambda}{\lambda} - \frac{\Delta\lambda_0}{\lambda_0}\right). \tag{105b}$$

Equations (105) indicate that the effect of the sample is proportional to its volume (see Fig. 10·53*c*). Because of the similarity to the equations previously discussed, the sources of experimental error need not be further investigated.

10·22. Summary. *Methods Tabulated.*—The great variety of experimental methods, which has been so often observed in the discussion, suggests that a brief summary will be of use, and such a summary is accordingly presented in Table 10·5. The descriptions given, which are suggestive only, are intended to aid recollection and are in no sense an adequate presentation of the method described. Because the emphasis has been on measurement procedure, a fine subdivision in Table 10·5 is used, despite the theoretical homogeneity. Thus, two methods are classified separately when they differ appreciably in experimental technique, even though they may be, in principle, entirely equivalent.

Consistency of Results.—Before the subject of dielectric measurement can be dropped, the order of accuracy that may be expected in typical

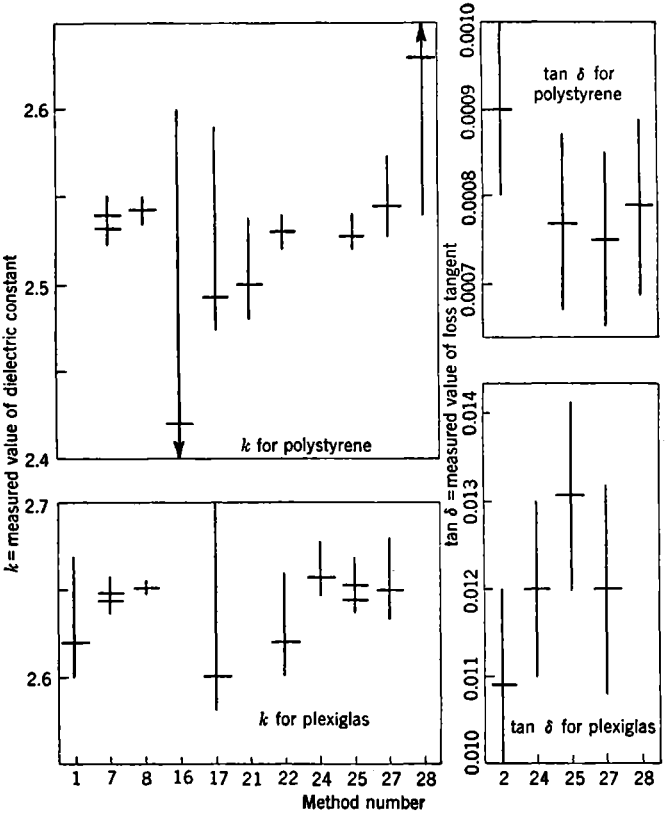

FIG. 10·54.—Comparison of values as measured by various methods. Horizontal line shows average value of k or tan δ for a given sample, vertical line shows estimated error.

TABLE 10·5.—SUMMARY OF METHODS

Method number	Quantity determined when loss is low	Procedure	Equipment	Discussed in section	References a	b	c
			Measurement from transmission in guide				
1	k	Set phase shifter for minimum with and without sample.	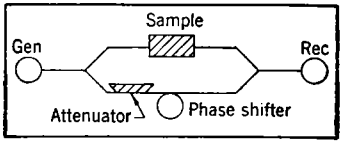	10·3, 10·5, 10·6	6		
2	tan δ	Take receiver reading with and without sample using tapered, $n\lambda_g/2$ or high-loss sample.	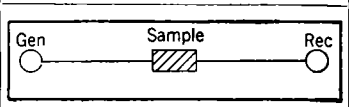	10·4, 10·5, 10·6	6		
3	tan δ	Take max. and min. with each probe, sample as in No. 2.	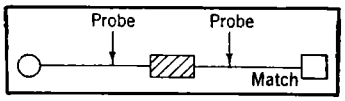	10·4, 10·5, 10·6.	17 7		
4	tan δ	Take max. and min. power as phase shifter is varied, sample as in No. 2.	Same as No. 1	10·4, 10·5, 10·6			
5	tan δ	Set calibrated attenuator to minimize the minimum with and without sample, sample as in No. 2.	Same as No. 1	10·4, 10·5, 10·6			
6	tan δ	Measure rate of temperature rise with power on, fall with power off.	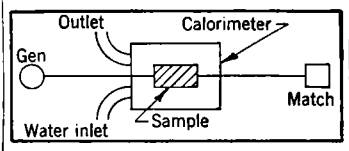	10·21	15		
			Measurement from transmission in free space				
7	k	Adjust micrometer for minimum with and without sample.	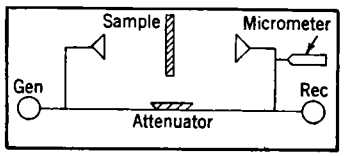	10·7, 10·8	6 7		6

TABLE 10·5.—SUMMARY OF METHODS.—(*Continued*)

Method number	Quantity determined when loss is low	Procedure	Equipment	Discussed in section	References		
					a	*b*	*c*
8	k	Adjust angle of incidence for minimum on each side of $\theta = 0$.	Same as No. 7	10·9	6		6
9	$\tan \delta$	Take receiver reading with and without half-wavelength or lossy sample.	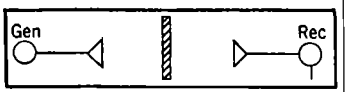	10·7 10·8	14		
10	$\tan \delta$	Same, ordinary sample at Brewster's angle.	Same as No. 9	10·9			
General methods depending on reflection							
11	k, $\tan \delta$	Measure interface reflection and phase shift with a traveling probe.	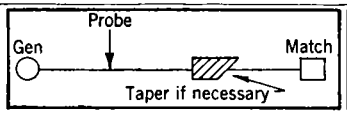	10·12	8 11		
12	k	Compare $(SWR)^2$ for sample and metal sheet. Sample should be an interface, or a quarter wavelength thick.	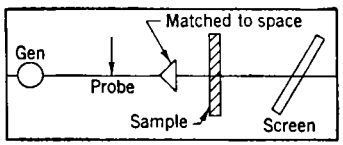	10·13	7 20		
13	k	Compare reflected with directly received power. Sample as in No. 12	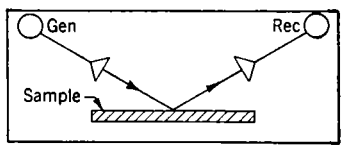	10·13	14 21		
14	k	Compare received power from sample and metal sheet in same position. Sample as in No. 12	Same as No. 13	10·13	14 20 7		
15	$\tan \delta$	Adjust antenna position for minimum with sample and metal sheet in same position.	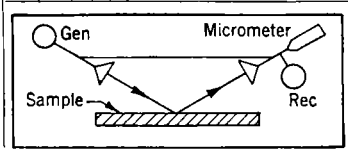	10·13	14		

TABLE 10·5.—SUMMARY OF METHODS.—(*Continued*)

Method number	Quantity determined when loss is low	Procedure	Equipment	Discussed in section	References		
					a	*b*	*c*
16	k	Measure reflection of a sheet, preferably a quarter wavelength thick.	Same as No. 11	10·14	6	21	
17	k	Take thickness for minimum reflection.	Same as No. 11	10·14	6		
18	k	Take maximum reflection of two or more samples.	Same as No. 11	10·14		8	
19	k, tan δ	Measure reflection and minimum position for two sample lengths.	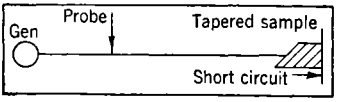	10·15			
		General methods depending on reflection					
20	k, tan δ	Measure distance between minima, and take width at twice minimum, probe being in sample.	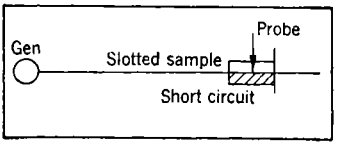	10·15			17
21	k	Take distance between minima, as sample moves past side arm.	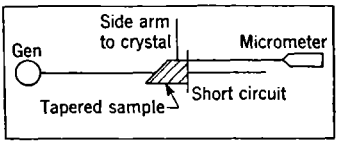	10·15	16 6		
22	k	Take difference of sample positions for resonance	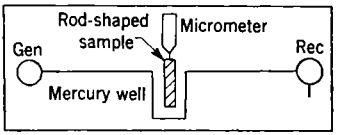	10·15	6		
23	tan δ	Take ratio of max. to min. power in each side arm as plunger is moved.	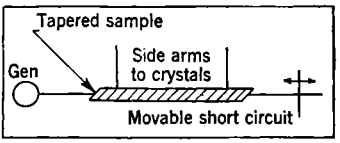	10.15	16		

TABLE 10·5.—SUMMARY OF METHODS.—(*Continued*)

Method number	Quantity determined when loss is low	Procedure	Equipment	Discussed in section	References a	b	c
			The short-circuited-line method				
24	k, tan δ	Measure minimum position and width at twice minimum with and without sample.	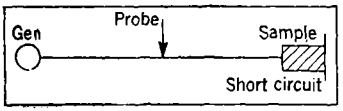	10·17 10·18	19 1	26 2 22 1 23 3 24 4 25 5 9	1 2 3 4
25	k, tan δ	Take plunger position for maximum and width of curve at half-maximum, or maximum power, with and without sample.	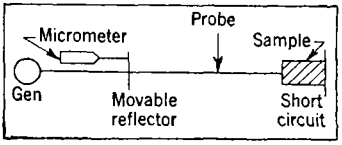	10·19	6		6
			Resonant-cavity methods				
26	k, tan δ	Same as No. 25	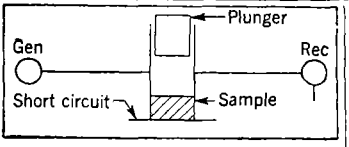	10·21	12		19
27	k, tan δ	Same as No. 25	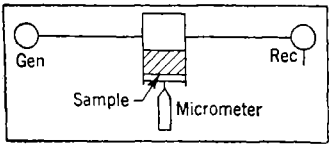	10·21	13		
28	k, tan δ	Adjust line length for resonance with and without sample. Take width or max. power.	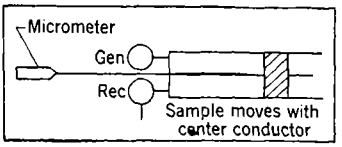	10.21		16 17 15 11 12	
29	k, tan δ	Same as No. 28	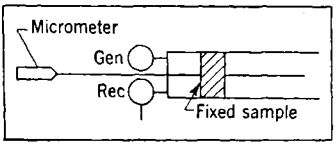	10.21		16 17 18	12 18
30	k, tan δ	Same, frequency varied instead of length.	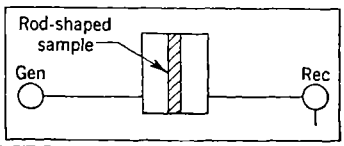	10.21	9 10	14 10	13 9

TABLE 10·6.—COMPARISON OF METHODS WITH REGARD TO INTERNAL CONSISTENCY FOR MEASUREMENT OF k

Method number	λ cm	Parameter varied	Number of measurements	Greatest value obtained	Least value obtained	Average deviation for all values	Material used	From Ref.
1	1.25	Sample thickness	10	2.65	2.59	0.02	Plexiglas	6*a*
7	1.25	Sample thickness	4	2.65	2.64	0.00	Plexiglas	6*a*
7	1.25	Sample thickness	2	2.54	2.53	0.00	Polystyrene	6*a*
7	1.25	Sample thickness	3	3.47	3.41	0.02	Dielectene	6*a*
8	1.25	Angle of incidence	8	2.659	2.648	0.002	Plexiglas	6*a*
8	1.25	Angle of incidence	9	2.550	2.542	0.002	Polystyrene	6*a*
8	1.25	Angle of incidence	3	3.41	3.40	0.00	Dielectene	6*a*
8	1.25	Angle of incidence	13	3.456	3.441	0.003	Dielectene	6*a*
12	9.1	Antenna size	5	2.72	2.63	0.03	Plexiglas	7*a*
21	1.25	.....	4	2.65	2.59	0.02	Plexiglas	6*a*
21	1.25	.....	2	2.50	2.50	0.00	Polystyrene	6*a*
22	1.25	.....	4	2.66	2.64	0.01	Plexiglas	6*a*
22	1.25	.....	2	2.53	2.53	0.00	Polystyrene	6*a*
24	1.25	Sample thickness	14	2.68	2.64	0.02	Plexiglas	6*a*
25	1.25	Sample thickness	2	2.65	2.64	0.01	Plexiglas	6*a*
25	1.25	Sample thickness	5	2.66	2.65	0.01	Plexiglas	6*a*
25	1.25	Sample thickness	6	2.67	2.65	0.01	Plexiglas	6*a*
25	1.25	Sample thickness	5	2.53	2.52	0.00	Polystyrene	6*a*
25	1.25	Sample thickness	6	3.45	3.42	0.01	Dielectene	6*a*

circumstances is to be considered. A precise investigation of this question presents considerable difficulty in that the accuracy of a given method depends on the nature of the sample. Thus, a method that is suitable for thick samples may be inaccurate for thin ones, and a method satisfactory for high loss may be almost useless when the loss is low. Added to the theoretical complication is the fact that experimental precision depends on the care with which the measurement is conducted. It is therefore clear at the outset that results only of the most qualitative kind will be presented. Because of the novelty of microwave procedures, however, it is believed that even such results have a certain value, in that they prevent serious misconceptions. With these preliminaries, it is noted that error appears in two forms: the results obtained with a given method disagree among themselves, to some extent, as the conditions are varied; on the other hand, the average results obtained for different methods are not exactly equal to each other. The error of the first type, which is concerned with reproducibility of the results in a given method, is illustrated in Table 10·6, where the variation of values is noted as various parameters are changed. The second error is considered in Fig. 10·54 where values as measured by the different techniques summarized in Table 10·5 are compared. The results for methods 21 and 22 were obtained with different samples from that used in the others and hence the agreement, or lack of it, has only doubtful significance. The materials used, plexiglas and more especially polystyrene, are known to be fairly uniform; but the evidence of this uniformity depends in no small measure on data of the type shown in Fig. 10·54, and it cannot validly be urged in the present case. With this reservation, however, the agreement is within the experimental error as estimated from Table 10·6 and from *a priori* considerations. Because of the lack of extensive data on tan δ with uniform samples, no result such as that of Table 10·6 or Fig. 10·54 is presented for loss. It is observed, however, that typical values for error would be perhaps ± 5 per cent or ± 0.0001, whichever is the larger. In exceptional cases, accuracies as great as ± 0.00001 may be achieved, although the techniques then become somewhat exacting. The accuracy with which k can be measured is of the order of ± 2 per cent to ± 0.2 per cent in typical cases, where only a high grade of engineering precision in the design and operation of the equipment is assumed. With the refinements that are to be expected in research work, this accuracy can no doubt be greatly exceeded.

BIBLIOGRAPHY

Because of the number of references dealing with the subject matter of this chapter, it has been thought best to present a classified bibliography, where the references are divided into classes dealing with

experimental techniques (*a* references), theory (*b* references), or tabulated values of k, tan δ (*c* references). If a report appeared to fit equally well into the *a* or *b* category, it was arbitrarily placed under *a*.

The following references are concerned chiefly with experimental procedures for finding the original data.

1*a*. VON HIPPEL, A., D. JELATIS, W. WESTPHAL, and M. HAUGEN, "Auxiliary Equipment for the MIT Coax Instrument and its Use," Laboratory for Insulation Research, MIT, NDRC 14-210, November, 1943.

2*a*. REDHEFFER, R. M., "Radome Bulletin Number 7: The Measurement of High Reflections at Low Power," RL Report 483-7, Nov. 20, 1944.

3*a*. REDHEFFER, R. M., "Radome Bulletin Number 9: The Matching of High Standing Wave Ratios," RL Report 483-9, Dec. 22, 1944.

4*a*. DOWKER, Y., and R. M. REDHEFFER, "Radome Bulletin Number 10: The Measurement of Small Reflections," RL Report 483-10, Feb. 6, 1945.

5*a*. DOWKER, Y., and R. M. REDHEFFER, "Radome Bulletin Number 14: An Investigation of R-F Probes," RL Report 483-14, Feb. 6, 1946.

6*a*. REDHEFFER, R. M., and E. D. WINKLER, "Radome Bulletin Number 15: The Measurement of Dielectric Constants in the One-Centimeter Band," RL Report 483-15, May 11, 1945.

7*a*. REDHEFFER, R. M., "Radome Bulletin Number 18: The Interaction of Microwave Antennas with Dielectric Sheets," RL Report 483-18, Mar. 1, 1946.

8*a*. TURNER, L. B., "Conductivities of Sea, Tap and Distilled Water at $\lambda = 10$ cm," Admiralty Signal Establishment, Lythe Hill House, Haslemere, Surrey, Report M496, April 1943.

9*a*. BORGNIS, F., "Measurement of the Dielectric Constants and Loss Factor of Dielectric Substances with a Wavelength of 17 cm. with the Help of Cavity-Resonators," *Phys. Z.*, **43**, 284–291 (Aug. 1942).

10*a*. SAXTON, J. A., "The Dielectric Constant and Absorption Coefficient of Water Vapour for Wavelengths of 9 cm. and 3.2 cm. (Frequencies 3,300 and 9,350 Mc/s.)," The National Physical Laboratory, Paper No. R.R.B./S.11., Apr. 12, 1943.

11*a*. COLLIE, C. H., "Preliminary Report on the Dielectric Properties of Water in the K-Band," The National Physical Laboratory, C.V.D. Report CL, Misc. 25.

12*a*. SAXTON, J. A., "The Dielectric Constant and Absorption Coefficient of Water Vapour for Radiation of Wavelength 1.6 cm. (Frequency 18,800 Mc/s.)," The National Physical Laboratory, Paper No. R.R.B./S.17., Apr. 22, 1944.

13*a*. PENROSE, R. P., Clarendon Laboratory, Oxford University. "A Method for the Determination of Permittivity for Power Factors of Low Loss Dielectrics in the K-Band," C.V.D. Report CL Misc. 32, Dec. 1944.

14*a*. SAXTON, J. A., and J. A. LANE, "The Dielectric Properties of Water in the Temperature Range 0°C. to 40°C. for Wavelengths of 1.24 cm. and 1.58 cm.," The National Physical Laboratory, Paper No. R. R. B./C.116, Mar. 7, 1945.

15*a*. CALBICK, C. J., "Ultra-High Frequency Attenuation in Liquids with Experimental Data for Water and Ethyl Alcohol," BTL MM-42-140-53, Sept. 16, 1942.

16*a*. YOUNKER, E. L., "Dielectric Properties of Water and Ice at K-band," RL Report 644, Dec. 4, 1944.

17*a*. LEITER, H. A,. "Dielectric Transmission Measurements," RL Report 244, Jan. 15, 1943.

18a. ENGLUND, C. R., "Series of Ultra Short Wave Dielectric Measurements," *Proc. Inst. Radio Engrs*, **23**, 114 (Jan. 1944).
19a. ALTAR, W., "Measurement of Dielectric Properties of Lossy Materials," Westinghouse Research Report R-94318-E, Sept. 13, 1944.
20a. REDHEFFER, R. M., "Radome Bulletin Number 2: An Outline of the Electrical Properties of Randomes," RL Report 483-2, Dec. 20, 1943.
21a. PFISTER and ROTH, *Hochfrequenztechn. u. Elektroakust.*, **51**, 156 (1938).
22a. REDHEFFER, R. M., "Radome Bulletin Number 13: Elliptical Polarization Produced by Streamlined Radomes," RL Report 483-13, Feb. 12, 1945.

The following references deal chiefly with the theoretical relations between the original data and the desired results, k, tan δ.

1b. STRATTON, J. A., *Electromagnetic Theory*, McGraw-Hill, New York, 1941.
2b. ROBERTS, S., and A. VON HIPPEL, "A New Method of Measuring Dielectric Constant and Loss in the Range of Centimeter Waves," Department of Electrical Engineering, MIT, Mar. 1941, pp. 1–19.
3b. VON HIPPEL, A., "Progress Report on Ultra-High Frequency Dielectrics," Laboratory for Insulation Research, MIT, NDRC Report 14-121, Jan. 1943.
4b. VON HIPPEL A., and R. BRECKENRIDGE, "The Interaction Between Electromagnetic Fields and Dielectric Materials," Laboratory for Insulation Research, MIT, NDRC Report 14-122, Jan. 1943.
5b. VON HIPPEL, A., D. G. JELATIS, and W. B. WESTPHAL, "Measurement of Dielectric Constant and Loss with Standing Waves in Coaxial Wave Guides," Laboratory for Insulation Research, MIT, NDRC Report 14-142, April 1, 1943.
6b. REDHEFFER, R. M., "Radome Bulletin Number 4: Transmission and Reflection of Single Plane Sheets," RL Report 483-4, July 12, 1944.
7b. REDHEFFER, R. M., "Radome Bulletin Number 11: Electrical Properties of Double-Wall and Sandwich Radomes," RL Report 483-11, Feb. 1, 1945.
8b. REDHEFFER, R. M., "Radome Bulletin Number 12: Transmission and Reflection of Parallel Plane Sheets," RL Report 483-12, Jan. 26, 1945.
9b. DOWKER, Y., "Radome Bulletin Number 19: Dielectric Constant and Loss Tangent Computation," RL Report 483-19, Aug. 7, 1945.
10b. TAYLOR, T. A., and W. JACKSON, "The Use of the Closed Cylindrical Resonator for Dielectric Loss Measurements," Ministry of Supply, Advisory Council on Scientific Research and Technical Development, R.D.F., Application Committee, Communications Committee, A.C. 1425, RDF. 100, Com. 70, Nov. 25, 1941.
11b. GENT, A. W., "Theory of Permittivity and Loss Factor Measurements Using Resonant Transmission Lines," Standard Telephones and Cables Limited, London, England, Valve Laboratory Report No. G.48, June 1942.
12b. GRANT, A. S., "The Measurement of Dielectric Constant and Power Factor of Insulating Materials at 10-cm. Wavelength," Standard Telephones and Cables Limited, London, England, Valve Laboratory Report No. G. 49, June, 1942.
13b. HANSEN, W. W., "A Type of Electrical Resonator," *J. Appl. Phys.*, **9**, 654–663 (1938).
14b. HORNER, F., and T. A. TAYLOR, "The Use of Cylindrical Resonators for Dielectric Measurements at Centimeter Wavelengths," Electrotechnics Department, Manchester University, Report No. 38, June 12, 1942.
15b. HORNER, F., "Measurement of Loss Factor of Low Loss Dielectrics at U.H.F." Extra-mural Research, Ministry of Supply, 287/Gen/35 D.S.R., Electro-Technics Dept., Manchester Univ., June 12, 1941.

16*b*. HORNER, F., and W. JACKSON, "Interim Report on Dielectric Loss Measurements at 3200 mc/sec.," Ministry of Research, D.S.R. Report No. 14, Feb. 15, 1941.

17*b*. DUNSMUIR, R., "The Resonant Frequency and Q Value of a Half Wave Coaxial Line Resonator Containing Dielectric Media with Transverse Discontinuities," Electrotechnics Department, Manchester University, June 20, 1944.

18*b*. SEAMAN, E. C. H., J. C. SIMMONDS and C. F. DAVIDSON, "A Resonant Cavity Method of Measuring Relative Permittivity and Loss Tangent," Radio Branch Laboratories, Wembley, England, Post Office Engineering Department, Radio Report No. 1240, Oct. 22, 1944.

19*b*. APKER, L., and L. TONKS, "Measurement of Dielectric Loss in the Microwave Region," GE, Schenectady, Nov. 18, 1942.

20*b*. FEENBERG, E., "Use of Cylindrical Resonator to Measure Dielectric Properties at Ultra-High Frequencies," Sperry Report GC 16907, July 21, 1942.

21*b*. BURROWS, C. R., "Transverse Dielectric Slab in a Wave Guide," BTL MM-43--160-46, Apr. 13, 1943.

22*b*. FEENBERG, E., "The Measurement of Dielectric Properties on an Impedance Meter," Sperry Report 5220-114, April 10, 1943.

23*b*. FEENBERG, E., "The Measurement of Dielectric Properties on an Impedance Meter," Supplement to Report No. 5220-114, Sperry Report 5220-124, Aug. 2, 1943.

24*b*. FEENBERG, E., R. LOUGHLIN, and R. MERCHANT, "The Measurement of Dielectric Properties on an Impedance Meter," Supplement to Report No. 5220-124, Sperry Report 5220-125, Sept. 15, 1943.

25*b*. DAKIN, T. W., "The Hollow Pipe Method of Measuring Dielectric Constant and Loss Factor," Westinghouse Research Report SR-134, Aug. 25, 1942.

26*b*. DAKIN, T. W., "Dielectric Constant and Dissipation Factor Calculation Methods from Wave Guide and Co-ax Standing Wave Measurements," Westinghouse Research Report R-94308-V, Oct. 5, 1944.

27*b*. SPERRY GYROSCOPE COMPANY, INC., *Microwave Transmission Design Data*, Publication No. 23–80, Sperry Gyroscope Company, Inc., Brooklyn 1, New York, 1944.

The following references give measured values of dielectric constant loss tangent, or both.

1*c*. VON HIPPEL, A., "Tables of Dielectric Materials," Laboratory for Insulation Research, MIT, NDRC Report 14-237, Feb. 1945.

2*c*. VON HIPPEL, A., "Tables of Dielectric Materials," Vol. II, Laboratory for Insulation Research, MIT, NDRC Report 14-425, June 1945.

3*c*. VON HIPPEL, A., L. G. WESSON, and S. L. WHITCHER, "The Polystyrene Plastics as High-Frequency Dielectrics," Laboratory for Insulation Research, MIT, NDRC Report 14-276, May 1944.

4*c*. BRECKENRIDGE, R. G., A. P. DE BRETTEVILLE, JR., J. M. BROWNLOW, F. G. CHESLEY, G. OSTER, L. TISZA, W. B. WESTPHAL, and A. VON HIPPEL, "High Dielectric Constant Ceramics," Laboratory for Insulation Research, MIT, NDRC Report 14-300, August 1944.

5*c*. EVERHART, E. M., "Radome Bulletin Number 5: Recent Dielectric Constant and Loss Tangent Measurements," RL Report 483-5, July 14, 1944.

6*c*. HEGARTY, M., Y. DOWKER, R. M. REDHEFFER, and E. D. WINKLER, "Radome Bulletin Number 17: Current Progress on R-f Research," RL Report 483-17, May 10, 1945.

7c. SUEN, T. J., and E. M. EVERHART, "Dielectric Constants and Loss Tangents of Radome Materials," RL Report 483-25, Jan. 11, 1946.

8c. BIRKS, J. B., "Expanded Dielectrics," TRE Report T.1812, Feb. 27, 1945.

9c. TAYLOR, T. A., and W. JACKSON, "The Electrical Properties of Ice," Ministry of Supply, Advisory Council on Scientific Research and Technical Development, R.D.F., Application Committee, Communications Committee, A.C. 1516, RDF. 110, Com. 78, Dec. 22, 1941.

10c. REDDISH, W., "The Use of a Cylindrical Cavity Resonator for Measurement of Permittivity and Power Factor of Low-Loss Dielectric Materials at 10,000 Mc/sec. (3 cms.)," Ministry of Supply, Advisory Council on Scientific Research and Technical Development, R.D.F., Application Committee, Communications Committee, A.C. 3056, Com. 140, RDF. 162, Nov. 21, 1942.

11c. JACKSON, W., "The Permittivity and Power Factor Values of a Range of Dielectric Materials Measured at Room Temperatures and 3000 Mc/sec. (approx.)," Ministry of Supply, Advisory Council on Scientific Research and Technical Development, Communications Committee, A.C. 3784, Com. 167, Mar. 31, 1943.

12c. HORNER, F., and T. A. TAYLOR, "Measurement at 3200 Mc/sec on a Series of Glasses Supplied by the B.T.H. Co.," Ministry of Supply, Extra-mural Research F 72/74, 287/gen/35 PSR, Electro-Technics Dept., Manchester Univ., Sept. 2, 1943.

13c. JACKSON, W., "The Permittivity and Power Factor Values of a Range of Dielectric Materials Measured at Room Temperature and 3000 Mc/sec (approx.)," Ministry of Supply, Advisory Council on Scientific Research and Technical Development, Communications Committee, Extra-mural Research F 72/74, Apr. 7, 1943.

14c. STRACHEY, C., "Dielectric Constant of Paraffin Wax-Rutile Mixtures," Standard Telephones and Cables Limited, London, England, Valve Laboratory Report No. G. 85, Aug. 1943.

15c. PENROSE, R. P., "Further Measurements on the Permittivity and Power Factor of Low Loss Dielectrics in the K-Band," Admiralty Department of Scientific Research and Experiment, Committee on Valve Development Report CL. Misc. 53; Clarendon Laboratory, Oxford University, July 1945.

16c. SAXTON, J. A., "The Dielectric Properties of Water at Wavelengths from 2 mm. to 10 cm., and over the Temperature Range 0°C. to 40°C.," The National Physical Laboratory, Radio Research Board Report C.115, Mar. 20, 1945.

17c. HUNT, L. E., "Dielectric Constant and Attenuation of Micalex at 3 cm," BTL MM-42-160-125, Oct. 20, 1942.

18c. ROBERTSON, S. D., "Properties of Dielectric Materials at K-Band Frequencies," BTL MM-43-160-131, Aug. 13, 1943.

19c. MEAHL, H. R., and R. F. WOOD, "Power Factors and Dielectric Constant Data at 10 cm and 3 cm Wavelengths," General Engineering Laboratory, GE, Schenectady, Data Folder No. 72335, Oct. 16, 1942.

PART IV

ATTENUATORS AND RADIATION MEASUREMENTS

CHAPTER 11

MICROWAVE ATTENUATORS. CUTOFF ATTENUATORS

By Rudolph N. Griesheimer

Microwave attenuators fall naturally into two groups which differ in the means by which the power is attenuated. The first group utilizes a waveguide operated at a frequency which is below the cutoff frequency characteristic of the size and shape of the waveguide. Electromagnetic fields excited at one end of the waveguide couple weakly to a receiving element at the other end of the waveguide, the amount of coupling depending on the length and size of the waveguide. This technique is particularly suitable for application in the microwave region, although it has been employed at frequencies as low as a few megacycles per second. In the second group of attenuators, power is absorbed in poorly conducting materials and transformed into heat as in a resistor used at low frequencies. In this chapter, cutoff attenuators are discussed. In the following chapter, resistive attenuators that are suitable for microwaves are described. In Chap. 13 the techniques by which attenuation may be measured are presented.

INTRODUCTION

11·1. Definitions of Attenuation.—The concept of attenuation is that of a reduction in the amplitude and a change in the phase of the voltage or current at the load impedance caused by the introduction of some circuit element, the attenuator, between the generator and the load. In most microwave transmission-line problems one is interested only in the amplitude reduction effected by the attenuator and can disregard the accompanying phase shift. On the other hand, when the attenuator causes no amplitude change but only a phase shift, it serves as a dissipationless "line stretcher."

Although the concept of attenuation is direct and elementary, there exists considerable confusion with regard to what constitutes a proper, quantitative definition of attenuation. Various authors have defined such quantities as insertion loss, transmission loss, attenuation, attenuation factor, attenuation constant, complex attenuation constant, transfer constant—all of which are rooted in the fundamental concept of an amplitude reduction and a phase shift of the wave. It is, therefore, necessary to establish the definitions and concepts on which subsequent discussion

within this chapter will be based. Despite the fact that microwave transmission is commonly discussed in terms of distributed-parameter transmission lines, it is sometimes advantageous to revert to concepts familiar in the lower frequency ranges, and to treat a relatively short, high-loss length of microwave transmission line as a dissipative, two-terminal-pair network. The term "attenuator" as used below may be considered to apply equally well to a distributed-parameter line or to a lumped-constant, dissipative, two-terminal-pair network.

The first quantity to be defined is insertion loss. If a generator of arbitrary impedance delivers an amount of power P_1 to a load of arbitrary impedance, and if the power to this same load is reduced from P_1 to P_2 when the attenuator is inserted in the line, the *insertion loss* L in decibels is given by

$$L = 10 \log_{10} \frac{P_1}{P_2}. \tag{1}$$

As so defined, insertion loss is not a quantity exclusively characteristic of the attenuator and will depend on the generator and load impedances. If the generator and load impedances are not equal, the insertion loss of the attenuator will, in general, be different, depending on which terminal-pair of the attenuator is considered as the input pair. If we further specify that the attenuator is to be installed in a transmission line of known, real characteristic impedance, which is terminated at both the generator and load ends in matched impedances, then we have a specific quantity which is characteristic of the attenuator. Insertion loss with these additional specifications will be defined as the attenuation A.

An equivalent way to define attenuation is

$$A = 10 \log_{10} \frac{P_1}{P_2}, \tag{2}$$

where P_1 is the maximum *available* power from the generator, and P_2 is the power delivered to a matched terminal load, with the attenuator inserted. Such a definition does not preclude the possibility of having the matched generator in a line of one characteristic impedance and the matched load in a line of different characteristic impedance. The equation can then specify, for example, the attenuation of a dissipative adaptor from waveguide to coaxial line.

There are several facts implicit in this definition of attenuation which deserve careful comment. It is important to note that a transmission-line element may produce attenuation, yet have no internal dissipation of power. For example, a dissipationless metal obstruction placed in a transmission line will cause a change in the power delivered

from generator to load. If the generator or load is not matched, this change can be such as to either increase or decrease the power to the load so that insertion loss L may be either a positive or negative quantity. However, the attenuation A of the metal obstruction can only be positive since a matched generator delivers maximum power to a matched load. In terms of waves traveling along the transmission line, it can be said that the metal obstruction introduces a reflected wave in the line, thereby reducing the amplitude of the wave which continues in the direction of the load. We shall speak of such attenuation as *reflective attenuation* in contrast to *dissipative attenuation*. Often the attenuator is mismatched

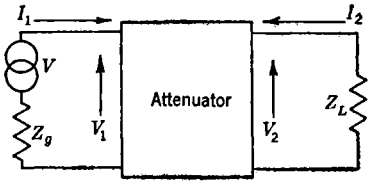

FIG. 11·1.—Four-terminal network.

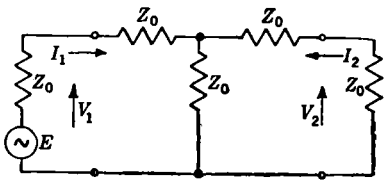

FIG. 11·2.—Example of attenuator network.

to the line, and may have different input impedances at the two pairs of terminals, that is, it is unsymmetrical. In such a case the attenuation it introduces is in part dissipative and in part reflective.

A rather common definition of attenuation is given by the expression

$$A' = 10 \log_{10} \frac{\mathrm{Re}(V_1 I_1^*)}{\mathrm{Re}(V_2 I_2^*)}, \tag{3}$$

where V_1, V_2, I_1, and I_2 are indicated on Fig. 11·1. Attenuation defined in this way is wholly dissipative as contrasted to our chosen definition of A which has both dissipative and reflective components. A simple example will serve to demonstrate this important difference. Consider the network shown in Fig. 11·2. The input impedance at terminal (1) is $2Z_0$, and the input power is $\frac{2}{9} E^2/Z_0$. The output power is $E^2/36Z_0$, and the attenuation given by Eq. (3) is

$$A' = 10 \log_{10} 8 = 9.03 \text{ db.}$$

Using our chosen definition of A, Eq. (2), we have

$$A = 10 \log_{10} 9 = 9.54 \text{ db.}$$

The reflective component of attenuation is therefore $9.54 - 9.03 = 0.51$ db. The reflective component can be calculated alternatively from the voltage standing-wave ratio r in the line connecting the matched generator and the attenuator. Here $r = 2$. The power drawn from the generator will be

$$1 - \left(\frac{r-1}{r+1}\right)^2 = \frac{8}{9}$$

of that which would be delivered to a matched load. The reflective component of attenuation is therefore equal to

$$10 \log_{10} \frac{9}{8} = 0.51 \text{ db.}$$

In a distributed-parameter transmission line there is defined a quantity γ which is called the *propagation constant* or complex attenuation constant of the line. The amplitude of the voltage wave is proportional to $e^{-\gamma z}$, where z is measured along the line and

$$\gamma = \alpha + j\beta, \qquad \beta = \frac{2\pi}{\lambda_g}.$$

The real part α is called the *attenuation constant* of the line and is measured in nepers per unit length of line. The imaginary part β is called the *wavelength constant* and is a measure of the phase shift along the line. It is expressed in radians per unit length of line. The attenuation constant is a measure of the *dissipative* attenuation per unit length of line, and is a quantity which is a function solely of the dissipative line.

The *attenuation constant* is not to be confused with the quantity we have chosen to define as attenuation. Both quantities are commonly used in the province of microwaves, and each has its place of importance. A dissipative line is often used as an attenuator. If α is small, the characteristic impedance of the dissipative line has only a small reactive component. If the resistive component of the characteristic impedance is nearly equal to the characteristic impedance of the line in which it is to be used as an attenuator, the reflective component of attenuation is then small. The attenuation is closely equivalent to the product of the attenuation constant and electrical line length of the attenuator. Cables and other relatively long lines with a low attenuation constant are commonly characterized by a value of the attenuation constant. This is often expressed in decibels per meter.

11·2. General Design Considerations.—One of the important requisites of a good attenuator is that the input impedance at both terminals shall be matched to the characteristic impedance of the transmission line in which it is to be used. It is not possible to match an attenuator perfectly over a band of frequencies, although it is relatively simple to accomplish this at any specific frequency through the use of reactive tuning elements. However, it is not uncommon to require that an attenuator be well matched over a band of frequencies, for example, that it have a voltage standing-wave ratio of less than 1.20. For the purposes of this chapter we shall speak either of a perfectly matched attenuator, that is, VSWR equal to unity within the limits of experimental error, or of an attenuator which is matched to a VSWR of 1.10, or less, over the band in question.

Our definitions of insertion loss and attenuation have shown that regardless of which quantity we consider, the measured magnitude of the quantity will be influenced by the extent to which the attenuator has been matched to the transmission line. If, in calibrating an attenuator, one is very careful to match the generator and load to the transmission line, the attenuation can be measured with good accuracy. However, when the carefully calibrated attenuator is placed in the transmission line in which it is to be used, it is often difficult to provide an equally well-matched generator and load, partcularly over a broad band. It therefore follows that calibration of the attenuator is no longer meaningful since the reduction in power received by the load is directly related to the insertion loss of the attenuator, and not to the quantity we have defined and measured as its attenuation. One calibrates the attenuator in terms of attenuation, and attempts when using it to meet the conditions of matched generator and matched load as closely as possible. Recognizing that one cannot meet these conditions exactly, the next best procedure is to minimize the mismatch contributed by the attenuator itself. The better matched the attenuator, the less error can result from failure to match the generator and load perfectly. Also, this error will be less sensitive to small variations (with frequency, for example) of the generator and load impedances. Therein lies the importance of impedance matching of the attenuator.

In a majority of cases the attenuator is used over a band of frequencies, and one must inquire into the frequency sensitivity of both its impedance match and its attenuation. When the utmost in accuracy is required, it is necessary to prepare a calibration curve showing the variation of attenuation with frequency. However, one is usually asked to design an attenuator which has an attenuation of X db, constant to $\pm Y$ db over the band. In general, the quantity Y has three components: (1) the inherent calibration error, (2) the frequency sensitivity of attenuation, and (3) the error that can arise from having a mismatched generator and mismatched load in the line in which the attenuator is to be used. In evaluating this third error, one usually calculates the greatest possible error from the known characteristics of the attenuator and an assumed set of maximum values for the voltage standing-wave ratios of generator and load. It is obvious that for a given allowable value of Y, the attenuator with greater frequency sensitivity of attenuation must be better matched. The problem of designing an attenuator with very small frequency sensitivity of attenuation is considerably more difficult (particularly for variable, resistive attenuators) than that of designing an attenuator matched over a broad band. The latter problem becomes serious only when dimensional limitations of the sort that preclude the use of long matching tapers are imposed.

Another factor of importance in the design of many attenuators is the maximum power capacity. Excessively high power levels can burn out an attenuator, or can change its calibration temporarily, or permanently. It is important to note that burnout may result either from arcing, when operating under pulsed-power conditions, or from the high temperatures associated with large average power. Consequently, it is essential in many cases to determine maximum values for both pulse and average power. Partial or complete burnout may lead to either increased or decreased attenuation. For example, a coaxial-line attenuator with a resistive center conductor will show increased attenuation for partial burnout, and nearly infinite attenuation for complete burnout. In contrast, a waveguide attenuator which uses a resistive film lying parallel to the narrow side of the guide will show decreased attenuation with partial burnout, and almost no attenuation with complete burnout. Some types of attenuators, particularly the resistive-film types, will change calibration with power level or temperature. Films with low temperature coefficients of resistance are chosen to circumvent this difficulty.

A practical consideration of occasional importance is the matter of deciding whether to use a single attenuator, or two in cascade. If the total attenuation required is as large as 70 or 80 db, it may be desirable to use a pair of attenuators. The sum of the calibration errors for two 40-db attenuators may easily be less than the calibration error associated with a single 80-db attenuator. Further, it is sometimes possible to use two cascaded attenuators of opposite frequency sensitivity so that the resultant combination is more accurate over a wide band than is a single attenuator.

Unfortunately, if there is a stringent restriction on the length of the attenuating element, the design problem, particularly for resistive-film attenuators, may become very difficult. Short lengths of film will necessarily have a high resistivity, and consequently a low power capacity. Further, so long as the r-f skin depth exceeds the film thickness, it is usually true that greater frequency sensitivity of attenuation and poorer matching result from decreasing the length of the attenuating element. The reasons for this will be made apparent in the subsequent discussion of specific attenuator designs.

In the design of a variable attenuator there are additional considerations of importance. For example, the shape of the calibration curve (db vs. displacement) is very often of interest. In a majority of problems one is asked to provide an attenuator with an approximately linear calibration curve. In some instances it has been possible to meet this requirement by a proper choice of the shape and resistivity gradients of the attenuating element; more frequently, it is accomplished by mechani-

cal means such as proper shaping of the cam which drives the movable element. If one is interested in greater accuracy at small attenuation levels, the calibration curve should have a slope which increases with the attenuation level. On the other hand, the calibration curve for attenuators used in microwave impedance bridges (see Chap. 9) should have a slope which decreases with increasing attenuation. The design of the drive mechanism for a variable attenuator is an important factor, and it is usually necessary to take great precautions against backlash, mechanical play, wear on moving parts, and r-f leakage.

CUTOFF ATTENUATORS

11·3. Principles of Cutoff Attenuators.—One of the most common types of microwave attenuator is that which utilizes a waveguide beyond cutoff. It is well known that, for a given frequency of oscillation, one can reduce the dimensions of either circular or rectangular waveguide to a point where energy of this frequency can no longer be propagated in the waveguide. Below the cutoff frequency, the fields decay exponentially along the waveguide, and the phase is changed a negligible amount by losses in the walls. It is possible to excite fields in a waveguide beyond cutoff in several ways, and to couple selectively to a mode of transmission whose attenuating characteristics can be calculated. For example, a simple means of constructing a cutoff attenuator is to terminate the inner conductor of a coaxial line by folding it back in a loop to the outer conductor. The outer conductor is continued as a length of waveguide beyond cutoff, and the receiving element consists of a similar loop-terminated coaxial line which slides in the cutoff tube. This construction is shown in Fig. 11·3. Circular waveguide is commonly used because simple mechanical arrangements can be provided to adjust the separation of the coupling elements.

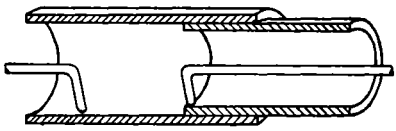

FIG. 11·3.—Simplest cutoff attenuator: *TE*-mode.

A cutoff attenuator may be designed for either a *TM*- or a *TE*-mode of transmission. In the *TM*-mode designs the coaxial lines are usually terminated in circular metal disks, the coupling between the two disks being capacitive. In *TE*-mode designs the coaxial lines are usually terminated by metal loops, and the coupling is inductive.

In circular waveguide the cutoff wavelength (the free-space wavelength corresponding to the cutoff frequency) is given by

$$\lambda_c = \frac{2\pi r \sqrt{k_e}}{s_{mn}}, \tag{4}$$

where r is the inside radius of the circular waveguide, s_{mn} is a dimensionless quantity characteristic of the specific mode (see Table 11·1), and k_e is the relative dielectric constant of the medium filling the waveguide. ($k_e = 1$ for free space.)

TABLE 11·1.—VALUES OF THE CUTOFF PARAMETER, s_{mn}, IN EQ. (4)

TM_{mn}-modes			
$s_{01} = 2.405$	$s_{02} = 5.520$	$s_{03} = 8.654$	$s_{04} = 11.79$
$s_{11} = 3.832$	$s_{12} = 7.016$	$s_{13} = 10.17$	$s_{14} = 13.32$
$s_{21} = 5.136$	$s_{22} = 8.42$	$s_{23} = 11.62$	$s_{24} = 14.80$
$s_{31} = 6.38$	$s_{32} = 9.76$	$s_{33} = 13.02$	$s_{34} = 16.22$
TE_{mn}-modes			
$s_{01} = 3.832$	$s_{02} = 7.016$	$s_{03} = 10.17$	
$s_{11} = 1.841$	$s_{12} = 5.33$	$s_{13} = 8.54$	
$s_{21} = 3.05$	$s_{22} = 6.71$	$s_{23} = 9.97$	
$s_{31} = 4.20$	$s_{32} = 8.02$	$s_{33} = 11.35$	

In rectangular waveguide the cutoff wavelength for either the TE_{mn}- or TM_{mn}-modes is given by

$$\lambda_c = \frac{2\sqrt{k_e}}{\sqrt{\left(\frac{m}{a}\right)^2 + \left(\frac{n}{b}\right)^2}}, \tag{5}$$

where a and b are, respectively, the wide and narrow inside dimensions of the waveguide. In the TE-mode series, m and n have integral values and either m or n may be zero. In the TM-mode series m and n have integral values equal to or greater than unity.[1]

When the frequency is varied from a value greater than the cutoff frequency to one less than the cutoff frequency, there is a continuous transition through the cutoff point from a slightly attenuated sinusoidal field to a highly attenuated exponential field. Expressions for the attenuation of either the traveling wave or the highly attenuated field are simple. The expression for the attenuation in the case in which λ is very slightly greater than λ_c is rather complicated, and is seldom used. For $\lambda/\lambda_c \geqq 1.05$, however, it is sufficiently accurate to write the following expression for the attenuation constant α

$$\alpha = \frac{2\pi}{\lambda_c}\sqrt{1 - \left(\frac{\lambda_c}{\lambda}\right)^2} \quad \text{nepers per unit length.} \tag{6}$$

This equation is valid for TE- or TM-modes, and for circular or rec-

[1] In this numbering system the TE_{10}-mode is the dominant mode in rectangular waveguide.

tangular waveguide, if the proper value of λ_c is used. Moreover, the value of α is independent of the material from which the waveguide is made if the material has a high conductivity.

It is interesting to note from Eq. (6) that α increases rapidly with λ for small values of λ/λ_c, but increases slowly with λ as λ/λ_c becomes large. In order to reduce the frequency dependence of α, it is customary to select a tube diameter such that λ/λ_c is large over the range of wavelengths in which the attenuator is to be used. For example, if the attenuator is to be used over a range of wavelengths from λ_1 to $1.5\lambda_1$, and if it is desired that α be constant to within one per cent over this wavelength range, then the tube diameter must be chosen so that

$$\lambda_c \leqq 0.19\lambda_1.$$

It is important to recognize that the dimensions of the waveguide must be known precisely if α is to be known with the accuracy customarily required. For example, for circular waveguide,

$$\frac{d\alpha}{\alpha} = -\left[\frac{1}{1-\left(\frac{\lambda_c}{\lambda}\right)^2}\right]\frac{dr}{r}.$$

Or, for $\lambda_c \ll \lambda$

$$\frac{d\alpha}{\alpha} = -\frac{dr}{r}.$$

Consequently, electroformed or carefully broached tubing is commonly used for these attenuators in order to avoid variations in α that may be caused by dimensional variations along the length of the tube.

11·4. Purity of Useful Mode.—The two major problems in the design of a cutoff attenuator are r-f impedance-matching of the antenna elements and mode purity. The importance of impedance-matching in any type of attenuator has been discussed in Sec. 11·2. The problem of mode purity, however, is peculiar to the cutoff attenuator.

One of the most attractive features of the cutoff attenuator is the fact that its attenuation constant can be predicted exactly by theory, and with certain limitations the attenuator may, therefore, be considered a primary standard. If only one mode exists in the cutoff tube, the attenuation constant is given exactly by Eq. (6), and is independent of the total attenuation. However, if more than one mode is excited in the cutoff tube, Eq. (6) is no longer sufficient to specify the attenuation constant. In this case α will vary with x, the separation of the antenna elements, and will approach a constant value only at large values of x. The variation of α with x is determined by the relative amplitudes and phases of the specific modes excited in the cutoff tube. Since the various modes have different values for α, their relative intensities vary with x.

As x increases, one mode after another decays into insignificance, until α becomes essentially independent of x when only the single mode with the smallest value of s_{mn} remains.

In most applications of cutoff attenuators it is desired to effect a known change in attenuation. Seldom is it necessary to know accurately the total attenuation introduced by the device. Consequently, greatest accuracy results from using the attenuator in the linear region—at large values of x where α is independent of x. Although it may not be necessary to know accurately the total attenuation under such circumstances, it is often desirable to keep it reasonably small. In order to obtain linearity in the calibration without having to accept objectionably large values of total attenuation, it is necessary to design at least one of the antennas so that it excites a single mode, the mode with the smallest value of s_{mn}.

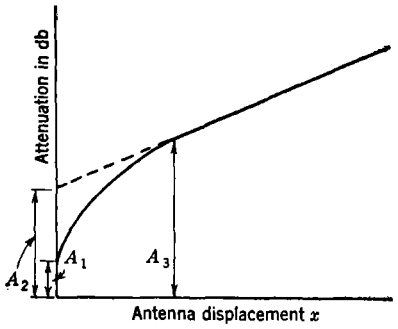

FIG. 11·4.—Representative calibration curve for a cutoff attenuator.

In Fig. 11·4 three quantities are indicated which are commonly used to characterize a cutoff attenuator.

The quantity A_1 represents the minimum attenuation that is available from the cutoff attenuator. The attenuation is minimized by bringing the antenna elements into contact, but, in general, cannot be made zero. Discontinuities in the transmission line at the antennas account for some reflective attenuation, and the impedance-matching devices commonly incorporated in a cutoff attenuator add a dissipative component to A_1.

A_2 is the attenuation value determined by extrapolating the linear part of the calibration curve to the x axis. The total attenuation at large values of x may be calculated from the simple linear equation

$$A = A_2 + \alpha x,$$

where α is the slope of the linear region of the curve.

A_3 is the smallest value of attenuation where the calibration curve is linear. Unfortunately, this definition is not specific, and there is lack of agreement with regard to how it should be further qualified. One may say either that the slope of the curve at this point is within a given percentage (for example, 1 per cent) of that of the linear portion of the curve, or that the attenuation at this point is within a given fraction of a decibel (for example, 0.5 db) of that associated with the extrapolated linear region of the curve. Any reference to A_3 in the following material

will be specifically qualified to avoid confusion. For most applications of cutoff attenuators it is important to have A_3 as small as possible. To meet this condition it is necessary to strive for high mode purity, and to design the impedance-matching networks in such a manner that satisfactorily low reflection can be obtained with networks having relatively small attenuation.

11·5. Separation of Undesirable Modes.—As previously mentioned, the nonlinearity of the calibration curve of a cutoff attenuator in the region of relatively close coupling between the antennas is largely a result of multimode coupling between the two antennas. Both antennas must be capable of exciting (or coupling to) more than a single mode in order for this nonlinearity to occur. Much of interest can be learned about cutoff attenuators by examining the mechanism of this multimode coupling.

Consider, for example, the case of a loop-coupled TE_{11}-mode attenuator. This mode is commonly used in cutoff-attenuator design because it has the smallest attenuation constant of all modes. The modes with larger α or s_{mn} values decay more rapidly, and the calibration curve for the attenuator must necessarily approach linearity at large values of loop displacement. By reference to Table 11·1 we note that the TM_{01}-mode is likely to be the most troublesome mode from a point of view of linearity since its s_{mn} value is closest to that of the TE_{11}-mode. Experience substantiates this prediction, particularly if the metal coupling-loop wires have diameters that are large enough for ruggedness. Referring now to Fig. 11·4, let us arbitrarily divide the curve into three regions: (1) the linear region where only the TE_{11}-mode exists, (2) an intermediate region where the curvature results from a combination of TE_{11}- and TM_{01}-modes, and (3) the region near $x = 0$ where the curvature is influenced by many modes and by other factors not yet mentioned. Let us concentrate on the intermediate region where only two modes need be considered. The TM_{01}-mode has a field intensity which is independent of the angle of rotation θ between the two loops; the intensity of the TE_{11}-mode (see Fig. 11·5) varies with $\cos\theta$, however, if both loops are grounded on the same generator of the cylinder where $\theta = 0$.

Let V_1 and V_2 represent, respectively, the voltages induced in the receiving loop by the TE_{11}- and TM_{01}-modes; then

$$V_1 = B_1 e^{-\alpha_1 x} \cos\theta, \tag{7}$$

$$V_2 = B_2 e^{-\alpha_2 x}, \tag{8}$$

where α_1 and α_2 are the corresponding attenuation constants.

In combining the vectors V_1 and V_2 it is necessary to take into consideration the fact that, in general, the two modes are separated in time phase by an angle ψ. Therefore, the resultant vector voltage V induced

in the receiving loop is given by

$$V^2 = V_1^2 + V_2^2 + 2V_1V_2 \cos \psi,$$

or

$$V^2 = (B_1e^{-\alpha_1 x})^2(1 + r^2e^{-2\rho x} + 2re^{-\rho x} \cos \theta \cos \psi - \sin^2 \theta), \qquad (9)$$

where

$$\rho = \alpha_2 - \alpha_1,$$

and

$$r = B_2/B_1.$$

If V_0^2 is defined as the value of V^2 for $x = 0$ and $\cos \theta = 1$, and if the attenuation in decibels is arbitrarily taken as zero for this case, then it

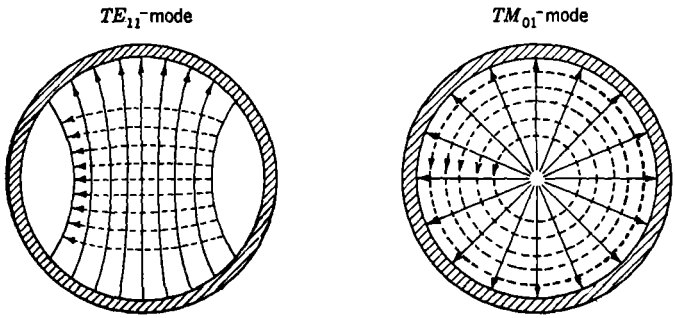

FIG. 11·5.—Field configurations of the TE_{11}- and TM_{01}-modes in circular waveguide.

follows from Eq. (9) that

$$A = 8.686\alpha_1 x + 10 \log_{10}\left(\frac{1 + r^2 + 2r \cos \psi}{1 + r^2e^{-2\rho x} + 2re^{-\rho x} \cos \theta \cos \psi - \sin^2 \theta}\right). \qquad (10)$$

Equation (10) is the general equation for the attenuation of the cutoff attenuator, except for an additive constant, resulting from a combination of the two modes. The equation includes the effects of both linear and angular displacement of the loops. The first term of Eq. (10) is the attenuation resulting from the desired TE_{11}-mode, and the second term is of the nature of a correction term which arises because of the existence of the TM_{01}-mode. Implicit in Eq. (10) are the assumptions that (1) the cutoff tube has a circular cross section with no elliptical eccentricity, (2) the plane of each of the two loops includes the center line of the cutoff tube, and (3) the transfer impedance effects, to be discussed later, are negligible.

For further considerations it is convenient to rewrite Eq. (10) for the special case, $x = 0$. The angular dependency of attenuation is thus

$$A = 10 \log_{10} \frac{1 + r^2 + 2r \cos \psi}{1 + r^2 + 2r \cos \theta \cos \psi - \sin^2 \theta}. \qquad (11)$$

Values for r and $\cos \psi$ may be calculated from measurements of A as a function of θ, taken at the arbitrarily chosen, $x = 0$ plane. As one loop is rotated with respect to the other, the power coupled from one loop to the other varies. It will have a maximum value at $\theta = 0$, by previous definition. As θ is increased, the power transferred will decrease, pass through a minimum, and will then increase again to a second maximum at $\theta = 180°$. This second maximum will be smaller than the first since in this case the electric-field vectors of the two modes oppose each other, whereas they reinforce each other in the case of larger maximum at $\theta = 0$. By differentiating the right-hand side of Eq. (11) with respect to θ and equating to zero, one obtains the condition that

$$\sin \theta \, (\cos \theta + r \cos \psi) = 0. \tag{12}$$

The maxima in power transfer occur for $\sin \theta = 0$, or $\theta = 0$ and $180°$, respectively. The minimum power transfer exists when

$$\cos \theta_m = -r \cos \psi. \tag{13}$$

Therefore, if we define A_{sm} as the attenuation when $\theta = 180°$, A_{mi} as the attenuation when $\theta = \theta_m$, we may rewrite Eq. (11) in the forms

$$A_{sm} = 10 \log_{10} \frac{1 + r^2 + 2r \cos \psi}{1 + r^2 - 2r \cos \psi}, \tag{14}$$

$$A_{mi} = 10 \log_{10} \frac{1 + r^2 + 2r \cos \psi}{1 + r^2 + 2r \cos \psi \cos \theta_m - \sin^2 \theta_m}. \tag{15}$$

Equations (13), (14), and (15) may be solved simultaneously to determine r, ψ and θ_m in terms of A_{sm} and A_{mi}. Thus

$$r = \left(\frac{1 - J}{1 + J}\right) \sqrt{1 + \frac{4g^2}{1 - t^2}\left(\frac{1 + J}{1 - J}\right)}, \tag{16}$$

$$\tan \psi = \pm \sqrt{\frac{4g^2}{1 - t^2}\left(\frac{1 + J}{1 - J}\right)}, \tag{17}$$

$$\cos \theta_m = \mp \left(\frac{1 - J}{1 + J}\right), \tag{18}$$

where

$$J \equiv \sqrt{\frac{t^2 - g^2}{1 - g^2}},$$

$$A_{mi} \equiv 20 \log_{10}\left(\frac{1}{g}\right), \tag{19}$$

$$A_{sm} \equiv 20 \log_{10}\left(\frac{1}{t}\right).$$

The calculation of θ_m from Eq. (18) may be checked by an experimental measurement of θ_m, provided that the assumed conditions are satisfied. An indication of the presence of other modes is asymmetry

of the angle calibration curve. For example, if the two minima (one between 0 and π and the other between π and 2π) are not symmetrically located or differ in the value of A_{mi}, at least one other mode is present. The choice of sign in Eq. (18) is dictated by whether the experimentally determined θ_m is in the first or second quadrant. The choice of sign in Eq. (17) is dictated by the fact that ψ is a second-quadrant angle if θ_m is in the first quadrant, and vice versa. This is apparent from Eq. (13).

If r and ψ have been found, Eq. (10) can be used to predict the attenuation as a function of θ and x. In particular, the value of x and the attenuation corresponding to the point A_3 of Fig. 11·4 may be determined. If we let Y equal the logarithmic correction term of Eq. (10), then the slope of the calibration curve is

$$\frac{\partial A}{\partial x} = 8.686\alpha_1 + \frac{\partial Y}{\partial x}. \tag{20}$$

By setting the ratio of $\partial A/\partial x$ to $8.686\alpha_1$ equal to 1.01, for example, one can determine the value of x at which the slope is within 1 per cent of the pure TE_{11}-mode slope; or one may calculate the value of x at which the attenuation is 0.5 db lower than that of the extrapolated linear portion of the curve. It will be remembered that these are the two alternatives for specifying the quantity A_3.

Several other bits of useful information may be extracted from the above equations. For example, referring to Eq. (20), the slope correction term $\partial Y/\partial x$ should be made as small as possible for best linearity. By differentiation,

$$\frac{\partial Y}{\partial x} = 8.686\rho r e^{-\rho x}\left(\frac{re^{-\rho x} + \cos\theta\cos\psi}{r^2e^{-2\rho x} + 2re^{-\rho x}\cos\theta\cos\psi + \cos^2\theta}\right). \tag{21}$$

For $\cos\psi = 0$ or unity, the value of $\partial Y/\partial x$ is minimized with respect to variations in θ by setting $\cos\theta =$ unity. Moreover, this condition on $\cos\theta$ holds, regardless of the value of x. To obtain the smallest possible A_3 value, the attenuator should be operated with the loops adjusted to meet the $\theta = 0$ condition.

If the cross section of the cutoff tube is not accurately circular, it is possible to get into peculiar difficulties. For example, in a slightly elliptical tube it is possible for the TE_{11}-mode to be excited as two modes, polarized at right angles with respect to each other. Since they have the same attenuation constant, the variation with x is not affected, but the variation with θ suffers a marked change. It is essential to guard against any twist along the length of a slightly elliptical tube. Such a twist rotates the plane of polarization of all modes that do not have circular symmetry, and this affects the coupling to these modes. Thus

it is possible to have a cutoff tube in which only the TE_{11}-mode exists, but which nevertheless has a nonlinear calibration curve because of the fact that the coupling to the mode varies with the twist angle of the tube. It is apparent that twist can be even more harmful in distorting the calibration curve if more than one mode is being coupled.

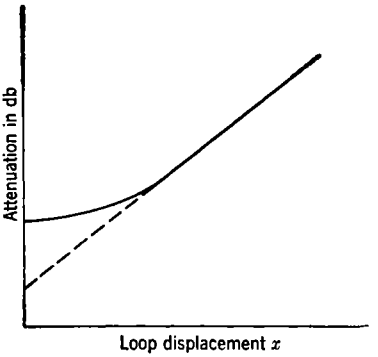

FIG. 11·6.—Calibration curve of a cutoff attenuator with TE_{11}- and TM_{01}-modes in opposite time phase.

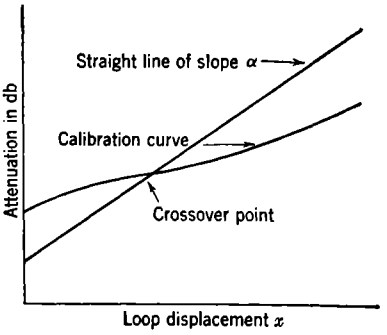

FIG. 11·7.—Calibration curve illustrating the crossover phenomenon.

The correction term Y may be either positive or negative; if it is positive, the general shape of the calibration curve is that shown in Fig. 11·4; if it is negative, the calibration curve approaches linearity by a decreasing slope, rather than by an increasing slope as in Fig. 11·6. The sign of the correction term Y changes from plus to minus for a value of ψ somewhat greater than 90°. If $\theta = 0$, then the sign of Y depends on whether the argument of the logarithm is greater or less than unity. Therefore, if $Y = 0$,

$$1 + r^2 + 2r \cos \psi = 1 + r^2 e^{-2\rho x} + 2re^{-\rho x} \cos \psi.,$$

and

$$\cos \psi = -\tfrac{1}{2}r(1 + e^{-\rho x}). \tag{22}$$

This equation states that it is possible to have $Y = 0$ at $x = 0$, an important observation. In other words, it permits the calibration curve to have a "crossover point" of the kind shown in Fig. 11·7.

The parenthetical quantity in Eq. (22) varies from 2 to 1 as x varies from 0 to ∞. Therefore, the crossover point occurs when $\cos \psi$ lies within the range between $-r/2$ and $-r$. As the value of $\cos \psi$ varies from $-r/2$ to $-r$, the crossover point moves out along the straight line toward infinity. Crossover from the opposite direction (that is, the mirror image of the calibration curve shown) is not possible if r is less than unity.

11·6. Principle of Mode Filtering.—A potentially powerful tool in the design of cutoff attenuators, and one which unfortunately has not been

utilized as often as it might have been, is the principle of mode filtering. One may select a waveguide such that, at the frequency of interest, propagation is possible only in the lowest, or dominant, mode. Modes of higher order will be beyond cutoff and will therefore be attenuated. A sufficient length of such a line can be used as an effective mode filter, maintaining unattenuated propagation of the fundamental mode while the higher modes decay into insignificance. After passing through the filter, the fundamental mode is used to excite a length of waveguide which is beyond cutoff for this mode. It is essential, of course, to design the junction between the filter and cutoff sections so that higher modes are not excited again. The principle is quite simple, but there are practical problems involved which are not always simple.

If the cutoff region for the dominant mode is to be in circular waveguide, the filter section is customarily designed for circular waveguide; similarly, rectangular filter sections are used with rectangular waveguides beyond cutoff. Consider, for example, the design of a circular-waveguide filter section for operation at a wavelength of 9.5 cm. From Eq. (4), it can be calculated that an air-filled tube of 2.93 cm radius will propagate the fundamental TE_{11}-mode at wavelengths of 10.0 cm or less and will propagate the next higher mode, the TM_{01}, at wavelengths of 7.6 cm or less. This tube radius would therefore be an acceptable one for use at 9.5 cm. There is no danger of cutoff attenuation in the fundamental mode, and the mode of the next higher order is sufficiently far beyond cutoff so that its attenuation constant is not too frequency-sensitive at this wavelength. The length of filter section used would depend on the time phases and intensities of the higher modes relative to those of the fundamental mode at the input end of the filter section. A waveguide diameter of 5.86 cm is apt to be objectionably large for some applications, so that it is desirable to fill the waveguide with a dissipationless material of relatively high permittivity. The reduction in tube radius, according to Eq. (4), is governed by the relation

$$a\sqrt{k_e} = \text{constant}.$$

Since it is possible to obtain a usable, easily machined TiO_2-impregnated polystyrene for which $k_e = 10$, the use of this dielectric permits reduction in radius of the tube by a factor of three or more.

The use of a dielectric-filled waveguide for the filtering section affords another advantage over an air-filled filter section. In using a filter with no dielectric, it is necessary to constrict the waveguide section following the filter in order to bring the fundamental mode beyond cutoff. This constriction might, for example, take the form of an abrupt decrease in the diameter of a circular waveguide, or an abrupt decrease in both the a and b dimensions of a rectangular waveguide.

Such a discontinuity in the waveguide will excite higher modes in the cutoff section, and much if not all of the usefulness of the mode filter will be lost. However, if a dielectric of high permittivity is used in the mode filter, there need be no discontinuity between the filter and cutoff sections aside from the simple dielectric-air interface which lies normal to the axis of the waveguide. The field boundary conditions at such an interface guarantee that if only the fundamental mode exists in the dielectric, adjacent to the interface, then only the fundamental mode can exist in the air region beyond. It is advantageous to use a material with a large dielectric constant in the filter section. In this case the fundamental mode will be far beyond cutoff in the air-filled cutoff section, and the attenuation constant for the mode will be relatively insensitive to frequency.

The use of a mode filter restricts the wavelength range in which the cutoff attenuator may be used. This range can at the most be the difference between the cutoff wavelengths for the fundamental and next higher mode. In practice it is necessary to sacrifice part of this range. For example, since there are small variations in the permittivity of the dielectric from one attenuator to the next, it is unwise to operate at wavelengths close to the cutoff wavelength of the fundamental mode. In working very close to the short-wavelength limit of the allowable range, variations in permittivity may allow the next higher mode to be propagated together with the fundamental. Also, the attenuation of this second mode will be slight in this wavelength region, and the filter section to be effective must be made objectionably long. It should be noted that the use of a dielectric-filled line in place of an air-filled line does not change the wavelength spread between the fundamental and next higher mode, provided that both arrangements have the same cutoff wavelength for the dominant mode.

Rectangular waveguide has an advantage over circular waveguide for mode filtering because the cutoff wavelengths (and cutoff attenuation constants) for the various modes are more widely separated when rectangular waveguide is used. Consequently, the rectangular mode-filtered cutoff attenuator is operable over a much broader wavelength range than is the circular mode-filtered attenuator. Reference to Table 11·2 should clarify this point. The data apply strictly for $\lambda \ll \lambda_c$, but are indicative of the situation when λ approaches λ_c closely.

In studying Table 11·2 note particularly the additional advantage gained from using a very flat waveguide. In such waveguide only the series of TE_{m0}-modes is of importance; all other modes have relatively large attenuation constants. However, regardless of the value of a/b, a considerably greater usable wavelength range is obtained with rectangular waveguide than with circular.

Because of the larger mode separation in rectangular waveguide, the input impedance for the filter section is less frequency-dependent and hence more susceptible to matching over a broad band. The higher modes that are attenuated in the filter section store power that is reflected back into the transmission line toward the generator. By no means all of the power associated with the main mode is coupled through the attenuator, and much of the total power reflection is from this mode. In the rectangular waveguide the phase shift in the dominant mode and the attenuation constants of the higher modes are less frequency-sensitive than in circular waveguide, and consequently the input impedance is less frequency-sensitive.

TABLE 11·2.—SPREAD IN CUTOFF WAVELENGTHS AND RATIO OF ATTENUATION CONSTANTS FOR VARIOUS WAVEGUIDE MODES

Circular Waveguide

Parameter (see notes)	TE_{11}	TE_{01}	TE_{21}	TM_{11}, TE_{01}	TE_{31}
X	....	0.23	0.40	0.52	0.56
Y	1.00	1.31	1.66	2.08	2.28

Rectangular Waveguide

Parameter (see notes)	TE_{10}	TE_{20}	$TE_{18,0}$	TE_{01}	TE_{11}, TM_{11}	TE_{21}, TM_{21}	TE_{02}	TE_{12}, TM_{12}
$\frac{a}{b} = \frac{9}{4}$								
X	....	0.50	0.94	0.56	0.59	0.67	0.78	0.78
Y	1.00	2.00	18.0	2.25	2.46	3.01	4.50	4.61
$\frac{a}{b} = \frac{9}{1}$								
X	....	0.50	0.94	0.89	0.89	0.89	0.94	0.94
Y	1.00	2.00	18.0	9.00	9.05	9.22	18.0	18.0

X represents the expression $\left[\frac{(\lambda_c)_f - (\lambda_c)_q}{(\lambda_c)_f}\right]$.

Y represents the expression $\left(\frac{\alpha_q}{\alpha_f}\right)$.

$(\lambda_c)_f$ is the cutoff wavelength for the fundamental mode.
$(\lambda_c)_q$ is the cutoff wavelength for the specific, tabulated mode.
α_f is the attenuation constant for the fundamental mode.
α_q is the attenuation constant for the specific, tabulated mode.

11·7. Variation of Input Impedance with Close Coupling.—Multimode coupling is not the only cause of nonlinearity in the calibration curve of a cutoff attenuator. A second source of nonlinearity is the variation in the input impedance of the attenuator, for a given load impedance, with a displacement of the coupling elements. For large separations of the

coupling elements the input impedance is wholly reactive, whereas for tight coupling the input impedance approaches the load impedance. The change in input impedance with antenna displacement is rapid for small separations, and very slight at large separations. This change in input impedance affects the power drawn from the generator, and consequently has an influence on the shape of the calibration curve. In many cutoff-attenuator designs the multimode coupling extends over such a large range of attenuation that the coupled-impedance effect is almost completely masked and can be ignored. However, in one or two of the specific designs to be discussed the mode purity is so good that impedance coupling becomes the limiting factor on linearity at the lower end of the calibration curve. Impedance coupling is also an

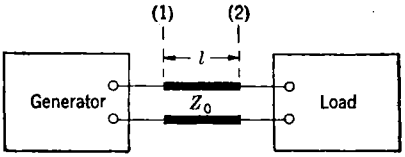

FIG. 11·8.—Diagrammatic representation of a transmission line.

important consideration in calculating the impedance-matching networks that are frequently built into cutoff attenuators.

The input impedance can easily be calculated as a function of the load impedance and the cutoff attenuation, either by formula or by reference to impedance-circle diagrams. In fact, the procedures are analogous to those used for a propagating waveguide. In the case of a propagating waveguide the magnitude of the voltage reflection coefficient Γ is not changed as the plane of reference is moved along the waveguide, but the phase angle of Γ varies twice as fast as the angle $2\pi l/\lambda_g$ through which the reference plane is moved. In contrast, the phase angle of Γ does not change with l in cutoff waveguides, but the magnitude of Γ does change with l.

In any transmission line, represented diagrammatically in Fig. 11·8, we can apply two fundamental formulas

$$\Gamma_1 = \Gamma_2 e^{-2\gamma l},$$
$$\Gamma = \frac{Z - Z_0}{Z + Z_0}.$$

For propagating waveguides, where the magnitude of Γ does not change with l,

$$\gamma = j\beta = j\frac{2\pi}{\lambda_g},$$
$$\Gamma_1 = \Gamma_2 e^{-2j\beta l}.$$

The characteristic impedance of the line is real, and we may write

$$Z_0 = R_0.$$

The transformation along the line may be represented graphically by the impedance-circle diagrams of Fig. 11·9. Here lines of constant $|\Gamma|$ are shown as solid lines, while lines of constant phase are dotted. To transform an impedance along the transmission line, moving θ degrees toward the generator, one moves 2θ degrees in a clockwise direction across the dashed constant-angle lines. Limiting the impedance to the right half of the Z-plane restricts the reflection coefficient to within the unit circle on the Γ-plane.

In the case of cutoff waveguides $\gamma = \alpha$ and Z_0 is pure imaginary. Let us write

$$Z_0 = jX_0,$$
$$\Gamma_1 = \Gamma_2 e^{-2\alpha l}.$$

The impedance diagrams for this case are shown in Fig. 11·9. Here also lines of constant Γ are solid, and the phase lines dotted. The characteristic impedances of the lines, whether or not they are operated at frequencies below cutoff, may be taken as proportional to the wave impedances in the line. For TE-modes the wave impedance is

$$Z_0 = \frac{j\omega\mu}{\gamma}.$$

If γ is imaginary, and we have propagation,

$$Z_0 = R_0 = \frac{\lambda_g}{\lambda}\sqrt{\frac{\mu}{\epsilon}}.$$

If γ is real,

$$Z_0 = jX_0 = j\frac{\omega\mu}{\alpha}.$$

For TM-modes, the wave impedance is $\gamma/j\omega\epsilon$, and

$$R_0 = \frac{\lambda}{\lambda_g}\sqrt{\frac{\mu}{\epsilon}},$$
$$X_0 = -\frac{\alpha}{\omega\epsilon}.$$

For cutoff waveguides having TM-modes, X_0 is negative, and the equation of transformation from the Z- to the Γ-plane becomes

$$\Gamma = \frac{Z + j|X_0|}{Z - j|X_0|}.$$

This corresponds to a geometrical reflection on the resistance axis of the

diagram in the impedance plane so that going toward the generator now corresponds to a clockwise rotation on the diagram. The diagrams can also be used for admittances. In this case there is a geometrical

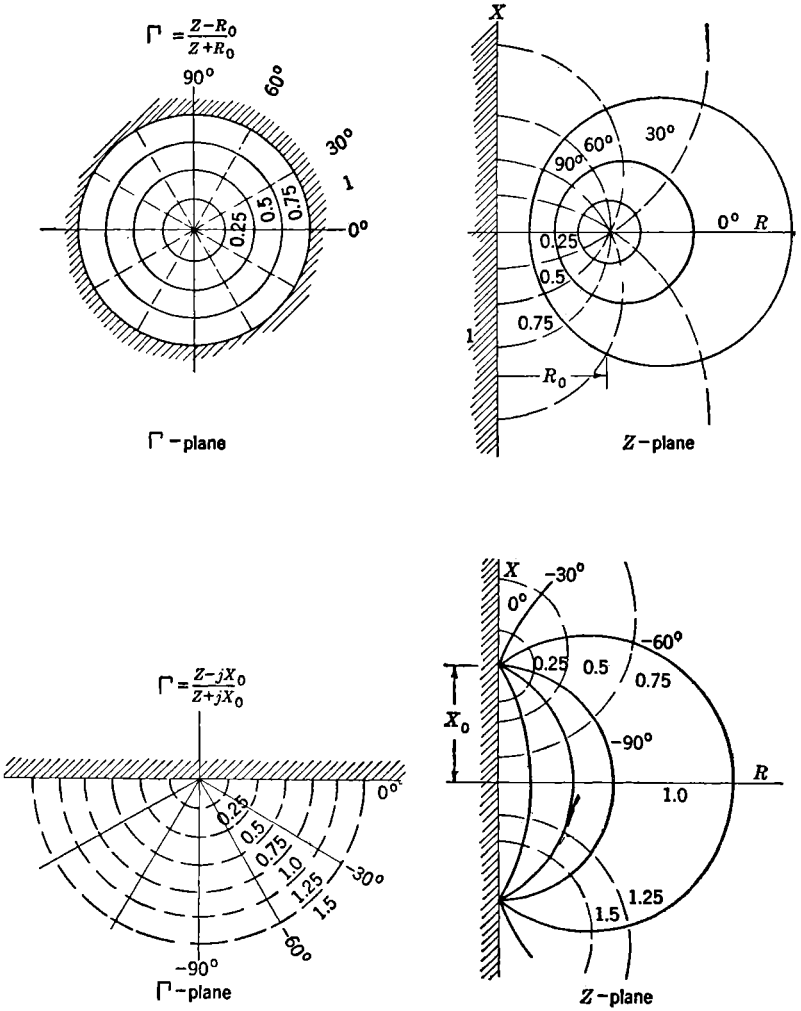

FIG. 11·9.—Γ- and Z-planes for a TE-mode beyond cutoff.

reflection on the resistance axis, and the angles are changed to their negative complements.

These calculations are applicable only for single-mode excitation

in the cutoff waveguide. In the event of multimode coupling, the situation is much more complicated, and we shall not discuss it here.

The junction between a propagating waveguide and one beyond cutoff may be represented as a four-terminal network whose parameters depend on the geometrical configuration of the junction as well as the characteristic impedances of the lines connected to the junction. Thus a complete cutoff attenuator has the equivalent circuit shown in Fig. 11·10. If the characteristics of the input and output junctions are known, the complete behavior of the attenuator can be calculated as outlined above. In Sec. 11·11 an attenuator is described for which this calculation has been carried out.

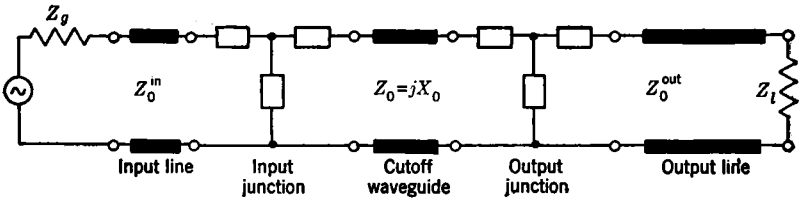

FIG. 11·10.—Equivalent circuit of a cutoff attenuator.

11·8. Impedance-matching Techniques.—In Sec. 11·2 an attempt was made to justify the importance of matching an attenuator. The cutoff attenuator particularly demands impedance-matching since its input impedance is wholly reactive for large separations of the coupling elements. The voltage standing-wave ratios are very high, around 40 or 50, and a small change in frequency can markedly affect the power drawn from the generator and delivered to the load which terminates the transmission line. There are several factors to be considered in the design of a matching network, and the choice of matching section depends on how one wishes to weight the various design factors. In general, the important factors are (1) maximum allowable input voltage standing-wave ratio, and the wavelength band over which the attenuator is to meet this maximum VSWR specification; (2) maximum reflections from the generator and load in the transmission line in which the attenuator is to be used; (3) magnitude of the dissipative attenuation introduced by the matching section; (4) relative importance of good matching at tight coupling and at loose coupling; (5) power-handling capacity of the matching section; (6) physical size of the matching section; (7) availability and ease of construction of the matching section; and, (8) reproducibility of the matching section.

The maximum allowable VSWR is, as previously explained, important from the viewpoint of ascertaining reflection errors when the generator and load are not perfectly matched. In attenuators which use matching

sections consisting of a lumped resistive element, the mismatched generator and load take on added significance. There is a power split between the matching element and the terminal load, this split being determined by the impedances of the two, and the effective dissipative attenuation of the matching element is therefore dependent on the load impedance. Consequently, a small change in load impedance can, under certain circumstances, exert a big influence on the over-all attenuation of the cutoff attenuator. More will be said about this in following paragraphs. Often one wishes to have good impedance-matching at the least possible cost in attenuation from losses in the matching section. The need for reducing this attenuation to a bare minimum will greatly influence the choice of the matching section. If the need for good impedance-matching is greatest under the condition of tight coupling, the design of a matching section is a much more severe problem than if the matching is to be made optimum at loose-coupling conditions. This follows from the fact that, at tight coupling, the impedance which is to be matched is varying much faster with antenna separation. The fact that the power level will be very low when the attenuator is in use does not allow one to neglect the power capacity of the matching section; relatively high-power levels must be used in calibrating the attenuator at large values of attenuation. The last three items in the above list are of relatively minor importance within the laboratory but can be quite troublesome if large-scale production of attenuators for field use is contemplated.

Most of the information available on resistive matching sections pertains to attenuators employing circular waveguide. In these designs the coupling elements terminate coaxial lines so that the matching sections are also in coaxial line. Matching sections of three types have been used in such attenuators: distributed-parameter resistive attenuators, i.e., microwave T-pads; resistive coupling loops; and a single, lumped-constant, series or shunt resistive element which is properly located with respect to the coupling element.

TABLE 11·3.—DATA ON CABLE ATTENUATION AND CHARACTERISTIC IMPEDANCE

Cable	λ, cm	Z_0, ohms	A, db/ft
RG-21/U	10.0	52	0.83
RG-21/U	3.3	52	1.6
RG-9/U	3.3	52	0.33

Undoubtedly the most commonly used matching device with distributed parameters is a long length of lossy cable. Typical data on cable attenuation and characteristic impedance are given in Table 11·3. In determining how much attenuation should be used, it is convenient to

refer to Fig. 11·11. This is a graph of the voltage standing-wave ratio of a short-circuited line which is "padded" with n db of matched attenuation. Thus, if the voltage standing-wave ratio looking into the attenuator is not to exceed 1.05, it is necessary to use at least 16 db of matched-cable attenuation. Actually, however, it is almost impossible to reduce the input VSWR to a value as small as 1.05 because of the reflections introduced by the cable fittings. If the cable attenuation reduces the VSWR of the short-circuited line to a value r_1, and if the cable fitting has a VSWR $= r_2$ when followed by a Z_0 load, then the actual or effective VSWR r' may lie anywhere within the range bounded by the product and quotient of r_1 and r_2. Thus the reflections from the connectors impose a limit on the goodness of matching.

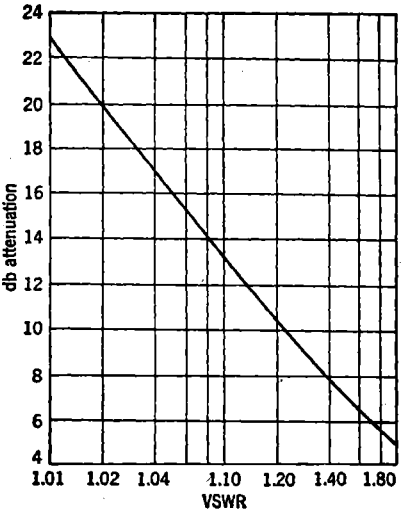

FIG. 11·11.—Change in VSWR with line attenuation.

It should be noted that r' need not be particularly small if the cutoff attenuator is used only to effect a known change in attenuation, and if it is operated in the range of relatively loose coupling where the previously discussed coupled-impedance effect is negligible. It is, nevertheless, safe practice to minimize r' since the attenuation error associated with a small and often unavoidable frequency drift will be less if r' is small.

Lossy cable has the advantage of being readily obtainable, but it is very bulky. Its attenuation constant is somewhat sensitive to changes of temperature and frequency, although if enough cable is used these variations are not disturbing. Flexion of the cable adjacent to the connectors can be very bothersome because it moves the center conductor pin of the plug (male) connector and changes the reflection. It is helpful to install a six-inch length of metal tube at the back end of the connector to prevent the cable from bending in this critical region. Lossy cable is capable of greater power dissipation than are most other types of matching sections.

There are many kinds of coaxial attenuators using metalized glass, polyiron, Bakelite, and other dissipative materials, that can be considered for use as cutoff-attenuator matching sections. In principle they do not differ from lossy cable but are often preferable because of their

compactness. Such designs will be discussed in detail in Chap. 12. In general, they are not well matched over as broad a wavelength band as is lossy cable.

The idea of using a resistive coupling loop which itself provides a satisfactorily matched termination for the coaxial line is an interesting one. This has been accomplished, in 0.5-in. 10-cm cutoff tubes, in two ways. The Carborundum Co. manufactures a midget carborundum resistor of 50-ohm nominal value in a 0.1-watt size. It is only $\frac{1}{16}$ in. in diameter and $\frac{1}{4}$ in. in length and has metalized ends for soldering. Figure 11·12 shows how such a resistor might be installed.

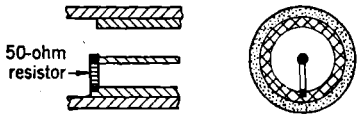

FIG. 11·12.—Coupling loop for a TE_{11}-mode cutoff attenuator with midget 50-ohm resistor.

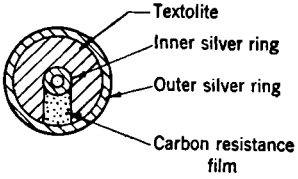

FIG. 11·13.—Resistive-stripe coupling loop for a TE_{11}-mode circular cutoff attenuator.

While rated for only 0.1 watt, the resistor will apparently carry several times this amount without harm. The standing-wave ratios obtained in the 10-cm band were considerably larger than those obtained using a "carbon stripe," so that the use of these resistors was abandoned except for a few instances where power capacity was of greater importance than low reflection. However, this method of matching would probably be very successful for application at longer wavelengths and would seem to deserve further investigation.

The carbon stripe is a coating of carbon on a thin $\frac{1}{32}$-in. textolite disk. The carbon material used is the same as that used in making the common carbon-strip potentiometers. The disk has a hole in its center through which the inner conductor of the coaxial line may protrude and silver-paste rings baked onto the disk to facilitate soldering or good pressure contact to the inner and outer conductors of the line. The hole diameter and disk diameter are chosen to be compatible with the coaxial-line size used. The construction is shown in Fig. 11·13.

The VSWR data in Table 11·4 indicate what can be expected in the impedance-matching of a resistive-stripe coupling loop. The cutoff tube is a 0.5-in. diameter tube; the sliding insert is a 50-ohm coaxial line terminated in the resistive stripe. The VSWR data were taken with the sliding insert installed in the cutoff tube but with no second loop to couple power from it. The resistivity of the carbon film was varied so that the d-c resistance of the stripe was 50 ohms in all cases.

TABLE 11·4.—IMPEDANCE-MATCHING DATA FOR A CARBON-STRIPE COUPLING LOOP

Stripe width, in.	VSWR less than	Over the band, cm
$\frac{1}{16}$	1.08	8.5 to 12.2
$\frac{3}{16}$	1.10	8.6 to 12.2
$\frac{9}{16}$	1.4	8.6 to 12.3
$\frac{3}{32}$	1.6	8.6 to 11.8

It will be noted from the data tabulated above that the wide stripes are preferable to the narrow ones from the viewpoint of broadband matching. The simplest explanation is that the wider stripes have less inductance, and thus contribute a smaller reactive component to the load impedance. An alternative, but perhaps less likely, explanation is that the inductance associated with the wide stripe, together with the inductive reactance which is reflected into the loop from the cutoff tube, is enough to resonate the capacitance of the high-permittivity textolite disk. Such a resonant circuit, heavily loaded by the resistance of the stripe, may be expected to have a very low Q and hence an impedance which is relatively insensitive to changes of frequency.

The carbon stripe unfortunately has a low power-handling capacity. Because of variations in the thickness of the resistive film, it is unwise to use such a stripe at power levels in excess of 0.1 watt. There seems to be no reason why the metalized-glass techniques used in making resistive attenuators could not be utilized in applying a metal-film stripe to a glass or a nonflaking synthetic-mica disk. Such techniques should produce a uniform, reproducible resistive coupling loop. The resistive stripe has two fundamental disadvantages: the appreciable width of the stripe enables it to couple well to the undesired TM-modes, and extremely tight coupling in the desired mode is impossible because of the difficulty of bringing two such stripes into intimate contact.

The third general procedure for matching the coaxial-line coupling element involves the use of a small, lumped-constant resistor in series or in shunt with the line. To idealize the situation, assume that the metal coupling loop in a design for the TE_{11}-mode is exactly equivalent to a short circuit at the loop, and that the metal disk used in the designs for the TE_{01}-mode is exactly equivalent to an open circuit at the metal disk. In the case of the short circuit at the loop, a tiny resistor of Z_0 ohms in series with the center conductor, at a distance of a half wavelength from the loop, would effect a matched termination. In other words, the load impedance is zero at this half-wavelength point, and a Z_0 series resistor installed at this point should provide a match. Similarly, if a shunt resistance is to be used, it would be installed at the quarter-wavelength point where its resistance would be in parallel with an open circuit

and would therefore present a match. Similar reasoning, applied to the design for the TM_{01}-mode, suggests that the series resistor should be inserted at the quarter-wavelength point and the shunt resistor at the half-wavelength point. Normally one would prefer the element placed at the quarter-wavelength point, as this obviously leads to a less frequency-sensitive load than would a half-wavelength spacing of the resistor. In any case, this third type of matching cannot be expected to be good over as broad a band as either of the first two mentioned.

Actually, conditions are not quite as we have assumed them to be. The reactive impedance of the cutoff tube must be considered and this may be inductive or reactive depending on whether the coupling is to *TE*- or *TM*-modes. In *TE*-mode designs the coupling loop has an appreciable inductance. In *TM*-mode designs there is a heavy capacitive loading from the fringing of the *E*-lines in the neighborhood of the periphery of the metal disk. Because of these factors, it is usually found that the resistors must be properly placed through trial and error to obtain the best results. The line distances are for this reason often far different from the simple quarter- and half-wavelength values. However, good impedance-matching is possible over limited wavelength bands.

In the above discussion of matching sections it is tacitly assumed that the optimum standing-wave ratio is required under loose-coupling conditions. As previously indicated, multimode coupling, in cutoff attenuators of most designs, discourages the use of these attenuators at small values of total attenuation. Since the attenuators are usually used in a loosely coupled condition, it is customary to match the impedances for this condition.

Series-matching resistors have been made from Erie[1] $\frac{1}{2}$-watt and 1-watt carbon resistors by cracking away the protective covering from the resistor material beneath it. The kernel of the $\frac{1}{2}$-watt resistor is approximately 0.11 in. by 0.5 in.; that of the 1-watt resistor is approximately 0.19 in. by 0.7 in. By use of a 0.500-in. OD, 0.217-in. ID coaxial line and a properly placed 50-ohm, 1-watt series resistor of this type, it was found possible to match a loosely coupled oscillator cavity to a VSWR of 2, or less, over the 8.9- to 11.1-cm band. Tolerances of ± 5 ohms on d-c resistance were found to affect the maximum standing-wave ratio very little. It is occasionally desirable to do most of the impedance-matching with such a lumped-resistor element and to reduce the VSWR further by using lossy cable.

The shunt resistor commonly used is a thin resistive disk since a disk presents a less serious discontinuity in the coaxial line than would a

[1] Erie Resistor Corp., Erie, Pa.

midget resistor installed across the line. The plane of the disk is normal to the axis of the coaxial line. Figure 11·14 shows the construction of a 50-ohm disk.[1] The disk is the correct size for installation in the coaxial sliding insert used with most 0.5-in. 10-cm cutoff attenuators. The construction is similar to that of the carbon stripe shown in Fig. 11·13, but, instead of a stripe, the entire annular region between the two silver rings is coated with carbon material. The resistance measured between the inner and outer rings is 50 ± 2.5 ohms with the dimensions as shown. The power capacity of such a disk is somewhat greater than 0.5 watt.

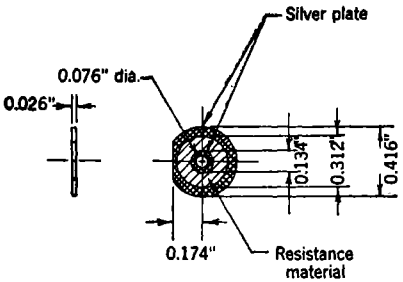

FIG. 11·14.—Resistive disk for matching attenuators.

Some idea of the effectiveness of the resistive disk as an impedance-matching device may be attained from the following data which apply to the use of the disk in a TM_{01}-mode circular cutoff design. Figure 11·15 shows the installation of the resistive disk behind the metal disk

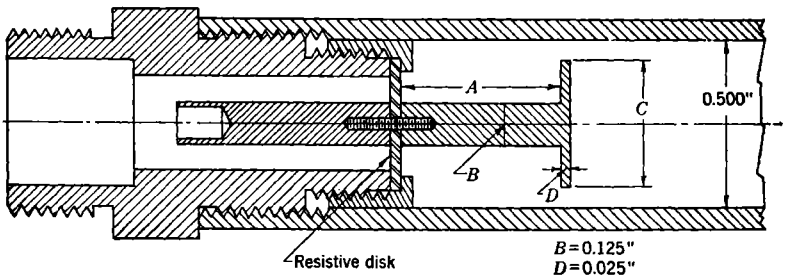

FIG. 11·15.—Installation of a resistive matching disk in a TM_{01}-mode cutoff attenuator.

which acts as the coupling element. The two most pertinent dimensions are the diameter C of the metal disk and the length A of the coaxial line between the metal disk and the resistive matching disk. The carbon side of the resistive disk is the side toward the right in the figure.

Impedance measurements were made by directing power from left to right. The VSWR-vs.-λ curves were found to be consistently parabolic. Holding the value of C constant at 0.400 in., a graph of A vs. the wavelength for minimum VSWR (λ_b) was plotted. The curve was found to be accurately a straight line for the entire range of A (0.85 in. to

[1] Manufactured by the International Resistance Company of Philadelphia (Catalogue number VC 14204).

1.60 in.) investigated. The value of $dA/d\lambda_b$ was found to be 0.178 in. per cm with λ_b being 10.0 cm for $A = 1.20$ in. Holding the value of A constant at 1.33 in., a graph of C vs. the wavelength for minimum VSWR (λ_b) was plotted. This curve was also found to be linear for the entire range of C (0.250 in. to 0.400 in.) investigated. The value of $dC/d\lambda_b$ was found to be 0.096 in. per cm. with λ_b being 10.0 cm for $C = 0.330$ in. The optimum VSWR (at λ_b) was, in almost all instances, between 1.05 and 1.10. The VSWR rose from its lowest value to a value of 1.20 at approximately $\lambda = (1 \pm 0.08)\lambda_b$. Ten different matching disks with d-c resistances in the range of 50 ± 8 ohms were used in taking these data. Disk variations appeared to be relatively unimportant.

Since a reasonably good impedance match can be obtained at a given wavelength by any one of a number of combinations of the A and C dimensions, an additional criterion is needed to specify the best combination. This criterion is concerned with mode purity of excitation in the cutoff region and will be discussed subsequently in Sec. 11·12. Assuming that the carbon disk is a pure 50-ohm shunt resistance, and having experimental data on λ_b for a given line length A, it is possible to calculate the value of capacitance which, representing the metal coupling disk in an equivalent circuit, produces an infinite impedance in shunt with the 50-ohm disk. The input VSWR of the over-all combination may then be calculated as a function of λ, and the calculated curve compares very well with the experimentally determined one. This is another way of saying that the disks have a small reactance, and that it is insensitive to frequency. Separate experiments involving impedance measurements on disks installed in short-circuited coaxial lines verify this conclusion.

11·9. Examples of Waveguide Attenuators for 3000 Mc/sec.—Having discussed most of the basic principles of cutoff-attenuator design, we may now consider the details of some specific designs that have been developed. First to be considered is a series of 10-cm circular TE_{11}-mode cutoff attenuators. These will be discussed in approximately the chronological order of their development so that the improvements effected can more easily be followed and understood. All attenuators in this series use a $\frac{1}{2}$-in. diameter cutoff tube.

The TPS-15 Attenuator.—The first 10-cm attenuator produced in quantity for use within the Radiation Laboratory was the TPS-15. An assembly sketch of the TPS-15 is shown in Fig. 11·16, and a photograph of the attenuator is shown in Fig. 11·17. The two coupling loops in this design are shown in contact in the figure. The rigidly mounted loop at the left terminates a short length of 50-ohm coaxial line. The loop at the right terminates the 50-ohm coaxial line in the sliding insert. Eight to ten fingers are cut into the left end of the sliding insert in the vicinity of its coupling loop, and the loop is grounded to one of these fingers. The

fingers are given sufficient spring to provide good electrical contact between the end of the slider and the wall of the cutoff tube. The slider is driven by a rack and pinion, and a dial is mounted on the shaft of the pinion gear. The spacing of teeth on the rack, the diameter of the

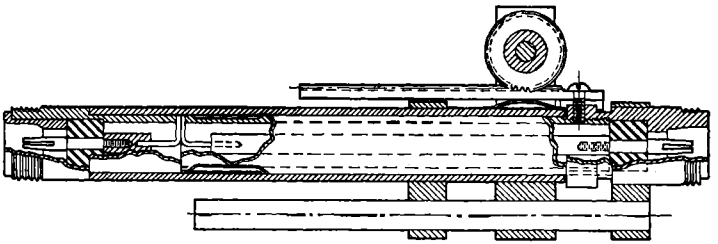

FIG. 11·16.—Assembly sketch of the TPS-15 cutoff attenuator.

pinion gear, and the dial engraving are so chosen that one dial division corresponds to one decibel of attenuation. Wobble of the insert is avoided by the use of a steel guide rod of large diameter which slides through oiled bearing holes in two brass blocks rigidly fastened to the cutoff tube. Note that no impedance-matching devices are designed

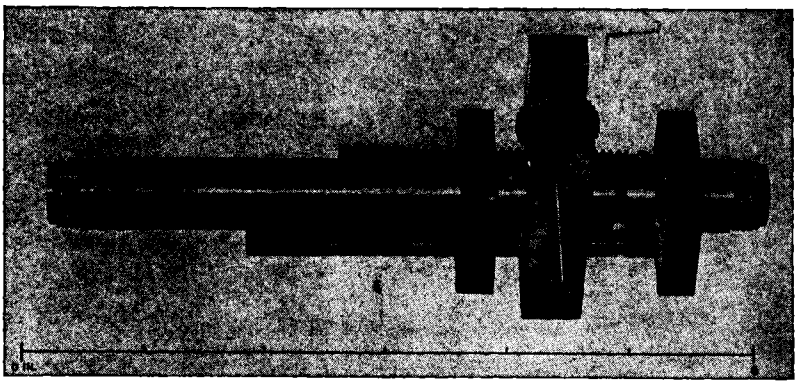

FIG. 11·17.—Photograph of the TPS-15 cutoff attenuator.

into this model; consequently, long lengths of lossy cable are required on each side of the attenuator.

Whereas the attenuator is simple to construct, it leaves much to be desired electrically. The coupling is by no means pure TE_{11}-mode coupling and the attenuation (exclusive of that in the cable) at a point within 0.5 db of linearity is approximately 30 db. When properly padded with lossy cable, the minimum attenuation that permits operation on the linear part of the calibration curve is, therefore, objectionably high for many purposes. The cutoff tube gradually becomes scored through wear

from the fingers and the finger contacts are not perfect enough to prevent r-f leakage between the sliding insert and the wall of the cutoff tube. R-f leakage either into or out of the attenuator can under certain circumstances (see Sec. 13·5) cause appreciable errors in measurements made with the attenuator.

A number of attempts to improve the purity of mode in this attenuator by radical changes in loop shape or by the use of solid silver contact fingertips on the slider were fruitless. Changes in the variation of attenuation with both distance and angle of loop orientation were effected in this manner, but none seemed to offer a sufficiently great improvement to suggest that the problem of nonlinearity could be solved in this way. Subsequently, there was conceived the idea of exciting the TE_{11}-mode by means of an iris instead of a loop, and later developments proved the merits of this suggestion.

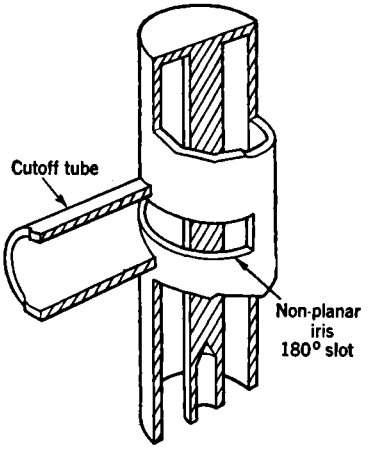

FIG. 11·18.—Iris-coupling mechanism used in the Model 0 attenuator.

The Model O Attenuator.—The first attenuator design making use of such an iris was called the Model O. The novel features of the design are shown in Fig. 11·18. The cutoff tube is joined at right angles to a coaxial line of comparable diameter, using a 180° circumferential slot in the outer coaxial conductor to couple the two lines electrically. The slot acts as a nonplanar iris which can excite or couple to a TE_{11}-mode in the cutoff tube, but discriminates against TM-modes. The coupling loop of the slider (not shown in the figure) lies in the plane which includes the axis of the coaxial line. The coaxial line is short-circuited a distance $\lambda/2$ from the coupling slot so that a current maximum exists at the slot. This facilitates tightest coupling. Because of the frequency sensitivity of the half wavelength of coaxial line, the attenuator has an obvious bandwidth limitation in so far as tight coupling is concerned. Also, higher-mode coupling still exists, although to a lesser degree than in the TPS-15 design. The calibration curve for the Model O reaches linearity to within 0.5 db at an attenuation (exclusive of lossy cable) of approximately 25 db.

The Model T Attenuator.—A further improvement in linearity was made in the Model T design shown in Fig. 11·19. A coaxial line of much larger diameter is used so that the cutoff tube can easily be projected

through its outer conductor. This permits the use of a planar iris at the end of the cutoff tube and also permits tighter coupling, since the iris is brought nearer the center conductor of the coaxial line where the field is more concentrated. The calibration curve reaches linearity within 0.5 db at an attenuation of approximately 20 db.

The Model S Attenuator.—The minimum attenuation of an iris attenuator can be reduced several decibels by coupling to the iris through a highly resonant cavity. The cavity has the function of building up the electric potential across the edges of the gap to a high value, and thereby tightens the coupling. The Model S attenuator makes use of this principle. It has proved to be a quite satisfactory design, and has served faithfully as a primary standard attenuator.

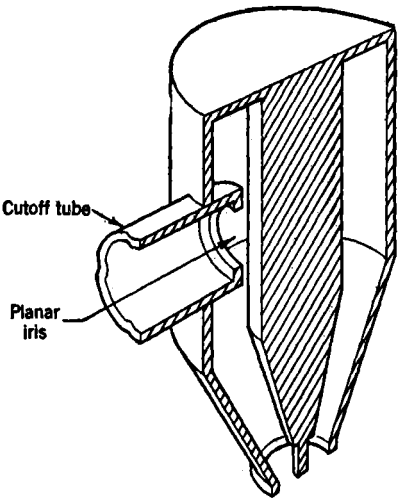

FIG. 11·19.—Iris-coupling mechanism used in the Model T attenuator.

Figure 11·20 shows a sketch of the pertinent features of the Model S attenuator. The cavity used is a round pillbox type with metal walls and an axial tuning rod. It normally resonates in a TM_{010}-mode although, possibly, the heavy capacitive loading associated with a small gap between the end of the tuning rod and the cavity bottom plate can make the cavity resonate in a coaxial mode at the long-wavelength end of its tuning range. It is good practice to keep the height of the cavity a little less than a half wavelength and the diameter somewhat greater than a half wavelength. The tuning rod may be either metal or a relatively high-permittivity (for example, glass) dielectric; the effect of either material is to concentrate the fields in the vicinity of the tuning rod. The dielectric tuning rod is preferable from the viewpoint of coherent-leakage protection since its diameter may be chosen so that the metal tube through which it slides is beyond cutoff. In contrast, one must depend on good electrical contact in the screw threads of the tuning mechanism to prevent leakage when a metal tuning rod is used. The cavity commonly used in this design will tune over a minimum wavelength band of 9 to 11 cm. Irregularities in the walls of the cavity show no appreciable effect on the shape of the calibration curve. Likewise, because of the relatively low loaded Q of the cavity, highly polished plating is unessential.

The input coupling loop is rigidly fixed with respect to the cavity and has dimensions which make it nearly resonant so that it couples tightly to the cavity. In contrast, the coupling through the planar iris to the loop of the slider in the cut-off tube is relatively weak. The large input coupling loop is approximately square, and oriented in a plane parallel to the tuning rod. It is grounded next to the flat bottom end of the cavity. The loaded Q of the cavity used in this design is of the order of 100 to 150, and decreases with the resonant frequency of the cavity. It was found preferable to locate the capacitive tuning gap at the bottom of the cavity, instead of at the center.

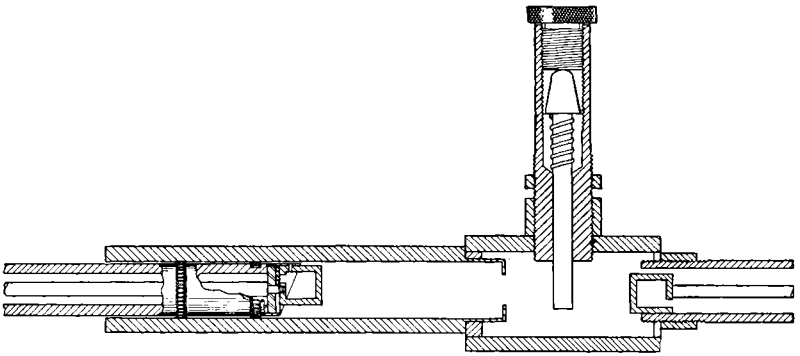

FIG. 11·20.—Sketch of the pertinent features of the Model S attenuator.

It is occasionally advantageous to install in the cavity another coupling loop which couples to a short length of coaxial line terminated by a crystal. The current induced in the loop is rectified by the crystal and measured by a d-c microammeter. For a given cavity, the crystal monitor provides a measure of the electric potential across the iris. Thus frequency-drift or output-power variations in the oscillator, either of which will affect the field intensity in the cavity, can easily be followed. The coaxial line should be extended a short distance beyond the crystal and filled with a tube of high-loss polyiron material. By bringing the d-c leads to the microammeter through such an attenuating line, one can avoid r-f leakage into or out of the cavity at this point.

The design of the planar iris terminating the cutoff tube is based on the necessity of a compromise between the purity of mode excitation and small cavity insertion loss. For a 0.5-in. cutoff tube, an iris width of $\frac{1}{8}$ in. to $\frac{1}{4}$ in. was found to provide good linearity. If the planar iris is approximately flush with the cylindrical wall of the cavity, the insertion loss is rather high, but the calibration curve reaches linearity almost immediately. On the other hand, if the cutoff tube and terminating iris are projected into the cavity a short distance, it is found that the insertion loss drops while the nonlinear part of the calibration curve is

extended. Consequently, the over-all attenuation level at which the calibration curve of the attenuator becomes linear to within a specified fraction of a decibel is not appreciably affected by the extent of projection of the iris. The best compromise is a projection into the cavity of approximately $\frac{3}{16}$ in. The iris is made $\frac{1}{32}$ in. thick, and the slot is carried all the way across the cutoff tube. Although, as indicated above, there is some latitude in choice of slot width, a $\frac{1}{4}$-in. width is commonly used.

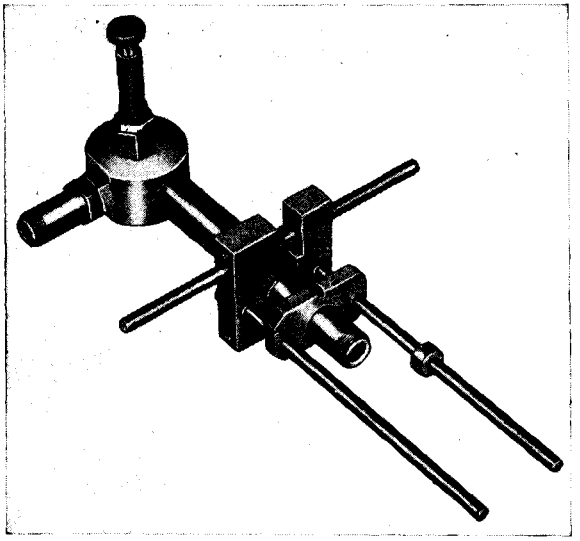

FIG. 11·21.—Photograph of the Model S attenuator.

The length of the slot lies in a direction normal to the plane of the coupling loop of the sliding insert.

The design of the sliding insert has likewise been given careful attention. The coupling loop (see Fig. 11·20) is a rather large one, and is formed from a thin metal strap of rectangular cross section. The 50-ohm IRC resistive disk used for impedance-matching is located at the base of the loop where it is easily installed. It is convenient for optimum impedance match that the sizable inductance associated with this large loop demands that the disk be placed at this point. Over the 9- to 11-cm band, the VSWR of the matched loop does not exceed 1.15. The cutoff tube in which the slider operates need not be built diametrically opposite the input coupling loop to the cavity, as shown in Fig. 11·20. Figure 11·21, a photograph of the Model S attenuator, shows the cutoff tube 90° from the input coupling loop.

It is not so easy to match the cavity loop because the position of the voltage maximum in the standing-wave pattern looking into the cavity

loop is critically dependent on tuning. To compensate for this two disks may be inserted. The first is in the normal position of the voltage minimum, and is inoperative when the cavity is tuned. The second disk is placed a quarter wavelength down the coaxial line from the first. When the cavity is detuned, the decreased effectiveness of the second disk is partially compensated for by the action of the first disk which is no longer located at the voltage minimum. With this arrangement the VSWR was reduced to 1.35 for a tuned cavity, and to 1.80 for a badly detuned cavity. The pair of disks introduced an additional attenuation of 4 to 6 db depending on the tuning. This represents a distinct improvement over the use of lossy cable, but the mechanical complication of installing the pair of disks may be too costly.

Sliding contacts which are electrically good are always difficult to obtain in the microwave region. The slider in the Model S offers no exception. The split-tubing finger construction, mentioned in connection with the TPS-15 attenuator, has many disadvantages. The finger to which the center conductor is grounded by the loop appears to be the important one, but unfortunately it is the least dependable because of the restraint put on it by the mechanical tie to the center conductor. The difficulty may be alleviated by stiffening the loop finger and bending it back so that it must be compressed slightly when inserted into the cutoff tube. Unless the insert is very tightly fitted in the cutoff tube (which is bad from other points of view), forces exerted on the slider can cause troublesome contact variations. Helical-spring contacts were designed for use in the Model S attenuator. Figure 11·22 shows in detail the method of constructing the helical springs and the method of installing them on the slider.

The wearing qualities of unoiled sliders are very poor, in general. No combination of brass, steel, solid silver, silver plate, or nickel plate evidenced good wearing qualities when operated dry. However, a good grade of low-viscosity motor oil used for slider lubrication effected a marked improvement. An attenuator design in which the slider must depend on pressure contact with the inside of the cutoff tube for mechanical support is particularly bad; rather severe gouging develops in time. It is desirable to use external guide rods to support the slider, although this procedure usually demands a larger tolerance between the slider and the cutoff tube. In turn, this larger tolerance invites greater r-f-leakage difficulties. However, the helical springs are not handicapped by this larger tolerance, as are the conventional split-finger contacts, and can serve simultaneously as effective leakage inhibitors and good electrical contactors. Optimum leakage protection is gained by using a pair of the springs, spaced $\lambda/4$ apart along the length of the slider. The springs have been shown to provide from 80 to 100 db of leakage pro-

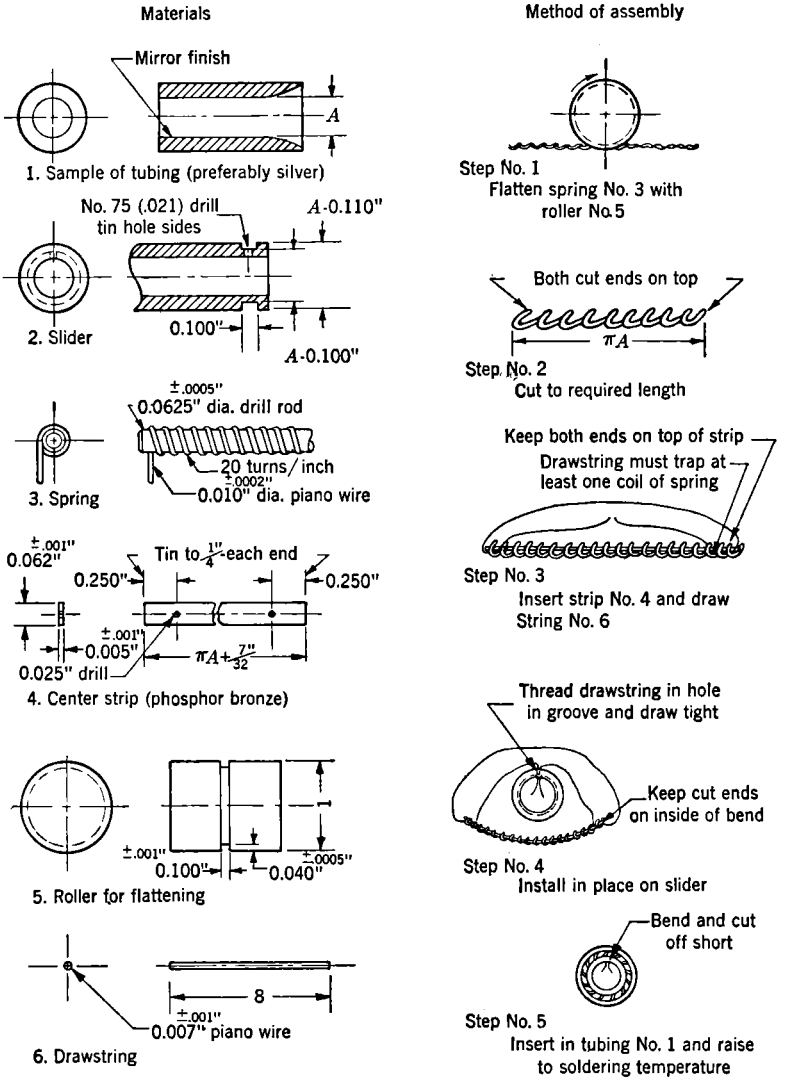

FIG. 11·22.—Method of constructing helical-spring r-f contacts.

tection when used in pairs. If desired, further leakage protection can be obtained by using a thin-walled tube of polyiron around the slider, locating it between the second helical spring and the r-f connector at the end of the slider. The polyiron should not touch the wall of the cutoff tube.

A spring-loaded rack with pinion gear is a commonly used drive mechanism for the slider. The dial attached to the pinion gearshaft may have an accurate vernier scale associated with it, or a dial indicator (Ames Gauge) may be used to indicate the position of the slider. The latter method escapes backlash troubles with the drive mechanism, and provides a least count of 0.001, or even 0.0001 in., of slider movement.

The Model S attenuator has a calibration curve which is within 0.5 db of linearity when the over-all attenuation (including loss in the slider matching disk) is 6 db, and is within 0.1 db of linearity at 14 db. The attenuators have been quite reproducible. The calibration curve includ-

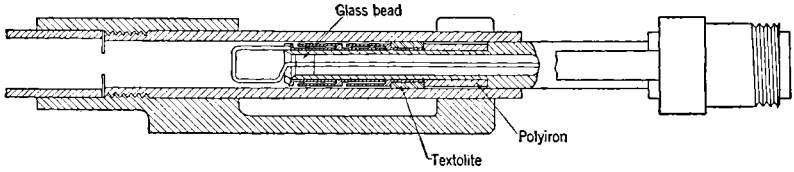

FIG. 11·23.—Sketch of a 3-cm-band TE_{11}-mode cutoff attenuator.

ing the nonlinear region is almost wholly independent of wavelength from 9 to 11 cm except for the slope change specified by Eq. (6). This is small: the slope is 0.975 db per dial division at 9 cm, and 0.985 db per dial division at 11 cm. Calibration curves taken with the cavity detuned by as much as 75 Mc/sec have shown that detuning to this degree has no appreciable effect on the extent of the nonlinear region. Of course, the insertion loss of the cavity is increased by such detuning.

11·10. A Waveguide Attenuator for 9000 Mc/sec.—The sketch of a design for frequencies near 9000 Mc/sec is shown in Fig. 11·23. It is somewhat dimensionally distorted to make possible the inclusion of all pertinent features in the single sketch. Figure 11·24 shows a photograph of the assembled attenuator.

The circular cutoff tube is approximately $\frac{1}{3}$ in. in diameter, and is coupled to the 0.400- by 0.900-inch rectangular waveguide by a planar iris similar to that used in the Model S designed for the 10-cm band. The circular and rectangular waveguides have a common axis. Experiments were conducted with a variety of iris shapes and the one finally selected as optimum for use over the band from 3.13 to 3.53 cm has a width approximately equal to the radius of the cutoff tube. The iris extends entirely across the cutoff tube, with its length parallel to the wide side of the rectangular waveguide.

The slider has a large rectangular loop of approximately resonant dimensions, and the loop is given rigidity at its base by a glass bead which mechanically supports the inner conductor of the coaxial line. No

impedance-matching network is built into the slider. A pair of stagger-tuned half-wavelength choke cups are installed on the slider immediately behind the coupling loop. Then follows a hard, smooth-surfaced textolite bushing which makes sliding contact with the cutoff tube. Behind the bushing is a polyiron sleeve of slightly smaller diameter to assist the tuned choke cups in providing adequate leakage protection. The minimum attenuation (with loop touching the iris) is 7 to 10 db over the above-mentioned wavelength band. The calibration curves require an additional 8 to 10 db to reach linearity within 0.5 db.

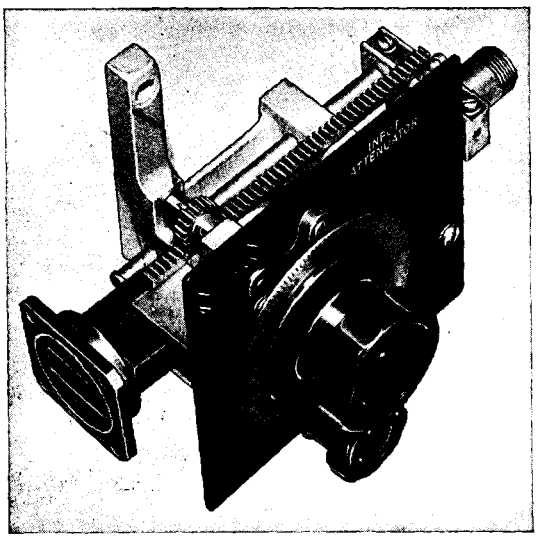

FIG. 11·24.—Photograph of the 3-cm-band cutoff attenuator.

11·11. An Attenuator for 24,000 Mc/sec.—Figure 11·25 shows the design of an attenuator for frequencies near 24,000 Mc/sec which utilizes a dielectric rod as the sliding member.

The $\frac{1}{2}$-in. by $\frac{1}{4}$-in. rectangular guide carries power from a generator to a power-monitoring termination (for example, a thermistor) or a matched load. A round waveguide beyond cutoff extends to the right, normal to the broad side of the rectangular waveguide. A polystyrene rod of approximately $\lambda_g/2$ in length is seated in the end of the cutoff tube. Its exact length is chosen such that, for loose coupling in the attenuator, the reactive impedance of the cutoff tube referred to the junction of the rectangular and cutoff waveguides is zero and no reflection is produced in the rectangular waveguide. A polystyrene rod is driven along the cutoff tube by a micrometer, thus varying the length of the air region which is beyond cutoff for the TE_{11}-mode. The TE_{11}-wave which is propagated

then couples into the rectangular waveguide and passes out of the attenuator. A tuned 1-cm-band choke facilitates coupling into the rectangular waveguide by preventing propagation further in the dielectric rod. A resistive matching disk is installed in the polystyrene rod, so that the wave moving through the dielectric rod proceeds from a matched generator. The extension of the rectangular waveguide and the location of its short-circuited end are carefully chosen so that the circular-to-rectangular-waveguide transition is reflectionless.

Resistive matching disks of several types have been tried, but none has been entirely satisfactory. Cloth soaked in Aquadag (a carbon suspension) has been used, for example. For the proper disk resistivity, a match can be obtained with a thin, uniform disk. Correction for an unfavorable resistivity can be made by cutting a hole of the proper size in the center of the disk. Since the disk is spliced between two dielectric rods, the adhesive presents a problem which has not been solved with entire satisfaction.

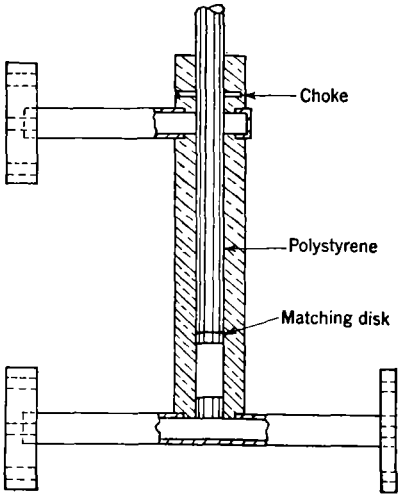

FIG. 11·25.—Attenuator with polystrene rod for 1-cm band.

The position of the matching disk with reference to the dielectric-air interface is important. The disk should be placed at a current node in the polystyrene rod. Since the reflected inductive reactance of the cutoff tube is approximately j, the polystyrene cap placed over the resistive disk should be approximately $\lambda_g/8$ in length.

A desirable feature of this variable attenuator is that it employs no sliding metal contacts. The diameter of the cutoff tube is so chosen that when it is filled with the dielectric it propagates the TE_{11}-mode but it is still below cutoff for the TM_{01}-mode. The short length of polystyrene, therefore, acts as a mode filter for energy coupled out of the main waveguide by the electric field. If the ends of the dielectric rods are accurately perpendicular to the cutoff tube, no higher modes are excited.

One of the big advantages inherent in the dielectric cutoff attenuator is that its calibration curve can be accurately predicted, including the nonlinear part that arises from interaction or reflection effects at the dielectric-air interfaces. The effect has been discussed in Sec. 11·7. The expression derived[1] for the attenuation (that is, ratio of power trans-

[1] N. H. Frank, private communication.

mitted through the air cutoff region to the power incident on the input dielectric-air interface) is

$$A = 10 \log_{10} \left\{ 1 + \frac{(k_e - 1)^2}{4\left[k_e - \left(\frac{\lambda}{\lambda_c}\right)^2\right]\left[\left(\frac{\lambda}{\lambda_c}\right)^2 - 1\right]} \sinh^2 \frac{2\pi l}{\lambda} \sqrt{\left(\frac{\lambda}{\lambda_c}\right)^2 - 1} \right\}, \tag{23}$$

where λ_c is the cutoff wavelength in the TE_{11}-mode for the tube when no dielectric is present. This equation can be simplified considerably if we choose the diameter of the waveguide beyond cutoff so that

$$W = \frac{(k_e - 1)^2}{4\left[k_e - \left(\frac{\lambda}{\lambda_c}\right)^2\right]\left[\left(\frac{\lambda}{\lambda_c}\right)^2 - 1\right]} = 1. \tag{24}$$

This condition is met when

$$\lambda_c = \lambda \sqrt{\frac{2}{1 + k_e}}. \tag{25}$$

In this case the simplified equation becomes

$$A = 10 \log_{10} \cosh^2 \left[\frac{2\pi l}{\lambda} \sqrt{\left(\frac{\lambda}{\lambda_c}\right)^2 - 1} \right]. \tag{26}$$

Since, for large x,

$$\sinh^2 x = \frac{e^{2x}}{4},$$

we can write Eq. (23), for $l \gg \lambda$, as

$$A = \frac{10}{\ln 10} \frac{4\pi l}{\lambda} \sqrt{\left(\frac{\lambda}{\lambda_c}\right)^2 - 1} + 10 \log_{10} \frac{W}{4}. \tag{27}$$

Thus the attenuation becomes a linear function of l with the slope

$$\alpha = \frac{40\pi}{\ln 10} \sqrt{\left(\frac{1}{\lambda_c}\right)^2 - \left(\frac{1}{\lambda}\right)^2}.$$

The term independent of l in Eq. (27) can be made independent of wavelength, if we impose the condition that

$$\frac{\partial W}{\partial \lambda} = 0. \tag{28}$$

This leads again to Eqs. (25) and (26), while Eq. (27) becomes

$$A = \frac{40\pi}{\ln 10} \sqrt{\left(\frac{1}{\lambda_c}\right)^2 - \left(\frac{1}{\lambda}\right)^2}\, l - 20 \log_{10} 2. \tag{29}$$

These relations have been verified to within the experimental error.

11·12. The Design of Cutoff Attenuators Using the TM_{01}-mode.— Until recently little attention has been given to the design of cutoff attenuators using the TM_{01}-mode. It was felt that the slightest amount of plate ellipticity or eccentricity in the centering of the plate in the cutoff tube would lead to excitation of modes in the TE-mode series. Even if the TE_{11}-mode is excited very weakly, it will cause trouble at large attenuations because it decays in intensity less rapidly than does the TM_{01}-mode. For example, if the TE_{11}-mode is excited with an intensity 40 db down from that of the TM_{01}, it will be only 20 db down after the TM_{01}-mode has been attenuated 80 db. It is, therefore, necessary to check calibration of such an attenuator over the entire range of attenuation for which it is to be used. If this range is 70 db or greater, such a procedure imposes severe experimental difficulties.

It has been pointed out that one should be able to circumvent the effects of TE_{11}-modes by properly orienting the two antenna plates. Two antenna plates which are slightly elliptical may be oriented in such a way that their major axes are at right angles to each other so that, if the first plate excites the TE_{11}-mode, the second one will not couple to it. This alignment cannot be based on mechanical measurements since the eccentricity is extremely small. However, an experimental determination of the proper alignment can be made. It is not unreasonable to suppose that proper orientation will reduce by 30 to 50 db the coupling to the TE_{11}-mode. Consequently, if the plates are turned down on a lathe after installation on their respective coaxial lines, and carefully oriented by means of an angle calibration, satisfactory freedom from TE-mode coupling can probably be achieved.

A brief investigation was made of a 10-cm-band TM_{01}-mode cutoff attenuator using 0.400-in.-diameter metal plates in a 0.5-in. cutoff tube. The inner conductors of the coaxial lines were supported by polystyrene beads located a short distance behind the plates. The minimum attenuation, plates touching, was less than 1 db in the wavelength range from 10 to 12 cm, and the calibration curve reached linearity within 0.5 db after 10 db of decoupling. The linearity was checked up to an attenuation of 50 db, and was found to be exact within the limits of experimental error.

In order to improve further the linearity of a TM_{01}-mode cutoff attenuator in the low-attenuation range, it would be necessary to suppress the excitation of the higher TM-modes. A means of accomplishing this has been suggested, but unfortunately has not been verified experimentally. The principle is to select different diameters for the two metal-disk antennas such that one disk cannot excite the TM_{02}-mode, and the other disk cannot excite or couple to the TM_{03}-mode.

CHAPTER 12

MICROWAVE ATTENUATORS. RESISTIVE ATTENUATORS

By E. Weber and R. N. Griesheimer

For general laboratory use, many devices are available which give fixed or variable attenuation of the main power flow, or which permit power sampling for power-monitoring purposes without reacting perceptibly upon the main power flow. For low power ranges it is usually permissible to insert in the main power path elements of dielectric base materials which have thin coatings of power-absorbing materials such as carbon or Aquadag. For larger powers, in order to provide for efficient heat transfer to the ambient air, power-absorbing materials in greater bulk and with proper metal casings are inserted. Finally, in order to separate the directly transmitted power from that absorbed in a properly designed terminal load, the principle of power division can be used.

The design of dissipative attenuators involves two problems of paramount importance: the choice of the material in which the power is to be lost, and the impedance-matching of the attenuator to the transmission line. These problems must also be solved in the design of a termination for a transmission line which will absorb without reflection all the power incident upon it. The design of a termination or load is often simpler than that of an attenuator because the impedance-matching need be done at one end only. The first part of this chapter is, therefore, devoted to a discussion of terminations.

Most of the general-purpose laboratory attenuators admit of calibration in a limited sense only, over narrow frequency ranges, either because of the frequency dependence of the loss characteristics of the materials, or because of the influences of temperature and humidity. For this reason, a separation is made between the general-purpose attenuators and the attenuators which by the use of precision metalized glass, justify higher accuracy in calibration and are therefore even useful as standards.

MATCHED TRANSMISSION-LINE TERMINATIONS

By R. N. Griesheimer

There are innumerable applications in microwave work for matched-impedance transmission-line terminations, or "loads" as they are more commonly called, and the number of materials and designs employed in

their construction has been as great as the number of applications. Terminations are commonly classed as either high-power or low-power terminations. High-power terminations are designed to take the full output power of a transmitter tube; that is, power ranging from a few watts to several hundred watts. They are used to replace the transmitting antenna under conditions where radiated power would violate secrecy or would interfere with neighboring receivers. In addition, the high-power load sidesteps the objection that within the confines of a laboratory an antenna offers a varying load impedance as objects move in its immediate vicinity. High-power loads are usually required to have a VSWR not greater than 1.05 to 1.10.

Low-power loads may be grouped into two classes. Some applications demand that the loads be almost perfectly matched; that is, their VSWR should be no greater than 1.01 or 1.02. The reference match in a magic T that is used for impedance measurement is such an application. Impedance measurements on lossless or low-loss line components are often conducted with a matched line termination placed after the component under test, and such a termination should also have a VSWR which is as small as 1.01. In contrast, the terminations used in the secondary lines of directional couplers, for example, can often be allowed a maximum VSWR as great as 1.1 or 1.2. In these applications a compromise is usually necessary between the allowable voltage standing-wave ratio and the allowable physical dimensions of the termination, with the directivity of the directional device being the determining factor in setting the maximum allowable voltage standing-wave ratio. Low-power loads are seldom designed to dissipate more than 0.5 watt.

In the design of a line termination there are a number of factors which must be taken into consideration. The most important electrical specifications are the maximum allowable voltage standing-wave ratio and the bandwidth over which the voltage-standing-wave ratio specification is to be met. The maximum safe power capacity of the load is also of considerable importance. For high-power loads it is necessary to consider both average power dissipation and pulse-power breakdown, or "arc-over." The impedance match should be independent of temperature within the stated safe average-power limit, and should not be affected by humidity variations or by aging. Many applications, for example the reference match for the magic T, demand that the loads be very carefully protected against r-f leakage. The impedance match of the load should be quite insensitive to shock and vibration, and, in the event that large-scale production is anticipated, it should also be reproducible from unit to unit. As previously suggested in the comments on directional couplers, the size, primarily the length, of the termination is important in some applications. In constructing very-

well-matched loads with VSWR less than 1.02, it is of particular importance to obtain precision waveguide or coaxial line for their construction. The reflection from a small discontinuity at the junction of the load and the line which it terminates can easily account for a VSWR of 1.01 or 1.02.

The metal housing for the load is customarily terminated by an r-f short circuit in order to avoid r-f leakage from the load. This imposes a lower limit on the attenuation of the termination if a broadband impedance match is to be obtained. Figure 11·11 shows that the VSWR of a short circuit, measured through 23 db of matched attenuation, is 1.01. Since the termination is not likely to be exactly matched, it is essential to have a minimum of 30 db of attenuation in the load if there is to be any hope of obtaining a load VSWR less than 1.01 over a sizable wavelength band.

The most difficult problem in load design is, of course, the impedance-matching problem. A number of techniques have been employed for impedance-matching; most of these techniques are also applicable to the matching of resistive attenuators. The most commonly used matching devices are long tapers, or one or more quarter-wavelength transformers. However, examples of other techniques will also be cited.

12·1. Low-power Coaxial-line Terminations.—Two coaxial-line terminations have been developed which meet a maximum VSWR specification of 1.02 to 1.04 over an 8 to 10 per cent band. One design utilizes a thermosetting plastic, Durez 7421, which is cast in a section of the line to be terminated. Then, because the temperature coefficient of expansion of Durez is greater than that of brass, it can be removed from the center conductor by heating and from the outer conductor by cooling. It is a relatively easy material to machine, and a conical matching taper of the correct length can be cut on a lathe. The taper is carried all the way to a knife edge at the center conductor, with the experimentally determined optimum taper length being approximately two wavelengths. The solid plastic provides a good support for the center conductor and consequently the load is a rugged one. A second well-matched load has been made from a resistive cloth, Uskon.[1] The cloth used has a resistivity of approximately 440 ohms per square. A long trapezoidal piece of the cloth is tightly wrapped around the inner conductor of the coaxial line in such a way that a conical matching taper, followed by a completely filled length of line, is formed. This is a less durable load than the one made from Durez, particularly since the cloth has a tendency to fray at the tip of the taper, and thereby produces a reflection. These loads may be made for a variety of sizes of coaxial lines but may become objectionably long at wavelengths longer than microwaves.

[1] Manufactured by the U. S. Rubber Co., Rockefeller Center, New York.

Various polyiron materials have been used effectively in making 10-cm-band and 3-cm-band step terminations in coaxial lines. Figure 12·1*a* shows a cross section of a polyiron cylinder commonly used for a $\frac{7}{8}$-in. coaxial line; Fig. 12·1*b* shows a preferable shape for a $\frac{5}{16}$- or $\frac{1}{2}$-in. line. In the smaller size the step shown in Fig. 12·1*a* is so thin that it is too easily broken. Polyiron has the advantage of having a very large attenuation constant for microwaves; consequently, polyiron terminations can be made relatively short. Moreover, polyiron terminations can be made for use at wavelengths considerably longer than microwaves. This material has the disadvantage, up to the present, that its microwave properties vary considerably from batch to batch, and the dimensions often need to be corrected when units are made from a new batch. Typical data on two coaxial polyiron terminations are given in Table 12·1.

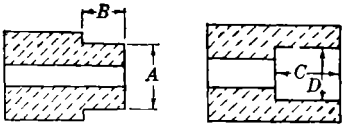

FIG. 12·1.—Cross section of polyiron cylinder for (*a*) large and (*b*) small coaxial lines.

TABLE 12·1.—DATA ON TWO COAXIAL POLYIRON TERMINATIONS

Crowley* material MP-1826

50-ohm, $\frac{7}{8}$-in. coaxial line	50-ohm, $\frac{5}{16}$-in. coaxial line
A = 0.511 in.	C = 0.188 in.
B = 0.295 in.	D = 0.228 in.
VSWR < 1.10 from 9 to 11 cm	VSWR < 1.10 from 3.1 to 3.5 cm

* Henry L. Crowley Co., West Orange, N. J.

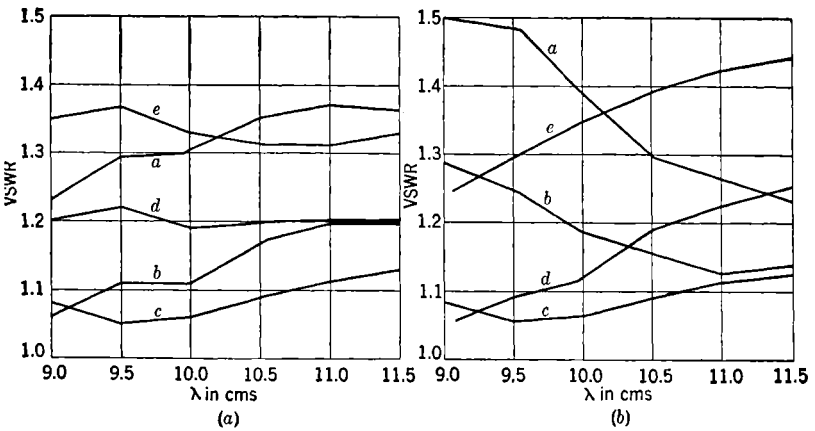

FIG. 12·2.—Tolerance study on a $\frac{7}{8}$-in. coaxial-line polyiron load of Fig. 12·1*a*. For curves *a*, dimension A = 0.511 in., dimension B for the various curves as follows (*a*) 0.220 in., (*b*) 0.260 in., (*c*) 0.295 in., (*d*) 0.350 in., (*e*) 0.400 in. For curves *b*, B = 0.295 in., A equals the following: (*a*) 0.570 in., (*b*) 0.530 in., (*c*) 0.511 in., (*d*) 0.500 in., (*e*) 0.480 in.

The tolerances on the step dimensions must be very small, even for loads made from a given batch of material. The graphs shown in Fig. 12·2 offer an indication of the criticalness of the dimensions. Such families of tolerance curves have proved to be very helpful in establishing dimensional corrections for a new batch of the material. Unfortunately polyiron is not an easy material to machine. Diamond-dust grinders and Carboloy-tipped drill bits and lathe tools are needed to cut it. An effective ventilating system is required to protect the machinist from the iron dust. Attempts have been made to match coaxial-line polyiron loads by machining conical tapers at the front ends of the pieces, but low standing-wave ratios with acceptably short taper lengths have not been obtainable.

Impedance data for cylinders of polyiron in 50-ohm, $\frac{7}{8}$-in. coaxial line (see Table 12·2) show that the impedance of the various materials is remarkably independent of wavelength. Although a termination of this design has not been built and tested, the tabulated data suggest that a broadband device could be made according to the construction shown in Fig. 12·3. The conical taper should be at least one-half wavelength long. There is a very good correlation between the degree of mismatch of the materials and the loss per unit length of the materials. For example, the attenuation constants for MP-1548, MP-1826, and MP-1822 are 20, 60, and 110 db/in. respectively.

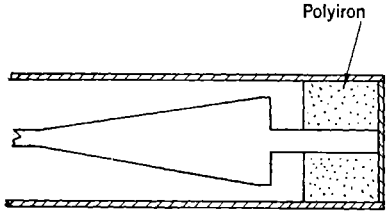

FIG. 12·3.—Proposed broadband polyiron coaxial termination.

TABLE 12·2.—IMPEDANCE DATA FOR CYLINDER OF POLYIRON IN 50-OHM, $\frac{7}{8}$-IN. COAXIAL LINE

Crowley material	Z/Z_0 at 11.5 cm	Z/Z_0 at 10.1 cm	Z/Z_0 at 8.9 cm
MP-1826	$0.39 - j0.16$	$0.38 - j0.15$	$0.39 - j0.21$
MP-1822	$0.14 - j0.09$	$0.13 - j0.09$	$0.13 - j0.16$
MP-2884D	$0.42 - j0.18$	$0.39 - j0.20$	$0.39 - j0.25$
MP-1529B	$0.42 - j0.08$	$0.41 - j0.10$	$0.43 - j0.10$
MP-1548	$0.53 - j0.16$	$0.52 - j0.19$	$0.49 - j0.16$
MP-2875D	$0.47 - j0.04$	$0.45 - j0.09$	$0.46 - j0.09$

A design for $\frac{7}{8}$-in. coaxial-line termination which shows promise of extreme bandwidth employs a short length of metalized-glass center conductor in a line with appropriately stepped or tapered outer conductor. Thus far it has been found possible to cover a bandwidth of 7.5 to 30 cm with a maximum VSWR well below 1.20. Such a design is

based on the following considerations. The impedance Z of a coaxial line with shunt conductance and series resistance losses is given as a function of distance along the line x by

$$\frac{dZ}{dx} = (GZ^2 - R) + j\omega(CZ^2 - L), \tag{1}$$

where R, G, L, and C are respectively the resistance, the conductance, the inductance, and the capacitance per unit length of line, and ω is the angular frequency. If it is desired to select a line taper such that Z will have no reactive component, Eq. (1) demands that

$$\frac{dZ}{dx} = GZ^2 - R, \qquad Z = \sqrt{\frac{L}{C}}. \tag{2}$$

Equation (2) dictates the spacing of the conductors as a function of x. If an inner conductor which is a dielectric rod coated with an extremely thin resistive film is considered, it may be said that $G = 0$, and R, because of the thinness of the film, is essentially frequency-independent. If the line is tapered by changing the diameter of the outer conductor b, while keeping the diameter of the inner conductor a constant, then

$$Z(x) = -Rx = 60 \ln \frac{b(x)}{z},$$

where $x = 0$ when $b = a$ and $z = 0$,
or

$$b(x) = ae^{-\frac{Rx}{60}}.$$

Therefore, if the outer conductor is tapered to make contact with the inner conductor at the end of the termination, and if the taper length l is chosen to be

$$l = \frac{Z_0}{R}, \tag{3}$$

the termination should absorb all incident power without reflection at all frequencies. Also, the power dissipation will be constant along the length of taper. It should be noted that, according to Eq. (3), the total resistance of the film should be equal to the characteristic impedance of the lossless coaxial line.

If, for constructional reasons, it is impossible to continue the taper until the outer and inner conductors meet, other means to terminate the tapered line may be used. For example, if the line is terminated in a short circuit, the impedance of the termination is given by[1]

[1] E. Feenberg, "Resistance Attenuators and Terminations," Sperry Report 117, Apr. 10, 1943.

$$\frac{4\pi}{\lambda R} Z(\eta) = \eta - \frac{\eta_0 e^{-j(\eta-\eta_0)}}{1 - \frac{j\eta_0}{2} e^{+j\eta_0} \int_0^{\eta} \frac{e^{-j\eta'}}{\eta'} d\eta'}, \tag{4}$$

where

$$\eta_0 = -\frac{4\pi x_0}{\lambda}, \qquad \eta = -\frac{4\pi x}{\lambda},$$

and the short circuit is placed at $x = x_0$. The real and imaginary parts of Eq. (4) for various values of η_0 may be plotted, and that point at which the short circuit should be placed in order to make Z real and equal to Z_0 may be observed. This construction is not as inherently broadband as the first construction mentioned, nor is the power dissipation constant along the length of taper.

12·2. Low-power Waveguide Terminations with Polyiron.—The variety of low-power waveguide terminations exceeds that of coaxial loads. Those to be discussed are grouped according to the materials used in their fabrication.

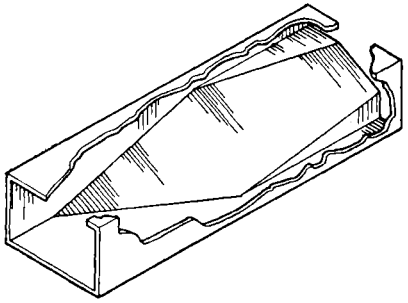

FIG. 12·4.—A well-matched polyiron termination for ½- by 1-in. waveguide.

An excellent polyiron termination has been made for ½-by 1 in. waveguide, using Crowley material MP-2884D, or Chromet 4. It has been found that the double-slant taper used in this construction (see Fig. 12·4) is better than a single taper to either the narrow or the wide side of the waveguide. It has a VSWR less than 1.01 over the 3.13- to 3.53-cm band. A similar termination, made from the same material, has an equally good impedance match in 1.25-cm-band waveguide. Polyiron waveguide terminations are capable of greater power dissipation than most of the terminations of other types that are to be considered, but the size and weight of a polyiron termination make it impractical for waveguides as large as those used at 10-cm band.

The step-matched polyiron piece shown in Fig. 12·5 may be used either as a load or as a bilaterally matched 40-db attenuator in ½- by 1-in. waveguide. It is made from Crowley material MP-2312 (D-1). Its

VSWR specifications are 1.02 or less at 3.3 cm, and 1.06 or less at the edges of a ±6 per cent wavelength band centered at 3.3 cm. As was shown to be true in the case of coaxial-line polyiron matching steps, the waveguide matching steps are also dimensionally critical. Furthermore, small dimensional corrections are usually necessary when loads are machined from a new batch of polyiron material. This must be taken into account when designing dies to be used in pressing the polyiron pieces into approximately the correct shape. A matching step which is centered in the waveguide has been found to be considerably more broadband than an unsymmetrically located step which rests on the broad side of the waveguide.

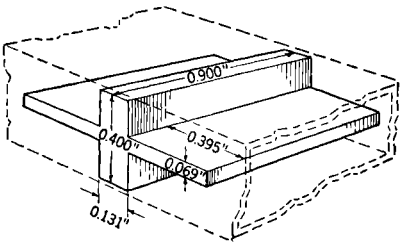

FIG. 12·5.—A step-matched polyiron termination for ½- by 1-in. waveguide.

A compact polyiron termination for use in a 3-cm-band directional coupler has been made from a rectangular block of MP-1826 polyiron, 0.458 in. in width, 0.183 in. in height, and 0.895 in. in length. The block is laid across the waveguide, and rests on a broad side of the waveguide. The waveguide is short-circuited by a metal plate soldered across its end, and *touches* the polyiron block which has been cemented in place. In this design, reflections from the front face of the block are canceled by those from the short circuit, and therefore, broadband matching cannot be expected. The VSWR of the termination is less than 1.15 over the 3.16- to-3.33-cm band. Such a load is to be recommended only when the space limitation is as severe as the impedance-matching requirement.

TABLE 12·3.—IMPEDANCE AND ATTENUATION DATA FOR BLOCKS OF POLYIRON IN ½- BY 1-IN. WAVEGUIDE

Crowley* material	λ = 3.13 cm		λ = 3.33 cm		λ = 3.53 cm	
	Z	db/in.	Z	db/in.	Z	db/in.
MP-2875D	$0.32 - j0.03$	30	$0.29 - j0.03$	30	$0.28 - j0.04$	30
MP-2325	$0.31 - j0.03$	40	$0.28 - j0.06$	30	$0.26 - j0.04$	30
MP-1529B	$0.27 - j0.02$	60	$0.23 - j0.02$	60	$0.22 - j0.04$	50
MP-1548	$0.29 - j0.07$	80	$0.27 - j0.08$	80	$0.26 - j0.08$	70
MP-2312	$0.23 - j0.12$	180	$0.22 + j0.02$	160	$0.20 + j0$	140
MP-2884D	$0.20 - j0.12$	180	$0.19 - j.01$	170	$0.19 - j0.02$	150
MP-1826	$0.21 - j0.12$	210	$0.20 + j0$	190	$0.19 - j0.02$	180
MP-1842	$0.08 - j0.11$	220	$0.07 + j0.06$	220	$0.07 + j0.03$	220

* Henry L. Crowley Co., West Orange, N. J.

Table 12·3 has been included to show the microwave differences among various polyiron materials that can be considered for attenuator or load design in $\frac{1}{2}$- by 1-in. waveguide. The impedance data were more carefully taken than the attenuation data. It is to be noted that, in general, the materials with larger conductance values have larger attenuation constants. The impedances have small reactive components, and while the reactances apparently vary somewhat more with wavelength than in the case of coaxial lines (see Table 12·2), the polyiron impedances are nevertheless surprisingly independent of wavelength.

Only scattered and incomplete data are available, but there is evidence for believing that the voltage standing-wave ratio of a well-matched polyiron load is subject to variation with humidity. The higher the frequency, the more likely this is to be true. Therefore, it is good practice to dry carefully the polyiron pieces in an oven after machining, and to impregnate them immediately with a moisture-resisting lacquer.

12·3. Low-power Waveguide Terminations Which Use Other Lossy Materials.—A well-matched termination for a circular E_0- or H_1-mode waveguide can easily be made by machining a long, sharp-pointed conical taper on a Durez or soft-pine rod of appropriate diameter. The taper length and the rod length for optimum broad-band matching are determined experimentally. For example, a Durez 7421 load for an H_1-mode waveguide of 0.350 in. ID, using a 2.5-in. taper length and a 4-in. over-all length, has a VSWR less than 1.01 over the 1.20- to 1.30-cm band. A soft-pine E_0-load for a tube of 1.150 in. ID, using a taper length of 14 in. and an over-all length of 28 in., has a VSWR less than 1.02 over the 3.13- to 3.53-cm band. An appreciable saving in length can be made by using a 400-ohms-per-square IRC resistance strip for the load element. If this strip is used, a symmetrical V is cut into the end of a rectangular strip of the material, so that the taper is toward the wall of the tube instead of toward its axis. If a taper length of 6 in. and an over-all length of 15 in. are used, the load VSWR can be held under 1.01 over the entire 3.13- to 3.53-cm band. The taper tips must touch the wall of the tube.

Well-matched terminations for rectangular waveguide may also be made from tapered IRC resistance strip. The strip is placed in the center of the waveguide, aligned in the direction of the electric field, and except for the tapered section, touches the two broad walls of the waveguide. The taper may be a single taper which touches one wall at the tip of the taper, or a double taper which tapers from both broad walls to the axis of the waveguide. A single taper is usually used except in flexible waveguide, but terminations of either type can be made which are well matched over a broad band. In order to combat the flexibility of the strips and to shorten the length required to provide the attenuation

necessary for low voltage standing-wave ratios, it is advisable to use a combination of two strips side by side, glued together, one shifted with respect to the other. Figure 12·6 illustrates these designs. The strips are supported mechanically by the short-circuiting block at the end of the waveguide.

If loads are made from IRC strip, care must be taken to obtain smooth edges, and to avoid chipping off the resistive coating. This can be done by using a shearing cutter similar to those used for cutting paper and sheet metals. It may be necessary to remove rough edges and chips by hand-smoothing the taper on emery cloth or sandpaper. The taper

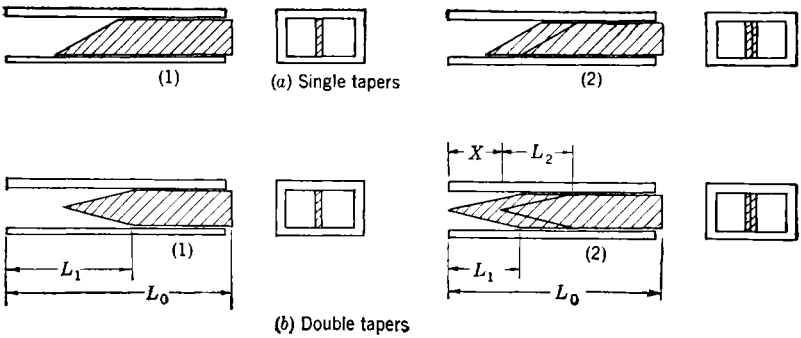

FIG. 12·6.—Various designs of IRC resistance loads for rectangular waveguide.

length is not critical except at wavelengths which are near the cutoff wavelength of the waveguide. Typical tolerances call for $\pm \frac{1}{2}°$ in the taper angle, and $\pm \frac{1}{4}$ in. in taper length, at 3-cm band. In general, the tolerances become larger as the taper length is increased. In all single-taper designs the end of the taper must rest flat against the waveguide wall. A small clearance, a few thousandths of an inch, is allowable between the other edge of the strip and the wall. The vertical position of the tip in the double-taper designs is not critical.

A taper length of one-half guide wavelength or slightly longer is satisfactory for single-taper designs. The attenuation per unit length A of an IRC strip in rectangular waveguide decreases linearly with increasing resistivity Ω measured in ohms per square. The following formulas have been determined empirically, and have been checked experimentally for the range of 100 to 800 ohms per square. For $\lambda_0 = 3.3$ cm, 1- by $\frac{1}{2}$-in. waveguide, 0.050-in. wall,

$$A = 15.7 - 1.5\frac{\Omega}{100} \quad \text{db/in.}$$

For $\lambda_0 = 10.0$ cm, 3- by $1\frac{1}{2}$-in. waveguide, 0.080-in. wall,

$$A = 5.0 - 0.38\frac{\Omega}{100} \quad \text{db/in.}$$

The over-all lengths of single-taper loads can be estimated by using these formulas and assuming that the attenuation contributed by the taper is one-half that of an equivalent length of strip which completely fills the waveguide. This assumption has been verified experimentally. It is advisable to allow a small additional length to compensate for the change of attenuation with wavelength. Table 12·4 summarizes the designs involving these strips. Reference should be made to Fig. 12·6 for the significance of the various dimensions.

A very compact termination from IRC strip material can be made by completely blocking off the waveguide with a strip placed normal to the axis of the waveguide. The waveguide is short-circuited at an experimentally determined position which is effectively one-quarter guide wavelength behind the resistive strip. If a 600 ohms per square strip in 1- by $\frac{1}{2}$-in. waveguide is used, it is possible to obtain a load VSWR less than 1.2 over a ± 6 per cent band. At the design wavelength, the VSWR can be brought below 1.05. The strip is introduced through a slot in the narrow side of the waveguide, and cemented in position.

TABLE 12·4.—SUMMARY OF IRC STRIP LOADS IN RECTANGULAR WAVEGUIDE

Line size	Strip material	Band, cm	VSWR over band	Dimensions*			
				L_1	L_2	L_0	X
$1\frac{1}{2}$-in. by 3-in. OD 0.080-in. wall	400 ohms	8 to 10.5	<1.01	$4\frac{1}{2}$ in.		10 in.	
Same	400 ohms	8 to 11.1	<1.02	$4\frac{1}{2}$ in.		10 in.	
Same	400 ohms	8 to 11.1	<1.01	$4\frac{3}{4}$ in.		10 in.	
Same	400 ohms	8 to 12	<1.02	$4\frac{3}{4}$ in.		10 in.	
Same	600-ohms long strip 400-ohms short strip	9 to 11.1	<1.01	$4\frac{3}{4}$ in.	$4\frac{1}{2}$ in.	8 in.	$2\frac{1}{8}$ in.
Same	600-ohms long strip 400-ohms short strip	8 to 12	<1.03	$4\frac{3}{4}$ in.	$4\frac{1}{2}$ in.	8 in.	$2\frac{1}{8}$ in.
$\frac{1}{2}$-in. by 1-in. OD 0.050-in. wall	100 ohms	3.13 to 3.53	<1.01	$3\frac{1}{4}$ in.		5 in.	
$\frac{5}{8}$-in. by $1\frac{1}{4}$-in. OD 0.062-in. wall	100 ohms	3.13 to 3.53	<1.01	$2\frac{1}{4}$ in.		5 in.	

* Refer to Fig. 12·6.

The IRC strip material can be easily damaged by the high temperatures associated with excessive average-power dissipation or soldering operations on the metal casing. It is usually easy to recognize an overheated strip by the small welts that rise on the resistive film. Because of this limitation it has been necessary in certain load designs for directional couplers to use other materials such as Uskon cloth, and Synthane. Uskon cloth of 6-ply lamination can be cut into a single-taper load

resembling the IRC strip loads shown in Fig. 12·6. In this application the material has an attenuation constant of approximately 30 db/in. at 3-cm band and 10 db/in. at 10-cm. band. Reasonably short taper lengths provide VSWR's less than 1.10 over a ± 5 per cent band. In addition to its ability to withstand higher temperatures than the IRC strip material, Uskon is more durable with respect to shock and vibration. However, the electrical properties of the material appear to vary con-

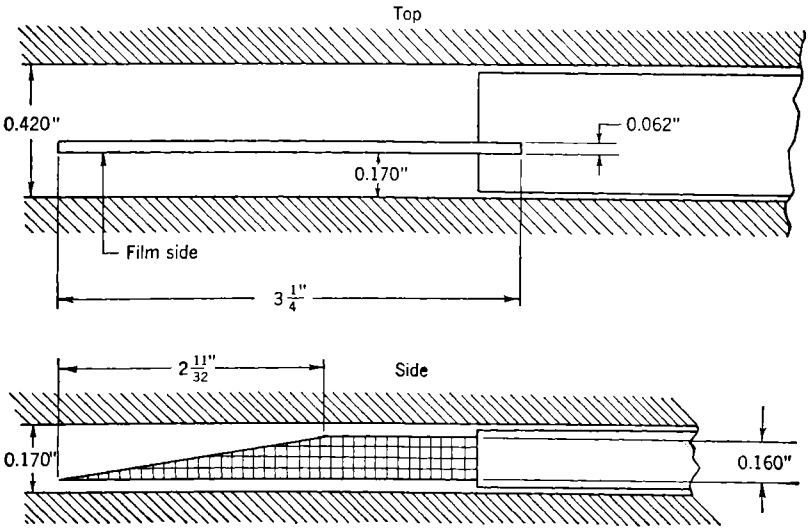

FIG. 12·7.—A metalized-glass load for 1.25-cm waveguide.

siderably from batch to batch. At high relative humidities the 6-ply cloth tends to split apart. The application of a silicone lacquer coating to the cloth would probably prevent this, but it has not yet been tried. Synthane is a material similar to Uskon, but it is mechanically stiffer than Uskon cloth of the same thickness and resistivity.

12·4. Low-power Terminations Using Metalized Glass.—A thin, evaporated Nichrome film sandwiched between a glass-plate support and a thin protective magnesium fluoride film can be used in place of the IRC strip material. It is more expensive than the IRC material although a preferable substitute since it has good mechanical rigidity and is unaffected by moisture, and aging. Figure 12·7 shows a 1.25-cm-band load of this type which has a VSWR less than 1.01 over the 1.215- to 1.285-cm band.

In developing this termination, tests were made first with a No. 774 Pyrex glass plate of 0.038 in. thickness. A film resistivity of approximately 300 ohms per square was found to be optimum according to

impedance-matching data taken with an untapered film. However, the taper length and over-all length required to meet a VSWR < 1.01 specification were found to be excessive, and not at all compatible with the mechanical strength of such a thin glass plate. In order to increase the mechanical strength, a thicker, soft-glass plate was tried. The thicker plate has a second advantage in that the guide wavelength is reduced because of the larger permittivity of soft glass as compared with Pyrex. If no detrimental field distortion is incurred, a reduction in the necessary taper length can be expected. Similar reasoning may be applied to the film resistivity. Although a film resistivity close to the characteristic impedance of the waveguide will, in general, match better than a smaller resistivity, its rate of attenuation will be much smaller. It may therefore have to be made objectionably long in order to provide sufficient attenuation to eliminate effectively reflections from the short circuit of the mechanical holder. The final soft-plate design is that shown in Fig. 12·7. The film resistivity is 110 ohms per square. Note that the strip is not centered with respect to the waveguide, but is displaced to the side where it has been found experimentally that lower voltage standing-wave ratios can be obtained.

12·5. High-power Coaxial-line Loads.—The first high-power 10-cm load made in $\frac{7}{8}$-in., 50-ohm coaxial line used Aquadag-coated sand as a dissipative medium. Two quarts of 20 to 30 testing sand[1] are stirred thoroughly in a fluid suspension consisting of $\frac{1}{2}$ pt. of Aquadag in $\frac{1}{2}$ gal. of water. The heavily-coated sand is then drained and allowed to dry in shallow trays at an elevated temperature. A 50-50 mixture of coated and uncoated sand is used as a filling material for the load. It is necessary to prepare a reflectionless, temperature-resisting bead to hold the sand within the line. Of the several bead designs investigated, the best appeared to be a $\frac{1}{16}$-in.-thick steatite washer which is held in place by Insalute Cement applied around its edges. After installation of the steatite bead, the sand is poured in from the rear end of the line and compacted by gentle tamping. A metal end plug is then soldered in place to terminate the line. In order to preserve the characteristic impedance of the line in the region of the sand which has a relatively high permittivity, the inner conductor of the line is undercut throughout the entire 9-in. length occupied by the bead and sand mixture. If a dozen 3-in.-diameter radiating fins equally spaced along the sand-filled section of line are used, it is possible to dissipate 60 watts average power and 50 kw pulse power. Unfortunately, the load was difficult to reproduce and the reject percentage was high even for a lenient maximum VSWR specification of 1.10 or less over the 8.5- to 11.5-cm band.

The sand load just described suffers in two respects because it does

[1] Ottawa Silica Co., Ottawa, Ill.

not make use of steps or of a continuous taper at its input end. Steps or a smooth taper facilitate impedance-matching and tend to allow a more uniform power dissipation along its length. In contrast, the sand load gets very hot at its input end where half of the power is dissipated in the first 3 db of attenuation. It may easily be shown that if the power dissipation is to be uniform along the length of the load, the attenuation constant must vary with position along the line according to the following formula

$$\alpha = 10 \log_{10} \frac{y + 1}{y}, \tag{5}$$

where $y = 0$ at the short-circuited end of the load, and where the total length of the load is large compared with the unit length. The formula may be applied either to steps or to a smooth taper. For example, if matching steps are used, the attenuation for successive steps of equal length, counting backwards from the short-circuited end of the load, should be ∞, 3 db, 1.8 db, 1.25 db, 1.0 db, and so forth, for as many steps as are to be used. The inclusion of additional steps does not alter the attenuation per step of the rear steps. Equation (9) offers an alternative expression for the attenuation constant of a line continuously tapered for uniform power dissipation along its length. This equation, unlike Eq. (5), had no restriction on the magnitude of a "unit length" as compared with the total length of the load. This equation is useful principally in step-matched constructions. It is customary to step or taper toward the outer rather than toward the inner conductor, since the outer conductor can more effectively carry away the heat developed in the load. Furthermore, a rough lip on the taper edge has less effect on the voltage standing-wave ratio of the load if the taper is carried to the outer conductor where the fields are weak rather than to the center conductor.

Figure 12·8 shows a $\frac{7}{8}$-in. coaxial-line load which makes use of a straight, conical taper to the outer conductor. The load material first used with this design was polyiron made resistant to high temperatures by a ceramic binder. However, it was impossible to mold the taper lip properly, and the machining of such a taper into polyiron was objectionably difficult in production. Consequently, it became necessary to choose another load material, and the final choice was a mixture of powdered flake graphite (Dixon's No. 2 grade) and X-Pandotite cement.[1] A mixture of 40 per cent graphite and 60 per cent cement by weight is ball-milled for two hours, care being taken to keep the cement dry to ensure satisfactory milling. Water is then added to the mixture—two parts

[1] X-Pando Corporation, Long Island City, N.Y.

of water to five parts of powder, by weight—and the whole is mixed thoroughly. The mixture is poured into a coaxial mold and allowed to set, partially before the tapered center mold is withdrawn to permit hard setting over a 24-hr period. The outer cylinder of this mold is the outer conductor of the load line. Then follows a 6-hr oven-drying treatment at 200°C. After the center conductor of the line is installed, the load material is impregnated with a fluid Dow-Corning resin No. 2102, allowed to air-dry for a few hours, and then oven-baked at 200° to 250°C for a period of 8 hr. At the end of this baking treat-

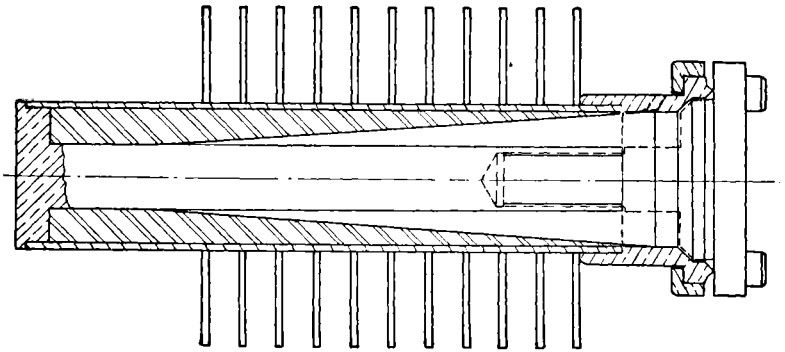

FIG. 12·8.—Sketch of a graphite-cement high-power coaxial-line load.

ment, all toluene from the resin should have evaporated. Benzene may be used to clean any resin from the coaxial-line coupling. The brass casing is painted with a dull black finish which is capable of withstanding a temperature of 200°C. The cement adheres well to the brass casing, and does not crack at temperatures of approximately 200°C. The load is rated at 100 watts average and 200 kw pulse power. The production VSWR specification is less than 1.10 over the 8-to-12-cm wavelength band. Laboratory-built models were all well within this specification. The high-temperature drying and the resin impregnation of the cement are essential, since absorbed water in the load has been found to affect appreciably the attenuation constant and to alter the impedance match.

Some helpful hints can be offered to facilitate the design of matching tapers for lines (coaxial or waveguide) which are filled with an attenuating dielectric. If the experimentally determined wavelength for smallest voltage standing-wave ratio for a given taper is *longer* than the wavelength at which optimum match is desired, a shorter taper and a material of higher conductivity (therefore larger attenuation constant) should be used in the line. Conversely, if the taper matches best at a wavelength

shorter than the design wavelength, a longer taper and a material of smaller attenuation constant should be used.

12·6. High-power Waveguide Loads.—In the microwave region more work has been done on high-power waveguide loads than on coaxial loads. There are several reasons for this. Waveguide has a greater pulse-power capacity than coaxial line, the skin loss in the metal walls of the line is smaller in waveguide than in a coaxial line, and the shortest wavelengths in the microwave region demand an unmanageably small coaxial line which is much more difficult to build than an appropriate rectangular waveguide. For these reasons there has been a growing trend, particularly for high powers and short wavelengths, to use waveguide loads.

A sand load for the 10-cm band in waveguide $1\frac{1}{2}$ by 3 in. by 0.080-in. wall has been made from the same sand mixture used in the previously described coaxial-line high-power load. Impedance-matching is obtained by tapering the input end of the sand load, holding the sand in the tapered position by a $\frac{1}{8}$-in. Transite plate which is made fast by Insalute cement. The taper is from narrow wall to narrow wall of the waveguide; the taper length, measured in the direction of the waveguide, is 12 cm. The load has a VSWR less than 1.1 over the 8.5- to 11.5-cm band, and is rated for 300 watts average and 300 kw pulse power. The power limitation of the load is the inability of the Transite material to withstand high temperature. The waveguide tapered sand loads have more reproducible impedance characteristics than do the coaxial sand loads, but all of them suffer from varying impedance as the moisture absorption of the sand changes. Moreover, their construction permits shock and vibration to break the sand seal, or even to change the match of the load because of a change in the compactness of the sand. A similarly constructed load for 3 cm with a thick sheet of mica replacing the Transite plate, has a VSWR less than 1.1 over a ± 5 per cent band. It is rated for 70 watts average and 150 kilowatts pulse power.

The Bell Telephone Laboratories have produced a satisfactory porcelain-silicon load[1] for use in $\frac{3}{8}$-in.-by-$1\frac{1}{4}$-in. waveguide. A combination of 30 per cent silicon in porcelain provides an attenuation of 50 db for a 6-in. length of load, $4\frac{1}{2}$ in. of which is a continuous linear taper from one broad side of the waveguide to the other. Silicon is not readily obtainable, but 220-mesh silicon carbide has been found to be a good substitute. This material withstands high temperatures without oxidation, and has good thermal shock and thermal conductivity characteristics. Because of the relatively large (10 per cent) shrinkage when the mixture is fired at 1250°C, the fired ceramic

[1] S. O. Morgan, "Ceramic Attenuators for Dummy Loads," BTL MM 44-120-36, Mar. 1, 1944, p. 2.

pieces must be ground to exact dimensions. The grinding operation is a rather tedious one, particularly in the vicinity of the taper tip. If the taper is sufficiently long, the standing-wave ratio depends primarily on the thickness of the tapered edge. Although it is desirable to make this edge as thin as possible, it is not feasible to grind it to a feather edge because of excessive breakage in manufacture and use. As a compromise, an edge thickness of $\frac{1}{64}$ in. was chosen. The VSWR of such a load can be less than 1.05 over an appreciable bandwidth. It is capable of dissipating 200 watts average and 200 kw pulse power. The ground ceramic pieces may be cemented into the waveguide with Insalute cement or Pliobond.

The most novel, and probably the most satisfactory, method of constructing a waveguide high-power load is to use waveguide walls which are poor conductors instead of using attenuating material which fills the waveguide. Such a construction facilitates a more effective removal of the heat generated in the load, and is not as subject to pulse-power breakdown (arcing) as are the designs which use filling materials in the waveguide. It has been shown experimentally that satisfactory impedance-matching can be obtained with this construction. Also, the waveguide walls may be tapered in order to effect a reasonably uniform power dissipation along the length of the load. The conditions under which a good impedance match in waveguide may be expected can be determined by comparison of the waveguide with a low-frequency transmission line.

The characteristic impedance of a dissipative transmission line is in general a complex quantity given by

$$Z_0 = \sqrt{\frac{R + j\omega L}{G + j\omega C}}.$$

However, Z_0 is real and equal to $\sqrt{L/C}$, the characteristic impedance of a nondissipative line of the same size, if

$$\frac{R}{L} = \frac{G}{C}. \tag{6}$$

The series resistance losses are proportional to the square of the current, and hence are proportional to the square of the magnetic field strength. The shunt conductance losses are proportional to the square of the voltage in the line and hence proportional to the square of the electric field strength. From these facts it can easily be shown that the condition expressed by Eq. (6) is equivalent to the statement that the series resistance losses are exactly equal to the shunt conductance losses in the dissipative medium.

The L and C of a line depend to a certain extent on R because of the skin effect which changes the dimensions of the line. Equation (6) is easily applied to the matching of a dissipative to a nondissipative line at low frequencies, since the dimensional adjustments necessary to make the ratio $\sqrt{L/C}$ of the dissipative line equal to that of the nondissipative line do not produce appreciable reflections. When the line dimensions are comparable with the wavelength, however, geometric discontinuities have an appreciable effect. Although it has not been possible to derive the condition for impedance match from theoretical considerations, it is likely that this relation is given by

$$\frac{\lambda_c}{\lambda} = \frac{2a}{\lambda} = \sqrt{1 + \frac{2b}{a}}. \tag{7}$$

Table 12·5 shows values of the parameters calculated from this equation.

TABLE 12·5.—APPLICATION OF EQ. 12·7 TO SEVERAL STANDARD WAVEGUIDES

Waveguide, in.	b, in.	a, in.	λ_c, cm	λ_c/λ	Calculated λ, cm
$1\frac{1}{2} \times 3$	1.340	2.840	14.4	1.40	10.3
$\frac{1}{2} \times 1$	0.400	0.900	4.57	1.38	3.32
$\frac{1}{4} \times \frac{1}{2}$	0.170	0.420	2.13	1.35	1.58

Data taken on loads of this type have verified the usefulness of Eq. (7) as a design formula. A typical 10-cm laboratory-made load gave VSWR's of 1.015 at 10 cm, 1.04 at 8 cm, and 1.06 at 12 cm. A typical 3-cm laboratory-made load gave VSWR's of 1.01 at 3.3 cm, and 1.025 at 3.1 and 3.5 cm. A load in $\frac{1}{4}$- by-$\frac{1}{2}$ in. waveguide gave a VSWR of approximately 1.07 at 1.25 cm, and progressively lower values as the wavelength was increased toward 1.58 cm. No oscillator was available that would operate in the wavelength range for which the voltage standing-wave ratio was a minimum. It has been observed that the input impedance of the lossy waveguide at the calculated wavelength is very nearly resistive, but slightly greater than unity. This can be accounted for by the effective increase of the b/a ratio caused by an appreciable skin depth in the dissipative walls of the load.

Figure 12·9 shows the broad-side and narrow-side views of the 3-cm-band load with dissipative walls. The 10-cm-band load has a similar construction. The dissipative material used in this design is a mixture of 35 per cent Portland cement and 65 per cent Dixon's No. 2 powdered flake graphite. It should be noted, however, that Eq. (7) assumed no specific dissipative material. The choice of Portland cement and graphite is dictated not so much by an impedance-matching consideration as by

considerations of thermal shock, durability of the load, the adhesive bond of the material to the metal walls of the waveguide, and ease of casting the mixture. Excessive graphite results in a crumbly material; too little graphite makes the attenuation constant too high.

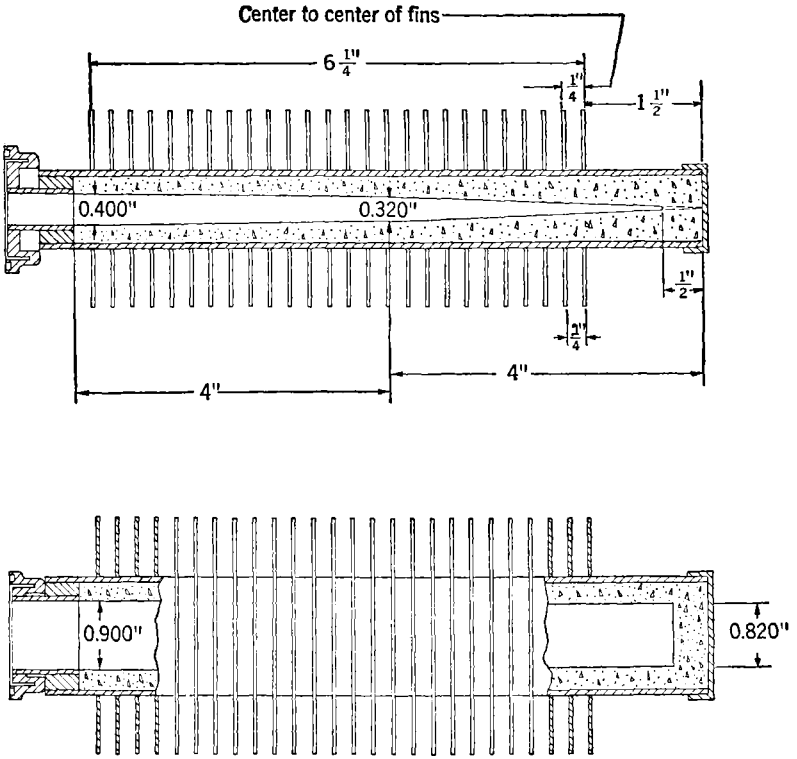

FIG. 12·9.—Construction of a 3-cm-band waveguide high-power load that uses attenuating walls.

The graphite-cement mixture is ball-milled for at least two hours and is then thoroughly mixed with water in the proportions of three parts water to four parts of dry mixture, by weight. A properly shaped center mold is inserted into the load casing, and the graphite-cement-water mixture is poured into the back end of the casing so as to fill the space between the waveguide walls and the center mold. The load should be shaken during the casting process to facilitate the removal of air bubbles. After the cement has set for approximately 4 hr, the center mold may be removed. After an additional 48-hr setting period, the load is allowed to dry for 6 hr in an oven at 200°C. This is followed

by impregnation with Dow-Corning Resin No. 2102. The baking of the impregnated load to remove the toluene, and the associated steps in this process are conducted according to the procedure outlined for the coaxial high-power load. It is extremely important that the transition between metal wall and graphite-cement wall inside the load should be smooth. No gap can be tolerated and small steps at the junction should be filed off.

If the transition has been made smoothly, as has been emphasized, the load accomodates, without breakdown, pulse-power levels almost as

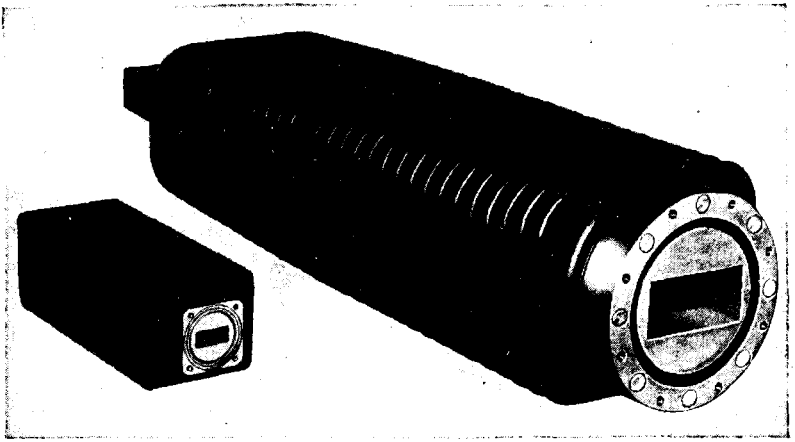

FIG. 12·10.—Photograph of the 10-cm-band and 3-cm-band dissipative-wall high-power loads.

great as those which the nondissipative waveguide accepts. Production specifications, however, have been made more lenient. The 10-cm-band load is rated for 2 Mw pulse power and 1 kw average. The 3-cm-band load is rated for 0.5 Mw pulse power and 0.2 kw average. As may be seen from Fig. 12·10, ample radiating fins are used to dissipate the heat generated in the load. Production voltage-standing-wave-ratio specifications have also been made rather lenient. The 10-cm-band load must have a VSWR less than 1.1 from 8 to 12 cms. The 3-cm-band load has a similar specification of 1.1 or less for the 3.13- to 3.53-cm band. The laboratory-made models were considerably better matched than these specifications require. The attenuation constant of the material is approximately 2 db/in. at 3-cm band, and 1 db/in. at 10-cm band. Experiments indicate that it is unaffected by the input-power level.

The dimensions of the load should be adjusted, in so far as it is possible. to obtain a uniform power dissipation on all four walls of the waveguide and throughout the length of the dissipative section. It may be shown

that the density of power dissipation is constant over the four walls of the waveguide when

$$\frac{\lambda_c}{\lambda} = \sqrt{2}. \tag{8}$$

When this condition is satisfied, the proper b/a ratio becomes equal to one-half, which is a very convenient value. It should be noted from Table 12·5 that λ_c/λ for standard waveguide sizes does not differ greatly from the preferred value given by Eq. (8).

In order to effect uniform power dissipation along the line, it is necessary to vary, in a prescribed manner, the attenuation constant with x, the distance along the waveguide. This can be done more easily by tapering the walls of the waveguide than by varying the composition of the material as a function of x. It is possible to derive an expression for the attenuation constant α as a function of x by starting with the well-known equation

$$\frac{dP_x}{dx} = -2\alpha P_x,$$

where P_x represents the power in the dissipative line at the point x. The equation is integrated from $x = 0$ to $x = x$, and the constant of integration is determined by setting $P_x = P_0$ when $x = 0$. Thus

$$P_d = 2\alpha P_x = 2\alpha P_0 \exp\left(-2\int_0^x \alpha\, dx\right),$$

where P_d represents the power dissipated per unit length of line. But

$$\frac{P_d}{2P_0} = \alpha_0,$$

where α_0 must be a constant if P_d is to be a constant, and is equal to the value of α at $x = 0$. This leads to the simplified form

$$\ln\left(\frac{\alpha}{\alpha_0}\right) = 2\int_0^x \alpha\, dx.$$

The solution to this equation is

$$\alpha = \frac{\alpha_0}{1 - 2\alpha_0 x}. \tag{9}$$

Equation (9) specifies how α should vary with x, but it is also necessary to have an expression for α as a function of a and b, the waveguide dimensions, if Eq. (9) is to be used effectively. This form is

$$\alpha = \frac{k}{a} \cdot \frac{\dfrac{a}{2b} + \left(\dfrac{\lambda}{2a}\right)^2}{\sqrt{1 - \left(\dfrac{\lambda}{2a}\right)^2}}, \tag{10}$$

where k is a constant that need not be evaluated.

At this point, it is wise to summarize the conditions which dictate the design of the load. Equation (7) specifies the impedance-matching condition. Equation (9) specifies α as a function of x for uniform power dissipation along the length of the load, and Eq. (10) dictates the tapering of the dimensions a and b in order to meet the condition stated by Eq. (9). Equation (8) specifies the condition necessary for all four walls of the dissipative waveguide to have the same density of power dissipation. There is also the additional consideration that the internal shape of the load must be such that the center mold used in the casting process can easily be withdrawn from the waveguide.

Since there are essentially only three variables with which to work, a, b, and x, all of the desired conditions cannot be met simultaneously. The compromises made in the design of the 3-cm- and 10-cm-band loads are the following. Since a low voltage standing-wave ratio is usually more essential than uniformity of power dissipation, the linear tapering of the dimensions a and b for the first 5 to 8 db of attenuation is made to conform with the condition expressed by Eq. (7). The tapering must be slight in order to avoid bringing the waveguide too near cutoff by making the a dimension too small. By taking differentials in Eq. (7) it may be shown that, to a first-order approximation, a linear tapering of the dimension a demands a linear tapering of the dimension b. If Eq. (7) is obeyed throughout the first few decibels of attenuation, no serious effect on the input voltage standing-wave ratio will be noticed if, for the remainder of the load, emphasis is given to distributing the losses more evenly along the length of the waveguide. In other words, Eq. (7) is discarded in favor of Eq. (9) for the remainder of the length. It should be noted from Eq. (10) that either a or b or both may be varied to get the value of α demanded by Eq. (9). Most of the variation is taken in the b dimension. In the final load design the a dimension is given a slight linear taper throughout the entire length of the load, whereas the taper on the b dimension changes abruptly after several decibels, when making the transition from an impedance-matching to a uniform-power-dissipation condition.

The same material used in constructing the dissipative-wall waveguide load can also be used for making a filled waveguide load. If the waveguide is properly tilted when the cement-graphite mixture is allowed to dry, the desired taper can be automatically cast. As previously mentioned, the filled waveguide load has less desirable electrical characteristics than the dissipative-wall load; however, it is more easily made.

A variation on the above theme was introduced in the design of a 1.25-cm-band waveguide load. It was felt that additional mechanical strength and a more gradual power dissipation could be achieved by introducing loss only in the narrow sides of the waveguide. Furthermore, lower voltage standing-wave ratios are possible in this design

because, as has been shown, the dimensions of standard 1.25-cm-band waveguide are not correct for impedance-matching at 1.25 cm if all walls of the waveguide are made to attenuate. To increase the mechanical strength of the load, the use of a continuous lossy wall was abandoned for a lattice structure in which sections of dissipative material $\frac{5}{16}$ in. long are separated by sections of conductor $\frac{1}{16}$ in. long. The attenuation

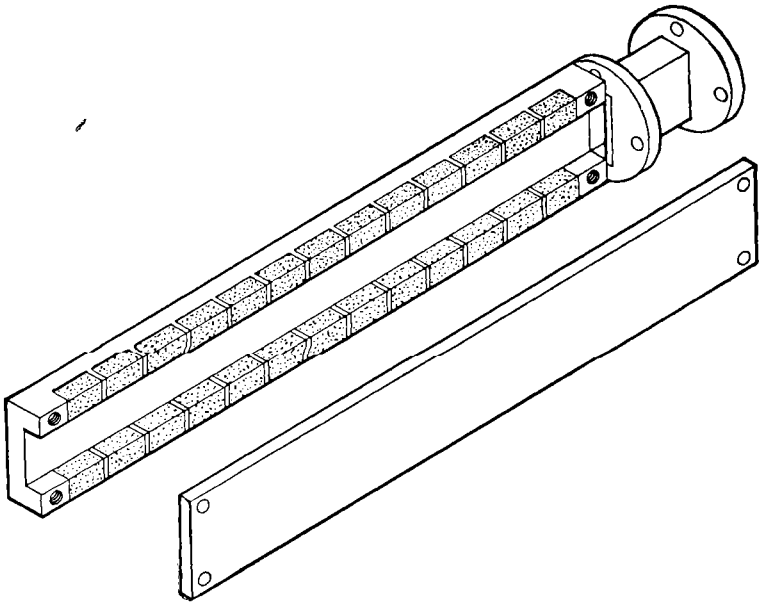

FIG. 12·11.—1.25-cm-band waveguide high-power load.

of a load 5 in. long was approximately 20 db. Figure 12·11, with a broad side of the waveguide removed, explains this construction.

The dissipative material consists of a mixture of a metal powder and a cement. Iron powder gave lower voltage standing-wave ratios than either nickel or nickel-copper mixtures. Consequently, a mixture of iron powder and X-pandotite was chosen as the attenuating material for the load. The iron powder is very fine, and presumably has grain dimensions which are less than the skin depth in iron at 1.25 cm. To a 4-to-1 mixture by weight of X-pandotite and iron powder (Cenco hydrogen-reduced iron) is added enough water to make a workable paste. After the load lattice is filled by the cement, the cement is allowed to harden for a few hours at 200°C. To protect the load material against moisture absorption it is coated with a 2 per cent solution of silicone (Dow-Corning Fluid No. 200) in carbon tetrachloride.

Production models of the load have a VSWR less than 1.1 over a band of ±2 per cent centered at 1.25 cm. The load absorbed, without breakdown or other ill effects, the highest pulse power, 115 kw, and the highest average power, 35 watts, available at the time of test. At these power levels no radiating fins need to be used.

GENERAL LABORATORY ATTENUATORS

By E. Weber

At microwave frequencies, practically all dielectric materials that are mechanically satisfactory absorb a considerable amount of electromagnetic power, and therefore, can be used as attenuating materials in either coaxial or waveguide transmission systems.

12·7. Cables as Coaxial Attenuators.—One of the most common, and also one of the most practical, dissipative attenuators is a piece of high-frequency coaxial flexible cable, usually constructed with a high-resistance inner conductor of nichrome wire. A description of cables of various types and their general characteristics as transmission lines is given in Vol. 9, Chap. 5. The old cables, with solid rubber dielectrics, had rather high power factors and the losses varied appreciably with changes in temperature. The recent cables have solid polyethylene insulation, a low-loss dielectric developed in England, which is much more stable and varies less with temperature.

Theoretically, attenuation should vary with wavelength in accordance with the form

$$\alpha = \frac{p}{\sqrt{\lambda}} + \frac{q}{\lambda}, \tag{11}$$

where p and q are constants; p indicates essentially the conductor losses which are proportional to the square root of frequency, whereas q indicates essentially the dielectric losses, which are directly proportional to frequency. Thus, for the low-loss cable RG-9/U, the coefficients are numerically $p = 0.392$, $q = 0.360$, for the wavelength λ in cm, which lead to values of α in db per foot.[1] For the high-loss cable RG-21/U, the coefficients are $p = 2.4$, $q = 0.81$, and indicate the larger contribution of the high-resistance inner conductor. The attenuation values were obtained at the Radiation Laboratory from measurements made at room temperature at two wavelengths, as shown in Table 12·6. The values of the coefficients can be used for approximate determination of α at other wavelengths down to wavelengths corresponding to several hundred megacycles per second.

[1] F. E. Ehlers, "Attenuation of RG-9/U Cable as a Function of Temperature and Frequency in the X-Band," RL Report 754, June 18, 1945.

TABLE 12·6.—CABLE ATTENUATION AS FUNCTION OF WAVELENGTH

Kind of cable	Type	Measured attenuation in db/ft		Coefficients of Eq. (11)	
		at λ = 10 cm	at λ = 3.30 cm	p	q
Low-loss cable	RG-9/U	0.16	0.326	0.392	0.360
High-loss cable	RG-21/U	0.83	1.60	2.40	0.81

TABLE 12·7.—MEASURED ATTENUATION VALUES OF MICROWAVE CABLES

Cable type	Manufacturer	Characteristic impedance Z_0 (ohms)	Attenuation in db/ft as function of	
			wavelength	temperature
D163296 (obsolete)	BTL	50 (nominal)	$9.55/\lambda$ 8.5 cm $< \lambda <$ 11.5 cm at T = 26°C	0.74 + 0.0082T 25°C $< T <$ 85°C at λ = 10 cm
RG-21/U	BTL	52 (approx.)	$2.64/\sqrt{\lambda}$ 8.7 cm $< \lambda <$ 12.6 cm at T = 26°C	$0.834 = 0.054 \times (T - \frac{8}{100})^{\frac{1}{2}}$ $-40°C < T <$ +60°C at λ = 10 cm
RC-21/U	BTL	52 (approx.)	$5.3/\lambda$ 3.12 cm $< \lambda <$ 3.53 cm at T = 26°C	$1.677 - 0.09 \times (T + \frac{50}{100})^{\frac{3}{4}}$ $-46°C < T <$ 89°C at λ = 3.23 cm
RG-9/U	Federal Tel. and Radio Co.	52 (approx.)	$1.08/\lambda$ 3.14 cm $< \lambda <$ 3.56 cm at T = 26°C	See text

However, as the empirical formulas in Table 12·7 indicate, the variation over narrower wavelength ranges can be simplified with closer approximation to measured values. This is particularly true for the shorter wavelengths where the braid of the outer conductor apparently influences the attenuation values rather markedly. For this reason, the cables must be securely anchored during measurements to avoid flexing. It was found that the attenuation could easily be varied from 5 to 10 per cent by moving the cable; it was also observed that if the cable were disturbed at all, a period of several minutes was required to allow the attenuation to stabilize. Flexure near the fittings can be particularly troublesome and can cause much larger errors in measurement.

The variation of attenuation with temperature is also indicated in Table 12·7 insofar as reliable results could be obtained. At the shorter wavelengths, temperature cycling produces hysteresis effects with permanent increases in the attenuation values. Thus, RG-9/U cable

showed, after about nine temperature cycles from room temperature to 65°C, a permanent increase of the losses of about 0.06 db per foot to a final value of about 0.40 db per foot. Similarly, a hysteresis effect occurs at low temperatures. Moving and shaking the cable after or during temperature cycling usually causes a sudden increase in the attenuation of about 0.01 db per foot. Such erratic values in the attenuation have been attributed to variation in the contact resistance between the braid wires, and have been observed only at the highest range of frequencies at which these cables can be used, namely at or near 9000 Mc/sec.

The input impedance of cables was originally chosen to be close to the standard characteristic-impedance values of coaxial transmission lines. However, the actual value of cable impedance varies from 52 to 48 ohms for cables with a nominal characteristic impedance of 50 ohms. If a cable of 52-ohm impedance is connected to a $\frac{5}{16}$-in. coaxial line of 49.6 ohms it leads to an unavoidable VSWR of 1.047. Careful measurements have also shown, particularly in low-loss cables, a periodicity

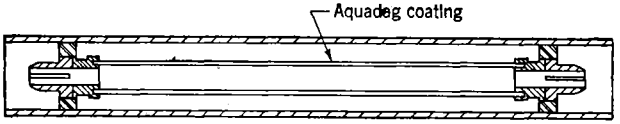

FIG. 12·12.—Carbon-coated coaxial attenuator.

effect introduced by the production method which causes large and rather sharp VSWR maxima of 1.4 or higher at some wavelengths between 8.4 cm and 10.6 cm. Lesser maxima occur at the harmonic multiples of the corresponding frequency. Finally, the input impedance can vary appreciably as a function of frequency since the connectors have to be considered an integral part of the cable assembly for testing and use. The characteristics of cable connectors are described in Vol. 9, Chap. 5.

Thus, while cable has the unquestioned advantage of simplicity for providing attenuation, care has to be exercised in any assumption of its attenuation or input-impedance value. It has the added advantage of large power capacity, but becomes bulky if large values of total attenuation are required.

12·8. Fixed Coaxial Pads.—One of the earliest attenuating materials used in the microwave region was Aquadag, a colloidal suspension of fine carbon powder. For use in coaxial lines, it is painted on a glass or ceramic rod of the same diameter as the inner conductor of a coaxial system and then dried in a baking oven at about 100°C. If the rod is furnished with standard end bullets and the outer casing with standard couplings for the particular line size, a fixed-value coaxial attenuator is obtained as shown in Fig. 12·12. The values of attenuation obtainable vary with the

thickness of the coating, but it is difficult to control the uniformity of the coating as well as its thickness. For attenuations up to about 8 db, the voltage standing-wave ratio is generally tolerable, and increases with attenuation for a fixed film length. The higher the value of attenuation the more dependent it is on frequency; it also depends on humidity and, to a slighter extent, on temperature. Although these attenuators, as laboratory instruments, are simple and convenient, they are restricted to low values of attenuation because of the difficulty of proper impedance-matching, and they are not suitable as standards because of possible changes with moisture.

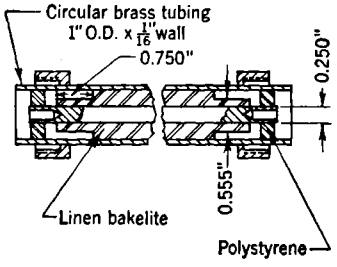

FIG. 12·13.—Coaxial attenuator.

Attenuators with higher values of attenuation in coaxial systems have been designed with good matching characteristics by combining carbonized shunt disks with series rods in II- or T-network fashion. The very close tolerances required in order to achieve desirable wideband performance have militated against more widespread use of these attenuators. Designs up to 500 and possibly 1000 Mc/sec are available at Bell Telephone Laboratories, and a few models have been built.

Fixed coaxial attenuators have also been produced by filling the space between inner and outer conductor with a lossy dielectric material or with a dispersion of conductive particles in a neutral binder. Practically all of these materials are described in greater detail in Secs. 1 to 6, inclusive, as illustrations of well-matched transmission-line terminal loads. For values of attenuation of 20 db of more, the matching shapes which have been described can be directly copied, since the reflection from the far end of the attenuator will be insignificant and without effect at the input end. For values of attenuation below 20 db, the matching sections must be modified in order to minimize or eliminate this reflection. As in the original design, only procedure by trial and error will lead to a satisfactory solution.

One illustration, Fig. 12·13 shows the construction of a fixed attenuator pad for a 75-ohm transmission system with linen Bakelite as the lossy dielectric.[1] The matching section is designed for a wavelength of 10 cm and a relative dielectric constant of approximately $k_e = 4$. Instead of Bakelite, either mahogany wood or Transite could be used. Both the wood and the Transite have about the same loss factor as Bakelite, but are even more subject to the influence of humidity than is Bakelite.

[1] Used by Sperry Gyroscope Co., Garden City, Long Island, N. Y.

Of course, a coating of a sealing, moisture-proof varnish can be used to reduce the effect of humidity, although usually its effect cannot be eliminated entirely.

Other materials that have been used are Durez 7421, which is a thermosetting plastic, and various polyiron materials.

12·9. Fixed Waveguide Attenuators.—A material of a somewhat different type is the IRC resistance card, a phenol fiber, approximately $\frac{1}{32}$ in. thick, on which is sprayed a mixture consisting of graphite and a binder; the latter volatilizes when heated to about 100°C and leaves a carbon coating of reasonable uniformity and adequate resistance values depending upon the length of baking. It is easy to cut this card material into different shapes and to use it, particularly in waveguides, as a power-

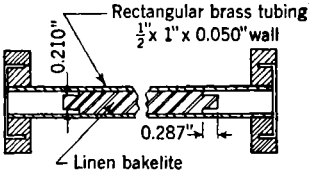

FIG. 12·14.—Waveguide attenuator.

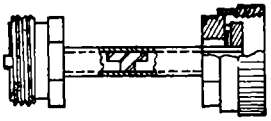

FIG. 12·15.—Polyiron waveguide pad for 1.25 cm.

absorbing element. In the form of a tapered vane, it can be placed in the center plane of the waveguide parallel to the small dimension and used for small power levels as a fixed attenuator. Data on the measured attenuation rates, voltage-standing-wave-ratio values for different waveguide sizes, and resistance values of the strips have been collected in Table 12·4; therefore, the design of simple waveguide pads is relatively easy. As has been indicated, the IRC strip might be replaced by a strip of Uskon cloth that has better mechanical strength.

For large power levels it is necessary to use material of greater bulk in order to provide proper heat exchange with the ambient air. A fixed waveguide pad of approximately 10 db attenuation at a wavelength of 3.2 cm, in which linen Bakelite is used as the lossy dielectric,[1] is shown in Fig. 12·14.

Polyiron materials have also been used very effectively in waveguides with stepped cross sections to provide proper matching. The characteristics of polyiron of several types have been determined (see Table 12·3) and therefore, the design of attenuator pads for the wavelength range from 3.13 cm to 3.53 cm in a waveguide of inner dimensions 0.400 by 0.900 in. is relatively simple. For other frequency ranges and other waveguide sizes, new designs would have to be made, although the values given can serve as a guide.

[1] Used by Sperry Gyroscope Co., Garden City, Long Island, N. Y.

The design of a waveguide pad for the wavelength range of 1.25 cm ± 1 per cent, with a nominal attenuation of 22 db, is shown in Fig. 12·15. The waveguide has inner dimensions of 0.169 by 0.419 in. and the polyiron used is material No. 1725. As a bilaterally matched pad, the VSWR was held to less than 1.2, but the dimensions had to be met very closely in order to stay within these specifications.

Of course, any lossy material can be used for the design of fixed pads as long as provision can be made for matching sections and machining, or if other suitable forming processes are applicable.

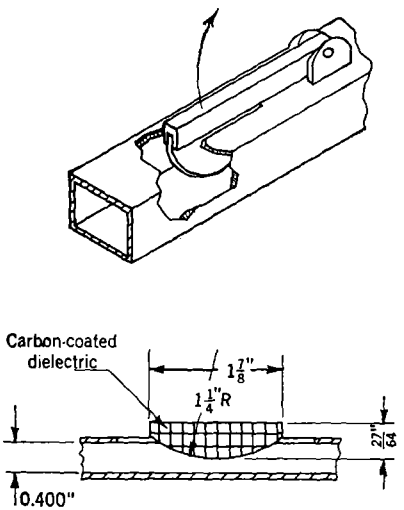

FIG. 12·16.—Variable waveguide attenuator of the flap type.

12·10. Variable Waveguide Attenuators.—The simplest type of variable attenuator for waveguides is the so-called flap attenuator, shown schematically in Fig. 12·16. The dissipative element is again an IRC resistance card, cut along a circle in order to achieve good voltage standing-wave ratio. A single strip, of resistivity 200 ohms per square, with the dimensions shown will give about 10 to 15 db attenuation in a waveguide whose inner dimensions are 0.400 by 0.900 in. In order to provide mechanical rigidity, two resistance cards of 200 ohms per square can be glued together back to back. This results in a combined film resistivity of 100 ohms per square and in a somewhat higher value of attenuation. Insertion into the guide is made through the broad top side of the guide and the vane swings about a hingelike holder. Because of the simplicity of its construction, an attenuator of this type is probably the most frequently used attenuator in test setups where the obvious leakage from the slot in the guide is of no particular concern. It is used near the oscillator as a buffer attenuator to avoid reaction of the load changes upon the oscillator; it is used as a variable buffer in the detector section of attenuation-measuring arrangements, but only if it cannot influence the input power to the detector through leakage coupling; it is also used to adjust power to predetermined levels where the amount of attenuation needed is of no interest. Building a casing over the central part of the waveguide and driving the resistive-strip holder suitably by means of a shaft extending through the casing, has produced calibrated

flap attenuators for about 24,000 Mc/sec and with maximum attenuation values of 90 db. These flap attenuators, however, were found to be very sensitive with respect to exact centering in the guide, parallelism to the guide walls, and exact shape of the resistive vane.

A variation of a flap attenuator of this type is shown in Fig. 12·17 where the resistance card is cut in spiral shape and is attached to a circular metal disk. This disk is centered on a shaft which penetrates a leakage-proof casing. The rotation of the shaft might also move a pointer or a dial calibrated directly in decibels of attenuation as measured against a comparison standard. By properly shaping the resistance card, a scale of attenuation which is almost linear can be attained with

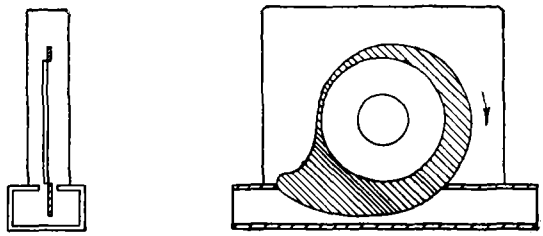

FIG. 12·17.—Attenuating strip moving vertically in guide.

rather good voltage standing-wave ratio. Although the construction is again simple, lack of mechanical rigidity and the possibility of a slight deformation under the influence of temperature and humidity would militate against the use of this card as a precision attenuator. Values of attenuation up to about 40 db are obtained easily, whereas higher values present considerable difficulties. These difficulties result from the coupling of the guide with the casing above, which permits much of the electromagnetic power to flow through the less attenuating path through the casing.

Instead of insertion through a slot in the guide, a vane can be fitted into the guide parallel to the small waveguide dimension as shown in Fig. 12·18. For mechanical reasons, two resistance cards can be used, cut either with tapered matching sections as shown in Fig. 12·18*a* or with notches as in Fig. 12·18*b* and glued back to back. Depending on the type of drive chosen, considerable accuracy of setting can be achieved.[1] However, temperature and humidity occasionally cause deformations of the strip which make reproducibility and reliability somewhat questionable particularly at the high values of attenuation where variation with position is very rapid. An illustration of this performance, Fig. 12·19, shows the attenuation versus position of a vane, as in Fig. 12·18*a*, at

[1] E. I. Green, H. J. Fisher, and J. F. Ferguson, "Techniques and Facilities for Microwave Radar Testing," AIEE Technical Paper No. 46-40, January, 1946, p. 22.

the three wavelengths 3.1, 3.32 and 3.5 cm and in a waveguide of inner dimensions 0.400 by 0.900 in. It can be observed from this figure, that the variation of attenuation with wavelength is large and not very systematic and therefore interpolation is very difficult. Another

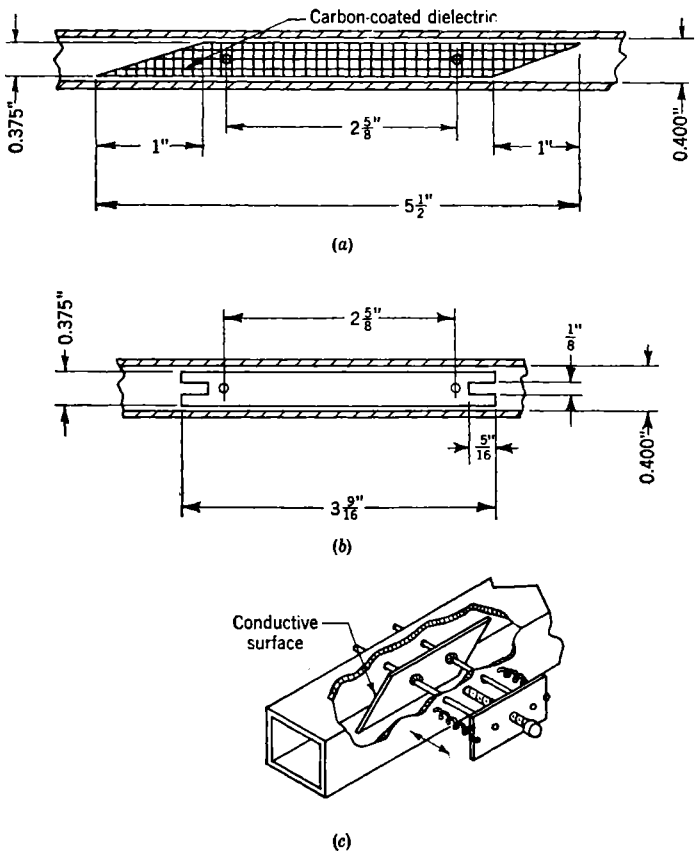

FIG. 12·18.—Variable waveguide attenuator of the vane type. (*a*) tapered vane, (*b*) notched vane, (*c*) perspective of assembly.

illustration of performance, Fig. 12·20, shows the calibration curves for the notched-end plate of Fig. 12·18 for different widths of the vane and for a fixed wavelength of 3.20 cm in a waveguide whose inner dimensions are 0.400 by 0.900 in. It is important to observe the critical influence of the width of the vane upon the attenuation curve which leads to a resonance peak for a width of 0.355 in. at a distance of $\frac{5}{32}$ in. from the

side wall. The design of the resistive strips is still an art, and from new applications unexpected results can be anticipated.

It is possible to obtain improved performance with respect to variation of attenuation with frequency if two vanes moving simultaneously from

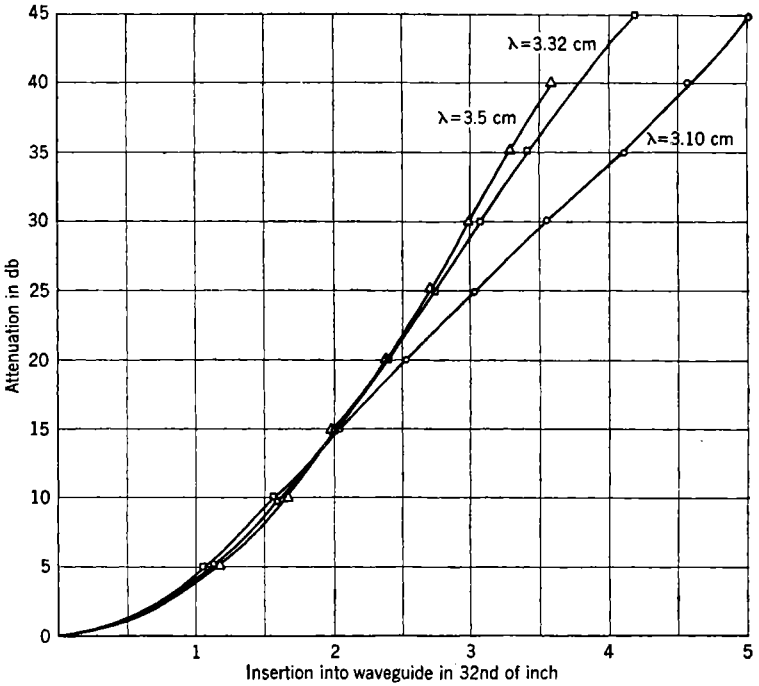

FIG. 12·19.—Calibration of tapered-end IRC resistive-vane attenuator.

the opposite small sides of the waveguide toward the center are used. The complication in construction is, however, considerable, and the increase in total attenuation is not uniform.

PRECISION METALIZED-GLASS ATTENUATORS

BY E. WEBER

The depth of the penetration of electromagnetic fields into metals can be derived by means of Maxwell's field equations as[1]

$$\delta = \sqrt{\frac{2}{\omega\mu\sigma}},$$

where $\omega = 2\pi f$ and f is the frequency of the oscillation in cycles per

[1] J. A. Stratton, *Electromagnetic Theory*, McGraw-Hill, New York, 1941, p. 504.

second, μ is the absolute permeability of the metal, and σ is its conductivity. For copper, at microwave frequencies of about 10,000 Mc/sec, a depth of penetration of 7×10^{-5} cm is obtained. Very thin metal films, appropriately applied to dielectric carriers, can be made of thicknesses of 10^{-6} to 10^{-5} cm; they will then exhibit essentially uniform current distribution even at the highest practical microwave frequencies.

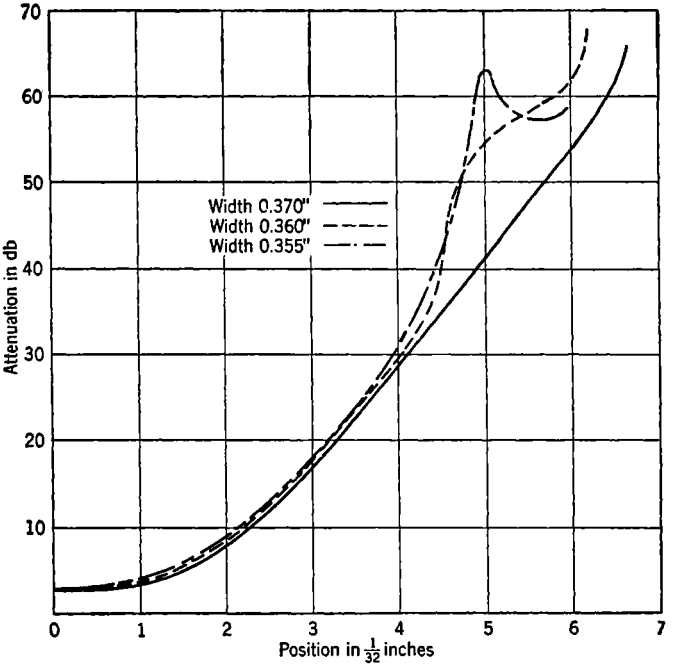

FIG. 12·20.—Calibration of notched-end IRC resistive-vane attenuator for varying widths of the vane.

Moreover, these metallic films, with glass as a foundation, can be made stable, unaffected by humidity, controllable as to resistance, and reproducible.

If these metal films on glass tubing are used as the inner conductor of a coaxial system, precision attenuators of fixed values can be obtained if suitable casings are provided which permit insertion in a standard coaxial line. With a variable metallic shunt path to the film, variable attenuators can be obtained which are of particular use as laboratory instruments.

12·11. Electrical Design of Coaxial-pad Inserts.—In the electrical design of the coaxial attenuator insert, dimensions and resistances of

film sections on insulators must be specified so that the over-all unit matches and has the required attenuation. In order to design units of various types, it is necessary to refer to the basic principles of transmission lines with series loss.

A section of uniform transmission line, in which the center conductor is a thin metallic film on a dielectric carrier, has a complex characteristic impedance with a real part greater than the characteristic resistance corresponding to the dimensions of the lossless line, and a capacitive reactive component; thus,

$$Z_c = \sqrt{\frac{R + j\omega L}{j\omega C}} = \sqrt{\frac{L}{C}}\sqrt{1 + \frac{R}{j\omega L}} = Z_0(u - jv), \tag{12}$$

where R, L, and C are the resistance, the inductance, and the capacitance, all per unit length (neglecting radiation resistance). The quantities u and v then are, respectively, the resistive component and the reactive component of the impedance normalized with respect to the geometric characteristic resistance, $Z_0 = \sqrt{L/C}$.

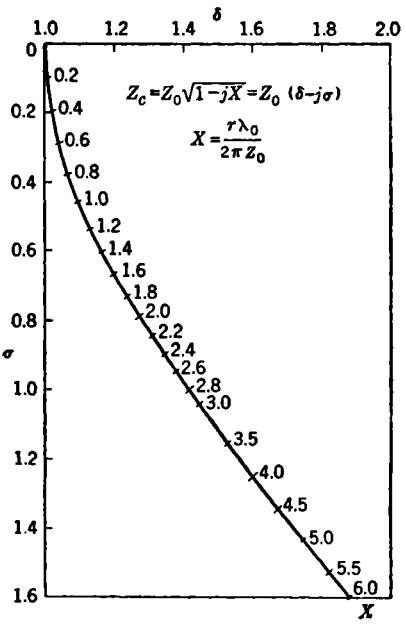

FIG. 12·21.—Normalized impedance chart for a line with series resistance.

If the quantities u and v are considered as functions of the resistance per unit length, they are related and define a curve on the impedance chart. For convenience, let

$$x = \frac{R}{\omega L} = \frac{R\lambda_0}{2\pi Z_0}, \tag{13}$$

where λ_0 is the wavelength for the lossless line in which $R = 0$. If the substitution

$$x = \sinh 2\theta \tag{14}$$

is used, there is obtained from Eq. (12)

$$u = \cosh\theta \quad \text{and} \quad v = \sinh\theta. \tag{15}$$

From this, it is seen that the real part of the characteristic impedance is always greater than the lossless ($R = 0$) characteristic resistance. The

locus of the normalized complex characteristic impedance, for a portion of the impedance chart, is shown in Fig. 12·21, with values of the parameter x indicated along the curve. For greater accuracy, special tables[1] of the functions in Eqs. (14) and (15), or conventional tables of the hyperbolic functions, may be used.

Similarly, the general expression for the propagation constant of a uniform transmission line can be reduced to functions of u and v,

$$\gamma = \sqrt{j\omega C(R + j\omega L)} = j\omega\sqrt{LC}\sqrt{1 - j\frac{R}{\omega L}} = \frac{2\pi}{\lambda_0}(v + ju). \quad (16)$$

With the general form $\gamma = \alpha + j\beta$, the attenuation constant becomes

$$\alpha = \frac{2\pi}{\lambda_0} v \qquad \text{nepers/meter}, \quad (17)$$

and the phase constant becomes

$$\beta = \frac{2\pi}{\lambda_0} u = \frac{2\pi}{\lambda_a}, \quad (18)$$

where $\lambda_a = \lambda_0/u$ is the actual wavelength in the resistive line, which is thus always shorter than the free-space wavelength.

Therefore, if any one of the three quantities, x, u, or v, and the lossless wavelength λ_0 are known, the calculation of the normalized line characteristics—characteristic impedance Z_c, attenuation constant α, and phase constant β—necessary for the design of the attenuator, can proceed. In fact, from Eq. (17) an expression for the attenuation per wavelength (measured in the lossless line) can be obtained

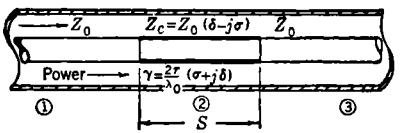

FIG. 12·22.—Schematic diagram of single metal-film section.

$$a = \lambda_0\alpha = 2\pi v. \quad (19)$$

This expression can be considered as a measure of all the design parameters, and it determines the performance that may be expected of an attenuator.

Let us assume first a single coaxial-line section of length s with metal film as shown schematically in Fig. 12·22, and with the same diameter ratio of conductor surfaces as the lossless line, so that the same geometric impedance holds for all three sections. From transmission-line theory, the expression for the input impedance to the film section is found to be

$$Z = \frac{1 - R_{23}e^{-2\gamma s}}{1 + R_{23}e^{-2\gamma s}} Z_c, \quad (20)$$

[1] R. W. P. King, *Electromagnetic Engineering*, Vol. I, Appendix II, McGraw-Hill, New York, 1945

where the reflection coefficient at the junction of lines (2) and (3) is defined by

$$R_{23} = \frac{Z_C - Z_0}{Z_C + Z_0}. \tag{21}$$

The over-all reflection coefficient at the beginning of the film section becomes

$$R_L = \frac{Z_0 - Z_L}{Z_0 + Z_L} = \frac{R_{12} + R_{23}e^{-2\gamma s}}{1 + R_{12}R_{23}e^{-2\gamma s}}, \tag{22}$$

where R_{12} is the (fictitious) reflection coefficient at the junction of lines (1) and (2), if line (2) is assumed of infinite length (or properly terminated); namely,

$$R_{12} = \frac{Z_0 - Z_C}{Z_0 + Z_C}. \tag{23}$$

By symmetry, $R_{12} = R_{23}$. Very frequently, especially in the design of attenuators,

$$|R_{12}R_{23} \cdot e^{-2\gamma s}| < 0.01,$$

and therefore, the approximate and very much simpler form

$$R_L \approx R_{12} + R_{23} \cdot e^{-2\gamma s} \tag{24}$$

can be used without appreciable loss in accuracy.

The design of the single metal-film section, which has a given attenuation $A = \alpha s$ and an ideal match $R_L = 0$, can now be attempted. From Eq. (24) together with Eqs. (21) and (23), there results, for $R_L = 0$,

$$e^{2\gamma s} = 1, \qquad 2\gamma s = j2\pi;$$

and with Eqs. (17) and (18)

$$4\pi \frac{s}{\lambda_0} \cdot v + j4\pi \frac{s}{\lambda_0} \cdot u = j2\pi,$$

which leads to $v = 0$, $u = \frac{1}{2}\lambda_0/s$. The exact solution is trivial, namely, $A = \alpha s = 0$. However, if the condition on the match is relaxed to permit an input VSWR of 1.02, $|R_L| = 0.01$, and therefore

$$\left|\frac{Z_0 - Z_C}{Z_0 + Z_C} 1 - e^{-2\gamma s}\right| = 0.01. \tag{25}$$

If the value of Z_C from Eq. (12) and of γ from Eq. (16) are introduced, there is obtained, for the condition for match,

$$\frac{(1-u)^2 + v^2}{(1+u)^2 + v^2} \cdot \left[1 - 2e^{-4\pi\frac{s}{\lambda_0}v} \cos\left(4\pi \frac{s}{\lambda_0} u\right) + e^{-8\pi\frac{s}{\lambda_0}v}\right] = 0.01, \tag{26}$$

while for the total attenuation Eq. (17) gives

$$A = \alpha s = 2\pi \frac{\lambda_0}{s} \cdot v. \tag{27}$$

By trial and error a combination of s/λ_0 and a proper pair (u,v) from Fig. 12·21 can be found, which satisfies simultaneously Eqs. (26) and 27). With this solution, it is possible to evaluate x according to Eq. (14)·

$$x = \sinh (2 \cosh^{-1} u). \tag{28}$$

Since s/λ_0 is now known, Eq. (13) is best rewritten as

$$x = \frac{1}{2\pi} \frac{\lambda_0}{s} \cdot \frac{R_s}{Z_0},$$

from which the value of the resistance R_s/Z_0 can be determined. For small values of attenuation A, satisfactory film sections can be designed.

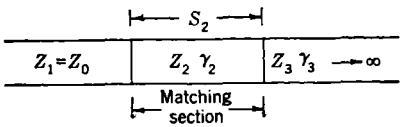

FIG. 12·23.—Schematic diagram of single matching section.

With proper modifications, the same relations can be used for the design of a metal-film transformer section interposed between the lossless line $Z_1 = Z_0$ and a main attenuating film of total attenuation large enough to make it appear of infinite electrical length, as shown in Fig. 12·23. The condition for match is again given, with slight modifications, by Eq. (24), namely,

$$R_L = R_{12} + R_{23} e^{-2\gamma_2 s_2} = 0, \tag{29}$$

$$R_{23} = \frac{Z_2 - Z_3}{Z_2 + Z_3}, \qquad R_{12} = \frac{Z_0 - Z_2}{Z_0 + Z_2}, \tag{30}$$

whereas the total attenuation of line section (2) is, in accordance with Eq. (27),

$$A_2 = \alpha_2 s_2 = 2\pi \frac{\lambda_0}{s_2} \cdot v_2. \tag{31}$$

By trial and error the complex equation (29) may be readily solved for the possible combinations of the pairs (v_2,u_2), (v_3,u_3), and s_2/λ_0. The solutions are unique if the restriction of shortest possible length, s_2/λ_0, is imposed. For this condition the results are plotted in Fig. 12·24 and the over-all attenuation A_2 follows from Eq. (31). It is observed that the length of the compensator approaches a quarter wavelength, and that v_2 approaches $\frac{1}{2}v_3$ as the resistances of both sections approach zero; these conditions are identical with those for the quarter-wave geometric-mean impedance transformer, and are to be expected. For

films of higher resistances, the length of the matching section increases beyond a quarter wavelength, and the ratio v_3/v_2 increases rapidly, and becomes 6.5 in the range covered by the curve. The ratio of the resistance value per unit length in line section (3) to the value in section (2) increases at a rate even more rapid than (v_3/v_2). This holds approximately for all attenuators with single matching sections.

An appropriate extension to n sections of metal film of different individual characteristics makes possible the design of more complex attenuator inserts for good matching conditions over broader frequency bands. In all cases, the trial-and-error method, if applied from the background of experience, yields the quickest results.

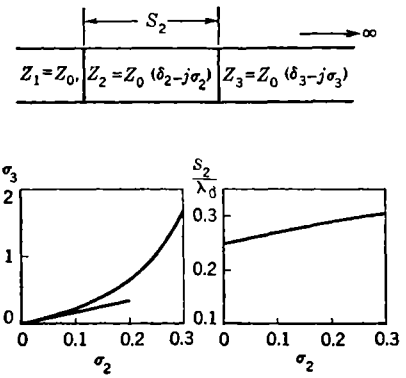

FIG. 12·24.—Attenuator design with single matching section.

12·12. Construction of Coaxial Fixed Pads.—A complete, fixed-value attenuator pad consists of the metalized-glass insert with metal bullets soldered to its ends for insertion into the metallic center conductor of the coaxial-line system; a support structure of the inner conductor; and a coaxial outer conductor or casing with suitable coupling elements with which to connect the pad rigidly to the adjoining line sections.

Metalized-glass Inserts.—Although several different methods have been developed for deposition of thin metallic films[1] on glass or similar nonmetallic carriers—for example, the Brashear and the Rochelle Salt methods of chemical deposition, cathode sputtering, spraying, and other methods—there are only two methods which by effective control provide the requisite precision for electrical applications: the burning-on method, and the evaporation method. Because of the broad range of its application, the burning-on method will be described in some detail here; the evaporation method will be discussed in Sec. 12·15.

The burning-on method of metal deposition has been known to china

[1] Strong, *Procedures in Experimental Physics*, Prentice-Hall, New York, 1943.

decorators and other artisans for a very long time; it is applicable only to noble metals, those metals that are reduced by heating. To form a resistive film on the glass, an oily solution of one of the metallic salts is painted, sprayed, brushed, or wiped on the glass. When heat is applied, the oil burns off and reduction of the salt occurs, leaving a metallic deposit on the glass. The glass is then heated to the softening point. This causes the deposit to form a compact adherent film on the glass. These films are mechanically sound; if they are formed on a clean glass surface they withstand considerable abrasion, are little affected by humidity changes, and retain good electrical characteristics. The ease with which such films are formed expedites production methods. The control of the resistance, however, is dependent on the metals used and upon their concentration in the original liquid coating, while the uniformity of the films is dependent on the method of application.

The most useful types of metallic solutions are those which contain mixtures of platinum and palladium with some rhodium. These are particularly useful for fairly high resistance values. For medium resistance values, platinum-gold solutions have been used, and for low resistances, pure platinum, gold, silver, or palladium solutions are available. Where it is necessary to make provisions for solderable connections, a paste of platinum- gold has been found most satisfactory. It is, however, not a thin film, and its resistance is negligible.

There are several ways in which the metallic solutions may be applied to the glass. In the case of tubing, four procedures have been tried: painting with a soft camel's-hair brush; spraying with an atomizer; drawing of the tubing through a cup filled with solution; and finally, applying by means of a saturated felt washer. Only the last-named method proved suitable for close and not too critical control of uniform film thickness. In this method, a felt washer is clamped between two metal washers. The diameter of the hole cut in the felt is about $\frac{1}{32}$ in. less than the diameter of the glass tubing to be coated. The metal washers used are approximately 2 in. in diameter, with $\frac{5}{8}$-in. holes, and are clamped together with four machine screws which pass through one washer and are threaded into the other. The washers and screws are made of brass. The felt is saturated with the solution used, and the glass tube to be coated, after thorough cleaning of the glass surface, is forced through the hole in the felt. The tube is run up and down through the hole two or three times and is rotated slightly while the washer is held in a horizontal position and the tube is held in a vertical position. On the final passage, as the tube is being withdrawn from the washer, the speed of withdrawal is held as constant as possible. The rotation of the tube and the constant speed of withdrawal tend to cause a uniform coating on the tube. This method of coating is affected by many variables; for

example, the concentration of the solution, the degree of saturation of the felt, the number of times the tube is passed through the felt, the speed of passage, and, particularly, the speed of the final withdrawal. However, this method for experimental work has proved to be the most successful of the methods tried.

After the glass tube has been coated with the metallic solution, it is placed immediately on a rotating spindle in a drying oven maintained at a temperature of approximately 100°C. During this drying period, which lasts about 5 min., the volatile oils in the solution evaporate and leave the surface film dry to the touch. The tube is then placed on a rotating spindle and inserted into a firing oven where it is kept from 5 to 7 min. at a temperature of 650°–680°C; the length of time and the temperature depend upon whether a metallic solution or a paste has been used. The rotating spindles in this step ensure uniform heating and maintain the alignment of the tube. The rods which form the spindles must be of some material that can withstand these temperatures for the time required without appreciable softening and consequent bending. During this period in the oven, the metallic salts are reduced, and the metal is deposited and then bonded onto the semiplastic surface of the glass.

After proper cooling, the resistance of the film is measured. If it is too high, another coating may be applied to form a second metallic layer on the first, and bonded with it. If the resistance is too low, it is advisable to vary the concentration of the solution by the addition of thinning agents. If it is necessary to produce resistive films on glass tubing in sections with different resistance values, then the higher resistance film is formed first over the entire tube. The section which now has the final desired resistance is covered with masking tape, and the sections that are to have a lower resistance are coated with additional solution. The unit is dried again, the tape removed, and the film cleaned with carbon tetrachloride.

After a film or complex films of correct resistance have been attained, collars of platinum-gold paste are burned on at the ends of the glass tube, which has previously been ground to the correct over-all length. The collars formed by this paste can be soldered readily; thus, they serve as a means by which the resistive film can be soldered to metal connectors, and thereby form a complete unit which may be inserted in, or removed from, a section of a coaxial line.

It is apparent that the attainment of exact resistance values by this "hand method" is almost an art. For better economy, an adaptation of the evaporation method has been developed. This consists of placing a special mechanical drive into the bell jar which revolves the individual spindles carrying the glass tubes. Since the process of

evaporation and the vacuum system with the bell jar will be described in Sec. 12·15, the discussion here will be restricted to the mechanical setup for evaporation on glass tubing. The machine consists of a cage which supports twenty spindles, and which turns in a horizontal plane about a center line drawn vertically through the center of the base plate and, therefore, through the center of the filaments. The spindles have small gears at their inner ends which are meshed with a fixed bevel

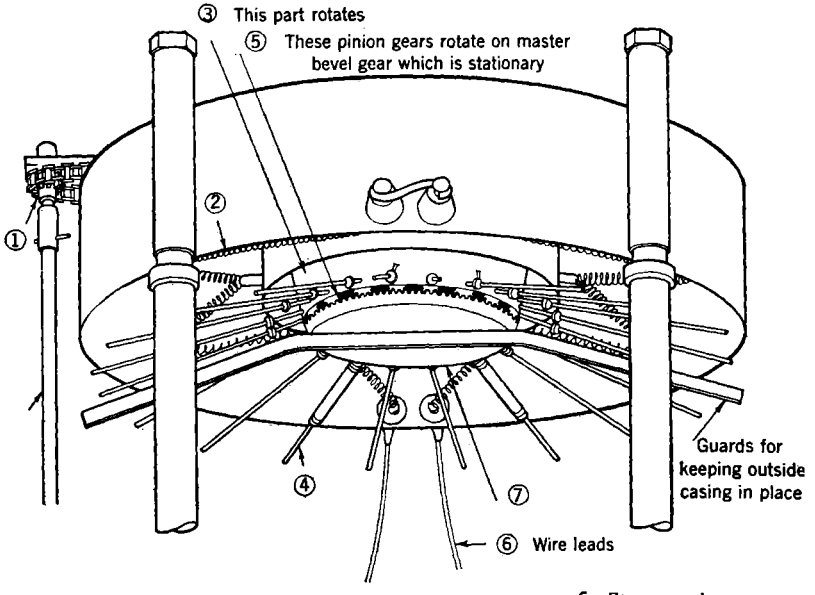

FIG. 12·25.—Mount for attenuator inserts in evaporation chamber.

gear. The supporting shaft of this bevel gear serves as the axis for the cage and spindles. The cage is turned by means of a chain drive which runs over a large sprocket wheel mounted over the cage and fastened rigidly to it, and also over a small sprocket wheel mounted vertically on a shaft offset to one side of the machine. To this small sprocket wheel is pinned a drive shaft that extends down, through a Wilson seal in the base plate, to a geared electric motor which drives it through a flexible coupling. When the cage is turned by the chain and sprocket drive, the spindles rotate on their axes and also revolve about their common center. The glass tubes, mounted on the spindles, are rotated on their axes and revolved, in a horizontal plane, about the central

vertical axis, and thus expose all of their outer surfaces to the molecular rays of the evaporating metal.

The assembly of this machine is shown in Fig. 12·25. In order to produce, in a single cycle of evaporation, a resistive film consisting of three sections—the end sections having a specified low resistance, and the center section a specified, relatively high resistance—a fixed mask made of curved sheet metal is mounted just beneath the spindles. The radial dimension of the mask is equal to that of the center section of the desired element, and its angular extent is about the same fraction of 2π as the ratio of the resistances per unit length of the center and end sections.

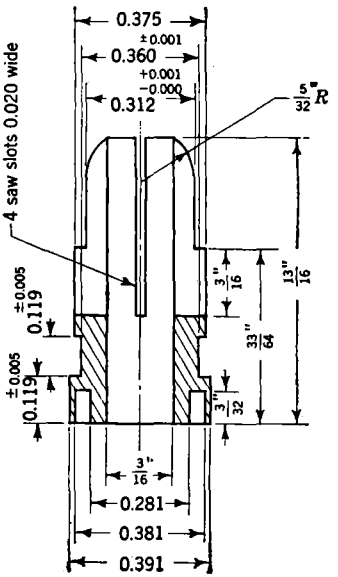

FIG. 12·26.—End bullet for metalized-glass insert of ⅜-in. diameter.

Assembly with End Connectors.—As an example of the brass end connectors directly soldered to the metalized-glass insert, Fig. 12·26 shows the bullet for ⅜-in.-diameter tubing and a midband frequency of 3000 Mc/sec. The cylindrical cup at the left end is the receptacle into which the collars at the ends of the metalized-glass tube are soldered. The outside wall of this cup is made very thin in order to minimize electrical reflections and to prevent an excessive strain on the glass as a result of the soldering process. To reduce still further the electrical effect of this increase in diameter, an adjacent corresponding decrease in diameter is provided. By this procedure, the voltage standing-wave ratio is reduced to less than 1.02 over a ±10 per cent frequency band. The remainder of the bullet is so constructed as to connect into a standard-line inner conductor. A hole is provided in the bullet to permit the escape of gas which is formed during the soldering of the glass tubing.

In order that the metalized-glass inserts may be mechanically strong and may fit interchangeably into various coaxial-line systems, the soldering technique must meet three requirements; the bullets must form a strong bond with the glass insert to which they are soldered, the bullets must be axially aligned, and the length between the bullet shoulders at the ends of the inserts must be maintained to the correct tolerance. The last two requirements are best met by the use of special jigs.

Protective Coating of Metalized-glass Inserts.—Although the metallic films, as produced by the burning-on method, are quite rugged, they can

be damaged by abrasion. To protect them during assembly in the casing that forms the outer conductor of the coaxial line, and to protect them from rough or thoughtless handling, a coat of wire varnish is usually painted on the completed element. This includes the glass tube with its metallic film and the soldered end connectors. This varnish is baked at 150°C for one hour, which causes it to set as a hard film that withstands all abrasion except that caused by sharp-pointed tools. It also serves as a protection against the effects of prolonged exposure to high humidity which might cause oxidation or corrosion of the metallic film. To prevent fungus growth which might occur in wire varnish if the units are to be used in tropical climates, a plastic, fungus-resistant varnish has been used. This also requires baking at 150°C.

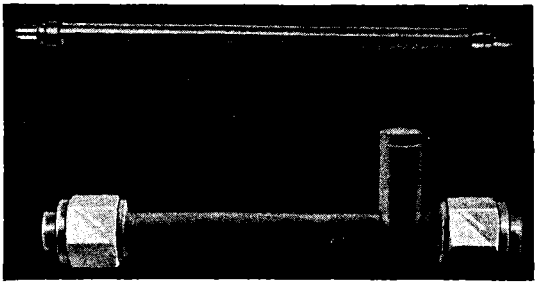

FIG. 12·27.—A $\frac{7}{8}$-in. coaxial-line attenuator and insert.

If the metal films have been formed with proper attention to the cleanliness of the glass surface and if care has been taken in all operations of coating, baking, and firing, these films are mechanically strong and can withstand considerable abrasion; they cannot be rubbed off the glass. Dirt, or contamination of the glass surface or of the solution, is always evidenced in poorly bonded films that are easily removed from the glass. A well-formed, well-bonded metal film resists removal by any means except forcible removal by a sharp-edged instrument. The metallic films are not permanently affected, either mechanically or electrically, by thermal changes between $-50°$ and 150°C, the baking temperature of the varnish. The temperature coefficient of resistance of the films has an average value of 0.0007 per degree C; slight variations probably result from differences in the composition of the solutions used.

Complete Assembly of Coaxial Pads.—The over-all length of the casing is short enough to be convenient and still ensure broadband operation. In the case of the $\frac{5}{8}$-in.-line and the $\frac{7}{8}$-in.-line units, casings of two types have been designed. One type has only one broadband (Pound) T-support as shown in Fig. 12·27; this casing is particularly convenient when frequent interchange of the attenuator elements is

desired. The other type of casing uses two broadband T-supports as shown in Fig. 12·28; this casing is recommended for standard attenuators which have been carefully calibrated and are to be used as reference attenuators. The small $\frac{5}{16}$-in.-line casing is made only as a complete unit, with the insert already bead-supported inside the casing. The construction is mechanically very rugged, and is shown in Fig. 12·29.

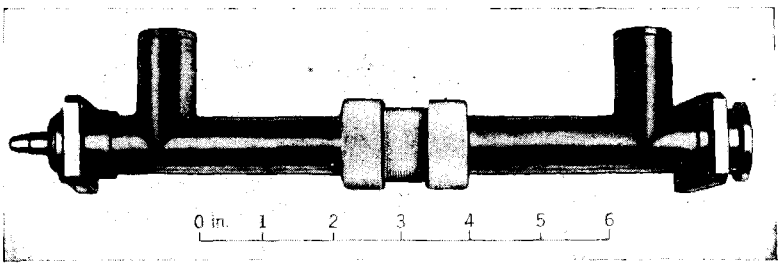

FIG. 12·28.—Standard coaxial attenuator.

FIG. 12·29.—A $\frac{5}{16}$-in. coaxial-line attenuator.

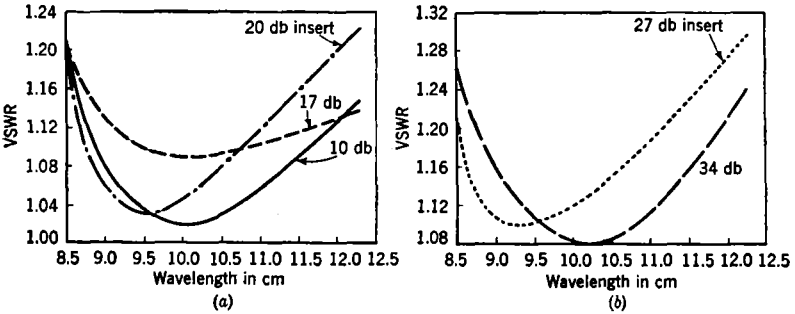

FIG. 12·30.—Voltage standing-wave ratio vs. wavelength of attenuator inserts for $\frac{7}{8}$-in. coaxial line.

All casings are provided with the proper coupling elements and they can be inserted easily in transmission systems of standard size.

12·13. Performance Characteristics of Fixed Coaxial Pads.—The most important characteristics of attenuators for broadband use are the variations of the voltage standing-wave ratio and of the attenuation with frequency. Their power capacity is also of considerable interest. The attenuator pads for $\frac{7}{8}$-in. coaxial line, which are used principally as laboratory units for precise measurements, have been studied in con-

siderable detail. As illustration of the results, Fig. 12·30, shows the variation, with wavelength, of the voltage standing-wave ratio for pad inserts designed for different values of attenuation. Each insert has a total film length of one wavelength at a center frequency of 3000 Mc/sec. Each curve represents an average of four measurements of voltage standing-wave ratio taken on a pair of attenuators; the voltage standing-wave ratio is measured at each end of the attenuator with a matched terminal at the output. Single-stub casings with especially low standing-wave ratios were used with each insert. The inaccuracy of the measurements is probably less than ± 0.03 in VSWR. The shape of the curves approximates that which is predicted theoretically. Since these attenuator inserts originally were designed for a ± 10 per cent frequency band, the performance is quite satisfactory. The inserts for higher values of attenuation have a center film of rather high specific resistance, and therefore nonuniformities in production tend to have a greater effect upon the resultant standing-wave ratio than at lower values of attenuation.

For these laboratory attenuators the variation of attenuation with frequency is very nearly linear. For the pads mentioned above, attenuation was very accurately measured at nine different wavelengths, ranging from 8.5 to 12.3 cm (3530 to 2440 Mc/sec). Straight lines could be drawn through the experimental points with less than ± 0.1 db deviation for any one point. The data at 8.5 cm and 12.3 cm are given in Table 12·8 with the measured slope and the theoretical slope calculated from the design theory.

TABLE 12·8.—ATTENUATION VS. WAVELENGTH FOR $\frac{7}{8}$-IN. COAXIAL-LINE ATTENUATORS

Nominal attenuation value, db	Measured attenuation in db		Measured slope, db per cm change of wavelength	Calculated slope, db per cm change of wavelength
	At 8.5 cm (3530 Mc/sec)	At 12.3 cm (2440 Mc/sec)		
10	9.9	9.7	0.05	0.05
10	11.0	10.6	0.10	0.05
17	16.6	15.7	0.20	0.20
17	17.1	16.1	0.20	0.20
20	20.0	18.6	0.30	0.33
20	21.5	20.3	0.40	0.33
27	28.0	25.8	0.60	0.65
27	29.5	27.2	0.60	0.65
34	35.4	32.4	0.80	0.95
34	36.0	33.0	0.80	0.95

The measured values are in good agreement with the calculated values. It can be observed that the frequency sensitivity increases with the attenuation value. This effect can be noted by comparing two 17-db units, connected in tandem so as to give 34 db, with a 34-db unit. The frequency sensitivity of the two 17-db units is 0.40 db/cm, whereas for the 34-db unit it becomes 0.80 db/cm, or twice that for the tandem connection.

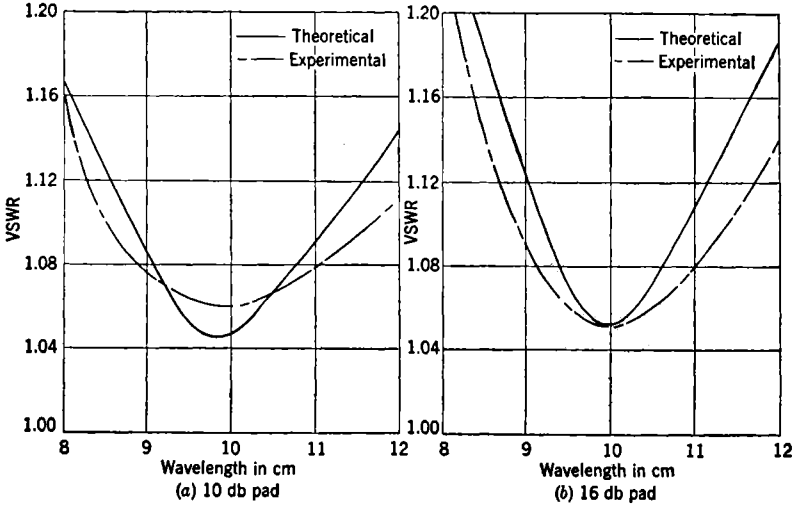

FIG. 12·31.—Wavelength vs. voltage standing-wave ratio for a $\frac{5}{16}$-in. coaxial line pad.

The attenuator pads for $\frac{5}{16}$-in. coaxial line, which are used principally in field instruments, have end-connectors in the form of cable fittings of essentially narrow-band design. To study the frequency sensitivity of these attenuators, the effects produced by the inserts must be distinguished from those produced by the casing. Fig. 12·31 shows the voltage standing-wave ratio vs. wavelength for the metalized-glass inserts of attenuation values of 10 and 16 db. These inserts were tested in special casings which permitted the evaluation of the performance of the inserts alone, and excluded the reflections of the cable fittings and the associated bead structures. Here, also, two inserts of each type were tested, which permitted four voltage standing-wave-ratio measurements per type to be averaged. The inaccuracy of measurement is considered to be less than ± 0.03 in VSWR. In addition to the experimental data, calculated curves are drawn according to the design theory of Sec. 12·11. Since the design is based on film length of one wavelength at a center wavelength of 10 cm, the agreement between theory and measurement

can be considered satisfactory. However, the cable fittings add reflections, particularly at the ends of the wavelength band, and consequently the over-all voltage standing-wave ratio of the completed pad may show values up to 1.34 either at the short or at the long wavelength end, depending on the type of cable fitting used. This demonstrates the frequency limitation of the existing cable fittings, which with proper redesign will eventually be removed.

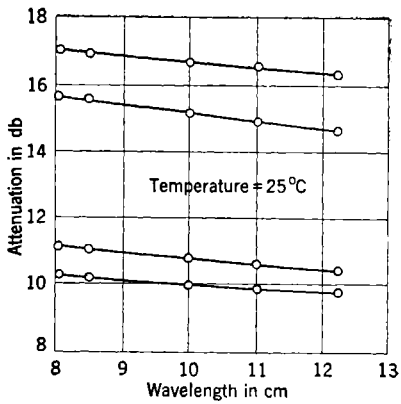

FIG. 12·32.—Attenuation vs. wavelength of inserts for $\frac{5}{16}$-in. coaxial line.

For the same attenuator pads, Fig. 12·32 shows the attenuation as a function of frequency, obtained by very careful measurements. Within experimental error, these curves can also be approximated by straight lines. The data on the rate of variation of attenuation with wavelength are given in Table 12·9. For use over rather broad frequency bands, a smaller frequency sensitivity would be required, and a better voltage standing-wave ratio would be needed. This indicates a need for a design which is basically new and on such a design work has already been begun.

TABLE 12·9.—ATTENUATION VS. WAVELENGTH FOR $\frac{5}{16}$-IN. COAXIAL-LINE ATTENUATORS

Nominal attenuation value, db	Measured slope, db per cm change of wavelength	Calculated slope, db per cm change of wavelength
10	0.15	0.1
10	0.10	0.1
16	0.25	0.3
16	0.20	0.3

With a film length of about two and one-quarter wavelengths, attenuation inserts for use at a center frequency of 9091 Mc/sec have been designed and built. An insert of this type has a considerably lower attenuation value per wavelength, which, according to Sec. 12·11, is a basic quantity for the electrical design. As a result, a lower voltage standing-wave ratio can be expected for the insert. However, for this insert also, the end connectors are of the cable-fitting type and, therefore, are inherently frequency-sensitive. Special improved end-fittings have been designed to reduce this frequency sensitivity, but the principal

requirement that they should mate with the existing cable connectors so restricted the freedom of design that only limited gain could be achieved. Thus, for ten samples of the 20-db unit, and six samples of the 10-db unit, the average voltage standing-wave ratio for the complete units with the improved casing was measured with the results given in Table 12·10.

TABLE 12·10.—VSWR VS. WAVELENGTH FOR ATTENUATORS FOR $\frac{5}{16}$-IN. COAXIAL LINE

Nominal attenuation value, db	VSWR values at		
	wavelength 3.5 cm (8570 Mc/sec)	wavelength 3.3 cm (9091 Mc/sec)	wavelength 3.1 cm (9680 Mc/sec)
10	1.21	1.17	1.20
20	1.10	1.10	1.14

The insert for the 10-db unit has no impedance-matching sections (compensators), and consequently has a VSWR of approximately 1.08 at the longest wavelength. For this reason, the 10-db units exhibit, on the average, a somewhat higher voltage standing-wave ratio than the 20-db units which do have compensators. From the design theory it is also predicted that only a slight variation in the voltage standing-wave ratio should occur over the frequency band and this contention is supported by the results of measurements.

For these same attenuators, the variation of attenuation over the frequency band of ± 6 per cent is theoretically predictable as about ± 0.02 db for the 20-db unit; measurements indicate practically unobservable variation of attenuation. This excellent result stems from the choice of the length of the attenuator inserts and suggests the possibility of further improvements.

Effect of Ambient Temperature.—If coaxial attenuators are used as standards in the laboratory, or if they are used over widely varying temperatures in the field, consideration must be given to the attenuation of the unit as a function of temperature. Although the temperature coefficient of resistance of the metal film is small, it is appreciable. The temperature coefficient of the film material of the main section is measured as 0.0006 per °C, while that of the compensator is 0.0008 per °C, for the majority of attenuators. With these values, the performance may be calculated as summarized in Table 12·11. The performance is substantially independent of line size and of the frequency at which the attenuators are used.

Attenuator inserts produced by means of the evaporation process (see Sec. 12·12) should be insensitive indeed to large variations in tem-

perature, since the nichrome film obtained by this process has a very low temperature coefficient, about $\frac{1}{10}$ of that of the burned-on films for which the above data are valid.

The effect of ambient-temperature changes upon the match characteristics of all coaxial attenuators is negligible.

TABLE 12·11.—EFFECT OF AMBIENT TEMPERATURE

Nominal attenuation value of units, db	Change in attenuation, db per 10°C rise in ambient temperature
10	+0.080
17	+0.124
20	+0.136
27	+0.167
30	+0.180
34	+0.196

Power Capacity.—In order to check the power capacity of the matalized-glass attenuators, tests of two types were made. In the first test, the power was increased slowly to the point of failure; this is a slow, tedious, and costly test, and invariably ends in the destruction of the unit. From the results of tests of this type it can be concluded that inserts of proper uniformity for $\frac{5}{16}$-in. coaxial lines at a center frequency of 3000 Mc/sec will withstand one watt of average power under any condition of pulsed operation; and attenuators for large line sizes will withstand larger amounts of average power, at least in the ratio of the insert diameters. In the second test, units were subjected to specified values of power and the number of failures were recorded. The results of tests on units for $\frac{5}{16}$-in coaxial line and center frequency 3000 Mc/sec are summarized in Table 12·12:

TABLE 12·12.—POWER TEST OF ATTENUATORS

Attenuation value, db	Number of units tested	Number of failures with 1.5 watts continuous r-f power	Number of failures with pulse power
20	4	0	1
16	5	0	0
10	5	0	1

In the 14 units tested by applying 1.5 watts of c-w power, no failures occurred. These 14 units were then tested at 1.0 watt average power with a pulse length of 1.0 μsec, and a repetition rate of 1000 cps. Two failures occurred. The fact that two units failed on 1 watt average power at a thousand-cycle repetition rate, after withstanding 1.5 watts of average continuous power, indicates that the pulse-power application is the more critical test.

Because of the reflections at the intersection of the first impedance-matching section (compensator) and the main film section, the current is not exponentially distributed along the metallic film. In the case of the 20-db insert one wavelength long, the theoretical distribution of the current was determined. The calculations show that in the first centimeter of the compensator the current remains virtually constant. This corresponds to the experimental fact that a large majority of the failures occur in the first centimeter of the leading end of the attenuator.

The actual failure of an insert is initiated by an arc which forms along its surface, travels at a rapid rate completely around the insert, and burns off an insulating ring. A d-c continuity test quickly indicates the failure which is always complete. The failure also causes bad mismatch and consequently the attenuation becomes appreciably higher.

All power tests so far described were restricted to attenuators which were not artificially cooled. With water cooling, sufficient to keep the temperature of the film to within several degrees of room temperature, 1 kw of continuous power has been dissipated in a film of 50-ohm resistance and of 3-in. length. This might indicate that the temperature rise of the film has an effect on the breakdown power.

Power Attenuators.—Under proper conditions the metallic films used in these attenuators can withstand considerable power. Special attenuators have been designed for powers ranging up to 30 watts average. This has been done by extending the length as far as convenient, and by arranging a low-attenuation section in front of a high-attenuation section. As a result, a large fraction of the power, about one-half, is absorbed in the first section. Such a design is necessary since the exponential decrease in voltage in a section of film causes most of the power to be dissipated in the leading parts of the film. For a special application at 7000 Mc/sec, an attenuator was designed in which the first section of 6-in. length had an attenuation of 6.67 db, whereas the second section, also of 6-in. length, had an attenuation of 13.33 db.

If air cooling can be arranged, the conventional 20-db unit in $\frac{7}{8}$-in. coaxial line, one wavelength long, at 3000 Mc/sec, can withstand continuous power up to 20 watts. For this high-power application, rather thick, low-resistance films are used. If an accurate knowledge of the attenuation is desired the attenuator must be calibrated against power.

12·14. Variable Metalized-glass Coaxial Attenuators.—The principle of very thin metal films on glass tubing as inner conductor of a coaxial system is also applicable to variable attenuators if a mechanism is arranged for effectively short-circuiting a part of the metal film. Two possible solutions have been suggested. In the first solution, a metal rod is inserted into the metalized-glass tubing from the far end of the attenuator, and coupling takes place through the glass wall to the metal

film; the attenuation is varied by varying the position of the metal rod. In the second solution, the short-circuiting member is a close-fitting metal tube which slides over the metalized-glass element and which is insulated from the metal film by a layer of varnish in order to avoid uncertain metallic contact.

The chief advantage of a metalized-glass variable attenuator lies in the possibility of a very low minimum attenuation of from 2 to 5 db, attained by permitting the movable element to short-circuit the entire attenuating metal film. In order to achieve this low loss and yet maintain a low input voltage standing-wave ratio to the attenuator at all positions of the movable metallic element over a reasonably broad frequency band, special types of matching were developed.

The input impedance to a long section of the main attenuating metal film was given by Eq. (12) and was seen to be complex. Broadband matching of the main film to a lossless line can, therefore, be obtained only by lossy matching elements, and again, two solutions have been found. In one case, there is interposed a short section of line which has a center conductor, the resistance of which varies gradually from zero to the resistance of the attenuating film. Such a transition film, or resistance-tapered transformer, provides a very good match in both directions over a wavelength band of ± 5 per cent, the VSWR being generally less than 1.05. In the other case, a film of uniform thickness is used, but applied in longitudinal stripes varying in width and number according to the required resistance. A resistance-tapered transformer of this type gives as good results as the first one, and is considerably simpler to apply. It is evident that these transformers absorb considerable power, but this is desirable in an attenuator.

A $\frac{5}{8}$-in.-line Variable Attenuator.—For application in a range near 3000 Mc/sec, a laboratory attenuator has been developed for rather coarse measurement work in $\frac{5}{8}$-in. coaxial line as shown in Fig. 12·33. Designed for use with type N connectors, its casing is made of standard $\frac{5}{8}$-in. line. The tubular element is made of glass coated with metal resistive film and is terminated at both ends by brass bullets whereby it is supported between a solid T-joint and a hollow joint. Through the center of the hollow joint and into the interior of the element is inserted the short-circuiting rod the motion of which is controlled by a rack and pinion. A central coupling unit is provided to facilitate installation of the element. The end shown on the left side of Fig. 12·33 is called the input end of the instrument. The tapered adaptor and the T-support are of proved design, therefore the first source of possible reflection is met at the input end of the element. A proper metal-film transformer is therefore inserted at that end. Reflections from the back end of the attenuator are generated both at the end of

the element and at the end of the sliding rod. The shape of the tip of the rod that gives the best results is that of an inverted cone as shown. A tip of this shape causes reflections which partially neutralize the

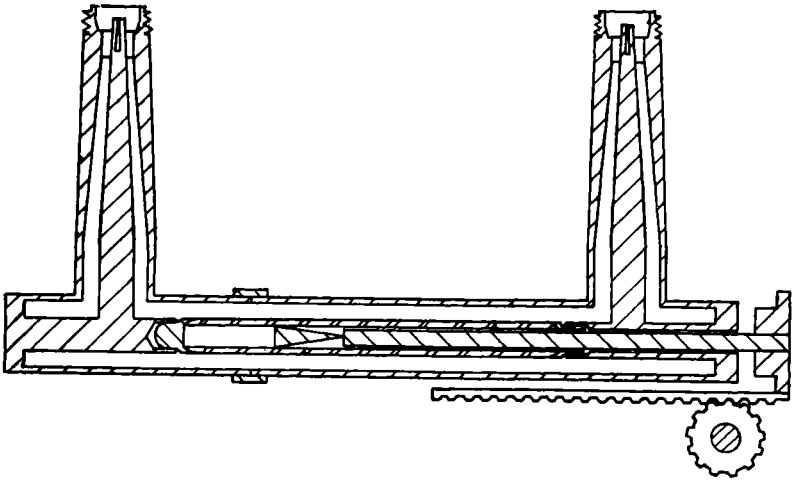

FIG. 12·33.—Schematic section of $\frac{1}{8}$-in. coaxial variable attenuator.

reflections at the end of the element. The compensation, however, is more or less imperfect according to the position of the slider, leading to variations in VSWR between 1.0 and 1.45. The total attenuation can be made to vary between 5 and 50 db, in a nearly linear manner over a considerable range.

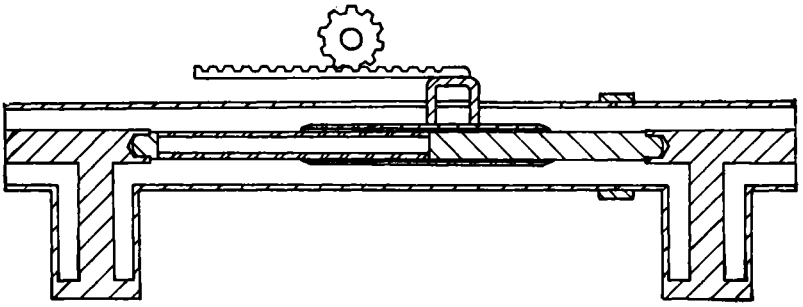

FIG. 12·34.—Schematic section of $\frac{7}{8}$-in. variable attenuator.

A $\frac{7}{8}$-in.-line Variable Attenuator.—For precise laboratory measurements, an attenuator in a $\frac{7}{8}$-in. coaxial line has been developed and has served both as a standard attenuator and as a general laboratory instrument. A schematic section is shown in Fig. 12·34. The element

consists of a metalized-glass tube equipped with brass-bullet terminals by which it is supported between two T-joints at the ends of a length of standard size $\frac{7}{8}$-in. line. Fitting over the element is a thin-walled metal tube or slider which serves to short-circuit the required length of the film on the element. This slider is controlled from the outside by a rack-and-pinion mechanism attached to it by an insulating handle which passes through a longitudinal slot in the outer conductor. The mechanism is concealed and protected by suitable metal covers and the only exposed moving parts are the control knob and the pointer by which the setting is indicated on an engraved scale.

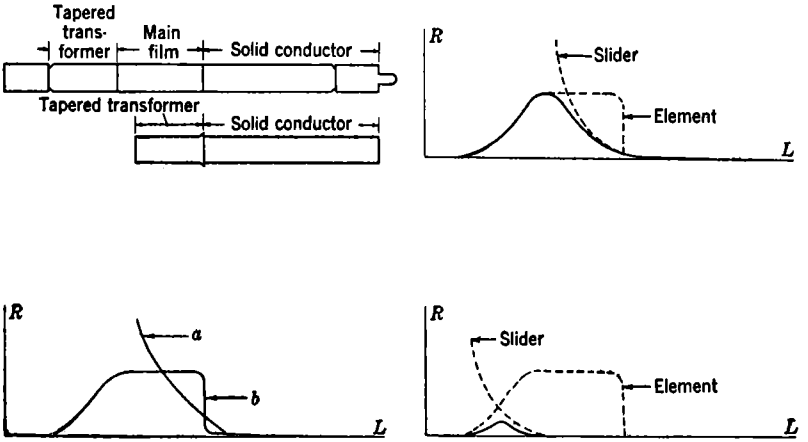

FIG. 12·35.—Diagrams to illustrate the matching of a variable coaxial-line attenuator. The curve at the upper right shows the combined resistance of element and slider at the position of maximum attenuation. On the lower left are the resistance characteristics of the slider (curve *a*) and the element (curve *b*). The curve at the lower right is the combined resistance at the position of minimum attenuation.

In this attenuator, the element is coated with metal film so as to produce the resistance distribution shown in Fig. 12·35. To the slider Fig. 12·34, is attached a short glass tube with stripes of film to form a tapered transformer as shown in the photograph, Fig. 12·36, and therefore the resistance distribution of the sliding system becomes as shown in Fig. 12·35. The slider transformer lies directly over the film of the element and the two films are separated only by a layer of baked enamel; consequently, at the frequencies employed the capacitance between them is very great. Therefore, the resistances of the two films may be added in parallel combination. If this be done, it is found that the effective resistance characteristic of the element and the slider combined is as shown in Fig. 12·35. But the characteristic there shown is simply that of a section of attenuating line joined at both ends by

tapered resistance transformers to normal lossless lines. The combination is therefore well matched in both directions even though the slider be moved, for this motion only varies the length of the central flat portion of the curve. When the slider system is moved all the way forward and the whole length of the uniform portion of the element film is covered by the metal slider, then the two tapered transformers are together, but

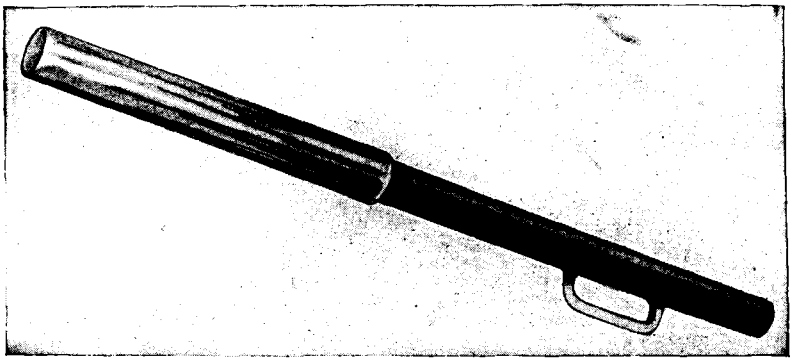

FIG. 12·36.—Slider assembly for $\frac{7}{8}$-in. variable attenuator.

face in opposite directions. Their added characteristic is as shown in Fig. 12·35 and is equivalent to two tapered transformers back-to-back with no intermediate attenuating line. A distinct advantage of the design is here evident, for the added characteristic, in this setting of minimum attenuation, shows that a very low insertion loss may be expected.

FIG. 12·37.—Side-outlet $\frac{7}{8}$-in. variable attenuator.

In Fig. 12·37 is shown a photographic view of the assembled attenuator with end sections that permit power flow into, and out of, the attenuating element at right angles to the element. The performance of an average standard unit is summarized by the following data: maximum attenuation, 40 db; minimum attenuation, about 3 db; VSWR less than 1.25 in both directions, at all settings and throughout a wavelength range of ± 10 per cent; power capacity, 10 watts continuous. A typical calibration curve shown in Fig. 12·38 indicates a parabolic variation of

attenuation with position of the slider, which is convenient if uniform relative accuracy of attenuation measurement is desired.

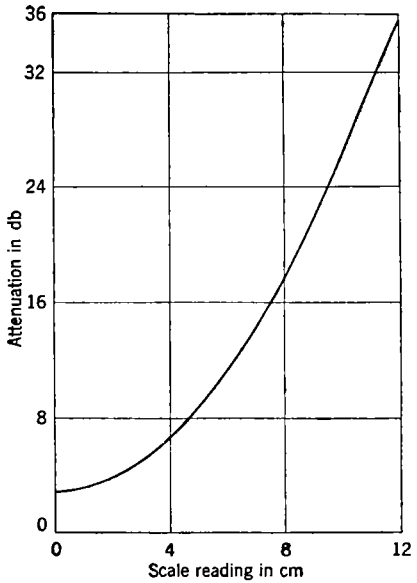

FIG. 12·38.—Calibration of typical $\frac{7}{8}$-in. coaxial variable attenuator.

12·15. Design of Elements for Waveguide Attenuators.—The use of metalized glass as a dissipative element in waveguide transmission systems is most convenient in the form of thin glass plates; usually, these plates carry metal film only on one side, and are suspended in the waveguide with the film parallel to the electric field lines. In the simplest construction, the glass plate has one or two holes drilled along its long center line and is cemented to one or two metal struts. These struts penetrate the guide wall, preferably at right angles to the electric field lines. These struts can, in turn, be made to move and carry the glass plate across the waveguide, as in the variable waveguide attenuators.

The most reliable cement to use in this construction is Sauereisen[1] Insalute Cement No. 1. It shows strong cohesion and permanence, easy applicability, and cold-drying qualities. Although this cement is not waterproof, a thick coating of Glyptol cement will minimize any detrimental effects from moisture. Humidity tests on cement-held plates of this type without the Glyptol coating have shown a "breathing" effect as large as ± 0.002 in. within several hours, during which time

[1] Made by Sauereisen Cements Co., Pittsburgh, Pennsylvania.

the relative humidity varied from 20 to 80 per cent. Although this effect apparently cannot be completely eliminated, the Glyptol-coated cement showed not only less but greatly retarded action. Figure 12·39 shows, schematically, the glass as it is cemented directly to continuous struts going completely across the waveguide.

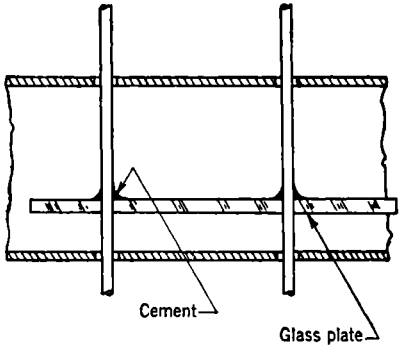

FIG. 12·39.—Cement mounting of glass plate in waveguide.

A much more satisfactory method of fastening the glass plate to the waveguide struts was developed by the Corning Glass Works. First, instead of drilling holes, which always causes slight chipping and thus weakens the glass section, Corning used a very fine gas flame to burn out or melt out the holes; the sides of these holes are perfectly smooth and fire-polished, and have a small crater of glass which actually strengthens the glass locally. Second, Corning designed German-silver eyelets as shown in Fig. 12·40 which are crimped onto the glass by special jigs; these eyelets permit soldering to the struts, which now have to be of solderable material. Shock and vibration tests on plates mounted

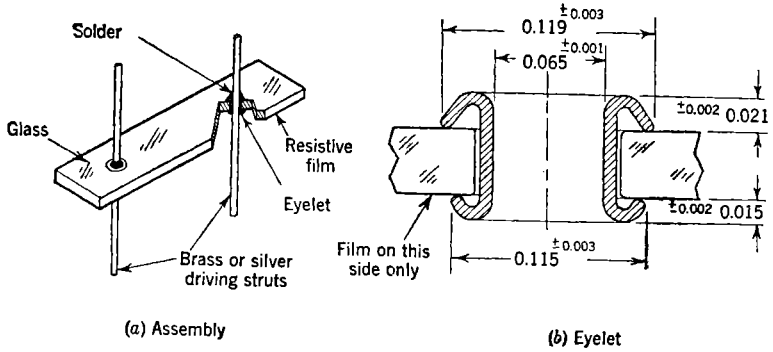

FIG. 12·40.—Eyelet mounting of glass plate on waveguide struts.

by this method have given completely satisfactory results; the effects of temperature and humidity are also eliminated.

Metalization of Glass Plates.—The metalization of the glass plates can be done by different chemical or mechanical processes of metal deposition. Utmost uniformity, together with the close control of thickness for the

proper rate of attenuation, can, however, be attained only with the evaporation process.[1]

In the evaporation process, the pieces to be coated with film are placed in an airtight chamber. In this chamber, and at a considerable distance from the pieces, is a heating element to which is attached a sufficient quantity of the material desired for the film. The chamber is evacuated to a low pressure during which time the filament is heated, which in turn melts and volatilizes the material to be evaporated. Molecular particles of the material deposit on relatively cool surfaces, and form a thin film. The amount of material required to produce a film of known resistance, and the rapidity at which it is formed, can be easily controlled by varying the temperature of the filament. The resistance of the film formed can be measured continually throughout the process by means of clips fastened to a glass plate placed in the chamber. Leads from the clips, brought out from the chamber through insulated and vacuum-tight seals, can be connected to an ohmmeter or other resistance-measuring device. By this means, the resistance of the film formed can be continually followed throughout the process, and the process can be stopped when the exact value of resistance is attained. The films formed on glass by this process are very adherent, are of considerable uniformity, and have excellent electrical properties for microwave work.

The equipment needed for evaporation of metals or nonmetals has already been described in detail in available literature.[2] The first, and most obvious, unit of equipment is a large, high bell jar with an accompanying oil diffusion pump and forepump. The pumps must have sufficient capacity to exhaust the bell jar fairly rapidly to an ultimate pressure of 10^{-4} to 10^{-5} mm Hg and they must have an ionization gauge for measurement of low pressures. To heat the filaments, a controllable power source, either d-c or a-c, of low voltage and high current is needed. This source is most conveniently provided by a low-voltage power transformer controlled by means of a Variac in the primary circuit. The glass plates should be supported from 10 to 15 inches above the filaments. As the distance between the filaments and the plates increases the degree of uniformity of deposition of the metal evaporated increases. The base plate of the vacuum system should be equipped with as many insulated and vacuum-sealed binding posts as are required to satisfy the demands for electrical connections within the bell jar.

It appears reasonable, at first, to use the noble metals, gold, platinum,

[1] A. A. S. Moore, "Production of Semi-reflecting Films of Chromium on Plane Mirrors," J. Sci. Instrum., Vol. 22, June 1945.

[2] J. Strong, *Procedures in Experimental Physics*, Prentice-Hall, New York, 1943.

and silver, for evaporation because of their immunity to oxidation and corrosion. However, in order to obtain a reasonable amount of electrical resistance of the film, the thickness of the film needs to be only a few times greater than the molecular diameter. For example, consider a film of platinum having a resistivity of 100 ohms per square and evaporated onto a glass plate 5 cm long and 1 cm wide. The resistance from end to end is then 500 ohms. Since

$$R = \frac{\rho l}{A} = \frac{\rho l}{wt}, \tag{32}$$

in which R is the resistance in ohms, ρ the resistivity in ohm cm, l the length of film, w the width of film, and t the thickness of film, then, under the assumed conditions

$$t = \frac{\rho l}{wR} = \frac{9.83 \times 10^{-6} \times 5}{1 \times 500} = 9.83 \times 10^{-8} \text{ cm} = 9.83\text{Å}.$$

This is an extremely thin film, approximately 5 molecules in thickness. Films of this thickness are difficult to obtain and are usually unstable. Of various metals and alloys which were tested, the most useful was found to be the resistive alloy nichrome. Films prepared by evaporation of nichrome exhibit the high resistivity and also the low temperature coefficient of resistivity which are characteristic of nichrome in bulk. The thickness of a nichrome film of the same type and value as that chosen in the above example is, however,

$$t = \frac{\rho l}{wR} = \frac{100 \times 10^{-6} \times 5}{500} = 100 \times 10^{-8} \text{ cm} = 100\text{Å}.$$

This film is approximately 50 molecules in thickness and is very stable. The only difficulty in producing uniform films of such resistance alloys arises from the large amounts of nickel that they contain. Nickel, when melted, dissolves most other metals, particularly the high-melting-point metals, such as tungsten, molybdenum, and others, which are suitable for use as heater elements in the evaporation process. This might cause a disintegration of the heater before a film of sufficient thickness is deposited, and furthermore, the dissolved heater material is also evaporated and has an adverse effect on the electrical properties of the film. It is, therefore, necessary to use tungsten wire of excessive thickness as a heater and a larger quantity of nichrome than is actually required for the film, so that, when it melts, the tungsten is coated with a nichrome layer so thick that a satisfactory film can be formed before tungsten has time to diffuse through the nichrome layer to the surface.

Because of the extreme thinness of the film, even the slightest deterioration of the surface seriously alters the resistance of the film. It is

therefore necessary to apply by evaporation a protective coating to the metal film before removing it from the vacuum. Magnesium fluoride was found to be the most convenient material for this purpose because of its low temperature of volatilization. A very thin coating of magnesium fluoride not only protects the metal film completely from chemical deterioration but, because of the great hardness and strength, it also prevents accidental mechanical injury of the film.

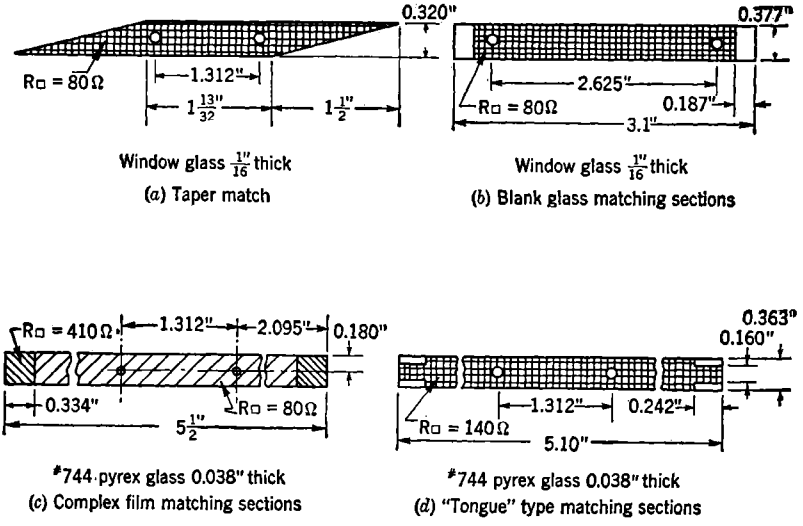

FIG. 12·41.—Types of matching of metalized-glass plates.

If all precautions have been taken in cleaning the surface of the plates, or tubes, the film deposit has considerable adherent strength. The combination of the film and the protective coating of magnesium fluoride which covers it has such great strength that ordinary abrasion from rubbing does not scratch the film; indeed, only a very sharp instrument pressed hard against the film, can penetrate the coating and damage the film. Further, since the fluoride coating completely covers the metallic film, the films are unaffected by change of humidity. The films also after having been subjected to temperature changes between $-50°C$ and $150°C$ show no permanent change in their resistance. Within this temperature range the temperature coefficient of resistance has been repeatedly checked and has an average value of 6×10^{-5} per degree C.

Matching Characteristics of Glass Plates.—Most attenuators require, in addition to stability, that the input impedance to the unit be almost equal to the characteristic impedance of the line or waveguide used. Unless the metallic-film resistance is very high and the supporting glass

dielectric is very thin, resistive plates will not match well without a transition or matching section preceding the active attenuating element. Four separate types of transitions, or matching sections, have been developed for use on the glass plates which are shown in Fig. 12·41. Two kinds of glass, either window glass $\frac{1}{16}$ in. thick or 0.038-in. No. 774 Pyrex glass, are used for all plates. Some of the matching arrangements prove more satisfactory with one of the glass types.

The possibilities of the taper match are perhaps most apparent. The taper section in Fig. 12·41 is actually a transition section and depends

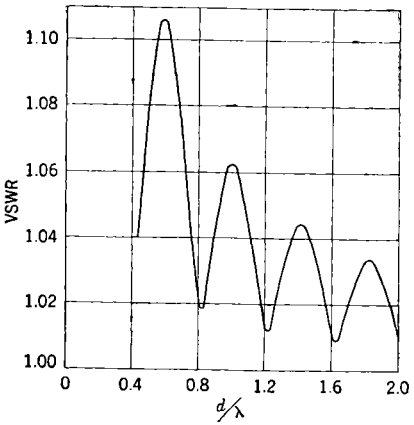

FIG. 12·42.—Variation of voltage standing-wave ratio with length of taper.

for match upon a small rate of transition, or change in characteristic impedance, per wavelength. The response curve shown in Fig. 12·42 is common for most taper transition sections and shows the variation of match as the taper is increased to several wavelengths in length. Film resistance, the dielectric constant of glass, and the thickness of the glass determine for a given wavelength the length of taper required for best match. Window-glass plates, with the relatively high dielectric constant $k_e = 7$, usually require a shorter taper than the Pyrex-glass plates. As an example of the results that can be expected with soft glass, plates 0.375 in. wide with a film resistance of 80 ohms per square and a taper length of $1\frac{1}{2}$ in. can be made to have VSWR's of less than 1.1 in a waveguide of 0.400 by 0.900 in. ID and over a frequency band of ± 6 per cent centered near 9000 Mc/sec. In fact, the VSWR can be below 1.1 for all positions of the plate in the guide, a very desirable characteristic for application in variable attenuators.

In order to reduce the length of the matching sections, the transformer shown in Fig. 12·41*b* has been developed for window-glass plates.

The theoretical details for this type of match have not been fully explored; it is known, however, that the blank glass present in the guide changes locally the characteristic impedance, which, together with the effective reactance provided by the shunt field distortion at the front edge of the glass, is apparently capable of matching window-glass plates with metal films which have a resistance of 100 ohms per square. This matching arrangement is most useful in narrow-band, variable attenuators. The dimensions have to be specifically determined for each frequency.

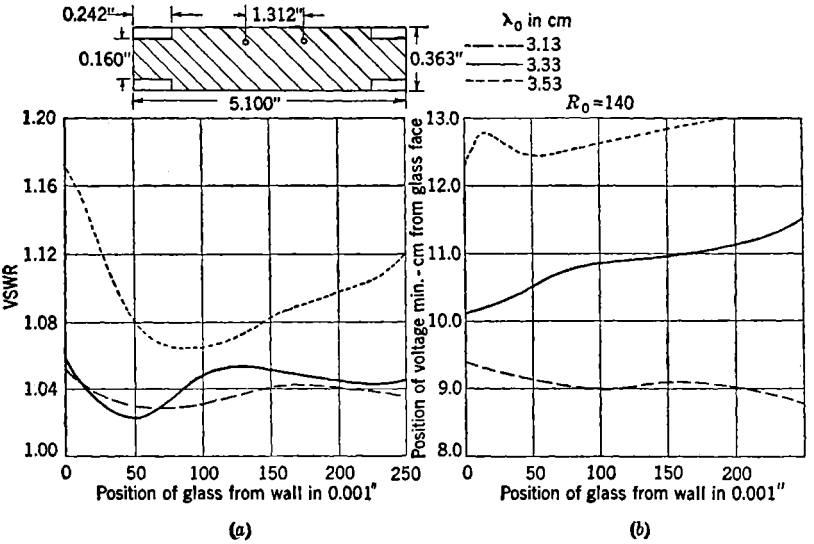

FIG. 12·43.—Impedance data for tongue-matched Pyrex plate.

The "complex film" transforming section shown in Fig. 12·41*c* is most useful for very thin Pyrex plates. The length and the resistance of the film transformer sections are determined experimentally. As an example, a main-film resistance of approximately 140 ohms per square could be matched by a transformer length of 0.330 in. with a matching-film resistance of approximately 400 ohms per square over a frequency range of about ±6 per cent centered at 9000 Mc/sec if used in a waveguide of 0.400 by 0.900 in. ID. The need of different film resistances on the same plate makes the use of the evaporation technique imperative. In order to metalize the element, the transforming sections are shielded, and the main section is evaporated first. When metalization has been completed, the shields are removed and the transformer section coated to the proper resistance. Since, for the second evaporation, the main

section is not shielded, two parallel coatings of resistive film exist in the main section, separated by a film of magnesium fluoride.

For broadband match on thin Pyrex plates a matching section of the type shown in Fig. 12·41*d* has proved to be the most satisfactory. The tongue section is made by suitable masking during evaporation. It provides a transforming section with a complex characteristic impedance similar to the complexfilm match. Film resistance is uniform, however, and the tongue width determines the difference in characteristic impedance between the matching and the main sections. The critical transformer dimensions have to be determined experimentally and differ for different film resistances of the main section. The broadband input impedance data for a typical plate using a match of this type are shown in Fig. 12·43 for a rectangular waveguide of 0.400 by 0.900 in. ID and used over a band of ±6 per cent with a center frequency of 9000 Mc/sec.

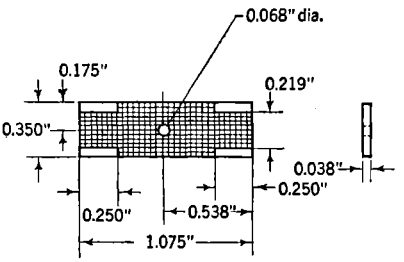

FIG. 12·44.—TMX-18PB film specifications.

12·16. Waveguide Pads of Fixed Values.—In the study of the dependence of attenuation at various frequencies on the position of a metalized-glass plate within the waveguide, it has been found by careful measurements that there exists a region of minimum frequency dependence of attenuation over a broad frequency band at a distance of about $a/8$ from the side wall of the guide. Usually, the glass plate carries the metal film facing the nearer side wall and the distance is measured from the film surface to the wall. If a properly designed glass plate is located in this region of minimum variation of attenuation with frequency, particularly desirable fixed waveguide pads are obtained, which can be used as calibrated attenuation "gauge blocks" to extend the range of power meters without appreciable loss of accuracy.

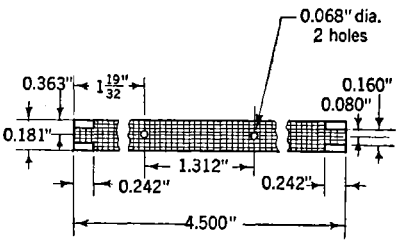

FIG. 12·45.—TMX-16PB film details.

Figure 12·44 shows the dimensions of a metalized-glass plate which gives an attenuation of 3 db in a waveguide of 0.400 by 0.900 in. ID when spaced 0.1 in. from the side wall and supported by a strut which, for mechanical reasons, extends completely across the waveguide. The design of the matching sections of this plate must take into account not only the match to the main attenuating film itself, but also the fact

that the main-film section is very short, has low attenuation, and therefore has an input impedance which depends on the termination of the pad. In addition, the supporting strut presents a local capacitive susceptance of appreciable value (see Sec. 12·18). Under these conditions, the accurate measurement of attenuation becomes an important problem

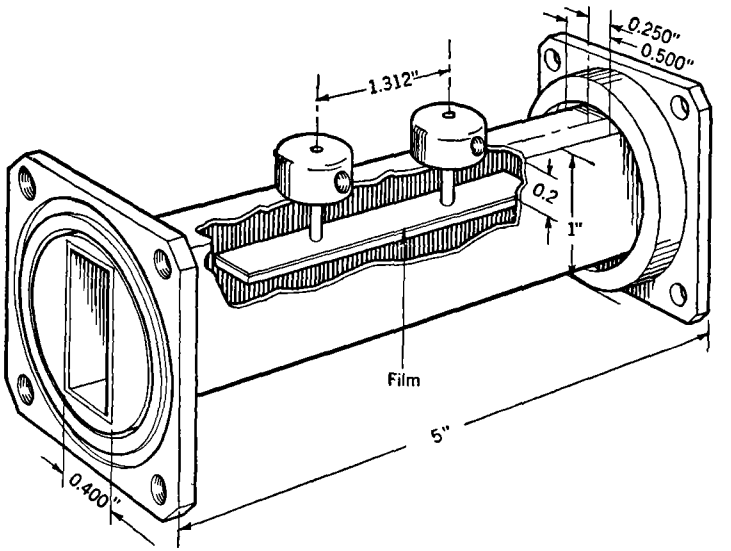

FIG. 12·46.—TMX-81PB fixed attenuator in casing.

and is discussed further in Chap. 13. Variation of attenuation with frequency over a 6 per cent band, centered at 9000 Mc/sec, is less than 0.2 db, and thus this pad makes a very accurate gauge block to establish the half-power point for measurements of Q. To demonstrate the influence of the positioning of the plate upon the variation of attenuation with frequency, a special casing was constructed with a fine micrometer drive and the same plate moved successively to positions giving 3, 4, 5

TABLE 12·13.—VARIATION OF ATTENUATION WITH FREQUENCY FOR DIFFERENT POSITIONS OF THE SAME PLATE

Position of plate	λ = 3.13 cm	λ = 3.33 cm	λ = 3.40 cm	λ = 3.53 cm	Spread of attenuation
3 db	3 03 db	2.97 db		2.86 db	0.17 db
4 db	4.0	4.0		3.7	0.30
5 db	4.90	5.01		4.50	0.51
6 db	6.1	6.0	5.67 db	5.55	0 55

and 6 db of attenuation at 9000 Mc/sec. The variation of attenuation with frequency is shown in Table 12·13, and the variation of the voltage standing-wave ratio is given in Table 12·14. For accurate measurements of voltage standing-wave ratio, it is also important to observe the effect of the coupling flanges, which cause additional frequency sensitivity beyond that of the metalized-glass plate itself. This effect is evident from the results given in Table 12·14.

Another example of the advantageous use of the frequency-insensitive region is the design of the metalized-glass plate shown in Fig. 12·45. This design is for a fixed waveguide pad of attenuation values between 25 and 30 db. In this case, the matching section can be designed to match the main film. To improve the voltage standing-wave ratio, the two struts used to support the plate do not continue beyond the glass plate, as shown in Fig. 12·46. The performance of this attenuator over the frequency band from 9000 to 9470 Mc/sec is given in Fig. 12·47 and shows particularly low voltage-standing-wave-ratio values for attenuations above 20 db.

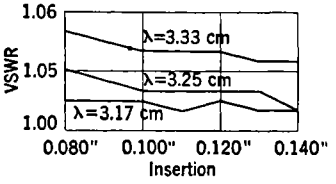

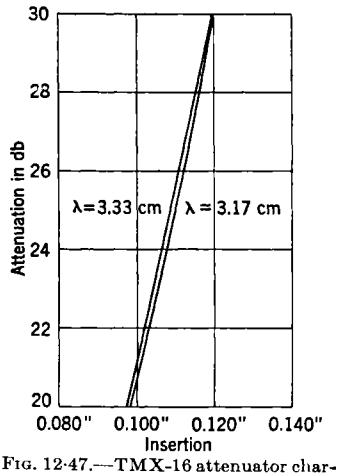

FIG. 12·47.—TMX-16 attenuator characteristics vs. insertion.

TABLE 12·14.—VARIATION OF VOLTAGE STANDING-WAVE RATIO WITH FREQUENCY FOR DIFFERENT POSITIONS OF THE SAME PLATE

Position of Plate	Direction of measurement*	λ = 3.13 cm	λ = 3.33 cm	λ = 3.53 cm
3 db	Choke end	1.065	1.041	1.055
	Flange end	1.03	1.062	1.079
4 db	Choke end	1.082	1.064	1.042
	Flange end	1.065	1.065	1.082
5 db	Choke end	1.09	1.10	1.045
	Flange end	1.07	1.105	1.09
6 db	Choke end	1.11	1.10	1.08
	Flange end	1.10	1.145	1.12

* Casing was furnished with one choke and one flange coupling. For "choke" reading, attenuator is coupled in through flange-choke combination. For "flange" reading, the coupling is through a flange-flange joint.

12·17. Construction of Variable Waveguide Attenuators.—In principle, the construction is of the same type for variable waveguide attenuators with metalized-glass inserts as for laboratory attenuators which use carbon paints or deposits on dielectric carrier plates (see Sec. 12·10). However, the driving mechanism for variable attenuators incorporating metalized-glass plates must be of considerable precision in order to avoid the imposition of undue mechanical stresses upon the glass. The result-

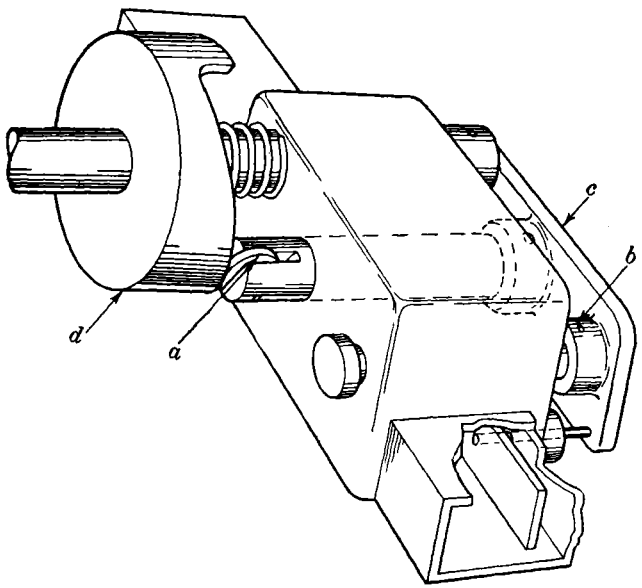

FIG. 12·48.—Cam drive for variable attenuator.

ing accuracy of positioning the dissipative metal film, together with the stability of the film itself, make these variable attenuators almost necessarily of the precision type suitable for permanent calibration.

The distinguishing features of the variation of attenuation have resulted in the development of three principal methods for the constructing of attenuators. These methods are incorporated in the single-vane type shown in Fig. 12·48, the double-vane type shown in Fig. 12·49, and the guillotine type, with either one plate in the center as shown in Fig. 12·50, or two plates symmetrically located, as shown in Fig. 12·51.

Single-vane Attenuators.—In attenuators of the single-vane type, two struts, accurately aligned, carry the single metalized-glass plate across a part of the guide. Special bosses on the side walls of the waveguide casing provide bearings as seen at *b* in Fig. 12·48. The actual driving

pin a is carefully aligned with the two struts and is attached to a heavy plate c which carries these struts. The driving pin in this model[1] is driven by a cam d against a restoring spring located within the superstructure. For accurate setting, the camshaft carries an engraved dial

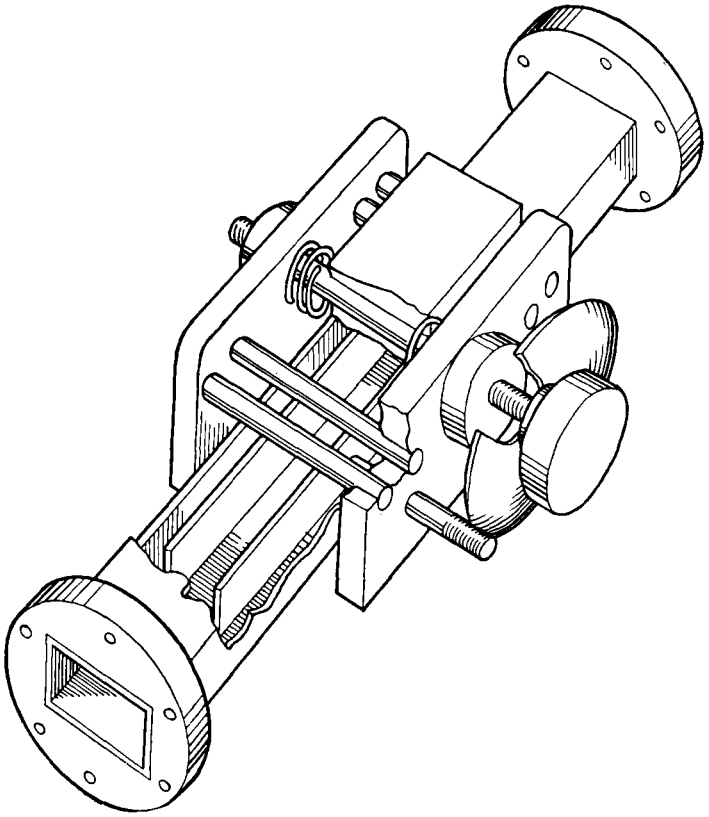

FIG. 12·49.—Double-vane attenuator.

while a gear-set vernier is usually attached directly to the casing. The cam drive has the advantages that the driving pin can be located in the center plane between the struts and that the cam can be designed to linearize the attenuation curve. It has the disadvantage, however, that any noticeable play of the camshaft makes resetting difficult. As an example, a metalized-glass insert designed for a maximum attenuation of 75 db in a waveguide of 0.400 by 0.900 in. ID has a change of attenua-

[1] This cam drive was designed by Philharmonic Radio Corporation, New York, N. Y.

tion of 0.8 db for each mil of displacement which occurs near a position corresponding to 66 db total attenuation. Obviously, the construction must be sufficiently sound to permit the resetting of the plate to small

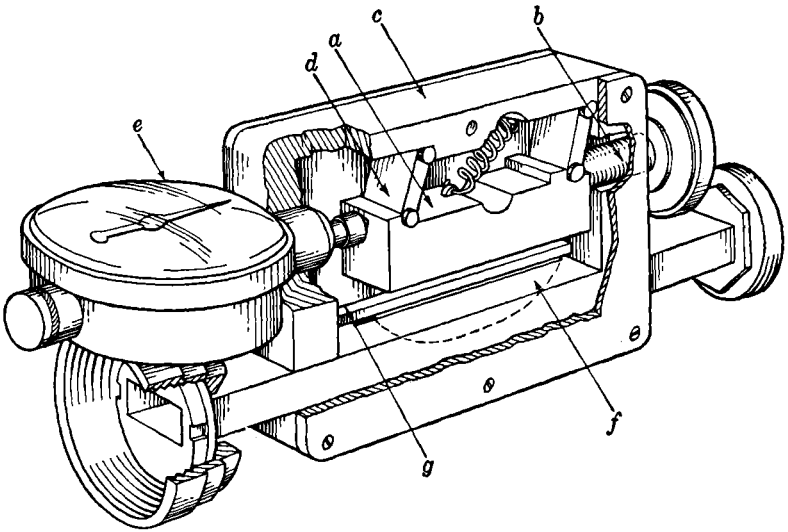

FIG. 12·50.—Precision 1-cm-band variable attenuator, TPK 35/PB/40.

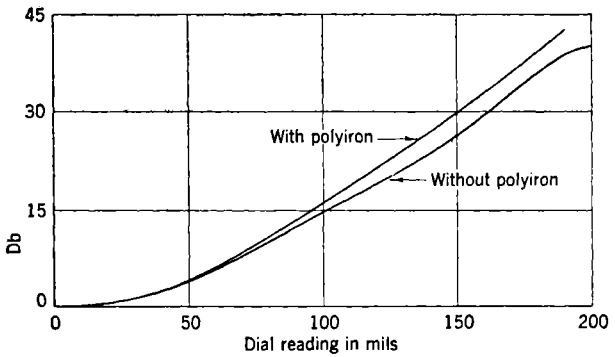

FIG. 12·51.—Effect of polyiron on attenuator loss. The ordinate scale is in decibels above the minimum insertion loss.

fractions of one mil. Frequently, a cam follower is built into the main pin *a* to avoid friction and wear; however, this follower must be accurately round in order to avoid errors in case of slippage. Furthermore, the restoring spring action must be strong enough to prevent the main pin from sticking when the cam is turned from higher to lower attenuation.

The cam drive can be replaced by a multithread screw drive.[1] The driving pin carries a very heavy plate, and the plate carries the struts supporting the glass plate. A guide pin keeps the plate from rotating or becoming misaligned. This casing is simple to construct, has directness of drive, and is easily reset. Hence, it has been widely used for attenuators where careful calibration is needed.

Instead of a dial and vernier, a micrometer drive can be installed and the position of the plate can be read on the micrometer head. Or, a counter device can be connected to the driving pin which has a fine screw thread so that each revolution corresponds to one mil advancement of the plate into the guide.

Another important consideration in the design of casings of the vane type is the exact spacing of the supporting struts. The strut-spacing tolerance and glass-hole-spacing tolerance must be kept small to permit ease of plate mounting. The struts should at no time exert undue pressure on the glass plate because pressure may cause breakage. This entails equal and exact strut spacing for all plate positions in the guide. It is important that no r-f power leak from the drive openings in the waveguide walls. Tests have shown little power leakage from the small $\frac{1}{16}$-in. driving holes in attenuators of the vane type. Although it is possible to provide small polyiron bushings to absorb the small leakage power, in most cases this is not necessary.

Double-vane Attenuator.—From theoretical considerations of the field distribution in the waveguide it can be shown that a symmetrical arrangement of two glass plates in the waveguide leads to a smaller voltage standing-wave ratio than is possible with a single glass plate, and it also results in a decreased frequency sensitivity of attenuation. Figure 12·49 gives a schematic view of the construction needed if two metalized-glass plates are driven simultaneously from opposite sides of the waveguide towards the center. The supporting struts cannot in this case extend across the waveguide. Although this construction affords an electrical advantage the mechanical construction is considerably weaker than the construction when one plate is used. For large plates, advanced far into the guide, the danger of mechanical resonance with impressed vibrations exists. This construction, therefore, has not been used for field-test attenuators.

Guillotine Attenuators.—An entirely different principle of variation of attenuation is the insertion of a metalized-glass plate through a slot in the broad side of the waveguide. Figure 12·50 shows the construction of a single-plate attenuator, for a center frequency of 24,000 Mc/sec, with a shape resembling that of a guillotine blade. On the broad side of the waveguide a frame c is built. From this frame the carrier a is

[1] Designed by F and R Machine Works, Long Island City, New York.

suspended by links *d* which are held in the bearing surfaces of the frame by a pair of strong springs. As a special feature of this construction, the glass plate *f* mounted on the carriage block *a* moves in the arc of a circle as the drive screw *b* is turned. During a constant turning of the drive screw, the vertical insertion of the glass in the guide is at first rapid, but its speed gradually tapers off as the glass swings to the lower extremity of the arc. If the dial indicator *e* is used, horizontal rather than vertical movement is measured. The form of variation of attenuation with plate insertion, combined with the nonlinear characteristic of the precision drive, results in an attenuation calibration which is nearly linear and which affords accurate setting.

Since the slot through which the glass plate is inserted is located in a region of strong electric field, the inserted glass acts as an antenna, and causes power to leak into the cavity formed by the attenuator casing. Thus energy is shunted from the main waveguide path, and the maximum attenuation obtainable is limited to the attenuation of this shunt path. In order to prevent this leakage, a frame of polyiron *g* is mounted on a metallic reinforcement of the top wall of the waveguide. Figure 12·51 demonstrates the effectiveness of the polyiron choking. Without polyiron, the maximum attenuation is about 40 db. The variation of the attenuation of the leakage path with glass insertion alters the shape of the calibration curve.

This single-plate guillotine attenuator can be contrasted with a double-plate guillotine attenuator of the symmetrical or balanced type.[1] Two plates are mounted on a common carrier as shown in Fig. 12·52. The carrier is driven by a cam which is mounted on a fixed frame of the casing, while the cam follower is affixed to a vertical structure of the carrier. Guidance is provided by a pin to avoid rotation about the vertical axis. Precise construction of this attenuator casing is necessary in order to avoid rocking of the carrier and to maintain strong contact between cam and cam follower. In order to avoid the shunt leakage provided by the metalized-glass plates, a polyiron frame closely surrounds the slots. Without this polyiron frame, the maximum attenuation obtainable is about 50 db, while with this frame, attenuation values up to 80 db can be obtained with very small variation of attenuation over a frequency band of ± 6 per cent centered at 9000 Mc/sec.

Mechanical Tests on Attenuators.—In many practical applications of attenuators, it is necessary that the complete attenuators withstand not only mechanical shock and vibration tests, but also corrosion tests under salt sprays. The cement mounting of the glass plates is satisfactory under dry conditions, but will not withstand salt spray. The

[1] Designed by Sperry Gyroscope Company, Garden City, N. Y.

eyelet mounting as described in Sec. 12·15 is completely satisfactory under all test conditions.

The mechanical strength of the glass plates might be a matter of concern under severe test conditions, particularly for long plates such as shown in Fig. 12·41*d*. For calculations on the strength of the cross section about the $\frac{1}{16}$-in. mounting hole, it was assumed that the plate was rigidly clamped at the point of strut support with a 4.8-cm length of

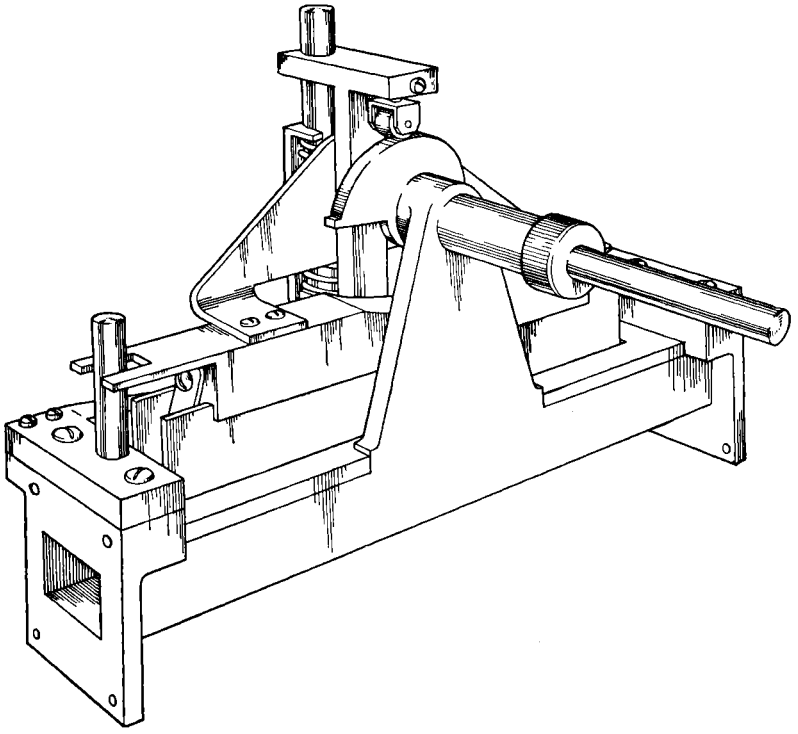

FIG. 12·52.—Double-plate guillotine attenuator.

glass extending out from the support. These calculations show that glass is strong enough to withstand the stress imparted by a sinusoidal vibration of the glass and the mounting with a maximum acceleration of 430*g*. The impressed vibration must have a frequency well below the natural frequency of 281 cps of the 4.8-cm length of extending glass. Static tests made on eleven plates with holes showed them to break when the stress applied corresponded to an acceleration of 200*g*. This reduction from the theoretical strength is probably caused by small fractures and strains in the glass.

Dynamic shake tests have been made on plates supported outside of casings, as well as on plates mounted in commercial casings of the type shown in Fig. 12·48 which use both cement and eyelet mounting. The shake tests were made by securely fastening the samples to the table of a vibration fatigue-testing machine.[1] In operation, the table had a sinusoidal vibration with a periodic change of frequency of from 10 to 50 cps over one-minute periods. Each sample was tested for vibration, in the plane of the glass and perpendicular to the plane of the glass, for ten minutes in each position. Four tests were made on each sample with different maximum accelerations ranging from 7.5 to 30g. In addition, all plates mounted in casings were tested with the plate close to the side wall and with the plate out in the center of the guide. There was no glass breakage nor did the joint between the glass and strut become loose. Several of the casings, however, were shaken so violently that the set screws on the drive mechanism were loosened, and indicated the necessity for cementing the set screws securely. Shock tests were conducted by directing severe hammer blows against a table on which the complete test set was mounted. No harm was done to the glass plates. Thus, with proper methods of mounting, the metalized-glass attenuators can be used as field instruments as well as for laboratory instruments.

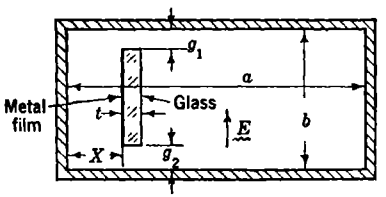

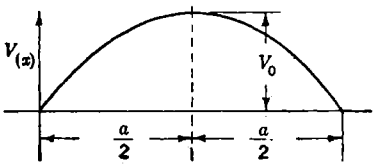

FIG. 12·53.—Coordinate system for circuit representation of attenuator.

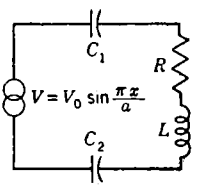

FIG. 12·54.—Simplified lumped-circuit representation of metal film in waveguide.

12·18. Performance Characteristics of Variable Waveguide Attenuators.—It is possible to devise a simple equivalent circuit for the dissipative action of an attenuator vane in a waveguide, and to explain, in a nearly quantitative manner, the variations of attenuation with the resistance of the metallic film, the position of the film in the guide, and the relative width of the glass plate carrying the film. Thus, if a transverse electric field is assumed, the designations in Fig. 12·53 used, and the current per unit length in the metallic film in the direction of the electric field

[1] Model 10-HA, manufactured by All-American Tool and Mfg. Company, Chicago, Ill.

defined as I, a shunt impedance to the local effective voltage V can be supposed as in Fig. 12·54. The resistance R and the inductance L are parameters per unit length of the resistive film, and the value of L varies with the plate position in the magnetic field of the guide. The condensers C_1 and C_2 represent the effective gap capacitances between the metalized-glass plate and the metal guide and depend inversely upon the gap values g_1 and g_2 and the resistance R of the film, since they represent the fringing effect of the electric field. This lumped-circuit representation is far from complete, but does allow for the possibility of the occurrence of resonance, which explains, at least partially, some of the attenuation characteristics experimentally observed.

Defining the effective voltage as

$$V = V_0 \sin \frac{\pi x}{a}, \tag{33}$$

and assuming, as a rough approximation,

$$\begin{aligned} L &= L_0 \sin \frac{\pi x}{a}, \\ C &= C_0 \frac{R_0}{R} \frac{g_0}{g} \sin \frac{\pi x}{a}, \end{aligned} \tag{34}$$

where L_0, R_0, g_0 and C_0 are quantities either empirically determined from tests or semiempirically determined from qualitative considerations, the current through the metallic film is

$$|I| = \frac{|V|}{|Z|} = \frac{V_0 \sin \frac{\pi x}{a}}{\left[R^2 + \left(\omega L - \frac{1}{\omega C}\right)^2\right]^{1/2}}$$

and the dissipated power per unit length is

$$|I|^2 R = \frac{V_0^2}{R_0} \cdot \frac{\left(\sin \frac{\pi x}{a}\right)^2}{\left(\frac{R}{R_0}\right) + \left(\frac{L_0}{R_0^2 C_0} \cdot \frac{g}{g_0}\right)\left(S - \frac{1}{S}\right)^2}, \tag{35}$$

where

$$S = \omega \sqrt{L_0 C_0} \sqrt{\frac{R_0}{R} \frac{g_0}{g}} \sin \frac{\pi x}{a}. \tag{36}$$

It is readily recognized that resonance occurs at the position x_0 for which

$$\sin \frac{\pi x_0}{a} = \frac{1}{\omega \sqrt{L_0 C_0}} \cdot \sqrt{\frac{R}{R_0} \frac{g}{g_0}}, \tag{37}$$

and that this resonance point is dependent on the width of the plate, on the resistance R, and on the frequency $\omega/2\pi$. No resonance exists if the right-hand term in Eq. (37) is larger than unity.

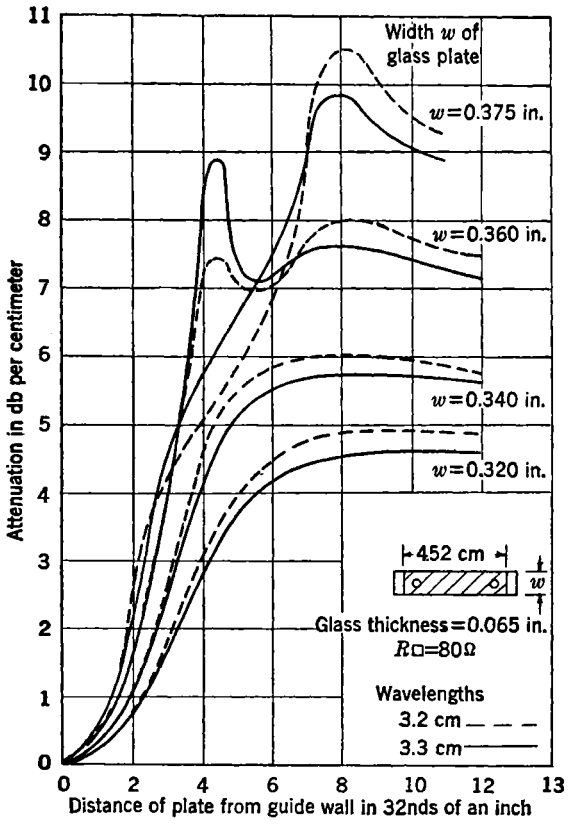

FIG. 12·55.—Attenuation characteristics of soft-glass vane coated with metallic film.

Figure 12·55 shows the measured values of specific attenuation of a metalized plate of soft glass in a waveguide the inner dimensions of which are 0.4 by 0.9 in. The match characteristics, over all tested values of width and for both frequencies, were good, with a VSWR of less than 1.15 even at the point of resonance, and therefore no possibility of a reflective resonance effect need be considered. The curves illustrate shift of resonance with increasing gap values g; they show the proper variation with frequency, and indicate that, in choosing a glass width for a certain film resistance, combinations close to resonance must be avoided. The change of attenuation with frequency usually becomes

large for plate widths near resonance. However, for some applications with the plate fixed in position, the attenuation-frequency crossover points caused by resonance can be used to reduce the variation of attenuation with frequency.

The curves in Fig. 12·56 illustrate the effect on attenuation, for various positions in the guide, as the film resistance is varied. The resistance

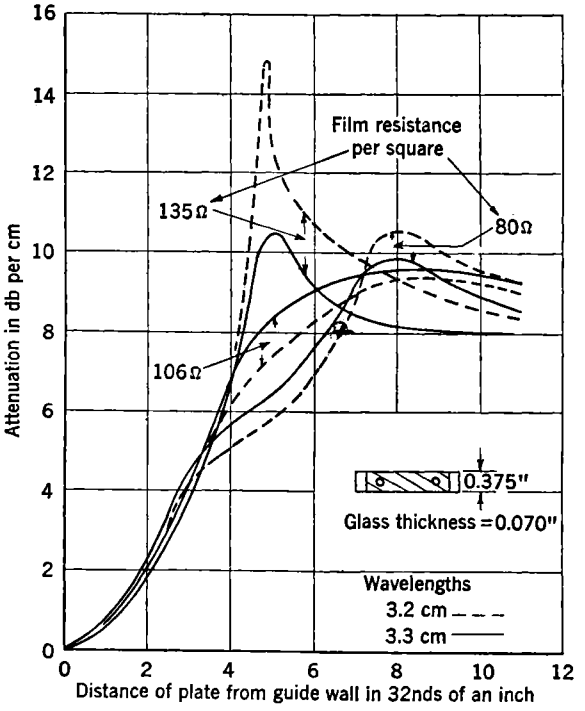

FIG. 12·56.—Attenuation characteristics of soft-glass vane coated with metallic film.

values shown are only approximate, since the metal films were not completely uniform. The shape and frequency characteristics of the curves justify the tentative acceptance of the equivalent series-resonant circuit. Thus, for a resistance of 135 ohms per square at a wavelength of 3.2 cm, the attenuation of the plate approaches the value for cutoff waveguide at the position corresponding to the cutoff width of the guide formed by the metal film and the larger section of the guide. As the plate moves out into the guide, the value of the attenuation decreases. However, a more complete equivalent circuit would be necessary to explain the shape of the attenuation curves of wide plates with a resistance of 80 ohms per square, particularly the hump in the curve at lower attenuation.

As an example of the over-all performance of a particular metalized-glass-plate design, Fig. 12·57 gives the voltage standing-wave ratio and the attenuation characteristics of the plate shown in Fig. 12·58. The design is for a frequency of 9000 Mc/sec, or a wavelength of 3.33 cm, and the inner dimensions of the waveguide are 0.4 by 0.9 in. The

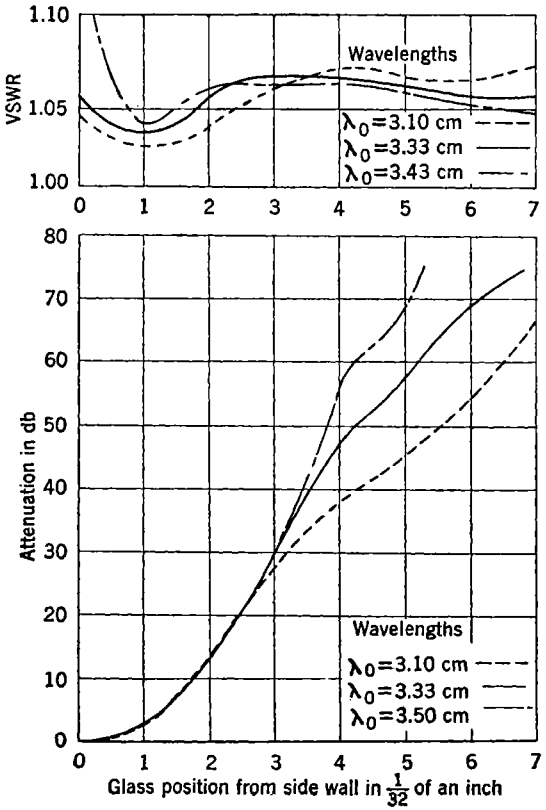

FIG. 12·57.—Attenuation characteristics of typical window-glass plate.

VSWR for this wavelength is less than 1.075 for all positions in the waveguide; and the attenuation curve, although not linear, is nearly so for high values of attenuation. The minimum value of attenuation, with the metal film very close to the side wall, is normally about 0.1 to 0.2 db. Although the match characteristics of the long taper are good over a rather broad band, the frequency dependence of attenuation is undesirably large. This is characteristic of vanes made of window glass.

The voltage standing-wave ratio of Fig. 12·57 shows the rise of the

voltage standing-wave ratio for small insertions of the metalized-glass plate into the guide, when only small effects from the plate itself might be expected. However, the glass plates in an attenuator of this type are usually supported by $\frac{1}{16}$-in. brass rods that extend across the guide in the plane normal to the electric lines of force (see Sec. 12·17). Since the supporting struts also reflect a small amount of power, the transforming section is designed to compensate for these reflections. If there is sufficient attenuation between the struts and the matching section to absorb this reflected power, then the strut problem is of no concern.

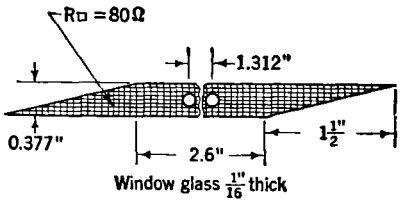

FIG. 12·58.—Metalized-glass plate dimensions for characteristics shown in Fig. 12·57.

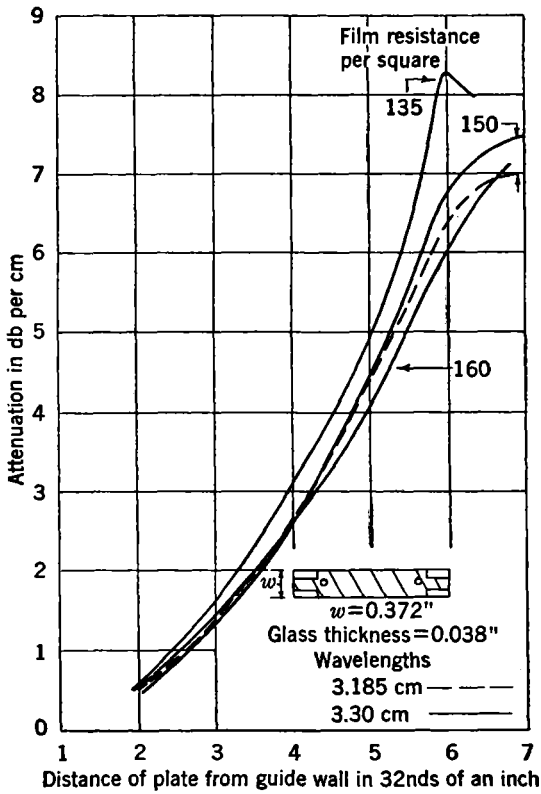

FIG. 12·59.—Attenuation characteristics of Pyrex glass with metallic film.

However, as the glass plate is also used in zero position or in positions of small attenuation, it is necessary to space the two struts an approximate distance apart of $n\lambda/4$, where n is an odd integer, in order to cancel the two strut reflections. Such cancellation can be perfect at only one wavelength, and in applications over a broad band of frequencies the strut effect becomes noticeable at the edges of the band, as seen in Fig. 12·57.

For the same waveguide size (0.4 by 0.9 in. ID), the thin pyrex plates with metal films should have a width of about 0.372 in. and a thickness

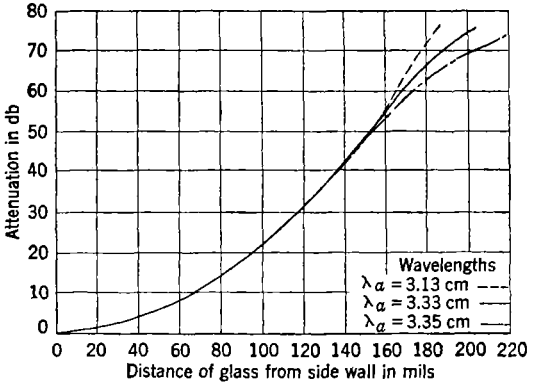

FIG. 12·60.—Attenuation characteristics for typical Pyrex plate with metallic film.

of about 0.038 in. in order to obtain a large range of attenuations, and at the same time to avoid the resonance characteristics shown in Figs. 12·55 and 12·56. The effect of the resistance is shown in Fig. 12·59, which indicates a resonance peak for a film of about 135 ohms per square at a position $\frac{3}{16}$ in. from the wall. It has been found that a film resistance of about 140 ohms per square gives best results with the above plate dimensions.

Figure 12·60 shows the over-all performance of the plate of Fig. 12·41*d*. The match characteristics are given in Fig. 12·43. This plate demonstrates very slight variations of attenuation with frequency up to values of 45 db and is therefore exceptionally well suited for broadband attenuators in low ranges of attenuation. In fact, if space permits, two of these can easily be placed in tandem in order to provide values of attenuation up to 90 db with a maximum variation of attenuation of about 2 db over the ± 6 per cent frequency band centered at 9000 Mc/sec. The minimum attenuation obtained with the metalized-glass plate close to the side wall of the guide and the metal film facing the wall, is practically negligible, in most instances less than 0.1 db.

For very small sizes of waveguide used for frequencies of about 24,000

Mc/sec, the use of metalized-glass vanes moving across the waveguide imposes extremely rigorous tolerances on the mechanical construction, and therefore, the desirable characteristics of the tongue-matched pyrex plate cannot be utilized. The most suitable attenuator construction is that of the guillotine, described in Sec. 12·17, with a metalized-glass plate, as shown in Fig. 12·61, whose matching characteristics depend on the gradual transition provided by its circular shape.

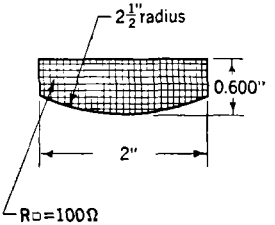

FIG. 12·61.—Metalized-glass plate dimensions for characteristics shown in Fig. 12·62.

An attenuator with a maximum attenuation of 40 db was designed for use over a band of ±2 per cent, centered at 24,000 Mc/sec, or for wavelengths from 1.225 to 1.275 cm, with a guide of inner dimensions

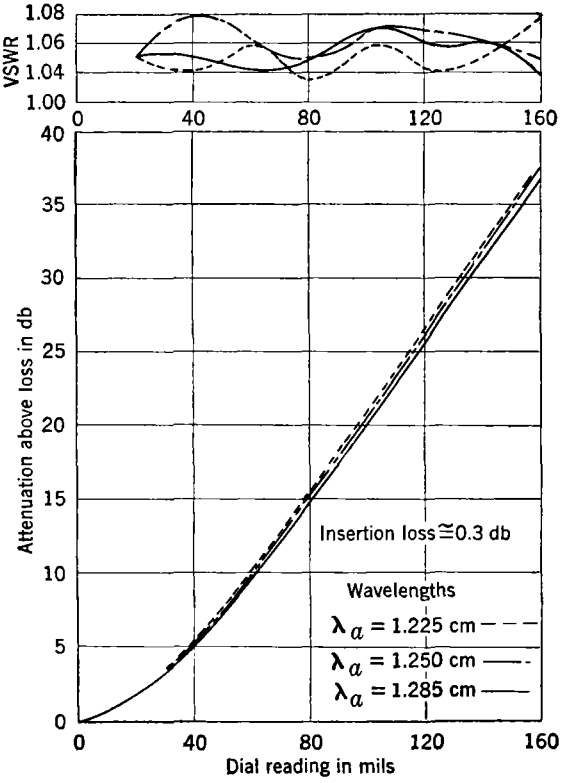

FIG. 12·62.—Performance characteristics of single-plate guillotine attenuator.

0.17 by 0.42 in. The minimum insertion loss of the complete unit was not more than 0.3 db and Fig. 12·62 shows the typical variation of attenua-

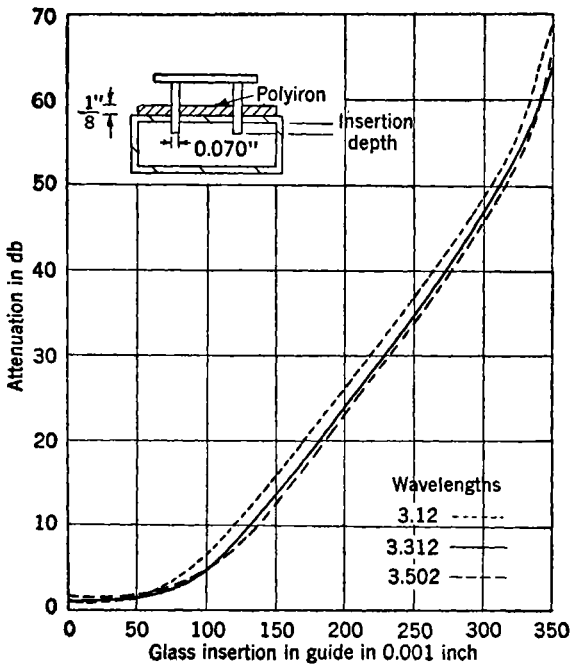

FIG. 12·63.—Attenuation characteristics of experimental model of 75-db balanced guillotine attenuator.

tion and voltage standing-wave ratio at three different frequencies. The maximum variation of attenuation between the edge frequencies is below ± 0.75 db.

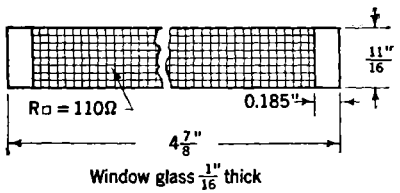

FIG. 12·64.—Metalized-glass plate dimensions for characteristics shown in Fig. 12·63.

An attempt to reduce the frequency sensitivity of attenuation for high values of attenuation in the range of 9000 Mc/sec resulted in the construction of the guillotine attenuator with two metalized-glass plates inserted into the guide as described in Sec. 12·17. Figure 12·63 shows the attenuation characteristics of this attenuator, and also indicates the schematic arrangement. Figure 12·64 shows the glass-plate dimensions with the clear glass matching sections used in this attenuator. The match characteristics are considerably poorer than those of the tongue-matched pyrex plate. They give VSWR values up to 1.24, but

the variation of attenuation with frequency over the band of ±6 per cent centered at 9000 Mc/sec is less than 3.5 db for all depths of insertion into the guide. This is the result of the interaction between the metalized-glass plates within the guide and the cavitylike casing which encloses the driving mechanism and superstructure as shown in Fig. 12·52. The attenuation curves in Fig. 12·63 show a second crossover region near 60-db attenuation values, which obviously tends to reduce the divergence found in the other regions. Such interaction is necessarily critical, however, in mechanical precision, metal film resistance, polyiron framing, and possibly other factors, and consequently, reproducibility under normal production processes is difficult to achieve.

POWER DIVIDERS AS ATTENUATORS

By E. Weber

In power measurements it is often convenient to use a sensitive power indicator because of its greater individual accuracy and also because of its quicker response. If a power indicator is used it is necessary to interpose between the input terminal of the power indicator and the main power flow an accurately known amount of attenuation. This attenuation is usually provided by radiation coupling either through appropriate holes or through pickup antennas. Power dividers of several types are used successfully; among those used are calibrated pickup probes, directional couplers, bifurcated lines, and branched lines.

12·19. Calibrated Pickup Probe.—A power-monitoring device of the very simplest type is a common slotted section with an adjustable bolometer-probe pickup, provided that this probe can be calibrated by

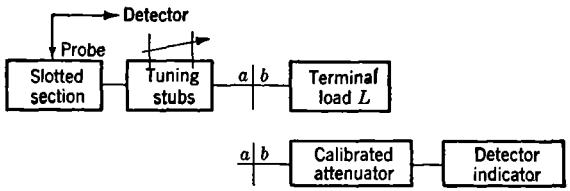

FIG. 12·65.—Use of calibrated bolometer probe with terminal load as attenuator.

an independent power measurement. Figure 12·65 shows an arrangement whereby the power into the terminal load L is to be measured by a sensitive power detector coupled through the probe to the main power flow. The calibration of the bolometer probe can be accomplished by substituting for the terminal load a well-matched calibrated attenuator and detector. For a certain fixed probe depth and for a fixed setting of the calibrated attenuator, the absolute probe indications over a selected frequency range can then be defined as the equivalent attenuation values.

By variation of the probe depth, different values of attenuation can be attained; but the probe depth must be so chosen that no appreciable reflection of power occurs since this reflection detracts from the accuracy of the power indication. Furthermore, in order to assure general validity of the calibration, the terminal load must be well matched; this can be achieved with the tuning stubs, and the bolometer probe in the slotted section can also be used to indicate proper match. If no matching stubs are available, then the forward power delivered into the terminal load can be computed from maximum and minimum values of power by

$$P = [\tfrac{1}{2}(\sqrt{P_{\max}} + \sqrt{P_{\min}})]^2. \tag{38}$$

If the bolometer-probe indications have been calibrated in terms of a well-matched calibrated attenuator, the assembly of the slotted section with the probe, the tuning stubs, and the terminal load represents an attenuator of adjustable values. These values of attenuation are usually large, above 30 db. This method is particularly useful for large powers, since the dissipation of the terminal load can be increased to absorb practically all the main power. If the terminal load is very well matched over the entire useful frequency band, then the probe can be kept in a fixed location and can be made an integral part of the load; for calibration purposes, however, it still has to be detachable. This method is, of course, equally applicable to waveguide and to coaxial transmission systems.

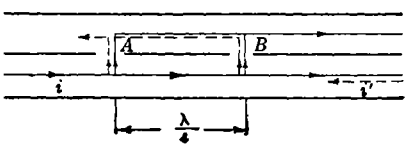

FIG. 12·66.—Principle of directional coupler.

12·20. Directional Couplers.—In Chap. 14, it is observed that directional couplers can be designed for broadband applications to measure voltage standing-wave ratio or to act as power monitors. In principle, two coupling holes between parallel transmission systems are spaced one-quarter wavelength apart as in Fig. 12·66, which shows a sketch for a waveguide system. The incident wave radiates through the holes A and B into the neighboring system; both forward waves are in time phase at B (having traveled the same distance) and support each other to form the outgoing wave O. The backward waves which issue from A and B travel to the left, but the phase difference between the waves from A and those from B at the point A is exactly 180°, and therefore cancellation results and no resultant wave issues to the left. For an incident wave i', the results are opposite, and therefore, the forward and the reflected wave intensities can be measured separately.

On the other hand, this simple directional coupler can be used as a fixed attenuator pad if the remaining incident wave i' is absorbed in the main system and the remaining reflected wave r' is absorbed in the other

system as shown in Fig. 12·67. In this way, it is easy to obtain attenuator pads for large power and for high attenuation values. Coaxial systems at approximately 3000 Mc/sec have been built for 30-db attenuation or more with small variations with frequency over a frequency band of 30 per cent.[1] For waveguide systems, such attenuator pads have

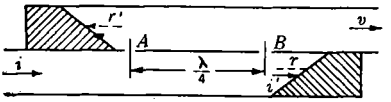

FIG. 12·67.—Use of directional coupler as attenuator.

been built for about 3000 Mc/sec down to values of 15 db, and at 9000 Mc/sec for values of 10- and 20-db attenuation. The variation in coupling was less than 0.3 db for a frequency band of 12 per cent. With well-matched terminations, the problem of the directivity of the coupler, that is, the fact that incomplete cancellation of the backward-traveling waves occurs, is of less importance. Of course, it is necessary to determine the attenuation values by accurate calibration, and it does not seem possible to control mechanical and material factors in such a way as to obviate this necessity.

12·21. Bifurcated Lines.—A very convenient power divider of fixed ratio is obtained by the introduction of a very thin partition into a transmission-line system, as shown in Fig. 12·68 for a waveguide. The

FIG. 12·68.—Bifurcation of a waveguide.

guide of small dimension b is divided into two guides of small dimensions b' and b''. If the characteristic impedances are chosen as

$$\frac{Z_0'}{Z_0} = \frac{b'}{b}, \qquad \frac{Z_0''}{Z_0} = \frac{b''}{b}, \tag{39}$$

and

$$Z_0 = Z_0' + Z_0'', \tag{40}$$

the three guides can then be considered in series combination and no power reflection takes place if the two smaller guides are individually terminated in their characteristic impedances. For use of this arrangement as an attenuator, one of the smaller guides would be terminated in a well-matched power-absorbing section and the other used as the

[1] R. S. Julian, "Directional Transmission Line Taps," BTL MM-44-170-6, Jan. 26, 1944.

output guide, connected to the transmission system with the reduced power. By the use of a proper taper transition section this output guide can, of course, be brought back to the characteristic impedance Z_0 of the input system. The actual value of attenuation can be determined from the power split. If the guide with impedance Z_0'' is the output guide, then the output power P'' is, in terms of the input power P_0,

$$P'' = \frac{Z_0'}{Z_0} P_0, \tag{41}$$

and therefore, the attenuation becomes

$$A = 10 \log_{10} \frac{P_0}{P''} = 10 \log_{10} \frac{Z_0}{Z_0'} = 10 \log_{10} \left(1 + \frac{Z_0''}{Z_0'}\right) \quad \text{db.} \tag{42}$$

This attenuation is defined directly in terms of the impedance ratio. If the termination in the guide Z_0' can be made frequency-insensitive and if the characteristic impedances are reasonably constant, the attenuation can be made substantially constant over a considerable range of frequencies. The termination must, of course, be able to absorb the power P' and this determines the material that can be used.

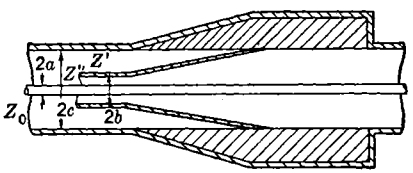

FIG. 12·69.—Attenuator using the bifurcation of a coaxial transmission line.

Figure 12·69 indicates a power split in a coaxial transmission system whereby the impedance must now be related according to

$$\frac{Z_0'}{Z_0} = \frac{\ln \frac{c}{b}}{\ln \frac{c}{a}}, \qquad \frac{Z_0''}{Z_0} = \frac{\ln \frac{b}{a}}{\ln \frac{c}{a}}, \tag{43}$$

and where

$$Z_0 = Z_0' + Z_0'' \tag{44}$$

in order to lead to the three lines in electrical series combination. To bring the output system to the same impedance as the input system a taper transition section is shown. This section, if made somewhat longer than the longest wavelength in the selected wavelength range, usually results in a satisfactorily low voltage standing-wave ratio over a considerable range.

The simple concept of direct series connection holds strictly for

infinitesimally thin partitions[1] and also for any chosen reference plane in the main guide, but practically, little disturbance is observed with thin but finitely thick partitions.

12·22. Branched Lines.—As an alternative to the series combination of transmission lines, two transmission lines in parallel to a main system can be connected as illustrated in Fig. 12·70 for a coaxial line. Since

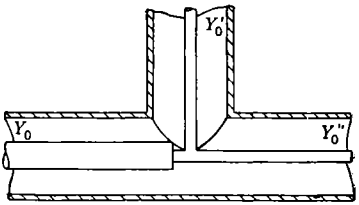

FIG. 12·70.—Attenuator using parallel power split.

the two branch lines are in parallel, they are best represented in terms of their characteristic admittances Y_0' and Y_0'', and again satisfy the condition that

$$Y_0' + Y_0'' = Y_0. \tag{45}$$

If one of the branches, Y_0', is terminated in a well-matched power absorber of proper characteristic impedance, and if the other branch Y_0'' is used as the power output system, the over-all attenuation is given as in Eq. (42) by

$$A = 10 \log_{10} \frac{P_0}{P''} = 10 \log_{10} \frac{Y_0}{Y_0'} = 10 \log_{10} \left(1 + \frac{Y_0''}{Y_0'}\right) \quad \text{db.} \tag{46}$$

In order to bring the output admittances again to standard coaxial-line values, impedance transformers can be added in the output section. The transformers may be either the quarter-wavelength type or the tapered type. From the point of view of frequency sensitivity, the bifurcated line has numerous advantages, while mechanically, both the bifurcated line and the branched line present moderate design difficulties.

[1] See Waveguide Handbook, Vol. 10.

CHAPTER 13

THE MEASUREMENT OF ATTENUATION

By Ernst Weber

To be meaningful the term "attenuation" must be associated with a measurable physical quantity, such as voltage, current, or power, which can be uniquely established at two terminal pairs of an otherwise unrestricted network (see Sec. 11·1). At microwave frequencies, the most readily measured quantity is power, whereas terms like voltage and current would in many cases require explanatory definitions. Attenuation has become associated principally with power and, furthermore, is, as demonstrated in Sec. 11·1, defined in terms of a measurement under ideally normalized conditions; namely, by inserting the pertinent micro-

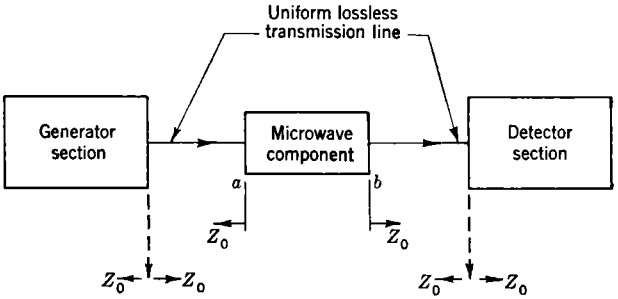

Fig. 13·1.—Schematic arrangement for measurement of attenuation at a microwave frequency.

wave component into a lossless transmission line of defined characteristic impedance Z_0 (see Fig. 13·1) terminated at one end by an ideally matched generator section, and at the other end by an ideally matched detector section. Maintaining these conditions, two principal methods of measurement can be devised; one in which the unknown microwave component is actually removed and the power ratio measured as "insertion loss," another, in which the unknown microwave component, together with a standard of comparison, establishes a fixed over-all power ratio by mutual substitution; both these methods will be described in detail. Other methods of attenuation measurement have been proposed and used; these, however, deviate from the above concept of attenuation and need qualifying elucidation.

13·1. Direct Measurement of Power Ratio.—The simplest arrangement for the direct measurement of the power ratio as insertion loss under normalized conditions involves the *use of two slotted sections* with probe detectors of identical characteristics. Figure 13·2 indicates schematically the arrangement of the equipment, and clearly indicates to the left of a the generator section, and to the right of b the detector section. In order to establish proper matching conditions in both directions, two complete modulated-oscillator assemblies with power supply and square-wave modulator are needed. With the oscillator unit A

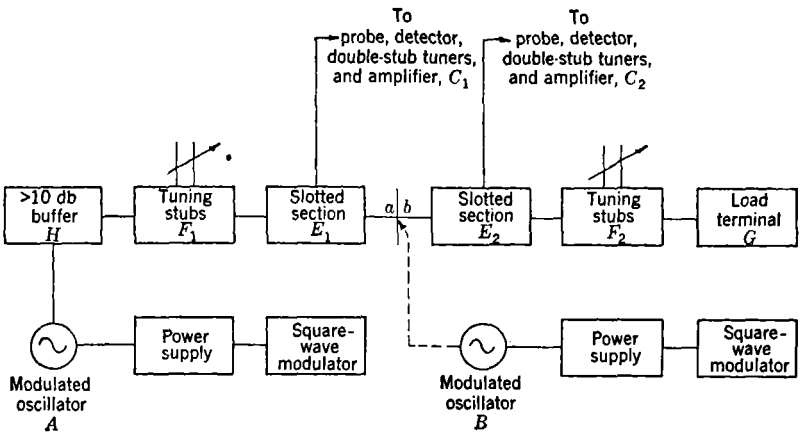

FIG. 13·2.—Schematic arrangement for measurement of attenuation with two slotted sections.

connected to the closed assembly joined at ab, the tuning stubs F_2 are adjusted to a VSWR < 1.02 as read in either slotted section E_1 or E_2. With the oscillator unit B connected to the left section of the assembly at b and with oscillator unit A inactive, the tuning stubs F_1 are adjusted to a VSWR < 1.05 as read in slotted section E_1. To assure no noticeable subsequent disturbance of the match looking back into the active oscillator unit A, the buffer attenuator H must have a minimum value of 10 db for most oscillators.

The measurement of attenuation proceeds by first normalizing the probes in slotted sections E_1 and E_2 to the same power level with a and b directly joined. Inserting then the unknown microwave component between a and b, and maintaining the *same* power level in the probe of slotted section E_1, the needed gain in the amplifier C_2 will be a direct measure of the power loss or attenuation caused by the unknown component. Obviously, the gain in the amplifier C_2 can be directly marked in decibel values and thus permit direct reading of attenuation as long as

the detector characteristic follows the square law, that is, is linearly related to the absorbed power. This is usually assured with Wollaston-wire bolometers which are therefore preferred to crystal detectors for attenuation measurements. If crystal detectors are used, it is best to determine their detection characteristics by calibration with a standard signal generator. In order to assure greater accuracy, the arrangement in Fig. 13·2 can be made perfectly symmetrical by placing the second modulated oscillator B behind the terminal load G, which can then take the form of a buffer attenuator similar to H, and which performs the

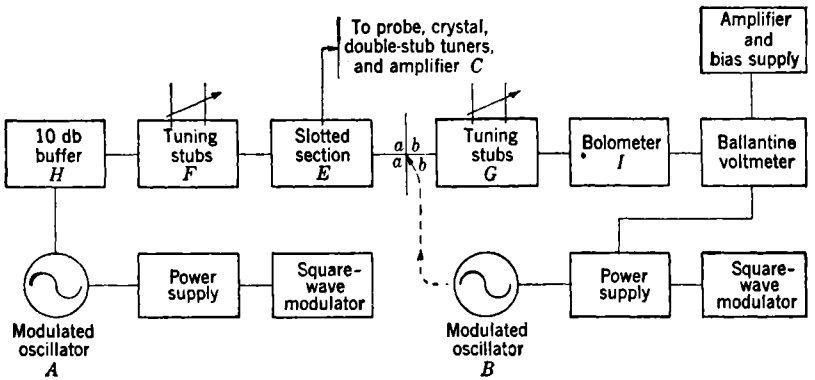

FIG. 13·3.—Schematic arrangement for measurement of attenuation with Ballantine voltmeter.

attenuation measurement alternately with source A active and B inactive, and vice versa. This requires complete identity of the probe-detector characteristics. This method can be used conveniently for attenuations up to 15 db and for frequency ranges for which the microwave accessories have been designed, since the ultimate indicator, namely, the amplifier, responds only to the modulating frequency of the oscillator which is usually chosen in the audio range.

This method will, however, not measure the value of attenuation as insertion loss according to the definition in Sec. 11·1 if the unknown component is badly mismatched. In this case, the reflective attenuation is disregarded by trying to keep the input power level constant; but even this becomes difficult to assure because the power level is actually determined from the VSWR of slotted section E_1.

Ballantine-voltmeter Method.—Another very convenient method of attenuation measurement replaces the detector section in Fig. 13·2 by a bolometer terminal in conjunction with a Ballantine voltmeter as shown schematically in Fig. 13·3. Here, detection of the modulated r-f power by the bolometer develops a voltage across the input terminals

of the special, tuned audio peaked amplifier which is amplified and indicated on the voltmeter. The basic assumption[1] is made that with the proper amount of d-c bias power in the bolometer, the a-c voltage developed across the amplifier input terminals is proportional to the r-f input power to the bolometer which therefore acts as a square-law detector. If the amplifier is strictly linear, a change on the voltmeter of n db indicates a change in attenuation in the transmission line of $n/2$ db. Since the calibrated voltmeter is actuated by the audio component of the bolometer output voltage, this method is not limited to a specific range of microwave frequencies unless difficulties are encountered in matching the bolometer at some frequencies.

The range on the voltmeter that may be used in practice is limited on the low-power end by noise and on the high-power end by nonlinearity of the bolometer. By checking the various scales of the voltmeter as well as the linearity of the amplifier, it has been found that the maximum safe range usually extends from 0.01 to 10 volts, permitting, together with the tuned amplifier, the measurement of power ratios up to 30 db. Larger ranges of attenuation may be measured in two steps by subdivision into two ranges, each of which is smaller than 30 db and by establishing the terminal point of the lower range as a new fixed reference point for the upper range. Of course, the error of measurement in such a procedure is doubled and the limit is probably set by the power capacity of the source as well as all the microwave components in the assembly. For greater accuracy, the voltmeter should be calibrated. The calibration may be made with an audio attenuator of negligible reactance which has in turn been calibrated with a potentiometer (see Sec. 13·7).

In order to establish proper matching conditions in both directions the same procedure should be followed as above. With source A inactive, source B connected at b, adjust the tuning stubs F for good match as read in the slotted section E; then, with source A active, the system closed at ab, adjust tuning stubs G for good match as again read in slotted section E. If the bolometer mount is tunable, it should be matched independently by using a slotted section with the proper d-c bias current circulating through the bolometer.

The actual measurement of attenuation then proceeds in the following manner: With the components assembled as in Fig. 13·3 and matched, the r-f power level is adjusted by means of the buffer H so that no more than the maximum permissible power enters the bolometer. The amount of buffering may be increased when necessary in order to fulfill this condition; however, a buffer of at least 10 db must be used, as

[1] The validity of this assumption is discussed in R. L. Report No. 55.1—10/16/45, "Notes on the Use of Bolometers for Pulsed R-f Power Measurements," by George Guthrie.

explained above. After the frequency of the oscillator is checked, the modulation frequency is set at 1000 cps to correspond with the frequency at which the preamplifier is peaked. This setting gives maximum deflection on the Ballantine voltmeter. The gain control on the preamplifier is adjusted so that the Ballantine voltmeter reads 20 on any range other than the 100-volt range. Switched to the next higher range, the meter should then read exactly 0. If it fails to do this, mechanical adjustment of the voltmeter must be made until this condition is met. By setting the gain control on the preamplifier, a reference level on the voltmeter is established, the system disconnected at points *a* and *b* and the unknown microwave component inserted and the new reading taken. One half of the difference between the reference and final readings gives the power attenuation of the unknown component. For better accuracy, repeated checks should be made on all initial adjustments, such as oscillator frequency, modulator frequency, reference power level, and matching conditions.

For various frequency ranges, different types of bolometers are available, which are described in Chap. 3. For frequencies in the range of 3000 Mc/sec or above, Littelfuse elements for $\frac{1}{200}$ amp can be used as bolometers; they require a d-c bias current of about 5.5 ma. Most Wollaston-wire bolometers can carry a permissible maximum power between 1 and 30 mw. Bolometers have been made with metalized-glass fibers which can carry up to 0.1 and 0.2 watt of maximum power. Further extension of the power range is possible by insertion of carefully calibrated precision attenuators between the bolometer and the tuning stubs *G* in Fig. 13·3. The accuracy of the attenuation measurement will then be influenced by the accuracy of the additional attenuator.

Water Calorimeter.—For still higher power capacities the bolometer-detector section in Fig. 13·3 is replaced by a water calorimeter, described in Secs. 3·32 to 3·36. The power-detecting medium is the circulating water absorbing the heat generated. With proper calibration and well-controlled water-pump speeds, the accuracy can be made satisfactory for most practical purposes.

13·2. Substitution Methods.—A different method of attenuation measurement particularly suitable for high values of attenuation is the *substitution method*, in which, at some point in the detector system, the power level is maintained constant upon insertion of the unknown microwave component by adjusting the attenuation of an appropriate standard attenuator, which can be a part of either the generator section or the detector section. Several schemes are possible based on the same principle and differing only with respect to the choice of the section in the detector system in which the power level is maintained constant. Thus, in the microwave substitution method, the microwave power at the

detector is maintained at a constant level with the aid of a microwave standard attenuator, located in series with the unknown attenuator, either in the generator section or in the detector section. In the intermediate-frequency substitution method, the power level is maintained constant at the i-f detector by adjusting an i-f standard attenuator to compensate for the insertion of the unknown microwave component. Finally, in the d-c substitution method, the power level in one arm of a d-c bridge circuit is maintained constant, as with the use of a bolometer bridge detector.

Microwave Substitution Methods.—The specific arrangement of equipment will in most cases depend on the power range of the microwave

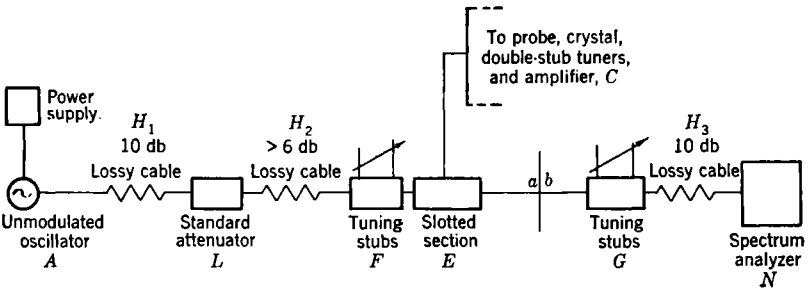

FIG. 13·4.—Schematic arrangement for measurement of attenuation at 3000 Mc/sec with microwave standard attenuator in generator section.

source, on the sensitivity of the detector, on the availability of a suitable standard, and on the over-all characteristics of the equipment. As will be pointed out in Sec. 13·6, the waveguide-beyond-cutoff standards can be considered primary standards, but they usually have a rather large minimum attenuation value necessitating very sensitive detectors to permit the measurement of large ranges of attenuation. Although the resistive precision attenuators have nearly zero minimum attenuation, they must be calibrated absolutely. Of the three principal types of power detectors that are commonly used; namely, the crystal, the bolometer, and the spectrum analyzer, only the spectrum analyzer has a sensitivity sufficiently high to permit attenuation measurements up to 70 or 80 db. The maximum sensitivity of the crystal or of the bolometer limits the range to about 30 db. In view of the fact that the substitution methods are particularly suitable for wide ranges of attenuation measurements, the spectrum analyzer primarily will be considered here.

As an illustration of an arrangement with the standard attenuator in the generator section, Fig. 13·4 shows the system used for frequencies of about 3000 Mc/sec, for which a special primary-standard attenuator has been developed with a tunable transmission cavity on one end that

must be tuned for maximum power transfer (see Sec. 11·9). It is advisable to use the cavity at the input end of the standard attenuator. The standard attenuator should be located near the oscillator since the effective load impedance at this point is constant and the frequency of the cavity will not be pulled. Power is coupled into the cavity with a loop and out of the cavity through an iris to the cutoff tube. If the attenuator is held in a position so that the rotating drive shaft is horizontal, the planes of both loops will be vertical and a line passing through the long dimension of the iris will be horizontal. The standard attenuator is isolated from the rest of the system by means of pieces of lossy cable so that the maintenance of a good match, looking towards the generator from point *a* after it has once been matched by means of the tuning stub *F*, is assured.

Similarly, the spectrum analyzer is isolated from the output end *b* of the unknown microwave component by a lossy cable of at least 10-db attenuation in order to maintain a match once a match has been established by the tuning stub *G*. The spectrum analyzer consists of a well-shielded superheterodyne receiver employing a crystal mixer and having a local oscillator that is frequency modulated in sawtooth fashion. A frequency spread of ± 20 Mc/sec about the frequency setting of the local oscillator is available. The sawtooth voltage that produces the frequency modulation of the local oscillator is also applied as the horizontal deflection voltage to a cathode-ray oscilloscope. The video output voltage of the receiver is connected to the vertical plates of the oscilloscope. Thus, when a signal is applied to the input terminals of the receiver, a pip appears on the screen. The receiver bandwidth is about 50 kc/sec. The magnitude of the pip is a measure of the input power to the receiver. To measure attenuation, the standard attenuator is set for a value that is a few decibels higher than the attenuation to be measured. By means of the gain control, the pip of the spectrum analyzer is set at a convenient level on the screen of the oscilloscope. The unknown microwave component is inserted at *ab* and the attenuation of the reference standard is reduced until the pip returns to the level previously set. As a check, removing the unknown component and returning the dial setting of the reference standard to the value initially selected should bring the pip to the same level again. If the level has changed, the measurement is to be discarded as erroneous. The error may be caused by instability either in the source or in the spectrum analyzer. The maximum usable range of this system for measuring attenuation is limited to about 54 db. The range of the power ratios that the spectrum analyzer can detect is of the order of 95 db. The various buffer-cable sections consume at least 26 db and the nonlinear region in the standard cutoff attenuator extends to 15 db resulting in an actual minimum attenuation in the system, exclusive of the unknown component, of 41 db.

Figure 13·5 shows the schematic arrangement of a system for the measurement of attenuation in the range of 9000 Mc/sec with the standard attenuator in the detector section. For better accuracy, rectangular

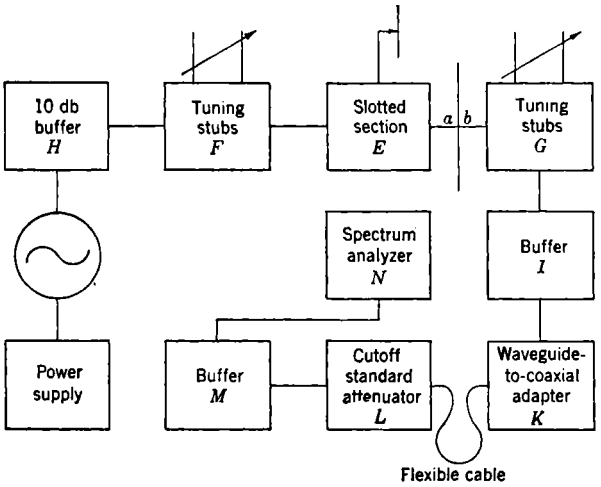

FIG. 13·5.—Schematic arrangement for measurement of attenuation at 9000 Mc/sec with microwave cutoff standard attenuator in detector section.

waveguide is used for the power-transmission system, necessitating an appropriate adaptor to permit insertion of the reference standard. The movable end of the cutoff attenuator is joined to the line by means of a flexible cable employing cable connectors. Since no cutoff standard has been designed for this frequency range which incorporates a frequency-sensitive cavity, it can be placed close to the receiver-type detector. As above, the over-all attenuation needed in the system, exclusive of the unknown component, is about 41 db so that the same range of attenuation measurements can be covered.

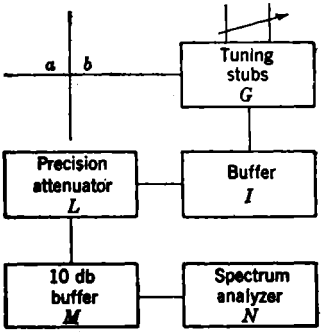

FIG. 13·6.—Schematic arrangement of detector section for measurement of attenuation at 9000 Mc/sec with microwave resistive attenuator in detector section (generator section same as Fig. 13·5).

A considerable extension of the range of attenuation measurements can be achieved by the use of a resistive variable attenuator standard such as is described in Secs. 12·18 and 13·6. The arrangement of the components is shown in Fig. 13·6. Essentially, the cutoff standard attenuator with the adaptor is replaced by the resistive precision

attenuator. The minimum attenuation of the resistive attenuator is almost zero, in any case less than 0.5 db. Since resistive attenuators are usually well matched, the buffer attenuator *I* can have very low attenuation. Therefore the minimum attenuation in the system, exclusive of the unknown component, can, in this case, be made about 20 db and the range of attenuation measurements can be extended to 75 db. With a proper r-f source or with reduced buffering and acceptance of loss of accuracy, this extension can possibly be carried even further.

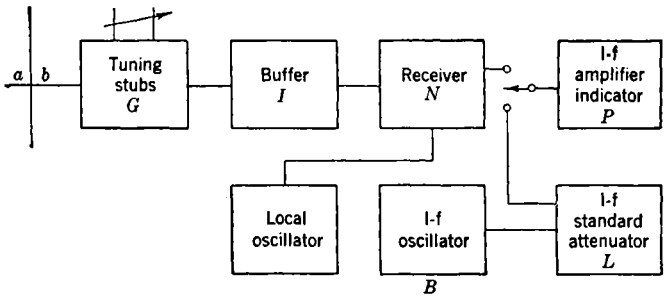

FIG. 13·7.—Schematic arrangement of detector section for measurement of attenuation with i-f standard attenuator.

I-f Substitution Method.—Instead of compensating for the attenuation of the unknown component in the microwave system itself, a receiver can be used as a detector and compensation can be made in the i-f part of the detector section. Figure 13·7 indicates one possible arrangement[1] whereby the i-f amplifier-indicator is designed for 20 Mc/sec and is used principally as a power-level indicator. The measurement of attenuation proceeds by first adjusting the gain control on the i-f amplifier to a convenient level for reception from the microwave line. The i-f amplifier-indicator is then connected to the i-f standard attenuator, which in turn is adjusted to give the *same* indication on the amplifier. The receiver is switched back to the microwave line, and the unknown microwave component inserted, the gain control on the i-f amplifier is adjusted to give a convenient reading; then the i-f amplifier is again switched over to the i-f standard attenuator and this is adjusted to bring the i-f amplifier to the new reading set by the microwave signal. The change in setting in decibels of the i-f standard attenuator is thus identical with the attenuation of the inserted microwave component at the microwave frequencies. In using the i-f standard attenuator, the frequency and power level of the i-f source should be carefully checked. It is advisable to use a special i-f amplifier with humped frequency

[1] See F. G. Gainsborough, "Notes on the Calibration of High-frequency Attenuators at the National Physical Laboratory," B.C.S.O. Report No. 343, Jan. 24, 1945.

response to make the tuning unambiguous. Likewise, the i-f standard attenuator should be very carefully constructed, preferably so that it can be calibrated with direct current to avoid additional sources of error.

The accuracy of the method depends on the linear relationship existing between the i-f beat-frequency amplitude and the power level of the microwave signal, which in turn depends on the mixer characteristics. If the local-oscillator input signal into the mixer can be kept at least 10 times stronger than the microwave signal, this linearity will be maintained with sufficient accuracy in diode mixers and even in crystals, as has been

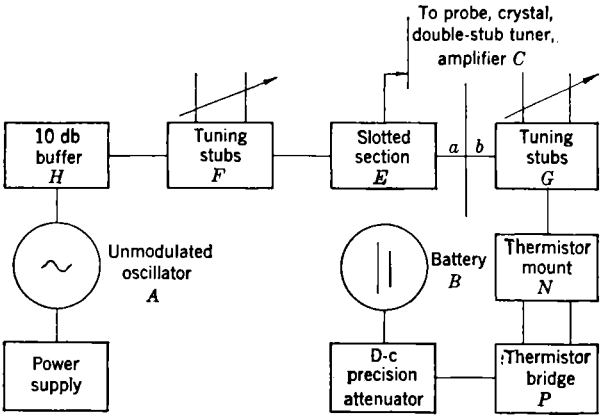

FIG. 13·8.—Schematic arrangement for measurement of attenuation with the thermistor bridge.

shown experimentally at the National Physical Laboratory.[1] The advantage of the method is, however, that the i-f attenuator standard can be the same for practically any microwave frequency if proper changes are made in the local oscillator of the receiver.

Thermistor-bridge Methods.—The use of thermistors as high-frequency power-measuring elements has been discussed in Chap 3. In almost all applications the basic assumption is made that equal amounts of d-c and microwave power have the same effect on the temperature rise of the element and therefore cause the same resistance change. This principle can be used to extend the substitution method to include d-c substitution by employing the thermistor as a power detector and a properly designed bridge circuit as a power-level indicator as shown schematically in Fig. 13·8.

The thermistor bridge itself consists of three 600-ohm resistors connected to a thermistor element to form a Wheatstone-bridge circuit

[1] See also L. C. Peterson and F. B. Llewellyn, "The Performance and Measurement of Mixers in Terms of Linear Network Theory," *Proc. I.R.E.*, 1, **33**, 458 (1945).

as shown in Fig. 13·9. The d-c voltage source supplies the bridge through several attenuators R_1, R_2, R_3, and R_4. Three of these attenuators are T-pads having a characteristic impedance equal to the input impedance of the bridge and calibrated in decibels. The resistor R_1 is an uncalibrated voltage divider that permits the effective input voltage of the bridge to be varied. The thermistor should preferably be mounted in a constant-temperature oven to minimize the effect of ambient-temperature changes. In order to measure microwave attenuation, first, with only direct current supplied to the bridge and the microwave source inactive, adjust the voltage divider R_1 until the bridge is balanced. The calibrated attenu-

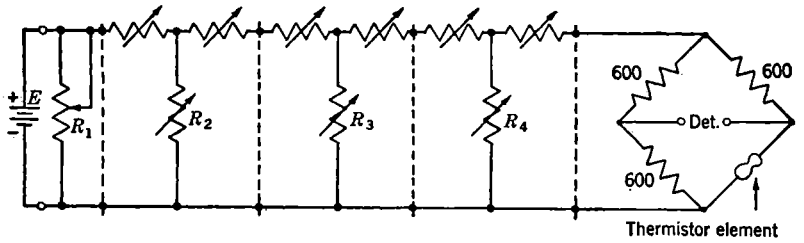

FIG. 13·9.—Thermistor-bridge circuit.

ators R_2, R_3, and R_4 should read zero during this adjustment of R_1. The d-c calibrated attenuators should then be set at least 4 db higher than the attenuation to be measured, for example, to A_1 db, thus reducing the d-c current through the thermistor to i_1. Turning on the microwave power and adjusting it by means of buffer H to such a value that the bridge will again be balanced establishes the reference microwave power P_1. The unknown microwave component is inserted into the line between points a and b, maintaining the established input power P_1 at the transmission line. The unknown component decreases the microwave power in the thermistor bead to P_2, so that the bridge must be rebalanced by adjusting the d-c calibrated attenuators R_2, R_3, and R_4. The new setting of these attenuators should be $A_2 < A_1$, whereas the d-c current should be increased to $i_2 > i_1$. Since direct substitution of d-c power for microwave power necessitates constant resistance values in all four arms of the bridge (precluding any heating effects in the three fixed arms), the attenuation of the unknown component can be defined as

$$A = 10 \log_{10} \frac{P_1}{P_2} = 10 \log_{10} \frac{1 - a_1}{1 - a_2}, \tag{1}$$

where

$$\frac{1}{a_1} = \text{antilog}_{10} \frac{A_1}{10}, \qquad \frac{1}{a_2} = \text{antilog}_{10} \frac{A_2}{10}. \tag{2}$$

Since the minimum power measurable to any degree of accuracy is about 50 μw, and the maximum power of the thermistor is in the neighbor-

hood of 4 mw, the largest attenuation range that can be measured is just under 20 db. To extend this range, standard attenuators can be used as gauge blocks. The power P_1 can be established with the standard attenuator in the microwave line and A can be set on the d-c attenuators. The unknown component can be substituted for the standard attenuator, and P_2 can be measured with the A_2 setting. The total attenuation of the unknown component is then the sum of the differential attenuation computed by Eq. (1) and the value of the standard attenuator. Although this method seems simple, it requires a powerful microwave source. The practical limit of measurements using this method and thermistor elements with no refinements is about 40 db with good accuracy, and 50 db with reasonable accuracy.

Instead of using accurately calibrated d-c attenuators, the d-c current measurements as indicated can be used and the measured attenuation can be defined

$$A = 20 \log_{10} \frac{i_2}{i_1}. \tag{3}$$

In order to preserve accuracy, however, the meter has to be of very high accuracy itself, although the d-c attenuating network can now be uncalibrated. Finally, if the low-resistance d-c attenuators are accurately calibrated, lower values of attenuated power P_2 can be measured and the range of measurement can be further increased. The practical limit in the measurement of very small powers lies in the necessity of using a sensitive galvanometer in the bridge circuit. If the thermistor element can be considered to be a linear detector of microwave power over a reasonably small resistance change, then the deflection of the galvanometer will be proportional to the input microwave power and an unbalanced bridge reading can be taken. The proportionality constant for this deflection can be obtained by calibration with a directly measurable small power. With a sensitive galvanometer of 1μa full-scale deflection and 50 ohms internal resistance, sizable deflections can be obtained with an input power of a microwatt or less. However, bridge-balance drifts make such measurements difficult and time consuming, and this method will usually be used only if microwave substitution methods cannot be applied.

Wire-bolometer-bridge Methods.—Instead of using the thermistor bead as a power detector, a hot-wire bolometer that employs a very thin Wollaston wire of a length that is small compared with a wavelength can be used. With a properly designed bridge circuit, attenuation measurements can be made in exactly the same manner as with the thermistor bridges, balanced or unbalanced. These bridges are described in detail in Chap. 3.

Similarly, thin metalized-glass fibers have been used as power-detector elements. Again with properly designed bridge circuits, these elements have been used for attenuation measurements.[1] Metalized-glass fibers have a higher power capacity than thermistor elements, their larger diameters permit better broadband matching than the hot-wire elements. They are, however, somewhat more difficult to produce.[2]

13·3. Measurement of Attenuation by Standing-wave Effects.—For measurement of small values of attenuation, neither substitution methods nor direct measurement of the power ratio with or without the unknown component are adequate if accuracies of 0.1 db or less are required. From basic transmission-line theory, however, it can be shown that the attenuation of any lossy four-terminal network may be determined from the knowledge of either of the following quantities: (1) the effect of the insertion of such a network on the voltage distribution and the phase shift in a short-circuited section of a lossless line following the unknown component, (2) the magnitude of the voltage standing-wave ratio of the unknown component terminated in a short circuit. Either effect can be made the basis for measurement of attenuation.[3]

Measurement of Power Ratios Referred to Line-voltage Distribution.—The methods of measuring attenuation discussed so far use either a defined standard attenuator, or square-law response of a detector, or correspondence between a-c and d-c voltage as a basis. Most of these assumptions are reasonably justified, but they have nevertheless been questioned from time to time. It seems desirable, therefore, to have still another method available which involves none of the previous assumptions, but rather measures attenuation in terms of a theoretically defined voltage distribution. Figure 13·10 shows the schematic arrangement for such a system in which the slotted section G_2, next to the short circuit, is the attenuation-measuring instrument. This apparatus must be particularly well constructed. Relative movement of its probe must be measurable to fractions of a mil; a 1-in. precision dial indicator with scale divisions of 1 mil, which is directly attached to the drive mechanism of the probe, is usually satisfactory.

In order to measure attenuation of an unknown component, both the detector and generator sections are first matched as well as possible by means of the slotted section G_1. The unknown component is then inserted between a and b. Maximum indication in the slotted section G_2 is determined and noted as a reference level. After removal of the

[1] J. Ebert, "Notes on the Use of Bolo-meters for Ultrahigh Frequency Attenuation Measurements," NDRC 14-219; PIB-7, June 2, 1943.

[2] S. A. Johnson, "Metalized-glass Bolometers," NDRC 14-524, Oct. 31, 1945.

[3] J. Ebert, "Notes on the Accurate Measurement of Small Attenuations," NDRC 14-439; PIB-43, Apr. 5, 1945.

unknown component, the distance is measured between two successive points about a voltage minimum in G_2 which give the same indication

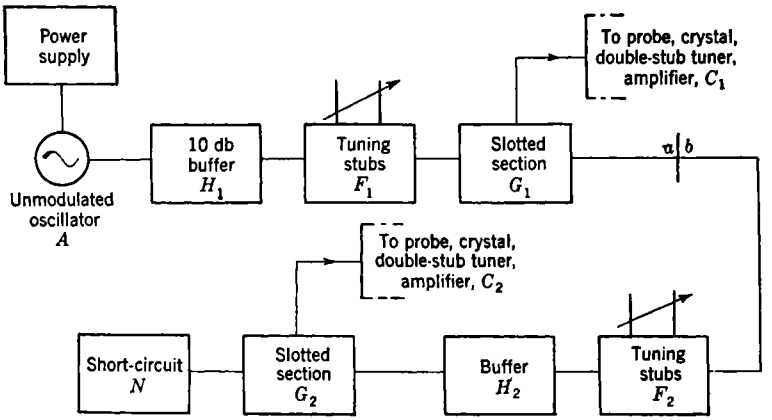

FIG. 13·10.—Schematic arrangement for measurement of attenuation by reference to line voltage distribution.

as the reference level previously noted. Knowing this distance, the frequency of the generator, and the voltage distribution, the power ratio or attenuation can be calculated in a simple manner. Assuming the entire detector section to be nearly lossless, the voltage distribution in the slotted section G_2 will be sinusoidal. Let E_1 represent the maximum voltage and reference level when the unknown component is inserted between a and b, and let E_2 be the maximum voltage when the unknown component is removed, as indicated in Fig. 13·11. Then the attenuation of the unknown component is by definition

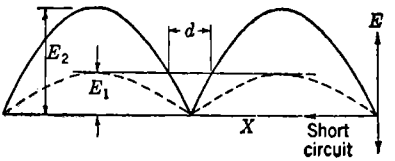

FIG. 13·11.—Voltage distribution in the slotted section G_2 of Fig. 13·10. The dotted line is the absolute value of the voltage with the unknown component present, the solid line is the voltage without the unknown.

$$A = 20 \log_{10} \frac{E_2}{E_1} \quad \text{db.} \tag{4}$$

Since the voltage distribution is sinusoidal, however,

$$E_2 \sin \frac{\pi d}{\lambda} = E_1,$$

where λ is the wavelength in the slotted section G_2. Thus, Eq. (4)

becomes

$$A = 20 \log_{10} \left(\frac{1}{\sin \pi d/\lambda} \right) \quad \text{db.} \tag{5}$$

Figure 13·12 gives the graphical representation of Eq. (5) for small values of attenuation.

The expression in Eq. (5) is an approximation since the short circuit and the transmission line are not lossless; the actual voltage distribution will therefore deviate appreciably from the assumed sinusoidal distribution. In the simple form given the method does not apply for attenuations much above 4 or 5 db. It is necessary, even at lower values of attenuation, to keep to a minimum the extension of the exploring probe into the active field in order to minimize its field-distorting effects and to maintain the voltage distribution close to sinusoidal. The main advantage of the method, however, is that the crystal or detector law of the exploring probe need not be known, because the same power level is used throughout.

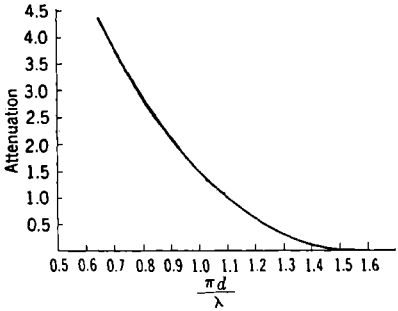

FIG. 13·12.—Attenuation values as measured by voltage distribution.

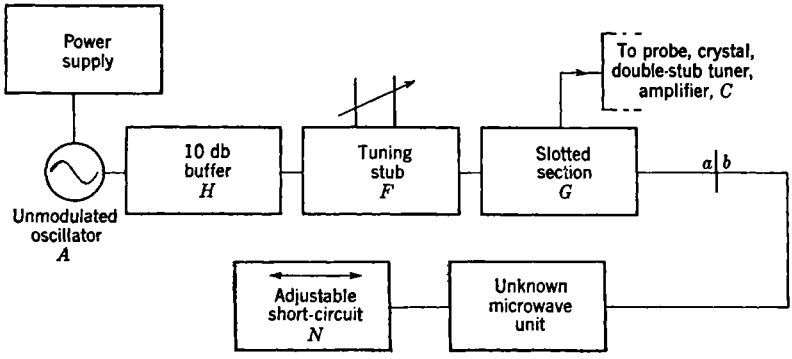

FIG. 13·13.—Schematic arrangement for measurement of power reflection ratio.

Measurement of Power-reflection Ratio.—If the unknown unit is terminated by a short circuit and if the ratio of incident to reflected power is known, the attenuation of the unknown unit can be computed. This power ratio may also be measured by determining the input standing-wave ratio in the arrangement shown in Fig. 13·13. The unknown

unit remains connected in the line system, making this method independent of the generator impedance.

Assuming a perfectly matched device to be measured, the relationship between voltage standing-wave ratio and attenuation can be found in the following way. Referring to Fig. 13·14, let P_1 represent the power incident on the unknown unit. Let the power transmitted by the unit be denoted by P_2. The power P_2, after being totally reflected from the short

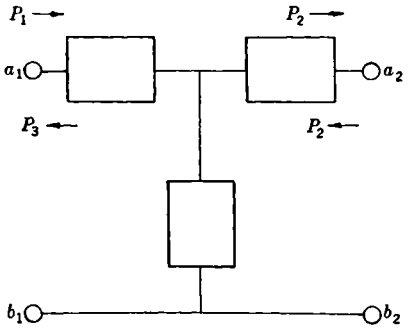

FIG. 13·14.—Power reflection from the terminals of short-circuited four-terminal network.

circuit, is again attenuated in passing through the unknown unit. If the power then emerging from the unit is represented by P_3, the attenuation of the unit can be written as

$$A = 10 \log_{10} \frac{P_1}{P_2} = 10 \log_{10} \frac{P_2}{P_3} = 5 \log_{10} \frac{P_1}{P_3} \quad \text{db.}$$

The quantity P_3/P_1 is, however, the ratio of incident to reflected power and is independent of generator impedance. If r is the input voltage standing-wave ratio, then

$$\frac{P_3}{P_1} = \frac{(r-1)^2}{(r+1)^2}.$$

Introducing this into the expression for A above,

$$A = 10 \log_{10} \frac{r+1}{r-1} \quad \text{db.} \tag{6}$$

This relationship is represented graphically in Fig. 13·15.

Most of the devices to be measured will not be perfectly matched, but will have reflections of their own, which will make the input standing wave dependent upon the phase of the reflection from the short circuit, and will make it vary from a maximum r_M to a minimum r_m. In this more general case, the relation

$$A = 10 \log_{10} \left[\left(\frac{r_M + 1}{r_M - 1} \right) \left(\frac{r_m + 1}{r_m - 1} \right) \right]^{1/2} \quad \text{db} \tag{7}$$

can be derived, or

$$A = \frac{1}{2}\left(10 \log_{10} \frac{r_M + 1}{r_M - 1} + 10 \log_{10} \frac{r_m + 1}{r_m - 1}\right) \quad \text{db.} \tag{8}$$

If r_M as well as r_m is measured with an adjustable short circuit, Fig. 13·15 can be used to determine the attenuation. Equation (8) is an expression for dissipative attenuation alone (see Sec. 11·1), and does

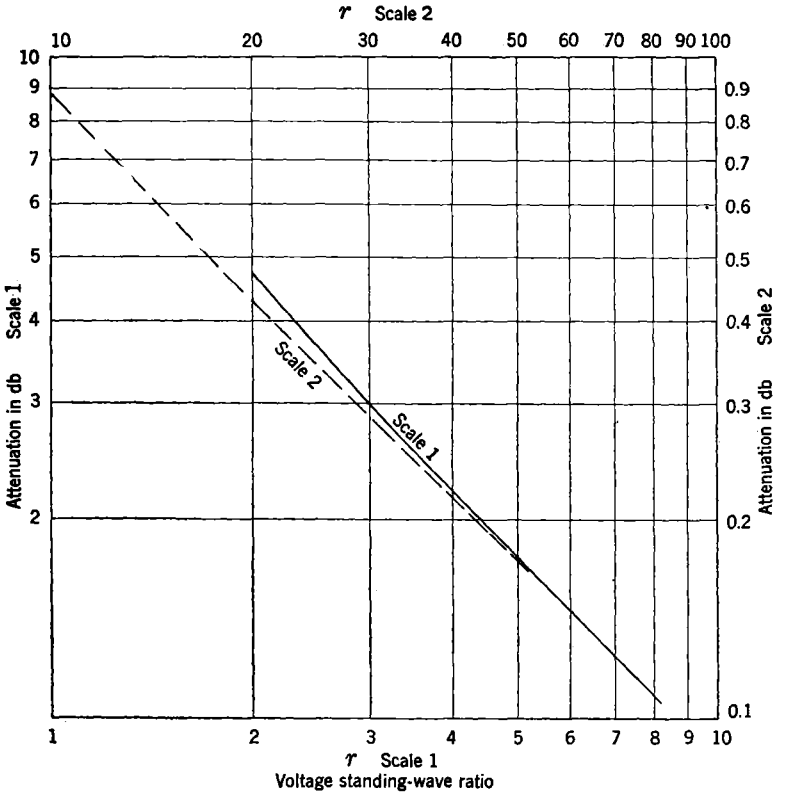

FIG. 13·15.—Plot of relation between attenuation and voltage standing-wave ratio.

not include the apparent increase of attenuation caused by power reflection from mismatches. Such reflection effects are included in all other measuring systems discussed above.

If the short circuit is imperfect, it can be regarded as a series combination of a perfect short circuit terminating a small fixed attenuating pad. The attenuation measured is the sum of the unknown unit and the attenuation of the imperfect short circuit. The attenuation value of

the hypothetical short-circuit pad can itself be measured by the method as outlined above.

In using this short-circuit method, it is necessary to measure input standing-wave ratios accurately. This can be done either with a hot-wire bolometer serving as a detector and as a standard in the slotted-section probe circuit, or by using some other sensitive microwave detector with a calibrated variable attenuator preceding it. When using the bolometer method, the powers at maximum- and minimum-voltage positions are measured and the ratio of the powers is the power standing-wave ratio r^2. When using the calibrated variable attenuator and detector in the probe circuit much larger standing-wave ratios can be measured. The change in attenuation necessary to equalize maximum and minimum indications is a measure of the reflection. Frequently a spectrum analyzer is used as the detector and a cutoff waveguide attenuator as the standard.

The advantage of using bolometers or standard attenuators in this method is the increase in sensitivity and accuracy of the measurements. Thus, measuring an unknown unit of 3-db attenuation, a change of approximately 0.3 db in power standing-wave ratio will correspond to a change of 0.1 db in the value of the unit. Measuring 1 db, the attenuation-sensitivity factor is roughly 8.4 and increases as the attenuation of the unknown unit decreases. However, since very large standing-wave ratios are difficult to measure accurately, some of this theoretical accuracy is usually lost, although the short-circuit method of measuring attenuation is the only convenient means available for measurements of attenuation below 0.1 db. Contrary to the power-measuring and substitution methods, the short-circuit method is independent of the generator impedance, thereby eliminating any mismatch error. Also, input power monitoring becomes unnecessary because of the ease and speed with which measurements may be checked.

13·4. Measurement of Very Small Attenuation Values.—An alternative method for the measurement of very small values of attenuation utilizes the resonance characteristics of metallically bounded field spaces as expressed in the definition of Q by

$$\frac{1}{Q} = \frac{\Delta f}{f} = \frac{R}{\omega L}, \tag{9}$$

where f is the resonance frequency at which maximum power is absorbed, and where Δf is defined as the interval between the upper and lower frequencies near f at which the magnitude of the admittance has fallen to one-half its peak value. The $\Delta f/f$ can also be taken as the ratio of dissipated to stored field energy analogous to the condition at lower frequencies.

Direct Measurement of Attenuation Constant of Transmission Lines.— Since the measurement of the Q of cavities is discussed in Chap. 5 only the modification of the method for measurement of conductive attenuation in transmission lines (coaxial or waveguide) will be given here. As shown in Slater,[1] the input admittance of a uniform, short-circuited, coaxial transmission line has periodic maxima and zeros. Near the maxima, it can be expressed in the first approximation as

$$|Y| = \frac{1}{Z_0} \frac{1}{\sqrt{(\alpha s)^2 + \delta^2}}. \tag{10}$$

In this form, Z_0 is the characteristic impedance of the line, assumed as real in this simplified case, α is the attenuation constant of the line, s is the length of the line to the short circuit, and δ is defined by

$$\beta s = n\pi + \delta, \tag{11}$$

where $\beta = 2\pi/\lambda = 2\pi f/v$ is the phase constant. Thus $|Y|$ regarded as a function of δ varies in the same way as a familiar resonance curve, as it should, since β is proportional to frequency. The spatial half-power points are indicated by the distances δ' for which the square of the admittance is reduced to one-half the maximum value for $\delta = 0$, since small attenuation has been assumed. This leads to

$$\frac{1}{Z_0^2} \frac{1}{(\alpha s)^2 + (\delta')^2} = \frac{1}{2} \frac{1}{Z_0^2} \frac{1}{(\alpha s)^2},$$

from which

$$\delta' = \pm \alpha s. \tag{12}$$

The measurement of the distance δ' gives directly, therefore, the total attenuation (αs) of length of the transmission line.

Because of the obvious symmetry, the interval between the two half-power points is $2\delta'$. Using Eqs. (9) and (12),

$$\frac{1}{Q} = \frac{\Delta f}{f} = \frac{2|\delta'|}{\beta s} = \frac{2\alpha}{\beta}. \tag{13}$$

Therefore the conventional methods of measuring Q will, if the phase constant is known, give the value of the attenuation constant of the transmission line.

A practical arrangement for this measurement is shown in Fig. 13·16. The slotted section G should preferably be of the same transmission-line size as the line to be measured in order to avoid spurious reflections. By means of the cutoff attenuator, the indication for maximum power in the probe is adjusted on the final detector (preferably a spectrum ana-

[1] J. C. Slater, *Microwave Transmission* McGraw-Hill, New York, 1942, p. 35.

lyzer) to a convenient magnitude; the distances δ' through which the probe has to be moved in either direction from the maximum in order to obtain half-power indication, are then recorded.

Although the derivation of Eq. (12) was based on the theory of the coaxial transmission line with real characteristic impedance, it can be shown that for small values of attenuation, such as encountered in transmission systems and low-loss cables, the same result is obtained with a

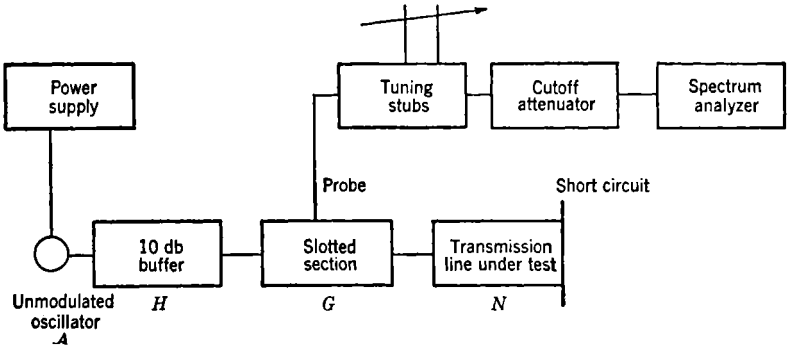

FIG. 13·16.—Schematic arrangement for measurement of attenuation constant of transmission lines.

complex characteristic impedance as is normally associated with a complex propagation constant. It is also irrelevant whether the losses are caused by series resistance, such as the losses in the conductors themselves, or whether they are caused by transverse conductance, such as the losses in dielectric materials filling the space between the conductors; the total attenuation α becomes the sum of these two separate contributions. Finally, the same analysis is directly applicable to waveguide transmission systems in which only one mode is utilized for power transmission.

Direct Measurement of Standing-wave Ratio.—The previous method requires a precision measurement of a very small distance if the attenuation is very slight. In order to improve the accuracy, the same physical arrangement may be used as is shown in Fig. 13·16 to measure directly the large VSWR by means of the cutoff attenuator. The VSWR is defined in terms of maximum and minimum values of the voltage distribution on the line by

$$r = \frac{|V_{\max}|}{|V_{\min}|}, \tag{14}$$

and can, of course, be converted into decibels of power ratio by taking $20 \log_{10} r$; this value is then directly read on the attenuator indicator.

Since the voltage distribution along a short-circuited transmission

line as referred to the short-circuit terminal is given by

$$V = V_0 \sinh \gamma x$$

with the absolute value

$$|V| = |V_0| \, (\sinh^2 \alpha x + \sin^2 \beta x)^{1/2}, \tag{15}$$

the maximum and minimum values may be easily found and the VSWR of Eq. (14) may be deduced for the approximation of slight attenuation,

$$r = \frac{\beta_0}{n\pi\alpha} = \frac{2Q}{n\pi}, \tag{16}$$

or also

$$\alpha = \frac{\beta_0}{n\pi r} = \left(n \frac{\lambda_0}{2} r\right)^{-1} \qquad \text{neper/m}, \tag{17}$$

where $n(\lambda_0/2)$ is the distance of the voltage minimum utilized in Eq. (14). It is irrelevant whether the VSWR is measured to the preceding or to the succeeding voltage maximum as long as the attenuation is small enough to justify the simplified derivation. This method is equally applicable to coaxial transmission lines and waveguides that utilize only one mode for the transmission of power. Of course, α will refer to this particular mode only.

For the measurement of the large VSWR, other suitable detector arrangements may be substituted, such as a crystal detector with galvanometer. A calibrated d-c attenuator would be placed between the crystal detector and the galvanometer in order to operate the galvanometer at optimum accuracy.

13·5. Common Sources of Error in Attenuation Measurements.—The most prominent sources of error in almost all methods of attenuation measurement are directly related to the physical arrangements. The attenuation of a microwave component has been defined in Sec. 11·1 in terms of normalized terminal conditions in either direction from the unknown component. Seldom, however, will these conditions be met exactly in practical measurements. The deviations constitute some of the most important sources of error. Other important sources are: leakage at the junctions of the microwave transmission system, which becomes particularly important in the measurement of large values of attenuation; reaction of the input impedance of the unknown component upon the generator power level or frequency if this impedance deviates from the standardized line impedance; and finally, instability in the detector section which usually contains an amplifier or heterodyne receiver.

Errors Caused by Reflection Interactions.—For a consideration of the effects caused by mismatches in the generator and detector sections, it is

most convenient to replace the unknown microwave component by a general, passive, linear four-terminal network of matrix $\begin{pmatrix} A & B \\ C & D \end{pmatrix}$. The general equivalent network arrangement of Fig. 13·1 then becomes that of Fig. 13 17. Performing the measurement according to the definition of attenuation, first, the power in load Z_L would be measured when it is directly connected to the generator section, then with the network inserted. The power ratio is given by conventional network theory as

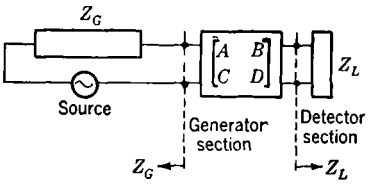

FIG. 13.17.—Equivalent network for attenuation measurement.

$$p = \left| \frac{(AZ_L + B) + (CZ_L + D)Z_G}{Z_L + Z_G} \right|^2. \tag{18}$$

Since attenuation is defined in terms of the power ratio with

$$Z_L = Z_G = Z_0,$$

the characteristic impedance of the transmission-line system,

$$p_0 = \left| \frac{(AZ_0 + B) + (CZ_0 + D)Z_0}{2Z_0} \right|^2 = \frac{1}{4} |A + \mathfrak{B} + \mathfrak{C} + D|^2, \tag{19}$$

if the convenient normalized parameters are used,

$$\mathfrak{B} = \frac{B}{Z_0}, \qquad \mathfrak{C} = CZ_0. \tag{20}$$

The error of measurement can now be expressed in terms of Eqs. (18) and (19) as a correction factor,

$$\frac{p}{p_0} = \left| \frac{(Aq_L + \mathfrak{B}) + (\mathfrak{C}q_L + D)q_G}{A + \mathfrak{B} + \mathfrak{C} + D} \cdot \frac{2}{q_L + q_G} \right|^2, \tag{21}$$

where the further abbreviations have been introduced

$$q_L = \frac{Z_L}{Z_0}, \qquad q_G = \frac{Z_G}{Z_0}. \tag{22}$$

It is most convenient to reduce all terms in Eq. (21) to directly measurable reflection factors, as for example:

$R_G = \dfrac{1 - q_G}{1 + q_G}$, reflection factor of generator section,

$R_L = \dfrac{1 - q_L}{1 + q_L}$, reflection factor of detector section,

$R' = \dfrac{1 - q'}{1 + q'}$ with $q' = \dfrac{Aq_L + \mathfrak{B}}{\mathfrak{C}q_L + D}$, reflection factor at the left terminals of a four-terminal network if its right terminals are connected to load impedance Z_L,

$R'_0 = \dfrac{1 - q'_0}{1 + q'_0}$, with $q'_0 = \dfrac{A + \mathfrak{B}}{\mathfrak{C} + D}$, reflection factor at the left terminals of a four-terminal network if its right terminals are connected to a matched load $Z_L = Z_0$,

$R'' = \dfrac{1 - q''}{1 + q''}$ with $q'' = \dfrac{Dq_G + \mathfrak{B}}{\mathfrak{C}q_G + A}$, reflection factor at the right terminals of a four-terminal network if its left terminals are connected to generator impedance Z_G,

$R''_0 = \dfrac{1 - q''_0}{1 + q''_0}$, with $q''_0 = \dfrac{D + \mathfrak{B}}{\mathfrak{C} + A}$, reflection factor at the right terminals of a four-terminal network if its left terminals are connected to a matched impedance $Z_G = Z_0$.

With these designations, the correction factor in Eq. (21) can be shown to take the alternative forms

$$\frac{p}{p_0} = \left|\frac{(1 - R''_0R_L)(1 - R'R_G)}{1 - R_LR_G}\right|^2 = \left|\frac{(1 - R'_0R_G)(1 - R''R_L)}{1 - R_GR_L}\right|^2. \quad (23)$$

From an exact knowledge of the R-values, which are in general complex, the deviation in any particular measurement may be computed as

$$\Delta A = 20 \log_{10} \left|\frac{(1 - R''_0R_L)(1 - R'R_G)}{1 - R_LR_G}\right| \text{ db.} \quad (24)$$

In most practical cases, however, the exact determination of the R-values is too cumbersome, if at all feasible, whereas the values of the voltage standing-wave ratio can be readily obtained. It is then possible to deduce only maximum errors in values obtained by accepting the measured power ratio as indicative of the attenuation of the tested component. The voltage standing-wave ratio is directly related to the absolute value of the reflection coefficient $|R|$ by the monotonic relations

$$r = \frac{1 + |R|}{1 - |R|}, \qquad |R| = \frac{r - 1}{r + 1}. \quad (25)$$

By choosing the worst phase combinations for the reflection factors R, the maximum error, either positive or negative, follows from Eq. (24) as

$$(\Delta A)_{max} = 20 [\log_{10} (1 \pm |R''_0||R_L|) + \log_{10} (1 \pm |R'||R_G|) - \log_{10} (1 \pm |R_L||R_G|)]. \quad (26)$$

From given values of the various standing-wave ratios, the absolute

values of the corresponding reflection coefficients are first calculated from Eq. (25); these values are then inserted in Eq. (26). The upper signs lead to the maximum positive error, the lower signs to the maximum negative error. It is not obvious which maximum will usually be the

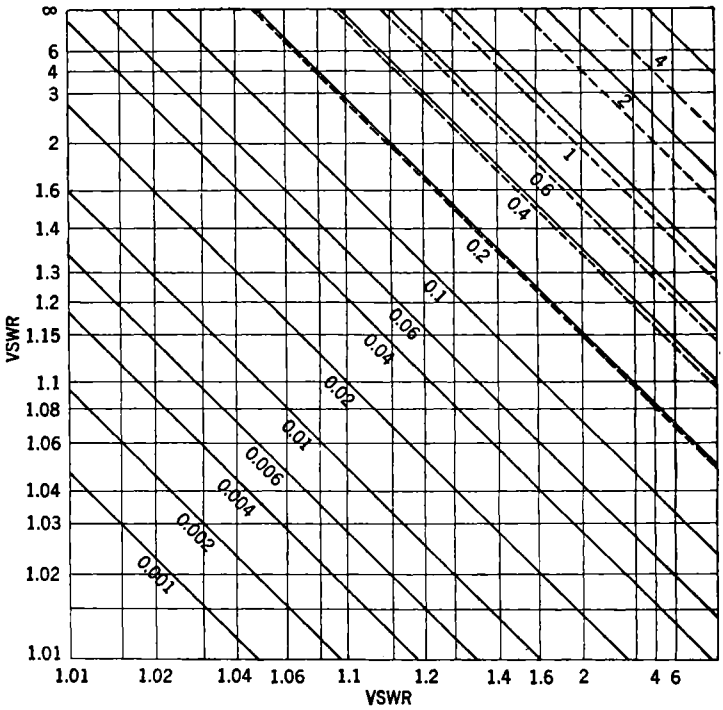

FIG. 13·18.—Values of $\pm 20 \log_{10}\left(1 \pm \frac{r_1 - 1}{r_1 + 1} \cdot \frac{r_2 - 1}{r_2 + 1}\right)$. The solid lines refer to the plus sign, the dotted lines to the negative sign.

larger one. To aid in the application to practical cases a chart of the general function

$$\pm 20 \log_{10} (1 \pm |R_1||R_2|) = \pm 20 \log_{10}\left(1 \pm \frac{r_1 - 1}{r_1 + 1} \cdot \frac{r_2 - 1}{r_2 + 1}\right)$$

is given in Fig. 13·18, whereby the solid diagonals refer to the upper sign and the dotted diagonals to the lower sign.

As a numerical example, assume that the VSWR values in the various combinations have been measured as

$$r' = 1.15, \qquad r_0'' = 1.1, \qquad r_G = 2, \qquad r_L = 1.4.$$

From Fig. 13·18, the values are found

$$\begin{aligned} +20 \log_{10} (1 \pm |R_0''||R_L|) &= +0.20, -0.21 \\ +20 \log_{10} (1 \pm |R'||R_G|) &= +0.07, -0.07 \\ -20 \log_{10} (1 \pm |R_L||R_G|) &= +0.51, -0.48 \\ \hline (\Delta A)_{\max} &= +0.78, -0.76 \quad \text{db.} \end{aligned}$$

The measured insertion loss can therefore be anywhere from 0.78 db higher to 0.76 db lower than the desired (matched) attenuation value.

From the general form of the correction factor in Eq. (21), it is obvious that reversal of the microwave component will lead to a different value of measured insertion loss, since, upon reversal, the parameters A and D interchange. If, on the other hand, $Z_L = Z_G$, but not matched, then reversal of the microwave component leaves the measured insertion loss unchanged because of the symmetrical form of Eq. (21).

A different and considerably simplified treatment[1] of the reflection effects on the input power level of attenuators is possible which permits the evaluation of deviations in the power level with fixed values, but varying phase relations, at any particular junction in a microwave system. It may be shown that the actual power level might differ in two separate measurements involving given VSWR values by a maximum amount of

$$\Delta P_{\max} = \pm 10 \left| \log_{10} \frac{q_1}{(1 - q_1)^2} - \log_{10} \frac{q_2}{(1 + q_2)^2} \right| \quad \text{db}, \qquad (27)$$

where

q_1 is the smaller of r'/r_G or r''/r_G,
q_2 is the larger of r'/r_G or r''/r_G,

and where r_G is the VSWR at the junction towards the generator section, and r' and r'' are the VSWR values at the same junction in two successive measurements towards the detector section. An alternative expression is

$$\Delta P_{\max} = \pm 10 \left| \log_{10} \frac{(1 + |R'||R_G|)^2}{(1 - |R''||R_G|)^2} \cdot \frac{1 - |R''|^2}{1 - |R'|^2} \right|, \qquad (28)$$

in which the reflection factors correspond to the VSWR values defined above.

Measurement of the VSWR of the Generator Section.—The actual evaluation of the VSWR of the generator section with the oscillator in operation is generally rather difficult. A simple scheme, which avoids substantial reaction on the output voltage of the oscillator (if proper buffering is used), is the following. A sliding reactance, such as a deeply penetrating probe of a slotted section, is introduced and the

[1] E. Weber, "Errors in Attenuation Measurements Caused by Reflection Losses," NDRC 14-365, PIB-39, Mar 16, 1945.

maximum and minimum indications on the detector are observed. If R_L and R_G are the reflection factors already defined, and if the detector measures voltage, then the ratio of maximum to minimum indication is

$$\frac{V_{\max}}{V_{\min}} = r = \frac{1 + |R_L||R_G|}{1 - |R_L||R_G|}. \tag{29}$$

If the value $|R_L|$ is known, it is easy to compute the value $|R_G|$ or to find it from Fig. 13·19.

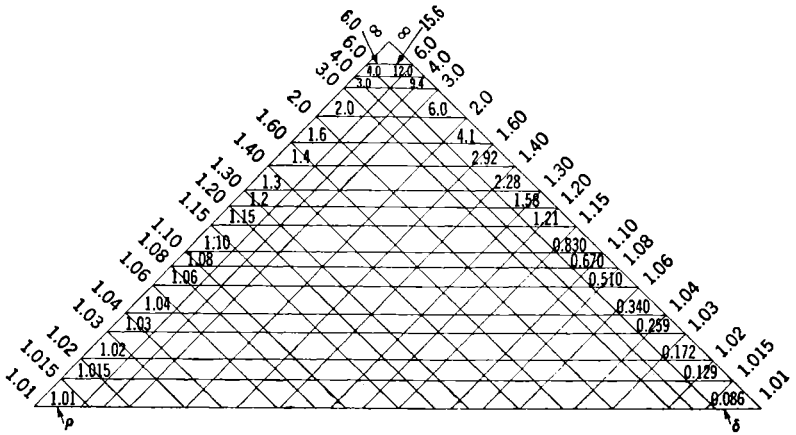

FIG. 13·19.—Values of $\delta = 20 \log_{10} \rho$ and

$$\rho = \frac{1 + \left(\frac{r_1 - 1}{r_1 + 1}\right)\left(\frac{r_2 - 1}{r_2 + 1}\right)}{1 - \left(\frac{r_1 - 1}{r_1 + 1}\right)\left(\frac{r_2 - 1}{r_2 + 1}\right)}$$

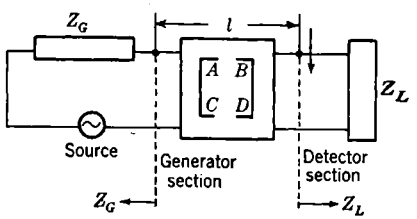

FIG. 13·20.—Schematic arrangement for the measurement of the VSWR of the generator section.

To demonstrate the validity of Eq. (29), assume as indicated in Fig. 13·20 that the probe forms part of the detector section, and that the transmission line of length l is a four-terminal network of variable insertion loss (caused by the phase of the probe reflection). The four-terminal-network parameters of the lossless transmission line of characteristic impedance Z_0 and propagation constant $\gamma = j\beta$ are

$$\begin{pmatrix} A & B \\ C & D \end{pmatrix} = \begin{pmatrix} \cos \beta l & jZ_0 \sin \beta l \\ j\frac{1}{Z_0} \sin \beta l & \cos \beta l \end{pmatrix}. \tag{30}$$

Using the previous definitions,

$$R' = R_L e^{-2j\beta l}, \qquad R_0'' = 0,$$

and therefore the correction factor of the insertion loss from Eq. (23) is

$$\frac{p}{p_0} = \left| \frac{1 - R_L R_G e^{-2j\beta l}}{1 - R_L R_G} \right|. \tag{31}$$

The maximum and minimum values, respectively, can be found, and their ratio leads to

$$\frac{p_{\max}}{p_{\min}} = \left(\frac{1 + |R_L||R_G|}{1 - |R_L||R_G|} \right)^2,$$

from which Eq. (29) is obtained.

Error Caused by Leakage.—The second important source of error is leakage at junctions in the microwave transmission system. Suppose the microwave power level in a transmission line at a particular point is P_0, and there exists, at that point, a source of power P_L as leakage from the generator or from other parts of the line. The extreme values of the resulting power level must, however, be computed from the superposition of the signal voltage E_0 and leakage voltage E_L. When attenuation is being measured, either by insertion of a microwave attenuator in the line or by changing a variable attenuator, the relative phase of the voltages E_0 and E_L may take any value whatsoever, so that the error in the final power measurement becomes

$$\Delta P = 10 \log_{10} \left(\frac{E_0 \pm E_L}{E_0} \right)^2 = 20 \log_{10} \left(\frac{E_0 \pm E_L}{E_0} \right) \quad \text{db.} \tag{32}$$

Assume that in the measurement of large attenuation, the final power is 70 dbm, and that the leakage power radiating back into the transmission line is 90 dbm, then the relative leakage power is $P_L = 0.01P_0$, and, therefore, the relative voltage $E_L = 0.1E_0$. The error in power measurement thus becomes

$$\Delta P = 20 \log_{10} (1.1) \quad \text{or} \quad 20 \log_{10} (0.9) = \begin{Bmatrix} +0.827 \\ -0.915 \end{Bmatrix} \quad \text{db},$$

a rather appreciable error affecting the accuracy of attenuation measurements. In order to make sure that the error is less than 0.1 db, the entering leakage power must be about 40 db below the main transmission-line power. Assuming a buffer attenuation of 10 db in the generator section, and another buffer of 10 db before the detector, then for the measurement of 75 db, the leakage path between generator and detector

must have at least 135 db attenuation. This indicates the seriousness of the problem. The following table gives the maximum errors in attenuation measurements with $L = 10 \log_{10} (P_L/P_0)$, a measure of the leakage power in decibels relative to P_0.

TABLE 13·1.—MAXIMUM ERROR IN ATTENUATION MEASUREMENT CAUSED BY LEAKAGE EFFECTS

L, db	Maximum error, in db	
	If leakage adds	If leakage subtracts
+ 6.0	.....	+9.6
+ 3.0	.....	+7.6
0.0	.....	+6.0
− 3.0	−10.7	+4.7
− 6.0	− 6.0	+3.5
−10.0	− 3.3	+2.4
−15.0	− 1.7	+1.4
−20.0	− 0.9	+0.8
−25.0	− 0.5	+0.4
−30.0	− 0.2	+0.2
−40.0	− 0.09	+0.09

Leakage may be detected by changing the relative phase and noting the variation of the signal. This may be done with a line stretcher or by moving a large sheet of metal in the vicinity of the transmission line. Leakage can usually be reduced sufficiently by putting the generator in a shield can, by using polyiron chokes on all d-c leads with access to the transmission line, by making all connections tight, and by covering joints with steel wool or conducting paint.

Errors Caused by Instability of Power Level.—Since most methods of attenuation measurement compare absolute power levels with and without the unknown microwave component, the measurements are very sensitive to variations in the power level of both the microwave power source and the local oscillator in the detector section, whether the detector is of microwave, intermediate, or audio frequency.

In order to minimize power-level fluctuations in the main oscillator, thermal stability, stability to supply-voltage variations, and stability of the cavity resonator are required. A number of schemes of automatic supply-voltage regulation, of cavity-resonator control, and of thermal compensations have been developed individually for the various types of oscillator tubes.

The importance of minimizing reflection interactions has already been stressed. The value and phase of the load impedance presented at the oscillator terminals greatly influences its output power, and

variations during attenuation measurement will cause errors of unpredictable magnitude. It is for this reason that the buffer H in Sec. 13·1 assumes considerable importance. Its value must be so chosen that variations of the impedance in its output plane are sufficiently reduced to cause only insignificant variations in its input plane. Usually about 10 db of attenuation proves sufficient. The allowable variations in the impedance of the input plane can best be gauged by the pertinent performance diagrams of the oscillator tube.

In a similar manner, power-level fluctuations of the local oscillator of the detector section will cause errors in attenuation measurements, and similar precautions must be taken. In addition, instability might occur in the amplifier, or in other associated circuits of the detector section with detrimental effects upon the accuracy of the indicator. Some of these effects will be treated more fully in connection with the calibration of attenuator standards, where they are, obviously, of greater concern.

13·6. Calibration of Attenuation Standards.—Even though absolute measurement of power ratios is possible, it is convenient to have available devices that may be calibrated for use as attenuation standards. The cutoff attenuator might be useful as a primary standard if freedom from higher modes could be assured. It seems safer, though, to verify by careful attenuation measurements or "absolute calibration," that it is usable as a primary standard; reliance on the accuracy of mechanical construction alone is not advisable. For most purposes of laboratory or field measurements, secondary standards of the dissipative type are preferable and are satisfactory if they have been calibrated either by absolute power measurements or by comparison with a cutoff attenuator certified as a primary standard.

In general, the suitability of an attenuating device as a standard is characterized by the accuracy, permanency, and range of validity of its calibration. In turn, the accuracy of calibration relies upon the method of measuring attenuation; the permanency of the calibration is subject to the stability of the attenuating element as affected by aging, by atmospheric influences, and by the precision of the mechanical movement to ensure extreme reliability in setting; whereas the range of validity refers to the variation of calibration values with ambient temperature, with frequency, with air pressure, or with other influencing factors.

Primary Standards.—The waveguide-beyond-cutoff attenuator with only one mode of electromagnetic-field distribution could well be used as a primary standard since its attenuation rate (exclusive of conductor losses) is theoretically defined (see also Sec. 11·3) by

$$\alpha = \frac{2\pi}{\lambda_c}\sqrt{1 - \left(\frac{\lambda_c}{\lambda}\right)^2} \tag{33}$$

with

$$\lambda_c = \frac{2\sqrt{k_e}}{\sqrt{\left(\frac{m}{a}\right)^2 + \left(\frac{n}{b}\right)^2}} \tag{34}$$

for rectangular waveguides of large inside dimension a and small inside dimension b; or with

$$\lambda_c = \frac{2\pi\sqrt{k_e}}{k_{m,n}} a \tag{35}$$

for circular waveguide of inside radius a. In both cases k_e is the relative dielectric constant referred to that of free space. As discussed in Secs. 11·4 to 11·6 it is difficult to ensure the presence of only one mode of field distribution. In fact, the theoretical values of the rate of attenuation α can be only approximately achieved by special selective microwave filter sections such as the iris coupling in the standard attenuators described in Secs. 11·10 and 11·11, or by special design of the coupling elements as described in Sec. 11·12, or, finally, by the most promising method of dielectric mode filters[1] as described briefly in Sec. 11·6. The most commonly encountered cutoff attenuatórs employ iris coupling, and only this type will be considered further.

Since the iris-coupled cutoff attenuator uses the dominant mode (TE_{11}) in the circular waveguide with $k_{11} = 1.841$, the effect of the other modes, if present, upon linearity will necessarily be limited to the region of lower attenuation. It is advisable, in fact necessary, to check the beginning of the linear region in each individual cutoff attenuator with a fixed position of the receiving loop, since the absolute value of α can be used only within the linear region. This requires a very accurate measurement of attenuation such as described in Sec. 13.7. Unfortunately, the large value of initial attenuation caused by the impedance-matching devices might cause the nonlinearity to extend as high as 40 or 50 db which makes it rather difficult in certain cases to verify the onset of the usable region.

Moreover, the accuracy of the value of α used depends on the mechanical measurement of the diameter of the tube and of its true circular cylindrical shape. It is best, then, to verify the exact value of α by accurate attenuation measurements, since according to Sec. 11.3.

$$\frac{d\alpha}{\alpha} = -\frac{da}{a} \tag{36}$$

for $\lambda_c^2 \ll \lambda^2$, the variations of the diameter have a directly proportional effect upon the attenuation rate α.

[1] A. B. Giordano, "Microwave Attenuation Standards," NDRC 14-531, Oct. 31, 1945.

Permanency of calibration is dependent only on mechanical features, particularly the exact angular position of the receiving loop. As to the range of validity of the calibration, variation of the calibration value of α is possible with frequency, temperature, humidity, and air pressure. From Eq. (35), assuming $\lambda_c^2 \ll \lambda^2$, one finds

$$\frac{d\alpha}{\alpha} = -\frac{1}{2}\frac{dk_e}{k_e}, \tag{37}$$

the effect of relative changes in the dielectric constant with temperature, humidity, or air pressure. Adequate corrections for these effects, however, can readily be made.

The variation of attenuation with wavelength can be obtained from Eq. (33) as

$$\frac{d\alpha}{\alpha} = 2\left(\frac{\lambda_c}{\lambda}\right)^2\frac{d\lambda}{\lambda}. \tag{38}$$

The variation is small for $(\lambda_c/\lambda)^2 \ll 1$, but has to be taken into account for wideband use of the cutoff attenuator (see Sec. 12·3). Equation (38) indicates a decreasing rate of change of α with increasing wavelength so that the design wavelength should be chosen closer to the short-wavelength end of the band considered. Assuming that λ_1 and λ_2 are the shortest and longest wavelengths, respectively, in the design wavelength band, and that $(\lambda_c/\lambda_1)^2 \ll 1$ to ensure minimum attenuation change over the band, then the design wavelength λ_d should be chosen in accordance with

$$\frac{1}{\lambda_d^2} = \frac{1}{2}\left(\frac{1}{\lambda_1^2} + \frac{1}{\lambda_2^2}\right), \tag{39}$$

in order to give symmetry with respect to attenuation variations. This total variation of attenuation is given by

$$\delta\alpha = \pm\frac{2\pi}{\lambda_c}\left[\left(\frac{\lambda_c}{\lambda_1}\right)^2 - \left(\frac{\lambda_c}{\lambda_2}\right)^2\right] \tag{40}$$

referred to the attenuation at the design wavelength. To illustrate, let $\lambda_1 = 8$ cm, $\lambda_2 = 12$ cm, and have $\lambda_c = 2$ cm so that

$$\left(\frac{\lambda_c}{\lambda_1}\right)^2 = 0.0625 \ll 1,$$

then $\lambda_d = 9.42$ cm, and $\delta\alpha = \pm 0.027$ neper/cm $= \pm 0.237$ db/cm, an appreciable value well above the accuracy of calibration.

Because of the exacting mechanical accuracies required, satisfactory primary standards have been developed principally for the longer wavelengths; none is available yet for wavelengths shorter than 3 cm. For accurate setting of a selected attenuation value or for recording

attenuation values in substitution measurements, the position of the receiver loop is read on a precision dial indicator with divisions of 0.001 in. In most measurements, only relative attenuation readings need be taken, namely, differences of indicator readings, which can be made very accurately. The knowledge of the theoretical attenuation rate makes the cutoff attenuator as accurate as the indicator reading can be made—makes it truly a primary standard for the linear range of attenuation.

Secondary Standards.—Any standard which requires calibration either by independent power measurement or by comparison with a primary standard is usually considered a secondary standard since its accuracy must be lower than that of a theoretically defined standard value. Thus, all cutoff attenuators in their nonlinear region are secondary standards. Because of their high minimum attenuation, these cutoff attenuators are not very useful as secondary standards, except that they can be built quite ruggedly and can be enclosed in a comparatively small space.

Dissipative attenuators have the advantage of practically vanishing minimum attenuation; the metalized-glass precision attenuators have, furthermore, the advantage of permanency and considerable range of validity of calibration, and, if variable, they can also be made very accurate by suitable precision drives. These metalized-glass attenuators have, therefore, gained considerable prominence as secondary standards in laboratories and for portable microwave test sets.

Fixed coaxial attenuators of the metalized-glass type in $\frac{7}{8}$-in. line size are particularly suitable as gauge blocks or fixed attenuation standards (see Sec. 12·13); they can also be used to extend the range of precise power measurements. The performance of these units has been extremely reliable. Similarly, broadband fixed waveguide attenuators with metalized-glass plates in the various standard sizes can be carefully calibrated for use as gauge blocks to verify linearity of cutoff attenuators, or for extending the range of precise power measurements (see Sec. 12·16). In order to ensure permanency of calibration, it is necessary to use metalized-glass plates with German-silver eyelets and to solder these to the supporting struts; the use of cements cannot be recommended because atmospheric conditions sooner or later cause deterioration with attendant drift of calibration.

Variable coaxial attenuators with metalized glass as power absorbing inserts have been used as secondary laboratory standards (see Sec. 12·14); the permanence of the calibration of well-made assemblies has been demonstrated, although moderate fragility prevents their use outside of laboratories. The internal mechanical structure makes the unit in the present form suitable only for narrow frequency bands that can be accommodated in the $\frac{7}{8}$-in. coaxial-line size.

Several very satisfactory designs of variable waveguide secondary attenuator standards have been developed using metalized-glass plates. One example suitable for the wavelength range from 3.1 to 3.6 cm is shown in Fig. 13·21. The waveguide casing of this precision attenuator is made of cast brass, accurately milled in two halves to attain a high degree of uniformity. The two halves are soldered together. The casing is pinned and screwed to a cast steel base. The struts supporting the

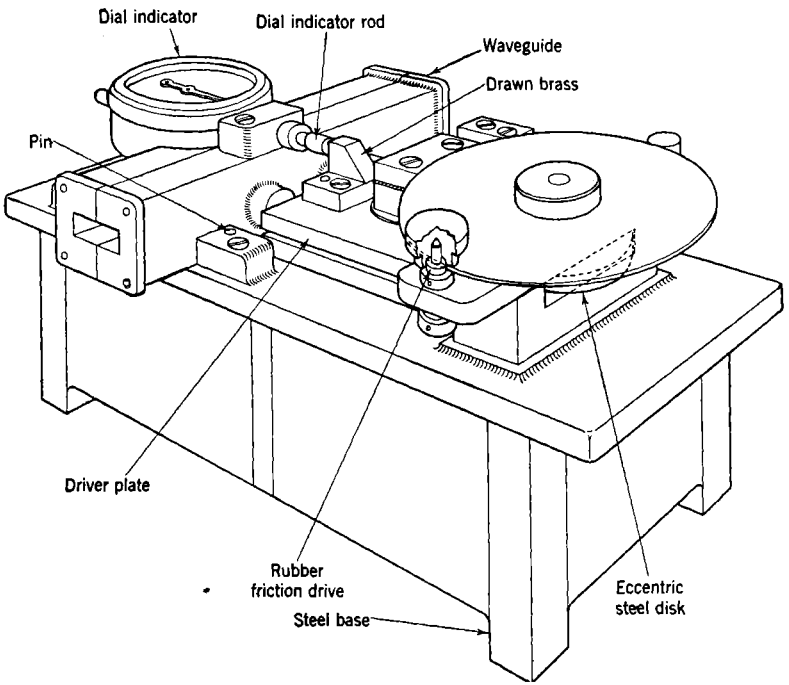

FIG. 13·21.—Waveguide metalized-glass attenuator standard.

glass plate are short and move freely through the side wall of the waveguide casing without contact bearing, the motion being supplied by a precision mechanical drive. This drive is kinematically designed and the carriage is supported on precision ball bearings. The movement of the plate in 1/10,000-in. steps is recorded on a dial indicator fastened securely to the waveguide casing. The front plane of the boss driving the rod of the indicator dial is also the driving plane of the struts so that only the differential expansion of the rod and strut materials can cause uncompensated temperature effects on the mechanical alignment. A typical calibration curve is shown in Fig. 12·60 indicating an over-all spread of attenuation with frequency of the same order as would be

expected from a corresponding cutoff attenuator; the VSWR over most of the frequency range is less than 1.1 because of the short supporting struts for the metalized-glass plate.

In order to check temperature sensitivity, special tests were performed with one sample attenuator. At room temperature, with the plate in its minimum position close to the guide wall, the movable dial of the gauge was set so that the indicating hand pointed to the zero of the dial. This will be referred to as the zero setting. By attenuation measurements, the dial reading for a 30-db change in attenuation at 3.2 cm was determined at room temperature. The attenuator was heated by using incandescent light bulbs distributed around and above the unit. The temperature was observed at various parts of the attenuator, and when a temperature equilibrium was reached, measurements were repeated to ascertain the dial reading corresponding to 30 db at the new temperature and the zero setting. The results of these tests are shown in Table 13·2.

TABLE 13·2.—CHECK OF TEMPERATURE SENSITIVITY OF SECONDARY ATTENUATION STANDARD

Temp., °C	Average dial reading of 4 tests, mils	Zero setting, mils	Temp. change, °C	Dial reading minus zero setting, mils	Deviation with reference to dial reading of 108.59 mils, db
25	108.59	0	0	108.59	0
30	108.37	−0.22	5	108.59	0.00
35	108.25	−0.37	10	108.62	0.015
40	108.08	−0.53	15	108.61	0.01
45	107.92	−0.70	20	108.62	0.015
25	108.59	0	0	108.59	0

The negative value of the zero setting signifies that the indicating hand read less than the zero value of the dial when the metalized-glass plate was returned to its minimum position. The average dial reading of the 30-db value is with respect to the zero of the dial. However, if the change in the zero setting is taken into account, the dial reading of the 30-db value of the attenuator remains practically constant with temperature. This leads to the conclusion that the change of zero setting with temperature is caused only by the temperature coefficient of the gauge and that temperature changes do not affect the attenuation calibration of this precision attenuator if the minimum position of the indicating hand is made to correspond to the zero of the dial when the unit is being used.

Another example suitable for frequencies near 24,000 Mc/sec has been described in Sec. 12·17 by the calibration curve shown in Fig. 12·62.

The special drive mechanism for this guillotine attenuator is accurate enough to permit resetting to better than ± 0.1 db.

13·7. Calibration with Absolute Power Measurement.—For the calibration of secondary standards as well as for the verification of linearity of a primary standard, very accurate methods of attenuation measurement must be chosen. The most reliable method based on direct measurement of the power ratio is the Ballantine-voltmeter method. Although the common errors in attenuation measurements have been described in Sec. 13·5, a more extensive and quantitative discussion of the specific errors in this particular method will be given in order to demonstrate possible improvements in accuracy as needed for careful calibration.

The circuit arrangement of the method is as shown in Fig. 13·3. The effects of instability of the generator and of variable contacts in the connectors of the transmission-line equipment, can with care be kept to less than ± 0.05 db. Particular care must be taken to establish proper and repeatable contacts at all junctions. To realize this condition, all contact surfaces should be cleaned with alcohol. In the case of $\frac{7}{8}$-in. coaxial lines, all male pins should be sprung. Coaxial fittings with type N couplings should be fastened securely to the table, so that no relative motion can occur between the components; the type N fittings themselves should also be thoroughly cleaned with alcohol and mechanically adjusted to afford the best possible contact. The importance of cleanliness is emphasized by the fact that dirty contact faces on $\frac{7}{8}$-in. couplings can increase the above error to 0.15 or 0.2 db. If the components of the setup are loosely connected, additional errors may result. These errors depend on the location of the loose connections and are erratic; errors as large as 1 db have been observed when loose connections are present and components are out of line. They may be attributed to leakage as well as the large reflections created at the discontinuities. It is, therefore, necessary to make all connections reasonably tight.

Specifically associated with the Ballantine-voltmeter arrangement is the error produced by the nonlinearity of the Wollaston-wire bolometer, and the total residual error of the Ballantine voltmeter after all known corrections have been made.

Nonlinearity of Bolometer Characteristic.—The nonlinearity of the static (d-c) characteristic of the bolometer element can easily be demonstrated as in Sec. 3·24. For practical evaluation of the bolometer characteristics it is more convenient to use an approximate empirical relation

$$R - R_0 = KP^n, \tag{41}$$

where R is the bolometer resistance in ohms at a specific d-c power level P in milliwatts, R_0 the bolometer resistance at $P = 0$, n the exponent

to be determined experimentally, and K a proportionality factor. The unknown parameters n and K of this expression may be determined by means of the method of least squares from experimental data of P and R for any particular bolometer element. With the actual units typical values for Sperry barretters are $n = 0.9$, $K = 7.57$.

Measuring attenuation, the bolometer will first carry the larger r-f power without the unknown attenuator inserted. Using symmetrical square-wave modulation the peak r-f power $(P_2 - P_1)$ superimposed on the bias d-c power P_1 is twice the average r-f power which defines the average over-all resistance. Inserting the unknown attenuator, the r-f power in the bolometer element is reduced considerably so that the total resistance will be close to the value R_1 corresponding to the power P_1. Since the audio amplifier utilizes only the a-c component of the voltage established across the bolometer resistance, the nonlinearity will cause an error in the power ratio. Figure 3·49 is a graph of the percentage deviation from square-law response as a function of the power increment $P_2 - P_1$.

Accuracy of Ballantine Voltmeter and Preamplifier.—In the analysis of the over-all error introduced by the Ballantine voltmeter and preamplifier, the problem can be divided into two parts: (1) the combined error caused by the nonlinearity of the preamplifier and voltmeter amplifier, by inaccurate meter graduations, by discrepancies introduced by the meter movement, and by personal error in the meter reading, and (2) the error introduced by the inaccuracy of the range switches on the Ballantine voltmeter.

The accuracy of the complete Ballantine-voltmeter circuit together with the preamplifier is best determined by measuring it with a well-calibrated Daven decade attenuator as a reference standard.

As an example, a Ballantine voltmeter Model No. 300 with a battery-operated preamplifier was selected. The combination has an over-all gain of 120 db. The preamplifier employs a highly selective feedback circuit such that only the modulation frequency is amplified; thus the noise level at the input terminals of the Ballantine voltmeter is reduced. The scale of the voltmeter is linear in decibels and is of such dimensions that it can be read accurately to 0.1 db. For its calibration a Daven decade attenuator box, Model T-692, with a range from 0 to 111 db was chosen.

The calibration of the Daven attenuator box was carried through with a Leeds and Northrup type K precision potentiometer using the circuit arrangement shown in Fig. 13·22. The input voltage to the decade attenuator is given by

$$e_{in} = \frac{R_{in}}{R_{std}} e'_{in}; \tag{42}$$

the attenuation for each step is found by

$$a_{\text{step}} = 20 \log_{10} \frac{e_{\text{in}}}{e_{\text{out}}}. \tag{43}$$

As indicated, the values of the resistor R_L, R_{in}, R_{std} were determined with good accuracy, the repeatability of the type K potentiometer for two successive runs being within ± 0.01 per cent on the 10-db and 1-db step dials, and ± 0.1 per cent on the 0.1-db step dial.

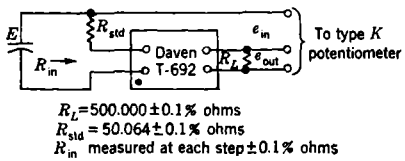

FIG. 13·22.—Calibration of Daven decade attenuator box.

The calibration of the Ballantine voltmeter and preamplifier was carried out with the calibrated Daven attenuator box connected to the unit under test, as shown in Fig. 13·23. With the 10-db step dial, the insertion loss of the decade attenuator was adjusted for 20 db, and the audio level set to full-scale reading on the Ballantine voltmeter. The decade attenuator was adjusted so that the voltmeter read the

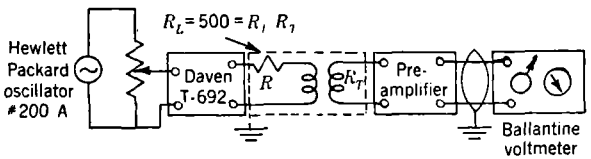

FIG. 13·23.—Calibration of the Ballantine voltmeter and preamplifier.

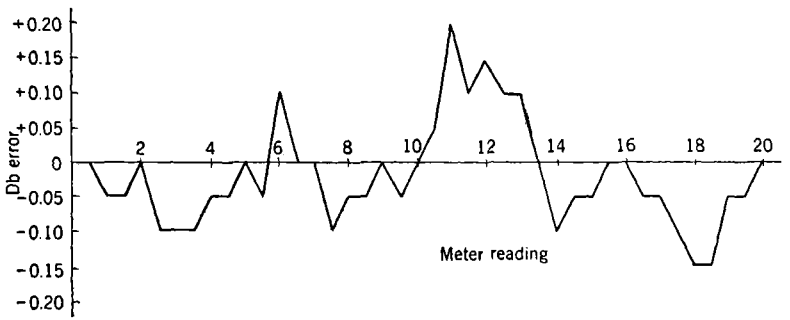

FIG. 13·24.—Correction curve for Ballantine voltmeter.

exact scale markings from 20 to 0 db in one-half-decibel steps. The corrected reading was taken at each scale graduation from the calibration data of the Daven attenuator box, T-692, and the correction plotted in Fig. 13·24.

The personal error was reduced to a minimum value, for each reading

was repeated by two different observers for three successive runs. From the figure, it can be seen that when this instrument is used with a square-law detector, the resulting error Δ_V will be ± 0.15 db. Interpolation of the curve in Fig. 13·24 will reduce this error to ± 0.05 db.

The range switches on the Ballantine voltmeter can be checked by a procedure similar to that described for the amplifier-linearity test. In the same example, the range-switch error was not detectable for any one step. It was estimated that the sum of the four range positions would not introduce an error greater than ± 0.05 db.

Total Accuracy of the Method.—If all the precautions enumerated above are properly taken, the over-all error can at worst be the sum of all the individual contributions. The errors are summarized in Table 13·3.

TABLE 13·3.—ACCURACY OF BALLANTINE-VOLTMETER METHOD

Individual error	Without calibration correction, db	With calibration correction, db
Generator instability and contact effects	± 0.05	± 0.05
Nonlinearity of bolometers	-0.07	.....
Ballantine voltmeter and preamplifier	± 0.15	± 0.05
Range switches of Ballantine voltmeter	± 0.05	± 0.05
Total	$+0.25$ -0.32	± 0.15

The importance of the calibration of the individual components is therefore emphasized for precision calibrations. By exercising great care, it is possible to achieve an over-all accuracy of ± 0.15 db in individual measurements, whereas for repeated measurements the probable accuracy should be not worse than $\pm 0.05\sqrt{3} = \pm 0.087$ db if the individual errors given in the table are assumed to be independent. This indicates that the above method is a most suitable calibration method.

With the introduction of a gauge block or precision fixed attenuator as discussed in Sec. 13·6, and with sufficient power available in the oscillator, the over-all attenuation range can be extended; the accuracy of the range is however, influenced by the accuracy of the gauge block itself.

13·8. Calibration of Secondary Standards by the Substitution Method.—The calibration of secondary standards is most conveniently done by comparison with a primary standard by means of the substitution method described in Sec. 13·2. The accuracy that can be achieved will be discussed in detail here, together with the sources of error peculiar to this method, and not already covered in Sec. 13·5.

An important point to observe is that the substitution method normally gives only relative values of attenuation referred to the minimum attenuation of the unknown component. For small values, the minimum attenuation certainly cannot be accurately determined by removing the unknown component and compensating the removed attenuation with adjustment of the standard; rather, this minimum attenuation must be determined by absolute measurement of the power ratio with and without the unknown component. This measurement has to be made very carefully since its value is additive to the relative values of the entire calibration curve.

Choice of the Buffer Sections.—The general test arrangement for the substitution calibration is that shown in Fig. 13·5 which indicates a waveguide setup such as used at about 9000 Mc/sec. The same block diagram applies with possible slight modifications for other frequency ranges and transmission-line systems. Buffer H, in the generator section, prevents reaction of load impedance changes upon the frequency and output power of the oscillator. The value of attenuation needed to keep the VSWR at a desired value close to unity can be ascertained from Fig. 11·11. Thus, if the maximum VSWR expected from the unknown attenuator is 1.30, the buffer H must be chosen as 10.15 db in order to keep the VSWR at the oscillator side to 1.025. Usually, if a value of 10 db or 12 db is chosen, the input impedance to the load system at the oscillator terminals will remain substantially constant.

Through the matching-stub section G, buffer I presents a matched termination to the attenuator undergoing calibration. In Fig. 13·5, this buffer is set for 10 db so that the power reflected from the cutoff attenuator and adapter section is completely absorbed. The matching stubs are employed to create a matched termination of VSWR equal to 1.03 or less, since the calibration is reliable only if the attenuator is terminated by a matched load. The VSWR must remain substantially constant throughout the process of calibration; it has been observed that with a variation from 1.03 to 1.1, only a negligible error is introduced into the calibration. However, if the VSWR is above 1.1, an appreciable error may be produced depending on the phase change introduced by the matching stubs and on the wavelength. For the worst phases, the conditions are depicted for a particular wavelength by the experimental curve shown in Fig. 13·25 where r_1 is the VSWR looking into the detector section, and r_2 is the VSWR looking into the unknown attenuator at an attenuation setting of 30 db so that r_2 is independent of r_1. As r_1 increases beyond 1.1, the error in attenuation rises rapidly above 0.1 db so that the calibration becomes meaningless.

Buffer M prevents power feedback from the local oscillator of the spectrum analyzer into the calibration line. It also serves to terminate

the reference cutoff standard by the characteristic impedance of the line Its value was chosen at 4 db and variation up to 15 db did not indicate any noticeable error. This is because the cutoff attenuator possesses an inherent termination that is highly reactive. The calibration of the cutoff attenuator is not, therefore, critically dependent on the setting of buffer M.

The total safe minimum insertion loss of the calibration system is, therefore, $12 + 10 + 4 = 26$ db in the three buffers alone, whereas the cutoff-attenuator standard has a minimum attenuation value of about 15 db. A total power loss of 41 db occurs and calibration can be con-

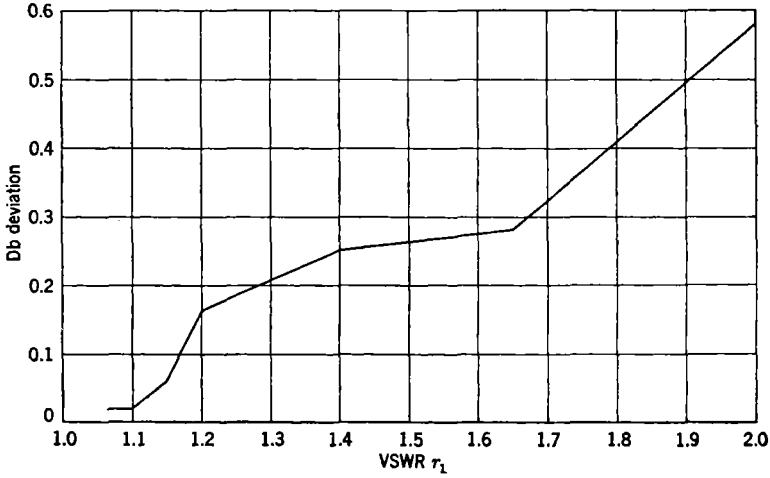

FIG. 13·25.—Influence of mismatch at input terminals of the detector upon measured attenuation. Attenuation level was 30 db and $r_2 = 1.07$.

ducted effectively only up to about a 90-db power-level difference between source and detector, hence a useful and accurate calibration range of 49 db remains.

The large minimum insertion loss with the cutoff-attenuator standard has led frequently to the use of a very well calibrated secondary dissipative standard as a reference standard. In this case, the arrangement of the detector section is shown in Fig. 13·6. Buffer H is chosen in the same manner as above, but buffer I need have a value of only 3 db since the input VSWR of the precision attenuator usually is less than 1.1 over the frequency range for which it is designed; otherwise it would be difficult to obtain an accurate calibration in accordance with the discussions of Sec. 13·5.

Buffer M terminates the dissipative-attenuator standard by a matched load. To ascertain the error caused by an improper termination, buffer

H and buffer M were both set at 15 db and two precision attenuators were chosen as reference values. These attenuators were calibrated at 30 db, one against the other. The 30-db value of the first standard was recalibrated for different attenuation values of buffer M and the deviation in decibels determined. The procedure was repeated at several wavelengths. The results are given in Table 13·4. Table 13·5 shows the deviation in decibels when the experiment was repeated for the 2-db setting of the same standards These data show that it is necessary to choose buffer M with a minimum value of 12 db of attenuation.

Following the same procedure as outlined above, the deviation in decibels can also be determined when both buffer H and buffer M are varied. This yields the effect of two sources of error. The resulting maximum errors were +0.03 db and −0.04 db with variations of each buffer between 15 db and 9 db. This clearly indicates that utmost attention must be paid to proper buffering in order to keep the calibration errors within tolerable limits.

TABLE 13·4.—INFLUENCE OF ATTENUATION VALUE OF BUFFER M UPON THE CALIBRATION WITH A DISSIPATIVE STANDARD AT THE 30-DB ATTENUATION LEVEL

Setting of buffer M, db	λ = 3.13 cm db deviation	λ = 3.20 cm db deviation	λ = 3.30 cm db deviation	λ = 3.53 cm db deviation
15	0	0	0	0
9	+0.02	−0.01	+0.01	−0.01
0.4	+0.02	−0.01	+0.08	−0.01
0	+0.01	−0.00	+0.05	+0.02

TABLE 13·5.—INFLUENCE OF ATTENUATION VALUE OF BUFFER M UPON THE CALIBRATION WITH A DISSIPATIVE STANDARD AT THE 2-DB ATTENUATION LEVEL

Setting of buffer M, db	λ = 3.13 cm db deviation	λ = 3.20 cm db deviation	λ = 3.30 cm db deviation	λ = 3.53 cm db deviation
15	0	0	0	0
9	−0.02	+0.03	−0.02	−0.03
0.2	−0.05	+0.03	−0.02	−0.00
0	−0.05	+0.01	−0.07	−0.04

The total safe minimum insertion loss of the calibration system is, in this case, 12 + 3 + 12 = 27 db, or 14 db less than when the cutoff-attenuator standard is used.

Accuracy in Setting the Reference Standard.—The mechanical accuracy in setting the cutoff-attenuator standard can be made as good as ±0.1 mil, which corresponds at 9000 Mc/sec to ±0.01 db, approximately. For the dissipative-attenuator standard at 9000 Mc/sec described in Sec. 13·6

the setting accuracy is ± 0.01 mil. Since the slope of the attenuation curve of this precision attenuator varies from 0.15 to 0.80 db/mil, the setting accuracy is from ± 0.002 to ± 0.008 db. It is, of course, desirable to make this mechanical adjustment as accurate as possible, since it can be most easily controlled.

Effects of temperature and humidity usually cause additional errors, which can be kept small with proper design particularly by utilizing inherent compensation features. The attenuation rate (db/cm) of the cutoff attenuator standard depends on the diameter of the cylindrical bore. Since the material is usually solid silver, the diameter change with temperature is about 0.00126 per cent/°C. For ordinary laboratory uses, this change is entirely negligible. A diameter variation of ± 0.063 per cent causes an equal change in the attenuation rate α according to Eq. (36). For values of 15 db/cm this change results in $\delta\alpha = \pm 0.0095$ db/cm. Therefore, in 60 db, the total error is ± 0.038 db, an error comparable with some of the other errors to be considered. Humidity will affect the dielectric constant of air; this effect is negligible unless condensation of water vapor takes place.

The effect of temperature and humidity on metalized-glass-attenuator standards is negligible if the metalized-glass plate is soldered on to the struts as pointed out in Sec. 13·6.

Effect of Detector Noise.—In the calibration of higher values of attenuation, about 40 db with the cutoff-attenuator standard and about 55 db with the dissipative standard, the total attenuation between the oscillator and the spectrum analyzer is 90 db or more, and the gain of the receiver must be set high. The noise of the receiver is amplified to such an extent that the signal or "pip" appearing on the screen of the cathode-ray oscilloscope fluctuates widely. Inherently, this fluctuation tends to introduce a calibration error. In order to determine the magnitude of this error, a series of tests was performed at about 9400 Mc/sec in which the attenuation at a constant dial setting of a calibrated attenuator was recalibrated as a function of the amplitude of the fluctuation, the average height of the pip being kept constant. The results indicate that attenuation measured with a fluctuating pip is always higher than attenuation measured with a steady pip. The deviation in decibels as a function of the height of the fluctuation has been plotted in Fig. 13·26; the values represent the averages of three independent tests.

In these tests, the amplitude of the fluctuation was varied by decreasing the input power to the spectrum analyzer and increasing the gain. This power decrease was accomplished by increasing the attenuation in buffer T and rematching the termination. Within the fluctuation range of 0 to 0.05 in. as shown in Fig. 13·26, an approximate error of $+0.04$ db can be made in measuring high values of attenuation. Actu-

ally, the calibration should not be carried into ranges of larger amplitudes of fluctuations because of the larger inaccuracies obtained.

Accuracy of Readings of the Unknown Component.—Individual observations of the setting of the unknown component will vary because

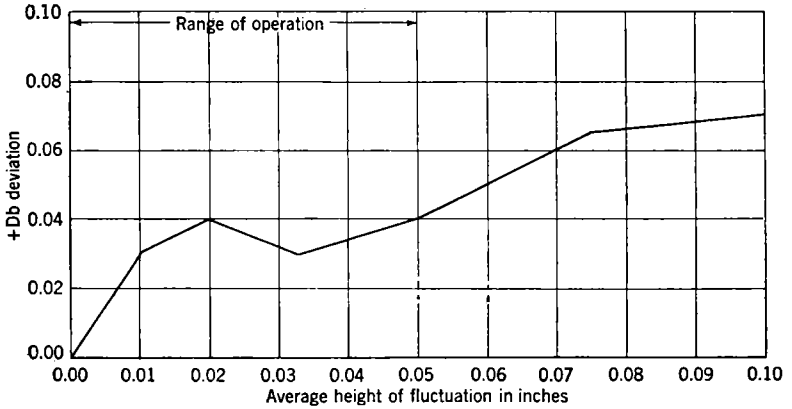

FIG. 13·26.—Calibration error contributed by signal fluctuation at high attenuation value.

of needed interpolation, parallax of indicator and scale, mechanical inaccuracies, and so forth. In order to minimize these influences, it is recommended to proceed as follows (refer to Figs. 13·5 or 13·6):

1. For the operating wavelength, match the buffer *I* (as termination of the unknown attenuator) to a VSWR of 1.03 or less by means of matching stubs *G*.
2. Set the reference standard for a value that is a few decibels higher than the attenuation to be measured.
3. By means of the receiver gain control, set the pip of the spectrum analyzer at a convenient level on the screen of the oscilloscope.
4. Reduce the attenuation of the reference standard by a known amount.
5. Insert attenuation of the unknown attenuator until the pip returns to the level set according to Step (3).
6. Return the dial setting of the reference standard to the value selected in Step (2).
7. Return the dial setting of the unknown attenuator to its original value.
8. View the pip level. If the pip returns to the same level as in Step (3), the dial reading obtained in Step (5) is accepted. If the level has changed, the dial reading is discarded.
9. This procedure is repeated for four acceptable dial readings and the average is taken to be the correct reading.

The dispersion of the four acceptable values will depend on all the factors enumerated above and particularly on the mechanical drive of the unknown attenuator. In the case of secondary standards of the metalized-glass type this accuracy can be made rather high. In the region of the maximum slope of this secondary standard at 9000 Mc/sec (see Sec. 14·6), the maximum spread has been found to be ± 0.04 db for careful calibration procedure.

TABLE 13·6.—COMPARISON OF MAXIMUM CALIBRATION ERRORS AT 9000 MC/SEC

Individual contributions	Calibration with cutoff standard, db	Calibration with metalized-glass standard, db
Combination of buffers H and M	+0.02 to −0.02	+0.03 to −0.04
Buffer I	+0.02 to −0.02	+0.02 to −0.02
Mechanical resettability of reference standard	+0.01 to −0.01	+0.008 to −0.008
Calibration error of reference standard	.....	+0.064 to −0.064
Effect of detector noise	+0.04	+0.04
Reading of the unknown component	+0.04 to −0.04	+0.04 to −0.04
Total	+0.13 to −0.09	+0.202 to −0.172

Total Error of Calibration Method.—The maximum total error incurred in the calibration of secondary standards is summarized in Table 13·6. With calibration against a cutoff standard, which has been certified to be truly linear, the error in the calibration can be anywhere between +0.13 and −0.09 db. However, the most probable measure of the reliability of the final result depends on the square root of the sum of the individual errors squared. This value is ± 0.064 db, approximately.

On the other hand, if the calibration is made against a secondary standard, the over-all calibration of this standard itself must be included and the maximum total error becomes +0.202 to −0.172 db. Again, the most probable error depends on the square root of the sum of the squares of the individual errors. This value, selecting the maximum deviations in each contribution, is ± 0.10 db, approximately.

These errors exist, of course, only under the conditions outlined, apply to the method of calibration, and presuppose good care in avoiding the more obvious general sources of error discussed in Sec. 13·5. The absolute values of attenuation may have still larger errors if the actual measurement of attenuation is not made under the proper conditions of termination. With the precautions indicated, however, and with the range of calibration restricted to the regions of small individual errors, the maximum deviation of absolute attenuation values should be small. As an illustration, take Eq. (26) and use the following values:

$r' = 1.10$, $r_0'' = 1.10$, assuming the maximum VSWR of a secondary standard,
$r_G = 1.03$, because of careful match of input buffer H,
$r_L = 1.03$, because of careful match of the detector section.

Then $(\Delta A)_{max.} = \pm 0.014$ db, a very small value indeed. The most probable error of a careful calibration measurement also gives the error in the value of the absolute attenuation.

13·9. Production Calibration.—Microwave test equipment frequently contains among its components attenuators of fixed or variable attenuation values. The calibration of these attenuators in a rapid and accurate manner is an important production problem.

Calibration of Fixed Attenuators.—Fixed-value attenuator pads are usually used to extend the range of power meters or other instruments in a manner similar to the equivalent range selectors at lower frequencies. The attenuation values, therefore, must be calibrated, yet they need not be calibrated as accurately as secondary standards. Because of the special need for rapid measurement of similar pieces, convenient modifications can be made in the substitution method of calibration. Figure 13·27 indicates a particularly useful arrangement whereby the unknown attenuators are inserted between the generator and detector section at *ab*. The microwave oscillator is modulated at audio frequency, and the output voltage of the first detector I can be either directly connected to the final audio amplifier and detector at C or connected to it at D over a carefully calibrated audio-frequency attenuator. With the unknown attenuator connected between a and b, and the audio selector switch at C, a convenient indication is obtained on the final detector-indicator by adjusting the gain of the audio amplifier. Leaving this gain adjustment fixed, and moving the audio selector switch to neutral position 0, the unknown component is removed and the detector section directly connected to the generator section. The audio selector switch is moved to D, and the a-f attenuator pad adjusted to restore the same indication on the final detector as previously selected. The dial reading of the audio pad gives directly the attenuation value of the unknown attenuator. For calibration of many attenuators of the same nominal value, this method is extremely rapid, since the audio pad can stay adjusted to the nominal value and only a fine adjustment is needed to the exact value of the particular unknown attenuator. If a tolerance range has been defined, this range can be marked on the fine-adjustment dial of the audio attenuator and any unknown attenuator outside this range can be rejected. Inasmuch as the first detector must carry the microwave power with and without the unknown attenuator inserted, the method is practically limited to about 20 to 30 db if good accuracy is desired.

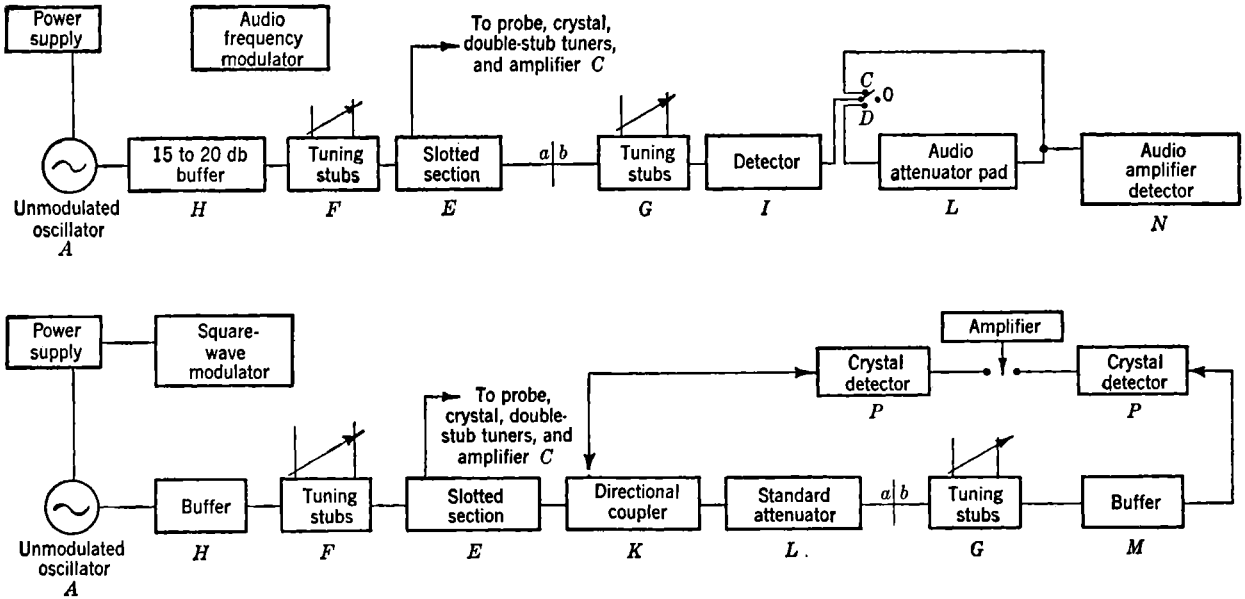

FIG. 13·27.—Top: Schematic arrangement for calibration of microwave fixed-value attenators by means of a-f attenuator pad. Bottom: Schematic arrangement for setting of attenuator pads to selected value.

Rather careful buffering of the oscillator is required in order to maintain output power and frequency setting; from time to time it is necessary to check these settings. A power monitor can easily be added for this purpose. One of the principal advantages of this method is that the audio pad can be calibrated at direct current with a precision potentiometer. By exercising care with all the other factors, this method can be made as accurate as the Ballantine-voltmeter method of absolute calibration. With proper modifications of the first detector I, the method can also be used for any microwave frequency desired.

Adjustment of Fixed Attenuators.—In many instances, particularly in the case of fixed waveguide attenuators, it is desired to set the insertion loss of each of a large number of similar pieces at a single value. A very suitable arrangement is that shown[1] in Fig. 13·27 where the output power of the side arm of a directional coupler K in the generator section is compared with the final power from buffer M. With the detector section connected directly to the generator section at the output terminal of the standard attenuator as shown, conditions are adjusted so that the input signals to the amplifier are equal. A push-button switch may be installed to facilitate comparisons between the two signals. If the standard attenuator is reduced by the desired amount, and if the unknown attenuator is inserted between a and b in Fig. 13·27 and adjusted so that the signals become equal, the proper setting has been obtained. The advantage of the method is that small changes in amplifier gain or oscillator output power do not necesitate recalibration. Both signals go through the same amplifier channel, and changes in gain affect both signals equally. If both crystals follow approximately the same law, small changes in the output power of the oscillator affect both signals about equally.

Because there is a small amount of coupling between the two input terminals of the amplifier, it is desirable that both input signals be of the same order of magnitude. To accomplish this, it may be necessary to insert an additional attenuator between the side arm of the directional coupler K and the monitoring crystal detector P.

Comparison of Directional Couplers.—It is often desired to measure the coupling of a large number of directional couplers of the same type. This may be done conveniently by comparison with one of the directional couplers which previously has been carefully calibrated as a standard. This standard coupler may again be K in Fig. 13·27, and the coupler to be measured is inserted in the detector section as shown in Fig. 13·28. The difference between the powers out of the two side arms is measured by means of bolometers and amplifiers with an audio attenuator. The

[1] W. E. Waller, "Microwave Attenuation Measurements," RL Report No. 55.5—11/12/45, p. 14.

bolometers replace the crystal detectors to ensure the same dependence on power in both detectors and the audio attenuator is used to bring the signal in the amplifier without gain adjustment to the same level in both cases. The difference in the audio-attenuator reading gives the difference in coupling of the two directional couplers.

If the couplers sample anything but a negligible portion of the power in the main line, compensation must be made for the reduction in the amount of power that enters the coupler under test, which can be done best by means of the audio attenuator.

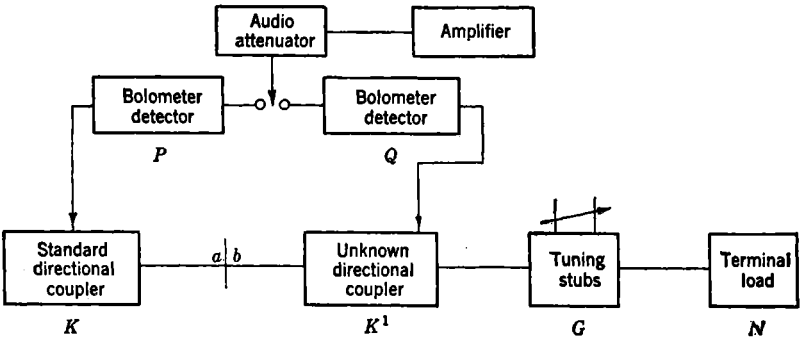

FIG. 13·28.—Modification of schematic arrangement in Fig. 13·27 (bottom) for comparison of directional couplers with standard.

Calibration of Variable Attenuators for Signal Generators.—Attenuators for signal generators for testing receivers and transmitters usually require wide ranges of adjustment, in most cases up to 75 or 85 db. As indicated in Sec. 13·2, such a range of attenuation calibration is difficult to achieve. It is not possible at present with a waveguide-beyond-cutoff primary standard because of its very high minimum insertion loss. The most common calibration procedure is, therefore, the substitution method with resistive precision attenuators as secondary standards, preferably of the metalized-glass type as described in Sec. 13·6. Calibration of these resistive standards over the entire range of 80 db must be done in pairs. One member of the pair is calibrated by a primary method, such as is described in Sec. 13·7, the other member of the pair is then calibrated by comparison with the first using the substitution procedure. As a detector, either a spectrum analyzer or a standard radar receiver with a frequency band of 2 Mc/sec and an intermediate frequency of 30 Mc/sec, may be used. The output signal of this receiver may be indicated either as a pip if the local oscillator is sawtooth-modulated, or as a deflection of a voltmeter connected to the second detector if the local oscillator is operated without modulation. Despite its wider pass band, such a receiver has at least as great a sensitivity and has more stability than

a spectrum analyzer. The high sensitivity expected from the narrow-band receiver in the analyzer is seldom realized, and a tendency for regeneration usually hampers stability. The optical advantage caused by the manner in which noise adds to the signal from the wider bandpass receiver when an oscilloscope is used, permits operation closer to noise. A signal that is equal to noise is about -125 dbw, and this is therefore the final limit of sensitivity.

The accuracy of the upper range of secondary standards is considerably lower than the accuracy of the lower range (see Sec. 13·8). Consequently, the absolute accuracy of calibration of the signal-generator attenuators is still lower, probably not better than ± 0.45 db at about 70 db total attenuation, since the mechanical drive is also less accurate than that of the standards. In the comparison of attenuators, possible deviations of twice this value must be expected.

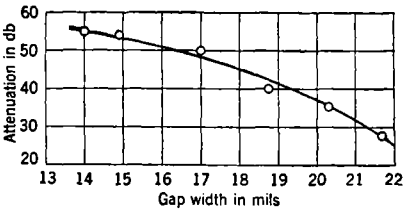

FIG. 13·29.—Shift of crossover of attenuation curves with variations in glass widths from $\lambda = 3.13$ and 3.53 cm.

In view of the unavoidable inaccuracies of individual calibrations the possibility of eliminating the calibration by careful quality control of the production of attenuators should be considered. This cannot be done, at least in the case of waveguide attenuators, as has been demonstrated clearly in experiments on metalized-glass attenuators by studying the influence of mechanical tolerances upon the variation of attenuation with frequency. It has been shown in Sec. 12·18 that the capacitances produced by the electric field fringing between the metalized-glass plate and the waveguide walls exert a strong influence on the attenuation characteristics. The metalized-glass plate shown in Fig. 12·58 was used with slightly varying widths in the same specially selected waveguide casing of 0.399 in. small dimension and of exceptional uniformity. The attenuation curves for the wavelengths 3.13 and 3.53 cm intersect with normal tolerances in the neighborhood of 40 db total attenuation. For glass plates of widths varying between 0.356 and 0.371 in., Fig. 13·29 indicates how the crossing point of these two attenuation curves shifts from about 28 db to 55 db. As this crossover shifts, the spread between the attenuation curves at a fixed medium value

of 40 db varies according to Fig. 13·30. Thus only a very small variation in the gap is allowed if an over-all spread of attenuation of 1 db or less between the wavelengths chosen is desired.

In order to reduce variations from attenuator to attenuator in production, the tolerances on waveguide dimensions as well as on glass width and thickness must be set close. If the glass plate shown in Fig. 12·58 with a width of 0.363 ± 0.001 in. is selected and if the inner dimension of the waveguide is set at 0.400 ± 0.002 in., a total maximum variation

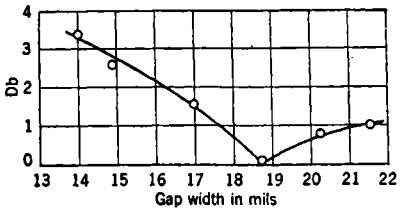

FIG. 13·30.—Total attenuation change at 40 db from λ = 3.13 to 3.53 cm.

of ±0.0015 in. in gap width will result centered about 18.5 mils as indicated in Fig. 13·29. This causes a variation of total attenuation change with frequency at 40 db from approximately 0.6 db at one tolerance extreme to 1.5 db at the other. A glass width of 0.3635 ± 0.001 in. reduces this to about 1 db. Other mechanical factors are also important, such as slight bowing of the glass plate, curvature in the waveguide casing, nonparallelism of the struts supporting the glass plates, and many others. Consequently any attempt to produce waveguide signal-generator attenuators of identical attenuation curves that would obviate calibration procedures seems utterly hopeless with present-day means.

CHAPTER 14

DIRECTIONAL COUPLERS

By R. L. Kyhl

14·1. Introduction.—In microwave systems it is often necessary to monitor the power which is being transferred through a transmission line, the line from a transmitter to an antenna, for example. Usually the monitoring must be accomplished by a simple device which does not add weight or complexity to the system. Such a device will employ a detector or detectors and some means of coupling power out of the transmission line in question. The simplest way of accomplishing the coupling is by means of a small probe such as that which is used in slotted-section measurements. Serious objections to this become evident at once. The voltage generated in such a probe is proportional to the electric intensity at the position of the probe; this intensity varies from point to point along the transmission line to give the familiar standing-wave pattern. The voltage generated in the probe is then by no means a unique measure of power transfer. The same objection may be made to a probe consisting of a small loop projecting into the line. In this case it is the magnetic intensity that is picked up; the standing-wave pattern, although displaced, will be of the same magnitude.

It is possible, of course, by means of a slotted section and sliding probe, or by means of a sufficient number of fixed probes, to determine completely the configuration of the electromagnetic waves in the transmission line, and in this way to determine, among other things, the net power transfer. This is far too complicated to be a satisfactory solution of the problem. What is desired is a type of coupling which will deliver, to a single detector, power which is proportional to the power transfer in the transmission line.

An attempt to answer this problem is the directional coupler, which measures the forward-going wave. Although this does not give exactly the power transfer, since there may be a reflected wave, it represents a much better approximation when the reflected power is small than does the simple probe. Equation (1) gives the dependence of power transfer on the amplitude of the forward wave,

$$P = \frac{|E|^2}{2Z_0}(1 - |\Gamma|^2), \tag{1}$$

where P is the power delivered to the load, E is the complex voltage amplitude of the wave in the forward direction, Z_0 is the characteristic impedance of the transmission line, and Γ is the complex voltage reflection coefficient of the terminating load. Since the directional coupler is sensitive only to the forward wave, the power reaching a detector connected to the coupler is proportional to the power transfer in the line, independently of the value of Γ, except for second-order terms in Γ.

$$P_d \propto \frac{P}{1 - |\Gamma|^2} \approx P(1 + |\Gamma|^2), \tag{2}$$

where P_d is the power extracted by a directional coupler. A simple probe, on the other hand, is sensitive to the total field strength $|E(1 + \Gamma)|$, so that

$$P'_d \propto P \frac{|1 + \Gamma|^2}{1 - |\Gamma|^2}, \tag{3}$$

where P'_d is the power extracted by a simple probe. The probe power is then independent of Γ only if first-order terms in Γ are neglected. Since, in practical transmission lines, values of $|\Gamma| = 0.2$ corresponding to a standing-wave ratio in voltage of 1.5 are common, these effects are by no means trivial.

It is often desired to monitor or to measure the available power of a matched generator which is driving a transmission line. In this case power carried by the forward wave is proportional to the available power, and the directional coupler gives the correct value independent of the standing-wave ratio in the line. If the generator is not matched, the forward wave will depend upon load and generator impedances, but in all cases the simple probe gives a coupling which is more dependent on load and generator impedances than does the directional coupler.

The above considerations also apply when the role of generator and detector are reversed, as can be seen from a consideration of reciprocity relations. This means that the directional coupler offers the same advantages when the problem is, for example, to put into a receiver a test signal which will be independent of the impedance of the antenna and of the other components in the transmission line. Then, too, there are many cases in which it is desirable to know the magnitude of a traveling wave for its own sake, as in the case of the reflectometer for measuring reflection coefficients. It has been assumed that the transmission line in question must remain operative. If it is possible to break the transmission line to insert detectors or generators, then the particular properties of the directional coupler are of no special value.

14·2. Equivalent Circuit of a Directional Coupler.—The problem of designing a device which is sensitive only to the wave in one direction

is equivalent to that of designing a device to excite a wave traveling in the reverse direction. From reciprocity considerations, a solution to one of the problems is automatically a solution of the other. This can be seen as follows: if a generator sends a wave down the transmission line in the rejected direction, that is, the direction in which the coupler is not sensitive, no power reaches the detector. Therefore, by reciprocity, if the detector and the generator are reversed and the probe generates, no power reaches the end of the transmission line containing the detector; therefore any wave generated must travel toward the other end of the transmission line. The same argument of course can also be applied in the opposite direction. This indicates that a simple probe cannot be used since it would radiate power into the line in both directions. It suggests the use of two or more probes driven in the appropriate phases to cancel the radiated waves in one direction in a manner analogous to that employed in certain directional antennas. Thus, since most directional couplers consist of a section of the main transmission line coupled to an auxiliary transmission line, the problem of sensitivity to power flowing in one direction in the main line is equivalent to the problem of exciting the transmission of power in a single direction in the auxiliary line.

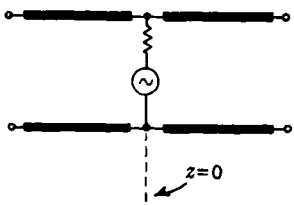

FIG. 14·1.—Electric probe coupling.

Consider, then, the generation of waves by a generator driving a probe or other device forming a weak coupling to the line. Such a generator can be represented in several equivalent ways. A single electric probe may be represented by a shunt generator, Fig. 14·1. The waves excited will be of the form

$$\left.\begin{aligned} e &= E_0 e^{j(\omega t - kz)} \\ i &= \left(\frac{E_0}{Z_0}\right) e^{j(\omega t - kz)} \end{aligned}\right\} \quad z > 0,$$

$$\left.\begin{aligned} e &= +E_0 e^{j(\omega t + kz)} \\ i &= -\left(\frac{E_0}{Z_0}\right) e^{j(\omega t + kz)} \end{aligned}\right\} \quad z < 0. \tag{4}$$

A probe may be generalized to include any device which couples to the transverse electric field of the waves in the transmission line. For this type of excitation the voltages at symmetrical points on the two sides of the probe have the *same phase*.

A simple loop may be represented by a series generator, Fig. 14·2. The waves excited will be of the form

$$\left.\begin{aligned} e' &= E_0' e^{j(\omega t - kz)} \\ i' &= \frac{E_0'}{Z_0} e^{j(\omega t - kz)} \end{aligned}\right\} \quad z > 0,$$

$$\left.\begin{aligned} e' &= -E_0' e^{j(\omega t + kz)} \\ i' &= +\frac{E_0'}{Z_0} e^{j(\omega t + kz)} \end{aligned}\right\} \quad z < 0. \tag{5}$$

A loop may be generalized to include any device which couples to the transverse magnetic field of the waves in the transmission line. For this type of excitation the voltages at symmetrical points on the two sides of the probe are *out of phase.*

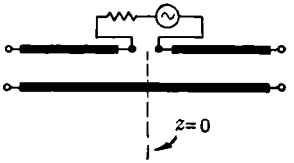

FIG. 14·2.—Magnetic loop coupling.

Next consider the problem of a transmission line excited by two probes. Both probes must be driven by the same generator, of course, so that the waves will be coherent. The resulting waves will be linear combinations of the individual waves. We shall consider two cases.

Case 1. A shunt and a series probe excite the line at the same point. Here,

$$\left.\begin{aligned} e &= (E_0 + E_0')e^{j(\omega t - kz)} \\ i &= \frac{1}{Z_0}(E_0 + E_0')e^{j(\omega t - kz)} \end{aligned}\right\} \quad z > 0,$$

$$\left.\begin{aligned} e &= +(E_0 - E_0')e^{j(\omega t + kz)} \\ i &= -\frac{1}{Z_0}(E_0 - E_0')e^{j(\omega t + kz)} \end{aligned}\right\} \quad z < 0. \tag{6}$$

If now the relative magnitudes and phases of the coupling are adjusted so that $E_0 = E_0'$, then $e = 0$ for $z < 0$, and the wave excited to the left will vanish.

Conversely, from reciprocity considerations, a wave falling on the probe combination from the left would not be detected at the terminal pair which drives the two probes. In other words, the probe combination is sensitive only to an incident wave traveling from the right to the left, and has the properties of a directional coupler. On the other hand, if we had made $E_0 = -E_0'$, the wave excited to the right would have vanished and the directional coupler would have been sensitive to waves traveling in the opposite direction.

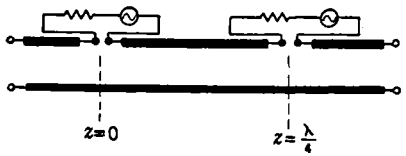

FIG. 14·3.—Probes spaced λ/4 apart.

Case 2. Two series probes drive the line at points separated by a quarter wavelength; Fig. 14.3. Here,

$$\left.\begin{aligned} e &= E_1 e^{j(\omega t - kz)} + E_2 e^{j\left[\omega t - k\left(z-\frac{\lambda}{4}\right)\right]} \\ i &= \frac{1}{Z_0} E_1 e^{j(\omega t - kz)} + \frac{1}{Z_0} E_2 e^{j\left[\omega t - k\left(z-\frac{\lambda}{4}\right)\right]} \end{aligned}\right\} \quad z > \frac{\lambda}{4},$$

$$\left.\begin{aligned} e &= -E_1 e^{j(\omega t + kz)} - E_2 e^{j\left[\omega t + k\left(z-\frac{\lambda}{4}\right)\right]} \\ i &= +\frac{1}{Z_0} E_1 e^{j(\omega t + kz)} + \frac{1}{Z_0} E_2 e^{j\left[\omega t + k\left(z-\frac{\lambda}{4}\right)\right]} \end{aligned}\right\} \quad z < 0, \tag{7}$$

giving

$$\left.\begin{aligned} e &= (E_1 + jE_2)e^{j(\omega t - kz)} \\ i &= \frac{1}{Z_0}(E_1 + jE_2)e^{j(\omega t - kz)} \end{aligned}\right\} \quad z > \frac{\lambda}{4},$$

$$\left.\begin{aligned} e &= -(E_1 - jE_2)e^{j(\omega t + kz)} \\ i &= +\frac{1}{Z_0}(E_1 - jE_2)e^{j(\omega t + kz)} \end{aligned}\right\} \quad z < 0. \tag{8}$$

If the relative magnitudes and phases of the couplings are adjusted so that $E_1 = jE_2$, the wave excited to the left will vanish, and by a similar argument, when a detector is used instead of a generator, the device is a directional coupler sensitive to a wave coming from the right. Notice that in this case the two probes must be connected so that there is a phase difference of 90° between them.

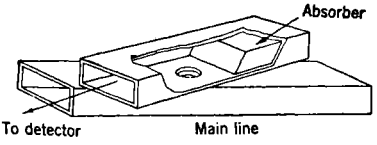

FIG. 14·4.—The Bethe-hole coupler.

These two examples will suffice to illustrate the general methods of obtaining directional properties. The various ways of obtaining the desired shunt and series excitation will be described subsequently. Actually any microwave junction can be represented either as a series or as a shunt circuit; however, the corresponding reference planes will be displaced one-quarter wavelength from one case to the other. Usually one of the choices has greater physical significance.

14·3. The Bethe-hole Coupler.—We shall now consider a particular example of a directional coupler. A typical Bethe-hole coupler is the design shown in Fig. 14·4 for rectangular waveguide. It consists of two waveguides with their broad sides adjoining and a single hole furnishing coupling between them. The lower guide is the main transmission line. The upper guide is terminated at one end to absorb unwanted power, and the other end is connected to the detector.

To describe the characteristics of a directional coupler, use is made of the terms "coupling," "directivity," and also standing-wave ratio in the main transmission line. These are defined in terms of the quantities

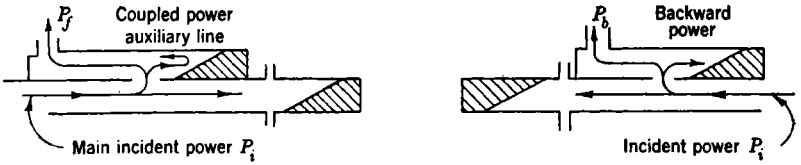

FIG. 14·5.—Definition of coupling and directivity.

shown schematically in Fig. 14·5. A coupler is designed so that ideally $P_b = 0$, but actually it may have some value which is small compared to P_f. Coupling is defined by

$$C = 10 \log_{10} \left(\frac{P_i}{P_f} \right). \tag{9}$$

Directivity is a measure of the quality of the coupler and is defined by

$$D = 10 \log_{10} \left(\frac{P_f}{P_b} \right). \tag{10}$$

The standing-wave ratio which is measured in the main line looking in the direction of the wave to which the coupler is sensitive, with the other end matched, is often used to specify one characteristic of a coupler. Usually the standing-wave ratio in the main line is the same looking in either direction with the main line terminated in a match.

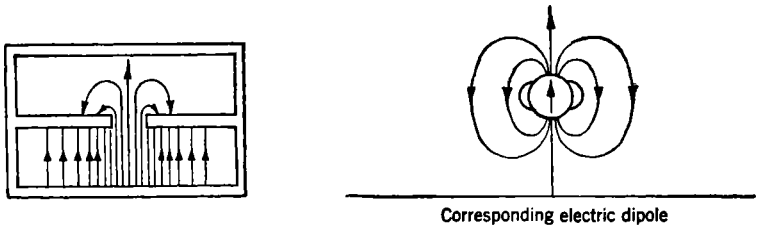

FIG. 14·6.—Electric coupling through a small hole.

In the Bethe-hole coupler, it can be seen that the hole provides coupling to both the electric and the transverse magnetic field components. This is illustrated in Figs. 14·6 and 14·7. The electric fields in the auxiliary guide in the neighborhood of the hole are similar to those generated by an oscillating electric dipole with its dipole moment parallel to the electric field of the incident wave in the main guide. Propagating waves will be set up in the auxiliary guide similar to those caused by such a dipole. In a like manner, the magnetic fields will behave as

though the hole contained a magnetic dipole moment which, however, is parallel to the transverse magnetic field in the main guide but in the direction opposite from it. In a pure traveling wave in the main line, the transverse electric and magnetic fields will be in phase. The electric dipole moment of the hole will also be in phase, while the magnetic dipole will be opposite in phase. Because of this reversal of sign of one type of coupling with respect to the other, the waves in the auxiliary line will cancel in the forward direction relative to the direction of propagation in the main line, and will reinforce in the backward direction. It is a general property of Bethe-hole couplers that the wave in the auxiliary line travels in the opposite direction from the wave in the main line.

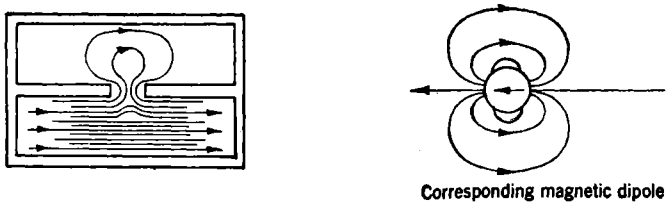

FIG. 14·7.—Magnetic coupling through a small hole.

As indicated in Sec. 14·2, the waves generated by the two types of coupling must be of equal amplitude in order to have complete cancellation and perfect directivity. The magnitude of the coupling through small holes has been calculated by Bethe,[1] and his results can be used for design purposes. Bethe assumes that the radius of the hole is small compared to a wavelength, and the hole is far from corners or other discontinuities in the plane containing the hole. The strength of the electric or magnetic dipole formed in the hole is proportional to the strength of the incident field and the polarizability of the hole. The polarizability depends on the shape of the hole and the direction of the incident field with respect to a line in the plane of the hole.

The voltage coupling is given by $(\pi j/\lambda_0 S)(E_1 E_2 P)$; E_1 and E_2 are the electric-field intensities corresponding to waves of unit amplitude in the primary and secondary guides respectively, which would have existed at the position of the hole if the hole had been absent. P is the electric polarizability of the hole, and S is a normalizing factor. Similarly, the magnetic coupling is given by $(\pi j/\lambda_0 S)(H_1 H_2 M)$, where M is the magnetic polarizability of the hole. The polarizabilities for a small round hole are given by $M = \frac{4}{3}r^3$ for the magnetic coupling, and $P = \frac{2}{3}r^3$ for the electric coupling, where r is the radius of the hole. It is seen that the ratio of the two kinds of coupling is independent of the size of the hole.

[1] H. A. Bethe, "Lumped Constant for Small Holes," RL Report No. 194, Mar. 24, 1943; "Theory of Side Windows in Waveguide," RL Report No. 199, Apr. 4, 1943.

The voltage coupling varies as the cube of r, so the coupled power varies as the sixth power of the hole radius.

To equalize the couplings, the axis of one guide is rotated with respect to the other as illustrated in Fig. 14·4. The magnetic dipole in the hole must now be resolved into a transverse and a longitudinal component in the auxiliary guide. Since only the transverse components couple, the magnetic coupling is reduced by a factor equal to a cosine function. The electric coupling is unchanged. This scheme is effective only if the magnetic coupling is stronger than the electric coupling when the guides are parallel. Fortunately, this is often the case. When the couplings are equal, the phase relations of the two components are such as to produce a wave in the auxiliary guide traveling in only one direction from the hole.

The wall thickness of the hole has the effect of reducing the coupling by a considerable amount. Moreover, it attenuates the two types of coupling by different factors. The hole may be regarded as a very short section of circular waveguide beyond cutoff. The electric coupling fields correspond to the TM_{01}-mode, and the magnetic coupling corresponds to the TE_{11}-mode in the round guide. Since the TM_{01}-mode is farther from cutoff, it is attenuated more rapidly than the TE_{11}-mode. Thus the effect of the wall thickness is always to increase the proportion of magnetic coupling.

If we let A_{inc} refer to the voltage amplitude of the wave incident in the main line, and A_E refer to the wave coupled into the auxiliary guide, then for the electric case

$$\frac{A_E}{A_{inc}} = \frac{\pi j}{\lambda_0 S}(E_1 E_2)\frac{2r^3}{3}F_E(t), \tag{11}$$

where $F_E(t)$ represents the attenuation in the hole of thickness t.

If the two guides are alike, $E_1 = E_2$, and if the hole is in the center of the broad side of the waveguide of dimensions a and b,

$$S = \frac{\lambda_g ab}{2\lambda_0} H_1^2 = \frac{\lambda_g ab}{2\lambda_0} E_1^2 \left(\frac{\lambda_0}{\lambda_g}\right)^2, \tag{12}$$

giving

$$\frac{A_E}{A_{inc}} = \frac{4\pi j r^3}{3\lambda_g ab}\left(\frac{\lambda_g}{\lambda_0}\right)^2 F_E(t). \tag{13}$$

Similarly, for the magnetic case,

$$\frac{A_H}{A_{inc}} = \frac{8\pi j r^3}{3\lambda_g ab}\cos\theta\, F_H(t). \tag{14}$$

The total coupled wave is then

$$\frac{A_E + A_H}{A_{inc}} = \frac{8\pi j r^3}{3ab\lambda_g}\left[\cos\theta\, F_H(t) + \frac{1}{2}\left(\frac{\lambda_g}{\lambda_0}\right)^2 F_E(t)\right]. \tag{15}$$

Coupling is then

$$C = 20 \log_{10} \left\{ \frac{\pi d^3}{3ab\lambda_g} \left[\cos \theta + \frac{1}{2} \left(\frac{\lambda_g}{\lambda_0} \right)^2 \frac{F_E}{F_H} \right] F_H \right\}, \tag{16}$$

where d is the diameter of the hole. The condition for equality of couplings becomes

$$\cos \theta = \frac{1}{2} \left(\frac{\lambda_g}{\lambda_0} \right)^2 \frac{F_E}{F_H}. \tag{17}$$

For this adjustment of the angle the coupling reduces to

$$C = 20 \log_{10} \left\{ \frac{2\pi d^3}{3ab\lambda_g} \cos\theta \, F_H \right\}. \tag{18}$$

The directivity is given by

$$D = 20 \log_{10} \left| \frac{\cos \theta + \frac{1}{2} \left(\frac{\lambda_g}{\lambda_0} \right)^2 \frac{F_E}{F_H}}{\cos \theta - \frac{1}{2} \left(\frac{\lambda_g}{\lambda_0} \right)^2 \frac{F_E}{F_H}} \right|. \tag{19}$$

The attenuation factors for the effect of the thickness of the hole are

$$F_E = e^{-2\pi \left[\left(\frac{1}{1.31d} \right)^2 - \frac{1}{\lambda^2} \right]^{1/2} t}, \tag{20}$$

and

$$F_H = e^{-2\pi \left[\left(\frac{1}{1.71d} \right)^2 - \frac{1}{\lambda^2} \right]^{1/2} t}, \tag{21}$$

for a hole of thickness t and diameter d. If the thickness is very small, so that F_E/F_H can be set equal to unity, then

$$\cos \theta = \frac{1}{2} \left(\frac{\lambda_g}{\lambda} \right)^2; \tag{22}$$

$\cos \theta$ is unity and the two waveguides are parallel when $(\lambda_g/\lambda)^2 = 2$ or when $\lambda = \sqrt{2}\, a$. This is very nearly the case for the standard 1-in. by $\frac{1}{2}$-in. waveguide at a wavelength of 3.2 cm.

The frequency sensitivity of the various properties of the directional coupler is usually of some concern. From the formula for directivity, it can be seen that frequency sensitivity appears in a term

$$\frac{1}{2} \left(\frac{\lambda_g}{\lambda_0} \right)^2 \left(\frac{F_E}{F_H} \right).$$

For thin walls the term F_E/F_H is relatively insensitive to frequency so that the frequency sensitivity is largely determined by the $(\lambda_g/\lambda_0)^2$ term. The directivity falls off rapidly in both directions with frequency, from an infinite value at the design frequency. It is simple to calculate the

bandwidth for a minimum directivity of 20 db. If a coupler is assumed for which $F_E/F_H = 1$, $\cos\theta = 1$, and $\lambda_g/\lambda_0 = \sqrt{2}$, the range of λ_0 for which $D > 20$ db is

$$\sqrt{\frac{13}{11}} > \frac{\lambda_0}{\lambda_{00}} > \sqrt{\frac{7}{9}}, \tag{23}$$

where λ_{00} is the design wavelength. The total bandwidth is thus approximately 20 per cent.

A coupling factor of 20 db in a Bethe-hole coupler requires a hole so large that the approximations of Bethe's theory do not hold. Rotation

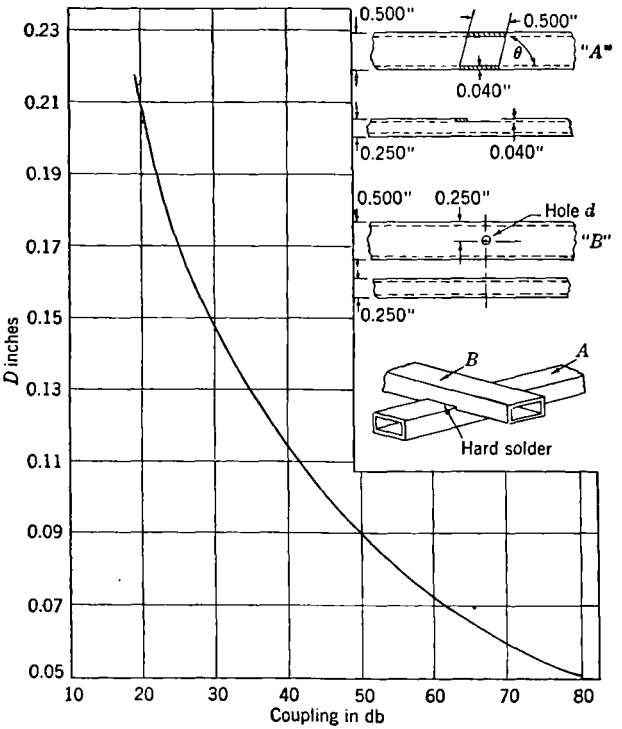

FIG. 14·8.—Design curve for Bethe-hole couplers in $\frac{1}{2}$- by $\frac{1}{4}$- by 0.040-in. wall waveguide, $\lambda_0 = 1.25$ cm.

of the guides from the angle predicted by the theory is necessary to obtain good directivity. The large hole in the guide wall sets up a reflection in the main transmission line. This is commonly matched out with a suitable iris. This problem becomes of importance for extremely tight coupling, 10 db or less.

It is readily seen that the directivity of a practical coupler is a function

not only of the coupling mechanism but also of the reflection from the termination in the auxiliary line, since energy from the backward direction can reach the detector by being reflected from this termination. An analysis of the effect of termination standing-wave ratio upon directivity is given in Sec. 14·10. The directivity of the actual coupler can be either better or worse than the directivity of the coupler with a perfect termina-

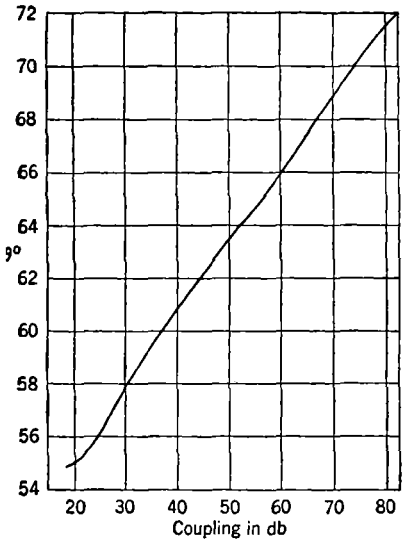

FIG. 14·9.—Design curve for Bethe-hole couplers in ¼- by ¼- by 0.040-in. wall waveguide, $\lambda_0 = 1.25$ cm.

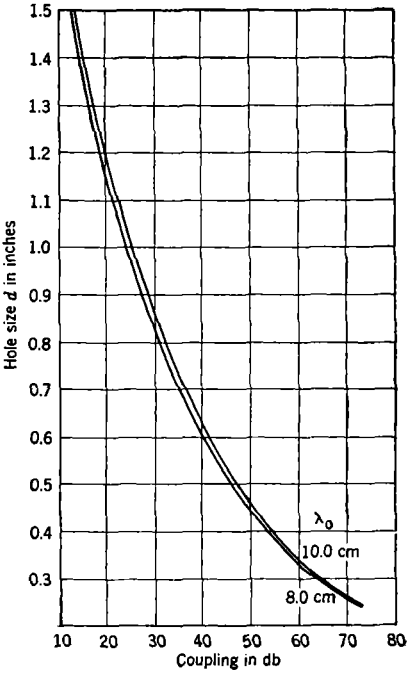

FIG. 14·10.—Design curves for Bethe-hole couplers in 3- by 1½- by 0.081-in. wall waveguide.

tion. It is not practical to compensate for an imperfect directivity by using a mismatched termination. This would be a critical procedure at best and in any case a narrow-band solution. A coupler is designed to give as good directivity as possible and the termination is matched within the tolerances of the over-all directivity required.

Figures 14·8, 14·9, 14·10, 14·11 give pairs of curves for designing Bethe-hole couplers in several sizes of waveguide which have been investigated. The hole size is first determined to give the desired coupling, and then the angle of rotation of the second guide is chosen to peak the directivity. The curves were obtained from theoretical calculations.

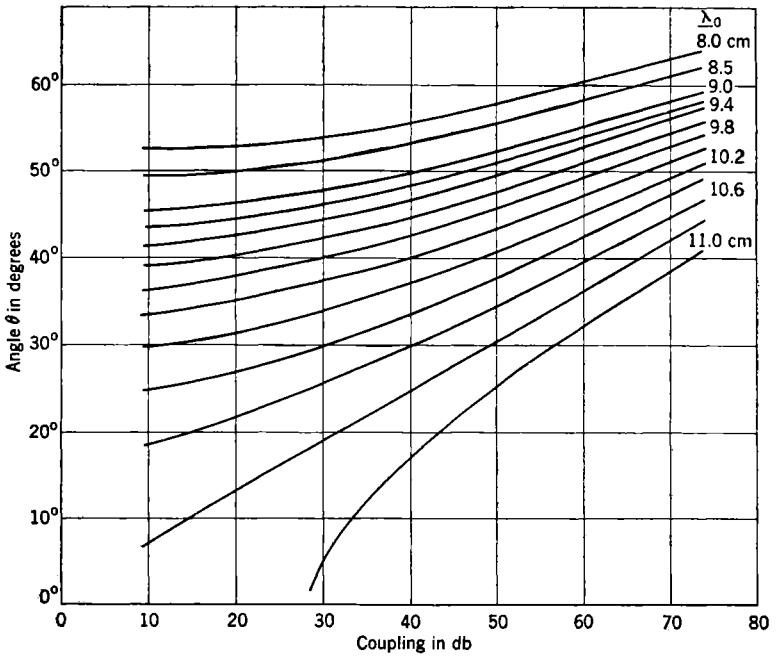

FIG. 14·11.—Design curves for Bethe-hole coupler in 3- by 1½- by 0.081-in. wall waveguide.

TABLE 14·1.—COUPLING AND DIRECTIVITY FOR BETHE-HOLE COUPLERS IN THE 10-CM BAND

Dimensions			Wavelength, cm	Coupling			Directivity, db	
Small hole, in.	Large hole, in.	Angle, deg.		Theory, db	Experiment, db	Theory minus experiment, db	Theory	Experiment,
0.740	1.375	52	8.5	34.13	35.7	−1.6	50.1	15
0.740	1.375	25	10.7	34.73	36.1	−1.4	50.9	24
0.740	1.5	38.5	10.0	34.6	35.7	−1.1		21
0.828	1.375	30	10.7	31.54	32.6	−1.1	30.2	23
1.105	1.5	30	10.7	22.84	24.4	−1.6	26.9	20
1.3	1.5	34.5	10.0	17.8	10.5	1.7		15
0.406	1.5	35	10.7	54.2	54.7	−0.5		19

For mechanical purposes, the hole for the 3- by 1½-in. waveguide is in a large recess in the second thickness of wall as is shown in Fig. 14·12. It is found empirically that it is necessary to design for a slightly larger value, by about 1 db, of coupling than is actually desired. Figure

14·12 shows the construction of this size of coupler. Table 14·1 gives a comparison of some of the experimental and theoretical values for the 3- by 1½-in. guide.

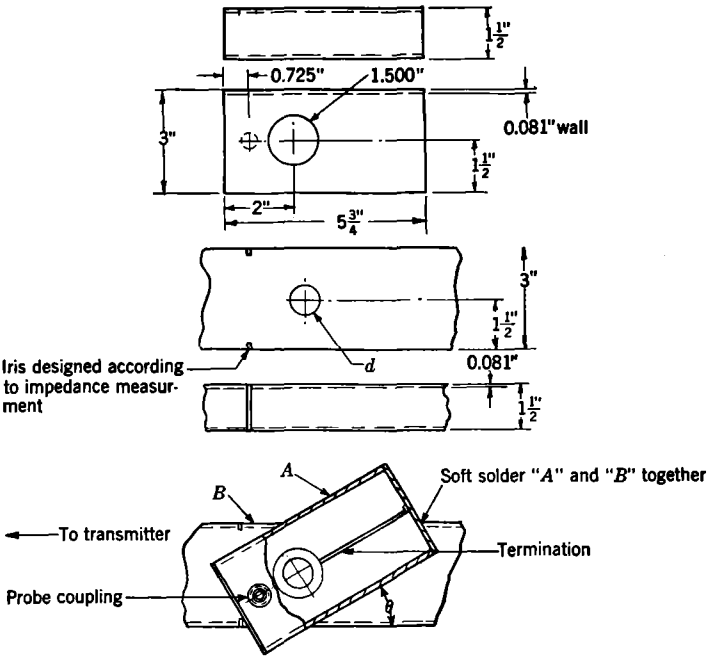

FIG. 14·12.—Bethe-hole couplers in 3- by 1½- by 0.081-in. wall waveguide. Choose d and θ according to design curves in Figs. 14·10 and 14·11.

14·4. Branched-guide Couplers.—The branched-guide coupler is a two-hole coupler which is particularly susceptible to exact analysis. Other types of two-hole couplers will be discussed in somewhat less detail in a later section. Figure 14·13 shows a branched-guide coupler in its usual form.

A qualitative idea of the operation of this coupler is obtained from the discussion of the two series probes in Sec. 14·2. If a pure traveling wave exists in one line, the relative phases of the waves in the small guides are exactly right to generate a pure traveling wave in the second guide in the *same* direction. In this respect, all two-hole couplers are different from the Bethe-hole coupler previously described.

In the following remarks the type of branched-guide coupler shown in Fig. 14·13 will be considered. The same analysis with only minor modifications can be applied as well to coaxial lines, or combinations of waveguide and coaxial lines; or indeed, to any type of transmission lines

arranged in this way. The representation of transmission lines as lumped circuits for purposes of analysis presents no difficulties. T-junctions present a more difficult problem, but it may be shown[1] that any symmetrical T-junction can be represented in the manner shown in Fig. 14·14. Four parameters are necessary to describe the symmetrical

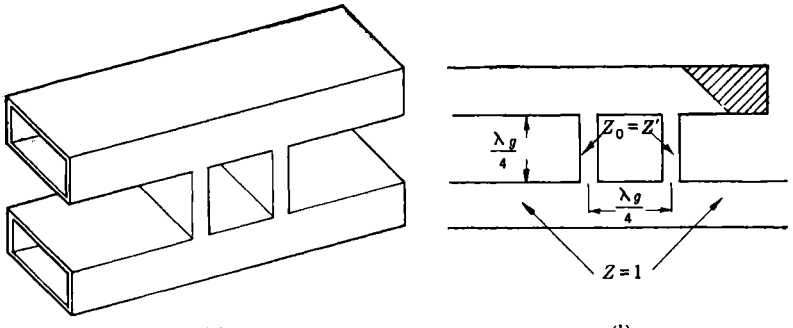

(a) Branched guide coupler (b) Schematic branched guide coupler

FIG. 14·13.—Branched-guide coupler.

junction: two to locate the three reference planes, and two to denote the values of the circuit elements. Similar circuits can be given for other types of T-junctions. The positions of these reference planes are not arbitrary. Only for certain positions is the simple equivalent circuit valid. For an E-plane T-junction, however, the change in the position

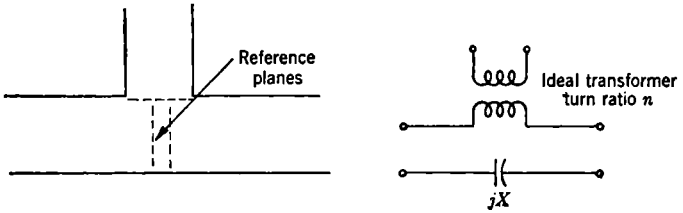

FIG. 14·14.—Equivalent circuit of T-junction.

of these reference planes with frequency is very small. As a first approximation, we shall assume that the positions of the reference planes at the junction are independent of frequency. In addition, we shall assume that $jX = 0$ and that the turns ratio of the ideal transformer is independent of frequency. This turns ratio will, in practice, be of the order of unity.

With these assumptions, the branched-guide coupler has the equivalent circuit of Fig. 14·15, where the quarter-wave branches have a charac-

[1] *Principles of Microwave Circuits*, Vol. 8, Chap. 8, Radiation Laboratory Series.

teristic impedance Z_0' relative to that of the main transmission line. Since all the transformers are alike, they serve only to change the imped-

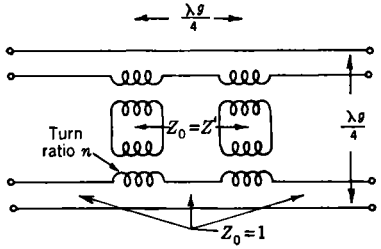

FIG. 14·15.—Equivalent circuit of branched-guide coupler.

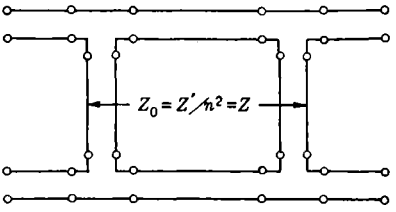

FIG. 14·16.—Modified equivalent circuit.

ance level of the stub lines so that we lose no generality in drawing the circuit as in Fig. 14·16, if we let

$$Z = \frac{Z'}{n^2}. \tag{24}$$

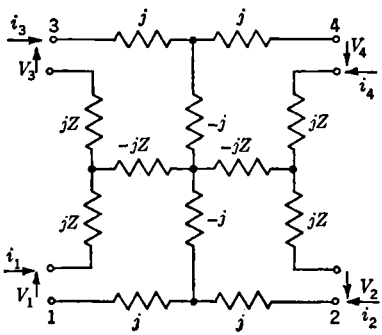

FIG. 14·17.—Equivalent circuit with lumped elements.

The equivalent circuit of a quarter-wavelength line of characteristic impedance Z_0 may be chosen to be a T-network with the series elements equal to jZ_0, and the shunt element equal to $-jZ_0$. The equivalent circuit of the coupler is then reduced to that in Fig. 14·17. The impedance matrix may be written down immediately by inspection, remembering that Z_{mn} is the voltage appearing at terminals m caused by a unit current at terminals n with all other terminals open-circuited.

$$\begin{pmatrix} V_1 \\ V_2 \\ V_3 \\ V_4 \end{pmatrix} = \begin{pmatrix} 0 & j & jZ & 0 \\ j & 0 & 0 & jZ \\ jZ & 0 & 0 & j \\ 0 & jZ & j & 0 \end{pmatrix} \begin{pmatrix} i_1 \\ i_2 \\ i_3 \\ i_4 \end{pmatrix}. \tag{25}$$

We now assume matched generators of voltages e_1, e_2, e_3, e_4 connected to guides 1, 2, 3, 4 respectively. Then, since $V_i = e_i - i_i$,

$$\begin{pmatrix} e_1 \\ e_2 \\ e_3 \\ e_4 \end{pmatrix} = \begin{pmatrix} 1 & j & jZ & 0 \\ j & 1 & 0 & jZ \\ jZ & 0 & 1 & j \\ 0 & jZ & j & 1 \end{pmatrix} \begin{pmatrix} i_1 \\ i_2 \\ i_3 \\ i_4 \end{pmatrix}. \tag{26}$$

If W is the determinant of the above matrix, and W^{ij} is the cofactor of the ij-element in the matrix, we may solve for i_j as

$$i_j = \sum_{k=1}^{4} \frac{e_k W^{kj}}{W} \qquad j = 1, 2, 3, 4. \tag{27}$$

We may now compute all the quantities of interest. It is sufficient to put

$$e_2 = e_3 = e_4 = 0 \tag{28}$$

to compute the effect of an incident wave at terminals 1. The currents produced by the other generators follow from symmetry considerations. We find the following expressions for the input impedance Z_{in}, the coupling C, and the directivity D:

$$Z_{in} = \frac{V_1}{i_1} = \frac{e_1}{i_1} - 1 = \frac{|W|}{W^{11}} - 1 = 1 - Z^2 \left(\frac{1 - \frac{Z^2}{2}}{1 + \frac{Z^2}{2}} \right), \tag{29}$$

$$\begin{aligned} C &= 10 \log_{10} \left(\frac{P_{\text{incident}}}{P_{\text{coupled}}} \right) = 10 \log_{10} \left| \frac{\frac{1}{4}(e_1)^2}{(i_4)^2} \right| \\ &= 10 \log_{10} \left[\frac{\frac{1}{4}|e_1|^2(4 + Z^4)^2}{|-2Z|^2|e_1|^2} \right] \\ &= 20 \log_{10} \left(\frac{4 + Z^4}{4Z} \right) \\ &= 20 \log_{10} \left(\frac{1}{Z} + \frac{1}{4} Z^3 \right), \end{aligned} \tag{30}$$

$$\begin{aligned} D &= 10 \log_{10} \left(\frac{(P_{\text{coupled forward}}}{P_{\text{coupled backward}}} \right) = 10 \log_{10} \left| \frac{(i_4)^2}{(i_3)^2} \right| \\ &= 10 \log_{10} \left(\frac{-2Z}{Z^3} \right)^2 = 20 \log_{10} \left(\frac{2}{Z^2} \right) \end{aligned} \tag{31}$$

It is seen that neither the voltage standing-wave ratio nor the directivity is perfect at the design frequency, but that both improve as the value of Z decreases.

The frequency sensitivity of the branched-guide couplers is the result of several factors of which only the change in the electrical length of the line sections can be readily analyzed. This is the principal cause of frequency sensitivity. Other causes are the change of the position of the reference planes of the junction with frequency (cf. Fig. 14·14) and the change in the turns ratio of the ideal transformer in the junction representation. Also, there is the reactive term jX shown in the equivalent circuit which has been ignored in the analysis. In practice this term is quite small.

To perform the analysis of change in line length we must replace the representation for a quarter-wave line by that of a line of length l shown in Fig. 14·18, where $\beta = 2\pi/\lambda_g$. The frequency sensitivity arises from the change in β. The same analysis can be used to predict effects caused by changes in line length l at a single frequency since these variables always occur as the product, βl. For $l \approx \lambda_g/4$ we approximate

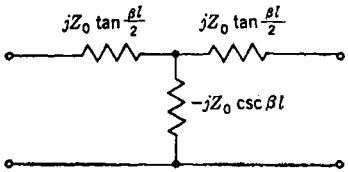

FIG. 14·18.—Equivalent circuit of a transmission line.

$$-jZ_0 \csc \beta l \approx -jZ_0$$

and

$$jZ_0 \tan \frac{\beta l}{2} \approx jZ_0(1 + \Delta\beta l), \quad (32)$$

where $\Delta\beta l$ represents the deviation of βl from $\pi/2$, its value when l is a quarter wavelength. The impedance matrix becomes

$$\begin{pmatrix} K & j & jZ & 0 \\ j & K & 0 & jZ \\ jZ & 0 & K & j \\ 0 & jZ & j & K \end{pmatrix}, \quad (33)$$

where $K = j(1 + Z)\Delta\beta l$. Proceeding as before with matched generators we have

$$\begin{pmatrix} e_1 \\ \cdot \\ \cdot \\ \cdot \end{pmatrix} = \begin{pmatrix} 1+K & j & jZ & 0 \\ j & 1+K & 0 & jZ \\ jZ & 0 & 1+K & j \\ 0 & jZ & j & 1+K \end{pmatrix} \begin{pmatrix} i_1 \\ \cdot \\ \cdot \\ \cdot \end{pmatrix}, \quad (34)$$

the only changes being in the diagonal elements. We may, as before, put $e_2 = e_3 = e_4 = 0$ corresponding to sending a wave into one arm of the coupler, and solve for the i's. We neglect all terms with higher powers of K than the first. The parameters of the coupler are then

$$Z_{in} = \frac{V_1}{i_1} = \frac{e_1}{i_1} - 1 = \frac{W}{W^{11}} - 1 = 1 - Z^2 + \cdots, \quad (35)$$

neglecting terms of order Z^4, K^2, KZ^2 and higher orders. Thus Z_{in}, to this order of approximation, is independent of frequency. The expression, of course, agrees with the exact expression previously derived, to the same order of approximation. The coupling is

$$C = 10 \log_{10} \left(\frac{\frac{1}{4}|e_1|^2}{|i_4|^2} \right), \quad (36)$$

$$C = 10 \log_{10} \left(\frac{\frac{1}{4}|4 + 8K|^2}{-4Z^2|1 + K|^2} \right). \quad (37)$$

Remembering that $K = -K^*$,

$$C = 10 \log_{10} \left[\frac{1 - 4K^2}{Z^2(1 + K^2)} \right] = 10 \log_{10} \left(\frac{1}{Z^2(1 + 3K^2 + \cdots)} \right), \quad (38)$$

so that the coupling also varies only with K^2, and is frequency-independent to the first order. Similarly, the directivity is

$$\begin{aligned} D &= 10 \log_{10} \left(\frac{|i_4|^2}{|i_3|^2} \right) \\ &= 10 \log_{10} \left[\frac{4Z^2(1 - K^2)}{Z^2(Z^4 - 4K^2)} \right] \\ &= 10 \log_{10} \left(\frac{1}{\frac{Z^4}{4} - K^2} \right) = 20 \log_{10} \left[\frac{2}{Z^2} \left(1 - \frac{4K^2}{Z^4} \right)^{-\frac{1}{2}} \right]. \end{aligned} \quad (39)$$

It should be pointed out that since K is imaginary, K^2 is negative, so the directivity given by the above formula is never perfect. The other causes of frequency sensitivity—changes in the parameters and in the reference planes of the junction—are important only for tight coupling and large Z.

Values of the Circuit Parameters.—If the height of the branched guide is small compared with the height of the main guide, several good approximations may be made. First, as before, the series reactance jX may be neglected. Second, the spacing of the reference planes in the main waveguide may be taken as zero, (see Fig. 14·14). The approximate reference planes are shown in Fig. 14·19. The parameter d may not be neglected, however. Relative to the small branched waveguide, the main guide appears as an open circuit at a distance d beyond the plane of junction. At the junction plane, the open circuit appears as a shunt capacitance on the branched line. Third, the turns ratio of the transformer may be taken equal to unity, so that the branch-line impedance Z is the ratio of the height of the branched guide b' to the height of the main guide b.

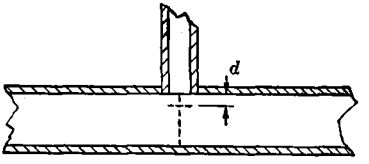

FIG. 14·19.—Approximate reference planes when $b' \ll b$.

The value of the shunt capacitive susceptance on the branched line is

$$B_c = \frac{2b'}{\lambda_g} \left(1 + \ln \frac{b}{2b'} \right). \quad (40)$$

This corresponds to a value of d given by

$$d = \frac{b'}{\pi} \left(1 + \ln \frac{b}{2b'} \right). \quad (41)$$

The design procedure in this simple case is straightforward. The height of the branched guide is chosen for the desired value of the coupling given by Eq. (30). To sufficient accuracy Eq. (30) reduces to

$$C = 20 \log_{10} \frac{b}{b'}. \tag{42}$$

The two branched guides are spaced a quarter of a wavelength apart along the main transmission line. The lengths of the branched guides are chosen to be smaller than a quarter wavelength by the amount $2d$.

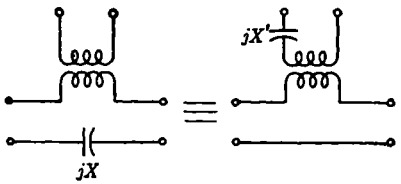

FIG. 14·20.—Alternative representation of T-junctions.

If a close coupling is desired, so that b' approaches b, the above approximations are no longer valid. The correct values of the circuit parameters, n, d, jX, and the separation of the reference planes in the main waveguide may be found in the *Waveguide Handbook* for the E-plane T-junction.

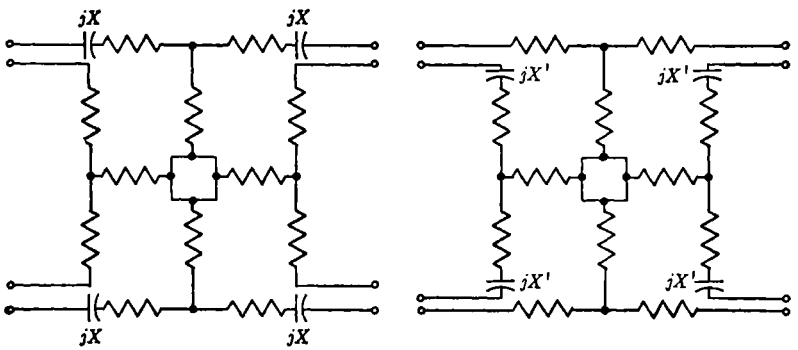

FIG. 14·21.—Lumped circuit for coupler with junction reactance.

Effect of Junction Reactance.—In addition to the method employed earlier in this section, the general representation of a T-junction can be made in another form as indicated in Fig. 14·20. If jX or jX' cannot be neglected, the lumped-circuit representation for the entire coupler can be of the form shown in Fig. 14·21. Since any lossless symmetrical T-network can be realized as a length of transmission line of real length and real characteristic impedance, correction for the effect of junction reactance can be accomplished by changing the length of one set of arms or even by changing both sets. There will be a corresponding change in coupling. If only the stub lines are changed, the coupler will still be of

the simple form treated above. The values of the parameter X are given in the *Waveguide Handbook*.

Modified Branched-guide Coupler.—It is useful at tight couplings to use a variation which has three different guide sizes instead of two. The ordinary type has a directivity of only 26 db at a coupling of 10 db, whereas the modification which is shown in Fig. 14·22 is perfect at the design wavelength. Unfortunately for the design of this type of coupler the parameters for unsymmetrical junctions have not been tabulated.

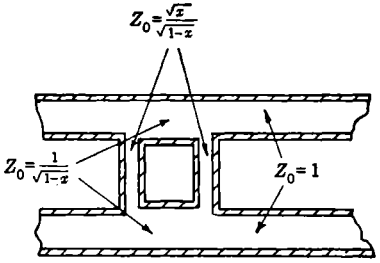

FIG. 14·22.—Modified branched-guide directional coupler.

Branched-guide couplers can be designed which have perfect directivity although none of the lines are a quarter wavelength long and all the branches are of different characteristic impedances. The investigation of these possibilities is too involved[1] to present here, and has not yet produced any forms of practical value.

14·5. Two-hole Couplers.—Two-hole couplers are included among those types which have a main transmission line, an auxiliary line, and two identical coupling devices spaced an odd number of quarter wavelengths apart. The branched-guide coupler treated in the previous section is one member of this class. Others are the two-hole coupler shown in Fig. 14·23 and the "inside-out" coaxial coupler shown in Fig. 14·24. The individual coupling devices should be nondirectional, or if directional, should favor the same direction as the complete coupler so that the directivity will be high. Two rectangular guides connected by holes in their broad sides would not operate satisfactorily since each hole is a Bethe-hole coupler transmitting primarily a backward wave and the cancellation of the backward waves would be imperfect. The frequency sensitivity of directivity is similar for all two-hole couplers. If the amplitude of the forward wave is unity, the amplitude of the wave in the backward direction is, to a first approximation, $\frac{1}{2}(1 + e^{2i\beta l})$, where l is the distance between the holes, assuming that the elements are nondirectional. The power in the backward wave is

$$|\tfrac{1}{2}(1 + e^{2i\beta l})|^2 = \cos^2 \beta l. \tag{43}$$

If we write

$$\beta l = (2n + 1)\left(\frac{\pi}{2} + \Delta\beta l\right), \tag{44}$$

[1] B. A. Lippmann, "Theory of Directional Couplers," RL Report No. 860, Dec. 28, 1945; also Principles of Morewave Circuits, Vol. 8, Chap. 8, Radiation Laboratory Series.

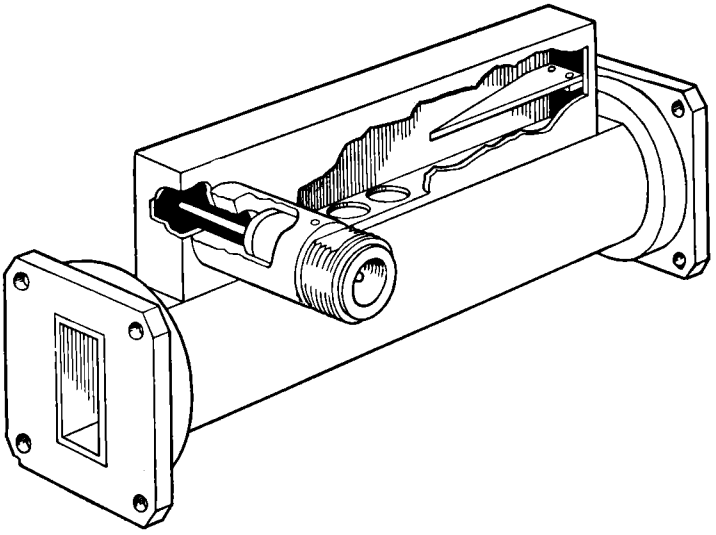

FIG. 14·23.—Two-hole directional coupler.

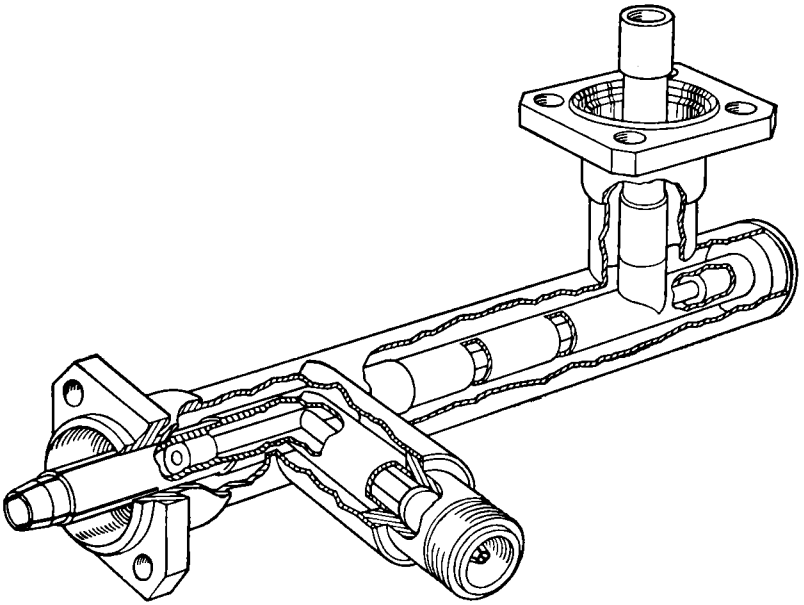

FIG. 14·24.—"Inside-out" coaxial coupler.

then the backward power is

$$\sin^2 [(\Delta\beta l)(2n + 1)], \tag{45}$$

where $(\Delta\beta l)$ is the departure of the hole spacing from an integral number of quarter wavelengths. Making the approximation $\sin \theta \approx \theta$, we have

$$D = 10 \log_{10} \frac{1}{(\Delta\beta l)^2(2n + 1)^2}. \tag{46}$$

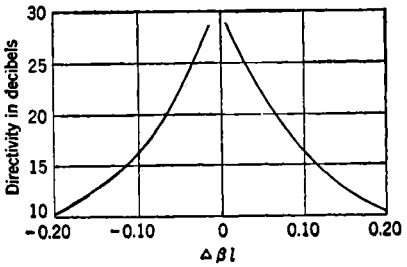

FIG. 14·25.—Frequency variation of directivity for two-hole couplers.

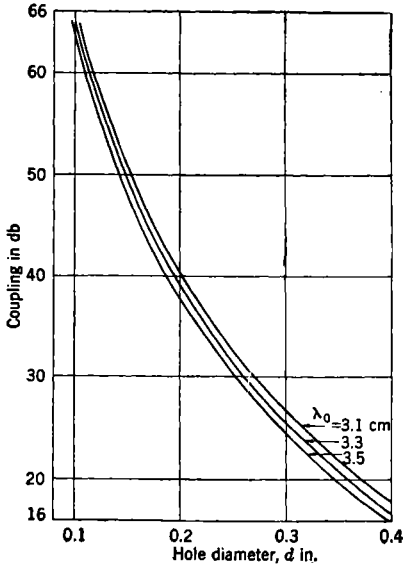

FIG. 14·26.—Design curves for two-hole couplers using round holes in the side of 1- by ½-in. waveguide with 0.050-in. wall.

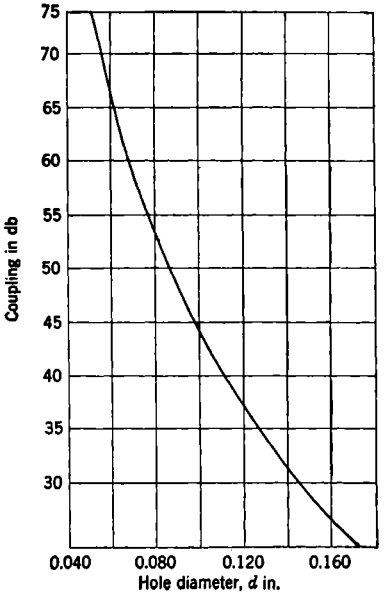

FIG. 14·27.—Design curve for two-hole couplers using round holes in the side of ½- by ¼-in. waveguide with 0.040-in. wall. for $\lambda_0 = 1.25$ cm.

This approximate formula gives an infinite directivity at the design wavelength which is generally not realized in practice because of reflections, inaccuracies, or interactions between coupling elements. Far from the design wavelength, where the directivity is determined primarily by the spacing of the coupling elements, this formula is a good approximation. A plot of D against $\Delta\beta l$ is shown in Fig. 14·25 for $n = 0$.

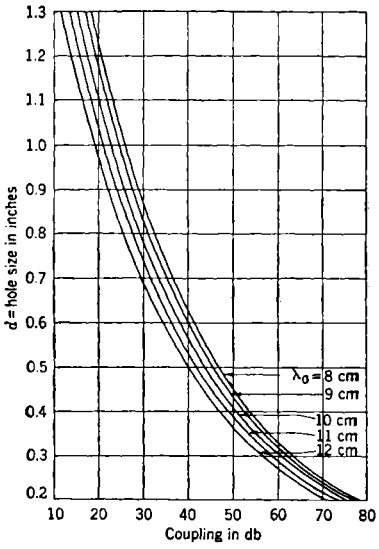

FIG. 14·28.—Design curves for two-hole couplers using round holes in the side of 3- by 1½-in. waveguide with 0.080-in. wall.

The frequency sensitivity of coupling is almost wholly dependent upon that of the individual coupling elements since the addition of waves in the forward direction depends only upon the equality of the two paths and thus does not depend upon frequency.

Design curves for an ordinary two-hole coupler such as that shown in Fig. 14·23 are given in Figs.

TABLE 14·2.—DIRECTIONAL COUPLERS USING TWO SLOTS
Data to accompany Fig. 14.30

Waveguide size	Slot length t, in.	Slot spacing s, in.	Slot height d, in.	Wall thickness l, in.	Curve in Fig. 14·30	Coupling, db
1¼ by ⅝ by 0.064 in.	0.350	0.385	0.094	0.187	..	24.6 at $\lambda_0 = 3.1$ cm 26.7 at $\lambda_0 = 3.5$ cm
	0.328	0.400	0.156	0.187	*A*	
	0.400	0.400	0.094	0.187	*B*	
1 by ½ by 0.050 in.	0.290	0.430	0.200	0.150	*C*	
	0.325	0.486	0.187	0.144	*D*	
	0.350	0.430	0.187	0.144	*E*	
	0.350	0.430	0.200	0.150	*F*	
½ by ¼ by 0.040 in.	0.070	0.152	0.062	0.080		34.3 at $\lambda_0 = 1.25$ cm
	0.100	0.152	0.062	0.080		29.0
	0.135	0.152	0.062	0.080		19.0
	0.166	0.152	0.062	0.080		8.5

14·26, 14·27, 14·28 for various sizes of waveguide. The curves show theoretical coupling from the formula given by Bethe,

$$C = 20 \log_{10}\left(\frac{\pi d^3 \lambda_g}{6a^3 b}\right) - 32.0\left[1 - \left(\frac{1.71d}{\lambda_0}\right)^2\right]^{\frac{1}{2}} \frac{t}{d}. \qquad (47)$$

The coupling can be increased and at the same time broadbanded by using slots instead of holes. The slots, which are about a quarter wavelength long, are staggered in the side wall of the guide to prevent over-

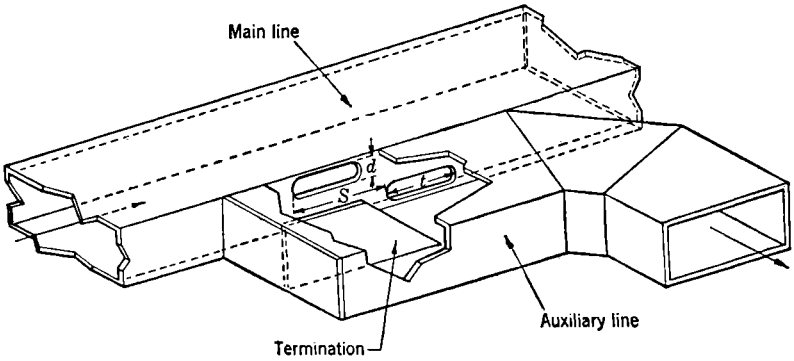

FIG. 14·29.—Coupler employing two slots.

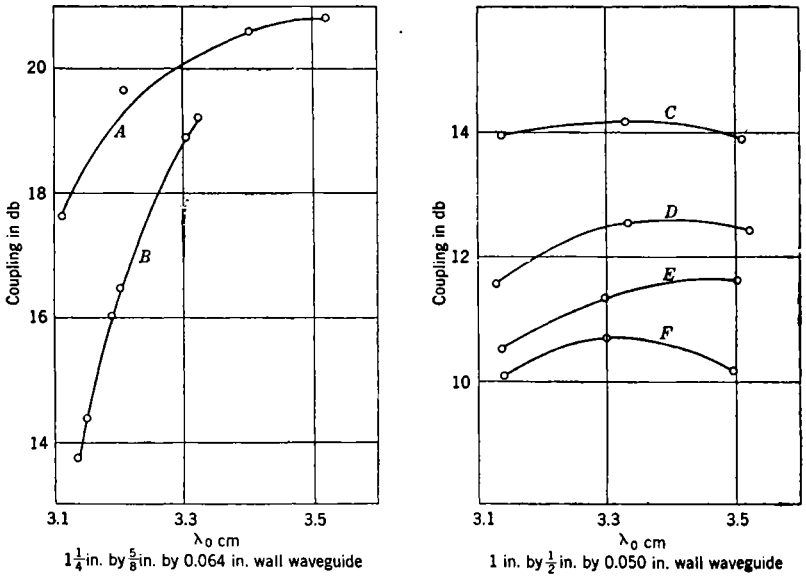

FIG. 14·30.—Experimental results on two-element couplers using slots in the side of guide.

lapping. Such a coupler is shown in Fig. 14·29. Figure 14·30 characteristics some of the couplers which have been made with this type of construction. The results are empirical. The theory of coupling through slots of this type has not been worked out. Table 14·2 gives the dimensions of the couplers whose characteristics are shown in Fig. 14·30 together with some additional observations.

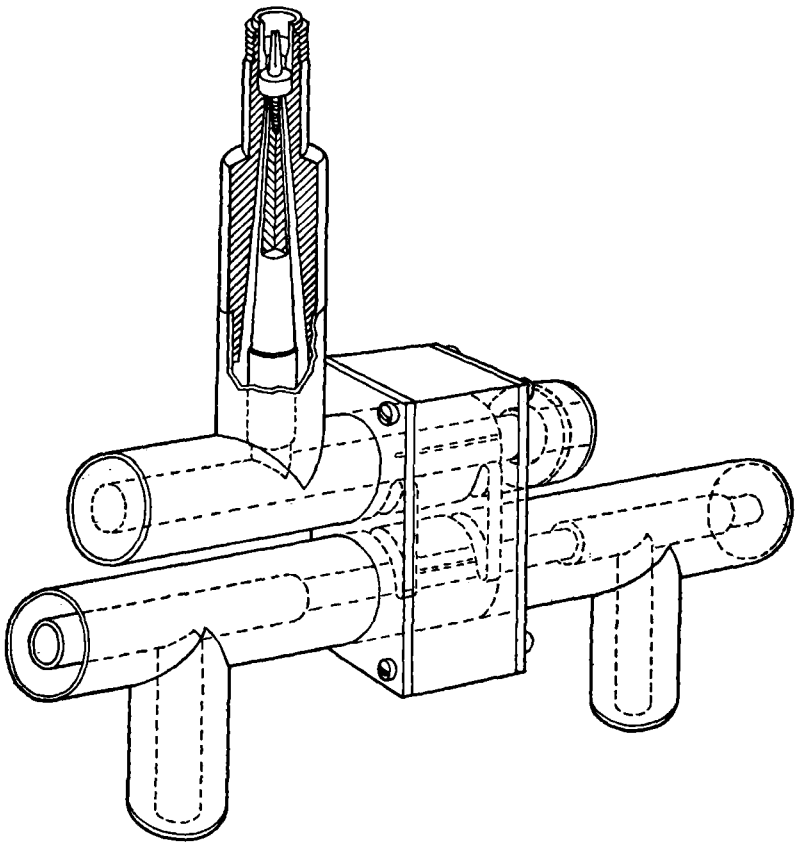

FIG. 14·31.—Slotted-block directional coupler for coaxial line.

Two-hole couplers have also been constructed in coaxial line. One method employs two coaxial lines side by side with slots joining them,[1] as shown in Fig. 14·31. It is difficult by this method to obtain sufficient coupling without introducing large reflections in the transmission lines.

[1] R. S. Julian, "Directional Transmission Line Taps," BTL MM-44-170-6, Jan. 26, 1944.

Experimental results for such a coupler are shown in Figs. 14·32 and 14·33.

A more satisfactory method is to place one coaxial line inside the center conductor of the second coaxial line. Coupling apertures are cut out between them. The inner line can be brought out to terminals through stub supports. Figure 14·24 shows an "inside-out" coaxial-line coupler of this type. In this way it is possible to obtain close couplings as is shown in the design curves of Figs. 14·34 and 14·35. In Fig. 14·35 the points represent experimental determinations; the curve is drawn on the assumption that the coupled power varies as θ^6. An approximate formula has been derived for the coupling of inside-out couplers by making the assumption that the coupling aperture is an elliptical hole in a plane conducting wall. This gives

$$C \approx 20 \log_{10} \left[\frac{5\pi r \theta^3}{2Z_0 \lambda \left(\ln \frac{4r\theta}{W} - 1 \right)} \right] + \frac{27t}{\theta r}, \tag{48}$$

where θ is the angular aperture of the slot in radians; r is the radius of the cylindrical surface between the two transmission lines; Z_0 is the line impedance; λ is the wavelength; t is the wall thickness; and W is the width of the aperture. The second term gives the attenuation through the aperture. The dashed line in Fig. 14·35 shows the results of applying this formula. The circled points are experimental.

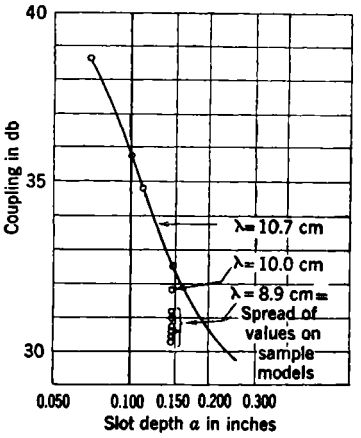

FIG. 14·32.—Design data on slotted-block coaxial couplers in ½-in. line.

Broadband coupling can be obtained by using a composite coupler composed of two units in cascade. If the frequency sensitivities of the two couplers are of opposite sign, it is possible to obtain an over-all coupling which is frequency-insensitive. For example, a coupler with two round holes and a slot coupler could be used together. This method is of course applicable only where weak coupling is desired.

14·6. Multiple-path Couplers.—An extension of the principle of the two-hole coupler is the multiple-path coupler. Waves add in the forward direction and cancel in the backward direction, but cancellation is obtained between waves excited by three or more coupling elements, usually spaced a quarter wavelength apart. A coupler of this type may

be used to increase the coupling in the forward direction or to improve the frequency sensitivity of the directivity. For this purpose a set of coupling elements for which the coupled voltages vary as the coefficients

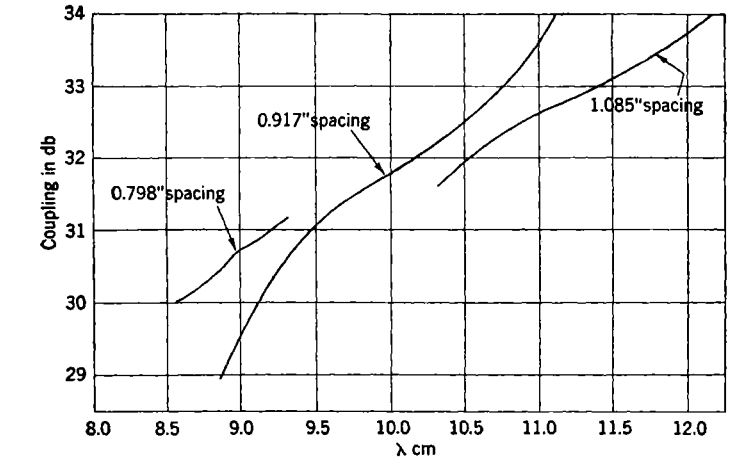

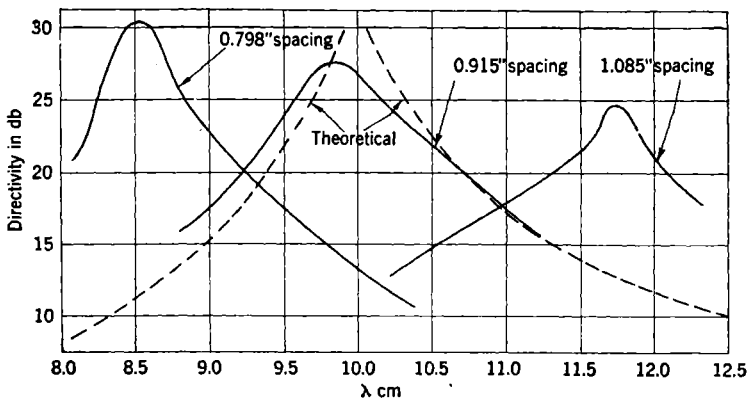

FIG. 14·33.—Experimental results on slotted-block directional coupler in $\frac{1}{8}$-in. coaxial line. Upper curves give the measured coupling for two-slot couplers with a nominal slot depth of 0.145 in. for different spacings between slots. The lower curves show the measured directivity.

in a binomial expansion may be used. This improves frequency sensitivity in much the same manner as the use of binomial tapers in impedance matching.[1]

[1] J. C. Slater, *Microwave Transmission*, McGraw-Hill, New York, 1942, p. 60.

Suppose we have two two-hole couplers spaced along a transmission line. If they do not have perfect directivity, each will produce a wave in the backward direction. If we space the couplers by an odd number of

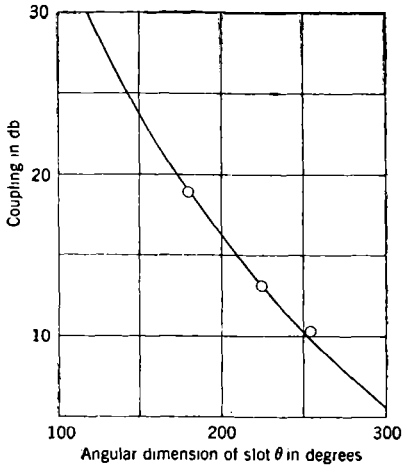

FIG. 14·34.—Design data for concentric coaxial coupler between $\frac{7}{8}$-in. OD and $\frac{3}{4}$-in. OD coaxial lines for $\lambda_0 = 10$ cm.

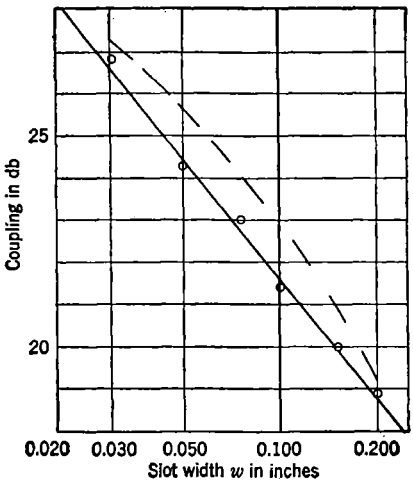

FIG. 14·35.—Design data for concentric coaxial coupler between $\frac{7}{8}$-in. OD and $\frac{3}{4}$-in. OD coaxial lines.

quarter wavelengths, the two backward waves will cancel. If we attempt to space them by one-quarter wavelength, the second hole of the first coupler will coincide with the first hole of the second coupler. We have a

three-hole coupler, with the center hole producing coupled waves of twice the amplitude of the waves produced by the outer holes. By repeating this process, we arrive at an $(n + 1)$-hole coupler with binomial coupling. We can calculate the relative couplings by this same argument as indicated schematically below.

$$\begin{array}{rl} & 1\ 1 \\ + & \underline{\ \ 1\ 1} \\ & 1\ 2\ 1 \\ + & \underline{\ \ 1\ 2\ 1} \\ & 1\ 3\ 3\ 1 \\ + & \underline{\ \ 1\ 3\ 3\ 1} \\ & 1\ 4\ 6\ 4\ 1 \\ + & \ldots\ldots \end{array}$$

Let $(n + 1)$ be the number of such holes. Then let the voltage coupling through these holes be proportional to the coefficients of the binomial expansion

$$1,\ n,\ \frac{n(n-1)}{1\cdot 2},\ \frac{n(n-1)(n-2)}{1\cdot 2\cdot 3},\ \ldots,\ \frac{n(n-1)\cdots(1)}{1\cdot 2\cdot 3\cdots n}.$$

In the forward direction these will add in phase to give a coupling proportional to 2^n. This does not mean that the coupling can be increased indefinitely since it is limited by the maximum coupling possible for the largest hole, and in order to materially increase the coupling the number of holes must be enormous.

In the backward direction the waves add with alternating signs so that at the design frequency the backward wave vanishes

$$1 - n + \frac{n(n-1)}{2} - \cdots (-1)^n \frac{n(n-1) - \cdots (1)}{1\cdot 2\cdot 3\cdots n} = (1-1)^n = 0. \quad (49)$$

To determine the frequency sensitivity of directivity we introduce a small deviation from quarter-wave spacing. The expression for the backward wave is then

$$1 - ne^{j\Delta} + \frac{n(n-1)}{1\cdot 2}e^{2j\Delta} - \frac{n(n-1)(n-2)}{1\cdot 2\cdot 3}e^{3j\Delta} + (-1)^n \frac{n(n-1)\cdots 1}{1\cdot 2\cdot 3\cdots n}e^{nj\Delta} = (1 - e^{j\Delta})^n. \quad (50)$$

For small values of Δ, the backward wave is $(-j\Delta)^n$, so that the backward wave vanishes to the n'th order of the frequency deviation. Some improvements over this method of broadbanding might be expected if

the spacings were staggered slightly so as to get the broadest bandwidth. However, interactions have been neglected in the analysis, and a more laborious calculation would be necessary to predict the optimum design. In addition, the frequency sensitivities of the coupling elements would have to be taken into consideration. Branched-guide couplers with many branches are also possible and form a type of multiple-path coupler.

14·7. Reverse-coupling Types.—An important variation of the two-hole coupler is the reverse-coupling type. This differs from the ordinary two-hole coupler in having a reversal of phase in one coupling element as compared to the other. This is accomplished by using the symmetry properties of the coupling and can be done only in certain

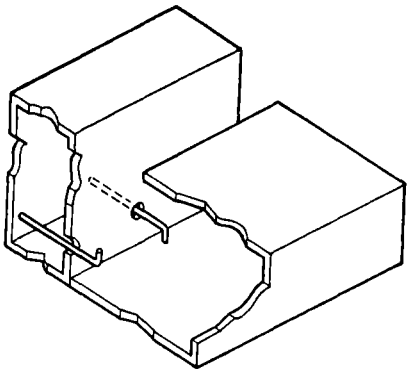

FIG. 14·36.—Reverse-coupling directional coupler.

cases. The advantage of a coupler of this kind is that the waves reinforce in the backward direction and cancel in the forward direction so that the cancellation is not so frequency-sensitive as in the simpler coupler. Because of the addition of the two waves in the backward direction, the coupling will have increased frequency sensitivity, but this is a slowly varying effect compared to the change in directivity of the usual variety of coupler. The individual coupling elements may have frequency sensitivity which can perhaps be used to balance out the other effect.

One method of obtaining the phase reversal is shown in Fig. 14·36. The action of this coupler may be easily understood from the cross sections shown in Fig. 14·37. Here identical currents are produced in the secondary line by fields which are opposite in phase in the primary line for the two elements.

Another method is shown in Fig. 14·38. The direction of the current lines across the slot, and hence the phase of coupling, will depend upon the side of the slot into which the screw is inserted. The strength of the

current and therefore the coupling will depend on the depth of insertion. This scheme has often been employed in antenna arrays.[1]

A third method which has proved useful in practice is known as the Schwinger reversed-phase coupler. This coupler is shown in Fig. 14·39.

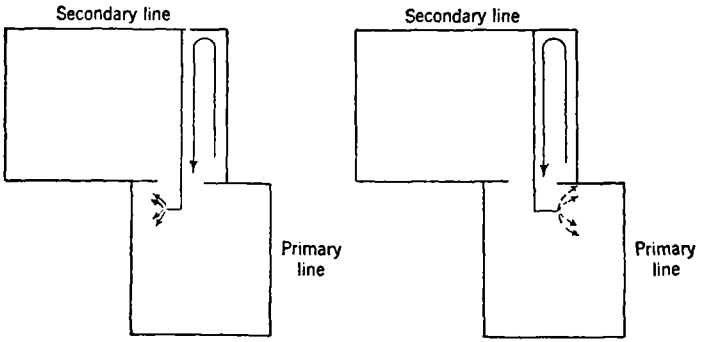

FIG. 14·37.—Action of RCA coupler.

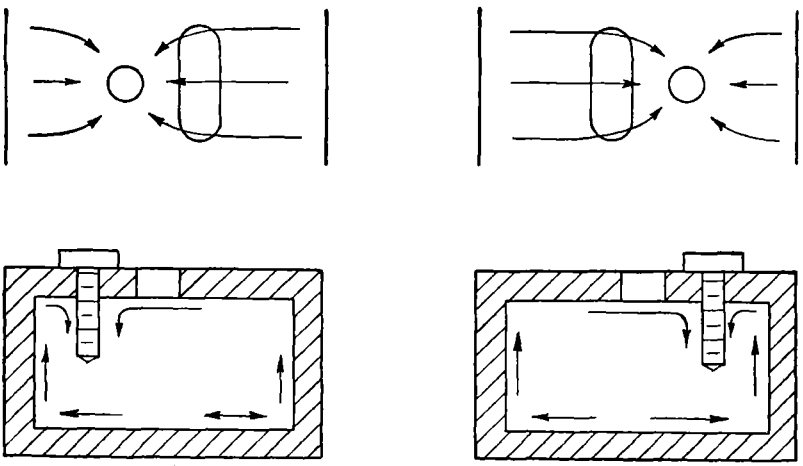

FIG. 14·38.—Second variety of reverse-phase coupling element.

The reversal of phase between the two elements is indicated in Fig. 14·40. The coupling is between the longitudinal magnetic field in one guide and the transverse magnetic field in the other. The use of a slot about a quarter-wavelength long results in broadband coupling (cf. Sec. 14·5). Experimental measurements on couplers of this type are shown in Fig. 14·41. Table 14·3 gives some results on a 10-cm-band model, built in 3- by 1½-in. waveguide.

[1] Microwave Antenna Theory and Design, Vol. 12 Radiation Laboratory Series.

TABLE 14·3.—10-CM-BAND SCHWINGER COUPLER

λ, cm	Coupling, db	Directivity, db
8.9	+19.6	22
9.24	+20.8	24
10.0	+22.1	30
10.55	+22.7	30
11.1	+22.9	26
11.55	+22.7	22

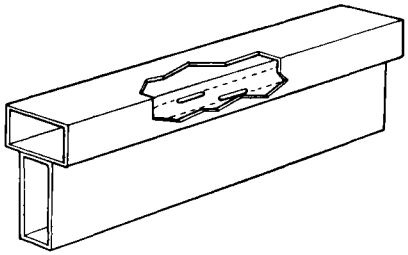

FIG. 14·39.—Schwinger directional coupler.

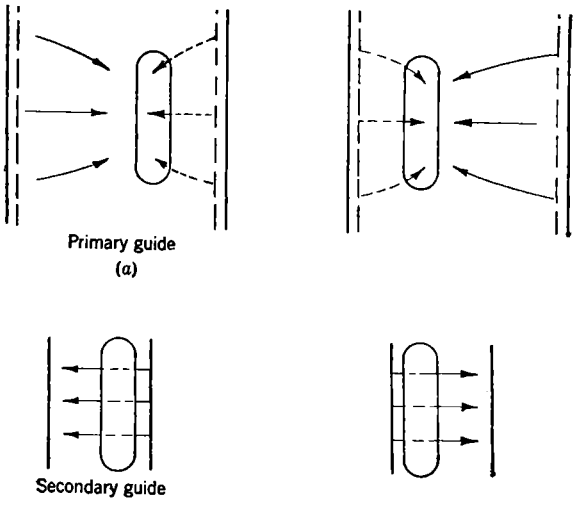

FIG. 14·40.—Reversal of phase in Schwinger coupler showing current lines.

Figure 14·42 shows the slot dimensions for the coupler whose characteristics are shown in the table.

14·8. Long-slot Couplers.—As the name implies, the long-slot coupler is formed of two transmission lines joined by a slot in the direction of

propagation. The slot is presumed to radiate or "leak" energy from one guide to the other at each point along its length. In the forward direction these incremental waves reinforce in phase. In the reverse

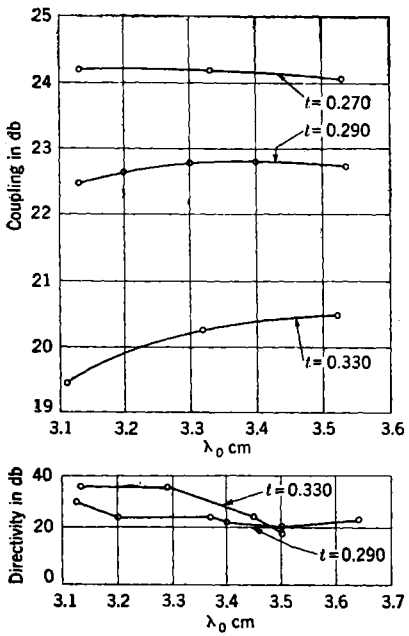

FIG. 14·41.—Schwinger directional coupler in 1- by ½- by 0.050-in. wall waveguide.

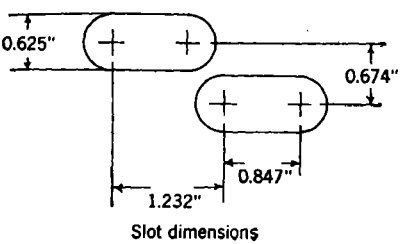

FIG. 14·42.—Slot dimensions of 10-cm-band Schwinger coupler.

direction the incremental waves are of all phases and tend to cancel. According to this simple picture, when the slot is an integral number of half wavelengths long, all phases are equally represented in the reverse direction so that there is no net wave and the directivity is perfect. In any case, the longer the slot, the greater the ratio of forward-to-backward coupling.

More sophisticated analysis shows that if the slot is carefully tapered

to prevent reflection from the ends, the directivity should be perfect even for very wide short slots. Further, it is possible to get all the energy into the auxiliary guide for any slot width by making the slot long enough. Making the slot still longer decreases the coupling. This limitation,

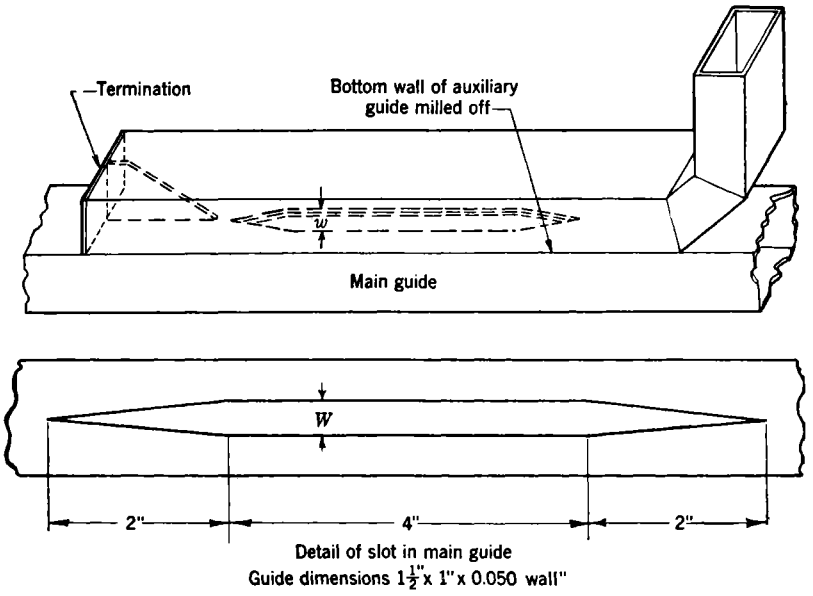

FIG. 14·43.—Construction of long-slot directional coupler.

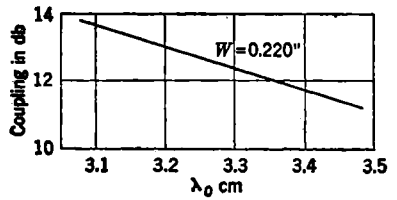

FIG. 14·44.—Frequency dependence of coupling for long-slot coupler in 1- by ½- by 0.050-in. wall waveguide.

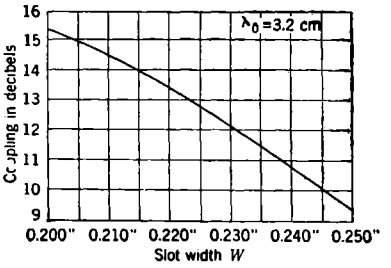

FIG. 14·45.—Design data for long-slot couplers in 1- by ½- by 0.050-in. wall waveguide.

however, is never reached in practice. For small coupling, the coupled power is proportional to the square of the slot length and to the sixth power of the slot width. It is possible to obtain high directivities in practice with this type of coupler so that it is suitable for reflectometer purposes (cf. Sec. 14·12). Its length, however, makes it unsuitable for most applications. The construction of a long-slot directional coupler

is shown in Fig. 14·43. The frequency sensitivity of coupling is large as shown in Fig. 14·44. The coupling obtained as a function of slot width is plotted in Fig. 14·45.

In order to demonstrate some of the properties of the long-slot coupler it may prove instructive to consider the problem from two widely different approaches. First, we shall consider infinitesimal sections of the length of the slot as separate radiators. As was shown in Sec. 14·3, fringing fields in the auxiliary guide will behave as if there were electric and magnetic dipoles in the slot in phase with the incident wave. These will radiate wavelets which will reinforce in the forward direction and tend to cancel in the reverse direction. We ignore any possible directional properties of the individual slot segments. Once a wave is set up in the auxiliary guide it will, in turn, radiate into the primary guide. It might be supposed that once half the power had entered the auxiliary guide a sort of equilibrium would be set up and further lengthening of the slot would produce no change. This is not the case, however. If the expression for dipole radiation into free space is recalled, it will be noticed that there is a 90° phase difference between the radiated field and the exciting field. The same holds for waveguides. The imaginary factor j in Eq. (11) represents the same phenomenon. The wave traveling in the auxiliary guide will hence be 90° behind the exciting wave. This is shown in Fig. 14·46. Figure 14·46 also shows that the wave reradiated into the primary guide is of such phase as to decrease the total intensity in the primary guide. One might almost say that the wave in the auxiliary guide "sucks" power out of the main guide. This process continues until all of the power has been transferred to the auxiliary guide, at which point the process reverses and power is transferred from the auxiliary guide back into the main guide. This action is exactly analogous to the behavior of two loosely coupled tuned circuits.

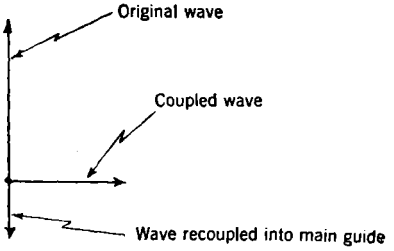

FIG. 14·46.—Operation of long-slot coupler.

For fairly short slot lengths, when the power transfer from the auxiliary guide to the main line can be neglected, the coupled voltage is proportional to slot length and hence coupled power varies as the square of slot length. As with coupling holes, the coupled power varies as the sixth power of the slot width (cf. Sec. 14·3). The directivity for short slot lengths is by this analysis

$$D = 10 \log_{10} \left(\frac{\beta l}{\sin \beta l} \right)^2, \tag{51}$$

if the possible directional effect of an incremental section of slot is ignored. Since, however, most long-slot couplers have tapered ends on the slots, this formula, as will be seen, is not particularly significant.

The second method of approach to these problems stems from a consideration of the two lines joined by the slot as a single transmission line of somewhat peculiar cross section. Figure 14·47 shows the types of modes which can be propagated in such a transmission line. Mode C

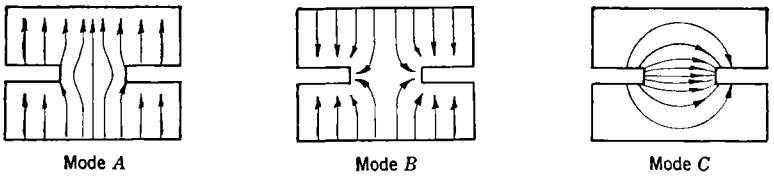

FIG. 14·47.—Normal modes in slotted guides.

cannot be excited except by irregularities, but it can cause the troublesome "slot resonance" in long-slot couplers, or in slotted sections, (cf. Sec. 8·3). It is totally reflected from the ends of the slot so that the slot behaves as a resonant section of line coupled to the rest of the system only by asymmetries. It is probably worth while to try to damp out this resonance, although this has not yet been investigated.

At the ends of the slots, modes A and B couple to the two guides only in certain symmetrical ways which we shall refer to as modes A' and B,

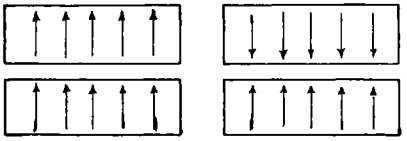

FIG. 14·48.—Normal modes in two guides.

respectively. These modes represent the two possible symmetries of the configuration and are shown in Fig. 14·48. There may also be reflections of these modes at the ends of the slot. We shall assume in this analysis that the ends of the slot have been carefully tapered to prevent reflections. Hence, if we simultaneously send waves down two guides to produce mode A', there will be a smooth transition to mode A along the slot and back to mode A' at the other end of the slot, without any reflections. Similarly with modes B and B'. This is illustrated in Fig. 14·49.

It can be seen from the figure that sending a wave down the primary guide from terminal 1, is equivalent to sending mode $(A' + B')$ in at terminals 1 and 3. The fields in arm 3 will cancel. Waves will come out at arms 2 and 4 only; and there will be no reflected waves. In other

words, the coupler will have perfect directivity and be perfectly matched, independently of everything except the quality of the tapering of the slot. The coupling comes about by virtue of the fact that modes A and B will have slightly different propagation velocities with the result that

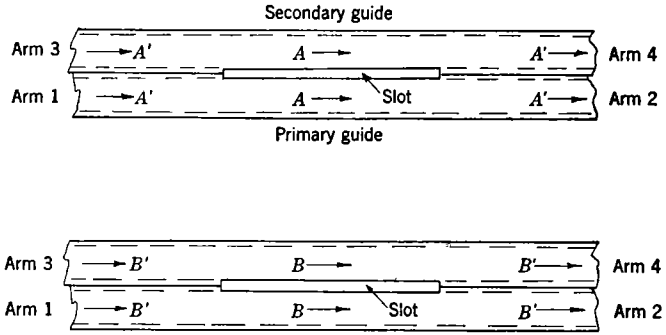

FIG. 14·49.—Modes in long-slot coupler.

modes A' and B' will no longer be in phase in arms 2 and 4. In arm 4 the amplitude will be

$$E_4 = e^{-j\beta_A l} - e^{-j\beta_B l} = e^{-j(\beta_B+\beta_A)\frac{l}{2}}\left[e^{j(\beta_B-\beta_A)\frac{l}{2}} - e^{-j(\beta_B-\beta_A)\frac{l}{2}}\right]$$

$$|E_4| = \left|2 \sin (\beta_B - \beta_A) \frac{l}{2}\right|. \tag{52}$$

In arm 2 similarly

$$|E_2| = \left|2 \cos (\beta_B - \beta_A) \frac{l}{2}\right|, \tag{53}$$

where β_A and β_B are the wave numbers of the corresponding modes and l is the length of the slot. The effect of slot width comes in by way of its effect on $\beta_A - \beta_B$.

Since β is dependent only on the cutoff wavelength, the behavior of such a long-slot coupler over a frequency range is given by two parameters in addition to length. Usually both cutoff wavelengths are near the cutoff wavelength for the unperturbed guide so that the only quantities necessary to specify the coupler are the length and the difference between the two cutoff wavelengths. Further analysis shows that care must be taken to ensure that the waves in the two guides have the same propagation velocity. Otherwise the running waves will get out of phase with each other, and it will not be possible to obtain maximum coupling. This is more critical for long slots than for short ones; the condition is that the difference in path lengths for the length of the slot should be negligible compared with a wavelength.

14·9. Resistive-loop Couplers.—It is well known that coupling loops have a tendency to couple to the electric as well as the magnetic field. This is exploited in the resistive-loop type of coupler shown in Fig. 14·50.[1]

Without the resistance the device could not have directive properties, since it would then be a three-terminal-pair *lossless* device, which can be rigorously represented as a pure shunt (or series) junction. This theorem is prove in Vol. 8, Chap. 9.

The relative strengths of magnetic and electric coupling can be adjusted by rotation of the loop. In addition, the value of resistance controls not only the relative magnitudes of the couplings but also their phases. This type of coupler can be inserted in either waveguide or coaxial transmission line.

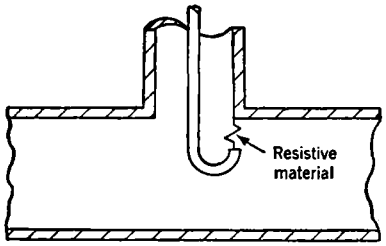

FIG. 14·50.—Resistive-loop coupler.

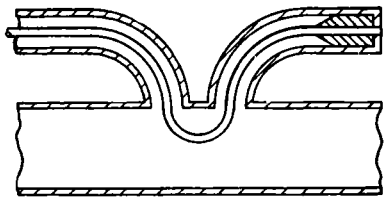

FIG. 14·51.—Resistive-loop coupler with fourth line brought out.

An unusual feature of the resistive-loop coupler is that the absorbing material is placed within the coupling region rather than in the end of a transmission line as is the case in the other couplers described. A variation which is more like the conventional design is shown in Fig. 14·51.

Little is known about the design of resistive-loop couplers. Since it is difficult to construct loops to close tolerances, it is probable that this design will find its most suitable applications at frequencies lower than 3000 Mc/sec.

14·10. General Theoretical Considerations.—For most purposes it is sufficient to describe a directional coupler in terms of directivity, coupling, and possibly its reflection coefficient in the main line. For some purposes, however, it may be necessary to describe the coupler more completely and exactly. It is sufficient to specify the impedance or admittance matrix of the coupler considered as a three-terminal-pair linear network containing loss. It will be more convenient to specify instead the scattering matrix, since the directional properties are more

[1] G. B. Myers and B. P. Charles, "The Reflectometer," Navy Report 521, Aug. 25, 1944.

evident in this form. Only the method of approach to the general problem will be indicated here.

The scattering matrix gives the relationship between the waves leaving the network and the waves entering the network. We write

$$\mathsf{b} = \mathsf{Sa},$$

$$\begin{pmatrix} b_1 \\ b_2 \\ b_3 \end{pmatrix} = \begin{pmatrix} S_{11} & S_{12} & S_{13} \\ S_{12} & S_{22} & S_{23} \\ S_{13} & S_{23} & S_{33} \end{pmatrix} \times \begin{pmatrix} a_1 \\ a_2 \\ a_3 \end{pmatrix}, \tag{54}$$

where the a's are the complex voltage amplitudes of the incident waves and the b's are the complex voltage amplitudes of the scattered waves. For a three-terminal-pair network, the scattering matrix (which is always symmetrical) has six complex parameters. The phases of the complex S_{ij} elements are functions of the positions of the arbitrarily selected reference planes.

The magnitudes of the scattering coefficients are immediately interpretable in terms of the previously defined quantities. If in Eq. (54), we call terminals 1 and 2 the terminals of the main transmission line with power going from 1 to 2 in the forward direction, and call 3 the probe terminal, then the various elements in the matrix have the following physical significance. The coefficients S_{11}, S_{22}, S_{33} represent reflection coefficients in the various arms, 1, 2, and 3, with the other arms matched, and in a good directional coupler they are all small. For the usual symmetrical coupler construction $S_{11} = S_{22}$. Ordinarily, only S_{11} is specified. The coefficient S_{12} represents the transfer of power in the main line past the coupling mechanism. The value of $|S_{12}|$ is slightly less than unity. The coefficient S_{13} represents the voltage coupled to the detector from a wave in the forward direction incident at terminal 1. It is a measure of the coupling C. The voltage coupled in the backward direction is represented by S_{23}. If the directivity is perfect, $S_{23} = 0$. More exactly

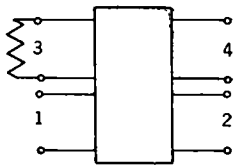

FIG. 14·52.—Four-terminal-pair representation.

$$\begin{aligned} C &= -20 \log_{10} |S_{12}|, \\ D &= 20 \log_{10} \left| \frac{S_{13}}{S_{23}} \right|. \end{aligned} \tag{55}$$

A more fruitful method of general approach is to consider the directional coupler as a four-terminal-pair nondissipative network with an external load (see Fig. 14·52). This representation is permissible since usually the resistive material is actually placed in an external line. This does not hold for the resistive-loop type of coupler, but here the resistance may be considered a single lumped element to a good approxi-

mation and as such can always be represented in this manner. This approach is valuable since it allows use of the theorems concerning nondissipative networks. Besides, there are a few applications in which directional couplers are used without the terminating resistance and all four terminal pairs are connected to other networks or components.

In this representation an ideal directional coupler is represented by the scattering matrix

$$\begin{array}{lc} & \begin{matrix} (1) & (2) & (3) & (4) \end{matrix} \\ \text{Main line} \quad \begin{matrix} (1) \\ (2) \end{matrix} & \begin{pmatrix} 0 & S_{12} & 0 & S_{14} \\ S_{12} & 0 & S_{23} & 0 \end{pmatrix} \\ \text{Auxiliary line} \quad \begin{matrix} (3) \\ (4) \end{matrix} & \begin{pmatrix} 0 & S_{23} & 0 & S_{34} \\ S_{14} & 0 & S_{34} & 0 \end{pmatrix} \end{array}, \tag{56}$$

where

$$|S_{12}| = |S_{34}|, \qquad \text{and} \qquad |S_{23}| = |S_{14}|,$$

and

$$|S_{12}|^2 + |S_{23}|^2 = 1,$$

so that by a suitable choice of reference planes we may write the scattering matrix as

$$\begin{pmatrix} 0 & \sqrt{1-\gamma^2} & 0 & \gamma \\ \sqrt{1-\gamma^2} & 0 & \gamma & 0 \\ 0 & \gamma & 0 & \sqrt{1-\gamma^2} \\ \gamma & 0 & \sqrt{1-\gamma^2} & 0 \end{pmatrix}, \tag{57}$$

where γ is a real quantity. The ideal coupler then has these properties: it is matched in all directions; the directivity is perfect both ways; and the coupling coefficient is the same both ways. Such ideal couplers are realizable in practice only at a single frequency.

The influence of the built-in termination upon the directivity of the coupler considered as a three-terminal-pair network can be determined in the following manner. In Sec. 14·3 directivity was defined as

$$D = 10 \log_{10} \left(\frac{P_f}{P_b} \right), \tag{58}$$

where P_f is the power coupled through the guide in the preferred direction. Since the amount of power reaching the termination from a forward wave is much smaller than this, the voltage standing-wave ratio of the termination cannot appreciably affect P_f. For P_b the situation is much different. The directional element alone contributes an amount P_0, caused by a unit backward wave. At the same time the termination receives an amount of power which is approximately equal to P_f since the directional element is symmetrically constructed. The amount of power to the termination is, in the case of a backward wave, large com-

pared to P_0. Any reflection from the termination will go largely to the output terminals and will contribute to P_b, in which it may indeed be the primary factor. If Γ_t is the reflection coefficient of the termination, then the output voltage will be a vector sum of the voltages from these two sources or

$$P_b = |P_0^{1/2} + \Gamma_t P_f^{1/2} e^{i\phi}|^2, \tag{59}$$

where $e^{i\phi}$ takes care of the possible phase relationship between the two waves. The extreme values of the directivity will be given by

$$\begin{aligned} D_{\text{extreme}} &= 10 \log_{10} \left(\frac{P_f}{|\sqrt{P_0} \pm \Gamma_t \sqrt{P_f}|^2} \right) \\ &= 10 \log_{10} \frac{P_f}{P_0} \left(\frac{1}{\left|1 \pm \Gamma_t \dfrac{\sqrt{P_f}}{\sqrt{P_0}}\right|^2} \right) \\ &= 10 \log_{10} \frac{P_f}{P_0} - 20 \log_{10} \left|1 \pm \Gamma_t \frac{\sqrt{P_f}}{\sqrt{P_0}}\right|. \end{aligned} \tag{60}$$

Letting $D_0 = 10 \log_{10} (P_f/P_0)$, we obtain

$$D = D_0 - 20 \log_{10} \left|1 \pm \Gamma_t \left(\frac{\sqrt{P_f}}{\sqrt{P_0}} \right)\right|. \tag{61}$$

The second term may be larger than the first. The magnitude and phase of Γ_t may always be chosen so as to make the directivity infinite. This is not feasible in practice. It is usually more convenient to design couplers with a satisfactory value of D_0 and to keep the effect of Γ_t small. This means in effect keeping

$$\Gamma_t \sqrt{\frac{P_f}{P_0}} \ll 1. \tag{62}$$

It is often convenient, instead of speaking of directivities, to define unbalance reflection coefficients as

$$\begin{aligned} \Gamma_D &= \sqrt{\frac{P_b}{P_f}} \\ \Gamma_0 &= \sqrt{\frac{P_0}{P_f}}. \end{aligned} \tag{63}$$

Equation (59) then becomes

$$\Gamma_D = |\Gamma_0 + \Gamma_t e^{i\phi}|. \tag{64}$$

Also

$$D = -20 \log_{10} \Gamma_D. \tag{65}$$

14·11. Measurements of the Properties of Directional Couplers.—The measurement of the various properties of directional couplers is not

appreciably different from other r-f attenuation and impedance measurements. Certain techniques, are, however, especially applicable. Distinction can be made between the measurement of a completed coupler including termination and adapters to particular types of fittings or line connections, and the measurement of the coupling element itself; that is, the hole, or slots, or other means of providing the directional property. Measurement of the coupling element would be, of course, primarily for purposes of research or design of new coupler types. This discussion will confine itself to the measurement of directivity, coupling, and VSWR.

Measurement of S_{11} does not need to be mentioned further. Obviously, in measuring VSWR in the main line, a termination should be used that is better than the desired accuracy of the measurement. The technique of a sliding termination described in Sec. 8·7 is useful here.

The measurement of coupling is a standard attenuation measurement. Since most couplers are designed to couple more closely than 40 db, no great difficulty should be met. Often the coupling must be measured between two different types of transmission lines which fact introduces a slight complication. Methods of making such measurements are described in detail in Chap. 13. Incidentally it should be pointed out that a directional coupler with well-matched terminations on two arms forms an excellent fixed-attenuation standard, especially for the higher attenuation ranges. Since the absorbing material appears only in the form of terminations, the device is completely stable and independent of power level, temperature, or humidity.

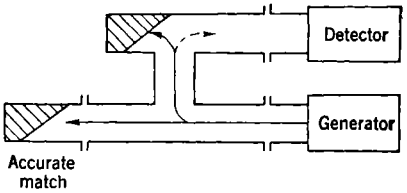

FIG. 14·53.—Measurement of directivity.

Directivity is somewhat more difficult to measure. In the first place, the attenuation is greater. If a 40-db coupler has a directivity of 30 db, to take an extreme case, the total attenuation from the main line is 70 db in the backward direction. This offers serious problems. In addition, for measuring completed couplers the termination which is connected to the far end of the main line must be very accurately matched. The effect on measured directivity is the same as that of the matched termination incorporated in the coupler. The experimental arrangement for measuring directivity is shown in Fig. 14·53.

The voltage reaching the output load from the forward wave as a result of the imperfect directivity of the coupler is

$$\sqrt{P_b} = \sqrt{\frac{P_b}{P_f}}\sqrt{P_f} = \Gamma_D \sqrt{P_f}. \tag{66}$$

If the termination used in the measurement has a reflection coefficient

Γ, then a portion of the reflected wave given approximately by $\Gamma\sqrt{P_f}$ in voltage will reach the output terminals. The resulting wave $\sqrt{P_b'}$ will be the vector sum of the two. If we define the measured unbalance reflection coefficient

$$\Gamma_M = \sqrt{\frac{P_b'}{P_f}} = \frac{1}{\sqrt{P_f}}\left(\Gamma_D\sqrt{P_f} + e^{i\theta}\Gamma\sqrt{P_f}\right), \tag{67}$$

then

$$\Gamma_M = |\Gamma_D + \Gamma e^{i\theta}|, \tag{68}$$

but this has exactly the same form as Eq. (64) describing the effect of the built-in termination on directivity. Another method of determining directivity is to use a tunable impedance to terminate the main line. This can now be tuned until no power reaches the detector. The reflection coefficient Γ of the variable impedance is now equal to the unbalance reflection coefficient Γ_D and can be measured with an ordinary slotted section. This method has the advantages of being a null method and of being independent of generator and detector impedances. It is suitable for the ordinary range of directivities. A directivity of 40 db corresponds to an unbalance voltage standing-wave ratio of 1.02, which is about as low a value of voltage standing-wave ratio as can be conveniently measured with a slotted section. Care must be taken to measure the tunable load at exactly the same frequency as was used in balancing the coupler.

14·12. The Reflectometer.—The application of directional couplers to the measurement of reflection coefficients of transmission-line components by measuring the magnitude of the reflected wave is an obvious one;[1] but the accuracy needed and the techniques used are sufficiently different from those used in measuring power transfer that a separate discussion is advisable. Directional couplers used for the measurement of reflected waves have commonly been called "reflectometers." Normally, two directional couplers are needed, one to measure the incident power, and the other the reflected power. A single directional coupler with a second detector substituted for the termination can perform both functions, but this places very stringent requirements on the match of both detectors so that it is usually more convenient to use two couplers.

The most critical requirement of a reflectometer is good directivity of the coupler used to measure reflected power. As was pointed out in Sec. 14·11 there is a relation between directivity and Γ. We interpret P_b as being caused by the reflected wave from the unknown impedance. Actually, however, there is a contribution from the imperfect directivity.

[1] R. S. Julian, "A Precision Impedance Comparator," BTL MM-44-170-18, Mar. 10, 1944.

By a method analogous to that used in the previous section we can obtain the result

$$\Gamma'_X = \Gamma_X \pm \Gamma_D e^{i\alpha}, \tag{69}$$

where Γ'_X is the observed reflection coefficient, Γ_X is the true unknown reflection coefficient, and α takes care of possible phase differences between the waves. An ordinary good coupler will have a directivity of 20 db which corresponds to a VSWR of 1.22, which is an intolerable error for a laboratory VSWR measurement. One might set up the requirement that the error caused by imperfect directivity should be of the order of 1.01 in VSWR which means a directivity of 46 db. The error caused by an imperfect termination in the coupler is given by the Γ_t of the termination itself, so that the termination would be required to have a VSWR of less than 1.01. For many field uses, these accuracy requirements can be relaxed to more reasonable values.

The long-slot type of coupler is preferred for reflectometers because of the high directivity obtainable, although the length is a disadvantage. The techniques used in conjunction with reflectometers are similar to those described in Chap. 9 for use with magic-T impedance bridges. Rather than to rely on calibrations of detector sensitivity to determine the reflected-wave amplitude with the reflectometer, it is convenient to have some "gauge blocks" in the form of standard mismatches which can be used to check the readings.

Since directivities of reflectometers must be high, the problem of directivity measurement becomes more difficult. Here again methods for measuring "balance" described in Chap. 9 will be found effective.

CHAPTER 15

R-F PHASE AND PATTERN MEASUREMENTS

By Harvey R. Worthington

The measurement of r-f phase and intensity in free space requires experimental procedures and circuits different from those used for analogous measurements in transmission lines. In order for the measurements to provide accurate and useful information it is necessary to observe certain optical requirements. The first purpose of this chapter is to show how the ideal optical conditions may be approximated in the experimental setup and to discuss the effect of these approximations on the various measurements. The second purpose is to describe the general procedures and circuits used for r-f intensity, gain, and phase measurements. The specialized applications of these techniques to such problems as antenna design will not be discussed.[1]

15·1. Terminology and Definitions.—In this chapter it will be necessary to use some new terms and to treat antenna properties not previously defined in this book. These are described briefly below to facilitate the subsequent discussion.

Near and Far Fields.—These fields are, respectively, the regions of Fresnel and Fraunhofer diffraction. The two regions are distinguished by the manner in which contributions from elements of the aperture surface add together at a distant point on the normal axis of the aperture. The Fraunhofer region is characterized by the condition that such contributions to the intensity at the distant point on the axis arrive with effectively their initial phase relationships. Since the transition between regions is gradual an arbitrary limit is defined. The limit between regions is given in terms of aperture diameter and wavelength by the equation

$$R = \frac{D^2}{\lambda}.$$

Pattern Parameters.—The principal parameters affecting the characteristics of the radiation pattern are the dimensions of the aperture and the functions that describe the distribution of illumination and phase over the aperture. For an aperture uniformly illuminated by a plane

[1] Volume 12 of this series discusses microwave antenna design and contains a chapter on antenna measurements.

wave the amplitude pattern in the far field is of the form

$$g(x) = g_0 \frac{\sin x}{x},$$

where x is a function of the aperture size, wavelength, and the angle of orientation with respect to the normal axis,

$$x = \frac{\pi D \sin \theta}{\lambda}.$$

When the illumination function is "tapered," the pattern is described by a different function having similar qualitative characteristics.

Gain.—The gain of an antenna expresses its effectiveness in concentrating power in a given direction. It is the ratio of the peak intensity of the pattern to the intensity of an isotropic radiator emitting the same amount of power. The maximum gain for an aperture of given area is obtained by uniform illumination with a plane wave,

$$G_0 = \frac{4\pi A}{\lambda^2}.$$

In practical antennas the gain is usually lower than this.

Efficiency can, therefore, be expressed conveniently as a ratio of the actual gain to the gain of a uniformly illuminated aperture of the same area. This ratio is called the "gain factor"

$$f = \frac{G}{G_0}.$$

Absorption Cross Section is a useful term describing an effective aperture area such that the gain calculated on the basis of uniform illumination of this area is equal to the actual gain of the full aperture,

$$G = \frac{4\pi(fA)}{\lambda^2}.$$

Scattering by an Antenna.—When radiation is intercepted by an antenna aperture only a part is absorbed. The remainder is reradiated or scattered. The fraction so scattered cannot be stated concisely in terms of simple antenna parameters, nor is it practical to undertake an accurate calculation. Roughly speaking it will be of the order of $(1 - f)$, where f is again the gain factor. The pattern of such scattered radiation is not capable of even a rough evaluation for general purposes. Therefore in anticipating the effect of scattering on intensity measurements it may be advisable to assume the unlikely possibility that the scattering gain factor is as large as $(1 - f)$.

Center of Phase.—For sources emitting spherical or cylindrical waves there is a geometric center point or line from which the rays appear to emanate. This is called the center of phase. Its location within the radiating element is of particular interest when this element is to be placed at the focus of some optical system.

15·2. Pattern Intensity Measurements.—To determine the intensity pattern of an antenna, the relative power received by a second antenna in the field is measured at the various positions of interest. The second antenna is maintained at a fixed range and is directed toward the center of the test antenna so as to subtend a constant solid angle at all orientations. The relative power received is then directly proportional to the intensity. A polar plot of the pattern in any given plane can be obtained by rotating either antenna about the proper axis through the center of the aperture of the test antenna. For short-range measurements in the laboratory it is usually most convenient to move the r-f pickup probe in a circular path while the test antenna remains fixed at the center. In the case of large antennas where long ranges are required it is necessary to rotate the test antenna about its own center keeping the second antenna stationary. Usually the fixed antenna is used as a transmitter so that the moving element need carry only the relatively small detecting apparatus.

The range of separation required for a given pair of antennas is an important factor in determining the physical features of the apparatus as well as the requirements of power and receiver sensitivity. Therefore it will be necessary, before proceeding, to establish some relationships between the range and the antenna diameters on the basis of optical requirements.

In most intensity measurements it is the far-field pattern that is of interest. This must be measured under far-field conditions because proper correction of the near-field pattern would require more information than is obtained by a single pattern measurement. On the other hand, the long ranges required for large antennas frequently make it necessary to work at the minimum range that will yield a satisfactory approximation of the far-field pattern. A convenient rule for determining the minimum range R for a given pair of antennas is

$$R = \frac{(D_1 + D_2)^2}{\lambda}, \tag{1}$$

where D_1 and D_2 are the aperture diameters and λ is the wavelength. This rule represents an approximation suitable for most developmental antenna measurements and for pattern testing of operational antennas. The basis for the relationship and the approximations involved in it may be shown by a brief analysis of the optical problem.

Since there is no single criterion on which to base a minimum range, several reasonable requirements may be satisfied. (1) The measured gain should not be more than 5 per cent lower than that which would be obtained under true far-field conditions. With the possibility of a calculated correction this is tolerable in most cases. (2) Relative intensity values should be maintained within 5 per cent. (3) The probe antenna must subtend a small enough angle to render good resolution of the pattern. (4) Errors in phase should not exceed $\pi/4$, in order to approximate Fraunhofer conditions. To facilitate the discussion it will be assumed that the antennas involved are circular and that they have the characteristics of uniformly illuminated apertures.

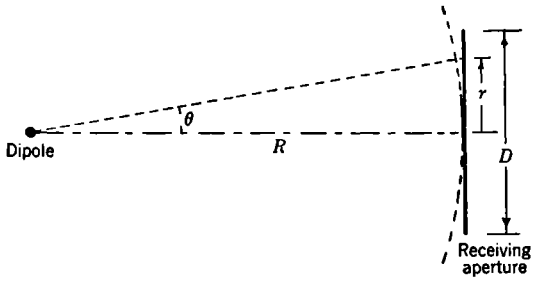

FIG. 15·1.—Dimensions for determining minimum range for pattern measurement.

A simple case in which only phase errors are significant is shown in Fig. 15·1. A small transmitter, such as a dipole, is shown illuminating the large circular aperture of a receiving antenna. The curved dashed line represents a spherical phase contour of the transmitted wave. Construction lines are also included to indicate the magnitude of the resultant phase errors in terms of the system parameters. The phase error ϕ will be a function of the angle off axis, θ,

$$\phi = \frac{2\pi R}{\lambda}(1 - \sec\theta). \tag{2}$$

For small values of θ,

$$\phi \approx \frac{2\pi R}{\lambda}\left[1 - 1 + \frac{1}{2}\left(\frac{r}{R}\right)^2 \cdots\right] = \frac{\pi r^2}{\lambda R}. \tag{3}$$

The phase error at the edge of the aperture is

$$\phi_D = \frac{\pi D_2^2}{4\lambda R}. \tag{4}$$

One effect of a spherical wave front can be seen from the ratio of the power received to that expected in the absence of phase errors,

$$\frac{P_r}{P_e} = \frac{\left|\int r \cos \phi \, dr\right|^2 + \left|\int r \sin \phi \, dr\right|^2}{\left|\int r \, dr\right|^2} \tag{5}$$

$$\frac{P_r}{P_e} \approx 1 - \frac{1}{12}\left(\frac{\pi D_2^2}{4\lambda R}\right)^2. \tag{6}$$

The relationship can be interpreted more easily if the range is expressed in terms of a multiple n of the Fresnel-Fraunhofer boundary range,

$$R = n\left(\frac{D_2^2}{\lambda}\right).$$

If this value is substituted in Eq. (6),

$$\frac{P_r}{P_e} = 1 - \frac{\pi^2}{12 \cdot 16}\left(\frac{1}{n}\right)^2$$

$$= 1 - 0.05\left(\frac{1}{n}\right)^2,$$

$$\frac{P_r}{P_e} = 0.95, \qquad \text{for } n = 1. \tag{7}$$

This reduction in received power is just within the arbitrary 5 per cent tolerance so that the minimum range for this case may be taken as

$$R = \frac{D^2}{\lambda}. \tag{8}$$

The corresponding phase error at the edge of the aperture is found to be

$$\phi_D = \frac{\pi D^2}{4\lambda R} = \frac{\pi}{4}, \tag{9}$$

which corresponds to a distance of $\lambda/8$. This degree of deviation from a plane phase front is the maximum which can safely be neglected.

The expression for the reduction in received power can be interpreted reciprocally to mean that the intensity at a point on the axis of a transmitter of aperture D_2 at a range D_2^2/λ would be down 5 per cent as a result of phase errors caused by the varying path length between different elements of the transmitter aperture and the point on the axis.

Where antennas of comparable size are used at inadequate range, errors would be expected from nonuniform intensity of illumination as well as phase. An expression for the power reduction in such a case is given below, neglecting higher-order terms,

$$\frac{P_r}{P_e} \approx 1 - 0.05\left(\frac{1}{\lambda R}\right)^2 (D_1^4 + 6D_1^2 D_2^2 + D_2^4), \tag{10}$$

where D_1 and D_2 are the aperture diameters. This is an approximate

relationship which applies only where $P_r/P_e > 0.9$. If the ratio P_r/P_e is set equal to 0.95, corresponding to a 5 per cent reduction in received power,

$$R^2 = \frac{1}{\lambda^2}(D_1^4 + 6D_1^2D_2^2 + D_2^4). \tag{11}$$

For the case of equal antenna diameters,

$$D_1 = D_2 = D,$$
$$R^2 = \frac{8D^4}{\lambda^2},$$
$$R = 2.83\left(\frac{D^2}{\lambda}\right). \tag{12}$$

This value for R indicates that the sum of the minimum ranges (D^2/λ) for the two separate antennas is not great enough for the combination, as might have been supposed. In fact even this range is not adequate to satisfy the other requirements that were initially stated. The full angular width β_1 of the main lobe for a uniformly illuminated aperture is $2\lambda/D$, whereas the angle β_2 subtended by the probe antenna is approximately D/R. From Eq. (12)

$$\frac{\beta_1}{\beta_2} = 5.66.$$

Such a ratio of angles results in an additional reduction in peak intensity of about 3 per cent whereas side lobes are reduced about 9 per cent. Moreover, at this range a phase difference of approximately $\pi/3$ can exist between components of the signal from different portions of the transmitter aperture because of path-length differences.

Accordingly, a longer range is necessary and the range given by Eq. (1) is a satisfactory minimum value. The limitations of this rule in two special cases are the following:

Case I. When the maximum antenna diameter for a given range is to be used, the second antenna must be very small and the expression reduces to Eq. (8), $R = D^2/\lambda$. This condition represents a maximum phase error of $\pi/4$ or $\lambda/8$ and a loss of 5 per cent in received power. The effect of the loss can be compensated to some extent by a calculated correction. The same relationship applies for noncircular apertures if D is the greatest linear dimension of the aperture. Although the errors arising from the reduction in power are less, the phase error is the same and determines the limit.

Case II. When $D_1 = D_2 = D$ the minimum range has its greatest value for a given D,

$$R = 4\frac{D^2}{\lambda}.$$

This range results in a reduction of about 2.5 per cent in received power caused by near-field effects. The angle subtended by the probe antenna is about $\frac{1}{8}$ of the full width of the main lobe. Discrepancies in phase among the various contributions from the transmitter aperture do not exceed $\pi/4$.

These approximations based upon uniformly illuminated circular apertures are not greatly changed when practical antennas with tapered illumination patterns are used. The reduction in received power is not so large because the contributions from the extreme edges of the aperture are less important. However, the loss is decreased only by a factor roughly equal to the gain factor. It may be repeated, also, that the expressions derived for power reduction caused by near-field effects are only approximations. They do not apply for reductions exceeding 10 per cent and do not hold where both antennas are small compared to the wavelength.

Having established the requirements upon range it is possible to determine the power and receiver-sensitivity requirements. For a pair of antennas having gains G_1 and G_2 the ratio of power received to power transmitted is given by the expression

$$\frac{P_r}{P_0} = \frac{G_1 G_2 \lambda^2}{(4\pi R)^2}.$$

This expression in terms of antenna area involves the gain factor f since for each antenna

$$G = \frac{4\pi f A}{\lambda^2}.$$

Therefore

$$\frac{P_r}{P_0} = \frac{(f_1 A_1)(f_2 A_2)}{\lambda^2 R^2}.$$

Again, for the purposes of illustration, assume that the antennas are of equal diameter D with an average value of f equal to $\frac{2}{3}$ and apply Eq. (1) for the minimum range,

$$f_1 A_1 = f_2 A_2 = \frac{\pi D^2}{6}$$

$$R = \frac{4D^2}{\lambda},$$

$$\frac{P_r}{P_0} = \frac{\pi^2}{36.16} = 0.0172.$$

In decibels this is

$$\left(\frac{P_r}{P_0}\right) = -17.6.$$

It is of interest to note that this expression is independent of D and λ under the minimum-range conditions. In practice, however, having

chosen the range for a certain measurement path on the basis of the maximum antenna diameter, it is likely that this range will be used with antennas of smaller area as well. For example, a line source with a length equal to the maximum permissable diameter, but with a width equal only to $\frac{1}{100}$ of the length would have an area equal to $\frac{1}{80}$ of the circular-aperture area. This would cause an additional power drop of -19 db. Since these figures apply to the peak sensitivity of the antennas, an additional 30 db would be required to render proper side-lobe detail. Thus a system for general use in testing antenna patterns should have power and receiver sensitivity enough for a 20-db drop in power plus a working range of 50 db, a total of 70 db.

The probe antennas may be of any design suited to the optical requirements. Where small apertures are desired, microwave horns are frequently used. These have the advantage that they are simple in construction and that their characteristics can be calculated without difficulty from their shape. Accurate formulas for such calculations are available. In cases where the length of the tapered section of the horn is made large with respect to the aperture dimensions, a simplified formula may be used for the gain,[1]

$$G = 4\pi \frac{fA}{\lambda^2},$$

where fA is the effective area of the aperture. The quantity f may be treated as a constant fraction of the actual aperture area A for long horns

$$f = \frac{8}{\pi^2}.$$

When coaxial line is used, a dipole or a coaxial probe may be employed as a small probe. A gain of about 3 db is obtained with such probes.

The characteristics of r-f power sources and detectors have been discussed elsewhere in this volume, so that it is possible to choose a suitable combination knowing the length of the transmitter-receiver path and the range of antenna gains to be used. Account must be taken of the additional power reduction which will be caused by padding attenuators. It is apparent that, in general, the sensitivity requirements are great enough to necessitate the use of a modulated source and an a-c receiver amplifier. A bolometer is indicated as the detecting element best suited for general application because of its linear behavior over a wide range of power levels. The response of a bolometer to pulsed power makes the use of an a-c amplifier simpler, whereas a crystal is easily saturated and great care must be taken. Superheterodyne receivers with calibrated attenuators in the r-f circuit are also suitable for these measurements.

[1] S. A. Schelkunoff, *Electromagnetic Waves*, McGraw-Hill, New York, 1943, p. 365.

The mechanical details of antenna mounts for pattern measurements will not be discussed here since this is a special problem depending upon the particular type of measurements to be made. Information about mounts as well as automatic pattern-recording equipment is presented in Vol. 12 dealing with antenna design. The problem of siting an antenna-measurement course is also treated.

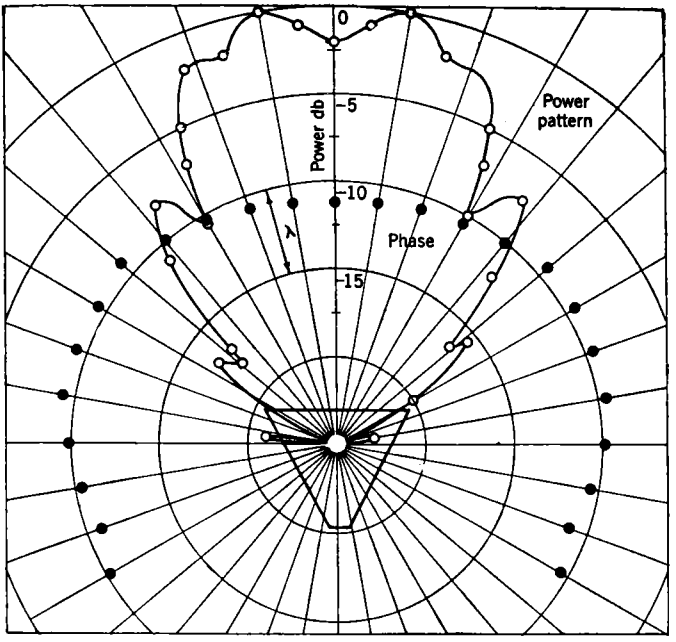

FIG. 15·2.—Radiation pattern of *E*-plane horn showing power pattern, phase front, and center of phase.

The general problem of interference from surrounding objects is met in practice by removing such objects as far as possible and by avoiding illumination of them. The use of poorly reflecting materials in the vicinity of antennas is necessary in some cases and this is best determined by experiment. The need for care in this matter is readily seen. When a receiving antenna is rotated during a pattern measurement, the main lobe may at times be pointed directly at some reflecting object. If the power received is from a −20-db side lobe of the transmitter and is reduced by another 20 db by scattering from the obstacle, it could still produce a serious effect on the measurements, because the directly received power would also be small. If a −20-db side lobe of the receiver were being measured under these conditions the ratio of amplitudes of the direct signal and the scattered signal would be 10.

This would produce a power variation of from $(1.0 + 0.1)^2$ to $(1.0 - 0.1)^2$ or ± 20 per cent. It is apparent, therefore, that particular care must be taken to avoid reflecting obstacles in the plane of rotation of the main lobe.

An example of a pattern measurement is shown in Fig. 15·2. The observations refer to a horn flared in the E-plane with aperture dimensions of 2.49 by 16.42 cm. The horn had a half angle of 30° and was used with waveguide $1\frac{1}{2}$ by 3 inches OD. The observations were made at a wavelength of 10 cm. The pattern is plotted in decibels down from the power at 0°. The oscillations in the pattern arise from the fact that the phase is not uniform over the mouth of the horn. The phase pattern is also shown on the figure, and the center of phase is indicated by the shape of the horn sketched in. The manner of observing the phase is described in Sec. 15·8.

15·3. The Measurement of Antenna Gain.—The gain of an antenna is a quantity of great practical interest. It is determined by methods

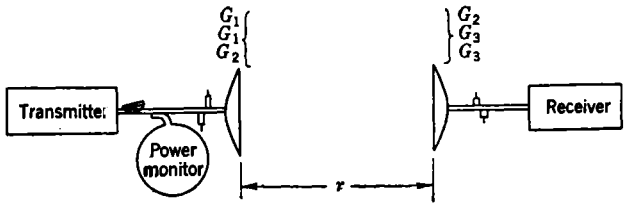

FIG. 15·3.—Measurement of gain by the three-antenna method.

which are essentially applications of power-measuring techniques, but these methods are sufficiently specialized as to merit some discussion. In practice, gain is usually measured with reference to a standard horn or to a parabolic antenna. A simple measurement of the ratio of the power received by the experimental antenna to that received by the standard gives the ratio of their respective gains. It is in the calibration of such gain standards and the measurement of other special antennas that the following techniques are employed.

The gain of an antenna may be measured by determining the fraction of power it receives from a transmitter at a known distance, provided the gain of the transmitting antenna is taken into account. In effect this is done by substituting a third antenna for each of the original pair in turn. Repetition of the experiment for each combination yields three expressions from which the three unknown gains can be evaluated.

The experimental setup is illustrated in Fig. 15·3. The transmitter consists of a stable c-w source, square-wave-modulated at an audio frequency. This source is loosely coupled to the line through a padding attenuator. In the waveguide line is a coupling for a power monitor and

for a matching device, if one is needed to match the particular antenna in use. Behind the receiving antenna is another matching device and the receiver consisting of a bolometer and an a-f amplifier. Three combinations of horns are represented according to their gains: $G_1 - G_2$, $G_1 - G_3$, and $G_2 - G_3$. Conditions governing the range of separation r have already been discussed.

The measurements of transmitted and received power are most conveniently made with the same bolometer. The transmitter power may be measured by attaching the bolometer to the transmitter line in place of the antenna. Sufficient padding attenuation must be used to prevent reaction on the oscillator because of the change of load.

In examining the optics of the system it will be convenient to refer to an effective absorbing cross section A' of the antenna, which is the area of a uniformly illuminated aperture having the same gain. Thus

$$G = \frac{4\pi A'}{\lambda^2}. \tag{13}$$

If the transmitted power is P_0, the power received with the first combination of horns is P_{12},

$$P_{12} = P_0 G_1 \left(\frac{A_2'}{4\pi r^2}\right). \tag{14}$$

But

$$A_2' = \frac{G_2 \lambda^2}{4\pi},$$

and hence

$$P_{12} = P_0 G_1 G_2 \left(\frac{\lambda}{4\pi r}\right)^2. \tag{15}$$

Accordingly, for the three combinations,

$$\left.\begin{aligned} G_1 G_2 &= \left(\frac{4\pi r}{\lambda}\right)^2 \frac{P_{12}}{P_0} \\ G_1 G_3 &= \left(\frac{4\pi r}{\lambda}\right)^2 \frac{P_{13}}{P_0} \\ G_2 G_3 &= \left(\frac{4\pi r}{\lambda}\right)^2 \frac{P_{23}}{P_0} \end{aligned}\right\}. \tag{16}$$

From these equations the value of gain for each antenna can be found, as for example,

$$G_1 = \frac{4\pi r}{\lambda} \sqrt{\frac{P_{12} P_{13}}{P_{23} P_0}}. \tag{17}$$

It has been assumed above that the value of P_0 was the same throughout the experiment.

For some purposes adequate results can be obtained by a simplified form of the three-antenna method. If two horns or parabolic antennas of identical mechanical construction are used, it may be assumed that their gains are equal,

$$G_1 = G_2 = G.$$

In this case the expression for received power is given by the expression

$$P_r = P_0 \left(\frac{G\lambda}{4\pi r}\right)^2,$$

whence,

$$G = \left(\frac{4\pi r}{\lambda}\right)\sqrt{\frac{P_r}{P_0}}.$$

If the two antennas are checked for equal gain by the use of a third transmitting antenna, the experiment becomes practically the same as the three-antenna method.

15·4. Effect of Antenna Scattering in Gain Measurements.—Thus far the effect of antenna scattering has not been considered. The amount of scattered power reaching the receiver in the above experiments is, in fact, almost negligible at a reasonable distance of separation. This might be expected since the radiation involved has been scattered twice, transversing the course r three times before reaching the receiver. An approximate evaluation of the effect is easily made.

To aid in the analysis it will be convenient to assign to the antenna an effective scattering cross section A''. This area is a fraction of the total area A corresponding to that fraction of the intercepted power that is scattered. Considering that the gain factor of an average antenna is approximately $\frac{2}{3}$, or $A'/A = G/G_0 = \frac{2}{3}$, it is reasonable to assume

$$A'' = \frac{A'}{2}.$$

This value has been experimentally corroborated by measurements using the mirror method to be described in the next section. With this scattered radiation, a certain pattern and a certain gain must be associated. No definite relationship between receiving gain and scattering gain can be stated, but for purposes of illustration a value of

$$G'' = \frac{G}{2}$$

will be assumed. Accordingly, the power initially scattered is

$$P_s = P_0 G \frac{A''}{4\pi r^2}.$$

Some of this radiation reaches the transmitter to be scattered a second time,

$$P_s' = P_s G'' \frac{A''}{4\pi r^2}.$$

Finally a portion of the power reaches the receiver,

$$P_s'' = P_s' G'' \frac{A'}{4\pi r^2}.$$

The ratio of scattered power received to direct power received may be expressed in terms of G,

$$P_s'' = P_0 G \left(\frac{A''}{4\pi r^2}\right) G'' \left(\frac{A''}{4\pi r^2}\right) G'' \left(\frac{A'}{4\pi r^2}\right),$$

$$P_s'' = P_0 \left(\frac{G''\lambda}{4\pi r}\right)^4 \left(\frac{G\lambda}{4\pi r}\right)^2,$$

$$P_s'' = \frac{1}{16} P_0 \left(\frac{G\lambda}{4\pi r}\right)^6.$$

But

$$P_r = P_0 \left(\frac{G\lambda}{4\pi r}\right)^2;$$

therefore,

$$P_s'' = \frac{1}{16} \frac{P_r^3}{P_0^2},$$

or

$$\frac{P_s''}{P_r} = \left(\frac{1}{4} \frac{P_r}{P_0}\right)^2.$$

To reduce this expression to definite terms another condition may be assumed. If a fixed relationship between the antenna diameter D and the separation r be maintained, it can be seen that the above ratio depends principally upon this relationship for a given type of antenna. For example let us try

$$r = \frac{nD^2}{\lambda}.$$

The received power is

$$P_r = P_0 G \frac{A'}{4\pi r^2},$$

or

$$\frac{P_r}{P_0} = \left(\frac{A'}{\lambda r}\right)^2.$$

Since

$$A' = \frac{2}{3} A = \frac{2}{3}\left(\frac{\pi D^2}{4}\right),$$

$$\frac{P_r}{P_0} = \left(\frac{\pi}{6} \frac{D^2}{\lambda r}\right)^2 = \left(\frac{\pi}{6n}\right)^2,$$

and

$$\frac{P_e''}{P_r} = \left(\frac{1}{4}\frac{P_r}{P_0}\right)^2 = \left(\frac{\pi}{12n}\right)^4.$$

In terms of the corresponding signal amplitudes,

$$\frac{E_e''}{E_r} = \left(\frac{\pi}{12n}\right)^2.$$

For $n = 4$,

$$\frac{E_e''}{E_r} = 0.004.$$

This corresponds to a negligible error of ± 0.04 db in the gain determination. With some antenna designs, however, the scattering may be appreciable. Moreover this error can be eliminated if necessary by measuring the maximum value of power, as r is varied. Since scattered power travels a distance $2r$ farther than the directly received power, the in-phase and out-of-phase conditions of E_e'' and E_r will occur at quarter-wavelength intervals of r.

15·5. The Mirror Method of Gain Determination.—A technique for gain determination involving more convenient measurements is the mirror method.[1] By reflecting the transmitted power from a large, plane mirror it is possible to use a single antenna as transmitter and receiver. The ratio of transmitted to received power can then be determined by means of standing-wave measurements in the waveguide. The antenna and its image in the mirror form a system analogous to that in the two-antenna method.

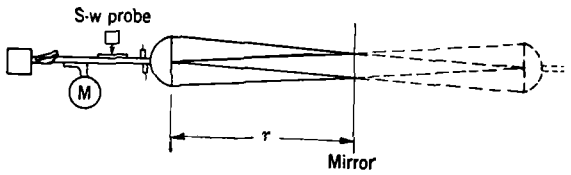

FIG. 15·4.—Mirror method for gain determination.

Figure 15·4 illustrates the apparatus required. The oscillator may provide either straight c-w power or square-wave-modulated power depending upon the power level available. A padding attenuator providing considerable decoupling (15 db) is used to prevent reaction of the reflected wave upon the oscillator. Included in the line also are a coupling for a wavemeter, a standing-wave probe, and a matching device for the antenna. The mirror is a first-surface reflector, flat in terms of the wavelength involved and placed normal to the axis of the disk or

[1] E. M. Purcell, "A Method for Measuring the Absolute Gain of Microwave Antennas," RL Report 168, No. Jan. 3, 1943.

horn. The size of the mirror should be sufficient to subtend an angle at the antenna which will include all side lobes of appreciable magnitude. Ideally the mirror need only include the main lobe, but to avoid appreciable currents at the boundary of the surface and to permit diversified use of the system it is preferable to have a mirror about ten times the antenna diameter. The requirement of flatness is of importance only in the region of the main lobe. The use of separations beyond the minimum value is limited by the sensitivity of standing-wave measurements.

The expression for power received by direct reflection is of familiar form,

$$P_1 = P_0 G \frac{A'}{4\pi(2r)^2},$$

$$P_1 = P_0 \left(\frac{G\lambda}{8\pi r}\right)^2.$$

If it is assumed again that

$$A' = \frac{2}{3} A = \frac{2}{3} \frac{\pi D^2}{4}$$

and

$$r = \frac{nD^2}{\lambda},$$

the power ratio may be written

$$\frac{P_1}{P_0} = \left(\frac{\pi}{12n}\right)^2.$$

For $n = 2$,

$$\frac{P_1}{P_0} = \left(\frac{\pi}{24}\right)^2.$$

The corresponding amplitude ratio is

$$\frac{E_1}{E_0} = \left(\frac{\pi}{24}\right) = 0.13.$$

The voltage standing-wave ratio is

$$\frac{E_0 + E_1}{E_0 - E_1} = 1.3,$$

which is easily measured accurately.

Scattered power in this experiment is much more serious than in the previous ones. In this case the scattering takes place only once, returning to the mirror and back again into the receiver. With the same assumptions as before, this effect may be examined. The power scattered after the first reflection is given by the expression

$$P_2 = P_0 G \frac{A''}{4\pi(2r)^2}.$$

The portion of this radiation reaching the receiver is

$$P_3 = P_2 G'' \frac{A'}{4\pi(2r)^2}$$
$$= \frac{1}{4} G P_1 \frac{A'}{4\pi(2r)^2}$$
$$= \frac{1}{4} \frac{P_1^2}{P_0}.$$

Thus

$$\frac{P_3}{P_1} = \frac{1}{4}\frac{P_1}{P_0},$$
$$\frac{E_3}{E_1} = \frac{1}{2}\frac{E_1}{E_0} = \frac{\pi}{24n}$$

or, if $r = 2D^2/\lambda$,

$$\frac{E_3}{E_1} = 0.065.$$

Since this amount of scattered radiation is not negligible, it is necessary to eliminate its effect by suitable experimental procedure. It is desirable to match the antenna into space as well as possible.

Since the path traversed by E_3 is greater than that traversed by E_1 by a distance of $2r$, it is possible to change the relative phase of the two signals by varying r. Therefore a position is sought which produces an in-phase relationship between E_1 and E_3, corresponding to a maximum VSWR.

$$R_1 = \frac{1 + E_1 + E_3}{1 - E_1 - E_3},$$

where the transmitter amplitude is taken as unity. A change of $\lambda/4$ in the length of r will give an out-of-phase condition of E_1 and E_3 and a minimum VSWR,

$$R_2 = \frac{1 + E_1 - E_2}{1 - E_1 + E_2}.$$

The value of E_1 can then be found in terms of R_1 and R_2,

$$E_1 = \frac{1}{2}\left(\frac{R_1 - 1}{R_1 + 1}\right) + \frac{1}{2}\left(\frac{R_2 - 1}{R_2 + 1}\right).$$

But

$$G = \frac{8\pi r}{\lambda} E_1,$$

therefore

$$G = \frac{4\pi r}{\lambda}\left(\frac{R_1 - 1}{R_1 + 1} + \frac{R_2 - 1}{R_2 + 1}\right).$$

This is the expression for the gain in terms of measured quantities under the condition that antenna mismatch is negligibly small. If for any reason the mismatch is not tuned out to a sufficient degree, it will be

necessary to make use of the information given by the minimum positions of each of the above standing-wave ratios, R_1 and R_2, to eliminate the mismatch amplitude from the calculations.

15·6. Gain Determination by Pattern Integration.—For practical purposes the definition of gain is somewhat loosely interpreted. Optically it is the ratio of the peak intensity of the pattern to the average or isotropic intensity of all the power *radiated.* In an actual antenna it is usually taken as the ratio of the peak intensity to the intensity that would exist if all power *incident* in the transmission line to the antenna were isotropically distributed. This effective gain is the quantity of practical interest in calculations of system performance and is the quantity determined in any method of direct measurement.

To determine the gain in the optical sense it is necessary to resort to integration of the radiation pattern. The accuracy of integration methods is not particularly high because of the inadequacy of detailed information concerning the pattern and the inaccuracy of techniques for graphical integration. For a rectangular aperture illuminated by a line source, reasonably good results can be obtained from only two patterns, one in the E-plane and the other in the H-plane, through the peak of the main lobe. This requires that it be possible to express the complete pattern as a product of two independent functions involving the two spherical angular coordinates.

$$I(\theta,\phi) = g(\theta) \cdot f(\phi).$$

For each plane the unidimensional gain of the pattern can be determined

$$\left[G_0 = \frac{I_{\max} \int_{-\pi}^{\pi} d\theta}{\int_{-\pi}^{\pi} g(\theta) f(\phi)\, d\theta} \right]_{\phi=0},$$

or

$$G_\theta = \frac{2\pi I_{\max}}{f(\phi = 0) \int_{-\pi}^{\pi} g(\theta)\, d\theta},$$

and

$$G_\phi = \frac{2\pi I_{\max}}{g\left(\theta = \frac{\pi}{2}\right) \int_{-\pi}^{\pi} f(\phi)\, d\phi}.$$

The value of the integrals may be obtained by graphical integration of the pattern plotted in rectangular coordinates as intensity vs. angle. The combination of these values to give the two-dimensional gain requires that the pattern be narrow in one plane so that all the power is concentrated within an angular range such that

$$\sin \theta \approx 1.$$

In this case the gain becomes

$$G_{\theta,\phi} = \frac{G_\theta G_\phi}{\pi}.$$

The usefulness of a gain value of this kind is limited. It is of some interest in studies of the optical characteristics of various types of aperture illumination. It also affords a means of evaluating losses in the antenna system caused by dissipation and leakage. The ratio of the measured gain to the integrated gain would ideally show the degree of attenuation of power.

15·7. R-f Phase Measurements.—The measurement of phase in microwave radiation fields is of principal importance in the development of microwave antenna components. Since certain phase conditions must be maintained for efficient performance, it is desirable in many cases to determine directly that the various elements of an antenna system have the proper characteristics. The measurements are, therefore, chiefly concerned with the determination of contours of constant phase, the location of centers of phase, and the examination of effects due to objects in the field.

In the several methods to be discussed the basic principle is the same. A sample of radiation picked up in the antenna field is compared in phase with a reference signal which comes directly from the source. Some means is provided for varying the phase of one signal with respect to the other so as to produce a recognizable interference condition between them, such as a minimum or maximum. The various types of apparatus differ in the means employed for this purpose, in their applicability to particular problems, and in ease of operation. A simple, versatile form of phase apparatus is one in which the pickup probe is connected by means of a coaxial cable to a mixer wherein the reference signal from the source is also present. The flexible cable permits the probe to be moved freely about in the antenna field, and allows the tracing of contours and the adjustment of the relative phase of the two signals to the reference condition.

Such an apparatus is shown in Fig. 15·5. Power from a square-wave-modulated oscillator is introduced into a waveguide section and radiated from the experimental antenna, shown as a horn. A sample of this radiation picked up by the probe is led back by cable to the mixer guide. In this same guide is a signal which is tapped off by a directional coupler from the transmitter line. The two signals interfere at the crystal detector terminating the section. The crystal output signal is amplified and indicated on a meter. By moving the probe back and forth along the line of propagation it is possible to find the position of an interference minimum.

The pickup probe is represented as a dipole terminating the coaxial line. It is supported by a mount attached well back from the dipole and made of a poorly reflecting material. To the base of the mount a marker may be attached directly below the dipole to permit direct plotting of the minimum position. A series of such points made by following a chosen minimum will give a detailed plot of the constant-phase contour. The location of the center of phase with respect to the horn aperture can then be found from the plot. The dipole is mounted so as to permit orientation about the longitudinal axis according to the polarization employed.

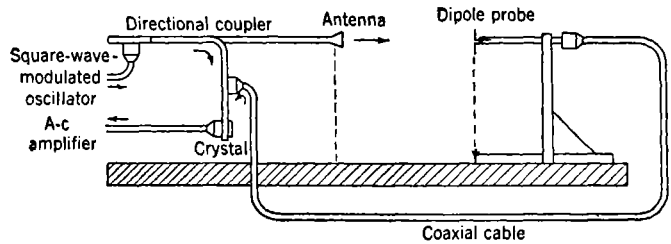

FIG. 15·5.—Simple phase apparatus.

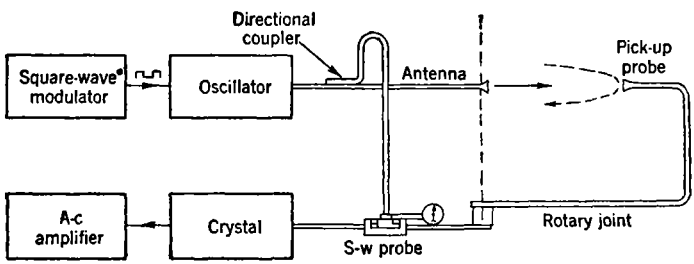

FIG. 15·6.—Phase apparatus in a waveguide system for circular phase contours.

15·8. Phase Apparatus for Point Sources.—If waveguide is used instead of coaxial cable, a different system is preferred in which it is not necessary to move the pickup itself in order to establish the reference condition of interference between the two signals. Instead, provision is made for adjusting the phase of the reference signal. This is conveniently done by using a standing-wave probe to introduce the reference signal into the mixer line. An arrangement of this type for studying circular phase contours is shown in Fig. 15·6. The pickup probe in this case is a small waveguide horn attached to a rotary joint so that it can be moved freely in a circular path. It is centered so that the experimental horn is approximately on the axis of rotation and the circular path corresponds fairly well with the circular contours to be studied.

In this apparatus the source is shown as a c-w oscillator modulated

by a square wave of audio frequency. Sufficient padding attenuation is used to eliminate the need for careful matching of experimental antennas. The reference signal is tapped off by means of a directional coupler with good directivity in order to prevent reflections from the antenna line from entering the reference line to disturb the phase and amplitude of that signal. A loop of waveguide leads from the coupler to the sliding probe. Its length and design are chosen to permit uninhibited movement of the probe through a distance of λ_g, or greater. With the sliding probe the reference signal is introduced into the mixer line. The coupling is nondirective with the ordinary probe and power is sent toward the field probe as well as toward the mixer. Consequently, it is necessary that the pickup probe and the rotary joint be well matched. The mixer itself may be either a crystal or bolometer connected to an a-c amplifier.

The matching required in the mixer line is not difficult to achieve and can be readily checked in the following way. With only the reference signal present in the mixer line, any reflected power from the pickup probe or rotary joint will produce an interference with the portion of the signal reaching the mixer directly. The interference will pass through a cycle with a displacement of the sliding probe equal to $\frac{1}{2}\lambda_g$. To avoid such mismatches, a properly designed horn and rotary joint should be used or a tuner should be incorporated in the line. The rotary joint in addition to being well matched should have a phase length that is independent of rotational angle. A well-designed joint employing a circularly symmetrical mode affords this characteristic.

In operation, the procedure with this apparatus is to measure the deviations of the minimum from the fixed circle described by the probe. At the initial point the position of the sliding probe is indicated on a scale or dial indicator. Variations in the phase ϕ of the probe signal are compensated by a measured displacement S of the sliding probe. In terms of the shift the phase change is

$$\Delta\phi = \frac{2\pi}{\lambda_g}\Delta S.$$

The results of these measurements may be plotted to give a constant-phase contour for the antenna. An example of such measurements is illustrated in Fig. 15·2 of Sec. 15·2.

15·9. Frequency Sensitivity of Phase.—Frequency sensitivity affecting phase is a problem to be dealt with in all two-channel systems of this type. It is desirable that the change in phase with frequency be identical in the two paths between their common points regardless of the variety of conductors making up the circuit. Usually the reference path will be corrected to suit the length of the probe signal path. The wavelength

in the air-gap is λ_0; the wavelength in the coaxial cable is $\lambda_0/\sqrt{k_e}$, where k_e is the relative dielectric constant of the cable. Thus if the two lines have lengths of waveguide, coaxial cable, and air gap corresponding to l_g, l_c, and l_0 and l'_g, l'_c, l'_0, respectively, it is desired to choose the value of l_g to satisfy the condition of equal phase shift with a change in frequency. The required length is given by the expression

$$l_g = l'_g + \frac{\lambda_0}{\lambda_g}(l'_c\sqrt{k_e} + l'_0 - l_c\sqrt{k_e} - l_0)$$

where λ_0 and λ_g are respectively the free-space wavelength and guide wavelength for the design frequency.

The compensating length of waveguide may conveniently be used as the flexible loop leading to the sliding probe. The accuracy of the correction can, of course, be checked directly by changing the frequency and noting whether a corresponding shift in the minimum position occurs.

15·10. Phase Apparatus for Line Sources.—The type of phase apparatus used for line sources may be the same in principle as that used for point sources. When waveguide is used, it is merely necessary to provide an additional rotary joint to permit straight-line motion of the probe. Two rotary joints suffice if the field probe is of a coaxial type with circular

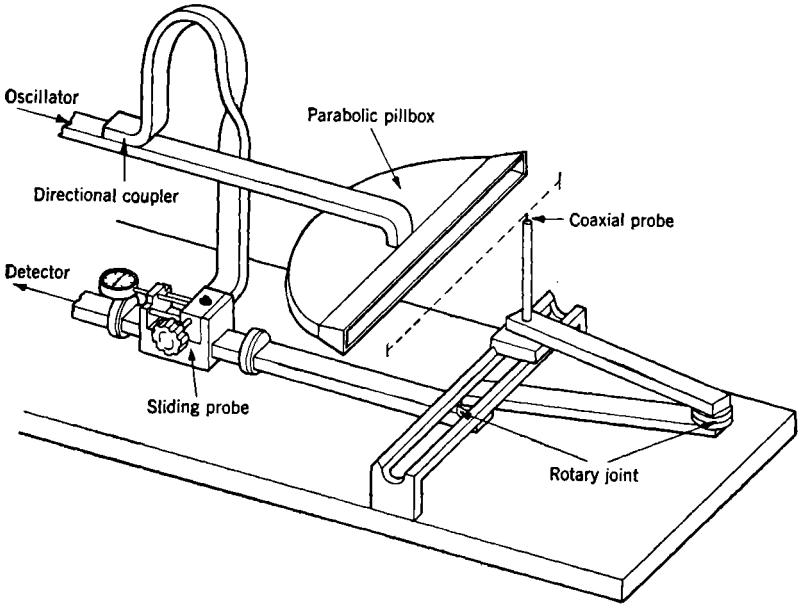

FIG. 15·7.—Phase apparatus suitable for linear phase contours.

phase symmetry. If a waveguide horn is used as a probe, a third rotary joint is required to permit orientation of the probe with respect to the wavefront.

An arrangement of components for use with the coaxial probe is shown in Fig. 15·7. The antenna is shown as a parabolic pillbox which is used as a line source for a reflector. The probe is located a short distance from the mouth of the pillbox and is articulated so as to move in a straight line parallel with it. To facilitate manipulation of the apparatus the probe is mounted on a track such as an optical bench. The track itself is well below the plane of the pillbox to minimize the disturbance of the field. The phase-measuring part of the system is identical with the previous model and is subject to the same conditions.

The plotting of wavefronts is also done in a similar manner, except that the variations in phase are measured with respect to the straight line. It should be remarked that for a center-fed parabola the phase contours will not be straight lines. The diffraction pattern due to the presence of the antenna feed, the superimposed pattern of the back wave from the feed and the fact that the probe is in the near field of the parabola combine to cause a wavy contour. The irregularities may be of the order of $\pm \frac{1}{8}\lambda$ and are largest at the center. With other types of line sources more nearly linear phase fronts would be observed.

15·11. Phase-modulation Method.—By employing phase modulation[1] of the reference signal it is possible to provide direct indication of phase on an oscilloscope. Either the position of a sinusoidal trace on the screen or the shape of a Lissajous figure serves to show instantaneously the phase of the field-probe signal at any point in the field. To determine the existence of a geometrically regular contour of constant phase it is simply necessary to traverse the desired curve with the probe. Deviations of the phase front from this line are indicated at once by a shift in the oscilloscope figure and without the need of detailed measurements. The centering of the antenna may readily be adjusted until the phase contour corresponds with the probe path.

In this method continuous phase modulation of the reference signal replaces the manual phase shift employed in the previous methods described. Instead of being adjusted to give an interference minimum or maximum, the phase is swept through the full cycle of interference, producing a sinusoidal interference signal of audio frequency. The position at which the minimum occurs within the modulation cycle indicates the relative phases of the two signals.

Linear modulation of phase at a suitable frequency for a-c amplification is the essential requirement of this method and it may be produced

[1] H. R. Worthington, "Measurements of Phase in Microwave Antenna Fields by Phase Modulation Methods," RL Report, No. 966, Mar. 14, 1946.

by many different means. The means thus far used has been the one requiring no special components. It involves frequency modulation in conjunction with a very long waveguide line in the reference-signal channel. A small change of frequency with a correspondingly small change in λ_g becomes sufficient to produce a full cycle of phase change when one line is many hundreds of wavelengths longer than the other.

To illustrate the principle, the simplest form of this apparatus is shown in bare outline in Fig. 15·8. Practical features such as rotary

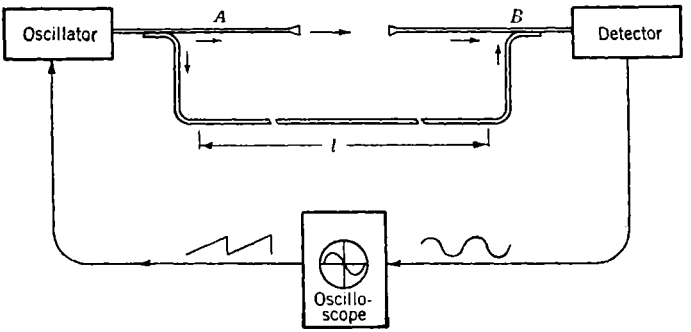

FIG. 15·8.—Phase-modulation system for phase determination.

joints have been omitted. The oscillator tube on the left is modulated by a sawtooth voltage from the oscilloscope sweep. The output power is frequency-modulated but of effectively constant amplitude. The power is divided into two channels at point A. One of these paths contains the antenna and pickup probe, the other the long waveguide line. The two channels rejoin at point B delivering both signals to the mixer. From the mixer an a-c voltage is obtained which is amplified and applied to the vertical plates of the cathode-ray tube.

The relative phase shift of the two signals is determined by the difference in length of the two paths. In previous systems the requirements for zero relative phase shift with frequency have been discussed. By taking the derivative of the phase change through the long line with respect to frequency a relationship is obtained for the change in phase for a given fractional change in frequency,

$$\Delta\phi = 2\pi l \left(\frac{\lambda_g}{\lambda_0^2}\right) \frac{\Delta f}{f},$$

where λ_g and λ_0 are the guide wavelength and free-space wavelength of the nominal frequency. The ratio is treated as a constant for standard guide within a particular frequency band.

Thus for a phase shift of 2π and a frequency change of 0.1 per cent

at 1.25 cm, the required length becomes

$$l = 1000\left(\frac{\lambda_0}{\lambda_g}\right)^2 \lambda_g,$$
$$= 660\lambda_g.$$

This is a considerable length but at 1.25 cm it is practical. The range of frequency modulation is easily obtained without causing appreciable amplitude modulation of the signal. It is important to avoid amplitude modulation since all alternating current at the crystal should be caused by interference only.

With an effectively continuous phase modulation taking place, the two signals arriving at the detector vary constantly and linearly in relative phase. The resultant power level is of the form

$$p = e_s^2 + e_r^2 + 2e_s e_r \cos \phi,$$

where e_s and e_r are the probe-signal and reference-signal amplitudes, respectively. Thus with a square-law detector the a-c component of output voltage is sinusoidal,

$$v \approx \cos \phi.$$

The phase angle is a function of the initial phase at the start of the modulation cycle and of $\Delta\phi$ as previously defined,

$$\phi = \phi_0 + \Delta\phi$$
$$= \phi_0 + 2\pi ft.$$

The choice of the modulation frequency f is governed by the requirements of sawtooth modulation and a-c amplification.

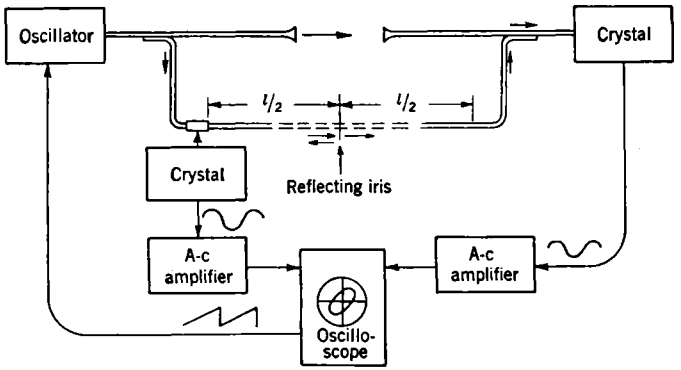

FIG. 15·9.—Phase-modulation system with frequency-drift compensation.

It will be noted that the system as it stands is sensitive to frequency drift. This can be taken into account in the measuring procedure by monitoring with a wavemeter. If the power passing through a high-Q

transmission wavemeter is applied to the vertical CRT plates through a second pair of input terminals to the amplifier, a sharp pip is obtained which can be used as a reference point on the sweep. The position of the phase signal with respect to this pip does not depend upon frequency.

A refinement of the above system can be made whereby inherent insensitivity to frequency is obtained and a Lissajous figure is provided as a very sensitive indicator of the "in-phase" condition for the two signals. Figure 15·9 shows the modifications involved. A standing-wave probe is inserted at the beginning of the long line and a diaphragm producing a partial reflection of power is introduced half-way down the line, a distance of $l/2$ beyond the probe. This arrangement gives rise to two signals at the probe which have the same path difference as the original interfering signals. Their frequency behavior will be identical with that of the other pair so that an a-c reference signal is obtained. The relative phase of the two signals is independent of frequency and varies directly as the phase of the r-f field signal. By moving the standing-wave probe it is possible to compensate for a shift in the field-signal phase quickly and accurately. The phase shift so compensated is measured in terms of the probe displacement.

$$\Delta\phi_0 = \frac{\pi\Delta s}{\lambda_g},$$

where Δs is the probe displacement.

This type of oscilloscope figure does not indicate directly the magnitude of phase shift as does the sine-wave figure, but it is extremely sensitive when a straight line is used for the reference condition. Accuracy of about $\pm 1.5°$ is provided in the measurement of phase over several cycles. Small deviations can be measured even more accurately. The sensitive, instantaneous indication is particularly useful in examining the effects of objects placed in the antenna field, for example, in locating flanges or baffles to take care of the back lobe from a feed horn.

For greater convenience in operation and electrical alignment of the apparatus itself a mechanical phase-modulating device can profitably be used to replace the frequency modulation and long-line system. At microwave frequencies lower than 24,000 Mc/sec this is particularly true.

APPENDIX A

MANUFACTURERS OF MICROWAVE EQUIPMENT

The sources of supply of most of the microwave equipment that was developed and used during the war are not well known to the public at large; nearly all of the equipment was made under military security regulations. In an effort to facilitate the procurement of measuring equipment the following list of manufacturers is presented. No attempt has been made to make the listing complete, and the omission of a company or item is not intended to imply anything concerning the nature of the product. The listing comprises some of the companies who supplied microwave equipment to the Radiation Laboratory during the war. It is not known whether this equipment will be manufactured or can be obtained from these sources in the future. The numbers in the right-hand column refer to the manufacturers' names listed on pages 925, 926, and 927.

1. *R-f Cables and Connectors*		Manufacturer
RG-5/U	Nonlossy, small-diameter cable	18 to 24
RG-9/U	Nonlossy, large-diameter cable	18 to 22, 24
RG-21/U	Lossy cable	18 to 20, 24
UG-18/U	Type N plug for RG-5/U and RG-21/U	34 to 38
UG-19/U	Type N jack for RG-5/U and RG-21/U	34 to 38
UG-24/U	Type N plug for RG-9/U	34 to 38
UG-25/U	Type N jack for RG-9/U	34 to 38

2. *Waveguide and Rigid Coaxial Line and Connectors*		
RG-44/U	10-cm-band stub-supported $\frac{7}{8}$" OD coaxial line	36
RG-48/U	$1\frac{1}{2}$- by 3- by 0.080-in. 10-cm-band waveguide	31 to 33
RG-52/U	$\frac{1}{2}$- by 1- by 0.050-in. 3-cm-band waveguide	31 to 33
RG-53/U	$\frac{1}{2}$- by $\frac{1}{4}$- by 0.040-in. 1-cm-band waveguide	31 to 33

CG-163/U	1-cm-band flexible waveguide	17
CG-164/U	3-cm-band flexible waveguide	17
CG-170/U	10-cm-band flexible waveguide	17
UG-45/U male, UG-46/U female	Connectors for RG-44/U	28, 29
UG-53/U cover, UG-54/U choke	Connectors for RG-48/U	41
UG-39/U cover, UG-40/U choke	Connectors for RG-52/U	41
UG-116/U cover, UG-117/U choke	Pressurized connectors for RG-53/U	41
Nonpressurized connectors for RG-53/U		30
Electroformed bends for 1-cm-band waveguide		46
Electroformed bends for 3-cm-band waveguide		46
Adaptor from waveguide coaxial line		45

3. *Amplifiers and Power Supplies*

Audio-frequency, narrow band	1, 5
20 and 40 Mc/sec, narrow band	9
30 Mc/sec, 2 to 3 Mc/sec wide	11
Power supplies with square-wave modulators for low power oscillators	4
Klystron power supplies	27
Signal generators	14

4. *Crystal Rectifiers*

1N21	10-cm band	9, 25
1N23	3-cm band	9, 25
1N26	1-cm band	9, 25

5. *Oscillator Tubes*

2K25 (type 723)	3-cm band	25, 26
2K28 (type 707)	10-cm band	9, 25, 26
2K33	1-cm band	26
419B	3-cm band	27
411	10-cm band	27
410R	10-cm band	27
417 and 2K41	10-cm band	27

6. *Power Measurements*

Thermistor bridges		9, 16
Bead Thermistors		
D-168527	3-cm band	25
D-163903	10-cm band	25

D-170575 1-cm band	25
Thermistor Mounts	
1-cm band	4
3-cm band	8, 15
10-cm band	16
7. *Attenuators*	
1-cm band	1, 2
3-cm band	2, 10, 6
10-cm band	2, 3
8. *Spectrum Analyzers*	9, 47
9. *R-f Components*	
1-cm components	
Crystal holder	1
Directional coupler	1
Termination	46
Slotted section	1
Squeeze section	1
Supports for waveguide	40
3-cm components	
Slotted section	8, 10, 13
Crystal mount	10
Tuner	10
2K25 tube mount	10
Termination	10
Plunger	10
Impedance bridges	14
10-cm components*	
Slotted section and probe	3, 7, 8, 43*
Wavemeter coupler	3, 7
Termination	2, 3, 28*, 42*
Mixer	44
2K28 oscillator-tube cavity	3
10. *Wavemeters*	
1-cm band	1, 15, 43
3-cm band	12, 6, 39
10-cm band	6

MANUFACTURERS

1. Humble Oil and Refining Co., Houston 5, Tex.
2. PIB Products Inc., 66 Court St., Brooklyn 2, N. Y.

* The items marked with an asterisk are in waveguide, the other 10-cm components are in coaxial line.

3. Diamond Instrument Co., Wakefield, Mass.
4. Browning Laboratories, Winchester, Mass.
5. Electronics Corp. of America, 45 West 18th St., N. Y. C., N. Y.
6. Maguire Industries, 342 W. Putnam Ave., Greenwich, Conn.
7. Nat'l. Silver Deposit Ware Co., 44 W. 18th St., N. Y. C., N. Y.
8. F-R Machine Works, 44-26 Purvis St., Long Island City, N. Y.
9. Sylvania Electric Co., 1221 W. 3rd St., P.O. Box 750, Williamsport, Pa.
10. Graham Mfg. Co., East Greenwich, R. I.
11. Harvey Radio, Cambridge, Mass.
12. Electric Corp., 150 Middle St., Pawtucket, R. I.
13. Yale and Towne Mfg. Co., Stamford Div., Stamford, Conn.
14. Boonton Radio Corp., Boonton, N. J.
15. Kannenstine Laboratories, 1922 W. Grey St., Houston, Tex.
16. Cover Dual Signal Systems, Inc., Div. of Electra Voice Corp., 5215 N. Ravenswood Ave., Chicago, Ill.
17. American Hose Branch of American Brass Co., Waterbury, Conn.
18. American Phenolic Corp., 1830 South 54th Ave., Chicago, Ill.
19. Anaconda Wire and Cable Co., 49 Federal St., Boston, Mass.
20. Federal Tel. and Radio Corp., 320 Orange St., Newark, N. J.
21. General Electric Co., 1 River Rd., Schenectady, N. Y.
22. Okonite Co., 1100 Statler Office Bldg., Boston, Mass.
23. Phelps Dodge Co., 143 Sidney St., Cambridge, Mass.
24. Simplex Wire and Cable Co., 79 Sidney St., Cambridge, Mass.
25. Western Electric Co., 120 Broadway, N. Y. C., N. Y.
26. Raytheon Mfg. Co., Foundry Ave., Waltham, Mass.
27. Sperry Gyroscope Co., Garden City, L. I., N. Y.
28. Lambert Meter Co., 715 W. Front St., Plainfield, N. J.
29. J. C. Rhodes Co., New Bedford, Mass.
30. Henry L. Crowley Co., 1 Central Ave., West Orange, N. J.
31. Chase Brass Co., Waterbury, Conn.
32. American Brass Co., Waterbury, Conn.
33. Revere Brass and Copper Co., 140 Federal St., Boston, Mass.
34. Mendelsohn Speedgun Co., 457-461 Bloomfield Ave., Bloomfield, N. J.
35. Astatic Co., 830 Market St., Youngstown, Ohio.
36. Selectar Mfg. Co., 21-10 49th Ave, Long Island, N. Y.
37. Ucinite Corp., 458 Watertown St., Newtonville, Mass.
38. M. Joseph Sewing Co., 5287 Washington St., West Roxbury, Mass.
39. Texas Co., Houston, Tex.
40. Central Scientific Co., 79 Amherst St., Cambridge, Mass.
41. Walworth Co., 60 E. 42nd St., N. Y. C., N. Y.

42. Gerstein and Copper, 1 West Third St., South Boston, Mass.
43. Chauncy Wing Co., 78 Pierce St., Greenfield, Mass.
44. Cundy-Bettoney, 96 Bradlee St., Hyde Park, Mass.
45. Wm S. Haynes Co., 108 Mass. Ave., Boston, Mass.
46. Bernard Rice's Sons, Inc., 325 Fifth Ave., N. Y. C. 16, N. Y.
47. Westinghouse Electric Manufacturing Co., East Pittsburgh, Pa.

Index

A

Admittance, 476
AFC, 58
Alpert, D., 307
Altar, W., 674
Amplifier, 924
  i-f, W-5, 555
  pulse, 550
  for standing wave measurements, 496–503
  twin-T, 501
Amplitude transmission measurement, 577–584
Angular frequency, 3
ANRFCCC, 9
Antenna, gain of, 899
  scattering by, 899
Apker, L., 675
Attenuation, 680
  angular dependency of, 690
  cable, 701
  definitions of, 679–682
  dissipative, 681
  frequency sensitivity of, 683
  as function of wavelength in coaxial-line attenuators, 764, 766
  in line, change in standing-wave voltage ratio resulting from, 702
  measurement of, 804–853
  of microwave cables, 744
  reflective, 681
  very small, measurement of, 821–824
  and voltage standing-wave ratio, 820
Attenuation calibration with absolute power measurement, 838–841
Attenuation constant, 3, 682, 686
  measurement of, 822
Attenuation measurement, with Ballantine voltmeter, 806
  with i-f standard attenuator, 812
  sources of error in, 824–832
  by standing waves, 816–821
Attenuation measurement, substitution method of, 808–816
  with thermistor bridge, 813
  with two slotted sections, 805
Attenuation standards, calibration of, 832–838
  secondary, calibration of, 841–848
Attenuator, coaxial, cable as, 743–745
    carbon-coated, 745–747
    variable metalized-glass, 769–774
  coaxial-line, $\frac{5}{16}$-in., 762
    $\frac{7}{8}$-in., 762
  cutoff, 685–719
    equivalent circuit of, 700
    input impedance of, 696–700
    mode purity of, 687–689
    principles of, 685–687
    3-cm-band TE_{11}-mode, 715
    with TM_{01}-mode, 719
  design considerations for, 682–685
  dissipative, 720
  double-vane, 785
  fixed, adjustment of, 850
    TMX-81 PB, 782
  flap, 748
  helical-spring r-f contacts for, 714
  impedance matching in, 700–707
  iris coupling in, 709
  loop-coupled TE_{11}-mode, 689
  metalized-glass, precision, 751–799
  microwave, 679–803
  model O, 709
  model S, 710
  model T, 709
  1-cm-band, 925
  power dividers as, 799–803
  production calibration of, 848–853
  for reflection reduction, 573
  resistive, 720–799
    general laboratory, 743–751
  separation of undesirable modes in, 689–693
  standard coaxial, 763

Attenuator, 3-cm-band, 925
10-cm-band, 925
TPK 35/PB/40, 786
TPS-15, 707
for 24,000 Mc/sec, 716–718
vane, 749
variable, calibration of, for signal generators, 851
cam drive for, 784
1-cm-band, 786
⅝-in.-line, 770
¾-in.-line, 771
variable coaxial-line, matching of, 772
waveguide, fixed, 747
for 3000 Mc/sec, 707–715
for 9000 Mc/sec, 715
variable, 748–751
construction of, 784–790
performance of, 790–799
Attenuator inserts, evaporation chamber for, 760
Attenuator pads (*see* Pads)
Attenuator standard, waveguide metalized glass, 836
Automatic frequency control (*see* AFC)

B

Bandwidth of cavity (*see* Cavity, bandwidth of)
Barretter, 81 156–171
direct-reading bridges for, 169–171
theory of operation of, 161–169
type 821, 160
Barretter-amplifier combinations, 171–175
Barretter demodulation, 166
Barretter mount, 175–179
type 82X, 178
Barrow, W. L., 297, 303, 307, 329
Beads, dielectric, 11
Becker, J. A., 141, 188
Beers, Y., 273
Beggs, H. E., 180
Bell Telephone Laboratories, 188, 201, 212, 512, 735
Beringer, R., 273
Bessel functions, roots of, 299
Bethe, H. A., 860
Bethe-hole coupler, 858–866
Bibliography of dielectric constant measurements, 673–676
Birks, J. B., 676
Bleaney, B., 168
Bode, H. W., 61
Bodtman, W. F., 198, 212
Bolometer, 81
a-f response of, 100–103
metalized-glass, 184–187
Bolometer bridges, temperature compensation of, 103–105
Boonton Radio Corporation, 552
Borgnis, F., 294, 297, 303, 307, 673
Breazeale, W. M., 273
Breckenridge, R., 674, 675
Bridge, self-balancing, 127–130
(*See also* type of bridge, Impedance; W-; etc.)
Bridge circuit, 84–89
operation of thermistor in, 97–100
(*See also* type of bridge)
Bridge sensitivity, 86
Brownlow, J. M., 675
Bunching, 24, 25
Burrows, C. R., 675

C

Cable attenuation, 701
Cables, 9
flexible, 8, 244
Calbick, C. J., 195, 202, 673
Calorimeter for measuring loss, 582
Cavity, bandwidth of, 291
beacon-reference, 377
as circuit element, 286–293
containing dielectric materials, 307
filter, 377
normal-mode fields in, 293–308
partial-coaxial, 377–379
resonant, 285–342, 375–384
standard, external temperature compensation for, 386–390
humidity effects for, 384, 390–392
temperature-compensated, 384
temperature effects, for, 384–390
for 24,000 Mc/sec, 383
standard measurement conditions for, 393
TE_{011}-mode, 325, 379–382
hybrid, 382–384
Cavity comparator, 403–407, 446
TFU-1RL, 406
Cavity-coupling system, 286, 330–342
single-line, equivalent circuit of, 286
two-line, equivalent circuit of, 289
transmission through, 289

Cavity oscillator, 707B, 250
Cavity Q-meter, 396–403, 447
Cavity systems, very-high-Q, 340
very-low-Q, 339
Chaloff, R. S., 175
Charles, B. P., 891
Chesley, F. G., 675
Clamping circuit, diode, 238
Coaxial resonator, 303
Coaxial T's, 527
Coaxial wavemeter, 320–322
Cole, P. A., 193
Collie, C. H., 673
Columbia Radiation Laboratory, 511
Condon, E. U., 294
Connector, 923
for coaxial line, 13
type N, 9
UHF, 10
Coupler, Bethe-hole, 858–866
branched-guide, 866–873
equivalent circuit of, 868
coaxial, inside-out, 874
directional (*see* Directional Coupler)
long-slot, 885–890
multiple-path, 879–883
resistive-loop, 891
two-hole, 873–879
Coupling, definition of, 859
measurement of, 895
(*See also* Line, coaxial; Waveguide; etc.)
Coupling coefficient, 487
Coupling loop, resistive-stripe, for cutoff attenuator, 703
for TE_{11}-mode cutoff attenuator, 703
Coupling parameters, 288
Crossover phenomenon, 693
Cross section, absorption, 899
Crystal, r-f impedance of, 498
silicon, rectification of, 498
Crystal barrier, equivalent circuit of, 279
Crystal boundary layer, 279
Crystal holder, 7, 925
Crystal oscillator (*see* Oscillator, crystal)
Crystal rectifier, 4, 924
harmonic generation by, 373
Crystal units, cartridge, properties of, 7
Cutoff attenuator (*see* Attenuator, cutoff)
Cutoff parameter, 686
Cutoff wavelength, 685

D

Dakin, T. W., 675
Davidson, C. F., 675
De Bretteville, A. P., Jr., 675
Decrement measurements, 340–342
Detector, coherent-signal, 546
for standing-wave measurements, 496–503
Detector nonlinearity, effects of, 635
Dicke, R. H., 271, 273
Dielectric constant, 3, 561
complex, 561
relations for analysis of data, 562–568
relative (*see* Specific inductive capacity)
Dielectric constant measurement, 561–676
bibliography of, 673–676
choice of method for, 568–570
comparison of, with optical methods, 604
comparison of methods for, 671
consistency of results in, 666
corrections for clearance of, 576
details of computation for, 584
by phase shift in guide, 571
by reflection, 606–625
by resonant-cavity methods, 657–665
by short-circuited-line method, 621, 625–656
gap between sample and short circuit, 631
measurement procedure, 633–640
method of, 646
modifications for low power, 644–654
sample thickness for, 630
sources of error in, 640–644
theory of, 625–633
uses of, 654–657
summary of methods for, 666–672
by transmission in free space, 591–606
by transmission in guide, 570–591
Diffraction, 898
Diode rectifiers, 193
Direct-reading bridge, 84
for barretter, 169–171
Directional coupler, 522, 800, 854–897, 925
branched-guide, modified, 873
comparison of types of, 850
equivalent circuit of, 855–858

Directional coupler, properties of, measurements of, 894
reverse-coupling, 883
Schwinger, 885
slotted block, for coaxial line, 878
theoretical considerations for, 891–894
two-hole, 873–879
with two slots, 876
(*See also* Coupler)
Directivity, definition of, 859
measurement of, 895
Discriminator, microwave, 63–67
employing two magic T's, 66
Double-probe coupling, 213
Dowker, Y., 488, 673–675
Du Mont K1017 oscilloscope, 469
Du Mont Laboratories, Allen B., 469
Dunsmuir, R., 675

E

E-plane horn, center of phase of, 906
phase front of, 906
power pattern of, 906
radiation pattern of, 906
E-plane T, wavemeter on, 314–316
Ebert, J., 816
Echo boxes, 192, 303, 325
OBU-3, 327
TS-218A, 447
Ehlers, F. E., 743
Electric field, 3
Electroforming, 524
Electronic-tuning hysteresis, 30
Englund, C. R., 674
Equivalence relations for free space and waveguide, 565
Equivalent circuit of lossless devices, 513
Everhart, E. M., 675, 676

F

Feenberg, E., 166, 374, 675, 725
Ferguson, J. F., 749
Fisher, H. J., 749
Frank, N. H., 718
Frequency, 3
standard, broadcasts of, 353
Frequency-difference measurements, 453
Frequency dividers, 354–357
regenerative-modulator, 356
Frequency measurements, 343–407, 453
spectrum-analyzer for, 393–395
Frequency measuring equipment and techniques, 392–407
Frequency multiplication, 33
Frequency multiplier, push-pull, 368
push-push, 368
vacuum-tube, 365–373
velocity-modulated, 373
Frequency-pulling, 291–293
Frequency stabilization (*see* Stabilization, frequency)
Frequency stabilizer, 67
Frequency standard, accuracy of, 375
microwave, 344
design considerations of, 345–347
Radiation Laboratory, 347–375
primary, 343–347
secondary, 375–384
Friis, H. T., 223

G

Gain, antenna, 899
measurement of, 907–909
Gain determination, mirror method of, 911–914
by pattern integration, 914
Gain factor, 899
Gain measurements, scattering in, effect of 909–911
Gainsborough, G. F., 136, 812
Galvanometer-amplifier, 499
General Electric Company, 180, 193, 443
Gent, A. W., 674
Ginzton, E., 374
Giordano, A. B., 833
GL-559, 193
GL-582 diode, 193
Grant, A. S., 674
Green, E. I., 749
Guillemin, E. A., 341
Guillotine attenuator, 787
Guthrie, G. B., 175, 807

H

Hansen, W. W., 272, 294, 307, 674
Harmonic generation, by crystal rectifiers, 373
frequency range covered by, 374
Harrison A., 374

Harrison, R. J., 175
Hatch, R., 374
Haugen, M., 673
Hegarty, M., 675
Helical-spring r-f contact for attenuator, 714
Hersberger, W. D., 214
Hollman, H. E., 468
Horner, F., 674–676
Hower, P. A., 350
Hughes, Rita, 212
Humidity-effect nomograph for cavities, 391
Hunt, L. E., 676
Hybrid coil, 546
Hysteresis, electronic-tuning, **30**

I

Image, higher-order, 416
Imaginary unit, 3
Impedance, 476
  of polyiron, in coaxial line, 724
    in waveguide, 727
Impedance bridge, 446, 515–560
  basic measuring techniques with, 530–537
  built-in calibrator for, 558
  calibration of, 556–559
  error for, 560
  with f-m discrimination, 543–548
  line components for, 540–545, 549, 554
  multifrequency, 537–543
    with panoramic receiver, 539
  with panoramic receiver, 552–556
  pulse-modulated, 538, 548–552
  single-frequency, 530
  sources of error for, 559
Impedance-bridge elements, 516–530
Impedance-circle diagrams, 476, 697
Incidence, angle of, measurement of, 602
  arbitrary, measurements at, 599–604
  far from normal, 613
  normal, measurements at, 593–599
Inductive capacity, specific, 561
Insertion loss, 680
Interface reflection, 600
Iris-coupling in attenuators, **709**

J

Jackson, W., 674–676
Jamieson, H. W., 180
Jelatis, D., 673, 674
Johnson, M. H., 216
Johnson, S. A., 184, 816
Johnson meter, 216
Julian, R. S., 801, 878, 896

K

Kallman, H. E., 512
Katz, S., 228
King, R. W. P., 754
Kinzer, J. P., 294, 297, 302, **303**
Kircher, R. J., 198
Klystron, double-cavity, **374**
  reflex, 21
    characteristics of, 35
    1-cm, 47–51
    oscillator, 23–33
    power supplies, 51–58
    tube types, 34–51
    2K28, 41
  723A/B, 31
  2K25, 37
  type 417, 43
Klystron power supplies, **924**
Konig, H., 308
Korman, N. I., 509
Krock, R., 109
Kuper, J. B. H., 193, **274**
Kyhl, R. L., 273

L

L4PD load lamp, 180
Lane, J. A., 673
Leakage, r-f, 240–243
  techniques to minimize, **242**
Lee, Gordon M., 468
Leiter, H. A., 673
Letter symbols, 3
Lighthouse diode, 2B22, 461
Lighthouse tube, 2C40, 22
Lighthouse-tube cavity, 256
Line, bifurcated, 801
  coaxial, 11–13
    connector for, 13
    rigid, 923
Lippmann, B. A., 873
Littelfuse mount, tunable, 176
Llewellyn, F. B., 813
Load, coaxial-line, high-power, 732–735
  gas, for power measurement, 214
  high-power, 721

Load, high-power, dissipative-wall, 739
1.25-cm-band, 742
3-cm-band, 738
hot transmission-line, 271
IRC resistance, for rectangular waveguide, 729
low-power, 721
matched, 503–505
water, 194–213
closed-flow system for, 209
for coaxial line, 195–199
flow systems for, 204–211
for 1-cm-band, 203
for 3-cm-band, 202
thermopiles for, 211
for waveguide, 199–204
waveguide, high-power, 735–743
Load lamps, 180–183
Loaded Q, 289
Loss tangent, 561
calculation of, 629
for distilled water, 195
of water, 587
Loughlin, R., 675

M

Magic T, 63, 237, 331, 517, 525, 546
Magic-T alignment, 535
Magnetic field, 3
Magnetic permeability, 3
Mann, L., 127
Manufacturers of microwave equipment, 923–927
Match, sliding, 534
Matching techniques for T's, 525
Mathison, W. W., 175
Meahl, H. R., 676
Measurement (*see* quantity to be measured)
Merchant, R., 675
Metalization of glass plates, 775
Metalized glass, coaxial-line termination of, 724
use of, with low-power terminations, 731
Metalized-glass plates, matching of, 778
Microwave attenuator (*see* Attenuator, microwave)
Microwave current, heating effects of, 166
Microwave equipment, manufacturers of, 923–927
Microwave oscilloscopes, 468
Microwave region, 1
Microwave wavemeters, 319–330
Microwaves, detection of, 4–8
Mie, G., 307
Mieher, W. W., 297, 303, 307, 329
Mismatches, adjustable reference, 557
Mode chart, 298
for coaxial cylinder, 304
for right circular cylinder, 298
for TFX-30 wavemeter, 324
Mode filtering, 693–696
Mode patterns, reflector, 26
Mode shapes, universal, 28
Model O attenuator, 709
Model S attenuator, 710
Model T attenuator, 709
Modes, in circular waveguide, 690
normal, of cavity, 285, 293
in coaxial resonator, 303–307
in rectangular parallelopiped cavity, 294–296
of right-circular cylinder, 297–303
in slotted guides, 889
Modulation, amplitude, 24
frequency, 24
velocity, 24
Modulator, single-sideband, 331
Moore, A. A. S., 776
More, K. R., 193
Moreno, T., 177
Morgan, S. O., 735
Mueller, G. E., 512
Multivibrator, pulse, 239
Myers, G. B., 891

N

National Bureau of Standards, 344, 347, 355, 393
National Physical Laboratory, 813
Neon tubes as power indicators, 218
Networks, ring, 527
Niemann, F. L., 149
Noise figure, receiver, 222–226
Noise-figure measurement, 224
with microwave noise source, 225
Noise generators, 222
Noise klystron, 274
Noise source, crystal, 278–281
microwave, 270–281
723A/B Klystron, 277
shot, 273–278

Noise source, Sperry 419, 277
sun as, 272
thermal, 271–273
Noise temperature, 225
of Sperry 417-A Klystron, 276
Nordsieck, A., 511
Normal incidence, 612

O

OBU-3 Echo Box, 327
Optical methods, comparison of, with other dielectric constant measurement, 604
Oscillator, audio interpolation, 359–361
crystal, for frequency standard, 352
crystal-controlled, for frequency standard, 350–353
frequency-marker, 437
microwave, 21–58
pulse modulation of, 237–240
stabilized, 331
tunable, 357–359
Oscillator tubes, 924
Oscilloscope, comparison, 361–365
Oscilloscope, Du Mont K1017, 469
r-f (*see* R-f oscilloscope)
Oster, G., 675

P

Pad inserts, coaxial, electrical design of, 752–757
Pads, coaxial, fixed, 745–747
construction of, 757–763
performance characteristics of, 763–769
polyiron waveguide, 747
waveguide, fixed, 781–784
Painter, N., 109
Pattern, radiation, of *E*-plane horn, 906
Pattern integration, gain determination by, 914
Pattern intensity measurements, 900–907
Pattern measurement, 898–915
minimum range for, 901
Pattern parameters, 898
Payne-Scott, Ruby, 272
Penrose, R. P., 673, 676
Permeability, complex, 561
magnetic, 3
Peskin, E., 161
Peterson, L. C., 813
Pfister, 674
Phase, center of, 900
of *E*-plane horn, 906
frequency sensitivity of, 917
Phase apparatus, for line sources, 918
for point sources, 916
Phase constant, 3
Phase front, of *E*-plane horn, 906
Phase measurement, in free space, 592
by phase-modulation method, 919–922
of *Q*, 336–340
Phase-shift measurement, 570–577
Phase shifter, 570
Plunger, 925
short-circuiting, 504
Polyiron, impedance of, in coaxial line, 724
in waveguide, 727
low-power waveguide termination with, 726–728
Polytechnic Institute of Brooklyn, 184
Pound, R. V., 331
Power, 3
average, 80
pulse, 80
Power divider, 799–803
adjustable, 214
for high-power measurements, 213–215
Power measurements, 924
at high level, 194–220
at low and medium levels, 84–194
microwave, 79–220
Power pattern, of *E*-plane horn, 906
Power ratio, measurement of, 805–808
Power supply for klystron, 51–58
Mark SX-12, 55
Probe, calibrated pickup, 799
design of, 488–496
distortion of standing-wave pattern by, 485
electric, 479
magnetic, 479
shielded, 489
10-cm, 495
traveling, 478–480, 483–488
Propagation constant, 3, 569
Pulse-forming circuits, 237
Pulse response, of receiver, 227
Pulsed modulation of oscillator, 237–240
Pulses, synchronization of, 239
Purcell, E. M., 911

Q

Q, loaded, 289
  phase measurements of, 336–340
  unloaded, 289
Q-factors, 288, 293
Q-meter, cavity, 396–403, 447

R

R6271 diode, 464
Radiation *Q*, 289
Radio Corporation of America, 214, 464
Radio Research Laboratory, 198
Rambo, W. R., 198
Receiver, comparison, 353
  pulse, measurements on, 226–234
    response of, to frequency-modulated signals, 230
  testing of, 222–234
  ultimate sensitivity of, 222
Recovery time of receiving system, 233
Rectifiers for power indication, 191–194
Reddish, W., 676
Redheffer, R. M., 488, 673–675
Reflection, interface, 565, 606–612
  large, measurement of, 536
  probe, 607–609
Reflection coefficient, 3, 475
  complex, 565
Reflection measurement in free space, 612–616
Reflectometer, 896
Reflector-mode pattern (*see* Mode pattern, reflector)
Resistive disk, 705
Resistivity, d-c, of common metals and alloys, 296
Resonant cavities, 285–342, 5–384
R-f cables, 8, 923
R-f envelope viewer, 193, 408, 455–468
  crystal, 458
  detector for, 459
  diode detectors for, 461
R-f oscilloscope, 408, 455, 467–469
R-f phase measurements, 898–900, 915–922
R-f source, modulation of, 500
Richtmeyer, R. D., 307
Rieke diagram, 31
Roberts, S., 223, 674
Robertson, S. D., 676
Roth, 674
RP-347 spectrum analyzer, 443
RP-392-K spectrum analyzer, 443

S

Saxton, J. A., 673, 676
Scaling theorems, 308
Scattering matrix, 517, 892
Schelkunoff, S. A., 905
Schneeberger, R. J., 203, 220
Seaman, E. C. H., 675
707B cavity oscillator, 250
707B characteristics, 35
723A/B characteristics, 35
723A/B klystron, 31
Shaw, R. C., 198, 212
Shive, J. N., 188
Short-circuited-line method, dielectric constant measurement by (*see* Dielectric constant measurement, by short-circuited-line method)
Shot noise, 270
Shot-noise sources, 273–278
Side-outlet T, 516–522
Signal generator, 221–281
  with magic T, 236
  microwave, design of, 234–270
  pulsed, 228
  pulsed-lighthouse-tube, 253–259
  pulsed-off, 229
  simple, 235
  TGS-5BL, 247–253
  for 3000-Mc/sec region, 247–253
  TS-147, 259–264
  for 24,000-Mc/sec region, 265–270
Signal generator calibration, 245
Similitude, principle of, 308
Simmonds, J. C., 675
Skin depth, 296
Slater, J. C., 822, 880
Slot waves, 482
Slotted guide, wavelength in, 481
Slotted line, characteristic impedance of, 480
Slotted section, 478–483, 925
  design of, 488–496
Smith, P. H., 478
Southworth, G. C., 273
Specific inductive capacity, 3

Spectrum, interpretation of, 448
power, 412
of pulse, 409
examples of, 449
Spectrum analyzer, 408, 925
beat-frequency indications of, 395
design considerations of, 416–423
for frequency measurement, 393–395
low-frequency, using microwave oscillators, 441–446
measurements with, 448–455
operation of, theory of, 411–416
principles and design of, 409–423
representative, 423–448
RP-347, 443
RP-347-K, 443
sensitivity of, 420
stability of, 422
TS-148/UP, 409, 429–434
TSK-2SE, 435, 440
TSK-3RL, 411, 423–429
TSS-4SE, 434–439
TSS-4SF, 411
TSX-4SE, 416, 429, 435, 439
Spectrum-analyzer principle, other instruments using, 446
Spectrum image, 415, 419
Sperry Gyroscope Company, 157, 162, 169, 177, 182, 307, 675, 788
Squeeze section, 507–510, 925
Stabilization, frequency, of microwave oscillator, 58–78
Stabilization factor, 62
Stabilization, frequency, i-f system, 69–75
results and limitations of, 75–78
Stabilizer, electronic frequency, 67
frequency, 67
Standing-wave detector, coaxial, 496
continuously indicating, 511
high-power, 510
for 1.25 cm, 490
for 3.2-cm wavelength, 492, 494
Standing-wave measurement, on cavities, 333–336
apparatus for, 503
detector for, 496–503
at high power, 510
on lossless devices, 512–514
Standing-wave minimum, shift in, 338
Standing-wave pattern, 475
Standing-wave ratio, direct measurement of, 634
Standing-wave ratio, high, measurement of, 505–507
voltage, VSWR, 3
Standing-wave voltage ratio, 3, 476
and attenuation, 820
of cavity, 335
change in, with line attenuation, 702
of TFX-30EC cavity, 335
Standing waves, fundamental relations of, 475–478
measurements of, 473–514
Strachey, C., 676
Stratton, J. A., 674
Strickland, A. C., 391
Strong, J., 776
Stub support, broadband, 13
Sturtevant, J. M., 218
Suen, T. J., 675
Sun, as noise source, 272
Superheating, 195
Sylvania Electric Products Co., 430, 434
Symbols, letter, 3
Synchroscope, 457

T

T (*see* type of T, e.g. Magic; Waveguide; etc.)
T-asymmetry, 532
T-junction, equivalent circuit of, 867
monitoring, 257
Tangential signal, 228
Taylor, T. A., 674, 676
TBX-1BR microwave impedance bridge, 446, 552
TE_{11}-mode in circular waveguide, 690
Telecommunications Research Establishment, 200, 218, 512
Temperature compensation, of bolometer bridges, 103–105
with two thermistor disks, 108–118
Terminations, 720, 925
coaxial-line, low-power, 722–726
of metalized glass, 724
coaxial polyiron, 723
low-power, with metalized glass, 731
transmission-line, matched, 720–743
waveguide, low-power, 726–731
with polyiron, 726–728
TFK-2 wavemeter, 327
TFS-5 coaxial wavemeter, 320
TFS-10, 377

TFU-1RL cavity comparator, 406
TFX-30 wavemeter, 323
TGS-5BL signal generator, 247–253
Thermistor, 81
  bead, 89, 924
    d-c characteristics of, 96
  disk, 90
  equivalent circuit for, 149
  operation of, in bridge circuit, 97–100
  V-519, 90
Thermistor bridge, 924
  self-balancing, 128
  two-disk, 117
Thermistor mount, 130–155, 925
  broadband coaxial-line, 136
  coaxial-line, 132
  double, 136
  fishtail, 150
  impedance variations of, 147
  1-cm-band, 151
  O-O, 140
  S-S, 140
  tri-tuner, 146
  waveguide, 139
Thermistor parameters, 89–97
Thermistor power monitors, 155
Thermocouple dipole, 190
Thermocouple power detectors, 187–191
  sensitivity of, 187
Tisza, L., 675
TM_{01}-mode in circular waveguide, 690
TMX-81 PB fixed attenuator, 782
Tonks, L., 675
TPK 35/PB/40 attenuator, 786
TPS-15 attenuator, 707
Transmission, measurement of, 577
Transmission coefficient, complex, 565
Transmission loss, 333
Transmission measurement, 332
  in free space, 592
TRE, (*see* Telecommunications Research Establishment)
Trigger pulses, 239
TS-218A echo box, 447
TS-148/UP spectrum analyzer, 409, 429–434
TS-155, 253–259
TS-270, 325–327
TSK-2SE spectrum analyzer, 435, 440
TSK-3RL spectrum analyzer, 411, 423–429
TSS-4SE spectrum analyzer, 411, 434–439
TSX-4SE spectrum analyzer, 416, 429, 435, 439
2B22 lighthouse diode, 193, 461
2C40 lighthouse tube, 22
2K25 klystron, 35, 37
2K25 mount, 39
2K28 reflex klystron, 35, 41
2K33, 47
  characteristics of, 36
2K45, 45
2K50, 47
Tung-Sol Lamp Works, 165
Tuning, electronic, 23, 29
    hysteresis, 30
  thermal, 46
Turner, L. B., 673
TVN-7BL, 52

U

Unitary matrix, 518
Units, system of, 2
Unloaded *Q*, 289

V

Van Vleck, J. H., 273
Vane, A. B., 273
V-bridge, 105–108
V-519 thermistor, 90
von Hippel, A. R., 590, 621, 673–675
VSWR (*see* Standing-wave voltage ratio)

W

Walker, R. M., 203
Waller, W. E., 515, 850
Waltz, M. C., 274
Water load (*see* Load, water)
Wattmeter, coaxial, for field use, 215
Wave number, 3
Waveguide, 923
  flexible, 244
  standard rectangular, 15
  wall losses in, 590
Waveguide coupling, 15
  choke-flange, 14
Waveguide T's, manufacture of, 524
Waveguide transmission lines, 13–16
Wavelength, 3
  measurement of, 285–342
  in waveguide, 3

Wavemeter, 925
cavity, transmission, 309–311
coaxial, TFS-5, 320
on coaxial stub, 318
on E-plane T, 314–316
microwave, 319–330
mode, TE_{011}, 322–325, 328–330
TE_{11n}, 327
reaction, 311–314
TFK-2, 327
TFX-30, 323
on top of waveguide, 316–318
for 24,000-Mc/sec region, 327
Wavemeter circuits, practical, 308–319
Wax, N., 202
W-bridge, 118–123
Webber, H. E., 166
Weber, E., 828
Wesson, L. G., 675
Westinghouse Electric Corporation, 176, 202, 220
Westinghouse Electric and Mfg. Co., 430
Westphal, W., 673–675
Whitcher, S. L., 675
Wiesner, J. B., 100
Winkler, E. D., 673, 675
Wollaston wire, 157
Wood, R. F., 676
Worthington, H. R., 919
WWV, Radio Station, 344, 353

X

X-bridge, 123–127

Y

Younker, E. L., 589, 673